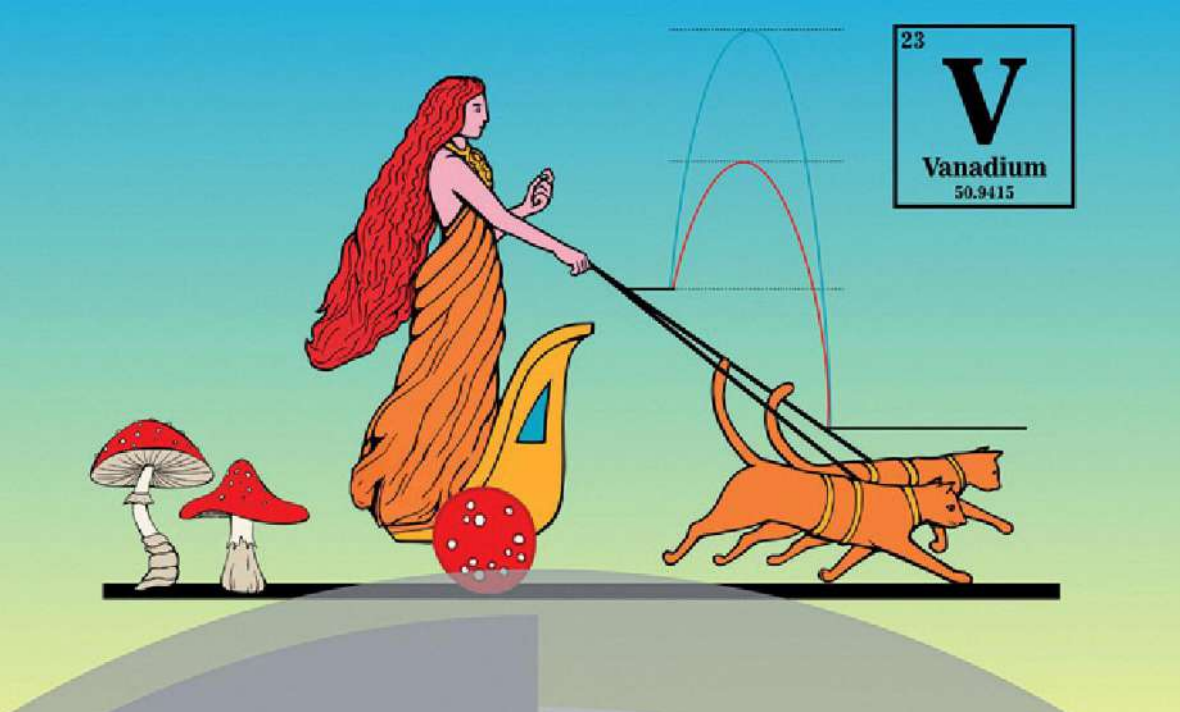

Catalysis Series

Vanadium Catalysis

Edited by Manas Sutradhar, José Armando L. da Silva and Armando J. L. Pombeiro

ROYAL SOCIETY OF CHEMISTRY

Vanadium Catalysis

Catalysis Series

Editor-in-chief:
Justin S. J. Hargreaves, *University of Glasgow, UK*

Series editors:
Bert Klein Gebbink, *Utrecht University, The Netherlands*
Jose Rodriguez, *Brookhaven National Laboratory, USA*

Titles in the series:
1: Carbons and Carbon Supported Catalysts in Hydroprocessing
2: Chiral Sulfur Ligands: Asymmetric Catalysis
3: Recent Developments in Asymmetric Organocatalysis
4: Catalysis in the Refining of Fischer–Tropsch Syncrude
5: Organocatalytic Enantioselective Conjugate Addition Reactions: A Powerful Tool for the Stereocontrolled Synthesis of Complex Molecules
6: N-Heterocyclic Carbenes: From Laboratory Curiosities to Efficient Synthetic Tools
7: *P*-Stereogenic Ligands in Enantioselective Catalysis
8: Chemistry of the Morita–Baylis–Hillman Reaction
9: Proton-Coupled Electron Transfer: A Carrefour of Chemical Reactivity Traditions
10: Asymmetric Domino Reactions
11: C-H and C-X Bond Functionalization: Transition Metal Mediation
12: Metal Organic Frameworks as Heterogeneous Catalysts
13: Environmental Catalysis Over Gold-Based Materials
14: Computational Catalysis
15: Catalysis in Ionic Liquids: From Catalyst Synthesis to Application
16: Economic Synthesis of Heterocycles: Zinc, Iron, Copper, Cobalt, Manganese and Nickel Catalysts
17: Metal Nanoparticles for Catalysis: Advances and Applications
18: Heterogeneous Gold Catalysts and Catalysis
19: Conjugated Linoleic Acids and Conjugated Vegetable Oils
20: Enantioselective Multicatalysed Tandem Reactions
21: New Trends in Cross-Coupling: Theory and Applications
22: Atomically-Precise Methods for Synthesis of Solid Catalysts
23: Nanostructured Carbon Materials for Catalysis
24: Heterocycles from Double-Functionalized Arenes: Transition Metal Catalyzed Coupling Reactions
25: Asymmetric Functionalization of C–H Bonds
26: Enantioselective Nickel-catalysed Transformations
27: N-Heterocyclic Carbenes: From Laboratory Curiosities to Efficient Synthetic Tools, 2nd edition
28: Zeolites in Catalysis: Properties and Applications
29: Biocatalysis: An Industrial Perspective

30: Dienamine Catalysis for Organic Synthesis
31: Metal-free Functionalized Carbons in Catalysis: Synthesis, Characterization and Applications
32: Modern Biocatalysis: Advances Towards Synthetic Biological Systems
33: NO_x Trap Catalysts and Technologies: Fundamentals and Industrial Applications
34: Alternative Catalytic Materials: Carbides, Nitrides, Phosphides and Amorphous Boron Alloys
35: Enantioselective Cobalt-catalysed Transformations
36: Noncovalent Interactions in Catalysis
37: Carbon Nanomaterials in Hydrogenation Catalysis
38: Nanoparticle Design and Characterization for Catalytic Applications in Sustainable Chemistry
39: Catalytic Aerobic Oxidations
40: Catalysis with Earth-abundant Elements
41: Vanadium Catalysis

How to obtain future titles on publication:
A standing order plan is available for this series. A standing order will bring delivery of each new volume immediately on publication.

For further information please contact:
Book Sales Department, Royal Society of Chemistry, Thomas Graham House, Science Park, Milton Road, Cambridge, CB4 0WF, UK
Telephone: +44 (0)1223 420066, Fax: +44 (0)1223 420247
Email: booksales@rsc.org
Visit our website at www.rsc.org/books

Vanadium Catalysis

Edited by

Manas Sutradhar
University of Lisbon, Portugal
Email: manas@tecnico.ulisboa.pt

José Armando L. da Silva
University of Lisbon, Portugal
Email: pcd1950@tecnico.ulisboa.pt

and

Armando J. L. Pombeiro
University of Lisbon, Portugal
Email: pombeiro@tecnico.ulisboa.pt

Catalysis Series No. 41

Print ISBN: 978-1-78801-857-9
PDF ISBN: 978-1-83916-088-2
EPUB ISBN: 978-1-83916-089-9
Print: ISSN: 1757-6725
Electronic ISSN: 1757-6733

A catalogue record for this book is available from the British Library

The Royal Society of Chemistry is a charity, registered in England and Wales, Number 207890, and a company incorporated in England by Royal Charter (Registered No. RC000524), registered office: Burlington House, Piccadilly, London W1J 0BA, UK, Telephone: +44 (0) 20 7437 8656.

For further information see our web site at www.rsc.org

Printed in the United Kingdom by CPI Group (UK) Ltd, Croydon, CR0 4YY, UK

Preface

Vanadium, named after the Scandinavian goddess of beauty and fertility, *Vanadis* (Freyja), with the atomic number 23, is the 22nd most abundant element in Earth's crust, being pervasively available in soil, crude oil, water, some living organisms (ascidians, a few fungi) and the vanadium-dependent enzymes nitrogenases and haloperoxidases whose actions involve biological catalytic processes. Besides being a biologically relevant element, its compounds have broad applications in catalysis. Accordingly, many original research articles and a considerable number of reviews on the application of vanadium compounds in catalysis have been published over the past few years. However, in spite of the availability of various books on Vanadium Chemistry, Bioinorganic Chemistry, Biochemistry and Biology, with applications in pharmacology and in industry, a book focused on Vanadium in Catalysis has not yet appeared.

This book intends to fill this gap and its cover image is inspired from the goddess *Vanadis* and on the *Amanita* mushroom, a natural source of *Amavadin*, a non-oxido vanadium complex with an unveiled intriguing catalytic activity.

Vanadium Catalysis provides a booming and broad area of research, and a book therein, contributing to the systematisation of the knowledge on this inter- and transdisciplinary field, namely covering chemical, biological and photochemical perspectives (either experimental or theoretical ones), appears to be quite timely.

This book addresses relevant topics on current Vanadium Catalysis, comprising 25 chapters organised in three parts following an Introduction: *Inorganic Catalysis* (with fourteen chapters), *Organometallic Catalysis* (five chapters) and *Biochemical and Biomimetic Catalysis* (also with five chapters). It covers extensive areas with well-documented research on relevant vanadium systems in catalysis, including chemical and biological and their respective models, addressing also the mechanisms involved, by gathering

Catalysis Series No. 41
Vanadium Catalysis
Edited by Manas Sutradhar, José Armando L. da Silva and Armando J. L. Pombeiro

Published by the Royal Society of Chemistry, www.rsc.org

contributions of well recognised authors from various countries in Europe, Asia and America. A detailed description of the contents of the book, including a brief summary of each chapter, is found in the Introduction (Chapter 1).

This book should provide reference documents for academic staff, students of various university levels and researchers at academia and in the industry. Hopefully it will be influential towards the introduction or establishment of interdisciplinary approaches, leading to new scientific developments in the use of vanadium in catalytic processes.

We hope readers will enjoy this book as much as we did while editing it, and will consider it as an inspiring source for future studies in the field of Vanadium Catalysis which is rapidly growing and promising, highly deserving further exploration.

We are thankful to all the authors for their worthy contributions, to the Royal Society of Chemistry for publishing the book, kind assistance and understanding along the arduous coronavirus pandemic, as well as the Fundação para a Ciência e Tecnologia (FCT), Portugal, through the 2020-2023 multiannual funding to Centro de Química Estrutural (project UIDB/00100/2020).

Manas Sutradhar
José Armando L. da Silva
Armando J. L. Pombeiro

Contents

Catalysis Series No. 41
Vanadium Catalysis
Edited by Manas Sutradhar, José Armando L. da Silva and Armando J. L. Pombeiro

Published by the Royal Society of Chemistry, www.rsc.org

CHAPTER 1

Introduction: Vanadium, Its Compounds and Applications

MANAS SUTRADHAR,* JOSÉ ARMANDO L. DA SILVA* AND ARMANDO J. L. POMBEIRO*

Centro de Química Estrutural, Instituto Superior Técnico, Universidade de Lisboa, Av. Rovisco Pais, 1049-001 Lisboa, Portugal
*Emails: manas@tecnico.ulisboa.pt; pcd1950@tecnico.ulisboa.pt; pombeiro@tecnico.ulisboa.pt

1.1 Vanadium

Vanadium is an early first-row transition metal (atomic number 23) that was discovered in 1801 by Andrés Manuel del Rio in Mexico City from a specimen of vanadinite, $Pb_5(VO_4)_3Cl$. However, it was wrongly identified as a chromium mineral by other chemists until in 1831 when the Swedish chemist Nil Gabriel Selfström in Stockholm ''discovered'' vanadium and separated it from a sample of cast iron. It was confirmed as a new chemical element in the 19th century after decades of uncertainty that followed its initial discovery. The current designation of this metal was coined from the name of a Scandinavian goddess of beauty and fertility, Vanadis, due to the beautiful colours of vanadium compounds in solution. The metal in pure form was first isolated in 1867 by the English chemist Henry Enfield Roscoe by hydrogen reduction of vanadium dichloride, VCl_2, and he showed that previously isolated samples were vanadium nitride (VN). In 1925 the American chemists John Wesley Marden and Malcolm N. Rich obtained 99.7% pure vanadium by reduction of vanadium pentoxide, V_2O_5, with calcium metal through a variety of smelting, leaching and roasting processes.

Catalysis Series No. 41
Vanadium Catalysis
Edited by Manas Sutradhar, José Armando L. da Silva and Armando J. L. Pombeiro

Published by the Royal Society of Chemistry, www.rsc.org

Vanadium is the 20th most abundant chemical element in the Earth's crust,[1] is found in *ca.* 65 different minerals and can be a significant constituent of some fossil fuels. The commercial sources of vanadium are the minerals carnotite, vanadinite, roscoelite and vanadium-bearing magnetite. Vanadium exhibits a wide range of oxidation states from -3 to $+5$ in inorganic compounds. In its higher oxidation states, it exhibits a good Lewis acidity. Oxophilicity is also an important property. The existence of multiple oxidation states, which often can be easily interconverted, its oxophilicity and Lewis acid character, ready hydrolysis and polymerization confer to this metal a richer chemistry than that of many other elements. These properties help in the formation of, *e.g.*, aggregated oxyanions and sulphur complexes, a diversity of types of oxido complexes, and in the broad application of its compounds in catalysis, as will be widely illustrated in the chapters of this book.

1.2 Applications of Vanadium and Its Compounds

Vanadium is a suitable metal for several technological applications. It is an important component of specific steel alloys since it promotes lightness and provides additional tensile strength of these materials, as well as providing extra protection against rust and corrosion. The vanadium oxides have important applications, *e.g.*, in manufacturing of ceramics, production of coatings for electrochemical tools of energy storage equipment, microelectronic devices and specific glasses used for the production of smart windows.[2,3] Vanadium has been applied as a component of batteries. A vanadium redox flow battery, used commercially for energy storage, is an electrochemical cell containing acid aqueous solutions of this metal with ions from $+5$ to $+2$ formal oxidation states (*i.e.*, the electrolyte in the positive half-cell is at oxidation state five and four, and in the negative side at oxidation state three and two).[4] Additionally, vanadium compounds have been proposed as constituents of lithium-ion batteries[5] and for bioinspired, nonaqueous redox flow batteries.[6]

Vanadium has a versatile chemistry with several oxidation states that are interchangeable under adequate conditions and is an essential metal for some living organisms. Curiously, the majority of biological roles of vanadium are associated with redox reactions, including alternative nitrogenase that has been identified in some diazotrophs,[7] specific haloperoxidases known from some seaweeds, fungi, lichen and bacteria,[8] as well as amavadin, a metallobiomolecule that is a complex found in a few *Amanita* fungi.[9] These cases have inspired models applied for catalytic purposes involving redox reactions.

Medicinal application of vanadium compounds is also a well-explored area of research. This biologically relevant element has many useful applications in vanadium-based therapeutic drugs for the treatment of several types of diseases, *e.g.*, diabetes, cancer and diseases caused by parasites.[10–12] The antidiabetic properties of vanadium compounds have been known for more than a century[13] and, thereafter, several vanadium compounds have been studied and explored in the search for attractive antidiabetic drugs.[14] Vanadium compounds as anticancer agents are of high interest in recent times on account of a combination of

beneficial properties for chemotherapy, *i.e.*, strong cytotoxicity, anti-metastatic activity and relatively low systemic toxicity.[15]

Various vanadium compounds have been identified in many modes of interactions including inhibition of protein phosphatases,[16–18] interactions with circulating proteins (*e.g.*, serum albumin and transferrin),[19] effects on reactive oxygen species (ROS) levels,[20,21] *etc.* The effects of vanadium compounds on the plasma membrane are also known.[22]

1.3 Vanadium in Catalysis

Vanadium, as a component of catalysts, participates in diverse chemical processes, *e.g.*, for the industrial production of sulphuric acid by the contact process, fabrication of maleic anhydride, oxidation of propane and propylene to acrylonitrile, toluene to benzonitrile, alkane oxydehydrogenation, olefin epoxidation, and in the reduction of sulphur and nitrogen oxide emissions resulting from human activities.[23]

Vanadium compounds have a broad range of applications in catalysis, and many research papers and a considerable number of reviews on specific topics of vanadium catalysts have been recently published.[9,24–33] For instance, various catalytic oxidation reactions, *e.g.*, oxidation of alkanes and alcohols, epoxidation, sulphoxidation, oxidative bromination, *etc.*, are efficiently catalysed by vanadium compounds using appropriate oxidants.[9,24–33] They are active catalysts under homogeneous or heterogeneous conditions. Several VO_x based organic–inorganic nanocomposites have potential photocatalytic properties.[34,35] Vanadium compounds are also widely used in olefin metathesis, olefin oligomerization, polymerization and copolymerization reactions.[36–41] They are involved in enantioselective C–C bond-forming and oxidative–reductive coupling reactions.[28,42]

Dioxygen activation by biomimetic vanadium complexes and vanadate-dependent haloperoxidases,[43–46] as well as vanadium nitrogenase[7,47–49] and *Amavadin*,[9,29] shows the potential of biologically relevant catalytic functions of vanadium compounds.

1.4 Structure of the Book

This book addresses relevant topics on current vanadium catalysis, comprising 25 chapters with contributions from internationally recognised authors from various parts of the world. It is organised in three self-explanatory parts that reflect the broad scientific areas in which vanadium has found applications in catalysis: *Inorganic Catalysis* (fifteen chapters), *Organometallic Catalysis* (five chapters), *and Biochemical and Biomimetic Catalysis* (also five chapters). Summaries of these chapters (often based on those provided by the corresponding authors) are as follows:

Ch. 1 – Introduction: vanadium, its compounds and applications (by M. Sutradhar, J. A. L. da Silva and A. J. L. Pombeiro)

An overall view about vanadium and its compounds, as well as on the structure of the book, is outlined.

Part I – Inorganic Catalysis

Ch. 2 – Amavadin and related complexes as oxidation catalysts (by J. A. L. da Silva, M. F. C. Guedes da Silva, M. Sutradhar and A. J. L. Pombeiro)

Amavadin, a metallobiomolecule with a rare coordination chemistry and particular *N*-oxyiminodicarboxylate ligand whose biological role is yet unknown, mediates water oxidation and exhibits nitrite reductase-, catalase- and peroxidase-type activity, this one towards thiols (*e.g.*, biological ones). It also mediates peroxidative oxidation, peroxidative halogenation and carboxylation of alkanes and other hydrocarbons, as well as oxidation of alcohols. Its models, non-oxido- and oxido-V complexes, namely with non-innocent ligands, are compared for the above catalytic oxidations.

Ch. 3 – Activating hydroperoxides by vanadium(V) compounds (by J. Hartung)

Vanadium(V) compounds, namely orthovanadates, promote oxygen atom transfer from hydroperoxides to various substrates, and examples for (i) bromide oxidation by H_2O_2 and (ii) alkenol oxidation by *tert*-butyl hydroperoxide (TBHP, a more nucleophilic oxidant) are discussed, illustrating two border mechanisms. In (i) catalysed by protonated ortho-vanadates in protic solvents (as in marine bromoperoxidases), H_2O_2 should be converted to an electrophile and the influence of its σ^*(O,O)-orbital energy is discussed. In (ii), shown by trialkyl orthovanadate-catalysed oxidations by TBHP in aprotic solvents, no effect on orbital energies of the peroxide is observed.

Ch. 4 – The vanadate–pyrazinecarboxylic acid–hydrogen peroxide reagent and similar systems for efficient oxidations with peroxides (by G. B. Shul'pin and L. S. Shul'pina)

The oxidation of alkanes (RH) and arenes (ArH) with aqueous H_2O_2 in acetonitrile solutions under mild conditions, at low temperature, leads to the formation of the corresponding alkyl hydroperoxides (ROOH) and phenols (ArOH), in the presence of adequate homogeneous V-catalysts and promoters (*e.g.*, pyrazine carboxylic acid or, in some cases, a strong inorganic or organic acid). This topic is addressed in this chapter, concerning different alkanes, including methane.

Ch. 5 – Peroxo-vanadium complexes as sustainable catalysts in oxidations, halogenations and other organic transformations (by F. Sabuzi, G. Pomarico, V. Conte and P. Galloni)

The application of V-peroxido complexes as catalysts in oxidation (of hydrocarbons, alcohols, phenols and sulphides) and bromination reactions is discussed, particularly in terms of sustainability (*e.g.*, use of H_2O_2 and solvents other than toxic VOCs, and avoidance of halides). Both homogeneous and two-phase systems are addressed. Examples of lignin valorisation, fuel desulphurization and clean synthetic methodologies are summarised.

Ch. 6 – Vanadium-scorpionate catalysed oxidations (by L. M. D. R. S. Martins and A. J. L. Pombeiro)

The selective catalytic oxidation of alkanes and other hydrocarbons can potentially provide important routes for preparing large-scale commodities in the chemical industry. In this chapter, recent advances on the use of V complexes with tris(pyrazolyl)methane (C-scorpionate) ligands as homogeneous or supported oxidation catalysts towards the development of industrially significant sustainable processes are reviewed. They include oxidations of alkanes and *p*-xylenes, and carboxylations of alkanes.

Ch. 7 – Vanadium-aroylhydrazone catalysed oxidations (by M. Sutradhar, V. B. Arion, T. Roy Barman and A. J. L. Pombeiro)

The catalytic activity of V complexes derived from hydrazone Schiff bases towards various oxidation reactions (of alkanes and alcohols, olefin epoxidation and bromination) is illustrated in this chapter. The importance of the ligand and the relevance of its eventual non-innocent redox behaviour is discussed in metal–ligand cooperation processes. The influence on their catalytic performance of oxidants, co-catalysts, temperature and other parameters is analysed.

Ch. 8 – Vanadium-oxide molecular catalysts in non-aqueous solution (by Y. Hayashi, M. Katayama and K. Ozutsumi)

This chapter compiles the diversity of V-oxide clusters that are spontaneously formed and transformed in solution, with significance for catalytic reactions, using a vanadate source. Transformations into versatile structures, including tubes, spheres, blocks, disks and bowls are discussed.

Ch. 9 – Catalysis by oxometalates and their microheterogeneous media (by J. Lodh and S. Roy)

In addition to archiving the chemistry of polyoxometalates in catalysing oxidative, reductive and photo-redox reactions along with acid- and base-catalysed reactions, this chapter also highlights examples of reactions that can harvest energy. It further addresses micro-heterogeneous media, or the state of soft-oxometalates, in site-specific catalysis and polymerization reactions.

Ch. 10 – Use of vanadium catalysts in epoxidation and sulphoxidation reactions with Green Chemistry criteria (by A. Galindo, A. Pastor, F. Montilla and M. del Mar Conejo)

Catalytic applications of V complexes in the oxidation of olefin and sulphide substrates, following green chemistry criteria, are reviewed in this chapter, with emphasis on the use of green oxidants and non-conventional solvents, and the immobilization of V species into several supports (inorganic materials, organic polymers, ionic liquids, *etc.*).

Ch. 11 – Supported vanadium catalysts: heterogeneous molecular complexes, electrocatalysis and biomass transformation (by C. Freire, C. Pereira, B. Jarrais, D. Fernandes, A. Peixoto, N. Cordeiro and Filipe Teixeira)

This chapter provides an overview of supported V complexes as eco-sustainable recyclable catalysts of several chemical reactions for the production of added-value products. Different strategies for V compounds' immobilization onto solid supports are reviewed, highlighting those that lead to enhanced catalytic performance. The application of V-based materials as electrocatalysts for reduction–oxidation reactions relevant to renewable energy storage and conversion technologies is also addressed, as well as V-mediated catalytic reactions for biomass valorisation.

Ch. 12 – Carbon-supported vanadium catalysis (by S. A. C. Carabineiro, L. M. D. R. S. Martins and M. Sutradhar)

Compared to the use of heterogenous V catalysts, much less work has been dedicated to the heterogenization (anchorage) of homogenous (soluble) V complexes on solid supports and their use as heterogenized catalysts with the advantages inherent to heterogenous catalysts. In this chapter, this interface area of research is reviewed by considering both V complexes (that can also act as soluble homogeneous catalysts) and V oxides supported on different types of C materials.

Ch. 13 – Molecularly dispersed vanadium oxide: structure-reactivity relationships for reducibility and hydrocarbon oxidation (by M. O. Guerrero-Pérez, M.V. Martínez-Huerta and M. A. Bañares)

Molecularly dispersed V oxide on oxide supports is a highly active material, and its redox and acidic properties can be tuned by its interaction with the support. The structure of the dispersed V oxide is characterised by V=O, V–O–H, V–O–V and V–O–support bonds, their reactivity depending on the coverage on the support, the cation of the support, the surface density of VO_x species and the degree of hydration. The studies on such themes, including the application of real-time catalytic spectroscopic methods (namely *operando* Raman spectroscopy), are discussed in this chapter.

Ch. 14 – Vanadium oxides in photocatalysis, including bare oxides and VO_x-based organic–inorganic nanocomposites (by E. Benavente, J. Aliaga and G. González)

This chapter provides a critical review on the use and potential of V oxides as photocatalysts under generally mild and environment-friendly conditions, as well as their advantages and limitations. Their preparation, chemical features and photocatalytic activity, as well as theoretical approaches to understand their role in the catalyst performance, are addressed. Pure, supported, doping, composites and inorganic–organic nanocomposites are analysed.

Ch. 15 – Theoretical mechanistic analysis on vanadium oxidation catalysis (by M. L. Kuznetsov)

Advances over the past 10 years in the field of V oxidation catalysis are discussed under theoretical perspectives. This chapter is focused on the mechanistic aspects of the V-catalysed oxidation reactions and on the

analysis of the main factors and driving forces which govern these processes, on the basis of theoretical methods.

Part II – Organometallic Catalysis

Ch. 16 – Vanadium-catalysed olefin oligomerization, polymerization and copolymerization (by S. Zhang and W. Zhang)

Olefin oligomerization, polymerization and copolymerization catalysed by V-based catalysts (including N-heterocyclic carbene V homogeneous catalysts) are presented in this chapter. It focuses on ethylene polymerisation and copolymerisation with α-olefins, showing the advantages of vanadium complex catalysts in controlling the molecular weight, molecular weight distribution, sequence and topological structure of the resulting ethylene–propylene copolymer.

Ch. 17 – Vanadium-catalysed olefin metathesis and related chemistry (by K. Nomura)

V-alkylidene catalysts are known to exhibit unique features that are different from those of conventional Ru and Mo complex catalysts for olefin metathesis, a widely employed method in the synthesis of fine chemicals and advanced polymeric materials. In this chapter, the basics in olefin metathesis, design of olefin metathesis catalysts with early transition metals, and recent progresses in V olefin ring-opening metathesis polymerization (ROMP) catalysis are discussed.

Ch. 18 – Vanadium-catalysed enantioselective C–C bond-forming reactions (by M. Sako, S. Takizawa and H. Sasai)

Recent advances in the enantioselective V mediated C–C bond-forming reactions *via* acid and redox catalysis are discussed in this chapter by addressing oxidative couplings of phenol derivatives catalysed by chiral V complexes. Catalysts with multidentate ligands prepared from salicylaldehyde derivatives and chiral amino acids are discussed, as well as applications in the synthesis of important chiral compounds, such as polycyclic biphenols, oxa[9]helicenes, bi(hydroxycarbazole)s and biresorcinols. The possible use of mild-reaction conditions under an air or oxygen atmosphere is emphasised.

Ch. 19 – Vanadium-induced oxidative and reductive coupling (by T. Amaya and T. Hirao)

V-induced oxidative and reductive couplings developed in the authors' group are surveyed. One-electron redox propensity and Lewis acidity of oxido-V^V compounds allow achieving oxidative C–C bond formation. The combination of B enolate and silyl enol ether towards selective cross-oxidative coupling is discussed. Ligand coupling reactions of organic substituents on main-group organometallic compounds are also induced by oxidation with such V catalysts and are described in this chapter. Moreover, reductive coupling reactions, namely of pinacol, and the use of V/Ti heterobimetallic catalysts for selective cross-coupling between aryl and aliphatic aldehydes are also addressed.

Ch. 20 – Vanadium-catalysed transformations of selected functional groups (by T. Moriuchi and T. Hirao)

Oxidative halogenation, oxidative aromatization, amination and oxidative deoxygenative coupling are discussed in this chapter. It focuses on V-catalysed oxidative aromatization of 2-cyclohexenones (to the corresponding phenol derivatives), and direct amination of allyl alcohols (with both aromatic and aliphatic amines) using oxido-V^V catalysts. Direct hydrazination of allyl alcohol and deoxygenative homocoupling reaction of alcohols depending on hydrazine derivatives, catalysed by oxido-V^V, are also addressed. The role in catalysis of the Lewis acidity, oxophilicity and redox properties of the oxido-V^V catalysts is discussed.

Part III – Biochemical and Biomimetic Catalysis

Ch. 21 – Vanadium compounds as indirect activators of a G protein-coupled receptor (by D. Althumairy, H. A. Murakami, R. Colclough, B. G. Barisas, D. A. Roess and D. C. Crans)

This chapter deals with a new mechanism for activation of luteinizing hormone receptors (LHR), a G-protein-coupled receptor which demonstrates that V compounds can initiate receptor-mediated intracellular signalling *via* indirect effects on membrane lipids. Bis(maltolato)oxovanadium(IV) (BMOV) and $VOSO_4$ decrease lipid packing, increase aggregation of LHR, and initiation of LHR signalling. Membrane lipid order effects and implications for BMOV or $VOSO_4$ internalization are also discussed.

Ch. 22 – Reductive dioxygen activation by biomimetic vanadium complexes (by C. Drouza and A. Keramidas)

Advances on O_2 activation by simple functional biomimetic V complexes are reviewed. The O_2 activation can involve coordination to V and direct reduction or, in rare cases, attack of O_2 on an activated non-innocent organic ligand (namely catecholate and hydroquinonate). V^{III}, V^{IV} compounds are shown to be efficient catalysts for $2e^-$ and $4e^-$ reductions of O_2, and mechanistic pathways are highlighted. The importance of peroxido-complexes and of biomolecules to compensate the thermodynamic and kinetic barriers is also discussed.

Ch. 23 – Vanadium in catalytically proceeding natural processes (by D. Rehder)

The naturally occurring enzymes vanadate-dependent haloperoxidases and V-dependent nitrogenases are addressed in this chapter. The vanadate–phosphate antagonism in the context of physiologically active phosphate-based enzymes is also discussed, as well as *Amavadin* with catalase and peroxidase activity.

Ch. 24 – Vanadium chloroperoxidases as versatile biocatalysts (by R. Wever, R. Renirie and F. Hollmann)

In this chapter, the catalytic and structural properties of the V chloroperoxidases (VCPO) are discussed with emphasis on their activity and stability under operational conditions which make them attractive catalysts for organic synthesis. The use of VCPO in the formation of singlet oxygen,

halogenation of phenols, alkenes, halocyclization of unsaturated alcohols and in the aza-Achmatowicz reaction is highlighted.

Ch. 25 – Vanadium catalysis relevant to nitrogenase (by H.-R. Pan and H.-F. Hsu)
This chapter is focused on V nitrogenase and V complexes showing nitrogenase-like reactivity. Structural and catalytic features of the enzyme are discussed. In addition, V complexes that show a reactivity relevant to nitrogen fixation, which includes N_2 reduction to ammonia, silylation of N_2 and reduction–disproportionation of hydrazine to NH_3, are also highlighted.

1.5 Final Remarks

The catalytic applications of vanadium compounds have been well documented in a rapidly growing number of research articles and reviews. Moreover, books on vanadium chemistry, bioinorganic chemistry, biochemistry and biology, with applications in pharmacology and in industry are available,[50–54] but a book devoted to catalysis has been missing. The current book intends to fill this gap, covering chemical, biological, photochemical and theoretical standpoints in vanadium catalysis, and providing a global and integrated view on catalysis based on research topics of current interest. This publication is expected to be a reference and inspiring tool for academic staff, researchers, students of different university levels, and will also be of significance to industry.

Acknowledgements

This work has been supported by the Fundação para a Ciência e Tecnologia (FCT) 2020–2023 multiannual funding to Centro de Química Estrutural (project UIDB/00100/2020). The authors are also grateful to the FCT for financial support to project PTDC/QEQ-QIN/3967/2014. M. S. acknowledges the FCT and IST for a working contract ''DL/57/2017'' (Contract no. IST-ID/102/2018).

References

1. E. Del Carpio, L. Hernandez, C. Ciangherotti, V. V. Coa, L. Jimenez, V. Lubes and G. Lubes, *Coord. Chem. Rev.*, 2018, **372**, 117.
2. Y. D. Wu, G. H. Zhang, R. Xu, Y. Wang and K. C. Chou, *Ceram. Int.*, 2019, **45**, 2117.
3. V. P. Prasadam, N. Bahlawane, F. Mattelaer, G. Rampelberg, C. Detavernier, L. Fang, Y. Jiang, K. Martens, I. P. Parkin and I. Papakonstantinou, *Mater. Today Chem.*, 2019, **12**, 396.
4. P. Alotto, M. Guarnieri and F. Moro, *Renewable Sustainable Energy Rev.*, 2014, **29**, 325.
5. Y. Yue and H. Liang, *Adv. Energy Mater.*, 2017, **7**, 1602545.
6. H. Huang, R. Howland, E. Agar, M. Nourani, J. A. Golen and P. J. Cappillino, *J. Mater. Chem. A*, 2017, **5**, 11586.

7. R. R. Eady, *Coord. Chem. Rev.*, 2003, **237**, 23.
8. C. Leblanc, H. Vilter, J. B. Fournier, L. Delage, P. Potin, E. Rebuffet, G. Michel, P. L. Solari, M. C. Feiters and M. Czjzek, *Coord. Chem. Rev.*, 2015, **301**, 134–146.
9. J. A. L. da Silva, J. J. R. F. da Silva and A. J. L. Pombeiro, *Coord. Chem. Rev.*, 2013, **257**, 2388.
10. J. C. Pessoa, E. Garribba, M. F. A. Santos and T. Santos-Silva, *Coord. Chem. Rev.*, 2015, **301–302**, 49.
11. D. C. Crans, J. T. Koehn, S. M. Petry, C. M. Glover, A. Wijetunga, R. Kaur, A. Levina and P. A. Lay, *Dalton Trans.*, 2019, **48**, 6383.
12. K. H. Thompson and C. Orvig, in *Metal Ions in Biological Systems, Metal Ions and Their Complexes in Medication*, ed. A. Sigel and H. Sigel, CRC Press, USA, **vol. 41**, 41, 2004, p. 221.
13. B. Lyonnet, F. Martz and E. Martin, *De l'emploi thérapeutique des dérivés du vanadium*, Assoc. Typogr, Lyon, France, 1899.
14. D. C. Crans, *J. Org. Chem.*, 2015, **80**, 11899.
15. D. C. Crans, L. Yang, A. Haase and X. Yang, in *Metallo-Drugs: Development and Action of Anticancer Agents*, ed. A. Sigel, H. Sigel, E. Freisinger and R. K.O. Sigel, De Gruyter, Berlin, Germany, ch. 9, 2018, pp. 251–274.
16. S. Trevino, A. Diaz, E. Sanchez-Lara, B. L. Sanchez-Gaytan, J. M. Perez-Aguilar and E. Gonzalez-Vergara, *Biol. Trace Elem. Res.*, 2019, **188**, 68.
17. E. Bellomo, K. B. Singh, A. Massarotti, C. Hogstrand and W. Maret, *Coord. Chem. Rev.*, 2016, **327**, 70.
18. L. Lu and M. Zhu, *Antioxid. Redox Signaling*, 2014, **20**, 2210.
19. C. G. Azevedo, I. Correia, M. M. dos Santos, M. F. Santos, T. Santos-Silva, J. Doutch, L. Fernandes, H. M. Santos, J. L. Capelo and J. C. Pessoa, *J. Inorg. Biochem.*, 2018, **180**, 211.
20. I. E. Leon, A. L. Di Virgilio, V. Porro, C. I. Muglia, L. G. Naso, P. A. M. Williams, M. Bollati-Fogolin and S. B. Etcheverry, *Dalton Trans.*, 2013, **42**, 11868.
21. U. Jungwirth, C. R. Kowol, B. K. Keppler, C. G. Hartinger, W. Berger and P. Heffeter, *Antioxid. Redox Signaling*, 2011, **15**, 1085.
22. P. W. Winter, A. Al-Qatati, A. L. Wolf-Ringwall, S. Schoeberl, P. B. Chatterjee, B. G. Barisas, D. A. Roess and D. C. Crans, *Dalton Trans.*, 2012, **41**, 6419.
23. M. O. Guerrero-Perez, *Catalysts*, 2018, **8**, 564.
24. M. Sutradhar, L. M. D. R. S. Martins, M. F. C. G. da Silva and A. J. L. Pombeiro, *Coord. Chem. Rev.*, 2015, **301**, 200.
25. H. Pellissier, *Coord. Chem. Rev.*, 2015, **284**, 93.
26. P. Schwendt, J. Tatiersky, L. Krivosudsky and M. Simunekova, *Coord. Chem. Rev.*, 2016, **318**, 135.
27. J. T. Grant, J. M. Venegas, W. P. McDermott and I. Hermans, *Chem. Rev.*, 2018, **118**, 2769.
28. R. R. Langeslay, D. M. Kaphan, C. L. Marshall, P. C. Stair, A. P. Sattelberger and M. Delferro, *Chem. Rev.*, 2019, **119**, 2128.

29. J. A. L. da Silva, J. J. R. Frausto, da Silva and A. J. L. Pombeiro, *Coord. Chem. Rev.*, 2011, **255**, 2232–2248.
30. V. Conte, A. Coletti, B. Floris, G. Licini and C. Zonta, *Coord. Chem. Rev.*, 2011, **255**, 2165.
31. M. Sutradhar and A. J. L. Pombeiro, *Cord. Chem. Rev.*, 2014, **265**, 89.
32. A. G. J. Ligtenbarg, R. Hage and B. L. Feringa, *Coord. Chem. Rev.*, 2003, **237**, 89.
33. M. Sutradhar and A. J. L. Pombeiro, in Vanadium Complexes in Catalytic Oxidations, *Elsevier Reference Module in Chemistry, Molecular Sciences and Chemical Engineering*, ed. J. Reedijk, Elsevier, Waltham, MA. 10.1016/B978-0-12-409547-2.13525-5, 2017.
34. J. M. Herrmann, *Top. Catal.*, 2005, **34**, 49.
35. N. Serpone, A. V. Emeline, S. Horikoshi, V. N. Kuznetsov and V. K. Ryabchuk, *Photochem. Photobiol. Sci.*, 2012, **11**, 1121.
36. K. Nomura and S. Zhang, *Chem. Rev.*, 2011, **111**, 2342.
37. H. Hagen, J. Boersma and G. van Koten, *Chem. Soc. Rev.*, 2002, **31**, 357.
38. J.-Q. Wu and Y.-S. Li, *Coord. Chem. Rev.*, 2011, **255**, 2303.
39. S. Gambarotta, *Coord. Chem. Rev.*, 2003, **237**, 229.
40. C. Redshaw, *Dalton Trans.*, 2010, **39**, 5595.
41. A. M. F. Phillips, H. Suo, M. F. C. Guedes, da Silva, A. J. L. Pombeiro and W.-H. Sun, *Coord. Chem. Rev.*, 2020, **416**, 213332.
42. T. Hirao, *Chem. Rev.*, 1997, **97**, 2707.
43. D. Rehder, M. Ebel, C. Wikete, G. Santoni and J. Gätjens, *Pure Appl. Chem.*, 2005, 77, 1607.
44. C. Leblanc, H. Vilter, J. Fournier, L. Delage, P. Potin, E. Rebuffet, G. Michel, P. L. Solari, M. C. Feiters and M. Czjzek, *Coord. Chem. Rev.*, 2015, **301–302**, 134.
45. R. Wever, B. E. Krenn and R. Renirie, *Methods Enzymol.*, 2018, **605**, 141.
46. R. Wever and P. Barnett, *Chem. Asian, J.*, 2017, **12**, 1997.
47. Z. Janas and P. Sobota, *Coord. Chem. Rev.*, 2005, **249**, 2144.
48. J. P. Bellenger, R. Darnajoux, X. Zhang and A. M. L. Kraepiel, *Biogeochemistry*, 2020, **149**, 53.
49. D. Sippel and O. Einsle, *Nat. Chem. Biol.*, 2017, **13**, 956.
50. *An Introduction to Vanadium: Chemistry, Occurrence and Applications*, ed. R. Bowell, Nova Science Publishers, NY, USA, 2019.
51. *Vanadium: The Versatile Metal*, ed. K. Kustin, J. C. Pessoa and D. C. Crans, American Chemical Society, 2007.
52. D. Rehder, *Bioinorganic Vanadium Chemistry*, Wiley, Chichester, UK, 2008.
53. *Vanadium-biochemical and Molecular Biological Approaches*, ed. H. Michibata, Springer, Dordrecht, The Netherlands, 2012.
54. *Vanadium: Chemistry, Biochemistry, Pharmacology and Practical Applications*, ed. A. S. Tracey, G. R. Willsky and E. S. Takeuchi, CRC Press, FL, USA, 2007.

CHAPTER 2

Amavadin and Related Complexes as Oxidation Catalysts

JOSÉ ARMANDO L. DA SILVA,* M. FÁTIMA C. GUEDES DA SILVA, MANAS SUTRADHAR AND ARMANDO J. L. POMBEIRO*

Centro de Química Estrutural, Instituto Superior Técnico, Universidade de Lisboa, Av. Rovisco Pais, 1049-001 Lisboa, Portugal
*Emails: pcd1950@tecnico.ulisboa.pt; pombeiro@tecnico.ulisboa.pt

2.1 Introduction

Amavadin (this term is probably derived from the combination of some syllables of *Amanita*, since this metallobiomolecule has been isolated from some species belonging to this genus, and vanadium[1]) or vanadium, bis[*N*-[(1*S*)-1-(carboxy-*kO*)ethyl]-*N*-(hydroxy-*kO*)-L-alaninato(2-)-*kN*,*kO*] (CAS 12705-99-6) has been identified in a few fungi, firstly in *A. muscaria* (L.:Fr.) Hook.[2–4] It is a vanadium(IV) complex bearing the basic form of (S,S)-*N*-oxyimino-(2,2′)-dipropionic acid (**1**), S,S-H_3HIDPA (Figure 2.1) with a ligand to metal ratio of 2 : 1 formulated as $[V(HIDPA)_2]^{2-}$.[2,5–7] It exhibits an unusual octa-coordinate geometry with single bonds of all eight donor atoms to the metal centre. It is a dianionic non-oxido complex with a molecular mass of 401.2.[8] The oxidation of amavadin leads to a monoanionic species with a metal centre at a formal oxidation state of five. Both oxidation states have a high level of similarity in terms of their coordination parameters.[9]

Catalysis Series No. 41
Vanadium Catalysis
Edited by Manas Sutradhar, José Armando L. da Silva and Armando J. L. Pombeiro

Published by the Royal Society of Chemistry, www.rsc.org

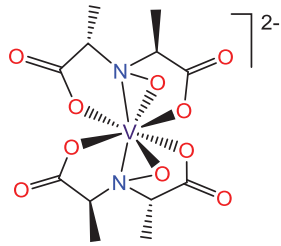

Figure 2.1 Schematic representation of amavadin at vanadium oxidation state four.

Amavadin is a particular case of vanadium(IV) coordination chemistry, which is quite rare compared with the common oxidovanadium(IV) core complexes.[10–23] Additionally, amavadin exhibits a higher coordination number (eight) than the great majority of the complexes with this metal (also rare for other first-row transition metals[14]) and with a high stability in aqueous solutions. These characteristics could explain some specificities of amavadin and its application as a catalyst.

Amavadin can be obtained from natural sources or by chemical synthesis, and its biosynthetic pathway has not yet been identified. It has a significant concentration in a few fungi (up to some hundreds of ppm, dry weight[1]) and therefore it can be extracted, although several steps are required to get pure amavadin.[2] Alternatively, its chemical synthesis does not involve very complex procedures and synthetic methodologies have been developed, allowing the production of this metallobiomolecule in significant amounts and with a high level of purity. Additionally, some of its models, using related proligands of amavadin, as well as related complexes with other transition metals, have been synthesised, amplifying the number of complexes of its type with potential catalytic activity. Some proligands of models of amavadin require fewer steps for their synthesis than for the metallobiomolecule.

2.2 Preparative Methods of Amavadin

The synthesis of the amavadin proligand (**1**, Figure 2.2) was inspired from[24] and carried out in 1973,[5] with improvements in 1986,[7,25] and in 2005 the pure enantiomer was achieved without purification by chromatography to eliminate non-natural steriosomers.[26] Other amavadin related proligands have been synthesised, such as *N*-oxyiminodiacetic acid (H_3HIDA) (CAS 87339-38-6) (**2**),[27] *meso-N*-oxyimino-2,2′-dipropionic acid (R,S-H_3HIDPA) (**3**),[28] *meso-N*-oxyimino-2,2′-dibutyric acid (R,S-H_3HIDBA) (**4**),[29] or by replacing a methyl group of the amavadin proligand by either a phenyl (**5**) or a benzyl (**6**) group (Figure 2.2).[30]

The synthesis of amavadin, the 2 : 1 vanadium(IV) complex $[V(HIDPA)_2]^{2-}$, was achieved[7] in aqueous solution by addition of a vanadyl [oxidovanadium(IV) ion, *i.e.,* VO^{2+}] salt to the proligand. Other vanadium(IV) complexes from the proligands H_3HIDA (**2**), H_3HIDPA, R,S-H_3HIDPA (**3**) and R,S-H_3HIDBA (**4**), were synthesised and their structures determined by X-ray diffraction.[28]

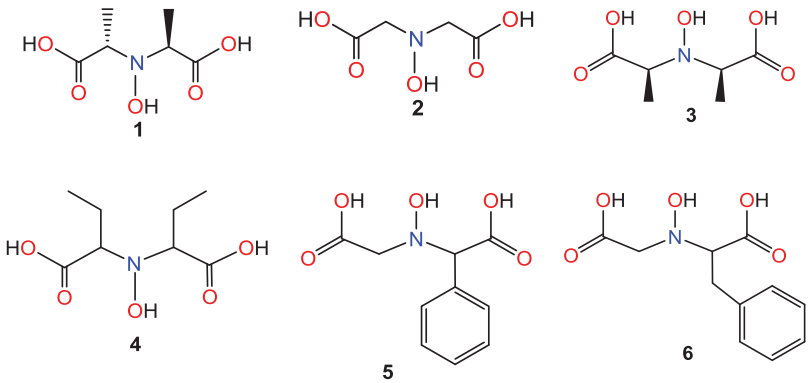

Figure 2.2 Amavadin proligand (**1**) and its related models.

Another type of amavadin model has been prepared from the proligand H_3HIDPA with some metal transition ions of the groups 4 [titanium(IV) and zirconium(IV)], 5 [niobium(V) and tantalum(V)] and 6 [molybdenum(V)],[29,31–35] as well as a chromium(III) complex from the proligand H_3HIDA (**2**).[36] However, their application as catalysts has not been reported, except for the titanium complex that does not seem to be suitable for redox reactions.[37] Their redox performance was studied for some cases by cyclic voltammetry, but only the molybdenum(V) complex from the proligand H_3HIDPA undergoes both reversible single-electron oxidation and reduction. This occurs in dichloromethane as solvent, but this complex exhibits an irreversible behaviour in aqueous solutions by the same electrochemical technique.[35]

Amavadin and related models containing vanadium as the metal centre display catalytic activity in electrochemical reactions (by mediating oxidation of some thiols), as well as in the oxidation of other substrates, including water and hydrocarbons (*i.e.*, for oxidations and other types of reactions).

2.3 Electrocatalytic Oxidation of Thiols

Electrochemical studies of amavadin-related molecules contribute to clarify their interaction with substrates (including biological ones) and can reveal information about the possible biological role of the vanadium metallobiomolecule. They can provide key information to understand the catalytic activity of amavadin and its models. Additionally, the design of new types of non-aqueous redox flow batteries was suggested on basis of the electrochemical performance of a model of amavadin.[38]

Meso-amavadin [racemic mixture of $[V(HIDPA)_2]^{2-}$ without optical activity, containing all stereoisomers of the metallobiomolecule ligand including the natural (S,S)-*N*-oxyimino-(2,2′)-dipropionate] and the related complex $[V(HIDA)_2]^{2-}$ exhibit a single-electron reversible oxidation by cyclic voltammetry (for the former at *ca.* 0.8 V *vs.* the standard hydrogen electrode in aqueous solution at neutral pH, whereas for the latter a slightly higher value by less than 0.1 V was determined)[39–42] and with a higher self-exchange rate

constant than other vanadium compounds.[43,44] In organic solvents (DMSO, DMF, acetonitrile or dichloromethane) the oxidation potential values are lower for the same process (*e.g.*, in DMSO it is *ca.* 0.3 V and 0.4 V for *meso*-amavadin and $[V(HIDA)_2]^{2-}$, respectively).[41] The reversible behaviour is a consequence of the molecular structure similarity between amavadin at oxidation state four[45] and five.[9]

Moreover, these complexes in aqueous solution[39–42] act as electrocatalysts of the oxidation of organic compounds with a thiol group (see Figure 2.3) and also a carboxylic or ester group in a suitable neighbourhood. This type of compound includes the biological thiols cysteine (**7**), glutathione (an antioxidant that is a tripeptide derived from the condensation reaction of glycine, glutamic acid and cysteine) (**8**) and penicillamine (**9**), as well as cysteine methyl ester (**10**) (a derivative of **7**). Substrates related with cysteine but upon replacement of the carboxylic group by an amine, a methyl, a methylenethiol, a sulphonate or a hydroxide[41,42] or a hydroxyl or an alkylthioether instead of a thiol, are not oxidised *via* electrocatalysis mediated by these complexes. In contrast, related substrates without the amino group, *i.e.*, 2-sulphanylacetic acid (**11a**) and 3-sulphanylpropionic acid (**11b**) undergo electrocatalytic oxidation mediated by amavadin related complexes.[41,42] Therefore, the additional carboxylate group [or its ester derivative, *e.g.*, in the case of methyl sulphanylacetate (**12**)] is indispensable for the oxidation reaction since it promotes the interaction of the thiol substrate with the vanadium atom of the complex.[46] By the end of reaction a disulphide compound (depending on the thiol used as the starting material) is formed (Scheme 2.1). For instance, a yield of *ca.* 85% by preparative scale controlled potential electrolysis is obtained with 8 equiv. of cysteine.[42]

A kinetic study based on digital simulation of cyclic voltammograms revealed a Michaelis-Menten-type mechanism for the electrocatalytic oxidation of the thiol mediated by amavadine. This was the first time that a Michaelis-Menten-type mechanism was recognized in electrocatalysis.[42] However, the

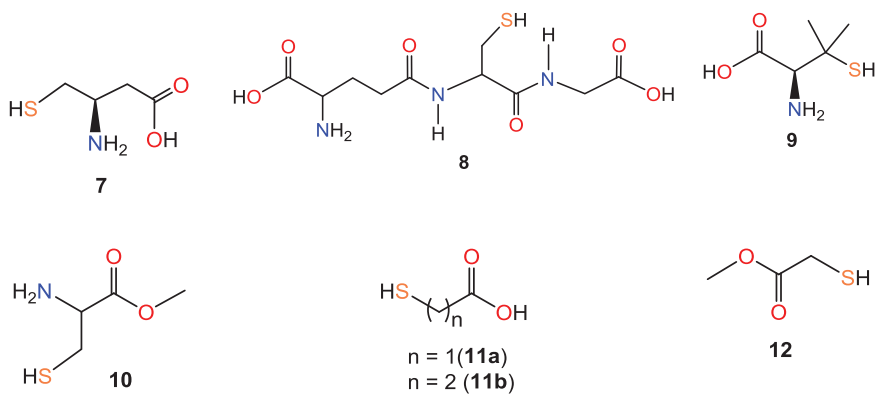

Figure 2.3 Substrates of amavadin and its models with a thiol group used for electrochemical oxidation reactions.

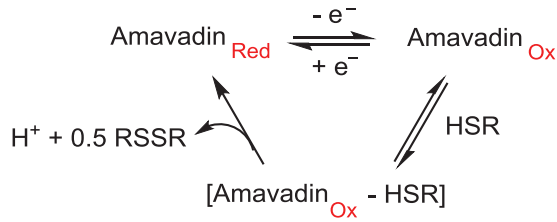

Scheme 2.1 Electrocatalytic oxidation of thiols to organodisulphides mediated by amavadin following a Michaelis-Menten-type mechanism (adapted from [42]); $Amavadin_{Red}$ and $Amavadin_{Ox}$ concern vanadium at oxidation state four and five, respectively.

Michaelis-Menten mechanism is common for reactions catalysed by enzymes, *i.e.*, the main group of biological catalysts, and is also followed in the case of amavadin, although it is not an enzyme since it does not contain a protein moiety. Therefore, the studied reaction follows an inner-sphere, electron-transfer process upon formation of a thiol-amavadin complex [$Amavadin_{Ox}$-HSR].[42] Oxidation of the RSH thiol ligand by the oxidised V^V centre leads to the thiol radical $RS^\bullet$ upon H^+ loss, which forms RSSR by S–S coupling.[42] The relevance of the presence of a carboxylic or derived ester group in the thiol molecule suggests the assistance of such a group to promote the interaction of the thiol with the electron-transfer mediator amavadin. This was rationalised by DFT calculations[46] on the catalytic oxidation of **12**, which indicate that protonation of the unbound oxygen atom of an $HIDPA^{2-}$ coordinated carboxylate group facilitates its uncoordination and substitution for the thiol which initially coordinates to the V^V centre *via* the ester group, assisted by a S–H···O hydrogen-bond. Thiolate is formed by thiol deprotonation, forming a thiolate complex in which the thiolate is oxidised by V^V to the radical $RS^\bullet$.[46]

2.4 Water Oxidation Using Sacrificial Oxidants

Water oxidation experiments with *meso*-$[V(HIDPA)_2]^{2-}$ or $[V(HIDA)_2]^{2-}$ were carried out using as oxidants the biological metabolites H_2O_2 and NO_2^- (for the sake of searching for a possible biological role of amavadin) or Ce^{4+} (the redox pair which does not require oxygen atoms that eventually could compete with the water oxidation) in aqueous solutions.

A blue aqueous solution of the amavadin models at a pH value of *ca.* 2, upon addition of the oxidant (either H_2O_2 or Ce^{4+}) turns red on account of the $V^{IV} \rightarrow V^V$ oxidation. However, it spontaneously returns slowly to the original blue colour, characteristic of the reduced V^{IV} complex with the final visible spectrum being identical to the initial one and the spectra crossing at an isosbestic point.[8,47,48] Hence, the reaction is carried out by a direct interconversion between the complexes with V^{IV} and V^V. It can be repeated with equivalent results. However, in the case of NO_2^- as oxidant, the absence of light is required for such a behaviour. At a higher pH value (4.6 and 7) by

addition of H_2O_2 as oxidant the same behaviour is observed, but the return to the original blue colour is faster.[47] Those results show that the V^V complex is unstable in aqueous solution. Moreover, the formation of small bubbles rich in molecular oxygen is detected.

Experiments with Ce^{4+} revealed that the oxidised amavadin is able to oxidise water (Ce^{4+} being reduced to Ce^{3+}) and with the other oxidants, H_2O_2 and NO_2^-, amavadin displays a catalase- and nitrite-reductase-type activity, respectively. Moreover, in the presence of an appropriate thiol (see above the electrocatalytic thiol oxidation) amavadin can catalyse, with H_2O_2 as oxidant, the thiol peroxidative oxidation, producing the dithio product, *i.e.*, it has a peroxidase-type activity.

The catalase activity of amavadin in aqueous conditions occurs with H_2O_2 and tetrabutylammonium hydroperoxyde (TBHP) and reduced amounts of water (by addition of a non-aqueous solvent the rate of decomposition of peroxides increases, *i.e.*, at high concentrations of water this solvent has an inhibitor effect).[37]

Nitrite, some thiols and water are biological substrates and biocatalytic behaviour of amavadin is suggested in Scheme 2.2. Two alternative procedures are indicated: (a) in the presence of a biological thiol and (b) in its absence (in this case water is the substrate). In the overall reaction, the ratio of consumption of hydrogen ions in the reduction of nitrite is higher than the formation of such ions in the oxidation of thiol or water (1.5 : 1).[48] Therefore, this process needs the supply of hydrogen ions to maintain a catalytic activity.

On the other hand, by using NO_2^- as oxidant, N_2O is produced as the reduction product.[48] Since it is a greenhouse gas contributor, if produced in considerable amount it could be collected in an appropriate reservoir to avoid its release into the atmosphere.[48]

Meso-$[V(HIDPA)_2]^-$ displays a lower reduction rate than $[V(HIDA)_2]^-$ but without a significant degradation—the latter complex undergoes a much more accentuated decomposition than the former.[8]

DFT calculations clarify the relevant steps of the water oxidation reaction, by using an appropriate model of amavadin (complex with HIDA) (Scheme 2.3).[8]

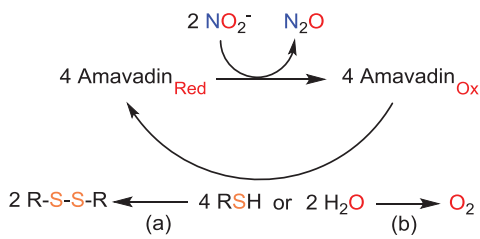

Scheme 2.2 Amavadin catalytic activity in water by using nitrite as oxidant, and a biological thiol (a) or water (b) as substrate (electrons, ligand, hydrogen ions and water formed from reduction of nitrite are absent for clarity) (adapted from [48]); $Amavadin_{Red}$ and $Amavadin_{Ox}$ concern vanadium at oxidation state four and five, respectively.

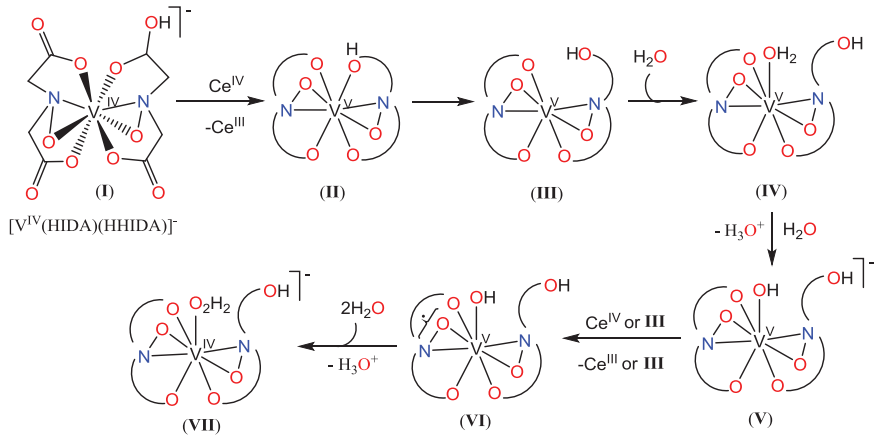

Scheme 2.3 Reaction mechanism of the formation of hydrogen peroxide as intermediate in the oxidation of water to molecular oxygen mediated by amavadin.[8]

The monoprotonated species $[V(HIDA)(HHIDA)]^-$ (**I**), at acidic pH, upon oxidation by Ce^{IV}, coordination and deprotonation of the H_2O ligand, forms the hydroxido-V^V complex $[V(OH)(HIDA)(HHIDA)]^-$ (**V**). In order to gain a sufficient oxidizing power, this V^V complex should undergo a further single-electron oxidation centred at an oxymate $\{>NO^-\}$ group to give $[V(OH)(HIDA)\cdot(HHIDA)]$ (**VI**) with the oxidized $\{>NO^\bullet\}$ moiety. Nucleophilic attack of H_2O to the hydroxide ligand in **VI** leads to O–O bond formation, followed by two-electron oxidation of the resulting O–O ligand by the V^V-$\{O\cdot N<\}$ centre, yields H_2O_2 in the V^{IV} complex $[V(HIDA)(HHIDA)(H_2O_2)]^-$ (**VII**). A redox active oxymate group in the non-innocent ligand has a key role since the oxidation state of metal changes only by one unit. The participation of ligand is required for the reaction process since this involves two electrons ($2O^{2-} \rightarrow {O_2}^{2-} + 2e^-$) whereas the metal centre has just one vanadium atom that changes its oxidation state by one unit. Therefore, the reversible contribution of the bound radical $ON^\bullet <$ form, accepting one electron, cooperates with V^V which accepts another electron in the key **VI** → **VII** conversion:

$$H_2O + HO\text{-}V^V\text{-}\{O\dot{N}<\} \rightarrow H_2O_2\text{-}V^{IV}\text{-}\{^-ON<\} + H^+$$

The subsequent steps (not represented in Scheme 2.3) involve the oxidation of H_2O_2 to O_2 that requires two additional electrons.[8]

The mechanism of Scheme 2.3 was unprecedented, involving a single metal and the cooperation between two reversible single-electron processes, one centred at the metal and other at a ligand.

The process also requires the direct participation of the sulphate (or probably bisulphate ion taking into account the pH value of the reaction) counterion that acts as a proton abstractor or donor.[8]

Complexes $[V(HIDPA)_2]^-$ and $[V(HIDA)_2]^-$ provide the first examples of molecular catalysts for water oxidation based on a metal out of groups 7–11

of the Periodic Table by using primary oxidants.[8] However, there is another example of a vanadium catalyst, the multicentred vanadium species $[V^{IV}{}_5V^{V})O_7(OCH_3)_{12}]^-$, but it needs to be photoinduced.[49]

As a final comment, regarding a biological standpoint, amavadin is the second biomolecule with capacity to mediate water oxidation and the first to be obtained from heterotrophic organisms.

2.5 Oxidation and Carboxylation of Hydrocarbons and Other Organic Compounds

Amavadin and its models have been used as catalysts for oxidation reactions of other species apart from water, mainly hydrocarbons, with potential industrial interest, and, based on these results, some patents have been registered.[50–53]

Catalytic functionalisation of light alkanes, *e.g.*, in natural gas, under mild or moderate reaction conditions can become a relevant topic since these compounds are an abundant carbon source and potential cheap, natural starting materials.[52–67] However, as they show a high inertness requiring an appropriate activation, they are currently mainly burned for energy production. Hence, the synthesis of high-value functionalised products from alkanes is a current challenge in chemistry and the subject (alkane functionalisation) has been widely treated in a recent book.[67]

Amavadin and its models have been used as catalysts for the hydroxylation, oxygenation, peroxidative halogenation of alkanes (gaseous and liquid) and benzene,[68] peroxidative oxygenation of benzene and 1,3,5-trimethylbenzene,[69] and even for the carboxylation of alkanes, including methane,[50,70,71] ethane,[72] propane,[73] as well as linear and cyclic pentanes and hexanes.[74] Additionally, amavadin was used as a catalyst for the oxidation of (methylsulphanyl)benzene and alcohols, epoxidation of allylic alcohols and cyanide addition to aldehydes.[37]

2.5.1 Peroxidative Oxidation of Hydrocarbons

Hydroxylations and oxygenations of cycloalkanes[68] to the corresponding alcohols and ketones (Scheme 2.4a), peroxidative oxygenation of benzene[68,69] to phenol (Scheme 2.4b) and of 1,3,5-trimethylbenzene or 3,5-dimethylphenylmethanol[69] to 3,5-dimethylbenzaldehyde (Scheme 2.4c) have been achieved with amavadin and its models. Differently from the case of benzene, the oxidation reaction of 1,3,5-trimethylbenzene as substrate does not lead to an alcohol, but to an aldehyde. These reactions are possible in acidified (by addition of a small amount of acid, typically nitric acid, as a promoter) water–acetonitrile solutions (but not in water as unique solvent), with an aqueous H_2O_2 solution as oxidant, typically at room temperature, during 6 h, and under an inert atmosphere (dinitrogen). Reactions at higher temperatures (up to 75 °C) can show a slight increase of the value of TON (moles product/mol catalyst), as for 1,3,5-trimethylbenzene oxidation.

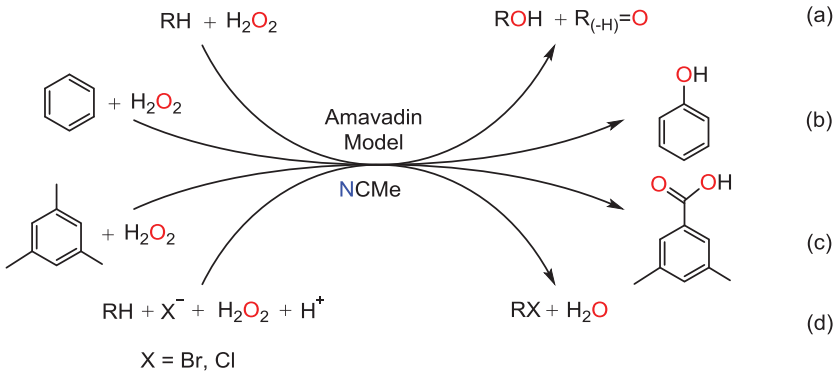

Scheme 2.4 Oxidations of hydrocarbons catalysed by amavadin models in mixed water acetonitrile: (**a**) hydroxylation and oxygenation of alkanes to the corresponding alcohols and ketones; (**b**) peroxidative oxygenation of benzene to phenol; (**c**) peroxidative oxygenation of 1,3,5-trimethylbenzene to 3,5-dimethylbenzaldehyde; (**d**) peroxidative monohalogenation of hydrocarbon to the corresponding organohalogen.

H_2O_2 is required for the reactions to proceed considerably. In its absence, HNO_3 can act as oxidant but the products are formed with a low yield, *i.e.*, the oxidising power of H_2O_2 in the presence of the catalyst is more relevant than that of HNO_3.[69] However, the amount of H_2O_2 should be controlled, since a too-high excess leads to a decrease of TON, conceivably as a result of overoxidation.[69]

Amavadin models led to TON values up to 16, 35 and 50 for oxidation of benzene, 1,3,5-trimethylbenzene and cyclohexane (mainly to cyclohexanol), respectively.[68,69]

The reactions proceed by radical mechanisms, as unveiled with radical trap and kinetic experiments.[75–78] That can be accounted for by the formation of the hydroxyl radical ($HO^{\bullet}$) from the catalyst-assisted reduction of H_2O_2, which acts as an H-atom abstractor from the alkane (RH) to form an alkyl radical ($R^{\bullet}$) that, upon reaction with O_2, leads to the organoperoxyl radical ($ROO^{\bullet}$). Decomposition of the derived hydroperoxide (ROOH) leads to the alcohol (ROH) and ketone $R_{(-H)}{=}O$ products.

2.5.2 Peroxidative Halogenation of Hydrocarbons

Amavadin and its models can also act as catalysts for peroxidative monobromination of saturated cycloalkanes (cyclohexane and cyclooctane) and benzene, at room temperature (Scheme 2.4d) leading to bromocyclohexane, bromocyclooctane and bromobenzene, respectively, with TON values up to 17 and 11 (for bromocyclohexane and bromobenzene, respectively) which are higher than for other studied oxidovanadium complexes.[68] The reactions are carried out in water–acetonitrile solutions with nitric acid as an acid promoter, aqueous hydrogen peroxide as the oxidant and KBr as the bromine source, under an inert atmosphere of molecular nitrogen and in the

absence of a phase-transfer agent.[68] Catalytic chlorination, with KCl instead of KBr as halogen source, was achieved with benzene as substrate.[68] The efficiency decreases for a high excess of H_2O_2, probably as a consequence of overoxidation of the substrate.[68]

These reactions probably proceed *via* radical pathways. Amavadin and its models have a coordinated oxyiminato group of each ligand, which is isoelectronic with the peroxido group.[70] In the halogenation reaction cycle catalysed by vanadium-haloperoxidases[1] of some terrestrial fungi, seaweeds, lichen and bacteria, a vanadium-peroxide complex is formed. The oxyiminato similarity to the peroxide moiety could eventually explain this catalytic activity of amavadin and its models concerning halogenation. A theoretical discrete Fourier transform (DFT) study supports the bromoperoxidase-type activity of amavadin at the vanadium oxidation state five,[79] *i.e.*, the same as that in haloperoxidases dependent of this transition metal.

2.5.3 Carboxylation of Alkanes

Carboxylations are not simple oxidations and typically the products (carboxylic acids) have one more carbon atom than the starting material.

Amavadin and its models, as well as the simpler vanadatrane complex [VO(L)] (L = triethanolaminate) catalyse the carboxylation of alkanes (Schemes 2.5–2.7) with peroxydisulphate $S_2O_8^{2-}$ (mainly the potassium salt, in an excess relative to substrate) as oxidising agent, under a CO atmosphere, in trifluoroacetic acid (TFA) as solvent, at 80 °C.[70–73] The reaction is carried out in a 316 stainless steel autoclave, with a Teflon-coated magnetic stirring bar, containing the required liquid and solid compounds. After closing, the autoclave is flushed with dinitrogen three times and then the gaseous reagents are inserted. This method was initially applied by Fujiwara *et al.*,[80] with other metal catalysts, typically based on palladium.

Carbon monoxide is a carbonyl source, but in its absence as in the vanadium systems discussed, TFA can behave as such, although much less effectively than CO[70,71] and usually producing the methyl ester of TFA in a low yield.[71]

These vanadium-catalysed reactions follow radical mechanisms (Scheme 2.6) as suggested by radical trap experiments, DFT calculations[71,72] and the product distribution. In fact, the carboxylation of linear alkanes occurs more favourably at the secondary carbon atoms than at the primary ones (*e.g.*, the higher relative amount of isobutyric relative to *n*-butyric acids,

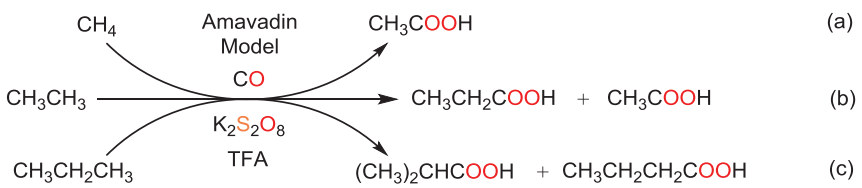

Scheme 2.5 Carboxylation of light gaseous alkanes catalysed by amavadin models: (**a**) methane; (**b**) ethane; (**c**) propane.

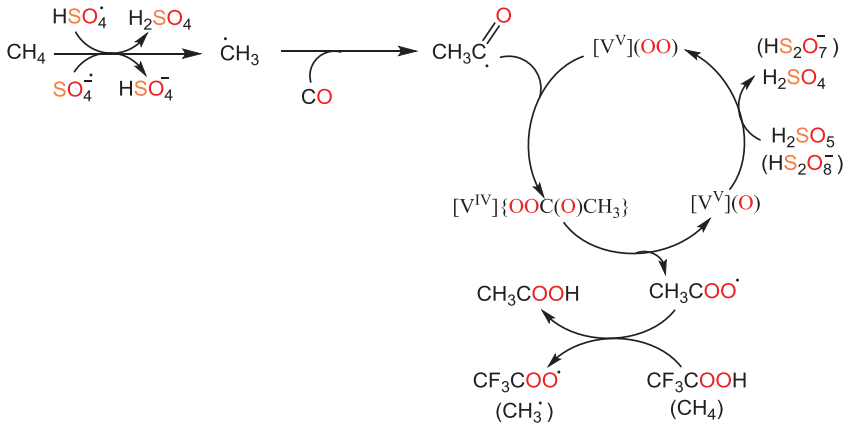

Scheme 2.6 Mechanism of the carboxylation of methane to acetic acid catalysed by amavadin models [71]. [V] represents V{N(CH$_2$CH$_2$O)$_3$} in the DFT calculations.

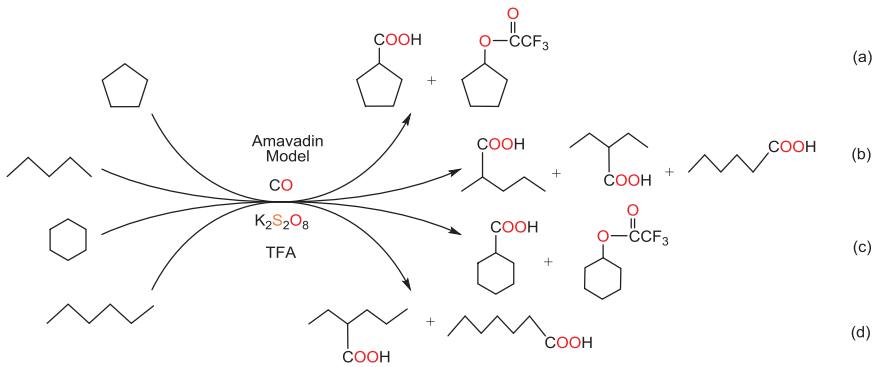

Scheme 2.7 Carboxylation of liquid alkanes catalysed by amavadin models: (**a**) cyclopentane; (**b**) pentane; (**c**) cyclohexane; (**d**) hexane.

by using propane as substrate, confirms this type of mechanism).[73] Consequently, the selectivity of the carboxylation depends on the number of carbon atoms and on the symmetry of the substrate (Schemes 2.5 and 2.7).

In the case of carboxylation of methane to acetic acid, the energetically most favourable mechanism based on synthetic and DFT studies (the latter on the simplified vanadatrane catalyst, Scheme 2.6)[71] suggests the initial formation of the sulphate radical $SO_4^{-\bullet}$ or ($HSO_4^{\bullet}$) upon thermolysis of peroxydisulphate (oxidant). This radical acts as hydrogen abstractor from the alkane, forming sulphuric acid and the methyl radical that reacts with carbon monoxide leading to the acyl radical $CH_3CO^{\bullet}$, which adds to a peroxide-vanadium catalyst from which the acetate radical $CH_3COO^{\bullet}$ is formed. Its reaction with a new molecule of alkane (H-abstraction) produces acetic acid

(CH_3COOH) and a new methyl radical to proceed the catalytic cycle.[71] The V-oxidation state varies between +5 and +4.

This type of mechanism is quite different from those proposed by Fujiwara *et al.*, in his systems,[80] which, for instance in the case of Pd catalysts, is based on the metal electrophilic attack to an alkane C–H bond to form, upon heterolytic cleavage, an alkyl-metal intermediate.

2.5.3.1 Gaseous Alkanes

All the three lighter alkanes, methane,[50,70,71] ethane[72] and propane,[73] are adequate substrates for carboxylation reactions (Scheme 2.5). The highest yields are obtained up to 10 atm of CO.[50,68–73] In spite of the inertness of these substrates, very high TONs (up to above 10^4) and yields (up to 92%) were accomplished,[70,71] *e.g.*, with $[V(HIDA)_2]^{2-}$ and using ethane as substrate, 92% yield of acetic and propionic acids was obtained,[72] whereas with catalyst $[V(HIDPA)_2]^{2-}$, a yield of 54% of acetic acid from methane was obtained (Scheme 2.5a).[71]

Propionic acid is usually the main product from ethane with a selectivity up to 95% but, depending on the experimental conditions (*e.g.*, for too-low CO pressures), acetic acid can become the predominant product, being formed upon oxidation of the substrate (Scheme 2.5b).[72]

Experiments with labelled ethane (at both carbon atoms) and labelled carbon monoxide confirmed that propionic acid is formed by carbonylation. However, acetic acid results mainly from ethane oxidation or, less significantly, upon C–C bond cleavage followed by carbonylation.[72]

In the case of propane, three products were obtained: isobutyric (the main one), *n*-butyric and acetic acids (the last one in a minor amount) (Scheme 2.5c).[73]

2.5.3.2 Liquid Alkanes

Cyclic and linear liquid alkanes (as typified in Scheme 2.7) can also be carboxylated under similar conditions as those used for gaseous alkanes, forming the corresponding carboxylic acids with one extra carbon atom.[74]

The amavadin model $[V(HIDA)_2]^{2-}$ is the most active catalyst precursor among all vanadium compounds tested, allowing a maximum yield and TON of 33% and 50 for cyclopentane carboxylation, and 50% and 74, respectively, for cyclohexane carboxylation (*i.e.*, cyclohexane is more reactive than cyclopentane). Trifluoroacetic esters can be the main products for the lowest and highest CO pressures, whereas without CO, carboxylic acid is not obtained.[74]

Carboxylation of linear alkanes with more than two carbon atoms leads to the formation of more than one product. Hence, for pentane and using $[V(HIDA)_2]^{2-}$ as catalyst, the products 2-methylpentanoic acid, 2-ethylbutanoic acid and hexanoic acid are formed (Scheme 2.7b) with partial yield ratios of *ca.* 4 : 2 : 1, respectively. Yields up to 54% are accomplished, comparable to the maximum obtained yields for the most efficient oxidovanadium complex.[74]

However, hexane leads to 2-ethylpentanoic acid and heptanoic acid (Scheme 2.7d) with a selectivity of the former up to *ca.* 95% and an overall yield up to 46%, for $[V(HIDA)_2]^{2-}$ as catalyst.[74] The carboxylation at a secondary carbon atom is always superior to that at a primary position, in accord with a radical mechanism for the reaction.

2.5.4 Other Oxidation Reactions

Preliminary results concerning amavadin as a catalyst precursor for the oxidation of alcohols (with an aromatic or linear group: phenylmethanol, (2*E*)-3-phenylprop-2-en-1-ol, heptan-1-ol, octan-1-ol and octan-2-ol) (Scheme 2.8a) and epoxidation of allylic alcohols (Scheme 2.8b) (2*E*)-3-phenylprop-2-en-1-ol and oxidation of (methylsulphanyl)benzene (Scheme 2.8c) were described.[37] Different conditions were tested for these reactions that were carried out in aqueous solutions, anhydrous media (heptane, ionic liquids or alcohols used as substrates) or two-phase solvent systems.[37]

Additionally, amavadin (with vanadium at oxidation state four or five) was tested as catalyst for asymmetric cyanations using benzaldehyde and cyanide (or trimethylsilylcyanide) and negative results (for both metal oxidation states) were obtained.[37]

2.5.4.1 Oxidation of Alcohols

Oxidation of alcohols to the corresponding aldehydes (Scheme 2.8a) was achieved in a bi-phasic water–alcohol mixture, at room temperature. The yields are very low[37] with higher values by using *tert*-butyl hydroperoxide (TBHP) instead of H_2O_2 as oxidant for phenylmethanol (benzyl alcohol). Heptan-1-ol (even at 80 °C) and octan-2-ol as substrates do not react and octan-1-ol leads to a low yield and TON with TBHP as oxidant. Reactions

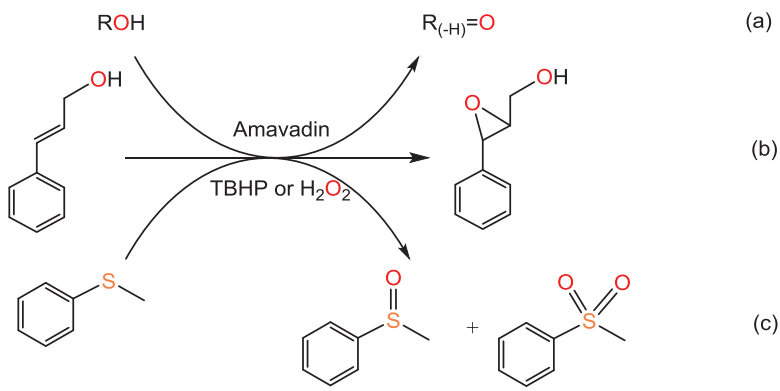

Scheme 2.8 Other oxidations mediated by amavadin: (**a**) oxidation of alcohols to their corresponding aldehydes; (**b**) epoxidation of cinnamyl alcohol; (**c**) oxidation of (methylsulphanyl)benzene.

carried out in one-phase system by addition of acetonitrile do not lead to the best results.[37]

Phenylmethanol in the ionic liquid [tri(*n*-hexyl)tetradecylphosphonium]-$[N(SO_3CF_3)_2]$ forms not only the aldehyde but also the acid that is the main product. The conversion is higher using TBHP as oxidant at 40 °C, instead of H_2O_2, with an overall yield up to 86%. For the other tested ionic liquids or in the absence of solvent, the conversion was very low for all products.

Oxidations under anhydrous conditions at 40 °C are more efficient if the solvent is the substrate. Under such conditions, phenylmethanol oxidation also forms the corresponding aldehyde and acid, the latter typically being the major product (maximum yield of 93% with TBHP as oxidant, after 18 h).

2.5.4.2 Epoxidation of Allylic Alcohols

For (2*E*)-3-phenylprop-2-en-1-ol (2*E*-cinnamyl alcohol) as substrate, amavadin (2.5 mol%) as catalyst leads to a yield up to 38% and a maximum TON of 15, with TBHP as oxidant (the use of H_2O_2 as oxidant is less effective) (Scheme 2.8b).[37] Aldehyde is also obtained at 40 °C, being the major product with H_2O_2, but not with TBHP as oxidant.

However, epoxidation of the same substrate leads to the corresponding epoxide in a higher yield (up to 90% with 40 h reaction time) under an inert atmosphere (molecular nitrogen) and in the presence of molecular sieves at 40 °C.[37]

2.5.4.3 Oxidation of (Methylsulphanyl)benzene

(Methylsulphanyl)benzene oxidation (Scheme 2.8c) leads to the corresponding sulphoxide and sulphone with a conversion of 100%, using 2.5 mol% of amavadin, at room temperature, after 8 h, in a water–acetonitrile mixture (by replacing the latter solvent with dichloromethane, forming a bi-phasic system, products are not detected).[37] One equivalent of oxidant (H_2O_2 or TBHP) is necessary for a good selectivity of 90% concerning sulphoxide. This selectivity decreases for higher oxidant amounts, with 50% conversion to sulphoxide and sulphone after 48 h.[37]

2.6 Final Remarks

Amavadin is a natural product with activity as catalyst in several reactions including biological ones. Hence, it can be considered as a biocatalyst and, in comparison with the most common ones (enzymes), its preparation follows a much easier synthetic methodology.

Amavadin is resistant to a broad range of conditions due to its high stability. This is confirmed by the vanadium complexes in oxidation state +4 with H_3HIDPA and H_3HIDA (**2**) proligands (1 : 2) *i.e.*, $[V(HIDPA)_2]^{2-}$ and $[V(HIDA)_2]^{2-}$, respectively, that show higher values of stability constants than

other vanadium complexes with polyaminocarboxylic acid proligands.[27,81–83] Additionally, those vanadium complexes related to amavadin have higher values of stability constants than the corresponding complexes with other transition metals and with the same ligands. The ligands have both hard *N* and *O* donor atoms (from oxyiminato and carboxylate groups) able to donate enough electron density (σ and π) to the metal ion leading to an unusual octacoordination that is quite rare for first-row transition metals.[14] These characteristics allow that amavadin and related complexes are stable in a wide range of pH values and they can catalyse reactions under acid environments. Biomolecules with redox activity containing a transition metal in a high-oxidation state can be used for oxidative reactions.[54,84,85] Amavadin and related molecules have characteristics that are associated with redox catalysis.[42,47,54,86]

Either in aqueous solution or as solids, amavadin and its related complexes are stable in air and water (or moisture) which allows their use under broad experimental conditions.[1]

In the solid state, these complexes can be prepared for catalytic purposes either *in situ*[86] or previously synthesized with a suitable counterion, *e.g.*, Ca^{2+}, $[NBu_4]^+$ or $[PPh_4]^+$ for the complex with vanadium in the oxidation state four,[37,86] and with $[PPh_4]^+$ for the oxidised form of the complexes.[37] These complexes are ionic (dianionic at the reduced form and monoanionic upon oxidation) and soluble in water. They are insoluble in many usual organic solvents, *e.g.*, propan-1-ol, propan-2-ol, butan-1-ol, diethyl ether, nitrobenzene, THF and toluene. The solubilities in some aromatic alcohols, such as phenylmethanol and (2*E*)-3-phenylprop-2-en-1-ol, are similar to those in methanol and ethanol.[37]

Methodologies can be followed to increase their solubilities, either by using vanadium complexes bearing ligands with large and apolar R groups (however, some of these complexes have low stability[30]) or by a suitable choice of counterions, thus extending the scope as catalysts for oxidation reactions.[84,85] The solubility is dependent on the counterion and, *e.g.*, for the complexes with V in oxidation state five, the use of $[PPh_4]^+$ as counterion leads to their solubility in dichloromethane or acetonitrile.[37] It should be noted that in contrast to amavadin, enzymes are easily denatured in organic solvents, thereby losing their catalytic activity.

Amavadin and related complexes are soluble in water exhibiting a blue solution, but in some non-aqueous organic solvents, such as DMSO, DMF and acetone, they convert to their oxidised form, *i.e.*, with V in oxidation state five, exhibiting a red solution.[86]

Amavadin and its models can be oxidised in aqueous solutions, *e.g.*, by hydrogen peroxide,[37,47] TBHP,[37] Ce(IV)[9] and NO_2^- (with this oxidant the reaction is light-dependent).[48] In aqueous solutions, the oxidised complexes (with V in oxidation state five) are not stable, leading to water oxidation in the absence of other more-reactive substrates. However, the complexes of vanadium with *N*-oxyiminodiacarboxylate ligands have different stabilities, and amavadin (with HIDPA ligand) is more stable than the complex with the

less bulky HIDA ligand. However, these complexes can require specific oxidants to act as catalysts for some reactions. Hence, peroxydisulphate is the most suitable oxidant for carboxylation of alkanes, whereas hydrogen peroxide is adequate for peroxidation (including halogenation) of hydrocarbons in acidic water–acetonitrile mixtures.[1]

Carboxylations catalysed by amavadin and its models[50–52,67,70–74,86] proceed *via* a radical pathway and display remarkably high TONs (up to 2×10^4) and yields. They are one-pot reactions, thus being much simpler than those applied in industry for the synthesis of carboxylic acids. Moreover, they are carried out under milder conditions and using a cheap catalyst metal. One can compare amavadin or its models, *e.g.*, with the catalysts of rhodium or iridium in the common industrial processes, Monsanto and Cativa, for the preparation of acetic acid by carbonylation of methanol, the overall process (since the steam reforming of methane or coal) requiring three separate stages with high energy needs.[87] Amavadin or its models, under comparable conditions with oxidovanadium catalysts, exhibit activities that typically are the highest or close to the maximum of the latter ones. However, in the carboxylation of linear alkanes with more than two carbon atoms, they lead to the formation of more than one product. Although the selectivity can be somehow controlled by the specific ratio of reagents, further developments are required, as well as the search of ''greener'' oxidant and solvent.

Amavadin and its models are also catalysts for halogenation reactions.[68] Their ligands have a oxyiminato group coordinated to the metal centre that is isoelectronic with the peroxido group[70] that is present in vanadium oxidation catalysts, including vanadium haloperoxidades, for the same reaction.[75–78,81,88–94] These enzymes promote peroxidative catalytic reactions with other substrates, in the absence of halides, *e.g.*, sulphoxidation of organic sulphides, with enantioselectivity for bromoperoxidases but not for chloroperoxidases.[95] Amavadin can mediate the oxidation of the organic sulphide (methylsulphanyl)benzene leading to a racemic mixture.[37] However, amavadin and its related models can be used for the synthesis of S–S-containing products with carboxylic or ester groups at specific positions since they are electrocatalytic mediators for the oxidation of the corresponding thiols.[41,42]

In the thiols oxidation, amavadin and its close models oxidise the substrate by an unprecedented electrocatalytic inner sphere mechanism of the Michaelis-Menten type.[42,46] However, such catalysts can also be involved in an outer-sphere mechanism as shown by their role as electron-transfer mediators between the anode and the thiol. In fact, only minor changes in geometry occur for the V(IV)–V(V) complex redox pair.[96] This double redox behaviour should be further explored.

In contrast to its common models, amavadin exhibits chiral properties that could be valuable for asymmetric catalysis.[26] The chirality results from its C_2 symmetry and five chirality centres, one at the metal and the other four at the carbon atoms bound to the nitrogen atoms. It displays S stereochemistry with two possible stereoisomers for the ligands.[43] However, enantioselectivity using amavadin as catalyst has not yet been conclusive.

Amavadin (as well its close models) starts to decompose at 170 °C and hence their application as catalysts at higher temperatures is not expected.[1] They have other limitations for the same purpose, *e.g.*, in terms of biological significance, concerning the oxidant and/or type of solvent used, that are different from those in the natural biological environments of the fungi.

The typical solvents for oxidation and carboxylations, acetonitrile and trifluoroacetic acid, respectively, are not ''green'', particularly the latter which, however, for hydrocarboxylations of alkanes can be replaced by the much more environmentally acceptable water–acetonitrile mixture at a lower temperature (even 25 °C).[97] However, amavadin and its models are not efficient as promoters for such a reaction (they can even act as inhibitors) as copper[98–104] and other metal[105–107] catalysts are.

Water can behave not only as a solvent but also as a substrate.[8] In fact, recently, amavadin and its models were found to promote water oxidation *via* an unprecedented type of mechanism.[8] This can inspire new approaches on catalyst design based on single-electron M^n/M^{n+1} redox pairs, with complexes containing other non-innocent ligands, to achieve a more efficient water oxidation catalysis *via* metal–ligand cooperation. An auxiliary ion, such as sulphate (or bisulphate), can also promote the reaction by participating in proton abstraction–donation. O_2 evolution from water oxidation has important potential applications, *e.g.*, associated with new approaches on energy production, with aerobic *in situ* treatment of water or with breathing air revitalization in enclosed environments with restrictions to carry out photochemical reactions, such as manned submersibles.[8] However, close homologues of amavadin could be employed to reduce nitrite contamination in aqueous environments.[48]

Alcohols (similarly to water) have a hydroxyl group and their oxidation could be a promising topic of amavadin research.

In summary, catalytic activity of amavadin and its models has already been disclosed for various important types of reactions, and the scope of the field can possibly be widely extended. Mechanistic proposals have been presented only in a few cases and they show unprecedented features that deserve to be further explored.

Catalysis based on amavadin and its models can provide promising multi- and interdisciplinary approaches, inspiring further studies, *e.g.*, on the design of new catalysts with related amavadin-ligands (or other non-innocent ligands) that should lead to developments with potential industrial application.

Acknowledgements

The authors are indebted to all co-authors cited in joint references, as well as to the Fundação para a Ciência e a Tecnologia (FCT), Portugal, for partial financial support (projects UIDB/00100/2020 of Centro de Química Estrutural, and PTDC/QEQ-QIN/3967/2014). M.S. acknowledges the FCT and IST for a working contract ''DL/57/2017'' (Contract no. IST-ID/102/2018).

References

1. J. A. L. da Silva, J. J. R. Fraústo da Silva and A. J. L. Pombeiro, *Coord. Chem. Rev.*, 2013, **257**, 2388.
2. E. Bayer and H. Kneifel, *Z. Naturforsch.*, 1972, **27b**, 207.
3. H.-U. Meisch, W. Reinle and J. A. Schmitt, *Z. Naturforsch.*, 1979, **66**, 620.
4. E. Koch, H. Kneifel and E. Bayer, *Z. Naturforsch.*, 1987, **42c**, 873.
5. H. Kneifel and E. Bayer, *Angew. Chem., Int. Ed. Engl.*, 1973, **12**, 508.
6. P. Krauß, E. Bayer and H. Kneifel, *Z. Naturforsch.*, 1984, **39b**, 829.
7. H. Kneifel and E. Bayer, *J. Am. Chem. Soc.*, 1986, **108**, 3075.
8. M. Domarus, M. L. Kuznetsov, J. Marçalo, A. J. L. Pombeiro and J. A. L. da Silva, *Angew. Chem., Int. Ed.*, 2016, **55**, 1489.
9. E. M. Armstrong, R. L. Beddoes, L. J. Calviou, J. M. Charnock, D. Collison, N. Ertok, J. H. Naismith and C. D. Garner, *J. Am. Chem. Soc.*, 1993, **115**, 807.
10. L. Vilas Boas and J. Costa Pessoa, in *Comprehensive Coordination Chemistry*, ed. G. Wilkinson, R. D. Gillard and J. A. McCleverty, Pergamon Press, Oxford, England, **vol. 3**, 1987, pp. 454–583.
11. D. C. Crans and J. J. Smee, in *Comprehensive Coordination Chemistry II*, ed. J. A. McCleverty and T. J. Meyer, Elsevier, **vol. 4**, 2003, pp. 175–239.
12. *Encyclopedia of Inorganic Chemistry*, ed. R. B. King, John Wiley & Sons, Chichester, UK, 2nd edn, **vol. 9**, (several issues concerning vanadium), 2005.
13. T. K. Paine, T. Weyhermuller, E. Bill, E. Bothe and P. Chaudhuri, *Eur. J. Inorg. Chem.*, 2003, 4299.
14. T. K. Paine, T. Weyhermuller, L. D. Slep, F. Neese, E. Bill, E. Bothe, K. Wieghardt and P. Chaudhuri, *Inorg. Chem.*, 2004, **43**, 7324.
15. B. Morgenstern, S. Steinhauser, K. Hegetschweiler, E. Garribba, G. Micera, D. Sanna and L. Nagy, *Inorg. Chem.*, 2004, **43**, 3116.
16. M. Rangel, A. Leite, M. J. Amorim, E. Garribba, G. Micera and E. Lodyga-Chruscinska, *Inorg. Chem.*, 2006, **45**, 8086.
17. H. F. Hsu, C. L. Su, N. O. Gopal, C. C. Wu, W. C. Chu, Y. F. Tsai, Y. H. Chang, Y. H. Liu, T. S. Kuo and S. C. Ke, *Eur. J. Inorg. Chem.*, 2006, 1161.
18. M. Sutradhar, G. Mukherjee, M. G. B. Drew and S. Ghosh, *Inorg. Chem.*, 2007, **46**, 5069.
19. K. Kanamori, K. Kusajima, H. Yachi, H. Suzuki, Y. Miyashita and K. Okamoto, *Bull. Chem. Soc. Jpn.*, 2007, **80**, 324.
20. T. Kajiwara, R. Wagner, E. Bill, T. Weyhermuller and P. Chaudhuri, *Dalton Trans.*, 2011, **40**, 12719–12726.
21. K. C. M. Westrup, T. Gregorio, D. Stinghen, D. M. Reis, P. B. Hitchcock, R. R. Ribeiro, A. Barison, D. F. Back, E. L. de Sá, G. G. Nunes and J. F. Soares, *Dalton Trans.*, 2011, **40**, 3198.
22. Y. H. Chang, C. L. Su, R. R. Wu, J. H. Liao, Y. H. Liu and H. F. Hsu, *J. Am. Chem. Soc.*, 2011, **133**, 5708.

23. N. Biswas, D. Patra, B. Mondal, S. Bera, S. Acharyya, A. K. Biswas, T. K. Mukhopadhyay, A. Pal, M. G. B. Drew and T. Ghosh, *Dalton Trans.*, 2017, **46**, 10963.
24. S.-C. J. Fu, S. M. Birnbaum and J. P. Greenstein, *J. Am. Chem. Soc.*, 1954, **76**, 6054.
25. E. Koch, H. Kneifel and E. Bayer, *Z. Naturforsch.*, 1986, **41b**, 359.
26. T. Hubregtse, E. Neeleman, T. Maschmeyer, R. A. Sheldon, U. Hanefeld and I. W. C. E. Arends, *J. Inorg. Biochem.*, 2005, **99**, 1264.
27. G. Anderegg, E. Koch and E. Bayer, *Inorg. Chem. Acta*, 1987, **127**, 183.
28. T. Hubregtse, H. Kooijman, A. L. Spek, T. Maschmeyer, R. A. Sheldon, I. W. C. E. Arends and U. Hanefeld, *J. Inorg. Biochem.*, 2007, **101**, 900.
29. P. D. Smith, R. E. Berry, S. M. Harben, R. L. Beddoes, M. Helliwell, D. Collison and C. D. Garner, *J. Chem. Soc., Dalton Trans.*, 1997, 4509.
30. T. Hubregtse, U. Hanefeld and I. W. C. E. Arends, *Eur. J. Org. Chem.*, 2007, 2413.
31. H. S. Yadav, E. M. Armstrong, R. L. Beddoes, D. Collison and C. D. Garner, *J. Chem. Soc., Chem. Commun.*, 1994, 605.
32. S. M. Harben, P. D. Smith, R. L. Beddoes, D. Collison and C. D. Garner, *Angew. Chem., Int. Engl.*, 1997, **36**, 1897.
33. S. M. Harben, P. D. Smith, M. Helliwell, D. Collison and C. D. Garner, *J. Chem. Soc., Dalton Trans.*, 1997, 4517.
34. P. D. Smith, S. M. Harben, R. L. Beddoes, M. Helliwell, D. Collison and C. D. Garner, *J. Chem. Soc., Dalton Trans.*, 1997, 685.
35. P. D. Smith, J. J. A. Cooney, E. J. L. McInnes, R. L. Beddoes, D. Collison, S. M. Harben, M. Helliwell, F. E. Mabbs, A. Mandel, A. K. Powell and C. D. Garner, *J. Chem. Soc., Dalton Trans.*, 2001, 3108.
36. A. M. Galvão, E. Levi, A. J. L. Pombeiro, M. F. C. Guedes da Silva, J. A. L. Silva and J. J. R. Fraústo da Silva, Models of amavadin – studies with the chromium(III) complex with hida (in Portuguese), *2nd Conference on Inorganic Chemistry of the Portuguese Chemical Society*, Monte Real-Portugal, **CP22**, 1995, pp. 91–92.
37. T. Hubregtse, *Structural Investigations of Amavadin-based Vanadium Complexes*, D. Phil. Thesis (Supervisor: R. A. Sheldon), Technical University of Delft, The Netherlands, 2007.
38. H. Huang, R. Howland, E. Agar, M. Nourani, J. A. Golen and P. J. Cappillino, *J. Mater. Chem. A*, 2017, **5**, 11586.
39. M. A. Nawi and T. L. Riechel, *Inorg. Chim. Acta*, 1987, **136**, 33.
40. R. D. Thackrey and T. L. Riechel, *J. Electroanal. Chem.*, 1988, **245**, 131.
41. J. J. R. Fraústo da Silva, M. F. C. Guedes da Silva, J. A. L. Silva and A. J. L. Pombeiro, in *Molecular Electrochemistry of Inorganic, Bioinorganic and Organometallic Compounds*, ed. A. J. L. Pombeiro and J. A. McCleverty, Kluwer Academic Publishers, The Netherlands, 1993, pp. 411–415.
42. M. F. C. Guedes da Silva, J. A. L. Silva, J. J. R. Fraústo da Silva, A. J. L. Pombeiro, C. Amatore and J.-N. Verpeaux, *J. Am. Chem. Soc.*, 1996, **118**, 7568.

43. J. M. Lenhardt, B. Baruah, D. C. Crans and M. D. Johnson, *Chem. Commun.*, 2006, 4641.
44. J. M. Lenhardt, B. Baruah, D. C. Crans and M. D. Johnson, *Pure Appl. Chem.*, 2009, **81**, 1241.
45. R. E. Berry, E. M. Armstrong, R. L. Beddoes, D. Collison, S. N. Ertok, M. Helliwell and C. D. Garner, *Angew. Chem., Int. Ed.*, 1999, **38**, 795.
46. L. Bertini, V. Barbieri, P. Fantucci, L. De Gioia and G. Zampella, *Dalton Trans.*, 2011, **40**, 7704.
47. C. M. M. Matoso, A. J. L. Pombeiro, J. J. R. Fraústo da Silva, M. F. C. G. da Silva, J. A. L. da Silva, J. L. Baptista-Ferreira and F. Pinho-Almeida, in *Vanadium Compounds – Chemistry, Biochemistry and Therapeutic Applications*, ed. A. S. Tracey and D. C. Crans, *American Chemical Society Symposium Series No 711*, American Chemical Society, Washington, 1998, pp. 241–247.
48. L. Dias, N. Bekhti, M. L. Kuznetsov, J. A. B. Ferreira, M. C. Bacariza and J. A. L. da Silva, *Chem. – Eur. J.*, 2018, **24**, 2474.
49. M. P. Santoni, G. La Ganga, V. M. Nardo, M. Natali, F. Puntoriero, F. Scandola and S. Campagna, *J. Am. Chem. Soc.*, 2014, **136**, 8189.
50. World Patent WO2004/037416-A2, May 6, 2004, A. J. L. Pombeiro, J. J. R. Fraústo da Silva, Y. Fujiwara, J. A. L. Silva, P. M. Reis and A. M. F. Palavra.
51. Portuguese Patent PT103131-Z, September 30, 2005, A. J. L. Pombeiro, J. J. R. Fraústo da Silva, J. A. L. Silva, M. V. Kirillova, P. M. Reis, A. M. F. Palavra and Y. Fujiwara.
52. Portuguese Paten PT103352, August 31, 2006, A. J. L. Pombeiro, J. J. R. Fraústo da Silva, J. A. L. Silva and M. V. Kirillova.
53. World Patent WO2008/088234-A1, July 24, 2008, A. J. L. Pombeiro, M. V. Kirillova, A. M. Kirillov, J. A. L. Silva and J. J. R. Fraústo da Silva.
54. J. A. L. da Silva, J. J. R. Fraústo da Silva and A. J. L. Pombeiro, *Coord. Chem. Rev.*, 2011, **255**, 2232.
55. G. B. Shul'pin, *Mini-Rev. Org. Chem.*, 2009, **6**, 95.
56. *Catalytic Activation and Functionalization of Light Alkanes*, ed. E. G. Derouane, J. Haber, F. Lemos, F. Ramôa Ribeiro and M. Guinet, *NATO ASI series*, Kluwer Academic Publishers, Dordrecht, The Netherlands, **vol. 44**, 1998.
57. *Activation and Functionalization of Alkanes*, ed. C. L. Hill, Wiley, New York, 1989.
58. *Methane Conversion by Oxidative Processes: Fundamental and Engineering Aspects*, ed. E. E. Wolf, Van Nostrand Reinhold, New York, 1992.
59. A. E. Shilov and G. B. Shul'pin, *Activation and Catalytic Reactions of Saturated Hydrocarbons in the Presence of Metal Complexes*, Kluwer Academic Publishers, Dordrecht, The Netherlands, 2000.
60. C. G. Jia, T. Kitamura and Y. Fujiwara, *Acc. Chem. Rev.*, 2001, **34**, 633.
61. R. H. Crabtree, *J. Chem. Soc., Dalton Trans.*, 2001, 2437.
62. G. B. Shul'pin, *C. R. Chim*, 2003, **6**, 163.
63. G. B. Shul'pin, *J. Mol. Catal. A: Chem.*, 2002, **189**, 39.

64. A. E. Shilov and G. B. Shul'pin, *Chem. Rev.*, 1997, **97**, 2879.
65. *Sustainable Strategies for the Upgrading of Natural Gas: Fundamentals, Challenges and Opportunities*, ed. E. G. Derouane, V. Parmon, F. Lemos, F. Ramôa Ribeiro and M. Guinet Springer, *NATO ASI Series II: Mathematics, Physics and Chemistry*, **vol. 191**, 2005.
66. G. B. Shul'pin, *Catalysts*, 2016, **6**, 50.
67. *Alkane Functionalization*, ed. A. J. L. Pombeiro and M. F. C. Guedes da Silva, John Wiley & Sons Ltd, 2019.
68. P. M. Reis, J. A. L. Silva, J. J. R. F. da Silva and A. J. L. Pombeiro, *Chem. Commun.*, 2000, 1845.
69. P. M. Reis, J. A. L. Silva, J. J. R. F. da Silva and A. J. L. Pombeiro, *J. Mol. Catal. A: Chem.*, 2004, **224**, 189.
70. P. M. Reis, J. A. L. Silva, A. F. Palavra, J. J. R. F. da Silva, T. Kitamura, Y. Fujiwara and A. J. L. Pombeiro, *Angew. Chem., Int. Ed.*, 2003, **42**, 821.
71. M. V. Kirillova, M. L. Kuznetsov, P. M. Reis, J. A. L. Silva, J. J. R. F. da Silva and A. J. L. Pombeiro, *J. Am. Chem. Soc.*, 2007, **129**, 10531.
72. M. V. Kirillova, M. L. Kuznetsov, J. A. L. da Silva, M. F. C. da Silva, J. J. R. F. da Silva and A. J. L. Pombeiro, *Chem. – Eur. J.*, 2008, **14**, 1828.
73. M. V. Kirillova, J. A. L. da Silva, J. J. R. F. da Silva, A. F. Palavra and A. J. L. Pombeiro, *Adv. Synth. Catal.*, 2007, **349**, 1765.
74. P. M. Reis, J. A. L. Silva, A. F. Palavra, J. J. R. F. da Silva and A. J. L. Pombeiro, *J. Catal.*, 2005, **235**, 333.
75. M. V. Kirillova, M. L. Kuznetsov, V. B. Romakh, L. S. Shul'pina, J. J. R. Fraústo da Silva, A. J. L. Pombeiro and G. B. Shul'pin, *J. Catal.*, 2009, **235**, 140.
76. T. F. S. Silva, K. V. Luzyanin, M. V. Kirillova, M. F. C. Guedes da Silva, L. M. D. R. S. Martins and A. J. L Pombeiro, *Adv. Synth. Catal.*, 2010, **352**, 171.
77. R. R. Fernandes, L. Jamal, M. F. C. Guedes da Silva, J. A. da Silva, J. J. R. Fraústo da Silva and A. J. L. Pombeiro, *Appl. Catal., A*, 2011, **402**, 110.
78. M. V. Kirillova, M. L. Kuznetsov, Y. N. Kozlov, L. S. Shul'pina, A. Kitaygorodskiy, A. J. L. Pombeiro and G. B. Shul'pin, *ACS Catal.*, 2011, **1**, 1511.
79. G. Zampella, L. Bertini and L. De Gioia, *Chem. Commun.*, 2014, **50**, 304.
80. C. Jia, T. Kitamura and Y. Fujiwara, *Acc. Chem. Res.*, 2001, **34**, 633.
81. J. Felcman, J. J. R. Fraústo da Silva and M. C. T. A. Vaz, *Inorg. Chim. Acta*, 1984, **93**, 101.
82. G. Bemski, J. Felcman, J. J. R. Fraústo da Silva, I. Moura, J. J. G. Moura, M. C. T. A. Vaz and L. F. Vilas-Boas in *Frontiers in Bioinorganic Chemistry*, ed. A. V. Xavier, VCH Verlagsgesellaschaft, Weinheim, 1986, pp. 97–105.
83. E. Bayer, E. Koch and G. Anderegg, *Angew. Chem., Int. Ed. Engl.*, 1987, **26**, 545.
84. C. M. Clouthier and J. N. Pelletier, *Chem. Soc. Rev.*, 2012, **41**, 1585.

85. M. S. Humble and P. Berglund, *Eur. J. Org. Chem.*, 2011, 3391.
86. J. A. L. da Silva, J. J. R. Fraústo da Silva and A. J. L. Pombeiro, in *Vanadium: Biochemical and Molecular Biological Approaches*, ed. H. Michibata, Springer, 2012, pp. 35–49.
87. *Applied Homogeneous Catalysis with Organometallic Compounds: A Comprehensive Handbook in Four Volumes*, ed. B. Cornils, W. A. Herrmann, M. Beller and R. Paciello, Wiley-VCH Verlag GmbH & Co, 3rd edn, 2018.
88. J. A. Guevara-García, N. Barba-Behrens, R. Contreras and G. Mendoza-Díaz, in *Vanadium Compounds – Chemistry, Biochemistry and Therapeutic Applications*, ed. A. S. Tracey and D. C. Crans, *American Chemical Society Symposium Series No. 711*, American Chemical Society, Washington, 1998, pp. 126–135.
89. V. Conte, F. Di Furia and S. Moro, in *Vanadium Compounds—Chemistry, Biochemistry and Therapeutic Applications*, ed. A. S. Tracey and D. C. Crans, *American Chemical Society Symposium Series No. 711*, American Chemical Society, Washington, 1998, pp. 136–145.
90. V. L. Pecoraro, C. Slebodnick and B. Hamstra in *Vanadium Compounds—Chemistry, Biochemistry and Therapeutic Applications*, ed. A. S. Tracey and D. C. Crans, *American Chemical Society Symposium Series No. 711*, American Chemical Society, Washington, 1998, pp. 157–167.
91. C. J. Schneider, G. Zampella, L. De Gioa and V. L. Pecoraro, in *Vanadium: The Versatile Metal*, ed. K. Kustin, J. C. Pessoa and D. C. Crans, *American Chemical Society Symposium Series No. 974*, American Chemical Society, Washington, 2007, pp. 148–162.
92. W. Plass, M. Bangesh, S. Nica and A. Buchholz, in *Vanadium: The Versatile Metal*, ed. K. Kustin, J. C. Pessoa and D. C. Crans, *American Chemical Society Symposium Series No. 974*, American Chemical Society, Washington, 2007, pp. 163–177.
93. M. R. Maurya, A. Kumar and J. C. Pessoa, *Coord. Chem. Rev.*, 2011, **255**, 2315.
94. J. J. R. Fraústo da Silva, *Chem. Speciation Bioavailability*, 1989, **1**, 139.
95. H. B. ten Brink, A. Tuynman, H. L. Dekker, W. Hemrika, Y. Izumi, T. Oshiro, H. E. Schoemaker and R. Wever, *Inorg. Chem.*, 1998, **37**, 6780.
96. D. C. Crans, J. J. Smee, E. Gaidamauskas and L. Yang, *Chem. Rev.*, 2004, **104**, 849.
97. M. V. Kirillova, A. M. Kirillov, M. L. Kuznetsov, J. A. L. Silva, J. J. R. F. da Silva and A. J. L. Pombeiro, *Chem. Commun.*, 2009, 2353.
98. A. Paul, A. P. C. Ribeiro, A. Karmakar, M. F. C. Guedes da Silva and A. J. L. Pombeiro, *Dalton Trans.*, 2016, **45**, 12779.
99. M.-F. Zaltariov, M. Alexandru, M. Cazacu, S. Shova, G. Novitchi, C. Train, A. Dobrov, M. V. Kirillova, E. C. B. A. Alegria, A. J. L. Pombeiro and V. B. Arion, *Eur. J. Inorg. Chem.*, 2014, 4946.
100. A. M. Kirillov, Y. Y. Karabach, M. V. Kirillova, M. Haukka and A. J. L. Pombeiro, *Cryst. Growth Des.*, 2012, **12**, 1069.

101. M. V. Kirillova, A. M. Kirillov, A. N. C. Martins, C. Graiff, A. Tiripicchio and A. J. L. Pombeiro, *Inorg. Chem.*, 2012, **51**, 5224.
102. M. V. Kirillova, A. M. Kirillov and A. J. L. Pombeiro, *Adv. Synth. Catal.*, 2009, **351**, 2936.
103. M. V. Kirillova, A. M. Kirillov and A. J. L. Pombeiro, *Chem. – Eur. J.*, 2010, **16**, 9485.
104. E. C. B. A. Alegria, E. Fontolan, A. P. C. Ribeiro, M. N. Kopylovich, C. Domingos, A. M. Ferraria, R. Bertani, A. M. Botelho do Rego and A. J. L. Pombeiro, *Mater. Today Chem.*, 2017, **5**, 52.
105. A. P. C. Ribeiro, L. M. D. R. S. Martins, S. A. C. Carabineiro, J. L. Figueiredo and A. J. L. Pombeiro, *Appl. Catal., A*, 2017, **547**, 124.
106. I. A. S. Matias, A. P. C. Ribeiro, E. C. B. A. Alegria, A. J. L. Pombeiro and L. M. D. R. S. Martins, *Inorg. Chim. Acta.*, 2019, **489**, 269.
107. E. Pakrieva, A. P. C. Ribeiro, L. M. D. R. S. Martins, I. A. S. Matias, S. A. C. Carabineiro, E. Kolobova, A. J. L. Pombeiro, J. L. Figueiredo and A. Pestryakov, *Catal. Today*, 2019, DOI: 10.1016/j.cattod.2019.05.050.

CHAPTER 3

Activating Hydroperoxides by Vanadium(V) Compounds

JENS HARTUNG

Fachbereich Chemie, Organische Chemie, Technische Universität Kaiserslautern, Erwin-Schrödinger-Straße, Kaiserslautern, Germany
Email: hartung@chemie.uni-kl.de

3.1 Introduction

Hydroperoxides, compounds with the general formula ROOH, are widely in use for valorising nucleophilic compounds of the type X (Schemes 3.1 and 3.2).[1–3] Combining high yields and selectivity for preparing targets XO in reasonable time frames requires specialized additives for activating hydroperoxides and narrowing pathways of oxygen-atom transfer to, if possible, exclusively monooxygention of X. Such additives, so-called oxidation catalysts, are of enormous economic value because they contribute to cutting costs of production lines by more effectively using raw materials, reducing energy input and limiting waste production.[4]

Nearly all hydroperoxide mediated syntheses provide stronger bonds between oxygen and carbon, sulphur, nitrogen or halogen from a nucleophilic and, thus, less-stabilized electron pair and a weak σ(O,O) bond. Although tabulated heats of formation predict considerable driving forces,[5] almost none of the reactions occurs spontaneously.[6] The reason for kinetic stability of hydroperoxide-nucleophile formulations arises from a barrier, preventing the peroxide group, being shielded by a set of four non-bonding electron pairs, to be approached by a reactant.[7,8]

Most additives in use for unleashing oxidative reactivity interact with a peroxide group for facilitating electron transfer into σ^*(O,O) and shifting

Catalysis Series No. 41
Vanadium Catalysis
Edited by Manas Sutradhar, José Armando L. da Silva and Armando J. L. Pombeiro

Published by the Royal Society of Chemistry, www.rsc.org

activating hydroperoxides by

• *Brønsted acids*: Maaß and Hiebert (1924)

HA = e.g. HBr, HCl, H_2SO_4

• *Lewis acids*: Brill and Indictor (1965) / Sheldon (1973)

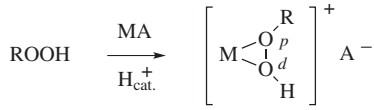

R = H, alkyl / MA = e.g. $Ti(OiPr)_4$, $VO(OEt)_3$, MoO_2Cl_2

Scheme 3.1 Concepts of activating hydroperoxides for two-electron reductions (descriptors *p* and *d* are used for distinguishing proximal from distal peroxide oxygen).[15–17]

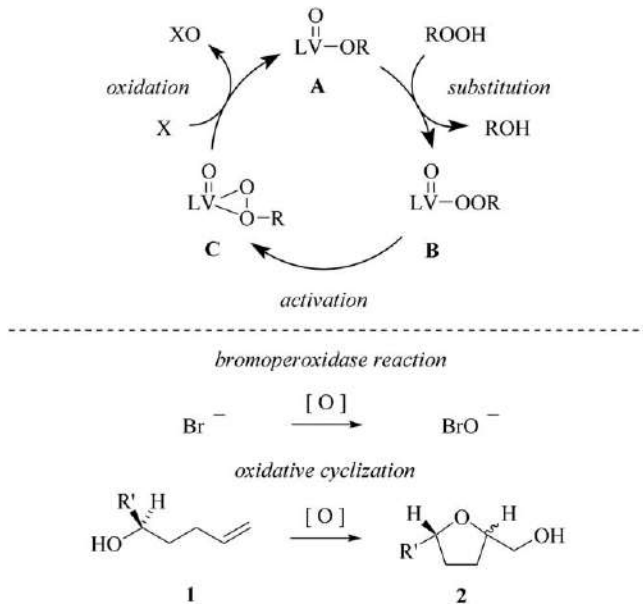

Scheme 3.2 Catalytic cycle for describing vanadium(v)-catalysed oxidation by the peroxy mechanism (top; R = H or alkyl; L = twofold negative donor group) and examples from bio-inspired synthesis proceeding accordingly {bottom; R′ and R″ = alkyl or aryl; [O] = VO(L)(OOR), *e.g.*, **C**}.

electron density from at least one non-bonding pair of oxygen to the periphery by forming an additional bond with the catalyst.

A second option for activating a hydroperoxide is transferring an electron from a metal-centred radical into σ^*(O,O), causing the peroxide bond to break

homolytically. This step splits the hydroperoxide into an anion and an oxyl radical. Oxyl radicals are demanding intermediates in synthesis, and guidelines for predicting selectivity in this chemistry are just evolving.[9]

Lewis acids cause a net stabilization of σ(O,O) *and* σ^*(O,O) when interacting with peroxides. Reagents in use for this purpose are early-transition metal ions,[10] silicate clusters,[11] heteropolyacids[12] and metalloenzymes[13] (Scheme 3.1). The simplest Lewis acid is the proton delivered from a Brønsted-acid HA. Almost all mineral acids are capable of protonating in chemical equilibria hydroperoxides to yield hydroperoxonium, a potent electrophilic oxygen atom donor.[14]

Among Lewis acids surveyed for activating hydroperoxides, esters of orthovanadium acid (H_3VO_4) stand out for reasons of otherwise unattainable reactivity and selectivity. Brill and Indictor in 1965 were the first to document rate effects of vanadium(v) compounds on hydrocarbon oxidation by hydroperoxides.[17] The progress achieved in this field of research ever since fills books,[11,18] book chapters[19,20] and, on a regular basis, reviews.[21,22]

Other transition metal compounds, particularly of titanium(IV),[23] chromium(VI),[24] molybdenum(VI)[25] and tungsten(VI)[26,27] exert similar activating effects on hydroperoxides, but none of the reagents combines reactivity and selectivity in the privileged manner orthovanadates do.

For rationalizing sometimes seemingly contradictory selectivity in oxidative chemistry, two mechanisms were proposed. Which of the mechanisms applies is guided by the chemical nature of the particular metal reagent–hydroperoxide couple.[11,28]

Early transition metals ions lacking by formal count in *d*-electrons, preferentially form Lewis-acid–base-adducts with alkyl hydroperoxides, thereby allowing transferring one of the peroxidic oxygens in S_N2-manner to a reductant (peroxy mechanism). The peroxy mechanism leaves the oxidation number at the metal unchanged (Scheme 3.2).[29,30]

Late transition metal compounds comprising two or more metal-oxo groups, *e.g.*, osmium(VIII)-tetroxide, perrhenate(VII), or permanganate(VII), accept electrons from nucleophiles by one or two π^*(M,O) orbital(s), causing the oxidation number of the metal to decline by two units. Regenerating the metal-based oxidant, in the so-called metal-oxo-route, occurs in a succeeding step using hydrogen peroxide, an alkyl hydroperoxide, an amine *N*-oxide, dioxygen or another suitable reagent as terminal oxidant.[30–33]

Distinguishing hydroperoxy- from metal-oxo-mechanism is feasible by tracing stereochemical fingerprints, particularly of C–O-bond formation. By these means, orthovanadate-catalysed oxidative cyclization of chiral 4-pentenols mediated with alkyl hydroperoxides in homogeneous solution was classified as hydroperoxy-mediated transformation (Scheme 3.2).[11,28]

At a moment when progress seemingly converged, input from biochemistry added unexpected momentum to orthovanadate-peroxide chemistry.[34,35] In 1983 Vilter discovered orthovanadate(v)-dependent enzymes able to activate hydrogen peroxide for oxidizing bromide in pH-neutral solution at ambient temperature.[36] Bromoelectrophiles generated accordingly offered an explanation for the chemical origin of brominated terpenes,

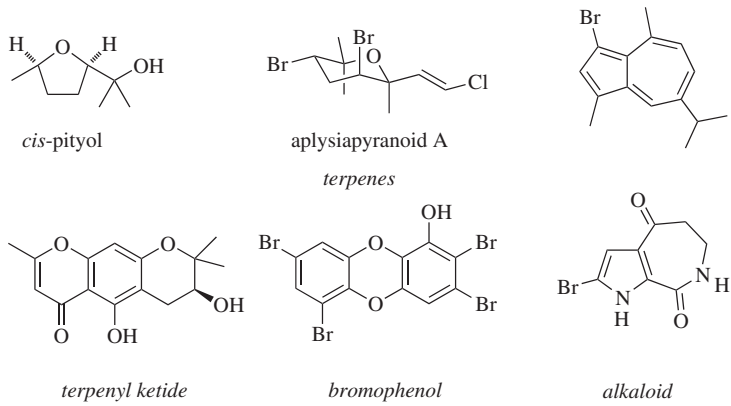

Figure 3.1 Classes and examples of natural products being synthetically accessible from hydroperoxide mediated C,O- and C,Br-bond formations.[37–39]

terpenyl-ketides, shikimates, polyketide-derived phenols and alkaloids in a marine environment (Figure 3.1).[37]

Pursuing biomimetic synthesis of brominated and hydroxylated secondary metabolites, *e.g.*, cyclic ethers (Figure 3.1) from potential biomimetic progenitors (*e.g.* **1**→**2**) required mechanistic understanding of the bromoperoxidase reaction, allowing predicting reactivity and selectivity of carbon–bromine- and carbon–oxygen-bond formation (Scheme 3.2).[34]

Earlier studies on the bromoperoxidase mechanism proposed anionic orthovanadates for activating hydroperoxides.[40] This approach, however, lacked physical reasoning since enhanced hydrogen peroxide reactivity from nucleophile–nucleophile contact is hardly explicable. In failing, this approach revealed that a physics-based theory on *activating* hydroperoxides did not exist.[41,42]

This chapter summarizes two recently elaborated mechanisms that explain how vanadium(v) reagents activate hydroperoxides.

The first reaction model focusses on the bromoperoxidase mechanism and emphasizes the need of adjusting polar effects for attaining reactivity.[41]

The second reaction model explains effects of trialkyl orthovanadates on alkyl hydroperoxides, exemplified by *tert*-butyl hydroperoxide [$(H_3C)_3COOH$, *t*BuOOH, TBHP] for oxyfunctionalising π(C,C) bonds. In this mechanism, donating effects from alkyl substitution level accepting contributions from vanadium(v), restrict the role of the metal to opening a pathway for transferring the distal peroxide oxygen (O^d) to a reductant.[42]

3.2 Basic Properties of Some Hydroperoxides

Neat hydrogen peroxide is a colourless, slightly viscous liquid and is used as rocket propellant. The mass fraction of transferrable oxygen atom accounts for 47.0% of the molecular weight (Table 3.1). Names also in use for

specifying the transferrable oxygen atom are *peroxidic oxygen (atom)* or *active oxygen*. The fraction of peroxidic oxygen declines in 30-weight percent aqueous solution to 14.1-mass percent, and is considered safe for storing and handling when free from acids, bases, redox active components or other contaminants.[10]

tert-Butyl hydroperoxide (TBHP) is commercially distributed as 70-weight percent aqueous solution, comprising an active oxygen content of 12.4-mass percent. A 5.5 molar solution of anhydrous TBHP in decane, being 10.6% by mass in active oxygen, is distributed by chemical suppliers and was used for conducting most experiments summarized in Section 3.8.

Working with hydroperoxides requires keeping in mind the thermochemical driving forces offered by the reagents for oxidizing hydrocarbons.[43] TBHP in concentrations above those available from commercial suppliers belong exclusively in the hands of experts. Increasing concentration, for instance, by distilling off solvent from solutions containing unspent oxidant increases propensity of TBHP for decomposing in violent explosion. Peroxide tests prior to working up reaction mixtures from oxidative transformations are routine to experts, as are methods for selectively decomposing unspent oxidant before beginning to isolate products.

Hydrogen peroxide is four orders of magnitude more acidic than water. TBHP exceeds *tert*-butanol by three orders of magnitude in acidity (Table 3.1, entry 2).[44] The ease with which corresponding bases form from both hydroperoxides should be a driving force for substituting hydroperoxy or alkyl peroxy for hydroxy or alkoxy in orthovanadates. Experimental data, however,

Table 3.1 Active oxygen content in mass percentage ([O]), acidity (pK_a), physical properties [boiling and melting points (bp, mp)], vertical ionization potentials (IP), minimum conformation, frontier molecular orbitals (from NBO-theory, see Text) and assignment of locators proximal (p) and distal (d) in hydroperoxides.

donor

$n(O) / \sigma(O,O)$

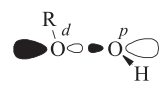

acceptor

$\sigma^*(O,O)$

Entry	Parameter	R = H	R = C(CH$_3$)$_3$
1	[O]/*w*/*w*/%[a]	14.1/47.0[b]	12.4/10.6[c]
2	pK_a	11.75	12.69
3	bp/°C	150.2	37[d]
4	mp/°C	−0.41	−3
5	IP/eV[e]	10.62	10.24

[a]Weight percent of transferable oxygen atom.
[b]First entry: 30% aqueous solution (*w*/*w*); second entry: neat hydrogen peroxide.
[c]First entry: 70% aqueous solution (*w*/*w*); second entry: 5.5 molar solution in decane.
[d]At a pressure of 20 mbar.
[e]IP = vertical ionization potential.

do not comply with this assumption. Perhydrolysing orthovanadates by hydrogen peroxide is only weakly exergonic (Section 3.3) and even endergonic for most substitutions by *tert*-butyl hydroperoxide (Section 3.6).

Orbital effects counterbalance oxidative and nucleophilic properties of hydroperoxides, requiring specialized reagents for unravelling one from the other. Nucleophilicity is apparent from an affinity towards electrophiles in substitutions, and physically obvious from vertical ionization potentials.

Hydroperoxide nucleophilicity arises from Coulomb repulsion between non-bonding electron pairs at oxygens, also affecting σ(O,O)-bond strength and conformational preference (Table 3.1, entry 5). Hydroperoxide electrophilicity arises from σ^*(O,O). Populating σ^*(O,O) by electrons from a reductant triggers peroxide decomposition and, thus, redox chemistry.

3.3 The Hydrogen Peroxide-orthovanadate System – Chemistry of Marine Bromoperoxidases

In acidic aqueous solution (pH 1–0) hydrogen peroxide exists in equilibrium with hydroperoxonium. The conjugated acid of hydrogen peroxide is a potent oxidant and reacts with bromide faster than any orthovanadate-derived peroxide.

At pH 6.2–6.5, hydrogen peroxide, being activated by an orthovanadate-dependent bromoperoxidase, surpasses in rate hydroperoxonium reactivity for oxidizing bromide by four orders of magnitude.[45]

The key to bromoperoxidase reactivity are the chemical changes the orthovanadate cofactor experiences upon binding *via* a network of cooperatively strengthened hydrogen bonds to a total of seven privileged amino acid side chains (*cf.* Figure 3.2).

Aspects of bromoperoxidases deserving additional mention are thermal and chemical stability. Most bromoperoxidases resist spontaneous denaturing at 90 °C, much as expected for enzymes from organisms living in the intertidal zone. Fractions of 50% by volume and more of alkanols, acetonitrile or dimethyl sulfoxide have minor effects only on oxidative reactivity of bromoperoxidases allowing to use such cosolvents attaining attractive yields and selectivity in oxidative hydrocarbon bromination.

Structurally unique is the fact that all bromoperoxidases characterized so far exist as even-numbered homomultimers, binding one molecule of orthovanadate per subunit at a structurally conserved site. In the monochlorodimedone (mcd) assay, this conserved binding site, surprisingly, leads to a dispersion of rates for turning over bromide, differing by factor 250 between *Macrocystis pyrifera* bromoperoxidase I, the most reactive enzyme characterized so far, to *Ceramium rubrum* I, the least reactive (Table 3.2, entries 1 and 5).[46]

In the resting state, the bromoperoxidase cofactor, most likely, adopts the dihydrogen orthovanadate configuration ($H_2VO_4^-$) and forms hydrogen bonds to side chains of two arginines, three histidines, one lysine and one serine. Arginine side chains, following thermochemical calculations using

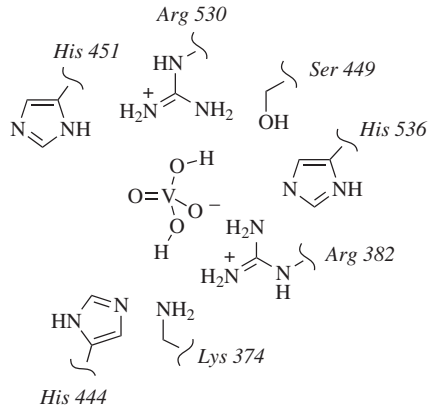

Figure 3.2 Model for co-factor bonding to amino acid side chains in $V_{Br}PO(AnII)$ (side chain positions were taken from the crystal structure of the bromoperoxidase).

Table 3.2 Quantifying enzymatic reactivity by the monochlorodimedone (mcd)-assay (U^0), source, quaternary organization and cofactor/monomer-ratio of selected bromoperoxidases.[47–50]

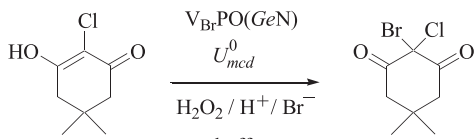

mcd

Entry	*Genus eptitet* isoenzyme X	$V_{Br}PO(GeN)^a$	Subunits	V/Subunit[b]	$U^0\,mg^{-1}$/[pH]
1	*Ceramium rubrum* I[51]	$V_{Br}PO(CrI)$	4[c]	1	7 [7.4]
2	*Ascophyllum nodosum* II[52]	$V_{Br}PO(AnII)$	6	1	90–120 [6.5]
3	*Ascophyllum nodosum* I[53]	$V_{Br}PO(AnI)$	2	1	130–170 [6.5]
4	*Corallina officinalis* I[54]	$V_{Br}PO(CoI)$	12	1	550 [6.4]
5	*Macrocystis pyrifera* I[55]	$V_{Br}PO(MpI)$	—[d]	1.5 (0.4)	1730 [6.0]

[a]Orthovanadate-dependent bromoperoxidase ($V_{Br}PO$) from organism specified by *G*enus, epitet *e* for defining a species (*Ge*) and isoenzyme number N.
[b]For proteins dialyzed against aqueous sodium orthovanadate; figure in brackets denotes vanadate-to-subunit ratio in the native bromoperoxidase.
[c]Calculated from molecular masses of 58 kDa for the monomer and 242 kDa for native bromoperoxidase.
[d]Not determined.

an assessed electronic structure theory, are the strongest attractors for anionic orthovanadates and orthovanadium acid (H_3VO_4).[41] The theory used for predicting ground-state properties, and aspects of peroxide chemistry, is Becke's three parameter Lee–Yang–Parr hybrid functional (B3LYP)[56,57] in combination with a set-basis set, abbreviated in the Gaussian system as 6-311++G**.[58] The basis set uses corrections for theoretically describing d-orbitals and allows predicting energy differences for chemical changes without causing energetic contributions from relativistic effects at

vanadium to exceed self-confined tolerance of ±5% compared to experimental references.[59–63]

Positive cooperativity in co-factor bonding arises from combining guanidinium from arginine as the electrophilic hydrogen bond donor with nucleophilic side chains from histidine, uncharged lysine or serine. The total hydrogen bond strength of, *e.g.*, an adduct between orthovanadium acid and *N*-methylguanidinium as truncated arginine side-chain model, imidazole in combination with methanamine as respective histidine and lysine mimics, exceeds in B3LYP/6-311++G**-theory, the sum of individual hydrogen-bond strengths by factor two. On an absolute scale, the predicted hydrogen-bond strength correlates with experimental affinity between co-factor and bromoperoxidase protein in V_{Br}PO(*An*I).[64]

Once dissociated from the bromoperoxidase protein, orthovanadate(v) exists in $\sim 10^{-5}$ molar pH neutral solution as equilibrium mixture of hydrogen orthovanadate (HVO_4^{2-}), dihydrogen orthovanadate ($H_2VO_4^-$) and minor fractions of derived dimeric and tetrameric homopolyacids. Below pH 3, proton-assisted hydrolysis transforms this equilibrium mixture into solvated *cis*-dioxovanadium(v) [$VO_2^+(H_2O)_n$; $n = 3$ to 4].[65]

Hydrogen peroxide interferes with the orthovanadate equilibrium in aqueous solution by preferentially perhydrolysing monomeric vanadium(v) compounds. The rate of orthovanadate perhydrolysis depends on proton concentration, gradually increasing as solutions become more acidic.[66] In aqueous perchloric acid (pH 2), a value of $3 \cdot 10^3$ M^{-1} for constant K^1 characterizing the first equilibrium (~20 °C and at an ionic strength I of 1.0 M) points to an exergonic process,[67] being one order of magnitude less favoured when argued on the basis of equilibrium constant K^2 than perhydrolyzing the solvated *cis*-dioxovanadium(v) cation at pH 1 ($K^2 = 3.7 \cdot 10^4$ M^{-1}, 25 °C, $I = 0.3$–1.0 M).[68,69]

Analysing kinetic data used for deriving K^2 at 25 °C in acidic solution at fixed ionic strength ($I = 3$ M) by varying reactant concentrations shows that second-order rate constant k^2 ($5 \cdot 10^3$ $M^{-1}\,s^{-1}$ in eqn (3.2))[70] may be split into three terms. One of the terms is directly proportional to proton concentration, the second indirectly and the third is independent from acid strength.

Analysing pressure dependence of rate constant k^2 in the pH range of 0–1.5 provides an activation enthalpy ($\Delta H^{\ddagger}$) for generating oxoperoxovanadium(v) cation (**4**) from *cis*-dioxovanadium(v) of 21 $kJ\,mol^{-1}$, an activation entropy ($\Delta S^{\ddagger}$) -69 $J\,mol^{-1}\,K^{-1}$ and an activation volume ($\Delta V^{\ddagger}$) of 15 $cm^3\,mol^{-1}$ (eqn (3.2)).[70]

When present in excess, hydrogen peroxide transforms peroxometavanadate(v) (**3**) into oxobisperoxovanadate(v) (**5**) (eqn (3.3)). In perchloric acid (pH 2), frequently added for investigating kinetics in the orthovanadate–hydrogen peroxide-system, the oxoperoxovanadium(v) cation (**4**) reacts with hydrogen peroxide in a rate constant k^4 of $3.5 \cdot 10^3$ $M^{-1}\,s^{-1}$ ($I = 3$ M, 25 °C) to yield oxobisperoxovanadate (**5**) (eqn (3.4)). The activation enthalpy ($\Delta H^{\ddagger} = 40$ $kJ\,mol^{-1}$) of the second peroxygenation is by factor two higher than the first, based on data obtained from studying pressure

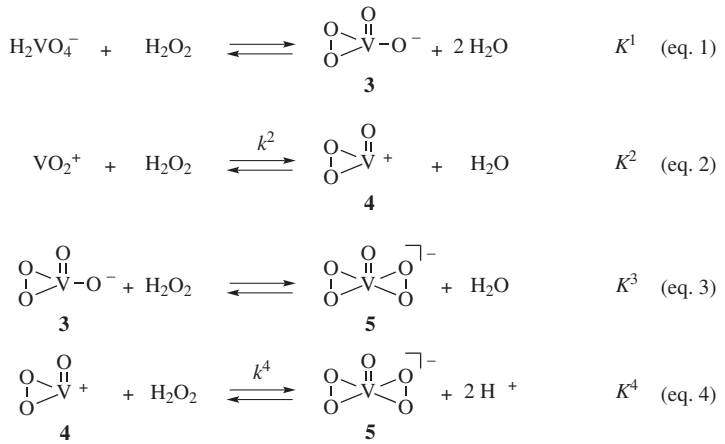

Scheme 3.3 Stoichiometry for peroxovanadate- (eqn (3.1)), oxoperoxovanadium(v) cation- (eqn (3.2)) and oxobisperoxovanadate formation (eqn (3.3) and (3.4); c_{H_2O} was treated as constant for calculating numbers and deriving dimensions of K^{1-4} provided in the text).[66–70]

dependence of k^4. Activation entropy ($\Delta S^{\ddagger} = -42$ J mol^{-1} K^{-1}) and activation volume ($\Delta V^{\ddagger}$) of 0 cm^3 mol^{-1} for the second peroxygenation show a less-uniform picture, thus pointing to additional elementary reactions, possibly responding to opposite effects. According to the data, $VO(O_2)_2^-$ (**5**) forms in approximately neutral solution more readily ($K^3 = 2 \cdot 10^5$ M^{-1}, pH 6.7, ~20 °C, $I = 1$ M)[67] than in acidic solution ($K^4 = 0.6$ M, pH 1.0, 25 °C, $I = 0.3$).[68]

Further increasing concentration and aliquots of hydrogen peroxide used for preparing bisperoxovanadate **5** afford tris- and tetra-kisperoxovanadates (Scheme 3.3).[71]

Monoperoxo orthovanadates exert in pH-neutral solution higher affinity for reacting with nucleophiles than bisperoxo orthovanadates. The reason for this seemingly contradictory finding is the elevated acidity of hydroperoxy(peroxo) orthovanadium(v) [$VO(O_2)_2H$] ($pK_a = 0.43$) existing in pH-neutral solution almost entirely as conjugate base, thus effectively repelling anions for electrostatic reasons. Protonation alters this situation, providing hydroperoxy(peroxo) orthovanadium(V), exceeding vanadium(v) monoperoxoic acid $VO(O_2)(OH)$ in rate for oxidizing sulphides by factor 10^4.[72]

A. nodosum bromoperoxidases $V_{Br}PO(AnI)$ and $V_{Br}PO(AnII)$ effectively bind hydrogen peroxide and rapidly oxidize bromide at pH 6–7.[52,73,74] Steady-state kinetic data comply for both bromoperoxidases with a bi-bi-ping-pong reaction model, a sequence of two-ordered bimolecular reversible elementary reactions [Scheme 3.4, eqn (3.5)–(3.8)].[75–77]

The first equilibrium of the bi-bi-ping-pong mechanism transforms resting-state PO and hydrogen peroxide in the presence of a proton source into activated state PO′ (eqn (3.5)). The second equilibrium furnishes upon bromide binding PO″ from PO′ (eqn (3.6)). In this model, PO″ represents the reactive state, generating oxygen atom transfer hypobromite (BrO^-) by

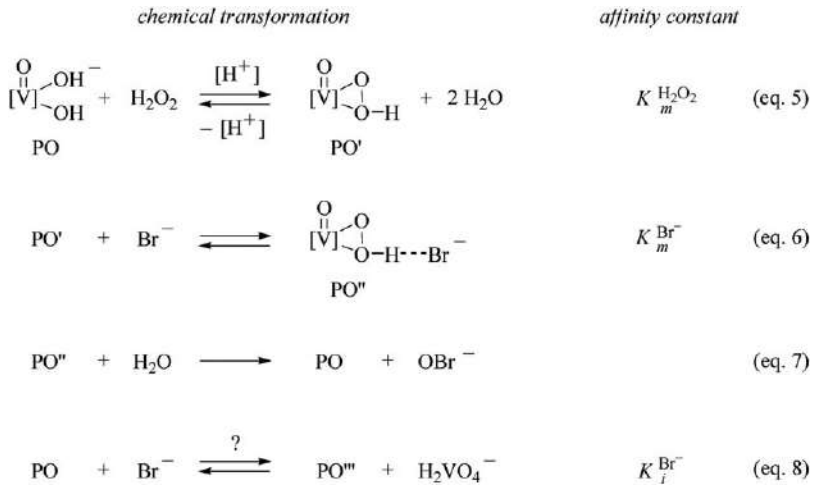

Scheme 3.4 Elementary steps (eqn (3.5)–(3.8)), states (PO–PO′′′), and Michaelis–Menten parameters ($K_m^{H_2O_2}$, $K_m^{Br^-}$, and $K_i^{Br^-}$) describing the mechanism of the bromoperoxidase mechanism on the basis of steady-state kinetic data (PO = peroxidase; PO′ = peroxo form of the peroxidase; PO″ = bromide adduct to protonated PO′; PO′′′ = bromide-inhibited state) and proposed structure formula for states PO, PO′ and PO″.[78]

Table 3.3 Steady-state kinetic data characterizing V_{Br}PO(*An*I)-catalysed bromide oxidation (pH 5.9, 1.65 molar ionic strength adjusted by adding sodium sulphate at a temperature of 22 ± 0.5 °C; 172 ± 2 U_{MCD}^0 mg^{-1}).

Entry	NaCl/mM	V_{max}/U mg^{-1}	$K_m^{Br^-}$/mM	$K_m^{H_2O_2}$/μM	$K_i^{Br^-}$[a]/mM
1	—	107 ± 7	2.9 ± 0.3	75 ± 7	557
2	10	130 ± 12	4.0 ± 0.6	58 ± 8	630

[a]Confidence level omitted due to considerable magnitude of standard deviation (±30–60%).

simultaneously regenerating resting-state configuration PO (eqn (3.7)). Higher concentrations of bromide competitively inhibit oxidative turnover, leading to kinetically defined state PO′′′, as obvious from inhibitory constant $K_i^{Br^-}$, being structurally subject to discussion (Table 3.3, eqn (3.8)).[78]

3.4 Activating Hydrogen Peroxide by Orthovanadate-dependent Bromoperoxidases

Chemical properties of the oxidant PO″ in the bromoperoxidase reaction are largely determined by supramolecular interactions between the hydrogen peroxide-loaded co-factor and a hydrogen-bonding network spanned by side chains of the seven prominent amino acids forming the binding site: serine, lysine, three histidines and two arginines. In aqueous solutions, guanidinium groups from arginine side chains are always protonated, generating

positively charged environment, which is thought to affect orthovanadate binding and the chemistry that follows.[41]

Electrostatics and electronic structure theory (*vide infra*) imply that a peroxide capable of oxidizing nucleophilic bromide at an outstanding rate exerts electrophilic properties. The only orthovanadium compound providing in a density functional theory-based model access to electrophilic vanadium(v)-derived oxidants, without being expelled from the cationic binding site, is orthovanadium acid (H_3VO_4; pK_a 3.5, 7.8, 12.5).[79]

Orthovanadium acid is a transient existing in aqueous solution in a narrow range slightly above and below pH 3.5. Above pH 3.8, the acid transfers a proton to water, yielding the dihydrogen orthovanadate anion. Below pH 3.5, the acid rearranges into hydrated *cis*-dioxovanadium(v).[79] Forming *cis*-dioxovanadium(V) at the twofold cationic bromoperoxidase binding site experiences a notable barrier, possibly extending the lifetime of hydrogen-bonded orthovanadium acid to participate as a sufficiently long-lived intermediate in the rapid catalytic reaction for oxidizing bromide (Scheme 3.5).[41]

In electronic structure theory, charge affects σ^*(O,O)-orbital energies of orthovanadium-derived peroxides by contracting or expanding electron shells. Nucleophiles are attracted by peroxides if energies from the nonbonding electron pair of the reductant and σ^*(O,O) of the oxidant nearly match, as specified by the third term of the Salem-Klopman equation.[41]

In hydrogen peroxide, σ^*(O,O) is too high in energy. Attractive forces between bromide and hydrogen peroxide, accordingly, do not suffice for compensating electron-pair repulsion between the reactants. Hydrogen

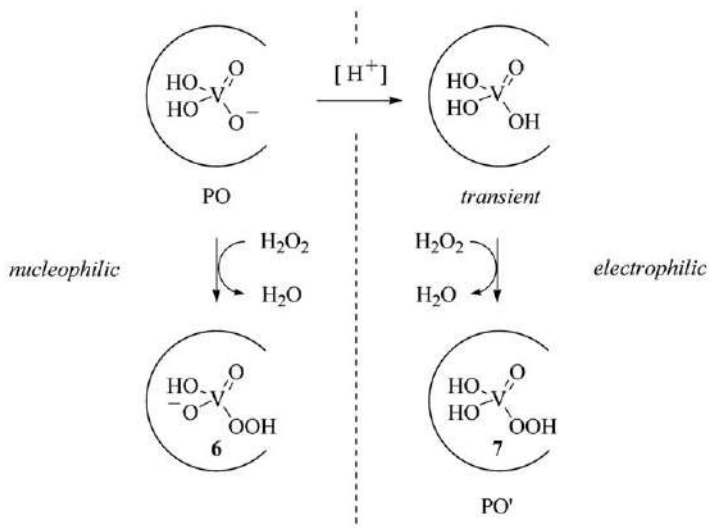

Scheme 3.5 Polarity of orthovanadium compounds serving as structural models for PO (top) and PO′ in the bromoperoxidase mechanism (*c.f.* Scheme 3.4; arcs symbolize the hydrogen bonding cavity of a bromoperoxidase protein).

Table 3.4 Properties of orthovanadium peroxoic acid and conjugated bases.[a]

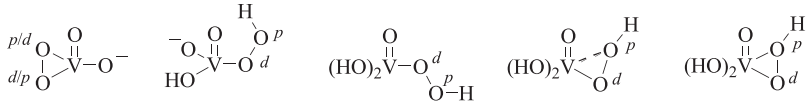

	3	*eo*-**6**	*eo*-**7**		*so*-**7**	*so*-**7**(active)
Entry	Compd.	$d(V,O^D)$/Å	$d(V,O^P)$/Å	$d(O,O)$/Å	$q(O^D)/e^-$	$q(O^P)/e^-$	$E - *(O,O)_{rel}$/eV
1	H_2O_2	—[b]	—[b]	1.454	−0.3	−0.3	−0.0
2	**3**	1.843	1.843	1.483	−0.4	−0.4	4.7
3	*eo*-**6**	1.869	2.699	1.464	−0.3	−0.3	4.7
4	*eo*-**7**	1.815	2.423	1.454	−0.2	−0.2	−0.7
5	*so*-**7**	1.844	2.270	1.462	−0.3	−0.1	−0.9
6	*so*-**7**(active)	1.877	1.876	1.454	−0.3	0.0	−1.6

[a]Bond lengths d and elementary charges e^- calculated on the B3LYP/6-311++G**-level of theory; σ^*-orbital energy taken from B3LYP/6-31G*//B3LYP/6-311++G**-NBO-analysis.
[b]Not available; experimental $d(O,O)$ in hydrogen peroxide: 1.453(7) Å.

peroxide and bromide in pH-neutral environment thus are inert towards one another (Figure 3.3).

Substituting bis(hydroxy)oxovanadium(v) for hydrogen in hydrogen peroxide stabilizes $\sigma^*(O,O)$ in the *end-on* (*eo*) conformer of orthovanadium peroxoic acid (**7**) by −0.7 electron volts. In molecular orbital theory, orbital energies customarily are given in electron volts (Table 3.4). One electron volt (eV) per molecule transforms into 96.4 kJ per mole of molecules.

A second conformer of peroxoic acid **7**, located 18.2 kJ per mole in Gibbs free energy on the potential energy surface above minimum structure *eo*-**7**, has the peroxide group bound *via* a long V,O^p-bond (2.270 Å) in *side-on* (*so*)-position. In local minimum (*so*)-**7** $\sigma^*(O,O)$ receives an extra stabilization of −0.2 eV from a second contact to vanadium, characterizing this conformer as a stronger electrophile.

Strengthening the second contact to vanadium by continuously shortening V,O^p until reaching a distance 1.877 Ångström the same length as V,O^d, affords an even more electrophilic transient, named *so*-**7**(active), located 53.0 kJ per mole in Gibbs free energy on the potential energy surface above peroxoic acid *eo*-**7**. In activated peroxide *so*-**7**(active), $\sigma^*(O,O)$ gains −1.6 eV in stabilization compared to hydrogen peroxide. Mulliken charges at oxygen dispersed to zero at O^p and −0.30 for O^d, thereby rendering proximal oxygen O^p of peroxide *so*-**7**(active) an ideal side for interacting with an anionic nucleophile.

Colinear approach of bromide from the backside of the peroxide bond at O^p, assisted by a guiding intramolecular hydrogen bond, furnishes in electronic structure theory stationary point **8**-O^p, having the peroxide bond extended by 24% in length (Scheme 3.6).

The barrier to be crossed for reaching intermediate **8**-O^p from the octahydrate of bromide of 34.4 kJ per mole reduces to almost zero by starting from peroxoic acid *so*-**7**(activated). A shallow energy barrier of this magnitude

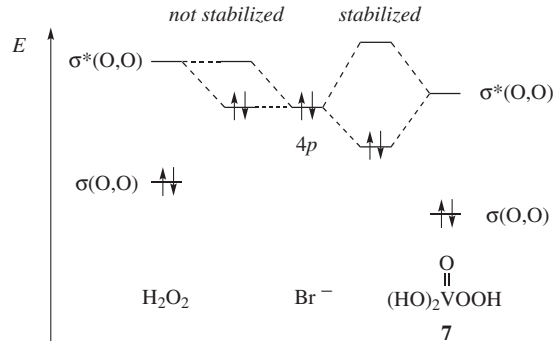

Figure 3.3 Correlation diagram displaying the role of σ^*(O,O)-orbital stabilization on frontier molecular orbital (FMO) attractions between orthovanadium peroxoic acid (**7**) and one of the non-bonding electron pairs of bromide (right), and an instance of negligible stabilizing FMO-interaction between hydrogen peroxide and the halide.

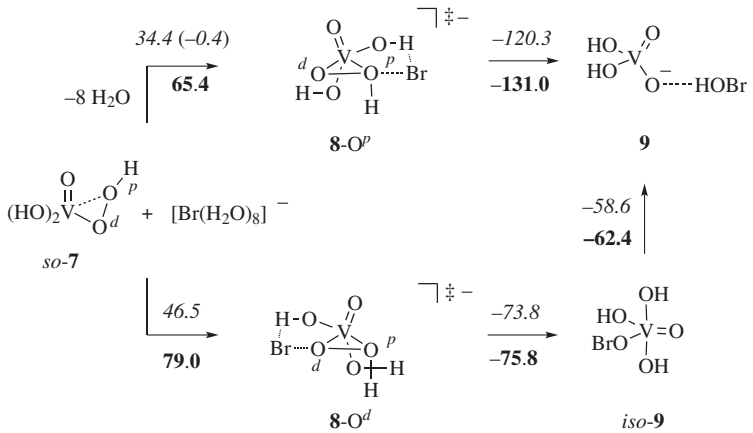

Scheme 3.6 Barriers and reaction energies for oxidizing bromide by orthovanadium peroxoic acid so-**7** [zero-point vibrational energy-corrected $\Delta_R E$ for 0 K printed in italics. The number in brackets refers to the barrier for transferring O^p from *so*-**7**(active) to bromide in the octahydrate, and ΔG^0 for a temperature of 298.15 K and a pressure of 1 atmosphere are printed in bold (all energies in kJ mol^{-1})].

points to a rate constant for the redox reaction close to the diffusion limit, providing a reasonable model for explaining the unusually high reactivity of orthovanadate-dependent bromoperoxidases (Schemes 3.4 and 3.6).

Bromide octahydrate serves in thermochemical calculations as a model for electronic effects imposed by hydrogen bonding of the halide, arising from amino acid side chains or water molecules close to the active site, or combinations of these.

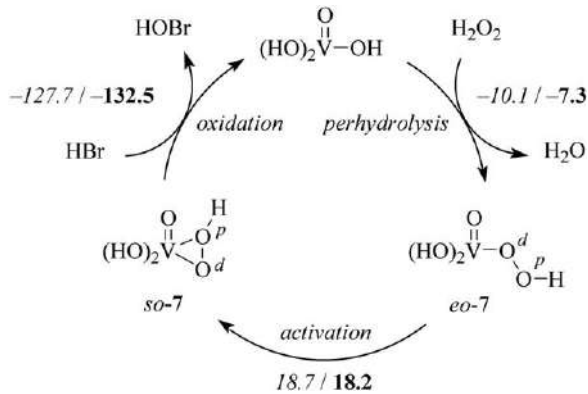

Scheme 3.7 Thermochemistry for oxidizing hydrogen bromide and hydrogen peroxide catalysed in orthovanadium acid-catalysed bromoperoxidase reaction (zero-point vibrational energy corrected reaction energies $\Delta_R E$ refer to 0 K; values printed in italics. Gibbs free energy changes ΔG^0 are provided for a temperature of 298.15 K at a pressure of 1 atmosphere; values printed in bold. All energy changes in kJ mol^{-1}; O^p = proximal oxygen; O^d = distal peroxide oxygen; for definition, refer to the text).

Proceeding the intrinsic reaction coordinate from transition structure **8**-O^p by unconstrained energy function minimization leads to hypobromous acid, hydrogen bonded to dihydrogen orthovanadate (**9**). This adduct fulfils all requirements imposed from kinetics for structurally modelling bromoperoxidase resting state PO.

The alternative mode for the backside attack of bromide at the peroxide bond in peroxoic acid *so*-**7** at distal oxygen O^d provides stationary point **8**-O^d, located 13.6 kJ per mole in Gibbs free energy above **8**-O^p. Proceeding from intermediate **8**-O^d along the intrinsic reaction coordinate leads to unconstrained energy function minimization to pentavalent mixed anhydride of hypobromous acid and dihydrogen orthovanadate (*iso*-**9**) as the local minimum, being −62.4 kJ per mole higher in Gibbs free energy than resting state model **9** (Scheme 3.6).

The amount of Gibbs free energy (45.7 kJ mol^{-1}) required for activating hydrogen peroxide in the proposed mechanistic scheme by generating transient orthovanadium peroxoic acid *so*-**7**(active) is balanced by the succeeding redox reaction.

When approximating solution chemistry of bromide and hydrogen peroxide by consuming one proton with a gas-phase reaction between hydrogen bromide and hydrogen peroxide, formation of water and hypobromous acid from the reagents is exergonic by 130.5 kJ per mole, based on tabulated standard Gibbs free energies of formation. The assessed electronic structure method predicts a Gibbs free energy change of −121.6 kJ per mole for the same transformation (Scheme 3.7).

When stored in the protein, *e.g.*, by changing the secondary conformation at the binding site, the surplus of energy is retrievable for assisting

conformation change from *eo*-**7** to *so*-**7**, and even on to *so*-**7**(active) in the succeeding catalytic cycle.[41]

3.5 Oxidative Transformations Mediated by Bromoperoxidases

3.5.1 Oxidative Bromination

Hypobromous acid, the initial product from the bromoperoxidase reaction, comproportionates in bromide-containing brines to molecular bromine. In excess of bromide, bromine forms tribromide as weakly bonded adduct.[80]

Molecular bromine, when dissolved in aqueous buffered solution of *tert*-butanol or acetonitrile, is sufficiently electrophilic for converting phenols, anilines, non-benzenoid π-nucleophilic arenes, heteroarenes and alkenes into brominated derivatives.[34]

Benchmarks for studying enzymatic oxidative hydrocarbon bromination are the *A. nodosum* bromoperoxidases I and II. Both enzymes retain structural integrity and chemical reactivity when stored *ex vivo* for up to three months at ~5 °C.[52] When heated to 90 °C, hexameric V_{Br}PO(*An*II) almost entirely resists thermal denaturation, isoenzyme V_{Br}PO(*An*I) slowly undergoes structural changes, as evident from UV-light scattering experiments and declining oxidative reactivity.[41,78]

Adding hydrogen peroxide in small batches, continuously in a flow system, or generating the oxidant *in situ*, *e.g.*, by a coupled glucoses-oxidase reaction, allows in-oxidative syntheses retaining 50% or more V_{Br}PO(*An*I) activity when conducted in morpholine ethanesulfonic acid-buffered solution, even in the presence of up to 0.75 molar concentration of π-nucleophilic hydrocarbon to be oxidatively brominated. At higher concentrations, hydrogen peroxide irreversibly terminates oxidative catalytic activity of V_{Br}PO(*An*I).[78]

3.5.1.1 Bromination of Aliphatic π(C,C)-bonds

Internal alkenes and alkenols comprising trialkyl-substituted π(C,C)-bonds, *e.g.*, hydrocarbons **1a** and **1b**, provide bromohydrins in synthetically attractive yields when added to reaction mixtures containing V_{Br}PO(*An*I), bromide and hydrogen peroxide. Introducing the bromo substituent always occurs at the most π-nucleophilic alkene carbon.

Dibromohydrin **10a** forms as a single diastereomer, presumably due to backside shielding by the already-existing σ(C,Br) bond. This observation provides a model for understanding the origin of stereoselectivity in biosynthesis of chiral brominated secondary metabolites (Scheme 3.8). Prenyl-type phenyl pentenol **1b** leads to a mixture of products, consisting of bromohydrin **10b** as principle organobromine. Bromo substituted tetrahydrofuran **11b** (47/53-mixture of diastereomers) and tetrahydropyran *trans*-**12b**, although formed in smaller fraction, are evidence that

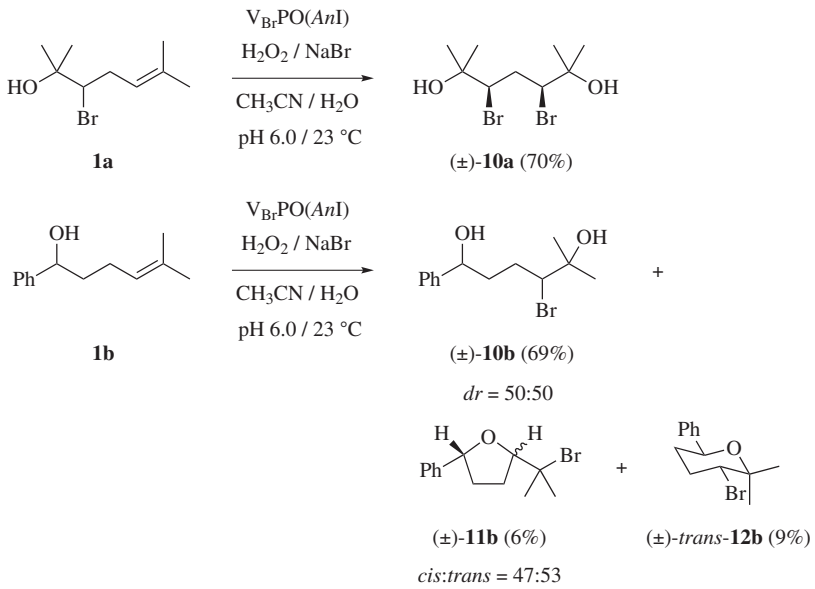

Scheme 3.8 Preparing bromohydrins and cyclic bromohydrin ethers from prenyl-type 4-pentenols from $V_{Br}PO$(AnI)-catalysed reactions.[82]

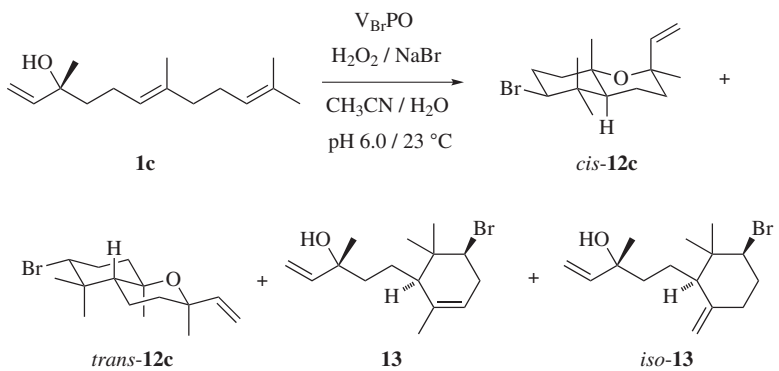

Scheme 3.9 Products obtained from oxidative bromination of (E)-nerolidol (**1c**).

bromoperoxidase reactivity is capable of transforming terpene-like progenitors into molecules comprising basic structural components of brominated secondary metabolites.[81]

A more complex biomimetic synthesis starts from nerolidol (**1c**), being converted in the presence of bromoperoxidase reactivity into a mixture of 5-(5-bromo-2,6,6-trimethylcyclohex-2-en-1-yl)-3-methylpent-1-en-3-ol **13**, constituent of the red alga *Laurencia obtusa*, and constitutional isomer *iso*-**13**, a compound isolated from *L. snyderae* (Scheme 3.9).[82]

3.5.1.2 Bromination of Aromatic and Heteroaromatic π(C,C)-Bonds

Phenol (**14a**), alkyl phenols **14b–c** and phenol ethers **14d–e** yield bromoarenes **15a–e**, and to a minor extent, dibromides **16a–e**, when subjected to enzymatic oxidative bromination. Some of the products serve in synthesis as substrates for preparing compounds of technical and medicinal use (Table 3.5).[80]

Fused arenes, for instance 1-naphtol (**17**) and 4,6,8-trimethylazulene (**18**), give products of selective σ(C,Br)-bond formation at the most π-nucleophilic site when present in solutions comprising V_{Br}PO(*An*I), hydrogen peroxide and bromide. Quantitative substrate conversion of the more lipophilic substrates causes the entire loss of oxidative V_{Br}PO(*An*I) activity (Scheme 3.10).[34]

Table 3.5 Oxidative bromination of phenols and phenol ethers mediated by V_{Br}PO(*An*I).

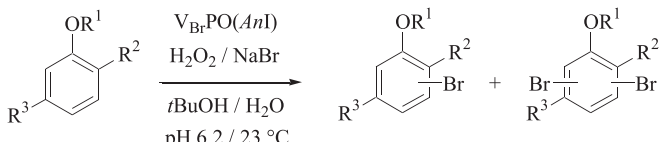

14 **15** **16**

Entry	**14**/conv./%[a]	R^1	R^2	R^3	**15**/% (*o*/*p*)[b]	**16**/% (*o*,*o*/*o*,*p*)[c]
1	**14a**/93	H	H	H	**15a:** 69 (9/91)	**16a:** 1 (<2/98)[d]
2	**14b**	H	*t*Bu	H	**15b:** 33 (30/70)	**16b:** 11 (<2/98)
3	**14c**	H	*i*Pr	CH_3	**15c:** 34 (18/82)	**16c:** 1 (<2/98)
4	**14d**	CH_3	H	H	**15d:** 18 (<2/98)	**16d:** —[e]
5	**14e**	CH_3	*i*Pr	CH_3	**15e:** 53 (<2/98)	**16e:** —[e]

[a] 34.6 U_T for 1.5 mmol of **14**.
[b] Referenced *versus* R^1; *o* = *ortho*; *p* = *para*.
[c] Referenced *versus* R^3; *o* = *ortho*; *p* = *para*.
[d] Additional product: 6% of 2,4,6-tribromophenol.
[e] Not detected.

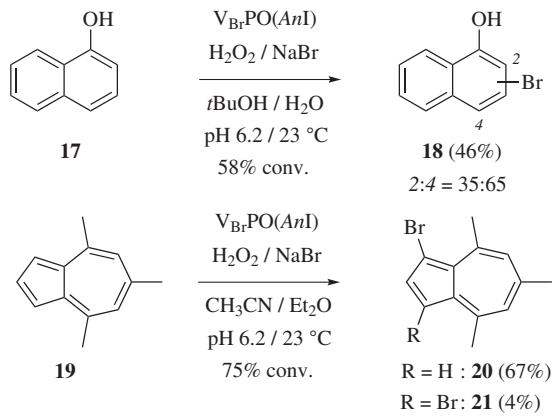

17 **19**

Scheme 3.10 Examples for oxidative enzymatic bromination of annulated arenes.

Table 3.6 Bromination of substituted pyrroles.

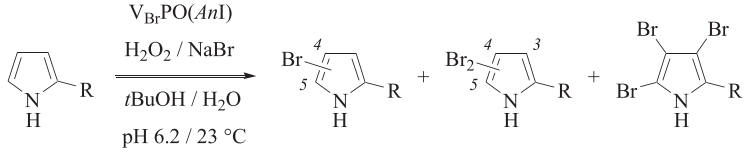

22 **23** **24** **25**

Entry	**22–25**	R	conv. **22**/%[a]	**23**/% (*4*/*5*)	**24**/%[b]	**25**/%
1	**A**	CO_2CH_3	95	53 (81/19)	33	—[c]
2	**B**	$CO_2C_3H_5$	quant.	24 (>98/2)	40	27
3	**C**	$CONH_2$	71	42 (71/89)	9	—[c]
4	**D**	CN	quant.	40 (>98/2)	—[c]	35

[a] 34.6 U_T corresponds to 32 μmol% of V$_{Br}$PO(*An*I) [611 U_T^0 mg^{-1}, except for entry 5 (558 U_T^0 mg^{-1})], 1.5 mmol of **22**, 3.3 equiv. of H_2O_2, 3.0 equiv. of NaBr.
[b] 4,5-substitution.
[c] Not detected (^{1}H NMR).

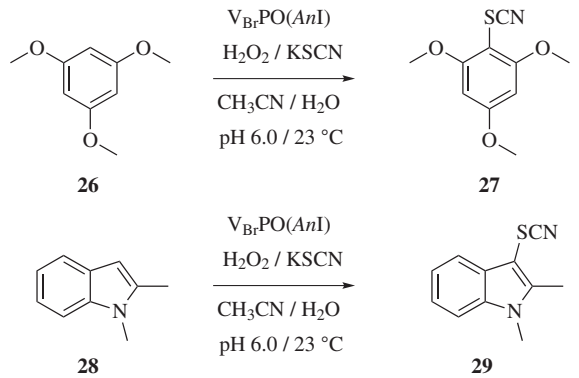

26 **27**

28 **29**

Scheme 3.11 Oxidative thiocyanation of π-nucleophilic substrates mediated by V$_{Br}$PO(AnI).[83]

O-Alkyl pyrrol-2-carboxylates **22a** and **22b**, pyrrole-2-carboxamide **22c** and carbonitrile **22d** are transformed into brominated derivatives with selectivity depending on the chemical nature of substituent R (Table 3.6). Marine sponges are sources of bromopyrroles, similar to compounds **23–24**.[78]

3.5.2 Oxidative Thiocyanation

A. nodosum bromoperoxidase I accepts thiocyanate (SCN^-) as a substitute for bromide, although with unknown affinity. Adapting the general procedure accordingly allows converting 1,3,5-trimethoxybenzol **26** into aryl thiocyanate **27**, and 1,2-dimethylindole (**28**) into derivative **29** (Scheme 3.11).[83]

3.6 Generation and Properties of *tert*-Butylperoxy(dialkyl) Orthovanadates

Oxidizing structurally more complex hydrocarbons often requires more demanding selectivity issues to be addressed by an oxidant. Achieving this goal in many instances is feasible by adapting electronic properties and stereochemical information of orthovanadium(V) compounds. Vanadium(V) reagents meeting such demands frequently are by substitution lipophilic, requiring polar-aprotic solvents and lipophilic hydroperoxides for undergoing sufficiently fast second-order peresterification.

Lipophilic equivalents to hydrogen peroxide in organic synthesis are cumene hydroperoxide and particularly *tert*-butyl hydroperoxide (TBHP), to name the most frequently applied reagents.[6] TBHP is the benchmark in physical organic experiments, and also the standard for exploring selectivity and product manifolds for converting alkenes into epoxides, alkenols into hydroxyl-substituted cyclic ethers,[42] thioethers into sulfoxides,[84] amines into nitro compounds[85] and halides into hypohalous acids.[86,87]

TBHP is inert towards most reductants given marked nucleophilicity arising from four non-bonding electron pairs and alkyl substitution at distal oxygen O^d. Utilizing TBHP for oxidizing nucleophilic substrates requires adapting the electronic structure of the peroxide. In most instances, early-transition metal compounds in high-oxidation states, characterized by d^0-electron configuration, are used for this purpose. In existing models, d^0-electron configuration is regarded as perquisite for Lewis acidity[28] of transition metal compounds. Support for this interpretation came from observing rate-retarding effects of acetone, dimethyl formamide or dimethyl carbonate when used as solvent in oxidations catalysed by d^0-transition metal complexes. Dichloromethane, chloroform and 1,2-dichlorethane show no such properties.[6,88]

Derivatives of orthovanadium acid combine in privileged manner rate and selectivity for mediating oxygen atom transfer from alkyl hydroperoxides to organic reductants. Disadvantages of organometallic vanadium(V) compounds in oxidative synthesis are their inherently low barriers for changing conformation, which poses a challenge for mediating stereoselective oxygen atom transfer by peresters of chiral orthovanadates. Compounds of vanadium(V) also show an obscure propensity of favouring homolytic hydroperoxide chemistry in later reaction phases.[84,89]

Almost all orthovanadates currently in use for activating hydroperoxides fit the general formula VO(L)Y, where O stands for the oxo oxygen, Y for a monovalent substituent and L for diolate or an entity of similar charge and donicity (Figure 3.4).

Compounds fitting the general structure formula **I** are accessible from aliphatic aminediols and trialkyl orthovanadates $VO(OR)_3$ by transesterification, or from vanadyl(IV) compounds $VO(OR)_2$ in the presence of dioxygen from air or a peroxide.[90–94]

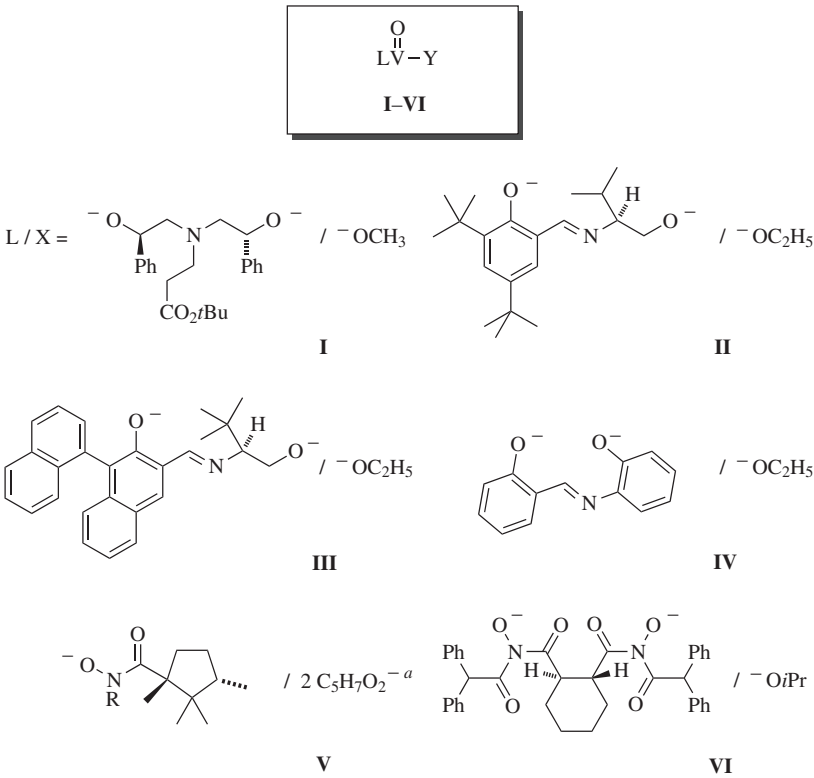

Figure 3.4 Representative examples for alkanediolates (in **I**) and alkylidene alkanamine diolates (in **II**) having one stereogenic centre, alkylidene alkanamine diolates (in **III**) comprising a stereogenic centre and an additional element of chirality, alkyldidene arenamine diolates (in **IV**), chiral monohydroxamates (in **V**) and bishydroxamates (in **VI**) in use for controlling reactivity and selectivity in TBHP-mediated oxidation catalysed by compounds use the general formula VO(L)Y.

Probably the largest fraction of vanadium(v) reagents in use for activating TBHP derive from alkylidene alkanaminediols (*i.e.*, for **II**–**IV**) that are available in manageable synthetic effort and considerable structural diversity from 2-aminoalcohols and hydroxyaldehydes.[88,91,95]

More specialized reagents for controlling stereoselectivity in epoxidation of prochiral propen-2-ols and but-3-enols by TBHP, are mixed anhydrides **V** and **VI** of a chiral hydroxamic acid and a trialkyl orthovanadate.[89,96–98]

Comparing strengths and weaknesses of reagents VO(L)Y (**I**–**VI**) from reports of the chemical literature does not lead to conclusive results since most reagents were developed by different groups for operating in a specific environment, using particular reactant concentration, oxidant-substrate ratio, a selected solvent, a possible additive, adjusted parameters from variation referred to by authors as *optimized* for solving a focused selectivity issue. None of the reports included kinetic and supplementary physical organic data

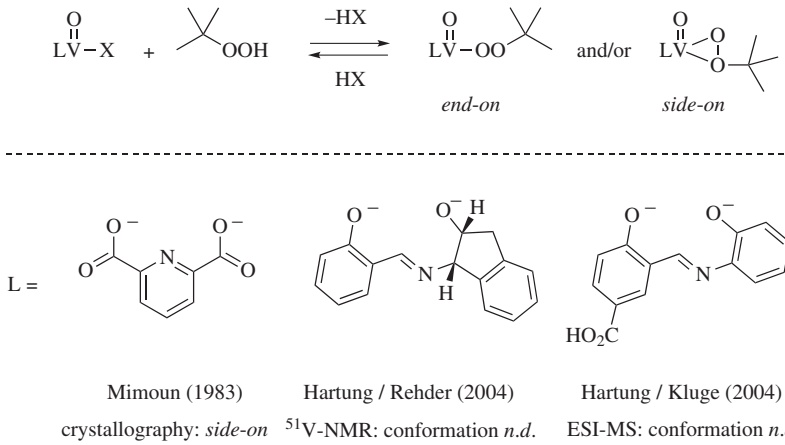

Scheme 3.12 Preparing and characterizing alkylperoxy orthovanadates(v) by physical methods (R = *e.g.*, ethyl, *cf.* Figure 3.4; n.d. = not determined).

allowing to identify whether structural differences in orthovanadates **I**–**VI** primarily affect perhydrolysis, substrate binding, rate and mechanism of oxygen atom transfer, two of these parameters, three, others or none.

Mimoun was the first to study structures of *tert*-butylperoxy vanadates and concluded, on the basis of a solid-state structure, that the perester group binds side-on to vanadium(v) (Scheme 3.12).[99]

Peresterification of orthovanadates in solution is apparent from changes in shielding of the vanadium-51 nucleus, frequently shifting resonances of parent alkyl vanadates towards higher field strength by about 50 ppm.[88,100] Further evidence for existence of *tert*-butyl peresters was presented from electron spray-ionization mass spectrometric studies in the gas phase, however without allowing deducing conformational details (Scheme 3.12).[87]

Mimoun also correlated mechanisms of transition metal-catalysed oxidation to peracid- and perester-mediated reactions.[101] In this model, properties of early-transition metal compounds resemble molecular rather than coordination compounds. Support for these ideas came recently from studying properties of chelated orthovanadates **32a**–**c** towards alkyl hydroperoxides. The set of these new reagents is accessible by transesterifying trialkyl orthovanadates with *cis*-2,6-(hydroxydialkyl)piperidines (*i.e.*, **31a**–**c** in Scheme 3.13).[42,102]

Thermochemical studies revealed a surprisingly small affinity for substituting ethanol from triethyl orthovanadate (**30**) by aminodiols **31a**–**c**, as evident from isothermal microcalorimetric titration.[42] Obtaining orthovanadates **32a**–**c** in adequate yields requires shifting chemical equilibria by distilling off ethanol, causing, at some point, the products to precipitate, particularly when allowed to rest in a refrigerator overnight.

For exploring thermochemical details from synthesis and physical aspects of alkyl hydroperoxide activation, chelated orthovanadates **32a** and **32b** were

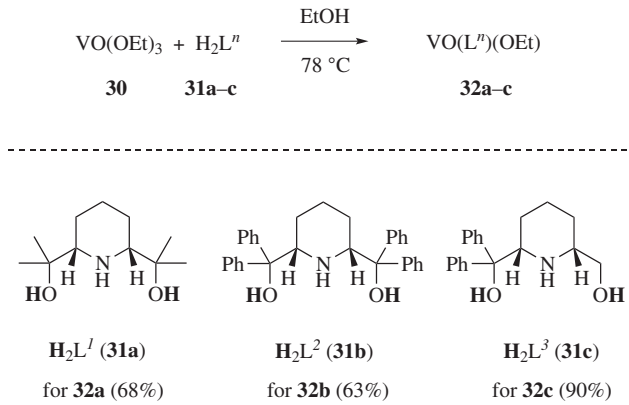

Scheme 3.13 Formation of chelated trialkyl orthovanadates **32a–c** from achiral of piperidine-2,6-dimethanols **31a** and **31b** and chiral congener **31c** (hydrogens displaced as proton in the course of transesterification are printed in bold).

subjected to X-ray diffraction analysis. The body of data generated from this study was then used for assessing electronic structure methods capable of reproducing ground-state properties of the reagents. Similar to findings summarized in Section 3.3, unconstrained energy function minimization in B3LYP/6-311++G** theory furnished structures agreeing with a precision of 97%–99% to interatomic distances, bond and torsion angles from solid state structures.[58] Interpreting density functional theoretical data in molecular orbital models requires conducting a separate population analysis in natural bond orbital (NBO) theory,[103] generally with a less-expanded basis set (B3LYP/6-31G*).

According to NBO theory, the non-bonding electron pair at piperidine nitrogen at a distance of 2.353 Ångström in the calculated minimum structure of orthovanadate **32a** experiences no stabilization by vanadium(v).[42] Strain induced by widening O,V,O-angles for bonding the chelated diol and compressing bond angles associated with the ethoxy oxygen counterbalance favourable entropy, rendering little-to-no driving force for substituting two molecules of ethanol by piperidine-2,6-bismethanol **31a** and presumably **31b–c** from triethyl orthovanadate (**30**) for preparing **32a–c** (Scheme 3.14, Figure 3.5).

NBO theory furthermore predicts a significant degree of π-bonding between *p*-type non-bonding orbitals of all four oxygens into appropriate unoccupied *d*-energy functions at vanadium, thereby transferring considerable electron density, *e.g.*, in triethyl orthovanadate (**30**) to the metal. Redistributing electrons accordingly reduces electrophilicity at vanadium, as expressed by a Mulliken charge of 0.80[42] and noted experimentally in low affinity of ester **30** for substituting stronger nucleophilic *tert*-butylperoxy by a group with less electron donicity, *i.e.*, ethoxy (Figure 3.6, Table 3.7, and Scheme 3.15).

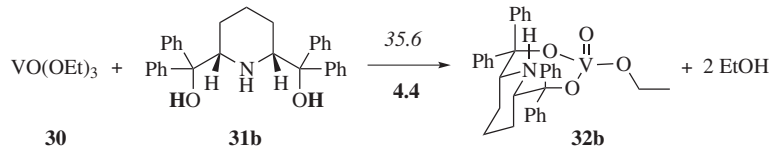

Scheme 3.14 Calculated energies in kJ mol^{-1} for synthesis of the lowest in energy conformers of ethyl *cis*-(piperidine-2,6-diyl)dimethyl vanadate **32b** ($\Delta_R E$ printed in italics and ΔG° in bold).

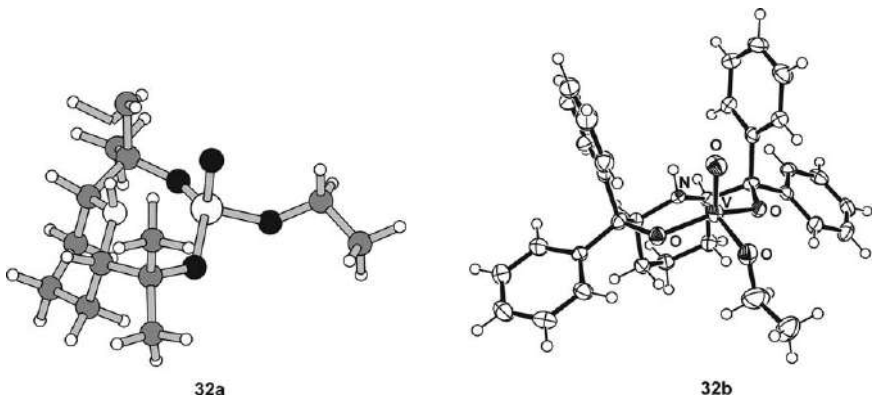

Figure 3.5 Modelled lowest in energy conformer of tetramethyl derivative **32a** [B3LYP/6-311++G**; oxygen is drawn in black, carbon in grey; vanadium (largest circle), nitrogen and hydrogen are drawn in white] and experimental structure of aminodiol-derived chelated trialkyl orthovanadate **32b** from X-diffraction (right, 100 K).

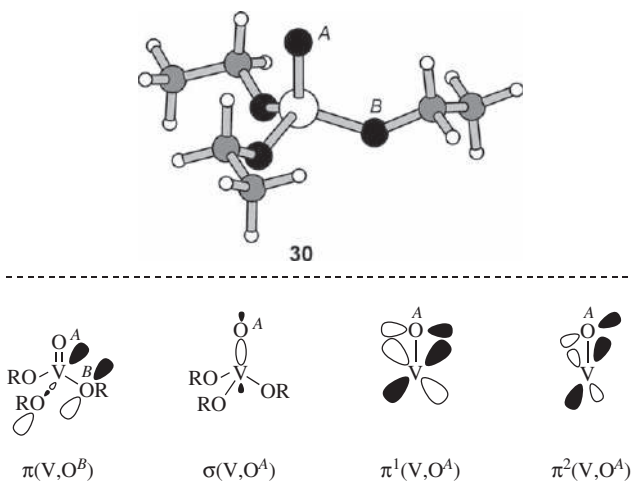

Figure 3.6 Intramolecular stabilization in the all-syn conformer of triethyl orthovanadate (**30**) by π-bonding [NBO-population analysis (B3LYP/6-31G*// B3LYP/6-311++G**); $R = C_2H_5$; ethoxy groups were omitted in the lower right of the graphic for the sake of clarity].

Table 3.7 Vanadium-51 chemical shifts of trialkyl orthovanadates **30** and **32** and derived *tert*-butyl peresters **33** and **34**.[42,102]

30 / **32** **33** / **34**

		$\delta^{51}V^a$	
Entry	L	**30**/**32**/ppm[b]	**33**/**34**/ppm[b]
1	2 OC_2H_5	**30:** −596	**33:** −551
2	L^1	**32a:** −486	**34a:** −553
3	L^2	**32b:** −512	**34b:** −552

[a]Referenced *versus* neat $VO(OtBu)_3$ ($\delta = -674$); chemical shift of $VO(OEt)_3$ (**30**) in EtOH/$CDCl_3$ for c(**30**) = 0.19 M.
[b]In ethanol/deuterochloroform = **1 : 1** (*v*/*v*).

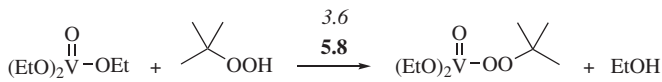

30 *eo*-**33**

Scheme 3.15 Calculated energies in kJ mol^{-1} for perhydrolyzing the all-syn conformer of triethyl orthovanadate (**30**) by TBHP ($\Delta_R E$ printed in italics and ΔG° in bold).

Adding an alkyl hydroperoxide in excess to a solution of a trialkyl orthovanadate experimentally occurs sufficiently slowly for being monitored by NMR spectroscopy. Evidence for an exchange of *tert*-butoxy for ethoxy is stronger shielding of the vanadium-51 nucleus by the peroxide group (*vide supra*), but exemptions from this guideline are known. Perhydrolyzing triethyl orthovanadate with TBHP, *e.g.*, leads to a net shielding of the vanadium-51 nucleus (Table 3.7). Triester **30** exists as dimer and perester **33** for steric reasons as monomer. Dissociation seems to affect shielding of the vanadium nucleus in a more pronounced manner than peresterification.

In density-functional theory, perhydrolyzing monomeric triethyl orthovanadate (**30**) by TBHP is endergonic by 5.8 kJ mol^{-1} (Scheme 3.15). This value confers with the experimentally determined equilibrium constant for the exchange process, measured in a solution of deuterochloroform at a temperature of −40 °C ($K = 6{\cdot}10^{-2}$).[104]

Substituting *tert*-butoxy for *syn*-oriented ethoxy in 2,6-bis(prop-2-diyl)-piperidine-substituted orthovanadate **32a** is similarly endergonic as the exchange process starting from triethyl orthovanadate (**30**) (Table 3.8, entry 1 and Scheme 3.15). Steric repulsion from four phenyl groups directs ethoxy in tetraphenyl-substituted chelated orthovanadate **32b** into *anti*-conformation, being for electronic reasons higher in energy than *syn*-conformation. Releasing the strain by substituting *tert*-butylperoxy for ethoxy adds to the chemical driving force, rendering perhydrolysis of **32b** exergonic. Support for this prediction comes from isothermal microcalorimetric studies indicating weakly

Table 3.8 Computed energies in kJ mol^{-1} for perester formation from TBHP and chelated vanadates **32a** and **32b**.[42]

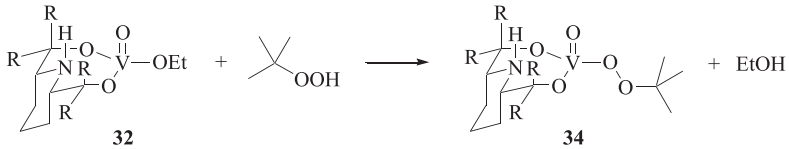

32 **34**

Entry	R	**32**/**34**	$\Delta_R E$/kJ mol^a	ΔG°/kJ mol^b
1	CH_3	**a**	2.6	6.8
2	Ph	**b**	−6.3	−9.1

[a]For 0 K, zero-point vibrational energy corrected.
[b]298.15 K and 1 atm; zero-point vibrational energy corrected; for preferred conformation of 36, refer to the text.

exergonic exchange reaction and from rates for turning over TBHP in oxidative synthesis catalysed by orthovanadate **32b** (Table 3.8 and Section 3.8).

3.7 Activating *tert*-Butyl Hydroperoxide by Trialkyl Orthovanadates

Substituting dialkoxy(oxo)vanadium(v) for hydrogen in TBHP exerts in NBO theory no stabilizing effect on orbital energies in *end-on* conformers of *tert*-butylperesters **33** and **34a**. At first glance, this finding seems to contradict information summarized for activating hydrogen peroxide *via* peracid *eo*-**7** (Table 3.9). In orthopervanadates **33** and **34a**, however, donating contributions from alkyl substitution at ester and perester oxygens largely compensate electron-withdrawing effects from the metal.[42] In the gas phase, and presumably also in hydrocarbon solvents of low polarity, the electrophile-nucleophile principle therefore fails to explain the activating effect of vanadium(v) compounds on alkyl hydroperoxides.

A weak stabilizing contribution from an overlapping *p*-type non-bonding electron pair at proximal oxygen O^p and $\sigma^*(V,O^A)$ in the ground state in, *e.g.*, perester *eo*-**33**, points to an aspect other than the polar effect playing a role for activating alkyl hydroperoxides by vanadium(v) compounds bearing at least one oxo-group. On shortening distance V,O^p, for instance by O^B,V,O^d-scissoring vibration, $n(O)^p \rightarrow \sigma^*(V,O^A)$ overlap but also molecular strain starts to increase in summary raising electronic energy of perester **33** (Figure 3.7). At a modelled V,O^p-distance of 1.93 Ångström, the peroxide group of perester **33** changes conformation to *side-on*, abbreviated by prefix *so* (Scheme 3.16).[42]

Structural response to shortening V,O^p is lengthening of V,O^d. Stabilizing $\sigma(V,O^p)$ weakens to similar extent $\sigma(V,O^d)$, facilitating O^d to be transferred to a reductant (Figure 3.8; Scheme 3.17).[42]

When approaching with π-electron density oriented towards $\sigma^*(O,O)$, ethene (**35**) is able to transfer electrons to *side-on* arranged *tert*-butyl perester *so*-**33** or to *so*-**34a**–**b**, thereby inducing $\sigma(O,O)$ and $\sigma(V,O^d)$ to

Table 3.9 Orbital energies and group electronegativity χ_{eq} of substituent X calculated for TBHP, orthovanadium peroxoic acid eo-(**7**), and chelated tert-butyl peresters eo-**33** and eo-**34**.[42]

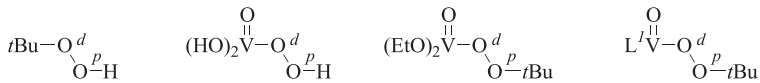

TBHP *eo*-**7** *eo*-**33** *eo*-**34a**

Entry	compd.	$E[\sigma^D)]$/ a.u.[a]	$E[\sigma^D,O^P)]$/ a.u.[a]	$E[\sigma^D,O^P)]$/ a.u.[a]	$E[n(O^D)]^b$/ a.u.[a]	$E[n(O^P)]^b$/ a.u.[a]	χ_{eq} for X[c]
1	TBHP	−0.72863	−0.69877	0.09190	−0.31217	−0.29931	2.20
2	*eo*-**7**	−0.52736	−0.74469	0.05778	−0.33364	−0.36239	2.42
3	*eo*-**33**	−0.46069	−0.70853	0.08366.	−0.30768	−0.33365	2.60
4	*eo*-**34a**	−0.34866	−0.70066	0.11157	—[d]	−0.29403	2.57

[a]1 atom unit (a.u.) = 1 Hartree = 27.2114 eV. 1 Hartree/particle = 2625.5 kJ mol^{-1}; NBO-analysis (B3LYP/6-31G*//B3LYP/6-311++G**.

[b]For the *p*-type, non-bonding (*n*) electron pair (>99% *p*).

[c]Based on the Pauling electronegativity scale. Iteratively calculated, assuming that the inductive effect propagates bond by bond. The equilibrium electronegativity χ_{eq} for X in **34a** was approximated by the value iterated for the dimethylamine adduct to (dimethoxy)(oxo)-vanadium(v).

[d]Delocalized towards vanadium forming a second bond $\{E[\pi(V,O^P)] = -0.35421$ a.u.$\}$.

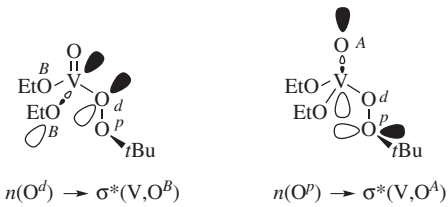

Figure 3.7 Visualization of orbital interactions associated with peroxide stabilization in the ground state (left), and onset of V,O^p-bonding in diethyl tert-butylorthopervanadate end-on (eo)-(**33**) (right).[42]

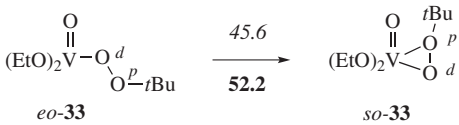

Scheme 3.16 Calculated energy for end-on-to-side-on conformational change of diethyl *tert*-butylorthopervanadate (**33**) (B3LYP/6-311++G**//B3LYP/6-311++G**).

being heterolytically broken. Regrouping of electron pairs shifts distal oxygen O^d from the perester to the alkene, forming two new σ(C,O)-bonds (Scheme 3.17).

Based on tabulated Gibbs free energies of formation, epoxidation of ethene (**35**) by TBHP is −282 kJ mol^{-1} exergonic when corrected for the oxirane ring strain (Scheme 3.18).[5,42,105]

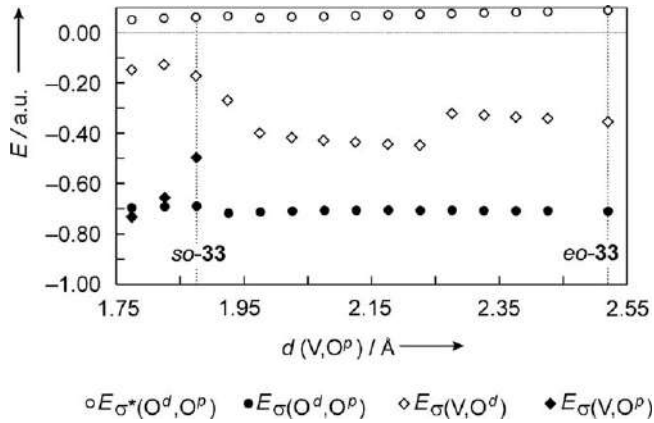

Figure 3.8 NBO-energies for the peroxide bond, the associated σ*-orbital and bonds between vanadium and peroxide oxygens O^d and O^p along the V,O^p-reaction coordinate [for structures of the compounds and indexing of oxygens, see Scheme 3.16; NBO-analysis; 1 atom unit (a.u.) = 1 Hartree = 27.2114 eV. 1 Hartree per particle = 2625.5 kJ mol^{-1}].[42]

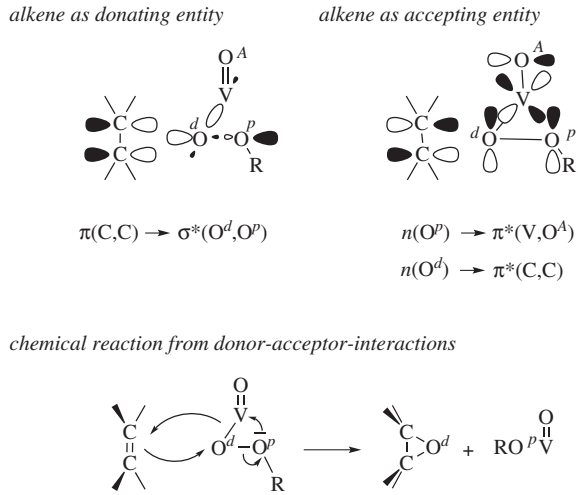

Scheme 3.17 Frontier molecular orbital description for interaction between an alkene and the side-on conformer of an alkylorthopervanadate (top) and mechanistic model for transferring distal oxygen O^d to an accepting alkene (bottom, see also Scheme 3.18) [R = *e.g.*, *t*Bu in **33** or **34a–b**; VO is short for $VO(OEt)_2$ or $VO(L^{1-2})$].

Oxidizing 5-methylhex-4-en-1-ol (**1d**) with TBHP provides *tert*-butanol and 2-(2-tetrahydrofuran-2-yl)-2-propanol (**2d**). Cyclic ether **2d** exerts structural details familiar from natural products, attributing biomimetic relevance to this chemistry. In a more sophisticated theoretical composite model named G3, the driving force for preparing ether **2d** is nearly identical to the experimentally

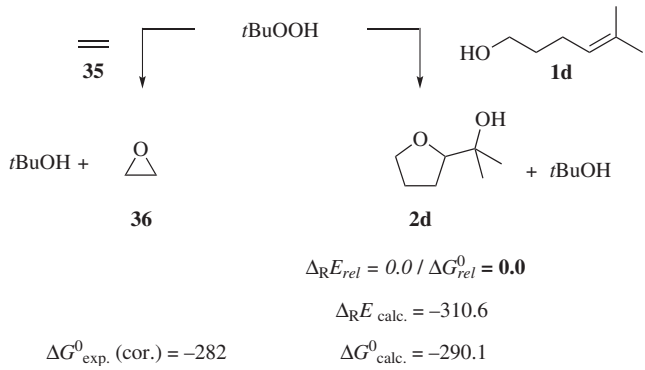

Scheme 3.18 Calculated (G3 theory) relative energies in kJ mol^{-1} for epoxidizing ethene (**35**) (left; cor. denotes, having the oxirane strain subtracted) and oxidative cyclization of 5-methylhex-4-en-1-ol (right).[42]

corrected value for ethene epoxidation. Thermochemical considerations of this kind indicate that barriers for changing conformation of *tert*-butyl orthopervanadates from *end-on* to *side-on* can readily be overcome by the surplus of energy released from TBHP-mediated monooxygenation (Scheme 3.18).[42]

3.8 Oxidizing Nucleophiles by TBHP in Alkyl Orthovanadate-catalysed Reactions

Conducting oxidative synthesis by TBHP in combination with a suitable alkyl orthovanadate catalyst over the past decade provided a great deal of information for understanding principles of chemo-, regio- and stereo-selective alkenol ring closure.[42,102] Some targets comprise σ(C,Br) bonds located at positions corresponding to π-nucleophilic sites in assumed terpene-, polyketide- or shikimate-derived progenitors, allowing devising models for predicting selectivity in biomimetic synthesis of brominated secondary metabolites when coupled with oxidative bromination.

3.8.1 Oxidative Bromination

Chelated orthovanadate **32b**, when added to solutions containing TBHP, 3-bromo-2,2-dimethyl propane acid (**37**) and sodium bromide, induce oxidative bromination of unsaturated hydrocarbons in polar-aprotic solvents. Sodium bromide in, *e.g.*, dialkyl carbonates is sufficiently basic for deprotonating 3-bromo-2,2-dimethyl propane acid (**37**), splitting the derived carboxylate into carbon dioxide, 2-methylprop-1-ene, hydrogen bromide and bromide. Hydrobromic acid is oxidized faster under such conditions than being formed, keeping acid concentration low and preventing acid-labile functional groups, as present π-basic alkenol **1e**, from being transformed. The sole product formed by oxidative bromination of substrate **1e** is hexasubstituted tetrahydropyran **12e**, serving as a building block for marine natural product aplysiapyranoid A

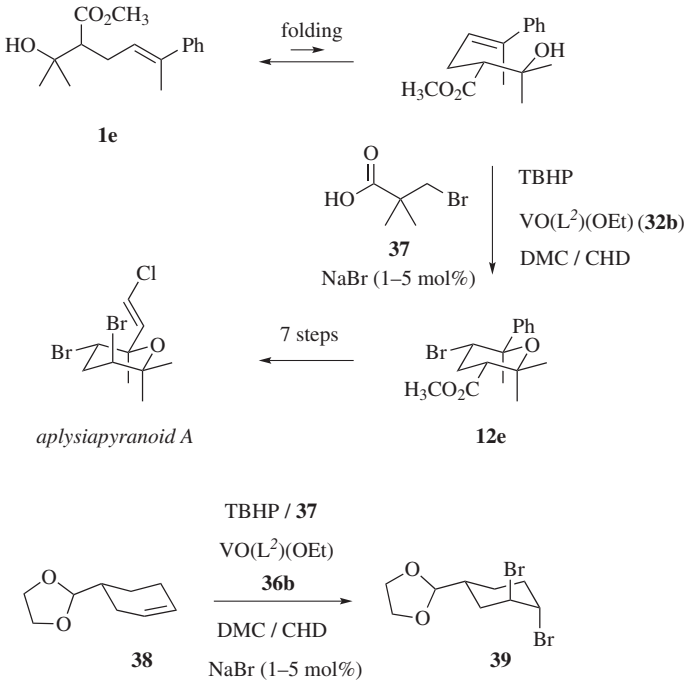

Scheme 3.19 Oxidative bromination of π-nucleophilic alkenes in oxidations catalysed by 5–10 mol% of chelated orthovanadate **32b**.[106]

(Scheme 3.19). A mild homolytic reductant, such as cyclohexa-1,4-diene (CHD), helps to improve yields and selectivity of oxidative alkene bromination.[106]

An acetal group, present for instance in substituted cyclohexene **38**, refrains from being hydrolysed in the new oxidative bromination. Water is always formed as co-product when oxidizing bromide with hydroperoxides. *Trans*-diaxial positioning indicates an *anti*-pathway for introducing the two bromine substituents of product **39**, pointing to molecular bromine as selectivity determining reagent.

3.8.2 π-Bond Monooxygenation

Oxyfunctionalizing substituted 4-pentenols with TBHP requires three selectivity issues to be addressed for use in bioinspired synthesis of hydroxy-substituted tetrahydrofurans: (i) stereoselectivity, (ii) π-bond selectivity and (iii) regioselectivity. Over the years, chelated orthovanadate **32b** has advanced as one of the most reactive and selective reagents for mediating oxidations of this kind.[102]

3.8.2.1 Stereoselectivity

Prenyl-type 4-pentenols, compounds bearing two methyl groups located in terminal position of the π(C,C) bond, and thus showing structural analogy

to terpenols, are quantitatively transformed within 8 hours in yields between 70% to 95% into 2-(hydroxy-2-propyl)-substituted tetrahydrofurans by TBHP in the presence of 1 mol% of chelated trialkyl orthovanadate **32b** at 20–25 °C.

Some alkenols require a longer time for being quantitatively turned over, which may be compensated by increasing the substrate-to-catalyst ratio to 5 mol%, and sometimes even to 10 mol%. Most oxidations summarized hereafter were conducted in chloroform. Some of the more recent experiments were performed using dimethyl carbonate (DMC) as solvent.[42]

Carbon substituents along the alkenol chain are the principle stereocontrolling elements in oxidative alkenol ring closures, in all instances explored so far overriding steric contributions from the trialkyl orthovanadate.

Alkyl and aryl groups at position 1 provide *cis*-2,5-substituted tetrahydrofurans from oxidative 4-pentenol cyclization, with the fraction of 2,5-*cis*-cyclized product rising as steric demand of the carbon substituent increases.[88,102]

When located in position 2, carbon substituents induce 2,4-*trans*-selective tetrahydrofuran-2-propanol syntheses. Two substituents cumulatively improve diastereoselection when arranged in matching relative configuration, as shown in tetrahydrofuran-synthesis from diphenyl-4-pentenol **1f**.[88,102]

Alkenols bearing a carbon substituent at position 3, *e.g.*, substrate **1g**, yield products of 2,3-*cis*-selective C,O-cyclization when treated with TBHP and trialkyl orthovanadate **32b** (Scheme 3.20).[102]

Chelated trialkylorthovanadate **32c**, prepared from enantiomerically pure 2,6-*cis*-substituted piperidine **31c**, induces enantioselective geraniol epoxidation (Scheme 3.20) but refrains from inducing similar selectivity in oxidative 4-pentenol cyclization.[102]

3.8.2.2 π-Bond Selectivity

Unlike other vanadium(v) catalysts,[89] chelated trialkyl orthovanadate **32b**, when loaded with TBHP, selectively induces π(C,C)-bond monooxygenation at position 4 of an alkenol, as evident from oxidizing phenyl-substituted dienols **1i** and **1j** (Scheme 3.21).[42]

Non-conjugated (*E*)- and (*Z*)-π(C,C)-bonds in dienol **1k** accept the peroxidic oxygen atom from TBHP in similar rates when activating the oxidant by chelated trialkyl orthovanadate **32b**. Conjugated (*E*)-C,C-double bonds, for instance in (+)-Laurediol (**1m**) react slower under standardized conditions than non-conjugated (*Z*)-double bonds (Scheme 3.22).[42]

3.8.3 Regioselectivity

Conformationally flexible prenyl-type 4-pentenol **1b**, selectively provides tetrahydrofuranyl-2-propanol **2b**, when oxidized with TBHP in the presence of orthovanadate ester **32b**. More rigid prenyl phenol **1n** affords under identical conditions annulated tetrahydropyran-3-ol **42n** (Scheme 3.23).[42]

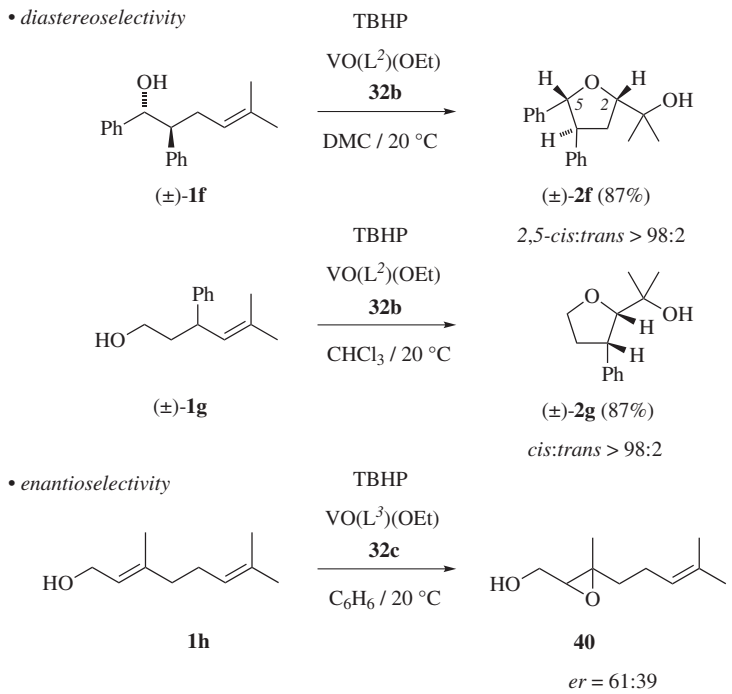

Scheme 3.20 Oxidation of prenyl-type alkenols with TBHP, catalysed by 5–10 mol% of chelated trialkyl orthovanadates **32b–c**.

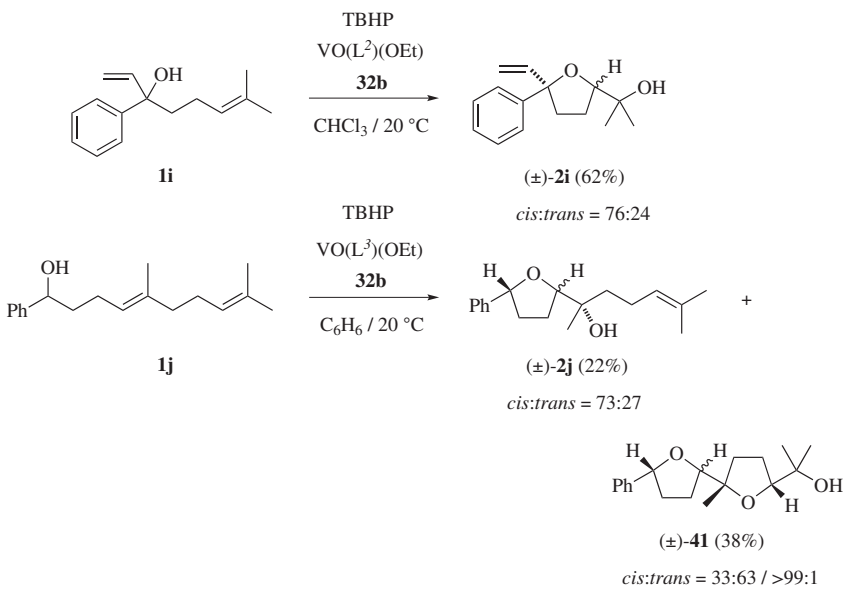

Scheme 3.21 Selectivity in TBHP-mediated oxidation of dienols, catalysed by 5–10 mol% of chelated trialkyl orthovanadate **32b**.

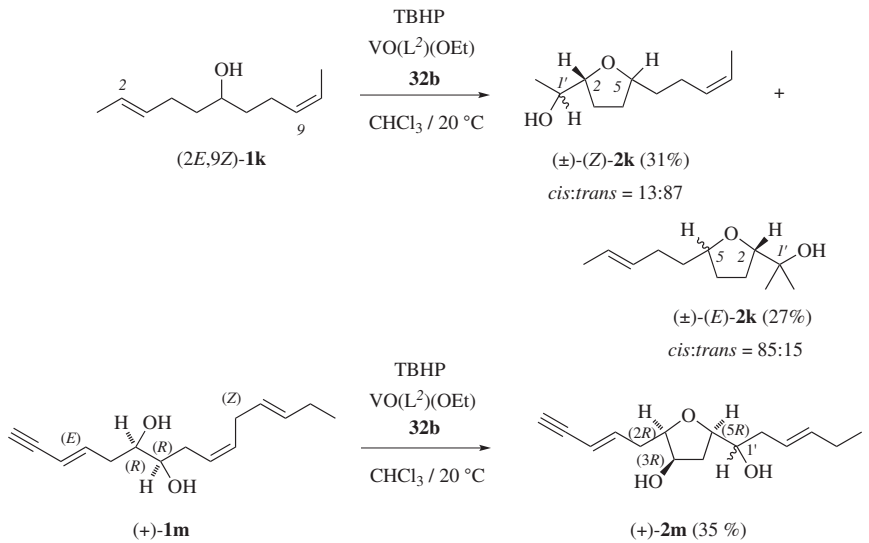

Scheme 3.22 Selectivity in oxidizing alkenols with (E)- and (Z)-double bonds, catalysed by 5–10 mol% of orthovandate(v) **32b**.

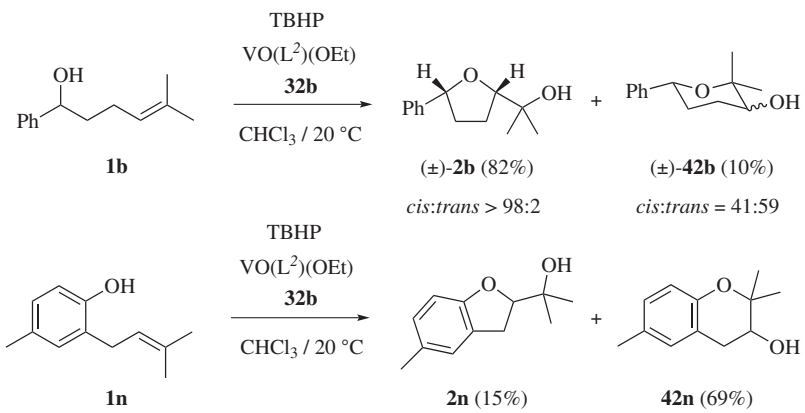

Scheme 3.23 Regioselectivity in oxidative cyclization of prenyl-type 4-pentenols by TBHP catalysed in oxidations mediated by orthovanadate **32b** [5 mol% of $VO(L^2)(OEt)$; quantitative alkenol conversion].

3.9 Epilogue

Although in use for more than half a century, compounds of vanadium(v), the orthovanadates, continue offering solutions to standing questions in oxidative synthesis, particularly at the interface of bioorganic, synthetic and physical chemistry.

Vital input for developing this field of research more recently came from theory, correlating with the enormous strength of existing methods for

predicting structure and energy changes. Reaction models developed by this approach helped, on a physical basis, understanding the role vanadium(v) compounds play for *activating* hydroperoxides.

When oxidizing strongly nucleophilic substrates in protic solvents by hydrogen peroxide, *activation* describes a reversal of polarity at the peroxide bond, as documented in reactivity–selectivity studies associated with the bromoperoxidase reaction. Scaling hydroperoxide reactivity in this model is feasible on the basis of frontier molecular orbital theory.

In oxidations of nucleophiles mediated by more nucleophilic oxidant *tert*-butyl hydroperoxide in combination with trialkyl orthovanadates, vanadium(v) compounds exert no effect on orbital energies of the peroxide. *Activation* of the hydroperoxide in the second mechanism means opening a reaction channel for transferring distal oxygen O^d to a reductant, which is not available in TBHP alone.

Both theories provide options for adapting properties of oxidants. The first mechanism offers ideas for developing truncated bromoperoxidases as potential catalysts for brominating substrates, using sea water as commodity. The second mechanism reveals how peroxide reactivity may be tuned, and even enhanced, by polar-substituent effects. Both aspects have not yet been pursued and require further study in continuing the path of scientific discovery.

References

1. C. W. Jones, *Applications of Hydrogen Peroxide and Derivatives*, Royal Society of Chemistry, Cambridge, 1999.
2. M. M. Faul and B. R. Huff, *Chem. Rev.*, 2000, **100**, 2407–2473.
3. T. Martín, J. I. Padrón and V. S. Martín, *Synlett*, 2014, 12–32.
4. R. A. Sheldon, in *Topics in Current Chemistry*, ed. W. A. Herrmann, Springer, Berlin, ch. 2, **vol. 164**, 1993, pp. 21–43.
5. *CRC Handbook of Chemistry and Physics*, ed. D. R. Lide, CRC Press, Boca Raton, 78th edn, 1997/1998, pp. 5–5 and 5–18.
6. K. B. Sharpless and T. R. Verhoeven, *Aldrichimica Acta*, 1979, **12**, 63–74.
7. K. Osafune and K. Kimura, *Chem. Phys. Lett.*, 1974, **25**, 47–50.
8. R. D. Bach, G. J. Wolwer and B. A. Coddens, *J. Am. Chem. Soc.*, 1984, **106**, 6098–6099.
9. J. Hartung, T. Gottwald and K. Špehar, *Synthesis*, 2002, 1469–1498.
10. R. A. Sheldon and J. K. Kochi, *Metal-catalyzed Oxidations of Organic Compounds*, Academic Press, New York, 1981.
11. H. Adolfson, in *Modern Oxidation Methods*, ed. J.-E. Bäckvall, Wiley-VCH, Weinheim, ch. 2, 2004, pp. 21–49.
12. N. Mizuno and K. Kamata, *Coord. Chem. Rev.*, 2011, **255**, 2358–2370.
13. H. L. Holland, *Organic Synthesis with Oxidative Enzymes*, VCH, New York, 1992.
14. F. Beer, G. Düsing and H. Pistor, in *Wasserstoffperoxid und seine Derivate*, ed. W. Weigert, Dr. Alfred Hüthig Verlag, Heidelberg, ch. 2, 1978, pp. 23–35.

15. O. Maass and P. G. Hiebert, *J. Am. Chem. Soc.*, 1924, **46**, 290–308.
16. J. Hartung and I. Svoboda, in *The Chemistry of Peroxides*, ed. Z. Rappoport, Wiley, Chichester, ch. 2, 2006, pp. 93–144.
17. N. Indictor and W. F. Brill, *J. Org. Chem.*, 1965, **30**, 2074–2075.
18. A. S. Tracey, G. R. Wilsky and E. S. Takeuchi, *Vanadium: Chemistry, Biochemistry, Pharmacology and Practical Applications*, CRC-Press, Boca Raton, 2007.
19. F. Freeman, in *Organic Synthesis by Oxidations with Metal Compounds*, ed. W. J. Mijs and C. R. H. De Jonge, Plenum Press, New York, ch. 1, 1986, pp. 1–39.
20. R. A. Sheldon, in *Aspects of Homogeneous Catalysis*, ed. R. Ugo, Reidel Publishing, Dordrecht, 4th edn, ch. 1, 1981, pp. 3–69.
21. A. G. J. Ligtenbarg, R. Hage and B. L. Feringa, *Coord. Chem. Rev.*, 2003, **237**, 89–101.
22. R. R. Langeslay, D. M. Kaphan, C. L. Marshall, P. C. Stair, A. Sattelberger and M. Delforro, *Chem. Rev.*, 2019, **119**, 2128–2191.
23. M. G. Finn and K. B. Sharpless, in *Asymmetric Synthesis*, ed. J. D. Morrison, Academic Press, Oxford, **vol. 5**, ch. 8, 1985, pp. 103–158.
24. J. Muzart, *Chem. Rev.*, 1992, **92**, 113–140.
25. V. Conte and B. Floris, *Dalton Trans.*, 2011, **40**, 1419–1436.
26. G. B. Payne and P. H. Williams, *J. Org. Chem.*, 1959, **24**, 54–55.
27. J. Prandi, H. B. Kagan and H. Mimoun, *Tetrahedron Lett.*, 1986, **27**, 2617–2620.
28. R. A. Sheldon, in *The Chemistry of Functional Groups: Peroxides*, ed. S. Patai, John Wiley, Chichester, ch. 6, 1983, pp. 161–200.
29. J. Hartung and M. Greb, *J. Organomet. Chem.*, 2002, **661**, 67–84.
30. H. E. B. Lempers, A. Pipollès i Garcia and R. A. Sheldon, *J. Org. Chem.*, 1998, **63**, 1408–1413.
31. H. C. Kolb, M. S. VanNieuwehnze and K. B. Sharpless, *Chem. Rev.*, 1994, **94**, 2483–2547.
32. E. Klein and W. Rojahn, *Tetrahedron*, 1965, **21**, 2353–2358.
33. T. B. Towne and F. E. Mc Donald, *J. Am. Chem. Soc.*, 1997, **119**, 6022–6028.
34. D. Wischang, O. Brücher and J. Hartung, *Coord. Chem. Rev.*, 2011, **255**, 2204–2217.
35. A. Podgoršek, M. Zupan and J. K. Iskra, *Angew. Chem., Int. Ed.*, 2009, **48**, 8424–8450.
36. H. Vilter, in *Vanadium and Its Role in Life*, ed. H. Sigel and A. Sigel, Marcel Dekker, New York, **vol. 31**, ch. 10, 1995, pp. 325–362.
37. G. W. Gribble, *Environ. Sci. Pollut. Res.*, 2000, **7**, 37–49.
38. K. Mori and P. Puapoomchareon, *Liebigs Ann. Chem.*, 1989, 1261–1262.
39. For pioneering studies on vanadium(v)-catalyzed oxidative cyclization, see:(a) M. Hashimoto, H. Harigaya, M. Yanagiya and H. Shirahama, *J. Org. Chem.*, 1991, **56**, 2299–2311; (b) D. A. Evans, R. P. Polniaszek, K. M. DeVries, D. E. Guinn and D. J. Mathre, *J. Am. Chem. Soc.*, 1991, **113**, 7613–7630.

40. A. Butler and J. N. Carter-Franklin, *Nat. Prod. Rep.*, 2004, **21**, 180–188.
41. M. Radlow, M. Czjzek, A. Jeudy, J. Dabin, L. Delage, C. Leblanc and J. Hartung, *ACS Chem. Biol.*, 2018, **13**, 1243–1259.
42. M. Dönges, M. Amberg, M. Niebergall and J. Hartung, *J. Inorg. Biochem.*, 2015, **147**, 204–220.
43. Y.-R. Luo, *Handbook of Bond Dissociation Energies in Organic Compounds*, CRC Press, Boca Raton, 2003.
44. W. H. Richardson, in *The Chemistry of Functional Groups, Peroxides*, ed. S. Patai, Wiley, Chichester, ch. 5, 1983, pp. 129–159.
45. M. J. Clague and A. Butler, *J. Am. Chem. Soc.*, 1995, **117**, 3475–3484.
46. D. Wischang, M. Radlow and J. Hartung, *Dalton Trans.*, 2013, **42**, 11926–11940.
47. H. S. Soedjak and A. Butler, *Biochim. Biophys. Acta*, 1991, **1079**, 1–7.
48. J. N. Carter, K. E. Beatty, M. T. Simpson and A. Butler, *J. Inorg. Biochem.*, 2002, **91**, 59–69.
49. C. Rush, A. Willetts, G. Davies, Z. Dauter, H. Watson and J. Littlechild, *FEBS Lett.*, 1995, **359**, 244–246.
50. M. N. Isupov, A. R. Dalby, A. A. Brindley, Y. Izumi, T. Tanabe, G. N. Murshudov and J. A. Littlechild, *J. Mol. Biol.*, 2000, **299**, 1035–1049.
51. B. E. Krenn, H. Plat and R. Wever, *Biochim. Biophys. Acta*, 1987, **912**, 287–291.
52. D. Wischang, M. Radlow, H. Schulz, H. Vilter, L. Viehweger, M. O. Altmeyer, C. Kegler, J. Hermann, R. Mueller, F. Gaillard, L. Delage, C. Leblanc and J. Hartung, *Bioorg. Chem.*, 2012, **44**, 25–34.
53. M. Weyand, H.-J. Hecht, M. Kieß, M.-F. Liaud, H. Vilter and D. Schomburg, *J. Mol. Biol.*, 1999, **293**, 595–611.
54. D. J. Sheffield, T. Harry, A. J. Smith and L. J. Rogers, *Phytochemistry*, 1992, **32**, 21–26.
55. H. S. Soedjak and A. Butler, *Biochemistry*, 1990, **29**, 7974–7981.
56. A. D. Becke, *J. Chem. Phys.*, 1993, **98**, 5648–5652.
57. C. Lee, W. Yang and R. G. Parr, *Phys. Rev.*, 1988, **B37**, 785–789.
58. M. J. Frisch, G. W. Trucks, H. B. Schlegel, G. E. Scuseria, M. A. Robb, J. R. Cheeseman, J. A. Montgomery, Jr., T. Vreven, K. N. Kudin, J. C. Burant, J. M. Millam, S. S. Iyengar, J. Tomasi, V. Barone, B. Mennucci, M. Cossi, G. Scalmani, N. Rega, G. A. Petersson, H. Nakatsuji, M. Hada, M. Ehara, K. Toyota, R. Fukuda, J. Hasegawa, M. Ishida, T. Nakajima, Y. Honda, O. Kitao, H. Nakai, M. Klene, X. Li, J. E. Knox, H. P. Hratchian, J. B. Cross, V. Bakken, C. Adamo, J. Jaramillo, R. Gomperts, R. E. Stratmann, O. Yazyev, A. J. Austin, R. Cammi, C. Pomelli, J. W. Ochterski, P. Y. Ayala, K. Morokuma, G. A. Voth, P. Salvador, J. J. Dannenberg, V. G. Zakrzewski, S. Dapprich, A. D. Daniels, M. C. Strain, O. Farkas, D. K. Malick, A. D. Rabuck, K. Raghavachari, J. B. Foresman, J. V. Ortiz, Q. Cui, A. G. Baboul, S. Clifford, J. Cioslowski, B. B. Stefanov, G. Liu, A. Liashenko, P. Piskorz, I. Komaromi, R. L. Martin, D. J. Fox, T. Keith, M. A. Al-Laham, C. Y. Peng, A. Nanayakkara,

M. Challacombe, P. M. W. Gill, B. Johnson, W. Chen, M. W. Wong, C. Gonzalez and J. A. Pople, Gaussian, Inc., Wallingford CT, 2004.
59. A. Bagno, V. Conte, F. Di Furia and S. Moro, *J. Phys. Chem. A*, 1997, **101**, 4637–4640.
60. P. Adão, J. C. Pessoa, R. T. Henriques, M. L. Kuznetsov, F. Avecilla, M. R. Maurya, U. Kumar and I. Correia, *Inorg. Chem.*, 2009, **48**, 3542–3561.
61. K. R. Geethalakshmi, M. P. Waller, W. Thiel and M. Bühl, *J. Phys. Chem. B*, 2009, **113**, 4456–4465.
62. V. Conte, A. Coletti, B. Floris, G. Licini and C. Zonta, *Coord. Chem. Rev.*, 2011, **255**, 2165–2177.
63. G. Zampella, J. Y. Kravitz, C. E. Webster, P. Fantucci, M. B. Hall, H. A. Carlson, V. L. Pecoraro and L. De Gioia, *Inorg. Chem.*, 2004, **43**, 4127–4136.
64. M. G. M. Tromp, G. 'Olafsson, B. E. Krenn and R. Wever, *Biochim. Biophys. Acta*, 1990, **1040**, 192–198.
65. L. Petterson, B. Hedman, A.-M. Nenner and I. Andersson, *Acta Chem. Scand.*, 1985, **A39**, 499–506.
66. A. Butler, M. J. Clague and G. E. Meister, *Chem. Rev.*, 1994, **94**, 625–638.
67. J. S. Jaswal and A. S. Tracey, *Inorg. Chem.*, 1991, **30**, 3718–3722.
68. F. Secco, *Inorg. Chem.*, 1980, **19**, 2722–2725.
69. M. Orhanović and R. G. Wilkins, *J. Am. Chem. Soc.*, 1967, **89**, 278–282.
70. S. Funahashi, K. Ishihara, M. Inamo and M. Tanaka, *Inorg. Chim. Acta*, 1989, **157**, 65–71.
71. T.-J. Won, C. L. Barnes, E. O. Schlemper and R. C. Thompson, *Inorg. Chem.*, 1995, **34**, 4499–4503.
72. A. F. Ghiron and R. C. Thompson, *Inorg. Chem.*, 1990, **29**, 4457–4461.
73. R. Wever, H. Plat and E. de Boer, *Biochim. Biophys. Acta*, 1985, **830**, 181–186.
74. R. R. Everett, H. S. Soedjak and A. Butler, *J. Biol. Chem.*, 1990, **265**, 15671–15679.
75. A. Cornish-Bowden, in *Fundamentals of Enzyme Kinetics*, Wiley-Blackwell, Weinheim, 4th edn, 2014.
76. C.-R. Yang, B. E. Shapiro, E. D. Mjolsness and G. W. Hatfield, *Bioinformatics*, 2005, **21**, 774–780.
77. W. W. Cleland, *Biochim. Biophys. Acta*, 1963, **67**, 104–137.
78. D. Wischang and J. Hartung, *Tetrahedron*, 2011, **67**, 4048–4054.
79. G. Schwarzenbach and G. Geier, *Helv. Chim. Acta*, 1963, **46**, 906–926.
80. D. Wischang and J. Hartung, *Tetrahedron*, 2012, **68**, 9456–9463.
81. J. Hartung, Y. Dumont, M. Greb, D. Hach, F. Köhler, H. Schulz, M. Časný, D. Rehder and H. Vilter, *Pure Appl. Chem.*, 2009, **81**, 1251–1264.
82. J. N. Carter-Franklin and A. Butler, *J. Am. Chem. Soc.*, 2004, **126**, 15060–15066.
83. J. V. Walker and A. Butler, *Inorg. Chim. Acta*, 1996, **243**, 201–206.
84. C. Bolm, *Coord. Chem. Rev.*, 2003, **237**, 245–256.
85. G. R. Howe and R. R. Hiatt, *J. Org. Chem.*, 1970, **35**, 4007–4012.
86. N. B. Barhate, A. S. Gajare, R. D. Wakharkar and A. V. Bedekar, *Tetrahedron*, 1999, **55**, 11127–11142.

87. J. Hartung, R. Kneuer, S. Laug, P. Schmidt, K. Špehar, I. Svoboda and H. Fuess, *Eur. J. Org. Chem.*, 2003, 4033–4052.
88. J. Hartung, S. Drees, M. Greb, P. Schmidt, I. Svoboda, H. Fuess, A. Murso and D. Stalke, *Eur. J. Org. Chem.*, 2003, 2388–2408.
89. R. C. Michaelson, R. E. Palermo and K. B. Sharpless, *J. Am. Chem. Soc.*, 1977, **99**, 1990–1992.
90. W. Prandtl and L. Hess, *Z. Anorg. Chem.*, 1913, **82**, 103–129.
91. D. C. Crans, H. Chen and R. A. Felty, *J. Am. Chem. Soc.*, 1992, **114**, 4543–4550.
92. P. Pfeiffer, T. Hesse, H. Pfitzner, W. Scholl and H. Thielert, *J. Prakt. Chem.*, 1937, **149**, 217–296.
93. J. C. Pessoa and I. Correia, *Coord. Chem. Rev.*, 2019, **388**, 227–247.
94. S. Hanessian, N. G. Cooke, B. DeHoff and Y. Sakito, *J. Am. Chem. Soc.*, 1990, **112**, 5276–5290.
95. H. Mimoun, L. Saussine, E. Daire, M. Postel, J. Fischer and R. Weiss, *J. Am. Chem. Soc.*, 1983, **105**, 3101–3310.
96. W. Zhang and H. Yamamoto, *J. Am. Chem. Soc.*, 2007, **128**, 286–287.
97. A. V. Malkov, L. Czemerys and D. A. Malyshev, *J. Org. Chem.*, 2009, **74**, 3350–3355.
98. C. Bolm and T. Kühn, *Synlett*, 2000, 899–901.
99. H. Mimoun, P. Chaumette, M. Mignard, L. K. Saussine, J. Fischer and R. Weiss, *Nouv. J. Chim.*, 1983, **7**, 467–475.
100. D. Rehder, *Angew. Chem., Int. Ed.*, 1991, **30**, 148–167.
101. H. Mimoun, *J. Mol. Catal.*, 1980, **7**, 1–29.
102. M. Dönges, M. Amberg, G. Stapf, H. Kelm, U. Bergsträßer and J. Hartung, *Inorg. Chim. Acta*, 2014, **420**, 120–134.
103. E. D. Glendening, J. K. Badenhoop, A. E. Reed, J. E. Carpenter, J. A. Bohmann, C. M. Morales, and F. Weinhold, NBO 5.9, 2009, http://www.chem.wisc.edu/∼nbo5. Theoretical Chemistry Institute, University of Wisconsin, Madison, WI.
104. F. Di Furia, G. Modena and R. Curci, *J. Mol. Catal.*, 1982, **14**, 219–229.
105. H. K. Eigenmann, D. M. Golden and S. W. Benson, *J. Phys. Chem.*, 1973, **77**, 1687–1694.
106. O. Brücher, U. Bergsträßer, H. Kelm, J. Hartung, M. Greb, I. Svoboda and H. Fuess, *Tetrahedron*, 2012, **68**, 6968–6980.

CHAPTER 4

The Vanadate–Pyrazinecarboxylic Acid–Hydrogen Peroxide Reagent and Similar Systems for Efficient Oxidations with Peroxides

GEORGIY B. SHUL'PIN*[a,b,c] AND LIDIA S. SHUL'PINA[d]

[a] Semenov Federal Research Center for Chemical Physics, Russian Academy of Sciences, ulitsa Kosygina 4, Moscow 119991, Russia; [b] Peoples' Friendship University of Russia, ulitsa Miklukho-Maklaya 6, Moscow 117198, Russia; [c] Chair of Chemistry and Physics, Plekhanov Russian University of Economics, Stremyannyi pereulok 36, Moscow 117997, Russia; [d] Nesmeyanov Institute of Organoelement Compounds, Russian Academy of Sciences, ulitsa Vavilova 28, Moscow 119991, Russia
*Email: gbsh@mail.ru

4.1 Introduction

The functionalization of saturated hydrocarbons – ''noble gases of organic chemistry'' – is an important area of metal complex catalysis. Particularly difficult is the task of obtaining products of partial oxidation of the most inert alkane methane. Vanadium derivatives are known to catalyse the oxidation and oxidative functionalization of alkanes, including methane.[1–13]

Catalysis Series No. 41
Vanadium Catalysis
Edited by Manas Sutradhar, José Armando L. da Silva and Armando J. L. Pombeiro

Published by the Royal Society of Chemistry, www.rsc.org

Obtaining products of the partial oxidation of the most inert alkane methane is an especially challenging problem.

4.1.1 Pyrazinecarboxylic Acid as a Unique Powerful Co-catalyst in the Oxidation of Organic Compounds by Hydrogen Peroxide

Oxygen and air are the most environment-friendly oxidising agents for chemical practice and production since they are not toxic, as is the by-product of their transformations – water. Hydrogen peroxide, which at a certain concentration does not adversely affect the organisms of warm-blooded animals and which can be converted only into water and molecular oxygen, can apparently be put in second place in terms of ''environmental friendliness''.[8–11] Simple transition metal salts seldom exhibit high activity in such processes. However, some additives have been found to dramatically increase the efficiency of the oxidising system. We will discuss these systems based on hydrogen peroxide and vanadium complexes. The publications of the authors of this chapter are mainly described here.

An effective reagent for the oxidation of organic compounds: ''H_2O_2–a derivative of vanadium–pyrazinecarboxylic acid (PCA)''

The vanadate anion, VO_3^- (complex **1**; see Figure 4.2) is not active as a catalyst in the oxidation of alkanes and other organic compounds with hydrogen peroxide. In 1993, Shul'pin and co-workers discovered that in a solution of acetonitrile this compound catalyses the effective oxidation of saturated and aromatic hydrocarbons, as well as alcohols and olefins, with hydrogen peroxide in air at temperatures of 20–70 °C if pyrazinecarboxylic acid (PCA or pcaH) is present as a co-catalyst, where pca is the anionic basic form of pyrazinic acid) in concentrations several times higher than the concentration of the vanadium complex[12] (see also subsequent publications[13–38]). Other (even similar in structure) amino acids turned out to be noticeably less active as co-catalysts.[31] The primary product of the alkane oxidation reaction by the reagent under discussion is alkyl hydroperoxide, which partly decomposes during the process to form the corresponding carbonyl compound (ketone or aldehyde) and alcohol. In the initial period of the reaction, especially at low temperature, only alkyl hydroperoxide is found in the solution. Benzene is converted to phenol. Not only simple vanadate **1** (used in the form of acetonitrile-soluble salt with tetra-*n*-butylammonium) but also vanadatran **2** and the binuclear complex **3** (Figure 4.1) are effective catalysts in the presence of PCA (Figure 4.2).

By lowering the concentration of catalysts, it was possible to significantly increase the number of catalytic cycles per molecule of catalyst (TON). Thus, the activity of binuclear complex **3** is exactly two-times higher than the activity of mononuclear complexes **1** and **2**. Figure 4.2 demonstrates the

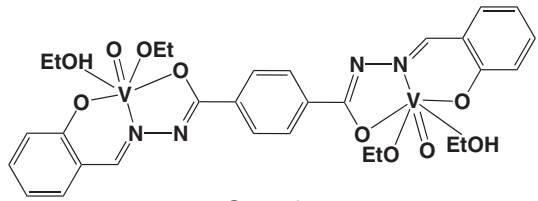

Complex **3**

Figure 4.1 Complex **3**: formula (top) and molecular structure determined by the method of X-ray diffraction analysis.
Reproduced from ref. 13 with permission from the Royal Society of Chemistry.

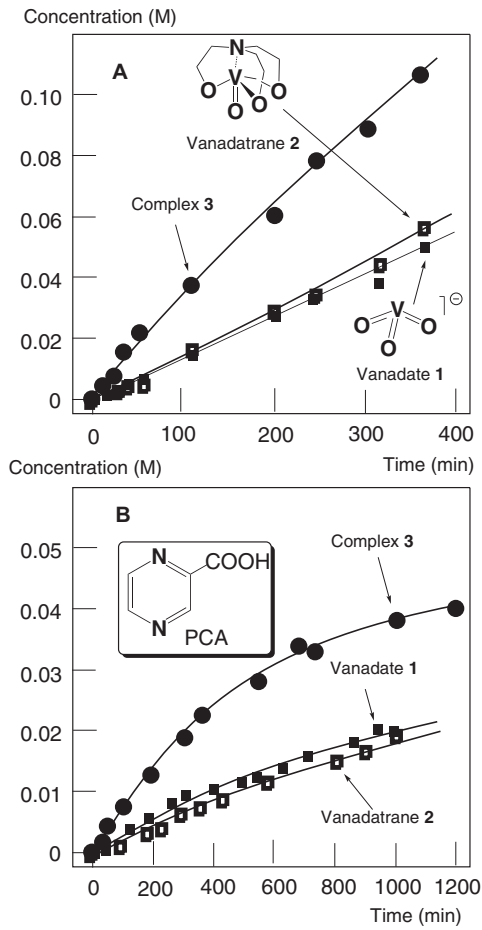

Figure 4.2 Kinetics of accumulation of cyclohexane oxidation products (total; the alcohol and ketone were determined after reduction with PPh_3) upon catalysis by vanadium complexes. Conditions: $[catalyst]_0 = 1.0\times10^{-5}$ (A) or 1.0×10^{-6} M (B); $[PCA] = 6\times10^{-4}$ M; $[H_2O_2]_0 = 0.4$ M (50% aqueous), $[H_2O]$ total = 0.76 M; $[cyclohexane]_0 = 0.40$ M; MeCN to a total volume of 5 mL; 50 °C.
Reproduced from ref. 13 with permission from the Royal Society of Chemistry.

kinetic curves of product accumulation for two different concentrations of catalysts. The values of the TON parameter per one vanadium ion for complexes **3**, **1**, and **2** are 5350, 5000 and 5700, respectively, after 360 min at a catalyst concentration of 1.0×10^{-5} M (Figure 4.2A). At a lower catalyst concentration (1.0×10–6 M), the corresponding values are 19 000, 20 000 and 19 000 after 1000 min (Figure 4.2B). In this case, for catalyst **1**, the initial rate (TOF, *i.e.*, TON per unit of time) reached 2100 h^{-1}. A study of the selectivities in the oxidation of various alkanes indicates that the oxidising effect of the studied system is due to the generation of hydroxyl radicals attacking the C–H bonds of the hydrocarbon. Using the spin-trap method, it was also possible to demonstrate that the interaction of hydrogen peroxide with a vanadium complex in the presence of PCA is accompanied by the formation of hydroxyl radicals.

When discussing the mechanism of the generation of hydroxyl radicals in the considered oxidising system, it should be noted first of all that the classical chain mechanism of the induced oxidation of cyclohexane with rates equal to experimentally observed for the described system (3×10^{-6} M s^{-1}) is impossible at 60 °C. This is due to the low reactivity of cyclohexyl peroxyl radicals. The non-chain nature of cyclohexane oxidation under the studied conditions is also evidenced by the fact that at a high concentration of hydrocarbon, when its oxidation rate ceases to depend on its initial concentration, the yield of hydroperoxide corresponds to the amount of hydrogen peroxide consumed. The observed dependence of the cyclohexane oxidation rate on its initial concentration (Figure 4.3, curve *1*) corresponds to the competition between cyclohexane and the acetonitrile solvent for the same oxidising species (the hydroxyl radical):

$$H_2O_2 \xrightarrow{W_g} HO^\bullet \; HO^\bullet + RH \xrightarrow{k_1} HO^\bullet + CH_3CN \xrightarrow{k_2} -\frac{d[RH]}{dt} = \frac{W_g}{1+\dfrac{k_2[CH_3CN]}{k_1[RH]}} \quad (4.1)$$

Kinetic processing of the data shown in Figure 4.3 (curve *1*), in accordance with eqn (4.1), allows to determine $Wg = 2.5\times10^{-6}$ M s^{-1} (as a segment cut off by straight line *2* on the ordinate axis) and the ratio of the rate constants k_2: $k_1 = 8.3\times10^{-3}$ (from the ratio of the values of the tangent of the angle of inclination to the segment on the ordinate axis for line *2*). The value of *Wg* corresponds to the maximum oxidation rate of cyclohexane at its high concentration, and $k_2 : k_1$ is close to the ratio of the rate constants of the interaction of acetonitrile and cyclohexane with $HO^\bullet$ radicals.

It was shown[13] that vanadate anions form complexes with one and two PCA molecules, and in the presence of hydrogen peroxide both vanadium(v) peroxo complexes and peroxo derivatives of vanadium complexes with PCA appear, since some of these compounds were isolated in crystalline state and their structures were determined by X-ray diffraction analysis. Their existence in the reaction solution was confirmed by ^{51}V NMR. Based on these

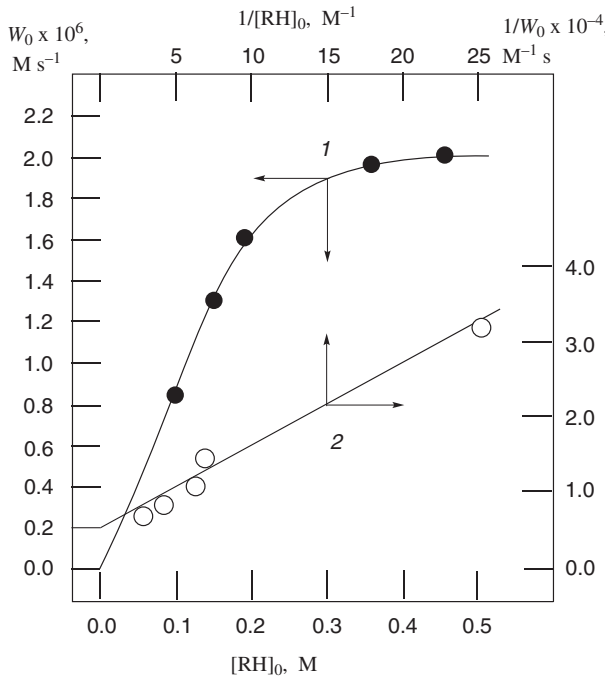

Figure 4.3 The dependence of the initial rate of oxidation of cyclohexane W_0 on its initial concentration (curve 1) and its anamorphosis (curve 2) obtained in accordance with eqn (4.1). Reaction conditions: $[n\text{-}Bu_4NVO_3]_0 = 1.0\times10^{-4}$ M, $[PCA]_0 = 1.0\times10^{-4}$ M, $[H_2O_2]_0 = 0.20$ M, 40 °C.

data, we can assume the following sequence of complexation stages in the system under consideration:

$$V + PCA \xrightarrow{K_2} V(PCA) \tag{4.2}$$

$$V(PCA) + PCA \xrightarrow{K_3} V(PCA)_2 \tag{4.3}$$

$$V(PCA) + H_2O_2 \xrightarrow{K_4} V(PCA)H_2O_2 \tag{4.4}$$

$$V(PCA)H_2O_2 \xrightarrow{K_5} V(H_2O_2) + PCA \tag{4.5}$$

$$V(PCA)_2 + H_2O_2 \xrightarrow{K_6} V(PCA)_2H_2O_2 \tag{4.6}$$

$$V(PCA)_2H_2O_2 \xrightarrow{K_7} V(PCA)H_2O_2 + PCA \tag{4.7}$$

Since at $[PCA]_0 > [V]_0$, there are practically no vanadium ions not associated with PCA in the solution, the concentration of [v] can be neglected in comparison with the concentration of its complexes in the balance equation. Eqs (4.2) and (4.3) deliberately simplify the situation.

Figure 4.4 shows the experimental dependence of cyclohexane-oxidation rate on PCA concentration. An increase in the reaction rate with small

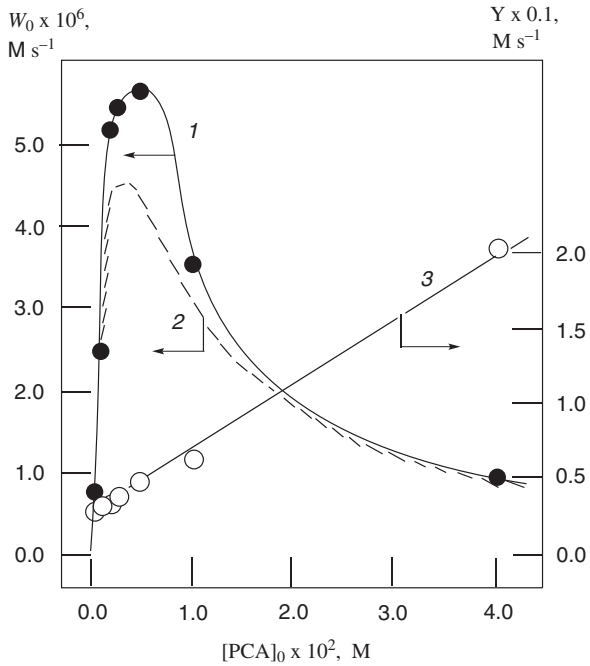

Figure 4.4 The experimental dependence of the initial oxidation rate of cyclohexane W_0 on the initial PCA concentration (curve 1) shows that the curve of this dependence is obtained in the calculation in accordance with eqn (4.12) (curve 2) and the linear anamorphosis of the experimental dependence (line 3), in the coordinates Y – $[PCA]_0$, where Y is given by eqn (4.14a). Reaction conditions: $[n\text{-}Bu_4NVO_3]_0 = 1.0 \times 10^{-4}$ M, [Cyclohexane]0 = 0.46 M, $[H_2O_2]_0 = 0.20$ M, 40 °C.
Reproduced from ref. 13 with permission from the Royal Society of Chemistry.

additions of co-catalyst clearly indicates that the generation of hydroxyl radicals is associated with the formation of vanadium complexes with PCA. The bell-shaped form of curve *1* in Figure 4.4 within the framework of eqn (4.2)–(4.7) corresponds to the fact that the vanadium complex containing one PCA molecule is involved in the limiting stage of the process. At the same time, vanadium complexes with two PCA molecules – or those without this ligand at all – are catalytically much less active. The dependence of the reaction rate on the concentration of hydrogen peroxide also has a maximum (Figure 4.5, curve *1*). As shown by specialised experiments, water additives inhibit the oxidation of cyclohexane. A decrease in the reaction rate at high H_2O_2 concentrations turned out to be associated with an increase of the H_2O concentration introduced into the reaction solution together with H_2O_2 (a 38% aqueous solution of hydrogen peroxide was usually used). Taking this effect into account showed that at a constant concentration of H_2O, the reaction rate tends to be a limiting value with an increase in the

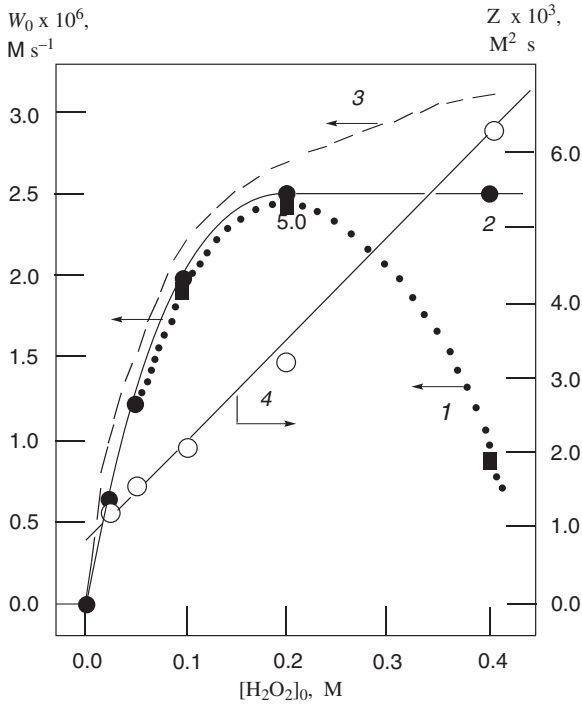

Figure 4.5 The dependence of the initial rate of oxidation of cyclohexane W_0 on the initial concentration of H_2O_2 (curve 1) – a curve of the same dependence – is obtained taking into account the inhibitory effect of water introduced together with H_2O_2 (curve 2), the calculated curve obtained using eqn (4.12) (curve 3) and a linear anamorphosis of the experimental dependence (line 4) in the coordinates Z–$[H_2O_2]_0$, where Z is given by eqn (4.12a). Reaction conditions: $[n\text{-}Bu_4NVO_3]_0 = 1.0\times10^{-4}$ M, $[PCA]_0 = 1.0\times10^{-4}$ M, $[cyclohexane]_0 = 0.46$ M, 40 °C.

concentration of H_2O_2 (curve *2* in Figure 4.5). This means that the vanadium monoperoxo complex is a catalytically active species.

The limiting stage of the process is the monomolecular transformation of the $V(PCA)\cdot H_2O_2$ complex. Thus, the appearance of hydroxyl radicals is possible as a result of a sequence of stages:

$$V^{V}(PCA)H_2O_2(PCA)H_2O_2 \rightarrow V^{IV}(PCA) + H^+ + HOO^{\bullet} \quad (4.8)$$

$$V^{IV}(PCA) + H_2O_2 \rightarrow V^{V}(PCA) + HO^{\bullet} + HO^- \quad (4.9)$$

$$V^{V}(PCA)H_2O_2 + HOO \rightarrow V^{V}(PCA) + HO^{\bullet} + H_2O + O_2 \quad (4.10)$$

The rate-limiting is reaction 4.8. Since at a high concentration of cyclohexane all the hydroxyl radicals arising in the system interact with this hydrocarbon, the reaction rate can be expressed as:

$$W = -\frac{d[RH]}{dt} = \frac{d[ROOH]}{dt} = 2kg\left[V(PCA)H_2O_2\right] \quad (4.11)$$

Thus, in order to obtain a kinetic expression for the rate of the process, it was sufficient to establish the dependence of $[V(PCA)H_2O_2]$ on the initial concentrations of the reagents. In the quasi-equilibrium approximation, the value of $[V^V\ (PCA)\ H_2O_2]$ can be obtained by taking $[PCA]_0/[V]_0 > 4$, *i.e.*, $[PCA]_0 - [V]_0 \approx [PCA]_0$, $[V]_0/[H_2O_2]_0 \ll 1$ and $[V^V] \gg [V^{IV}]$. Using the obtained expression for the quasi-equilibrium species concentration $V^V{\cdot}(PCA){\cdot}H_2O_2$, we obtain the following kinetic expression for the initial reaction rate:

$$-\frac{d[ROOH]}{dt} = \frac{2k_8K_4[H_2O_2]_0[PCA]_0[V]_0}{K_3\left(1+K_6[H_2O_2]_0\right)[PCA]_0^2 + \left(1+K_4[H_2O_2]_0\right)[PCA]_0 + K_4K_5[H_2O_2]_0} \tag{4.12}$$

To verify the correspondence of the proposed kinetic expression to experimental data, we studied the dependence of $d[ROOH]/dt$ on $[V]_0$ under the condition $[V]_0/[PCA]_0 \leq \frac{1}{4}$ and the data in Figures 4.4 and 4.5. First, in accordance with the kinetic expression (4.12), according to our data, the reaction rate is proportional to the concentration of vanadium. Second, experimental data confirm the dependence of the reaction rate on the H_2O_2 concentration predicted by expression eqn (4.12). According to eqn (4.12) the dependence of the function

$$Z = [H_2O_2]_0\ [V]_0\ [PCA]_0/W \tag{4.12a}$$

on $[H_2O_2]_0$ should be linear. Line 4 in Figure 4.5 demonstrates a good agreement with the model, *i.e.*, eqn (4.12) and (4.12a) with experimental data. Third, the dependence of the reaction rate on PCA concentration also corresponds to the proposed kinetic expression eqn (4.12). Indeed, according to eqn (4.12) the maximum value of the reaction rate at a given concentration of hydrogen peroxide is achieved at a PCA concentration determined by the expression:

$$[PCA]_{max} = \sqrt{\frac{K_4K_5[H_2O_2]_0}{K_3\left(1+K_6[H_2O_2]_0\right)}} \tag{4.13}$$

Using relation eqn (4.13) and the kinetic expression for the reaction rate eqn (4.12) we can obtain eqn (4.14):

$$\frac{[V]_0[H_2O_2]_0}{[PCA]_0 - [PCA]_{max}}\left\{\frac{[PCA]_0}{W} - \frac{[PCA]_{max}}{W_{max}}\right\} = \frac{1}{2kgK_4} \times \left\{\left(1+K_4[H_2O_2]_0\right) + K_3\left(1+K_6[H_2O_2]_0\right)\left([PCA]_0 + [PCA]_{max}\right\}\right. \tag{4.14}$$

In accordance with this expression, the value of the left-hand side of eqn (4.14) calculated from the experimental data, should be a linear function of

the PCA concentration at a fixed concentration of H_2O_2. This dependence of the parameter

$$Y = \frac{[V]_0[H_2O_2]_0}{[PCA]_0 - [PCA]_{max}} \left\{ \frac{[PCA]_0}{W} - \frac{[PCA]_{max}}{W_{max}} \right\} \quad (4.14a)$$

on PCA concentration is observed in Figure 4.4 (straight line *3*).

Last, the dependences of the reaction rate on $[V]_0$, $[H_2O_2]_0$ and $[PCA]_0$ are satisfactorily described if we take the following values for the equilibrium constants: $K_3 = 0.16$; $K_4 = 0.55$; $K_5 = 8\times10^{-3}$; $K_6 = 5.7\times10^3$ and the rate constant $k_8 = 0.4\ s^{-1}$. The results of such calculations are illustrated by curve *2* in Figure 4.4 and curve *3* in Figure 4.5. Thus, the proposed kinetic scheme of the process satisfactorily describes the entire set of experimental data, *i.e.*, correctly reflects the main features of the investigated process. At low concentrations of H_2O_2 and PCA ($[H_2O_2]_0 \le 0.1\ M^{-1}$, $[PCA]_0 \le 2\times10^{-3}\ M^{-1}$) and $10 \ge [PCA]_0/[V]_0 \ge 4$, the kinetic expression (4.12) can be simplified as:

$$\frac{d[ROOH]}{dt} = \frac{2k_8K_4[H_2O_2]_0[PCA]_0[V]_0}{[PCA]_0 + K_4K_5[H_2O_2]_0} \quad (4.15)$$

Taking into account the numerical values of the constants obtained, it takes the form

$$\frac{d[ROOH]}{dt} = \frac{0.44[H_2O_2]_0[PCA]_0[V]_0}{[PCA]_0 + 0.44\times10^{-3}[H_2O_2]_0} \quad (4.16)$$

and can be used to calculate the expected values of the cyclohexane oxidation rates. At a low concentration of H_2O_2, the expression for the reaction rate is even more simple:

$$\frac{d[ROOH]}{dt} = 2kgK_4[H_2O_2]_0[V]_0 \quad (4.17)$$

Under such conditions, the temperature dependence of the oxidation rate of cyclohexane was studied. According to the data obtained, the effective activation energy of the process, defined as the sum of the true activation energy of the monomolecular decomposition of the $V(PCA)H_2O_2$ complex, equilibrium (4.4) enthalpy is 17.6 ± 2 kcal mol^{-1}, and the effective value of the pre-exponential factor for the effective rate constant (k_8K_4) is $3.6\times10^{11}\ M^{-1}\,s^{-1}$.

The decomposition rate of hydrogen peroxide in acetonitrile, catalysed by the vanadate anion and PCA, decreases markedly when alkane (cyclohexane, *n*-heptane, isooctane) is introduced into the reaction solution, which is oxidised to alkyl hydroperoxide by the catalytic system. This was explained by the fact that the oxidation of acetonitrile to the final products, which is largely suppressed by the addition of the necessary amounts of alkane, consumes a much larger number of hydrogen peroxide molecules than the

oxidation of cyclohexane to cyclohexyl hydroperoxide. For example, at $[CyH] = 0.92$ M employing 38% H_2O_2 in the initial reaction period, approximately half of the total amount of H_2O_2 is used to oxidize CyH, and the second half is spent for the CH_3CN oxidation and O_2 formation. This conclusion confirms that the decomposition of H_2O_2 in an organic solvent proceeds as a radical non-chain process.

The hydroxyl radical formed in the reaction of H_2O_2 with the vanadium complex interacts with the CyH cyclohexane molecule:

$$HO^{\bullet} + CyH \rightarrow H_2O + Cy^{\bullet} \tag{4.18}$$

$$Cy^{\bullet} + O_2 \rightarrow CyOO^{\bullet} \tag{4.19}$$

$$CyOO^{\bullet} + V^{4+} + H^{+} \rightarrow CyOOH + V^{5+} \tag{4.20}$$

$$CyOO^{\bullet} + HOO^{\bullet} \rightarrow CyOOH + O_2 \tag{4.21}$$

$$CyOO^{\bullet} + H_2O_2 \rightarrow CyOOH + HOO^{\bullet} \tag{4.22}$$

The formation of CyOOH by reaction (4.21) is not excluded, but reaction (4.22) is unlikely. Therefore, the scheme satisfactorily describes the experimental data.

It has been concluded on the basis of the kinetic study of benzene hydroxylation by the "O_2–H_2O_2–*n*-Bu_4NVO_3–PCA" reagent in acetonitrile at various temperatures that oxidation is induced by the attack of the hydroxyl radical on the benzene molecule. The rate-limiting step of the reaction is the monomolecular decomposition of the complex containing one coordinated PCA molecule as well as one hydrogen peroxide molecule: $V^{V}(PCA)(H_2O_2) \rightarrow V^{IV}(PCA) + HOO^{\bullet} + H^{+}$. The V(IV) species thus formed reacts further in a non-limiting stage with the second H_2O_2 molecule to generate the hydroxyl radical: $V^{IV}(PCA) + H_2O_2 \rightarrow V^{V}(PCA) + HO^{\bullet} + HO^{-}$. The effective activation energy is 19 ± 3 kcal mol^{-1}.

It was especially interesting to study the oxidation of the most-inert alkane, methane, by the reagent under discussion. Acetonitrile is also oxidised by a vanadium reagent. In the case of an aqueous solution, it turned out that the system works most efficiently at a low (0.1 mM) concentration of vanadate ion, but using a 100-fold excess of PCA over the vanadate ion. In this case, the TON reaches 45 (mainly formic acid is formed). The reason for the need to introduce a large excess of PCA into the reaction solution became clear after studying the PCA behaviour during the process. It was shown by ^{1}H NMR that, in contrast to the oxidation in acetonitrile solution, during the oxidation of methane by the described system in water, intense oxidative degradation of PCA occurs that leads to a rapid loss of activity of the system with respect to methane. At a temperature of 50 °C and 60 °C over 4 hours, the concentration of PCA drops by almost half. In this case, PCA, competing with methane in the oxidation process, oxidises much faster than alkane and its oxidation products are almost not detected. At 80 °C, although the concentration of PCA decreases by a factor of 7 over 4 hours, the system manages to produce a significant amount of methane oxidation products

(TON = 45). The competing oxidation of methane and PCA is even more intense at 90 °C, *i.e.*, within 8 hours the concentration of PCA decreases by a factor of 20, but TON in methane oxidation reaches 79. It is obvious that PCA is oxidised by hydrogen peroxide, since even at 90 °C in its absence no decrease in PCA concentration is observed.

Some strong inorganic and organic acids added to the aqueous solution noticeably increase the yield of formic acid as the main product of methane oxygenation. Interestingly, this yield depends on the mixing order of PCA and sulphuric acid. If sulphuric acid is first added to the reaction solution, and then only PCA, the yield is two-times higher than in the reverse order. The best result was obtained when PCA and sulphuric acid are used as co-catalysts, although sulphuric acid itself is an effective oxidation promoter.

Based on this material, a simplified scheme for the hydroperoxidation of alkane RH with the reagent "O_2–H_2O_2–vanadium derivative–PCA" was proposed, which is shown in Figure 4.6. Under the plane are the molecules entering the catalytic cycle, and above the plane are the substances leaving the system. The catalytic cycle involving vanadium complexes is depicted lying in the plane. Two hydrogen peroxide molecules and an oxygen molecule from the atmosphere participate in the oxidation (this fact was proved in experiments with labelled $^{18}O_2$). Vanadium changes valency from V to IV and *vice versa*.

The cycle shown in Figure 4.6 tells us nothing about the possible accelerating role of the PCA process. It was assumed that PCA plays the role of mediator in proton transfer from a coordinated H_2O_2 molecule to the oxygen atom of the ligand of the complex. This mechanism is called the robot's arm mechanism. Figure 4.7 schematically illustrates this idea.

In 2005, Alexis Bell *et al.*, published a paper[14] in which the authors examined the discussed oxidising system (and the "robot's arm" mechanism) using the density functional method (DFT) and showed that the direct proton transfer from the H_2O_2 molecule to the oxygen atom of the

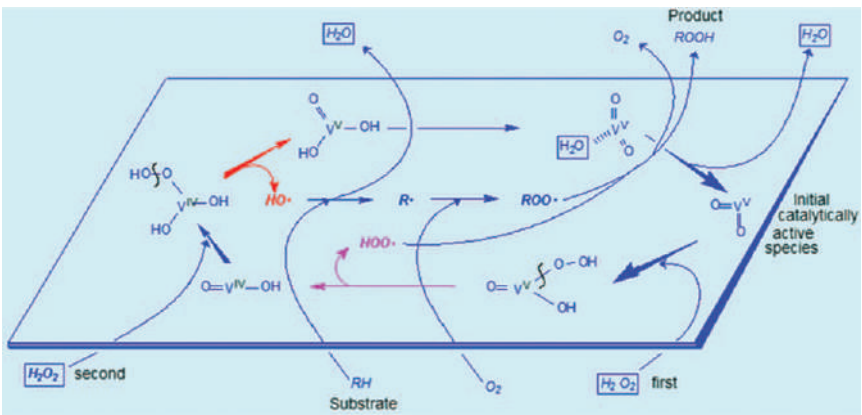

Figure 4.6 A simplified scheme for the generation of hydroperoxyl HOO• and hydroxyl HO • radicals and the reaction of hydroxyl radicals with alkane RH.

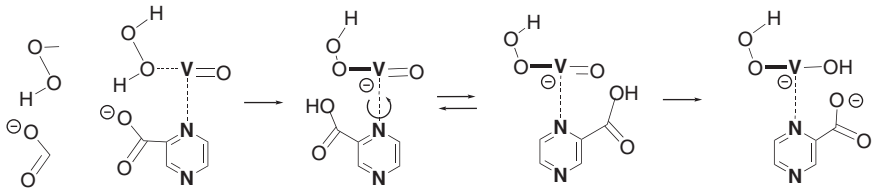

Figure 4.7 The idea of a PCA-assisted proton transfer in a vanadium complex (robot's arm mechanism).

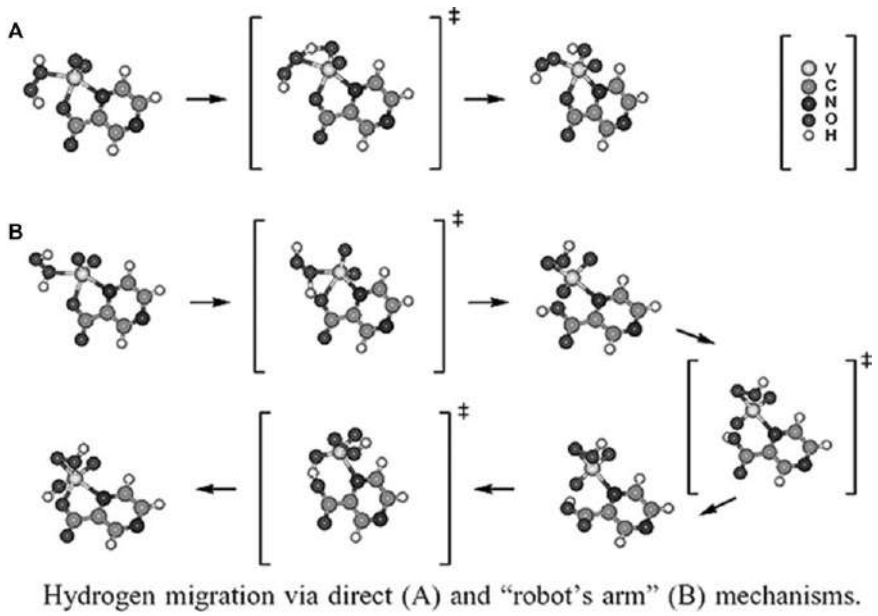

Figure 4.8 Two mechanisms of hydrogen migration.
Reproduced from ref. 14 with permission from American Chemical Society, Copyright 2005.

vanadium-containing fragment is noticeably a higher barrier compared to proton migration, the first step from hydrogen peroxide to the carboxyl group of the pca anion (coordinated with the vanadium ion at the nitrogen atom) and only then to the V = O fragment (Figure 4.8). Bell concluded that the hydrogen transfer step can also become a rate-determining step for the whole process. ''This is in agreement with the hypothesis of Shul'pin and others that the catalytic activity of the catalyst is determined by the ability to transfer the proton from hydrogen peroxide to the vanadyl group''.[14] The effective activation energy of the process experimentally determined by Shul'pin *et al.*, (63–80 kJ mol^{-1})[32] also agrees well with the value of E_a calculated by Bell *et al.* (67–81 kJ mol^{-1}). It is interesting to note that, based on the calculations, Bell *et al.*, suggested that ''it is impossible to find a co-catalyst better than PCA.''

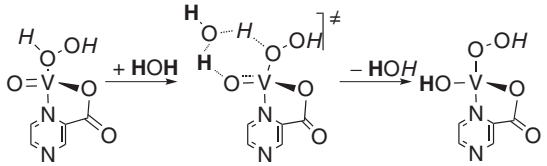

Figure 4.9 Scheme of a water-assisted mechanism for the transfer of hydrogen with a 6-membered transition state.
Reproduced from ref. 16 with permission from Elsevier, Copyright 2009.

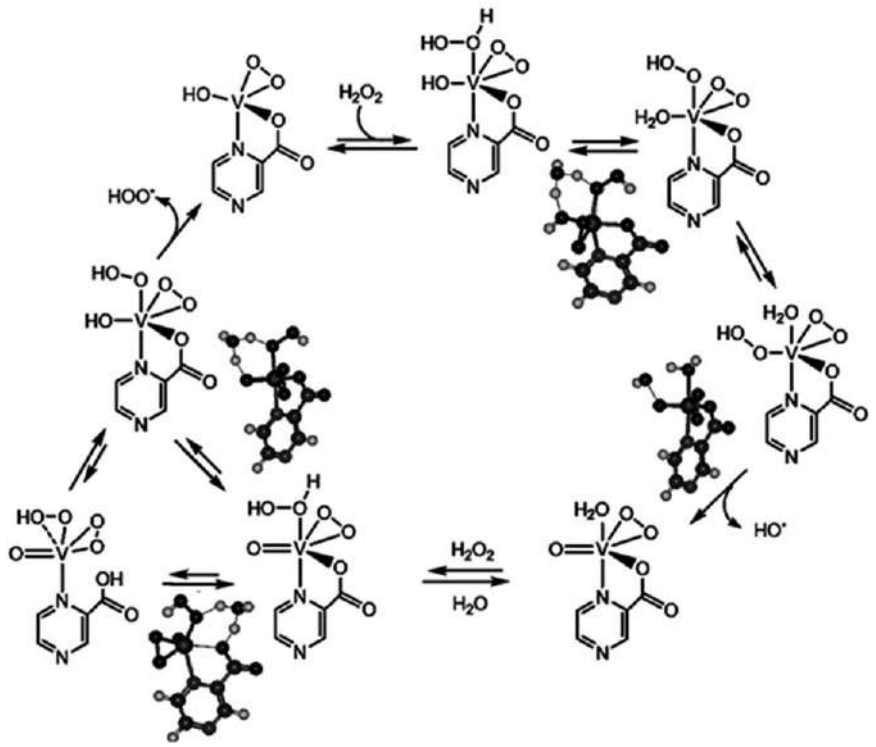

Figure 4.10 A simplified presentation of the most advantageous catalytic cycle for generating radicals in the system ''vanadium complex–PCA–H_2O_2''. The structures of some transition states are shown.
Reproduced from ref. 16 with permission from Elsevier, Copyright 2009.

A general mechanism for generating radicals by the reagent was proposed (Figure 4.9). It is based on the kinetic data obtained on the oxidation of cyclohexane and isopropanol with the reagent ''H_2O_2–vanadium–PCA complex'' (where the vanadium complex is **1** or **2**) and data on the composition of the reaction solution obtained by electron spectroscopy and nuclear NMR ^{1}H, ^{13}C and ^{51}V, and calculations using the density functional method (DFT) (Figure 4.10).[16]

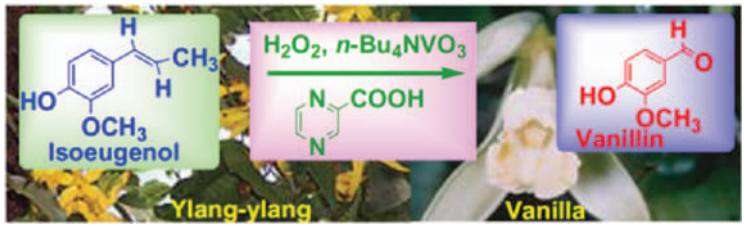

Scheme 4.1 The oxidation of isoeugenol to vanillin.
Reproduced from ref. 15 with permission from Elsevier, Copyright 2012.

Gusevskaya[15] has applied the H_2O_2–vanadate–PCA reagent to the practically very important oxidation of isoeugenol into vanillin (see Scheme 4.1). The mechanism of this oxidation has also been studied.

4.2 Oligovanadates Formed from Monovanadate by the Action of Acid Effectively Generate Hydroxyl Radicals from Hydrogen Peroxide

Monovanadate VO_3^- in a solution in acetonitrile under the influence of a small amount of strong acid (sulphuric, oxalic, *etc.*) is converted into a mixture of oligovanadates, which effectively catalyse the oxidation of alkanes with hydrogen peroxide. As expected, the complex $[n\text{-}Bu_4N]_4[V_{10}O_{26}]$ (complex **A**) specially synthesised and characterised by the data of X-ray diffraction analysis and EPR spectra, contains eight vanadium(V) ions and two vanadium(IV) ions (the latter are distinguished by a larger font) and catalyses the oxidation of alkanes, without requiring the addition of acid.

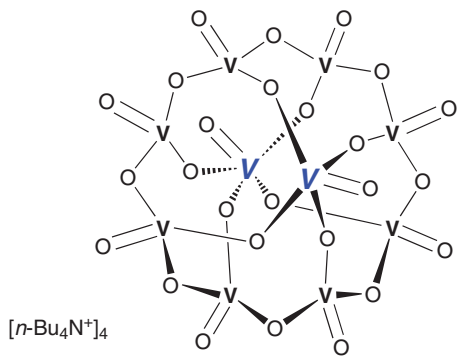

Complex A

The activity of the polyvanadate ion, in contrast to monovanadate, can be explained by the fact that, in the presence of an adjacent V=O fragment in polyvanadate, the formation of a hydroperoxyl complex from a complex with a coordinated H_2O_2 molecule with the participation of a six-membered transition state is facilitated (Scheme 4.2).

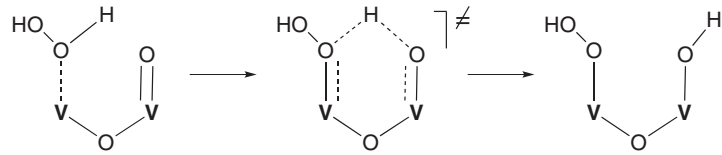

Scheme 4.2 Proton transfer between two vanadium-containing fragments.

Kuznetsov, together with the authors of this chapter,[16] has analysed the possible catalytic cycles for generating radicals $HOO^{\bullet}$ and $HO^{\bullet}$ with the participation of model divanadate (Figure 4.11A) and monovanadate (Figure 4.11B) using the density potential method (DFT). The calculated Gibbs free energy $\Delta G_s^{\neq}$ for the formation of hydroxyl radicals with the participation of divadate turned out to be 24.8 kcal mol^{-1}, which is noticeably less than that value (29.0 kcal mol^{-1}) for the process catalysed by monovanadate. The difference in these parameters is 4.2 kcal mol^{-1} and this corresponds to a ratio of rate constants of the order of 1200. Thus, the calculated data explain why the monovanadate ion is not active in a neutral medium. It should be noted that the observed activation energies for catalysis with monovanadate in the presence of acid and complex **A** without acid addition are very close (22 ± 2 kcal mol^{-1}). This value is larger than the parameter measured for the H_2O_2/VO_3^-/PCA system (17 ± 2 kcal mol^{-1}). The $\Delta G_s^{\neq}$ values calculated by the DFT method are 19.8 kcal mol^{-1} (*cf.* $E_a = 67$–81 kJ mol^{-1} calculated by Bell *et al.*) and 24.8 kcal mol^{-1}, respectively. Thus, it can be seen that the calculated parameters agree well with the experimental data. The following conclusion can be made: unlike monovanadate, in the case of polyvanadate, there can be ways of an energetically more-favourable transfer of hydrogen to the oxo-ligand in a rate-limiting stage. Moreover, the adjacent second vanadium-containing fragment plays the role of a stabiliser of key transition states due to the formation of six-membered dimetallic structures (the middle structure in equation B).

Gushchin *et al.* recently[17,18] found high activity of complexes **1–4** shown in Scheme 4.3 in oxidation of hydrocarbons with peroxides.

The chloride complexes **1** and **2** shown in Scheme 4.3, exhibited a high catalytic activity in the oxidation of alkanes with hydrogen peroxide in an acetonitrile solution. For example, stirring at 20 C a solution of **2** ($5 \cdot 10^{-4}$ M), cyclohexane (0.46 M), H_2O_2 (aqueous, 2 M) after 150 h gave 0.011 M of cyclohexanone and 0.041 M of cyclohexanol (analysis after the reduction of the solution with PPh_3). An analogous reaction catalysed by complex **1** ($5 \cdot 10^{-4}$ M; Scheme 4.3) afforded cyclohexanone (0.015 M) and cyclohexanol (0.12 M). At higher temperature (40 C) the reactions proceeded faster. After 6 h, yields of cyclohexanone and cyclohexanol were 0.01 M and 0.112 M, respectively, in the case of catalyst **2** (Scheme 4.3). Complex **1** (Scheme 4.3) turned out to be more efficient, affording 0.02 M and 0.16 M of cyclohexanone and cyclohexanol, respectively, after the reduction of the solution with PPh_3 (compare Figures 4.4 and 4.5). This activity is comparable with that

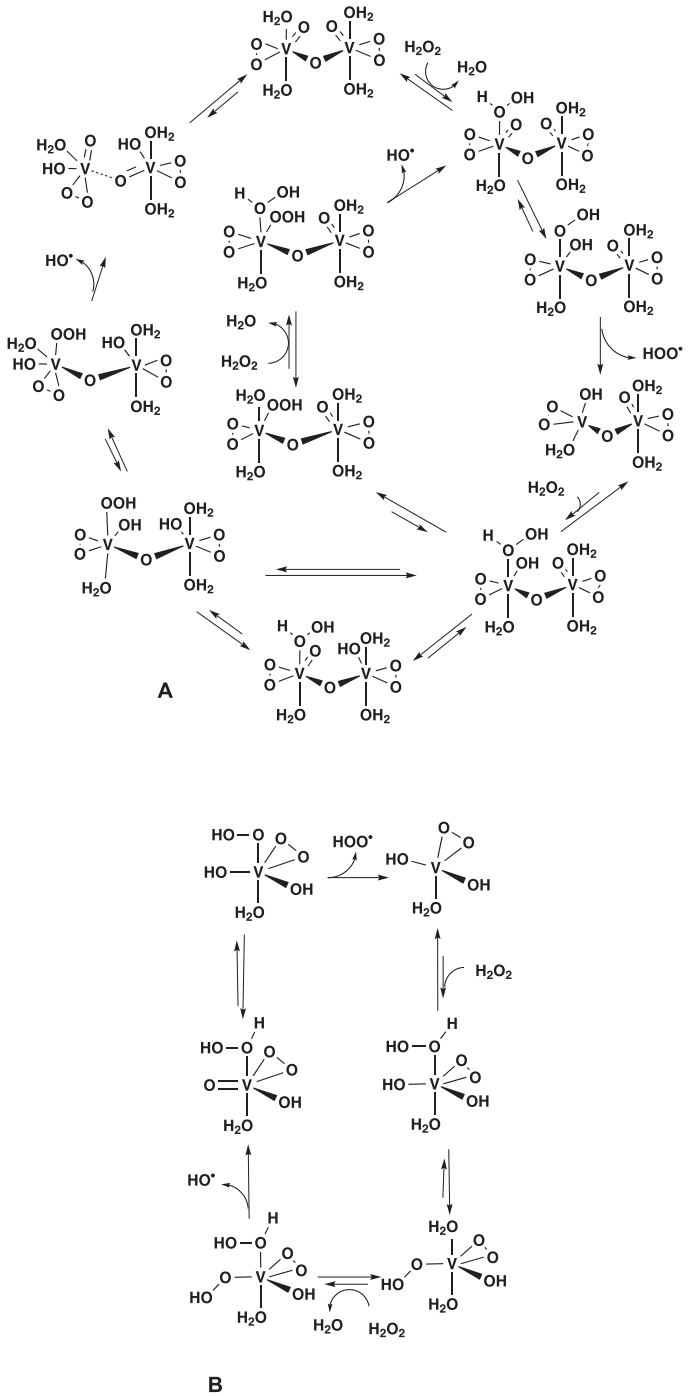

Figure 4.11 Catalytic cycles of radical generation involving divanadate (A) and monovanadate (B).
Reproduced from ref. 16 with permission from Elsevier, Copyright 2009.

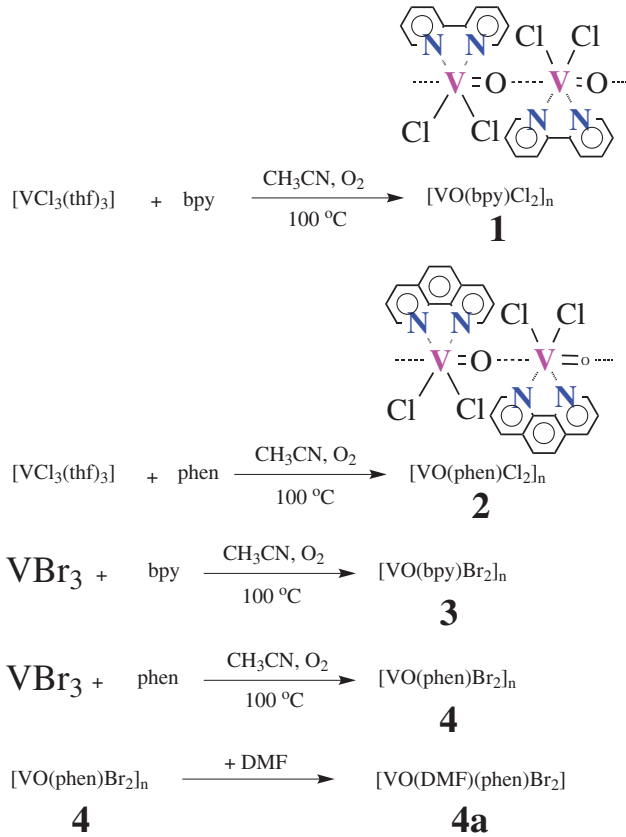

Scheme 4.3 Preparation of certain vanadium complexes.[17,18] Reproduced from ref. 18, https://doi.org/10.3390/catal9030217, under the terms of the CC BY 4.0 licence, https://creativecommons.org/licenses/by/4.0/.

found previously for the other vanadium complexes in the alkane oxidations with peroxides.[19–38] The oxidation reactions catalysed by compound **2** (Scheme 4.3) have been studied in more detail. Figure 4.12 clearly demonstrates that reduction of the reaction solution with PPh_3 gives rise to a higher concentration of cyclohexanol and a decrease of cyclohexanone concentration (compare Graphs A and B). These changes indicate alkyl hydroperoxides are formed in the course of the oxidation (the so-called Shul'pin method (see Figure 4.12).[39–53]

The selectivity parameters for the oxidation of certain alkanes catalysed by complexes **1–4** are summarised in Table 4.1. The parameters measured in the oxidation of linear and branched alkanes are close to the parameters typical for the reactions of alkanes with hydroxyl radicals.[54,55] Taking this fact into account, we can consider the simplest scheme of the concurrent oxidation by involving eqn (4.23) and (4.24).

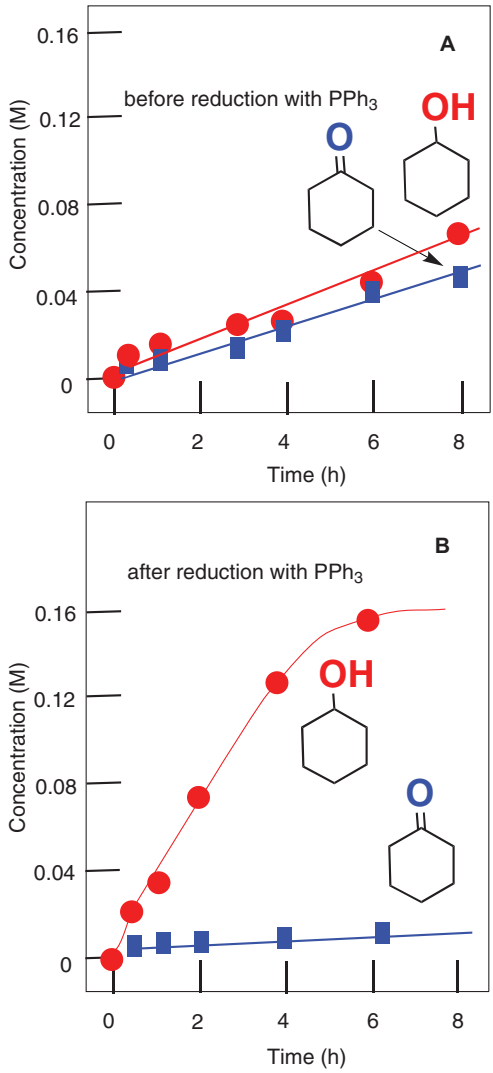

Figure 4.12 Accumulation of cyclohexanol and cyclohexanone in the oxidation of cyclohexane (0.46 M) with H_2O_2 (2.0 M) catalysed by complex (Scheme 4.3) (5×10^{-4} M) at 40 °C. Concentrations of products were measured by GC before (Graph A) and after (Graph B) the reduction of the reaction sample with solid PPh_3.
Reproduced from ref. 18, https://doi.org/10.3390/catal9030217, under the terms of the CC BY 4.0 licence, https://creativecommons.org/licenses/by/4.0/.

The oxygenation of *cis*-1,2-dimethylcyclohexane with H_2O_2 catalysed by complex **3** (Scheme 4.3) gave the corresponding isomeric tertiary alcohols in a *trans*/*cis* ratio of 0.8 (Table 4.1). These data as well as the character of dependence of the initial cyclohexane oxidation rate on the initial hydrocarbon

Table 4.1 Selectivity parameters for the oxidation of certain alkanes with H_2O_2. Reproduced from ref. 55 with permission from Elsevier, 2017.

n-Heptane			Methylcyclohexane	1,2-*cis*-DMCH
Entry	Catalyst	C(1) : C(2) : C(3) : C(4)	1 : 2 : 3	*trans*/*cis*
1	**1**	1.0 : 5.6 : 5.6 : 5.2	1.0 : 5.3 : 17.5	0.7
2	**2**	1.0 : 5.6 : 5.8 : 5.2	1.0 : 5.9 : 16.0	0.84
3	**3**	1.0 : 5.7 : 6.2 : 5.6	1.0 : 5.0 : 12.6	0.8
4	**4**	1.0 : 5.9 : 6.2 : 5.9	1.0 : 5.4 : 12.9	0.9

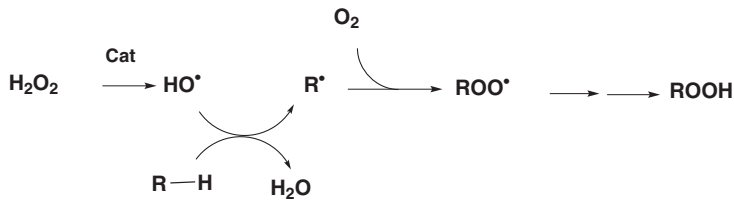

Scheme 4.4 A radical mechanism of the alkane oxidation with H_2O_2.

concentration (approaching a plateau at $[\text{Cyclohexane}]_0 > 0.3$ M) indicate that the reaction occurs with the participation of hydroxyl radicals, and alkyl hydroperoxides are formed as the main primary products.

Let us consider the simplest scheme of the concurrent oxidation of the alkane and acetonitrile solvent:

$$H_2O_2 + \text{Cat} \rightarrow HO^\bullet \quad W_i$$

$$HO^\bullet + RH \rightarrow R^\bullet \rightarrow \rightarrow \text{ ROOH} \quad k_1 \tag{4.23}$$

$$HO^\bullet + CH_3CN \rightarrow \rightarrow \text{ products} \quad k_2 \tag{4.24}$$

Here W_i is the rate of generation of hydroxyl radicals formed in the process of catalytic H_2O_2 decomposition; eqn (4.23) and (4.24) are transformations of RH into ROOH and CH_3CN into products and rate-limiting steps are interaction of $HO^\bullet$ with RH (k_1) and CH_3CN (k_2), respectively.

Assuming that the concentration of hydroxyl radicals is quasi-stationary during the reaction, we can obtain the term for the initial rate of ROOH formation as:

$$\frac{[RH]}{\left(\frac{d[ROOH]}{dt}\right)_0} = \left(\frac{k_2}{k_1}[CH_3CN] + [RH]\right)\frac{1}{W_i} \tag{4.25}$$

In the case of the alkane oxidation catalysed by the simple vanadate, the reactions in the presence of some vanadium complexes do not require the addition of PCA. Moreover, when PCA was added, the initial reaction rate was halved.

Theoretical DFT calculations have been performed for the monomeric form of the catalyst **II** (Schemes 4.4 and 4.5). In accord with experimental kinetic,

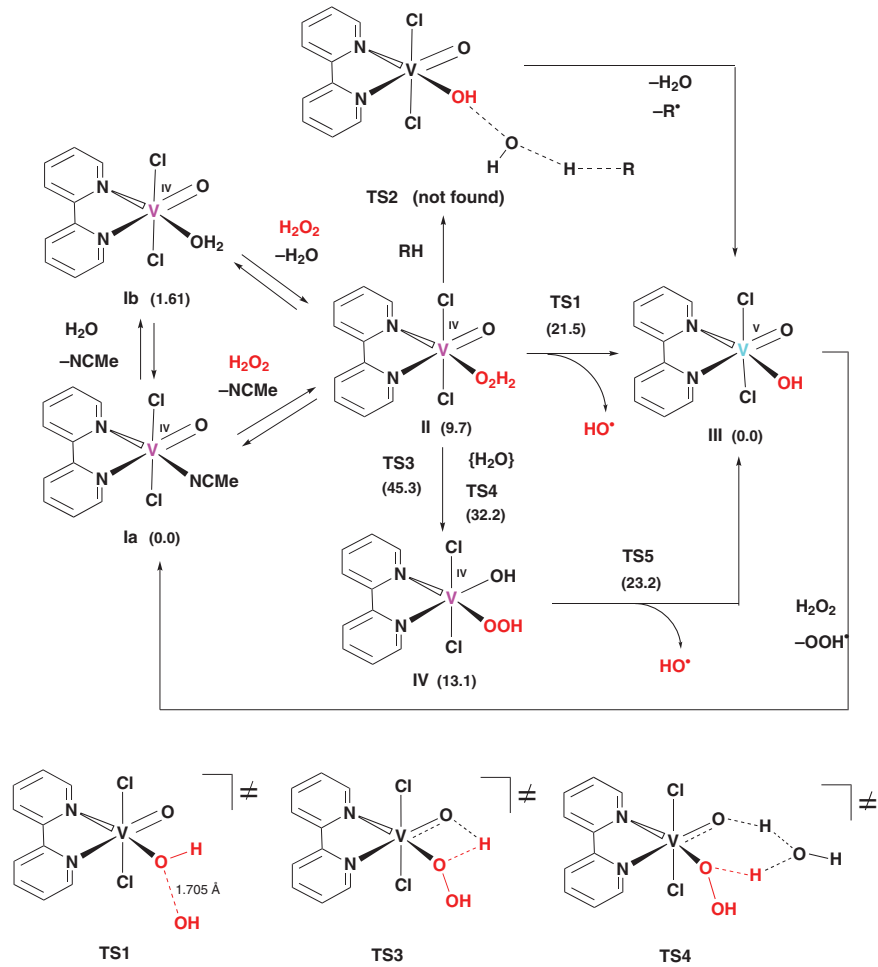

Scheme 4.5 The mechanism of the HO• generation from H_2O_2 catalysed by **I** (Gibbs free energies are indicated in parentheses relative to **Ia** in kcal mol^{-1}). Reproduced from ref. 18, https://doi.org/10.3390/catal9030217, under the terms of the CC BY 4.0 licence, https://creativecommons.org/licenses/by/4.0/.

selectivity and radical trap data, the global reaction mechanism is radical involving the generation of the HO• species which then oxidize alkane molecules RH to give, upon hydrogen abstraction, the corresponding alkyl radicals R• (Scheme 4.4). The latter react with molecular oxygen producing the alkylperoxo radicals ROO• and then the corresponding alkyl hydroperoxide ROOH experimentally detected by GS-MS. In accord with kinetic studies, the rate-limiting step of the whole process is the generation of the HO• radicals.

A mechanism has been proposed for the generation of hydroxyl radical (see Scheme 4.5). In the presence of hydrogen peroxide, the acetonitrile or water ligands in **I** may be replaced for H_2O_2 to give $[V(=O)(bpy)(H_2O_2)Cl_2]$ (**II**)

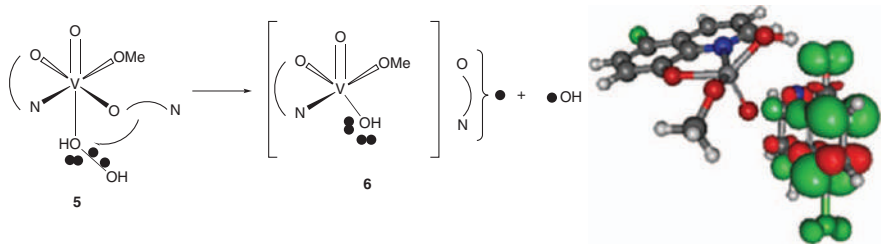

Scheme 4.6 Cleavage of the HO–OH bond and intramolecular electron transfer in a vanadium complex (left) **5** and spin density distribution in structure **6** (right).
Adapted from ref. 56 with permission from American Chemical Society, Copyright 2005.

(Scheme 4.5). Such a substitution is endoergonic by 8.1–9.7 kcal mol^{-1}. Coordination of H_2O_2 to the V(IV) centre tremendously activates this molecule towards the O–O homolysis. Indeed, energy of the homolytic O–O bond cleavage in **II** leading to **III** and HO$^{\bullet}$ is −9.7 kcal mol indicating that this process is exoergonic. Meanwhile, the activation barrier for the HO$^{\bullet}$ generation from **II** *via* TS1 is 11.8 kcal mol^{-1}. The overall activation barrier of the HO$^{\bullet}$ formation relative to the most stable complex **Ia** is 21.5 kcal mol^{-1} in terms of $\Delta G^{\neq}$ and 19.6 kcal mol^{-1} in terms of $\Delta H^{\neq}$. The latter value is in a good agreement with the experimentally obtained activation energy for this reaction catalysed by **I** (20.2 ± 2 kcal mol^{-1}).

Machura, Kuznetsov *et al.*,[56] described the alkane oxidation of inert alkanes to alkyl hydroperoxides by H_2O_2 catalysed with monomeric oxovanadium(V) complexes with non-innocent 8-hydroxyquinoline derivatives VO(OMe)(N–O)$_2$ (where N–O is nitro or chloro substituted quinolin-8-olate) (Scheme 4.6 and Figure 4.13).

4.3 Conclusions

Vanadium complexes are promising catalytic systems. Some exhibit catalytic activity in the oxidation of hydrocarbons and alcohols with hydrogen peroxide. The oxidising system consisting of a simple vanadate anion ($VO3^-$), 2-pyrazinecarboxylic acid (PCA) and hydrogen peroxide is especially attractive. Acetonitrile most often serves as solvent, but water can also be used. This is an effective system and was first described in 1993. It is also cheap and environment-friendly. The addition of PCA to a solution containing a vanadate anion significantly accelerates the oxidation reactions through decomposition of H_2O_2, which is confirmed by DFT calculations. Kinetic studies have shown that the reaction mechanism consists in breaking the O–O bond with the formation of a hydroxyl radical that attacks the substrate. The alkyl hydroperoxides resulting from the oxidation of alkanes is partially decomposed, giving a mixture of their corresponding ketones and alcohols. Under the action of triphenylphosphine, the alkyl hydroperoxides are transformed into alcohols.

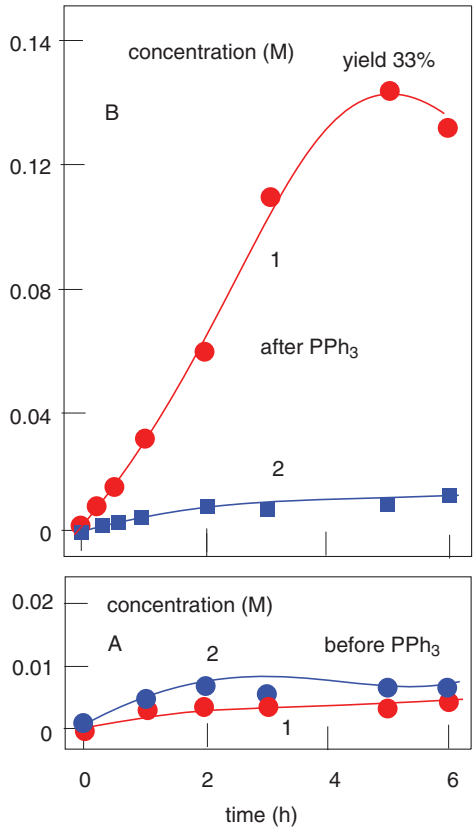

Figure 4.13 Oxidation of cyclohexane (0.46 M) with H_2O_2 (50%, 2 M) catalysed by complex **5** (2×10^{-4} M) at 40 °C. Concentrations of cyclohexanol (curves 1) and cyclohexanone (curves 2) were measured both before and after reduction with PPh_3.
Adapted from ref. 56 with permission from American Chemical Society, Copyright 2005.

Acknowledgements

The publication of this chapter was prepared with the support of RUDN University Program 5–100 and funded by RFBR according to Research Project 19-03-00142. This work was performed within the framework of the Program of Fundamental Research of the Russian Academy of Sciences for 2013–2020 on the research issue of IChP RAS No. 47.16. Theme number in Federal Agency for Scientific Organizations: 0082-2014-0004. State registration number of Center of Information Technologies and Systems for Executive Power Authorities (CITIS): AAAA-A17-117040610283-3. The authors thank the A. N. Nesmeyanov Institute (INEOS RAS) for the support, and particularly Dr Y. N. Kozlov, Dr A. N. Bilyachenko and Prof. D. Mandelli for their help in preparation of this chapter.

References

1. *Alkane Functionalization*, ed. A. J. L. Pombeiro and M. F. C. Guedes da Silva, J. Wiley & Sons, Hoboken, NJ, USA, (ISBN: 9781119378808), 2019.
2. (a) J. A. L. da Silva, J. J. R. Frausto da Silva and A. J. L. Pombeiro, *Coord. Chem. Rev.*, 2011, **255**, 2232–2248; (b) M. Sutradhar, L. M. D. R. S. Martins, M. F. C. Guedes da Silva and A. J. L. Pombeiro, *Coord. Chem. Rev.*, 2015, **301–302**, 200–239.
3. N. Xing, H. Shan, H.-Y. Zhao and Y.-H. Xing, *J. Coord. Chem.*, 2012, **65**(5), 898–910.
4. T. F. S. Silva, T. C. O. Mac Leod, L. M. D. R. S. Martins, M. F. C. Guedes da Silva, M. A. Schiavon and A. J. L. Pombeiro, *J. Mol. Catal. A: Chem.*, 2013, **367**, 52–60.
5. Y. Tanabe and Y. Nishibayashi, *Coord. Chem. Rev.*, 2019, **381**, 135–150.
6. M. R. Maurya, A. Arya, P. Adao and J. Costa Pessoa, *Appl. Catal., A*, 2008, **351**, 239–252.
7. A. Pappalardo, R. Puglisi and G. T. Sfrazzetto, *Catalysts*, 2019, **9**, 630.
8. R. A. Sheldon, *Green Chem.*, 2005, **7**, 267.
9. G. Duca, *Homogeneous Catalysis with Metal Complexes: Fundamentals and Applications*, Springer, Berlin, Heidelberg, 2012, p. 478.
10. G. Duca, Y. Skurlatov and A. Sychev, *Redox Catalysis and Ecological Chemistry*, CEP USM, Chisinau, 2002, p. 316.
11. G. B. Shul'pin, Metal-catalyzed Oxidation of C–H Compounds with Peroxides in Unconventional Solvents, in *Frontiers of Green Catalytic Selective Oxidation*, ed. K. P. Bryliakov, *Series Green Chemistry and Sustainable Technology*, Springer Nature, Singapore Pte Ltd. **ch. 1**, 2019, pp. 1–35.
12. G. B. Shul'pin, Thesis, Semenov Institute of Chemical Physics, Moscow, 2013.
13. M. Sutradhar, N. V. Shvydkiy, M. F. C. G. da Silva, M. V. Kirillova, Y. N. Kozlov, A. J. L Pombeiro and G. B. Shul'pin, *Dalton Trans.*, 2013, **42**, 11791–11803.
14. R. Z. Khaliullin, A. T. Bell and M. Head-Gordon, *J. Phys. Chem. B*, 2005, **109**, 17984–17992.
15. E. V. Gusevskaya, L. Menini, L. A. Parreira, R. A. Mesquita, Y. N. Kozlov and G. B. Shul'pin, *J. Mol. Catal. A: Chem.*, 2012, **363–364**, 140–147.
16. M. V. Kirillova, M. L. Kuznetsov, V. B. Romakh, L. S. Shul'pina, J. J. R. Fraústo da Silva, A. J. L. Pombeiro and G. B. Shul'pin, *J. Catal.*, 2009, **267**, 140–157.
17. I. S. Fomenko, A. L Gushchin, L. S. Shul'pina, N. S. Ikonnikov, P. A. Abramov, N. F. Romashev, A. S. Poryvaev, A. M. Sheveleva, A. S. Bogomyakov, N. Y. Shmelev, M. V. Fedin, G. B. Shul'pin and M. N. Sokolov, *New J. Chem.*, 2018, **42**, 16200–16210.

18. I. S. Fomenko, A. L. Gushchin, P. A. Abramov, M. N. Sokolov, L. S. Shul'pina, N. S. Ikonnikov, M. L. Kuznetsov, A. J. L. Pombeiro, Y. N. Kozlov and G. B. Shul'pin, *Catalysts*, 2019, **9**, 217.
19. G. B. Shul'pin, D. Attanasio and L. Suber, *J. Catal.*, 1993, **142**, 147–152.
20. G. B. Shul'pin, D. Attanasio and L. Suber, *Russ. Chem. Bull.*, 1993, **42**, 55–59.
21. G. B. Shul'pin, A. N. Druzhinina and G. V. Nizova, *Russ. Chem. Bull.*, 1993, **42**, 1327–1329.
22. G. V. Nizova and G. B. Shul'pin, *Russ. Chem. Bull.*, 1994, **43**, 1146–1148.
23. G. B. Shul'pin and G. Süss-Fink, *J. Chem. Soc., Perkin Trans. 2*, 1995, 1459–1463.
24. G. B. Shul'pin, R. S. Drago and M. Gonzalez, *Russ. Chem. Bull.*, 1996, **45**, 2386–2388.
25. G. B. Shul'pin, M. C. Guerreiro and U. Schuchardt, *Tetrahedron*, 1996, **52**, 13051–13062.
26. M. C. Guerreiro, U. Schuchardt and G. B. Shul'pin, *Russ. Chem. Bull.*, 1997, **46**, 749–754.
27. G. V. Nizova, G. Süss-Fink and G. B. Shul'pin, *Tetrahedron*, 1997, **53**, 3603–3614.
28. U. Schuchardt, M. C. Guerreiro and G. B. Shul'pin, *Russ. Chem. Bull.*, 1998, **47**, 247–252.
29. G. Süss-Fink, G. V. Nizova, S. Stanislas and G. B. Shul'pin, *J. Mol. Catal. A: Chem.*, 1998, **130**, 163–170.
30. G. B. Shul'pin, Y. Ishii, S. Sakaguchi and T. Iwahama, *Russ. Chem. Bull.*, 1999, **48**, 887–890.
31. G. Süss-Fink, S. Stanislas, G. B. Shul'pin, G. V. Nizova, H. Stoeckli-Evans, A. Neels, C. Bobillier and S. Claude, *J. Chem. Soc., Dalton Trans.*, 1999, **18**, 3169–3175.
32. G. B. Shul'pin, Y. N. Kozlov, G. V. Nizova, G. Süss-Fink, S. Stanislas, A. Kitaygorodskiy and V. S. Kulikova, *J. Chem. Soc., Perkin Trans. 2*, 2001, **8**, 1351–1371.
33. M. H. C. De la Cruz, Y. N. Kozlov, E. R. Lachter and G. B. Shul'pin, *New J. Chem.*, 2003, **27**, 634–638.
34. G. B. Shul'pin and Y. N. Kozlov, *Org. Biomol. Chem.*, 2003, **1**, 2303–2306.
35. L. G. Cuervo, Y. N. Kozlov, G. Süss-Fink and G. B. Shul'pin, *J. Mol. Catal. A: Chem.*, 2004, **218**, 171–177.
36. Y. N. Kozlov, G. V. Nizova and G. B. Shul'pin, *J. Mol. Catal. A: Chem.*, 2005, **227**, 247–253.
37. M. J. D. M Jannini, L. S. Shul'pina, U. Schuchardt and G. B. Shul'pin, *Petroleum Chem.*, 2005, **45**, 413–418.
38. Y. N. Kozlov, V. B. Romakh, A. Kitaygorodskiy, P. Buglyó, G. Süss-Fink and G. B. Shul'pin, *J. Phys. Chem. A*, 2007, **111**, 7736–7752.
39. G. B. Shul'pin and A. N. Druzhinina, *React. Kinet. Catal. Lett.*, 1992, **47**, 207–211.
40. G. B. Shul'pin and Nizova, *React. Kinet. Catal. Lett.*, 1992, **48**, 333–338.
41. G. B. Shul'pin, *J. Mol. Catal, A: Chem.*, 2002, **189**, 39–66.

42. G. B. Shul'pin, *C. R. Chim*, 2003, **6**, 163–178.
43. G. B. Shul'pin, Y. N. Kozlov, L. S. Shul'pina, A. R. Kudinov and D. Mandelli, *Inorg. Chem.*, 2009, **48**, 10480–10482.
44. G. B. Shul'pin, Y. N. Kozlov, L. S. Shul'pina and P. V. Petrovskiy, *Appl. Organometal. Chem.*, 2010, **24**, 464–472.
45. P. P. Knops-Gerrits, C. A. Trujillo, B. Z. Zhan, X. Y. Li, P. Rouxhet and P. A. Jacobs, *Top. Catal.*, 1996, **3**, 437–449.
46. E. Fornal and C. Giannotti, *Photochem. Photobiol. A: Chem.*, 2007, **188**, 279–286.
47. G. B. Shul'pin, *Mini-Rev. Org. Chem.*, 2009, **6**, 95–104.
48. G. B. Shul'pin, *Org. Biomol. Chem.*, 2010, **8**, 4217–4228.
49. G. B. Shul'pin, *Dalton Trans.*, 2013, **42**, 12794–12818.
50. G. B. Shul'pin, *Catalysts*, 2016, **6**, 50.
51. G. Olivo, O. Lanzalunga and S. Di Stefano, *Adv. Synth. Catal.*, 2016, **358**, 843–863.
52. I. Garcia-Bosch and M. A. Siegel, *Angew. Chem. Int. Ed.*, 2016, **55**(41), 12873–12876.
53. A. L. Maksimov, Y. S. Kardasheva, V. V. Predeina, M. V. Kluev, D. N. Ramazanov, M. Y. Talanova and E. A. Karakhanov, *Petroleum Chem.*, 2012, **52**(5), 318–326.
54. D. S. Nesterov, E. N. Chygorin, V. N. Kokozay, V. V. Bon, R. Boča, Y. N. Kozlov, L. S. Shul'pina, J. Jezierska, A. Ozarowski, A. J. L. Pombeiro and G. B. Shul'pin, *Inorg. Chem.*, 2012, **51**(16), 9110–9122.
55. G. B. Shul'pin, D. S. Nesterov, L. S. Shul'pina and A. J. L. Pombeiro, *Inorg. Chim. Acta*, 2017, **455**, 666–676.
56. I. Gryca, K. Czerwińska, B. Machura, A. Chrobok, L. S. Shul'pina, M. L. Kuznetsov, D. S. Nesterov, Y. N. Kozlov, A. J. L. Pombeiro, I. A. Varyan and G. B. Shul'pin, *Inorg. Chem.*, 2018, **57**, 1824–1839.

CHAPTER 5

Peroxo-vanadium Complexes as Sustainable Catalysts in Oxidations, Halogenations and Other Organic Transformations

F. SABUZI,[a] G. POMARICO,[b] V. CONTE[a] AND P. GALLONI*[a]

[a] Department of Chemical Science and Technologies, University of Rome Tor Vergata, Via della Ricerca Scientifica snc, 00133 Rome, Italy; [b] Department of Molecular and Translational Medicine, University of Brescia, Viale Europa, 11 – 25123 Brescia, Italy
*Email: galloni@scienze.uniroma2.it

5.1 Introduction

Peroxides are powerful tools to perform the oxidation of organic and inorganic substrates under mild conditions and with significant yields and high selectivity.[1–3] Hydrogen peroxide, organic peracids and alkyl hydroperoxides are the most exploited sources of peroxides.[4] Regrettably, the cheapness and low toxicity of H_2O_2 are counterbalanced by its weak oxidising power. Vanadium, as well as other transition metals in high oxidation state, is able to activate H_2O_2, raising its oxidising strength[5] and making more feasible its exploitation. The general working scheme of oxidation by peroxide is shown in Scheme 5.1.

Vanadium derivatives containing an oxido moiety such as V^{+4} ($[V^{IV}O]$), V^{+5} ($[V^{V}O]$ or $[V^{V}O_2]$) are exploited in different fields, such as biology,[6,7]

Catalysis Series No. 41
Vanadium Catalysis
Edited by Manas Sutradhar, José Armando L. da Silva and Armando J. L. Pombeiro

Published by the Royal Society of Chemistry, www.rsc.org

Scheme 5.1 General scheme of oxidation reactions with peroxides.

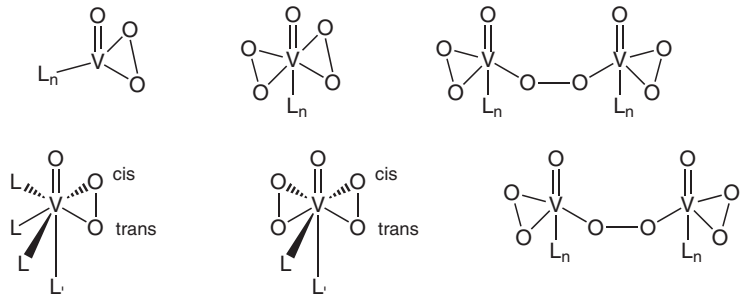

Figure 5.1 Different coordination modes for peroxo-complexes.[21]

pharmacology[8,9] and catalysis.[10–13] For the latter application, the most reactive species entails vanadium d^0 containing one or more peroxide units; bi- or poly-metallic complexes can also be prepared, with the O_2^{2-} bridging two metal atoms. Many of these compounds have been characterised in solution and in the solid state.[14,15] UV–vis, IR, ^{51}V NMR and electrochemical data provide data on the nature of the complexes in terms of number of peroxide units, geometry and the oxidation state of the central metal.[16–20]

The most common V-derivatives have one or two peroxide groups, namely oxidoperoxidovanadium(v) and oxidodiperoxidovanadium(v) complexes. The preferred geometry is triangular bidentate, and, when the central metal binds one or two peroxides, they are located on an equatorial plane with respect to the oxido ligand. Consequently, the corresponding geometrical arrangement of the molecule is pentagonal bipyramidal (Figure 5.1).

The acidity of the medium plays a fundamental role in the insertion of one or two peroxide groups. In solution, the formation of peroxido complexes is pH-dependent: at pH = 1 the monoperoxido derivatives are exclusively obtained, while lowering the acidity leads to an equilibrium between monoperoxido and diperoxido derivatives.

In this chapter, the role of peroxido-vanadium complexes as catalysts in promoting sustainable organic transformation is discussed.

5.2 Oxidation

Vanadium peroxido-complexes in their high oxidation state are widely used in catalytic oxidation reactions, and their use is considered one of the most promising alternatives to traditional methods.[20,22–24] In fact, conventional approaches involving stoichiometric amounts of toxic and heavy metal-based oxidants, like dichromate or permanganate, have to be stopped, making space for sustainable catalytic pathways. Therefore, clean synthetic methodologies,

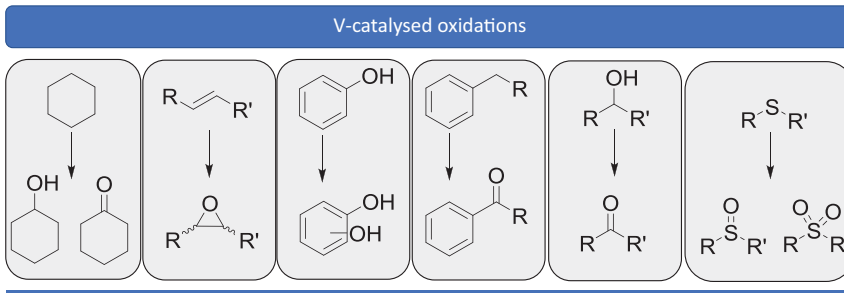

Figure 5.2 Examples of oxidation reactions of organic substrates catalysed by V-peroxocomplexes.

high atom economy and low E-factor are the key notions for developing new, appealing and easily scalable oxidative processes. To this purpose, molecular oxygen is extensively adopted at the industrial level as a clean primary oxidant, nevertheless, oxidation processes using H_2O_2 are also widespread. Oxidations performed with hydrogen peroxide properly respect *green chemistry* requirements, *i.e.*, characterised by a very high atom economy and safety of use. Moreover, water is the only by-product, thus the generation of harmful or difficult-to-dispose wastes is prevented. However, in order to be adopted in oxidation processes, peroxides need activation. Various vanadium complexes have been synthesised over the past few decades and some resulted in suitable species to activate H_2O_2, as well as other peroxides. In the presence of ROOH species, vanadium-peroxo complexes form in solution[11,18,21,25] and have been widely used as effective oxidants in the selective oxidation of different substrates, like saturated, unsaturated and aromatic hydrocarbons, alcohols and phenols, sulphides, bromides and other substrates, usually leading to high added-value compounds, which is interesting from a synthetic, industrial and pharmaceutical point of view (Figure 5.2).[11,20,22–24,26]

5.2.1 Oxidation of Hydrocarbons

Several systems have been proposed to perform sustainable alkanes oxidation using vanadium-based catalysts. In particular, V-oxido and dioxido complexes, in the presence of different peroxides (H_2O_2, benzoyl peroxide, *tert*-butyl hydroperoxide or *m*-chloroperbenzoic acid) and acid promoters (*i.e.*, HNO_3, H_2SO_4 or organic acids like 2-pyrazinecarboxylic or oxalic acid) have been adopted to oxidize model substrates such as cyclohexane, cyclopentane or adamantane to their corresponding alcohols or ketones.[20,24,27] In the reaction conditions, alkanes oxidation generally occurs through a radical pathway, in which $RO^{\bullet}$ and $ROO^{\bullet}$ radicals are involved. Reactions are usually performed in CH_3CN and proceed with high-turnover frequencies, in mild conditions. Notably, the use of H_2O_2 instead of other peroxides is preferred for the sake of atom economy. Moreover, commercially available V(v) salts or simple V-complexes (such as vanadyl acetylacetonate, or V-complexes with

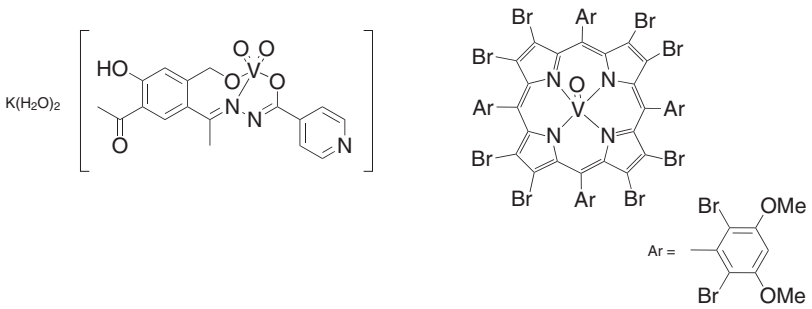

Figure 5.3 Recent examples of V-complexes adopted in the epoxidation on alkenes.[28,29]

picolinate-based ligands) constitute readily available and efficient alternatives to more sophisticated synthetic complexes.[21]

A number of mono-nuclear and di-nuclear vanadium complexes have also been studied as catalysts in the selective epoxidation of different alkenes (Figure 5.3).[28,29]

Reactions proceed with good yields and high selectivity in mild conditions, mainly using acetonitrile as the solvent. Interestingly, in some examples, even better yields and shorter reaction times can be achieved performing the reaction in water–ionic liquid biphasic systems rather than the organic solvent.[30] It has been observed that by raising the temperature, good results can be achieved in solvent-free conditions. Several studies have been carried out, in conjunction with DFT calculations, to understand the mechanism of such reactions, but different pathways have been proposed to justify experimental results.[11]

Likewise, the stereoselective epoxidation of allylic alcohols can been attained using vanadium peroxo-complexes. With these substrates, chiral epoxides can be obtained, which are fundamental building blocks in the synthesis of important biologically active compounds.[20,22]

Among others, oxidation of arenes constitute a challenging process in organic synthesis as the reaction leads to the formation of largely used products for industrial applications. For example, obtaining phenol from benzene through sustainable oxidative procedures is attracting the interest of several research groups involved in vanadium chemistry (Figure 5.4). Hence, suitable V-based catalysts have been developed to selectively hydroxylate benzene in mild conditions.

Similarly, hydroxylation of anisole and ethylbenzene can be achieved. Notably, in appropriate conditions, toluene and ethylbenzene oxidation can occur at the benzylic position, leading to benzaldehyde and acetophenone, respectively, as the main valuable products.[20,33]

5.2.2 Alcohols Oxidation

V(v)-oxido and dioxido complexes resulted as highly effective in the sustainable oxidation of primary and secondary alcohols with O_2 in aqueous

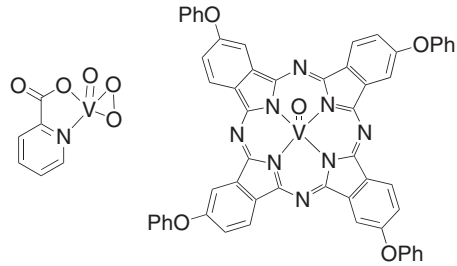

Figure 5.4 Examples of V-complexes adopted in the hydroxylation of aromatics.[24,31,32]

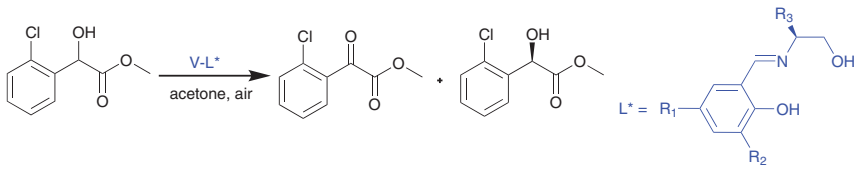

Scheme 5.2 Oxidation of an α-hydroxyesters catalysed by a V-complex.

media. Reactions lead to the formation of aldehydes or ketones, respectively, with high conversions and selectivities. The substrate scope is broad, and it can be extended to differently substituted benzylic, allylic and propargylic alcohols.[20,34] Moreover, selective phenol hydroxylation to catechol has been proposed using H_2O_2 as primary oxidant, with good yields.

The use of chiral catalysts resulted as strategic to perform the enantioselective oxidation of α-hydroxyketones and α-hydroxyesters, leading to the corresponding ketones, as well as to the kinetic resolution of racemic substrates (Scheme 5.2).

From an applicative point of view, much interest is devoted to the V-catalysed oxidation of natural sources, such as lignin. Oxidation of phenolic and non-phenolic lignin model compounds have been performed, and is generally accomplished with the oxidative cleavage of C–C bonds.[35–37] High conversions to interesting aromatic products can be achieved in moderately mild conditions (Scheme 5.3).

5.2.3 Sulphides Oxidation

Sulphides oxidation constitutes an appealing topic in organic chemistry, since the oxidised products, namely sulfoxides and/or sulfones, are important building blocks for several synthetic pathways.[22,38] Indeed, differently substituted alkyl–aryl or aromatic sulphides can be oxidised in mild conditions using V-based catalysts (Scheme 5.4).

Variegated catalysts with Schiff base ligands have been adopted to perform sulphide oxidation, eventually generating chiral sulfoxides.[20,22] Notably, chiral sulfoxides are relevant products in organic chemistry since they are

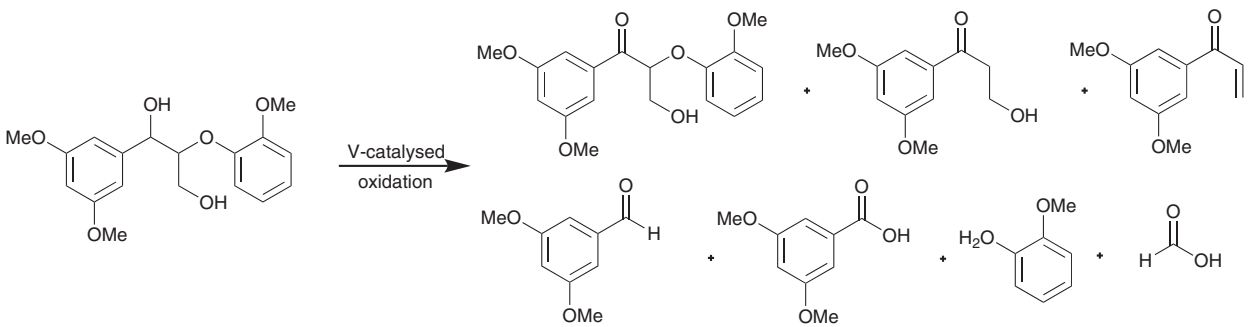

Scheme 5.3 Oxidation of a lignin model catalysed by V-based complexes.[36]

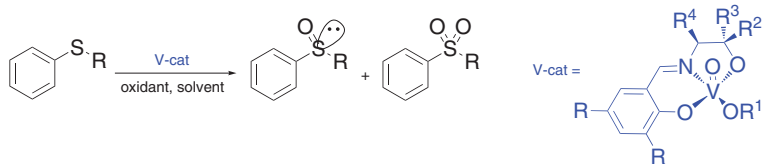

Scheme 5.4 General scheme of sulphide oxidation catalysed by V-based complexes.[22]

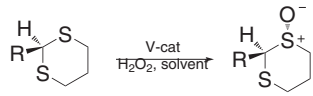

Scheme 5.5 V-catalysed sulfoxidation of a chiral dithiane.[20]

widely used as chiral auxiliary in asymmetric synthesis and, more importantly, they find application in different pharmaceutical fields. Similarly, the enantioselective oxidation of 1,3-dithianes (Scheme 5.5) can be performed using V-catalysts.[20]

Notably, aromatic sulphide oxidation constitutes a key step for a highly attractive topic, namely fuel desulfurization. In fact, over the past few decades, several catalytic systems, the majority based on vanadium complexes, have been proposed to selectively oxidize sulphides in model fuels.[23,26,30,39,40] The main advantage of this method is that the oxidised S-containing products can be easily removed from the fuel without altering the hydrocarbon compounds content. To this aim, vanadium peroxo- or oxo-hydroperoxo complexes with pyridine, hydrazine, Schiff bases, salen and salophen ligands have been proposed, in order to accomplish the conversion of model, difficult-to-oxidize, aromatic sulphides, such as dibenzothiophene and methyl-*p*-tolyl sulphide, to their corresponding sulfoxide and sulfone, with excellent results. In one of the most recent examples, oxidative fuel desulfurization was successfully performed in a three-phase system (fuel/H_2O_2/ionic liquid) using V^VO-salophen complexes.[40] With this method, the selective conversion of dibenzothiophene to the corresponding sulfone was achieved and the oxidised product could be readily extracted by the ionic liquid, thus immediately lowering the amount of sulphur in the fuel. The process could be also accelerated performing the reaction under microwave irradiation. Notably, control experiments performed in the presence of cyclooctene demonstrated that no alkene oxidation occurred in the experimental conditions; hence, the selective oxidation and removal of sulphur compounds from the fuel could be fruitfully achieved, without altering the double bond content.

5.3 Halogenation

5.3.1 General Mechanism of V-catalysed Halogenation

Exploitation of oxido-peroxido vanadium complexes for the halogenation of organic substrates started almost three decades ago.[41] However, these were mainly bromination reactions, since chlorination is usually carried out by enzymatic catalysis (by chloroperoxidses) or by different metal-based systems. Conversely, vanadium complexes are suitable for successfully mimicking the mode of action of bromoperoxidase, an enzyme containing a vanadium centre that converts bromide ion into an electrophilic ''Br^+'' species, which then functionalizes organic substrates. The halogen oxidation takes place by H_2O_2 as primary oxidant and a vanadium-based

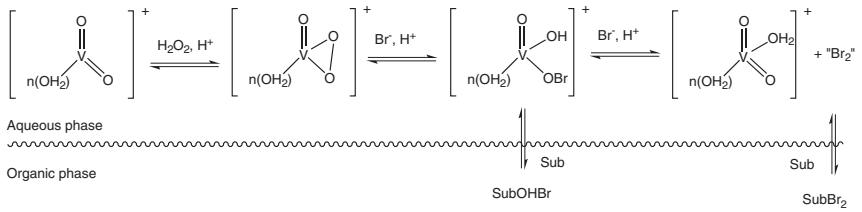

Scheme 5.6 Mechanism of the V-catalysed bromination of organic substrates.

catalyst, whose role into the catalytic cycle is to enhance the oxidising ability of H_2O_2. The active species is the oxido-peroxido vanadium (V) complexes formed in an acidic medium (pH = 1). Since that first paper, much research has been carried out to clarify the role of the variables involved, such as bromide source, reactants ratio, temperature, pH, mode of addition of H_2O_2, *etc.* The detailed mechanistic aspects, as shown in Scheme 5.6, can be found in several books and reviews.[11,24,26]

Since this synthetic approach exploits cheap and low- or non-toxic substances, vanadium-catalysed halogenation is considered a sustainable process and is in accordance with many of the 12 principles of green chemistry.[42]

5.3.2 Bromination of Aromatic Substrates

Catalysis operated by vanadium may be performed in homogeneous and heterogeneous systems. Many sustainable procedures for the bromination of a wide range of organic substrates have been reviewed.[43] Vanadium-based catalysts can be used as simple V-salt, coordinated to an organic ligand (Schiff base, macrocycle) or polymer-supported.

Recently, simple NH_4VO_3 has been used to promote the bromination of tetraphenylporphyrin derivatives.[44] In a biphasic CH_2Cl_2–aqueous system, accurate tuning of substrate-to-reactants ratio allowed to selectively obtain macrocycles functionalised onto the β-pyrrolic positions with a variable number of bromines, ranging from 1 to 8. In particular, porphyrins free base modified with 3 or 4 Br units and the Cu-complex of the fully β-brominated macrocycle have been obtained in satisfactory yields (**a–c**, Figure 5.5) with the advantage that the use of unsafe substances has been avoided. Vanadium complexes of two different tetraphenylporphyrin derivatives have been used as catalysts.[29] The authors investigated a planar macrocycle (**d**, Figure 5.5) and a distorted tetrapyrrole (**e**, Figure 5.5) where the deviation form planarity is induced by the bromines onto the peripheral positions.

The macrocycle confers a good efficiency to the metal centre, as highlighted by the high turnover frequency and the short reaction time, better than those of many other systems reported in the literature. A noticeable stability was observed since the catalyst can be recovered at the end of the reaction. The distortion of the macrocycle as well as the presence of electron-withdrawing groups enhances the catalytic ability of **e** making the oxidovanadium(IV) centre more electrophilic and, thus, facilitating the formation of the oxidoperoxido

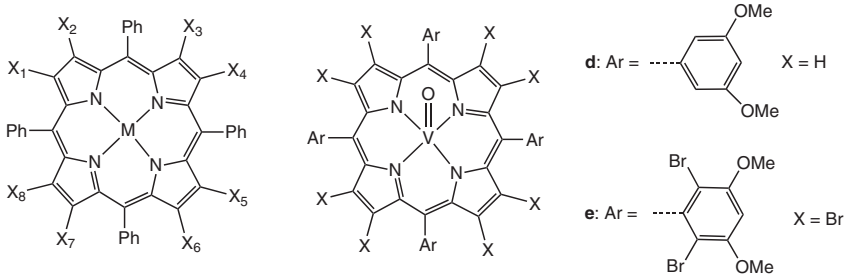

a: M = 2H, $X_{1,2,5}$ = Br; $X_{3,4,6,7,8}$ = H
b: M = 2H, $X_{1,2,5,6}$ = Br; $X_{3,4,7,8}$ = H
c: M = Cu, $X_{1\text{-}8}$ = Br

Figure 5.5 Examples of brominated porphyrins.

intermediate. As a result, it yielded >90% conversion in many attempts of bromination of activated phenol, *p*-cresol, salicylaldehyde and thymol.[43]

Particular emphasis has been devoted to the preparation of polydentate ligands. The presence of electron-withdrawing groups generally raises the Lewis acidity of the metal centre, while bulky substituents may drive the selectivity of the reaction. Many N- or O-based organic ligands structurally close each other and different numbers and/or positions of electron-active or bulky groups have been prepared. The catalytic activity of these complexes has usually been verified by performing the bromination of activated aromatics such as thymol or salicylaldehyde. A conversion rate higher than 80% is the common result and the major product is the expected monobrominated derivative. By changing the reaction conditions, a larger amount of polybrominated substances can be obtained. For example, Debnath *et al.*,[45] compared the performances of mononuclear (**f**, Figure 5.6) and di-nuclear (**g**, Figure 5.6) oxidovanadium complexes with amine-bis(phenolate) ligand for the bromination of salicylaldehyde that yielded the monobrominated species as a major product together with polyfunctionalised arylaldehydes in a minor extent.

Computational studies were performed to investigate the role of the active catalytic species. A three-step mechanism was conjectured where the first step is the formation of the side-on peroxido species, followed by oxidation of Br^- to HOBr and finally bromination of the substrate. O–O– bond-breaking was identified as the rate-determining step. Homobimetallic complexes were also investigated by Syiemlieh *et al.*,[46,47] who reported preparation of oxaloyldihydrazone, a hetero O–N–O ligand (**h**, Figure 5.6). The compounds were fully characterised by means of different techniques such as IR, UV–vis and ^{1}H and ^{13}C NMR. Analysis of the electrochemical behaviour by cyclic voltammetry highlighted the presence of different peaks for the redox processes involving any of the $V^{(IV)}/V^{(V)}$ centres. The complexes were also subjected to titration with HCl and the effects of the protonation observed by UV–vis spectroscopy. All the changes were reversible after back-titration with KOH, suggesting good stability of the catalyst under reaction conditions. A salicylaldehyde derivative was chosen as model substrate to

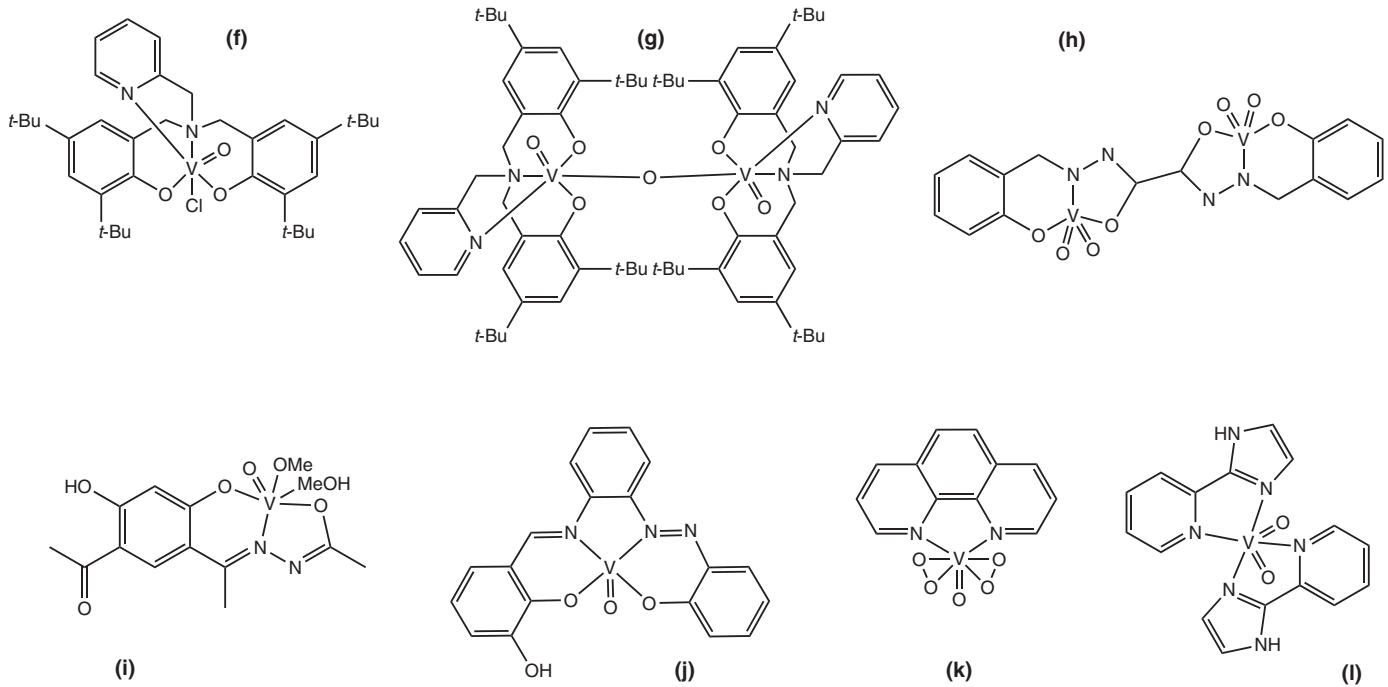

Figure 5.6 Structure of different oxidovanadium complexes adopted in the bromination of aromatic substrates.

prove the performance of the catalysts, which were compared to those of common V-based salts, with respect to which the synthesised catalyst yielded better results, with generally high conversion grade (over 80%) and quick reaction (30–60 minutes). Recently, Maurya[28] reported the preparation and exploitation of a resorcinol derivative (**i**, Figure 5.6) as ligand for V. Almost quantitative conversion has been reported for bromination of thymol rings and a large value for the dibrominated products have been obtained.

The electrochemical, catalytic and cytotoxic properties of aza-salophen ligands (**j**, Figure 5.6) have been described.[48] In the structure of these molecules there is a free –OH that is not involved in the transition-metal binding, *i.e.*, it is available for the interaction by hydrogen bond with the molecules approaching the catalytic site.

The ability of a simple phenanthroline ligand (**k**, Figure 5.6) to bind the transition metal has been investigated.[49] The characteristic IR signal of the V=O stretching around 970 cm^{-1} as well as the X-ray crystal structure confirmed the ligand chelation of the metal ion. This complex has been used for the bromination of phenol-red. The large colour variation occurring as a result of the bromination of phenol red (converted into the bromophenol blue) allows the use of this system as a colorimetric sensor for the detection of H_2O_2. Finally, the low-dissociation constant suggests the good stability of the complex. Another example of a nitrogen-based ligand has been described by Sun *et al.*[50] Many N,O heteroligands containing a pyridine or an imidazole moiety have been explored as building blocks for the preparation of coordinating systems; for this reason the authors speculated that a ligand containing both pyridine and imidazole heterocycles (**l**, Figure 5.6) could act as a good unit for vanadium coordination. The ability of this system to promote the bromination reaction was verified with the functionalization of activated rings such as phenol and aniline; depending on the substrate, mono- or poly-brominated rings were obtained within 30–120 minutes.

5.4 Supported V-peroxocomplexes

Numerous studies have emerged on the immobilization of metal catalysts on different solid supports, with the aim to generate new heterogeneous systems. The main goal of this approach is to combine the advantages of homogeneous and heterogeneous catalysis, thus creating efficient metal-based catalysts that can be easily recovered and reused after regeneration. Very different supports – like inorganic oxides[51,52] or organic polymers[13,53–56] – have been designed to immobilise homogeneous vanadium-complexes. Further catalytic studies have also been carried out, obtaining very encouraging results in the oxidation of various hydrocarbons, alcohols and sulphides, as well as in bromination reactions.

5.5 Conclusions

In this chapter, a brief overview of various V-peroxido-complexes has been presented. Sustainable catalytic halogenation and oxidation reactions have

been principally discussed, eventually highlighting the feasibility of such V-systems for fundamental applicative purposes.

References

1. *The Chemistry of Functional Groups, in Peroxides*, ed. S. Patai, Wiley, Chichester, 1983.
2. *Peroxide Chemistry. Mechanistic and Preparative Aspects of Oxygen Transfer*, ed. W. Adam, Wiley, Weinheim, 2000.
3. V. Conte and O. Bortolini, in *The Chemistry of Eroxides*, ed. and Z. Rappoport, Wiley Interscience, **vol. 2**, Part 1, 2006.
4. *Organic Peroxides*, ed. D. Swern, Wiley Interscience, New York, **vol. II**, 1971.
5. N. A. Milas and L. S. Malorey, *J. Am. Chem. Soc.*, 1940, **62**, 1841.
6. E. Kioseoglou, S. Petanidis, C. Gabriel and A. Salifoglou, *Coord. Chem. Rev.*, 2015, **301–302**, 87.
7. C. Rozzo, D. Sanna, E. Garribba, M. Serra, A. Cantara, G. Palmieri and M. Pisano, *J. Inorg. Biochem.*, 2017, **174**, 14.
8. D. Gambino, *Coord. Chem. Rev.*, 2011, **255**, 2193.
9. D. Rehder, *Future Med. Chem.*, 2012, **4**, 1823.
10. M. R. Maurya and J. Costa Pessoa, *J. Organomet. Chem.*, 2011, **696**, 244.
11. V. Conte, A. Coletti, B. Floris, G. Licini and C. Zonta, *Coord. Chem. Rev.*, 2011, **255**, 2165, and references cited therein.
12. J. A. L. da Silva, J. J. R. Fraústo da Silva and A. J. L. Pombeiro, *Coord. Chem. Rev.*, 2011, **255**, 2232.
13. J. Costa Pessoa and M. R. Maurya, *Inorg. Chim. Acta*, 2017, **455**, 415, and references cited therein.
14. N. J. Campbel, A. C. Dengel and W. P. Griffith, *Polyhedron*, 1989, **8**, 1379.
15. M. Bhattacharjee, S. K. Chettri, M. K. Chaudhuri, N. S. Islam and S. R. Barman, *J. Mol. Catal.*, 1993, **78**, 143.
16. J. Tatiersky, S. Pacigová, M. Sivák and P. Schwendt, *J. Arg. Chem. Soc.*, 2009, **97**, 181.
17. *Vanadium in Biological Systems*, ed. D. Rehder and N. D. Chasteen, Kluwer Academic Publishers, Dordrecht, 1990.
18. P. Schwendt, J. Tatiersky, L. Krivosudský and M. Šimuneková, *Coord. Chem. Rev.*, 2016, **318**, 135, and references cited therein.
19. V. Conte, F. Di Furia and S. Moro, *J. Mol. Catal.*, 1994, **94**, 323.
20. M. Sutradhar, L. M. D. R. S. Martins, M. Fátima, C. Guedes da Silva and A. J. L. Pombeiro, *Coord. Chem. Rev.*, 2015, **301–302**, 200, and references cited therein.
21. V. Conte and B. Floris, *Dalton Trans.*, 2011, **40**, 1419, and references cited therein.
22. G. Licini, V. Conte, A. Coletti, M. Mba and C. Zonta, *Coord. Chem. Rev.*, 2011, **255**, 2345, and references cited therein.
23. B. Floris, F. Sabuzi, A. Coletti and V. Conte, *Catal. Today*, 2017, **285**, 49, and references cited therein.

24. R. R. Langeslay, D. M. Kaphan, C. L. Marshall, P. C. Stair, A. P. Sattelberger and M. Delferro, *Chem. Rev.*, 2019, **119**, 2128, and references cited therein.
25. O. Bortolini and V. Conte, *J. Inorg. Biochem.*, 2005, **99**, 1549.
26. V. Conte and B. Floris, *Inorg. Chim. Acta*, 2010, **363**, 1935, and references cited therein.
27. X. T. Ma, N. Xing, Z. D. Yan, X. X. Zhang, Q. Wu and Y. H. Xing, *New J. Chem.*, 2015, **39**, 1067.
28. M. R. Maurya, N. Jangra, F. Avecilla and I. Correia, *Eur. J. Inorg. Chem.*, 2019, 314.
29. T. A. Dar, B. Uprety, M. Sankar and M. R. Maurya, *Green Chem.*, 2019, **21**, 1757.
30. V. Conte, F. Fabbianesi, B. Floris, P. Galloni, D. Sordi, I. W. C. E. Arends, M. Bonchio, D. Rehder and D. Bogdal, *Pure Appl. Chem.*, 2009, **81**, 1265.
31. M. Bonchio, V. Conte, F. Di Furia, G. Modena and S. Moro, *J. Org. Chem.*, 1994, **59**, 6262.
32. J. K. Joseph, S. Singhal, S. L. Jain, R. Sivakumaran, B. Kumar and B. Sain, *Catal. Today*, 2009, **141**, 211.
33. P. Galloni, M. Mancini, B. Floris and V. Conte, *Dalton Trans.*, 2013, **42**, 11963.
34. S. D. Kurbah, M. Asthana, I. Syiemlieh and R. A. Lal, *Appl. Organomet. Chem.*, 2018, **32**, 4299.
35. C. Díaz-Urrutia, B. Sedai, K. C. Leckett, R. T. Baker and S. K. Hanson, *ACS Sustainable Chem. Eng.*, 2016, **4**, 6244.
36. M. D. Kärkäs, B. S. Matsuura, T. M. Monos, G. Magallanes and C. R. J. Stephenson, *Org. Biomol. Chem.*, 2016, **14**, 1853, and references cited therein.
37. C. Cheng, J. Wang, D. Shen, J. Xue, S. Guan, S. Gu and K. Hong Luo, *Polymers*, 2017, **9**, 240, and references cited therein.
38. A. Coletti, P. Galloni, A. Sartorel, V. Conte and B. Floris, *Catal. Today*, 2012, **192**, 44.
39. H. M. Gobara, M. I. Nessim, M. T. Zaky, F. H. Khalil and A. V. Anisimov, *Catal. Lett.*, 2014, **144**, 1043.
40. A. Coletti, F. Sabuzi, B. Floris, P. Galloni and V. Conte, *J. Fuel Chem. Technol.*, 2018, **46**, 1121.
41. V. Conte, F. Di Furia and S. Moro, *Tetrahedron Lett.*, 1994, **35**, 7429.
42. P. T. Anastas and J. C. Warner, *Green Chemistry: Theory and Practice*, Oxford University Press, Oxford, 1998.
43. F. Sabuzi, G. Pomarico, B. Floris, F. Valentini, P. Galloni and V. Conte, *Coord. Chem. Rev.*, 2019, **385**, 100, and references cited therein.
44. G. Pomarico, F. Sabuzi, V. Conte and P. Galloni, *New J. Chem.*, 2019, **43**, 17774.
45. M. Debnath, M. Dolai, K. Pal, S. Bhunya, A. Paul, H. M. Lee and M. Ali, *Dalton Trans.*, 2018, **47**, 2799.
46. I. Syiemlieh, M. Asthana and R. A. Lai, *Appl. Organometal Chem.*, 2019, **33**, e4984.

47. I. Syiemlieh, M. Asthana, S. D. Kurbah and R. A. Lai, *Polyhedron*, 2019, **170**, 202.
48. U. Das, P. Pattanayak, M. K. Santra and S. Chattopadhyay, *J. Chem. Res.*, 2018, **42**, 57.
49. H. Adhikari and K. Mukherjea, *J. Coord. Chem.*, 2018, **71**, 542.
50. M. Sun, S. Zhang, J. Zhang, W. Xia, J. Chen and X. Yu, *J. Coord. Chem.*, 2019, **72**, 1899.
51. See as an example:J. Xu, Y. Hong, M.-J. Cheng, B. Xue and Y.-X. Li, *Micropor. Mesopor. Mater.*, 2019, 223
52. See as an example:T. O. Dembaremba, R. van Der Westhuizen, W. Welthagen, E. Ferg, A. S. Ogunlaja and Z. R. Tshentu, *Energy Fuels*, 2019, **33**, 7595
53. See as an example:M. R. Maurya, B. Uprety, N. Chaudhary and F. Avecilla, *Inorg. Chim. Acta*, 2015, **434**, 230
54. N. S. Islam and J. Jyoti Boruah, *J. Chem. Sci.*, 2015, **127**, 777, and references cited therein.
55. M. R. Maurya, *Top. Catal.*, 2018, **61**, 1500, and references cited therein.
56. See as an example:P. Paul, A. Ghosh, S. Chatterjee, A. Bera, S. M. Alam and Sk. M. Islam, *Inorg. Chim. Acta*, 2019, **492**, 198

CHAPTER 6

Vanadium-scorpionate Catalysed Oxidations

L. M. D. R. S. MARTINS* AND A. J. L. POMBEIRO

Centro de Química Estrutural and Departamento de Engenharia Química, Instituto Superior Técnico, Universidade de Lisboa, Portugal
*Email: luisammartins@tecnico.ulisboa.pt

6.1 Introduction

Tripodal nitrogen poly(pyrazol-1-yl)-methane or -borate type scorpionate ligands, $[R_{(4-n)}X(R'pz)_n]^m$ (pz = pyrazol-1-yl; X = C, $m = 0$; X = B, $m = -1$; $n = 2$ or 3; see Figure 6.1), discovered by Hückel *et al.*, (1937)[1] and Trofimenko (1966),[2] respectively, are of the most versatile and widely used class of ligands in coordination chemistry. Indeed, they are able to (i) stabilise transition metals in a wide range of oxidation states; (ii) combine the tripodal architecture needed for efficient three-point biding with a chelating coordination site, leaving up to three sites to other coordinations; and (iii) provide a degree of steric bulk, avoiding *e.g.*, dimerisation reactions. Variation of the substituents at different positions on the pyrazolyl rings leads to a range of steric and electronic effects, this tunability being one of the most important advantages of poly(pyrazol-1-yl)-methane or -borate ligands. Moreover, tris(pyrazolyl)borates [not of tris(pyrazolyl)methanes] are also of easy synthetic access: it is a solvent-free and temperature-controlled selective synthesis by reacting the corresponding pyrazole with a borohydride anion.[3–5]

The organometallic and coordination chemistry of scorpionates has been extensively developed, with a particular interest in the modification of the

Catalysis Series No. 41
Vanadium Catalysis
Edited by Manas Sutradhar, José Armando L. da Silva and Armando J. L. Pombeiro

Published by the Royal Society of Chemistry, www.rsc.org

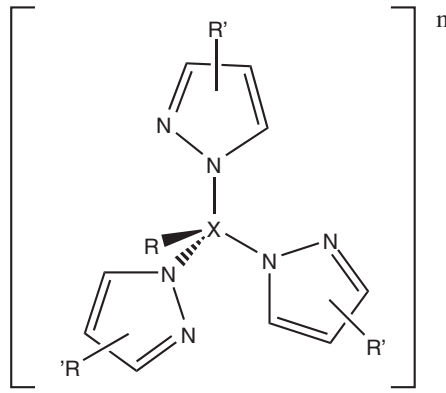

Figure 6.1 General structure of a C- or B-scorpionate ligand.

functional groups connected to the pyrazolyl moiety, in order to control or modify the steric and electronic environment surrounding the metal centre.

Studies have found increasing applications in bioinorganic chemistry (particularly in metalloenzyme modelling studies mimicking of histidine nitrogen coordination by pyrazole to the metal ion binding sites), materials science and in homo- and heterogeneous catalysis as reviewed[3–12] by several researchers.

Regarding the application of C-scorpionates on catalytic processes, metal complexes with heteroscorpionate ligands $R(R')C(pz)_2$ (pz = pyrazol-1-yl) based on the bis(pyrazol-1-yl)methane moiety (H_2Cpz_2) have been mainly applied in catalytic polymerisation reactions,[13] whereas coordination compounds bearing homoscorpionate tris(pyrazol-1-yl)methane type ligands were mostly used in oxidative reactions.

Oxidation reactions, in particular the challenging selective oxidations of hydrocarbons into oxygenated derivatives (*e.g.*, alcohols, aldehydes, ketones or carboxylic acids) are extensively studied[14,15] primarily because such products are important industrial commodities and there is still a need to improve their industrial production processes. In fact, industrial oxidation reactions are usually not selective. One example is the well-studied catalytic industrial oxidation of cyclohexane to cyclohexanol and cyclohexanone (KA oil), one of the most important large-scale processes (~4 million ton per year, growing *ca.* 5% per year)[16] is its involvement in Nylon 6,6 production.[17] By this process, besides KA oil as the desired product, the oxidation of cyclohexane may lead to hundreds of additional species, mostly due to the higher reactivity of KA oil compared to cyclohexane.[17] Although temperatures up to 165 °C and O_2 pressures of 8–15 bar are applied in the industrial (*e.g.*, BASF, DOW Chemicals) liquid-phase oxidation of cyclohexane to shorten retention time and avoid oxidative side reactions, cyclohexane conversion must be limited to 10%–11% per cycle, requiring sequential separation and re-feeding the non-converted substrate to the oxidation reactor.

Another example of large-scale commodity production requiring process improvement is the oxidation of *para*-xylene to terephthalic acid, a very

important process in the polyester industry,[18,19] such as polyethylene terephthalate (PET) manufacturing. The industrial homogeneous oxidation of *para*-xylene (AMOCO process)[18] requires the highly corrosive medium with bromide dissolved in aq. acetic acid and, therefore, a halogen-free efficient catalytic system to produce terephthalic acid is needed.

Thus, one of the main aims of transition-metal catalysis is finding efficient systems, based on coordination compounds as catalysts, able to selectively oxidise alkanes and other organic compounds under sustainable conditions (*e.g.*, using environment-friendly oxidants such as dioxygen or peroxides, not producing hazardous or wasteful by-products, and operation under mild conditions). In this chapter, an overview of scorpionate-vanadium catalysed oxidation of alkanes and other hydrocarbons is presented.

6.2 Homogeneous Scorpionate-vanadium Catalytic Systems

The knowledge that vanadium catalysts can provide a significant advance in the oxidation of alkanes towards their potential application as raw materials for organic synthesis, led to the design and preparation of new carbon and boron scorpionate-vanadium complexes aiming to act as homogeneous catalysts for the oxidation of light cycloalkanes.[20–24]

A series of C-scorpionate vanadium(III or IV) complexes bearing hydrotris(pyrazol-1-yl)methane ($HCpz_3$, Tpm), tris(pyrazol-1-yl)methanesulfonate ($SO_3Cpz_3^-$, Tpms), tris-2,2,2-(1-pyrazol-1-yl)ethanol ($HOCH_2C(pz)_3$, Tpm^{OH}) or 2,2,2-tris(pyrazol-1-yl)mesyloxymethyl ($MeSO_2OCH_2C(pz)_3$, Tpm^{OMs}) was easily synthesised directly from VCl_3 under mild conditions: $[VCl_3(Tpm)]$ (**1**)[21] and $[VCl_3(Tpms)]$ (**2**),[22] the first examples of half-sandwich Tpms complexes of vanadium; $[VOCl_2(Tpm^{OH})]$ (**3**),[23] the first example of a vanadium(IV) complex bearing the hydroxo-functionalized tris(pyrazolyl)ethanol ligand; and $[VOCl_2(Tpm^{OMs})]$ (**4**)[24] (see Figure 6.2). In all the complexes, the C-scorpionate ligand is κ^3-coordinated to vanadium by the N atoms of the pyrazolyl rings. The coordination of oxygen as an oxido ligand was tuned by the reaction conditions used: absence (**1** and **2**)[21] or presence (**3** and **4**)[23,24] of dioxygen in the reaction medium.

These mononuclear V-complexes have shown relevant catalytic activity towards the homogeneous peroxidative[21] or aerobic[25] oxidation of cyclohexane (**1–3**) or cyclooctane (**4**)[24] to the corresponding alcohols and ketones (see Figure 6.3).

For example, complexes **1** and **2** selectively catalyse the oxidation of neat cyclohexane with dioxygen (the cheapest and greenest oxidant) to cyclohexanol (as the main product) and cyclohexanone. At an O_2 pressure of 15 atm and at 140 °C during 18 h, 13% conversion of cyclohexane into KA oil was achieved in the presence of $[VCl_3(Tpm)]$ (**1**).[25] The reaction can be further promoted by adding pyrazine carboxylic acid (HPCA) to the reaction

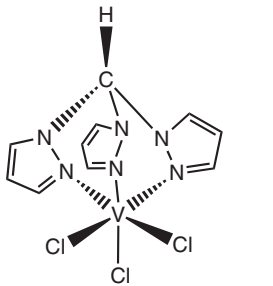

$[VCl_3(Tpm)]$ (**1**)

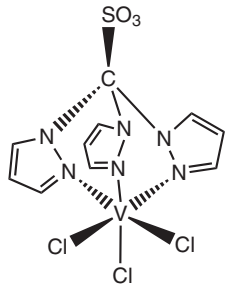

$[VCl_3(Tpms)]$ (**2**)

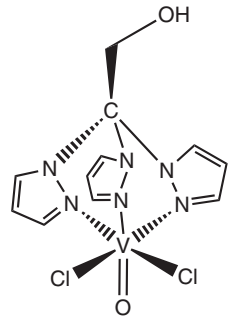

$[VOCl_2(Tpm^{OH})]$ (**3**)

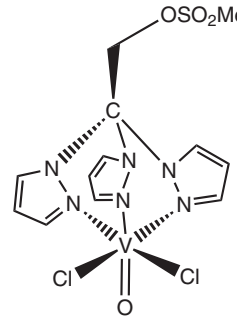

$[VOCl_2(Tpm^{OMs})]$ (**4**)

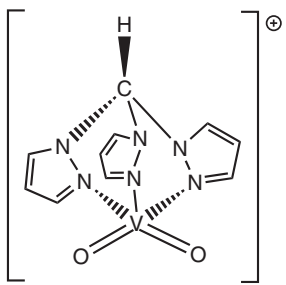

$[VO_2(Tpm)]^+$ (**5**)

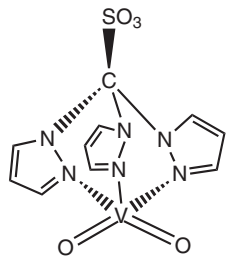

$[VO_2(Tpms)]$ (**6**)

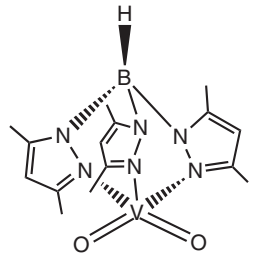

$[VO_2(Tp^{Me})]$ (**7**)

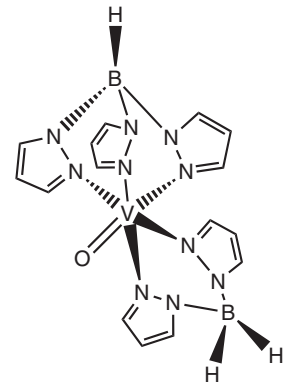

$[VO(Tp)(Bp)]$ (**8**)

Figure 6.2 Structures of C- and B-scorpionate complexes $[VCl_3(Tpm)]$ (**1**),[20] $[VCl_3(Tpms)]$ (**2**), [20] $[VOCl_2(Tpm^{OR})]$ (R = H (**3**)[21] or SO_2Me (**4**)[22]), $[VO_2(Tpm)][BF_4]$ (**5**),[20] $[VO_2(Tpms)]$ (**6**),[20] $[VO_2(Tp^{Me})]$ (**7**)[20] and [VO(Tp)(Bp)] (**8**).[21]

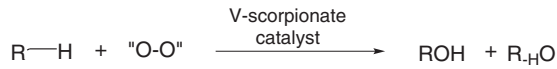

Figure 6.3 Oxidation of alkanes to the corresponding alcohols and ketones, catalysed by V-scorpionate complexes.

medium. Although the mechanistic path was not established, a free-radical mechanism was proposed[25] involving the formation of the cyclohexyl radical by reaction of dioxygen with the cyclohexane (homolytic C–H bond rupture). The oxidation of the cyclohexyl radical by O_2 forms the cyclohexylperoxyl radical that could further react leading to the desired products, cyclohexanol and cyclohexanone.

Complexes $[VCl_3(Tpm)]$ (**1**) and $[VCl_3(Tpms)]$ (**2**) were also able to act as homogeneous catalysts for the peroxidative (with aqueous hydrogen peroxide) oxidation of cyclohexane[21] (and cyclooctane in the case of **4**)[24] in acetonitrile, at ambient or mild temperature (60 °C for **4**) and leading, typically after 6 h, to the corresponding alcohols and ketones *via* formation of the cycloalkyl hydroperoxide as the primary product. KA-oil yield (relative to cycloalkane) values up to 24% or 27% (for cyclohexane and cyclooctane, respectively) and turnover number (TON; moles of desired product per mole of catalyst) values up to 200 were reached.[21,24] A catalytic-promoter effect upon addition of nitric acid to the oxidation media was found for complexes **1–3**. Besides leading to higher KA-oil yields, the peroxidative catalytic system presents the advantage of performing under mild conditions, namely at room temperature, which is not possible when dioxygen (or air) is the chosen oxidant.

The search for efficient catalysts for the functionalisation of light alkanes was extended to scorpionate dioxido-vanadium(v) complexes taking into account that high oxidation state dioxido-vanadium species bearing the VO_2^+ moiety have been used to mimic the V-centre of haloperoxidases.[26]

The half-sandwich C-scorpionate dioxidovanadium(v) complexes $[VO_2(Tpm)][BF_4]$ (**5**) and $[VO_2(Tpms)]$ (**6**) as well as the B-scorpionate dioxidovanadium(v) compound $[VO_2(Tp^{Me})]$ (**7**) [$Tp^{Me} = HB(3,5\text{-}Me_2pz)_3$, pz = pyrazol-1-yl] were obtained[22] by reaction of triethyl vanadate $[VO(OEt)_3]$ with hydrotris(pyrazol-1-yl)methane ($HCpz_3$), lithium tris(pyrazol-1-yl)methanesulfonate $\{Li[SO_3Cpz_3]\}$ and potassium hydrotris(3,5-dimethylpyrazol-1-yl)borate $\{K[HB(3,5\text{-}Me_2pz)_3]\}$, respectively. Complex **6** represents the first example of a dioxidovanadium complex bearing the tris(pyrazol-1-yl)methanesulfonate ligand, whereas **7** is the first reported mononuclear vanadium complex bearing a tris(pyrazol-1-yl)borate ligand.[22] In complexes **5–7**, the C- or B-scorpionate is ligated to the vanadium centre in the *N,N,N*-coordination mode (see Figure 6.2).

In addition to the half-sandwich V-complexes, a mixed κ^3-tris(pyrazol-1-yl)borate and κ^2-bis(pyrazol-1-yl)borate oxidovanadium(IV) complex $[VO(Tp)(Bp)]$ (**8**) (Bp = dihydrobis(pyrazol-1-yl)borate, H_2Bpz_2) was obtained[22] from the reaction of triethyl vanadate with potassium hydrotris(pyrazol-1-yl)borate, which undergoes a partial conversion into the corresponding bis(pyrazol-1-yl)borate ligand (see Figure 6.2).

Among the C- and B-scorpionate oxidovanadium(IV or V) complexes **5**–**8**, $[VO_2(Tpms)]$ (**6**) led to the highest cyclohexanol and cyclohexanone yield and TON values (19% and 117, respectively)[22] from oxidation of cyclohexane with aq. hydrogen peroxide in acetonitrile, during 6 h at room temperature. This catalytic behaviour is in accord with the very easy V(V) to V(IV) reduction ($E_p^{red} = -0.5$ V *vs.* SCE)[22] detected for **6** by cyclic voltammetry and controlled potential electrolysis at platinum electrodes.

Also, in the case of oxidovanadium scorpionate complexes, addition of nitric acid to the oxidation medium has a catalytic-promoter effect, as found *e.g.*, for $[VO_2(Tpms)]$ (**6**) and [VO(Tp)(Bp)] (**8**).[22] Under the tested reaction conditions, vanadium C-scorpionate complexes exhibited better catalytic performance than the borate ones. Moreover, the latter are more prone to undergo hydrolysis and other decomposition reactions, increasing their instability under oxidation conditions and, thus, hampering better catalytic performances.

Most of the known vanadium complexes behaving as catalysts for alkane oxidation are believed to act through an indirect activation of the alkane;[27,28] reaction of the V-complex with the oxidant (*e.g.*, ROOH) can lead to a reactive radical species (*e.g.*, hydroxyl radical) which abstracts a hydrogen from the alkane without the direct participation of the vanadium catalyst. The low alcohol–ketone selectivity found for the product mixtures catalysed by C- or B-scorpionate vanadium complexes **1**–**8**, as well as the products yield decrease when the reaction was performed in the presence of radical traps, suggests that the oxidation of cycloalkanes in the presence of **1**–**8** proceeded *via* the overall mechanistic path described. For example, where hydrogen peroxide was used as oxidant, the reaction takes place through the formation of the highly reactive hydroxyl radical ($HO^{\bullet}$) upon vanadium-catalysed decomposition of H_2O_2, and accordingly displays low bond-, regio- and stereoselectivities.

The metal-promoted formation of the hydroxyl radical from H_2O_2 involves proton-shifts[29,30] which can be assisted by the basic pyrazolyl groups of the scorpionate ligands, apart from other promoters such as water or pyrazinecarboxylic acid.

The oxidation of other hydrocarbons, besides alkanes, catalysed by the C-scorpionate vanadium(IV) complexes $[VCl_3(Tpms)]$ (**2**), $[VOCl_2(Tpm^{OH})]$ (**3**) or $[VOCl_2(Tpm^{OMs})]$ (**4**) was also explored.[31] *p*-Xylene was the chosen substrate (see Section 6.1) for the halogen- and solvent-free, mild (80 °C) homogeneous microwave-assisted oxidation with aqueous *tert*-butyl hydroperoxide (TBHP). Activation at one of the methyl groups of *p*-xylene was selectively achieved, providing toluic acid (up to 28% yield after 12 h reaction time, Figure 6.4)[31] in the absence of any additive.

The addition of nitric acid as co-catalyst increases the product yield, whereas the microwave irradiation allowed shortening the reaction time, when compared with a conventional (oil bath) heating mode, as it generates heat evenly throughout the reactor, thereby enhancing product yield, selectivity and purity.

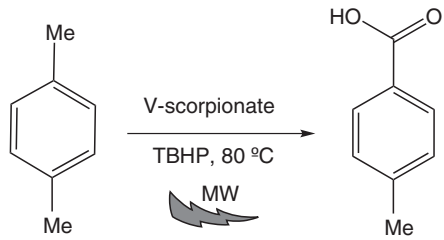

Figure 6.4 Microwave-assisted oxidation of *p*-xylene to toluic acid catalysed by V-scorpionate complexes.

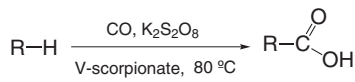

Figure 6.5 Carboxylation of gaseous alkanes to the corresponding carboxylic acids, catalysed by V-scorpionate complexes.

Besides acting as catalysts for the liquid-phase oxidation of hydrocarbons, C- or B-scorpionate vanadium(III to V) complexes **1**, **2** and **5**–**8** have been used as efficient catalysts for the carboxylation (formation of a C–CO bond) of gaseous (methane and ethane) alkanes (carboxylic acid yields up to 40%, TONs up to 157), typically undertaken under a CO atmosphere with peroxydisulfate as the oxidant, at 80 °C in trifluoroacetic acid (Figure 6.5).[22]

The tris(pyrazol-1-yl)methanesulfonate complexes $[VCl_3(Tpms)]$ (**2**) and $[VO_2(Tpms)]$ (**6**) are the most effective towards methane carboxylation to acetic acid (37% and 39%, respectively for **2** and **6**)[22] whereas the catalytic performance decreases on replacement of Tpms by Tpm at the vanadium centre: 20% and 16% of acetic acid for $[VCl_3(Tpm)]$ (**1**) and $[VO_2(Tpm)][BF_4]$ (**5**), respectively. Ethane carboxylation to propionic acid occurred while competitive oxidation produced acetic acid, reaching a maximum of 14% of propionic acid in the presence of $[VO_2(Tpms)]$ (**6**).[22]

In spite of their good catalytic activity, the scorpionate complexes cannot achieve for alkane carboxylation the remarkably high activity displayed by the natural vanadium complex amavadin $[V(HIDPA)_2]^{2-}$ (HIDPA = basic form of *N*-hydroxyiminedipropionic acid), its model $[V(HIDA)_2]^{2-}$ (HIDA = basic form of *N*-hydroxyiminediacetic acid) and related vanadium catalysts such as vanadatrane.[32–35]

6.3 Heterogeneous Scorpionate-vanadium Catalytic Systems

Although exhibiting good catalytic performances, C- or B-scorpionate vanadium homogeneous catalysts lack reusability. Thus, the immobilisation of a C- or B-scorpionate vanadium catalyst on an inert support could allow its easier separation and recycling, apart from eventually improving the

catalytic activity and selectivity, which are required conditions in sustainable processes. Therefore, a combination of the properties of the vanadium complexes with the advantages of heterogeneous systems would be obtained. In fact, in heterogenized catalysts the support has been recognised to play an active role,[36] whether physically stabilizing the active (metallic) phase dispersion or by modifying its electronic properties, apart from allowing the catalyst recycle.

Functionalized silica or carbon materials, as well as polymeric structures and hierarchical zeolites were the selected types of solids to act as supports for the C- or B-scorpionate vanadium complexes heterogenisation since they are inert in the oxidative reactions catalysed by the scorpionate complexes.

Complexes $[VOCl_2(Tpm^{OH})]$ (**3**) and $[V(acac)(Tpm^{OH})]$ (**9**, acac = acetylacetonate)[37] were immobilised at functionalized silica (by reaction with chlorosulfonylphenylethyltrimethoxysilane) and used as catalysts for the selective oxidation of cyclohexane with molecular oxygen under relatively mild conditions. TON values up to 2.6×10^3 and cyclohexanol plus cyclohexanone yields up to 27% were reached with a 95% selectivity. Moreover, the stability of the materials under oxidation conditions allowed their reuse up to six catalytic cycles.[37]

The heterogenisation of B-scorpionate vanadium complexes at porous inorganic materials was also tested.[38] Complex $[VO_2(Tp^{Me})]$ (**7**) was anchored on a modified (through a surfactant mediated technology) hierarchical MOR zeolite providing three different catalysts, 7@MOR, 7@MOR_NaOH and 7@MOR_TPAOH, according to the basic treatment applied, NaOH or tetrapropylammonium hydroxide (TPAOH), to promote the development of a mesopore network (Figure 6.6). The catalytic activity of the materials was evaluated for the oxidation of cyclohexane to KA oil using aq. TBHP, at room temperature, in a slightly acidic medium. KA-oil yields up to 52% were obtained with TON values up to 6.2×10^2 for 7@MOR_NaOH (the most efficient catalyst).[38] Its stability allowed its recovery at the end of each catalytic cycle and its re-use in consecutive (up to four) cycles. The first decrease (18%)[38] on the oxidation yield observed occurred without significant leaching of the

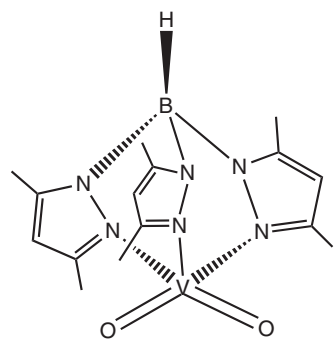

Figure 6.6 Anchorage of complex $[VO_2(Tp^{Me})]$ (**7**) on a modified (through a surfactant mediated technology) hierarchical MOR zeolite treated with NaOH (TEM image).[38]

V complex. This is most likely due to some adsorption phenomena causing diffusional constraints and restricting the access of reactants to the immobilised V-catalyst, and/or to catalyst decomposition to unleached species.

C-scorpionate vanadium(IV) complexes were also supported on functionalized carbon materials.[31] C-materials as catalyst supports have the advantage of being easily functionalized with a variety of surface groups (carboxylic acid, phenol, carbonyl, lactone, *etc.*) that can be tailored, including their physical (surface area and porosity) properties, to meet the requirements of a desired application. Thus, the complexes $[VCl_3(Tpms)]$ (**2**), $[VOCl_2(Tpm^{OH})]$ (**3**) or $[VOCl_2(Tpm^{OMs})]$ (**4**), that act as homogeneous catalysts for the MW-assisted oxidation of *p*-xylene to *p*-toluic acid with TBHP (see Section 6.2) were immobilised on functionalized multi-walled carbon nanotubes (MWCNTs) most likely through the formation of a covalent V–O bond with the MWCNT surface carboxylate or phenolate groups, thus, displacing a chloride ligand or replacing one of the scorpionate pyrazolyl rings bound to the vanadium centre. The catalytic activity of the hybrid materials was evaluated under homogeneous conditions (see Section 6.2) in the absence of any bromine source. A *p*-toluic acid yield of 43% with a selectivity of 73% and TON of 1.34×10^3 was obtained when catalysed by $[VOCl_2(Tpm^{OH})]$@MWCNT. Reuse of the hybrid catalysts with preservation of their activity was found for up to six consecutive cycles. After the sixth cycle, vanadium leaching was detected and the material activity started to decrease.[31]

In addition, $[VOCl_2(Tpm^{OH})]$ (**3**) was anchored at another type of material,[23] a polymeric membrane synthesised by Sn-catalysed crosslinking silanol-terminated poly(dimethylsiloxane) (PDMS) with tetraethoxysilane (TEOS). This V-membrane-supported catalyst exhibited for the peroxidative oxidation of cyclohexane, under the same reaction conditions (see Section 6.2), lower activity than **3**. Moreover, although allowing an easy product separation, the re-use of $[VOCl_2(Tpm^{OH})]$@PDMS/TEOS was hampered by the chemical instability of the membrane under the studied conditions.[23]

6.4 Conclusion

In recent years, significant developments have been accomplished in oxidative catalysis with vanadium complexes. However, the application of mononuclear V-catalysts for the oxidation of hydrocarbons, in particular of challenging alkanes, still needs further advancement. Among the known examples, vanadium complexes bearing C- or B-scorpionate ligands are experiencing a significant development. The basicity of the scorpionate ligands, their hemilability, and, in the case of C-based ones, their stability under the reaction conditions are properties that favour the catalytic activity of their vanadium complexes. Moreover, the scorpionate complexes can be water soluble, particularly when displaying an hydrosoluble scorpionate ligand (*e.g.*, tris(pyrazol-1-yl)methanesulfonate, Tpms) that fosters their catalytic behaviour in aqueous–watered medium such as that typically used in the peroxidative oxidations in acetonitrile with an aqueous peroxide.

There are challenges that are still to be addressed, especially towards the development of sustainable reaction conditions (*e.g.*, the use of microwave or ultrasound irradiation, supercritical fluid or ionic liquid media) and extension of the V-scorpionate complexes to other types of catalytic reactions.

Acknowledgements

This work was supported by the Fundação para a Ciência e Tecnologia (FCT), project UIDB/00100/2020 of Centro de Química Estrutural and projects PTDC/QEQ-ERQ/1648/2014 and PTDC/QEQ-QIN/3967/2014.

References

1. W. Hückel and H. B. Chneider, *Ber. Dtsch. Chem. Ges.*, 1937, **70**, 2024.
2. S. Trofimenko, *J. Am. Chem. Soc.*, 1966, **88**, 1842.
3. S. Trofimenko, *Chem. Rev.*, 1993, **93**, 943.
4. S. Trofimenko, in *Scorpionates: The Coordination Chemistry of Polypyrazolylborate Ligands*, Imperial College Press, London, 1999.
5. C. Pettinari, *Scorpionates II: Chelating Borate Ligands*, Imperial College Press, London, 2008.
6. H. R. Bigmore, S. C. Lawrence, P. Mountford and C. S. Tredget, *Dalton Trans.*, 2005, 635.
7. C. Pettinari and R. Pettinari, *Coord. Chem. Rev.*, 2005, **249**, 525.
8. A. Otero, J. Fernández-Baeza, A. Lara-Sánchez and L. F. Sánchez-Barba, *Coord. Chem. Rev.*, 2013, **257**, 1806.
9. L. M. D. R. S. Martins and A. J. L. Pombeiro, *Coord. Chem. Rev.*, 2014, **265**, 74.
10. L. M. D. R. S. Martins and A. J. L. Pombeiro, *Eur. J. Inorg. Chem.*, 2016, 2236.
11. L. M. D. R. S. Martins, *Catalysts*, 2017, **7**, 12.
12. L. M. D. R. S. Martins, *Coord. Chem. Rev.*, 2019, **396**, 89.
13. A. Otero, J. Fernández-Baeza, A. Lara-Sánchez and L. F. Sánchez-Barba, *Coord. Chem. Rev.*, 2013, **257**, 1806.
14. *Alkane Functionalization*, ed. A. J. L. Pombeiro and M. F. C. G. Silva, J. Wiley & Sons, New Jersey, 2019.
15. *Advances in Organometallic Chemistry and Catalysis: The Silver/Gold Jubilee ICOMC Celebratory Book*, ed. A. J. L. Pombeiro, J. Wiley & Sons, New Jersey, 2014.
16. Adipic acid (ADPA): 2016 world market outlook and forecast up to 2020, Merchant Research and Consulting, Birmingham, UK, 2016.
17. M. L. Campbell, *Ullmann's Encyclopaedia of Industrial Chemistry*, Wiley-VCH: Weinheim, Germany, 2011.
18. R. A. F. Tomás, J. C. M. Bordado and J. F. P. Gomes, *Chem. Rev.*, 2013, **113**, 7421.
19. R. J. Sheehan, *Ullmann's Encyclopaedia of Industrial Chemistry*; Wiley-VCH: Weinheim, Germany, **vol. 35**, 6th edn, 2003, p. 639.

20. M. Sutradhar, L. M. D. R. S. Martins, M. F. C. Guedes da Silva and A. J. L. Pombeiro, *Coord. Chem. Rev.*, 2015, **301–302**, 200.
21. T. F. S. Silva, E. C. B. A. Alegria, L. M. D. R. S. Martins and A. J. L. Pombeiro, *Adv. Synth. Catal.*, 2008, **350**, 706.
22. T. F. S. Silva, K. V. Luzyanin, M. V. Kirillova, M. F. C. G. Silva, L. M. D. R. S. Martins and A. J. L. Pombeiro, *Adv. Synth. Catal.*, 2010, **352**, 171.
23. T. F. S. Silva, T. C. O. Mac Leod, L. M. D. R. S. Martins, M. F. Guedes da Silva, M. A. Schiavon and A. J. L. Pombeiro, *J. Mol. Catal. A: Chem.*, 2013, **367**, 52.
24. T. F. S. Silva, B. G. M. Rocha, M. F. C. Guedes da Silva, L. M. D. R. S. Martins and A. J. L. Pombeiro, *New J. Chem.*, 2016, **40**, 528.
25. G. S. Mishra, T. F. S. Silva, L. M. D. R. S. Martins and A. J. L. Pombeiro, *Pure Appl. Chem.*, 2009, **81**, 1217.
26. *Vanadium: The Versatile Metal*, ed. K. Kustin, J. C. Pessoa and D. C. Crans, American Chemical Society, Washington, DC, 2007.
27. M. Sutradhar, L. M. D. R. S. Martins, M. F. C. Guedes da Silva and A. J. L. Pombeiro, Alkane Oxidation with Vanadium and Copper Catalysts, in *Alkane Functionalization*, ed. A. J. L. Pombeiro and M. F. C. Guedes da Silva, J. Wiley & Sons, Hoboken, New Jersey, **Ch. 16**, 2019, pp. 319–336.
28. G. B. Shul'pin, in *Alkane Functionalization*, ed. A. J. L. Pombeiro and M. F. C. Guedes da Silva, J. Wiley & Sons, Hoboken, New Jersey, ch. 3, 2019, pp. 47–72.
29. M. V. Kirillova, M. L. Kuznetsov, V. B. Romakh, L. S. Shul'pina, J. J. R. Fraústo da Silva, A. J. L. Pombeiro and G. B. Shul'pin, *J. Catal.*, 2009, **267**, 140.
30. M. Kuznetsov and A. J. L. Pombeiro, *Inorg. Chem.*, 2009, **48**, 307.
31. J. Wang, L. M. D. R. S. Martins, A. P. C. Ribeiro, S. A. C. Carabineiro, J. L. Figueiredo and A. J. L. Pombeiro, *Chem. – Asian J.*, 2017, **12**, 1915.
32. J. A. L. da Silva, J. J. R. Fraústo da Silva and A. J. L. Pombeiro, *Coord. Chem. Rev.*, 2013, **257**, 2388.
33. M. V. Kirillova, M. L. Kuznetsov, P. M. Reis, J. A. L. Silva, J. J. R. Fraústo da Silva and A. J. L. Pombeiro, *J. Am. Chem. Soc.*, 2007, **129**, 10531.
34. M. V. Kirillova, M. L. Kuznetsov, J. A. L. Silva, M. F. C. Guedes da Silva, J. J. R. Fraústo da Silva and A. J. L. Pombeiro, *Chem. – Eur. J.*, 2008, **14**, 1828.
35. M. V. Kirillova, A. M. Kirillov, P. M. Reis, J. A. L. Silva, J. J. R. Fraústo da Silva and A. J. L. Pombeiro, *J. Catal.*, 2007, **248**, 130.
36. *Green Chemistry: An Inclusive Approach*, ed. B. Török and T. Dransfield, Elsevier Inc., Amsterdam, The Netherlands, 2017.
37. K. Machado, S. Mukhopadhyay and G. S. Mishra, *J. Mol. Catal. A: Chem.*, 2015, **400**, 139.
38. D. Ottaviani, V. Van-Dúnem, A. P. Carvalho, A. Martins and L. M. D. R. S. Martins, *Catal. Today*, 2019, DOI: 10.1016/j.cattod.2019.09.034.

CHAPTER 7

Vanadium-aroylhydrazone Catalysed Oxidations

MANAS SUTRADHAR,*[a] VLADIMIR B. ARION,[b] TANNISTHA ROY BARMAN[a] AND ARMANDO J. L. POMBEIRO[a]

[a] Centro de Química Estrutural, Instituto Superior Técnico, Universidade de Lisboa, Av. Rovisco Pais, 1049-001 Lisboa, Portugal; [b] Institute of Inorganic Chemistry, University of Vienna, Währinger Strasse 42, 1090 Vienna, Austria
*Email: manas@tecnico.ulisboa.pt

7.1 Introduction

Vanadium catalysts have been applied on various oxidation transformations of organic compounds under homogeneous or heterogeneous conditions that can play a vital role in the manufacture of fine and bulk chemicals.[1–3] Vanadium is also present in several enzymes, *e.g.*, in vanadium nitrogenases and vanadium-dependent haloperoxidases (VHPOs).[4] Furthermore, hydrazone-based ligands (Scheme 7.1) can stabilise vanadium complexes in various oxidation states (including mixed-valence states) with different oxidovanadium cores and coordination numbers (up to eight).[5] Vanadium complexes derived from hydrazone ligands can act as good catalysts for peroxidative oxidation reactions. Some trigonal-bipyramidal dioxidovanadium(v) complexes, particularly with benzimidazole-, imidazole-, pyridyl- and hydrazone-derived ligands, can act as functional models of vanadium haloperoxidades (VHPOs) as these complexes can mimic oxidative halogenations and sulfoxidations.[6,7]

Catalysis Series No. 41
Vanadium Catalysis
Edited by Manas Sutradhar, José Armando L. da Silva and Armando J. L. Pombeiro

Published by the Royal Society of Chemistry, www.rsc.org

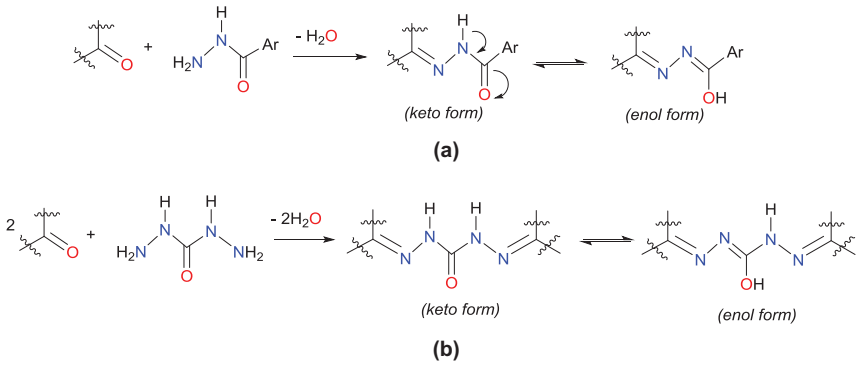

Scheme 7.1 Synthesis of aroylhydrazones (a) and carbohydrazones (b).

The Lewis acidic character of high oxidation state (IV or V) vanadium compounds and their strong affinity for oxygen favour their use as catalysts or pre-catalysts in various peroxidative oxidation reactions. Aroylhydrazone-based oxidovanadium complexes are important members in the catalysts series as environment-friendly oxidants (O_2 or H_2O_2) are commonly used.

In this chapter, some useful vanadium-aroylhydrazone catalysed peroxidative oxidation reactions, *e.g.*, oxidations of alkanes and alcohols, epoxidations and sulfoxidation, under homogeneous and supported heterogeneous conditions, are discussed. Some microwave-assisted oxidations are also presented. The effects of several factors (*e.g.*, acid promoter, temperature, catalyst amount, *etc.*) on the catalytic activity of vanadium compounds are also discussed and the proposed mechanisms are illustrated.

7.2 Oxidative Functionalisation of Alkanes

Alkanes are saturated hydrocarbons that are often used as fuels and important raw materials in the petrochemical industry. These carbon-rich compounds have high potential interest for the synthesis of added-value functionalised organic products upon their functionalisation.[1–3,8] However, their chemical inertness (*e.g.*, they require the use of harsh reaction conditions, which lead to low product yields and/or selectivities) limits their application as raw materials. Therefore, the development of environment-friendly efficient catalytic systems under mild conditions for selective oxidation of alkanes is highly challenging. Various vanadium complexes have already been tested as efficient catalysts or catalyst precursors for the oxidative functionalisation of alkanes.[1–3] In this chapter, the catalytic activity of a number of oxidovanadium complexes derived from aroylhydrazone or carbohydrazone ligands towards the functionalisation of alkanes are discussed.

7.2.1 Oxidation of Alkanes under Conventional Mild Conditions

Condensation of aromatic acid hydrazides or carbohydrazide with suitable aldehydes or ketones leads to the formation of aroylhydrazones or

carbohydrazones (Scheme 7.1) which are useful pro-ligands for the synthesis of stable oxidovanadium(IV) and oxidovanadium(V) complexes. Examples of several oxidovanadium(V) complexes of different nuclearities, *e.g.*, mononuclear (**1**),[9] binuclear (**2**-**8**),[10] trinuclear (**9**),[11] the heterometallic coordination polymers (**10**-**12**)[12] as well as the mixed-valence (IV/V) species (**13**)[13] derived from aroylhydrazones or carbohydrazones, are catalysts for the oxidative functionalisation of alkanes.

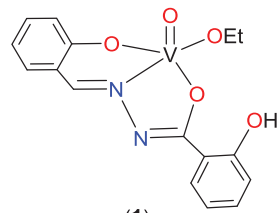

(**1**)

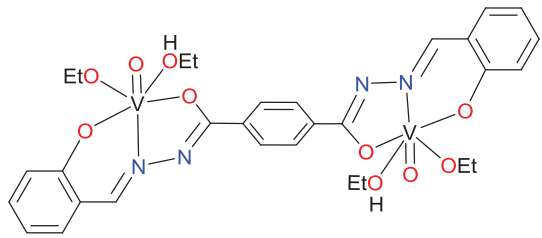

(**2**)

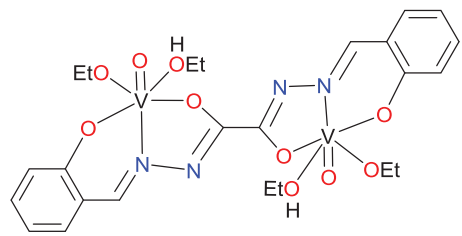

(**3**)

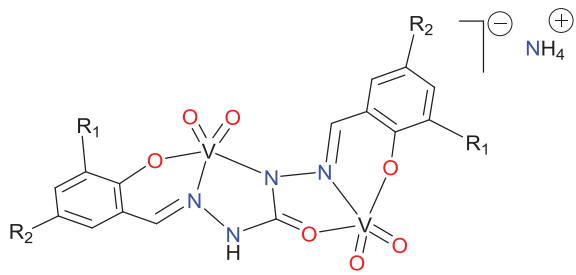

$R_1 = R_2 = H$ (**4**)
$R_1 = R_2 =$ *tert*-Bu (**5**)

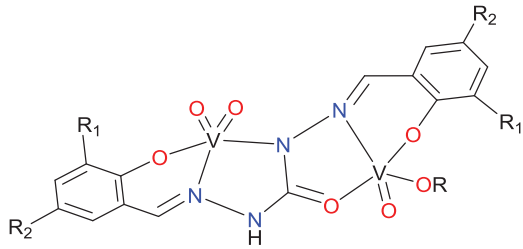

$R_1 = R_2 = H$, R = Me (**6**)
$R_1 = R_2 =$ *tert*-Bu, R = Et (**7**)

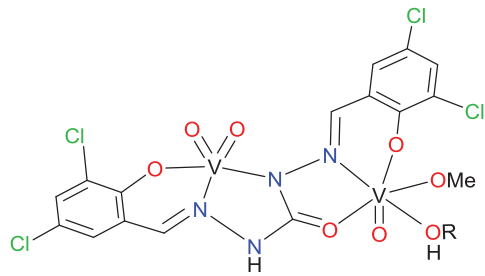

R = Me or H (**8**)

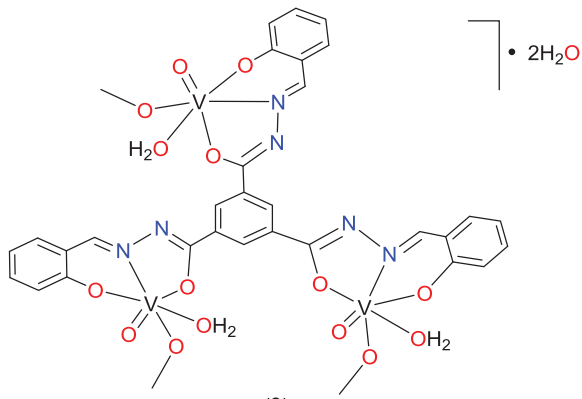

(**9**)

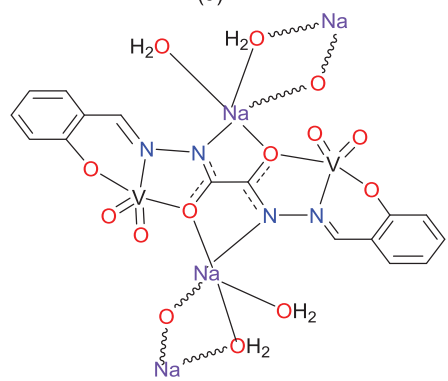

(**10**)

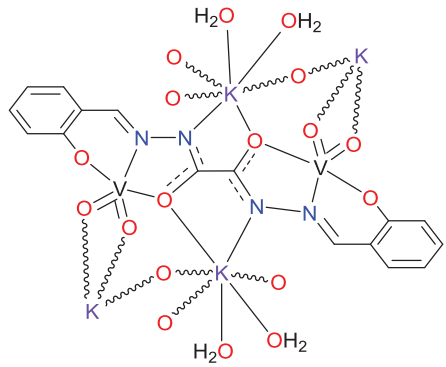

(**11**)

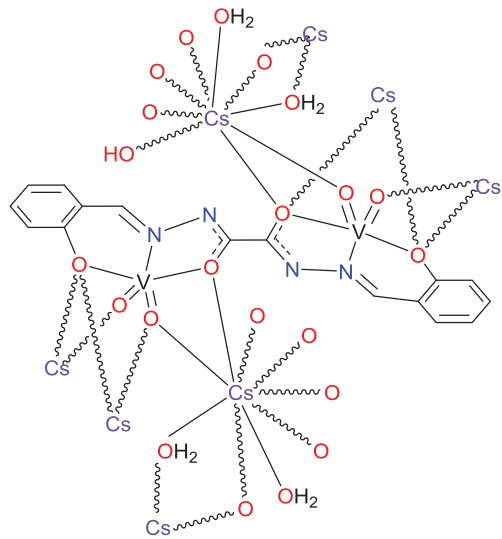

(**12**)

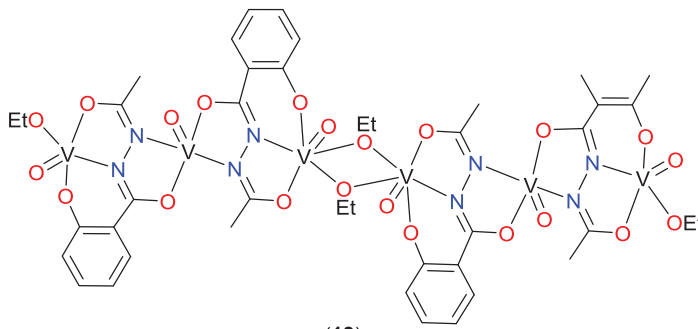

(**13**)

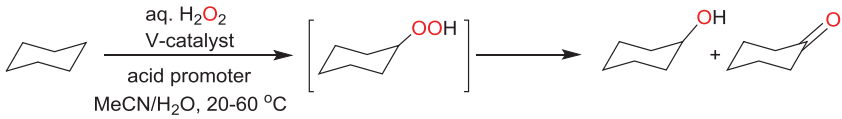

Scheme 7.2 Vanadium-catalysed peroxidative oxidation of cyclohexane.

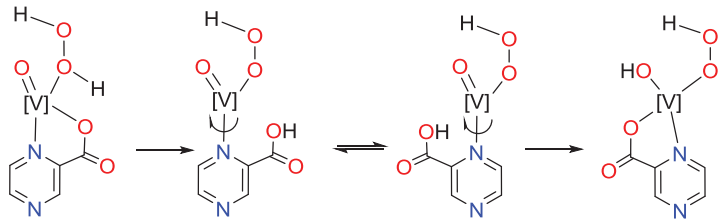

Scheme 7.3 PCA-assisted proton shift from a coordinated H_2O_2 molecule to an oxido ligand at a vanadium centre [V] ("robot's arm mechanism").[15]

Cyclohexane, which is commonly used as a raw material in the manufacture of Nylon-6,6, is usually chosen as a model substrate for studying the oxidative functionalisation of alkanes using H_2O_2 as the oxidant under mild conditions (Scheme 7.2).

Several vanadium complexes efficiently catalyse the oxidation of alkanes under mild conditions and their efficiency can be dramatically improved by the addition of a small amount of an acid as promoter, such as 2-pyrazinecarboxylic acid (PCA),[14–16] nitric,[17] sulfuric[18] or oxalic[18] acid. In fact, in 1993, Shul'pin and co-workers discovered that PCA can enhance activity of the vanadium catalytic systems towards the oxidation of organic compounds (alkanes, arenes, alcohols) with hydrogen peroxide as an oxidant under mild conditions (20–60 °C, in acetonitrile solution).[15] This has been further confirmed by several vanadium-catalysed systems for the peroxidative oxidation of liquid and gaseous alkanes under mild conditions.[5,9–13] The vanadium complexes **1–3** and **9–13** contain aroylhydrazone ligands with the azine fragment (C=N–N=C) and exhibit an efficient catalytic activity.[5,9–13] During the catalytic action, as a promoter, PCA accelerates the proton transfer from a coordinated hydrogen peroxide molecule to an oxido, hydroxido or peroxido ligand *via* the so-called robot's arm mechanism (Scheme 7.3)[15] which is involved in the generation of the hydroxyl radical from H_2O_2.

Oxidovanadium(v) complexes of various nuclearities, such as the mononuclear compound [VO(OEt)(L)] (**1**) (H_2L = 2-hydroxy-(2-hydroxybenzylidene)-benzohydrazide), the dinuclear complexes [{VO(OEt)(EtOH)}$_2$L] (**2**, H_4L = bis(2-hydroxybenzylidene)terephthalohydrazide; **3**, H_4L = bis(2-hydroxybenzylidene)oxalohydrazide), the trinuclear [{VO(OMe)(H_2O)}$_3$(L)]·2H_2O (**9**) (H_6L = tris(2-hydroxybenzylidene)benzene-1,3,5-tricarbohydrazide), the heterometallic dioxidovanadium(v)/alkali metal coordination polymers derived from the same ligand as used in **2** $[(VO_2)_2(\mu_4\text{-L})\{Na_2(\mu\text{-}H_2O)_2(H_2O)_2\}]_n$ (**10**),

$[\{V(\mu\text{-}O)_2\}_2(\mu_4\text{-}L)\{K_2(\mu\text{-}H_2O)_2(H_2O)_2\}]_n$ (**11**), $[\{V(\mu\text{-}O)(\mu_3\text{-}O)\}_2(\mu_8\text{-}L)\{Cs_2(\mu\text{-}H_2O)_2(H_2O)_2\}]_n$ (**12**)[12] and the mixed-valence $[V_3O_3(OEt)(ashz)_2(\mu-OEt)]_2$ (**13**) ($H_3ashz = N$-acetylsalicylhydrazide)[13] are good catalysts or catalyst precursors for the mild peroxidative oxidation of alkanes.

The dinuclear oxidovanadium(V) complex **3**, the heterometallic V^V/Cs coordination polymer **12** and the mixed-valence oxidovanadium(IV/V) complex **13** lead to the highest yields (≥25%) of cyclohexanol and cyclohexanone for the oxidation of cyclohexane in the presence of an acid promoter (mainly PCA) under mild conditions (50 °C) in MeCN/H_2O medium.[10a,12,13] The most efficient catalytic system in terms of turnover number (TON) is **2**/PCA/H_2O_2, with a maximum TON of 4.4×10^4 at 50 °C, for 1×10^{-6} M of **2** (low catalytic amount).

Under optimised conditions, the activity of the water-soluble coordination polymers **10** – **12** having identical $[(VO_2)_2(\mu_{4/8}\text{-}L)]^{2-}$ (H_4L = bis(2-hydroxybenzylidene)oxalohydrazide) cores follows the trend **10** < **11** < **12** in the presence of PCA, which correlates with the ionic radius and the coordination number of the alkali cation.[12] A maximum yield of 36% (based on substrate) of cyclohexanol and cyclohexanone with a TON value of 5.7×10^3 was achieved by the **12**/PCA catalytic system.[12]

7.2.2 Oxidation of Alkanes under Microwave Irradiation

The effect of microwave (MW) irradiation on solvent-free peroxidative oxidation of cyclohexane (with aq. H_2O_2) to cyclohexanol and cyclohexanone was examined with oxidovanadium(V) complexes with different nuclearities (mononuclear **1**, binuclear **2** and trinuclear **9**).[11] Under optimised conditions, the solvent- and additive-free systems – 60 °C and 1.5 h of low power (25 W) MW irradiation – produce the maximum yield of 24% (for **1**), 33% (for **2**) and 39% (for **9**) of the oxygenated products using a low catalyst load (0.2% molar ratio relatively to substrate). They are highly efficient catalysts. In a short period of reaction time (15 min) under MW irradiation, 15 (**1**), 23 (**2**) and 26% (**9**) yield of oxygenates were achieved.[11]

MW-assisted solvent-free peroxidative (with aqueous TBHP) oxidation of cyclohexane to cyclohexanol and cyclohexanone was also studied with the series of dinuclear oxidovanadium complexes $NH_4[(VO_2)_2(^{H}LH)]$ (**4**), $NH_4[(VO_2)_2(^{t\text{–}Bu}LH)]$ (**5**), $[(VO_2)(VO)(^{H}LH)(CH_3O)]$ (**6**), $[(VO_2)(VO)(^{t\text{–}Bu}LH)\text{-}(C_2H_5O)]$ (7) and $[(VO_2)(VO)(^{Cl}LH)(CH_3O)(CH_3OH/H_2O)]$ (**8**) (where $^{H}LH_4$ = 1,5-bis(2-hydroxybenzaldehyde)carbohydrazone, $^{t\text{–}Bu}LH_4$ = 1,5-bis(3,5-di-*tert*-butyl-2-hydroxybenzaldehyde)carbohydrazone, and $^{Cl}LH_4$ = 1,5-bis(3,5-dichloro-2-hydroxybenzaldehyde)carbohydrazone) with the ligand as trianion (using two different binding sites, ONN and ONO, separated by a diazine unit).[10c] Complexes **4**–**8** exhibit good catalytic activity under MW irradiation. A good yield of oxygenated products can be achieved in a short reaction time under MW irradiation (at 100 °C), *e.g.*, 19% yield with a TON value of 93 after 1.5 h for **6**. The low-power, MW-assisted reaction provides a much more efficient and simpler method than conventional heating (which, *e.g.*, requires 24 h of reaction in the presence of **4** under the same conditions to achieve 20% yield of cyclohexanol and cyclohexanone).[10c]

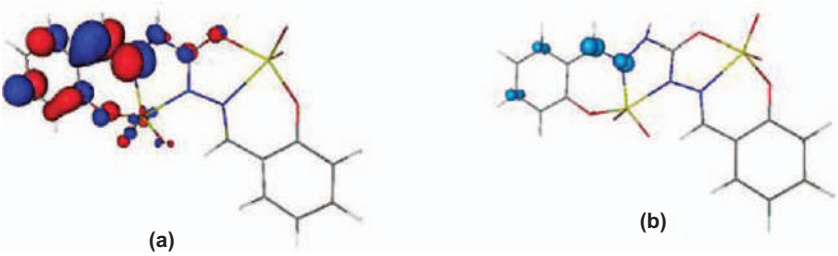

Figure 7.1 (a) LUMO of ^{1}[4] in vacuum; (b) spin density of its reduced form in vacuum. (Reused with copyright permission).[10c]
Reproduced from ref. 10*c*, https://pubs.acs.org/doi/10.1021/acs.inorgchem.6b01011, with permission from American Chemical Society, Copyright 2016.

The redox non-innocent character of the carbohydrazone ligand was established by cyclic voltammetry, spectroelectrochemistry and DFT studies which show that these complexes are reducible, but the reduced form preserves the +5 vanadium oxidation state.[10c] Figure 7.1a represents the LUMO of the starting anionic framework of **4**, which is mainly ligand localised. Figure 7.1b shows that the spin density of the reduced dianionic form is also located on the ligand. Therefore, the existence of metal–ligand cooperation is observed in the alkane oxidation with these carbohydrazone-vanadium catalysts.

Oxidovanadium(v) complexes derived from aroylhydrazone ligands were also studied in the functionalisation of gaseous alkanes (methane, ethane, propane and *n*-butane). Alcohols, aldehydes, ketones and/or carboxylic acids are the oxygenated products obtained upon the peroxidative oxidation of these light alkanes. Under homogeneous reaction conditions, the V-cat/PCA/aq. H_2O_2/CH_3CN systems (V-cat = **2** or **3**) efficiently catalyse the oxidation of gaseous alkanes at 50 °C.[10a,b] The simplest alkane (methane) is less reactive and produces methanol with a lower yield in comparison with the other gaseous alkanes. In the case of ethane, the oxidation leads to acetaldehyde as the main product as well as ethanol. A smaller amount of acetic acid is also obtained, probably due to the oxidation of the acetaldehyde.[10a,b] Oxidation of propane produces acetone and isopropanol as the main products, apart from some minor amounts of propanal, propanol and propionic acid.[10a,b] Butanone-2 and butanol-2 are obtained as the major products and butanal, 1-butanol and butyric acid are the minor products of the peroxidative oxidation of *n*-butane.[10a,b] A very high TON (in the 1×10^3–3×10^3 range) was observed in the case of ethane and propane oxidations. The presence of the secondary carbon atom makes propane more reactive towards oxidation.[10a,b]

7.3 Mechanism: Vanadium-catalysed Peroxidative Oxidation of Alkanes

To elucidate the type of mechanism for the vanadium-catalysed peroxidative oxidation of alkanes, selectivity parameters for the oxidations of different

linear and branched alkanes were analysed by using various vanadium-catalytic systems, such as V-cat/PCA/aq. H_2O_2/CH_3CN[10–13,17,18] and V-cat/HNO_3/aq. H_2O_2/CH_3CN,[19] *etc.* Low bond- and regioselectivities were observed for the oxidation of *n*-heptane and methylcyclohexane. The oxidation of the *cis* and *trans* isomers of 1,2-dimethylcyclohexane show non-stereoselectivity. All these low-selectivity features support the involvement of the highly reactive hydroxyl radical during the course of the oxidation reaction.

Based on selectivity, kinetic and theoretical studies, the oxidation of alkanes is proposed to proceed *via* generation of the hydroxyl radical ($HO^{\bullet}$) upon metal-catalysed decomposition of H_2O_2.[14] This $HO^{\bullet}$ abstracts an hydrogen atom from the alkane (RH) to form the alkyl radical ($R^{\bullet}$) which reacts with O_2 (*e.g.*, from air) yielding the alkyl peroxyl radical $ROO^{\bullet}$, followed by the formation of the alkyl hydroperoxide ROOH as a primary product. Finally, the decomposition (metal-assisted) of ROOH afforded the corresponding alcohol (ROH) and ketone.

A likely catalytic mechanism of the formation of $HO^{\bullet}$ by a V^{V} complex is presented in Scheme 7.4.[14]

The metal-promoted, proton-transfer steps from H_2O_2 to oxido or hydroxido ligands can possibly occur *via* four different transition states, as depicted in Scheme 7.5.[16b]

The role of H_2O (Scheme 7.5c)[20] or of an oxido-vanadium group (Scheme 7.5d)[16b] is markedly favourable due to the formation of 6-membered metallacycles, which substantially lower the energy of the transition state in comparison with direct proton-transfer (Scheme 7.5a) or PCA-assisted proton-transfer (Scheme 7.5b). This extra stability of the transition state effectively promotes the reaction, as supported by DFT calculations.[16b,20] Hence, a controlled amount of water present in the system can play a relevant promoting role as a catalyst for proton-shift steps.

The rate of the oxidation process for the **2**/H_2O_2/PCA system has been determined, showing the dependences of the initial oxidation rates on the initial concentrations of the various components of the reaction mixture.[10a] The kinetic data also support the generation of hydroxyl radicals during the

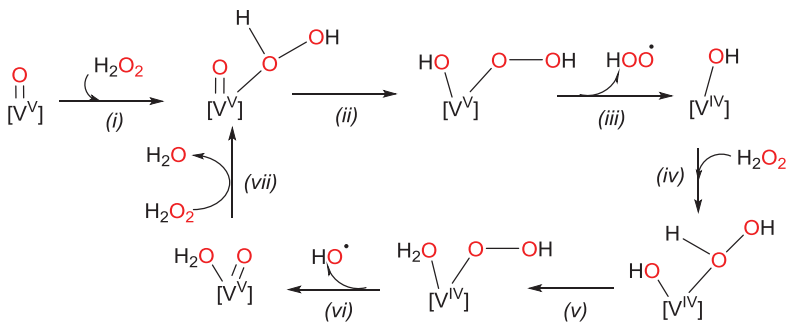

Scheme 7.4 Proposed catalytic mechanism for vanadium-catalysed hydroxyl radical generation from H_2O_2.[14]

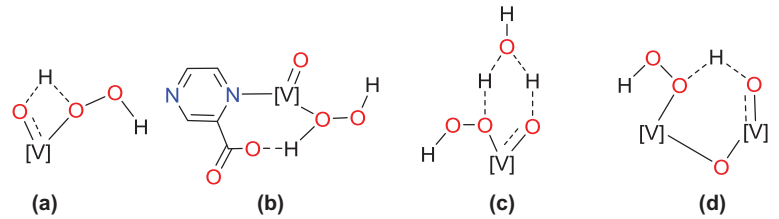

Scheme 7.5 Four different transition states likely involved in proton-shift from H_2O_2: direct proton-transfer (a), assisted by PCA (b), assisted by H_2O (c) and assisted by a second V centre (d).

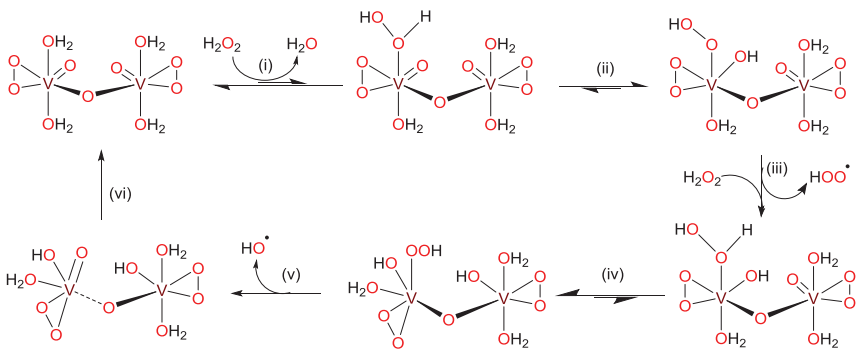

Scheme 7.6 Proposed catalytic cycle for the hydroxyl radical generation from H_2O_2 based on an oxidodivanadate.[16b]

reaction process[10a,21] and suggest that acetonitrile is the main competitor for cyclohexane in the reaction with hydroxyl radical.[16b]

The generation of the HO• radical is also established in the case of oligovanadates (generated in acidic medium from monovanadate) as shown in Scheme 7.6 for an oxidodivanadate catalytic system, as supported by theoretical DFT calculations.[16b] In this case, the second vanadium fragment stabilises the key transition state [step (iv), Scheme 7.6] *via* formation of a 6-membered cyclic structure (Scheme 7.5d).[16b]

In these mechanistic proposals for the formation of the hydroxyl radical, the overall reactions (7.1) and (7.2) are involved in which the vanadium oxidation state in the catalyst is variable (V or IV).

$$[V^{V}] + H_2O_2 \rightarrow [V^{IV}] + H^+ + HOO^{\bullet} \quad (7.1)$$

$$[V^{IV}] + H_2O_2 \rightarrow [V^{V}] + HO^- + HO^{\bullet} \quad (7.2)$$

However, in the case of a vanadium catalyst with a suitable redox active carbohydrazone ligand, as illustrated by complex **4**, such a non-innocent ligand can play the redox role of the metal which can keep a unique oxidation state (eqn (7.3) and (7.4)). A convenient metal–ligand cooperation effect can thus be achieved.

$$[V]-L+H_2O_2 \rightarrow [V]-L^{red}+H^+ + HOO^{\bullet} \quad (7.3)$$

$$[V]-L^{red}+H_2O_2 \rightarrow [V]-L+HO^- + HO^{\bullet} \quad (7.4)$$

7.4 Vanadium Catalysed Oxidation of Alcohols

Oxidations of alcohols to ketones concern relevant strategies for diverse applications.[22,23] In particular, the selective oxidations of secondary alcohols to ketones can be aerobic[24] or peroxidative,[25] and the use of microwave (MW) irradiation instead of conventional heating can provide a convenient synthetic method.[26] Oxidovanadium complexes derived from aroylhydrazones are efficient catalysts or catalyst precursors for such oxidation reactions.

7.4.1 Catalytic Oxidation of 1-Phenylethanol under Conventional Heating

The oxidovanadium(v) complexes [VO(ap-bhz)(OMe)(MeOH)] (**14**), [VO(ap-fah)-(OMe)(MeOH)] (**15**), [VO(ap-nah)(OMe)(MeOH)] (**16**) and [VO(ap-inh)(OMe)-(MeOH)] (**17**) derived from four different aroylhydrazone ligands act as efficient catalysts for oxidation of 1-phenylethanol (Scheme 7.7).[27] The pro-ligands, *i.e.*, H_2ap-bhz, H_2ap-fah, H_2ap-nah and H_2ap-inh, respectively, were obtained by the condensation of acetylpyrazolone (H_2ap) with benzoyl hydrazide (bhz), furoyl hydrazide (fah), nicotinoyl hydrazide (nah) and isonicotinoyl hydrazide (inh).[27]

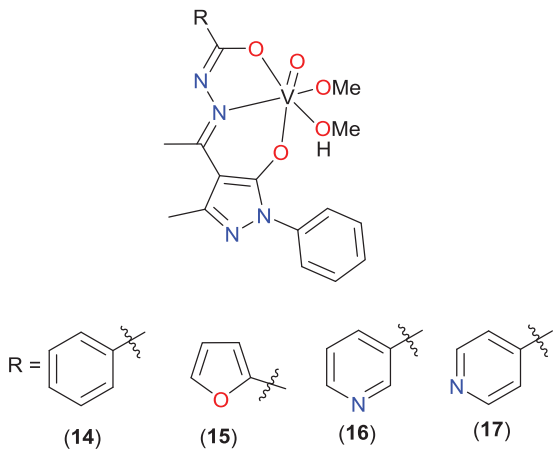

(**14**) (**15**) (**16**) (**17**)

Under optimised reaction conditions (0.01 mol of 1-phenylethanol, 4.4 μmol of catalyst, 0.02 mol of H_2O_2, 5 mL MeCN at 80 °C, 6 h) complex **14** exhibits the highest conversion to acetophenone (86%) with a TOF value of 651 h^{-1}. In the case of complexes **15–17**, the obtained maximum conversion is *ca.* 80%.[27] Based on UV/Vis and ^{51}V NMR studies, a possible catalytic cycle (Scheme 7.8) was proposed.[27]

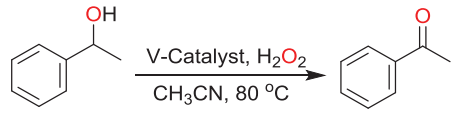

Scheme 7.7 Catalytic oxidation of 1-phenylethanol to acetophenone under conventional conditions.

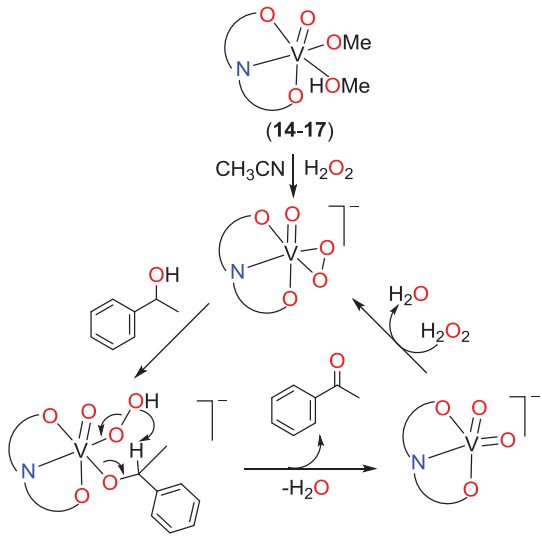

Scheme 7.8 Proposed catalytic cycle for the oxidation of 1-phenylethanol to acetophenone under conventional heating.[27]

7.4.2 Microwave-assisted Oxidation of Secondary Alcohols

A set of four different oxidovanadium(IV) and oxidovanadium(V) complexes derived from salicylaldehyde-2-hydroxybenzoylhydrazone (H_2L) were tested as catalysts for solvent-free MW-assisted oxidation of aromatic and alicyclic secondary alcohols with *tert*-butylhydroperoxide as oxidant. The complexes are the oxidoethoxidovanadium(V) [VO(OEt)L] (**1**), the dioxidovanadium(V) $(NH_3CH_2CH_2OH)^+[VO_2L]^-$ (**18**), the oxidovanadium(V) [VO(hq)L] (Hhq = 8-hydroxyquinoline) (**19**) and the oxidovanadium(IV) [VO(phen)L] (phen = 1,10-phenanthroline) (**20**).[28]

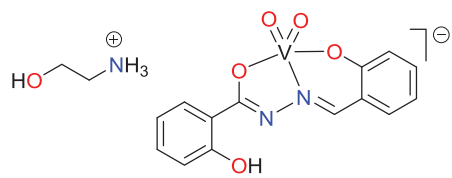

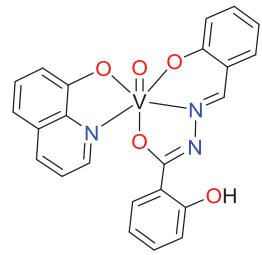

(**19**)

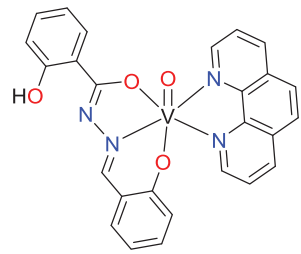

(**20**)

1-Phenylethanol and cyclohexanol (Scheme 7.9) were chosen as model substrates for the oxidation of aromatic and alicyclic secondary alcohols. Under neat solvent- and additive-free conditions [30 min, low power (25 W) MW irradiation] these complexes exhibited good catalytic activity with TON (TOF) values up to 1.8×10^3 (3.6×10^3 h^{-1}) (**3**) leading to yields of acetophenone (from 1-phenylethanol) and cyclohexanone (from cyclohexanol) in the ranges of 77–94% and 30–38%, respectively. This catalytic transformation shows a high selectivity towards the formation of ketones as no traces of other products were detected by GC–MS analysis.[28]

A strong inhibition effect was observed when the catalytic reaction was carried out in the presence of a carbon-radical trap ($BrCl_3$) or an oxygen-radical trap (Ph_2NH). Therefore, a possible mechanism may proceed *via* formation of ^{t}BuO$^\bullet$ and ^{t}BuOO$^\bullet$ radicals produced in the vanadium promoted decomposition of TBHP according to the proposed eqn (7.5) – (7.10).[28]

$$VO^{3+} + {}^t\text{BuOOH} \rightarrow VO^{2+} + {}^t\text{BuOO}^\bullet + H^+ \qquad (7.5)$$

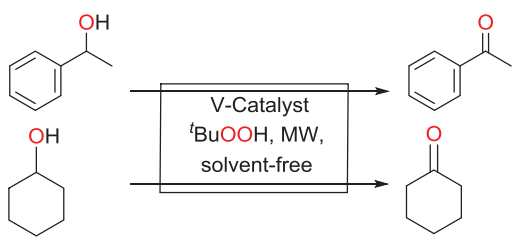

Scheme 7.9 Microwave-assisted, neat, solvent-free oxidation of 1-phenylethanol and cyclohexanol to acetophenone and cyclohexanone.[28]

$$VO^{2+} + {}^{t}BuOOH \rightarrow VO^{3+}\text{–}OH + {}^{t}BuO^{\bullet} \quad (7.6)$$

$$VO^{3+}\text{–}OH + {}^{t}BuOOH \rightarrow VO^{3+}\text{–}OO\text{–}{}^{t}Bu + H_2O \quad (7.7)$$

$${}^{t}BuO^{\bullet} + R_2CHOH \rightarrow {}^{t}BuOH + R_2C^{\bullet}\text{–}OH \quad (7.8)$$

$${}^{t}BuOO^{\bullet} + R_2CHOH \rightarrow {}^{t}BuOOH + R_2C^{\bullet}\text{–}OH \quad (7.9)$$

$$VO^{3+}\text{–}OO\text{–}{}^{t}Bu + R_2C^{\bullet}\text{–}OH \rightarrow R_2C{=}O + {}^{t}BuOOH + VO^{2+} \quad (7.10)$$

The catalytic oxidation of 1-phenylethanol by oxidovanadium(v)-aroylhydrazone complexes anchored on carbon materials as catalysts is discussed in Chapter 12.

7.5 Epoxidation of Alkenes

Epoxidation of alkenes or olefins leading to alkene oxides is an important reaction in chemical industry since they can be useful raw materials in the production of fine chemicals, surfactants, epoxy resins and paints as well as being vital intermediates in organic synthesis for the manufacture of other important commercial products.[29] Organic peroxides and organic peracids have been widely used for a large number of catalytic epoxidation processes.[30] However, metal-catalysed epoxidation of alkenes using milder oxidants, including O_2, H_2O_2 and alkyl hydroperoxides, has gained high interest.[31] Vanadium-aroylhydrazones can also play a significant role as catalysts for the epoxidation of alkenes.

The aroylhydrazones obtained by the condensation of 4,6-diacetylresorcinol with isonicotinoyl hydrazide (H_2dar-inh), nicotinoyl hydrazide (H_2dar-nah), benzoyl hydrazide (H_2dar-bhz) and 2-furoyl hydrazide (H_2dar-fah) in MeOH have been used to synthesise the set of dioxidovanadium complexes $[K(H_2O)_2][VO_2(darinh)]$ (**21**), $[K(H_2O)_2][VO_2(dar\text{-}nah)]$ (**22**), $[K(H_2O)_2][VO_2(dar\text{-}bhz)]$ (**23**) and $[K(H_2O)_2][VO_2(dar\text{-}fah)]$ (**24**), respectively.[32] These oxidovanadium complexes (**20**–**24**) act as catalysts for the epoxidation of various alkenes such as styrene, cyclohexene, *cis*-cyclooctene, 1-hexene, 1-octene, cyclohexenone and *trans*-stilbene as model substrates with H_2O_2 in the presence of $NaHCO_3$ as promoter.[32]

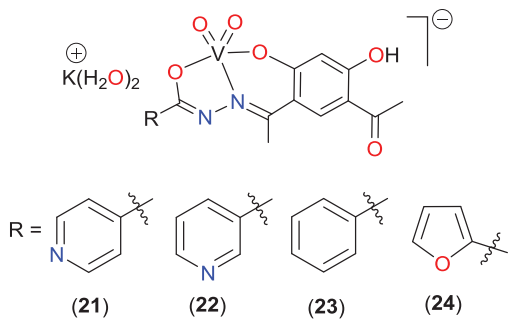

Under optimal reaction conditions – catalyst (0.0005 g), 30% H_2O_2 (1.70 g, 15 mmol), $NaHCO_3$ (2 mmol), MeCN (7 mL) and 80 °C – *cis*-cyclooctene

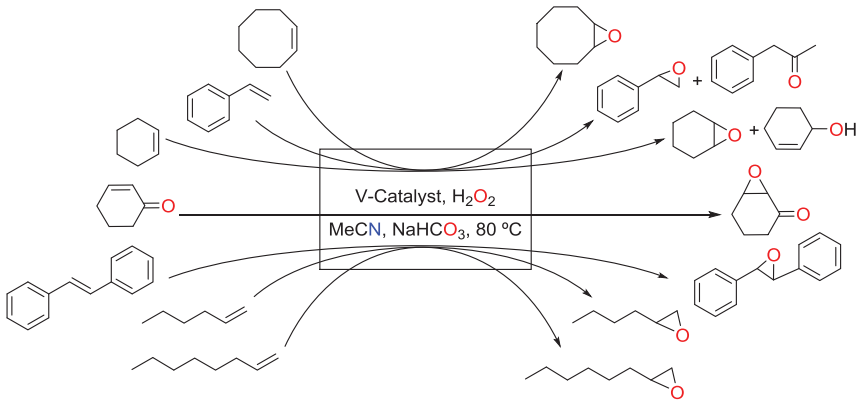

Scheme 7.10 Vanadium-catalysed epoxidation of alkenes.[32]

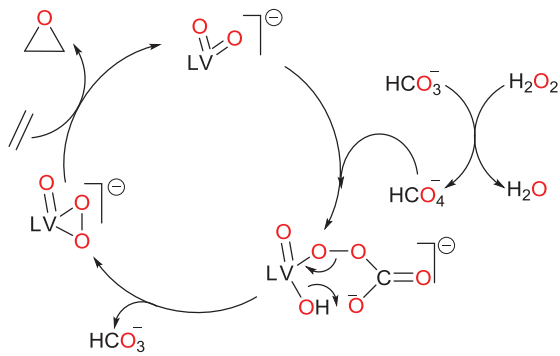

L represents the corresponding ligand in **21-24.**

Scheme 7.11 Proposed mechanism for the epoxidation of alkenes by oxidoperoxidovanadium(v) complex with H_2O_2 in the presence of $NaHCO_3$.[33]

produces a maximum of 85% conversion with 100% selectivity (using **21** and **24** as catalysts) to cyclooctene oxide in 6 h.[32] Lower conversions were realised in other solvents compared to MeCN, following the order: EtOH (78%) > MeOH (56%) > $CHCl_3$ (29%) > CH_2Cl_2 (20%) > *n*-hexane (12%) > toluene (10%).

With other alkenes, 86%–97% conversions were obtained in 6 h, except for the linear alkanes (52%–73% conversions). Within 24 h, 100% conversions were achieved except for styrene and 1-hexene where by-products were formed. The reaction products are shown in Scheme 7.10.[32]

The proposed mechanism is supposed to proceed *via* formation of HCO_4^- (peroxymonocarbonate) which upon the reaction with the dioxidovanadium complex (catalyst) forms an oxido-peroxido species (Scheme 7.11).[33] This oxido-peroxido species then reacts with the alkene and produces epoxide with the regeneration of the dioxidovanadium catalyst.

7.6 Oxidative Bromination

Haloperoxidases and halogenases are special enzymes that catalyse the formation of C–X bonds in biology. The oxidative halogenation of hydrocarbons catalysed by haloperoxidases (using peroxide as oxidant) occurs *via* formation of hypohalous acids (HOX) according to eqs. (11) and (12).[4b,4c,34] This is also an important reaction in organic chemistry with relevance to the chemical industry. Oxidovanadium(v) and oxidovanadium(iv) complexes with mixed O,N-donor atoms can act as functional models of vanadate-dependent haloperoxidase enzymes (VHPO) and can catalyse the oxidative bromination of organic substrates in the presence of H_2O_2 and bromide ion.

$$X^- + H_2O_2 + H^+ \rightarrow HOX + H_2O \tag{7.11}$$

$$RH + HOX \rightarrow RX + H_2O \tag{7.12}$$

7.6.1 Oxidative Bromination of Styrene

Several oxidovanadium(v) complexes derived from aroylhydrazones served as functional models of VHPO. Oxidomonoperoxido $[VO(O_2)]^+$ or oxidodiperoxido $[VO(O_2)_2]^-$ species are generated during the catalytic cycle by the reaction of the vanadium complex with 1 or 2 equiv. of H_2O_2, which ultimately oxidise KBr to Br_2 and/or HOBr. These latter species further react with the organic substrate to yield the brominated product.[35]

Examples of such complexes are discussed for the oxidative bromination of styrene.

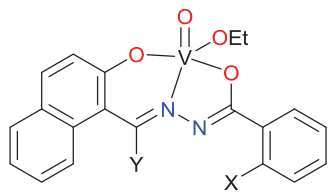

X = NH_2, Y = H (**25**)
X = OH, Y = H (**26**)
X = H, Y = CH_3 (**27**)
X = NH_2, Y = CH_3 (**28**)

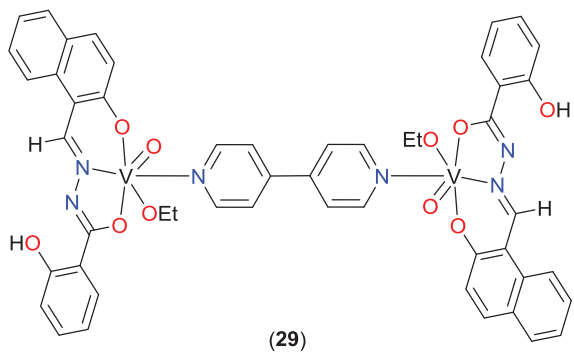

(**29**)

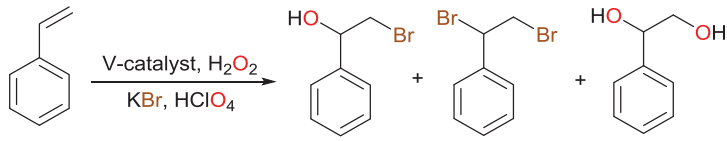

Scheme 7.12 Oxidative bromination of styrene catalysed by vanadium-aroylhydrazone complexes.

The mononuclear oxidoethoxidovanadium(v) complexes (**25**–**28**) and the dinuclear compound **29** act as catalyst precursors towards the oxidative bromination of styrene in the presence of H_2O_2, KBr and $HClO_4$ (Scheme 7.12). Three main products, *viz.*, 2-bromo-1-phenylethan-1-ol, 1,2-dibromo-1-phenylethane and 1-phenylethan-1,2-diol, are obtained along with a small amount (*ca.* 4%) of minor products (benzaldehyde, styrene epoxide, benzoic acid and 4-bromostyrene). The addition of $HClO_4$ promotes the oxidative bromination. At room temperature, under optimised conditions (10 mmol KBr, 30 mmol H_2O_2, 20 mmol $HClO_4$ and 0.0005 g catalyst in 1 h), 96% to 99% of conversion was achieved with a TOF value of 8000 h^{-1} (or above) in CH_3CN/water (20/5 mL). Complex **27** gives the highest conversion, but the dinuclear complex **29** yields a maximum yield of 33% of 2-bromo-1-phenylethane-1-ol.[35]

The oxidovanadium(v) and dioxidovanadium(v) complexes [VO(OMe)(MeOH){Hdfmp(inh)$_2$}] (**30**), [VO(OMe)(MeOH){Hdfmp(nah)$_2$}] (**31**) and [VO(OMe)(MeOH){Hdfmp(bhz)$_2$}] (**32**) [VO_2{H_2dfmp(inh)$_2$}]$_n$·5nH_2O (**33**), K[VO_2{Hdfmp(nah)2}] (**34**) and K[VO_2{Hdfmp(bhz)$_2$}] (**35**) are also catalysts for the same reaction, *i.e.*, oxidative bromination of styrene in the presence of H_2O_2, KBr and $HClO_4$. The aroylhydrazone Schiff bases H_3dfmp(L)$_2$ were synthesised by the condensation of 2,6-diformyl-4-methylphenol with the appropriate hydrazone [L = isonicotinoylhydrazide (inh), nicotinoylhydrazide (nah) and benzoylhydrazide (bhz)].[36]

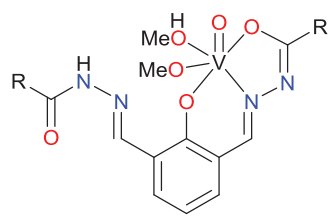

R = 4-pyridyl (**30**)
R = 3-pyridyl (**31**)
R = phenyl (**32**)

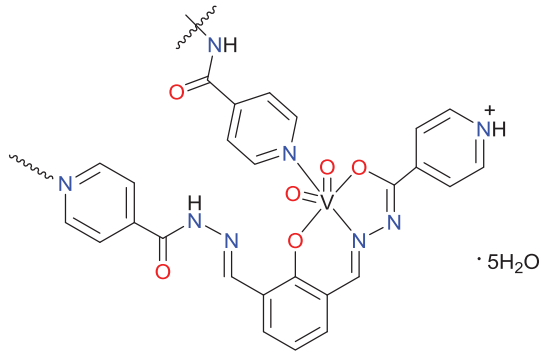

(**33**)

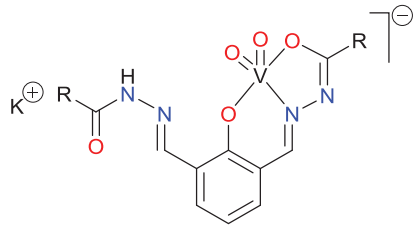

R = 3-pyridyl (**34**)
R = phenyl (**35**)

The optimised reaction conditions were standardised using **33** and these are 0.001 g of catalyst precursor, 10 mmol of styrene, 20 mmol of 30% H_2O_2, 20 mmol of KBr and 30 mmol of $HClO_4$ in 40 mL of dichloromethane–water (1 : 1 v/v) mixture at room temperature after 1 h. All these catalyst precursors (**30**–**35**) render closely similar conversions (*ca.* 97%–99%) into the oxidative brominated products, and **35** shows a slightly better conversion (99%) compared to other catalyst precursors.[36]

7.6.2 Oxidative Bromination of Salicylaldehyde

The oxidovanadium(v) complexes **25**–**29** also catalyse the oxidative bromination of salicylaldehyde in the presence of H_2O_2 in water as the solvent, yielding 5-bromosalicylaldehyde, 3,5-dibromosalicylaldehyde and 2,4,6-tribromophenol (Scheme 7.13).[35]

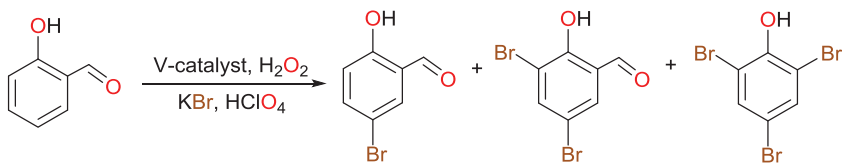

Scheme 7.13 Oxidative bromination of salicylaldehyde catalysed by vanadium-aroylhydrazone complexes.

The reaction was performed under the following conditions: salicylaldehyde (5 mmol), V-catalyst (0.0005 g), KBr (5 mmol), 30% aqueous H_2O_2 (10 mmol), 70% aqueous $HClO_4$ (15 mmol) and water (20 mL). A maximum of 99% conversion was achieved with **27** as catalyst and the selectivities of different products are as follows: 5-bromosalicylaldehyde (74%) > 2,4,6-tribromophenol (21%) > 3,5-dibromosalicylaldehyde (5%).[35]

7.7 Conclusions

This chapter illustrates the importance of oxidovanadium(IV) and oxidovanadium(V) complexes derived from aroylhydrazones in various catalytic transformations of organic substrates. These complexes can play a crucial role as catalysts or catalyst precursors in various catalytic oxidation reactions, such as oxidations of alkanes and of alcohols, as well as epoxidation of alkenes and oxidative brominations. Aroylhydrazone ligands can stabilise the vanadium high oxidation states (IV or V) of the complexes. Moreover, the redox activity of the coordinated aroylhydrazones allows them to engage in cooperative effects with vanadium, promoting the catalytic activity of the metal catalyst, as observed for alkane oxidation. The activity of the catalysts increases markedly in the presence of 2-pyrazinecarboxylic acid (PCA) as promoter towards the oxidation of alkanes, but water and an oxidovanadium moiety of a dinuclear catalyst can also promote the reaction, even in a more effective way. The alkane oxidation occurs *via* radical pathways, as supported by selectivity, kinetic and theoretical studies.

The aroylhydrazone oxidovanadium(IV and V) complexes are also catalysts for the oxidation of primary and secondary alcohols. The use of microwave irradiation can be advantageous compared to conventional heating in terms of catalytic activity and energy efficiency. A very good catalytic activity is found towards the selective epoxidation of various alkenes. Some of the complexes with mixed O,N-donor atom ligands can act as potential functional models of vanadate-dependent haloperoxidases by catalysing the bromination of organic substrates in the presence of hydrogen peroxide, a bromide salt and perchloric acid.

Oxidovanadium-aroylhydrazones are promising catalysts for oxidations of organic species, and the scope of the field deserves to be further extended and explored in terms of achieving more sustainable and greener catalytic systems.

Acknowledgements

This work has been supported by the Fundação para a Ciência e Tecnologia (FCT) 2020–2023 multiannual funding to Centro de Quimica Estrutural (project UIDB/00100/2020). The authors are also grateful to the FCT for financial support to project PTDC/QEQ-QIN/3967/2014. M. S. acknowledges the FCT and IST for a working contract ''DL/57/2017'' (Contract no. IST-ID/102/2018).

References

1. (a) M. Sutradhar, L. M. D. R. S. Martins, M. F. C. Guedes, da Silva and A. J. L. Pombeiro, *Coord. Chem. Rev.*, 2015, **301–302**, 200; (b) V. Conte, A. Coletti, B. Floris, G. Licini and C. Zonta, *Coord. Chem. Rev.*, 2011, **255**, 2165; (c) J. A. L. da Silva, J. J. R. Fraústo, da Silva and A. J. L. Pombeiro, *Coord. Chem. Rev.*, 2011, **255**, 2232–2248; (d) A. E. Shilov and G. B. Shul'pin, *Chem. Rev.*, 1997, **97**, 2879.
2. (a) G. Licini, V. Conte, A. Coletti, M. Mba and C. Zonta, *Coord. Chem. Rev.*, 2011, **255**, 2345; (b) J. A. L. da Silva, J. J. R. Frausto da Silva and A. J. L. Pombeiro, *Coord. Chem. Rev.*, 2011, **255**, 2232; (c) M. Sutradhar and A. J. L. Pombeiro, Vanadium Complexes in Catalytic Oxidations, in *Elsevier Reference Module in Chemistry, Molecular Sciences and Chemical Engineering*. ed. J. Reedijk, Elsevier, Waltham, MA, 2017.
3. (a) M. R. Maurya, A. Kumar and J. C. Pessoa, *Coord. Chem. Rev.*, 2011, **255**, 2315; (b) C. Bolm, *Coord. Chem. Rev.*, 2003, **237**, 245; (c) T. Hirao, *Chem. Rev.*, 1997, **97**, 2707; (d) L. M. D. R. S. Martins and A. J. L. Pombeiro, *Coord. Chem. Rev.*, 2014, **265**, 74.
4. (a) J. N. Carter-Franklin, J. D. Parrish, R. A. Tchirret-Guth, R. D. Little and A. Butler, *J. Am. Chem. Soc.*, 2003, **125**, 3688; (b) D. Rehder, *Bioinorganic Vanadium Chemistry*, John Wiley & Sons, New York, ;, 2008; (c) R. Wever and W. Hemrika, Vanadium Haloperoxidases, in *Handbook of Metalloproteins*, ed. A. Messerschmidt, R. Huber, T. Poulos and K. Wieghardt, John Wiley & Sons, Ltd, Chichester, ch. 7, 2001, pp. 1417–1428.
5. M. Sutradhar and A. J. L. Pombeiro, *Coord. Chem. Rev.*, 2014, **265**, 89.
6. (a) D. C. Crans, A. D. Keramidas, S. S. Amin, O. P. Anderson and S. M. Miller, *J. Chem. Soc., Dalton Tans.*, 1997, 2799; (b) M. R. Maurya, A. Arya, A. Kumar, M. L. Kuznetsov, F. Avecilla and J. Costa Pessoa, *Inorg. Chem.*, 2010, **49**, 6586.
7. (a) M. R. Maurya, N. Chaudhary and F. Avecilla, *Polyhedron*, 2014, **67**, 436; (b) M. R. Maurya, A. Arya, U. Kumar, A. Kumar, F. Avecilla and J. Costa Pessoa, *Dalton Trans.*, 2009, 9555; (c) M. R. Maurya, M. Bisht, A. Kumar, M. L. Kuznetsov, F. Avecilla and J. Costa Pessoa, *Dalton Trans.*, 2011, **40**, 6968.
8. *Alkane Functionalization*, ed. A. J. L. Pombeiro and M. F. C. Guedes da Silva, Wiley, Hoboken, NJ, USA, 2019.
9. M. Sutradhar, G. Mukherjee, M. G. B. Drew and S. Ghosh, *Inorg. Chem.*, 2006, **45**, 5150.
10. (a) M. Sutradhar, N. V. Shvydkiy, M. F. C. Guedes da Silva, M. V. Kirillova, Y. N. Kozlov, A. J. L. Pombeiro and G. B. Shul'pin, *Dalton Trans.*, 2013, **42**, 11791; (b) S. Gupta, M. V. Kirillova, M. F. C. Guedes, da Silva and A. J. L. Pombeiro, *Appl. Catal., A*, 2013, **460–461**, 82; (c) D. Dragancea, N. Talmaci, S. Shova, G. Novitchi, D. Darvasiová, P. Rapta, M. Breza, M. Galanski, J. Kožíšek, N. M. R. Martins, L. M. D. R. S. Martins, A. J. L. Pombeiro and V. B. Arion, *Inorg. Chem.*, 2016, **55**, 9187.

11. M. Sutradhar, L. M. D. R. S. Martins, T. Roy Barman, M. L. Kuznetsov, M. F. C. Guedes da Silva and A. J. L. Pombeiro, *New J. Chem.*, 2019, **43**, 17557.
12. S. Gupta, M. V. Kirillova, M. F. C. Guedes da Silva, A. J. L. Pombeiro and A. M. Kirillov, *Inorg. Chem.*, 2013, **52**, 8601.
13. M. Sutradhar, M. V. Kirillova, M. F. C. Guedes da Silva, L. M. D. R. S. Martins and A. J. L. Pombeiro, *Inorg. Chem.*, 2012, **51**, 11229–11231.
14. (a) G. B. Shul'pin, Y. N. Kozlov, G. V. Nizova, G. Suss-Fink, S. Stanislas, A. Kitaygorodskiy and V. S. Kulikova, *J. Chem. Soc., Perkin Trans. 2*, 2001, **2**, 1351; (b) M. V. Kirillova, M. L. Kuznetsov, V. B. Romakh, L. S. Shul'pina, J. J. R. Fraústo da Silva, A. J. L. Pombeiro and G. B. Shul'pin, *J. Catal.*, 2009, **267**, 140; (c) G. B. Shul'pin, *Dalton Trans.*, 2013, **42**, 12794.
15. (a) G. B. Shul'pin, D. Attanasio and L. Suber, *J. Catal.*, 1993, **142**, 147; (b) G. B. Shul'pin, D. Attanasio and L. Suber, *Russ. Chem. Bull.*, 1993, **42**, 55; (c) G. B. Shul'pin, A. N. Druzhinina and G. V. Nizova, *Russ. Chem. Bull.*, 1993, **42**, 1327.
16. (a) R. Z. Khaliullin, A. T. Bell and M. Head-Gordon, *J. Phys. Chem. B*, 2005, **109**, 17984; (b) M. V. Kirillova, M. L. Kuznetsov, Y. N. Kozlov, L. S. Shul'pina, A. Kitaygorodskiy, A. J. L. Pombeiro and G. B. Shul'pin, *ACS Catal.*, 2011, **1**, 1511.
17. (a) P. M. Reis, J. A. L. Silva, J. J. R. Frausto da Silva and A. J. L. Pombeiro, *Chem. Commun.*, 2000, 1845; (b) T. F. S. Silva, E. C. B. A. Alegria, L. M. D. R. S. Martins and A. J. L. Pombeiro, *Adv. Synth. Catal.*, 2008, **350**, 706.
18. L. S. Shul'pina, M. V. Kirillova, A. J. L. Pombeiro and G. B. Shul'pin, *Tetrahedron*, 2009, **65**, 2424.
19. T. F. S. Silva, K. V. Luzyanin, M. V. Kirillova, M. F. C. Guedes da Silva, L. M. D. R. S. Martins and A. J. L. Pombeiro, *Adv. Synth. Catal.*, 2010, **352**, 171.
20. M. L. Kuznetsov and A. J. L. Pombeiro, *Inorg. Chem.*, 2009, **48**, 307.
21. A. E. Shilov and G. B. Shul'pin, *Activation and Catalytic Reactions of Saturated Hydrocarbons in the Presence of Metal Complexes*, Kluwer Academic Publishers, Dordrecht, 2000.
22. R. A. Sheldon, I. Arends and U. Hanefeld, *Green Chemistry and Catalysis*, Wiley-VCH, Weinheim, Germany, 2007.
23. (a) J.-E. Bäckvall, *Modern Oxidation Methods*, Wiley-VCH, Weinheim, 2004, pp. 83–118; (b) *Ullmann's Encyclopedia of Industrial Chemistry*, Wiley-VCH, Weinheim, 6th edn; 2002; (c) R. A. Smiley and H. L. Jackson, *Chemistry and the Chemical Industry*, CRC Press, Boca Raton, FL, 2002.
24. (a) R. Chakrabarty, P. Sarmah, B. Saha, S. Chakravorty and B. K. Das, *Inorg. Chem.*, 2009, **48**, 6371; (b) I. E. Markó, A. Gautier, R. Dumeunier, K. Doda, F. Philippart, S. M. Brown and C. J. Urch, *Angew. Chem., Int. Ed.*, 2004, **43**, 1588; (c) S. S. Stahl, *Angew. Chem., Int. Ed.*, 2004, **43**, 3400; (d) G.-J. ten Brink, I. W. C. E. Arends and R. A. Sheldon, *Science*, 2000,

287, 1636–1639; (e) Y. Uozumi and R. Nakao, *Angew. Chem., Int. Ed.*, 2003, **42**, 194.
25. (a) D. S. Bailie, G. M. A. Clendenning, L. McNamee and M. J. Muldoon, *Chem. Commun.*, 2010, **46**, 7238; (b) D. Sloboda-Rozner, P. L. Alsters and R. Neumann, *J. Am. Chem. Soc.*, 2003, **125**, 5280; (c) V. R. Choudary, D. K. Dumbre, B. S. Uphade and V. S. Narkhede, *J. Mol. Catal. A: Chem.*, 2004, **215**, 129; (d) J. Boudreau, M. Doucette and A. N. Ajjou, *Tetrahedron Lett.*, 2006, **47**, 1695.
26. (a) M. N. Kopylovich, A. P. C. Ribeiro, E. C. B. A. Alegria, N. M. R. Martins, L. M. D. R. S. Martins and A. J. L. Pombeiro, *Adv. Organomet. Chem.*, 2015, **63**, 91; (b) Y. Y. Karabach, M. N. Kopylovich, K. T. Mahmudov and A. J. L. Pombeiro, in *Advances in Organometallic Chemistry and Catalysis*, ed. A. J. L. Pombeiro, John Wiley & Sons, Hoboken, NJ, USA, ch. 18, 2014, pp. 233–245.
27. M. R. Maurya, B. Sarkar, F. Avecilla and I. Correia, *Eur. J. Inorg. Chem.*, 2016, 4028.
28. M. Sutradhar, L. M. D. R. S. Martins, M. F. C. Guedes da Silva and A. J. L. Pombeiro, *Appl. Catal., A*, 2015, **493**, 50.
29. (a) K. Yuan, T. Song, D. Wang, Y. Zou, J. Li, X. Zhang, Z. Tang and W. Hu, *Nanoscale*, 2018, **10**, 1591; (b) X. Chen, B. Gao, Y. Su and H. Huang, *Adv. Synth. Catal.*, 2017, **359**, 2535; (c) N. A. Grosso-Giordano, C. Schroeder, A. Okrut, A. Solovyov, C. Schottle, W. Chasse, N. Marinkovic, H. Koller, S. I. Zones and A. Katz, *J. Am. Chem. Soc.*, 2018, **140**, 4956; (d) Y. Zhu, Q. Wang, R. G. Cornwall and Y. Shi, *Chem. Rev.*, 2014, **114**, 8199.
30. (a) K. A. Jørgensen, *Chem. Rev.*, 1989, **89**, 431; (b) S. T. Oyama, *Mechanisms in Homogeneous and Heterogeneous Epoxidation Catalysis*, Elsevier Science, 2008; (c) A. Blanckenberg and R. Malgas-Enus, *Catal. Rev.*, 2019, **61**, 27–483.
31. M. Costas, in *Green Oxidation in Organic Synthesis*, ed. N. Jiao and S. S. Stahl, John Wiley & Sons Ltd., Hoboken, NJ, USA, ch. 4, 2019, pp. 123–157.
32. M. R. Maurya, N. Jangra, F. Avecilla and I. Correia, *Eur. J. Inorg. Chem.*, 2018, 314.
33. S. Pasayat, M. Böhme, S. Dhaka, S. P. Dash, S. Majumder, M. R. Maurya, W. Plass, W. Kaminsky and R. Dinda, *Eur. J. Inorg. Chem.*, 2016, 1604.
34. D. Rehder, G. Santoni, G. M. Licini, C. Schulzke and B. Meier, *Coord. Chem. Rev.*, 2003, **237**, 53.
35. S. P. Dash, A. K. Panda, S. Dhaka, S. Pasayat, A. Biswas, M. R. Maurya, P. Kumar Majhi, A. Crochet and R. Dinda, *Dalton Trans.*, 2016, **45**, 18292.
36. M. R. Maurya, C. Haldar, A. Kumar, M. L. Kuznetsov, F. Avecilla and J. C. Pessoa, *Dalton Trans.*, 2013, **42**, 11941.

CHAPTER 8

Vanadium-oxide Molecular Catalysts in Non-aqueous Solution

Y. HAYASHI,*[a] M. KATAYAMA[b] AND K. OZUTSUMI[b]

[a] Department of Chemistry, Kanazawa University, Kakuma, Kanazawa 920-1192, Japan; [b] Applied Chemistry, College of Life Science, Ritsumeikan University, Kusatsu, Shiga 525-8577, Japan
*Email: hayashi@se.kanazawa-u.ac.jp

8.1 Fundamental Vanadium-oxide Cluster Chemistry

Metal-oxide clusters concern vast series of molecular-oxide compounds composed by oxygen and transition-metal atoms. When they are limited to vanadium ion, vanadium-oxide clusters may be defined by the formula of $[V_xO_y]^{n-}$. They may be called iso-vanadium-oxide clusters. When there is the presence of heteroatoms, with the formula of $[V_xO_yX_z]^{n-}$ where X represents a heteroatom or a multi-atomic group, they are called hetero-vanadium-oxide clusters. In this chapter, the oxidation state of vanadium atoms is either +5 or +4, but the name of vanadium-oxide clusters usually implies that the oxidation state of vanadium atoms is +5. When some of the vanadium atoms are reduced to the V(IV) oxidation state, those species are referred as mixed-valence vanadium-oxide clusters or reduced vanadium-oxide clusters.

Catalysis Series No. 41
Vanadium Catalysis
Edited by Manas Sutradhar, José Armando L. da Silva and Armando J. L. Pombeiro

Published by the Royal Society of Chemistry, www.rsc.org

8.1.1 Building Blocks: Four Types of Coordination Modes

A fundamental building block of vanadium-oxide clusters is a tetrahedral VO_4 unit, a pyramidal VO_5 unit, a trigonal-bipyramidal VO_5 unit, or an octahedral VO_6 unit (see Figure 8.1). The structures often range between the two ideal different VO_5 units, *i.e.*, the pyramidal unit and the trigonal-bipyramidal unit. To categorize a structure, the τ-value is used to distinguish the two extremes.[1]

The VO_5 coordination mode is characteristic of high-valence vanadium cations. The small ionic radius of V(v) makes it difficult to bind six negative oxygen atoms that are repelling each other, resulting in the rejection of one oxygen atom out of the coordination sphere. Each building block may share the peripheral oxygen atoms and forms a dimer or even larger cluster. Those are constructed by interconnecting the polyhedra through bridging oxygen atoms. The joining of two coordination polyhedra has several patterns (see Figure 8.2). Two polyhedra may join by a mono-bridged oxygen atom and it is referred to as an apex-sharing or a corner-sharing mode. Doubly bridged oxygen atoms mean that two polyhedra are sharing their polyhedral edges and the joining is called an edge-sharing mode. Triply-bridging oxygen atoms provide an example of face-sharing polyhedra. The face-sharing mode is usually energetically unfavourable due to the repulsive interaction between the cations at the centre of the T_d-unit, especially when the cation is at its highest valence state.

To illustrate the structure, a polyhedral model is often used for the purpose of simplifying the structure by omitting metal and oxygen atoms although it is an unfamiliar description for organic chemists. In this chapter, the ''ball-and-stick model'' (see Figure 8.3) is mainly used because it is easier to understand.

8.1.2 Principle Reaction Mechanism of Vanadium-oxide Clusters

Research on oxide-molecules lags many years behind organic chemistry. The chemistry of vanadium-oxide molecules involves constantly changing

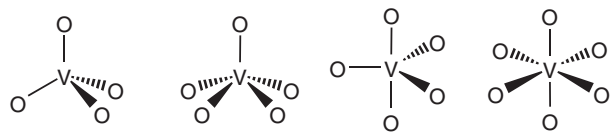

Figure 8.1 Four types of coordination modes in vanadium-oxide clusters.

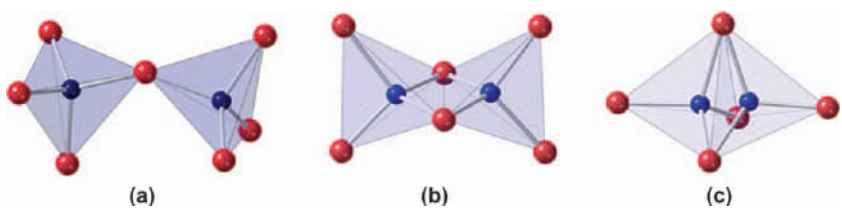

Figure 8.2 Three connecting modes in T_d-based metal-oxide clusters.

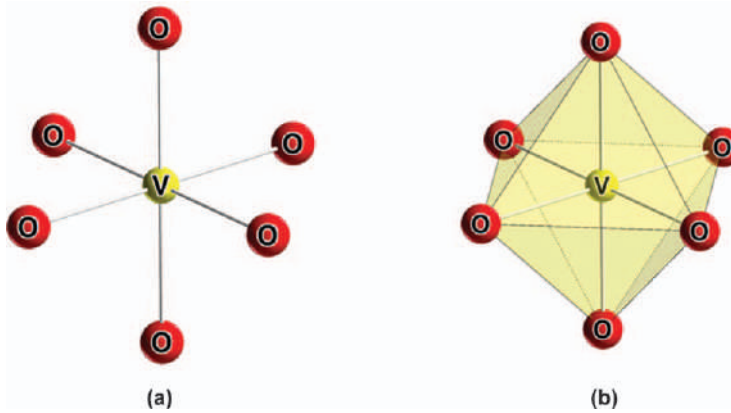

Figure 8.3 Ball-and-stick model, and polyhedral model.

molecular-surface reactions and each molecule exchanges its peripheral oxygen atoms with water. In contrast, organic reaction proceeds by a stepwise bond-breaking or bond-making at only a few bonds in a particular reaction – the reaction of vanadium-oxide clusters involves multiple bond-breaking and bond-making simultaneously. In other words, weak ionic bonds allow a chemical transformation to occur relatively easily because it has far less bond energy than the energy of covalent bonds. In a structure transformation, a series of reactions is involved such as protonation and deprotonation, water dissociation or association, nucleophilic attacks of hydroxido-group to make the cluster framework growth and dissociation of mononuclear units or even a multinuclear unit to make a cluster unit smaller. However, this does not mean metal-oxide molecules are easy to decompose. Instead they are considered to be robust molecules that eventually cannot be burnt further. They exhibit a sort of a self-healing structure under specific conditions. Even if some molecules break apart, the ionic-charge balance requires a reconstruction of the original framework because it is the most electrostatically balanced form. The resurrection of the framework has a stark difference from organic compounds: when organic materials are decomposed, the reconstruction of the original structure is often hard work. The decomposition reaction tends to be a spontaneous, one-way reaction in organic chemistry. This is why vanadium-oxide clusters can be good catalysts. A catalyst has to change the structure quickly by adopting specific requirements: (i) to accept a substrate, it has to provide a coordination site by a dissociation of a ligand on a catalytic precursor; (ii) the reactants also require an approach to the substrate on the surface of the catalyst by making a way by rearranging the structure; (iii) the reaction between the substrate and the reactant usually needs a different coordination number at an active site before the reaction and after the reaction; and (iv) the dissociation of the product leaves an uncoordinated site that prompts a rearrangement to prepare for the next reaction step. These multiple series of events on a catalytic-active centre have to proceed smoothly and without interruption by the formation of a thermodynamically stable inactive form.

Vanadium-oxide molecules have a reactive surface that can be appropriate for a particular catalytic reaction, and it is also very easy to reproduce the original structure – a fundamental requirement for a catalyst.

The building-up of those units connected by a different bridging mode allows a vanadium cluster to build an infinite combination of different cluster frameworks. Thus, theoretically, there is an infinite number of vanadium-oxide cluster structures available to a particular reaction. However, in aqueous solution, isolated species are quite restricted to a few species, such as orthovanadates, $[VO_4]^{3-}$, metavanadates, $[VO_3]^-$, and decavanadates, $[V_{10}O_{28}]^{6-}$ and their protonated species. These species are considered to be thermodynamically stable and are very easy to transform each other in water. The growth of an oxide-cluster is explained by an acid-condensation reaction, while the reverse reaction is a hydrolysis reaction. A mononuclear orthovanadate may be protonated to produce $[HVO_4]^{2-}$ which has a hydroxido-group. The hydroxido-group is usually highly nucleophilic and attacks the cationic centre of the nearest molecule to produce a dimer (see Figure 8.4).

A terminal oxygen atom on vanadium-oxide clusters may be protonated to different degrees, resulting in the formation of three types of terminal groups – an oxido-group, a hydroxido-group and an aqua-group. The bond energy between a terminal oxido-group and a vanadium atom is especially strong and is considered to be a double or triple bond. The very-short V=O bond is called a *vanadyl-bond* and shows a characteristic IR band in the region of 900 cm^{-1}. The protonated species are distributed in the solution depending on the pH value. The repulsive force between a metal cation and the proton on the hydroxido-group is an important factor for distribution. Here, the valence state of the metal cation strongly influences the degree of protonation: higher valence (such as 6+) metal cations have a significant cation–proton repulsive force, favouring deprotonation, and the equilibrium shifts to the left in the equation. At a lower valence state, metal cation allows more protonation favouring and the equilibrium shifts to the right side of the equation (see Figure 8.5).

The simple form of vanadate monomer, orthovanadate (VO_4^{3-}) exists only at an extremely high pH value. Protonation on orthovanadate gives HVO_4^{2-}

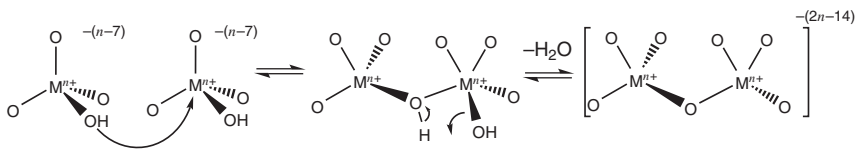

Figure 8.4 Condensation mechanism of metal-oxo-acids.

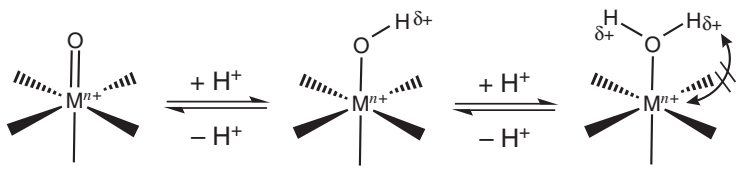

Figure 8.5 Protonation and deprotonation equilibrium.

and prompts the production of metavanadate species (VO_3^-) that may be a dimer, trimer or tetramer with protonation, or without protonation and is either in a linear or cyclic form. The chemistry is similar to phosphates. Decavanadates, $[V_{10}O_{28}]^{6-}$, are under an equilibrium with metavanadates and orthovanadates.[2] In aqueous solution, these three species are equilibrated. The reaction conditions, such as acidity and concentration, are extremely important since the dominant species depends on them.

Vanadium-oxide clusters are easy to react in water through a multi-step process. Protonation and deprotonation are relatively rapid. Formation of a hydroxido-group triggers a nucleophilic attack against a cationic metal centre. It leads to a new chemical bond formation and may respond to create a new structure after rearrangement to cope with its new charge balance. However, it might do the opposite and repel each other, resulting in a decrease of the size of the cluster. The formation of a new molecule requires a multi-step reaction, but it proceeds rapidly because of the weak ionic bonds. In organic solvents, those reactions are restricted because of the limited amount of water in solution, and a distinct series of vanadium-oxide clusters are formed.

8.2 Typical Reactions in Vanadium-oxide Molecules

Contrary to an organic reaction, a reaction of inorganic clusters is dynamic and may change the structure into a different framework or a cluster of different size. The uniqueness of the chemical principles governing vanadium-oxide clusters may be demonstrated in the transformation reaction among decavanadates, $[V_{10}O_{28}]^{6-}$, dodecavanadates, $[V_{12}O_{32}]^{4-}$, and tridecavanadates, $[V_{13}O_{34}]^{3-}$ (see Figure 8.6). When a protonated decavanadate is refluxed in acetonitrile solution, a mixture of dodecavanadates and tridecavanadates forms and the reaction is categorized as an acid-condensation reaction. However, by carefully adjusting the stoichiometry, decavanadates are converted to dodecavanadates exclusively and further adjustment of the stoichiometry affords tridecavanadates. The stepwise acid-condensation reaction increases the number of vanadium from 10 to 13. The reverse reaction is hydrolysis and decavanadates can be synthesized from the hydrolysis reaction of dodecavanadates or tridecavanadates. The number of vanadium atoms in decavanadates, dodecavanadates and tridecavanadates is V_{10}, V_{12}, and V_{13}, respectively. In these reactions, V_{10} grows to V_{13} through V_{12}, and the hydrolysis reaction of V_{13} produces V_{10}.

However, according to organic chemistry theory, an addition of vanadium atoms is necessary when the cluster increases the number of vanadium atoms, because in organic reaction, no scrambling of molecular formulae is possible, which is unlike silicon chemistry. You may wonder that without adding vanadium sources, these reactions may not make sense at all. In ionic compounds, when a hydroxido-group attacks a near molecule, it spontaneously scrambles the composition and drives a structure transformation in the kinetically most-favoured form by either discarding water to form an oxido-bridge or a hydroxido-bridge, thereby resulting in growth of the number of vanadium

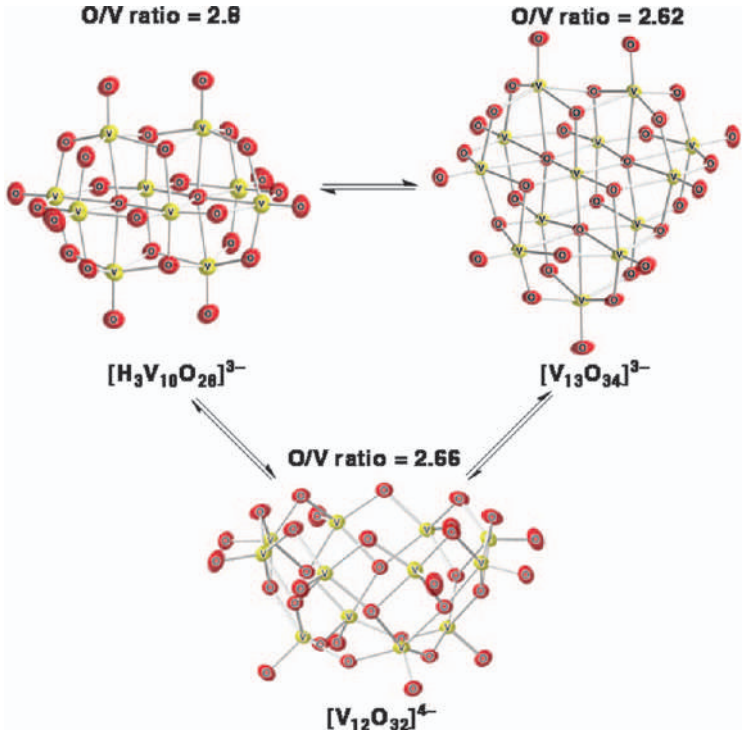

Figure 8.6 Mutual conversion reactions by condensation and hydrolysis of vanadium-oxide clusters.

$$\{(n\text{-}C_4H_9)_4N\}_3[H_3V_{10}O_{28}] + 2\{(n\text{-}C_4H_9)_4N\}OH \longrightarrow 5\{n\text{-}C_4H_9)_4N\}_4[V_{12}O_{32}] + 10H_2O \quad (1)$$

$$13\{(n\text{-}C_4H_9)_4N\}_3[H_3V_{10}O_{28}] \longrightarrow 10\{(n\text{-}C_4H_9)_4N\}_3[V_{13}O_{34}] + 9\{(n\text{-}C_4H_9)_4N\}OH + 15H_2O \quad (2)$$

$$13\{(n\text{-}C_4H_9)_4N\}_4[V_{12}O_{32}] + 8H_2O \longrightarrow 12\{(n\text{-}C_4H_9)_4N\}_3[V_{13}O_{34}] + 16\{(n\text{-}C_4H_9)_4N\}OH \quad (3)$$

Scheme 8.1 Stoichiometry of the reactions.

atoms, or by accepting a water molecule followed by a vanadate group dissociation, with decreasing the number of vanadium atoms. The resulting compounds may have different numbers of vanadium atoms, and an unstable intermediate does not survive in the reaction because it may further condense or hydrolyse until it reaches a kinetically stable form.

There is no requirement to add or subtract vanadium atoms for maintaining the math of the chemical formula. If the scrambling of a molecular composition is allowed, these reactions may follow an exact stoichiometry as shown in Scheme 8.1.

In fact, the series of reactions proceeds quantitatively and isolated yields have achieved almost 90%. These reaction schemes emphasise that the stoichiometry of acid–base as well as the amount of water molecules in the solution is critical in vanadium-oxide cluster synthesis.[3]

Inorganic oxide molecules allow composition scrambling. The oxygen-to-vanadium ratio is an important factor, and it is just like the carbon-to-hydrogen ratio in organic chemistry, but it is far more critical. When the oxygen–vanadium ratio decreases, it is a condensation growth reaction and when it increases, it is a hydrolysis reaction. The oxygen–vanadium ratio of decavanadates, dodecavanadates and tridecavanadates is 2.80, 2.66 and 2.62, respectively. A smaller value means a more condensed structure, as the number of vanadium atoms increases from 10 to 12 and then to 13, along with a decrease of the ratio. By adjusting the acid–base concentration to alter the oxygen–vanadium ratio, the scrambling of the composition proceeds through the reaction to reassemble the framework. The equilibrium drives the series of reactions until all the clusters in the solution become settled into a charge-balanced species as homogeneous as possible. It is not necessary to consider the addition or the subtraction of the number of vanadium atoms according to the molecular formula. However, this does not mean that the reaction proceeds according to any equations. When the adjustment of proton concentration is between the stable compositions, it gives a mixture of the compounds.

8.3 Representative Vanadium-oxide Cluster Frameworks

The building blocks of vanadium-oxide clusters consist of three fundamental units: VO_6 octahedron, VO_5 square pyramid and VO_4 tetrahedron. By using these building blocks, three types of structures are formed. The first type of structure is a block type. It is composed of the edge-sharing of VO_6 octahedra to give a part of rock-salt(NaCl)-type closed-packing structure by V and O atoms. The second structure is a spherical-, bowl- or tube-type structure through the arrangement of the bottom of the square pyramidal units to the same side. The third structure is formed from tetrahedral units that connect each other at the apex and form a linear or a cyclic structure. The cyclic-vanadates act as an inorganic macrocyclic ligand for cations to form a disk-shape structure. The representative vanadium-oxide complexes are categorized in one of these criteria, and are discussed in the following section.[4]

8.4 Vanadium-oxide Clusters Consisting of Tetrahedral VO_4 Units

Orthovanadate has the same structure as phosphate, with the same three minus charges. For the condensation of phosphate anions, a considerable amount of energy is required to build diphosphates or triphosphates, *i.e.*, a reaction to serve as an energy-storage mechanism in living organisms.

Orthovanadates spontaneously condense into their oligomers such as a divanadate, and are called pyrovanadates, trivanadates or tetravanadates. These chemical species are equilibrated in aqueous solution. In alkaline conditions, these monomers to oligomers with the number of vanadium atoms from 1 to 5 are distributed in water and the mixture of these species is called the methavanadate solution. In non-aqueous solution, the equilibrium slows down, and one of those species as a pure substance may be isolated. Cyclic-tetravanadates, $[V_4O_{12}]^{4-}$ are the most important species in organic solvents. The tetravanadates bind a metal cation with different charges from M^+ to M^{3+} through the coordination by oxygen atoms.

The addition of heterometal cations in a solution of cyclic-tetravanadate in an organic solvent may coordinate to the cation. The tetravandates can be monodentate to tetradentate as an inorganic ligand, and may coordinate up to four metal cations at its peripheral oxido-moiety on each vanadium atom. Cyclic-tetravanadate tends to work as a multidentate ligand to exhibit various sandwich-type structures as bidentate or tridentate ligands.

Two cyclic-tetravanadates in tridentate mode, sandwich M^{3+} cation to form octahedral coordination sphere at its M^{3+} centre, as exemplified by $[Y(V_4O_{12})_2]^{5-}$. To avoid steric repulsion, the coordination arrangement of two cyclic-tetravanadates was observed in *trans*-fashion (see Figure 8.7(a)). Due to the weak coordination ability of tetravanadates, they may accept further water coordination to form a monoaqua complex, $[Y(OH_2)(V_4O_{12})_2]^{5-}$ (see Figure 8.7(b)) or a diaqua complex, $[Y(OH_2)_2(V_4O_{12})_2]^{5-}$ (see Figure 8.7(c)) by leaving the coordination of one of the VO_4 units.[5] The VO_4 unit and aqualigands interact through hydrogen bonds. This indicates that even though tetravanadate is a multidentate chelate ligand, the addition of a large amount of water gradually competes with the coordination of tetravanadates. By dissociating an oxido-moiety, an association of water proceeds and ultimately tetravanadates are susceptible to dissociate through a stepwise dissociative process. However, as long as the presence of water is limited, various all-inorganic coordination complexes between a T_d-vanadate ring, $(VO_3)_n^{n-}$, and cations are possible. Most transition elements from d-block

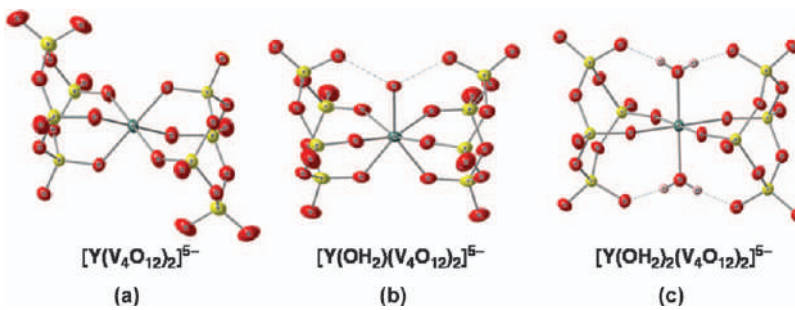

Figure 8.7 Sandwich coordination of tetravanadates with or without water ligands. Yellow, red, green, pink ellipsoids represent vanadium, oxygen, yttrium, and hydrogen atoms, respectively. Dotted line indicates hydrogen bonds.

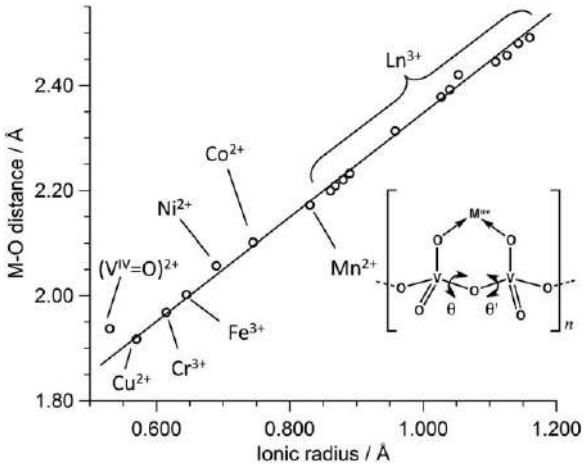

Figure 8.8 The plot of ionic radius *vs* M–O bond distances of all-inorganic complexes for various transition metal cations shown in Figure 8.9. By adjusting two V–O rotational angles, θ and θ', a macrocyclic vanadium ligand is able to adopt a different ion from all-sort of cations in the periodic table. The conformation of the ring and ring sizes are another variable to allow cation clusters in the ring.

transition to lanthanide cations form an all-inorganic macrocyclic vanadate complex, and the ring flexibility allows it to accommodate a cation in a different size (see Figure 8.8).[6]

A Lewis-acidic cation prompts the increase of the ring size, n, in $(VO_3)_n^{n-}$ rings. Because the adjustment of two V–O rotation angles, θ and θ', is able to vary the bite angle against the M^{n+} centre, it allows the vanadium macrocycle to work as a versatile ligand for any cation on the periodic table. Among d-block transition cations, a cation with three plus charges, M^{3+}, can assemble more negatively charged VO_4 units to make the ring complete as a macrocycle. But in the case of M^{2+}, it only attracts a limited number of VO_4 units, *e.g.*, half way around the metal coordination sphere in the range of four to five vanadium atoms that is not large enough to complete the ring to cover the coordination sphere. Because of the incomplete coordination sphere, M^{2+} vanadate complexes have to form a dimer by combining two units to form a di-heterometallic complex in the completed-ring. As a result, d-block transition metal cations form a mono-heterometallic or a di-heterometallic complex alternatively in the order of the periodic table (see Figure 8.9): a diheterometallic complex in the case of manganese (Figure 8.9 (b)) and a monoheterometallic complex in the chromium or iron cases (Figure 8.9 (c)).

8.5 XAFS Analysis of Vanadium-oxide Clusters

Unlike molybdates or tungstates that have been studied in the past, these all-inorganic coordination vanadium complexes have been established recently. These new complexes have been examined through various analytical methods

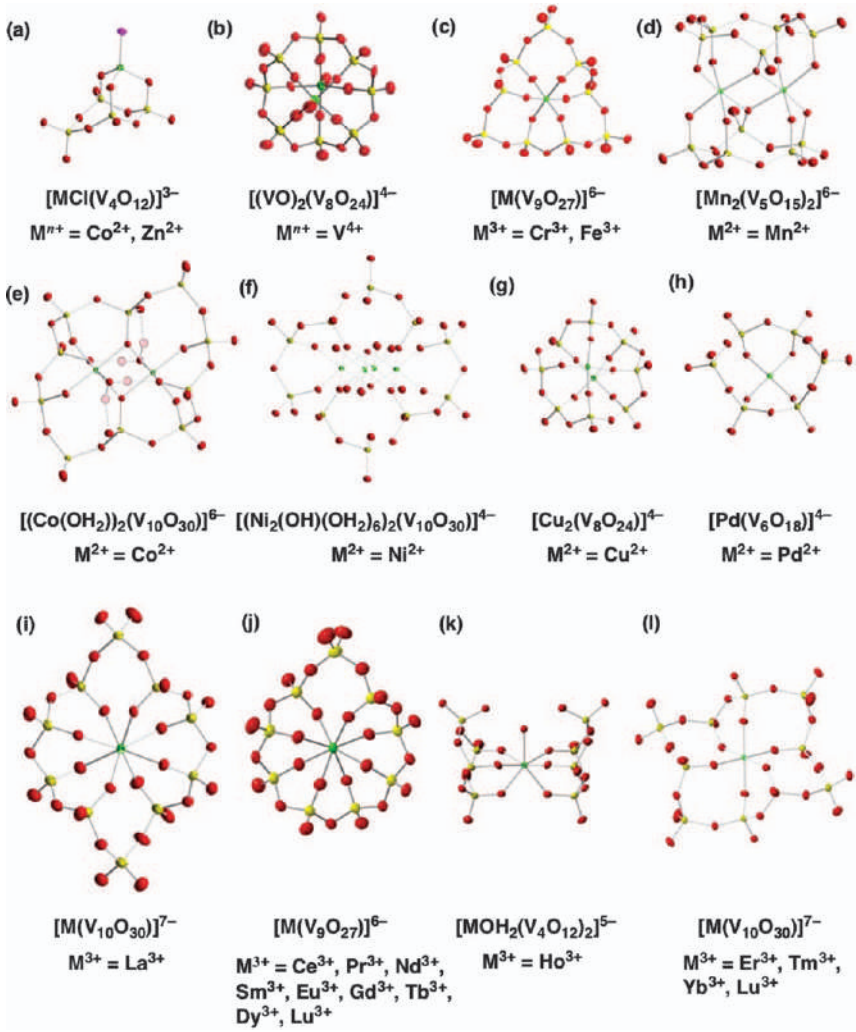

Figure 8.9 Structures of all-inorganic macrocyclic complexes of transition metal cations. Yellow, red, pink, purple ellipsoids represent, vanadium, oxygen, hydrogen, halogen atoms, respectively. Transition metal cations other than V(v) are shown in green ellipsoids.

and are stable in acetonitrile solution, even with the presence of a stoichiometric amount of water. To further elucidate the solution-state chemistry, XAFS spectroscopy was employed as the only possible method to estimate bond-distances, angles and coordination numbers directly. The all-inorganic complexes of the type $[(M^{n+})_a(VO_3)_b]^{c-}$ [M = 3d-transition elements as shown in Figure 8.9 (b–g)] have been investigated through XAFS analysis at the SR centre in Ritsumeikan University (see Figure 8.10). The crystalline sample that was already analysed by single-crystal X-ray analysis has been used as a strong

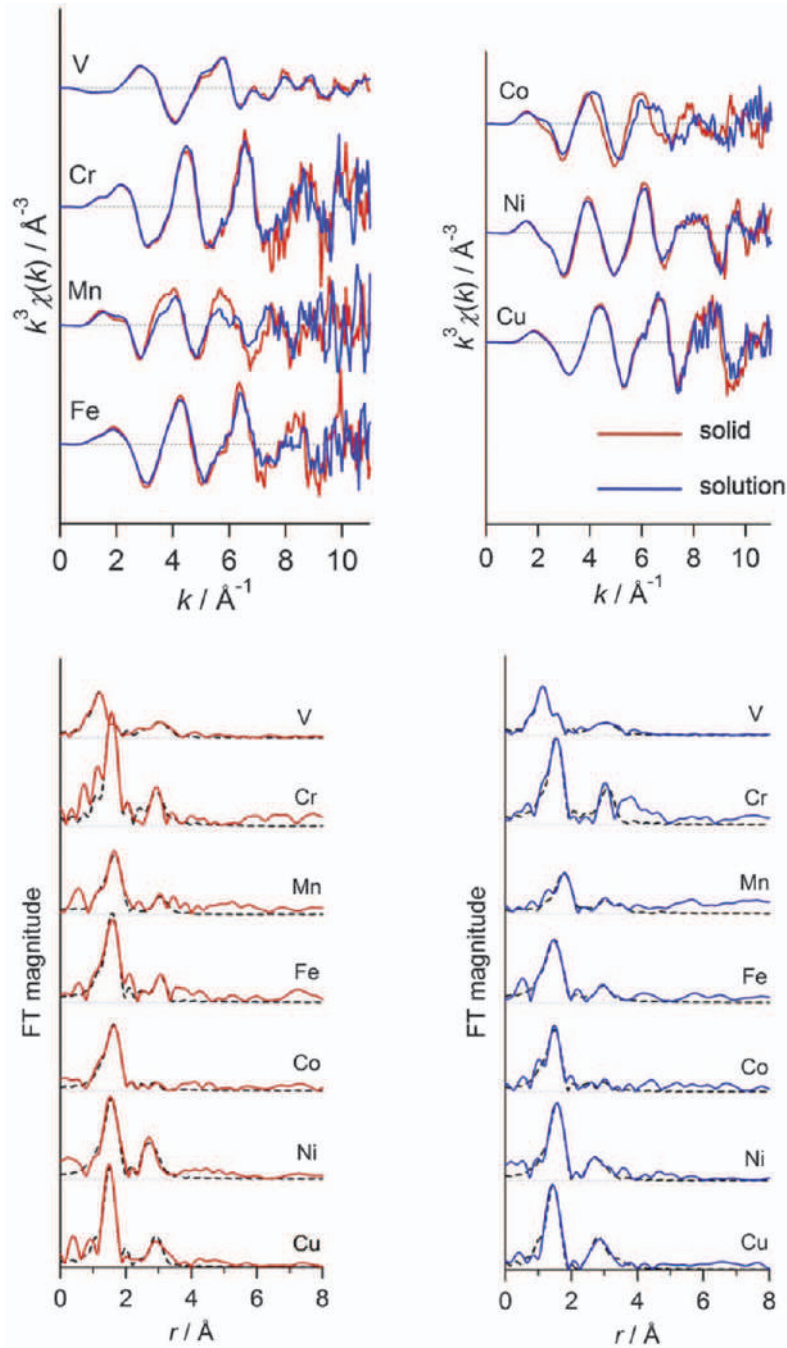

Figure 8.10 Comparison of solid and solution state EXAFS data of all-inorganic complexes of 3d-metal cations ((b), (c), (d), (e), (f) and (g) in Figure 8.9). Top two graphs are EXAFS oscillations, and the bottom two graphs are Fourier transforms of solid state and solution state data. Red is solid state and blue is solution state data, dotted black line is simulated data by FEFF program.

reference sample. The EXAFS data of the corresponding crystalline sample and solution sample matched well, showing almost identical oscillation patterns. The comparison of the XAFS oscillations between the solid BN pellet sample and acetonitrile solution is a powerful method to confirm the structural retention in the solution state, because there is no room for an artificial interpretation problem that may arise from data manipulation and distortions in EXAFS analysis. The Fourier transform of each spectrum shows clear peaks at the first coordination sphere (M–O) as well as the second coordination sphere (M···V). For the accurate estimation of the bond information, the FEFF program has been used to simulate the results along with single crystallographic data. The estimated bond information of the first and second coordination spheres is compiled in Table 8.1. The EXAFS estimation of bond lengths in the solid state and solution state agrees well, along with the single-crystal data, clearly indicating that even in acetonitrile solution, these all-inorganic complexes maintain their structures.

However, when the oscillation patterns were scrutinized, a minor deviation was observed in Mn and Co complexes (for the complex in Figure 8.9 (d) and (e)). The Fourier transforms of Mn and Co complexes also indicated an ambiguity in the second coordination sphere peaks. When the bond-information for the first coordination sphere that is estimated from FEFF simulation is plotted, the deviations for Mn and Co complexes become obvious.

In most of the 3d-complexes, the EXAFS estimations of bond parameters in solid and solution state and crystallographic data were almost identical, with

Table 8.1 Estimated bond distances by EXAFS and single crystal data.

Interaction	Coordination number	EXAFS (solid)	*r*/Å	
			EXAFS (solution)	Single-crystal
V^{IV}–O	1.8	1.66(2)	1.64(1)	1.645
V^{V}–O	2.4	1.84(3)	1.82(2)	1.859
$V^{IV}\cdots V$	1.6	3.26(2)	3.27(2)	3.247
$V^{V}\cdots V$	1.6	3.41(2)	3.42(2)	3.582
Cr–O	6	1.98(2)	1.98(2)	1.968
Cr···V	6	3.38(4)	3.44(4)	3.405
Mn–O	6	2.14(2)	2.22(3)	2.172
Mn···Mn	1	3.17(29)	3.45(9)	3.308
Mn···V	6	3.45(12)	3.69(11)	3.502
Fe–O	6	2.02(1)	1.99(2)	2.002
Fe···V	6	3.47(5)	3.43(9)	3.439
Co–O	6	2.088(8)	1.97(2)	2.101
Co···Co	1	2.98(7)	3.05(11)	3.104
Co···V	5	3.20(8)	3.27(12)	3.389
Ni···O	6	2.04(1)	2.05(1)	2.057
Ni···Ni	2.5	3.01(4)	3.06(3)	3.048
Ni···V	3	3.31(4)	3.36(5)	3.370
$Cu–O_{eq}$	4	1.92(1)	1.90(2)	1.917
$Cu–O_{ax}$	1	2.66(22)	2.41(12)	2.658
Cu···Cu	1	3.21(16)	3.18(5)	3.209
Cu···V	4	3.55(16)	3.65(7)	3.391

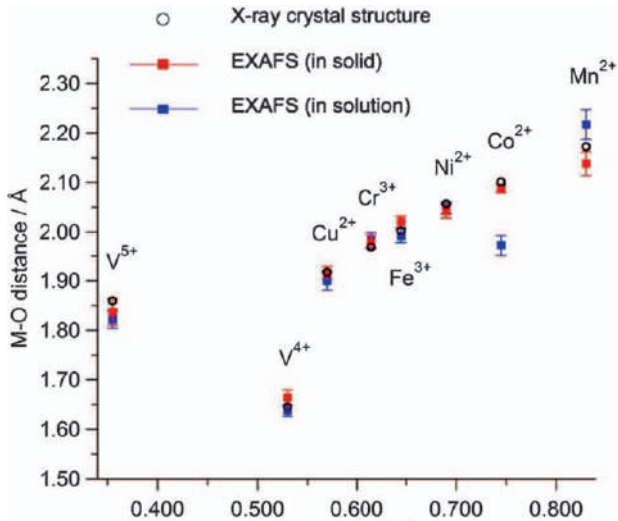

Figure 8.11 Plot of ionic radii vs M–O distances for all-inorganic macrocyclic complexes of 3d-transition metal cations. Data from single crystal X-ray analysis are plotted in circles, and red is solid state and blue is solution state data estimated by EXAFS analysis with an estimated error-bar.

the exception of Co and Mn complexes (see Figure 8.11). There are two reasons for these subtle differences. When all-inorganic lanthanide complexes were examined by variable temperature ^{51}V NMR, a fluxional movement of the vanadate ring was revealed (see Figure 8.12). In those relatively larger vanadate-rings, there are coordinating VO_4 units and non-coordinating VO_4 units to the heterometallic cation. By coordinating or non-coordinating VO_4 units alternatively, a macrocyclic vanadate ring is able to switch a coordination site without an overall structural change (see Figure 8.12).[7] At room temperature, these moves are averaged due to the fluxional behaviour. At low-temperature, down to -20 °C, the motion is frozen and the chemical shifts are clearly separated according to the chemical environment.[8]

This fluxionality is a first reason of the difference in solid-state and solution-state structures of manganese and cobalt complexes.

The second reason is the existence of a coordination water molecule on Co complexes causing a significant deviation of the bond data because of the dissociation and association equilibrium of the aqua ligands. When the aqua ligand dissociates, bond lengths at the first coordination sphere have to shrink, and when the aqua ligand associates, bond lengths have to expand. The EXAFS data for V, Cr, Fe, Ni and Cu complexes show a good agreement between solution- and solid-state data, suggesting these series of complexes are inert in solution state. Furthermore, the slight discrepancy observed in Mn and Co EXAFS data suggests a dynamic move of the clusters in solution state although the overall structures are maintained. By utilizing this dynamic nature of the cluster framework, further modification of Mn

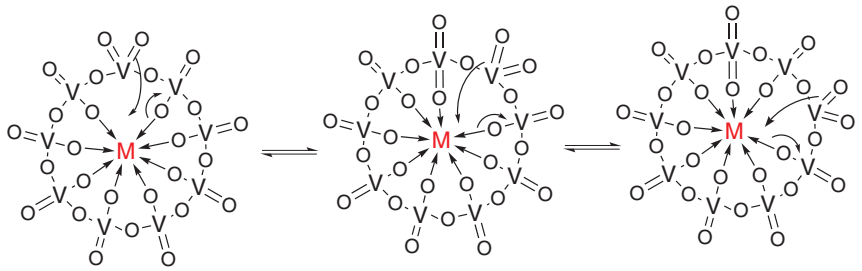

Figure 8.12 Fluxional movements of an all-inorganic macrocyclic complex of vanadium-oxide clusters.

and Co complexes becomes possible. The dimanganese complex has two pentavanadate rings and the ring size can be switched between two pentavanadate rings and one decavanadate ring.[9] The existence of cyclic pentavanadate in water had been postulated by Pettersson's group.[10] By addition of one equivalent of Mn^{2+} cation, the dimanganese cluster grows to a trimanganese cluster and the growth of the metal-core requires a larger ring to accommodate three manganese atoms, resulting in an expansion of the ring into a decavanadate ring by linking two cyclic-pentavanadates in one ring (see Figure 8.13). The Co complex also allows the expansion of the dinuclear cluster to the trinuclear form and the additional coordination spheres are occupied by an acetate ligand. The facile conversion between those species is possible by adjusting the Mn/V or Co/V ratios.[11] The trimanganese cores may be linked by diacetate connected by a straight alkyl chain binding a nonpolar cation like tweezers through non-covalent interaction.[12]

8.6 Vanadium-oxide Clusters Forming Cage-type Structures

The versatility of VO_4 tetrahedral units is not only limited to the ring structures. It can also share further apexes on a VO_4 unit to branch the main ring leading to the formation of a cage-type structure. Pentavandate, $[V_5O_{14}]^{3-}$, is a typical example and has the smallest cage and so there is no room to incorporate a guest inside the cage.[13] When the cage expands in size, it becomes a host molecule and the incorporation of a guest molecule in the cage becomes possible. Heptavanadate, $[V_7O_{19}F]^{4-}$, has a fluoride anion in the cavity[14] and an icosavanadate, $[V_{20}O_{58} \supset Ln_4(OH)_4]^{8-}$($Ln = Y^{3+}$, Er^{3+}, Yb^{3+}), incorporates a tetranuclear cubane cluster, $Ln_4(OH)_4$, in the cage, which is luminescent (see Figure 8.14).[4] The icosavanadate has an adamantine-like cage structure.

8.7 Vanadium-oxide Clusters with Unique Structures

A unique structure in vanadate chemistry arises from building a structure using a pyramidal VO_5 unit. A typical V_2O_5 structure is similar to a graphite

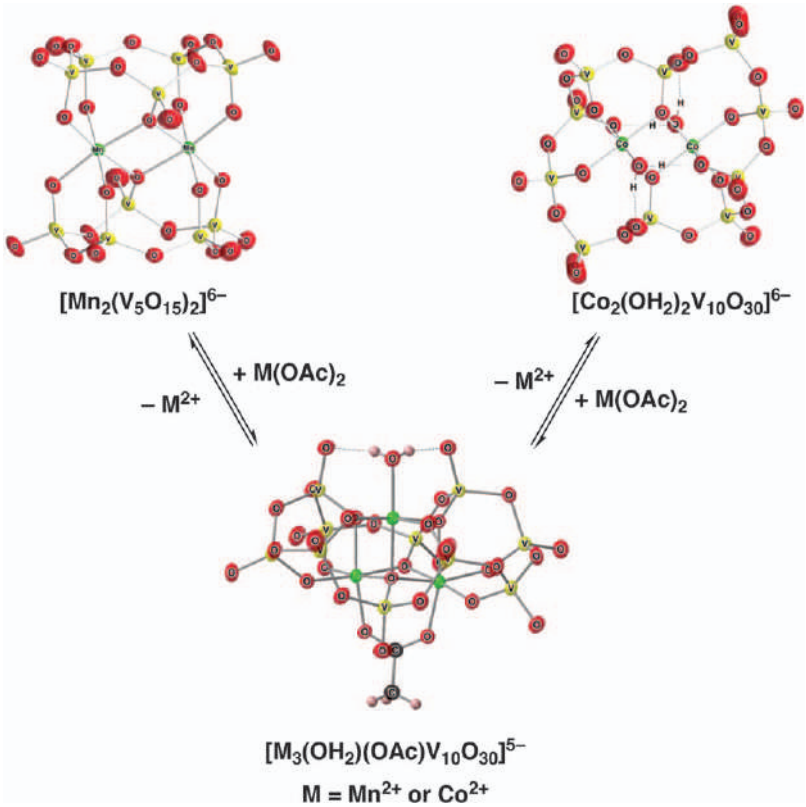

Figure 8.13 Structure conversions of cyclic-decavanadate complexes between dimanganese and trimanganese or dicobalt complexes and tricobalt complexes.

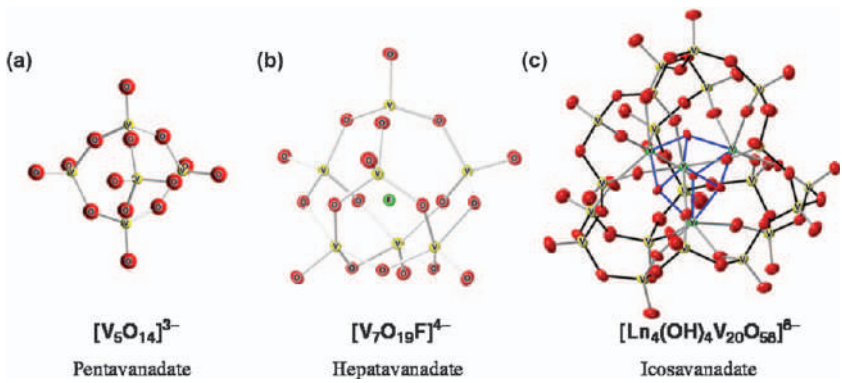

Figure 8.14 Cage-type structures. Red ellipsoids indicate oxygen atoms. Fluorine and lanthanide atoms are shown in green ellipsoids.

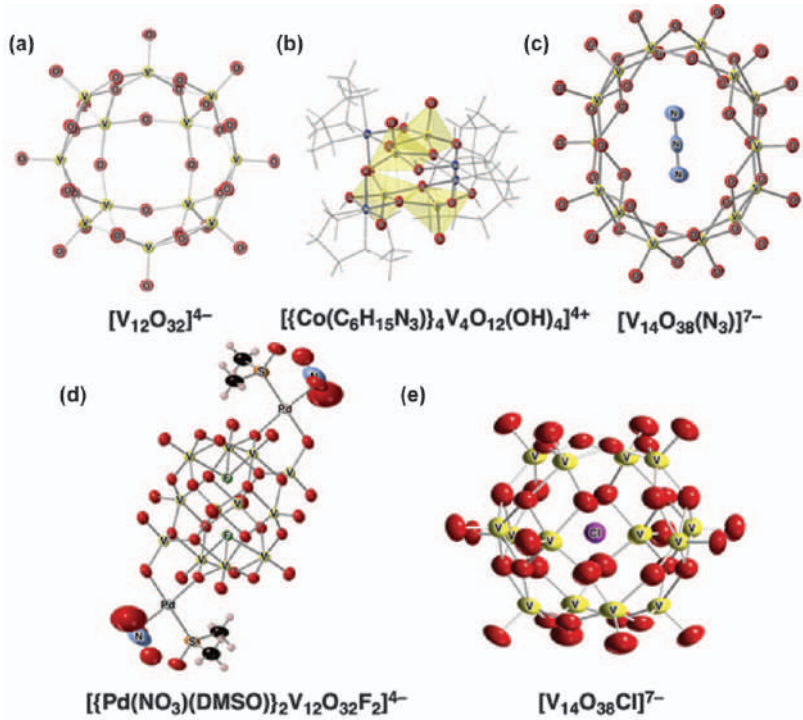

Figure 8.15 Unique structures in vanadium-oxide clusters. Red ellipsoids indicate oxygen atoms. Line drawings represent an organic ligand.

sheet: the edge and corner sharing VO_5 pyramids form 2D-sheets, and the structure of V_2O_5 is described as a stack of those sheets. As a result, a vanadium cluster based on VO_5 units can construct a structure similar to carbon chemistry, such as graphenes, nano-tubes and fullerenes. One unique example is dodecavanadate (see Figure 8.15(a)). The inorganic, bowl-type molecule is able to incorporate a guest molecule in the cavity.[15] Surprisingly, it prefers an anion guest despite the host itself having four negative charges, because of a positive nature of the cavity that is constructed by twelve V(v) cations arranged in the form of a bowl. Interestingly, the rate of the incorporation reaction of a multiatomic anion, such as nitrate, was higher when compared with that of a monoatomic anion like a chloride, because of the spreading of the charges on multiatomic nitrate that makes anion–anion repulsion smaller.[16] The incorporation of an halide is slower, but once it is incorporated, the dissociation reaction was not observed in the ^{51}V NMR since the halogen anion is trapped inside the cavity.

A minimum layer of V_2O_5 sheet may be isolated as a molecule by utilizing a capping strategy by an inorganic ligand (see Figure 8.15(b)).[19] The tube-type clusters are another interesting example[17,18] as they can incorporate various anions in the tube (see Figure 8.15(c)).[20] Supporting palladium cations on a vanadium-oxide framework is also possible (see Figure 8.15(d)) and exhibits

square-planer, tetrahedral, square-pyramid and octahedaral coordination sites observed in one molecule – *i.e.*, various coordination modes of transition elements are shown in one molecule.[21] The available coordination sites on Pd atoms may provide an application in inorganic MOF construction and in supramolecular chemistry as a cross-linker unit. A spherical structure is also formed by incorporating an anion at the centre (see Figure 8.15(e)).[22] The spherical cage looks like the Buckminster-fullerene, but the cage can be constructed step-wise by utilizing umpolung of a guest from cations to an anion, to give guest-incorporated, bowl-type dodecavanadates.[23] Because of the stepwise synthesis, an appropriate guest anion can be introduced selectively. The valence state of vanadium atoms in these series of clusters is the diamagnetic V(V) and the reaction or host–guest interaction can be monitored through ^{51}V NMR spectra. When V(IV) is involved, various spherical vanadium-oxides are reported, but the reduced species are omitted here.

8.8 Vanadium-oxide Clusters Including a NaCl-type Closed-packing Structure

The Lindqvist-type hexavanadate structure is one of the fundamental frameworks that is constructed by edge-sharing of six VO_6 octahedral units forming an even larger octahedron (see Figure 8.16(a)). Because of the building up of charges on the core, it does not exist on its simple form of $[V_6O_{19}]^{8-}$. The first hexavanadate was isolated with organometallic capping groups to compensate the too-large negative charges.[24] Alternatively, by replacing a terminal-oxido moiety by a methoxido-group that is also able to disperse the charges, it becomes isolable but it is susceptible to hydrolysis through an exchange reaction with water.[25,26] Reduction of hexavanadates makes the core much more stable and enables the study of mixed-metal hexametalate chemistry.[27,28] The most important vanadium-oxide cluster and a species soluble in water is a decavanadate. It is often protonated and the presence of an aggregate in the dimer supported by hydrogen bonding has been elucidated even in solution (see Figure 8.16(b)).[29] Similar intermolecular hydrogen bonding dimers are also known in tridecavanadates (see Figure 8.16(c)).[30,31] Heptadecavanadate with a super-cubane unit has a unique structure in which the main framework is constructed by $3\times3\times3$ NaCl type cores and the four peripheral vanadates and vanadium atom at the centre are reduced to V(IV) with an arrangement of five V(IV) atoms sitting as far as possible in the core (see Figure 8.16(d)).[32] These types of reduced species exhibit multistep reversible waves in electrochemistry.

8.9 Rearrangement Reaction of Vanadium-oxide Clusters

In vanadium-oxide cluster chemistry, the electrostatic balance on the structure framework is an important factor rather than an arrangement of relatively weak bonds. The swift structure conversion allows the cluster to suit catalytic

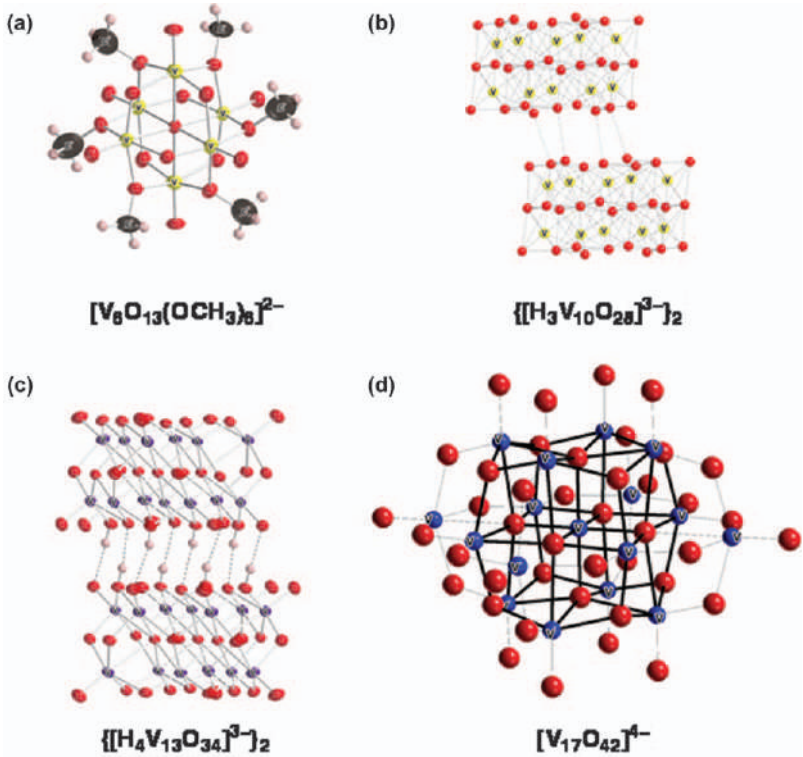

Figure 8.16 Structures containing a NaCl-type close-packing module. Red and pink ellipsoids indicate oxygen and hydrogen atoms, respectively. Dotted lines indicate hydrogen bonds.

applications. In addition to the fluxional behaviour observed in T_d-based vanadates in Section 8.5, a structural rearrangement of a cluster framework is also possible. A transformation reaction may proceed at a particular vanadium unit, or the whole structure may be rearranged in a different form. The simple flipping of a VO_5 unit is possible in bowl-type dodecavanadate. The dodecavanadate may include a guest at its cavity. When a guest is not available in solution, a capping solvent sits on top of the cavity in the solid state. When the capping molecule is a volatile solvent such as dichloromethane, it can be removed by heating at the solid state resulting in exposure of the cavity. An empty cavity with a vacant space may be formed, but it triggers the flipping of one VO_5 at the bottom to give a flipped dodecavanadate that is considered to be an empty dodecavanadate (see Figure 8.17(a)).

After the flipping, the original cavity of the bowl is occupied by the flipped oxygen atom from the upside-down VO_5 unit. When it is exposed to a guest molecule, the reverse reaction makes the cavity ready to capture a guest selectively.[33] Another unique feature of dodecavanadates is a total-rearrangement of the bowl structure in a completely different shape. When dodecavanadates catches a halide in the cavity, an addition of one equivalent of proton requests

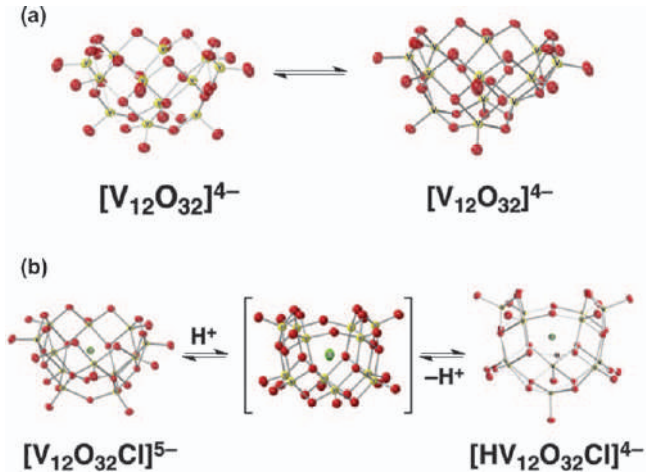

Figure 8.17 Reversible structure rearrangement of dodecavanadates. Red ellipsoids indicate oxygen atoms. Dotted lines indicate hydrogen bonds.

a vanadium framework rearrangement in a spherical form. The first step is a protonation, the second step is a rearrangement to a tube-type dodecavanadate and the third step completes the formation to a spherical dodecavanadate with a crack on its surface and it is zipped by a hydrogen bond (see Figure 8.17(b)). Each transformation process is elucidated through ^{51}V NMR. Unzipping the binding by removing a proton triggers the burst of the sphere and it goes back to the original bowl form. The rearrangement is reversible and controlled by the presence or absence of a proton.[34] In this way, the whole structure can be rearranged in a completely different form maintaining the formula $[V_{12}O_{32}(Cl)]^{5-}$, as if it plays ''catch'' with a molecular ''mitt'' in the baseball game.

8.10 Summary

Vanadium-oxide clusters are redox-active species, and a rearrangement reaction is feasible. In its highest oxidation state, it is easy to monitor the cluster framework by ^{51}V NMR and a quick structure conversion makes the cluster ideal as a platform for catalytic reactions. The introduction of any cation on its oxide framework is possible in a particular molar ratio at a particular site. Most of the clusters discussed in this chapter were recently discovered and further investigation in catalytic application is expected. The important parameter necessary to control is the ratio of oxygen to vanadium through the adjustment of the amounts of water, acids or bases. As long as the reaction conditions are controlled in a way that allows the oxygen–vanadium ratio to stay the same, the structure may resurrect because the most electrostatically balanced structure is the original form. Vanadium-oxide clusters display various structures of spheres, cages, tubes, bowls and blocks. Good catalysts can change their structure quickly to accept a

substrate and reactant. Rearrangement reactions and quick-exchange reactions allow vanadium clusters to be applied in versatile catalytic chemistry with similarities to carbon-based new structures such as nano-tubes, but it is far easier to modify their structures on account of their ionic bonds.

References

1. C. C. McLauchlan, H. A. Murakami, C. A. Wallace and D. C. Crans, *J. Inorg. Biochem.*, 2018, **186**, 267–279.
2. D. Rehder, *Bioinorganic Vanadium Chemistry*, *A Wiley Textbook Series*, John Wiley & Sons Ltd., England, 2008.
3. Y. Kikukawa, K. Ogihara and Y. Hayashi, *Inorganics*, 2015, **3**, 295–308.
4. T. Maruyama, H. Kawabata, Y. Kikukawa and Y. Hayashi, *Eur. J. Inorg. Chem.*, 2019, **2019**, 529–533.
5. Y. Hayashi, *Bull. Jpn. Soc. Coord. Chem.*, 2015, **66**, 12–25.
6. Y. Hayashi, *Coord. Chem. Rev.*, 2011, **255**, 2270–2280.
7. M. Nishio, S. Inami, M. Katayama, K. Ozutsumi and Y. Hayashi, *Inorg. Chem.*, 2012, **51**, 784–793.
8. M. Nishio, S. Inami and Y. Hayashi, *Eur. J. Inorg. Chem.*, 2013, **2013**, 1876–1881.
9. S. Inami, M. Nishio, Y. Hayashi, K. Isobe, H. Kameda and T. Shimoda, *Eur. J. Inorg. Chem.*, 2009, **2009**, 5253–5258.
10. L. Pettersson, *Coord. Chem. Rev.*, 2003, **237**, 77–87.
11. T. Maruyama, Y. Kikukawa, H. Sakiyama, M. Katayama, Y. Inada and Y. Hayashi, *RSC. Adv.*, 2017, **7**, 37666–37674.
12. T. Maruyama, Y. Kikukawa, K. Kawamoto and Y. Hayashi, *Eur. J. Inorg. Chem.*, 2017, **2017**, 596–599.
13. V. W. Day, W. G. Klemperer and O. M. Yaghi, *J. Am. Chem. Soc.*, 1989, **111**, 4518–4519.
14. Y. Kikukawa, T. Yokoyama, S. Kashio and Y. Hayashi, *J. Inorg. Biochem.*, 2015, **147**, 221–226.
15. S. Kuwajima, Y. Ikinobu, D. Watanabe, Y. Kikukawa, Y. Hayashi and A. Yagasaki, *ACS Omega*, 2017, **2**, 268–275.
16. S. Kuwajima, Y. Kikukawa and Y. Hayashi, *Chem. – Asian J.*, 2017, **12**, 1909–1914.
17. K. Kastner, J. T. Margraf, T. Clark and C. Streb, *Chem. – Eur. J.*, 2014, **20**, 12269–12273.
18. K. Kastner, J. Forster, H. Ida, G. N. Newton, H. Oshio and C. Streb, *Chem. – Eur. J.*, 2015, **21**, 7686–7689.
19. K. Sugiarto, Kawamoto and Y. Hayashi, *Front. Chem.*, 2018, **6**, 375.
20. S. Kuwajima, Y. Arai, H. Kitajima, Y. Kikukawa and Y. Hayashi, *Acta Crystallogr., Sect. C: Struct. Chem.*, 2018, **74**, 1295–1299.
21. M. Khair, Y. Kikukawa and Y. Hayashi, *Chem. Lett.*, 2017, **46**, 1406–1408.
22. T. Kurata, Y. Hayashi and K. Isobe, *Chem. Lett.*, 2010, **39**, 708–709.
23. S. Kobayashi, T. Kuwajima, Kurata and Y. Hayashi, *Inorg. Chim. Acta*, 2014, **420**, 69–74.

24. Y. Hayashi, Y. Ozawa and K. Isobe, *Inorg. Chem.*, 1991, **30**, 1025–1033.
25. D. Hou, G.-S. Kim, K. S. Hagen and C. L. Hill, *Inorg. Chim. Acta*, 1993, **211**, 127–130.
26. K. Domae, D. Uchimura, Y. Koyama, S. Inami, Y. Hayashi, K. Isobe, H. Kameda and T. Shimoda, *Pure Appl. Chem.*, 2009, **81**, 1323–1330.
27. L. E. VanGelder, A. M. Kosswattaarachchi, P. L. Forrestel, T. R. Cook and E. M. Matson, *Chem. Sci.*, 2018, **9**, 1692–1699.
28. B. E. Petel, W. W. Brennessel and E. M. Matson, *J. Am. Chem. Soc.*, 2018, **140**, 8424–8428.
29. T. Kojima, M. R. Antonio and T. Ozeki, *J. Am. Chem. Soc.*, 2011, **133**, 7248–7251.
30. D. Hou, K. S. Hagen and C. L. Hill, *J. Am. Chem. Soc.*, 1992, **114**, 5864–5866.
31. T. Kurata, Y. Hayashi, A. Uehara and K. Isobe, *Chem. Lett.*, 2003, **32**, 1040–1041.
32. Y. Hayashi, K. Fukuyama, T. Takatera and A. Uehara, *Chem. Lett.*, 2000, **29**, 770–771.
33. Y. Kikukawa, K. Seto, S. Uchida, S. Kuwajima and Y. Hayashi, *Angew. Chem., Int. Ed.*, 2018, **57**, 16051–16055.
34. Y. Inoue, Y. Kikukawa, S. Kuwajima and Y. Hayashi, *Dalton Trans.*, 2016, **45**, 7563–7569.

CHAPTER 9

Catalysis by Oxometalates and Their Microheterogeneous Media

J. LODH AND S. ROY*

EFAML, Materials Science Center, Department of Chemical Sciences, Indian Institute of Science Education & Research, Mohanpur Campus, Kolkata, India
*Email: s.roy@iiserkol.ac.in

9.1 Introduction

Catalytic processes are of great interest, can have a long-lasting effect and can even change the dynamics and demographics of global population.[1] Catalytic processes, thus, have been of immense economic importance, and include the Haber–Bosch process for activation of nitrogen,[2] oxidation of sulphur-dioxide for synthesis of sulphuric acid,[3] epoxidation catalysis,[4] Ziegler–Natta catalysis,[5] olefin metathesis[6–8] and hydrogenation reactions.[9,10] Using supramolecular interactions, supramolecular catalysis has also led to several possibilities including, but not limited to, self-organisation and complex matter.[11] Using the multiplicity of weaker interactions and entities with diffuse interfaces, soft-matter systems became important in micellar catalysis and related processes.[12] All such catalytic reactions had an immediate effect on the human condition by addressing hunger alleviation and significant life-style changes. In many of these catalytic processes, metals and especially transition metals and their oxides play a significant role. Thus, transition metals and their oxides have

Catalysis Series No. 41
Vanadium Catalysis
Edited by Manas Sutradhar, José Armando L. da Silva and Armando J. L. Pombeiro

Published by the Royal Society of Chemistry, www.rsc.org

been an agent of choice for carrying out important catalytic processes. In recent examples of catalytically important reactions ranging from C–X activation,[13] C–C coupling,[14] OER,[15] ORR[16] to small molecule activation,[17] transition metals and, at times, their oxides, continue to play an important role as catalysts. In this chapter, a closer look on transition metal-based model systems, oxometalates in both molecular state of oxometalates and in their colloidal state of soft-oxometalates in the context of catalysis is undertaken. In doing so, we explore the effects of the physical state of oxometalates (molecular and microheterogeneous or soft-matter) on catalysis.

Polyoxometalates (POMs) can be viewed as a crystalline state of discrete molecular anionic clusters constituted of early transition metals (M = V, Nb, Ta, Mo, W) in their highest oxidation state, which might also include certain main group heteroatoms (X) such as B,[18] P,[19] Al[20] and Ge.[21] The incorporation of these heteroatoms in the molecular cluster renders these oxometalates $[X_aM_bO_c]^{n-}$ highly stable, but can also, at times, be highly reactive. Some of these early transition metals (M) can be substituted with other metals like Cr,[22] Mn,[23] Fe,[24] Co,[25] Ni[26] and Cu[27] and affects their properties and reactivity.[28] This stability coupled with reactivity of such systems renders the field of oxometalates as an area of immense importance and has been the subject of several books and reviews.[29–34] We now give a brief overview of recent design strategies of oxometalates.

The design of oxometalates was performed by Patzke from a molecular building block to an extended structure.[35] Understanding the formation of molecular POMs from sub-molecular precursors has been studied by Cronin and Poblet[36,37] and also by the authors of this chapter.[38] Using simple systems like Keggins, Bera and Antonio have demonstrated the formation of liquid like microheterogeneous media of oxometalates (soft-oxometalate or SOM phases)[39–42] and their formation in great detail.[43,44] Going a step further, crystallisation of POMs in isopoly Mo_7 and Mo_8 *en route* to a micro-heterogeneous medium of the soft-oxometalates have been studied.[45,46] More specifically, in the context of compartmentalisation and catalysis, the Crans group has developed a very elegant method for effective reactions and studying their pathways in great detail.[47,48] Exploring the SOMs, the Wu group has very elegantly demonstrated peptide-based adhesive SOM coacervate for environment-responsive underwater adhesion.[49] SOM-based water cleaning systems employed as active matter exploring their photo-redox behaviour have been explored.[50] From the ongoing developments in the literature, such oxometalate-based entities seem to be important in various catalytic processes. The reason for this importance can be attributed to: (i) their nature as acids, (ii) their capacity as an oxidation and reduction catalyst, and (iii) the possibility of catalysis in the soft-matter state, thus acting as a model system to understand molecular and heterogeneous catalysis. In this chapter, we explore these facets in more detail. We first describe the rationale of using POMs and their SOM states as catalysts.

9.2 The Rationale of Using Oxometalates as Catalysts

Over the years, oxometalates (OMs) have been used as catalysts for a wide range of reactions such as oxidation, reduction, electrocatalysis and photocatalysis. The redox properties of these oxometalates ensure great catalytic efficacy, as well as their stability over a pH range of 2–12 and their resistance to oxidants. Oxometalates are considered green catalysts due to their high-oxygen content and high-atom efficiency.[51,52] OMs carry multiple proton sites or metal centres with Lewis acidity. These sites work as catalytic centres in acid catalysis. Owing to this reason, they have been used to catalyse major acid catalysed reactions such as Friedel–Crafts acylation and Fries rearrangement for the synthesis of aromatic ketones. Instead of using strong mineral acids or traditional Lewis acids, the oxometalates can be considered as attractive alternatives, being more acidic than solid acids such as zeolite or mixed metal oxide,[53] which makes these polyoxometalate moieties even more favourable for acid-catalysed reactions. Over the years, major attention has been given to their acidic as well as redox properties. In fact, in the absence of protons they act as efficient base catalysts since electron-rich oxygen atoms are present on the surface of oxometalates and carry a high-negative charge. In this regard, lacunary oxometalates need a special mention since the lacunary sites carry a high-negative charge, making it possible to extract protons from organic reactants. In order to act as base catalysts, oxometalates should satisfy the following criteria: (1) The thermal and oxidative stabilities of the oxometalates need to be higher than the organic bases; (2) the metal-oxo moieties should be able to activate the nucleophilic sites; and (3) the design of basic sites should be electrically and structurally controlled.

POMs can be used as oxidation catalysts instead of conventional oxidation catalysts such as H_2SO_4, HNO_3 and other peroxy acids, as the latter produce more side products. Additionally, the focus has shifted towards greener oxidants. Oxometalates are an attractive choice for versatile catalysis owing to their thermal and hydrolytic stability compared to organometallic catalysts. POMs are responsive to light and can be excited from their ground state, which facilitates the charge transfer from oxygen to the transition metal d-orbitals.[54] This forms the basis of several photocatalytic reactions such as CO_2 reduction and water oxidation. These polyanions (POMs) have well-separated HOMO and LUMO band gaps that are able to resist the electron and hole recombination while being irradiated with light higher or equal to their band-gap energy. The photogenerated electrons and holes are capable to initiate chemical reactions due to the strong photo-reductive and photo-oxidative ability of electrons and holes, respectively. The metals in these clusters in higher oxidation states easily undergo one- or two-electron transfer. The potential of these redox couples is dependent on pH value. It is possible to tune the catalytic activity of POMs by tuning the pH and redox states and engineering the band gaps. Several reviews have highlighted catalysis by POMs exploring these facets or related aspects in the context of

catalysis by POMs. (See Table 9.1 for an overview of various reactions catalysed by oxometalates.)

Catalysis by POMs refers to the molecular state (homogenous) of the oxometalates and the colloidal state (heterogeneous) of oxometalates. The latter state, referred to as soft-oxometalates (SOMs) has certain advantages in the context of catalysis. These advantages are: (1) the presence of a large number of M=O centres; (2) these states can be kinetically trapped active states in catalysis; and (3) they can act as a model system to study the transition from homogenous (molecular) to heterogeneous (soft-matter state) in catalysis. Keeping such advantages of SOMs in mind, our group has been exploring the catalytic activity of these states in detail. We now describe the catalysis by POMs and SOMS (the types of reactions are illustrated in Table 9.1).

9.3 POMs in Acid Catalysis

9.3.1 Friedel–Crafts Reactions and Fries Rearrangement

Oxometalates have always been well-known for their acidic properties due to the presence of one or more acidic sites or protons. Early studies used oxometalates as solid catalysts for liquid-phase reactions.[55,56] Using Keggin-type heteropolyphosphotungstic acid in water, Michael-type Friedel–Crafts alkylation of *N,N*-dialkylanilines with nitroalkanes[57] has been shown. Further, studies on electron-rich arenes and different nitroalkanes showed that *N,N*-dimethylanilines and *N,N*-diethylanilines gave maximum yield. 12-phosphotungstic acid, a Keggin, and its composite have been used for catalysing Friedel–Crafts reactions. Another Keggin-type heteropolyanion, 12-phosphotungstic acid based ionic liquid-functionalized mesoporous copolymer P(VB–VMS)PW, was developed and shown to lead to excellent yield for Friedel–Crafts benzylation of arenes with benzyl alcohol.[58] Owing to its mesoporous copolymeric structure it could be easily recovered, as well as the functionalization of heteropolyanion with the copolymer enhancing the structural stability and the acidity, thus promoting the acid catalysis. Along similar lines, works have been done on functionalizing heteropolyphosphotungstic acid with acid leached porous kaolin for Friedel–Crafts acylation of anisole.[59] There have also been works featuring Fe-based heteropolytungstate supported on activated carbon, whose activated carbon porous structure played a significant role on benzylation reaction.[60] The activated carbon structure not only facilitated the dispersion of heteropolytungstate during benzylation due to high-surface area, but also ensured easy recovery from the reaction mixture. Later works encapsulated phosphotungstic acid in MIL-100, mesoporous metal organic framework and showed its application on acid-catalysed acetalization.[61] Zeolite frameworks have also been popular as a support to HPAs for efficient Friedel–Crafts acylation.[62] Going a step further from the extended porosity of framework materially, in molecular Keplerate capsules the porosity was explored in the context of catalysis. In 2016, using the confined space in $\{Mo_{132}\}$ Keplerate the encapsulation of benzene, phenol,

Table 9.1 Different organic reactions catalysed by oxometalates.

Category	Representative catalyst	Reaction	References
Acid Catalysed Reactions	 $H_3PW_{12}O_{40}$	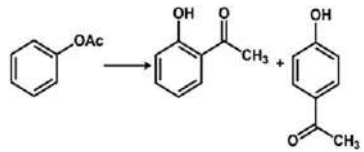	66
	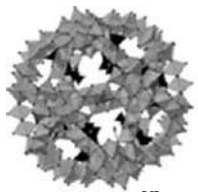 $(NH_4)_{42}[Mo^{VI}{}_{72}Mo^{V}{}_{60}O_{372}(CH_3COOH)_{30}(H_2O)_{72}]$.ca 300 H_2O	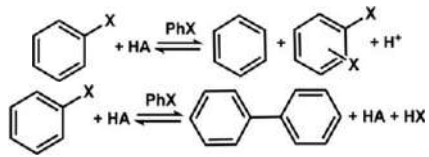	63
	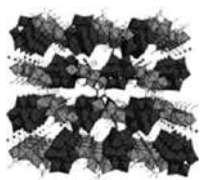 $Cs_2[Cr_3O(OOCC_2H_5)_6(H_2O)_3]_2[\alpha\text{-}SiW_{12}O_{40}]$	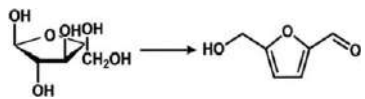	71

Table 9.1 (*Continued*)

Category	Representative catalyst	Reaction	References
Base Catalysed Reactions	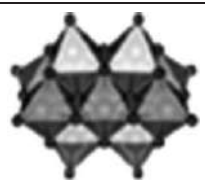 $(TMA)_6$-$[Nb_{10}O_{28}]\cdot 6H_2O$	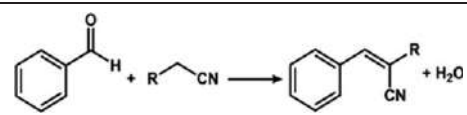	87
	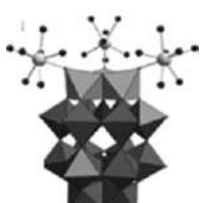 $[RE(H_2O)_7]_{3-}$ $P_2W_{15}Ta_3O_{62}\cdot nH_2O$	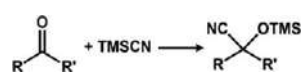	92
	 $[Sm(H_2O)_5][Sm(H_2O)_7][Co_2Mo_{10}H_4O_{38}].6H_2O$	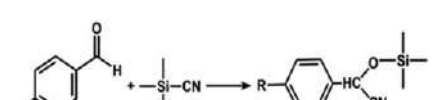	91

Oxidation Reactions

$THA_3[SbW_9O_{33}(^tBuSiO)_3Ti(O^iPr)]$

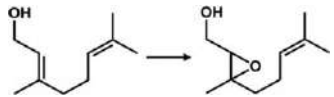

148

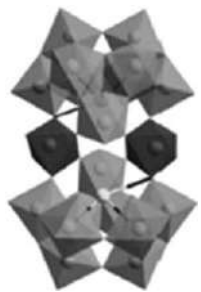

$Na_2H_2[(CH_3)_4N]_6[Te_2W_{20}O_{70}\{Re(CO)_3\}_2]\cdot 20H_2O$

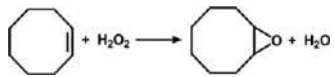

150

(3-aminopropyl)triethoxysilane linked to anthracene and a monovacant polyoxometalate, $(SiW_{11}O_{39})$

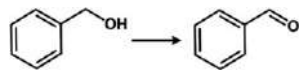

171

Table 9.1 (*Continued*)

Category	Representative catalyst	Reaction	References
CO_2 reduction coupled with hydration of phenylacetylene	 $(NH_4)_{42}[Mo^{VI}{}_{72}Mo^{V}{}_{60}O_{372}(CH_3COOH)_{30}(H_2O)_{72}]$.ca 300 H_2O	 $CO_2 + 2e^- + 2H^+ \rightarrow HCOOH$	84
Water Oxidation coupled with click reaction	 $\{[K_{6.5}Cu(OH)_{8.5}(H_2O)_{7.5}]_{0.5}[K_3PW_{12}O_{40}]\}$	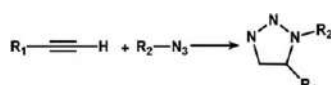 $2H_2O \rightarrow O_2 + 4H^+ + 4e^-$	230

halobenzenes, phenols have been studied, as well as for chloroarenes of the Friedel–Crafts arylation.[63] Keggin, phosphomolybdic acid ($H_3PMo_{12}O_{40}$), has been identified as a bifunctional catalyst for Friedel–Crafts type dehydrative coupling, *i.e.*, C–C bond formation *via* the dehydrative reaction of diarylmethanols with nuclepohiles such as indoles, benzothiophene, benzofuran, *etc.*[64] The protons in the oxometalates help in the activation of alcohol, whereas polyanion helps in stabilizing the carbocation species. Reports related to Fries rearrangement catalysed by several POMs/HPAs are found in the literature.[65–67] In this context, we now know that Keggin of the type $H_3PW_{12}O_{40}$ with or without a supported network has been a catalyst of choice for Friedel–Crafts reactions for the reason that it is a stronger acid than conventional mineral acids in homogenous media.

9.3.2 Biomass Utilisation

Biomass has always generated great interest in energy research and 5-(hydroxymethyl)furfural has been the most important molecule in the utilisation of biomass. Here again, Keggins like $H_3PW_{12}O_{40}$ (PW_{12})-, $H_3PMo_{12}O_{40}$ (PMo_{12})- and $H_4SiW_{12}O_{40}$ (SiW_{12})-based ionic liquids have shown great catalytic activity for conversion of fructose to 5-hydroxymethylfurfural and alkyl levulinate.[68] Reports on the synthesis of levulinic acid and formic acid from fructose using various ionic liquid POM-based salt are reported in the literature.[69] The effect of a counter-ion substituent has also been studied by partially substituting H^+ in $H_3PMo_{12}O_{40}$ with Cs^+ for one pot, one-step synthesis of 2,5-diformylfuran from carbohydrates.[70] Along similar lines, Cr-based heteropolyacid crystal $Cs_2[Cr_3O(OOCC_2H_5)_6(H_2O)_3]_2[\alpha\text{-}SiW_{12}O_{40}]$ has been proven as an efficient catalyst for the same reaction. Cr is responsible for the Lewis acidity of the catalyst whereas dissociation of the polyoxometalate unit from the coordinated water under the polarising effect of cation generates shows Bronsted acidity.[71] The presence of dual acidic sites in the catalyst ensures isomerization and dehydration of glucose to hydroxymethylfurfural (HMF).

The strategy of encapsulation of an oxometalates framework material has been employed to enhance the acidity of the catalyst. Encapsulating phosphomolybdic acid in MIL-101, leading to high Bronsted acidity and moderate redox potential of the catalyst, facilitates conversion of fructose to 2,5-diformylfuran.[72] Several acid site-carrying catalysts have been popular in this regard.[73] Further, various works have also demonstrated bifunctional acid–base catalysts using amino acids and HPAs such as $(C_6H_{15}O_2N_2)_{3-x}H_xPW_{12}O_{40}$ to catalyse the selective conversion of glucose to levulinic acid.[74] The amino acid in these cases, like lysine, helped the polyanions in forming micellar assemblies in eutectic solvents.[75] Such works can be taken as early examples of micellar catalysis. Oxide- or silica matrix-supported POMs have been used as support to solid acid catalysts for selective conversion of glucose to 5-HMF as well as oxidation of biomass.[76,77] In the matter of biomass utilisation, Keggin-type POMs seem to be the chosen catalysts.

9.3.3 Isomerization of Alkanes

POMs also have an important role in catalysing the isomerization of alkanes.[78,79] $H_3PW_{12}O_{40}$ (PMo_{12}) and $H_4SiW_{12}O_{40}$ (SiW_{12}) had been impregnated into SBA-15 type silica and the resultant monofunctional hybrid material based on Keggin-type oxometalates supported on silica was used for isomerization of n-hexane.[80] The polyoxometalate used has a broader reaction temperature window and higher di-branching selectivity than the zeolites.[81] $H_4SiW_{12}O_{40}$ is preferred over $H_3PW_{12}O_{40}$ owing to its greater selectivity. Metals such as Pt were also impregnated in HPW/SBA-15 and it has been observed that carbocations in this case hydrogenated faster on Pt particles, thus making bifunctional Pt/HPA/SBA-15 more efficient catalysts than monofunctional HPA/SBA-15.[82] Recently, isomerization of cyclohexane using bifunctional metal-acid catalysts based on Cs salt of $H_3PW_{12}O_{40}$ with Pt and Au as metallic components have been developed. Here also, Keggin-type POMs seem to be the preferred catalysts. Similar results were obtained with PtAu/CsPW that exhibited two-fold higher activity for n-hexane isomerization.[83]

9.3.4 Carbon Dioxide Reduction Coupled with Proton Facilitated Hydration Reaction

Combining the intrinsic acidity of oxometalates and their nature of photo-redox catalysis, an unusual activity can be observed. For instance, our group has reported coupling of CO_2 reduction with hydration of phenylacetylene. Keplerate $\{Mo_{132}\}$ catalysed reduction of CO_2 to formic acid with organic transformation from phenylacetylene to acetophenone. The protons generated in the process are taken up for oxidation of organic substrates. Since the reduction of carbon dioxide takes up protons in the medium released by water oxidation, we can conclude that with decreasing pH, the concentration of the reduced product would increase. CO_2 reduction can thus be considered as a proton-coupled process. Further, during hydration of phenylacetylene, the triple bonds act as a Lewis basic site and are attacked by the protons in the medium and generate a vinylic carbocation. This addition of protons is Markovnikov's addition. The water then reacts with the carbocation and tautomerization gives acetophenone. The whole reaction is thus favoured by protons generated in the medium due to the water oxidation catalysed by the $\{Mo_{132}–CO_2\}$ unit under visible light irradiation.[84] Thus, in short, this reaction demonstrates the acidity and photo-redox capacity of OMs as a key factor in driving catalytic reactions (Figure 9.1).

9.4 Base Catalysis and Oxometalates

The base catalysis by oxometalates has been less explored compared to other catalytic reactions. However, there have been some noteworthy base catalytic reactions facilitated by oxometalates that will be discussed here.

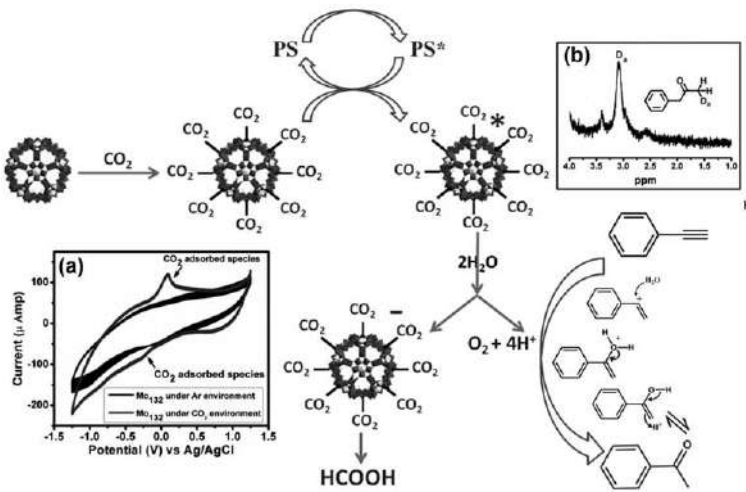

Reagent	Product	Yield
		79
		83
H_3CO	H_3CO	86
		91
Cl	Cl	8
Br	Br	7
F	No reaction	-

Figure 9.1 (a) A probable pathway for coupling carbon dioxide reduction with hydration of phenylacetylene catalysed by $\{Mo_{132}\}$. [Inset: Cyclic voltammogram for CO_2 adsorbed species (bottom-left corner) and NMR spectra for deuterium-substituted product (top-right corner).] (b) Effect of substitution on the reaction yield is shown in the table.

$Na_8H[A\text{–}PW_9O_{34}]\cdot 7H_2O$ and $Na_8H[B\text{–}PW_9O_{34}]\cdot 19H_2O$ and tri-lacunary POMs have been reported as efficient Lewis base catalysts for Knoevenagel condensation and cyanosilation of aldehydes and ketones.[85] These lacunary POMs have greater efficiency compared with the Keggins such as $Na_3[PW_{12}O_{40}]$. From a molecular point of view, $Na_8H[A\text{–}PW_9O_{34}]\cdot 7H_2O$ and $Na_8H[B\text{–}PW_9O_{34}]\cdot 19H_2O$ carry three lacunary sites and nine negative charges, compared to monolacunary Keggin. Thus, the former can abstract protons from ethyl cyanoacetate more easily than the latter in case of Knoevenagel reaction. An alkaline, highly negatively charged, Keggin-type oxometalate $Na_{16}[SiNb_{12}O_{40}]\cdot xH_2O$ for catalysing CO_2 cycloaddition and Knoevenagel condensation reaction has been reported.[86] Usually, Keggin-type POMs such as $[H_3PW_{12}O_{40}]$ are acidic and the sodium or potassium counterparts [*e.g.*, $Na_3PW_{12}O_{40}$] are weakly basic, thus making them unsuitable for base-catalysed reactions. The basicity of $[SiNb_{12}O_{40}]^{16-}$ has been supported theoretically, which shows that NBO (natural bond orbital, which depicts the natural atomic orbitals – a complete orthonormal set to describe the constituents within the molecular environment) changes for two crystallographically distinct $[SiNb_{12}O_{40}]^{16-}$ α-Keggin ions from −0.9 to −1, which is an index of high basicity.[86] Further, the decaniobate $(TMA)_6[Nb_{10}O_{28}]\cdot 6H_2O$ was found to catalyse base-promoted, aldol-type condensation.[87] Lindqvist-type polyoxoniobate $K_7HNb_6O_{19}\cdot 13H_2O$ has been observed to successfully catalyse Knoevenagel condensation of benzaldehyde and ethyl cyanoacetate to ethyl (*E*)-acyanocinnamate experimentally and theoretically.[88] Mizuno and co-workers have reported a γ-Keggin germanodecatungstate $[\gamma\text{-}HGeW_{10}O_{36}]^{7-}$ synthesised *via* the reaction of $[\gamma\text{-}H_2GeW_{10}O_{36}]^{6-}$ with one equivalent of $[(n\text{-}C_4H_9)_4N]OH$ under non-aqueous conditions.[89] The catalytic efficiency was found to increase dramatically for base-catalysed reactions as the negative charge increased from −6 to −7.

Ester, being a valuable chemical, makes the base-catalysed acylation of alcohols with acyl chlorides, acid anhydrides and esters as acylating agent important and promising. Using $[\gamma\text{-}HGeW_{10}O_{36}]^{7-}$ as the catalyst for acylation of benzyl alcohol with vinyl acetate, the yield of the product increased up to 86% (from 5%) compared to $[\gamma\text{-}H_2GeW_{10}O_{36}]^{6-}$ as catalyst. Metal (M = Ti, Ln) substituted Keggin polyoxometalate-based hybrid dimers have also shown considerable reactivity towards catalysing cyanosilylation.[90] In another work, the synthesis of the Sm-based catalyst $[Sm(H_2O)_5][Sm(H_2O)_7][Co_2Mo_{10}H_4O_{38}]\cdot 6H_2O$ for catalysing cyanosilylation of benzaldehyde has been reported.[91] The higher yield of the product has been obtained due to the synergistic effect of Lewis acid (Sm^{3+}) and Lewis base, and the surface oxygen atoms ($[Co_2Mo_{10}H_4O_{38}]^{6-}$) lead to activation of aldehyde and trialkylsilyl cyanides (TMSCN). Similar reports of catalysing a cyanosilylation reaction have been obtained for rare earth-POMs with chemical formulae $[RE(H_2O)_7]_3\text{–}P_2W_{15}Ta_3O_{62}\cdot nH_2O$ [RE = Y, Eu, Gd, Tb, Dy, Ho, Er, Tm, Yb and Lu].[92] Knoevengael condensation and CO_2 fixation to epoxide was studied in order to understand the basicity of POMs with group 5 $[M(V)_6O_{19}]^{8-}$ and

group 6 $[M(VI)_6O_{19}]_{2-}$ metals.[93] The base-catalysed activity increased in the order of $[Mo_6O_{19}]^{2-}$, $[W_6O_{19}]^{2-} \ll [H_4Nb_6O_{19}]^{4-} < [H_4Ta_6O_{19}]^{4-}$, which is in accordance with the NBO charges on the surface of oxygen atoms. It is to be noted that in the context of base-catalysed reactions, in addition to substituted Keggins, hexadecaoxometalates seem to be the chosen catalysts. It seems reasonable to state that charges on the surface oxygen controlling the basicity of the catalysts play a crucial role in the choice of these oxometalates as base catalysts.

9.5 Oxidation Catalysis and Oxometalates

Oxometalates are used as oxidation catalysts instead of traditional oxidation catalysts such as H_2SO_4, HNO_3 and peroxy acids, as the latter catalysts produce more side products. With changing times, the focus has shifted more towards green oxidants. POMs are an attractive choice as metal catalysts owing to their thermal and hydrolytic stability compared to organometallic catalysts.

9.5.1 Epoxidation Catalysis

The oxidation of alkenes to epoxides using POMs and H_2O_2 as oxidant was achieved in the early 1980s.[94] A large body of work exists on the epoxidation of alkenes.[95–116] Over the past five years, there has been a significant development in the field of the epoxidaton of alkenes. Using Keplerate nano-sphere of the type $\{Mo_{72}(M)_{30}\}$ as an efficient catalyst, epoxidaton of olefins in ethanol with hydrogen peroxide has been achieved (M = Mo, V, Cr, Fe).[117,118] The process showed excellent selectivity. Stereoselectivity was observed for norborene and other cis- and trans-olefins. Later, incorporating polyoxometalate with an organotriphosphonate ligand $K_4H_6[H_4\{(As\text{-}W_9O_{33})Zn(H_2O)W_5O_{11}(N\text{–}(CH_2PO_3)_3)\}_2(\mu_2\text{-}O)_2]\cdot 27H_2O$ type catalyst has been used to investigate its efficacy for alkene epoxidation in acetonitrile using H_2O_2 as the oxidant.[119] A green method for epoxidation of olefins using polyoxometalate over gold nanoparticle support, wherein the reaction can be carried out with or without using solvent and by using a stoichiometric amount of oxidant, in presence of *t*-butyl hydroperoxide as an initiator,[120] has been developed. Similar works[121–126] have also been reported in this regard, using amphiphillic polyoxometalate nanoparticles as catalysts. Composites of $[\gamma\text{-}H_2PV_2W_{10}O_{40}]^{3-}$ and $[\alpha\text{-}SiW_{12}O_{40}]^{4-}$ supported on Fe_2O_3 acted as catalysts for selective oxidation using hydrogen peroxide.[127] Encapsulated Zn substituted polyoxometalate $[PW_{11}Zn(H_2O)O_{39}]^{5-}$ ($PW_{11}Zn$) in silica nanoparticles as a model catalyst for oxidation of alkene[128] led to a complete conversion within 24 h. The integration of POM into silica leads to enhancement of the catalysis. Layered double hydroxides (LDHs) pillared with POMs have been used for epoxidation for a long time.[129–134] Organic–inorganic hybrid polyoxometalate-based materials act as effective catalysts for epoxidation of alkenes. Several such organic–inorganic polyoxometalate

based frameworks HSiW-MOF, PMo-MOF, HPMo-MOF and PW-MOF[135] show excellent chemoselectivity. The hydroxyl group sensitive to oxidation remained completely intact in the presence of the catalyst. Cyclo-octene was converted to 1, 2-epoxycyclooctane with a high yield and selectivity using $KH[(CH_3)_4N]_3\{[[Re(CO)_3]_4[(\mu_2\text{-}OH)(\mu_3\text{-}O)(W_5O_{18})]]\}\cdot 6H_2O$.[136] Phase-transfer agents such as alkylaminophosphazenes (RPN) can be used for oxidation using H_2O_2 catalysed by polyoxometalates.[137] These phosphazene cations render the oxometalate soluble in organic media. The activity of the OMs in decreasing order in the medium is found to be: $PMo_{12}O_{40}^{3-} > PW_{12}O_{40}^{3-} \gg SiW_{12}O_{40}^{4-}$. Keggin type transition-metal-substituted phosphotungstates $[PW_{11}M(L)O_{39}]^{m-}$($PW_{11}M$, M = Co, Cu, Fe, Ni and Mn) have been used with H_2O_2 in acetonitrile as efficient catalysts for oxidation of cyclohexene.[138] Lanthanide-substituted oxometalates have also been a particularly popular choice for epoxidation.[139,140] Aromatic sulfonium octamolybdate hybrids using aromatic sulfonium counterions and sodium molybdate have been used as self-separating catalysts for olefin epoxidation.[141] Aromatic sulfonium octamolybdates are known to combine homogenous and heterogeneous properties in a single moiety. A novel polymer-supported decatungstate catalyst bearing a poly(isopropylacrylamidealkylammonium) matrix has been reported as a catalyst for aerobic oxidation of alkene to epoxide or chlorohydrins with moderate to excellent yield.[142] Phosphomolybdic acid-based hybrid material was synthesised using polyamine-mediated bioinspired assembly *via* noncovalent interactions of PMA with PAH–citrate aggregates for selectivity towards epoxidation.[143] A series of seven compounds based on $[P_2W_{18}O_{62}]^{6-}$ and transition metal mixed organic ligand complexes was synthesised and characterised for high catalytic performance for styrene epoxidation.[144] Also, HPA/POM encapsulated in a metal organic framework gives excellent yield due to the uniform distribution of HPA/POM clusters within the MOF coupled with multiple interactions.[145] Sandwich-type oxometalates are familiar catalysts for epoxidation of olefins.[146] Similar observations for catalysing sulphoxidation and epoxidation were made for Mg_3Al–ILs–$La(PW_{11})_2$.[147] Further, there have been reports of functionalized catalysts synthesised by reacting silanol functionalized polyoxometalate $[XW_9O_{34-x}(^tBuSiOH)_3]^{3-}$ and $[Ti(^iPrO)_4]$ acting as a model catalyst for olefin epoxidation.[148] Cyclooctene epoxidation has also been known to be catalysed by vanadium-substituted, Lindqvist-type polyoxotungstate[149] $[VW_5O_{19}]^{3-}$. It not only catalyses epoxidation, but also facilitates decomposition of H_2O_2, as a significant amount of O_2 evolves. Even the isolated monomeric tellurotungstate(IV)-supported rhenium carbonyl derivative $Na_2H_2[(CH_3)_4N]_6[Te_2W_{20}O_{70}\{Re(CO)_3\}_2]\cdot 20H_2O$ has been exploited for epoxidation. Selective epoxidation of various alkenes including different cycloalkenes, styrene derivatives and internal and long-chain alkenes were carried out.[150] There have been many significant reports[151,152] of epoxidation of olefin using polyoxometalate or polyoxometalate-supported catalysts. Using optically patterned trails, our group has been successful in carrying out site-specific epoxidation catalysis using 1-octadecene and styrene as substrates.[153]

9.5.2 Alkene and Alcohol Oxidation Catalysis

In addition to epoxidation, alkenes have also been oxidised to aldehydes or ketones using POMs as catalysts. Here we give a few examples. Oxometalates show significant activity towards selective oxidation of alkene to aldehyde. The group of Neumann and Poblet employed a Cu-substituted polyoxometalate, such as $\{\alpha_2\text{-Cu(L)P}_2\text{W}_{17}\text{O}_{61}\}^{8-}$ or $\{[(\text{Cu–(L)}]_2\text{WZn(ZnW}_9\text{O}_{34})_2\}^{12-}$ (L = NO_2) as a catalyst for C–C bond cleavage reaction in alkenes to yield the corresponding aldehydes or ketones.[154] In another work, the synthesis of the sandwich-type polyoxometalate $\text{Na}_{10}\text{H}_4[\text{Bi}^{\text{III}}\text{Bi}^{\text{V}}\text{O}[\text{Zn}_2(\text{ZnW}_9\text{O}_{34})_2]\cdot 37\text{H}_2\text{O}$ was reported whose terminal position was substituted with a Lewis basic centre Bi^{III}, leading to a change in chemoselectivity of catalytic oxidation reactions of alkenes and α,β-unsaturated alcohols.[155] The high reactivity towards oxidation of allylic alcohol is due to the fact that in the base catalysed reaction, the Bi(III) site leads to the generation of an alkoxide intermediate, which is oxidised by a peroxo species *via* oxidative β-elimination to yield the carbonyl product. Dispersing oxo-metalates into metal–organic frameworks to catalyse selective oxidation of alkenes to aldehydes has been achieved.[156]

The selective oxidation of alcohol to carboxyl is of utmost importance to the industry due to the significance of carboxyl compounds in our daily life, starting from perfumes to medicine. A hybrid catalyst $[\text{TMGHA}]_{2.4}\text{H}_{0.6}\text{PW}$ by assembling alcohol, $H_3PW_{12}O_{40}$ and guanidinium ionic liquid [TMGHA]Cl [*N*″-(3-amino-2-hydroxypropyl)-*N*,*N*,*N*′,*N*′-tetramethylguanidinium chloride] as a triphasic catalyst, effectively mediates the oxidation of benzyl alcohol.[157] Keggin-type oxometalates[158–162] have been found to be extremely effective as catalysts for the selective oxidation of alcohols, and have therefore been polyoxometalate-supported on various matrixes.[163–170] Another catalyst was synthesised by attaching (3-aminopropyl)triethoxysilane linker to the anthracene and a monovacant polyoxometalate, $(SiW_{11}O_{39})$ for catalysing the oxidation of different benzylic and aliphatic alcohols to the corresponding carbonyl compounds using O_2 as an oxidant under visible light.[171] Room temperature-catalytic oxidation using oxovanadate, *i.e.*, $Cs_5(V_{14}As_8O_{42}Cl)$, as a catalyst for conversion of secondary alcohol to ketones[172] has been achieved. In another example, the sandwich-type POM $\{Zn_3Cu_2W_{19}\}$ with highly oxophilic Gd^{3+} ions was used to form a 2D inorganic porous POM framework material CZJ-11, consisting of redox copper(II) sites inside the pore space wherein CZJ-11 was simply transformed into a stable 3D porous POM framework CZJ-12 by partial dehydration to realise the biomimetic activation of molecular oxygen for aerobic oxidation of aliphatic alcohols.[173]

Furthermore, incorporation of double catalytic sites into a single molecule has been shown to result in an intramolecular, cooperative reaction pathway, thus generating an enhanced reaction rate and higher selectivity in the selective oxidation of benzyl alcohol with H_2O_2 in water. The di-imidazolium IL cations have been shown to induce a controlled phase transfer function to P-based hybrids.[174] A nanocomposite made of PdNi/RGO/oxometalate has been used as a promising electrocatalyst for electrochemical alcohol

oxidation. The long-term stability and excellent catalytic activity of the catalyst can be compared to the commercial Pd/C catalyst.[175] Many such nanocomposites using oxometalates have been able to successfully catalyse the oxidation of alcohols.[176] A hybrid surfactant with catalytic activity prepared by integrating $[PW_{11}O_{39}]^{7-}$ anion and an alkoxysilane by a covalent bond was reported for catalysing selective oxidation of alcohol.[177] The epoxidation of olefin and oxidation of alcohol was catalysed by the praseodymium(III)-containing arsenotungstate $K_{16}H_{15}Li_7[Pr_2(H_2O)_3(pzdc)As_3W_{29}O_{103}]_2{\cdot}38H_2O$.[178] Oxidation of 1-phenylethanol, in particular, attains a turnover frequency of 10 170 h^{-1}. There also have been studies on the effect of mono- and multi-valent cations on the acidity of a catalyst, which ultimately influences reactions such as the oxidation of alcohols.[179] Even OM encapsulated in MOF has been a popular choice for catalysing the oxidation of alcohols.[180]

9.5.3 Olefin Oxidation and Polymerisation Reaction

Photoactivity of oxometalates (OM) can be explored in the context of organic oxidation and polymerisation catalysis. Exciting a Keggin-type unit photochemically and generating a radical *in situ* has been a strategy that we used for the polymerisation of a series of industrially important monomers. In doing so, we incorporated BMIm (1-butyl-3-methylimidazolium) type IL (ionic liquid)-based counterions that enable and facilitate a HAT type reaction and thereby induce a polymerisation cascade[181] (Figure 9.2). In another reaction, we have homo-coupled the generated radicals with concomitant oxidation to synthesise di-one from an aromatic olefin[182] (Figure 9.2).

9.5.4 Site-specific Oxidation Catalysis on an Optically Patterned Catalyst Chip

By using patterned microchips of POMs, synthesised by directed self-assembly induced in the microheterogeneous medium or SOM state of Mo_7 type units, epoxidation catalysis was carried out.[153] Such catalysis gives the possibility of spatially localising the catalytic site (Figure 9.3). We showed

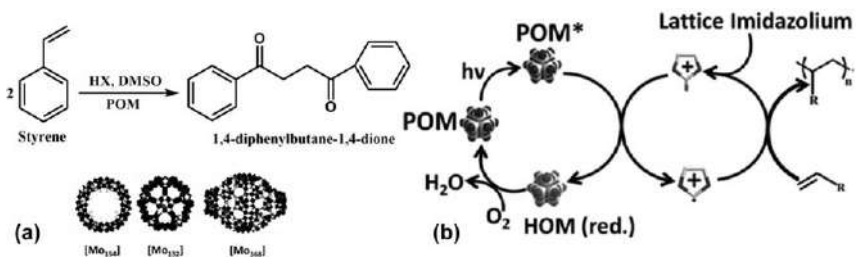

Figure 9.2 (a) Schematic representation of synthesis of di-one from styrene using different POMs. (b) Mechanistic pathway for polymerisation reaction.

that epoxidation catalysis only takes place on the specific catalytic site of the heterogenized substrate (*i.e.*, glass slide). Likewise, in another work, exploiting the same concept of spatial localisation, site-specific oxidation of benzaldehyde to benzoic acid was carried out using a supramolecular complex of a porous organic framework based on phosphonium (JUC-Z4) with Mo_7 (Figure 9.3).[44] In another work, polymerisation of pyrrole, aniline with concomitant doping by the Mo_7 based SOM pre-catalyst, led to the design of plastic conductors.[183]

9.5.5 Water Oxidation Catalysis

There have been ample examples of oxometalates as water oxidation catalysts.[184–188] Co-based POMs have been a popular choice as water

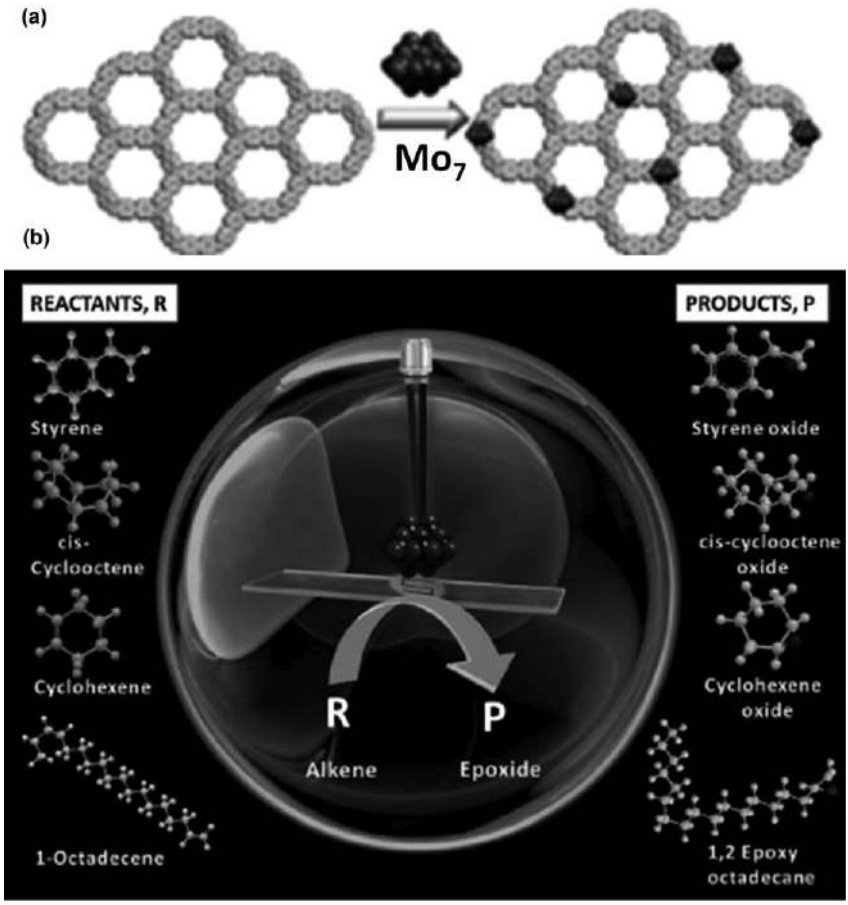

Figure 9.3 (a) Incorporation of ammonium heptamolybdate on JUCZ-4 (porous organic framework). (b) Schematic representation of epoxidation of alkenes ammonium heptamolybdate patterned trail.

oxidation catalysts.[189–196] In 2014, the Wang group reported four high nuclearity POM-based cobalt–phosphate (Co–Pi) molecular catalysts for water oxidation.[197] The oxidatively and thermally stable catalyst $Na_{10}[Co_4(H_2O)_2(VW_9O_{34})_2]\cdot 35H_2O$ synthesised by the Hill group was found to catalyse water oxidation in visible and dark conditions.[198] Under mild conditions, its turnover frequency was reported to be greater than 1×10^3 s^{-1}. Along similar lines, cobalt(II) substituted-silicotungstate[199] was used as a visible light-driven water oxidation catalyst (WOC) where $[Ru(bpy)_3]^{2+}$ acted as photosensitizer. The Wang group further synthesised three polyoxometalate based nickel clusters for visible light-driven water oxidation experiments, the highest reported TON among the three clusters was 204.5. The photocatalytic behaviour can be explained by virtue of structural motif of OM, band-gap structure and number of active sites.[200] Nickel-based OMs have been one of the choices for water oxidation catalysts.[201] The groups of Scandola, Kortz and Bonchio reported tetramanganese-substituted tungstosilicate $[Mn^{III}_3Mn^{IV}O_3(CH_3COO)_3(A\text{-}\alpha\text{-}SiW_9O_{34})]^{6-}$ (Mn_4POM) to mimic the functional core of oxygenic photosynthesis for water oxidation. It is known to be the first Mn POM to be catalytically active towards photoinduced water oxidation.[202] Since Mn-based WOCs generate a low turnover number, an active WOC based on a Mn platform was designed by using the complex $[Mn^{V}(N)(CN)_4]^{2-}$ and employing $(NH_4)_2[Ce(NO_3)_6]$ as the terminal oxidant.[203] Further, Mn substituted POMs have been known to catalyse visible light-driven water oxidation reaction effectively.[204] In another work, the 11 iron-containing nanoscale inorganic polyanionic oxide cluster $[Fe_{11}(H_2O)_{14}(OH)_2(W_3O_{10})_2\text{–}(\alpha\text{-}SbW_9O_{33})_6]^{27-}$ (Fe_{11}) was reported as an exceptional water-oxidation catalyst with a remarkable TON of 1815 ± 50.[24] Along similar lines, coupling the iron-containing polyoxometalate (Fe_{11}) with a semiconductor $BiVO_4$, photocatalytic water oxidation under acidic conditions was reported where the semiconductor acts as the light-harvesting unit.[205] The first efforts on designing WOC-containing vanadium as a catalyst $[(V^{IV}_5V^{V}_1)O_7(OCH_3)_{12}]^{-}$ were by Santoni, Scandola, Campagna and others. The reaction occurred in the presence of $Ru(bpy)_3{}^{2+}$ (bpy = 2,2′-bipyridine) and $Na_2S_2O_8$, in an acetonitrile–aqueous phosphate buffer generating a quantum yield of 0.20.[206] Plasmonic gold nanoparticles (AuNPs) when derivatized with polyoxometalate ($H_3PMo_{12}O_{40}$) and incorporated into WO_3 resulted in a large increase in water photo-oxidation currents.[207] Carbon quantum dots (CQDs)/Ag/$Ag_3PW_{12}O_{40}$ nanocomposites are also known to be effective WOCs.[208] There are reports of photocatalytic water oxidation using nanomaterial doped with oxometalates confined in a metal–organic framework. The presence of nanocrystals allows the catalyst to be fine-tuned to increase the water-oxidation efficiency.[209] The group of Bonchio and Prato in 2019 reported a system where self-assembly of multi-perylene-bisimide chromophores (PBI) were designed to function by interacting with a polyoxometalate water-oxidation catalyst (Ru_4POM) resulting in the formation of $[PBI]_5Ru_4POM$ to participate in photo-assisted water oxidation.[210] In another work, a tetra Ru-substituted polyoxometalate, $Na_{10}[\{Ru_4O_4(OH)_2(H_2O)_4\}$

(γ-$SiW_{10}O_{36})_2$] (Ru_4POM), was immobilised on glassy carbon electrodes and indium tin oxide (ITO) coated glass slides by employing a conducting polypyrrole matrix assembled by the layer-by-layer (LBL) technique and exhibited electrochemical water oxidation at high pH.[211] Cobalt-based POMs have also been particularly popular as electrocatalysts.[212–217] A multilayer covalent cobalt porphyrin framework on multi-walled carbon nanotubes ((CoP)n-MWCNTs) was reported as an excellent electrocatalyst for water oxidation. In addition to great durability, the Faradaic efficiency for oxygen production was greater than 86%.[218] Hexaniobate Lindqvist $[Nb_6O_{19}]^{8-}$ was used to develop a method[219] for efficient electrodeposition of cobalt and nickel nanostructures to study catalytic activity in water oxidation. Another work demonstrated that anionic POM WOCs and cationic polyelectrolytes (PEs) can be efficiently incorporated on the surface of various photoelectrodes with complex geometries such as Fe_2O_3, $BiVO_4$ and TiO_2, and their properties can be tuned to increase the efficacy of photoanodes towards water splitting.[220] Photoanodes have been designed and fabricated using cobalt POM and graphene oxide into a nacre-like, multilayer architecture on a haematite photoanode. The polymeric base layer improves the catalytic activity by facilitating the transfer of photogenerated holes for water oxidation through modification of the flat-band potential of the underlying photoelectrode.[221] Thus, modified and heterogeneous photoanodes are becoming popular for photo-electrochemical water oxidation or splitting.[222,223] The polyoxometalate-based Ni coordination compound $[Ni^{II}(2,2'\text{-bpy})_3]_3[\{Ni^{II}(2,2'\text{-bpy})_2(H_2O)\}\{HCo^{II}W^{VI}_{12}O_{40}\}]_2\cdot 3H_2O$ has been reported as an excellent electrocatalyst for water oxidation reaction,[224] where Ni(II) acts as the catalytic centre and the reaction follows a proton-coupled electron transfer pathway generating a high turnover frequency of 18.49 s^{-1}. Electrochemical water oxidation has been tested using Cu-substituted oxometalates; in this regard, work has been done wherein $[(\alpha\text{-}SbW_9O_{33})_2Cu_3(H_2O)_3]^{12-}$ acts as an electrochemical WOC at neutral pH.[225] The Das group rendered the Keggin anion $[CoW_{12}O_{40}]^{6-}$ active for electrochemical water oxidation by confining it in the well-defined void space of ZIF-8, a metal organic framework (MOF).[226] In a significant development, the Mascaros group recently reported a WOC-based on earth-abundant metals,[227] *i.e.*, barium salt of a cobalt-phosphotungstate polyanion, which is highly effective in acidic conditions (pH < 1) with an overpotential of 189 mV at 1 mA cm^{-2}.

The fields of photocatalytic[228] and electrocatalytic water oxidation[229] have undergone significant development over the past five years. In the matter of low overpotential, POMs seem to be good electrocatalysts. In the context of photo- and electro-catalysis, clearly oxometalates and their heterogenized media emerge as candidates of choice. This raises possibilities for exploring further coupled processes. For instance, we have reported light driven-water oxidation coupled with C–N coupling using a Cu-based SOM, $\{[K_{6.5}Cu\text{–}(OH)_{8.5}(H_2O)_{7.5}]_{0.5}[K_3PW_{12}O_{40}]\}$. The electrons generated from photochemical water oxidation reduced Cu(II) to Cu(I). Cu(I) further acts as the active catalyst for click reaction[230] (Figure 9.4). Thus, oxometalates hold promise as

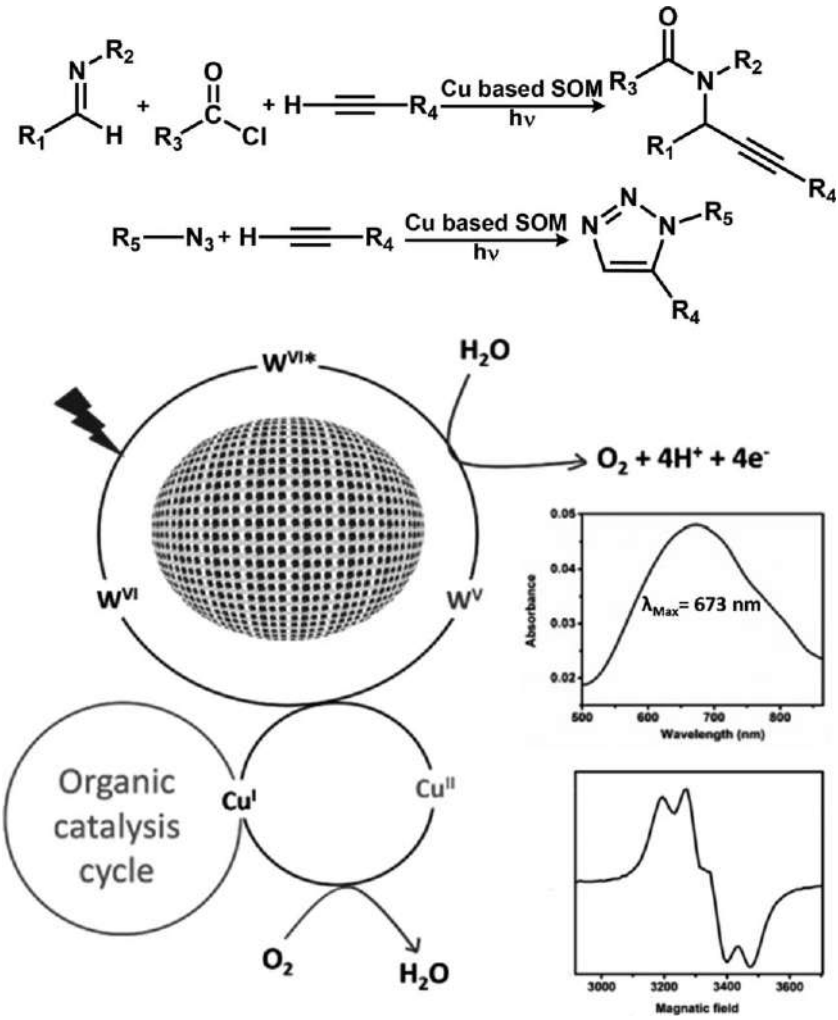

Figure 9.4 A pathway for water oxidation reaction coupled with C–N coupling. [Inset: EAS and EPR for probing the catalyst.] See ref. 230 for more details.

catalysts for coupled processes not just limited to photo-redox. Having highlighted the oxometalates as oxidation catalysts we now archive their roles in reduction catalysis.

9.6 Reduction Catalysis and Oxometalates

OMs have been reported majorly for oxidation catalysis. Reductions catalysed by them have been less explored. In this section, we highlight the

development in POM-catalysed reductive reactions over the past five years. Other leading efforts using different important catalyst types will be touched upon.

9.6.1 CO_2 Reduction Catalysis

Over the past three decades there has been a significant increase in the emission of greenhouse gases (GHG), which has created a great challenge for the scientific community to reduce GHG, primarily CO_2 and high-energy fuels, using solar energy. CO_2 has very low Gibbs free energy owing to the double bond between carbon and oxygen atoms, thus making it thermodynamically stable. The real challenge to activate an unreactive molecule such as CO_2 can be overcome by the introduction of a binding site for CO_2 in the cluster since the interaction between CO_2 moiety and the negatively charged polyoxometalate is unfavourable. The reduction of CO_2 *via* two-, four-, six-, eight- or twelve-electron processes yields HCOOH, HCHO, CH_3OH, CH_3COOH and CH_3CH_2OH,[231] respectively. The reduction can proceed photochemically, electrochemically or photoelectrochemically.[232–234] Lehn and Sauvage, during 1980s, pioneered the field of photoelectrochemical CO_2 reduction using {*Re*-(2,2′-bipyridine)},[235] Ni-cyclams[236] and polyporphyrins. The electrochemical reduction of CO_2 has been popular over a long period of time. Different aspects of electrochemical CO_2 reduction have been studied, such as electrodes, catalysts and methods generating product selectivity, such as formic acid, methanol and ethanol. POMs, owing to their tuneable size, reversible redox process, robust structure and charge distribution make them efficient catalysts for the electrochemical and photochemical reduction of CO_2. The Isaacs group reported electrochemical and photoelectrochemical CO_2 reduction using an ITO/multilayer modified electrode where the multilayer formation was by LBL using Mn(III), Ni(II) and Zn(II) in the central cavity coordinated to μ-(meso-5,10,15,20-tetra(pirydil)porphyrin)tetrakis{bis(bipyridine)chloride ruthenium(II)} and anionic $[SiW_{12}O_{40}]^{4-}$ polyoxometalate moiety.[237] These multilayer modified electrodes $[MTRP]^{n+}/[SiW_{12}O_{40}]^{4-}$ act as efficient electrocatalysts and their activity was found to be increased by light and applied potential where light produces excited state sites on the multilayer which are more sensitive towards carbon dioxide reduction. Electrochemical reduction of CO_2 by $(TOA)_6[\alpha\text{-}SiW_{11}O_{39}Co(\_)]$ (TOA = tetraoctyl ammonium; _ = vacant position in the coordination sphere of Co) resulted in the formation of CO and formaldehyde.[238] It has been observed that the shape of cyclic voltammogram of $(TOA)_6[SiW_{11}O_{39}Co(\_)]$ changed with a six-fold increase in the reduction peak intensity in the presence of CH_2Cl_2. In the first step, the POM gets reduced, followed by a transfer of electrons from POM to CO_2 leading to two- or four-electron process giving Co and formaldehyde. Another interesting work by the Zhang group features bioinspired electrocatalytic reduction of CO_2 by bovine serum albumin capped silver nanoclusters[239] mediated by $[\alpha\text{-}SiW_{12}O_{40}]^{4-}$, where AgNC@BSA in conjunction with

$[\alpha\text{-}SiW_{12}O_{40}]^{4-}$ displayed major selectivity towards CO with a faradic efficiency greater than 75%. A catalyst with polyoxometalate and metalloporphyrin framework for electrochemical CO_2 reduction has also been designed by the Lan group.[240] The integration of metalloporphyrin and the $\{\varepsilon\text{-}PMo_8{}^{v}Mo_4{}^{vi}O_{40}Zn_4\}$ polyoxometalate moiety lends them a greater efficiency due to electron donating and accepting capabilities and electron migration. This is because: (a) metalloporphyrins, which are π-electrons conjugated macrocycles, facilitate electron mobility; (b) reduced POMs consisting of low valent metal ions such as $\{\varepsilon\text{-}PMo_8{}^{v}Mo_4{}^{vi}O_{40}Zn_4\}$ are majorly electron-rich aggregates and easily donate electrons when acted upon by a stimulus; and (c) the integration of metalloporphyrin with POMs creates a directed electron transport system under an applied electric field which is extremely feasible for accomplishing a multi-electron transfer process for electrochemical reduction of CO_2 to CO. Co-PMOF displays an excellent Faradic efficiency (greater than 94%) over a broad potential range of −0.8 to −1.0 V. The system shows a turnover frequency of 1656 h^{-1} and the catalyst is stable for more than 36 h. It is worth noting that without the more oxidising oxometalate component, just employing a more reducing Co-corrole and employing covalent and non-covalent interactions on the corrole with PEG side chains we were able to achieve 12 electron reduction of CO_2 to ethanol with a high Faradaic efficiency.[241] Therefore, to obtain more reduced products from CO_2 (like ethanol), alone oxometalates may not suffice.

The groups of Blanchard and Proust had designed a catalyst $[\alpha\text{-}H_2PW_{11}O_{39}\{Rh^{III}Cp^*(OH_2)\}]^{3-}$ which closely resembles $[Cp^*Rh^{III}(bpy)Cl]^{+}$ by substituting the mono-vacant $[PW_{11}O_{39}]^{7-}$ Keggin-based POM for the bipyridine ligand.[242] The electrochemical behaviour suggested deviation in the presence of CO_2, indicating interaction with the POM derivative in spite of the presence of the solvent. In the presence of water, the electrochemical reduction of CO_2 favoured the catalytic formation of dihydrogen, with the formate being the minor product. To ensure the atom economy of the process, coupled low-energy electroreduction of CO_2 with glycerol oxidation using chemical regenerative phosphomolybdic acid (PMo_{12}), which acts as electron coupled proton carrier, was achieved.[243] Glycerol, a by-product from biodiesel synthesis, acts as a reducing agent to provide electrons to phosphomolybdic acid under light irradiation. The novelty of the process involves a low-electrolysis potential and the use of a noble metal free anode owing low overpotential of $H\text{–}PMo_{12(red)}$ oxidation on the anode.

The Sun and Wang groups introduced noble metal free polyoxometalate (Co_4) into g-C_3N_4 resulting into a hybrid material (Co_4@g-C_3N_4) for visible light-driven photochemical CO_2 reduction.[244] The material showed greater activity towards CO_2 reduction than bare g-C_3N_4. The polyoxometalate Co_4 facilitates charge transfer to g-C_3N_4 and increases the surface catalytic oxidative ability. $H_5PW_2{}^{v}W_{10}O_{40}$, an acidic reduced polyoxometalate, was used to act as a photoactive electron and proton donor with visible light *via* excitation of intervalence charge-transfer band for light-driven reduction of CO_2 to CO.[245] This polyoxometalate was integrated with dirhenium

molecular catalyst, resulting in a cascade of transformation where polyoxometalate is reduced electrochemically at the low potential of 1.3 V *vs.* $Ag/AgNO_3$. Visible light was used to transfer electrons from polyoxometalate to dirhenium catalyst for selectively reducing CO_2 to CO. CO_2 reduction using a catalyst based on Ti substituted polyoxometalate $[PTi_2W_{10}O_{40}]^{7-}$, Au nanoparticles and HKUST-1, where PTiW serves as the reactive centre and a reservoir for electrons and protons placed in HKUST-1, was achieved.[246] Here the incorporated Au nanoparticles help in harvesting visible light and the HKUST-1 cage functions as a microreactor to concentrate CO_2 molecules. A porous material containing reductive polyoxometalate has been found to catalyse photochemical CO_2 reduction successfully. The group of Lan and Huang further synthesised $TBA_5[P_2Mo_{16}{}^{V}Mo_8{}^{VI}O_{71}(OH)_9Zn_8(L)_4]$ (NNU 29), a polyoxometalate-based metal organic framework (MOF) where L is a hydrophobic organic ligand ensuring chemical stability and restrain in hydrogen generation for NNU 29.[247] Formic acid produced has a yield of 35.2 μmol with selectivity of 97.9% after 16 h. Two cobalt-based polyoxometalates, *i.e.*, a binuclear cobalt cluster $[Co_{2.67}(SiW_{12}O_{40})(H_2O)_4(Htrz)_4]\cdot Cl_{1.33}$ (Htrz = 1,2,4-triazole) and a trinuclear cobalt cluster $[Co_3(SiW_{12}O_{40})(H_2O)_3(Htrz)_6Cl]\cdot Cl\cdot 6H_2O$, were used for visible light-driven CO_2 reduction to CO.[248] The trinuclear cluster was more catalytically active in this case. Thus, from the above studies we note a pattern in the matter of electrocatalytic CO_2 reduction efforts with POMs and porphyrins: (1) Presence of Co seems to play a role; (2) POMs and porphyrins appear to be effective as ligands; and (3) for obtaining less reduced products like CO, formic acid and formaldehyde, POMs seem to be the catalyst of choice. On the other hand, for more reduced products like ethanol and acetic acid, porphyrins and corroles seem to be the efficient catalyst. We now explore oxygen reduction reactions.

9.6.2 Oxygen Reduction Reaction Catalysis

The oxygen reduction reaction (ORR) has an important role as cathode in energy-converting systems such as fuel cells that contribute to harvesting sustainable energy. $\{[FeTPyP(Crphen_2Cl)_4]^{8+}/SiW_{12}O_{40}{}^{4-}\}n_i$ (1) and $\{[NiTPyP(Crphen_2Cl)_4]^{8+}/SiW_{12}O_{40}{}^{4-}\}n_i$ (2), where TPyP = 5,10,15,20-tetra(4-pyridyl)porphyrin, phen = 1,10-phenanthroline, $SiW_{12}O_{40}{}^{4-}$ = silicontungstate and n_i = number of multilayers were assembled onto different electrode surfaces for oxygen reduction.[249] Both systems reduce oxygen differently with respect to the applied potential, $\{[FeTPyP(Crphen_2Cl)_4]^{8+}/SiW_{12}O_{40}{}^{4-}\}n_i$/GC (where n_i = 1, 2) reduced oxygen by [2e − + 2e −] steps and direct 4e-reduction. On the other hand, for the n_i = 3 system, direct transfer of 4 electrons occurs.

Green, facile electrochemical reduction of oxygen has been reported using Ag nanoparticles, oxometalates and graphene oxide (GO).[250,251] Here, polyoxometalate serves not only as an electrocatalyst but also as bridging catalyst. The oxygen reduction followed a four-electron pathway due to the

synergistic effect of Ag nanoparticles and reduced graphene oxide. The Wei group reported a novel reduced POM on Pd-catalyst substrate, *i.e.*, $Pd/H_nMo_n^{VI}Mo_{12-n}^{V}O_{40}$, for oxygen reduction reaction.[252] The high efficiency of the catalyst is observed due to electron delocalisation between the Pd and the reduced POM, causing a down-shift in the d-band structure of the Pd NPs. The reduced POM centre acts as an assisting catalyst, thus supporting the decomposition of the peroxide intermediate. Further, a Co_7Zn/C cathode made of noble metal-free polyoxometalate $Co_7(AlePyZn)_2$ and Vulcan XC-72, a low-cost carbon material, has also been reported as a highly efficient oxygen reduction catalyst.[253] The group of Freire, Mbomekalle and Fernandes reported vanadium-substituted phosphomolybdate $[PMo_{11}VO_{40}]^{4-}$ incorporated into carbon-based materials [Graphene (GF), SWCNTs, CBV] as ORR catalysts.[254] All of them showed promising catalytic activity in acidic material in a 2-electron mechanism. Zhang, He and co-workers synthesised large-scale, carbonaceous-supported, precious metal-free POM-based composites for highly efficient oxygen reduction in a neutral or basic media *via* the four-electron reduction mechanism.[255] Along similar lines Fernandes and co-workers synthesised $(TBA)_7H_3[Co_4(H_2O)_2(PW_9O_{34})_2]$ (TBA–$Co_4(PW_9)_2$) polytungstate-based, sandwich-type nanocomposites immobilised on carbonaceous material as an ORR catalyst.[256] Similarly, there have been reports of $[PW_{11}MO_{39}]^{5-}$ decorated on Ru-reduced graphene oxide nanosheets as ORR catalysts where M = Co, Ni and Cu.[257] $[SiW_{11}O_{39}]^{8-}$ (SiW_{11}) covalently combined with graphitic carbon nitride (g-C_3N_4) through an organic linker has been demonstrated as an excellent catalyst for promoting photocatalytic H_2O_2 production *via* two-electron reduction of O_2 to H_2O_2.[258] Next, we describe a few examples of HERs with POMs.

9.6.3 Hydrogen Evolution Reaction

The copper cation and hexa-capped Keggin oxoniobates based 3D framework $[Cu(en)_2]_4[PNb_{12}O_{40}(VO)_6](OH)_5{\cdot}8H_2O$ and $[Cu(enMe)_2]_4[PNb_{12}O_{40}(VO)_6](OH)_5{\cdot}6H_2O$ is reported as an efficient catalyst for photocatalytic water reduction leading to hydrogen evolution.[259] Likewise, a gigantic Co_{14} containing 36 niobates, $Na_{12}K_8[Co_{14}(OH)_{16}(H_2O)_8Nb_{36}O_{106}]{\cdot}71H_2O$ shows photocatalytic H_2 evolution activity using Pt loading in methanol solution under irradiation using a 300 W Xe lamp.[260] Copper-based polyoxometalate complexes, such as $Na_3K_7[Cu_4(H_2O)_2(B\text{-}\alpha\text{-}PW_9O_{34})_2]{\cdot}30H_2O$ (Na_3K_7–Cu_4P_2), work as efficient visible light-driven hydrogen evolution catalysts when coupled with (4,4′-di-*tert*-butyl-2,2′-dipyridyl)-bis(2-phenylpyridine(1H))-iridium(III) hexafluorophosphate ($[Ir(ppy)_2(dtbbpy)][PF_6]$) as a light absorber and triethanolamine (TEOA) as sacrificial electron donor.[261] A tetra-nickel containing polyoxometalate $Na_6K_4[Ni_4(H_2O)_2(PW_9O_{34})_2]{\cdot}32H_2O$ (Na_6K_4–Ni_4P_2) has also been known to be an efficient catalyst for photocatalytic H_2 evolution with a turnover number as high as 6500.[262] The Patzke group reported nickel containing polyoxometalate $([Ni(H_2O)XW_{11}O_{39}]^{n-}$ for photocatalytic H_2 evolution.[263] The turnover number for the reaction depended on

the heteroatom X and the highest turnover number in the series was recorded for $[Ni(H_2O)GeW_{11}O_{39}]^{6-}$. An assembly of noble metal free POM inside a metal organic framework $[P_2W_{18}O_{62}]^{6-}$@UiO has been found to be capable of visible light-driven proton reduction.[264] It is one of the first reported examples of light driven-proton reduction by Wells Dawson type POM through synergistic photoexcitation of MOF framework and multi-electron injection from the excited states of the $[Ru(bpy)_3]^{2+}$-based bridging ligands to the encapsulated POMs. The Lin group encapsulated $[Ni_4(H_2O)_2(PW_9O_{34})_2]^{10-}$ into porous and phosphorescent MOFs.[265] The vicinity of Ni_4P_2 to the photosensitizers in Ni_4P_2@MOF facilitates the multi-electron transfer to facilitate visible light-driven HER. The Ta/W mixed addendum POMs $Cs_5K_2[(Si_2W_{18}Ta_6O_{78})Cr(H_2O)_4]\cdot 8H_2O$ and $Cs_3K_4H_2[(Si_2W_{18}Ta_6O_{78})FeCl_2(H_2O)_2]\cdot 15H_2O$ were shown to increase the rate of H_2 evolution.[266]

Hill and co-workers found the self-assembly of oxometalates (POM), metal organic framework (MOF) and Pt nanoparticles (NP) to a hybrid material that shows synergistic activity for visible light-driven catalytic H_2 evolution due to binding of POM-stabilised Pt nanoparticles with NH_2-MIL-53.[267] The POMs play four roles here, namely: (1) reduction of H_2PtCl_6 to Pt NPs, (2) stabilise Pt NPs, (3) association of Pt NPs with cationic support, and (4) facilitating H_2 evolution by electron transfer from NH_2-MIL-53 to Pt-NPs. Oxometalates have also been integrated with a porphyrin system such as zinc(II) mesotetrakis(*N*-methyl-pyridinium-4-yl)porphyrin ($ZnTMPyP^{4+}$)[268] or organosilica framework[269] to increase its efficiency as a photocatalytic HER catalyst. The groups of Liu, Bao and Lan synthesised a novel polyoxometalate decorated g-C_3N_4-wrapping snowflake-like CdS nanocrystal photocatalyst, which displays high activity towards hydrogen production.[270] The introduction of $Ni_4(PW_9)_2$ POM not only serves as redox electron modulator but also as co-catalyst. It has been found that the synergistic effect from the multicomponent system increases the activity towards HER. A polyoxometalate consisting of tetradecanuclear nickel biphosphonate cluster capping a $\{SiW_9\}$ displays a high hydrogen evolution reaction under visible light *via* a reductive quenching mechanism.[271] $K_{12.5}Na_{1.5}[NaP_5W_{30}O_{110}]$ (P_5W_{30}) type Preyssler anion and graphene oxide was integrated to form a polyoxometalate–graphene nanocomposite multilayer along with protonated polyethylenimine through LBL assembly for catalysing electrochemical hydrogen evolution.[272] A highly active hydrogen evolution reaction electrode with low Pt loading on glassy carbon prepared using co-deposition of polyoxometalate and anodic platinum dissolution[273] was reported. It shows an overpotential of 65 mV at 20 mA cm^{-2}, comparable to commercial working Pt electrodes. Furthermore, a porous Mo-based composite derived from POMOFs (polyoxometalate-based metal–organic framework) and graphene oxide exhibits low Tafel slope of 41 mV dec^{-1}, which is a very positive onset potential close to that of 20% Pt/C and high exchange current density of 4.8×10^{-4} A cm^{-2}, making it one of the best performing electrocatalysts for HER.[274] In another effort, a catalyst comprising a POM

anion encapsulated MOF was coated with carbon nitride polymer on the surface and was annealed.[275] Its hollow structure and unique composition make it a remarkable catalyst for electrochemical HER. Fe_3C/Mo_2C-containing N, P co-doped graphitic carbon derived from POM@MOF-100 (Fe) (denoted as Fe_3C/Mo_2C@NPGC) was reported and displays great electrocatalytic ability towards HER with a low onset overpotential of 18 mV (*vs.* RHE), small Tafel slope of 45.2 mV dec^{-1}, as well as long-term durability for 10 h.[276] $[H_7P_8W_{48}O_{184}]^{33-}$ (P_8W_{48}) fixed in a 3D configuration on reduced graphene oxide sheets (rGO) was found to display excellent electrocatalytic H_2 evolution with a quantitative Faradic yield and high turnover frequency of 11 s^{-1} at 295 mV overpotential.[277] In another report, a catalyst consisting of Mo_2C NPs, NPC and NPRGO, was obtained by carbonizing a ternary PMo_{12}–PPy/RGO nanocomposite.[278] It displays outstanding electrocatalytic activity for the hydrogen evolution reaction and excellent stability in acidic media, the best among the reported non-noble-metal catalysts. Another stable electrocatalyst for HER by encapsulating P-modified tungsten carbide in N-doped carbon (P-W_2C@NC) has been prepared by annealing $H_3PW_{12}O_{40}$ and dicyandiamide.[279] There have been many such hybrids reported to be efficient catalyst for photochemical and electrochemical hydrogen evolution reactions. We now outline CO_2 reduction coupled with water oxidation using microheterogeneous media of oxometalates, also called soft-oxometalates.

9.6.4 Carbon Dioxide Reduction Coupled with Water Oxidation

By exploring the intrinsic, optical, semiconductor nature of oxometalates, it is possible to oxidise water and generate reducing equivalents. Such reducing equivalents can, in turn, be transiently stored and injected into a suitable substrate (Figure 9.5a). Our efforts have centred around using water and CO_2 as substrates. In 2016, we reported simultaneous CO_2 reduction coupled with water oxidation using three soft-oxometalates catalysts based on $\{Mn_6P_3W_{24}\}$, $\{Mo_{154}\}$ and $\{Mo_{132}\}$ to efficiently catalyse the reduction of CO_2 to formaldehyde and formic acid.[280] These metal oxide-based clusters are photoactive towards UV light and, hence, do not need an external photosensitizer. The water used in the reaction medium gets oxidised to generate oxygen, protons and electrons. These generated protons and electrons further assist in reducing CO_2 with a maximum turnover number and turnover frequency as high as 1.4×10^6 and 610 s^{-1}, respectively. The real nature of the active catalyst in these cases is yet unknown. It is reasonable to state that perhaps SOMs or the microheterogenized state is the pre-catalyst state, which upon activation carries out catalysis.[281] The exact pathway of activation of these and other related SOM-based catalysts are now being investigated in our laboratory. The question whether these catalysts are in state of kinetic arrest has to be explored. Further, we have reported other

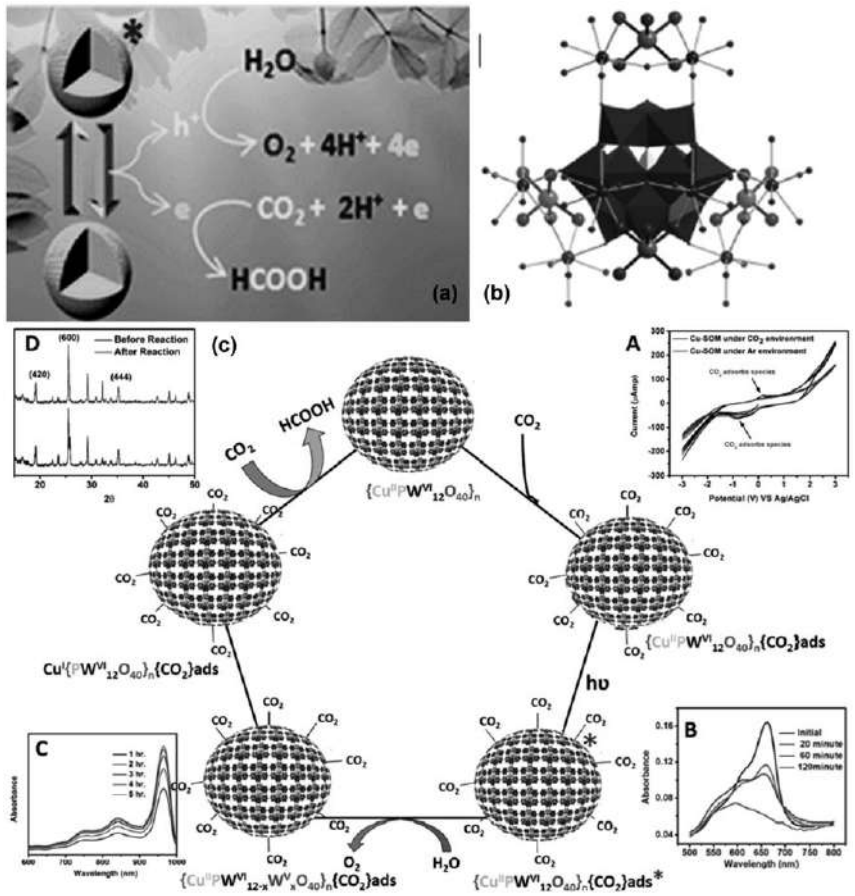

Figure 9.5 (a) Representative pathway for water oxidation coupled carbon dioxide reduction reaction. (b) Pictorial representation of $[Cu(H_2O)_5]^{2+}$ moiety coordinated to Keggin ion. (c) Mechanistic route for photochemical carbon dioxide reduction using $\{[K_{6.5}Cu\text{-}(OH)_{8.5}(H_2O)_{7.5}]_{0.5}[K_3PW_{12}O_{40}]\}$ as a catalyst. [Insets: A (CV), B, C (EAS) and D(XRD) represent different states for probing the catalytic pathway.] For details refer to ref. 282.

soft-oxometalate catalysts based on $\{[K_{6.5}Cu\text{–}(OH)_{8.5}(H2O)_{7.5}]_{0.5}[K_3PW_{12}O_{40}]\}$ for photocatalytic reduction of CO_2 to formic acid[282] (Figure 9.5b). On purging CO_2 in the medium, it gets adsorbed on the catalyst species. On photoexcitation, the CO_2 adsorbed catalyst species get excited due to the $\{PW_{12}O_{40}\}$ core going into $\{PW_{12}O_{40}\}^*$ state. It oxidises water to O_2 and the electrons released during water oxidisation reduce the $\{W_{12}O_{40}\}$ core. Thus, W^{VI} centres get reduced to W^{V}, leading to the emergence of an inter-valence charge transfer from W^{V} to W^{VI}. Photochemical CO_2 reduction takes place on the Cu centre wherein Cu^{II} is reduced to Cu^0 by reduced tungsten, which

is oxidised to (+VI) oxidation state (Figure 9.5c). In turn, Cu^0 likely goes back to Cu^{II} after carrying out the reduction. We synthesised a reduced OM, $[\{(CH_3)NH_2\}_4\{(Mo_2{}^{V}O_4)_6(\mu_2\text{-}OH)_{10}(\mu_2\text{-}O)_2(\mu_3\text{-}OH)_2(\mu_3\text{-}O)_2(Mo^{VI}O_3H)_4\}]_{0.94}$ $[\{(Mo_2{}^{V}O_4)_6(\mu_2\text{-}OH)_{10}(\mu_2\text{-}O)_2(Mo^{VI}O_3H)_4\}\{Mo^{VI}(\mu_3\text{-}O)_4\}]_{0.06} = \{Mo_{16}\}$ and have shown that by tuning the reduced metal centre of the synthesised OM, one can achieve selectivity for formaldehyde in CO_2 reduction over formic acid. $\{Mo_{16}\}$ is sensitive to light and, hence, no external photosensitizer is used and water acts as the electron donor, making the reaction environment-friendly.[283]

9.7 Conclusions and Perspectives

To summarise, in this chapter recent endeavours in the context of catalysis with oxometalates centres concerning certain key features of these catalysts are provided. These are: (i) acid–base properties, (ii) redox properties, and (iii) the existence of these entities in heterogenized state. Exploration of the first two properties of the oxometalates has led to an extremely rich literature. Interest is now increasing to understand and exploit the richness of the phases and states of the oxometalates, especially in the heterogenized (liquid or soft-matter) state. In this chapter, setting out to overview the literature on reactions as diverse as Friedel–Crafts to Fries rearrangement and to alkene isomerization, we have presented the efforts on processes for energy harvesting and catalysis. All the examples are stitched together on the two aspects of oxometalates: acid-base properties and redox properties.

Recent endeavours raise the question of possibility and challenge of transferring oxometalates from the crystalline (polyoxometalate) or homogeneous phase of molecular liquid to heterogeneous (liquid or soft-matter) phase. Open and challenging questions emerge. What is the nature of these catalysts in general? How can one delineate and thus exploit and understand their behaviour in the heterogeneous phase? Are the catalysts in heterogeneous phase responsive, dynamic and self-healing? Are the probed states of these catalysts in heterogeneous phase pre-catalysts? What is the nature of the active catalyst? What are the active sites? Finally, the what is the efficiency and atom economy of catalytic processes involving oxometalates in heterogenized media? By asking these questions, one faces the typical conundrum on facets of heterogeneous catalysis. How can these processes be understood down to every step and at the same time their efficiency be further improved so that a scalable, rapidly converting catalytic system can be designed? Perhaps the answer to these challenges lies in designing a hybrid catalyst system where homogeneous, heterogeneous and patterned catalysts can co-operate and act in unison. For such a realisation to become reality, the first step would be to understand the processes that activate a pre-catalyst and initiate the catalysis, giving the system the active catalyst – the true nature of which remains elusive and challenging to delineate, especially in the context of oxometalates.

References

1. V. Smil, *Nature*, 1999, **400**, 415.
2. G. Ertl, *Angew. Chem. Int. Ed.*, 2008, **47**, 3524–3535.
3. D. M. P. Mingos, *Essentials of Inorganic Chemistry*, Oxford University Press, Oxford, 1995.
4. K. B. Sharpless, *Angew. Chem. Int. Ed.*, 2002, **41**, 2024–2032.
5. G. Odian, *Principles of Polymerization*, John Wiley & Sons, New York, 2004.
6. R. R. Schrock, *Angew. Chem. Int. Ed.*, 2006, **45**, 3748–3759.
7. Y. Chauvin, *Angew. Chem. Int. Ed.*, 2006, **45**, 3740–3747.
8. R. H. Grubbs, *Angew. Chem. Int. Ed.*, 2006, **45**, 3760–3765.
9. J. G. de Vries and C. J. Elsevier, *Handbook of Homogeneous Hydrogenation*, Wiley-VCH, Weinheim, 2007.
10. P. Sabatier, *Nobel Lectures*, 1912.
11. J.-M. Lehn, *Supramolecular Chemistry: Concepts and Perspectives*, Wiley-VCH, Weinhiem, 1995.
12. P. -G. de Gennes, *Angew. Chem., Int. Ed. Engl.*, 1992, **31**, 842–845.
13. B. Li and P. H. Dixneuf, *Chem. Soc. Rev.*, 2013, **42**, 5744–5767.
14. A. Suzuki, *Angew. Chem. Int. Ed.*, 2011, **50**, 6722–6737.
15. Y. Surendranath and D. G. Nocera, *Prog. Inorg. Chem.*, 2011, **57**, 505–560.
16. D. G. Nocera, *Acc. Chem. Res.*, 2012, **45**, 767–776.
17. H. Frei, *Curr. Opin. Electrochem.*, 2017, **2**, 128–135.
18. Y. Niu, B. Liu, G. Xue, H. Hu, F. Fu and J. Wang, *Inorg. Chem. Commun.*, 2009, **12**, 853–855.
19. M. Fournier, C. Feumi-Jantou, C. Rabia, G. Hervé and S. Launay, *J. Mater. Chem.*, 1992, **2**, 971–978.
20. J. J. Cowan, A. J. Bailey, R. A. Heintz, B. T. Do, K. I. Hardcastle, C. L. Hill and I. A. Weinstock, *Inorg. Chem.*, 2001, **40**, 6666–6675.
21. U. Kortz, S. Nellutla, A. C. Stowe, N. S. Dalal, U. Rauwald, W. Danquah and D. Ravot, *Inorg. Chem.*, 2004, **43**, 2308–2317.
22. N. I. Gumerova, A. Roller, G. Giester, J. Krzystek, J. Cano and A. Rompel, *J. Am. Chem. Soc.*, 2020, **142**, 3336–3339.
23. B. S. Bassil, M. Ibrahim, R. Al-Oweini, M. Asano, Z. Wang, J. van Tol, N. S. Dalal, K. Y. Choi, R. Ngo Biboum, B. Keita, L. Nadjo and U. Kortz, *Angew. Chem. Int. Ed.*, 2011, **50**, 5961–5964.
24. X. Du, Y. Ding, F. Song, B. Ma, J. Zhao and J. Song, *Chem. Commun.*, 2015, **51**, 13925–13928.
25. J. M. Clemente-Juan, E. Coronado, A. Gaita-Ariño, C. Giménez-Saiz, H.-U. Güdel, A. Sieber, R. Bircher and H. Mutka, *Inorg. Chem.*, 2005, **44**, 3389–3395.
26. J. -W. Zhao, J. Zhang, Y. Song, S. -T. Zheng and G. Y. Yang, *Eur. J. Inorg. Chem.*, 2008, **2008**, 3809–3819.
27. Z. Luo, P. Kögerler, R. Cao, I. Hakim and C. L. Hill, *Dalton Trans.*, 2008, 54–58.

28. S.-T. Zheng and G.-Y. Yang, *Chem. Soc. Rev.*, 2012, **41**, 7623–7646.
29. M. T. Pope, *Inorganic Chemistry Concepts*, Springer, Berlin, **vol. 8**, 1983.
30. C. L. Hill, *Chem. Rev.*, 1998, **98**, 1–2.
31. L. Cronin and A. Müller, *Chem. Soc. Rev.*, 2012, **41**, 7333–7334.
32. D. C. Crans and S. Roy, *New J. Chem.*, 2016, **40**, 882–885.
33. S. Roy, D. C. Crans and T. N. Parac-Vogt, *Front. Chem.*, 2019, **7**, 646.
34. S. Uchida, *Porous Ionic Crystals Based on Polyoxometalates*, Springer, Berlin, 2017, pp. 65–87.
35. F. Song, K. Al-Ameed, M. Schilling, T. Fox, S. Luber and G. R. Patzke, *J. Am. Chem. Soc.*, 2019, **141**, 8846–8857.
36. L. G. Christie, S. Asche, J. S. Mathieson, L. Vilà-Nadal and L. Cronin, *J. Am. Chem. Soc.*, 2018, **140**, 9379–9382.
37. J. M. Cameron, L. Vilà-Nadal, R. S. Winter, F. Iijima, J. C. Murillo, A. Rodríguez-Fortea, H. Oshio, J. M. Poblet and L. Cronin, *J. Am. Chem. Soc.*, 2016, **138**, 8765–8773.
38. S. Biswas, D. Melgar, A. Srimany, A. Rodríguez-Fortea, T. Pradeep, C. Bo, J. M. Poblet and S. Roy, *Inorg. Chem.*, 2016, **55**, 8285–8291.
39. S. Roy, *CrystEngComm*, 2014, **16**, 4667–4676.
40. S. Roy, *Comments Inorg. Chem.*, 2011, **32**, 113–126.
41. S. Biswas and S. Roy, *J. Mater. NanoSci.*, 2014, **1**, 1–6.
42. A. Mallick and S. Roy, *Metal Nanoparticles: Synthesis and Applications in Pharmaceutical Sciences*, Wiley-VCH, Weinheim, 2018, pp. 49–61.
43. B. Roy, M. Arya, P. Thomas, J. K. Jürgschat, K. Venkata Rao, A. Banerjee, C. Malla Reddy and S. Roy, *Langmuir*, 2013, **29**, 14733–14742.
44. P. Thomas, C. Pei, B. Roy, S. Ghosh, S. Das, A. Banerjee, T. Ben, S. Qiu and S. Roy, *J. Mater. Chem. A*, 2015, **3**, 1431–1441.
45. P. Thomas, S. Chandel, A. Mallick, S. S. Sreejith, N. Ghosh and S. Roy, *Cryst. Growth Des.*, 2018, **18**, 4068–4075.
46. S. Paul, S. S. Sreejith and S. Roy, *Acta Crystallogr. Sect. C: Struct, Chem.*, 2018, **C74**, 1274–1283.
47. D. C. Crans, B. J. Peters, X. Wu and C. C. McLauchlan, *Coord. Chem. Rev.*, 2017, **344**, 115–130.
48. N. Samart, J. Saeger, K. J. Haller, M. Aureliano and D. C. Crans, *J. Mol. Eng. Mater.*, 2014, **2**, 1440007.
49. X. Li, T. Zheng, X. Liu, Z. Du, X. Xie, B. Li, L. Wu and W. Li, *Langmuir*, 2019, **35**, 4995–5003.
50. A. Mallick and S. Roy, *Nanoscale*, 2018, **10**, 12713–12722.
51. P. T. Anastas and J. C. Warner, *Green Chemistry: Theory and Practice*, Oxford University Press, New York, 1998, pp. 29–56.
52. P. T. Anastas, L. B. Bartlett, M. M. Kirchhoff and T. C. Williamson, *Catal. Today*, 2000, **55**, 11–22.
53. I. Kozhevnikov, *Appl. Catal. A: Gen.*, 2003, **256**, 3–18.
54. Y. Guo and C. Hu, *J. Mol. Catal. A: Chem.*, 2007, **262**, 136–148.
55. Y. Izumi, *Catal. Today*, 1997, **33**, 371–409.
56. Y. Izumi, K. Urabe and M. Onaka, *Zeolite, Clay, and Heteropoly Acid in Organic Reactions*, Kodansha, Tokyo, 1992, p. 99.

57. A. Z. Halimehjani, M. V. Farvardin, H. P. Zanussi, M. A. Ranjbari and M. Fattahi, *J. Mol. Catal. A: Chem.*, 2014, **381**, 21–25.
58. J. Li, Y. Zhou, D. Mao, G. Chen, X. Wang, X. Yang, M. Wang, L. Peng and J. Wang, *Chem. Eng. J.*, 2014, **254**, 54–62.
59. N. M. Basir, H. O. Lintang and S. Endud, *J. Teknol.*, 2015, **76**, 27–34.
60. C. R. Kumar, N. Rambabu, K. C. Maheria, A. K. Dalai and N. Lingaiah, *Appl. Catal. A: Gen.*, 2014, **485**, 74–83.
61. F. Zhang, Y. Jin, J. Shi, Y. Zhong, W. Zhu and M. S. El-Shall, *Chem. Eng. J.*, 2015, **269**, 236–244.
62. M. Ammar, S. Jiang and S. Ji, *J. Solid State Chem.*, 2016, **233**, 303–310.
63. B. B. Sarma, L. Avram and R. Neumann, *Chem.– Eur. J.*, 2016, **22**, 15231–15236.
64. G. P. Yang, D. Dilixiati, T. Yang, D. Liu, B. Yu and C.- W. Hu, *Appl. Organomet. Chem.*, 2018, **32**, e4450.
65. E. F. Kozhevnikova, J. Quartararo and I. V. Kozhevnikov, *Appl. Catal. A: Gen.*, 2003, **245**, 69–78.
66. E. F. Kozhevnikova, E. G. Derouane and I. V. Kozhevnikov, *Chem. Commun.*, 2002, 1178–1179.
67. E. F. Kozhevnikova, E. Rafiee and I. V. Kozhevnikov, *Appl. Catal. A: Gen.*, 2004, **260**, 25–34.
68. J. Chen, G. Zhao and L. Chen, *RSC Adv.*, 2014, **4**, 4194–4202.
69. K. Li, L. Bai, P. N. Amaniampong, X. Jia, J. -M. Lee and Y. Yang, *ChemSusChem*, 2014, **7**, 2670–2677.
70. Y. Liu, L. Zhu, J. Tang, M. Liu, R. Cheng and C. Hu, *ChemSusChem*, 2014, **7**, 3541–3547.
71. X. Yi, I. Delidovich, Z. Sun, S. Wang, X. Wang and R. Palkovits, *Catal. Sci. Technol.*, 2015, **5**, 2496–2502.
72. J. Zhao, J. Anjali, Y. Yan and J. M. Lee, *ChemCatChem*, 2017, **9**, 1187–1191.
73. F. Shen, R. L. Smith Jr, L. Li, L. Yan and X. Qi, *ACS Sustain. Chem. Eng.*, 2017, **5**, 2421–2427.
74. Z. Sun, S. Wang, X. Wang and Z. Jiang, *Fuel*, 2016, **164**, 262–266.
75. S. Körner, J. Albert and C. Held, *Front. Chem.*, 2019, **7**, 661.
76. S. Yan, Y. Li, P. Li, T. Jia, S. Wang and X. Wang, *RSC Adv.*, 2018, **8**, 3499–3511.
77. H. Yan, Y. Yang, D. Tong, X. Xiang and C. Hu, *Catal. Commun.*, 2009, **10**, 1558–1563.
78. K. Na, T. Okuhara and M. Misono, *J. Chem. Soc., Faraday Trans.*, 1995, **91**, 367–373.
79. S. Suzuki, K. Kogai and Y. Ono, *Chem. Lett.*, 1984, **13**, 699–702.
80. T. Pinto, V. Dufaud and F. Lefebvre, *Appl. Catal. A: Gen.*, 2014, **483**, 103–109.
81. B. C. Gagea, Y. Lorgouilloux, Y. Altintas, P. A. Jacobs and J. A. Martens, *J. Catal.*, 2009, **265**, 99–108.
82. T. Pinto, P. Arquillière, V. Dufaud and F. Lefebvre, *Appl. Catal. A: Gen.*, 2016, **528**, 44–51.

83. A. Alazman, D. Belic, E. F. Kozhevnikova and I. V. Kozhevnikov, *J. Catal.*, 2018, **357**, 80–89.
84. J. Lodh, A. Mallick and S. Roy, *J. Mater. Chem. A*, 2018, **6**, 20844–20851.
85. S. Zhao, Y. Chen and Y.-F. Song, *Appl. Catal. A: Gen.*, 2014, **475**, 140–146.
86. W. Ge, X. Wang, L. Zhang, L. Du, Y. Zhou and J. Wang, *Catal. Sci. Technol.*, 2016, **6**, 460–467.
87. S. Hayashi, S. Yamazoe, K. Koyasu and T. Tsukuda, *RSC Adv.*, 2016, **6**, 16239–16242.
88. Q. Xu, Y. Niu, G. Wang, Y. Li, Y. Zhao, V. Singh, J. Niu and J. Wang, *Mol. Catal.*, 2018, **453**, 93–99.
89. K. Sugahara, N. Satake, K. Kamata, T. Nakajima and N. Mizuno, *Angew. Chem. Int. Ed.*, 2014, **53**, 13248–13252.
90. H. An, Y. Zhang, Y. Hou, T. Hu, W. Yang, S. Chang and J. Zhang, *Dalton Trans.*, 2018, **47**, 9079–9089.
91. H. An, L. Wang, Y. Hu and F. Fei, *CrystEngComm*, 2015, **17**, 1531–1540.
92. S. Li, Y. Zhou, Q. Peng, R. Wang, X. Feng, S. Liu, X. Ma, N. Ma, J. Zhang, Y. Chang, Z. Zheng and X. Chen, *Inorg. Chem.*, 2018, **57**, 6624–6631.
93. S. Hayashi, N. Sasaki, S. Yamazoe and T. Tsukuda, *J. Phys. Chem. C*, 2018, **122**, 29398–29404.
94. C. Venturello, E. Alneri and M. Ricci, *J. Org. Chem.*, 1983, **48**, 3831–3833.
95. C. L. Hill and R. B. Brown, *J. Am. Chem. Soc.*, 1986, **108**, 536–538.
96. X. Zhang, T. M. Anderson, Q. Chen and C. L. Hill, *Inorg. Chem.*, 2001, **40**, 418–419.
97. D. C. Duncan, R. C. Chambers, E. Hecht and C. L. Hill, *J. Am. Chem. Soc.*, 1995, **117**, 681–691.
98. R. Prabhakar, K. Morokuma, C. L. Hill and D. G. Musaev, *Inorg. Chem.*, 2006, **45**, 5703–5709.
99. R. Neumann and M. Gara, *J. Am. Chem. Soc.*, 1994, **116**, 5509–5510.
100. R. Ben–Daniel, L. Weiner and R. Neumann, *J. Am. Chem. Soc.*, 2002, **124**, 8788–8789.
101. G. Maayan and R. Neumann, *Chem. Commun.*, 2005, 4595–4597.
102. R. Neumann and M. Gara, *J. Am. Chem. Soc.*, 1995, **117**, 5066–5074.
103. R. Neumann and M. Dahan, *Polyhedron*, 1998, **17**, 3557–3564.
104. R. Ben-Daniel, A. M. Khenkin and R. Neumann, *Chem.– Eur. J.*, 2000, **6**, 3722–3728.
105. M. V. Vasylyev, D. Astruc and R. Neumann, *Adv. Synth. Catal.*, 2005, **347**, 39–44.
106. R. Neumann and M. Dahan, *J. Chem. Soc., Chem. Commun.*, 1995, 171–172.
107. K. Kamata, R. Ishimoto, T. Hirano, S. Kuzuya, K. Uehara and N. Mizuno, *Inorg. Chem.*, 2010, **49**, 2471–2478.
108. K. Kamata, K. Sugahara, K. Yonehara, R. Ishimoto and N. Mizuno, *Chem. – Eur. J.*, 2011, **17**, 7549–7559.
109. Y. Nakagawa and N. Mizuno, *Inorg. Chem.*, 2007, **46**, 1727–1736.
110. K. Kamata, Y. Nakagawa, K. Yamaguchi and N. Mizuno, *J. Catal.*, 2004, **224**, 224–228.

111. K. Yamaguchi, C. Yoshida, S. Uchida and N. Mizuno, *J. Am. Chem. Soc.*, 2005, **127**, 530–531.
112. Y. Nakagawa, K. Kamata, M. Kotani, K. Yamaguchi and N. Mizuno, *Angew. Chem. Int. Ed.*, 2005, **44**, 5136–5141.
113. K. Kamata, K. Yonehara, Y. Sumida, K. Yamaguchi, S. Hikichi and N. Mizuno, *Science*, 2003, **300**, 964–966.
114. Y. Nishiyama, Y. Nakagawa and N. Mizuno, *Angew. Chem. Int. Ed.*, 2001, **40**, 3639–3641.
115. N. Mizuno and K. Yamaguchi, *Chem. Rec.*, 2006, **6**, 12–22.
116. N. Mizuno, K. Yamaguchi and K. Kamata, *Coord. Chem. Rev.*, 2005, **249**, 1944–1956.
117. A. Rezaeifard, R. Haddad, M. Jafarpour and M. Hakimi, *ACS Sustain. Chem. Eng.*, 2014, **2**, 942–950.
118. F. Jalilian, B. Yadollahi, M. R. Farsani, S. Tangestaninejad, H. A. Rudbari and R. Habibi, *RSC Adv.*, 2015, **5**, 70424–70428.
119. Y. Huo, Z. Huo, P. Ma, J. Wang and J. Niu, *Inorg. Chem.*, 2015, **54**, 406–408.
120. E. Tebandeke, C. Coman, K. Guillois, G. Canning, E. Ataman, J. Knudsen, L. R. Wallenberg, H. Ssekaalo, J. Schnadt and O. F. Wendt, *Green Chem.*, 2014, **16**, 1586–1593.
121. A. Mouret, L. Leclercq, A. Mühlbauer and V. Nardello-Rataj, *Green Chem.*, 2014, **16**, 269–278.
122. Y. Leng, J. Liu, P. Jiang and J. Wang, *ACS Sustain. Chem. Eng.*, 2015, **3**, 170–176.
123. Y. Leng, J. Liu, C. Zhang and P. Jiang, *Catal. Sci. Technol.*, 2014, **4**, 997–1004.
124. Y. Leng, J. Zhao, P. Jiang and J. Wang, *ACS Appl. Mater. Interfaces*, 2014, **6**, 5947–5954.
125. Y. Leng, J. Zhao, P. Jiang and J. Wang, *RSC Adv.*, 2015, **5**, 17709–17715.
126. J. Zhao, Y. Leng, P. Jiang, J. Wang and C. Zhang, *New J. Chem.*, 2016, **40**, 1022–1028.
127. Y. Wang, K. Kamata, R. Ishimoto, Y. Ogasawara, K. Suzuki, K. Yamaguchi and N. Mizuno, *Catal. Sci. Technol.*, 2015, **5**, 2602–2611.
128. L. S. Nogueira, S. Ribeiro, C. M. Granadeiro, E. Pereira, G. Feio, L. Cunha-Silva and S. S. Balula, *Dalton Trans.*, 2014, **43**, 9518–9528.
129. T. Kwon and T. J. Pinnavaia, *Chem. Mater.*, 1989, **1**, 381–383.
130. E. Narita, P. D. Kaviratna and T. J. Pinnavaia, *J. Chem. Soc., Chem. Commun.*, 1993, 60–62.
131. T. Kwon, G. A. Tsigdinos and T. J. Pinnavaia, *J. Am. Chem. Soc.*, 1988, **110**, 3653–3654.
132. S. K. Yun and T. J. Pinnavaia, *Inorg. Chem.*, 1996, **35**, 6853–6860.
133. F. Kooli and W. Jones, *Inorg. Chem.*, 1995, **34**, 6237–6238.
134. K. Chibwe and W. Jones, *Chem. Mater.*, 1989, **1**, 489–490.
135. H. Haddadi, S. M. Hafshejani, M. R. Farsani and A. K. Babahydari, *New J. Chem.*, 2015, **39**, 9879–9885.
136. J. Li, J. Guo, J. Jia, P. Ma, D. Zhang, J. Wang and J. Niu, *Dalton Trans.*, 2016, **45**, 6726–6731.

137. M. Craven, R. Yahya, E. F. Kozhevnikova, C. M. Robertson, A. Steiner and I. V. Kozhevnikov, *ChemCatChem*, 2016, **8**, 200–208.
138. Y. Song, F. Xin, L. Zhang and Y. Wang, *ChemCatChem*, 2017, **9**, 4139–4147.
139. J. Guo, Y. Niu, L. Song, Q. Xu, J. Lu, P. Ma, D. Zhang, C. Zhang, J. Niu and J. Wang, *Dalton Trans.*, 2017, **46**, 12981–12987.
140. H. Aoto, K. Matsui, Y. Sakai, T. Kuchizi, H. Sekiya, H. Osada, T. Yoshida, S. Matsunaga and K. Nomiya, *J. Mol. Catal. A: Chem.*, 2014, **394**, 224–231.
141. A. Kumar, A. K. Gupta, M. Devi, K. E. Gonsalves and C. P. Pradeep, *Inorg. Chem.*, 2017, **56**, 10325–10336.
142. T. S. Symeonidis, A. Athanasoulis, R. Ishii, Y. Uozumi, Y. M. A. Yamada and I. N. Lykakis, *ChemPhotoChem*, 2017, **1**, 479–484.
143. R. Chilivery and R. K. Rana, *ACS Appl. Mater. Interfaces*, 2017, **9**, 3161–3167.
144. Y. Lü, X. Zhang, X.-B. Cui and J.-Q. Xu, *Inorg. Chem.*, 2018, **57**, 11123–11134.
145. X. Song, D. Hu, X. Yang, H. Zhang, W. Zhang, J. Li, M. Jia and J. Yu, *ACS Sustain. Chem. Eng.*, 2019, **7**, 3624–3631.
146. W.-W. Li, S.-N. Cai, Z.-F. Tian, Y.-H. Fan, Z.-P. Xu, Y. Bai and D.-B. Dang, *Inorg. Chem. Commun.*, 2019, **104**, 36–39.
147. T. Li, W. Zhang, W. Chen, H. N. Miras and Y. F. Song, *ChemCatChem*, 2018, **10**, 188–197.
148. T. Zhang, L. Mazaud, L.-M. Chamoreau, C. Paris, A. Proust and G. Guillemot, *ACS Catal.*, 2018, **8**, 2330–2342.
149. E. Ishikawa, D. Kihara, Y. Togawa and C. Ookawa, *Eur. J. Inorg. Chem.*, 2019, **2019**, 402–409.
150. J. Lu, X. Ma, P. Wang, J. Feng, P. Ma, J. Niu and J. Wang, *Dalton Trans.*, 2019, **48**, 628–634.
151. M. Bagherzadeh, H. Hosseini, S. Akbayrak and S. Özkar, *ChemistrySelect*, 2019, **4**, 5911–5917.
152. R. Sadasivan, A. Patel and A. Ballabh, *Inorg. Chim. Acta*, 2019, **487**, 345–353.
153. P. Thomas, S. Ghosh and S. Roy, *ChemistrySelect*, 2016, **1**, 805–811.
154. A. Rubinstein, P. Jiménez-Lozanao, J. J. Carbó, J. M. Poblet and R. Neumann, *J. Am. Chem. Soc.*, 2014, **136**, 10941–10948.
155. S. R. Amanchi, A. M. Khenkin, Y. Diskin-Posner and R. Neumann, *ACS Catal.*, 2015, **5**, 3336–3341.
156. Y. Ma, H. Peng, J. Liu, Y. Wang, X. Hao, X. Feng, S. U. Khan, H. Tan and Y. Li, *Inorg. Chem.*, 2018, **57**, 4109–4116.
157. G. Chen, Y. Zhou, Z. Long, X. Wang, J. Li and J. Wang, *ACS Appl. Mater. Interfaces*, 2014, **6**, 4438–4446.
158. S. Pathan and A. Patel, *Catal. Sci. Technol.*, 2014, **4**, 648–656.
159. X. Huang, X. Zhang, D. Zhang, S. Yang, X. Feng, J. Li, Z. Lin, J. Cao, R. Pan, Y. Chi, B. Wang and C. Hu, *Chem.– Eur. J.*, 2014, **20**, 2557–2564.
160. S. Hasannia and B. Yadollahi, *Polyhedron*, 2015, **99**, 260–265.

161. L. M. Dornan and M. J. Muldoon, *Catal. Sci. Technol.*, 2015, **5**, 1428–1432.
162. Q. Xu, S. Li, M. K. Banks, W. Xu and R. Wu, *Catal. Commun.*, 2018, **114**, 24–27.
163. N. Narkhede, A. Patel and S. Singh, *Dalton Trans.*, 2014, **43**, 2512–2520.
164. J. Zhu, M. n. Shen, X. j. Zhao, P. c. Wang and M. Lu, *ChemPlusChem*, 2014, **79**, 872–878.
165. M. R. Farsani and B. Yadollahi, *J. Mol. Catal. A: Chem.*, 2014, **392**, 8–15.
166. E. Assady, B. Yadollahi, M. Riahi Farsani and M. Moghadam, *Appl. Organomet. Chem.*, 2015, **29**, 561–565.
167. T. S. Symeonidis, I. Tamiolakis, G. S. Armatas and I. N. Lykakis, *Photochem. Photobiol. Sci.*, 2015, **14**, 563–568.
168. J. Tong, L. Su, W. Li, W. Wang, H. Ma and Q. Wang, *Polyhedron*, 2016, **115**, 282–287.
169. A. Rezaeifard, A. Khoshyan, M. Jafarpour and M. Pourtahmasb, *RSC Adv.*, 2017, **7**, 15754–15761.
170. M. Mohammadi, A. Rezaei, A. Khazaei, S. Xuwei and Z. Huajun, *ACS Appl. Mater. Interfaces*, 2019, **11**, 33194–33206.
171. D. Karimian, B. Yadollahi and V. Mirkhani, *Dalton Trans.*, 2015, **44**, 1709–1715.
172. M. L. Campbell, D. Sulejmanovic, J. B. Schiller, E. M. Turner, S.-J. Hwu and D. C. Whitehead, *Catal. Sci. Technol.*, 2016, **6**, 3208–3213.
173. M. Zhao, X.-W. Zhang and C.-D. Wu, *ACS Catal.*, 2017, **7**, 6573–6580.
174. P. Hao, M. Zhang, W. Zhang, Z. Tang, N. Luo, R. Tan and D. Yin, *Catal. Sci. Technol.*, 2018, **8**, 4463–4473.
175. J. Hu, X. Wu, Q. Zhang, M. Gao, H. Qiu, K. Huang, S. Feng, T. Wang, Y. Yang, Z. Liu and B. Zhao, *Langmuir*, 2018, **34**, 2685–2691.
176. K. Darvishi, K. Amani and M. Rezaei, *Appl. Organomet. Chem.*, 2018, **32**, e4323.
177. X. Bai, X. Huang, L. Wen, N. Song, J. Zhang, Y. Zhang and Y. Zhao, *Chem. Commun.*, 2019, **55**, 3598–3601.
178. X. Ma, P. He, B. Xu, J. Lu, R. Wan, H. Wu, Y. Wang, P. Ma, J. Niu and J. Wang, *Dalton Trans.*, 2019, **48**, 12956–12963.
179. T. Wilke and M. A. Barteau, *Ind. Eng. Chem. Res.*, 2019, **58**, 14752–14760.
180. D. Li, Q. Xu, Y. Li, Y. Qiu, P. Ma, J. Niu and J. Wang, *Inorg. Chem.*, 2019, **58**, 4945–4953.
181. D. Chen, A. Sahasrabudhe, P. Wang, A. Dasgupta, R. Yuan and S. Roy, *Dalton Trans.*, 2013, **42**, 10587–10596.
182. S. Das, D. Lai, A. Mallick and S. Roy, *ChemistrySelect*, 2016, **1**, 691–695.
183. S. Ghosh, S. Das, S. Paul, P. Thomas, B. Roy, P. Mitra, S. Roy and A. Banerjee, *J. Mater. Chem. C*, 2017, **5**, 6718–6728.
184. J. M. Sumliner, H. Lv, J. Fielden, Y. V. Geletii and C. L. Hill, *Eur. J. Inorg. Chem.*, 2014, **2014**, 635–644.
185. J. R. Galán-Mascarós, *ChemElectroChem*, 2015, **2**, 37–50.
186. Q. Han and Y. Ding, *Dalton Trans.*, 2018, **47**, 8180–8188.

187. M. Stuckart and K. Y. Monakhov, *J. Mater. Chem. A*, 2018, **6**, 17849–17853.
188. P. Li, R. Zhao, H. Chen, H. Wang, P. Wei, H. Huang, Q. Liu, T. Li, X. Shi, Y. Zhang, M. Liu and X. Sun, *Small*, 2019, **15**, 1805103.
189. R. Schiwon, K. Klingan, H. Dau and C. Limberg, *Chem. Commun.*, 2014, **50**, 100–102.
190. C. Zhang, X. Lin, Z. Zhang, L.-S. Long, C. Wang and W. Lin, *Chem. Commun.*, 2014, **50**, 11591–11594.
191. D. Barats-Damatov, L. J. W. Shimon, L. Weiner, R. E. Schreiber, P. Jiménez-Lozano, J. M. Poblet, C. De Graaf and R. Neumann, *Inorg. Chem.*, 2014, **53**, 1779–1787.
192. J. Wei, Y. Feng, P. Zhou, Y. Liu, J. Xu, R. Xiang, Y. Ding, C. Zhao, L. Fan and C. Hu, *ChemSusChem*, 2015, **8**, 2630–2634.
193. W.-C. Chen, X.-L. Wang, C. Qin, K.-Z. Shao, Z.-M. Su and E.-B. Wang, *Chem. Commun.*, 2016, **52**, 9514–9517.
194. B. Liu, E. N. Glass, R.-P. Wang, Y.-T. Cui, Y. Harada, D.-J. Huang, S. Schuppler, C. L. Hill and F. M. F. de Groot, *Phys. Chem. Chem. Phys.*, 2018, **20**, 4554–4562.
195. G. Paille, M. Gomez-Mingot, C. Roch-Marchal, B. Lassalle-Kaiser, P. Mialane, M. Fontecave, C. Mellot-Draznieks and A. Dolbecq, *J. Am. Chem. Soc.*, 2018, **140**, 3613–3618.
196. Y. Choi, D. Jeon, Y. Choi, J. Ryu and B.-S. Kim, *ACS Appl. Mater. Interfaces*, 2018, **10**, 13434–13441.
197. X.-B. Han, Z.-M. Zhang, T. Zhang, Y.-G. Li, W. Lin, W. You, Z.-M. Su and E.-B. Wang, *J. Am. Chem. Soc.*, 2014, **136**, 5359–5366.
198. H. Lv, J. Song, Y. V. Geletii, J. W. Vickers, J. M. Sumliner, D. G. Musaev, P. Kögerler, P. F. Zhuk, J. Bacsa, G. Zhu and C. L. Hill, *J. Am. Chem. Soc.*, 2014, **136**, 9268–9271.
199. R. Xiang, Y. Ding and J. Zhao, *Chem.–Asian J.*, 2014, **9**, 3228–3237.
200. X.-B. Han, Y.-G. Li, Z.-M. Zhang, H.-Q. Tan, Y. Lu and E.-B. Wang, *J. Am. Chem. Soc.*, 2015, **137**, 5486–5493.
201. L. Yu, Y. Ding, M. Zheng, H. Chen and J. Zhao, *Chem. Commun.*, 2016, **52**, 14494–14497.
202. R. Al-Oweini, A. Sartorel, B. S. Bassil, M. Natali, S. Berardi, F. Scandola, U. Kortz and M. Bonchio, *Angew. Chem. Int. Ed.*, 2014, **53**, 11182–11185.
203. L. Ma, Q. Wang, W. L. Man, H. K. Kwong, C. C. Ko and T. C. Lau, *Angew. Chem. Int. Ed.*, 2015, **54**, 5246–5249.
204. K. Tsuji, O. Tomita, M. Higashi and R. Abe, *ChemSusChem*, 2016, **9**, 2201–2208.
205. Q. Hu, X. Meng, Y. Dong, Q. Han, Y. Wang and Y. Ding, *Chem. Commun.*, 2019, **55**, 11778–11781.
206. M.-P. Santoni, G. La Ganga, V. Mollica Nardo, M. Natali, F. Puntoriero, F. Scandola and S. Campagna, *J. Am. Chem. Soc.*, 2014, **136**, 8189–8192.
207. R. Solarska, K. Bienkowski, S. Zoladek, A. Majcher, T. Stefaniuk, P. J. Kulesza and J. Augustynski, *Angew. Chem. Int. Ed.*, 2014, **53**, 14196–14200.

208. J. Liu, H. Zhang, D. Tang, X. Zhang, L. Yan, Y. Han, H. Huang, Y. Liu and Z. Kang, *ChemCatChem*, 2014, **6**, 2634–2641.
209. Q. Lan, Z. M. Zhang, C. Qin, X. L. Wang, Y. G. Li, H. Q. Tan and E. B. Wang, *Chem.–Eur. J.*, 2016, **22**, 15513–15520.
210. M. Bonchio, Z. Syrgiannis, M. Burian, N. Marino, E. Pizzolato, K. Dirian, F. Rigodanza, G. A. Volpato, G. La Ganga, N. Demitri, S. Berardi, H. Amenitsch, D. M. Guldi, S. Caramori, C. A. Bignozzi, A. Sartorel and M. Prato, *Nat. Chem.*, 2019, **11**, 146.
211. N. Anwar, A. Sartorel, M. Yaqub, K. Wearen, F. Laffir, G. Armstrong, C. Dickinson, M. Bonchio and T. McCormac, *ACS Appl. Mater. Interfaces*, 2014, **6**, 8022–8031.
212. S. J. Folkman and R. G. Finke, *ACS Catal.*, 2017, **7**, 7–16.
213. G. Y. Lee, I. Kim, J. Lim, M. Y. Yang, D. S. Choi, Y. Gu, Y. Oh, S. H. Kang, Y. S. Nam and S. O. Kim, *J. Mater. Chem. A*, 2017, **5**, 1941–1947.
214. M. Blasco-Ahicart, J. Soriano-López and J. R. Galán-Mascarós, *ChemElectroChem*, 2017, **4**, 3296–3301.
215. S. D. Adhikary, A. Tiwari, T. C. Nagaiah and D. Mandal, *ACS Appl. Mater. Interfaces*, 2018, **10**, 38872–38879.
216. S. J. Folkman, J. Soriano-Lopez, J. R. Galán-Mascarós and R. G. Finke, *J. Am. Chem. Soc.*, 2018, **140**, 12040–12055.
217. A. Haider, B. S. Bassil, J. Soriano-López, H. M. Qasim, C. Sáenz de Pipaón, M. Ibrahim, D. Dutta, Y.-S. Koo, J. J. Carbó, J. M. Poblet, J. R. Galán-Mascarós and U. Kortz, *Inorg. Chem.*, 2019, **58**, 11308–11316.
218. H. Jia, Z. Sun, D. Jiang and P. Du, *Chem. Mater.*, 2015, **27**, 4586–4593.
219. Y. Liu, S.-X. Guo, L. Ding, C. A. Ohlin, A. M. Bond and J. Zhang, *ACS Appl. Mater. Interfaces*, 2015, **7**, 16632–16644.
220. D. Jeon, H. Kim, C. Lee, Y. Han, M. Gu, B.-S. Kim and J. Ryu, *ACS Appl. Mater. Interfaces*, 2017, **9**, 40151–40161.
221. Y. Choi, D. Jeon, Y. Choi, D. Kim, N. Kim, M. Gu, S. Bae, T. Lee, H.-W. Lee, B.-S. Kim and J. Ryu, *ACS Nano*, 2019, **13**, 467–475.
222. D. Jeon, N. Kim, S. Bae, Y. Han and J. Ryu, *ACS Appl. Mater. Interfaces*, 2018, **10**, 8036–8044.
223. S. Bae, H. Kim, D. Jeon and J. Ryu, *ACS Appl. Mater. Interfaces*, 2019, **11**, 7990–7999.
224. C. Singh, S. Mukhopadhyay and S. K. Das, *Inorg. Chem.*, 2018, **57**, 6479–6490.
225. L. Yu, J. Lin, M. Zheng, M. Chen and Y. Ding, *Chem. Commun.*, 2018, **54**, 354–357.
226. S. Mukhopadhyay, J. Debgupta, C. Singh, A. Kar and S. K. Das, *Angew. Chem. Int. Ed.*, 2018, **57**, 1918–1923.
227. M. Blasco-Ahicart, J. Soriano-López, J. J. Carbó, J. M. Poblet and J. Galan-Mascaros, *Nat. Chem.*, 2018, **10**, 24.
228. Y. Wang, X. Cao, Q. Hu, X. Liang, T. Tian, J. Lin, M. Yue and Y. Ding, *ACS Appl. Mater. Interfaces*, 2019, **11**, 23135–23143.

229. Y. Li, X. -R. Chang, X. -J. Sang, J. -S. Li, Y. -H. Luo, Z.- M. Zhu and W.- S. You, *Eur. J. Inorg. Chem.*, 2019, **2019**, 3597–3604.
230. S. Das, K. Das, C. Kübel and S. Roy, *ChemistrySelect*, 2019, **4**, 1994–2000.
231. Q. Zhu, X. Sun, D. Yang, J. Ma, X. Kang, L. Zheng, J. Zhang, Z. Wu and B. Han, *Nat. Commun.*, 2019, **10**, 3851.
232. J. Artz, T. E. Müller, K. Thenert, J. Kleinekorte, R. Meys, A. Sternberg, A. Bardow and W. Leitner, *Chem. Rev.*, 2018, **118**, 434–504.
233. R. Francke, B. Schille and M. Roemelt, *Chem. Rev.*, 2018, **118**, 4631–4701.
234. F. N. Al-Rowaili, A. Jamal, M. S. Ba Shammakh and A. Rana, *ACS Sustain. Chem. Eng.*, 2018, **6**, 15895–15914.
235. J. Hawecker, J.-M. Lehn and R. Ziessel, *J. Chem. Soc., Chem. Commun.*, 1984, 328–330.
236. M. Beley, J.-P. Collin, R. Ruppert and J.-P. Sauvage, *J. Chem. Soc., Chem. Commun.*, 1984, 1315–1316.
237. M. García, M. J. Aguirre, G. Canzi, C. P. Kubiak, M. Ohlbaum and M. Isaacs, *Electrochim. Acta*, 2014, **115**, 146–154.
238. M. Girardi, S. Blanchard, S. Griveau, P. Simon, M. Fontecave, F. Bedioui and A. Proust, *Eur. J. Inorg. Chem.*, 2015, **2015**, 3642–3648.
239. S.-X. Guo, D. R. MacFarlane and J. Zhang, *ChemSusChem*, 2016, **9**, 80–87.
240. Y.-R. Wang, Q. Huang, C.-T. He, Y. Chen, J. Liu, F.-C. Shen and Y.-Q. Lan, *Nat. Commun.*, 2018, **9**, 4466.
241. S. Gonglach, S. Paul, M. Haas, F. Pillwein, S. S. Sreejith, S. Barman, R. De, S. Müllegger, P. Gerschel, U.-P. Apfel, H. Coskun, A. Aljabour, P. Stadler, W. Schöfberger and S. Roy, *Nat. Commun.*, 2019, **10**, 3864.
242. M. Girardi, D. Platzer, S. Griveau, F. Bedioui, S. Alves, A. Proust and S. Blanchard, *Eur. J. Inorg. Chem.*, 2019, **2019**, 387–393.
243. L. Yang, W. Liu, Z. Zhang, X. Du, L. Dong and Y. Deng, *J. Power Sour.*, 2019, **420**, 99–107.
244. J. Zhou, W. Chen, C. Sun, L. Han, C. Qin, M. Chen, X. Wang, E. Wang and Z. Su, *ACS Appl. Mater. Interfaces*, 2017, **9**, 11689–11695.
245. E. Haviv, L. J. W Shimon and R. Neumann, *Chem. – Eur. J.*, 2017, **23**, 92–95.
246. S. M. Liu, Z. Zhang, X. Li, H. Jia, M. Ren and S. Liu, *Adv. Mater. Interfaces*, 2018, **5**, 1801062.
247. X.-X. Li, J. Liu, L. Zhang, L.-Z. Dong, Z.-F. Xin, S.-L. Li, X.-Q. Huang-Fu, K. Huang and Y.-Q. Lan, *ACS Appl. Mater. Interfaces*, 2019, **11**, 25790–25795.
248. W. Yao, C. Qin, N. Xu, J. Zhou, C. Sun, L. Liu and Z. Su, *CrystEngComm*, 2019, **21**, 6423–6431.
249. C. García, C. Díaz, P. Araya, F. Isaacs, G. Ferraudi, A. G. Lappin, M. J. Aguirre and M. Isaacs, *Electrochim. Acta*, 2014, **146**, 819–829.
250. R. Liu, Z. Xian, S. Zhang, C. Chen, Z. Yang, H. Li, W. Zheng, G. Zhang and H. Cao, *RSC Adv.*, 2015, **5**, 74447–74456.
251. Z. Xian, R. Liu, H. Li, S. Zhang, Z. Yang, W. Zheng, C. Chen, H. Cao and G. Zhang, *J. Cluster Sci.*, 2016, **27**, 241–256.

252. X. Xie, Y. Nie, S. Chen, W. Ding, X. Qi, L. Li and Z. Wei, *J. Mater. Chem. A*, 2015, **3**, 13962–13969.
253. G. Rousseau, S. Zhang, O. Oms, A. Dolbecq, J. Marrot, R. Liu, X. Shang, G. Zhang, B. Keita and P. Mialane, *Chem. – Eur. J.*, 2015, **21**, 12153–12160.
254. M. Nunes, D. M. Fernandes, I. M. Rocha, M. F. Pereira, I. M. Mbomekalle, P. de Oliveira and C. Freire, *ChemistrySelect*, 2016, **1**, 6257–6266.
255. S. Zhang, O. Oms, L. Hao, R. Liu, M. Wang, Y. Zhang, H.-Y. He, A. Dolbecq, J. Marrot, B. Keita, L. Zhi, P. Mialane, B. Li and G. Zhang, *ACS Appl. Mater. Interfaces*, 2017, **9**, 38486–38498.
256. D. M. Fernandes, H. C. Novais, R. Bacsa, P. Serp, B. N. Bachiller-Baeza, I. Rodríguez-Ramos, A. Guerrero-Ruiz and C. Freire, *Langmuir*, 2018, **34**, 6376–6387.
257. A. A. Ensafi, E. Heydari-Soureshjani and B. Rezaei, *Chem. Eng. J.*, 2017, **330**, 1109–1118.
258. S. Zhao, X. Zhao, S. Ouyang and Y. Zhu, *Catal. Sci. Technol.*, 2018, **8**, 1686–1695.
259. J.-Q. Shen, Y. Zhang, Z.-M. Zhang, Y.-G. Li, Y.-Q. Gao and E.-B. Wang, *Chem. Commun.*, 2014, **50**, 6017–6019.
260. J. Niu, F. Li, J. Zhao, P. Ma, D. Zhang, B. Bassil, U. Kortz and J. Wang, *Chem.–Eur. J.*, 2014, **20**, 9852–9857.
261. H. Lv, Y. Gao, W. Guo, S. M. Lauinger, Y. Chi, J. Bacsa, K. P. Sullivan, M. Wieliczko, D. G. Musaev and C. L. Hill, *Inorg. Chem.*, 2016, **55**, 6750–6758.
262. H. Lv, W. Guo, K. Wu, Z. Chen, J. Bacsa, D. G. Musaev, Y. V. Geletii, S. M. Lauinger, T. Lian and C. L. Hill, *J. Am. Chem. Soc.*, 2014, **136**, 14015–14018.
263. K. von Allmen, R. More, R. Müller, J. Soriano-López, A. Linden and G. R. Patzke, *ChemPlusChem*, 2015, **80**, 1389–1398.
264. Z.-M. Zhang, T. Zhang, C. Wang, Z. Lin, L.-S. Long and W. Lin, *J. Am. Chem. Soc.*, 2015, **137**, 3197–3200.
265. X. J. Kong, Z. Lin, Z. -M. Zhang, T. Zhang and W. Lin, *Angew. Chem. Int. Ed.*, 2016, **55**, 6411–6416.
266. P. Huang, X.-G. Han, X.-L. Li, C. Qin, X.-L. Wang and Z.-M. Su, *CrystEngComm*, 2016, **18**, 8722–8725.
267. W. Guo, H. Lv, Z. Chen, K. P. Sullivan, S. M. Lauinger, Y. Chi, J. M. Sumliner, T. Lian and C. L. Hill, *J. Mater. Chem. A*, 2016, **4**, 5952–5957.
268. A. Panagiotopoulos, A. M. Douvas, P. Argitis and A. G. Coutsolelos, *ChemSusChem*, 2016, **9**, 3213–3219.
269. E. D. Koutsouroubi, I. T. Papadas and G. S. Armatas, *ChemPlusChem*, 2016, **81**, 947–954.
270. X. -L. Zhai, J. Liu, L. -Y. Hu, J. -C. Bao and Y. -Q. Lan, *Chem. – Eur. J.*, 2018, **24**, 15930–15936.
271. G. Paille, A. Boulmier, A. Bensaid, M.-H. Ha-Thi, T.-T. Tran, T. Pino, J. Marrot, E. Rivière, C. H. Hendon, O. Oms, M. Gomez-Mingot,

M. Fontecave, C. Mellot-Draznieks, A. Dolbecq and P. Mialane, *Chem. Commun.*, 2019, **55**, 4166–4169.
272. M. Jiang, D. Zhu, J. Cai, H. Zhang and X. Zhao, *J. Phys. Chem. C*, 2014, **118**, 14371–14378.
273. C. Zhang, Y. Hong, R. Dai, X. Lin, L.-S. Long, C. Wang and W. Lin, *ACS Appl. Mater. Interfaces*, 2015, **7**, 11648–11653.
274. Y. -J. Tang, M. -R. Gao, C. -H. Liu, S. -L. Li, H. -L. Jiang, Y. -Q. Lan, M. Han and S. -H. Yu, *Angew. Chem. Int. Ed.*, 2015, **54**, 12928–12932.
275. X. Xu, F. Nosheen and X. Wang, *Chem. Mater.*, 2016, **28**, 6313–6320.
276. J.-S. Li, Y.-J. Tang, C.-H. Liu, S.-L. Li, R.-H. Li, L.-Z. Dong, Z.-H. Dai, J.-C. Bao and Y.-Q. Lan, *J. Mater. Chem. A*, 2016, **4**, 1202–1207.
277. R. Liu, G. Zhang, H. Cao, S. Zhang, Y. Xie, A. Haider, U. Kortz, B. Chen, N. S. Dalal, Y. Zhao, L. Zhi, C. -X. Wu, L. -K. Yan, Z. Su and B. Keita, *Energy Environ. Sci.*, 2016, **9**, 1012–1023.
278. J.-S. Li, Y. Wang, C.-H. Liu, S.-L. Li, Y.-G. Wang, L.-Z. Dong, Z.-H. Dai, Y.-F. Li and Y.-Q. Lan, *Nat. Commun.*, 2016, **7**, 11204.
279. G. Yan, C. Wu, H. Tan, X. Feng, L. Yan, H. Zang and Y. Li, *J. Mater. Chem. A*, 2017, **5**, 765–772.
280. S. Das, S. Biswas, T. Balaraju, S. Barman, R. Pochamoni and S. Roy, *J. Mater. Chem. A*, 2016, **4**, 8875–8887.
281. S. Roy, *J. Mater. Chem. A*, 2019, **7**, 23241–23245.
282. S. Das, S. Kumar, S. Garai, R. Pochamoni, S. Paul and S. Roy, *ACS Appl. Mater. Interfaces*, 2017, **9**, 35086–35094.
283. S. Barman, S. S. Sreejith, S. Garai, R. Pochamoni and S. Roy, *ChemPhotoChem*, 2019, **3**, 93–100.

CHAPTER 10

Use of Vanadium Catalysts in Epoxidation and Sulphoxidation Reactions with Green Chemistry Criteria

AGUSTÍN GALINDO,* ANTONIO PASTOR,
FRANCISCO MONTILLA AND MARÍA DEL MAR CONEJO

Departamento de Química Inorgánica, Universidad de Sevilla, Aptdo 1203, 41071 Sevilla, Spain
*Email: galindo@us.es

10.1 Introduction

The search of environment-friendly processes for traditional organic transformations is a priority and a challenge in modern chemistry.[1–5] In oxidation reactions, traditional processes, in which stoichiometric inorganic oxidants and conventional organic solvents were used, are far from current needs in oxidation technology.[6,7] Obviously, catalysis offers solutions, but some additional requirements are necessary to achieve sustainable oxidation processes. Organic solvents are generally needed for oxidation reactions and usually the ratio of solvent to reagents is high.[8,9] Additionally, they are employed in extraction and purification processes in large quantities. The excessive consumption of non-renewable solvents is an environmental problem and, consequently, the use of non-conventional solvents is a topic of extraordinary interest at academic and industrial level.[10] Catalyst separation and its

Catalysis Series No. 41
Vanadium Catalysis
Edited by Manas Sutradhar, José Armando L. da Silva and Armando J. L. Pombeiro

Published by the Royal Society of Chemistry, www.rsc.org

subsequent recyclability is another issue of great importance and the heterogeneisation of catalysts on solid supports may offer advantages over the conventional homogeneous reactions.[11,12] Well-defined inorganic solids, organic polymers[13] or organic–inorganic hybrid materials have been used as supports for the heterogeneisation of homogeneous catalysts, which can be immobilised to the support by formation of a covalent bond, by adsorption or by encapsulation. Thus, key characteristics of a green-oxidation reaction can be summarised in the use of a recyclable catalyst compatible with a green oxidant in an alternative reaction medium. Green oxidants commonly used are molecular oxygen,[14] hydrogen peroxide[15,16] and organic peroxides.[17]

High oxidation state vanadium complexes containing typically oxido and peroxido[18] ligands are well-known catalysts for oxidation of organic substrates. A vast amount of literature is available in this regard that has been conveniently reviewed over the past few decades.[14–16,19–27] In this chapter, we will specifically discuss vanadium-catalysed epoxidation and sulphoxidation reactions with selected key characteristics of a green process. Concerning epoxidation, a great number of vanadium compounds have been shown to be active catalysts in this process and the resulting products, epoxides, are of great interest because they have industrial and pharmaceutical significance. On the one hand, vanadium compounds generally employed as catalyst precursors are in high oxidation state (V or IV) and their typology is ample, from simple compounds such as $[VO(acac)_2]$ to complexes containing oxido moiety and other co-ligands with N- and O-donor atoms such as Schiff bases and salen-type ligands. On the other hand, the interest in sulphoxidation is due to the versatility of sulphoxides as precursors for chemically and biologically added-value products.[28–33] The use of vanadium catalysts in this process is well-established and has been revised over the past few decades.[34–36] Moreover, the elimination of sulphur residues in fuels and wastes by oxidation has gained major attention due to environmental concerns.[37]

The development of new procedures for the V-catalysed oxidation of olefins and sulphides with green chemistry criteria is, consequently, an area of expansion in which the adequate catalyst design may control the selectivity towards the epoxide or the sulphoxide species. Particularly, we have centred our attention on (a) non-conventional solvents as reaction media[10] (such as ionic liquids,[38] ILs, or supported ionic liquid phases, supercritical carbon dioxide, $scCO_2$, water[39] and solvent-free conditions) and (b) easily recyclable catalysts (through the heterogeneisation on inorganic or organic supports, polymers, *etc.*). Advances in the field of heterogeneisation have been recently reviewed for V-catalysed oxidations.[40,41]

10.2 Non-conventional Solvents

10.2.1 Ionic Liquids (ILs)

The nature of vanadates and peroxovanadates in ILs were initially studied by Conte *et al.*, through ^{51}V NMR experiments,[42] but the first report in which ILs

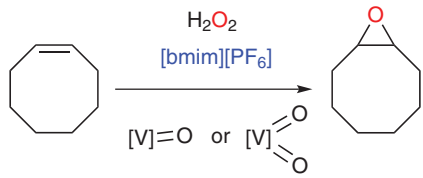

Scheme 10.1

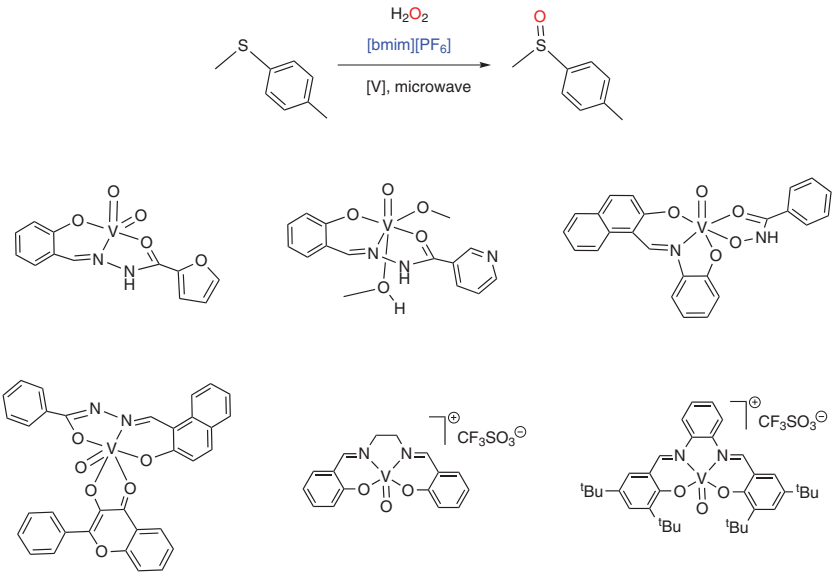

Scheme 10.2

were employed as reaction media appeared in 2009.[43] The oxidation of *cis*-cyclooctene with H_2O_2 was selected as model reaction and was investigated for the catalytic activity of several oxido and dioxido vanadium(v) complexes (13 examples) containing polydentate ligands based on different combinations of nitrogen–oxygen donor atoms. Faster reactions, but lower yields, were observed in 1-butyl-3-methylimidazolium hexafluorophosphate, [bmim][PF_6], in comparison with the reaction in acetonitrile (Scheme 10.1). In other hydrophobic ILs much lower yields of cyclooctene epoxide were obtained, while no epoxidation was observed in hydrophilic ILs. Other alkenes (cyclohexene and 1-octene) were much less reactive than cyclooctene.[43] Using selected oxidovanadium complexes (Scheme 10.2) in [bmim][PF_6] Conte and Floris were also capable to oxidise the *p*-tolyl methyl sulphide with H_2O_2, at 25 °C. Conversions of >99% and selectivities to sulphoxide higher than 82% were achieved after 3 h of reaction. However, if the reaction was microwave-assisted (power 2 W) the reaction time was reduced to 20–100 s, with a concomitant increment of conversions close to 100%.[15,43]

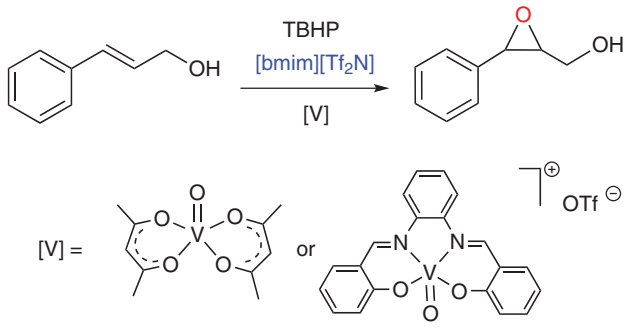

Scheme 10.3

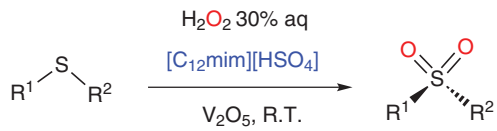

R^1 = aryl, alkyl; R^2 = H, aryl, alkyl

Scheme 10.4

The specific epoxidation of cinnamyl alcohol to 3-phenylglycidol in different ILs was investigated by Arends and co-workers.[44] The use of hydrophobic 1-butyl-3-methylimidazolium bis(trifluoromethylsulphonyl)imide, [bmim][Tf_2N], is required to reach reasonable selectivities to 3-phenylglycidol at 25 °C and using 1.5 equiv. of *tert*-butyl hydroperoxide, ^{t}BuOOH (TBHP), with 3 mol% [$VO(acac)_2$] (conversion 90%, selectivity 65%). The use of hydrophilic ILs induces alcohol oxidation to cinnamaldehyde, while catalyst [VO(Salophen)](TfO) (1 mol%, under the same reaction conditions) affords similar selectivity but lower conversion (Scheme 10.3).[44]

Simple V_2O_5 was used for the desulphurisation of model oils in combination with H_2O_2 (30% aq.) and 1-butyl-3-methylimidazolium tetrafluoroborate, [bmim][BF_4]. Benzothiophene (BT), dibenzothiophene (DBT) and 4,6-dimethyldibenzothiophene (4,6-DMDBT) were extracted into the IL and oxidised into their corresponding sulphones by the *in situ* formed peroxidovanadium complex. The removal of DBT can reach 98.7% only if the IL is present. Interestingly, the system could be recycled seven times without a significant decrease in activity.[45] Hu and co-workers, also using V_2O_5 as simple catalyst, have demonstrated the efficient oxidation of sulphides to sulphones with H_2O_2 in different ILs. Optimal results were obtained with 3-dodecyl-1-methylimidazolium hydrogen sulphate, [C_{12}mim][HSO_4] (Scheme 10.4). The products were obtained in high yields (82%–95%) separated by simple extraction, and the system could be recycled and reused without loss of activity.[46]

An interesting alternative to the use of ILs as solvents is the incorporation of the IL functionality onto the ligand. Thus, Yin and co-workers presented

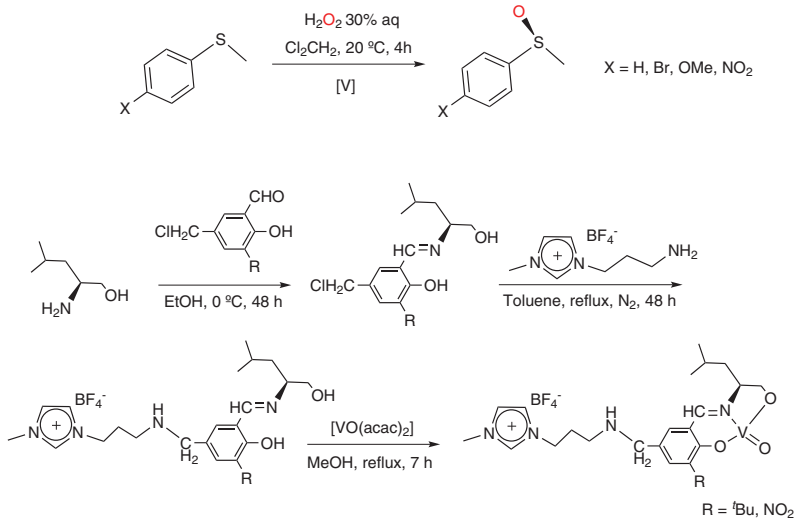

Scheme 10.5

the preparation of an oxidovanadium(IV) Schiff base complex covalently grafted with an IL functionality. The complex was an efficient catalyst in the enantioselective oxidation of methyl aryl sulphides to sulphoxides with aqueous H_2O_2 as an oxidant (Scheme 10.5). The best result was 85% yield of the *S*-sulphoxide (43% ee). The vanadium complex with the IL-functionalised ligand can be easily recovered by simple hexane precipitation and reused for at least six cycles without loss of activity and enantioselectivity.[47]

10.2.2 Supercritical CO_2 ($scCO_2$)

Liquid and supercritical CO_2 has been demonstrated to be appropriate solvents for the selective epoxidation of allylic alcohols.[48–50] Rates measured in liquid CO_2 (103 bar) for the $[VO(O^iPr)_3]$-catalysed epoxidation of allylic alcohols (12 examples) using TBHP (5.6 M in decane) are comparable to those measured in conventional organic solvents (24 h at 25 °C).[48,49] The activity of $[VO(acac)_2]$ in such a solvent was found to be substantially lower than in organic solvents, presumably due to its low solubility in CO_2. The use of fluorinated acac-type ligands increased the reactivity of V-catalysed epoxidations by enhancing catalyst precursor solubility (best result: 99% conversion and 99% selectivity in the epoxidation of *trans*-2-hexen-1-ol, by using the 6,6,7,7,8,8,8-heptafluoro-2-methyloctane-3,5-dione ligand; Scheme 10.6).[49] Related epoxidation reactions of allylic alcohols (11 examples) with TBHP (70% aq.) were investigated in $scCO_2$ (220 bar) by using as catalyst the complex [VO(salen′)] containing a substituted salen ligand. For example, 99% yield and 99% of diastereoselectivity was obtained in the epoxidation of 3,7-dimethylocta-2,6-dien-1-ol (Scheme 10.7).[50]

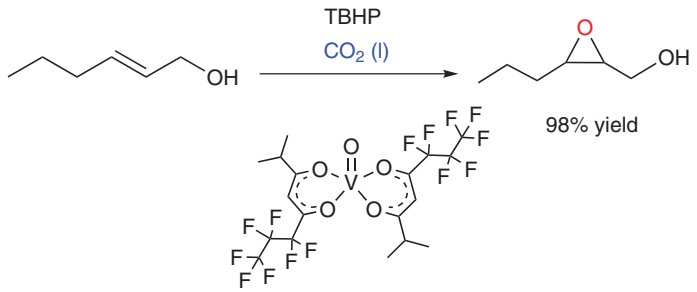

Scheme 10.6

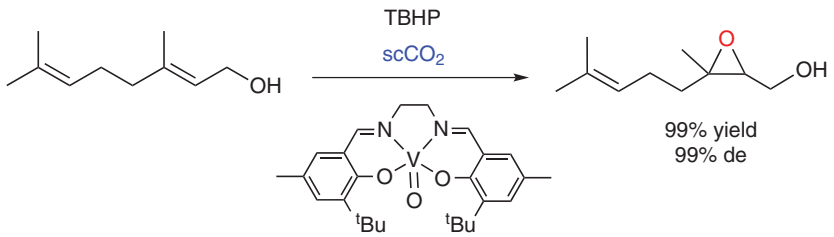

Scheme 10.7

10.2.3 Solvent-free

Epoxidation under solvent-free conditions has been studied for several vanadium systems. For example, *cis*-cyclooctene epoxidation occurred with aqueous TBHP at 80 °C using 1 mol% $[VO(SAP)]_2O$ (SAP = salicylideneaminophenolate) as catalyst, in the absence of organic solvents. Under these conditions, 94% of the *cis*-cyclooctene was converted in 5.5 h with a selectivity to epoxide of 83% (Scheme 10.8).[51] The same authors reported the synthesis of a series of dinuclear and mononuclear oxidovanadium(v) complexes (7 examples) containing tridentate Schiff base ligands derived from pyridoxal and appropriate thiosemicarbazide or hydrazide. These complexes were tested as pre-catalysts for the *cis*-cyclooctene epoxidation with TBHP under solvent-free conditions at 80 °C. The cyclooctene conversion was moderate to very good after 5 h (60%–87%), but the selectivity towards the formation of cyclooctene oxide is low due to the formation of cyclooctanediol product.[52]

Compounds $[R_3SnVO_3]$ (R = Me, Et) are demonstrated to be remarkable catalysts in the epoxidation of olefins (6 examples) with TBHP in decane without additional organic co-solvents.[53,54] These compounds act as solid reservoirs for soluble, catalytically active species that promote high selectivities to the epoxide. The addition of an organic co-solvent reduces the reaction yield. Cyclooctene oxide was the only product formed at 24 h reaction and 55 °C with 82% yield for R = Et. Lower yields were observed for other alkenes (for instance, 45% for *trans*-2-octene with selectivity of 100%; Scheme 10.9).[53]

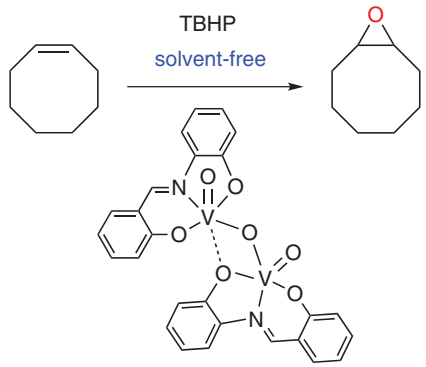

Scheme 10.8

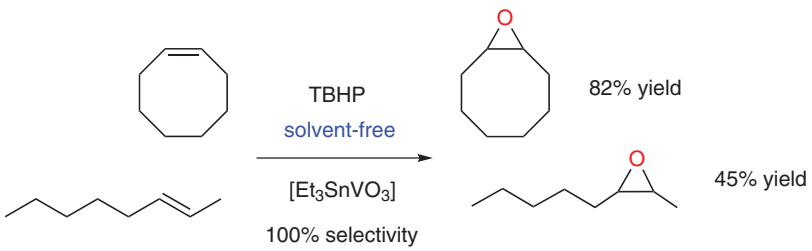

Scheme 10.9

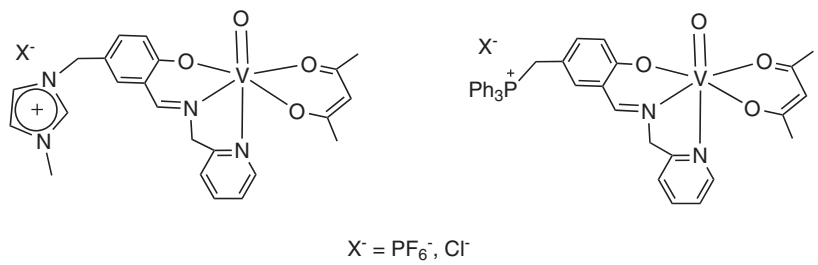

Scheme 10.10

Grivani and co-workers adopted the methodology of preparing Schiff bases with bounded IL fragments for the preparation of six-coordinated vanadium(IV) complexes (Scheme 10.10). They are active in the oxidation of methyl phenyl sulphide under solvent-free conditions. For example, by using TBHP a conversion of 85% and 100% selectivity to sulphoxide was obtained in 2 min with the phosphonium-chloride derivative, while lower conversions were observed with H_2O_2. The presence of phosphonium or imidazolium cation in the functionalised ligand, with chloride as counter anion, does not change the catalytic activity. However, changing the chloride by PF_6^- anion drastically decreases the activity.[55]

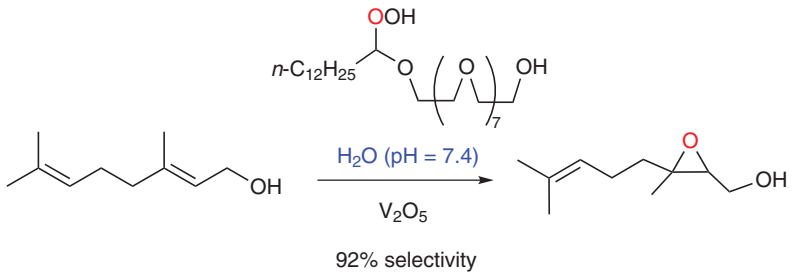

Scheme 10.11

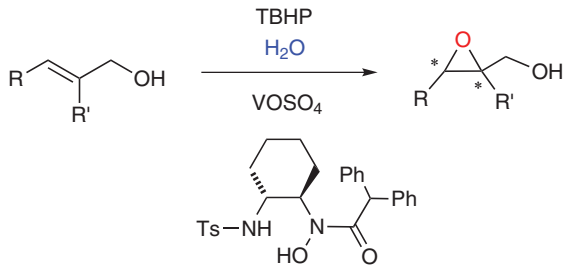

Scheme 10.12

10.2.4 Water

An interesting approach to carry out oxidation reactions in water is the use of micellar systems in which the hydroperoxide oxidant has amphiphilic properties. Masuyama and co-workers described the preparation of a series of novel amphiphilic hydroperoxides that behave as new oxidising agents bearing a micelle-forming character in water. The epoxidation of geraniol with these hydroperoxides occurred in water with $VOSO_4 \cdot nH_2O$ as catalyst at 30 °C for 24 h, but formation of triols indicated that hydrolysis of the epoxides took place simultaneously. However, this hydrolysis was avoided by adjusting the pH of the reaction media to 7.4. In this way, the epoxides at the 2- or 6-position were exclusively obtained. By using V_2O_5, under the same experimental conditions, good conversions and selectivities to the epoxide at the 2-position were obtained (best result: conversion 67%, selectivity 92%; Scheme 10.11).[56] Water can also be used as solvent in the asymmetric V-catalysed epoxidation of allylic alcohols by using chiral ligands with sulphonamide and hydroxamic acid fragments. The reaction, notorious for its ligand-deceleration effect, turned into a ligand-accelerated process in this solvent. By using this procedure, a range of allylic alcohols (12 examples) were epoxidised using TBHP at 0 °C with up to 94% ee and good to very good yields (Scheme 10.12).[57,58]

Recently, Maurya, Sankar *et al.*, reported oxidovanadium-porphyrin catalysts that were active for the selective epoxidation of several alkenes (8 examples) in a mixture of water–acetonitrile as the reaction medium. Epoxidations were carried out with aqueous H_2O_2 in the presence of

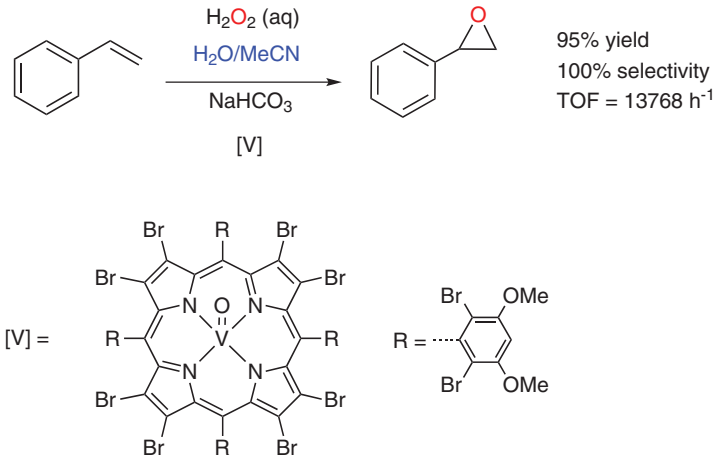

Scheme 10.13

$NaHCO_3$ at 50 °C (Scheme 10.13). Very high conversions, selectivities and TOF numbers were observed, even with low-catalyst loadings.[59]

10.3 Heterogeneisation

10.3.1 Mesoporous Silica

Vanadium catalysts anchored on several types of mesoporous silica (SBA-3, SBA-15, MCM-41, silicalite and amorphous silica) have been prepared, and the effect of the support and the vanadium concentration in the epoxidation of propene using N_2O as oxidant have been studied. Vanadium species was introduced by impregnation of inorganic matrices with an aqueous solution of $VOSO_4 \cdot 5H_2O$. The reported highest conversion was 30% for a vanadium species supported on SBA-3, although the yield to propene oxide was only of 8%.[60] Other inorganic supports such as Al_2O_3, MgO and TiO_2 provided lower conversions and selectivities.[61] Modification of several vanadium catalysts supported in silica with different amounts of potassium ions causes the conversion to decrease, but the selectivity to epoxide improves.[62] The highest propene-oxide productivity was obtained with samples prepared from NH_4VO_3 that showed a high vanadium content.[63] Another reported method for the preparation of vanadium catalysts is the deposition of a vanadium oxido on SBA-15 and FDU-15 (phenol–formaldehyde resin) by atomic layer deposition. This is a powerful method to control the growth of monolayers on the surface of the mesoporous support. These compounds were tested in the epoxidation of cyclohexene using TBHP in decane as an oxidant (highest conversion 63% after 8 h).[64] Epoxidation of styrene with H_2O_2 using UV-irradiation and a silica (SBA-15) impregnated with aqueous solutions of nitrates of alkaline-earth metals and NH_4VO_3 as a catalyst have also been described. The addition of alkaline-earth metals to vanadium-impregnated

silica has been shown to improve selectivity from styrene to epoxide.[65] A catalyst, prepared by impregnation with $VOSO_4 \cdot 5H_2O$ of mesoporous silica synthesised with the aid of sucrose as porogeneous agent, has been used with N_2O as the oxidant. The presence of sucrose changed the morphology and structure of the resulting porous silica support. The best results in the propene epoxidation were obtained using silica SBA-3 (13% conversion).[66]

In these examples, simple compounds were used as the vanadium source and catalyst materials were obtained by simple impregnation methods. The alternative to these processes is the immobilisation of a vanadium complex by using (3-aminopropyl)alkoxysilane linkers. Thus, Bhunia and Koner reported a new hybrid heterogeneous catalytic system obtained by the immobilisation of $[VO(acac)_2]$ complex into MCM-41 by using (3-aminopropyl)triethoxysilane, **$[VO(acac)_2]$@MCM41** (Scheme 10.14). The epoxidation of several alkenes (6 examples) with TBHP catalysed by **$[VO(acac)_2]$@MCM41** was studied in different solvents. The best results were obtained in acetonitrile. The catalyst can be recycled up to three cycles without significant loss in their activity.[67]

With the aim of improving the catalytic system, various authors have reported the preparation of magnetically recoverable nanoparticles containing covalently grafted vanadium complexes. For the heterogeneisation of the catalysts, they used Fe_3O_4 magnetic nanoparticles that were coated with a dense silica layer. The silica-layered system (SiO_2@Fe_3O_4) was then grafted on the surface by using the vanadium complexes, affording the organic–inorganic hybrid materials. Using this strategy, the vanadium(v) complex $[VO_2(bpca)]$ (bpca = dipicolinoylamide) can be immobilised onto modified silica coated Fe_3O_4 nanoparticles. The resulting material **$[VO_2(bpca)]$@SiO_2@Fe_3O_4** (Scheme 10.15) has been reported as an effective catalyst for the epoxidation of several olefins and allylic alcohols (8 examples) with aqueous TBHP (70%). The catalyst can be easily separated by means of an external magnet and can be reused at least three times without significant decrease in selectivity.[68]

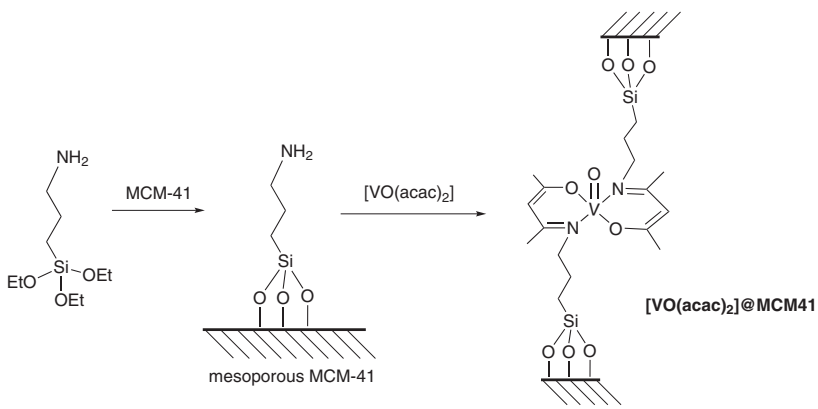

Scheme 10.14

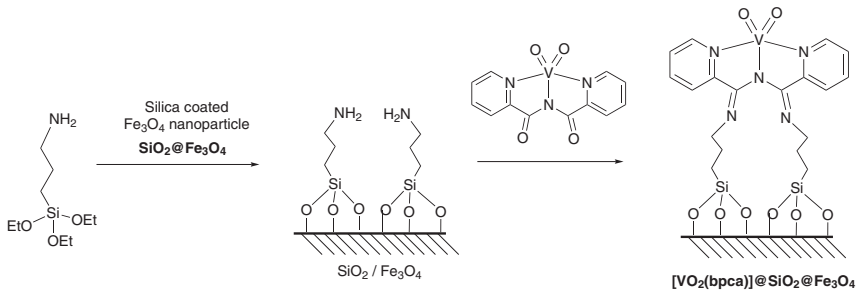

Scheme 10.15

Khedher *et al.,* reported a chiral vanadyl salen catalyst immobilised on mesoporous silica by a covalent grafting method using 3-amino-propyl triethoxysilane. The resulting organic–inorganic hybrid material **VO(salen)@SiO_2** (Scheme 10.16) was tested as catalyst, in combination with H_2O_2 as terminal oxidant and Cl_2CH_2 as solvent, for the oxidation of methyl phenyl sulphide. The observed enantioselectivity was modest, in the 8%–10% ee range.[69] Dabiri *et al.*, using a similar strategy, prepared a vanadyl Schiff base complex supported on mesoporous silica as an organic–inorganic hybrid catalyst. The catalyst, abbreviated here as **VO(2,4-dhba)@SiO_2** (Scheme 10.16), was synthesised by covalent grafting on mesoporous silica using 3-amino-propyltriethoxysilane, subsequent reaction with 2,4-dihydroxybenzaldehyde and then reaction with $[VO(acac)_2]$. **VO(2,4-dhba)@SiO_2** was used as an efficient heterogeneous catalyst for the selective oxidation of different aryl sulphides to the corresponding sulphoxides with H_2O_2 as oxidant and methanol as solvent. Moreover, the catalyst was shown to be reusable for the oxidation of methyl phenyl sulphide (up to five runs) without significant loss of its catalytic activity.[70] A closely related hetereogenised vanadyl Schiff base complex **VO(3,4-dhba)@MCM41** (Scheme 10.17) has been reported by Nikoorazm's group, which supported the $V^{IV}O$ complex on mesoporous silica MCM-41 using a Schiff base ligand based on 3,4-dihydroxybenzaldehyde.[71] The catalytic activity of **VO(3,4-dhba)@MCM41** was evaluated for the oxidation of various alkyl and/or aryl substituted sulphides using urea hydroperoxide (UHP) as oxidant in ethanol with excellent conversions to sulphoxide (14 examples, yield range: 89%–98%). The reusability of this catalyst was also evaluated in the oxidation of dibenzyl sulphide. The results show only an 11% decrease in the conversion after four cycles. The same research group also described another vanadyl complex covalently anchored into organic-modified MCM-41 silica. In this example, the hybrid material catalyst **VO(2A3HP)@MCM41** (Scheme 10.17) was synthesised by covalent grafting on the silica surface using 3-chloropropyltriethoxysilane, following reaction with 2-amino-3-hydroxypyridine and then complexation with $[VO(acac)_2]$. Several types of alkyl and/or aryl substituted sulphides (12 examples) were efficiently oxidised to the corresponding sulphoxides with good to excellent yields (86%–98%) using **VO(2A3HP)@MCM41** as catalyst and H_2O_2 as terminal oxidant under solvent-free conditions at room temperature. Moreover, it is

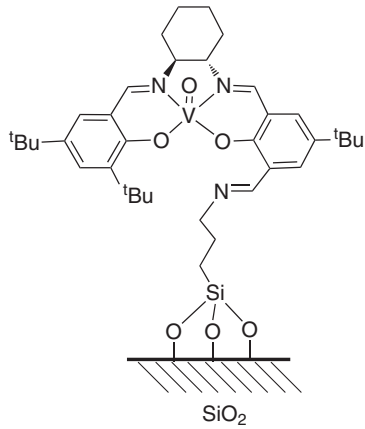

VO(salen)@SiO_2 **VO(2,4-dhba)@SiO_2**

Scheme 10.16

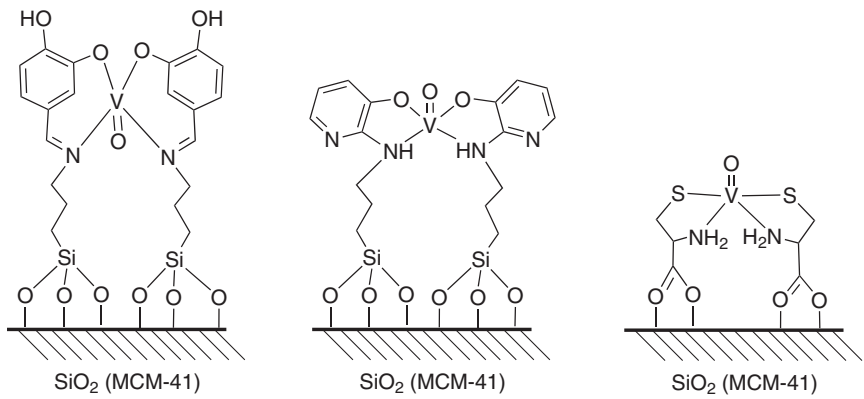

VO(3,4-dhba)@MCM41 **VO(2A3HP)@MCM41** **VO(Cys)@MCM41**

Scheme 10.17

noteworthy that functional groups, such as OH groups or alkenes, were not oxidised.[72] Nikoorazm *et al.,* also reported the synthesis and characterisation of an oxidovanadium complex containing L-cysteine anchored to mesoporous silica MCM-41. The resultant heterogeneised vanadyl complex **VO(Cys)@MCM41** (Scheme 10.17) can act as an efficient catalyst in the oxidation of various sulphides, with different functional groups, into their corresponding sulphoxides with excellent yields (94%–98%). H_2O_2 was used as an oxidant at room temperature under neat conditions. Furthermore, the catalyst was shown to be reusable for the oxidation of methyl phenyl sulphide (seven runs) under optimised conditions.[73]

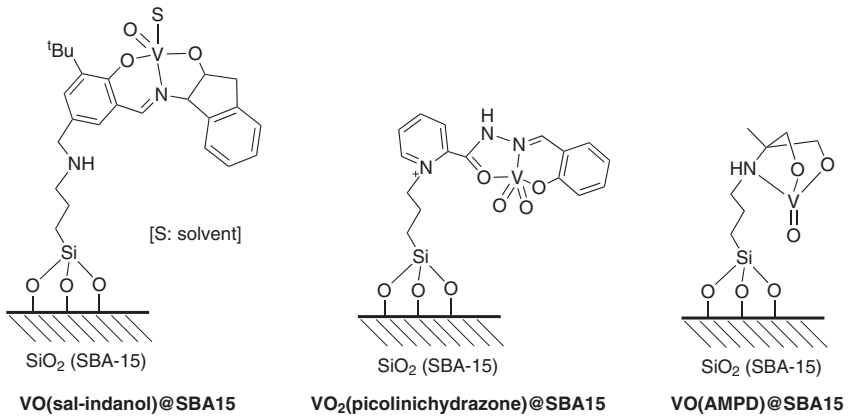

Scheme 10.18

Similarly, mesoporous silica SBA-15 has been used as inorganic support for various vanadyl complexes used as catalysts in sulphoxidation. For instance, the heterogeneous vanadyl complex **VO(sal-Indanol)@SBA15** (Scheme 10.18) has been synthesised by a grafting method on the silica surface using 3-aminopropyltriethoxysilane, reaction with Schiff base ligand based on (1*R*,2*S*)-(+)-*cis*-1-amino-2-indanol and then complexation with [VO(acac)$_2$]. Catalytic evaluation in asymmetric sulphoxidation of several thioanisols showed that **VO(sal-Indanol)@SBA15** exhibited high catalytic activity and enantioselectivities in the range of 30%–35%, in the presence of H_2O_2 as oxidant and CH_2Cl_2 as solvent at 0 °C. The reusability of **VO(sal-Indanol)@SBA15** was successfully tested four times in the asymmetric sulphoxidation of thioanisol.[74] Analogously, supported dioxidovanadium complex **VO$_2$(picolinichydrazone)@SBA15** (Scheme 10.18) was obtained by a covalent grafting on the SBA-15 surface using 3-chloropropyltriethoxysilane and reaction with a VO_2–picolinic hydrazine Schiff base complex. The resultant heterogeneised dioxidovanadium complex can act as an efficient catalyst in the oxidation of various alkyl and/or aryl substituted sulphides into their sulphoxides, with good to excellent yields (70%–94%), in the presence of H_2O_2 as oxidant and $C_2H_4Cl_2$ as solvent at room temperature. The narcolepsy drugs, modafinic and modafinil, were also prepared by using this catalytic system.[75] Similarly, Tamoradi *et al.*, synthesised the hybrid material catalyst **VO(AMPD)@SBA15** (Scheme 10.18) by a covalent grafting on the silica surface using 3-chloropropyltriethoxysilane, subsequent reactions with 2-amino-2-methyl-1,3-propanediol (AMPD) and then with [VO(acac)$_2$]. In order to investigate the catalytic activity of this material, the authors investigated it for the oxidation of a wide range of sulphides with different functional groups (20 examples) into their corresponding sulphoxides. Excellent yields (89%–99%) were obtained in the presence of H_2O_2 as oxidant at room temperature under neat conditions. The reusability of **VO(AMPD)@SBA15** was also demonstrated for the oxidation of tetrahydrothiophene (9 cycles) without significant loss of catalytic activity.[76]

Bagherzadeh *et al.*, prepared a magnetically recyclable vanadyl catalyst **VO(salen)@SiO_2@Fe_3O_4** (Scheme 10.19) by covalent anchoring of [VO(salen)Cl] complex on SiO_2@Fe_3O_4. These nanoparticles were efficient catalysts for oxidation of sulphides (7 examples) to corresponding sulphoxides with urea hydrogen peroxide as oxidant and a mixture CH_2Cl_2–methanol as solvent at room temperature. Recycling experiments showed that the hybrid catalyst could be used for nearly complete oxidation of three different substituted sulphides for at least five successive cycles.[77] The same research group used 3-aminopropyltriethoxysilane to functionalise silica-coated magnetite nanoparticles, which were reacted with 5-bromosalicylaldehyde to form Schiff base and then with [$VO(acac)_2$]. The resulting material **VO(acac)(Schiff)@SiO_2@Fe_3O_4** (Scheme 10.19) was used as catalyst for epoxidation of alkenes (9 examples) with TBHP as an oxidant (conversions in the range 40%–95%).[78] Rostami and co-workers also used magnetic nanoparticles. They synthesised a supported chiral vanadyl-pseudoephedrine complex **VO(pseudoephedrine)@SiO_2@Fe_3O_4** (Scheme 10.19) by the complexation of *N*-(3-trimethoxysilane)propyl pseudoephedrine with [$VO(acac)_2$] and subsequent grafting on the silica surface of SiO_2@Fe_3O_4 nanoparticles. The catalytic activity of **VO(pseudoephedrine)@SiO_2@Fe_3O_4** as reusable organic–inorganic hybrid catalyst was tested in the chemo- and enantioselective oxidation of several sulphides, using H_2O_2 under solvent-free conditions at room temperature. The overall product yields were in the range of 80%–97% and enantiomeric excesses of 9%–15% of the sulphoxide were obtained (9 examples). Notably, the catalyst could be recycled up to 20 runs for the oxidation of methyl phenyl sulphide without any significant loss of activity and enantioselectivity.[79] Ghorbani-Choghamarani *et al.*, have prepared the heterogeneous hybrid **VO(SPATB)@SiO_2@Fe_3O_4** (Scheme 10.19) by a covalent grafting on the silica surface using 3-mercaptopropyltrimethoxysilane, reaction with isatoic anhydride and then complexation with [$VO(acac)_2$]. The resultant heterogenised vanadyl complex could act as an efficient catalyst in the oxidation of various alkyl and/or aryl-substituted sulphides into their sulphoxides in excellent yields (10 examples, yields range: 86%–96%) in the presence of H_2O_2 as oxidant at room temperature under neat conditions.[80]

10.3.2 Supported Ionic Liquid Phases (SILPs)

When an IL is covalently immobilised on a high surface-area porous solid, the resulting material, SILP, combines the interesting features of ILs as reaction media with the benefits of heterogeneous catalysis.[81] A SILP based on 1-methyl-3-(3-(trimethoxysilyl)propyl)-1*H*-imidazol-3-ium chloride and mesoporous silica MCM-41 has been used as support of a vanadium-containing phosphopolymolybdate, $[PMo_{10}V_2O_{40}]^{5-}$ (Scheme 10.20). The resulting material catalyses the oxidation of alkenes (7 examples) with TBHP with medium-to-high conversions and acceptable epoxide selectivities (from 40% to 100%). The catalyst can be easily separated from the reaction mixture and reused 10 times without apparent loss of its catalytic performance.[82]

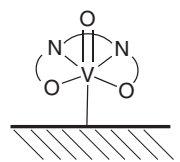

VO(salen)@SiO_2@Fe_3O_4

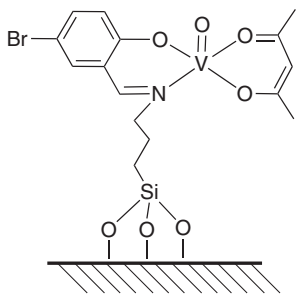

VO(acac)(Schiff)@SiO_2@Fe_3O_4

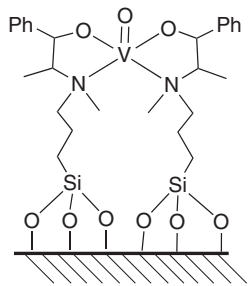

VO(pseudoephedrine)@SiO_2@Fe_3O_4

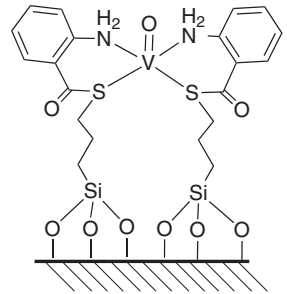

VO(SPATB)@SiO_2@Fe_3O_4

Scheme 10.19

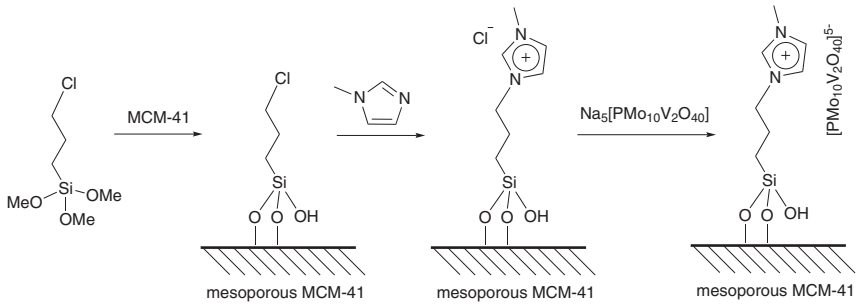

Scheme 10.20

10.3.3 Metal Oxide Nanoparticles

The direct grafting of oxidovanadium complexes on the surface of Fe_3O_4 nanoparticles has been investigated. For instance, Ghorbani-Choghamarani's group synthesised the hybrid material catalyst **VO(TEDETA)@Fe_3O_4** by a covalent grafting on Fe_3O_4 nanoparticles using 3-aminopropyltriethoxysilane as connector, subsequent reaction with acryloyl chloride, then reaction with *N*,*N*,*N*′,*N*′-tetraethyldiethylenetriamine (TEDETA) and, finally, complexation with [VO(acac)$_2$]. The resulting magnetically recyclable vanadyl catalyst, in combination with H_2O_2 as terminal oxidant under solvent-free conditions at room temperature, was tested for the oxidation of a variety of functionalised sulphides (13 examples) into respective sulphoxides with high selectivity (yields range: 70%–97%). The reusability of **VO(TEDETA)@Fe_3O_4** was confirmed in the oxidation of methyl phenyl sulphide under the optimised reaction conditions (12 cycles).[83] Veisi *et al.,* prepared a vanadyl Schiff base complex supported on magnetic Fe_3O_4 nanoparticles **VO(BINE)@Fe_3O_4** (Scheme 10.21) by a covalent grafting using 3-aminopropyltriethoxysilane, subsequent reactions with 1,2-bis(2-formylnaphthoxy)ethane (BINE) and then with [VO(acac)$_2$]. **VO(BINE)@Fe_3O_4** was used as an efficient heterogeneous catalyst for the selective oxidation of different functionalised sulphides (10 examples) in high yields (78%–96%) and short times, at room temperature using H_2O_2 as oxidant under solvent-free conditions. Moreover, it is noteworthy that the functional groups, such as OH, CHO and COOMe, were not oxidised. The catalyst could be also recovered up to 8 cycles in the oxidation of methyl phenyl sulphide without a significant loss of its catalytic activity.[84] Eftekhari-Sis reported the synthesis of **VO_3(GlyPyr)@Fe_3O_4** material (Scheme 10.21), an oxidoperoxidovanadium complex anchored on Fe_3O_4 magnetic nanoparticles, by a covalent grafting on the oxide surface using glycine and subsequent reaction with 2-pyridinecarboxaldehyde, followed by *in situ* reduction of the imine bond with $NaBH_4$ and, finally, complexation with NH_4VO_3. **VO_3(GlyPyr)@Fe_3O_4** was found to be an efficient heterogeneous catalyst for the oxidation of sulphides (3 examples) using H_2O_2 as oxidant in toluene at 70 °C, to give respective sulphoxides (88%–100% conversion and 58%–79% selectivity).[85]

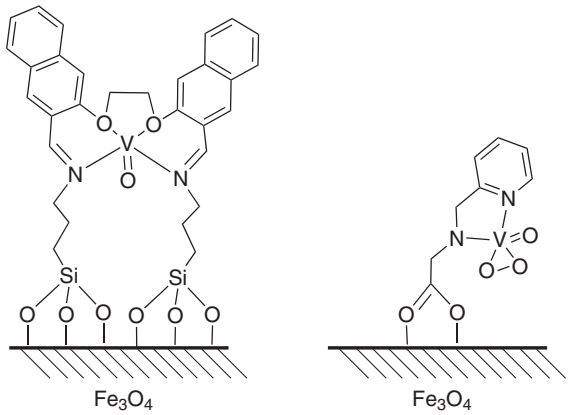

VO(BINE)@Fe_3O_4 **VO_3(GlyPyr)@Fe_3O_4**

Scheme 10.21

10.3.4 MOFs

Vanadium-based metal–organic frameworks (MOFs) have also been used as catalysts in epoxidation reactions. For example, Voort and co-workers used **V-MIL-47**, a MOF-containing coordinatively saturated V^{IV} site bridged by terephthalic linkers. This MOF was tested in the epoxidation of cyclohexene with TBHP as an oxidant. The best results were obtained using decane as the TBHP solvent. In this case, leaching is negligible and the structural integrity of **V-MIL-47** is maintained during successive runs.[86] The study was extended to **V-MIL-47-X** series (X = OH, Br, Cl, F, CH_3, NH_2) and these substituted materials are much more prone to leaching during the epoxidation catalysis than the parent **V-MIL-47**.[87] It has also evaluated the use of a bimetallic V/Ti MOF based on **NH_2-V-MIL-47**. This MOF exhibits a significantly higher cyclohexene conversion compared to the non-functionalised material and leaching of V or Ti was not detected.[88] For the Materials of the Institute Lavoisier (MIL) series, the **V-MIL-101** have also been employed in epoxidation. Farzaneh and Sadeghi described the immobilisation of this MOF on modified iron-oxide nanoparticles and the successful application of the resulting material in the epoxidation of allylic alcohols and alkenes with TBHP. Conversion and selectivity of 100% have been reported for geraniol and *trans*-2-hexen-1-ol. By using a magnet, the separation of the catalyst is easy. It can be recycled up to five times with the loss of 100% to 98% of conversion without any changes in selectivity.[89]

Alternatively, the vanadium centre can be covalently anchored to the organic linker of a preformed MOF. Using this strategy, Dehghanpour *et al.,* have used **UiO-66(NH_2)** (UiO = University of Oslo) and **UiO-66-SI** (functionalisation of UiO-66(NH_2) with salicylaldehyde) and treated them with [VO(acac)$_2$]. The resulting materials, **UiO-66-SI/VO(acac)** and **UiO-66-N/VO(acac)$_2$**, were used in the epoxidation of geraniol with aqueous TBHP as oxidant. Conversion of 100% and selectivity to 2,3-epoxygeraniol of 100% have been achieved. The catalysts based

on UiO-66-SI were reused four times without loss of activity.[90] Analogously, the MOF **UiO-66(Zr)-V**, prepared by reaction of UiO-66(Zr) with VCl_3, was found to be active for epoxidation of some allyl alcohols (4 examples) with conversions within the range 46%–97% and 100% selectivity.[91]

10.3.5 Other Inorganic Materials

10.3.5.1 Montmorillonite

Titanium-pillared montmorillonite impregnated with vanadium has been tested in the catalytic epoxidation of (*E*)-hex-2-en-1-ol, with TBHP used as oxidant. The inorganic support without vanadium is inactive, while with a 3% vanadium loading the conversion of alcohol to epoxide increases up to 96% (5 h at 65 °C). When more than 1% vanadium is used, a partial leaching of vanadium occurs.[92] In the same way, Bezaatpour described a catalyst prepared by impregnation of sodium montmorillonite with a vanadyl Schiff base complex (Scheme 10.22), which can be reused four times without appreciable loss of activity, with conversion for cyclohexene of 98% and selectivity to epoxidation close to 100%.[93]

10.3.5.2 Zeolites

When a vanadium-exchanged faujasite zeolite is used in a mixture of DMF and the ionic liquid 1-ethyl-3-methylimidazolium bis(trifluoromethylsulphonyl)-imide, [emim][NTf_2] (optimal ratio of 1:4 DMF/IL), a high *cis*-cyclooctene conversion (94.6%) and high epoxide selectivity (91%) was achieved. The improvement of conversion and epoxide selectivity is observed when [emim][NTf_2] is present as co-solvent. The catalyst was recycled up to four times without significant loss of activity except for a slight gradual decrease in cyclooctene conversion after each test that was attributed to partial leaching.[94] Mesoporous vanadium silicate-1-zeolites have also been used in the study of styrene oxidation using TBHP as an oxidant (conversions range from 49% to 85% with epoxy selectivity from 20% to 54%). In some cases, the main product is benzaldehyde. It has been shown that a lower content of vanadium produces a higher selectivity to epoxide.[95] Similarly, hierarchical ZSM-5 zeolite has been used for the preparation of a vanadium catalyst, obtained by impregnation with [$VO(acac)_2$]. The resulting material was used in the catalytic oxidation of cyclohexene by TBHP without the use of any solvent and the catalytic activity

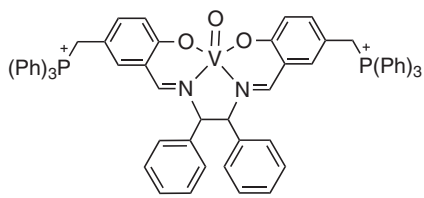

Scheme 10.22

was retained after five runs.[96] Zeolite-Y has been used for the encapsulation of [VO_2(pydx–aepy)] complex (Hpydx–aepy = Schiff base obtained by the condensation of pyridoxal and 2-aminoethylpyridine). The resulting catalyst, **VO_2(pydx–aepy)@zeoliteY**, has been tested in the oxidation of styrene and cyclohexene with H_2O_2, showing high conversions but low selectivities to the corresponding epoxide.[97] The same catalyst was employed for the oxidation of methyl phenyl sulphide and diphenyl sulphide using aqueous H_2O_2 in acetonitrile. For instance, methyl phenyl sulphoxide was obtained with a conversion of 93% and a selectivity of 71% after 3.5 h with a 1 : 2 ratio of substrate:oxidant.[97]

Immobilisation of the catalyst can be achieved by encapsulation on a mesoporous inorganic material. For instance, the Maurya group has reported the encapsulation in the nanocavity of zeolite-Y of an oxidovanadium(v) complex with the tribasic pentadentate ligand hap–dahp (Schiff base ligand derived from 2-hydroxyacetophenone and 1,3-diamino-2-hydroxypropane). The encapsulated complex, **VO(hap–dahp)@zeoliteY**, catalysed the oxidation of methyl phenyl sulphide and diphenyl sulphide to the corresponding sulphoxides using H_2O_2 as oxidant in good yield (98% and 81%, respectively) (Scheme 10.23). Furthermore, the encapsulated complex was recyclable at least up to two cycles of catalytic oxidation, but with a partial loss of activity.[98] In another example, Ben Zid and co-workers reported the preparation of several bis(oxazoline)vanadyl complexes supported by electrostatic interaction with aluminosilicate sheets in laponite clay as heterogeneous catalysts for asymmetric oxidation of methyl phenyl sulphide, using TBHP as oxidant in Cl_2CH_2 at room temperature. The corresponding sulphoxide was obtained in good yield (91%), but with a modest 22% ee value (Scheme 10.24).[99]

10.3.5.3 Alumina, boehmite, brucite-like layers

Tanase, Rothenberg *et al.,* reported epoxidation of limonene using V_2O_5 supported on an alumina–magnesia compound (60 : 40 Al_2O_3/MgO) using

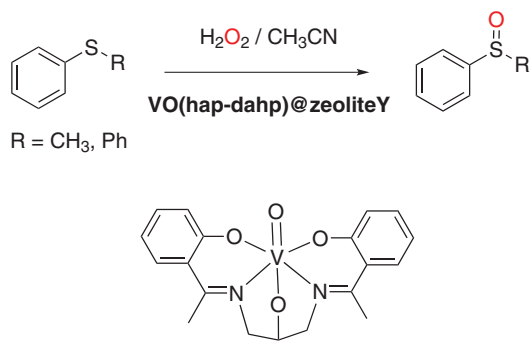

Scheme 10.23

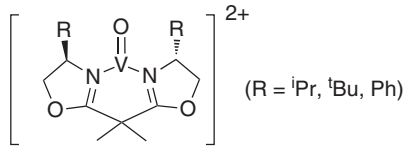

VO(box)

Scheme 10.24

H_2O_2 as oxidant. The conversion is low (13.7% to 18.3%) but the selectivity to epoxide is high (95%). The main product is the 1,2-epoxide (69% to 74%) and the minor product is the 8,9-epoxide (26% to 20%).[100] Mirzaee and co-workers have used boehmite nanoparticles (γ-Al(O)OH) as support of selected vanadium complexes.[101–103] These materials have been used as catalysts in the epoxidation of *cis*-cyclooctene and other olefins with high conversions and yields. The best yield and selectivity were obtained using **V-IFB@boehmite** (Scheme 10.25) and TBHP as oxidant in the case of *cis*-cyclooctene (92% conversion and 92% selectivity after 3.5 h) and cyclohexene epoxidation (92% conversion and 84% selectivity). The catalyst can be recycled up to 10 times with a decrease in epoxide yield from 92% to 75%.[101] More recently, the related **$VO(acac)_2$(en)@boehmite** catalyst has been used, in which complex $[VO(acac)_2]$ was the vanadium source, with similar epoxide yields (Scheme 10.25).[102] An additional recent progress was the use of Fe_3O_4 core nanoparticles coated with functionalised boehmite that supports vanadium species, **V@boehmite@Fe_3O_4** (Scheme 10.25). This strategy, as stated before, allows the easy recovery of the catalyst using a magnet.[103]

He and co-workers described heterogeneous catalysts containing $[VO(O^iPr)_3]$ and amino acids intercalated in a double-hydroxide layer with a brucite-type structure. These materials have been used in the asymmetric epoxidation of allylic alcohols, using TBHP as an oxidising agent.[104–106] In this system, the amino acid was first attached to the double hydroxide layer through by H-bonding and electrostatic interactions, and then coordinated to the vanadium centre.[106] The inorganic brucite-like layers behave as a planar substituent, enhancing the enantioselectivities in the vanadium-catalysed epoxidation of allylic alcohols (up to 99% ee with moderate to high yields).[104,105]

10.3.5.4 Zirconia

The oxidovanadium(IV) complex, $[VO(L)_2(H_2O)]$, containing the 1-phenyl-3-methyl-4-toluoyl-5-pyrazolone ligand, L (Scheme 10.26), was supported on hydrous zirconia and the resulting material was used for the solvent-free oxidation of styrene to benzaldehyde. Several reaction parameters were investigated and full conversion with >99% selectivity for benzaldehyde (1151 TON) was achieved under optimised reaction conditions. The catalyst material can be recovered by simple filtration and reused three times without any substantial loss in the activity.[107]

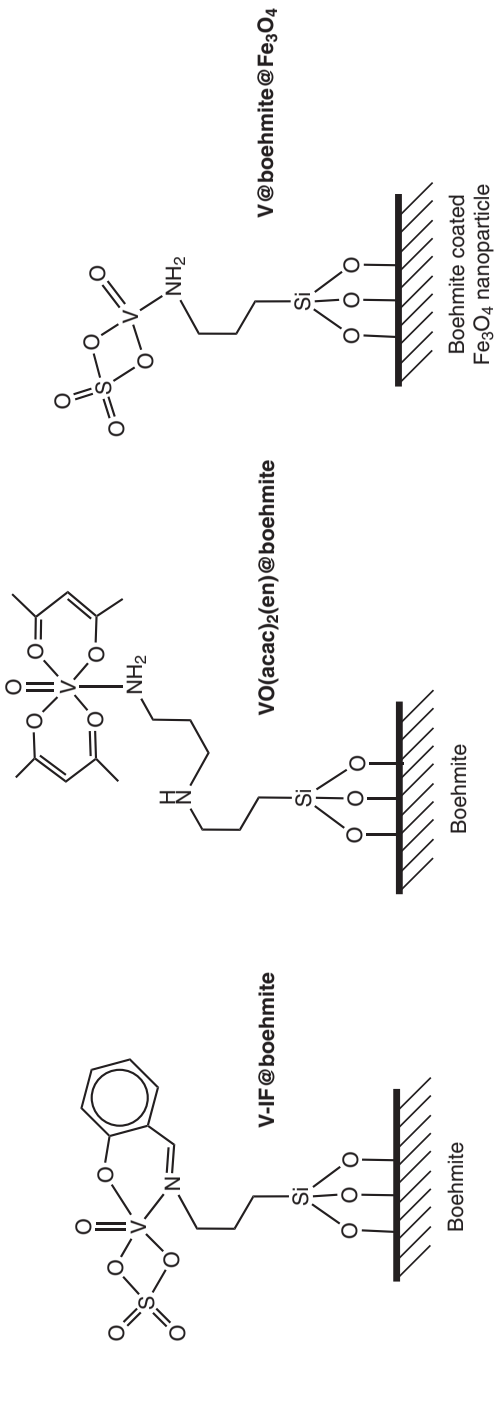
V-IF@boehmite
Boehmite
VO(acac)2(en)@boehmite
Boehmite
V@boehmite@Fe3O4
Boehmite coated
Fe3O4 nanoparticle

Scheme 10.25

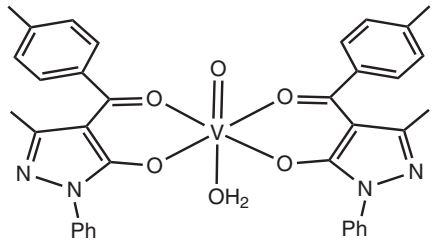

$[VO(L)_2(H_2O)]$

Scheme 10.26

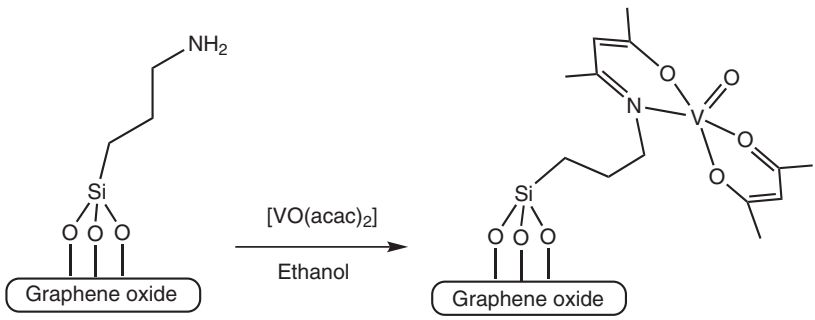

Scheme 10.27

10.3.5.5 Graphene oxide

Immobilisation of an oxido-vanadium Schiff base onto graphene oxide (Scheme 10.27) produces a catalyst used in the epoxidation of fatty acids (8 examples) and esters without solvent, with TBHP in dodecane as oxidant. A range of conversion from 80% to 99% and selectivity to epoxide from 98.4% to 99.2% was obtained, while isolated yield varied from 78% to 97%. In the case of oleic acid, the catalyst can be recycled up to six times without loss of activity.[108]

10.3.6 Organic Polymers

Heterogeneisation can be also attained by grafting on organic polymers. The main advantages of heterogenised organic support respecting the organic–inorganic mesoporous hybrids is that the linkage of the chelating ligand to an organic support via a strong C–C or C–heteroatom bond is less sensitive against cleavage than a Si–O–Si linkage to a silica support. A polymer-supported vanadium-binaphtyl bishydroxamic acid, **PS-VBHA** (Scheme 10.28), was used as catalyst for the asymmetric epoxidation of allylic alcohols using TBHP with high yields and enantioselectivities (up to 85% ee). The

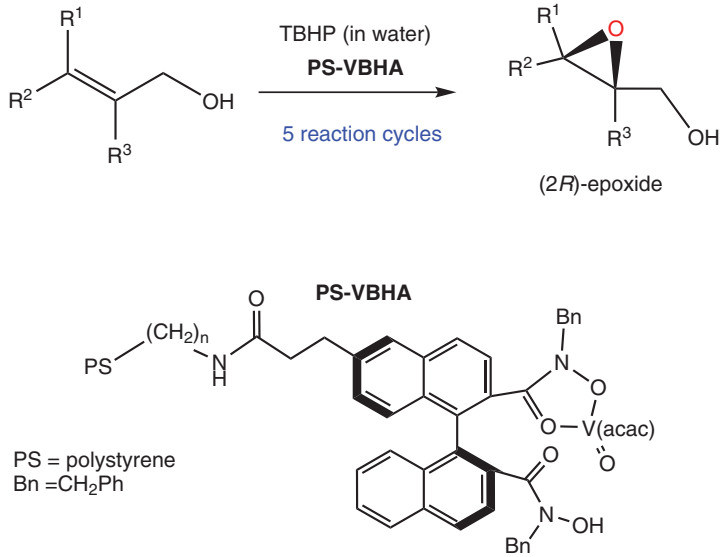

Scheme 10.28

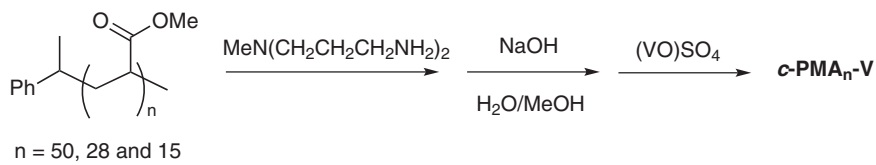

Scheme 10.29

epoxidation is procedurally simple and was carried out at 20 °C without the need for anhydrous conditions. The catalyst was recycled up to five times without appreciable loss of yield and enantioselectivity.[109]

Liu and co-workers immobilised vanadium complexes onto cross-linked polyacylates, ***c*-PMA$_n$–V** (Scheme 10.29) and studied their behaviour as catalysts for bishydroxylation and oxidative cleavage of selected alkenes in water. For example, benzoic acid was obtained in 84% yield and 100% conversion from styrene, using TBHP in water at 100 °C. Furthermore, these materials catalyse the epoxidation of *cis*-cyclooctene with TBHP in water (92% yield at 60 °C in 12 h) and the catalyst can be recycled without losing their activity (five reaction cycles).[110]

Maeda studied the functionalisation of a Merrifield resin (chloromethyl polystyrene, PS-Cl) with the vanadyl Schiff base complexes [VO(OH–salae)], [VO(OH–slapheol)] and [VO(OH–salhisol)] to give polystyrene-bound systems, **VO(salae)@PS** and **VO(salpheol)@PS** and **VO(salhisol)@PS**, respectively (Scheme 10.30). The Schiff base ligands were synthesised by the reaction of 2,4-dihydroxybenzaldehyde and the corresponding 2-amino alcohol. The performance of these polymer-bound systems as catalysts in the oxidation of

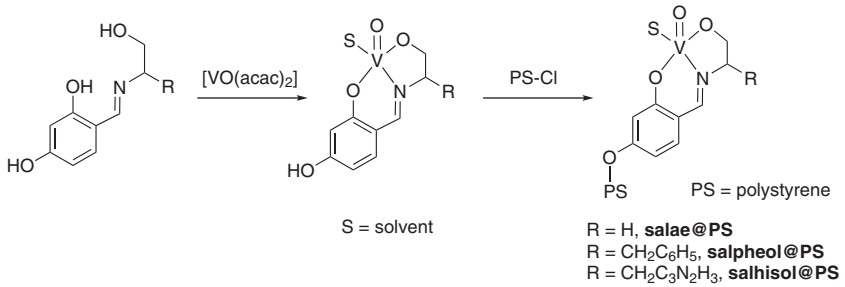

Scheme 10.30

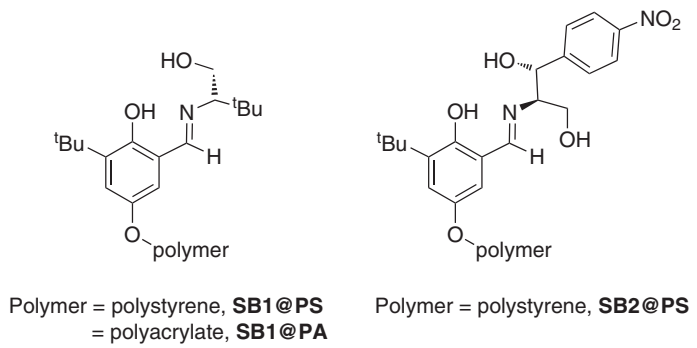

Scheme 10.31

methyl phenyl sulphide with aqueous TBHP (70 vol%) was evaluated. They converted the sulphide to the corresponding sulphoxide in 80%–90% yields in $CDCl_3$ during 90 min at 18 °C. Interestingly, chiral catalysts **VO(salpheol)@PS** and **VO(salhisol)@PS**, converted methyl phenyl sulphide in a stereoselective manner yielding the sulphoxide in enantiomeric excess (highest value of 40%).[111] The closely related hetereogenised vanadyl Schiff base complexes, **VO(SB1)@PS, VO(SB1)@PA** and **VO(SB2)@PS** (Scheme 10.31), have been reported by the Sartori group, which supported the $V^{IV}O$ complexes on polystyrene (PS) or polyacrylate (PA) using a Schiff base ligand based on 2,5-dihydroxybenzaldehyde. These heterogeneous complexes have been employed to catalyse the enantioselective oxidation of different methyl aryl sulphides (6 examples) with H_2O_2 as oxidant in CH_2Cl_2 at 0 °C. The procedure affords the sulphoxides in good yields (range: 54%–80%) and with acceptable ee values (45%–57%). Furthermore, the catalyst can be used for at least four cycles without any significant decrease in both efficiency or enantioselectivity.[112]

Ligand Hsal–his, derived from salicylaldehyde and histamine, has been covalently bound to chloromethylated polystyrene cross-linked with 5% divinylbenzene. Upon treatment with $[VO(acac)_2]$ and then oxidation, the polystyrene-bound ligand (abbreviated as **Hsal–his@PS**) resulted in the stable polystyrene-bound oxidovanadium(v) complex **VO_2(sal-his)@PS** (Scheme 10.32). This compound was found to be an efficient heterogeneous

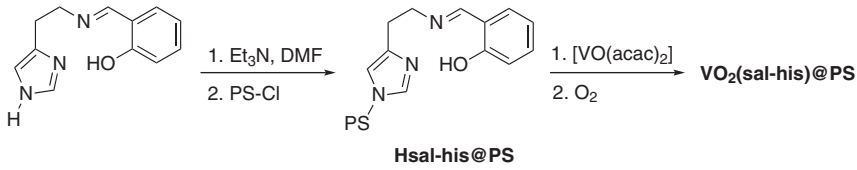

Scheme 10.32

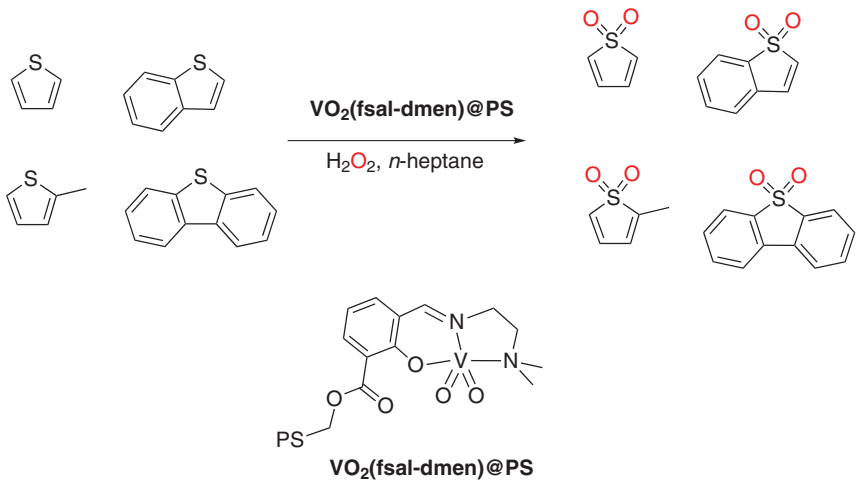

Scheme 10.33

catalyst for the oxidation of methyl phenyl sulphide and diphenyl sulphide using H_2O_2 as oxidant in acetonitrile at room temperature, to give respective sulphoxides in moderate yields (60%).[113] Maurya and co-workers also synthesised the polymer-bound dioxidovanadium complex **VO_2(fsal–dmen)@PS** by a covalent grafting of Schiff base ligand (Hfsal–demen, derived from 3-formylsalicyclic acid and *N*,*N*-dimethylethylenediamine) on chloromethylated polystyrene, subsequent complexation with [VO(acac)$_2$] and followed by aerobic oxidation. The catalytic oxidative desulphurisation of organosulphur compounds thiophene, dibenzothiophene, benzothiophene and 2-methylthiophene (model of fuel diesel) was carried out using **VO_2(fsal–dmen)@PS** as catalyst and H_2O_2 as oxidant in *n*-heptane at 60 °C (Scheme 10.33). All substrates were converted almost quantitatively to the corresponding sulphones.[114]

In another example, reported by Tshentu group, the ligand 2-(2′-hydroxyphenyl)-1*H*-imidazoline (Hpimin) was covalently linked to chloromethylated polystyrene (PS-Cl) to afford the polymer-anchored ligand **pimin@PS** as a mixture of two isomers. This resin was then allowed to react with vanadyl sulphate to afford the polymer-bound vanadyl complex, **VO(pimin)@PS** (Scheme 10.34). This hetereogenised material was investigated for their catalytic efficiency for the oxidation of methyl phenyl sulphide using

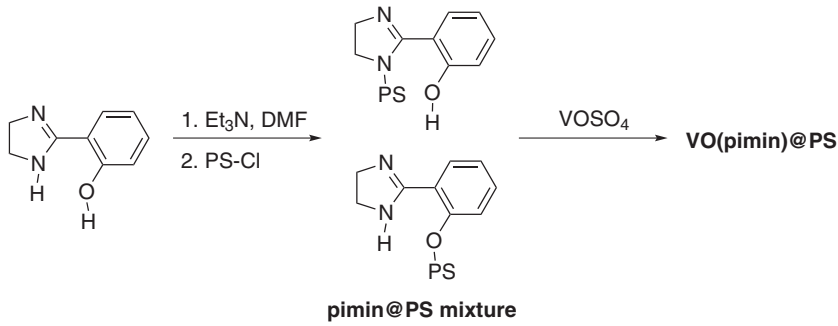

Scheme 10.34

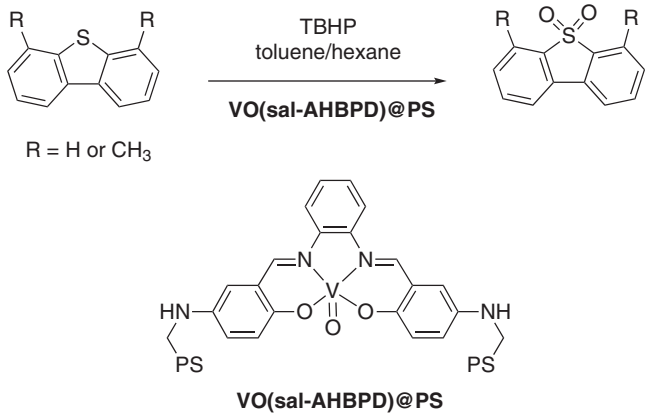

Scheme 10.35

acetonitrile as a solvent and H_2O_2 as the oxidant at room temperature. The sulphide conversion was almost quantitative, but with a moderate selectivity to the respective sulphoxide.[115] The same authors reported the synthesis of **VO(sal–AHBPD)@PS**, a vanadyl complex covalently anchored on polystyrene, by the reaction of $VOSO_4$ and the polystyrene-supported tetradentate N_2O_2-donor Schiff base ligand (**sal–AHBPD@PS**). The preparation of this ligand proceeded by nitrosation reaction of sal–HBPD, obtained by the condensation of salicylaldehyde and *o*-phenylenediamine, followed by the reduction with hydrogen to form an amine group that was then linked to Merrifield resin. **VO(sal–AHBPD)@PS** was found to be an efficient heterogeneous catalyst for the oxidation of dibenzothiophene and 4,6-dimethyldibenzothiophene, using TBHP as oxidant in a mixture toluene/hexane at 40 °C, to give respective sulphones with a conversion of 88% and 72%, respectively (Scheme 10.35).[116]

Besides cross-linked synthetic organic polymers, chitosan, a natural co-polymer of 2-amino-2-deoxy-D-glucopyranose and 2-acetamido-2-deoxy-D-glucopyranose, has also received interest as support for immobilisation

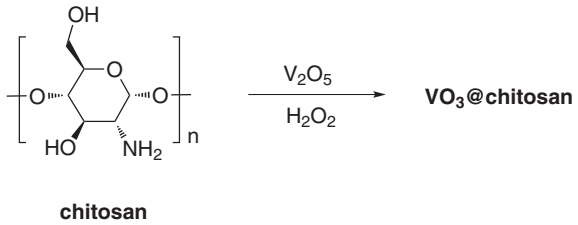

Scheme 10.36

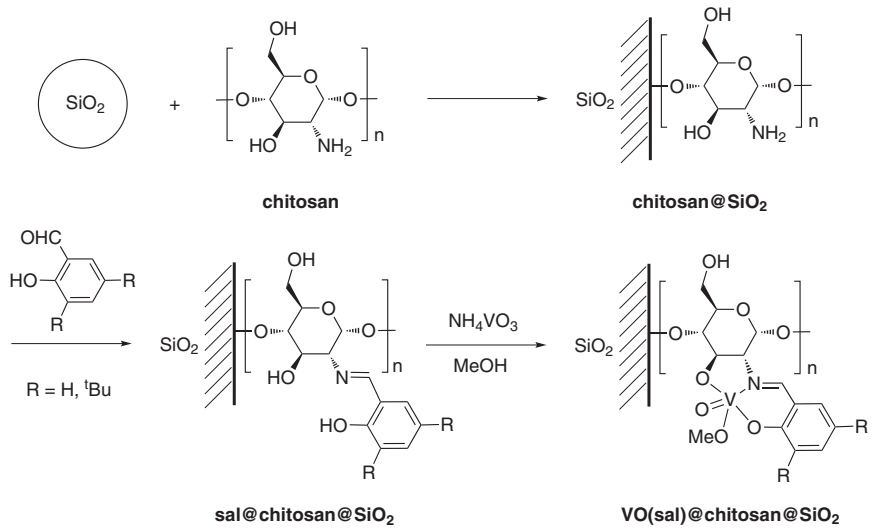

Scheme 10.37

and heterogeneisation of vanadium compounds. Thus, Islam and co-workers synthesised the chitosan-supported oxidodiperoxidovanadium(v) complex **VO_3@chitosan**, which was obtained by reaction of V_2O_5 and chitosan in the presence of hydrogen peroxide (Scheme 10.36). The compound effectively facilitated chemoselective oxidation of a range of structurally diverse sulphides to the respective sulphoxides, using H_2O_2 as terminal oxidant, in experiments conducted independently in water (9 examples, yield range: 39%–98%) as well as acetonitrile (9 examples, yield range: 47%–97%) under mild reaction conditions. Furthermore, the heterogeneous catalyst was recyclable for five catalytic cycles without significant loss in selectivity, using methyl phenyl sulphide as the model substrate.[117]

In addition, chitosan was used in combination with an inorganic support to give the corresponding organic–inorganic hybrid that has been used as support for the vanadium species. For instance, the heterogeneous **VO(sal)@chitosan@SiO_2** material has been prepared by Shen's group (Scheme 10.37). For the heterogeneisation of the catalyst, they used SiO_2 nanoparticles that were grafted with chitosan. The silica-layered system

(**chitosan@SiO_2**) was grafted on the surface by the reaction with a salicylaldehyde in the presence of acetic acid to give the corresponding supported Schiff base ligand and then complexation occurred by reaction with NH_4VO_3. The resulting material was used as an active heterogeneous catalyst for asymmetric oxidation of different aryl alkyl sulphides (8 examples) with H_2O_2 as oxidant in CH_3OH/H_2O at 0 °C. The procedure affords the corresponding sulphoxides in good yields (range: 63%–95%) and with satisfactory ee values (42%–67%). In addition, the catalyst was efficiently applied to the asymmetric oxidation of pyrmetazole to esomeprazole (92% yield, 68% ee). The catalyst could be used for at least five cycles in the asymmetric sulphoxidation of methyl phenyl sulphide using the optimised reaction conditions without any significant decrease in both yield or enantioselectivity.[118]

In another recent example, Veisi *et al.* prepared a vanadyl complex immobilised on chitosan coated-magnetic nanoparticles (Fe_3O_4). For the heterogeneisation they used freshly prepared Fe_3O_4 nanoparticles that were grafted with chitosan and subsequent reaction with $[VO(acac)_2]$ to afford the heterogeneous **VO@chitosan@Fe_3O_4** (Scheme 10.38). The catalytic activity of **VO@chitosan@Fe_3O_4** was studied as a reusable organic–inorganic hybrid catalyst for the selective oxidation of functionalised sulphides (10 examples) to sulphoxides in high yields (70%–90%) and short reaction times. Aqueous H_2O_2 was used as oxidant, under solvent-free conditions at room temperature. Recycling experiments showed that the hybrid catalyst could be used for nearly complete oxidation of methyl phenyl sulphide for at least nine successive cycles.[119] In a similar strategy, the same group prepared a vanadyl complex immobilised on polydopamine coated-magnetic nanoparticles. In this example, the heterogeneous system, abbreviated as **VO@pda@Fe_3O_4**, was prepared by grafting on the Fe_3O_4 nanoparticle surface with chitosan and subsequent complexation with $[VO(acac)_2]$ (Scheme 10.38). The organic-

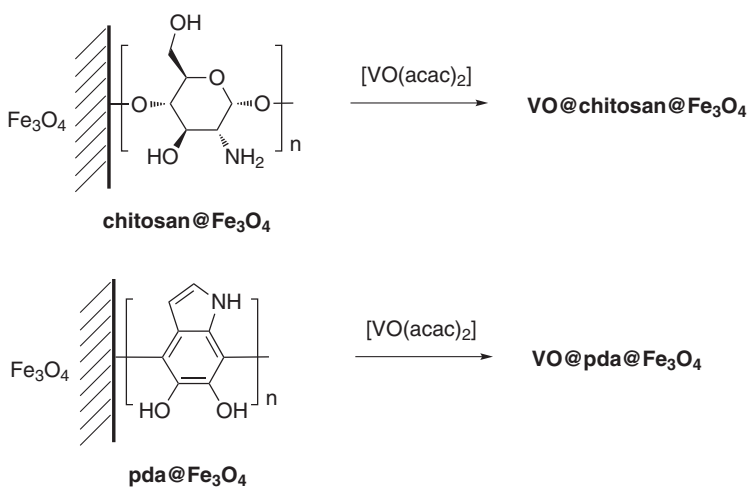

Scheme 10.38

inorganic hybrid presented high catalytic activity as a recyclable catalyst in the chemoselective oxidation of several functionalised sulphides (10 examples) to sulphoxides in high yields (82%–96%), using aqueous H_2O_2 as oxidant under solvent-free conditions at room temperature.[120]

10.3.7 Other Organic Supports

Besides the examples of organic polymers, other more specific organic-based supports have been used for the heterogeneisation of vanadium complexes. Huang and co-workers have recently synthesised an efficient catalyst by anchoring a vanadyl unit onto an amino-functional microporous organic nanotube frameworks (MONFs). The amino groups were used to immobilise the vanadyl complex into the MONF through the formation of a Schiff base ligand by reaction with salicylaldehyde and complexation using $VOSO_4$ (Scheme 10.39). The resulting heterogeneous system, **VO(SA)@MONF**, has a network based on mesoporous tubular channels that improves mass transfer in the catalytic system and facilitates the accessibility of active sites, which is beneficial for good catalytic performance in heterogeneous catalysis. Thus, the prepared vanadyl heterogeneous catalyst shows high activity and excellent stability in the selective oxidation reactions of thiols to disulphides (6 examples, range yield: 86%–99%).[121]

Covalent organic framework (COFs) are an emerging class of porous crystalline materials, built by strong covalent bonds in a periodic arrangement, that display permanent high porosity, structural versatility and chemical and thermal stability. Ma *et al.* have recently reported the preparation of a system based on vanadyl units anchored in a COF, **VO@COF** (Scheme 10.40). This material was synthesised by the Schiff base condensation reaction of 2,4,6-tris(4-aminophenyl)-1,3,5-triazine (TAPT) and

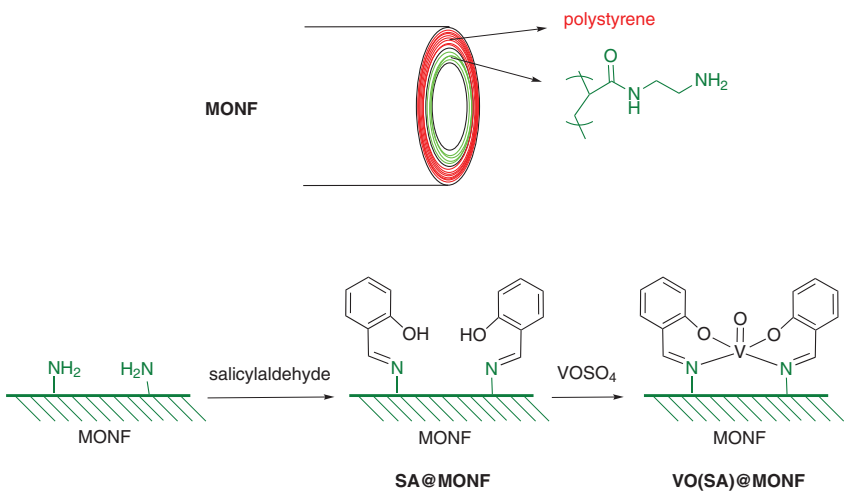

Scheme 10.39

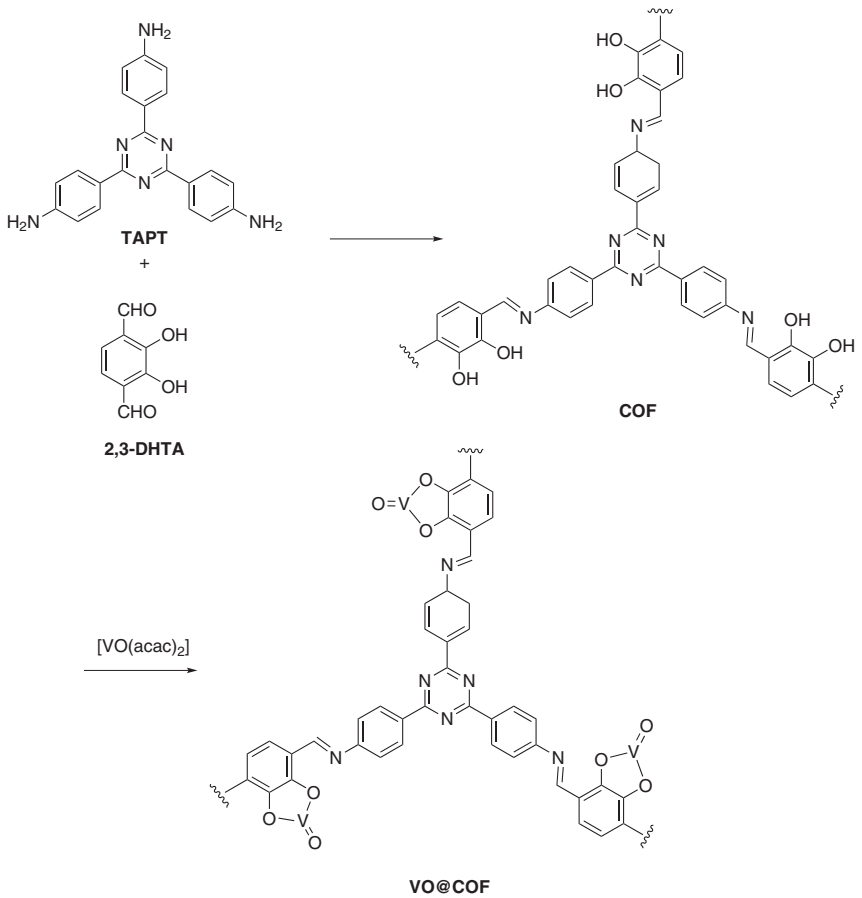

Scheme 10.40

2,3-dihydroxyterephthaldehyde (2,3-DHTA), followed by complexation with $[VO(acac)_2]$. The vanadyl moiety coordinates through the O, O′ moieties in the pores of mesoporous framework (Scheme 10.40). **VO@COF** presented high catalytic activity in the selective oxidation of a range of functionalised sulphides (7 examples) to sulphoxides. High yields were obtained (75%–96%), using TBHP as oxidant in CH_3CN at 40 °C.[122]

Others supports employed for the immobilisation of vanadium species are polysiloxanes. In particular, Trapp *et al.* have immobilised chiral vanadium(IV)–salen complexes with variable spacer lengths onto polydimethylsiloxanes (Scheme 10.41). These materials were used as catalytically active stationary phase in on-column reaction gas chromatography, on-column reaction electrophoresis and in flow-through reactors for asymmetric sulphoxidation using H_2O_2 as the oxidant.[123] Interestingly, this approach combines catalysis and chromatographic analysis in a single step. For the oxidation of benzyl phenyl sulphide, conversion was always around 75%, while a drastic influence of the

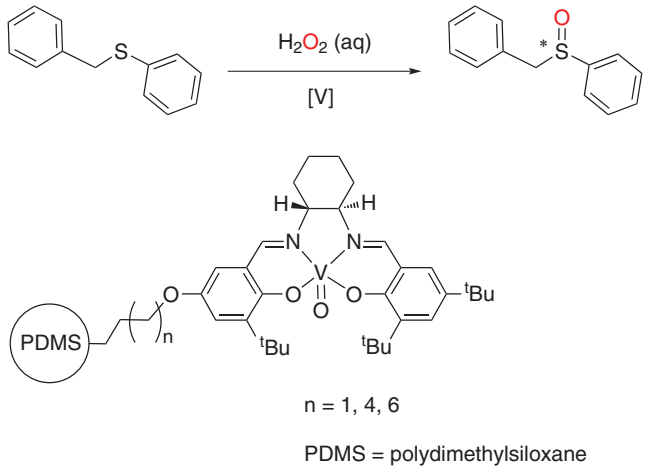

Scheme 10.41

spacer length on the enantioselectivity was observed. The maximum ee value of 38% was observed with the longest spacer ($n = 6$, Scheme 10.41).[123]

References

1. P. J. Dunn, *Chem. Soc. Rev.*, 2012, **41**, 1452–1461.
2. C.-J. Li and P. T. Anastas, *Chem. Soc. Rev.*, 2012, **41**, 1413–1414.
3. M. Poliakoff and P. Licence, *Nature*, 2007, **450**, 810–812.
4. R. A. Sheldon, *Chem. Commun.*, 2008, 3352–3365.
5. R. A. Sheldon, *Green Chem.*, 2007, **9**, 1273–1283.
6. J.-E. Bäckvall, *Modern Oxidation Methods*, Wiley-VCH, Weinheim, 2nd edn, 2011.
7. R. A. Sheldon and J. K. Kochi, *Metal-catalyzed Oxidations of Organic Compounds*, Academic Press, New York, 1981.
8. E. Buncel, R. A. Stairs and H. Wilson, *The Role of the Solvent in Chemical Reactions*, Oxford University Press, Oxford, 2003.
9. C. Reichardt and T. Welton, *Solvents and Solvent Effects in Organic Chemistry*, Wiley-VCH, Weinheim, 2011.
10. C. J. Clarke, W.-C. Tu, O. Levers, A. Bröhl and J. P. Hallett, *Chem. Rev.*, 2018, **118**, 747–800.
11. J. H. Clark, *Catalysis of Organic Reactions by Supported Inorganic Reagents*, Wiley-VCH, Weinheim, 1994.
12. J. H. Clark and D. J. Macquarrie, *Chem. Commun.*, 1998, 853–860.
13. N. E. Leadbeater and M. Marco, *Chem. Rev.*, 2002, **102**, 3217–3274.
14. M. Kirihara, *Coord. Chem. Rev.*, 2011, **255**, 2281–2302.
15. V. Conte and B. Floris, *Inorg. Chim. Acta*, 2010, **363**, 1935–1946.
16. B. Floris, F. Sabuzi, A. Coletti and V. Conte, *Catal. Today*, 2017, **285**, 49–56.

17. V. Conte, A. Coletti, B. Floris, G. Licini and C. Zonta, *Coord. Chem. Rev.*, 2011, **255**, 2165–2177.
18. P. Schwendt, J. Tatiersky, L. Krivosudský and M. Šimuneková, *Coord. Chem. Rev.*, 2016, **318**, 135–157.
19. J. A. L. da Silva, J. J. R. F. da Silva and A. J. L. Pombeiro, *Coord. Chem. Rev.*, 2011, **255**, 2232–2248.
20. V. Conte and B. Floris, *Dalton Trans.*, 2011, **40**, 1419–1436.
21. M. L. Ramos, L. L. G. Justino and H. D. Burrows, *Dalton Trans.*, 2011, **40**, 4374–4383.
22. G. Licini, V. Conte, A. Coletti, M. Mba and C. Zonta, *Coord. Chem. Rev.*, 2011, **255**, 2345–2357.
23. M. Sutradhar, L. M. D. R. S. Martins, M. F. C. Guedes, da Silva and A. J. L. Pombeiro, *Coord. Chem. Rev.*, 2015, **301–302**, 200–239.
24. H. Pellissier, *Coord. Chem. Rev.*, 2015, **284**, 93–110.
25. M. Sutradhar and A. J. L. Pombeiro, *Reference Module in Chemistry, Molecular Sciences and Chemical Engineering*, Elsevier, Amsterdam, 2017, pp. 1–17.
26. M. R. Maurya, *Coord. Chem. Rev.*, 2019, **383**, 43–81.
27. R. R. Langeslay, D. M. Kaphan, C. L. Marshall, P. C. Stair, A. P. Sattelberger and M. Delferro, *Chem. Rev.*, 2019, **119**, 2128–2191.
28. S. Patai and Z. Rappoport, *Syntheses of Sulphones, Sulphoxides and Cyclic Sulphides*, John Wiley & Sons, Ltd., Chichester, UK, 1995.
29. E. Wojaczyńska and J. Wojaczyński, *Chem. Rev.*, 2010, **110**, 4303–4356.
30. G. E. O'Mahony, A. Ford and A. R. Maguire, *J. Sulfur Chem.*, 2013, **34**, 301–341.
31. H. B. Kagan, in *Organosulfur Chemistry in Asymmetric Synthesis*, ed. T. Toru and C. Bolm, Wiley-VCH Verlag GmbH & Co. KGaA, Weinheim, Germany, 2008, pp. 1–29.
32. R. Bentley, *Chem. Soc. Rev.*, 2005, **34**, 609–624.
33. M. Madesclaire, *Tetrahedron*, 1986, **42**, 5459–5495.
34. K. P. Volcho and N. F. Salakhutdinov, *Russ. Chem. Rev.*, 2009, **78**, 457–464.
35. F. Van De Velde, I. W. C. E. Arends and R. A. Sheldon, *Top. Catal.*, 2000, **13**, 259–265.
36. J. C. Pessoa, I. Correia and P. Adão, in *Advances in Organometallic Chemistry and Catalysis*, ed. A. J. L. Pombeiro, John Wiley & Sons, Inc., Hoboken, NJ, USA, 2013, pp. 227–232.
37. J. M. Campos-Martin, M. C. Capel-Sanchez, P. Perez-Presas and J. L. G. Fierro, *J. Chem. Technol. Biotechnol.*, 2010, **85**, 879–890.
38. D. Betz, P. Altmann, M. Cokoja, W. A. Herrmann and F. E. Kühn, *Coord. Chem. Rev.*, 2011, **255**, 1518–1540.
39. T. Kitanosono, K. Masuda, P. Xu and S. Kobayashi, *Chem. Rev.*, 2018, **118**, 679–746.
40. M. R. Maurya, A. Kumar and J. Costa Pessoa, *Coord. Chem. Rev.*, 2011, **255**, 2315–2344.

41. J. Costa Pessoa and M. R. Maurya, *Inorg. Chim. Acta*, 2017, **455**, 415–428.
42. I. Bányai, V. Conte, L. Pettersson and A. Silvagni, *Eur. J. Inorg. Chem.*, 2008, **2008**, 5373–5381.
43. V. Conte, F. Fabbianesi, B. Floris, P. Galloni, D. Sordi, I. W. C. E. Arends, M. Bonchio, D. Rehder and D. Bogdal, *Pure Appl. Chem.*, 2009, **81**, 1265–1277.
44. S. Kazemi, Á. B. Martín, D. Sordi, M. C. Kroon, C. J. Peters and I. W. C. E. Arends, *Green Process. Synth.*, 2012, **1**, 509–516.
45. D. Xu, W. Zhu, H. Li, J. Zhang, F. Zou, H. Shi and Y. Yan, *Energy Fuels*, 2009, **23**, 5929–5933.
46. Y. L. Hu, X. B. Liu and D. Fang, *Catal. Sci. Technol.*, 2014, **4**, 38–42.
47. D. Yin, R. Tan, C. Li, Z. Peng and D. Yin, *Catal. Commun.*, 2011, **12**, 1488–1491.
48. D. R. Pesiri, D. K. Morita, W. Glaze and W. Tumas, *Chem. Commun.*, 1998, 1015–1016.
49. D. R. Pesiri, D. K. Morita, T. Walker and W. Tumas, *Organometallics*, 1999, **18**, 4916–4924.
50. G. R. Haas and J. W. Kolis, *Tetrahedron Lett.*, 1998, **39**, 5923–5926.
51. C. Cordelle, D. Agustin, J. C. Daran and R. Poli, *Inorg. Chim. Acta*, 2010, **364**, 144–149.
52. J. Pisk, J. C. Daran, R. Poli and D. Agustin, *J. Mol. Catal. A: Chem.*, 2015, **403**, 52–63.
53. A. C. Gomes, M. M. Antunes, M. Abrantes, A. A. Valente, F. A. A. Paz, I. S. Gonçalves and M. Pillinger, *ChemCatChem*, 2018, **10**, 3481–3489.
54. M. Abrantes, M. S. Balula, A. A. Valente, F. A. A. Paz, M. Pillinger, C. C. Romão, J. Rocha and I. S. Gonçalves, *J. Inorg. Organomet. Polym. Mater.*, 2007, **17**, 215–222.
55. S. A. Talouki, G. Grivani and A. D. Khalaji, *Appl. Organomet. Chem.*, 2018, **32**, e4078.
56. A. Masuyama, K. Fukuoka, N. Katsuyama and M. Nojima, *Langmuir*, 2004, **20**, 82–89.
57. A. V. Malkov, L. Czemerys and D. A. Malyshev, *J. Org. Chem.*, 2009, **74**, 3350–3355.
58. Z. Bourhani and A. V. Malkov, *Chem. Commun.*, 2005, 4592–4594.
59. T. A. Dar, B. Uprety, M. Sankar and M. R. Maurya, *Green Chem.*, 2019, **21**, 1757–1768.
60. A. Held, J. Kowalska-Kuś and K. Nowińska, *Catal. Commun.*, 2012, **17**, 108–113.
61. A. Held, J. Kowalska-Kuś, A. Łapiński and K. Nowińska, *J. Catal.*, 2013, **306**, 1–10.
62. A. Held, J. Kowalska-Kuś, K. Nowińska and K. Góra-Marek, *J. Catal.*, 2017, **347**, 21–35.
63. E. Janiszewska, A. Held, K. Nowińska and S. Kowalak, *RSC Adv.*, 2019, **9**, 4671–4681.
64. I. Muylaert, J. Musschoot, K. Leus, J. Dendooven, C. Detavernier and P. Van Der Voort, *Eur. J. Inorg. Chem.*, 2012, **2012**, 251–260.

65. G. Wang, S. Zhang, Y. Huang, F. Kang, Z. Yang and Y. Guo, *Appl. Catal. A: Gen.*, 2012, **413–414**, 52–61.
66. E. Janiszewska and S. Kowalak, *New J. Chem.*, 2017, **41**, 2955–2963.
67. S. Bhunia and S. Koner, *J. Porous Mater.*, 2011, **18**, 399–407.
68. Z. Azarkamanzad, F. Farzaneh, M. Maghami, J. Simpson and M. Azarkish, *Appl. Organomet. Chem.*, 2018, **32**, e4168.
69. T. Ben Zid, I. Khedher and A. Ghorbel, *React. Kinet., Mech. Catal.*, 2010, **100**, 131–143.
70. M. Dabiri, M. Koohshari, F. Shafipour, M. Kasmaei, P. Salari and D. MaGee, *J. Iran. Chem. Soc.*, 2016, **13**, 1265–1272.
71. M. Nikoorazm, A. Ghorbani-Choghamarani and N. Noori, *Appl. Organomet. Chem.*, 2015, **29**, 328–333.
72. M. Nikoorazm, A. Ghorbani-Choghamarani and M. Khanmoradi, *Appl. Organomet. Chem.*, 2016, **30**, 236–241.
73. N. Noori, M. Nikoorazm and A. Ghorbani-Choghamarani, *Microporous Mesoporous Mater.*, 2016, **234**, 166–175.
74. A. Lazar, P. Sharma and A. P. Singh, *Microporous Mesoporous Mater.*, 2013, **170**, 331–339.
75. M. J. Taghizadeh, H. Karimi and H. S. Abandansari, *Res. Chem. Intermed.*, 2016, **42**, 8201–8215.
76. T. Tamoradi, M. Ghadermazi, A. Ghorbani-Choghamarani and S. Molaei, *Res. Chem. Intermed.*, 2018, **44**, 4259–4276.
77. M. Bagherzadeh, M. M. Haghdoost and A. Shahbazirad, *J. Coord. Chem.*, 2012, **65**, 591–601.
78. M. Bagherzadeh, M. Bahjati and A. Mortazavi-Manesh, *J. Organomet. Chem.*, 2019, **897**, 200–206.
79. A. Rostami and B. Atashkar, *J. Mol. Catal. A: Chem.*, 2015, **398**, 170–176.
80. M. Nikoorazm, F. Ghorbani, A. Ghorbani-Choghamarani and Z. Erfani, *J. Iran. Chem. Soc.*, 2019, **16**, 553–562.
81. Y. Gu and G. Li, *Adv. Synth. Catal.*, 2009, **351**, 817–847.
82. R. Hajian, S. Tangestaninejad, M. Moghadam, V. Mirkhani, I. Mohammadpoor-Baltork and A. R. Khosropour, *J. Coord. Chem.*, 2011, **64**, 4134–4144.
83. M. Norouzi and A. Ghorbani-Choghamarani, *React. Kinet., Mech. Catal.*, 2016, **119**, 537–554.
84. H. Veisi, S. Hemmati, A. Rashtiani, A. Rostami and M. Shirinbayan, *Polyhedron*, 2019, **157**, 358–366.
85. B. Eftekhari-Sis, M. Akbari, A. Akbari and M. Amini, *Catal. Lett.*, 2017, **147**, 2106–2115.
86. K. Leus, M. Vandichel, Y.-Y. Liu, I. Muylaert, J. Musschoot, S. Pyl, H. Vrielinck, F. Callens, G. B. Marin, C. Detavernier, P. V Wiper, Y. Z. Khimyak, M. Waroquier, V. Van Speybroeck and P. der Voort, *J. Catal.*, 2012, **285**, 196–207.
87. M. Vandichel, S. Biswas, K. Leus, J. Paier, J. Sauer, T. Verstraelen, P. Van Der Voort, M. Waroquier and V. Van Speybroeck, *ChemPlusChem*, 2014, **79**, 1183–1197.

88. K. Leus, G. Vanhaelewyn, T. Bogaerts, Y.-Y. Liu, D. Esquivel, F. Callens, G. B. Marin, V. Van Speybroeck, H. Vrielinck and P. Van Der Voort, *Catal. Today*, 2013, **208**, 97–105.
89. F. Farzaneh and Y. Sadeghi, *J. Mol. Catal. A: Chem.*, 2015, **398**, 275–281.
90. M. Pourkhosravani, S. Dehghanpour, F. Farzaneh and S. Sohrabi, *React. Kinet., Mech. Catal.*, 2017, **122**, 961–981.
91. E. Geravand, F. Farzaneh and M. Ghiasi, *J. Mol. Struct.*, 2019, **1198**, 126940.
92. J. Arfaoui, L. K. Boudali and A. Ghorbel, *Appl. Clay Sci.*, 2010, **48**, 171–178.
93. A. Bezaatpour, *React. Kinet., Mech. Catal.*, 2014, **112**, 453–465.
94. L. Bai, K. Li, Y. Yan, X. Jia, J.-M. M. Lee and Y. Yang, *ACS Sustain. Chem. Eng.*, 2016, **4**, 437–444.
95. B. Singh and A. K. Sinha, *J. Mater. Chem. A*, 2014, **2**, 1930–1939.
96. M. Nandi and A. K. Talukdar, *J. Porous Mater.*, 2016, **23**, 1143–1154.
97. M. R. Maurya, M. Bisht and F. Avecilla, *J. Mol. Catal. A: Chem.*, 2011, **344**, 18–27.
98. M. R. Maurya, M. Bisht, N. Chaudhary, F. Avecilla, U. Kumar and H. F. Hsu, *Polyhedron*, 2013, **54**, 180–188.
99. T. Ben Zid, M. Fadhli, I. Khedher and J. M. Fraile, *Microporous Mesoporous Mater.*, 2017, **239**, 167–172.
100. Z. Strassberger, E. V. Ramos-Fernandez, A. Boonstra, R. Jorna, S. Tanase and G. Rothenberg, *Dalton Trans.*, 2013, **42**, 5546–5553.
101. M. Mirzaee, B. Bahramian and A. Amoli, *Appl. Organomet. Chem.*, 2015, **29**, 593–600.
102. M. Mirzaee, B. Bahramian, J. Gholizadeh, A. Feizi and R. Gholami, *Chem. Eng. J.*, 2017, **308**, 160–168.
103. M. Mirzaee, B. Bahramian, P. Gholampour, S. Teymouri and T. Khorsand, *Appl. Organomet. Chem.*, 2019, **33**, e4792.
104. J. Wang, L. Zhao, H. Shi and J. He, *Angew. Chem. Int. Ed.*, 2011, **50**, 9171–9176.
105. L. W. Zhao, H. M. Shi, J. Z. Wang and J. He, *Chem. – Eur. J.*, 2012, **18**, 9911–9918.
106. H. Liu, L. Zhao, J. Wang and J. He, *J. Catal.*, 2013, **298**, 70–76.
107. S. Parihar, S. Pathan, R. N. Jadeja, A. Patel and V. K. Gupta, *Inorg. Chem.*, 2012, **51**, 1152–1161.
108. S. Verma, M. Aila, S. Kaul and S. L. Jain, *RSC Adv.*, 2014, **4**, 30598–30604.
109. M. Noji, H. Kondo, C. Yazaki, H. Yamaguchi, S. Ohkura and T. Takanami, *Tetrahedron Lett.*, 2019, **60**, 1518–1521.
110. M. C. Hsiao and S. T. Liu, *Catal. Lett.*, 2010, **139**, 61–66.
111. R. Ando, T. Yagyu and M. Maeda, *Inorg. Chim. Acta*, 2004, **357**, 2237–2244.
112. A. Barbarini, R. Maggi, M. Muratori, G. Sartori and R. Sartorio, *Tetrahedron: Asymmetry*, 2004, **15**, 2467–2473.
113. M. R. Maurya, A. Arya, A. Kumar and J. C. Pessoa, *Dalton Trans.*, 2009, 2185–2195.

114. M. R. Maurya, A. Arya, A. Kumar, M. L. Kuznetsov, F. Avecilla and J. Costa Pessoa, *Inorg. Chem.*, 2010, **49**, 6586–6600.
115. Z. R. Tshentu, C. Togo and R. S. Walmsley, *J. Mol. Catal. A: Chem.*, 2010, **318**, 30–35.
116. A. S. Ogunlaja, W. Chidawanyika, E. Antunes, M. A. Fernandes, T. Nyokong, N. Torto and Z. R. Tshentu, *Dalton Trans.*, 2012, **41**, 13908–13918.
117. G. Saikia, K. Ahmed, S. R. Gogoi, M. Sharma, H. Talukdar and N. S. Islam, *Polyhedron*, 2019, **159**, 192–205.
118. J. Jin, K. Zheng, J. Qiao, C. Shen, P. Zhang and L. Zhao, *Catal. Commun.*, 2017, **92**, 114–118.
119. H. Veisi, S. Sajjadifar, P. M. Biabri and S. Hemmati, *Polyhedron*, 2018, **153**, 240–247.
120. H. Veisi, P. Safarimehr and S. Hemmati, *J. Taiwan Inst. Chem. Eng.*, 2018, **88**, 8–17.
121. H. Zhang, M. Zhou, L. Xiong, Z. He, T. Wang, Y. Xu and K. Huang, *Microporous Mesoporous Mater.*, 2018, **255**, 103–109.
122. H. Vardhan, G. Verma, S. Ramani, A. Nafady, A. M. Al-Enizi, Y. Pan, Z. Yang, H. Yang and S. Ma, *ACS Appl. Mater. Interfaces*, 2019, **11**, 3070–3079.
123. S. Sandel, S. K. Weber and O. Trapp, *Chem. Eng. Sci.*, 2012, **83**, 171–179.

CHAPTER 11

Supported Vanadium Catalysts: Heterogeneous Molecular Complexes, Electrocatalysis and Biomass Transformation

CRISTINA FREIRE,* CLARA PEREIRA,* BRUNO JARRAIS,* DIANA FERNANDES, ANDREIA PEIXOTO, NATÁLIA CORDEIRO AND FILIPE TEIXEIRA

REQUIMTE/LAQV, Departamento de Química e Bioquímica, Faculdade de Ciências da Universidade do Porto, Rua do Campo Alegre s/n, 4169-007 Porto, Portugal
*Emails: acfreire@fc.up.pt; clara.pereira@fc.up.pt; bjarrais@fc.up.pt

11.1 Introduction

Over the years, there has been an unceasing interest in oxidovanadium complexes owing to their remarkable activity and (enantio)selectivity as homogeneous catalysts for the synthesis of valuable fine and bulk chemicals and chemical intermediates. A plethora of catalytic transformations has been efficiently catalyzed by these compounds, namely the oxidation of alkanes, alkenes, arenes, alcohols and carbonyl groups, namely epoxidation reactions, hydroxylations, sulfoxidations, halogenations, cyanosilylations, hydrogenations, olefin polymerizations, among others.[1–8] However, the high cost, low chemical and thermal stabilities, and difficult separation from the reaction medium of homogeneous oxidovanadium-based catalysts are major

Catalysis Series No. 41
Vanadium Catalysis
Edited by Manas Sutradhar, José Armando L. da Silva and Armando J. L. Pombeiro

Published by the Royal Society of Chemistry, www.rsc.org

economic and environmental barriers for their practical implementation in industry. Moreover, they can undergo degradation or decomposition phenomena at the end of the catalytic reaction, contaminating the end products and thus compromising the sustainability of the whole process.[9,10]

The global concern with environmental protection and energy saving boosted the development of eco-sustainable and economically viable vanadium-based catalytic systems. In particular, the immobilization of oxidovanadium complexes onto solid supports – the so-called *heterogenization of homogeneous catalysts* – constitutes a potential strategy to overcome the limitations of homogeneous catalysts, while at the same time facilitating their separation from the reaction medium and enabling their recycling and reuse.[9,10] The main challenge has been to design vanadium-based heterogeneous catalysts that present similar or higher activity and (enantio)selectivity than their homogeneous counterparts and that can be simultaneously reused multiple times, with no leaching of the catalytically active phase.

Although earlier studies reported a decrease of the activity and/or (enantio)selectivity upon the immobilization of oxidovanadium complexes onto solid supports, more recent works have demonstrated that improved catalytic performance can be achieved, combined with high catalyst stability, recyclability and negligible metal leaching. The existence of synergistic effects between the support and the grafted complex moieties, the prevention of possible complex polymerization due to the isolation of the catalytic active centres throughout the supporting matrix and the confinement effect have been identified as the main factors for these improvements. This topic has been extensively reviewed in the literature over the past few years.[9–12]

Among the different types of solid supports for the heterogenization of oxidovanadium complexes, organic polymers and bulk inorganic porous materials such as zeolites, clays, mesoporous silicas, metal oxides and carbon-based materials have been of particular interest owing to their high surface area, chemical and thermal robustness, easy surface modification and, in many cases, possibility of tailoring their porosity. Nevertheless, in many cases, lower catalytic performance of the supported catalysts has been reported in the literature – *i.e.*, higher reaction times and/or lower substrate conversions and (enantio)selectivities – in part due to diffusion constraints imposed by the support porosity.

More recently, nanometre-sized supports – such as graphene, carbon nanotubes, silica nanoparticles, magnetic iron oxide and ferrite nanoparticles – emerged as potential alternatives to bulk supports. It is envisaged that their nanometre dimensions, high surface area-to-volume ratio and high colloidal stability in several solvents can lead to an improvement of the dispersion of the catalytic active sites in the reaction medium and of their accessibility to all reagents, as well as to the immobilization of higher complex loadings, thus overcoming the diffusion limitations related with heterogeneous catalysts.[13] In this sense, they gave rise to a new generation of *recyclable hybrid nanocatalysts* that cross the frontiers between homogeneous and heterogeneous catalysts. Magnetically recyclable vanadium-based nanocatalysts

have been of particular interest since they can be easily recovered from the reaction medium through magnetic separation, which is an eco-friendly route for catalyst recycling. By minimizing the use of additional solvents and mass losses, this process offers promising prospects for catalytic industrial applications in terms of cost, time and waste management.[14,15]

Various strategies have been developed for the grafting of oxidovanadium complexes onto bulk and nano solid supports, which can be classified according to the type of interaction between the support and the complex: (i) covalent bonding, either directly or through a linker, (ii) non-covalent interactions (physical adsorption and electrostatic interactions) and (iii) encapsulation.[13,16] The covalent bonding has been the most frequently used strategy, since it can minimize the leaching of the metal complex, thus giving rise to more robust heterogeneous catalysts. A distinct methodology has also been proposed which consists on the assembly of vanadium complexes and polyfunctional ligands in a three-dimensional network, leading to a family of self-supported catalysts, named metal–organic catalysts or metal–organic frameworks (MOFs).

More recently, with the emergence of the new paradigms of circular economy, sustainable development and clean energy, research on supported vanadium materials has been directed towards new applications, namely as electrocatalysts for water splitting and in biomass transformation. Besides supported oxidovanadium complexes, supported vanadium oxides and other solid-state compounds containing vanadium, such as vanadium-based polyoxometalates, vanadium phosphates, vanadium carbides and vanadium nitrides have been highlighted as promising (electro)catalysts for these chemical transformations owing to the multiplicity of oxidation states of vanadium and rich elemental abundance.

Electrochemical water splitting has been reported as the most effective technology to produce clean hydrogen fuel. The main challenge has been to develop highly efficient, cost-effective and durable bifunctional electrocatalysts for hydrogen evolution and oxygen evolution reactions, since the most promising methods for hydrogen evolution reactions (in acidic medium) have low electrocatalytic efficiency on oxygen evolution reactions (alkaline medium), or *vice versa*.[17–19]

On the other hand, the replacement of fossil fuels by cost-effective and abundant renewable energy sources, such as biomass, has been a major quest in order to reduce their environmental impact. In particular, the transformation of non-edible biomass (lignocellulose) into high value-added chemicals and fuels through catalytic processes mediated by vanadium-based compounds has become a hot topic of research, particularly for the selective oxidation of biomass-derived furans, including furfural and 5-hydroxymethylfurfural, to produce 2,5-diformylfuran.[20,21]

This chapter provides an overview of the wide variety of catalytic applications of supported vanadium-based catalysts and other solid-state compounds containing vanadium for the production of high value-added products. In the second section, the catalytic applications of oxidovanadium complexes supported onto different types of bulk and nano-sized materials, or

integrated on MOF or covalent organic framework structures will be reviewed. The selected examples aim to demonstrate the different strategies used for the immobilization of oxidovanadium complexes onto solid supports and their application in the most representative types of catalytic reactions, with special emphasis on the most recent works. Moreover, the highlighted examples are focused on robust catalytic systems with performances that compete or surpass those of the corresponding homogeneous counterparts. In the third section, vanadium-based electrocatalysts for hydrogen and oxygen evolution reactions are reviewed, focusing on the examples where vanadium seems to be the active site or has the greatest contribution. In the fourth section, the application of vanadium-based materials as highly active and selective heterogeneous catalysts for the aerobic oxidation of sugars and derivatives for the production of 2,5-diformylfuran is reviewed. In the fifth section, some insights on the latest theoretical findings on supported vanadium catalysts will be provided.

Finally, the chapter ends with some concluding remarks and future challenges of eco-sustainable vanadium-based catalytic systems for the different key areas that were explored throughout the chapter.

11.2 Recyclable Oxidovanadium-based Heterogeneous Catalysts

11.2.1 Oxidation Reactions

11.2.1.1 Oxidation of Alkenes

In the literature, a wide variety of supported oxidovanadium catalysts have been prepared for the oxidation of aliphatic and aromatic alkenes. For instance, an oxidovanadium(IV) Schiff base complex bearing chloromethyl groups (*N,N′*-bis(5-chloromethyl-salicylidene)ethylenediamine ligand) was immobilized on the surface of SBA-15 mesoporous silica functionalized with 3-aminopropyltriethoxysilane (APTES) and tested in the aerobic oxidation of styrene.[22] The complex was covalently grafted to the support through condensation reaction between its chloromethyl groups and the amine groups of the APTES-functionalized support. The best catalytic results were achieved at 80 °C in acetonitrile when using air as oxidant: 78.6% styrene conversion (%C) after 8 h (turnover frequency, TOF = 63.0 h^{-1}) and 71.2% selectivity (%S) towards styrene oxide. In contrast, the homogeneous catalyst presented lower activity and selectivity, leading to 69.0% substrate conversion (TOF = 63.4 h^{-1}) and 58.2% styrene oxide selectivity. The improved performance of the heterogeneous catalyst was probably due to the isolation of the catalytic active species, preventing their dimerization, and to cooperative effects between the metal complex and the support. The heterogeneous catalyst was reused three times, with a small decrease of the activity (%C = 64.6%; TOF = 54.7 h^{-1}) and selectivity (51.6%) probably due to a slight decrease of the complex loading.

This type of support has been also successfully used for the immobilization of VO(IV) complexes bearing different chlorinated ligands, namely 4-(2-chloroacetyl)-3-methyl-1-phenyl-1*H*-pyrazol-5(4*H*)-one (H-AP) and 5-chloromethyl-8-quinolinol hydrochloride (H-HQ).[23] First, SBA-15 was functionalized with 3-aminopropyltrimethoxysilane (APTMS) or bis[3-(trimethoxysilyl)propyl]-amine and then with the chlorinated ligands, followed by immobilization of vanadyl cations (VO^{2+}) by using $VOSO_4{\cdot}5H_2O$ or oxidovanadium(IV) acetylacetonate ([$VO(acac)_2$]) as precursor. For comparison, a pre-formed VO(IV) complex containing the H-AP ligand was directly grafted onto APTMS-functionalized SBA-15. All catalysts were tested in the H_2O_2-promoted oxidation of styrene, α-methyl and β-methylstyrene at 50 °C in acetonitrile. In the case of styrene, all hybrid materials led to high conversion values (from 86% to >98%), affording high yields of benzaldehyde (75%–95%; %S of up to 95%) and could be recycled and reused twice. Only trace amounts of acetophenone and acetic acid were produced. The most efficient catalysts were the H-HQ/[$VO(acac)_2$] and the H-AP/$VOSO_4{\cdot}5H_2O$-based systems using APTMS-functionalized SBA-15 as support, albeit the former being slightly more stable upon reuse in two further cycles. The catalyst prepared by grafting the preformed VO(IV) complex onto SBA-15 presented slightly lower activity (%C = 90%; %Yield = 92%), but was also stable upon reuse. The heterogeneous catalysts presented higher selectivity than their homogeneous congeners, indicating that the mesostructured support played an active role on the selectivity of the catalytic reactions. In the case of α-methylstyrene and *cis*-β-methylstyrene oxidation, the H-HQ- and H-AP-based catalysts also presented very high activity (%C = > 98%) and stability over three cycles, affording 98% and 90%–92% of acetophenone or benzaldehyde, respectively, after the first cycle.

Zeolite-supported oxidovanadium catalysts have been also developed for the aerobic oxidation of alkenes. For instance, Maurya *et al.* encapsulated several oxidovanadium(IV) complexes bearing tetradentate ligands (*N*,*N*′-ethylenebis(pyridoxyliminato, H_2pydx-en; *N*,*N*′-propylenebis(pyridoxyliminato), H_2pydx-1,3-pn and H_2pydx-1,2-pn) within the nanocavities of zeolite-Y and tested them in the oxidation of styrene, cyclohexene and methyl phenyl sulphide using acetonitrile as solvent and H_2O_2 as oxidant.[24] The catalysts were prepared by the flexible ligand approach, *i.e.*, through metal exchange of Na^+ cations of the zeolite by VO^{2+}, followed by reaction between the metal-exchanged zeolites and the ligands. The [VO(pydx-en)]-Y catalyst presented the best performance, leading to maximum conversions of styrene (at 80 °C), cyclohexene (at 80 °C) and methyl phenyl sulphide (at room temperature) of 85.5% (TOF = 490 h^{-1}), 95.9% (TOF = 1374 h^{-1}) and 85.5% (TOF = 980 h^{-1}), respectively, after 6 h, 6 h and 2.5 h. In the case of styrene oxidation, benzaldehyde was the main product and the products selectivity varied in the order of: benzaldehyde (74.7%) > 1-phenylethane-1,2-diol (9.4%) > benzoic acid (6.8%) > styrene oxide (3.9%) > phenyl acetaldehyde (3.4%) > other (1.8%). In the case of cyclohexene substrate, the products selectivity order was 2-cyclohexen-1-one (50.8%) > 2-cyclohexen-1-ol (32.9%) > cyclohexane-1,2-diol

(9.7%) > others (4.9%) > cyclohexene oxide (1.6%). Finally, the catalyst oxidized methyl phenyl sulphide with 79.6% selectivity to sulfoxide and 20.4% selectivity to sulphone. All catalysts were recycled and reused in one further cycle, presenting a slight decrease of the activity and selectivity, but with no metal leaching. Moreover they were significantly more active than the corresponding neat complexes, which presented distinct selectivities: in the case of styrene oxidation, the relative amount of benzoic acid was higher and that of 1-phenylethane-1,2-diol was lower, whereas for cyclohexene oxidation, the product selectivity order was 2-cyclohexen-1-ol ≫ 2-cyclohexen-1-one > cyclohexene oxide > cyclohexane-1,2-diol. The improved performance of the heterogeneous catalysts could be due to favorable adsorption of water and H_2O_2 oxidant on the polar surface of the zeolite cages, making the oxidant more readily available to the substrates.

A more efficient and selective heterogeneous catalyst for the oxidation of cyclohexene in acetonitrile, with H_2O_2 as oxidant, has been reported, consisting on VO(IV) porphyrin (5,10,15,20-tetrakis-(4-methoxy carboxy phenyl) vanadyl porphyrin) complex immobilized onto APTES-functionalized SBA-15.[25] The catalyst led to 85% substrate conversion after 4 h, with high selectivity towards 2-cyclohexen-1-one (70%). Additionally, the catalytic reaction could be performed at room temperature. No significant decrease of the activity and selectivity was detected upon reuse four times, with only a slight vanadium leaching.

Another substrate that has been efficiently oxidized by supported oxidovanadium complexes is limonene. For instance, VO(IV) complexes with Schiff base ligands derived from vanillin thiophene-2-carboxylic hydrazone (VTCH), vanillin furoic-2-carboxylic hydrazone, salicylaldehyde thiophene-2-carboxylic hydrazone and salicylaldehyde furoic-2-carboxylic hydrazone encapsulated in the nanopores of zeolite-Y presented higher catalytic activity than the corresponding free complexes and higher selectivity towards limonene glycol. Carveol, carvone and inorganic polymers were the by-products formed.[26] In particular, when the reaction was performed at 80 °C in acetonitrile using *tert*-butyl hydroperoxide (TBHP) as oxidant, the zeolite-supported $[VO(VTCH)_2]$ catalyst presented the best performance, leading to 97.70% substrate conversion, a TOF of 33.43 h^{-1} and 45.10% selectivity towards limonene glycol after 24 h (*vs.* %C = 85.89%; TOF = 12.76 h^{-1}; %S = 34.15% and 49.97% for limonene glycol and apolar inorganic polymers, respectively, for the homogeneously catalyzed reaction). The improved performance of the heterogeneous systems relative to the homogeneous counterparts was assigned to the poor solubility of the neat complexes in the solvent used in the catalytic reaction and to the hydrophilic nature of the support, which presented higher affinity for the adsorption of polar products. Finally, the zeolite-supported $[VO(VTCH)_2]$ catalyst was recycled and reused three times, presenting a small decrease of activity and vanadium leaching after the second cycle, but then preserving the activity and stability in the following cycles. In this sense, the zeolite matrix prevented the decomposition and dimerization of the complex under the catalytic reaction conditions.

11.2.1.2 Selective Oxidation of Alcohols into Aldehydes and Ketones

An oxidovanadium Schiff base complex grafted onto graphene nanosheets revealed to be an efficient catalyst for the oxidation of several primary and secondary alcohols to the corresponding aldehydes and ketones, at 65 °C in acetonitrile, using anhydrous TBHP as oxidant (Figure 11.1).[27] A multi-step procedure was developed for the fabrication of the hybrid catalyst, consisting on the: (i) functionalization of the graphene nanosheets with APTMS; (ii) reaction of the amine groups of APTMS-modified support with a salicylaldehyde ligand; (iii) addition and reaction of $VOSO_4$ with the Schiff base functionalized graphene nanosheets. The material catalyzed the oxidation of benzhydrol in 20 min, leading to 94% of benzophenone, which was similar to the behaviour of the homogeneous catalyst (%C = 95% after 20 min). Moreover, it presented high activity and stability upon recycling and reuse in five consecutive cycles, with no metal leaching. Finally, when tested with other substrates, the hybrid catalyst revealed to be more active in the oxidation of aromatic substituted alcohols and of 1,2-diols than of aliphatic/alicyclic secondary alcohols, leading to substrate conversions of up to 98% and product yields of up to 95% in 20–30 min. It also oxidized borneol and 1-menthol with 80% and 75% conversion/yield in 30 and 35 min, respectively.

A photoactive $[VO(acac)_2]$@g-C_3N_4 catalyst has been also reported for the selective oxidation of alcohols into the corresponding aldehydes and ketones by immobilization of the complex onto the surface of graphitic carbon nitride through non-covalent interactions.[28] The catalytic reactions were performed at room temperature, in acetonitrile, under the effect of visible light, using H_2O_2 as co-oxidant. The photocatalyst was highly active and selective in the oxidation of benzyl alcohol

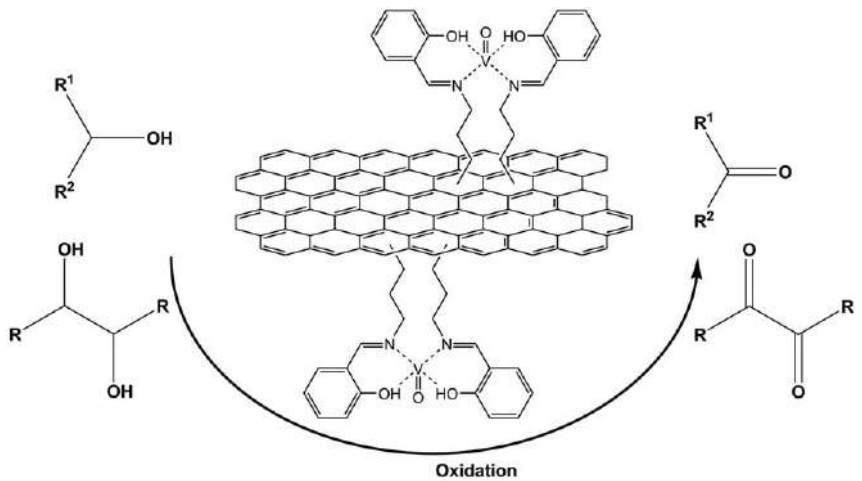

Figure 11.1 Oxidation of primary and secondary alcohols catalyzed by an oxidovanadium Schiff base complex anchored onto graphene nanosheets. Adapted from ref. 27 with permission from the Royal Society of Chemistry.

and its derivatives to the corresponding aldehydes in 1 h (Yield = 95%–98%; %S = > 99%) and of secondary alcohols to the corresponding ketones in 1.5–2 h (Yield = 87%–97%; %S = > 99%). For instance, it afforded 98% of product yield in the oxidation of benzyl alcohol after 1 h, preserving the performance in 10 consecutive cycles (Yield = 97%–99%), with no metal leaching. In contrast, the free complex only led to 21% of the desired product after 12 h and the blank test with the support resulted in 10% substrate conversion after 24 h. The improved performance of the hybrid photocatalyst was assigned to a synergistic effect arising from the combination of the complex and the support. 2-Thiophenemethanol and furfuryl alcohol were also efficiently converted into the corresponding aldehydes, resulting in 96% of product yields after 1 h (%S = > 99%). The oxidation of aliphatic dihydroxy compounds and α-hydroxy ketones resulted in 85% and 96% product yields, respectively, after 2.5 and 1.5 h (%S = > 99%).

The influence of the type of support and surface treatment on the catalytic performance of the resulting supported oxidovanadium complexes has been studied by Sutradhar *et al.*[29] The authors anchored VO(V) aroyl hydrazone complexes derived from (3,5-di-*tert*-butyl-2-hydroxybenzylidene)-2-hydroxybenzohydrazide (H_2L^1) and (3,5-di-*tert*-butyl-2-hydroxybenzylidene)-2-aminobenzohydrazide (H_2L^2) onto four types of carbon supports – activated carbon (AC), multi-walled carbon nanotubes (MWCNT), nanodiamonds and carbon xerogel – unmodified, oxidized with HNO_3 and oxidized with HNO_3 followed by treatment with NaOH. The resulting hybrid catalysts were tested in the solvent-free microwave-assisted oxidation of 1-phenylethanol to acetophenone, at 90 or 125 °C, using TBHP as oxidant. The catalytic activity depended on the type of support, while the selectivity was preserved. MWCNT-ox-Na (MWCNTs oxidized with HNO_3 and subsequently treated with NaOH) was the most promising support, with the corresponding heterogeneous catalysts leading to higher activity than the homogeneous analogues. In particular, the most active heterogeneous system was based on the μ-oxido bridged VO(v) complex $[(VOL^2)_2(\mu\text{-}O)]$ bearing $V_2O_3^{4+}$ cores, which yielded a maximum of 96% of acetophenone in 0.5 h with a TOF of 1.92×10^{-3} h^{-1} (at 90 °C) *vs.* a product yield of up to 92% in 1 h and a TOF of 920 h^{-1} for the homogeneously catalyzed reaction. Moreover, the catalyst preserved its catalytic efficiency (yield over 90%) in nine consecutive cycles, with only very small metal leaching. The higher performance could probably be explained by the formation of phenolate and carboxylate groups on the CNTs surface that acted as coordination sites for the complex. The authors also highlighted that, based on their previous works, MWCNT-ox-Na was usually the best match of support and treatment to achieve enhanced catalytic activity, recycling and heterogenization efficiency.

A distinct group of catalytic supports often used for this type of reaction is the group of mesoporous silicas. For instance, Verma *et al.* immobilized an oxidovanadium Schiff base complex onto a periodic mesoporous organosilica (PMO) containing diimine functionalities through covalent grafting.[30] The resulting hybrid catalyst presented high activity and stability in the selective oxidation of a variety of primary, secondary and α-hydroxy carbonyl compounds to the corresponding aldehydes, ketones and 1,2-dicarbonyl

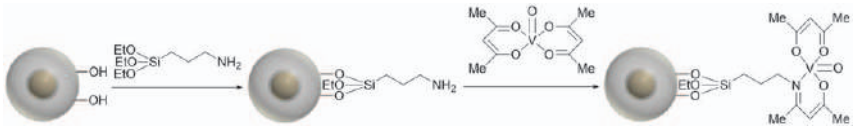

Figure 11.2 Schematic representation of the covalent immobilization of $[VO(acac)_2]$ complex onto superparamagnetic silica-coated iron oxide nanoparticles functionalized with APTES.
Reproduced from ref. 13 with permission from the Royal Society of Chemistry.

compounds, at 65 °C in acetonitrile, using TBHP as oxidant. High to excellent product yields in the range of 75%–96% were obtained after 2.5–5 h, with the most reactive substrates being α-hydroxy carbonyl compounds and aromatic secondary alcohols. Moreover, the performance of the heterogeneous catalyst was comparable to that of the homogeneous counterpart in the oxidation of benzhydrol (Yield = 95%–96% *vs.* 96%; reaction time: 3.0 h *vs.* 2.0 h), preserving the activity upon recycling and reuse for seven times with no metal leaching.

Magnetically recyclable oxidovanadium-based catalysts have been also reported for the selective oxidation of alcohols. For instance, Rostami *et al.* grafted a chiral oxidovanadium (+)-pseudoephedrine complex onto silica-coated Fe_3O_4 magnetic nanoparticles (MNPs) and studied its catalytic properties in the selective oxidation of alcohols to carbonyl compounds at 80 °C, using TBHP as oxidant and polyethylene glycol as solvent.[31] Benzyl alcohol was oxidized to benzaldehyde in 3 h, with 98% product yield and could be reused six times with no significant loss of activity. Various types of primary and secondary benzylic and allylic alcohols were also selectively oxidized, leading to good to high product yields in the range of 85%–98% after 2–55 h.

11.2.1.3 Epoxidation of Alkenes and Allylic Alcohols

Oxidovanadium complexes have been grafted onto several types of bulk and nano supports in order to develop efficient and recyclable heterogeneous catalysts for the epoxidation of allylic alcohols. In particular, our research group has developed several works in this field through the immobilization of $[VO(acac)_2]$ onto clays (LAPONITE® and K10-Montmorillonite),[32] a porous clay heterostructure (PCH),[33] mesoporous silicas (SBA-15 and hexagonal mesoporous silica, HMS),[33,34] a nanostructured ordered carbon material CMK-3,[35] silica-coated MNPs (240 nm particle size)[36] and silica nanoparticles (45 nm size).[37] In all cases, the support was previously functionalized with APTES through reaction between the hydroxyl groups of the support and the ethoxy groups of the organosilane, followed by covalent grafting of $[VO(acac)_2]$ through Schiff condensation between the amine groups of the APTES-functionalized support and the carbonyl group of the acac ligand (Figure 11.2).

The resulting hybrid materials were tested as heterogeneous catalysts in the epoxidation of geraniol at room temperature, in dichloromethane, using TBHP as oxidant.[32–37] The catalysts presented high regioselectivity towards

2,3-epoxygeraniol product (81%–99%), being comparable to that achieved with the homogeneous catalyst (100%), except for the SBA-15 and PCH-based catalysts. However, the reaction time and maximum substrate conversion depended on the type of support. Among all bulk heterogeneous [$VO(acac)_2$] catalysts, the complex grafted onto the amine-functionalized CMK-3 support presented the best performance and the highest stability upon reuse in a further cycle (lowest leaching), leading to a geraniol conversion comparable to that obtained under homogeneous conditions (98% *vs.* 100%) with only a small increase of the reaction time from 0.5 to 2.5 h.[32] The lower reaction time when compared with other bulk heterogeneous [$VO(acac)_2$] catalysts reported in the literature (typically 48 h) was attributed to an effective mass transport promoted by the rod-like structure of the support.

In the case of the [$VO(acac)_2$]-based nanocatalysts, the complex grafted to the 45 nm silica nanoparticles presented the highest catalytic activity, leading to 100% geraniol conversion and 99% selectivity towards 2,3-epoxygeraniol, after only 2 h *vs.* 0.25 h for the reaction catalyzed by the free complex.[37] Additionally, it was highly stable upon recycling and reuse, preserving its performance in four subsequent cycles. In this sense, this catalytic system revealed to be the most efficient heterogeneous [$VO(acac)_2$]-based catalyst reported in the literature for this particular reaction. The enhanced performance was assigned to the nanometre dimensions of the support, which improved the dispersion of the catalytic active centres in the reaction medium and enabled the immobilization of a higher amount of complex when compared with the remaining hybrid catalysts (295 *vs.* 35–137 $\mu mol\, g^{-1}$). This work highlighted the importance of nanosized supports, especially those with dimensions lower than 100 nm, for the design of eco-sustainable recyclable catalysts with performances that resemble those of the corresponding homogeneous counterparts.

[$VO(acac)_2$] has been also immobilized onto different types of supports for application in the epoxidation of alkenes. For instance, Verma *et al.* immobilized the complex onto APTES-functionalized graphene oxide (GO).[38] The resulting heterogeneous catalyst was highly active and selective in the solvent-free epoxidation of fatty acids and esters at 65 °C, using anhydrous TBHP as oxidant, leading to substrate conversions in the range of 80%–100% and epoxide selectivities of 98%–99% after 5 h. In particular, it led to a maximum of 99.8% oleic acid conversion and 99.1% epoxide selectivity after 5 h. In contrast, when the reaction was performed under homogeneous conditions, it led to lower oleic acid conversion and epoxide selectivity (92.5% and 96.5%, respectively). The improved performance of the heterogeneous catalyst was assigned to the type of support, which presented many oxygen-containing groups on its surface that interacted with the substrate and oxidant, facilitating the reaction. The hybrid catalyst was highly stable upon recycling and reuse in five further cycles, with no metal leaching, leading to almost comparable substrate conversion and epoxide selectivity (%C = 97.8% and %S = 99.1% after the sixth cycle). Finally, the oleic acid epoxidation catalyzed by the GO-based material could be scaled-up (20×), reaching a substrate conversion of 98%, 99% epoxide selectivity and an epoxide isolated yield of 97.4%.

More recently, Mirzaee *et al.* anchored [VO(acac)$_2$] onto boehmite nanoneedles ($l \times w = 50$ nm$\times$10 nm) previously functionalized with 3-chloropropyltrimethoxysilane, followed by reaction with ethylenediamine to replace the terminal chlorine groups of the functionalized support.[39] The resulting catalyst was tested in the epoxidation of *cis*-cyclooctene under reflux conditions, in CCl_4, using TBHP as oxidant, leading to an epoxide yield of 95% after 60 min and a TOF of 60 h^{-1}. Moreover, it was more active than the free complex (Yield = 81%), which could be related to the homogeneous dispersion of the catalytic active sites on the surface of the support. Additionally, it led to higher epoxide yield and TOF values than those achieved with the heterogeneous vanadium(IV) Schiff-base analog (epoxide yield = 92%; TOF = 29 h^{-1})[40] and with oxo-sulphate vanadium(IV) supported on boehmite nanoparticles functionalized with APTMS (epoxide yield = 93%; TOF = 39 h^{-1}).[41] Nevertheless, the catalytic activity decreased ~15% upon reuse in six further cycles (epoxide yield: from 95% to 81%; TOF: from 60 to 51 h^{-1}), which was assigned to a poisoning effect of water vapour which may be adsorbed during the recovering process and block the catalytic active sites, since no metal leaching was detected. The nanocatalyst was tested in the epoxidation of other alkenes, namely cyclohexene, 1-octene, 1-hexene, styrene, α-methyl styrene and α-pinene, yielding 81%, 60%, 65%, 86%, 91% and 90% of epoxide, respectively, after 60, 240, 240, 210, 90 and 90 min, respectively.

Very recently, a magnetically recyclable [VO(acac)$_2$] nanocatalyst was prepared by Farzaneh and Asgharpour by covalent grafting of a Schiff base ligand derived from melamine and 2-hydroxylnaphtaldehyde on the surface of superparamagnetic silica-coated iron oxide nanoparticles (10–15 nm) followed by complexation with [VO(acac)$_2$].[42] The nanocatalyst was tested in the epoxidation of geraniol in acetonitrile under reflux conditions, using TBHP as oxidant, and gave rise to 100% geraniol conversion after 2 h, with 100% selectivity to the corresponding epoxide and a TOF of 417 h^{-1}. Moreover, it could be magnetically recycled and reused in four subsequent cycles, with only a slight decrease of the substrate conversion from 99% to 96% and with negligible metal leaching. The nanocatalyst was also able to catalyze the epoxidation of trans-2-hexen-1-ol and 1-octen-3-ol into the corresponding epoxides, with 100% conversion and selectivity after 3 and 5 h, respectively. Finally, it was tested with other alkene substrates, such as norbornene, cyclooctene, cyclohexene, α-methyl styrene and styrene. In the case of norbornene and cyclooctene epoxidation, 100% selectivity to the corresponding epoxides was achieved (%C = 92% and 80% after 8 h, respectively), while in the case of cyclohexene, α-methyl styrene and styrene epoxidation, other side products were formed besides the epoxides (%C = 45%–75%; $\%S_{epoxide}$ = 58%–74%; reaction time: 8 h).

11.2.1.4 Bayer–Villiger Oxidation of Ketones

The Bayer–Villiger oxidation of ketones is a type of reaction with great interest in organic synthesis for the fabrication of valuable lactone and ester

intermediates applied on the production of pharmaceuticals, agrochemicals, polymers and perfumes. Recently, zeolites have been used for the development of heterogeneous VO-based catalysts for this type of reaction. In this framework, [VO(mpamp)] (mpamp = 2,2′-((1*E*,1′*E*)-((methylenebis-(4,1-phenylene)) bis(azanylylidene))bis(methanylylidene))diphenol)) complex was entrapped in the nanopores of zeolite-Y by the flexible ligand approach.[43] The resulting hybrid catalyst was active and selective in the Bayer–Villiger oxidation of cyclic ketones, namely cyclopentanone, cyclohexanone and 2-adamantanone at 80 °C in acetonitrile, for 12 h, using H_2O_2 as oxidant (Figure 11.3). It converted 46% of cyclopentanone into δ-valerolactone, with a selectivity of 71.5% and a TOF of 132 h^{-1}, almost preserving the activity upon reuse twice with similar selectivity and no metal leaching. Moreover, it presented higher catalytic activity than the neat complex due to site-isolation of the metal complexes, which prevented their dimerization. Cyclohexanone and 2-adamantanone were also successfully oxidized into the corresponding lactones, with conversions of 43.3% and 57% and lactone selectivities of 89% and 90%, respectively (TOF = 124 and 164 h^{-1}, respectively).

Later on, improvements of the cyclopentanone conversion and δ-valerolactone selectivity were reported by Modi *et al.*, when using a VO(IV) complex bearing the Schiff base ligand (*Z*)-2-((2-hydroxybenzylideneamino)-phenol entrapped in the same type of zeolite by a similar procedure.[44] A maximum of 80.22% conversion of cyclopentanone (TOF = 1746.76 h^{-1}) with 83.56% selectivity towards δ-valerolactone was achieved with the heterogeneous catalyst at 70 °C in methanol, using H_2O_2 as oxidant. Nevertheless, small decreases of the activity and selectivity were detected upon reuse for three times. The catalyst also oxidized cyclohexanone to the corresponding lactone with 56.87% conversion and 84.67% product selectivity (TOF = 1238.99 h^{-1}).

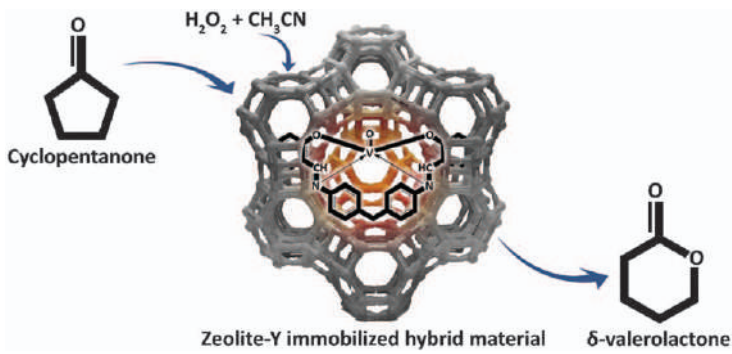

Figure 11.3 Bayer–Villiger oxidation of cyclopentanone to δ-valerolactone catalyzed by [VO(mpamp)] complex entrapped in the nanopores of zeolite-Y. Reproduced from ref. 43 with permission from Elsevier, Copyright 2017.

11.2.1.5 Hydroxylation of Aromatic Compounds

Supported oxidovanadium(IV) complexes also revealed to be promising recyclable catalysts for the selective hydroxylation of aromatic compounds, namely of benzene to phenol. It can be highlighted the pioneering work of Borah and co-authors that incorporated $[VO(acac)_2]$ in a PMO framework by a strategy that ensured that the $[VO(acac)_2]$ moieties were embedded and homogeneously distributed throughout the PMO structure, consisting on the: (i) preparation of an organic $[VO(acac)_2]$-based precursor through Schiff base condensation between the amine group of APTES and the carbonyl group of $[VO(acac)_2]$, followed by the (ii) synthesis of the PMO and simultaneous immobilization of the organic precursor prepared in (i), through co-condensation between tetraethyl orthosilicate and the precursor, using cetyltrimethylammonium bromide as structure-directing template.[45] The resulting catalyst led to a benzene conversion of 27.4% with 100% selectivity towards phenol, after 8 h, at 50 °C in acetonitrile, in the presence of H_2O_2. In contrast, when the reaction was performed under homogeneous conditions, although the substrate conversion was similar (28.6%), the epoxide selectivity was only of 76.8%. Finally, the PMO-based catalyst was stable upon reuse in two further cycles, with no metal leaching, leading to similar selectivity (100%) with only a slight decrease of the substrate conversion (from 27.4% to 25.9%).

Two distinct types of active, highly selective and recyclable heterogeneous oxidovanadium-based catalysts for this particular reaction have been produced by immobilization of $[VO(acac)_2]$ onto APTES-functionalized AC and HMS.[46] The resulting AC and HMS-based heterogeneous catalysts allowed reaching higher benzene conversions than the aforementioned PMO-based catalyst,[45] of 56% and 52%, respectively, with phenol selectivities of 90% and 95% and a phenol yield of 50%. Moreover, they presented higher selectivity towards phenol than the corresponding homogeneous complex (%S = 87%; Yield = 48%) and led to comparable benzene conversion (56% with the neat complex). The materials could be recycled and reused at least three times, leading to comparable or higher phenol yields (AC-based: 48%–54%; HMS-based: 58%–66%).

A distinct type of substrate that has been selectively hydroxylated using supported oxidovanadium catalysts is phenol. For instance, Salavati-Niasari reported the liquid-phase selective hydroxylation of phenol into a mixture of catechol and hydroquinone at 80 °C in acetonitrile, catalyzed by VO(IV) tetraaza complexes encapsulated in NaY zeolite, using H_2O_2 as oxidant.[47] A maximum substrate conversion of up to 38.4% after 6 h could be achieved for $[VO(Bzo_2[14]aneN_4)]^{2+}$-NaY (where $Bzo_2[14]aneN_4$ = dibenzo-1,5,8,12-tetraaza-2,9-dioxo-4,11-diphenylcyclotetradecane), with a selectivity towards catechol of 86.7% (hydroquinone selectivity: 13.3%). In contrast, in the case of the homogeneous phase reaction, although the phenol conversion could reach 43.2%, the corresponding selectivity towards catechol was only of 78.5%. The host–guest catalyst was reused in three cycles, with only a slight

decrease of the substrate conversion from 38.4% to 36.0% and of the catechol selectivity from 86.7% to 82.2%. The encapsulation of the complexes in the nanopores of zeolite NaY reduced the occurrence of dimerization of the complexes, that can be observed under homogeneous conditions, by isolating the metal N_4-macrocyclic complexes from each other.

11.2.2 Miscellaneous Reactions

In this sub-section, other types of reactions catalyzed by heterogeneous oxidovanadium systems will be addressed, such as sulfoxidations, oxidative aminations, Strecker-type reactions, and oxidative desulphurization. For the sake of clarity, this sub-section will only be focused on covalently bonded molecular complexes, with some insights on recent developments on well-defined single-site heterogeneous catalysts, namely vanadium-containing metal–organic frameworks.

11.2.2.1 Supported Oxidovanadium Complexes

An oxidovanadium(IV) Schiff base complex having two terminal trimethoxysilyl groups peripheral to the ligand has been used to obtain an MCM-41-like PMO. The resulting material efficiently catalyzed the cyanosilylation of carbonyl groups, namely the addition of trimethylsilyl cyanide (TMSCN) to benzaldehyde at 0 °C in $CHCl_3$ under N_2 atmosphere, with 80% conversion and 30% enantiomeric excess (ee).[48] One of the prepared catalysts was reused in four consecutive runs, only presenting a minor decrease in the conversion during the final run, which stated its good recyclability as an efficient heterogeneous catalyst for the formation of cyanohydrins. Interestingly, it was observed that the free silanol groups on the PMO support were not deleterious to the enantioselectivity, contradicting previous observations by the same authors.[49]

In another work, styryl functionalized oxidovanadium(IV) Schiff base has been covalently anchored on mercapto-modified single-walled carbon nanotubes (SWCNTs) through a radical chain mechanism.[50] The oxidovanadium-modified SWCNT material was tested in the catalytic cyanosilylation of aldehydes with TMSCN (at room temperature, in $CHCl_3$ under N_2 atmosphere), having achieved an impressive substrate conversion of 93%, which was comparable to that achieved with the homogeneous counterpart (98%). Moreover, the system did not present any decrease of the activity after five consecutive runs, yielding a minimum productivity of 317 mol of product per mole of complex. An asymmetric version of this catalytic reaction was also performed using a SWCNT supported chiral oxidovanadium(IV) complex, giving rise to 66% ee (at 0 °C, in $CHCl_3$, N_2 atmosphere) which, albeit being lower than the value obtained with the homogeneous counterpart (around 90% ee), was still encouraging and higher than the values obtained for other metal salen complexes supported on inorganic oxides for which much lower ee's have been reported.

New heterogeneous catalysts obtained by covalent immobilization of vanadium(V) salen complexes on organic polystyrene resins (JandaJel and Merrifield) were tested in the asymmetric addition of hydrogen cyanide (generated *in situ* from TMSCN) to *N*-benzyl benzylimine (Strecker type reaction; reaction conditions: dry toluene, CH_3OH, N_2 atmosphere, -40 °C).[51] Their catalytic performance was found to be similar to that of the corresponding homogeneous catalyst, and the ee value was slightly inferior. The JandaJel-V(V) heterogeneous catalyst could be used in three consecutive runs without significant loss of conversion or enantioselectivity, thus opening a route for the preparation of chiral amino acids through a heterogeneous process. Oxidovanadium(IV) Schiff base complexes covalently attached on the surface of MCM-41 have been synthesized by anchorage of a Schiff base ligand, with subsequent reaction with $[VO(acac)_2]$, for application in the oxidation of sulphides.[52] The resulting heterogeneous catalysts were able to achieve 85% thioanisole sulfoxidation conversion and 81% sulfoxide selectivity at 30 °C in CH_3CN but, unfortunately, the authors did not present any recyclability data.

A chiral oxidovanadium(IV) salen complex has been also immobilized onto MCM-41 by covalent grafting, using APTES as a reactive surface modifier, and tested in the asymmetric sulfoxidation of thioanisole at 25 °C in CH_2Cl_2, using cumene hydroperoxide as oxidant.[53] Slight improvements in sulphide conversion (95% conversion with 98% sulfoxide selectivity) and mainly in the ee value could be achieved (17% ee), when compared to the results obtained with the homogeneous [VO(salen)] complex (89% conversion with 96% sulfoxide selectivity and 13% ee). However, upon reuse, the conversion and ee values dropped to 73% and $<5\%$, respectively, being attributed to the blocking of the pores either by inactive V-oxo species formed during the catalytic process or by other insoluble side reaction products which could not be removed from the materials.

More recently, L-cysteine has been used as an MCM-41 surface modifier to anchor an oxidovanadium(IV) complex, and the resulting material was evaluated in the catalytic oxidation of sulphides and oxidative coupling of thiols (30% H_2O_2, room temperature), leading to excellent yields of the target products, and showing great stability and reusability, as it retained almost the same activity during seven consecutive catalytic cycles.[54]

A silica supported chitosan–vanadium complex has been prepared as depicted in Figure 11.4 and used as an heterogeneous catalyst for the asymmetric oxidation of aryl alkyl sulphides at 0 °C in H_2O/CH_3OH, using H_2O_2 as oxidant and HOAc as additive.[55] The oxidation products were obtained in high yields (up to 95%) with good enantioselectivities (up to 68% ee). Moreover, this catalyst could be reused five times without losing its catalytic activity.

A novel magnetic nanocatalyst has been prepared through immobilization of an oxidovanadium(IV) Schiff base complex on Fe_3O_4 nanoparticles (Figure 11.5) and tested in the solventless sulfoxidation of sulphides at room temperature, using H_2O_2 as the oxygen source.[56] The nanocatalyst presented a remarkable catalytic performance with TOFs of up to 1280 h^{-1} (for thioanisole sulfoxidation) and was reused for eight catalytic cycles with minimal metal

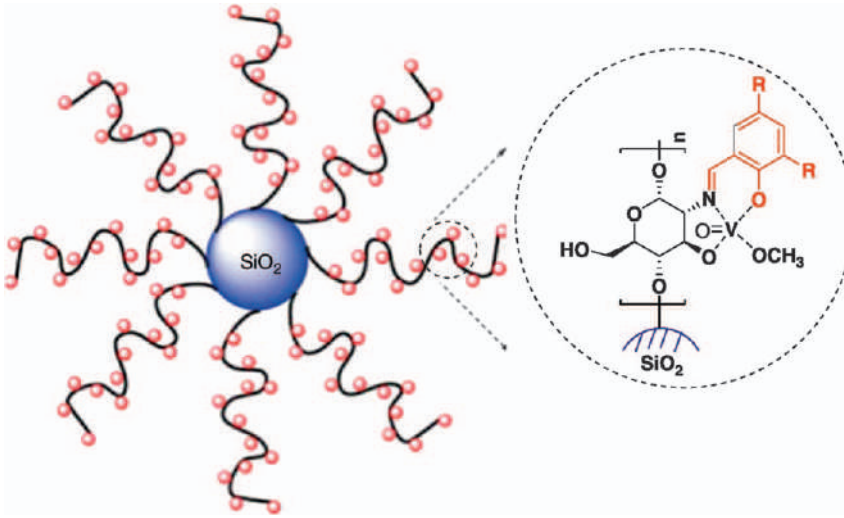

Figure 11.4 The structure of silica supported chitosan@vanadium catalyst.
Reproduced from ref. 55 with permission from Elsevier, Copyright 2017.

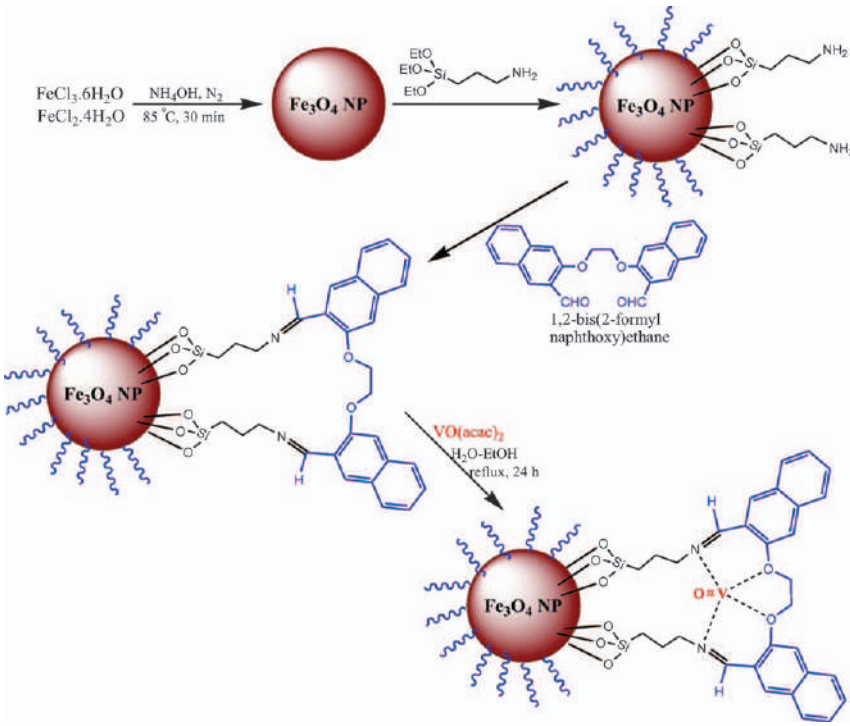

Figure 11.5 Immobilization of an oxidovanadium(IV) Schiff base complex on Fe_3O_4 nanoparticles.
Reproduced from ref. 56 with permission from Elsevier, Copyright 2019.

leaching. The magnetic nanocatalyst also had the advantage of facile separation from the reaction medium through the application of an external magnetic field and decantation.

Vanadium monomers with chiral tridentate Schiff base ligands have been supported on fumed SiO_2 through reaction with its surface silanols, where self-dimerization of the oxidovanadium complexes took place.[57] These chiral self-dimerized vanadyl complexes exhibited remarkable catalytic performance for the asymmetric oxidative coupling of 2-naphthol at 20 °C in toluene, using 101.3 kPa O_2 as oxidant: 96% conversion, 100% selectivity to 1,1′-binaphthol, and 90% ee, which was equivalent to the maximum ee reported for the homogeneous phase reaction. Furthermore, the silica supported vanadium dimers were reusable without loss of the catalytic performance.

Oxidovanadium(IV) complexes with Schiff bases derived from salicylaldehyde and cysteine have been immobilized onto chloromethylated polystyrene and employed as heterogeneous catalysts in the oxidative amination of styrene with secondary amines (diethylamine, imidazole, and benzimidazole) at 75 °C in CH_3CN with O_2 bubbling, yielding a mixture of two aminated products, in which the anti-Markovnikov product was favored over the Markovnikov one due to the steric hindrance posed by the secondary amines.[58] The polymer-anchored complexes actually performed better than their homogeneous counterparts, with TOFs of 39 and 21 h^{-1}, respectively (for diethylamine), and higher anti-Markovnikov selectivity (71.2% *vs.* 67.4%, respectively). Although no catalytic data regarding recyclability was presented, electron paramagnetic resonance analysis revealed that the coordination sphere around VO(IV) remained unaltered after the catalytic cycle. This work was further developed by varying the Schiff base, this time derived from 3-formylsalicylic acid and 2-(2-aminoethyl)pyridine.[59] The resulting polymer-bound oxidovanadium(IV) materials were tested in the catalytic hydroamination of styrene and vinylpyridine with amines, at 90 °C in toluene, yielding a mixture of two enamines in good yields (styrene: %C = up to 76%, with 86% selectivity to anti-Markovnikov product; vinylpyridine: %C = up to 92%, with 81% selectivity to anti-Markovnikov product) and being free from leaching during three consecutive catalytic cycles.

Another variation of the salen ligand derived from 3-formylsalicylic acid and *N*,*N*-dimethyl ethylenediamine has been covalently bonded to chloromethylated polystyrene, and tested in the catalytic oxidative desulphurization of model fuel diesel mixtures of organosulphur compounds such as thiophene, dibenzothiophene, benzothiophene, and 2-methyl thiophene, at 60 °C using heptane as solvent.[60] The hybrid catalyst efficiently oxidized the substrates to the corresponding sulphones in the presence of H_2O_2, without loss of efficiency for at least up to three catalytic cycles.

11.2.2.2 Oxidovanadium Incorporated Onto Metal–Organic Frameworks

Metal–organic frameworks (MOFs) can be defined as crystalline, porous solids, whose structure is defined by nodes of metal ions or clusters of metal

ions held in the lattice by bi- and multi-podal rigid organic linkers. A great advantage of MOFs is that the molecular-level structural control and possible modularity allow molecule-like catalyst design in the solid state.

A chiral porous MOF has been constructed from [VO(salen)]-derived dicarboxylate and dipyridine bridging ligands.[61] After oxidation of V(IV) to V(V), the material was found to be an effective, recyclable and reusable heterogeneous catalyst in the asymmetric cyanosilylation of aldehydes with TMSCN at 0 °C in dichloroethane using Ph_3PO, boasting 93% conversion and 92% ee for benzaldehyde. It was found that the catalytic reaction mainly occurred inside the pores of the MOF, since bulkier aldehyde substrates with sizes larger than the MOF pore diameters were tested and a very reduced conversion was obtained.

Another two-dimensional covalent organic framework (COF) that featured eclipsed stacking structure, large pores and hydroxyl functionalities has been post-synthetically modified with $[VO(acac)_2]$ to yield a vanadium docked COF (VO-TAPT-2,3-DHTA).[62] The resulting material was tested as heterogeneous catalyst in the Prins reaction (in CH_3CN, 80 °C) and sulphide oxidation (in CH_3CN, 25 °C) with excellent efficiency and reusability. The percentage yield of nopol *via* Prins condensation reaction of β-pinene and paraformaldehyde over $[VO(acac)_2]$ and $[VO(catechol)_2]$ was moderate (19% and 21%, respectively), whereas in the presence of VO-TAPT-2,3-DHTA it increased to 69%, which was due to the mesoporous nature, large diameter of pore channel and presence of active vanadium sites uniformly distributed in the framework. This catalyst was also tested in the sulfoxidation of various aliphatic and aromatic sulphides, and achieved up to 99% conversion and 95% sulfoxide selectivity for thioanisole oxidation. Furthermore, it was reused for three consecutive cycles with negligible loss of catalytic activity.

A vanadium-based MOF, MIL-47, has been synthesized using VCl_3 and 1,4-benzenedicarboxilic acid, and its catalytic activity was tested in the oxidative desulphurization of heterocyclic aromatic sulphur compounds in the presence of TBHP in the temperature range of 60–100 °C in decane.[63] Although the catalytic results were promising, it was found that the MOF underwent degradation into V_2O_5 and 1,4-benzenedicarboxilic acid under the catalytic reaction conditions.

Bottlebrush polymers have been synthesized by ''graft from'' approach and further hyper-cross-linked to produce amino functional microporous organic nanotube frameworks (MONFs) *via* the Friedel–Crafts alkylation reaction.[64] Afterwards, the MONFs were reacted with salicylaldehyde *via* the aldimine condensation to prepare a salicylaldehyde-modified MONFs ligand (Figure 11.6). As a Schiff base, the salicylaldehyde-modified MONFs were then coordinated with oxidovanadium(IV) moieties to obtain MONFs-based oxidovanadium(IV) complexes (VO-MONFs). The VO-MONFs catalyst was tested in the selective oxidation of *p*-chlorobenzenethiol to disulphides at ambient temperature in CH_3CN, using urea peroxide as the oxidant, and after 6 min, the conversion was nearly up to 100% with a TOF of 4305 h^{-1}. The high catalytic activity of the VO-MONFs was attributed to its high hierarchical porosity and distribution of active sites.

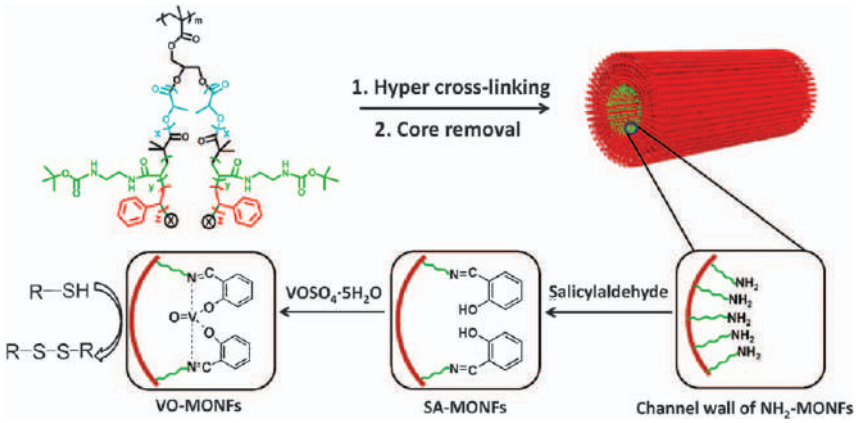

Figure 11.6 Illustration of the synthesis of VO-MONFs and application in selective oxidation of thiols to disulphides.
Reproduced from ref. 64 with permission from Elsevier, Copyright 2018.

A MOF with vanadium in a molecule-like coordination environment has been prepared by cation exchange in MFU-4*l* (a Zn-based MOF).[65] This material formed a single-site heterogeneous catalyst with methylaluminoxane for olefin polymerization and provided polyethylene with low polydispersity and the highest activity (TOF of up to 148 000 h^{-1}) reported for a MOF-based polymerization catalyst. The resulting polyethylene was obtained as a free-flowing powder, as desired industrially, and the catalyst showed good structural integrity and retained polymerization activity for over 24 hours.

11.3 Vanadium-based Electrocatalysts for Water Splitting

Electrocatalysts play an essential role in energy conversion and storage technologies, such as fuel cells, batteries and water electrolysis.[66,67] Electrochemical water splitting has been regarded as the most effective technology to produce clean hydrogen fuel. Even though the theoretical water-splitting voltage is 1.23 V, this demanding reaction always requires a large overpotential in real life applications.[68] Therefore, developing highly efficient, cost-effective and durable hydrogen evolution reaction (HER) and oxygen evolution reaction (OER) electrocatalysts is a top priority. Platinum, iridium and ruthenium precious metals and their derivatives have been found to be the most active OER and HER electrocatalysts, but their extensive use is hindered due to their high cost and poor stability.[17,66] As a result, tremendous efforts have been undertaken on the investigation and development of highly efficient electrocatalysts (ECs) based on earth-abundant elements, both for HER (carbides, phosphides, nitrites, chalcogenides) and OER (oxides, hydroxides) and several review papers can be found in the

Table 11.1 Vanadium-based electrocatalysts for HER and OER.[a]

		HER		OER		
Electrocatalyst	Electrolyte	η_{10} (mV *vs.* RHE)	TS (mA dec^{-1})	η_{10} (mV *vs.* RHE)	TS (mA dec^{-1})	Ref.
VC-NS	0.5 M H_2SO_4	98	56	—	—	75
VC@NCNT	1 M KOH	159	39	—	—	77
	0.5 M H_2SO_4	161	95			
V_8C_7NMs/GF	1 M KOH	156	89.4	—	—	78
	0.5 M H_2SO_4	52	48.3			
V/NF	1 M KOH	176	82	292	68	72
$Ni_3(VO_4)_2$@$NiCo_2O_4$/NF	—	113	101	—	—	73
NiFeVS/NF	1 M KOH	161	96	—	—	74
$Ni_3Fe_{1-x}V_x$/CFP	1 M KOH	—	—	200	39	92
Ni-VC@C/Ti	1 M KOH	146	97	—	—	76
	0.5 M H_2SO_4	138	61			
$Ni_3V_2O_8$/NRGO	1 M KOH	43	—	—	—	71
Ni_3S_2/VS_2	1 M KOH	—	—	227	59.9	91
N-Ni_3S_2/VS_2	1 M KOH	151	107.5	—	—	91
MoVN	1 M KOH	108	60	—	—	161
	0.5 M H_2SO_4	153	76			
CVN/CC	1 M KOH	118	73.6	263	64.1	80
CoVO/C	1 M KOH	—	—	350	75	95
$CoVO_x$/FTO	0.5 M KOH	—	—	310	75	90
a-$CoVO_x$	1 M KOH	—	—	347	65	88
CoV_2O_6-600	1 M KOH	—	—	324	113	87
CoV_2O_6-V_2O_5/NRGO	1 M KOH	—	—	239	49.7	86
$Co_3(VO_4)_2$-ethanol	1 M KOH	—	—	330	55	89
$CoV_{1.5}Fe_{0.5}O_4$	1 M KOH	—	—	300	38	83
VCoN	1 M KOH	179	123	—	—	82
VN-Co-P	1 M KOH	137	—	335	—	81
$Fe_{0.5}V_{0.5}$	1 M KOH	—	—	360	36.7	84
Zn-Fe-VO_4	0.5 M KOH	—	—	310	75	94
Lepidocrite VOOH	1 M KOH	164	104	270	68	85

[a]VC – vanadium carbide; NS – graphitic carbon network nanosheets; NCNT – N-doped carbon nanotubes; GF – graphene; NF – Nickel foam; CFP – carbon fibre paper; NRGO – N-doped reduced graphene oxide; CC – carbon cloth; FTO – fluorine-doped tin oxide.

literature.[18,19,66,69] In this section we will focus on vanadium-based ECs owing to their advantages, namely their richer elemental abundance, smaller relative atomic mass when compared to other similar elements and, more importantly, the multiple valence oxidation states of vanadium, which make them promising materials for water splitting.[70,71] Table 11.1 lists a summary of the vanadium-based materials used as HER and OER ECs that will be discussed next.

11.3.1 HER Electrocatalysts

In 2016, Yu and co-workers reported that nickel foam (NF) coated with vanadium nanobelts (V/NF) was an efficient EC for water splitting in alkaline medium, with $\eta_{10} = 176$ mV *vs.* RHE, Tafel slope of 82 and an overall water-splitting voltage of 1.80 V at $j = 20$ mA cm^{-2}.[72] Mixed transition metal oxides ($Ni_3(VO_4)_2$, $NiCo_2O_4$)[73] and multiple transition metal sulphides (NiFeVS)[74] have also been deposited on nickel foams giving rise to ECs with superior HER electroactivity. In the latter, the authors suggested the occurrence of a synergistic effect on ternary metals sulphides, as these showed superior HER activity than binary NiFeS/NF and NiVS/NF.

Another type of vanadium-based materials that has been applied as HER ECs are vanadium carbides (VC), owing to their excellent hydrogen adsorption properties. For instance, X. Peng *et al.* reported the successful application of VC nanoparticles encapsulated in graphitic carbon network nanosheets (VC-NS) as HER ECs in acidic medium.[75] The material was prepared by a hydrothermal reaction using V_2O_5 nanosheets as precursor and template, followed by a low-temperature and environmentally-friendly magnesium thermic reduction. The VC-NS presented very low overpotential at a current density (j) of 10 mA cm^{-2} ($\eta_{10} = 56$ mV *vs.* the reversible hydrogen electrode, RHE), small Tafel slope (TS = 98 mV dec^{-1}) and excellent durability.

In a distinct work, Peng and co-workers were able to surpass VC common disadvantages like the need for high synthesis temperature and uncontrollable morphologies.[76] The authors designed a chemical vapour carbonization method to prepare Ni-VC@C/Ti ECs, which were composed of Ni-modified VC nanoboscages with a graphitic carbon coating supported *in situ* on a Ti plate. The ECs presented HER activity in both alkaline ($\eta_{10} = 146$ mV *vs.* RHE, TS = 97 mV dec^{-1}) and acidic media ($\eta_{10} = 138$ V, TS = 61 mV dec^{-1}), with excellent stability (20 h without significant changes). Later, VC nanoparticles embedded within N-doped carbon nanotubes (VC@NCNT) *via* a metal-triggered confinement strategy have been reported as efficient HER ECs over a wide pH range, with $\eta_{10} = 161$, 159 and 266 mV *vs.* RHE in acidic, alkaline and neutral medium, respectively.[77] The better performance was attributed to a synergistic effect between pyridinic N-doping, CNT support and ultra-small VC nanoparticles. Remarkable durability (100 h) and almost 100% faradaic yield were also achieved in both acidic and alkaline media. More recently, a V_8C_7 nanomesh/graphene EC has been prepared by epitaxial growth of graphene.[78] The energy barriers of hydrogen generation have been considerably reduced due to the strong electronic interactions between V_8C_7 and graphene, leading to excellent HER activity ($\eta_{10} = 52$ and 156 mV, and TS = 48.3 and 89.4 mV dec^{-1}, in 0.5 H_2SO_4 and 1 M KOH, respectively).

Almost at the same time, bimetallic vanadium-molybdenum nitride (MoVN) thin films have been reported as HER ECs, delivering low overpotentials ($\eta_{10} = 108$ and 153 mV in 1 M KOH and 0.5 H_2SO_4, respectively), TS values of 60 and 76 mV dec^{-1} and excellent long-term durability.[79] A 3D

nanohybrid (CVN/CC) of cobalt nitride (Co_4N) and vanadium oxynitride ($VN_{1-x}O_x$) has been fabricated by pyrolyzing Co-V precursor grown on polyaniline (PANI)-coated carbon cloth (CC) and applied towards HER and OER (see Table 11.1 for OER parameters) in 1 M KOH.[80] The resulting EC showed $\eta_{10} = 118$ mV and a TS of 73.6 mV dec^{-1} along with a remarkable stability (100 h). It was established that the variation of the Co/V ratio not only significantly affected the HER and OER features since V played a crucial role on the enhancement of the electrocatalytic performance of CVN/CC, but also facilitated the charge transfer process and assisted the transformation of Co centres into electrocatalytically active species. Dual-doping approach of vanadium nitride has also been reported to achieve high-performance HER ECs.[81,82] This method was employed in order to create more active sites during the entire electrocatalytic process and promising results were obtained in alkaline medium for VN-Co-P ($\eta_{10} = 137$ mV *vs.* RHE).[81]

The most recent report describes the application of nickel vanadate ($Ni_3V_2O_8$) anchored on N-doped reduced graphene oxide (NRGO) as HER EC.[71] This EC was applied in alkaline medium, achieving a low η_{10} of 43 mV *vs.* RHE, a small TS (54.8 mV dec^{-1}) and a high exchange current density ($j_0 = 1.24$ mA cm^{-2}). It was established that the NRGO content influenced the homogeneous distribution of nickel vanadate over NRGO sheets and, consequently, the HER performance. Additionally, the study of the HER activity of nickel vanadate ($\eta_{10} = 97$ mV) and NRGO sheets ($\eta_{10} = 194$ mV) suggested a synergistic effect in the $Ni_3V_2O_8$/NRGO hybrid.

11.3.2 OER Electrocatalysts

One of the first examples of vanadium-based ECs towards OER was the V/NF for HER.[72] This EC led to a η_{10} of 292 mV and a low TS (68 mV dec^{-1}) in alkaline solution. The performance of highly dispersed cobalt vanadium iron spinel nanoparticles ($CoV_{2-x}Fe_xO_4$, with $x = 0$, 0.5, 1, 1.5 and 2) towards OER has been also evaluated.[83] The study showed that the electrocatalytic activity was strongly influenced by the V/Fe ratio, with $CoV_{1.5}Fe_{0.5}O_4$ showing the most promising results ($\eta_{10} = 300$ mV and TS = 38 mV dec^{-1}). At the same time, hollow $Fe_{0.5}V_{0.5}$ composites were successfully applied as OER ECs with low overpotential ($\eta_{10} = 360$ mV) and small TS (36.7 mV dec^{-1}), demonstrating that efficient water oxidation ECs could be prepared without the involvement of commonly used Ni or Co.[84] Studies with lepidocrocite VOOH hollow nanospheres showed that by varying the reaction temperature, the surface area could be readily tuned and, consequently, the corresponding electrocatalytic activity.[85] In 2017, a composite based on bimetallic oxides (CoV_2O_6 and V_2O_5) anchored on NRGO (CoV_2O_6-V_2O_5/NRGO) has been reported, with an ultralow η_{10} of 239 mV *vs.* RHE, a TS of 49.7 mV dec^{-1} and excellent stability in alkaline medium.[86] This work showed that CoV_2O_6 acted as active sites, while the hydrogen bond between V_2O_5 and the HOO* intermediate of OER greatly decreased the composite adsorption energy, thus reducing the overpotential. Above all, it demonstrated for the first time that intermolecular hydrogen

bonding played a crucial role on the improvement of OER electrocatalytic properties. This (CoV_2O_6)[87] and other cobalt vanadates ($Co_yV_{1-y}O_x$,[88] $Co_3(VO_4)_2$,[89] $CoVO_x$[90]) have also been tested towards OER either alone or as thin films, with overpotentials ranging from 310 to 347 mV *vs.* RHE.

In 2018, the study of the effect of vanadium and N-doping on Ni_3S_2 nanosheets towards water splitting revealed that N-doping was only beneficial for HER, while the presence of V increased the efficiency for OER, decreasing the η_{10} by 93 mV and the TS from 76.2 to 59.9 mV dec^{-1} (from Ni_3S_2 to Ni_3S_2/VS_2).[91] Various $Ni_3Fe_{1-x}V_x$ (oxy)hydroxide ($1 \geq x \geq 0$) materials have been also evaluated as OER ECs, with $Ni_3Fe_{0.5}V_{0.5}$ presenting the best results, with $\eta_{10} = 200$ mV and a TS of 39 mV dec^{-1}.[92] In the same year, a polyoxovanadate was intercalated into nickel hydroxide $Ni(OH)_2$ 2D nanosheets, resulting in a unique structure effective for the improvement of OER activity, while contributing towards a potential method to prepare novel, porous hydroxide-based nanohybrid materials.[93] Vanadate ions intercalated into Zn–Fe layered double hydroxides (Zn–Fe–VO_4-LDH) have also exhibited good OER activity, expressed as low η_{10}, small TS and large exchange current density.[94]

More recently, a novel composite based on the thermal conversion of a metal organic framework (ZIF-67) functionalized with molecular vanadium oxide clusters ($[V_{10}O_{28}]^{6-}$) has been applied as OER electrocatalyst, presenting an overpotential of 350 mV *vs.* RHE and a TS of 75 mV dec^{-1}.[95] The use of vanadium oxide clusters modified the pore formation process, enlarging the specific surface area of the final compound and improving the OER properties.

11.4 Vanadium-based Heterogeneous Catalysts for Biomass Transformation

The transformation of non-food biomass (lignocellulose) to chemicals and fuels has become an area of recent research focus due to the concerns over the environmental impact of fossil fuels.[96] Biomass has been considered the only sustainable source of organic carbon on Earth that can replace fossil carbon sources due to its abundance and low cost.[97] Considerable efforts have been devoted to the transformation of biomass into simple building blocks, the so-called platform molecules, and their subsequent transformation into high value-added chemicals using catalytic processes, such as oxidation, hydrogenation, dehydration and deoxygenation. The development of new and efficient catalysts to improve the selectivity and yield production of biomass derivatives is still a challenge. Vanadium-based catalysts have attracted much attention for biomass transformation catalytic processes due to their high efficiency in homogeneous and heterogeneous selective oxidation of light alkanes.[98,99] In recent years, many approaches have been proposed for the oxidation of lignin to generate aromatic compounds,[100–103] for the conversion of ethyl lactate to ethyl pyruvate[104,105] and for the oxidation of biomass-derived furans, including furfural (FUR)[106–109] and 5-hydroxymethylfurfural (HMF)[20,106,110] using vanadium-based heterogeneous catalysts. In particular, the catalytic oxidation of HMF to obtain 2,5-diformylfuran (DFF) is one of the

prominent biomass transformation reactions and hence has been deeply explored over the past few years with great interest for academia and industry.[20]

11.4.1 2,5-Diformylfuran Production

Based on the scope of this chapter, this section provides an overview on the articles published over the past few years focused on the selective oxidation of HMF for the production of DFF as an example of the noticeable efficiency of vanadium-containing heterogeneous catalysts in biomass transformation. This section is divided in two sub-sections: 11.6.1.1 – Selective oxidation of HMF to DFF; and 11.6.1.2 – One-pot/one-step *vs.* one-pot/two-step reactions for the production of DFF from biomass sugar derivatives (fructose).

11.4.1.1 Selective Oxidation of HMF to 2,5-Diformylfuran

The selective oxidation of HMF is one of the most important transformations to produce DFF, which is considered a highly significant furan derivative, with extensive applications in many fields, including as intermediate for pharmaceuticals and as building block for the synthesis of heterocyclic ligands, drugs, antifungal agents, furan-containing polymers and fluorescent materials.[21]

However, the oxidation of HMF can easily undergo many side reactions, as shown in Figure 11.7. To face this drawback, many efforts have been carried out to selectively convert HMF to DFF using greener and more efficient catalytic systems, namely molecular oxygen as a cheaper and greener alternative to classical oxidants,[111] and efficient heterogeneous catalysts, including vanadium-based materials due to their noticeable multiple oxidation states. Table 11.2 summarizes the vanadium-based heterogeneous catalysts employed in the DFF production by HMF selective oxidation and by one-pot fructose conversion in the presence of air or oxygen as green oxidants.

In 1997, Moreau *et al.* reported the oxidation of HMF to DFF in a batch reactor at 90 °C in the presence of supported V_2O_5/TiO_2 catalysts, using toluene as solvent.[112] Substrate conversions and DFF selectivity around 90% were obtained within 4 h under 1.6 MPa air pressure, although a high

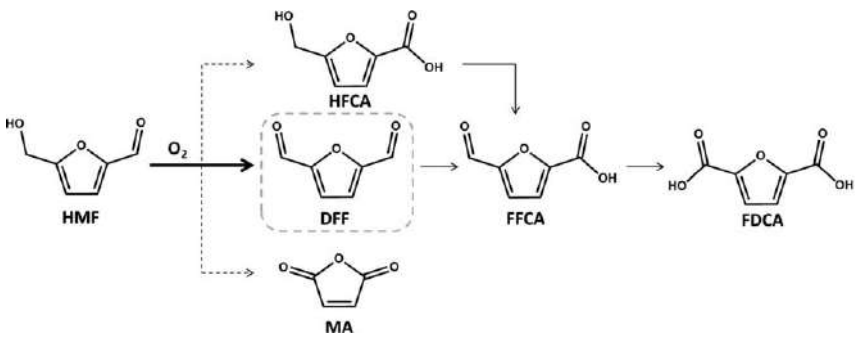

Figure 11.7 HMF oxidation products.

Table 11.2 DFF production using vanadium-based heterogeneous catalysts.[a]

Vanadium-based Catalyst	Reaction Conditions	HMF Conversion (%)	DFF Selectivity (%)	Ref.
HMF oxidation to DFF				
V_2O_5/TiO_2 (15 wt% V)	Toluene; 363 K; air (1.6 MPa); 4 h;	91	93	112
$VOPO_4{\cdot}2H_2O$ (VOP)	DMSO; 150 °C; air (0.1 MPa); 6 h	84.0	97.0	123
	DMF; 100 °C; O_2 (0.1 MPa); 6 h	56.0	93.0	
VOP/SiO_2 (14 wt% VOP)		84.0	23.3	
MgVOP	DMF; 100 °C; O_2 (0.1 MPa); 8 h	74.0	78.0	
$C_{14}VOPO_4$	Toluene; 110 °C; 1 atm O_2; 6 h	99	82	124
$C_{14}VOHPO_4$		99	83	
PVP1-VO (2.4 wt% V)	Trifluorotoluene; 130 °C; air (1 MPa); 4 h	77	100	126
SBA-Py-VO + pyridine additive		50	98	
VO_x/ZrO_2 (8.0 wt%)	Toluene; 363 K; air (1.6 MPa)	~30	70.3	113
VO_x/TiO_2 (5.1 wt%)			69.6	
VO_x/Nb_2O_5 (3.0 wt%)			72.0	
V_2O_5/H-beta	DMSO; 125 °C; O_2 (10 bar); 3 h	84	>99	114
0.93%V–0.26%Cu-CS	Acetonitrile; 140 °C; air (40 bar); 4 h	99	98	128
V_2O_5/AC	MIBK; 100 °C; O_2 (0.28 MPa); 4 h	95.2	96.4	116
10% V_2O_5/SBA-15	Toluene; 110 °C; O_2 (0.28 MPa)	88.6	57.9	120
VO_2-PANI/CNT (9.5 wt% V)	DMSO, 120 °C; O_2 (1.0 MPa); 11 h	>99	96	118
PA–$VO(acac)_2$	4-Chlorotoluene; 110 °C; O_2; 12 h	99.2 (>99)	86.2	162
V–g-C_3N_4(1.39)	DMSO; 130 °C; O_2 (0.1 MPa), 6 h	>99	92	117
Fe_3O_4@SiO_2–NH_2–VO^{2+} (100 mg) and Fe_3O_4@SiO_2–NH_2–Cu^{2+} (30 mg)	Toluene; 110 °C; O_2 (0.28 Mpa); 1 h	98.7	87.4	131
10V_2O_5@Cu-MOR (125)	DMSO; 120 °C; O_2 (balloon); 7 h	99.9	72.1	115
MCM-NH_2-VO^{2+} and MCM-NH_2-Cu^{2+} (co-catalyst)	Toluene; 110 °C;	98.1	61.2	163
VPO	DMSO; 120 °C; air; 10 h	100	83.6	125
V-CS-800	DMSO; 120 °C; O_2; 9 h	100	99	119
VO_x-ms[b]	H_2O; 130 °C; O_2 (3.0 MPa); 1 h	93.7	95.4	121
10% V_2O_5/ceramic	DMSO; 140 °C; O_2 (balloon); 5 h	100	85.7	122

Table 11.2 (*Continued*)

Vanadium-based Catalyst	Reaction Conditions	HMF Conversion (%)	DFF Selectivity (%)	Ref.
One-pot production of DFF from biomass derived fructose[c]				
g-$C_3N_4(H^+)$ + V-g-C_3N_4(1.39)	130 °C; DMSO; O_2 (0.1 MPa); 6 h	99	63	117
V–g-$C_3N_4(H^+)$[d]			45	
PA–$VO(acac)_2$ + Amberlyst-15	DMSO/4-chlorotoluene (1 : 4); 110 °C; O_2; 12 h	100.0	71.0	162
Pd-V(3:2)-MIL-101 + sulphonic resin	DMSO; 140 °C; O_2 (1 bar); 10 h	100.0	34	135
VSi-Beta(100) + H_2SO_4	DMSO; 130 °C; O_2 (balloon); 3 h	>99.9	93.3	132
V_2O_5@Si-Beta		>99.9	80.3	
WO_3H-VO(Salten)-SiO_2@Fe_3O_4	Isopropanol; H_2O_2; 60–80 °C; 16 h	100	71	134
10 V_2O_5@MOR(60) + HCl	DMSO; 130 °C; O_2 (balloon); 4 h	100	96	133
10% V_2O_5/ceramic + H_2SO_4	DMSO; 140 °C; O_2; 5 h	100	68.4	122

[a]TFT – triflurotoluene; DMSO – dimethyl sulfoxide; DMF – *N*,*N*-dimethylformamide; MIBK – Methyl isobutyl ketone; PVP – poly(4-vinylpyridine) 33% cross-linked with divinylbenzene; PANI – polyaniline; CNT – carbon nanotubes; AC – Activated carbon; g-C_3N_4 – graphitic carbon nitride; Salten – *N*,*N*-bis-3-(salicylidenamino)ethyltriamine; MOR – mordenite zeolite.
[b]Vanadium oxide nanobelt-arrayed microspheres.
[c]0.78 mmol g^{-1} (V) and 0.58 mmol g^{-1} (H^+).
[d]Conversion calculated for fructose.

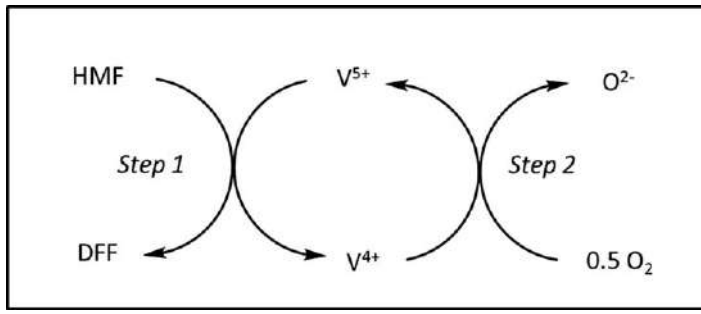

Figure 11.8 Mars–van Krevelen mechanism involving V^{5+}/V^{4+} redox cycles.

catalyst/substrate ratio (of 2) was required. Later on, Nie and Liu evaluated the influence of the VO_x surface density and support type on the activity and selectivity of the resulting catalysts for the HMF oxidation.[113] The supports included Nb_2O_5, ZrO_2, TiO_2, MgO and Al_2O_3 with different acid–base and redox properties. ZrO_2, TiO_2 and Nb_2O_5 led to higher selectivities (69.6%–72.0%). The authors proposed the domain of a Mars–van Krevelen redox mechanism for the HMF oxidation to DFF, involving the surface lattice oxygen atoms of VO_x, Figure 11.8.

Sadaba *et al.* took advantage of the excellent features of zeolites including their high thermal stability and surface area and prepared four V_2O_5 catalysts supported on different zeolites: H-Y, H-mordenite, H-beta and H-ZSM-5.[114] The most active catalyst was V_2O_5 supported on H-beta zeolite (1 wt% V_2O_5/H-beta), which presented higher acidity, leading to 84% HMF conversion with more than 99% DFF selectivity, at 125 °C and 10 bar O_2 pressure in DMSO. Later on, V_2O_5 has been efficiently supported on Cu-containing mordenite-type zeolite (Cu-MOR).[115] The catalyst was used in the heterogeneous oxidation of HMF in ambient pressure of O_2, leading to high DFF yield (91.5%) after 4 h, at 130 °C in DMSO. The catalyst also presented good reusability. The analysis of structure–activity relationship showed a remarkable effect of the strong interaction between the support framework Cu species and the grafted V sites on the catalytic performance.

Metal or metal oxide catalysts supported on carbon-based materials have been also applied in this type of reaction. For instance, Antonyraj *et al.* reported the preparation of an AC-supported V_2O_5 catalyst.[116] During the preparation the authors noticed an *in situ* oxidation of V^{3+} to V^{5+}, which contributed to highly dispersed V_2O_5 supported over AC and, consequently, to a highly stable and active catalyst for the selective oxidation of HMF into DFF. In particular, it afforded >95% HMF conversion and DFF selectivity after 4 h, at 100 °C, using methyl isobutyl ketone (MIBK) as solvent and O_2 as oxidant. Chen and co-authors prepared vanadium-doped graphitic carbon nitride (V-g-C_3N_4) as an environmentally benign catalyst for the oxidation of HMF to DFF.[117] V-g-C_3N_4 (1.39 mmol g^{-1} V) showed excellent activity, leading to quantitative HMF conversion and 82% DFF selectivity after 6 h, at 130 °C in DMSO, using O_2

(atmospheric pressure) as oxidant. The replacement of V by other metals, namely Mo, Fe, Ni, Co, Mn and Cu, drastically reduced the DFF yield (<25%), suggesting the involvement of the $V^{5+} - V^{4+}$ redox cycle, Figure 11.8.

Later on, the same authors immobilized vanadium oxide, in different loadings, on PANI-functionalized CNTs (VO_2-PANI/CNT) using a bicomponent assembly method.[118] The prepared catalysts were efficiently used in the aerobic oxidation of HMF, with VO_2-PANI/CNT (9.5 wt% V) showing complete conversion and a maximum DFF yield of 96% after 11 h, at 120 °C using DMSO as solvent and O_2 (1.0 MPa) as oxidant. The high selectivity was attributed to the synergistic effect between both components, VO_2 and PANI. The reusability of VO_2-PANI/CNT was investigated and a decrease of the catalytic performance was observed after five cycles (from 96% to 75% DFF yield) mainly due to some vanadium leaching (~30%). In a similar way, Zhao *et al.* prepared VO_2 embedded on mesoporous carbon spheres (V-CS) by a hydrothermal method.[119] The V-CS materials were used as heterogeneous catalysts in the aerobic oxidation of HMF using atmospheric oxygen as the oxidant and optimized reaction conditions (at 120 °C in DMSO). A DFF yield of 99% and quantitative substrate conversion were obtained after 9 h when using the V-CS-800 catalyst (calcined at 800 °C), evidencing the remarkable positive effect of the micro-mesoporous structure of the carbon spheres combined with the highly dispersed vanadium dioxide species. The catalyst showed to be reusable with no significant loss of activity in the recycling test.

Liao *et al.* prepared a series of V_2O_5/SBA-15 catalysts by molecular designed dispersion method with different V_2O_5 loadings of 5, 10, 15 and 20 wt%.[120] The 10 wt% V_2O_5/SBA-15 catalyst led to 88.6% HMF conversion with 57.9% DFF yield at 110 °C, employing molecular oxygen (0.28 MPa) as oxidant and toluene as solvent. The improved performance of the catalyst was attributed to a uniform sized nanovanadium species distribution on the pore surfaces of the hexagonally well-ordered mesoporous silica support.

Nanobelt-arrayed vanadium oxide hierarchical microspheres (VO_x-ms) synthesized through solvothermal method and calcination at 350 °C selectively catalyzed the oxidation of HMF to DFF at 130 °C in water using O_2 as oxidant, with high substrate conversion and selectivity, 93.7% and 95.4%, respectively, after 1 h.[121] The high performance was attributed to the major exposure of the (010) facet of the material with higher hydrogen adsorption capability of vanadyl (V=O) sites and to the highly oriented morphology of the material for HMF contact and residence time control.

A V_2O_5/ceramic catalyst has been prepared by Cui and co-authors by co-sintering V_2O_5 with a ceramic matrix (SiO_2, Al_2O_3, Na_2SiO_3, MgO, CaO).[122] Complete conversion of HMF into DFF at 140 °C in DMSO under atmospheric pressure of oxygen was achieved after 5 h, yielding 85.7% of DFF. After five times of catalyst recycling, only a slight decrease of the catalyst performance was observed, affording 70% of DFF.

Vanadyl phosphates, $VOPO_4 \cdot 2H_2O$ (VOP), have been investigated by Carlini *et al.* as heterogeneous catalysts. An HMF conversion of 84% with DFF selectivity of 97% were achieved after 6 h at 150 °C using dimethyl sulfoxide

(DMSO) as solvent and O_2 (0.1 MPa) as oxidant.[123] When VOP was supported on silica, an increase of the substrate conversion was observed (84%), while the DFF selectivity decreased (23%). This behaviour was attributed to the substrate degradation favored by the presence of hydroxyl groups at the silica surface. The authors also checked the effect of a partial substitution of VO^{3+} by different metal cations (Fe^{3+}, Cr^{3+}, Ga^{3+}, Mg^{2+}, Cu^{2+} and Pd^{2+}) at 0.1 MPa in DMF. The best activity (%C = 74%) and moderate selectivity (78%) were observed for MgVOP catalyst after 8 h, at 100 °C and 0.1 MPa of O_2. Nevertheless, it presented lower catalytic performance than the unmodified VOP.

Later on, Grasset's group also prepared vanadium phosphate oxide (VPO)-based heterogeneous catalysts by intercalation of alkyltrimethylammonium ions in $VOPO_4{\cdot}2H_2O$.[124] The authors concluded that the length of the intercalated alkyl ammonium chain did not significantly affect the catalytic performance, leading to 90% substrate conversion and product yields of 76%–87% when increasing the alkyl chain from C_{10} to C_{16}. $C_{14}VOPO_4$ was the most active (%C = 99%) and selective (82%) catalyst after 6 h of reaction at 110 °C in toluene using 1 atm of oxygen as oxidant. Under the same conditions, the non-intercalated VPO precursor only presented <7% DFF selectivity with 82% substrate conversion. Recycling studies for $C_{14}VOPO_4$ catalyst were undertaken and a decrease of the performance was observed after the second cycle, being attributed to some leaching of intercalated ammonium ions and to changes on the catalyst structure. Heterogeneous VPO catalysts with different V/P molar ratios have been prepared by Lai and co-authors and used for the selective oxidation of HMF to DFF.[125] The VPO catalyst with V/P molar ratio of 0.25 revealed the best catalytic performance, leading to a high DFF yield of 83.6% and quantitative HMF conversion after 10 h reaction, at 100 °C in DMSO under atmospheric pressure.

Navarro *et al.* immobilized vanadyl pyridine complexes onto poly(4-vinylpyridine) cross-linked with 33% divinylbenzene (PVP) and onto APTES-functionalized SBA-15 capped with hexamethyldisilazane.[126] PVP1-VO (2.4 wt% vanadium content) led to 77% HMF conversion and 100% selectivity to DFF after 4 h reaction, at 130 °C in triflurotoluene (TFT) using air as oxidant (1 MPa). This catalyst showed to be more active than other PVP-metal-based catalysts and the homogeneous $[VO(acac)_2]$ catalyst. Indeed, $[VO(acac)_2]$ presented significant lower activity (%C = 50%) and selectivity (57%) after 10 h, being mainly attributed to the strong Lewis acidity of vanadium when it was not coordinated to pyridine, which favored the formation of other side products. Nevertheless, 28% of metal leaching was observed after the first cycle. The metal leaching could be practically suppressed by preparing a similar type material in a longer reaction time, which led to a catalyst with higher vanadium loading (5.1 wt%, PVP2-VO catalyst). However, it presented lower catalytic activity (%C = 78% and %S = 98% after 24 h), which was assigned to the existence of less free pyridine moieties close to redox sites or to the inaccessibility of the internal metal active sites that are required for the activation of the proton abstraction of the -OH groups of HMF and, consequently, to favour the oxidative conversion to DFF. On the other hand, the SBA-15-based catalyst

(SBA-Py-VO) led to lower substrate conversion (50%) with 98% DFF selectivity after 24 h even in the presence of pyridine additives. The authors ascribed these results to the higher distance between the pyridine–VO active sites and to a possible inaccessibility of the active sites owing to the capping of the SBA-15 surface with trimethyl functionalities.

Xu and Zhang immobilized [$VO(acac)_2$] onto PANI and used this catalyst in the oxidation of HMF at 110 °C in 4-chlorotoluene, under atmospheric oxygen pressure.[127] A high HMF conversion of 99.2% was obtained after 12 h, yielding 86.2% of DFF. The catalyst was reused in five additional cycles, with only a slight loss of activity (%C = 85.3% and Yield = 77.2%) due to minor metal leaching.

Several types of heterogeneous VO^{2+} and Cu^{2+} supported catalysts have been reported for this type of reaction. For instance, Le *et al.* immobilized VO^{2+} and Cu^{2+} ions on sulfonated carbon prepared by carbonization of Amberlyst-15, a commercial ion-exchange resin.[128] The addition of copper in low concentrations to the vanadyl-based catalyst (V–Cu–CS) led to high DFF selectivity and good reusability. In particular, the catalyst with the composition 0.93%V–0.26%Cu–CS exhibited the best performance, with a near quantitative substrate conversion and 98% DFF selectivity after 4 h, at 140 °C under air (40 bar) using acetonitrile as solvent. Moreover, it was stable during three cycles of reusability without loss of activity or selectivity.

The excellent catalytic activity obtained by Ma and co-authors[129,130] when using an equimolar ratio of $Cu(NO_3)_2/VOSO_4$ inspired Liao *et al.* to design a novel type of heterogeneous catalyst which contained VO^{2+} and Cu^{2+} ions anchored onto APTES-modified silica-coated MNPs ($Fe_3O_4@SiO_2$).[131] The resulting hybrid material was tested as catalyst in the HMF oxidation reaction with oxygen. The best substrate conversion and selectivity to DFF, 98.7% and 87.4% respectively, were obtained after 1 h using a mixture of $Fe_3O_4@SiO_2–NH_2–VO^{2+}$ and $Fe_3O_4@SiO_2–NH_2–Cu^{2+}$ (co-catalyst), at 110 °C and 0.28 MPa of O_2 in toluene.

11.4.1.2 *One-pot Production of DFF from Biomass-derived Sugars*

In recent years, some efforts have been performed to replace HMF by sugar derivatives in order to directly prepare 2,5-DFF (fructose or glucose, Figure 11.9) using several metal-containing catalysts including vanadium-based catalysts.[20]

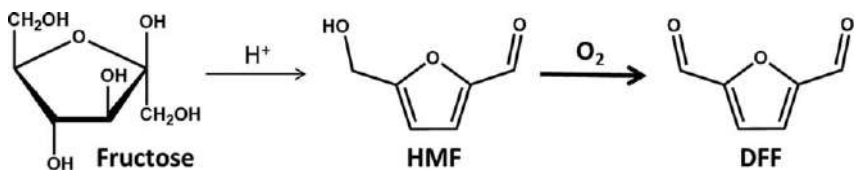

Figure 11.9 One-pot synthesis of DFF from fructose.

For instance, Chen *et al.* successfully combined an acid-based g-$C_3N_4(H^+)$ and a vanadium-doped g-C_3N_4 (V-g-C_3N_4) to promote the direct synthesis of DFF from fructose through a one-pot/two-step process consisting on: (i) g-$C_3N_4(H^+)$-promoted fructose dehydration followed by the (ii) V-g-C_3N_4-catalyzed aerobic oxidation of HMF to DFF.[117] An almost complete fructose conversion was achieved, leading to 63% DFF yield after 6 h, at 130 °C in DMSO with O_2 as oxidant. The reusability of V–g-C_3N_4 catalyst was evaluated in five consecutive cycles, leading to a slight decrease of the DFF yield, which was attributed to some V leaching. The authors also prepared a bifunctional catalyst – the protonated vanadium-doped g-C_3N_4 [V–g-$C_3N_4(H^+)$] – to promote the one-pot/one-step transformation of fructose into DFF at 130 °C in DMSO and atmospheric pressure of molecular oxygen. Although a high substrate conversion (>99%) was obtained after 6 h, the catalyst presented lower selectivity for DFF (up to 45%).

Later on, Cui and co-workers proposed a cascade two-step dehydration/oxidation catalysis of fructose for the one-pot synthesis of DFF at 140 °C under molecular oxygen, using DMSO as solvent. The one-pot method to convert fructose into DFF used the V_2O_5/ceramic catalyst (described in subsection 11.4.1.1) and sulphuric acid.[122] The fructose was firstly completely converted into HMF by dehydration reaction and, afterwards, converted into DFF with 68.4% yield after 2 h.

A direct synthesis of DFF from fructose *via* one-pot and one-step reaction has been proposed by Zhang *et al.,* using vanadium-containing silica beta zeolites (VSi-Beta).[132] The VSi-Beta catalyst (silicon to vanadium molar ratio of 50) demonstrated high activity at 130 °C in the presence of sulphuric acid and DMSO and using atmospheric oxygen as oxidant, affording a high yield of 86.3% of DFF with 100% of fructose conversion after 3 h. In another publication, the same authors reported the direct synthesis of DFF from fructose using vanadium oxide supported on high-silica MOR zeolites in the presence of hydrochloric acid and using atmospheric O_2 as oxidant, which afforded 96.0% of DFF yield after 4 h at 130 °C in DMSO, with good reusability.[133]

A bi-functional tungstic acid–vanadium oxide magnetic nanocatalyst (WO_3HO-VO(Salten)-SiO_2@Fe_3O_4), prepared by vanadium oxide complexation with Salten-Cl-SiO_2@Fe_3O_4 and subsequent tungstic acid functionalization, has been used as catalyst in the direct one-pot/two-step conversion of fructose into DFF. The catalyst yielded 82% HMF in the first step and 71% DFF after the addition of H_2O_2, in isopropanol at relatively low temperatures, after 16 h.[134] Tao *el al.* observed a quantitative conversion of fructose, with 40% yield of HMF intermediate and a final DFF yield of 34% after 10 h, using 5%Pd-V(3 : 2)-MIL-101 in DMSO at 140 °C and 1 bar O_2 pressure in the presence of sulphonic resin. The HMF intermediate could not be efficiently converted into DFF mainly due to active sites deactivation by humins formed during the reaction.[135]

Xu and Zhang reported the direct oxidation of fructose to DFF in DMSO/4-chlorotoluene solvent system (1 : 4 V/V) at 110 °C under atmospheric oxygen pressure by two different routes: (i) one-pot reaction simultaneously

catalyzed by two binary catalysts, Amberlyst-15 and PANI-supported [VO(acac)$_2$], with Amberlyst-15 being used as the acid catalyst for the dehydration of fructose into HMF and PANI–[VO(acac)$_2$] being used for the oxidation of HMF to DFF; (ii) in two consecutive steps, *i.e.*, production of HMF from the dehydration of fructose catalyzed by Amberlyst-15, followed by the Amberlyst-15 removal from the reaction medium and addition of PANI–[VO(acac)$_2$].[127] In method (i) the maximum DFF yield was 42.1% after 12 h, whereas method (ii) was faster and more efficient, leading to a higher DFF yield of 71.1% after the same reaction time.

11.5 Theoretical Modelling of Supported Vanadium Catalysts

While the latter half of the 20th century witnessed the development of many important theoretical methods, the first decade of the 21st century brought forth the manufactures and deployment of computational technologies capable of applying said methods to chemical systems large enough to represent solid-state catalysts.[136,137] In particular, Density Functional Theory (DFT) has become the method of choice for studying medium-sized systems. However, some situations commonly found in transition metal chemistry are known to be particularly challenging for DFT,[136,137] with additional difficulties being raised when modelling immobilized transition metal catalysts.[138] Such issues can be addressed by a number of diagnostic procedures[139] and (semi-)empirical corrections[140] at the expense of additional complexity and cost, thus limiting the size and complexity of the studied catalytic systems, and fostering the use of simplified models. Because of this, theoretical studies tend to apply increasingly accurate methods on simplified model chemistries, rather than attempting to model larger, more complex, ones. In the case of immobilized vanadium catalysts, the mechanistic aspects of the catalytic cycle are usually evaluated using non-immobilized analogues (*i.e.*, most omitting the supporting material),[141–143] as well as using simple alcohols (usually methanol) to model the Hydrogen Evolution Reaction (HER) from biomass.

Indeed, most theoretical works devoted to the chemistry of supported vanadium catalysts focus on the deposition of vanadium and/or vanadium oxides on top of metal, metal oxide and silica surfaces,[144–152] whereas the study of the mechanistic aspects of these catalysts has been mostly confined to the oxidative dehydrogenation of simple alcohols,[147,149,152–155] as models for the catalytic production of H_2 from biomass.

In 2018, Zang *et al.*[152] studied the suitability of silanol-decorated polyoxotungstates as models for describing an isolated vanadium atom deposited at silica surfaces (V@SiO_2), thus replacing the silica surface by a cluster of atoms. The DFT calculations in their work helped elucidating the spectroscopic data obtained from the synthesized species, and the results from both approaches pointed towards a good accordance between these vanadium-polyoxotungstate derivatives and the properties of V@SiO_2. The

application of vanadium-polyoxotungstate model as a surrogate for $V@SiO_2$ was further explored by Liu *et al.*[156] by studying the activation of H_2O_2 towards the formation of a vanadium-peroxo complex by DFT, using a divanadium–polyoxotungstate catalyst. Their results indicated the formation of a hydroperoxo intermediate *via* a vanadium-assisted proton transfer pathway with an energetic barrier of about 100 kJ mol^{-1}, followed by a water-assisted proton transfer to form the vanadium–peroxo complex responsible for the oxidation and epoxidation of alkene moieties.[142,143]

More recently, Sauer and co-workers have addressed the structure and stability of vanadium oxide oligomers on the $CeO_2(111)$ surface.[150] Their results highlighted that oligomeric VO_2 and V_2O_5 monolayer structures were thermodynamically more stable than taller cluster structures, indicating a preference for a complete two-dimensional coverage of the ceria support. Moreover, vanadium oxide showed a tendency to aggregate, with the formation of larger oligomers being preferred over the formation of isolated smaller monomers and oligomers over the ceria surface. This was in sharp contrast with the gas-phase behaviour of V_nO_m clusters, where a preference towards cage-like clusters was observed.[150] This behaviour was also distinct from that of V_nO_m on other surfaces, such as Al_2O_3/NiAl, where taller bilayer clusters were thermodynamically preferred.[157,158] Despite the surface effects leading to different topologies of the adsorbed vanadium oxide moieties, there is a core chemistry governing the coordination of vanadium. Indeed, the most common coordination number of vanadium in vanadium oxide is four, and six-member rings are the preferred structural motif, regardless of the cage-like, monolayer or bilayer preference dictated by the environment.[150] Indeed, both periodic (crystalline mesh) and cluster approaches have been applied to model the catalytic activity of supported vanadium oxides towards the oxidative dehydrogenation of alcohols.

As discussed by Paier,[137] early theoretical studies suggest that the oxidation of methanol at ceria-supported vanadium oxide sites requires the existence of oxygen defects, with a single VO_2 site on the $CeO_2(111)$ surface being the most promising active site. These results align with the observation that the adsorption of methanol on the pristine $CeO_2(111)$ surface is thermodynamically unfavourable. Moreover, the energy barriers predicted by DFT calculation are coherent with the kinetic data obtained from temperature-programmed spectroscopic experiments. Herrera and co-workers[149,159] later showed that monomeric vanadium oxide nanoclusters were the most active species involved in the partial oxidation of alcohols using TiO_2 supported vanadium oxide. In addition to this, DFT calculations carried under periodic boundary conditions showed that the formation enthalpy for oxygen defect formation was lower on monomeric vanadium oxide, suggesting that the alcohol oxidation turnover mostly took place on these smaller nanoclusters. A similar DFT approach was also used by Kropp *et al.*[153] to study the oxidative dehydrogenation of methanol on trimeric vanadium oxide clusters supported on the $CeO_2(111)$ surface. Their results showed that the adsorption of methanol at the VO_2 trimer was dissociative,

with the methoxide moiety binding to three vanadium atoms while the proton was transferred to a surface oxygen atom. The adsorption energy of 130 kJ mol^{-1} revealed that methanol bound less tightly to these trimeric VO_2 clusters (compared with their respective monomers)[160] and it was also close to the experimentally observed intrinsic energy barrier of 133 kJ mol^{-1}, being in good accordance with the fact that methanol adsorption was the rate-determining step for this reaction.

More recently, González-Navarrete *et al.*[154] approached the oxidative dehydrogenation of methanol using a remarkably small cluster model ($VTi_4H_5O_{10}$) to represent a reduced vanadium oxide on TiO_2. This eased exploring a large number of possible reaction pathways, showing good accordance with older studies carried out using larger VO/TiO_2 clusters. In general, the oxidative dehydrogenation was found to be more favourable on these reduced vanadium species than on vanadium(v) clusters. Although the full effect of the TiO_2 surface remained unexplored, this work suggested some common ground with the trimeric VO_2 catalysts studied by Kroop *et al.*,[153] as both systems preferred the dissociative adsorption of methanol.

11.6 Conclusions and Future Perspectives

Vanadium, like its neighbours titanium and chromium, is a first-row transition metal more abundant and cheaper than precious metals further down the Periodic Table. Such a simple, yet pragmatic, statement surely inspired the foray on the design of new vanadium-based catalysts. Throughout the decades, we have witnessed a tremendous effort on the development of recyclable and eco-sustainable supported oxidovanadium-based catalysts for a myriad of reactions with synthetic relevance, such as (ep)oxidation of alkenes, alcohols, aldehydes and ketones, oxidative amination, sulfoxidation, Strecker-type reactions, among others.

Although several vanadium-based heterogeneous catalysts offer competitive reactivity to that of their homogeneous congeners, a more comprehensive understanding of structure – activity relationship is still lacking. In fact, many reports with new vanadium-based heterogeneous catalysts often lack detailed mechanistic studies and reaction pathways are sometimes inferred from previous works. Moreover, the catalytic behaviour of immobilized complexes is generally more complex than that of their homogeneous counterparts and, in most cases, the reasons for the improved or decreased performance of the immobilized catalysts remain unclear. Features of the supporting solid materials, such as the effect of the particle size and textural properties, the preparation methods and the possible occurrence of side reactions or synergistic effects arising from for instance, surface groups, deserve a greater understanding, in order to avoid the establishment of general but still misleading concepts. Additionally, when a supported metal complex is recycled numerous times in a catalytic reaction, it is imperative to know whether the catalyst used in subsequent cycles remains the same as the one initially prepared, and if leaching is occurring.

Despite these challenges, heterogeneous vanadium catalysts continue to be a key component for many catalytic applications, and their deeper understanding will certainly pave the way to the discovery and development of new catalytic routes. To achieve this goal, the scientific community should thrive on the design of new heterogeneous catalysts with homogeneous functions, allowing for detailed correlations of mechanistic features between homogeneous and heterogeneous catalysts, make use of promising emerging solid matrices, namely COFs, expand the scope of vanadium catalysis in underexplored areas, such as hydrogenation and carbon–carbon bond formation. In parallel, advanced spectroscopic techniques should be applied, in order to gain deeper insights into the catalyst behavior under the catalytic reaction conditions.

Concerning the field of electrocatalysis, even though promising results have been achieved with vanadium-based ECs for water splitting, much is yet to be done. One of the major drawbacks of most vanadium-based ECs is the fact that they are still unable to match with noble metal-based ones in terms of electrochemical activities. Still, they are promising as lower cost alternatives for practical applications, which frequently demand a trade-off between activity and cost. The combination of experimental and theoretical calculations will also speed up the engineering of vanadium-based ECs towards the envisaged energy-related reactions as it may shed light on parameters such as electronic structures, energy barriers and active sites.

In the field of biomass valorization, the aerobic oxidation of HMF for the production of 2,5-DFF using heterogeneous catalysts is very promising from economic and environmental points of view, with great potential for applications on a biorefinery concept. The use of vanadium-based heterogeneous catalysts has become an attractive route due to their high activity and selectivity for DFF. However, most of the processes reported in the literature use organic solvents, including DMSO, DMF and toluene, lacking further development and optimization to replace these solvents by ''greener'' ones. Furthermore, in order to be industrially applicable, the catalyst should be stable for several catalytic cycles without loss of activity or DFF selectivity. Therefore, the development of robust catalysts is still a challenge and their use in continuous-flow reactors has not been well-explored yet. On the other hand, the one-pot production of DFF from sugar derivatives is an excellent alternative to overcome the high cost of HMF. In general, the product yield and selectivity using bifunctional or multiple catalysts for DFF production directly from fructose still need further improvements, including in the used solvents and reusability of the multiple catalysts in the two-step processes.

The field of theoretical modelling supported vanadium catalysts remains relatively unexplored despite the accomplishments over recent years. The tendency for improving the used models, together with the increased availability in computational power, allow us to postulate that novel theoretical insights on more complex systems will be forthcoming in the upcoming years.

Finally, it is worth mentioning that at present, most catalytic studies reported in the literature have only been performed at a laboratorial scale, with no information on reproducibility upon scale-up. Therefore, the fabrication

of vanadium-based hybrid catalysts on a medium-to-larger scale as well as the development of scaling-up experiments of the catalytic processes is urgently needed, so that their implementation in industry and commercialization may become a reality in the near future.

Abbreviations

AC	activated carbon
APTES	3-aminopropyltriethoxysilane
APTMS	3-aminopropyltrimethoxysilane
%C	substrate conversion
CC	carbon cloth
CFP	carbon fibre paper
CNT	carbon nanotubes
COF	covalent-organic framework
DFF	2,5-diformylfuran
DFT	Density Functional Theory
DMF	*N*,*N*-dimethylformamide
DMSO	dimethyl sulfoxide
EC	electrocatalyst
ee	enantiomeric excess
FDCA	2,5-furandicarboxylic acid
FTO	fluorine-doped tin oxide
GF	graphene
GO	graphene oxide
HER	hydrogen evolution reaction
HFCA	5-hydroxymethyl-2-furancarboxylic acid
HMF	5-hydroxymethylfurfural
HMS	hexagonal mesoporous silica
j	current density
j_0	exchange current density
MA	maleic anhydride
MIBK	methyl isobutyl ketone
MNPs	magnetic nanoparticles
MOF	metal–organic framework
MONF	microporous organic nanotube framework
MOR	mordenite zeolite
MWCNT	multi-walled carbon nanotubes
NCNT	N-doped carbon nanotubes
NF	nickel foam
NRGO	N-doped reduced graphene oxide
NS	graphitic carbon network nanosheets
OER	oxygen evolution reaction
PANI	polyaniline
PCH	porous clay heterostructure
PEG	polyethylene glycol

PMO	periodic mesoporous organosilica
PVP	poly(4-vinylpyridine)
%S	selectivity
SWCNT	single-walled carbon nanotube
TBHP	*tert*-butyl hydroperoxide
TFT	triflurotoluene
TMSCN	trimethylsilyl cyanide
TOF	turnover frequency
TS	Tafel slope
VC	vanadium carbide
VN	vanadium nitride
$[VO(acac)_2]$	oxidovanadium(IV) acetylacetonate
VOP	vanadyl phosphate
η_{10}	overpotential

Acknowledgements

This work was supported by National Funds through Fundação para a Ciência e a Tecnologia (FCT)/MCTES and co-supported by Fundo Europeu de Desenvolvimento Regional (FEDER) throughout COMPETE 2020 – Programa Operacional Competitividade e Internacionalização within the scope of the projects UIDB/50006/2020, PTDC/BII-BIO/30884/2017 and PTDC/QUI-QIN/30649/2017. CP thanks FCT for the FCT Investigator contract IF/01080/2015. DF and AP acknowledge FCT/MCTES for their work contracts (in the scope of the framework contract foreseen in the numbers 4, 5 and 6 of the article 23, of the Decree-Law 57/2016, of August 29, changed by Law 57/2017, of July 19) supported by national funds (OE).

References

1. R. R. Langeslay, D. M. Kaphan, C. L. Marshall, P. C. Stair, A. P. Sattelberger and M. Delferro, *Chem. Rev.*, 2019, **119**, 2128–2191.
2. H. Pellissier, *Coord. Chem. Rev.*, 2015, **284**, 93–110.
3. M. Sutradhar, L. M. D. R. S. Martins, M. F. C. Guedes and A. J. L. Pombeiro, *Coord. Chem. Rev.*, 2015, **301–302**, 200–239.
4. J. A. L. da Silva, J. J. R. F. da Silva and A. J. L. Pombeiro, *Coord. Chem. Rev.*, 2011, **255**, 2232–2248.
5. G. Licini, V. Conte, A. Coletti, M. Mba and C. Zonta, *Coord. Chem. Rev.*, 2011, **255**, 2345–2357.
6. K. C. Gupta and A. K. Sutar, *Coord. Chem. Rev.*, 2008, **252**, 1420–1450.
7. C. Bolm, *Coord. Chem. Rev.*, 2003, **237**, 245–256.
8. A. Butler, M. J. Clague and G. E. Meister, *Chem. Rev.*, 1994, **94**, 625–638.
9. J. Costa Pessoa and M. R. Maurya, *Inorg. Chim. Acta*, 2017, **455**, 415–428.
10. M. R. Maurya, A. Kumar and J. Costa Pessoa, *Coord. Chem. Rev.*, 2011, **255**, 2315–2344.

11. Q. H. Fan, Y. M. Li and A. S. C. Chan, *Chem. Rev.*, 2002, **102**, 3385–3466.
12. I. W. C. E. Arends and R. A. Sheldon, *Appl. Catal., A*, 2001, **212**, 175–187.
13. C. Freire, C. Pereira and S. Rebelo, in Green Oxidation Catalysis with Metal Complexes: From Bulk to Nano Recyclable Hybrid Catalysts, ed. J. Spivey and M. Gupta, *Catalysis*, Royal Society of Chemistry, **vol. 24**, 2012, pp. 116–203.
14. V. Polshettiwar, R. Luque, A. Fihri, H. Zhu, M. Bouhrara and J. M. Basset, *Chem. Rev.*, 2011, **111**, 3036–3075.
15. S. Shylesh, V. Schünemann and W. R. Thiel, *Angew. Chem., Int. Ed.*, 2010, **49**, 3428–3459.
16. *Chiral Catalyst Immobilization and Recycling*, ed. D. E. De Vos, I. F. J. Vankelecom and P. A. Jacobs, John Wiley & Sons, Ltd, Weinheim, Germany, 2000.
17. Y. Jiao, Y. Zheng, M. T. Jaroniec and S. Z. Qiao, *Chem. Soc. Rev.*, 2015, **44**, 2060–2086.
18. J. R. Galan-Mascaros, *ChemElectroChem*, 2015, **2**, 37–50.
19. M. Zeng and Y. G. Li, *J. Mater. Chem. A*, 2015, **3**, 14942–14962.
20. P. Pal and S. Saravanamurugan, *ChemSusChem*, 2019, **12**, 145–163.
21. P. V. Rathod, S. D. Nale and V. H. Jadhav, *ACS Sustainable Chem. Eng.*, 2017, **5**, 701–707.
22. Y. Yang, Y. Zhang, S. Hao, J. Guan, H. Ding, F. Shang, P. Qiu and Q. Kan, *Appl. Catal., A*, 2010, **381**, 274–281.
23. A. Di Giuseppe, C. Di Nicola, R. Pettinari, I. Ferino, D. Meloni, M. Passacantando and M. Crucianelli, *Catal. Sci. Technol.*, 2013, **3**, 1972–1984.
24. M. R. Maurya, P. Saini, A. Kumar and J. Costa Pessoa, *Eur. J. Inorg. Chem.*, 2011, 4846–4861.
25. S. Farahmand and M. Ghiaci, *Microporous Mesoporous Mater.*, 2019, **288**, 109560.
26. C. K. Modi, J. A. Chudasama, H. D. Nakum, D. K. Parmar and A. L. Patel, *J. Mol. Catal. A: Chem.*, 2014, **395**, 151–161.
27. H. P. Mungse, S. Verma, N. Kumar, B. Sain and O. P. Khatri, *J. Mater. Chem.*, 2012, **22**, 5427–5433.
28. S. Verma, R. B. N. Baig, M. N. Nadagouda and R. S. Varma, *ACS Sustainable Chem. Eng.*, 2016, **4**, 1094–1098.
29. M. Sutradhar, L. M. D. R. S. Martins, S. A. C. Carabineiro, M. F. C. Guedes da Silva, J. G. Buijnsters, J. L. Figueiredo and A. J. L. Pombeiro, *ChemCatChem*, 2016, **8**, 2254–2266.
30. S. Verma, M. Nandi, A. Modak, S. L. Jain and A. Bhaumik, *Adv. Synth. Catal.*, 2011, **353**, 1897–1902.
31. A. Rostami, O. Pourshiani, N. Darvishi and B. Atashkar, *C. R. Chim*, 2017, **20**, 435–439.
32. C. Pereira, A. R. Silva, A. P. Carvalho, J. Pires and C. Freire, *J. Mol. Catal. A: Chem.*, 2008, **283**, 5–14.
33. C. Pereira, K. Biernacki, S. L. H. Rebelo, A. L. Magalhães, A. P. Carvalho, J. Pires and C. Freire, *J. Mol. Catal. A: Chem.*, 2009, **312**, 53–64.

34. B. Jarrais, C. Pereira, A. R. Silva, A. P. Carvalho, J. Pires and C. Freire, *Polyhedron*, 2009, **28**, 994–1000.
35. S. Dorbes, C. Pereira, M. Andrade, D. Barros, A. M. Pereira, S. L. H. Rebelo, J. P. Araújo, J. Pires, A. P. Carvalho and C. Freire, *Microporous Mesoporous Mater.*, 2012, **160**, 67–74.
36. C. Pereira, A. M. Pereira, P. Quaresma, P. B. Tavares, E. Pereira, J. P. Araújo and C. Freire, *Dalton Trans.*, 2010, **39**, 2842–2854.
37. C. Pereira, J. F. Silva, A. M. Pereira, J. P. Araújo, G. Blanco, J. M. Pintado and C. Freire, *Catal. Sci. Technol.*, 2011, **1**, 784–793.
38. S. Verma, M. Aila, S. Kaul and S. L. Jain, *RSC Adv.*, 2014, **4**, 30598–30604.
39. M. Mirzaee, B. Bahramian, J. Gholizadeh, A. Feizi and R. Gholami, *Chem. Eng. J.*, 2017, **308**, 160–168.
40. M. Mirzaee, B. Bahramian and A. Amoli, *Appl. Organomet. Chem.*, 2015, **29**, 593–600.
41. M. Mirzaee, B. Bahramian and M. Mirebrahimi, *Chin. J. Catal.*, 2016, **37**, 1263–1274.
42. F. Farzaneh and Z. Asgharpour, *Appl. Organomet. Chem.*, 2019, **33**, 1–11.
43. J. P. Mehta, D. K. Parmar, H. D. Nakum, D. R. Godhani and N. C. Desai, *Microporous Mesoporous Mater.*, 2017, **247**, 198–207.
44. C. K. Modi, N. Solanki, R. Vithalani and D. Patel, *Appl. Organomet. Chem.*, 2018, **32**, 1–13.
45. P. Borah, X. Ma, K. T. Nguyen and Y. Zhao, *Angew. Chem., Int. Ed.*, 2012, **51**, 7756–7761.
46. L. Carneiro and A. R. Silva, *Catal. Sci. Technol.*, 2016, **6**, 8166–8176.
47. M. Salavati-Niasari, *Inorg. Chim. Acta*, 2009, **362**, 2159–2166.
48. C. Baleizão, B. Gigante, D. Das, M. Álvaro, H. Garcia and A. Corma, *J. Catal.*, 2004, **223**, 106–113.
49. C. Baleizão, B. Gigante, H. Garcia and A. Corma, *J. Catal.*, 2003, **215**, 199–207.
50. C. Baleizão, B. Gigante, H. Garcia and A. Corma, *J. Catal.*, 2004, **221**, 77–84.
51. M. A. Esteves, B. Gigante, C. Santos, A. M. Guerreiro and C. Baleizão, *Catal. Today*, 2013, **218–219**, 65–69.
52. G. Gao, J. Gao, L. Lu, W. Zhou and M. He, *J. Porous Mater.*, 2008, **15**, 127–132.
53. T. Ben Zid, I. Khedher, Z. Ksibi and J. M. Fraile, *J. Porous Mater.*, 2016, **23**, 507–516.
54. N. Noori, M. Nikoorazm and A. Ghorbani-Choghamarani, *Microporous Mesoporous Mater.*, 2016, **234**, 166–175.
55. C. Shen, J. Qiao, L. Zhao, K. Zheng, J. Jin and P. Zhang, *Catal. Commun.*, 2017, **92**, 114–118.
56. H. Veisi, A. Rashtiani, A. Rostami, M. Shirinbayan and S. Hemmati, *Polyhedron*, 2019, **157**, 358–366.
57. M. Tada, N. Kojima, Y. Izumi, T. Taniike and Y. Iwasawa, *J. Phys. Chem. B*, 2005, **109**, 9905–9916.

58. M. R. Maurya, U. Kumar, I. Correia, P. Adão and J. C. Pessoa, *Eur. J. Inorg. Chem.*, 2008, 577–587.
59. M. R. Maurya, A. Arya, U. Kumar, A. Kumar, F. Avecilla and J. C. Pessoa, *J. Chem. Soc., Dalton Trans.*, 2009, 9555–9566.
60. M. R. Maurya, A. Arya, A. Kumar, M. L. Kuznetsov, F. Avecilla and J. C. Pessoa, *Inorg. Chem.*, 2010, **49**, 6586–6600.
61. W. Xi, Y. Liu, Q. Xia, Z. Li and Y. Cui, *Chem. – Eur. J.*, 2015, **21**, 12581–12585.
62. H. Vardhan, G. Verma, S. Ramani, A. Nafady, A. M. Al-Enizi, Y. Pan, Z. Yang, H. Yang and S. Ma, *ACS Appl. Mater. Interfaces*, 2019, **11**, 3070–3079.
63. N. D. McNamara, G. T. Neumann, E. T. Masko, J. A. Urban and J. C. Hicks, *J. Catal.*, 2013, **305**, 217–226.
64. H. Zhang, M. Zhou, L. Xiong, Z. He, T. Wang, Y. Xu and K. Huang, *Microporous Mesoporous Mater.*, 2018, **255**, 103–109.
65. R. J. Comito, Z. Wu, G. Zhang, J. A. Lawrence, M. D. Korzyński, J. A. Kehl, J. T. Miller and M. Dincă, *Angew. Chem., Int. Ed.*, 2018, **57**, 8135–8139.
66. N. T. Suen, S. F. Hung, Q. Quan, N. Zhang, Y. J. Xu and H. M. Chen, *Chem. Soc. Rev.*, 2017, **46**, 337–365.
67. C. Freire, D. M. Fernandes, M. Nunes and V. K. Abdelkader, *ChemCatChem*, 2018, **10**, 1703–1730.
68. K. Zeng and D. K. Zhang, *Prog. Energy Combust. Sci.*, 2010, **36**, 307–326.
69. D. J. Chen, C. Chen, Z. M. Baiyee, Z. P. Shao and F. Ciucci, *Chem. Rev.*, 2015, **115**, 9869–9921.
70. Y. Zhong, X. H. Xia, F. Shi, J. Y. Zhan, J. P. Tu and H. J. Fan, *Adv. Sci.*, 2016, **3**, 28.
71. A. Karmakar and S. K. Srivastava, *J. Mater. Chem. A*, 2019, **7**, 15054–15061.
72. Y. Yu, P. Li, X. F. Wang, W. Y. Gao, Z. X. Shen, Y. N. Zhu, S. L. Yang, W. G. Song and K. J. Ding, *Nanoscale*, 2016, **8**, 10731–10738.
73. X. Shang, J. Q. Chi, S. S. Lu, B. Dong, Z. Z. Liu, K. L. Yan, W. K. Gao, Y. M. Chai and C. G. Liu, *Electrochim. Acta*, 2017, **256**, 100–109.
74. X. Shang, J. Q. Chi, Z. Z. Liu, B. Dong, K. L. Yan, W. K. Gao, J. B. Zeng, Y. M. Chai and C. G. Liu, *Electrochim. Acta*, 2017, **256**, 241–251.
75. X. Peng, L. S. Hu, L. Wang, X. M. Zhang, J. J. Fu, K. F. Huo, L. Y. S. Lee, K. Y. Wong and P. K. Chu, *Nano Energy*, 2016, **26**, 603–609.
76. L. S. Peng, J. J. Shen, L. Zhang, Y. Wang, R. Xiang, J. Li, L. Li and Z. D. Wei, *J. Mater. Chem. A*, 2017, **5**, 23028–23034.
77. L. Y. Cao, N. Zhang, L. L. Feng, J. F. Huang, Y. Q. Feng, W. B. Li, D. Yang and Q. Q. Liu, *Nanoscale*, 2018, **10**, 14272–14279.
78. W. Fu, Y. Wang, H. Zhang, M. He, L. Fang, X. Yang, Z. Huang, J. Li, X. Gu and Y. Wang, *J. Catal.*, 2019, **369**, 47–53.
79. B. B. Wei, G. S. Tang, H. F. Liang, Z. B. Qi, D. F. Zhang, W. S. Hu, H. Shen and Z. C. Wang, *Electrochem. Commun.*, 2018, **93**, 166–170.

80. S. Dutta, A. Indra, Y. Feng, H. Han and T. Song, *Appl. Catal., B*, 2019, **241**, 521–527.
81. H. Yang, Y. Hu, D. Huang, T. Xiong, M. Li, M. S. Balogun and Y. Tong, *Mater. Today Chem.*, 2019, **11**, 1–7.
82. N. Zhang, L. Y. Cao, L. L. Feng, J. F. Huang, K. Kajiyoshi, C. Y. Li, Q. Q. Liu, D. Yang and J. J. He, *Nanoscale*, 2019, **11**, 11542–11549.
83. K. Chakrapani, G. Bendt, H. Hajiyani, T. Lunkenbein, M. T. Greiner, L. Masliuk, S. Salamon, J. Landers, R. Schlogl, H. Wende, R. Pentcheva, S. Schulz and M. Behrens, *ACS Catal.*, 2018, **8**, 1259–1267.
84. K. Fan, Y. F. Ji, H. Y. Zou, J. F. Zhang, B. C. Zhu, H. Chen, Q. Daniel, Y. Luo, J. G. Yu and L. C. Sun, *Angew. Chem., Int. Ed.*, 2017, **56**, 3289–3293.
85. H. H. Shi, H. F. Liang, F. W. Ming and Z. C. Wang, *Angew. Chem., Int. Ed.*, 2017, **56**, 573–577.
86. F. C. Shen, Y. Wang, Y. J. Tang, S. L. Li, Y. R. Wang, L. Z. Dong, Y. F. Li, Y. Xu and Y. Q. Lan, *ACS Energy Lett.*, 2017, **2**, 1327–1333.
87. G. M. Thorat, H. S. Jadhav, A. Roy, W. J. Chung and J. G. Seo, *ACS Sustainable Chem. Eng.*, 2018, **6**, 16255–16266.
88. L. Liardet and X. L. Hu, *ACS Catal.*, 2018, **8**, 644–650.
89. M. F. Hao, M. S. Xiao, L. H. Qian and Y. Q. Miao, *Front. Chem. Sci. Eng.*, 2018, **12**, 409–416.
90. M. A. Ehsan, A. S. Hakeem, M. Sharif and A. Rehman, *ACS Omega*, 2019, **4**, 12671–12679.
91. X. W. Zhong, J. Tang, J. W. Wang, M. M. Shao, J. W. Chai, S. P. Wang, M. Yang, Y. Yang, N. Wang, S. J. Wang, B. M. Xu and H. Pan, *Electrochim. Acta*, 2018, **269**, 55–61.
92. J. Jiang, F. F. Sun, S. Zhou, W. Hu, H. Zhang, J. C. Dong, Z. Jiang, J. J. Zhao, J. F. Li, W. S. Yan and M. Wang, *Nat. Commun.*, 2018, **9**, 12.
93. J. L. Gunjakar, B. Hou, A. I. Inamdar, S. M. Pawar, A. T. A. Ahmed, H. S. Chavan, J. Kim, S. Cho, S. Lee, Y. Jo, S. J. Hwang, T. G. Kim, S. Cha, H. Kim and H. Im, *Small*, 2018, **14**, 10.
94. K. Nejati, A. R. Akbari, S. Davari, K. Asadpour-Zeynali and Z. Rezvani, *New J. Chem.*, 2018, **42**, 2889–2895.
95. Y. C. Ji, Y. Ma, R. J. Liu, Y. J. Ma, K. C. Cao, U. Kaiser, A. Varzi, Y. F. Song, S. Passerini and C. Streb, *J. Mater. Chem. A*, 2019, **7**, 13096–13102.
96. Y. Liu, Y. Nie, X. Lu, X. Zhang, H. He, F. Pan, L. Zhou, X. Liu, X. Ji and S. Zhang, *Green Chem.*, 2019, **21**, 3499–3535.
97. S. Zhou, L. Zhou, Y. Zhang, J. Sun, J. Wen and Y. Yuan, *J. Mater. Chem. A*, 2019, **7**, 4217–4229.
98. W. Chu, J. Luo, S. Paul, Y. Liu, A. Khodakov and E. Bordes, *Catal. Today*, 2017, **298**, 145–157.
99. S. Bagheri and N. M. Julkapli, *Int. J. Hydrogen Energy*, 2017, **42**, 2116–2126.
100. S. K. Hanson and R. T. Baker, *Acc. Chem. Res.*, 2015, **48**, 2037–2048.
101. S. Lotfi, D. C. Boffito and G. S. Patience, *ChemSusChem*, 2015, **8**, 3424–3432.

102. S. Lotfi, D. C. Boffito and G. S. Patience, *React. Chem. Eng.*, 2016, **1**, 397–408.
103. C. Diaz-Urrutia, B. B. Hurisso, P. M. P. Gauthier, B. Sedai, R. D. Singer and R. T. Baker, *J. Mol. Catal. A: Chem.*, 2016, **423**, 414–422.
104. W. Zhang, G. Innocenti, P. Oulego, V. Gitis, H. H. Wu, B. Ensing, F. Cavani, G. Rothenberg and N. R. Shiju, *ACS Catal.*, 2018, **8**, 2365–2374.
105. W. Zhang, B. Ensing, G. Rothenberg and N. R. Shiju, *Green Chem.*, 2018, **20**, 1866–1873.
106. G. Lv, C. Chen, B. Lu, J. Li, Y. Yang, C. Chen, T. Deng, Y. Zhu and X. Hou, *RSC Adv.*, 2016, **6**, 101277–101282.
107. X. K. Li, J. G. Ko and Y. G. Zhang, *ChemSusChem*, 2018, **11**, 612–618.
108. X. K. Li, B. Ho and Y. G. Zhang, *Green Chem.*, 2016, **18**, 2976–2980.
109. X. Li, P. Jia and T. Wang, *ACS Catal.*, 2016, **6**, 7621–7640.
110. Z. Du, J. Ma, F. Wang, J. Liu and J. Xu, *Green Chem.*, 2011, **13**, 554–557.
111. X. Tong, Y. Ma and Y. Li, *Appl. Catal., A*, 2010, **385**, 1–13.
112. C. Moreau, R. Durand, C. Pourcheron and D. Tichit, in *Studies in Surface Science and Catalysis*, ed. H. U. Blaser, A. Baiker and R. Prins, Elsevier, **vol. 108**, 1997, pp. 399–406.
113. J. Nie and H. Liu, *Pure Appl. Chem.*, 2012, **84**, 765–777.
114. I. Sadaba, Y. Y. Gorbanev, S. Kegnaes, S. S. R. Putluru, R. W. Berg and A. Riisager, *ChemCatChem*, 2013, **5**, 284–293.
115. W. Zhang, J. Y. Xie, W. Hou, Y. Q. Liu, Y. Zhou and J. Wang, *ACS Appl. Mater. Interfaces*, 2016, **8**, 23122–23132.
116. C. A. Antonyraj, B. Kim, Y. Kim, S. Shin, K. Y. Lee, I. Kim and J. K. Cho, *Catal. Commun.*, 2014, **57**, 64–68.
117. J. Z. Chen, Y. Y. Guo, J. Y. Chen, L. Song and L. M. Chen, *ChemCatChem*, 2014, **6**, 3174–3181.
118. Y. Y. Guo and J. Z. Chen, *ChemPlusChem*, 2015, **80**, 1760–1768.
119. J. Zhao, X. P. Chen, Y. H. Du, Y. H. Yang and J. M. Lee, *Appl. Catal., A*, 2018, **568**, 16–22.
120. L. F. Liao, Y. Liu and S. B. Wu, *J. Biobased Mater. Bioenergy*, 2018, **12**, 321–329.
121. Y. B. Yan, K. X. Li, J. Zhao, W. Z. Cai, Y. H. Yang and J. M. Lee, *Appl. Catal., B*, 2017, **207**, 358–365.
122. M. Cui, R. L. Huang, W. Qi, R. X. Su and Z. M. He, *RSC Adv.*, 2017, **7**, 7560–7566.
123. C. Carlini, P. Patrono, A. M. R. Galletti, G. Sbrana and V. Zima, *Appl. Catal. A Gen.*, 2005, **289**, 197–204.
124. F. L. Grasset, B. Katryniok, S. Paul, V. Nardello-Rataj, M. Pera-Titus, J.-M. Clacens, F. De Campo and F. Dumeignil, *RSC Adv.*, 2013, **3**, 9942–9948.
125. J. H. Lai, K. Liu, S. L. Zhou, D. Zhang, X. X. Liu, Q. Xu and D. L. Yin, *RSC Adv.*, 2019, **9**, 14242–14246.

126. O. C. Navarro, A. C. Canós and S. I. Chornet, *Top. Catal.*, 2009, **52**, 304–314.
127. F. Xu and Z. Zhang, *ChemCatChem*, 2015, **7**, 1470–1477.
128. N. T. Le, P. Lakshmanan, K. Cho, Y. Han and H. Kim, *Appl. Catal., A*, 2013, **464**, 305–312.
129. J. Ma, Z. Du, J. Xu, Q. Chu and Y. Pang, *ChemSusChem*, 2011, **4**, 51–54.
130. X. Jia, J. Ma, M. Wang, Z. Du, F. Lu, F. Wang and J. Xu, *Appl. Catal., A*, 2014, **482**, 231–236.
131. L. Liao, Y. Liu, Z. Li, J. Zhuang, Y. Zhou and S. Chen, *RSC Adv.*, 2016, **6**, 94976–94988.
132. W. Zhang, W. Hou, T. S. Meng, W. X. Zhuang, J. Y. Xie, Y. Zhou and J. Wang, *Catal. Sci. Technol.*, 2017, **7**, 6050–6058.
133. W. Zhang, T. S. Meng, J. J. Tang, W. X. Zhuang, Y. Zhou and J. Wang, *ACS Sustainable Chem. Eng.*, 2017, **5**, 10029–10037.
134. N. Mittal, G. M. Nisola, L. B. Malihan, J. G. Seo, H. Kim, S.-P. Lee and W.-J. Chung, *RSC Adv.*, 2016, **6**, 25678–25688.
135. F. Tao, Y. Cui, P. Yang and Y. Gong, *Russ. J. Phys. Chem. A*, 2014, **88**, 1091–1096.
136. F. Neese, *Coord. Chem. Rev.*, 2009, **253**, 526–563.
137. J. Paier, *Catal. Lett.*, 2016, **146**, 861–885.
138. F. Teixeira and M. N. D. S. Cordeiro, *Catalysts*, 2017, **7**, 2.
139. C. A. Bauer, A. Hansen and S. Grimme, *Chem. – Eur. J.*, 2017, **23**, 6150–6164.
140. A. D. Laurent and D. Jacquemin, *Int. J. Quantum Chem.*, 2013, **113**, 2019–2039.
141. M. Vandichel, K. Leus, P. Van der Voort, M. Waroquier and V. Van Speybroeck, *J. Catal.*, 2012, **294**, 1–18.
142. F. Teixeira, R. Mosquera, A. Melo, C. Freire and M. N. D. S. Cordeiro, *Inorg. Chem.*, 2016, **55**, 3653–3662.
143. F. Teixeira, R. Mosquera, A. Melo, C. Freire and M. N. D. S. Cordeiro, *Inorg. Chem.*, 2017, **56**, 2124–2134.
144. J. Sauer, M. Pritzsche and J. Döbler, *J. Phys. Chem. C*, 2014, **118**, 29159–29163.
145. M. Lankelma, J. de Boer, M. Ferbinteanu, A. L. D. Ramos, R. Tanasa, G. Rothenberg and S. Tanase, *Dalton Trans.*, 2015, **44**, 11380–11387.
146. B. J. H. Sheppard, M. P. Shaver and J. K. Pearson, *J. Phys. Chem. A*, 2015, **119**, 8537–8546.
147. X.-P. Wu and X.-Q. Gong, *J. Am. Chem. Soc.*, 2015, **137**, 13228–13231.
148. A. K. Agegnehu, C.-J. Pan, M.-C. Tsai, J. Rick, W.-N. Su, J.-F. Lee and B.-J. Hwang, *Int. J. Hydrogen Energy*, 2016, **41**, 6752–6762.
149. D. Yun, Y. Song and J. E. Herrera, *ChemCatChem*, 2017, **9**, 3655–3669.
150. C. Penschke, J. Paier and J. Sauer, *J. Phys. Chem. C*, 2018, **122**, 9101–9110.
151. Y.-X. Xu, X.-R. Cao, L.-H. Xu, J.-H. Zhang, S.-Q. Wu and Z.-Z. Zhu, *Nanoscale Res. Lett.*, 2018, **13**, 199.

152. T. Zhang, A. Solé-Daura, S. Hostachy, S. Blanchard, C. Paris, Y. Li, J. J. Carbó, J. M. Poblet, A. Proust and G. Guillemot, *J. Am. Chem. Soc.*, 2018, **140**, 14903–14914.
153. T. Kropp, J. Paier and J. Sauer, *J. Catal.*, 2017, **352**, 382–387.
154. P. González-Navarrete, J. Andrés and M. Calatayud, *J. Phys. Chem. A*, 2018, **122**, 1104–1113.
155. V. V. Kaichev, Y. A. Chesalov, A. A. Saraev and A. M. Tsapina, *J. Phys. Chem. C*, 2019, **123**, 19668–19680.
156. C. Liu and Y. Chu, *J. Mol. Graphics Modell.*, 2018, **85**, 56–67.
157. V. Brázdová, M. V. Ganduglia-Pirovano and J. Sauer, *J. Phys. Chem. B*, 2005, **109**, 394–400.
158. V. Brázdová, M. V. Ganduglia-Pirovano and J. Sauer, *J. Phys. Chem. C*, 2010, **114**, 4983–4994.
159. D. Yun, Y. Wang and J. E. Herrera, *ACS Catal.*, 2018, **8**, 4681–4693.
160. T. Kropp, J. Paier and J. Sauer, *J. Am. Chem. Soc.*, 2014, **136**, 14616–14625.
161. B. Wei, G. Tang, H. Liang, Z. Qi, D. Zhang, W. Hu, H. Shen and Z. Wang, *Electrochem. Commun.*, 2018, **93**, 166–170.
162. F. H. Xu and Z. H. Zhang, *ChemCatChem*, 2015, **7**, 1470–1477.
163. C. L. Liu, L. F. Liao, Z. Y. Li, Y. Liu, S. B. Wu and J. P. Zhuang, *J. Biobased Mater. Bioenergy*, 2017, **11**, 414–423.

CHAPTER 12

Carbon-supported Vanadium Catalysis

SÓNIA A. C. CARABINEIRO,*[a,b] LUÍSA M. D. R. S. MARTINS[a] AND MANAS SUTRADHAR[a]

[a] Centro de Química Estrutural, Instituto Superior Técnico, Universidade de Lisboa, Portugal; [b] LAQV-REQUIMTE, Departamento de Química, Faculdade de Ciências e Tecnologia, Universidade NOVA de Lisboa, Largo da Torre, 2829-516 Caparica, Portugal
*Emails: sonia.carabineiro@tecnico.ulisboa.pt; sonia.carabineiro@fct.unl.pt

12.1 Introduction

The remarkable catalytic activities of vanadium complexes in solution are already described in Chapters 1 to 10 and also reported in several reviews on the topic.[1,2] It is well-known that homogeneous catalysts have high activity, enantioselectivity and well-characterised structures, but heterogeneous systems show longer lifetimes, easier separation of the catalyst from the products, possible catalyst recycling and adaptation to continuous flow processes. The possibility to combine the remarkable properties of homogeneous catalysts with the well-known advantages of heterogeneous systems by anchoring soluble complexes on porous materials, is therefore a is a very promising interface area of research.[3,4]

Chapter 11 dealt with vanadium complexes anchored on several kinds of supports. The present chapter deals with vanadium complexes heterogenised on a particular type of supports – carbon materials. These can have advantages, since their texture and surface chemistry can easily be tuned to fit the desired applications.[5–10] Several carbon supports, such as activated carbon, mesoporous

Catalysis Series No. 41
Vanadium Catalysis
Edited by Manas Sutradhar, José Armando L. da Silva and Armando J. L. Pombeiro

Published by the Royal Society of Chemistry, www.rsc.org

carbon xerogels, carbon nanotubes, graphenes, nanodiamonds, *etc.*, have been used. Such use, although promising, is still scarce, as reported in this chapter.

Much more work has been performed on vanadium oxides supported on carbon materials for catalysis for several reactions, such as selective catalytic reduction of nitrogen oxides and selective oxidation reactions, among others. This chapter also briefly reviews this topic.

12.2 Heterogenisation of Vanadium Complexes on Carbon Materials

Although homogenous vanadium complexes have been extensively used in catalysis (see Chapters 1 to 10) their anchorage on carbon materials is still not very abundant. A Web of Science search on the topic, performed when this chapter was being written (October 2019), revealed only around 20 articles dealing with different carbon supports. Such works are briefly summarised below.

12.2.1 2D Graphene Materials

Graphene is a two dimensional (2D) layer of sp^2 hybridised carbon atoms produced from graphite (a low-cost material)[11] from which several types of carbon nanostructures can be obtained, as shown in Scheme 12.1. Ideally, graphene should be a single-layer material, but graphene samples with two or more layers are quite common (like graphene nanoplatelets). Graphene oxide is an oxidised form of graphene with various oxygen-containing functionalities such as epoxide, carboxyl and hydroxy groups. On the other hand, carbon nanotubes are 3D structures derived from graphene and are discussed in the next section (12.2.2). In this section, only 2D supports will be referred to.

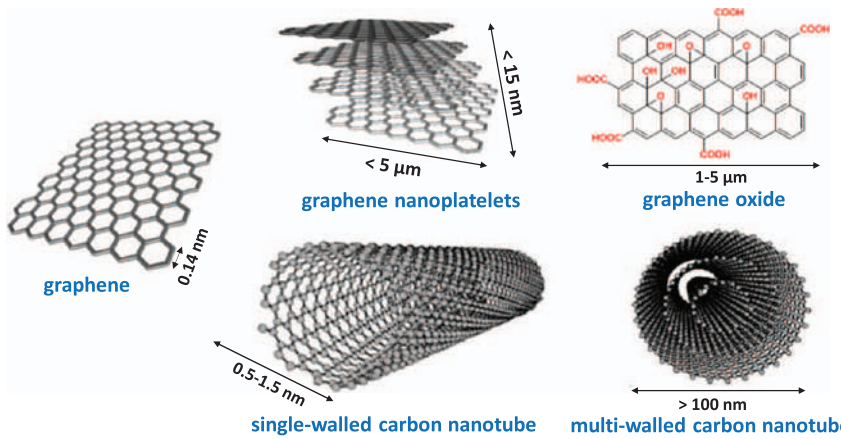

Scheme 12.1 Simplified models of several carbon nanostructures derived from graphene.
Adapted from ref. 12 with permission from John Wiley and Sons, © 2018 Wiley–VCH Verlag GmbH & Co. KGaA, Weinheim.

Mungse *et al.*,[13] bounded an oxo-vanadium Schiff base on graphene nanosheets and used it for the oxidation of various primary and secondary alcohols to carbonyl compounds using *tert*-butylhydroperoxide (TBHP) as oxidant (Scheme 12.2). The immobilised complex was found to be highly efficient and showed catalytic reactivity comparable to its homogenous analogue, with the added benefits of easy recovery. Aromatic alcohols were more reactive compared to aliphatic or alicyclic secondary alcohols. 1,2-diols gave the corresponding 1,2-diketones in high yields. Non-activated alcohols, such as borneol and l-menthol, were also oxidised in high yields. The graphene-bound oxo-vanadium Schiff base was successfully reused for several runs of benzhydrol oxidation without significant loss in its catalytic activity.

Li *et al.*,[14] used an oxovanadium(IV) salen complex (also a Schiff base) grafted onto amino-modified graphene oxide (Scheme 12.3) in the epoxidation of styrene (Scheme 12.4), using acetonitrile as solvent and air as oxidant. The heterogenised catalyst showed 88% conversion of styrene after 8 h with a turnover frequency (TOF) of 186.4 h^{-1} and 21% selectivity for styrene oxide, being more active than its homogeneous analogue (TOF 63.4 h^{-1}, 69% conversion). The supported catalyst probably isolates the active species and prevents the formation of μ-oxo, μ-peroxo dimeric or other polymeric species.

The same authors also studied this reaction with the same complex immobilised onto carbon-coated Fe_3O_4 nanoparticles hybridised with graphene sheets,[15] obtaining an inferior TOF value of 149.4 h^{-1} (72% styrene conversion).

Su *et al.*,[16] covalently grafted another oxovanadium(II) Schiff base complex (vanadyl acetylacetonate, a typical compound, shown in Scheme 12.5) onto graphene oxide, previously functionalised with 3-aminopropyltriethoxysilane and used the material in the epoxidation of styrene, using air as the oxidant. 70% conversion with 55% selectivity to epoxide at 80 °C and 8 h reaction was

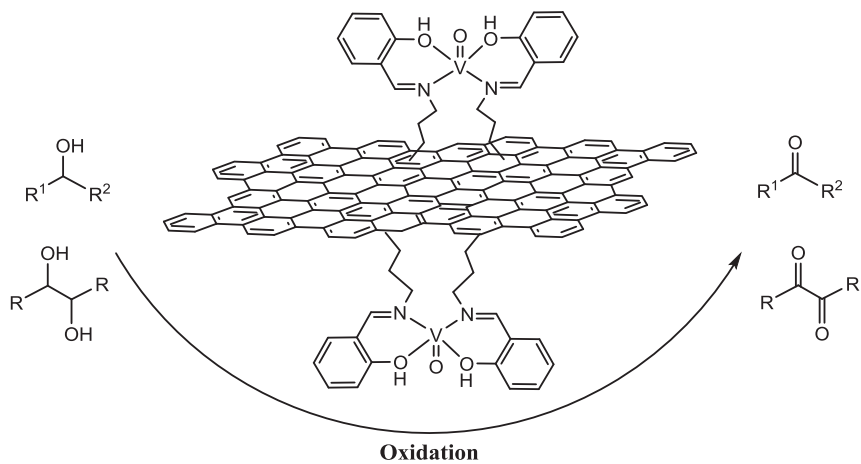

Scheme 12.2 Oxidation of alcohols catalysed by an oxo-vanadium Schiff base bound to graphene nanosheets.
Adapted from ref. 13 with permission from the Royal Society of Chemistry.

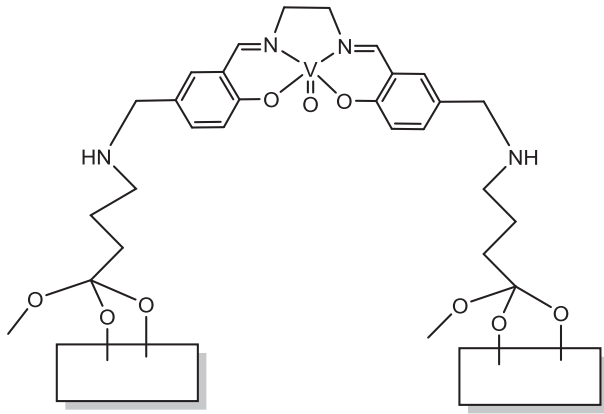

Scheme 12.3 VO(IV) complex immobilised on graphene oxide. Adapted from ref. 14 with permission from the Royal Society of Chemistry.

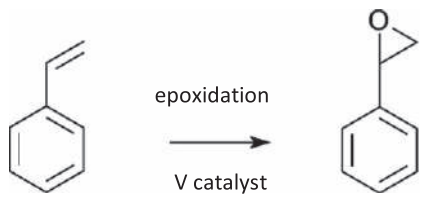

Scheme 12.4 Epoxidation of styrene to styrene oxide.

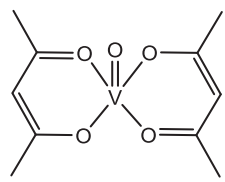

Vanadyloxo acetyleacetonate

Scheme 12.5 Vanadyl acetylacetonate complex.

achieved, which was higher than the obtained with the homogenous analogue (45% conversion, 53% selectivity, under the same conditions). The recycling results of the heterogeneous catalyst showed good recoverability without significant loss of activity and selectivity within four successive runs (~64% conversion, ~50% selectivity).

Another oxo-vanadium Schiff base was also covalently immobilised onto amino-functionalised graphene oxide (Scheme 12.6), also using 3-aminopropyltriethoxysilane as a coupler, by Verma *et al.*[17] The catalyst was efficient and selective for the epoxidation of fatty acids and esters using TBHP as an oxidant, showing higher catalytic efficiency than the homogeneous analogue. The recycling experiments showed that the material was able to maintain high activity and selectivity even after six cycles of use.

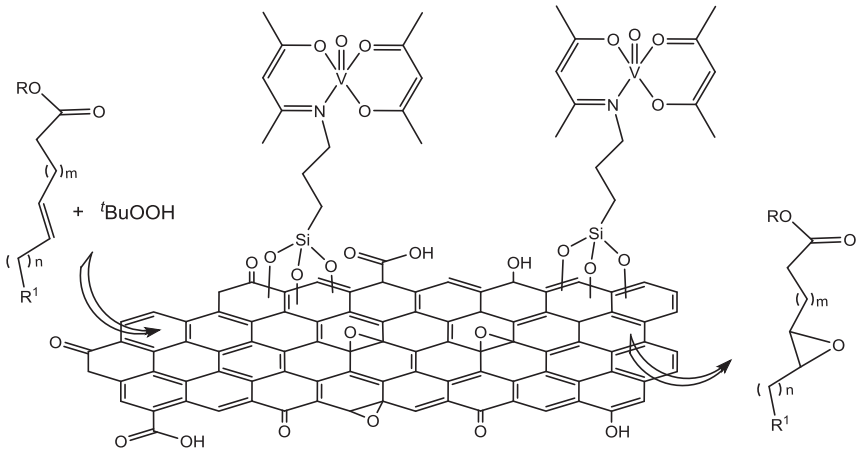

Scheme 12.6 Epoxidation of fatty acids and esters using an oxo-vanadium Schiff base immobilised on functionalised graphene oxide.
Adapted from ref. 17 with permission from the Royal Society of Chemistry.

In all these studies it was shown that the graphitic structures were well preserved after immobilisation of the V complexes and that anchorage was successful.

12.2.2 Carbon Nanotubes

Carbon nanotubes (CNT) are cylindrical molecules consisting of rolled-up sheets of graphene (Scheme 12.1). They can be single-walled (SWCNT) with a diameter of less than 1 nm, or multi-walled (MWCNT) and consisting of several concentrically interlinked nanotubes, with diameters reaching more than 100 nm.[12] Their length can reach several micrometres or even millimetres. Like their building block, graphene, CNTs are chemically bonded with sp^2 bonds, an extremely strong form of molecular interaction. This feature, combined with CNT's natural inclination to rope together *via* van der Waals forces, provide the opportunity to develop unique materials.

Salimi *et al.*,[18] immobilised a vanadyl tetradentate Schiff base complex (bis-salicylaldehyde-ethylenediimine oxovanadium(IV), shown in Scheme 12.7) on MWCNTs to be used as electron-transfer mediator onto a glassy carbon-electrode surface. The modified electrodes showed excellent catalytic activity towards the reduction of BrO_3^-, IO_4^-, IO_3^- and NO_2^- ions at unusually positive potential in acidic solution.

Salavati-Niasari *et al.*, synthesised a vanadium-containing polyphosphomolybdate ($Na_5[PV_2Mo_{10}O_{40}]\cdot 14H_2O$).[20,21] The Keggin-type polyoxometalate (PVMo) was supported on MWCNT (yielding a PVMo-CNT composite prepared by a one-step solid-state reaction) and used as a catalyst for the epoxidation of olefins with hydrogen peroxide (Scheme 12.8).[21] The use of ultrasonic (US) irradiation increased the conversions and

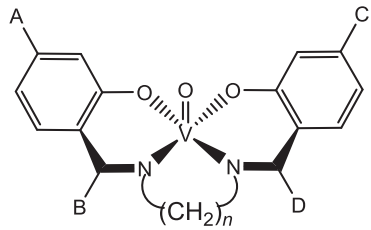

A=C=H, B=D= CH_3, n=2

Scheme 12.7 Bis-salicylaldehyde-ethylenediimine oxovanadium(IV) used by Salimi *et al.*[18,19]

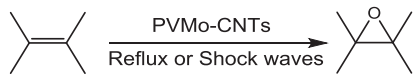

Scheme 12.8 Epoxidation of olefins with hydrogen peroxide using PvMo as catalyst. Adapted from ref. 21 with permission from Elsevier, Copyright 2010.

reduced the reaction times. The best result was obtained for cyclooctene epoxidation with 400 W US irradiation (95% conversion, 40 min reaction time, 100% epoxide selectivity, TOF = 402.6 h^{-1}), being much higher than in reflux conditions (80% conversion, 10 h reaction time, 100% epoxide selectivity, TOF = 22.4 h^{-1}) or with homogeneous PVMo (78% conversion, 20 h reaction time, 96% epoxide selectivity, TOF = 10.9 h^{-1}). Similar improvement was found for other alkenes, such as cyclohexene, styrene and α-methyl styrene 1-dodecene and 1-octene. Shock waves induced by the collapsing bubbles lead to strong movements in the liquid and to particle collisions, reducing particle size, increasing the mass transfer and reducing the diffusion layer at the particle's surface, as also stated by other authors.[22,23] Additionally, the produced bubbles generate high temperatures.[21]

Salavati-Niasari *et al.*,[24] covalently anchored a hydroxyl functionalised oxovanadium(IV) Schiff-base; *N*,*N*′-bis(4-hydroxysalicylidene)-ethylene-1,2-diamineoxovanadium(IV), [VO($(OH)_2$-salen)] shown in Scheme 12.9; on modified MWCNTs. The material was used as catalyst for the liquid-phase oxidation of cyclohexane with H_2O_2 to yield a mixture of cyclohexanone, cyclohexanol and cyclohexane-1,2-diol in CH_3CN, being more selective towards cyclohexanol formation.

The same authors[25] covalently anchored an hydroxyl functionalised oxovanadium(IV) Schiff-base; (*N*,*N*-bis(4-hydroxysalicylidene)phenylene-1,2-diamine)oxovanadium(IV), [VO($(OH)_2$-salophen)], shown in Scheme 12.10 on modified MWCNT. The composites were used as catalysts for the liquid-phase oxidation of cyclooctene with O_2 in CH_3CN. The best result was 91.6% conversion for 96 h time reaction, at 78 °C temperature, with a mixture of cyclooctene epoxide (12%), cyclooctene-1-ol (45.7%) and cyclooctene-1-one (42.3%) being obtained.

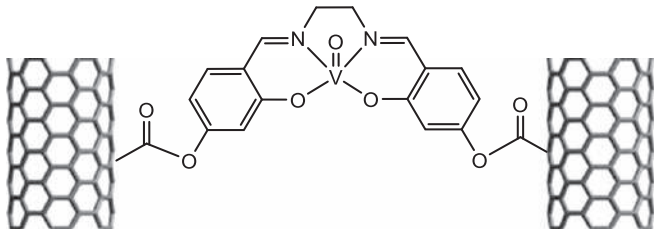

Scheme 12.9 *N*,*N*′-bis(4-hydroxysalicylidene)-ethylene-1,2-diamineoxovanadium(IV) used by Salavati-Niasari *et al.*[24]

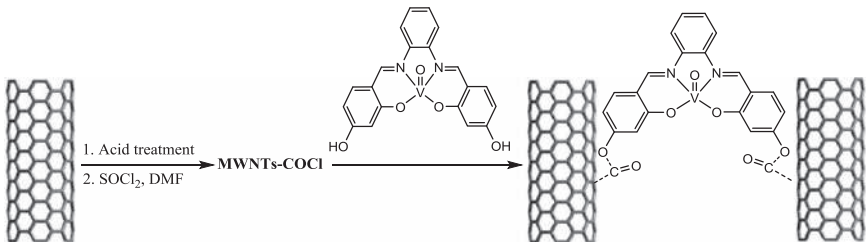

Scheme 12.10 Anchorage of *N*,*N*-bis(4-hydroxysalicylidene)phenylene-1,2-diamine)-oxovanadium(IV) complex on functionalised MWCNT.[25]

Sutradhar *et al.*,[26] supported several oxidovanadium (V) complexes (Scheme 12.11) on functionalised MWCNT (pristine sample: CNT; oxidised with nitric acid in reflux: CNT-ox, and oxidised with nitric acid and subsequently treated with NaOH: CNT-ox-Na). The materials were used as catalysts for the oxidation of 1-phenylethanol (Scheme 12.12), using low power (10W) microwave (MW) irradiation. The best results were obtained with AC-ox-Na; however, the corresponding homogenous complexes showed better performance.

Wang *et al.*,[27] reported on CNT-supported scorpionate vanadium(IV) pyrazol-1-yl complexes, used in the oxidation of *o*-, *m*- or *p*-xylene to the corresponding toluic acids (main products), tolualdehydes and methylbenzyl alcohols. This work is discussed in more detail in Chapter 6.

In all cases reported in this section, characterisation of the obtained CNT composite materials showed the retention of MWCNT structure and the covalently anchored complexes on modified MWCNTs. The MWCNT were able to keep the complexes dispersed and prevent their dimerisation, retaining the catalytic activity.

12.2.3 Activated Carbon

Activated carbon is a highly porous material that can be prepared from several carbon-containing precursors by pyrolysis in inert atmosphere and then physical or chemical activation to increase the porosity.[28] Activated carbon has an interesting structure that is shown in Figure 12.1. It consists of crystallites formed by stacked graphitic planes, randomly oriented,

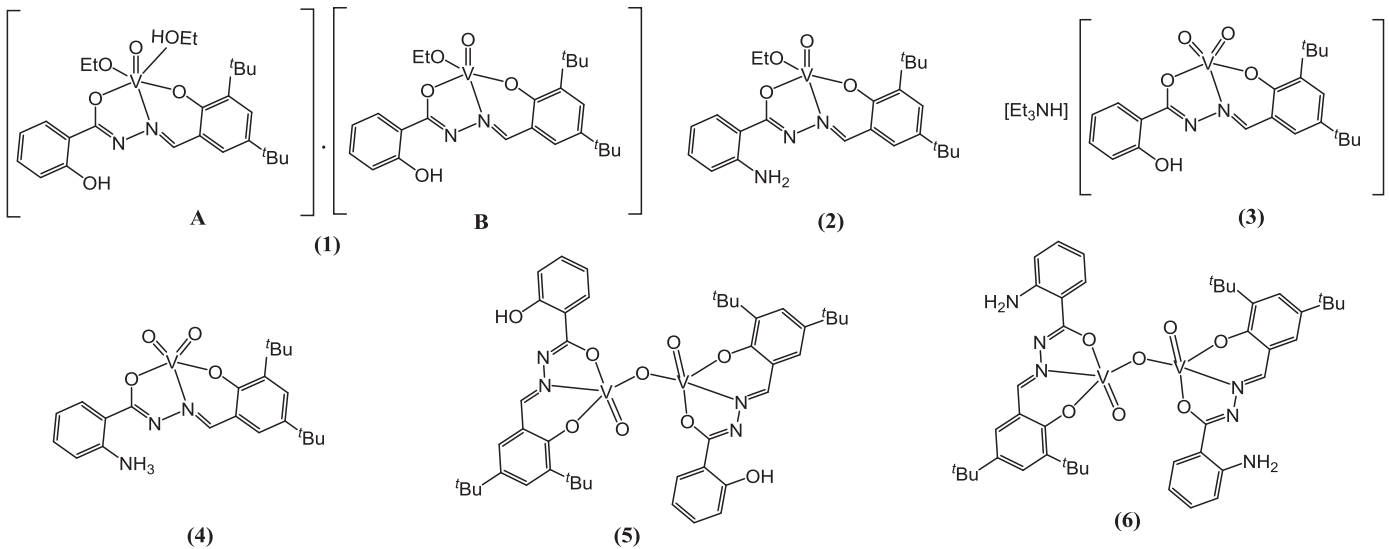

Scheme 12.11 Oxidovanadium(v) aroylhydrazone complexes derived from (3,5-di-*tert*-butyl-2-hydroxybenzylidene)-2-hydroxybenzohydrazide (H_2L^1) and (3,5-di-*tert*-butyl-2-hydroxybenzylidene)-2-aminobenzohydrazide (H_2L^2), namely, $[VOL^1(OEt)][VOL^1(OEt)(EtOH)]$ (**1**), $[VOL^2(OEt)]$ (**2**), $[Et_3NH][VO_2L^1]$ (**3**), $[VO_2(HL^2)]\cdot 2EtOH$ (**4**), $[(VOL^1)2(m\text{-}O)]$ (**5**), and $[(VOL^2)2(m\text{-}O)]$ (**6**). Redrawn from ref. 26.

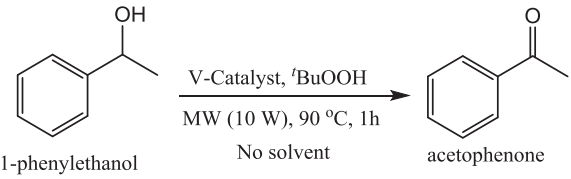

Scheme 12.12 MW-assisted oxidation of 1-phenylethanol to acetophenone.[26]

Figure 12.1 Microstructure of activated carbon.
Redrawn from ref. 29 with permission from the authors and editor, Copyright 1997.

resulting in a disordered structure, similar to wrinkled sheets of paper.[29] The spaces between the graphitic planes of the crystallites create the microporous structure, which has a high internal surface area, providing activated carbons with their remarkable adsorption properties.[30,31]

Freire and co-workers reported on the anchorage of vanadyl acetylacetonate (shown in Scheme 12.5) onto amine-functionalised activated carbons that were efficiently used in the epoxidation of an allylic alcohol.[32] This work is described in more detail in Chapter 11.

Sutradhar *et al.*,[26] also supported the oxidovanadium(v) complexes shown in Scheme 12.11 on functionalised activated carbon (AC), with the same treatments for CNT (obtaining AC-ox and AC-oxNa samples). The catalytic results for 1-phenylethanol oxidation were not as good as those obtained on CNT materials. Nevertheless, high selectivity to acetophenone was obtained (no trace of by-products).

12.2.4 Ordered Mesoporous Carbons

Nanostructured ordered mesoporous carbon materials (CMK-n) have been prepared either by nanocasting ordered mesoporous silica or zeolite templates, or directly by templating triblock copolymer structure-directing

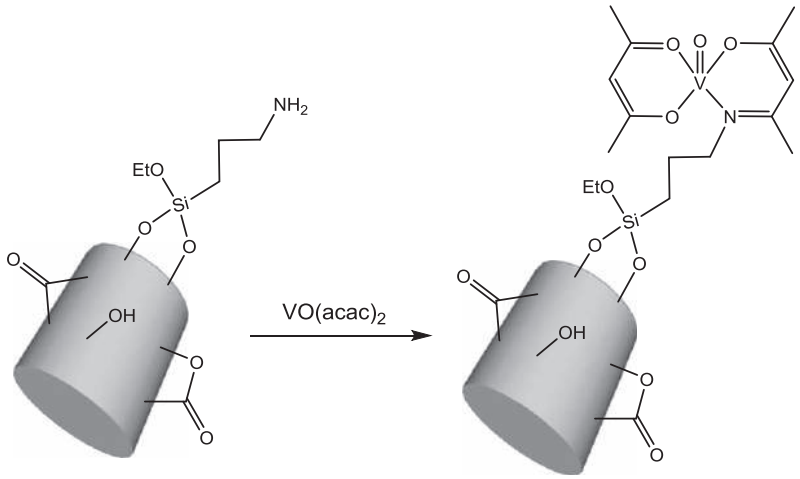

Scheme 12.13 Synthetic schematic outlines of NH_2-CMK-3 and V-NH_2-CMK-3.[34]

species.[33] Some work on the heterogenisation of V complexes has been performed on the ordered nanostructured carbon CMK-3, a SBA-15 (mesoporous silica) replica, and is discussed next.

Freire and co-workers reported on the immobilisation of oxovanadium(IV) acetylacetonate complex (shown in Scheme 12.5) on the CMK-3 and its test in the epoxidation of geraniol using TBHP as oxidant. This work is described in more detail in Chapter 11.

Wang *et al.*,[34] also grafted the oxovanadium(IV) acetylacetonate complex (shown in Scheme 12.5) on amino-modified CMK-3 (NH_2-CMK-3, Scheme 12.13) and tested the obtained material in the aerobic oxidation of styrene (reaction shown in Scheme 12.4). The heterogenised complex displayed a relatively good catalytic performance with 94.6% of styrene conversion, with a selectivity of 70.5% to styrene oxide, using air as oxidant.

The same authors[35] used a similar procedure to immobilise a VO(II) Schiff base complex (VO-Sal-CMK-3, shown in Scheme 12.14). A styrene conversion of 91.8% was obtained with a selectivity of 63.7% to styrene oxide, showing that the acetylacetonate complex was more favourable for the reaction.

In all cases, the characterisation methods showed that the structure of CMK-3 was well preserved and that the V complexes were successfully incorporated onto the support.

12.2.5 Polymer-based Carbon Materials

Polymer-based carbon materials can be obtained by sol–gel processes yielding different structures: (1) xerogels, when conventional (subcritical) solvent evaporation is used, and (2) aerogels, when supercritical drying is employed. It has been shown that carbon xerogels have textural properties that can easily be tuned by changing the parameters of the preparation procedure (such as preparation pH).[36–38] Xerogels can be prepared by sol–gel

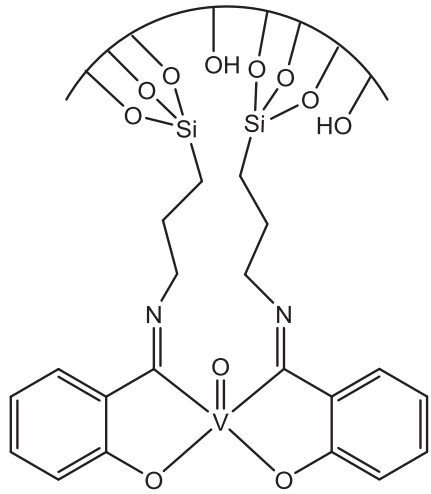

Scheme 12.14 VO(II) salicylaldehyde Schiff base complex grafted on NH_2-CMK-3.[35]

polymerisation of resorcinol with formaldehyde followed by carbonisation at a high temperature under inert atmosphere.[36–38]

Sutradhar *et al.*,[26] supported the oxidovanadium(V) complexes of Scheme 12.11) on functionalised carbon xerogel (CX, CX-ox and CX-ox-Na), prepared in this way. Just like with AC, catalytic results were inferior to those obtained with CNT, although still with high selectivity to acetophenone.

Yazdely *et al.*,[39] also used a xerogel prepared from resorcinol and formaldehyde for direct immobilisation a vanadium(IV) complex [VIVO(HL)-(H_2O)(CH_3OH)] with an extended ligand π system and reactive hydroxyl groups on the L-tyrosine fragment. The heterogenised complex had better activity and selectivity than the homogeneous counterpart and showed high catalytic performance for the epoxidation of unfunctionalised olefins with molecular oxygen in the presence of isobutyraldehyde. It was also easily recovered from the reaction medium and could be reused for another five runs without significant loss of activity.

Graphitic carbon nitride (g-C_3N_4) is a polymeric material consisting of C, N and some impurity H, connected *via* tris-triazine-based patterns.[40] It is often produced by polymerisation of cyanamide, dicyandiamide or melamine.[11]

Vanadyl(IV) acetylacetonate was immobilised on g-C_3N_4 by Xu *et al.*,[41] by the reaction between the carbonyl group of the acetylacetonate and the amino groups. The heterogeneous catalyst showed high performance in the direct hydroxylation reaction of benzene to phenol (Scheme 12.15), with maximum phenol yield of ~20.0%. Phenol is a commercially important chemical compound, often synthesised by complicated chemical procedures and side products. Thus its direct hydroxylation from benzene to phenol with green oxidants (H_2O_2, O_2) is very appealing. However, the C–H bonds are quite strong and inert.[42]

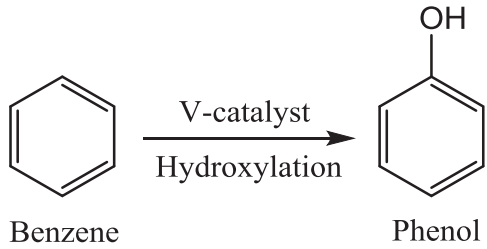

Scheme 12.15 Direct hydroxylation of benzene to phenol.

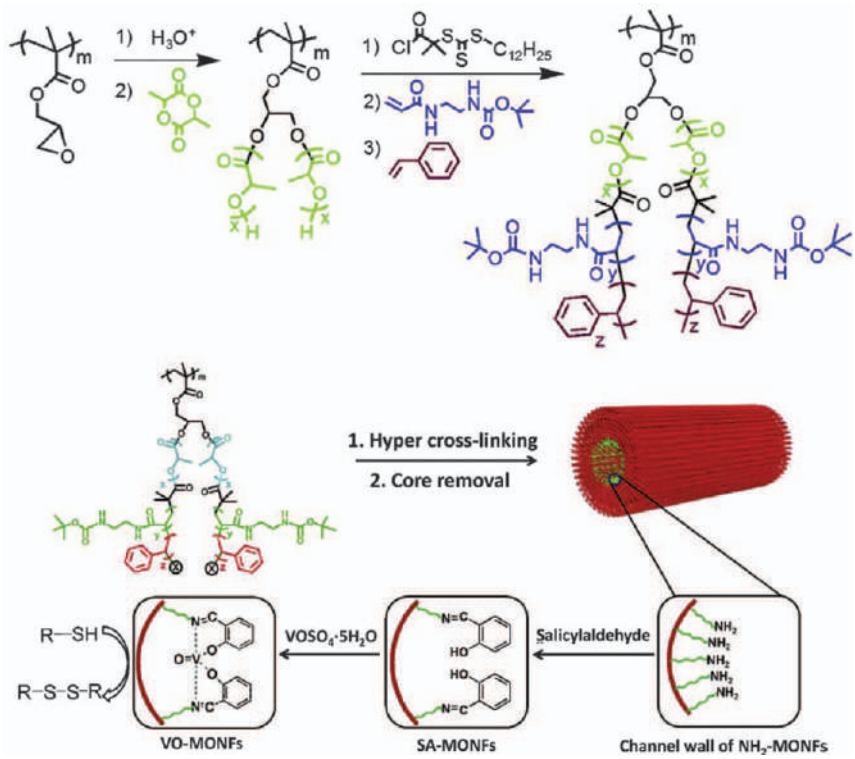

Scheme 12.16 Synthesis of the precursors of VO-MONFs and their use in selective oxidation of thiols to disulphides.
Reproduced from ref. 43 with permission from Elsevier, Copyright 2018.

The catalytically active site for hydroxylation was proposed to be the grafted complex while the support played a crucial role in activating benzene.

Porous organic polymers are an emerging class of materials with high surface area and excellent chemical modifiability. Zhang *et al.*,[43] anchored an oxo-vanadium(IV) complex on amino functional microporous organic nanotube frameworks (NH_2-MONFs, Scheme 12.16). The prepared

oxo-vanadium heterogeneous catalyst shows high catalytic activity and excellent stability in the selective oxidation reactions of thiols to disulphides. The selective oxidation of *p*-chlorobenzenethiol was investigated as a model reaction using urea peroxide as the oxidant at ambient temperature. At room temperature, after 6 min, the conversion was already around 100% with TOF of 4305 h^{-1}, which is one of the highest values ever reported for oxidation of the thiols in various vanadium heterogeneous catalysts. The excellent catalytic performance of the material can be attributed to its special nanotube framework structure, high surface area and highly dispersed vanadium(IV) species within the walls of the nanotubes. Moreover, the material proved to be stable since there was no apparent decrease in catalytic activity after recycling for more than eight times, and porous structure, surface area and pore volume were preserved with the use.

12.2.6 Nanodiamonds

Nanodiamonds (NDs) are monocrystalline diamond particulates originated from a detonation process.[44,45] They exhibit a narrow particle size distribution, small particle size (<10 nm) and have a highly developed chemically active surface.[44] Also they have different sp^2 or sp^3 hybridisations (they are sp^2 in the surface but the core is sp^3).

Sutradhar *et al.*,[26] anchored oxidovanadium(V) complexes (shown in Scheme 12.11) on functionalised nanodiamonds (ND, ND-ox and ND-ox-Na). Better results were obtained, compared to the homogenous counterparts, especially for complexes **3** and **4** (Scheme 12.11) on ND. Acetophenone yield up to 91% (with 98% selectivity) was obtained in 0.5 h reaction time, and 125 °C temperature. **4**@ND could be recycled but preserved its catalytic performance only for two consecutive runs.

12.3 Carbon-supported Vanadium Oxides

As mentioned, there are more works dealing with vanadium oxides supported on carbon materials, especially on activated carbon (but also, more recently, on other supports like carbon nanotubes and graphitic carbon nitride). Carbon plays a role of V-reducing agent that allows the preparation of such composites under ''green'' conditions (like aqueous solutions).[46,47] The works dealing with V oxides on carbon supports will be briefly reviewed in this section (but vanadium oxides supported on other materials are dealt with in Chapter 13).

12.3.1 Activated Carbon

Nitrogen oxides are some of the major pollutants of the atmosphere and their selective catalytic reduction (SCR), using ammonia or carbon monoxide as the reducing agent, is an effective method for their removal. V-based catalysts have advantages of wide operation-temperature windows and superior low-temperature activity in reduction of NO_x in the oxidising atmosphere.[48]

Activated carbon-supported vanadium oxide (V_2O_5) catalyst was used for the SCR of NO (nitric oxide) with NH_3 (ammonia), eqn (12.1), from 90 to 250 °C, by Zhu *et al.*[49]

$$4NO + 4NH_3 + O_2 \rightarrow 4N_2 + 6H_2O \quad (12.1)$$

V_2O_5/AC was much more efficient than unsupported V_2O_5. A pre-oxidised catalyst showed higher and more stable activity, with NO conversions of ~8% (for 5% wt. V V_2O_5/AC). Activated carbon was a good support for the vanadium catalysts because its high surface area and inability to react with SO_2 (often present in the flue gas).

The same authors[50,51] studied the effects of SO_2, V_2O_5 loading and reaction temperature on the activity of V/AC catalyst for the same reaction at low temperatures (150–250 °C). The optimum V_2O_5 loading was in the range of 1–5% wt, as loadings above 7% wt were detrimental. SO_2 significantly promoted the catalyst activity (180–250 °C) due to the formation of SO_4^{2-} on the catalyst surface, which increases the surface acidity. Other authors achieved similar results on SO_2 promotion of SCR of NO with NH_3, using V_2O_5/SiC (1% wt.) catalysts at 250 °C.[52]

Viscose-based activated carbon fibres (VACF) treated by oxygen plasma modification (OPM) and nitric acid modification (NAM) were used as supports for vanadium oxide (mostly V_2O_5).[53] Materials were used in the SCR of NO with NH_3 at low temperature (120–240 °C). The results showed that the OPM and NAM could increase the oxygen functional groups on the VACF surface which contributed to a higher vanadium loading and dispersion, exhibiting high activity (NO conversion around 85% for sample doped with 12% V).

Gálvez *et al.*, used V_2O_5/AC for SCR of NO with NH_3 at low temperatures (100–300 °C).[54] The presence of 10% (v/v) water vapour caused a considerable decrease in activity. The presence of 200 ppmv SO_2 in the reactant gas mixture did not influence catalytic activity. Previous oxidation of AC with HNO_3 and H_2O_2 produced more active catalysts due to the positive effect of the new oxygen-containing groups created. The same authors proposed that the reaction mechanism involved adsorbed species of ammonia, which reacted with the NO from the gas phase, while the role of oxygen was to regenerate the used catalytic sites.[55]

Lei *et al.*, also studied the SCR of NO by NH_3 from 120 °C to 250 °C on V_2O_5/AC.[56] The intrinsic kinetic measurements obtained fitted more accurately the Eley–Rideal model. The same authors performed similar experiments in the presence of water and found out that this model was also the most adequate.[57]

Sun *et al.*, studied the SCR of NO with NH_3 on an activated coke-supported V_2O_5 catalyst at 200 °C by *in situ* diffuse reflectance infrared Fourier transform spectroscopy.[58] Results indicated that NH_3 was adsorbed in the forms of coordinated NH_3, NH_4^+ and $-NH_2$. V_2O_5 promoted formation of $-NH_2$, while NO was oxidised to NO_2 in the presence of O_2. Thus, $-NH_2$ and NO_2 were the intermediates of the reaction.

Sun *et al.*, also studied the SCR of NO and NO_2 with NH_3 over V_2O_5/AC catalysts.[59] NO_2 and NO can react with the adsorbed ammonia (NH_{3ads}) in the absence of oxygen, but the activity of NO_2 is superior to that of NO. NO_2 can react with NH_{3ads} to form N_2, but NO shows little activity unless oxygen is present.

The SCR of NO and NO_2 with NH_3 over V_2O_5/AC was also studied by Gao *et al.*[60] NO_x conversion to N_2 increases from 26% to 75% and 94%, at 150 °C, with increasing NO_2 to NO_x ratio from 0 to 0.5 and 1, respectively. NH_4NO_3 could be deposited on the catalyst at 100 °C and decomposed to NH_3, N_2O and NO around 130 °C. NH_4NO_3 was reduced to N_2 by AC instead of NO.

Activated carbons obtained from a Spanish coal were doped with V_2O_5, NH_4VO_3 and petroleum coke ashes (PCA) as V sources, and used as SCR catalysts for the reduction of NO with NH_3 at low temperatures by Lázaro *et al.*[61] Significant conversions of NO (above 50%) with almost 100% selectivity toward N_2 at 150 °C were obtained for all V materials supported on the char activated at 750 °C, showing that PCA is an effective V source (containing around 23% v/v of V). The activity of the catalysts was maintained at least over 24 h of reaction.

The same authors used low-rank coal for the preparation of carbon briquettes, using V_2O_5 and PCA as V sources, for NO SCR with NH_3.[62,63] NO reductions between 40% and 80% were obtained from 75 to 350 °C.[62]

The group also studied the influence of previously treating carbon with sulphuric and nitric acids, comparing activities for the same reaction.[63,64] Treatment with HNO_3 increased the catalytic activity due to the presence of acidic surface groups such as carboxyl and lactone, which help not only to create a reservoir of reactants on the catalysts surface but also to improve the dispersion – or even increase – the amount of vanadium loading. Materials showed considerable activity from 75 to 350 °C (40%–90% conversion) and total selectivity towards N_2.[64]

A commercial cordierite-made cellular monolith (honeycomb) was impregnated with a polymeric solution (liquid phenolic resin), dried and carbonised at 700 °C, to obtain a carbon ceramic support, which was impregnated with VO_2^+ and thermally treatment by Valdes-Solis *et al.*[65,66] A V-catalyst for low-temperature SCR of NO_x with NH_3 was obtained, with resistance to SO_2 poisoning and inhibition by water being reversible, but after subjecting the catalyst to the outlet gas stream of a power plant, deactivation was found, possibly due to arsenic poisoning and the formation of superficial sulphates.[65] The authors concluded that the reaction proceeds *via* a mechanism in which NO reacts from the adsorbed phase with NH_{3ads}.[66]

Lázaro and co-workers used carbon-coated cordierite monoliths, loaded with V, in SCR of NO with NH_3.[67–78] V_2O_5 was dispersed as overlayers from 3 to 6% wt. loading; for higher loadings crystallites appeared.[69,70] In fact, crystalline V_2O_5 phase appears when V loading exceeded the dispersion limit loading on the support, typically known as the ''monolayer'' coverage, and such critical loading is reached at *ca.* 4 V atoms per nm^2 of AC support.[79] The monolith shape performed better than the fixed bed.[70] It was found that

mesoporous supports had more oxygenated surface groups, which allowed a better dispersion of V_2O_5 and better activity, while microporosity was detrimental.[68,74] For mesoporous materials, addition of 400 ppm SO_2 caused a three-fold increase in the specific activity of the catalyst, being more effective that the addition of a second metal.[71]

V-supported carbon-coated monoliths were also sulphated with a mixture of SO_2 and O_2 at 200 °C by the same authors.[72] Those materials showed a two-fold higher conversion for SCR of NO with NH_3 than the fresh catalyst below 200 °C. Sulphates were anchored to carbon in the vicinity of vanadyl sites and the enhancement of the materials redox properties led to the superior performance of the sulphated catalysts.

The effect of oxidation of the carbon–ceramic monoliths was also tested by the same group.[73–75,78] Treatment with 10% O_2 at 530 °C produced to the highest V loading and dispersion, that had reflection on catalytic activity. Treatments with HNO_3 were also effective, but treatment with ozone led to the lowest dispersion (as O_3 generated a high amount of carboxylic groups that decomposed below the calcination temperature of 350 °C).[73] Treatment with HNO_3 was also more effective than with H_2SO_4 or H_2O_2, as it produced the highest number of active surface complexes, as carboxyls and lactones, which enhanced V dispersion and catalytic activity.[75,78]

The authors also compared using PCA and NH_4VO_3 as V sources on the same supports.[76] Catalysts prepared with PCA had a slightly lower catalytic activity than those prepared with NH_4VO_3, but similar selectivity towards N_2 was found.

The same authors also compared AC and alumina coated monoliths and found out that the carbon washcoat was much thinner, better adhered to ceramic support, provided a higher surface area and presented a higher thermal shock and vibration resistance.[77]

Activated carbon honeycomb (ACH) supported V_2O_5 catalysts were studied for simultaneous SO_2 and NO removal (by SCR with NH_3) at temperatures of 150–250 °C by Wang *et al.*[80] The material with 2% wt. V_2O_5 showed high activities at 200 °C. Regeneration of the used catalyst in 5% vol. NH3/Ar resulted in a slight increase in SO_2 removal activity, and significantly increased SCR activity.

The same group showed that V_2O_5 might transform into $V_2O_3(SO_4)_2$ during SO_2 oxidation over V_2O_5/AC.[81] SO_2 promoted NO reduction in the range of 180–240 °C. The authors proposed that the promising SO_2-tolerance found for V_2O_5/AC for SCR of NO with NH_3 is likely related with the catalytic activity of $V_2O_3(SO_4)_2$ at low temperatures.

Activated carbon-supported V_2O_5 catalysts were used to investigate the selective catalytic reduction of NO (coming from incineration flue gas) with CO (Eqn (12.2)).[82]

$$NO + CO \rightarrow \tfrac{1}{2} N_2 + CO_2 \qquad (12.2)$$

The materials showed high activity and the presence of SO_2 in the incineration flue gas significantly promoted the catalytic activity. The authors

considered that using CO as reducing agent was more effective than using NH_3, since ammonia may be partially oxidised in the presence of excess O_2, to form N_2, which can decrease the NO reduction efficiency.

Carbon materials impregnated with V_2O_5 and NH_4VO_3 can also be efficiently used as low-cost catalytic sorbents for NO_x.[83,84]

V_2O_5/AC was also effective for the simultaneous removal of SO_2 and NO from flue gas at 200 °C.[85,86] The SO_2-adsorbed V_2O_5/AC catalyst-sorbent could be regenerated in the presence of 5% NH_3/Ar at 300 °C, and the carbon burn-off is much less than that in an inert atmosphere as NH_3 reacts with the surface oxygen-containing groups of the material, producing H_2O and nitrogen-containing groups such as $-CONH_2$, C–N, and C≡N.[85] The regenerated catalyst showed higher and more stable SO_2 adsorption capacity and higher NO removal activity.[86] During regeneration, reduction of the adsorbed sulphur species by carbon to SO_2 and CO_2 and oxidation of carbon by oxygen in the V_2O_5/AC to CO_2 occurred.

Carabineiro *et al.*, also used AC impregnated with a precursor salt of vanadium (ammonium monovanadate) as catalyst for the reduction of NO and N_2O by carbon between 300–900 °C.[87] The main products obtained were N_2, N_2O, CO and CO_2. The catalytic effect of vanadium could be explained by the occurrence of redox processes in which the catalyst was reduced to lower oxidation states such as V_2O_5/V_6O_{13}.

NO reduction was also studied by Carabineiro *et al.*, using binary V mixtures on AC.[88,89] The best synergetic effects were observed for samples doped with V + Cu and V + Fe (Figure 12.2). The synergistic effect observed with addition of V was related with its ability to wet and spread on carbon surface and with enhancement of oxygen–carbon complexes on carbon surface, increasing CO_2 production and generating new active sites.

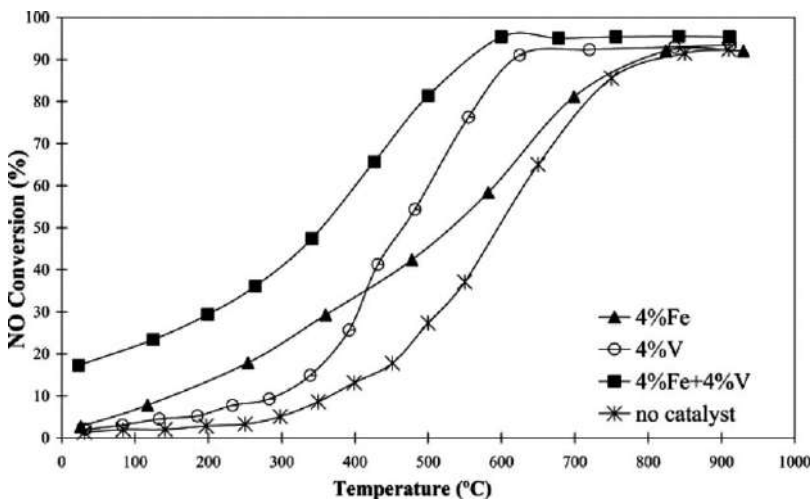

Figure 12.2 NO conversion for samples doped with V, Fe and V + Fe on AC. Reproduced from ref. 88 with permission from Elsevier, Copyright 2003.

The activity for NO reduction of a vanadium supported acid nitric activated carbon catalyst (2.8% wt. V/AC-HNO_3) prepared by impregnation with an aqueous solution of NH_4VO_3, followed by drying and heat treatment at 400 °C, was also studied.[90] The NO reduction reactions were conducted with and without 3% O_2. With oxygen, 84% NO conversion was obtained at 360 °C, but the catalyst began to burnout above 300 °C. Without O_2, NO conversion reached 78% at 450 °C.

Lázaro *et al.*, used carbon briquettes obtained from low-rank coal, in which V_2O_5 and PCA were impregnated, for NO reduction with and without O_2, from 100 to 300 °C.[62,74] V_2O_5 gave slightly better results than PCA below 300 °C. Higher NO reduction efficiencies were achieved for the catalysts prepared using pre-oxidised briquettes, due to the presence of oxygen groups and with increased microporosity.[62,74]

Carabineiro *et al.*, also studied CO_2 reduction to CO (300 to 900 °C) with binary mixtures of V with other metals on AC. The best synergetic effects were observed for samples doped with Ba + V, Mg + V, Fe + V and Cu + V.[91] The detected phases were metal carbonates and metal oxide phases. Those results were being much better than those obtained with only vanadium on AC.[87]

The AC supported V, Cu and Cu + V materials also showed good behaviour in SO_2 adsorption at 20 °C (adsorption isotherms were reasonably fitted by the Langmuir model), as shown by Carabineiro *et al.*[92] The good behaviour of V is related with its catalytic activity in the SO_2 oxidation process as shown by Davini.[93]

Activated carbon-supported V_2O_5 catalysts were used for the catalytic oxidation of sulphur dioxide/hydrogen chloride from incineration flue gas.[82] They showed higher activities for SO_2 (and HCl oxidation) than traditional γ-Al_2O_3–supported catalysts, acting as catalysts instead of sorbents, decomposing sulphate with evolution of SO_2 and then regenerating for more SO_2 adsorption to take place.

It was shown that elemental sulphur could be obtained through regeneration in H_2 of a V_2O_5-CoO/AC material with SO_2 from flue gas adsorbed.[94] The regeneration efficiency was maximum at 330 °C, with SO_2 as product. The production of elemental sulphur occurred at 350–380 °C.

$V_2O_3(SO_4)_2$/AC (prepared by AC impregnation with $VOSO_4$) was used for SO_2 oxidation.[81] A sulphur capacity of 50.1 mg g^{-1} was found at 100 °C.

Other reactions were also studied on V/AC catalysts, namely, the synthesis of vinyl chloride monomer (from the acetylene and HCl, eqn (12.3). It is essential to industrial polyvinyl chloride (PVC) production, but often carried out using a $HgCl_2$ that leads to environmental pollution.

$$C_2H_2 + HCl \rightarrow CH_2CHCl \qquad (12.3)$$

Dai *et al.*,[95] used a V nitride load into AC that allowed to achieve a 20% conversion and was able to keep 98% selectivity for the reaction, although not as active as Mo and W analogues.

7 nm vanadium nanoparticles on activated carbon were synthesised by the reduction of $VCl_3 \cdot 3THF$ with $K[BEt_3H]$ and their catalytic activity was studied

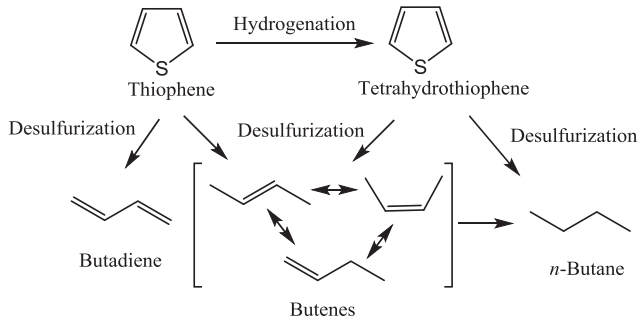

Scheme 12.17 Thiophene hydrodesulphurisation reactions. Reproduced from ref. 97 with permission from Elsevier, Copyright 2010.

for thiophene hydrodesulphurisation at 300 °C.[96] VO_2, V_2O_3 and V_8C_7 (or V_4C_3) were detected. The catalytic activity of the V/AC catalyst is 2-fold larger than that of the commercial $NiMoS/Al_2O_3$, being more selective towards the formation of *n*-butane and olefins (Scheme 12.17).

Dehydrogenation of isobutane in the presence of carbon dioxide was tested over supported vanadium oxide catalysts, with the best results being obtained with the VO_x/AC material (55% conversion, 80% isobutene yield at 600 °C, 0.2 h time), compared to (Ce, La, Si, Ti, Al, Zr and Zn) oxide supports.[98] This activity was also higher than the obtained for vanadium magnesium binary oxides supported AC (35% yield) for the same reaction (lower activities were obtained for Mg–V on other supports, like SiO_2, γ-Al_2O_3 or ZnO).[99]

Methane oxidative coupling (eqn (12.4) and (12.5)) and dehydrogenation of C_2–C_4 alkanes to olefins (eqn (12.6)), in the presence of carbon dioxide, were studied by Ogonowski and Skrzynska on a VO_x/AC catalyst.[100] Increasing the surface acidity decreased both methane and ethane conversion, as they require basic sites for activation. Higher hydrocarbons (like propane, *n*-butane and isobutane) were activated on the acid sites.

$$n\mathrm{CH_4} + (n-1)\mathrm{CO_2} = \mathrm{C}_n\mathrm{H}_{2n+2} + (n-1)\mathrm{CO} + (n-1)\mathrm{H_2O} \qquad (12.4)$$

$$n\mathrm{CH_4} + n\mathrm{CO_2} = \mathrm{C}_n\mathrm{H}_{2n} + n\mathrm{CO} + n\mathrm{H_2O} \qquad (12.5)$$

$$\mathrm{C}_n\mathrm{H}_{2n+2} + \mathrm{CO_2} = \mathrm{C}_n\mathrm{H}_{2n} + \mathrm{CO} + \mathrm{H_2O} \qquad (12.6)$$

AC obtained from sugar cane straw was used as a support for vanadium catalysts (prepared by impregnation with NH_4VO_3) in the propane oxidation with O_2.[101] A conversion of 30%, with 10% selectivity to propylene (10%), with a high amount of CO_x products was obtained, similarly to the V catalyst on commercial AC.

Dehydrogenation of ethylbenzene (Scheme 12.18) to produce styrene (an important intermediate for petrochemical industries) over AC supported V_2O_3 catalysts was carried out at 450–650 °C by Sakurai *et al.*[102] The 1.0 mmol $V\,g_{AC}^{-1}$ material gave the highest ethylbenzene conversion of 67.1%, with a styrene yield of 54.2% and a styrene selectivity of 80.8% at

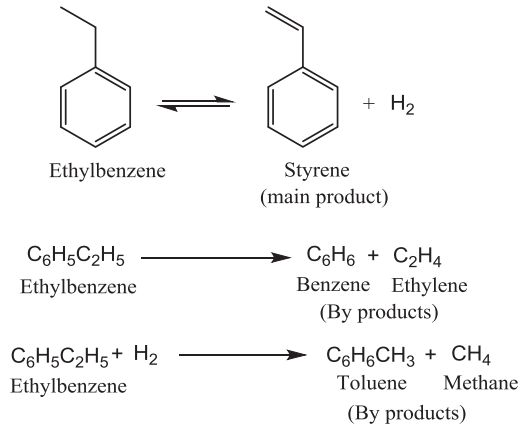

Scheme 12.18 Dehydrogenation of ethylbenzene.

277 °C in CO_2 atmosphere (results are 14.0% higher than in Ar), compared to other supports like Si, Al, Ce or Ti oxides, or charcoal (which did not show any activity). For vanadium(v)-based catalysts, the active phase of V for this reaction was observed to be V^{5+} species.[103]

Activated carbon obtained from the sulphonated styrene-divinylbenzene copolymer loaded with vanadium was tested for ethylbenzene dehydrogenation by Holtz *et al.*[104] AC was active and selective to styrene, due to the presence of quinone groups on the surface. The addition of V increased the activity even more due to the activity of V in dehydrogenation reactions and the increase of the amount of oxygen groups on the surface. The catalyst with 5% of vanadium was the most promising sample, showing the highest ethylbenzene conversion, which was three times the value obtained with a commercial catalyst in the presence of steam. This is advantageous since the addition of steam can be avoided, thereby saving energy.

Sakurai *et al.*, also studied the dehydrogenation of isopropylbenzene to α-methylstyrene (an important monomer in the petrochemical industry) in the presence of CO_2.[105] An AC-supported vanadium oxide (V_2O_5) catalyst gave a high activity in CO_2 as the yield was twice as large than in Ar at 450 °C, as CO_2 could keep the surface of vanadium oxide at a high oxidation state.

The benzene hydroxylation to phenol (Scheme 12.15) with H_2O_2 was carried out over 0.5% wt. V impregnated on AC, followed by calcination.[106,107] V performed better than other transition metals, and AC was better MCM-41 as support giving a higher yield of phenol, due to the hydrophobic nature of the AC surface and also its acidity and basicity enhanced the catalyst performance. V_2O_3 was detected by XRD.[107]

The selective oxidation of alcohols to the corresponding aldehydes and ketones is an important organic transformation, as the obtained carbonyl products have extensive applications in plastic, dyes, perfumes, flavour, pharmaceutical and agro-chemical industry.[108]

The selective oxidation of benzyl alcohol (phenylmethanol) to benzaldehyde using molecular oxygen over AC supported Mn and V catalysts was investigated by Chen *et al.*[109] The catalytic activities were significantly improved after pre-oxidising the AC supports materials, due to the specific variety and increased density of oxygen-containing groups. The best result was 93% conversion (99% selectivity to benzaldehyde) over V on AC oxidised for 3 h in O_2.

Vanadium and phosphorous mixed phases (VPO) bulk catalysts with spherical morphology were prepared using a template consisting on AC prepared by a hydrothermal method, using cellulose as starting material by Valero-Romero *et al.*[110] Materials were used in methanol oxidation reaction (44% conversion was achieved) and oxidative dehydrogenation of propane, being selective to propylene and stable. At 500 °C, a high selectivity (80%) to propylene was found with a low propane conversion (5%). For higher temperatures, conversion is higher, but CO_x products are also formed, decreasing propylene selectivity. The same authors also prepared a promising VPO carbon-supported material with fibrous morphology by electrospinning.[111]

V/AC catalysts were synthesised by a wet-impregnation method used for the catalytic oxidation of aromatic alcohols (such as 4-methyl-, 4-methoxy-, 4-nitro-, and 4-bromobenzyl alcohols) with O_2.[112] Highly dispersed V^{5+} species were found up to 10% wt. V. For 4% wt. V, at 100 °C, up to 3 h reaction, 99% conversion with 99% selectivity to the corresponding aldehydes was obtained.

Pt–V_2O_5/C composite performed better than Pt/C catalyst for the electrochemical oxidation of methanol due to a synergistic effect between Pt and V_2O_5.[113,114] The presence of V_2O_5 contributed to the formation of O-containing species that can transform CO-like poisoning species for Pt into CO_2, which helped in regenerating active sites on Pt for further electrochemical oxidation of methanol.[113]

The oxygen reduction reaction (ORR) is very important in several electrochemical systems but is slow in kinetics and Pt catalysts are needed. A heat-treated Pt–V/C catalyst was found to be more active than heat treated Pt/C.[115] The enhancement was assigned to a lowering of the adsorption strength of adsorbed oxygen species.

V_2O_5/AC was prepared by wetness impregnation method from an aqueous solution of NH_4VO_3 and used as catalyst for the liquid-phase oxidation of glyoxal to glyoxylic acid.[116] The conversion of glyoxal and the yield of glyoxalic acid were 29.2% and 13.6%, respectively, without pH regulation, at 40 °C, in oxygen, after 10 h reaction.

VO^{2+} and Cu^{2+} ions were immobilised on a sulphonated previously carbonised resin (CS) and used in the selective aerobic oxidation of biomass-based 5-hydroxymethyl-2-furfural (HMF), a versatile hexoses-derived compound, to obtain 2,5-diformylfuran (DFF), a high-value chemical (Scheme 12.19).[117] The highest DFF yield (98%) with a relative concentration of DFF (>98%) was observed at 140 °C with the 0.93%V–0.26%Cu–CS catalyst.

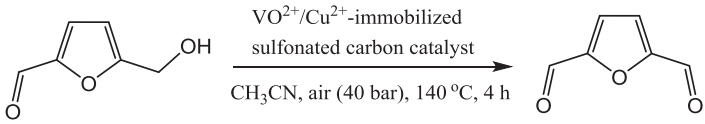

5-hydroxymethyl-2-furfural (HMF)

2,5-diformylfurfural (DFF)

Scheme 12.19 Oxidation of hydroxymethyl-2-furfural. Reproduced from ref. 117 with permission from Elsevier, Copyright 2013.

Another report deals with selective oxidation of HMF into DFF using O_2 on a V_2O_5/AC catalyst.[118] A maximum HMF conversion of >95% with >96% DFF selectivity was achieved and the catalyst could be used four times without any significant loss of activity.

The polymerisation of α-pinene using vanadium oxide (5% wt. metal) supported on activated carbon was carried by Encarnação *et al.*[119] Polymers of low molecular weight were obtained after 100 h of reaction and 30% conversion was attained. The phases identified were a mixture of V_2O_5/V_6O_{13}. The catalyst increased the formation of radical species such as peroxides, which acted as polymerisation initiators.

The Fischer–Tropsch synthesis is a process to convert coal or natural gas-derived syngas (CO/H_2 mixture) in high quality clean liquid fuels and high-value chemicals, often catalysed by cobalt catalysts. Wang *et al.*, found that the CO conversion increased from 39% to 87% when 4% wt. V was added to the Co/AC catalyst.[120] V increased the concentration of surface-active carbon species by enhancing CO dissociation and improved the selectivity towards of long-chain C_{10}–C_{20} hydrocarbons, suppressing the formation of light hydrocarbons.

12.3.2 Carbides

Metal carbides are of particular interest because of their potential as high-surface area, low-cost catalysts, specially the vanadium carbide V_8C_7.[121] They have been used mostly in electrocatalysis, as described next.

Vanadium carbide on carbonised resin composites (C–VC_x) were synthesised by an ionic exchange process.[122] Pt/C–VC_x were highly active and stable for methanol oxidation and ORR, due to the synergistic effect between Pt and VC_x. The kinetic mass current for the Pt/C–VC_x electrocatalyst two-folder higher than that of a commercial Pt/C electrocatalyst for ORR. The onset potential for methanol oxidation on Pt/C–VC_x was also negatively shifted by more than 100 mV compared with that of commercial Pt/C.

Pt nanoparticles were dispersed on V carbide incorporated on resorcinol-formaldehyde resin carbon (V_8C_7@RFC).[123] The catalyst exhibited a negative shift of over 100 mV in the onset potential for CO_{ads} electro-oxidation and a dramatically enhanced activity in methanol oxidation reaction, due to the electronic effect between Pt and V_8C_7 and the mesoporous structure.

A nanocomposite of Pt and vanadium carbide nanoparticles loaded onto graphitised carbon was reported by He *et al.*, as an effective electrocatalyst for the ORR.[124] The stability and the durability of the nanocomposite were improvement compared with the usual Pt/C material.

Huang *et al.*, provided the first report on using graphene oxide as the carbon source in the synthesis of transition-metal carbides as ORR catalysts.[125] The catalytic performance of the Pt on nitrogen-doped graphene–vanadium carbide hybrids in alkaline solutions was superior to that of commercial Pt/C catalysts in terms of the oxygen-reduction half-wave potential and the mass activity. The stability study of the catalyst also shows less degradation in catalytic activity after 3000 cycles compared with Pt/C and the hybrid catalyst structure remains virtually unchanged.

V carbide particles were synthesised by a ionic exchange process on a graphitised resin (GC-V_8C_7) and Pd particles are loaded on it, to be used as catalysts for ethanol electrooxidation in alkaline media.[126] The Pd/GC-V_8C_7 electrocatalyst showed improved catalytic performance in activity, stability and overpotential, compared with Pd/C.

Reduction of $VCl_3{\cdot}3THF$ supported on activated carbon allowed to obtain vanadium carbide nanopowders with good dispersion and uniform sizes at room temperature.[127] The material was used in hydrotreatment reactions, namely hydrodesulphurisation of thiophene, hydrogenation of toluene and hydrodenitrogenation of pyridine and more efficient than the bulk V_8C_7 solid and industrial catalysts.

Mesoporous vanadium carbide encapsulated in graphitic carbon (m-VC@C) was synthesised by a single-step, environment-friendly route using V_2O_5, Mg and C_3H_{60} as precursors.[128] V carbide acts as a catalyst for graphitisation and also for the formation of a mesoporous structure. The material was used in the photo-degradation of salicylic acid (SA) under ultraviolet irradiation (254 nm wavelength). SA concentration decreased 31.2% after 180 min.

12.3.3 Graphene-based Materials

Pt was deposited on a graphene–vanadium carbonitride material (obtained from reduction of GO-supported V_2O_3 under ammonia atmosphere) and used as catalyst in methanol electro-oxidation.[129] The activity was larger and better stability was obtained during long-term operation, compared with the commercial Pt/C catalyst.

V_2O_5 catalysts were supported on graphene and used for oxidative dehydrogenation of propane to propylene.[130] The main products were propylene, ethylene and CO_x. The graphene catalyst had better performance at 450 °C, than V on MWCNT and SWCNT, with 54% propylene selectivity and 51% propane conversion.

Choi *et al.*,[131] investigated the characteristic of V_2O_5 deposited on reduced graphene oxide (RGO) and concluded it had potential to be used in SCR of NO_x.

V_2O_5–WO_3–TiO_2 supported on RGO was used for SCR of selective catalytic reduction of NO_x with NH_3 from 250 to 500 °C by Lee *et al.*[132] The best value obtained was 90% at 450 °C for 1V6WTi/rGO (1% wt. V, 6% wt. W).

Lee *et al.*, used V_2O_5/RGO for the low-temperature SCR of NO with NH_3.[133] The NO conversion reached 54% at 100 °C, being 75% when the temperature was 220 °C. The catalyst had good low-temperature denitrification performance due to the chemical adsorption oxygen and low-valent vanadium oxide present, which was beneficial to the redox reaction between V_2O_5 and graphene.

10% wt. Pt on a vanadium nitride/graphitic carbon composite was used as an effective electrocatalyst for the ORR, showing better results (more positive onset potential, higher mass activity and better cyclic stability towards ORR than the commercial 20% Pt/C.[134]

Pt on a vanadium nitride/porous graphitic nanocarbon composite (Pt–VN/PGNC) was also an efficient electrocatalyst for the same reaction.[135] The 10% Pt–VN/PGNC catalyst exhibited excellent ORR performance also with better results than the commercial 20% Pt/C catalyst, due to the porous structure of the support, which facilitates strong synergistic effects between the Pt and VN nanoparticles.

Cathodes were fabricated with V_2O_5 nanorods supported on RGO for application in microbial fuel cells.[136] This low-cost material showed higher power output and organic matter removal than the V_2O_5-AC analogue and the expensive Pt cathodes.

12.3.4 Graphitic Carbon Nitride

Graphitic carbon nitride-supported V catalysts (xV/g-C_3N_4) with different V contents were prepared by impregnation and used for the direct oxidation of benzene to phenol (Scheme 12.15) using H_2O_2.[137] 8%V/g-C_3N_4 exhibited the highest activity and showed stable recyclability with a benzene conversion of 24.6% and phenol selectivity of 99.2%, at 70 °C, after 4 h reaction.

The selective oxidation of toluene to give benzaldehyde was studied by Huang *et al.*, using a vanadium oxide (V_2O_5) supported on g-C_3N_4 and TiO_2.[138] The best results were obtained with 0.3% wt. V/g-C_3N_4 (7% conversion, 43% selectivity to benzaldehyde), with no marked deactivation at 330 °C for 6 h. This result was much better than the obtained with the traditional V/TiO_2 (3% conversion, 29% selectivity). The nitrogen-rich properties of this support provide abundant anchoring sites, leading to high dispersion of V oxide.

V_2O_5/g-C_3N_4 was used for solar-light-driven photocatalytic hydrogen production from concentrated lactic acid aqueous solution.[139] The optimised material (with a g-C_3N_4/V_2O_5 ration of 0.3) achieved a high initial H_2 evolution rate 2.44-times larger than pristine g-C_3N_4, under simulated solar light irradiation, and was relatively stable for 5 h H_2 evolution reactions, due to its large specific surface area.

12.3.5 Carbon Nanotubes

CNTs have unique electronic and structural properties, making them very good catalytic supports, and are also good NO_x adsorbents. Unless, otherwise stated the studies described below on CNTs were performed on MWCNTs.

Compared to other carbon nanostructures, V doped CNTs showed better activity for NO reduction.[140] The low temperature SCR of NO with NH_3 was studied over V_2O_5/CNT catalysts from 100 °C to 250 °C.[141] The Lewis acid sites on the surface of 2.35% wt. V_2O_5/CNT are the active sites for the reaction. 92% NO conversion was obtained at 190 °C.

V_2O_5/CNT also showed very high stability in the presence of SO_2, their activities being significantly promoted instead of being poisoned by SO_2, and higher than V_2O_3/AC.[142] The reaction of V_2O_5/CNT for low-temperature SCR of NO followed an Eley–Rideal mechanism.

SCR of NO with NH_3 was also studied over V_2O_5–MnO_x/TiO_2-CNT and V_2O_5/TiO_2–CNT composites synthesised by a solvothermal method.[143] A NO_x removal efficiency of 99% was observed over V_2O_5–MnO_x/TiO_2-CNTs at 275 °C. The increase of reducibility and acidic strength by including Mn on V_2O_5/TiO_2–CNT contributed to the improvement of catalytic activity.

$V^{x+}{}_yO^{2-}{}_z$/CNT catalysts, prepared by pore volume impregnation with ammonium metavanadate of CNTs modified with carboxyl/hydroxyl groups, were used for NO reduction with NH_3 at low temperature.[144] In the absence of SO_2 and H_2O, the hydroxyl groups promoted the reaction. In the presence of SO_2, carboxyl groups gave better results. These effects can be attributed to the VO_x species with different oxidation states (V^{5+}, V^{4+} and V^{3+}) and the variation of the microscopic environment of the carbons adjacent to the VO_x species.

V_2O_5 catalysts were supported on MWCNTs and single-wall carbon nanotube (SWCNTs) and graphene were used for oxidative dehydrogenation of propane to propylene.[130] The main products were propylene, ethylene and CO_x. The SWCNT composite had better activity (around 45% propane conversion and 45% selectivity to propylene at 450 °C) than the corresponding MWCNT (around 23% conversion, 35% selectivity, under similar conditions).

VO_2 immobilised on polyaniline-functionalised carbon nanotubes (VO_2-PANI/CNT) was used for the aerobic oxidation of HMF to DFF with O_2 (Scheme 12.20).[145] The best results were obtained with the 9.5% wt. catalyst that showed excellent performance with a DFF yield of 96% and a full HMF conversion, at 120 °C, for 11 h.

Polychlorinated dibenzo-*p*-dioxins and polychlorinated dibenzofurans (PCDD/Fs) are stable, persistent, highly toxic, severely hazardous to the environment and public health chlorinated organic compounds. The simultaneous decomposition of gaseous PCDD/Fs and NO (with or without NH_3) using V_2O_5/TiO_2-CNTs catalysts was studied by Wang *et al.*[146] The removal efficiency of PCDD/Fs reached 99.9% at 150 °C and adsorption was the main

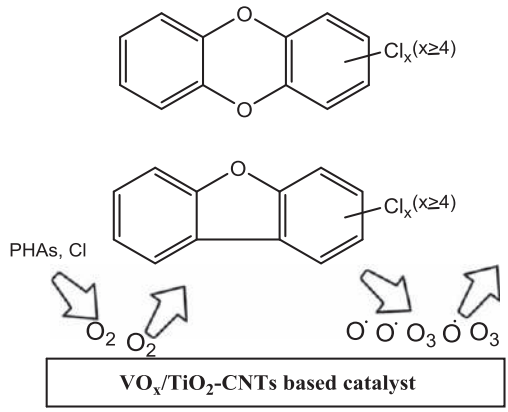

Scheme 12.20 Decomposition of PCDD/Fs. PHAs – Polyaromatic hydrocarbons. Adapted from ref. 147 with permission from American Chemical Society, Copyright 2016.

mechanism at this temperature. Addition of NO had a positive effect, due to the oxidation of NO to NO_2 that increased the catalyst reoxidation. The addition of NO and NH_3 restricted the adsorption of PCDD/Fs, reducing the removal efficiency.

VO_x/TiO_2-CNT modified with MnO_x and CuO_x were used as catalysts for the decomposition of 130 tetra- to octa-PCDD/Fs congeners (Scheme 12.20).[147] In an O_3-containing atmosphere, low chlorination level PCDD/Fs congeners were well removed with VO_x-MnO_x/TiO_2-CNT, while high chlorination level PCDD/Fs congeners were better removed over VO_x-CuO_x/TiO_2-CNT. All PCDD/Fs congeners decomposed well over VO_x-MnO_x-CuO_x/TiO_2-CNT.

A V_2O_5/CNTs-TiO2 catalyst was used for degradation of hexachlorobenzene. The presence of V^{5+} and Ti^{4+} increased the concentration of the surface oxygen species, resulting in a higher catalytic activity because of promotion of the electron mobility and oxygen transfer. 94.8% conversion was achieved at 250 °C in 20% O_2 in N_2. The conversion remained above 90% for 24 h batch test, showing the catalyst stability.

Koohestani *et al.*, prepared vanadium oxide (V_xO_y) nanoparticles on CNT (CNT-V_xO_y), CNTs-V_xO_y template coated with γ-Al_2O_3 (CNTs-V_xO_y/Al_2O_3), γ-Al_2O_3/V_xO_y nanoparticles and V_xO_y nanotubes (V_xO_y-NTs) and tested them in the oxidation of styrene with anhydrous hydrogen peroxide.[148] CNT-V_xO_y showed better performance for styrene conversion and benzaldehyde selectivity.

VO_2 was supported on CNT with defects, originating a VO_2-defects/CNT composite that was used for the hydroxylation of benzene to phenol (Scheme 12.15).[149] Defects were used as promoters for preventing the oxidation of phenol and transferring electrons in the catalysis. 24% conversion was achieved with 94% selectivity.

V_2O_5/CNT composites were investigated for electrochemical activity with lithium ion, showing both high power density and high energy density as supercapacitor electrode.[150]

Pt nanoparticles were dispersed on VO_x-CNTs nanocomposites and used as electro-catalyst in methanol electro-oxidation.[151] Compared to Pt/CNTs, the Pt/VO_x-CNTs electro-catalyst exhibited high activity and very good stability. The presence of VO_x in the composite dramatically increased the electrochemical active surface area of Pt nanoparticles.

3 nm V carbide (VC) nanoparticles on N-doped carbon nanotubes (VC@NCNT) were used as electrocatalysts for water splitting.[152] The catalyst exhibited low overpotentials, remarkable durability at least for 100 h and similar to 100% faradaic yield in both acid and alkaline media, due to the synergistic contribution of high pyridinic N-doping, good conductivity of CNT and exposed abundant catalytic active sites of small VC nanoparticles.

12.3.6 Diamond Materials

A recent review deals with oxygen treated diamond used as a catalyst support for several catalysts, including V_2O_5.[153]

Oxidised diamond was used as support for V_2O_5 catalysts for the dehydrogenation of light alkanes to alkenes in the presence of CO_2.[154] The presence of this gas showed to be very important, especially in the dehydrogenation of propane, as nearly two-fold higher activities in CO_2 than without it. This effect was smaller with *n*-butane and iso-butane. CO_2 kept the surface V_2O_5 in a higher oxidation state, that was beneficial for the reaction.

Ethane was selectively oxidised with CO_2 over various metal oxide-loaded catalysts supported on oxidised diamond.[155] 3% wt. V_2O_5 afforded the highest activity towards acetaldehyde production at 650 °C. In the absence of CO_2, no aldehydes were obtained, indicating that oxygen was supplied from CO_2 through the V_2O_5 surface.

12.3.7 Ordered Mesoporous Carbons

V_2O_5 supported-CMK-3 catalysts with V loadings of 1–7% wt. were studied in the oxidative desulphurisation of dibenzothiophene, using H_2O_2 as oxidant.[156] The best catalysts were obtained with 7% loading, with 100% of DBT attained at short time (~20 min) in mild conditions (60 °C). Moreover, the catalyst showed to be recyclable, with a small activity loss after three cycles.

12.3.8 Nitrogen-doped Carbon Materials

V-supported N-doped carbon materials (designated as V–N–C), obtained by polymerisation of PANI and VO(acetylacetonate)$_2$, were used for the direct hydroxylation of benzene to phenol (Scheme 12.15) using O_2.[157] Up to 12.6% yield of phenol with selectivity as high as 97.8% was achieved employing V–N–C-600 catalyst (pyrolised at 600 °C) at 80 °C, for 12 h reaction. The catalytic recycling tests demonstrated that this material could be reusable up to six cycles.

Hu *et al.*, obtained a nitrogen-doped mesoporous carbon (NC) using the low-toxic hexamethylenetetramine (HMTA) as the precursor and KIT-6 (a ordered mesoporous silica) as the hard template, calcined at different temperatures

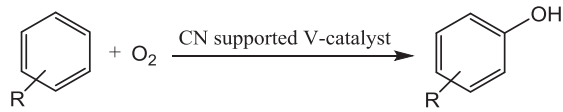

R = H, CN, COOH, NO_2, CF_3, $COCH_3$, Cl, Br and F

Scheme 12.21 Hydroxylation of aromatic compounds with O_2.[160]

and impregnated with diverse amounts of NH_4VO_3 to obtain V/NC materials.[158] The integration of a highly ordered 3D mesostructure, the hydrophobic surface with an open π-conjugated system, the abundant defects introduced by nitrogen related functionalities, and the highly dispersed V species made the catalysts highly efficient in the benzene hydroxylation to phenol using H_2O_2 as an oxidant. A maximum benzene conversion of 31.0% and a phenol selectivity of 97.2% were obtained over a 4.2%V/NC-600 catalyst.

The same authors obtained a highly ordered mesoporous carbon of body-centred cubic structure using Pluronic F127 (a non-ionic copolymer surfactant) as template and phenolic resol as carbon source in which vanadium was doped.[159] Ordered mesoporous carbon nanoparticles of the same body-centred cubic structure were also synthesised, followed by V impregnation. The materials were tested in the direct benzene hydroxylation reaction using H_2O_2 as an oxidant. The V supporting mesoporous carbon nanoparticles, due to the open framework and short channels for fast reactants diffusion and the easily accessible active V species for reactants activation, exhibited superior catalytic activity. The best results were 38.2% conversion and phenol selectivity of 96.1%, along with good recyclability during five cycles.

Li *et al.* used V catalysts supported on N-doped carbon materials (CN), obtained from 1,10-phenanthroline, $H_3PW_{12}O_{40}$ (or $H_4SiW_{12}O_{40}$) and $VOCl_3$ (or VCl_3) precursors.[160] VOSiW (obtained from $H_4SiW_{12}O_{40}$ and $VOCl_3$, containing both V^{4+} and V^{5+} species) showed high activity for the hydroxylation of various aromatics with O_2 (Scheme 12.21). Compounds with electron-withdrawing groups such as CN, NO_2, COOH, CF_3, $COCH_3$ and aromatic halides (F, Cl and Br) were oxygenated to the corresponding phenols in considerable yields (namely, 27% for benzene, 33% for chlorobenzene). The CN materials allowed reusability of the vanadium catalyst VOSiW but also improved due to the high catalytic activity.

12.4 Conclusions

Much work has been done with supported-V oxides (mostly V_2O_5) on AC and the most studied reaction has been SCR of NO with NH_3. AC showed to be a good support for this reaction, with the emphasis on special tolerance for SO_2 (shown also on other carbon materials like SiC and CNT). Moreover, the presence of surface oxygenated groups also showed to be beneficial.

In terms of V carbides, the studies performed so far dealing with electrocatalysis are promising as, in all cases, better results were obtained than with the traditional and expensive Pt catalysts.

Less research has been done on other carbon materials, but graphene derivatives are now especially promising, not only as V oxide supports but also for immobilisation of V complexes for a wide variety of reactions, as shown in this chapter.

Research in the heterogenisation of V complexes on carbon supports is still not abundant; however, carbon materials have the potential to be more used in such applications in the near future.

Acknowledgements

This work has been supported by the Fundação para a Ciência e Tecnologia (FCT) 2020–2023 multiannual funding to Centro de Quimica Estrutural (project UIDB/00100/2020) and by the Associate Laboratory for Green Chemistry – LAQV which is financed by national funds from FCT/MCTES (UIDB/50006/2020). Authors are also grateful to the FCT for financial support to project PTDC/QEQ-QIN/3967/2014. M. S. acknowledges the FCT and IST for a working contract ''DL/57/2017'' (Contract no. IST-ID/102/2018).

References

1. J. A. L. da Silva, J. da Silva and A. J. L. Pombeiro, *Coord. Chem. Rev.*, 2011, **255**, 2232–2248.
2. M. Sutradhar, L. M. D. R. S. Martins, M. F. C. Guedes da Silva and A. J. L. Pombeiro, *Coord. Chem. Rev.*, 2015, **301–302**, 200–239.
3. M. P. de Almeida and S. A. C. Carabineiro, *ChemCatChem*, 2012, **4**, 18–29.
4. M. Peixoto de Almeida and S. A. C. Carabineiro, in *New and Future Developments in Catalysis, B. Catalytic Hybrid Materials, Composites, and Organocatalysts*, ed. S. L. Suib, Elsevier, Amsterdam, 2013, pp. 105–121.
5. J. L. Figueiredo, M. F. R. Pereira, M. M. A. Freitas and J. J. M. Órfão, *Carbon*, 1999, **37**, 1379–1389.
6. J. L. Figueiredo, M. F. R. Pereira, M. M. A. Freitas and J. J. M. Órfão, *Ind. Eng. Chem. Res.*, 2007, **46**, 4110–4115.
7. J. L. Figueiredo and M. F. R. Pereira, *Catal. Today*, 2010, **150**, 2–7.
8. S. A. C. Carabineiro, M. F. R. Pereira, J. J. M. Órfão and J. L. Figueiredo, in *Activated Carbon: Classifications, Properties and Applications*, ed. J. F. Kwiatkowski, Nova Science Pub Inc., New York, 2011, pp. 125–168.
9. J. L. Figueiredo, *J. Mater. Chem. A*, 2013, **1**, 9351–9364.
10. J. L. Figueiredo and M. F. R. Pereira, *J. Energy Chem.*, 2013, **22**, 195–201.
11. M. R. Axet, J. Durand, M. Gouygou and P. Serp, in *Advances in Organometallic Chemistry*, ed. P. J. Pérez, Academic Press, **vol. 71**, 2019, pp. 53–174.
12. A. P. C. Ribeiro, L. M. D. R. S. Martins, S. A. C. Carabineiro, J. G. Buijnsters, J. L. Figueiredo and A. J. L. Pombeiro, *ChemCatChem*, 2018, **10**, 1821–1828.
13. H. P. Mungse, S. Verma, N. Kumar, B. Sain and O. P. Khatri, *J. Mater. Chem.*, 2012, **22**, 5427–5433.

14. Z. Li, S. Wu, H. Ding, H. Lu, J. Liu, Q. Huo, J. Guan and Q. Kan, *New J. Chem.*, 2013, **37**, 4220–4229.
15. Z. F. Li, S. J. Wu, D. F. Zheng, H. Ding, X. F. Wang, X. Y. Yang, Q. S. Huo, J. Q. Guan and Q. B. Kan, *ChemPlusChem*, 2014, **79**, 716–724.
16. H. Su, S. Wu, Z. Li, Q. Huo, J. Guan and Q. Kan, *Appl. Organomet. Chem.*, 2015, **29**, 462–467.
17. S. Verma, M. Aila, S. Kaul and S. L. Jain, *RSC Adv.*, 2014, **4**, 30598–30604.
18. A. Salimi, H. Mamkhezri and S. Mohebbi, *Electrochem. Commun.*, 2006, **8**, 688–696.
19. D. M. Boghaei and S. Mohebi, *J. Mol. Catal. A*, 2002, **179**, 41–51.
20. K. Nomiya, S. Matsuoka, T. Hasegawa and Y. Nemoto, *J. Mol. Catal. A*, 2000, **156**, 143–152.
21. H. Salavati, S. Tangestaninejad, M. Moghadam, V. Mirkhani and I. Mohammadpoor-Baltork, *Ultrason. Sonochem.*, 2010, **17**, 453–459.
22. L. A. Crum, *Ultrason. Sonochem.*, 1995, **2**, S147–S152.
23. K. S. Suslick, Y. Didenko, M. M. Fang, T. Hyeon, K. J. Kolbeck, W. B. McNamara Iii, M. M. Mdleleni and M. Wong, *Philos. Trans. R. Soc., A*, 1999, **357**, 335–353.
24. M. Salavati-Niasari and M. Bazarganipour, *Bull. Korean Chem. Soc.*, 2009, **30**, 355–362.
25. M. Salavati-Niasari, A. Badiei and K. Saberyan, *Chem. Eng. J.*, 2011, **173**, 651–658.
26. M. Sutradhar, L. M. D. R. S. Martins, S. A. C. Carabineiro, M. da Silva, J. G. Buijnsters, J. L. Figueiredo and A. J. L. Pombeiro, *ChemCatChem*, 2016, **8**, 2254–2266.
27. J. Wang, L. M. D. R. S. Martins, A. P. C. Ribeiro, S. A. C. Carabineiro, J. L. Figueiredo and A. J. L. Pombeiro, *Chem. – Asian J.*, 2017, **12**, 1915–1919.
28. I. A. S. Edwards, in *Introduction to Carbon Science*, ed. H. Marsh, Butterworths, University of Newcastle upon Tyne, 1989.
29. F. Rodríguez-Reinoso, in *Introduction to Carbon Technologies*, ed. H. Marsh, U. Heintz and F. Rodríguez-Reinoso, Universidad de Alicante, 1997.
30. A. Linares-Solano, in *Science and Technology of Activated Carbon (short course)*, Alicante, Spain, 1994, pp. 57–67.
31. H. Benaddi, T. J. Bandosz, J. Jagiello, J. A. Schwarz, J. N. Rouzaud, D. Legras and F. Béguin, *Carbon*, 2000, **38**, 669–674.
32. B. Jarrais, A. R. Silva and C. Freire, *Eur. J. Inorg. Chem.*, 2005, 4582–4589.
33. P. Serp and J. L. Figueiredo, *Carbon Materials for Catalysis*, Wiley, Hoboken, New Jersey, 2009.
34. X. F. Wang, S. J. Wu, Z. F. Li, X. Y. Yang, J. Hu, Q. S. Huo, J. Q. Guan and Q. B. Kan, *Appl. Organomet. Chem.*, 2015, **29**, 698–706.
35. X. F. Wang, S. J. Wu, Z. F. Li, X. Y. Yang, H. L. Su, J. Hu, Q. S. Huo, J. Q. Guan and Q. B. Kan, *Microporous Mesoporous Mater.*, 2016, **221**, 58–66.
36. N. Job, R. Pirard, J. Marien and J.-P. Pirard, *Carbon*, 2004, **42**, 619–628.

37. P. V. Samant, F. Gonçalves, M. M. A. Freitas, M. F. R. Pereira and J. L. Figueiredo, *Carbon*, 2004, **42**, 1321–1325.
38. N. Mahata, M. F. R. Pereira, F. Suárez-García, A. Martínez-Alonso, J. M. D. Tascón and J. L. Figueiredo, *J. Colloid Interface Sci.*, 2008, **324**, 150–155.
39. T. M. Yazdely, M. Ghorbanloo and H. Hosseini-Monfared, *Desalin. Water Treat.*, 2019, **158**, 256–265.
40. J. Zhu, P. Xiao, H. Li and S. A. C. Carabineiro, *ACS Appl. Mater. Interface*, 2014, **6**, 16449–16465.
41. J. Xu, Q. Jiang, J.-K. Shang, Y. Wang and Y.-X. Li, *RSC Adv.*, 2015, **5**, 92526–92533.
42. C. L. Hill, *Activation and Functionalization of Alkanes*, Wiley, 1989.
43. H. Zhang, M. H. Zhou, L. F. Xiong, Z. D. He, T. Q. Wang, Y. Xu and K. Huang, *Microporous Mesoporous Mater*, 2018, **255**, 103–109.
44. A. Krueger, *J. Mater. Chem.*, 2008, **18**, 1485–1492.
45. A. Schrand, S. Ciftan Hens and O. Shenderova, *Crit. Rev. Solid State Mater. Sci.*, 2009, **34**, 18–74.
46. J. Skubiszewska-Zieba, *Appl. Surf. Sci.*, 2010, **256**, 5520–5527.
47. J. Goscianska, P. Nowicki, I. Nowak and R. Pietrzak, *Thermochim. Acta*, 2012, **541**, 42–48.
48. J. Q. Xu, G. R. Chen, F. Guo and J. Q. Xie, *Chem. Eng. J.*, 2018, **353**, 507–518.
49. Z. P. Zhu, Z. Y. Liu, S. J. Liu and H. X. Niu, *Appl. Catal., B*, 1999, **23**, L229–L233.
50. Z. P. Zhu, Z. Y. Liu, H. X. Niu and S. J. Liu, *Sci. China, Ser. B: Chem.*, 2000, **43**, 51–57.
51. Z. P. Zhu, Z. Y. Liu, H. X. Niu, S. J. Liu, T. D. Hu, T. Liu and Y. N. Xie, *J. Catal.*, 2001, **197**, 6–16.
52. S. L. Bai, Z. B. Wang, H. Y. Li, X. Xu and M. C. Liu, *Fuel*, 2017, **194**, 36–41.
53. H. C. Huang, D. Q. Ye, B. C. Huang and Z. L. Wei, *Catal. Today*, 2008, **139**, 100–108.
54. M. E. Galvez, M. J. Lazaro and R. Moliner, *Catal. Today*, 2005, **102**, 142–147.
55. M. E. Galvez, A. Boyano, M. J. Lazaro and R. Moliner, *Chem. Eng. J.*, 2008, **144**, 10–20.
56. Z. G. Lei, A. B. Long, C. P. Wen, J. Zhang and B. H. Chen, *Ind. Eng. Chem. Res.*, 2011, **50**, 5360–5368.
57. Z. G. Lei, B. Han, K. Yang and B. H. Chen, *Chem. Eng. J.*, 2013, **215**, 651–657.
58. D. K. Sun, Q. Y. Liu, Z. Y. Liu, G. Q. Gui and Z. G. Huang, *Catal. Lett.*, 2009, **132**, 122–126.
59. D. K. Sun, Z. Y. Liu, G. Q. Gui, Z. G. Huang, Q. Y. Liu and Y. Xiao, *Chin. J. Catal.*, 2010, **31**, 56–60.
60. X. Gao, S. J. Liu, Y. Zhang, X. S. Du, Z. Y. Luo and K. F. Cen, *Catal. Today*, 2011, **175**, 164–170.

61. M. J. Lazaro, M. E. Galvez, C. Ruiz, R. Juan and R. Moliner, *Appl. Catal., B*, 2006, **68**, 130–138.
62. M. J. Lazaro, A. Boyano, M. E. Galvez, M. T. Izquierdo and R. Moliner, *Catal. Today*, 2007, **119**, 175–180.
63. A. Boyano, M. E. Galvez, R. Moliner and M. J. Lazaro, *Fuel*, 2008, **87**, 2058–2068.
64. M. E. Galvez, A. Boyano, R. Moliner and M. J. Lazaro, *J. Anal. Appl. Pyrol.*, 2010, **88**, 80–90.
65. T. Valdes-Solis, G. Marban and A. B. Fuertes, *Appl. Catal., B*, 2003, **46**, 261–271.
66. T. Valdes-Solis, G. Marban and A. B. Fuertes, *Ind. Eng. Chem. Res.*, 2004, **43**, 2349–2355.
67. E. Garcia-Bordeje, L. Calvillo, M. J. Lazaro and R. Moliner, *Ind. Eng. Chem. Res.*, 2004, **43**, 4073–4079.
68. E. Garcia-Bordeje, L. Calvillo, M. J. Lazaro and R. Moliner, *Appl. Catal., B*, 2004, **50**, 235–242.
69. E. Garcia-Bordeje, M. J. Lazaro, R. Moliner, J. F. Galindo, J. Sotres and A. M. Baro, *Appl. Surf. Sci.*, 2004, **228**, 135–142.
70. E. Garcia-Bordeje, M. J. Lazaro, R. Moliner, J. F. Galindo, J. Sotres and A. M. Baro, *J. Catal.*, 2004, **223**, 395–403.
71. E. Garcia-Bordeje, A. Monzon, M. J. Lazaro and R. Moliner, *Catal. Today*, 2005, **102**, 177–182.
72. E. Garcia-Bordeje, J. L. Pinilla, M. J. Lazaro, R. Moliner and J. L. G. Fierro, *J. Catal.*, 2005, **233**, 166–175.
73. E. Garcia-Bordeje, M. J. Lazaro, R. Moliner, P. M. Alvarez, V. Gomez-Serrano and J. L. G. Fierro, *Carbon*, 2006, **44**, 407–417.
74. M. J. Lazaro, A. Boyano, M. E. Galvez, M. T. Izquierdo, E. Garcia-Bordeje, C. Ruiz, R. Juan and R. Moliner, *Catal. Today*, 2008, **137**, 215–221.
75. A. Boyano, M. C. Iritia, I. Malpartida, M. A. Larrubia, L. J. Alemany, R. Moliner and M. J. Lazaro, *Catal. Today*, 2008, **137**, 222–227.
76. A. Boyano, N. Lombardo, M. E. Galvez, M. J. Lazaro and R. Moliner, *Chem. Eng. J.*, 2008, **144**, 343–351.
77. A. Boyano, M. J. Lazaro, C. Cristiani, F. J. Maldonado-Hodar, P. Forzatti and R. Moliner, *Chem. Eng. J.*, 2009, **149**, 173–182.
78. A. Boyano, C. Herrera, M. A. Larrubia, L. J. Alemany, R. Moliner and M. J. Lazaro, *Chem. Eng. J.*, 2010, **160**, 623–633.
79. M. O. Guerrero-Perez, J. M. Rosas, R. Lopez-Medina, M. A. Banares, J. Rodriguez-Mirasol and T. Cordero, *J. Phys. Chem. C*, 2012, **116**, 20396–20403.
80. Y. L. Wang, Z. Y. Liu, L. A. Zhan, Z. G. Huang, Q. Y. Liu and J. R. Ma, *Chem. Eng. Sci.*, 2004, **59**, 5283–5290.
81. W. Jing, Q. Q. Guo, Y. Q. Hou, G. Q. Ma, X. J. Han and Z. G. Huang, *Catal. Commun.*, 2014, **56**, 23–26.
82. H. H. Tseng, M. Y. Wey, Y. S. Liang and K. H. Chen, *Carbon*, 2003, **41**, 1079–1085.

83. S. V. Vassilev, C. Braekman-Danheux, R. Moliner, I. Suelves, M. J. Lazaro and T. Thiemann, *Fuel*, 2002, **81**, 1281–1296.
84. M. J. Lazaro, M. E. Galvez, I. Suelves, R. Moliner, S. V. Vassilev and C. Braekman-Danheux, *Fuel*, 2004, **83**, 875–884.
85. Y. X. Guo, Z. Y. Liu, Q. Y. Liu and D. K. Sun, *Chin. J. Catal.*, 2007, **28**, 514–520.
86. Y. X. Guo, Z. Y. Liu, Q. Y. Liu and Z. G. Huang, *Catal. Today*, 2008, **131**, 322–329.
87. S. A. Carabineiro, F. B. Fernandes, A. M. Ramos, J. Vital and I. F. Silva, *Catal. Today*, 2000, **57**, 305–312.
88. S. A. Carabineiro, F. B. Fernandes, J. S. Vital, A. M. Ramos and I. M. Fonseca, *Appl. Catal., B*, 2003, **44**, 227–235.
89. S. A. C. Carabineiro and L. S. Lobo, *Energ. Fuel.*, 2016, **30**, 6881–6891.
90. L. C. Chen, T. Y. Yen and G. J. Peng, *J. Chin. Inst. Chem. Eng.*, 2007, **38**, 35–41.
91. S. A. Carabineiro, D. W. McKee and I. F. Silva, *Carbon*, 2001, **39**, 451–463.
92. S. A. C. Carabineiro, A. M. Ramos, J. Vital, J. M. Loureiro, J. J. M. Orfão and I. M. Fonseca, *Catal. Today*, 2003, **78**, 203–210.
93. P. Davini, *Carbon*, 2001, **39**, 419–424.
94. X. Y. Xing, Z. Y. Liu and J. C. Wang, *Fuel Process. Technol.*, 2007, **88**, 717–722.
95. H. Dai, M. Y. Zhu, H. Y. Zhang, F. Yu, C. Wang and B. Dai, *J. Ind. Eng. Chem.*, 2017, **50**, 72–78.
96. S. Pinto, L. D'Ornelas and P. Betancourt, *Appl. Surf. Sci.*, 2008, **254**, 5390–5393.
97. H. Wang and E. Iglesia, *J. Catal.*, 2010, **273**, 245–256.
98. J. Ogonowski and E. Skrzynska, *React. Kinet. Catal. Lett.*, 2006, **88**, 293–300.
99. J. Ogonowski and E. Skrzynska, *Catal. Lett.*, 2006, **111**, 79–85.
100. J. Ogonowski and E. Skrzynska, *Catal. Lett.*, 2008, **124**, 52–58.
101. V. Neto, T. D. B. Costa, A. L. L. Magalhaes, A. B. Gaspar, P. G. P. de Oliveira and F. M. T. Mendes, *Mol. Catal.*, 2018, **458**, 317–325.
102. Y. Sakurai, T. Suzaki, N. Ikenaga and T. Suzuki, *Appl. Catal., A*, 2000, **192**, 281–288.
103. I. Kainthla, J. T. Bhanushali, R. S. Keri and B. M. Nagaraja, *Catal. Sci. Technol.*, 2015, **5**, 5062–5076.
104. R. D. Holtz, S. B. de Oliveira, M. A. Fraga and M. D. Rangel, *Appl. Catal., A*, 2008, **350**, 79–85.
105. Y. Sakurai, T. Suzaki, K. Nakagawa, N. Ikenaga and T. Suzuki, *Catal. Lett.*, 2000, **69**, 59–64.
106. J. S. Choi, T. H. Kim, M. B. Saidutta, J. S. Sung, K. I. Kim, R. V. Jasra, S. D. Song and Y. W. Rhee, *J. Ind. Eng. Chem.*, 2004, **10**, 445–453.
107. J. S. Choi, T. H. Kim, K. Y. Choo, J. S. Sung, M. B. Saidutta, S. D. Song and Y. W. Rhee, *J. Porous Mater.*, 2005, **12**, 301–310.

108. M. A. Hussain, N. Joseph, O. Kang, Y. H. Cho, B. H. Um and J. W. Kim, *Appl. Chem. Eng.*, 2016, **27**, 227–238.
109. Y. T. Chen, W. Chen, Q. H. Tang, Z. Guo, Y. H. Yang and F. B. Su, *Catal. Lett.*, 2011, **141**, 149–157.
110. M. J. Valero-Romero, A. Cabrera-Molina, M. O. Guerrero-Pérez, J. Rodríguez-Mirasol and T. Cordero, *Catal. Today*, 2014, **227**, 233–241.
111. R. Berenguer, J. Fornells, F. J. García-Mateos, M. O. Guerrero-Pérez, J. Rodríguez-Mirasol and T. Cordero, *Catal. Today*, 2016, **277**, 266–273.
112. Q. H. Tang, Y. T. Chen and Y. H. Yang, *J. Mol. Catal. A: Chem.*, 2010, **315**, 43–50.
113. P. Justin and G. R. Rao, *Catal. Today*, 2009, **141**, 138–143.
114. T. Maiyalagan and F. N. Khan, *Catal. Commun.*, 2009, **10**, 433–436.
115. L. Santos, K. S. Freitas and E. A. Ticianelli, *Electrochim. Acta*, 2009, **54**, 5246–5251.
116. Y. L. Niu, Z. Xu, M. Li and R. F. Li, *Chin. Chem. Lett.*, 2008, **19**, 245–248.
117. N.-T. Le, P. Lakshmanan, K. Cho, Y. Han and H. Kim, *Appl. Catal., A*, 2013, **464–465**, 305–312.
118. C. A. Antonyraj, B. Kim, Y. Kim, S. Shin, K. Y. Lee, I. Kim and J. K. Cho, *Catal. Commun.*, 2014, **57**, 64–68.
119. A. C. Encarnacao, A. Flores, S. I. Mota, C. Palma, A. M. Ramos, J. Vital and I. M. Fonseca, *Catal. Today*, 2003, **78**, 197–201.
120. T. Wang, Y. J. Ding, J. M. Xiong, L. Yan, H. J. Zhu, Y. Lu and L. W. Lin, *Catal. Lett.*, 2006, **107**, 47–52.
121. S. M. Schmuecker and B. M. Leonard, *Inorg. Chem.*, 2015, **54**, 3889–3895.
122. Z. X. Yan, M. Cai and P. K. Shen, *J. Mater. Chem.*, 2011, **21**, 19166–19170.
123. K. Li, J. B. Zhu, M. L. Xiao, X. Zhao, S. K. Yao, C. P. Liu and W. Xing, *ChemCatChem*, 2014, **6**, 3387–3395.
124. G. Q. He, Z. X. Yan, M. Cai, P. K. Shen, M. R. Gao, H. B. Yao and S. H. Yu, *Chem. – Eur. J.*, 2012, **18**, 8490–8497.
125. T. Z. Huang, S. Mao, H. H. Pu, Z. H. Wen, X. L. Huang, S. Q. Ci and J. H. Chen, *J. Mater. Chem. A*, 2013, **1**, 13404–13410.
126. Z. X. Yan, M. M. Zhang, J. M. Xie and P. K. Shen, *J. Power Sources*, 2013, **243**, 336–342.
127. S. Pinto-Castilla, S. Marrero, Y. Diaz, J. L. Brito, P. Silva and P. Betancourt, *React. Kinet., Mech. Catal.*, 2012, **107**, 321–332.
128. M. Mahajan, N. P. Lalla, K. Singh and O. P. Pandey, *Mater. Chem. Phys.*, 2015, **160**, 48–58.
129. T. Z. Huang, S. Mao, G. H. Zhou, Z. L. Zhang, Z. H. Wen, X. K. Huang, S. Q. Ci and J. H. Chen, *Nanoscale*, 2015, **7**, 1301–1307.
130. M. Fattahi, M. Kazemeini, F. Khorasheh and A. M. Rashidi, *Ind. Eng. Chem. Res.*, 2013, **52**, 16128–16141.
131. J. Y. Choi, B. Jeong, E. S. Kim, H. Y. Chun, D. W. Shin, D. H. Kim and H. D. Kim, *J. Nanosci. Nanotechnol.*, 2015, **15**, 9083–9087.

132. M. Lee, B. Ye, B. Jeong, H. Y. Chun, D. H. Lee, S. S. Park, H. Lee and H. D. Kim, *Korean J. Chem. Eng.*, 2018, **35**, 1988–1993.
133. M. Y. Li, Y. Y. Qi, W. Jin, B. Q. Jiao and J. Zhao, *J. Wuhan Univ. Technol., Mater. Sci. Ed.*, 2019, **34**, 572–578.
134. J. Yin, L. Wang, C. G. Tian, T. X. Tan, G. Mu, L. Zhao and H. G. Fu, *Chem. – Eur. J.*, 2013, **19**, 13979–13986.
135. J. Yin, L. Wang, P. Yu, L. Zhao, C. G. Tian, B. J. Jiang, D. D. Zhao, W. Zhou and H. G. Fu, *ChemElectroChem*, 2015, **2**, 1813–1820.
136. M. T. Noori, C. K. Mukherjee and M. M. Ghangrekar, *Electrochim. Acta*, 2017, **228**, 513–521.
137. C. Wang, L. Y. Hu, M. Y. Wang, Y. H. Ren, B. Yue and H. Y. He, *Chin. J. Catal.*, 2016, **37**, 2003–2008.
138. Z. J. Huang, F. W. Yan and G. Q. Yuan, *Catal. Lett.*, 2017, **147**, 509–516.
139. S. V. P. Vattikuti, P. A. K. Reddy, J. Shim and C. Byon, *J. Mater. Sci.: Mater. Electron.*, 2018, **29**, 18760–18770.
140. H. Y. Li, S. L. Bai, W. P. Jia and F. Li, in *Materials Processing Technology, Pts 1-3*, ed. X. H. Liu, Z. Jiang and J. T. Han, **vol. 418–420**, 2012, pp. 629–632.
141. B. C. Huang, R. Huang, D. J. Jin and D. Q. Ye, *Catal. Today*, 2007, **126**, 279–283.
142. S. L. Bai, S. T. Jiang, H. Y. Li and Y. J. Guan, *Chin. J. Chem. Eng.*, 2015, **23**, 516–519.
143. Q. Li, H. S. Yang, A. M. Nie, X. Y. Fan and X. B. Zhang, *Catal. Lett.*, 2011, **141**, 1237–1242.
144. L. Wang, J. H. Zhao, S. L. Bai, H. Zhao and Z. P. Zhu, *Chem. Eng. J.*, 2014, **254**, 399–409.
145. Y. Guo and J. Chen, *ChemPlusChem*, 2015, **80**, 1760–1768.
146. Q. L. Wang, P. C. Hung, S. Y. Lu and M. B. Chang, *Chemosphere*, 2016, **159**, 132–137.
147. R. X. Zhao, D. D. Jin, H. S. Yang, S. Y. Lu, P. M. Potter, C. C. Du, Y. Q. Peng, X. D. Li and J. H. Yan, *Environ. Sci. Technol.*, 2016, **50**, 11424–11432.
148. B. Koohestani, A. L. Ahmad, S. Bhatia and B. S. Ooi, *Curr. Nanosci.*, 2011, **7**, 781–789.
149. S. Q. Song, S. J. Jiang, R. C. Rao, H. X. Yang and A. M. Zhang, *Appl. Catal., A*, 2011, **401**, 215–219.
150. M. Sathiya, A. S. Prakash, K. Ramesha, J. M. Tarascon and A. K. Shukla, *J. Am. Chem. Soc.*, 2011, **133**, 16291–16299.
151. A. Nouralishahi, A. A. Khodadadi, A. M. Rashidi and Y. Mortazavi, *J. Colloid Interface Sci.*, 2013, **393**, 291–299.
152. L. Y. Cao, N. Zhang, L. L. Feng, J. F. Huang, Y. Q. Feng, W. B. Li, D. Yang and Q. Q. Liu, *Nanoscale*, 2018, **10**, 14272–14279.
153. T. Suzuki and K. Nakagawa, *J. Jpn. Pet. Inst.*, 2011, **54**, 66–79.
154. K. Nakagawa, C. Kajita, N. Ikenaga, M. Nishitani-Gamo, T. Ando and T. Suzuki, *Catal. Today*, 2003, **84**, 149–157.

155. K. Okumura, K. Nakagawa, T. Shimamura, N. O. Ikenaga, M. Nishitani-Gamo, T. Ando, T. Kobayashi and T. Suzuki, *J. Phys. Chem. B*, 2003, **107**, 13419–13424.
156. L. Rivoira, J. Juarez, H. Falcon, M. G. Costa, O. Anunziata and A. Beltramone, *Catal. Today*, 2017, **282**, 123–132.
157. S. S. Shang, B. Chen, L. Y. Wang, W. Dai, Y. Zhang and S. Gao, *RSC Adv.*, 2015, **5**, 31965–31971.
158. L. Y. Hu, C. Wang, B. Yue, X. Y. Chen and H. Y. He, *RSC Adv.*, 2016, **6**, 87656–87664.
159. L. Y. Hu, C. Wang, B. Yue, X. Y. Chen and H. Y. He, *Mater. Today Commun.*, 2017, **11**, 61–67.
160. Y. Li, B. Li, L. F. Geng, J. Wang, Y. Wang and J. Huang, *Catal. Lett.*, 2015, **145**, 1014–1021.

CHAPTER 13

Molecularly Dispersed Vanadium Oxide: Structure–Reactivity Relationships for Reducibility and Hydrocarbon Oxidation

M. OLGA GUERRERO-PÉREZ,[a] MARÍA V. MARTÍNEZ-HUERTA[b] AND MIGUEL A. BAÑARES*[b]

[a] Universidad de Málaga, Departamento de Ingeniería Química, E29071 Málaga, Spain; [b] CSIC-Instituto de Catálisis y Petroleoquímica, 28049 Madrid, Spain
*Email: miguel.banares@csic.es

13.1 Supported Vanadia

Vanadia may be present as a bulk oxide phase, but it may also spread on surfaces of other materials, like metal oxides or activated carbon, generating a composite material. The spreading of bulk vanadia as molecularly dispersed vanadium oxide species is a natural tendency due to its lower surface free energy. As a result, dispersed vanadia is characterized of new kind of bonds, connecting vanadium with the cation of the support, V–O–[S] (Scheme 13.1). This bond is directly related with the stabilization of dispersed vanadia and also endows the vanadia-support composite system with

Catalysis Series No. 41
Vanadium Catalysis
Edited by Manas Sutradhar, José Armando L. da Silva and Armando J. L. Pombeiro

Published by the Royal Society of Chemistry, www.rsc.org

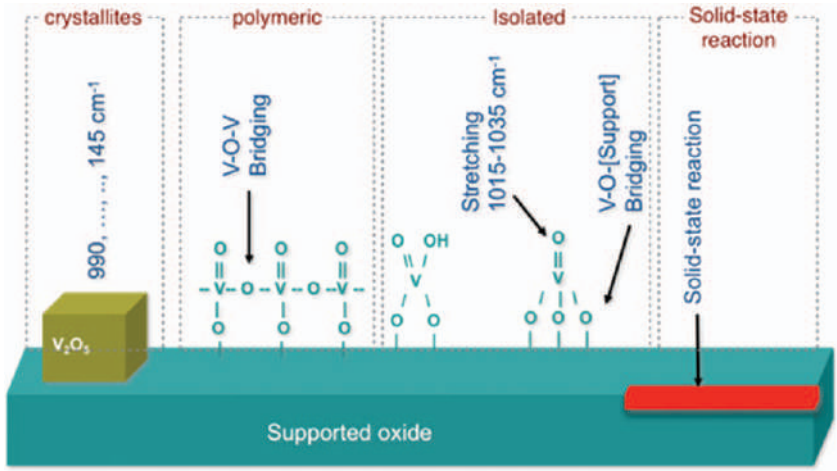

Scheme 13.1 Concept structure of supported vanadium oxides.

properties unlike those of the components. The new properties range from chemical to mechanical or thermal. The presence of a support is a way to maximize exposure of the active phase related with vanadium sites, but it also provides mechanical properties and may help tuning heat conductivity along the catalyst bed. This chapter will focus on the chemical site of these phenomena: how the presence of a support and vanadia coverage determines chemical properties related with vanadia structure, reducibility and polymerization degree that, in turn, tune the properties of supported vanadium oxides.

13.2 Stabilization of Dispersed Vanadia

Dispersion of vanadia is due to a stabilization of vanadia moieties by titration of support hydroxyl groups, as is the case for other supported oxides.[1,2] Thus, the hydroxyl bonds of the support [S]–O–H change into [S]–O–V bonds, releasing water. The maximum loading that can be attained by vanadia on an oxide support is related to the presence of surface hydroxyl groups on the support. This degree is different from support oxide to support oxide; most support oxides are quite well hydroxylated, like alumina, titania, zirconia, ceria and may thus stabilize a high surface density of dispersed vanadia moieties, typically up to *ca.* 7 V atoms per nm^2 of oxide support;[3] this surface coverage corresponds to the physical coverage of the support by VOx moieties and is at the core of the term ''*monolayer coverage*''. Monolayer coverage is not fully accurate since the maximum surface density is limited by anchorage sites, which may be few. Silica is a good example – while silica exhibits a typically elevated surface area, its hydroxylation is significantly lower than that of the oxides discussed. Silica hydroxylation can be almost an order of magnitude lower than that of those oxides; this is evident when

the infrared signal of hydroxyl groups of silica is compared with that of the other oxides. Highly isolated hydroxyl groups dominate on silica and no hydrogen bonding is typically apparent. That limits the number of VOx moieties that may disperse, *e.g.*, fumed silica may stabilize less than 1 VOx moiety per nm^2 of silica support. In this case, the term "*monolayer*" coverage is clearly far-fetched. Actually, the right term should be "*dispersion limit loading*", which is understood as the maximum coverage at which an oxide may spread on a support before three-dimensional structures become apparent.

The structure of a supported oxide is determined by the nature of the supported oxide (vanadia in this contribution), the nature of the support and its surface chemistry and area. Since surface coverage is a critical factor, it is more informative to describe it as surface density (atoms per nm^2 of support) than as weight percent. This brings better comparability among samples and provides a descriptor directly related to properties of the system.

13.3 Characterizing Supported Oxides

Multiple techniques can be used to characterize supported oxides, the most convenient being textural (like BET area), surface analysis (like XPS), diffraction analyses (like XRD) and molecular analysis (like Raman and infrared spectroscopies). Detailed insight can be obtained by additional characterization, like solid-state NMR, EPR, transmission electron microscopy or those based on X-ray absorption at synchrotron facilities. However, most insight can be obtained by the former, which are quite accessible in most research facilities. Some examples of the latter will be given for specific cases later in this chapter.

BET area provides the surface area of the support and of the supported vanadium oxide system. BET area of the support is instrumental to know at what vanadia weight loading the system reaches its dispersion limit loading.

Photoelectron spectroscopy, XPS, provides information about the elements, their oxidation state and their environment. It is possible to assess whether the supported oxide is mainly at the outermost surface of the support or diffuses into its bulk. The XPS vanadium to cation of the support ratios provides an estimate on the degree of dispersion of supported oxides. This is not the most accurate measurement since escape depth of photoelectrons is of several atomic layers, thus, the early formation of aggregates will not be apparent to XPS atomic ratios until those possess a significant size.

X-ray diffraction provides valuable insights into the long-range order of the system, mainly on the phases of the support phase. Little is typically reported by XRD on the supported vanadia, since it is molecularly dispersed. Supported vanadia may also be present as V_2O_5 domains above the dispersion-limit loading; however, these are nanocrystals, typically smaller than 4 nm, which may not generate a diffraction pattern. In most cases, the key catalytic properties of supported oxides are delivered when these

are present as molecularly dispersed or when they build nano-scaled crystallites.

Molecular spectroscopies are particularly valuable to characterize supported oxides, since these are typically amorphous phases. Raman and infrared elegantly blend into very convenient and complementary insight.

Infrared spectroscopy is a bulk technique; but supported oxides species are on the surface. Infrared may also provide information on the molecular states of supported oxides and with high sensitivity. However, infrared high sensitivity to supported oxides is hampered by the concomitant overlap of the absorption of the oxide supports, typically in the region below 1000 or 900 cm^{-1}, depending on the oxide. This generates signal saturation below *ca.* 900 cm^{-1} obscuring information on the oxide support. Fortunately, in many cases, the vanadyl can be observed in the *ca.* 1000 cm^{-1} region, and its harmonic above 2000 cm^{-1} is free of this constraint. The impossibility to observe modes below *ca.* 950 cm^{-1} seriously limits infrared spectroscopy to investigate supported oxides' structures during reaction. The most important capacity of infrared is associated with *in situ* and *operando* studies, where the adsorption and evolution of reactants, intermediates and spectators can be investigated during reaction. Infrared is most informative on the states of adsorbed molecules, ammonia-based, nitrogen oxide-based or hydrocarbons. For these, infrared is highly sensitive to oxygen-containing carbon species and less sensitive to polyolefinic carbon species; but can be well-monitored with Raman spectroscopy. Multimodal IR-Raman *operando* reactors thus provide the perfect blend of information during catalytic operation.[4]

Raman spectroscopy is also a bulk technique; however, Raman signal of the supported phase originates essentially from the surface. Raman spectroscopy is particularly sensitive to the states of supported vanadia for it can describe the state of vanadium as isolated, polymerized or crystalline. Raman can describe solid-state reactions between vanadia and the support and can tell interaction of supported vanadia with other species at the surface. Furthermore, Raman can characterize the interaction of dispersed vanadia with gases and vapors, *e.g.*, water (dehydrated, hydroxylated, hydrated).[3,5–7] There is, in addition, a particularly valuable feature of Raman spectroscopy: it is ideally suited for *in situ* and *operando* characterization of supported oxides since it typically words with visible light and in backscattering mode.[8,9] Thus, any quartz, sapphire or glass cell, cuvette or reactor is adequate to observe changes of supported vanadia in real time during treatments or reactions.[3] The catalyst changes during reaction affect not only to the state of the oxide system but also to the adsorption of reactants at the surface (nitrogen oxides, ammonia, hydrocarbons) or the buildup of carbon deposits (*e.g.*, coke) these can be observed by Raman spectroscopy. In a complementary fashion to infrared, Raman is more sensitive to polyolefinic carbon species than to oxygen containing ones. For this reason, complementary multimodal IR-Raman *operando* reactors provide the perfect blend of information during catalytic operation.[4]

13.4 Role of the Support

Vanadia binds to the cation support, [S], *via* V–O–[S] bridging oxygen bonds. This has dramatic effects on the properties of molecularly dispersed vanadia. The most apparent is the strength of the vanadyl (V=O) mode, which change is clearly monitored with Raman spectra of the dehydrated catalysts. The dramatic changes of the V=O mode strength with support and the dramatic (orders of magnitude) changes in activity per vanadium site (turnover frequency) in different oxidation reactions (methanol, ethane, propane) has led some authors to suggest that the vanadyl mode is the site directly involved in the rate-determining step. However, a plot of the V=O strength (Raman mode) *vs.* TOF numbers show that there is no correlation at all (Figure 13.1). The effect of the support on V–O–[S] bonds is apparent to reactivity tests, such as catalytic oxidation reactions, like oxidative dehydrogenation of ethane, which runs $ZrO_2 > TiO_2 > Al_2O_3 > CeO_2 > SiO_2$.[10,11] The reducibility of the oxide support typically reflects on vanadia reducibility and seems to correlate with the activity per surface vanadium site for ethane oxidation, where vanadia would undergo redox cycles. There is, however, an exception: ceria stabilizes vanadium as pentavalent by reducing itself to Ce^{3+} [12] and the redox cycle is run on the ceria cations.[13] The rationale for this was provided by Sauer and co-workers,[14] who modeled dispersed vanadia on ceria at the request of Bañares' group, and calculated that ceria reduced at the interface with vanadia, which in turn is dramatically stabilizes in its pentavalent state.

The interaction with the support may lead to solid-state reactions between vanadia and the oxide supports, as is the case for niobia, ceria, alumina or zirconia where mixed phases form.

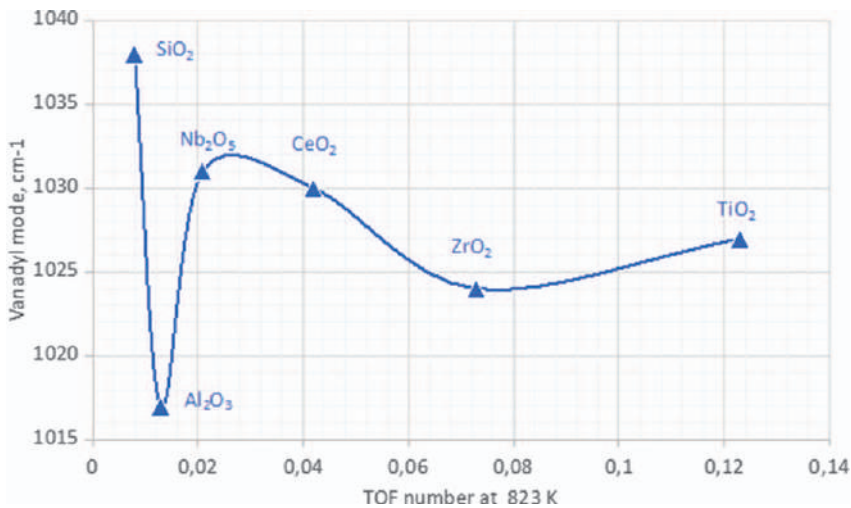

Figure 13.1 Role of the oxide support on the V=O mode and on the TOF numbers (s–1) for ethane oxidative dehydrogenation reaction. Generated with data from ref. 11.

Ceria. Vanadium oxide on ceria reacts forming cerium vanadate,[15] its formation is facilitated by reducing conditions,[16] which is consistent with the presence of reduced ceria at the interface with vanadia.[13]

Niobia. Vanadium oxide on niobia is an interesting system since vanadia first blends with niobia support making a solid-solution. Surface dispersed vanadium oxides are only present when the bulk of niobia support saturates with vanadium;[17] bulk V–Nb–O phases form at higher loadings.

Alumina. Vanadium oxide on alumina may result in the formation of aluminum vanadate,[18] which presence is clearly reported by Raman spectra. Aluminum vanadate (Raman modes at 281, 322, 397, 463, 514, 557, 851, 900, 918, 947, 984 and 1012 cm^{-1})[19,20] does not typically form and its formation typically occurs at high vanadia loadings, close to the dispersion limit loading.

Zirconia. Vanadia reacts with zirconia into zirconium vanadate, ZrV_2O_7, characterized by intense Raman modes, particularly at 780 and 990 cm^{-1}.[21] The solid-state reaction between ZrO_2 and vanadia requires some.

Titania is different as it will host tetravalent vanadium cations replacing titanium cations, this triggers the titania anatase-to-rutile transition at temperatures significantly lowers that pure titania: *ca.* 500 °C *vs.* > 1000 °C.[22]

Silica is also different as hardly any reaction occurs between vanadia and the silica support. The low hydroxylation of silica results in dispersion limit loadings far below those observed for the support oxides commented above, *ca.* 1 *vs. ca.* 7 $V_{at}\,nm^{-2}$. Little interaction not only exhibits a moderate dispersion limit loading for vanadia, but it also hardly stabilizes dispersed vanadia species. Reducing conditions tend to aggregate dispersed oxides, like vanadia. Thus, increasing their polymerization degree. Silica low hydroxylation does not allow the presence of polymeric vanadia and only isolated vanadium oxides are apparent. Reducing treatments of vanadia on silica leads to rearrangement of dispersed vanadia into V_2O_5 crystallites,[23] while oxidative ones promote its dispersion.[24]

The structure–activity relationships for ethane ODH on supported oxides was reviewed in detail;[25] more recently, a thorough revision for propane ODH on supported vanadia can also be found.[26]

13.5 Role of Coverage

The structure of molecularly dispersed vanadia depends on its coverage. Vanadia binds to the cation support, [S], *via* V–O–[S] bridging oxygen bonds. Supported vanadium oxide is comprised, at least, of V=O bonds and V–O–[S] bonds. As vanadia loading increases, its higher surface density results in distances among vanadia sites that enable its polymerization *via* the V–O–V bonds, and the population grows at the expense of the V–O–[S] bonds. The progressive polymerization of supported oxides with coverage can be observed by different techniques, *e.g.*, the V=O Raman mode of dehydrated samples is sensitive to the progressive polymerization of supported vanadia, blueshifting its mode with coverage. Some broad bands near 900 cm^{-1} grow

increasingly stronger with coverage in dehydrated samples and is associated with V–O–V modes. On some occasions it is possible to quantify the polymerization degree of supported oxides with the use of UV–vis spectroscopy; the alumina-supported vanadia polymerization degree was quantified and show clearly the evolution from isolated to fully polymerized vanadia[18] – this work also provides an interesting correlation between vanadia polymerization on alumina and the presence of Brønsted acid sites.

It is expected that the properties impinged by the support to supported vanadia will be maximum at lower coverages, where the (V–O–V)/(V–O–[S]) population ratio is lower. A good example of this is provided by the effect of vanadia coverage on titania and on alumina supports. The reducibility can be measured with H_2 Temperature Programmed Reduction (TPR), which defines a temperature for maximum reduction (T_{max}). Titania makes supported vanadia more reducible than alumina support does: 550 °C[18] *vs.* 406 °C[22] at low coverage (*ca.* 1 V nm^{-2}). However, as vanadia loading increases, the reducibility of vanadia, measured (T_{max} values during TPR) changes differently for both systems (Figure 13.2). Vanadium oxide on titania becomes increasingly less reducible as vanadia coverage increases up to *ca.* 7 V_{at} nm^{-2},[22] which is the dispersion limit loading. Conversely, vanadium oxide on alumina becomes increasingly reducible as vanadia coverage increase up to *ca.* 7 V_{at} nm^{-2} (dispersion limit loading). Why are these trends apparently opposite? The reason is that titania makes supported vanadia more reducible than alumina. As vanadia coverage increases, the (V–O–V)/(V–O–[S]) population ratio increases, which dilutes the support effect. Ultimately, this population distribution would tend to a predominance of V–O–V species. This scenario happens at the dispersion limit loading, since crystalline vanadia develops above this loading. It is interesting to note that vanadia on titania and vanadia on alumina tend to reduce at very similar temperatures as we approach the dispersion limit loading (459 °C on titania and 469 °C on alumina). In many reactions, polymeric surface vanadia species break into smaller oligomeric species.[27]

Coverage also has an effect on reactivity, since some reactions run on single sites; on these reactions, coverage has a negligible effect on activity, keeping the rate per vanadium site (turnover frequency) essentially constant (like the oxidative dehydrogenation of ethane or propane). Others require an arrangement of sites, and such ensembles may be afforded upon polymerization with higher vanadia loading. A good example of this is presented by Deo and Wachs,[28] where the TOF number from butane to maleic anhydride increases with vanadia loading on titania, in direct relationship with the polymerization of surface vanadia sites (Figure 13.3). This is due to the need of simultaneously oxidize both ends of butane molecule.

13.6 Role of Additives

Supported vanadia interact preferably with the support and then among them as surface coverage increases, evolving from isolated to polymerized species. The presence of additives is typically to modulate the properties of

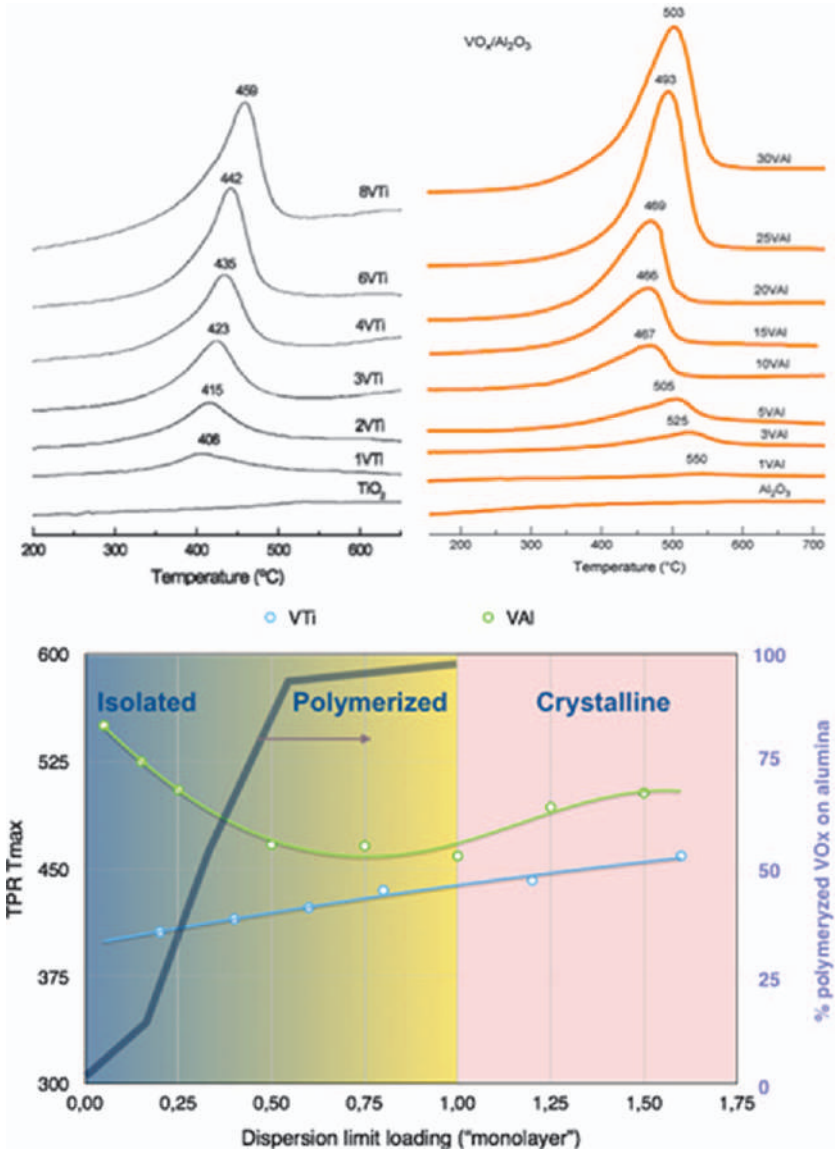

Figure 13.2 H_2-TPR profile for VOx/TiO_2 (left), VOx/Al_2O_3 (right), and effect of vanadia coverage on reducibility and acidity (bottom).
Reproduced from ref. 18 (right) and ref. 22 (left), with permission from Elsevier, Copyright 2006, 2009.

supported vanadia, and typical additives can be alkali cations, phosphorus, other transition oxides, *etc.* As a general rule, additives may be classified as ''interacting'' and ''non-interacting'' additives. This classification is based on their affinity with supported vanadia. Interacting additives will interact with supported vanadia, even at very low loadings since there is a clear

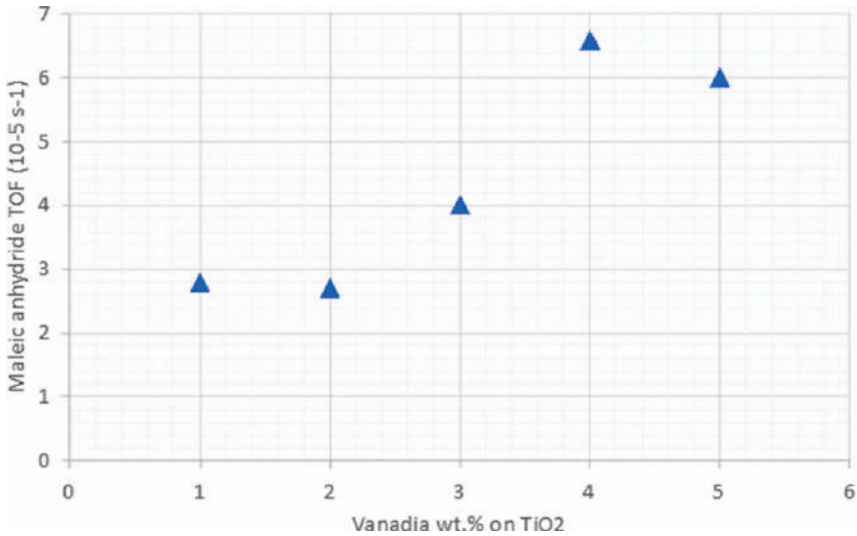

Figure 13.3 Butane to maleic anhydride TOF numbers *vs.* vanadia loading on titania. Generated with data from ref. 28.

affinity; alkali cations constitute a good example of interacting additives. Non-interacting additives will interact with vanadia when the total loading of vanadia plus additive is above the dispersion limit loading. Supported molybdena is a good example of a non-interacting additive.

Interacting Additives. Potassium is a good example of an interacting additive. It will maximize its entanglement with vanadia, and DFT calculations show that the energy of the system is minimum with a maximum interaction between K and V on TiO_2 support.[29] The presence of little amounts of potassium has a clear effect on supported vanadia structure and reactivity. Raman spectra show a redshift of the vanadyl mode, which is associated with a weakening of the V=O bond.[29] Still, this system becomes increasing less reducible as the alkali cation progressively weakens the V=O bond. This is a clear indication that the reactive oxygen site on supported vanadia for its reduction is not the V=O bond. DFT calculations show that it is the V–O–Ti bond the one where oxygen is removed from vanadia upon reduction; this bond grows stronger with increasing addition of potassium. In a more general scope, alkali cations decrease vanadia reducibility in the order $Li < Na < K < Rb < Cs$.[29] Another interacting additive is phosphorus, which also has a great affinity for vanadia.

Non-interacting Additives. Molybdenum or antimony are good examples of non-interacting additives. When surface coverage of $Mo + V$[30,31] or $Sb + V$[32] is below the dispersion limit loading, both elements share the support, there is an increasing crowding as coverage approaches the dispersion limit, but no mixed oxide phases are apparent. However, above that loading, when three-dimensional structures form, both elements blend into mixed oxide phases, *e.g.*, Mo–V–O mixed oxide phases and $VSbO_4$.

13.7 *In Situ* Characterization of Supported Vanadia

Water, Water Everywhere. Supported vanadium oxide is most sensitive to environmental conditions, with dramatic effects on its structure; thus, it is critical to characterize supported vanadia under the conditions relevant to our study. Before we consider reactive conditions, we should step into more simple and adventitious molecules: water. Water molecules are ubiquitous, they are very reactive and have a major effect (Scheme 13.2). A typical supported vanadium oxide exposed to ambient moisture will adsorb water readily, experimental observation demonstrating that supported vanadia is actually totally solvated.[5] Even if the samples look dry and behave as a dry loose powder, the supported oxides typically have some 10 wt.% as molecular. Supported oxides under ambient conditions are actually hydrated. The structure they have is determined by liquid phase chemistry, thus, ruled by concentration and pH;[5] these parameters are defined by the specific oxide support and vanadia loading; *e.g.*, silica support will provide an acidic support while MgO will provide a basic support. The structures will range from monovanadates at high pH values to decavanadate species at low pH values and high concentration (Figure 13.4).[3]

Since most supported-vanadia materials are used for catalysis in reactions that typically occur at temperatures high enough to evaporate water, this would lead to a scenario of dehydrated supported oxides. The transition from hydrated to dehydrated supported oxides is reversible. A dehydrated supported oxide is characterized by V–O–[S] bonds along with vanadyl and V–O–V bonds. The presence of water leads to hydrolysis of the bridging oxygen, progressively decoupling supported vanadia moieties, and the solvation process ultimately leads to dissolved vanadates.

The concept of hydrated samples is accurate; however, the concept of dehydrated sample is not fully accurate. Hydroxyls are the third character in this scenario that ranges from liquid water to water vapor. Hydroxyls result

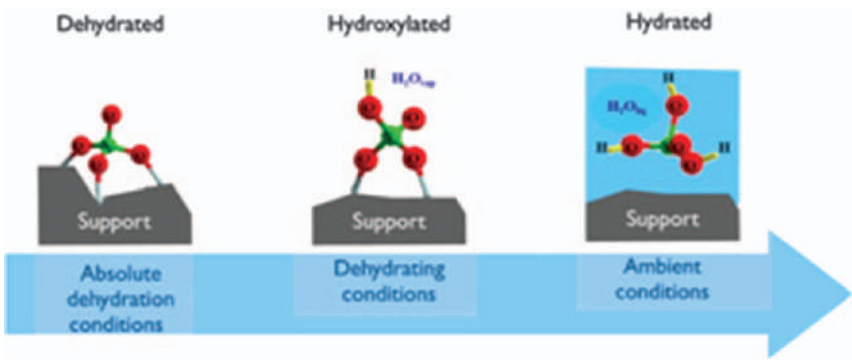

Scheme 13.2 States of supported vanadia upon increasing exposure to humidity, dehydrated (left), hydroxylated (middle), solvated-hydrated (right).

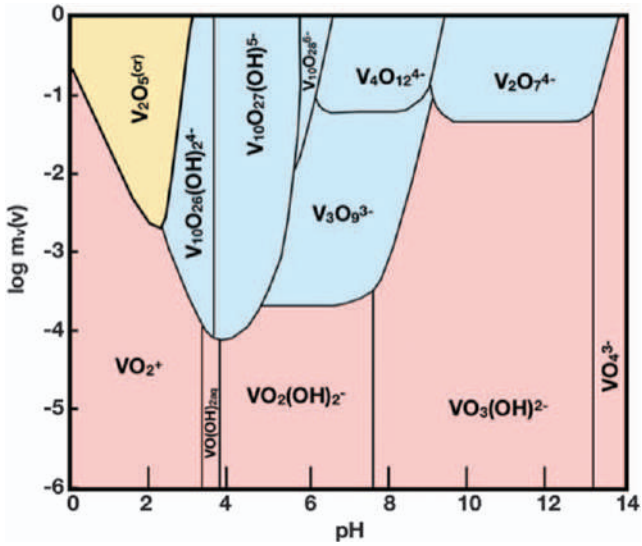

Figure 13.4 Phase diagram of aqueous vanadium(v) solution species, present in aqueous solutions at 25 °C, on the basis of data in Baes C. F., Jr., and Mesmer R. E., ''The Hydrolysis of Cations,'' Wiley, New York, 1970. Yellow solid, red monomeric, blue polymeric.

from dissociative adsorption of water during hydrolysis of V–O–[S] bonds. The actual state of a catalyst will actually range from dehydrated, hydroxylated and hydrated. A Molecular Dynamics and Density Functional Theory series of studies have addressed this for vanadium oxide molecularly dispersed on titania at low coverage, mainly monomeric,[7] and close to the dispersion limit loading, mainly polymerized;[6] showing that absolute dehydrated supported vanadia exist only in the absolute absence of water. If water is present, some hydroxylation will occur and if water partial pressure is high enough or temperature is low enough, solvation will occur (Figure 13.5). As supported-vanadia hydroxylates, two phenomena become apparent – its polymerization decreases for high coverage samples,[6] and the vanadyl Raman mode redshifts at any coverage.[6,7]

If Raman spectroscopy can clearly tell the difference between hydrated and dehydrated supported oxides, it may also estimate the degree of hydroxylation of supported oxides. There is a systematic trend, the vanadyl mode shifts to lower frequencies upon hydration, *e.g.*, 1030 cm^{-1} towards 960 cm^{-1}. If we avoid hydrated conditions, there is a consistent redshift of the V=O mode of any supported vanadia, the redshift is stronger as the temperature decreases and/or as the partial pressure of water vapor increases (Figure 13.6). This is associated with progressive hydroxylation of supported vanadia, and the MD-DFT model provides the rational for this since the hydroxylation weakens the vanadyl mode and its calculated Raman mode exhibits lower frequencies.[6,7]

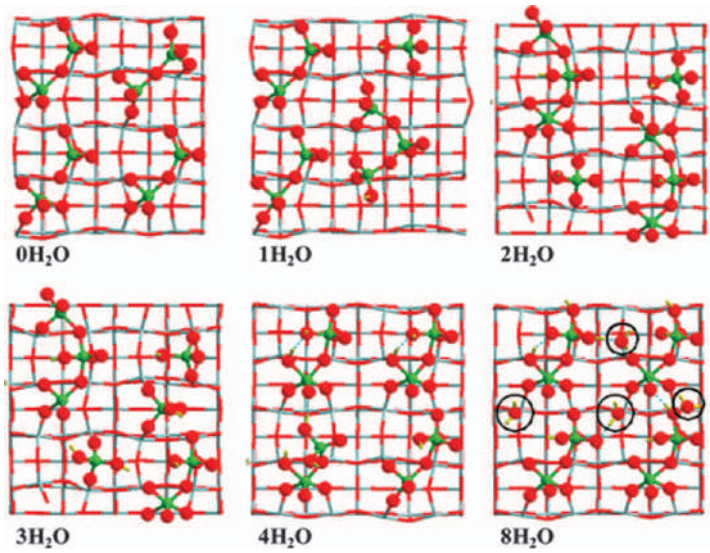

Figure 13.5 Most stable models of the high loading vanadia–titania catalyst after water molecules addition; optimized at 0 K. Water molecules are marked by a black circle.
Reproduced from ref. 6 with permission from American Chemical Society, Copyright 2013.

Reactive Environment, Reduction, Oxidation. Temperature-programmed reduction (TPR) and oxidation (TPO) are typical means to characterize supported vanadia catalysts, *in situ* spectroscopic characterization during TPR/TPO provides valuable insight on the dynamic states of supported vanadia; for instance, the solid-state reaction between ceria support and vanadia species on the surface occurs at *ca.* 600 °C in air during an *in-situ* TPO-Raman study (Figure 13.7); however, the same transition occurs slightly above 400 °C in hydrogen, as reported by *in-situ* TPR-Raman. This solid-state, in both cases, leads to the formation of $CeVO_4$, which oxidation states are Ce(III) and V(V), the starting materials, VOx/CeO_2 is characterized by oxidation states of V(V) and Ce(III) at the interface with vanadia and Ce(IV) in the bulk of ceria. Cerium vanadate net oxidation degree is lower than that of VOx/CeO_2; thus, the formation of $CeVO_4$ is promoted by reducing environment. This is an interesting case for multiple reasons. One reason is because it is the only supported vanadia system which does not undergo redox cycle on the vanadium cation,[13] which is stabilized as pentavalent. The other reason is because typical H_2-TPR profiles of supported vanadia associate the reduction peak in the 400–500 °C with the reduction of dispersed vanadia. *In-situ* TPR-Raman shows that this system is different, there is indeed reduction in the 400–500 °C region, but it is due to the reduction of ceria and the concomitant formation of $CeVO_4$. This case provides a clear example of the value of real-time characterization in reactive conditions. This paves the ground to characterize catalytic materials during reaction conditions since it will provide valuable information of the state of the catalyst during reaction.

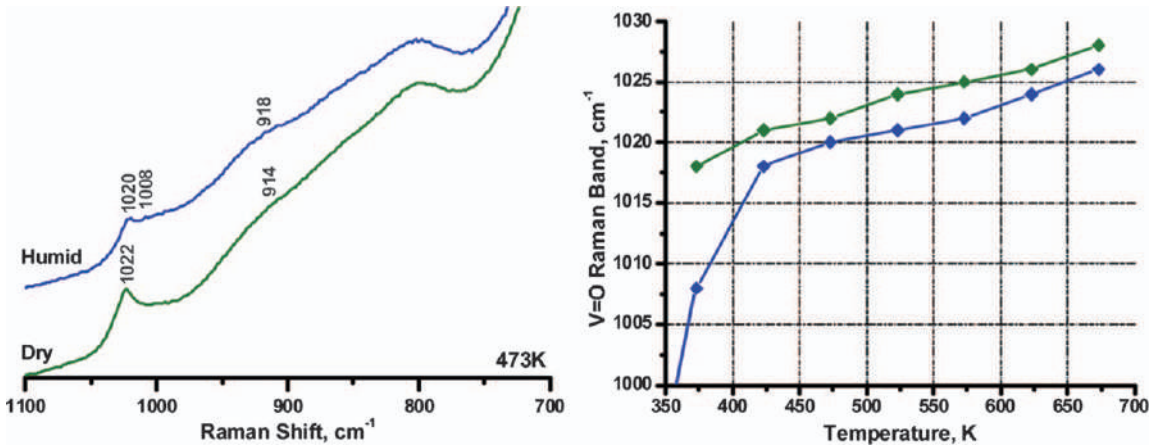

Figure 13.6 (left) Representative Raman spectra of a catalyst containing 1.2 V atoms per nm^2 of TiO_2 in dry (green trace) and humid (blue trace) air flow at 473 K. (right) Raman vanadyl vibration mode *vs.* temperature for such catalyst in dry (green trace) and humid (blue trace) air.
Reproduced from rref. 7 with permission from American Chemical Society, Copyright 2011.

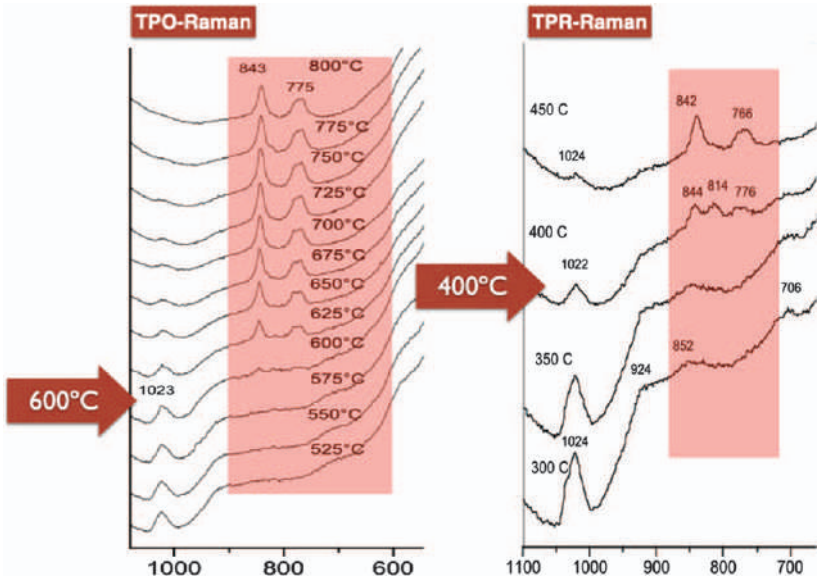

Figure 13.7 *In-situ* TPO-Raman (left) and *in-situ* TPR-Raman (right) of 2 wt.% V_2O_5/CeO_2. Adapted from rref. 15 with permission from American Chemical Society, Copyright 2008.

13.8 *Operando* Study of Supported Vanadia

Mimicking catalysis in an *in-situ* cell is a valuable approach to understand the state of a catalyst during reaction; however, most *in-situ* cells perform poorly as a catalytic reactor.[33] This is a major hurdle if we aim at determining structure-activity relationships. The past 20 years have experienced a major transformation to transform *in-situ* cells into catalytic reactors that allow acquiring spectra during reaction. Thus, both spectra and activity data have quality; this is the concept of *operando* methodology, which was first proposed in 2002.[34,35] *Operando* studies are a particular case of hyphenated *in-situ* studies in which the catalyst is characterized while it is really working ("*operando*" in Latin), and the activity is simultaneously measured. *This hyphenation makes sense only if the operando reactor behaves like the reactor in which the catalyst under study typically operates*.

A good *operando* example is related with the solid-state reaction between vanadia and ceria during the oxidative dehydrogenation of ethane to produce ethylene.[16] Ceria-supported vanadia catalyst deactivates during this reaction; the deactivated catalyst has no dispersed vanadia, which has transformed into $CeVO_4$. An *operando* Raman-GC study a solid-state reaction occurs at 500 °C during reaction. This is an interesting temperature, it is clearly above the 400 °C at which the solid-state reaction takes place in the presence of air (*in-situ* TPO-Raman study, Figure 13.7-left) and it is clearly below the 600 °C limit at which the solid-state reaction takes place in the

presence of hydrogen (*in-situ* TPR-Raman, Figure 13.7-right). TPO and TPR actually define the boundary conditions of the ethane oxidative dehydrogenation reaction. This is an oxidation redox reaction that operates on Mars-van-Krevelen mechanism;[36,37] such a mechanism implies that the catalyst lattice oxygen is directly involved in the catalytic cycle. While it is an oxidation reaction with net oxidizing reaction conditions, the catalyst reduces oxidizing the hydrocarbon molecule and the gas-phase molecular oxygen feed reoxidizes the catalyst. Mars-van-Krevelen mechanism implies continuous reduction and oxidation cycles. 500 °C is high enough to trigger the solid-state reaction to $CeVO_4$ when the catalyst is reduced by the hydrocarbon. This irreversible solid-state reaction accounts for the deactivation of the catalyst at 500 °C in oxidizing environment.

Operando spectroscopy can also monitor the evolution of supported oxides and how they blend with additives during reaction, creating the active phase. That is the case of propane ammoxidation to acrylonitrile on alumina-supported V–Sb–O catalysts.[34] Figure 13.8a shows the state of the catalyst as synthesized. The fresh catalyst is constituted by dispersed vanadia and antimony oxide on alumina support. Dispersed amorphous SbOx has very weak Raman bands[32,38] so the presence of the Raman bands of supported vanadium oxide overwhelm those of SbOx. As ammoxidation reaction temperature increases, significant changes are apparent in the Raman bands of dispersed vanadia, these changes illustrate the progressive formation of $SbVO_4$ (Figures 13.8b–e). Simultaneous activity measurements show the increasing production of acrylonitrile as the $VSbO_4$ phase becomes apparent. This figure illustrates the genesis of a catalytic active phase. Also, a comparison between *operando* spectra during ammoxidation and upon reoxidation show changes in the states of dispersed vanadia and of segregated antimony oxide, while $VSbO_4$ remains essentially unaltered. A detailed study blending operando Raman studies with DFT calculations[39] shows that ammoxidation takes advantage of the high structural reactivity of $VSbO_4$, as confirmed by HR-TEM[40] and theoretically,[41] facilitating the interconversion between dispersed vanadia and segregated antimony oxide. Dispersed vanadia would activate propane to propylene, which would subsequently react with ammonia that adsorbs on isolated vanadium sites at the surface of $VSbO_4$ surface.[39,42]

13.9 Concluding Remarks

The scope of this chapter addresses supported vanadium oxide catalysts, their structure and their activity, mainly for alkane oxidation and ammoxidation reactions; it also addresses the reducibility of supported oxides. In all these cases, the reactivity is associated with oxygen species coordinated with vanadia. The conclusions drawn here will be relevant for these cases, where there is experimental evidence. Supported vanadium oxide catalysts activity is affect by the support, additives and surface coverage. In all cases – reducibility, oxidation of hydrocarbons and ammoxidation of

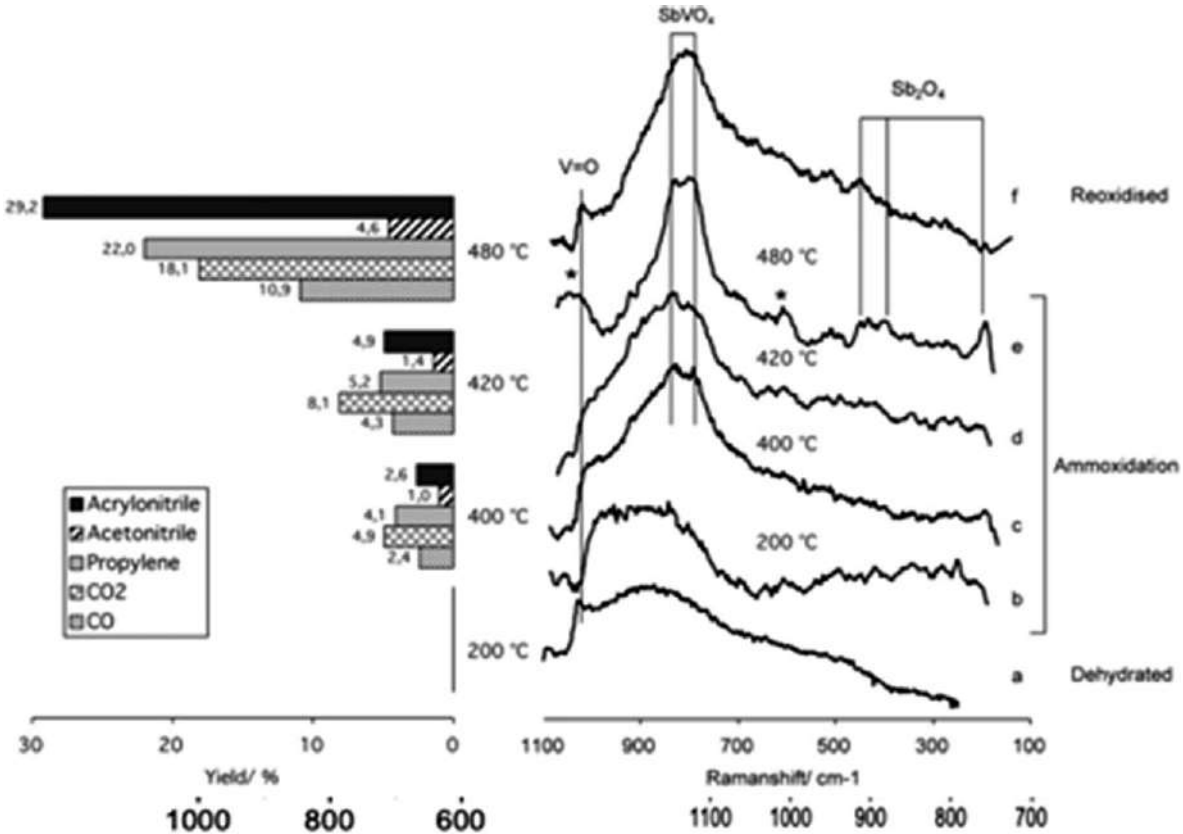

Figure 13.8 Raman spectra of Sb–V–O/Al_2O_3 catalyst during propane ammoxidation reaction and other conditions: dehydration at 200 °C (a); ammoxidation at 200 °C (b), 400 °C (c), 420 °C (d) and 480 °C (e), reoxidation at 440 °C (f). The corresponding yield values are presented in the left panel. Reaction conditions: 200 mg of catalyst, total flow 20 ml min^{-1}; feed composition (% volume); C_3H_8–O_2–NH_3–H_2O–He $(9.8 + 25 + 8.6 + 0 + 56.5)$.
Reproduced from ref. 34 with permission from the Royal Society of Chemistry.

hydrocarbons – there is no correlation with the bond strength of the vanadyl bond. Thus, the role of this site as participating in the critical rate-determining step is ruled out. A common feature is also that the support has a dramatic effect on reducibility and alkane (am)oxidation activity, which underlines the relevance of the V–O–[Support] bond as the critical site for the rate-determining steps. Finally, supported vanadia polymerization degree increases with coverage, triggering the (V–O–V)/(V–O–[Support]) population ratio. The presence of polymeric vanadia affects its reactivity and properties. In some reactions, *e.g.*, where an arrangement of sites rather than a single site is needed, the turnover frequencies will increase.

Additives have an effect on the structure of supported oxide, alkali dopants have very high affinity for vanadia, they are ''interacting'' additives and their effect is apparent from very low loadings. The major effect of alkali cations is strengthening of the V–O–[support] bond making the system less reactive and less reducible. Alkali cations also weaken the vanadyl bond, which in any case is much stronger than bridging oxygens and does not make it more reactive than other available sites. Structurally, alkali cations tend to maximum entanglement with supported vanadia, minimizing its polymerization. Other additives show less affinity to react with supported vanadia; ''non-reacting'' additives will blend once that coverage is above monolayer dispersion limit, where bulk structures form.

Real-time spectroscopy, in particular *operando* methodology, allows characterizing the structure and reactivity of supported vanadia (and many oxides, in general) in a simultaneous fashion. This places us in an ideal situation to assess structure–activity relationships at a molecular level, which, in turn, enables knowledge-based design of better performing materials.

Acknowledgements

This chapter is devoted to the memory of Prof. J. L. G. Fierro (d.2020); the authors are among those who were lucky enough to have him as their PhD advisor (M.A.B.) and PhD co-advisor (M.V.M.H. and M.O.G.P.).

References

1. R. D. Roark, S. D. Kohler, J. G. Ekerdt, S. Du Kim and I. E. Wachs, *Catal. Lett.*, 1992, **16**, 77.
2. M. Galán-Fereres, L. J. Alemany, R. Mariscal, M. A. Bañares, J. A. Anderson and J. L. G. Fierro, *Chem. Mater.*, 1995, **7**, 1342.
3. M. A. Bañares and I. E. E. Wachs, *J. Raman Spectrosc.*, 2002, **33**, 359.
4. J. J. Ternero-Hidalgo, M. O. Guerrero-Pérez, J. Rodríguez-Mirasol, T. Cordero, M. A. Bañares, R. Portela, P. Bazin, G. Clet and M. Daturi, *Anal. Chem.*, 2020, **92**, 5100–5106.
5. G. Deo and I. E. Wachs, *J. Phys. Chem.*, 1991, **95**, 5889.

6. A. E. Lewandowska, M. Calatayud, F. Tielens and M. A. Bañares, *J. Phys. Chem. C*, 2013, **117**, 25535.
7. A. E. Lewandowska, M. Calatayud, F. Tielens and M. A. Bañares, *J. Phys. Chem. C*, 2011, **115**, 24133.
8. A. Chakrabarti, M. E. Ford, D. Gregory, R. Hu, C. J. Keturakis, S. Lwin, Y. Tang, Z. Yang, M. Zhu, M. A. Bañares and I. E. Wachs, *Catal. Today*, 2017, **283**, 27.
9. J. Strunk, M. A. Bañares and I. E. Wachs, *Top. Catal.*, 2017, **60**, 1577.
10. M. A. Bañares, M. Martínez-Huerta, X. Gao, I. E. Wachs and J. L. G. Fierro, *Stud. Surf. Sci. Catal.*, 2000, **130**, 3125.
11. M. A. Bañares, M. V Martínez-Huerta, X. Gao, J. L. G. Fierro and I. E. Wachs, *Catal. Today*, 2000, **61**, 295.
12. M. V. Martínez-Huerta, J. M. Coronado, M. Fernández-García, A. Iglesias-Juez, G. Deo, J. L. G. Fierro and M. A. Bañares, *J. Catal.*, 2004, **225**, 240.
13. A. Iglesias-Juez, M. V. Martínez-Huerta, E. Rojas-García, J.-M. Jehng and M. A. Banares, *J. Phys. Chem. C*, 2018, **122**, 1197.
14. M. Baron, H. Abbott, O. Bondarchuk, D. Stacchiola, A. Uhl, S. Shaikhutdinov, H.-J. Freund, C. Popa, M. V. Ganduglia-Pirovano and J. Sauer, *Angew. Chem., Int. Ed.*, 2009, **48**, 8006.
15. M. V. Martínez-Huerta, G. Deo, J. L. G. Fierro and M. A. Bañares, *J. Phys. Chem. C*, 2007, **111**, 18708.
16. M. V. Martínez-Huerta, G. Deo, J. L. G. Fierro and M. A. Bañares, *J. Phys. Chem. C*, 2008, **112**, 11441.
17. L. E. Briand, O. P. Tkachenko, M. Guraya, X. Gao, I. E. Wachs and W. Grünert, *J. Phys. Chem. B*, 2004, **108**, 4823.
18. M. V. Martínez-Huerta, X. Gao, H. Tian, I. E. Wachs, J. L. G. Fierro and M. A. Bañares, *Catal. Today*, 2006, **118**, 279.
19. J. M. Kanervo, M. E. Harlin, A. O. I. Krause and M. A. Bañares, *Catal. Today*, 2003, **78**, 171.
20. H. Tian, I. E. Wachs and L. E. Briand, *J. Phys. Chem. B*, 2005, **109**, 23491.
21. C. L. Pieck, M. A. Bañares, M. A. Vicente and J. L. G. Fierro, *Chem. Mater.*, 2001, **13**, 1174.
22. M. V. Martínez-Huerta, J. L. G. Fierro and M. A. Bañares, *Catal. Commun.*, 2009, **11**, 15.
23. M. A. Bañares, J. H. Cardoso, F. Agulló-Rueda, J. M. Correa-Bueno and J. L. G. Fierro, *Catal. Lett.*, 2000, **64**, 191.
24. M. Hävecker, P. Düngen, S. Buller, A. Knop-Gericke, A. Trunschke and R. Schlögl, *Catal. Struct. React.*, 2017, **3**, 104.
25. M. A. Bañares, *Catal. Today*, 1999, **51**, 319.
26. C. A. Carrero, R. Schloegl, I. E. Wachs and R. Schomaecker, *ACS Catal.*, 2014, **4**, 3357.
27. P. Waleska, S. Rupp and C. Hess, *J. Phys. Chem. C*, 2018, **122**, 3386.
28. I. E. Wachs, J. M. Jehng, G. Deo, B. M. Weckhuysen, V. V Guliants and J. B. Benziger, *Catal. Today*, 1996, **32**, 47.

29. A. E. Lewandowska, M. Calatayud, E. Lozano-Diz, C. Minot and M. A. Bañares, *Catal. Today*, 2008, **139**, 209.
30. S. J. Khatib, R. Guil-López, M. A. Peña, J. L. G. Fierro and M. A. Bañares, *Catal. Today*, 2006, **118**, 353.
31. M. A. Bañares and S. J. Khatib, *Catal. Today*, 2004, **96**, 251.
32. M. O. Guerrero-Pérez, J. L. G. Fierro, M. A. Vicente and M. A. Bañares, *J. Catal.*, 2002, **206**, 339.
33. M. A. Bañares and G. Mestl, *Adv. Catal.*, 2009, **52**, 43.
34. M. O. Guerrero-Pérez and M. A. Bañares, *Chem. Commun.*, 2002, 1292.
35. M. A. Bañares, M. O. Guerrero-Pérez, J. L. G. Fierro and G. G. Cortez, *J. Mater. Chem.*, 2002, **12**, 3337.
36. P. Mars and D. W. van Krevelen, *Chem. Eng. Sci.*, 1954, **3**, 41.
37. C. Doornkamp and V. Ponec, *J. Mol. Catal. A: Chem.*, 2000, **162**, 19.
38. M. O. Guerrero-Pérez, J. L. G. Fierro, M. A. Vicente and M. A. Bañares, *Chem. Mater.*, 2007, **19**, 6621.
39. E. Rojas, M. Calatayud, M. A. Bañares and M. O. Guerrero-Pérez, *J. Phys. Chem. C*, 2012, **116**, 9132.
40. A. R. Landa-Cánovas, F. J. García-García and S. Hansen, *Catal. Today*, 2010, **158**, 156.
41. B. Irigoyen, A. Juan, S. Larrondo and N. Amadeo, *Catal. Today*, 2005, **107–108**, 40.
42. H. Seitz, E. Germán, A. Juan and B. Irigoyen, *Appl. Surf. Sci.*, 2012, **258**, 3617.

CHAPTER 14

Vanadium Oxides in Photocatalysis, Including Bare Oxides and VOx-based Organic–Inorganic Nanocomposites

E. BENAVENTE,[a,b] J. ALIAGA[a,b] AND G. GONZÁLEZ*[c]

[a] Departamento de Química, Facultad de Ciencias Naturales, Matemática y del Medio Ambiente, Universidad Tecnológica Metropolitana, Santiago, Chile; [b] Programa Institucional de Fomento a la Investigación, Desarrollo e Innovación (PIDi), Universidad Tecnológica Metropolitana, Santiago, Chile; [c] Departamento de Química, Facultad de Ciencias, Universidad de Chile, Santiago, Chile
*Email: ggonzale@uchile.cl

14.1 Introduction

14.1.1 Heterogeneous Photocatalysis

Heterogeneous photocatalysis has aroused growing interest over the past few decades, mainly due to the potential of this field of catalysis to become a powerful tool to address the threatened sustainability of the planet. Although humanity is only a small part of the biosphere, population growth, energy consumption and waste production associated with its development

Catalysis Series No. 41
Vanadium Catalysis
Edited by Manas Sutradhar, José Armando L. da Silva and Armando J. L. Pombeiro

Published by the Royal Society of Chemistry, www.rsc.org

are affecting the balance of this work of art of nature, created and preserved over time by the energy of the sun. Consequently, much research on heterogeneous photocatalysis carried out refers to the processes of oxidative degradation or mineralization of natural or artificial wastes.[1] However, although photocatalysis looks primarily as a non-selective process, there are also many studies focused on photocatalytic processes for the production of organic materials, such as fuels and industrial chemical intermediates under environment-friendly conditions.[2] Most of the published reports have so far focused mainly on photocatalysts based on TiO_2.[3,4] However, vanadium oxide-based photocatalysis is becoming an interesting alternative.

Heterogeneous photocatalysis, like conventional heterogeneous catalysis, refers to the acceleration of a biphasic fluid (gas or liquid)–solid chemical reaction by the action of a catalyst using light as a primary activation energy source instead of thermal energy.[5–7] This is by using a semiconductor as a catalyst, the photocatalyst, which converts light into chemical energy.[8,9] The energy conversion capacity of semiconductors lies in their peculiar electronic frontier structure consisting of two electronic bands separated by an energy gap (E_G). In the fundamental state, the lowest energy band, the valence band (VB), is full of electrons, while the highest energy band, the conduction band (CB), is empty, Figure 14.1.

When the semiconductor interacts with light of energy equal to or greater than its band gap, it absorbs energy-promoting photoexcited electrons (in femtoseconds) from VB to CB leaving in the VB an excess of positive charge, known as photo-holes (h^+). The generated electron–hole pair (e^-–h^+) is considered a complex particle, called exciton (Figure 14.1a). Due to the lack of electronic states between bands, direct charge recombination is slow, allowing the exciton to migrate and/or dissociate in its components. Both free holes and free electrons that manage to prevent their recombination reach the surface of the catalyst where they stay trapped in the atoms, or defect off the catalyst near (or at the interface) with the fluid medium. There, photogenerated charge carriers define two types of redox centres, electron donor sites and electron receptors, capable of reducing or oxidizing the adsorbed species on the catalyst surface, respectively.[10] Alternatively, photogenerated charges can react directly with adsorbed species through charge transfer (Figure 14.1b).

The role of the photocatalyst in a given chemical reaction consists in triggering appropriate redox processes to accelerate its development. In order that the semiconductor behaves as photocatalyst and not as a reagent in a redox photochemical reaction, oxidation and process reduction must occur simultaneously, allowing the catalyst to return to its original state after each reaction cycle. The semiconductor choice primarily considers its ability to harvest light from a given spectral range and generating active sites with proper redox potential.[11] The band gap defines the photon minimal energy to excite the semiconductor ($h\nu \geq E_G$), while the positions of the VB and CB state the redox potential of photo-holes and photoelectrons, respectively.[12]

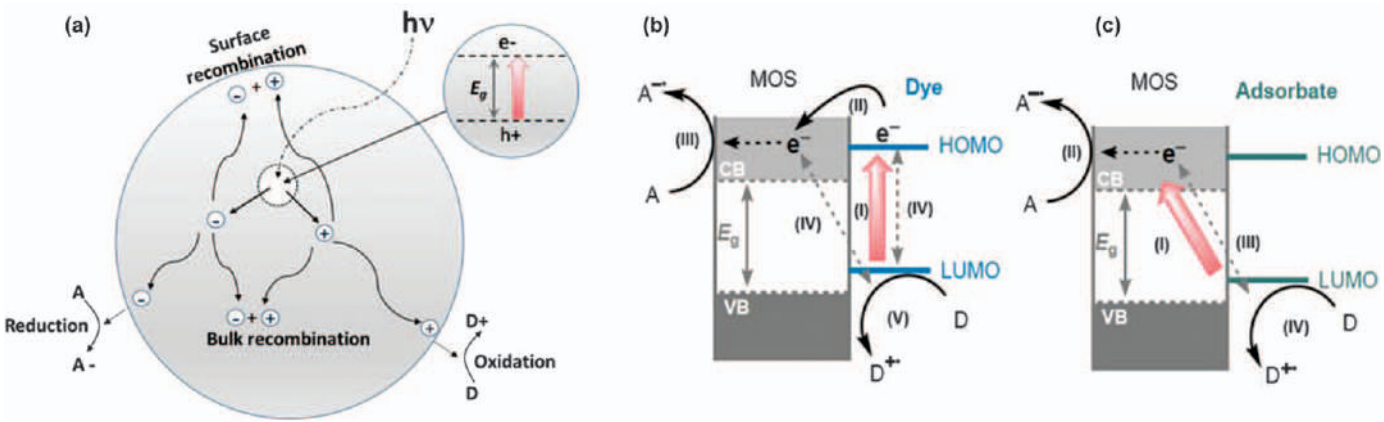

Figure 14.1 Schematic illustration of the semiconductor photoactivation process generation of an electron–hole pair. (h^+: hole, e^-: electron, A: electron acceptor, D: electron donor. CB: conduction band, VB: valence band, hν: energy of impinging photon, HOMO: highest occupied molecular orbital, LUMO: lowest unoccupied molecular orbital.) (a) general metal-oxide semiconductor photocatalysis (MOS) mechanism. (b) Dye photosensitization. (c) LMCT (ligand-to-metal charge transfer) photosensitization.
Reproduced from ref. 12 with permission from the Royal Society of Chemistry.

Furthermore, the photocatalyst performance is attainable, for example, through its quantum yield or by the conversion rate to produce active redox sites or produce–degrade certain products in a model reaction. However, the dispersion of the observed results for apparently identical systems reveals the complexity of heterogeneous photocatalytic processes.[1,13] This generally seems to be due to subtle changes in the preparation, composition or morphology of the photocatalysts that, by affecting photophysical processes of the semiconductor, such as the light absorption cross-section, charge carrier diffusion or charge recombination features, influence the overall performance of the process. In this sense, the nanostructured nature of the photocatalyst certainly has a significant impact on its properties.[14] The nanostructuring changes the electronic boundary structure of the semiconductor and, in addition, being intrinsically defective materials, they can create new levels of photoactive electrons as well as traps for photogenerated charges.

Since the pioneering article by Fujishima[15] reporting the photocatalytic H_2 generation using a thin film of TiO_2, the use of heterogeneous photocatalyst particles where at least one of its size dimensions is in the nanometre range, became a necessary condition to achieve photocatalysis. The typical properties of nanostructured materials, such as increased surface area, short pathlength charge carriers or the exciton wave function that extends over complete semiconductor particles, are particularly useful for photocatalysis phenomena.[14,16]

14.1.2 Vanadium Oxides

Vanadium is a transition metal widely distributed in the Earth's crust that is found in a variety of colourful minerals, which led to its controversial discovery and designation, Erythronium (M. Del Rio, 1801) and Vanadium (Sëfstrom, 1831).[17] Vanadium's electronic configuration Ar[$4s^2 3d^3$], characterized by energetically close valence orbitals, leads to rich redox and coordination chemistries. This is particularly appropriate to produce versatile vanadium oxide-based materials that are sensitive to low-energy stimuli, whose understanding, handling and applicability remain a challenge. Figure 14.2 shows the complexity of the oxo-vanadium species in solution solids – expressed by the known phase diagrams[18] – is apparent in the solution. In fact, between each pair of vanadium stoichiometric oxides phases – VO, V_2O_3, VO_2 and V_2O_5 – there are a series of thermodynamic or kinetically stable homogeneous phases, where vanadium atoms coexist in different oxidation states. Such phases are generically expressed as VO_x species. Without considering vanadium(II) oxide, VO_x phases identified in the diagram in Figure 14.2 belong to two homologous series. VO_x suboxides with $1.5 \leq x \leq 2.0$ correspond to the so-called vanadium oxide Magnéli phases, V_nO_{2n-1}.[19] Meanwhile, the VO_x suboxides in the range $2.0 \leq x \leq 2.5$, V_2O_5 suboxides such as VO_3, V_3O_7, V_4O_9, V_6O_{13} and the same V_2O_5 (Figure 14.2)

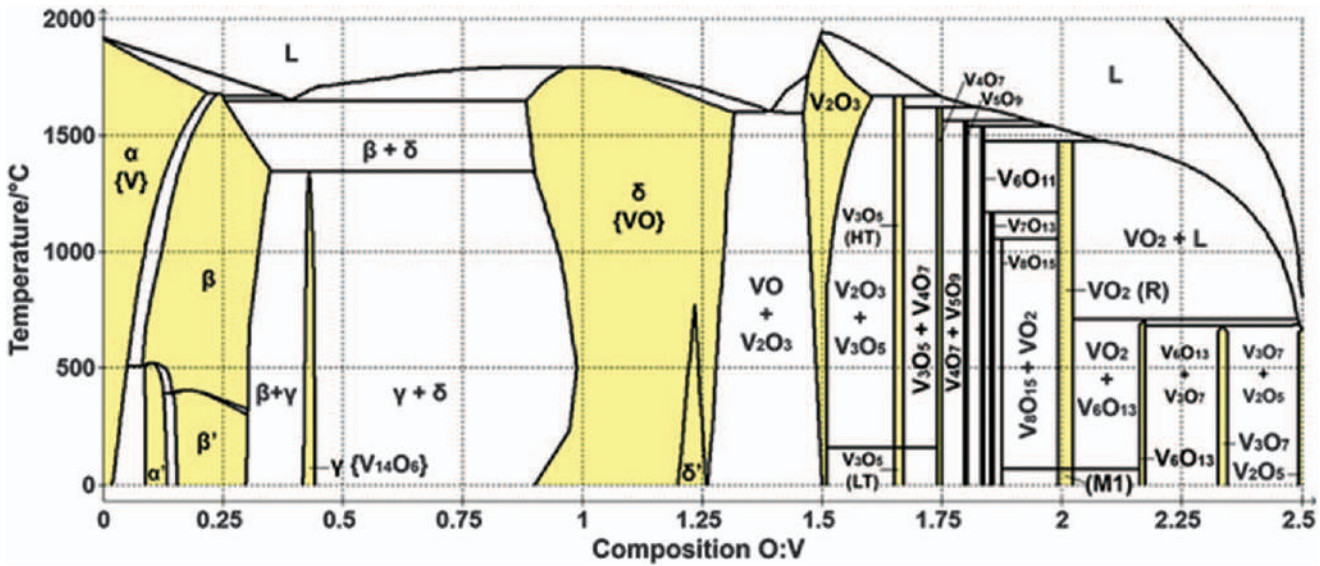

Figure 14.2 Diagram vanadium-oxygen phase.
Reproduced from ref. 18 with permission from John Wiley and Sons, © 2019 John Wiley & Sons, Ltd.

follows the formula V_nO_{2n+1}. Katze *et al.*,[20] proposed a unified description of both homologous series, suggesting that the constructive phase transition processes between adjacent homogeneous phases would occur by a symmetry-breaking mechanism of involved structures.

VO_2, a low-valence oxide, is the most widely studied due to its stability, but also because of some VO_2 polymorphs present metal insulation transition (MIT) at accessible temperature, facilitating the exploit of the electrical and thermal features associated to this transition. Indeed, VO_2 appears as an auspicious material for emerging ''oxide electronic'',[21] as well as for the development of energy-efficient smart windows.[22] The use of VO_2 would also be promising as a cathode material for lithium-ion batteries.[23] In addition, as discussed in the next section, photocatalytic properties of VO_2 are beginning to emerge. Beyond its thermal and chemical stability, V_2O_5 has some peculiar properties that have aroused growing interest due to its possible applications. They include a particularly small band gap, a layered structure capable of intercalating different species and the ability, under appropriate conditions, to become a variety of nanostructured, functional materials.[24] This makes V_2O_5 interesting for applications in fields such as lithium-ion[25,26] or sodium-ion[27] batteries; photochromic[28] and electrochromic[29] devices; heterogeneous catalysis;[30] and in heterogeneous photocatalysis.

14.2 Pure Vanadium Oxide Photocatalysts

14.2.1 α-V_2O_5 Photocatalysts

α-V_2O_5, with its peculiar structural features, is the polymorph most used due to its stability and availability.[31] The orthorhombic structure of α-V_2O_5 possesses a van der Waals gap (Figure 14.3a) that gives it a laminar character that, like other lamellar solids such as graphene or molybdenum disulphide (MoS_2), allows it to easily transform into functional flat nanostructures (2D), tubular (1D) or as fullerenes (0D)[24] (Figure 14.3b). Liu *et al.*,[32] recently reviewed preparation methods, structural properties and applications in energy conversion of vanadium-oxide nanostructures.

The relevance of vanadium-oxide devices for energy conversion, even in photovoltaic solar cells,[33] contrasts with their relatively late and slow development in photocatalysis. Reversing this trend is a significant challenge, especially in the design and development of new photocatalysts taking into account the leading causes that prevent vanadium oxides from realizing their real photocatalytic potential. We hope this chapter contributes in some way in that direction.

The activity of nanostructured pure vanadium oxide photocatalysts (Table 14.1), beyond their chemical nature, depends on numerous factors including crystal structure, morphology and preparation strategies.[34,35]

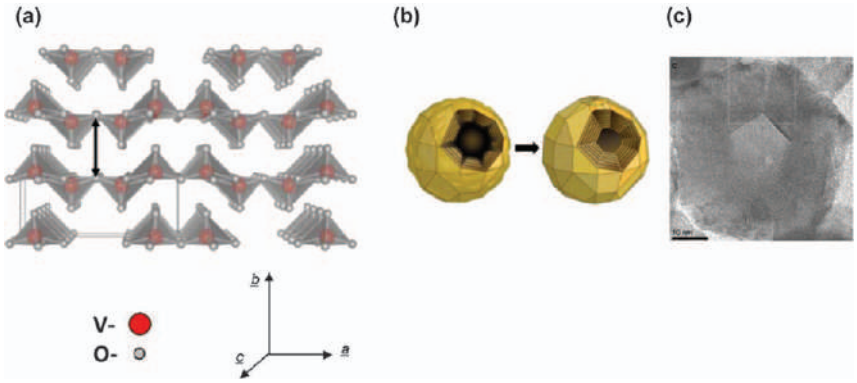

Figure 14.3 (a) Crystal structure of α-V_2O_5. (b) Schematic formation mechanism of fullerene-like hollow V_2O_5 nanoparticles. (c) TEM images of the hollow core V_2O_5 nanoparticles.
Reproduced from ref. 24, https://doi.org/10.3390/ma3084428, under the terms of the CC BY 4.0 licence, https://creativecommons.org/licenses/by/4.0/.

Laminar V_2O_5, xerogel (hydrated V_2O_5) or organogels show poor-to-acceptable performance in dye removal under visible light.[36] However, by a simple hydrothermal treatment (HT) of the mentioned V_2O_5 gels, it is possible to improve their photocatalytic performance. For example, under HT treatment at 180 °C it is possible to achieve low hydrated V_2O_5-nanostructures, nanobelt or nanorolls,[35] able to degrade over 70% Rhodamine B (RhB) after 80 min under visible light irradiation. The performance even becomes almost quantitative after calcining the samples at 500 °C.

These results suggest that water has a detrimental photocatalytic effect on V_2O_5 photocatalysts, which agrees with a recent report by Zengin *et al.*,[37] who prepared pure α-V_2O_5 nanoparticle powders by grinding previously calcined commercial V_2O_5 in absolute ethanol. Theses α-V_2O_5 nanoparticles are shown to efficiently photocatalyse the degradation of bisphenol, 90% after 45 min UV-light irradiation. Dry ethanol prevents the hydration excess and also is useful in gel-coagulating for obtaining flower-like V_2O_5 nanostructures with an 88% superior performance than sol-gel V_2O_5 (33%) or P25 (46%) under visible light.[38] Liu *et al.*, prepared films of V_2O_5 flower-like nanorods oriented on fluorine-doped tin oxide (FTO) obtained by calcination of a hard-template nanostructured VO_2 (B). They show a good photocatalytic performance for methyl blue (MB) degradation under UV and visible light.[39]

Beyond dye degradation, α-V_2O_5 nanosheet particles obtained by templated sol-gel procedure demonstrate to have visible-light (vis) generated active redox sites able to produce H_2 from methanol solutions in a quite high yield ($\approx 8.8\ mm^{-1}\ g^{-1}$, 50% MeOH)[40] and the reduction ability of the catalyst strongly increases when it is sensitized with Eosyn ($\approx 19.7\ mm^{-1}\ g^{-1}$, 30% ethanolamine).

Table 14.1 Vanadium oxides photocatalysts.

Vanadium	Structure	Band gap	Method	Irrad-Model reagent	Process	Ref.
V_2O_5	Nano 1D nanowires and nanorods	2.55–2.60 eV	Sol-gel, V_2O_5, H_2O_2 HT[a]	Vis, MB (methylene blue)	adsorption–photocatalytic	35
V_2O_5	Flower-like	2.19 eV	$VOSO_4$ Sol-gel EtOH 100% ST[b] Crystallization 450 °C	Vis, TBOT (Toluidine blue)	degradation 88% in 10 h	40
V_2O_5 Orthorh. crystalline	Powder nanorods flower-like on FTO	2.1 eV	Templated with VO_2(B)	UV and Vis, MB	degradation 74.6% UV and 63% vis in 210 min	41
V_2O_5	Mesoporous-assembled V_2O_5 nanosheet	2.25 eV	Sol-gel Vanadium(V) tri-ethoxide oxide, $C_6H_{15}O_4V$ LAHC surfactant	Vis, methanol	H_2 production	42
$V_2O_5{\cdot}xH_2O$ annealing to V_2O_5	Nanobelts and nanorolls	2.8 eV	NH_4VO_3 and H_2SO_4 180 °C for 24 h $V_2O_5xH_2O$ heated to 500 °C for 3 h	UV, Rh B (rhodamine B)	nanobelts and nanorolls 95% of degradation in 80 min	36

[a]HT: Hydrothermal.
[b]ST: Solvothermal.

14.2.2 Low- and Mixed-valence Vanadium Oxide Species

VO_2, beyond serving as a successful template to prepare improved α-V_2O_5, room-temperature VO_2 semiconductor polymorphs also can serve as photocatalysts. Initially, VO_2 phases appear to be inappropriate for photocatalysis because of their high conductivity; currently, many examples show that through adequate nanostructuring, pure VO_2 as well as in composites or mixed-valence compounds, may absorb UV or visible light to induce redox processes.[22,39]

Wang *et al.*[41] reported a promising example of VO_2-based photocatalysts, synthesizing cone-shaped VO_2-nanorods crystalized in a bcc structure, with an optical band gap of 2.7 eV. Photocatalytic activity of this product, tested for hydrogen evolution from an ethanol–water solution under UV light, showed a quantum yield efficiency of about 38.7% and an exceptionally high hydrogen generation rate (800 mmol m^{-2} h^{-1}). The ability of mixtures of vanadium oxides with different oxidation states for photocatalytic H_2 production under UV-light is observed, for instance, in the activity shown by VO_x-nanostructure films fabricated by oxidation of fuzzy fibre-form nanostructures previously obtained from subjecting vanadium metal to helium plasma irradiation.[42] The catalytic activity arises from the synergic effect of a mix of low-valence vanadium species, V(III) and V(IV), covered by a thin layer of V_2O_5.

Mixed-valence, vanadium-oxide nanostructures have proved to possess electronic structures appropriate for developing visible-light-driven photocatalysts. Combustion of a solution of ammonium metavanadate and diethyl imidazole in ethanol at 500 °C leads to a mixture of VO_2 and mixed-valence V_6O_{13} ($VO_x \approx 1.85$). The total mineralization of atrazine after 2 h of visible light irradiation points to a semiconductor heterojunction (Figure 14.4a) that, synergically, optimizes light harvesting and simultaneously avoids

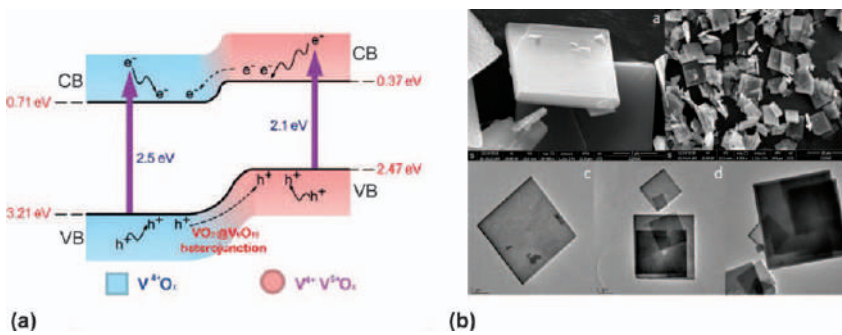

Figure 14.4 (a) The energy band structure of the vacuum level of the composites with the VO_2@V_6O_{13}. Reproduced from ref. 43 with permission from John Wiley and Sons, Copyright 2014. (b) $(NH_4)V_7O_{16}$ microsquares morphology SEM and TEM images.
Reproduced from ref. 55 with permission from the Royal Society of Chemistry.

photoinduced charge-carriers recombination.[43] Another example of V(IV)-V(V) mixed-valence vanadium oxides is the layered V_7O_{16} vanadates family,[18] which appears to be outside the VO_x classification discussed (Figure 14.2). Almost all V_7O_{16} nanostructures are known to consist of hybrid organic–inorganic nanocomposites. Recently, we prepared V_7O_{16}-microsquares,[44] a pure inorganic product that according to experiments (Figure 14.4b), shows interesting photocatalytic activity.

14.3 Metal Oxide-supported Vanadium-oxide Photocatalysts

This section focuses on vanadium oxide-photocatalysts where the active material is VO_x species that form a thin molecular layer on photocatalytic inactive metal oxides such as silica, alumina, aluminosilicates and, as an exception, titania. These photocatalysts are substantially akin to those used in conventional catalysts widely studied over several decades. Therefore, before commenting on selected examples of reactions assisted by vanadia photocatalysts supported by metal oxides, we will briefly highlight general aspects that arise from thermal substitution by photonic activation, particularly the working conditions typically used in photocatalysis.

The preparation of supported vanadium-oxide photocatalysts as conventional catalysts mainly comprises two consecutive stages; the incorporation by subtle interaction (impregnation) or graft of vanadia on the surface of the support and then a heat treatment at 500–600 °C where the VO_x species are anchored to the support surface (Figure 14.5a).[45] Under anhydrous conditions and vanadium loading below the monolayer surface coverage,[46] vanadium oxide spontaneously forms tetrahedral units of VO_4 which, isolated and/or oligomerized, define functional sites on the support surface.[47]

However, under environmental conditions, the metal-oxide surface comprises a shell of more than 10 layers of water,[46] making the supported-vanadium species behave as if they were in an aqueous solution undergoing restructuring processes that depend on its concentration and the pH of the medium, akin to those described in the Pourbaix diagram[48] (see Figure 14.5b). Therefore, the chemical structure of the VO_x species depends on the point of zero charge (PZC) of the support[46,49] (Table 14.2). The molecular nature of the active VO_x sites supported is the bridge that would allow photocatalysis to exploit the ability of conventional V_2O_5 catalysts to promote selective chemical transformations.[50] This was achieved in the photocatalytic oxidation of methanol, a ''smart'' model molecule frequently used in thermal catalysis,[51] and will be discussed next.

14.3.1 Selective Oxidation of Methanol

Recently, Korteville *et al.*,[52,53] reported the activity of vanadia photocatalysts with silica support for the oxidative conversion of methanol in

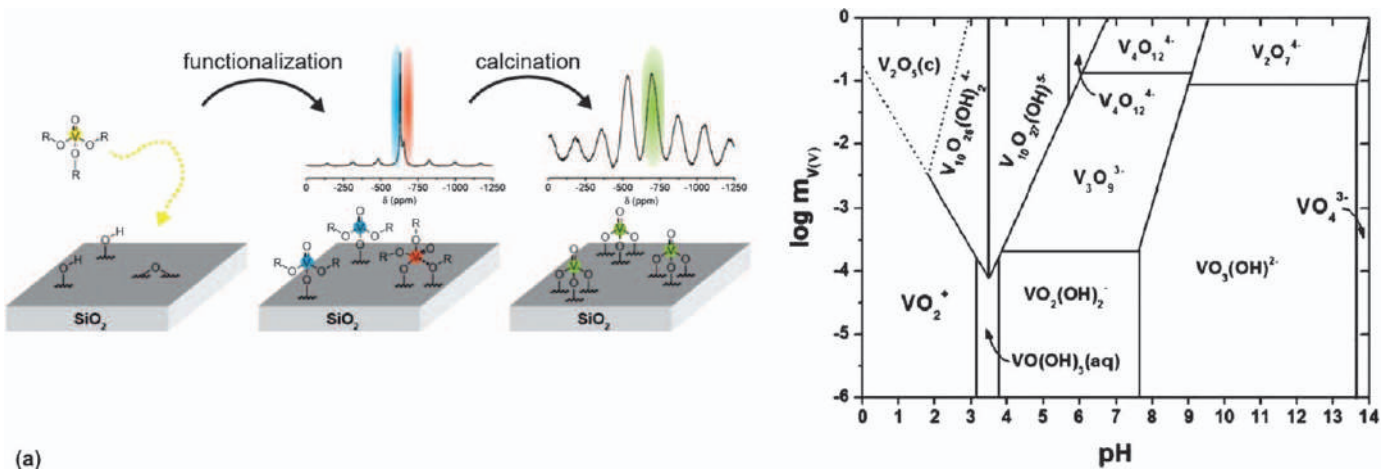

Figure 14.5 (a) Anchoring and subsequent thermal reconstruction of vanadium oxide on amorphous silica. Reproduced from ref. 45 with permission from American Chemical Society, Copyright 2016. (b) Aqueous phase equilibrium chemistry of vanadium. Reproduced from ref. 48 with permission from the Royal Society of Chemistry.

Table 14.2 Surface vanadium oxides dependence on the net pH at the point of zero charge (PZC) on different hydrated inorganic oxides. Adapted from ref. 46 with permission from American Chemical Society, Copyright 1991. Adapted from ref. 49 with permission from Elsevier, Copyright 2003.

Support oxide	pH at PZC of pure oxides	V oxides at low V loading	V oxide at high V loading
MgO	11	VO_4, V_2O_7, $(VO_3)_n$	VO_4, V_2O_7, $(VO_3)_n$
Al_2O_3	8.9	$(VO_3)_n$	$(VO_3)_n$, $V_{10}O_{28}$
TiO_2	6.0–6.4	$(VO_3)_n$, $V_{10}O_{28}$	$V_{10}O_{28}$
ZrO_2	5.9–6.1	V_2O_7, $(VO_3)_n$, $V_{10}O_{28}$	$V_{10}O_{28}$
SiO_2	3.9	O_h (Decavanadate-like)	V_2O_5

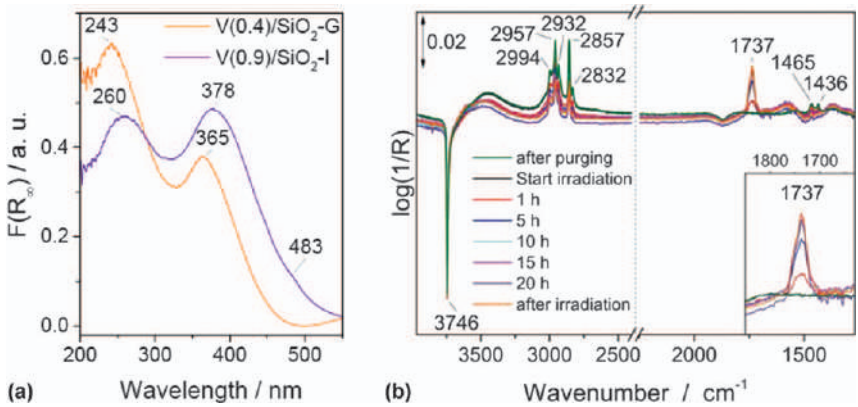

Figure 14.6 (a) Kubelka-Munk function of the catalysts under ambient conditions derived from UV-Vis DR spectra, (b) DRIFT spectra of V(0.4)/SiO_2-G of photocatalytic oxidation of absorbed methanol recorded during irradiation with a 150 W Hg/Xe lamp equipped with water-based IR filter (240–950 nm).
Reproduced from ref. 52 with permission from John Wiley and Sons, © 2018 Wiley–VCH Verlag GmbH & Co. KGaA, Weinheim.

environmental conditions, focusing on the equivalence between thermal and photonic catalysts and the correlation between photoactivity and the photocatalytic performance of two catalysts that differ in preparation process and vanadium content. Photocatalyst V(0.4)SiO_2-G prepared by an anhydrous graft procedure has a vanadium surface density of 0.4 V nm^{-2} and a second one, V(0.9)SiO_2-I, with higher surface coverage (0.9 V nm^{-2}) obtained by wet impregnation. Raman and UV-Vis DR spectroscopy indicate that both samples have a mixture of isolated sites consisting of monomers O=V(–OH)(O–Si)$_2$ and dimers O=V(–O–Si)$_2$–O–(–O–Si)$_2$V=O respectively.[54] The comparison of the electronic spectra of both catalysts (Figure 14.6a) reveals differences between the samples, which is attributable to the different hydration effects arising from their preparation methods and

composition. Both the redshift of the absorption band at 243 nm corresponds to the hydrated VO_4, and the increase in the relative intensity of the band at 378 nm indicates an incipient oligomerization by the hydration effect. Also, the feature at approximately 483 nm assignable to the incipient formation of V_2O_5 NP reinforces the hypothesis.

Photocatalytic oxidation of gaseous methanol adsorbed on the catalysts monitored by time-resolved *in-situ* diffuse reflectance infrared Fourier transform spectroscopy (DRIFT) as a function of the irradiation time (see, for instance, Figure 14.6b), together with the analysis of the effluent by mass spectrometry allowed to follow the reaction progress, illustrates the evolution of the difference spectrum of the catalyst. Results indicate the photocatalytic oxidation of methanol to formaldehyde with 100% selectivity. However, formaldehyde remains adsorbed at the catalyst. The same experiments (Figure 14.6b), but illuminating in the wavelength range of 320–700 nm, indicate that among all the optically active species detected, only the VO_4 species absorbing in the deep UV-range are photocatalytically active in the oxidation of methanol.[52] Studies performed using V-grafted samples with different vanadia loadings show similar results until almost full surface coverage (0.7 V nm^2).[55] As demonstrated by Le Roz *et al.*,[56] selective oxidation of photocatalytic methanol is also achievable by visible-light-driven photocatalysis using as catalyst vanadium oxide species supported on a nanocrystalline Beta-zeolite with low aluminium content. The authors prepared this new catalyst, P-VO_x@Beta, by treating the aluminosilicate with a cold plasma (120 K) of VCl_3 followed by oxidation with O_2 plasma at the same temperature. Interestingly, based on ^{27}Al, ^{29}Si and ^{51}V MAS NMR spectra, the authors suggest the presence of vanadium in a lower oxidation state (VO_x, $x < 2.5$). FTIR monitored the photocatalytic process under *operando* conditions. The measured conversion rate (V_{MeOH} mmol g^{-1} min^{-1}) using P-VO_x@Beta is 1.9 and 3.7-times higher than that of V_2O_5 photocatalysts prepared by impregnation of Beta-Zeolite and SiO_2, respectively, and 9.0-times than that of non-supported V_2O_5. Concerning the selectivity with respect to conversion to formaldehyde, P-VO_x@Beta at 20% methanol concentration of 1200 ppm and irradiance of *ca.* 200 mW/cm^2 shows a performance of about 70% (Figure 14.7a), while V_2O_5@SiO_2 and V_2O_5@Beta leads to mixtures of formaldehyde (FA) with methyl formate (MF) and with dimethoxymethane (DMM) and dimethyl ether (DME), respectively. However, the selectivity of P-VO_x@Beta depends on the concentration of MeOH (Figure 14.7b) as well as on the irradiance rate. With a MeOH flow of 1200 ppm, but at an irradiance of 100 mW/cm^2, a selectivity for DMM of approximately 75% is achieved, while with 5000 ppm MeOH it becomes less selective for leading DMM and MF (61% and 36%, respectively).

14.4 Vanadium-doped Titanium-oxide Photocatalysts

This section is about titania photocatalysts doped with vanadium (V-TiO_2) in which the crystalline network of TiO_2 contains a small amount of

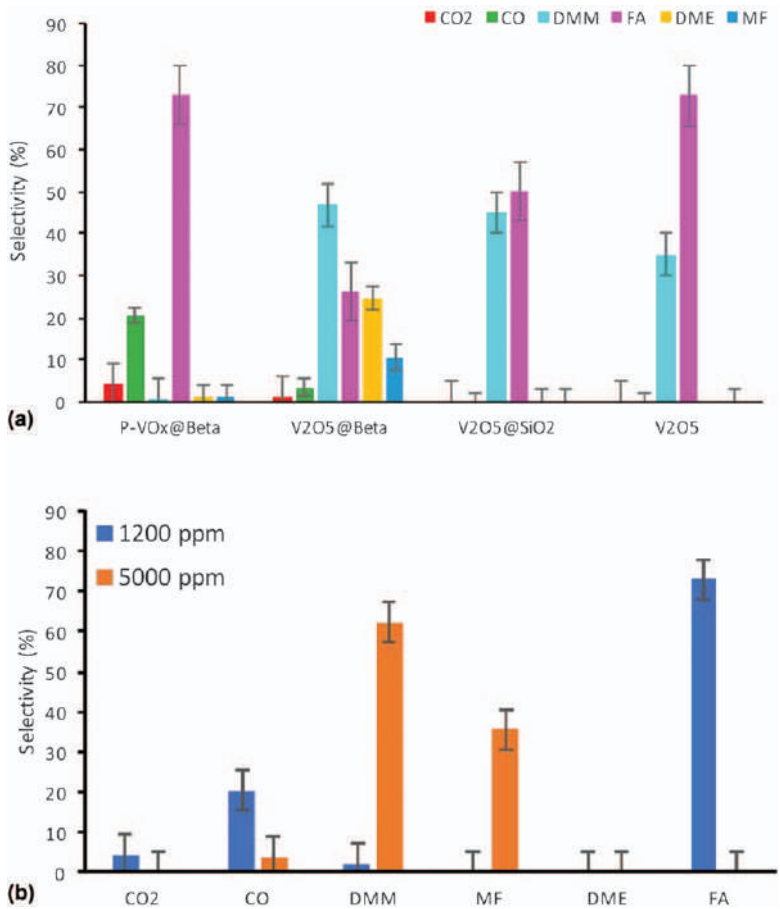

Figure 14.7 (a) Reaction selectivity of P-VO_x@Beta, V_2O_5@Beta, V_2O_5@SiO_2 and V_2O_5 photocatalysts. (b) Selectivity of P-VOx@Beta a 1200 and 5000 ppm of methanol.
Reproduced from ref. 56 with permission from American Chemical Society, Copyright 2017.

vanadium atoms. This research field focuses on improving the photocatalytic activity of TiO_2 by increasing the harvest of visible light and reducing the recombination of photoinduced charges. In that direction, transition metal (TM) doped titania proves to be a valuable approach[57] in which vanadium-doped catalysts play an increasingly attractive role.[58] In this section, we present a general description of the performance of V–TiO_2 catalysts in the degradation of environmental pollutants[58–69] (Table 14.3). Additionally, we discuss the polymerization of ethylene driven by visible-light assisted, vanadium-doped titanosilicate catalysts (V–ETS–10) which, beyond being an interesting example of heterogeneous photocatalysis in organic synthesis, helps to better understand some peculiarities of V–TiO_2 photocatalysts.

Table 14.3 Vanadium-doped titanium oxide photocatalysts.

Synthesis	Compositions explored	Special characterization	Illumination model reagent	Band Gap	Ref.
Combustion method at 350 °C $Ti(NO_3)_4$ and NH_4VO_3 in glycine + water	1–10%	UV–vis	Solar, 4-nitrophenol	—	60
$TiCl_3 \rightarrow Ti(OH)_4H_2O_2 + NH_4VO_3$ 100 °C	0–3%	XPS, PL	Vis and UV, methyl orange (MO)	3.25 eV 0% to 1.67 eV	59
Sol-gel 450 °C $Ti[OCH(CH_3)_2]_4$, VCl_3 in isopropanol thin films	0.05 to 1.00%V V-TiO_2 metal basis	—	UV, MB and rhodamine B (RhB)	3.43 eV for 0.05	60
Aqueous solution of $VO(OiPr)_3$ $Ti[OCH(CH_3)_2]_4$, and DDA 606 °C for 6d 726 °C for 10d	V/Ti atomic ratio of 1 : 21.	XAFS	Vis, ethanol	—	72
Sol-gel $Ti(OBu)_4$, ethanol, glacial acetic acid, and NH_4VO_3	0.5–1.0–1.5	XRD BET	Vis, formaldehyde	—	61
Sol-gel (i) $VO(C_5H_7O_2)_2$. in-butanol and Acetic acid mixed in $Ti(OBu)_4$. calcined at 400 °C (ii) VCl_4 in ethanol, in $Ti(OBu)_4$ 110 °C	(i) 0.01, 0.02, 0.029, 0.035, 0.052 (ii) 0.25, 0.05, 0.08	XANES	Vis MB and crystal violet (CV)	—	62
TTIP + $VOSO_4(H_2O) + HNO_3$	0.5–5	Specific surface area SSA	UV LEDs, Caffeine	3.1	63
Spray flame	0.25, 0.50, 1, 3, 5%	EPR	UV and Vis, MB and 2,4-dichlorophenol (2,4-DCP)	—	64

Sol-gel $NH_4VO_3Ti(OiPr)_4$ different surfactants	0.0184 V/Ti % 0.186	—	Solar, MO	—	65
ETS-10 is a microporous titanosilicate $VOSO_45H_2O$	0.13, 0.33, 0.43 and 1.00	NEXAFS and RAMAN	UV, polymerization of ethylene	4.32 to 3.58 eV	77
NH_4VO_3 and P25 TiO_2 (200, 300, 400, 500, 600 °C)	0.5, 1, 2, 4, 7 and 10 mol% of V-doped	XPS electrochemical	Hg oxidation simulated flue gas system	3.21–2.14	66
Sol-gel method TiO_2 with $Ti[OCH(CH_3)_2]_4$ and V_2O_5	1 and 5%	—	Solar, Red	1.79–1.69	67
V-TiO_2 NPs were grown *via* gas-phase condensation	V/Ti ratio of 3.0%	Transient-absorption spectroscopy (TAS).	NO_2 reduction and $\lambda_{ex} = 330$, 400, and 530 nm.	—	68
Sol-gel method $Ti[OCH(CH_3)_2]_4$ $VOSO_4$ reflux 50–60 °C calcination 600 °C undoped at 450 °C	0.2, 0.09, 0.05, 0.01, 0.005	BET	Vis, MB	—	58
$VOSO_4$ onto TiO_2 surface calcination at 300 °C	0.22 to 3.5 mmol dm^{-3}	EPR	UV, RhB	—	73
Sol-gel X, Y-TiO_2, and V_2O_5 NPs RT dried 100 °C 24h. Calcination 450–550 °C	5%	—	Vis, Cr(VI) reduction	2.79–2.74 2.73 450 2.54 2.57 2.71 550	69

14.4.1 Vanadium-doped Titania

The incorporation of TM atoms in a titania network can alter its electronic properties, and thereby its photocatalytic properties. This through the modification of band-edge positions and/or the creation of new energy levels between bands that lead to band gap narrowing, often allowing TM-doped TiO_2 to absorb visible light.[57,70] In the V–TiO_2 catalyst, the O2p character of titania VB remains unchanged after doping due to its energy difference with the vanadium frontier 3D orbitals positioned within the TiO_2 band gap slightly below the catalyst CB, defining impurity energy levels within the TiO_2 band gap. This often produces noticeable changes in the electronic spectrum of the V–TiO_2 photocatalysts, detectable in redshifts of titanium band-edge and/or new broadened absorption bands within the visible range (Figure 14.8a). The results strongly suggest that the vanadium-doping effect, in this case, is due to charge transfer from the valence band of V–TiO_2 to vanadium t_{2g} energy levels.[71]

Such UV-vis spectrum features, though sometimes interpreted as photocatalyst activity signal, frequently fail as a catalyst performance descriptor. This lack of correlation arises from the influence of vanadium d-levels on the availability of redox centres on the surface of the photocatalyst by acting as traps for photoinduced free charges, scavenging electrons and holes in the case of V(v) and V(iv), respectively, which can hinder the photocatalytic process. Consequently, understanding photocatalysis based on vanadium-doped material necessarily implies to consider the actual oxidation state of vanadium in the catalyst, due to the ease redox changes even by subtle stimuli. For example, the sample preparation for the experiment in Figure 14.8b, which initially contains only V(iv), was prepared using a 1 : 1 sol-gel mixture of two precursors of V(iv) and V(v), respectively.[72] Furthermore, the redox states of vanadium over mesoporous TiO_2 during the ethanol dehydration reaction excited in visible-light suggested the presence of V (iii) and V(iv).

Despite the latter, many reports often focus primarily on photocatalyst performance, paying little or no attention to this problem. The replacement of Ti(iv) ions in the TiO_2 network is an energetically plausible process due to the similarity of the ionic radii (Ti(iv), 0.745 Å *vs.* V(iv), 0.72 Å and V(v), 0.68 Å) what makes it easily achieved using a V(iv) or V(v) precursor. The substitution with V(iv), isovalent with Ti in the TiO_2 network, as single dopant is possible, as in the example just mentioned.[72] On the other hand, the incorporation of V(v) due to the difference in charge with Ti(iv) implies the participation of Ti(iii) to maintain the electroneutrality of the catalyst, being its presence as a single dopant energetically unfavourable. The excess V(v) is considered detrimental to the photocatalyst activity because the Ti(iii) would act as a trap of photogenerated holes to reoxidate to Ti(iv). Recently, Kokorin *et al.*,[73] employing EPR, analyzed differences in the distribution of both types of vanadium between bulk and surface doping. Also, the authors studied the effect of the presence of a reductant in the solution that allows such a

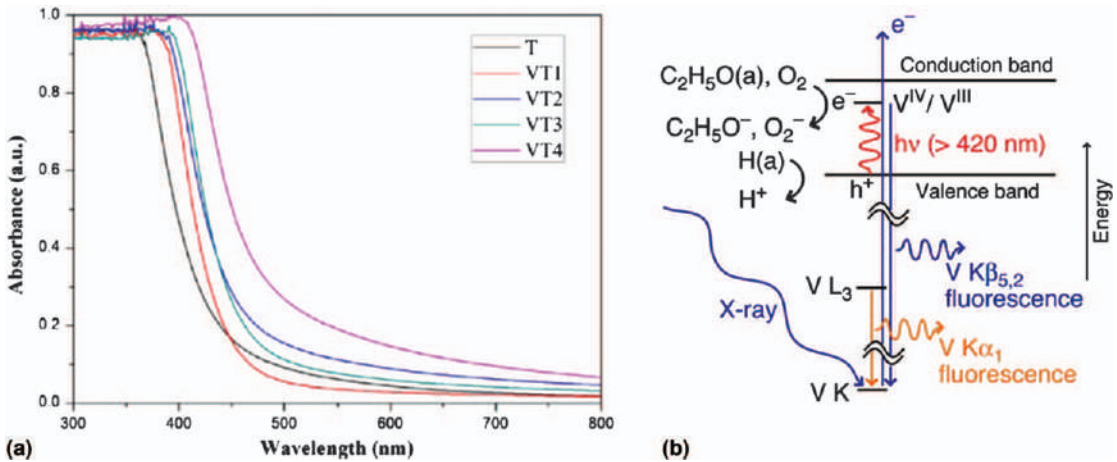

Figure 14.8 (a) Electronic spectra of V-TiO_2 photocatalysts with different vanadium loading. The insert shows the band gap values dependence according to vanadium loading. Adapted from ref. 70 with permission from Elsevier, Copyright 2015. (b) Energy diagram scheme for V-TiO_2 catalyst proposed by XAFS ''on-reaction'' measurements, describing the presence of V(III) and V(IV) redox states in photocatalytic ethanol dehydration reaction under visible light.
Reproduced from ref. 72 with permission from American Chemical Society, Copyright 2007.

surface distribution to change using the degradation of rhodamine B (RhB) under UV as well as visible light.

The complexity of these processes is observable, among others, in the dispersion of the reported results for apparently similar systems. Among them is the level of doping necessary to maximize the catalyst activity, after which the activity begins to decrease again.[58,74]

Although here we mainly refer to vanadium mono-doped catalysts, there are some examples showing that additional non-metal doping is an alternative for further improving V–TiO_2 photocatalyst performance. For example, the co-doped V, nitrogen-TiO_2 catalyst, exhibits activity for RhB degradation under visible light superior to those of either V- or N-TiO_2 single-doped photocatalysts.[75] Under similar illumination conditions, TiO_2 co-doped with vanadium and carbon shows an improved activity compared to that of V-doped TiO_2 for degradation of acid orange 7 (AO7).[76] In both examples, the authors suggest that vanadium active species would be V(IV).

14.4.2 Vanadium-substituted Zeolite-ETS-10

The 3D structure of the ETS-10 synthetic zeolite consists of a stack of 2D titanosilicate sheets, constituted by corning-sharing TiO_6-octahedra and SiO_4-tetrahedra at a Ti to Si ratio of 1 : 5, joined by Si–O–Si bonds.[77] The functional importance of ETS-10 mainly arises from the presence of interchangeable cations in the pores balancing the negative charge excess coming from the TiO_6 units, as well as from the distribution of the Ti and Si atoms in the sheets (Figure 14.9a), which defines regular arrangement of pores of twelve silicon rings and atypical segregation of Ti atoms in the network. The peculiar linear grouping of Ti in ETS-10 appears as a wire-like titania cluster confined into an inert matrix is an interesting model for studying V–TiO_2 catalysts.[78]

Nash *et al.*[77] studied the partial and total replacement of Ti(IV) in the Ti–O–Ti chains of ETS-10 per vanadium. The authors prepared pristine ETS-10 and partially substituted samples (ETSV-10) by the same procedure,[79] adding in the case of the latter the corresponding amount of $VOSO_4$, and obtaining the totally substituted sample (AM-6). Measurements of near-edge X-ray fine structure spectroscopy (NEXAFS) made it possible to demonstrate that V(IV) and V(V) coexist in all ETSV-10 samples as well as in AM-6. The effect of vanadium substitution on the ETS-10 electronic structure was evidenced in UV-vis DRS as indicated by the samples' band gap.

In order to assess the photocatalytic activity of ETSV-10 and AM-6, the authors chose the polymerization of ethylene under polychromatic light at 25 °C. The formation of polyethylene was followed by *in-situ* DRIFTS measurements, under irradiation over six hours, evaluating the rate of conversion by the area under the peaks to 2825 and 2854 cm^{-1}. The comparison of area profiles obtained for the ETSV-10 and AM-6 photocatalysts with those of ETS-10 and P25 measured under the same conditions (Figure 14.9b) shows that vanadium substitution improves, in general, the performance of ETS-10,

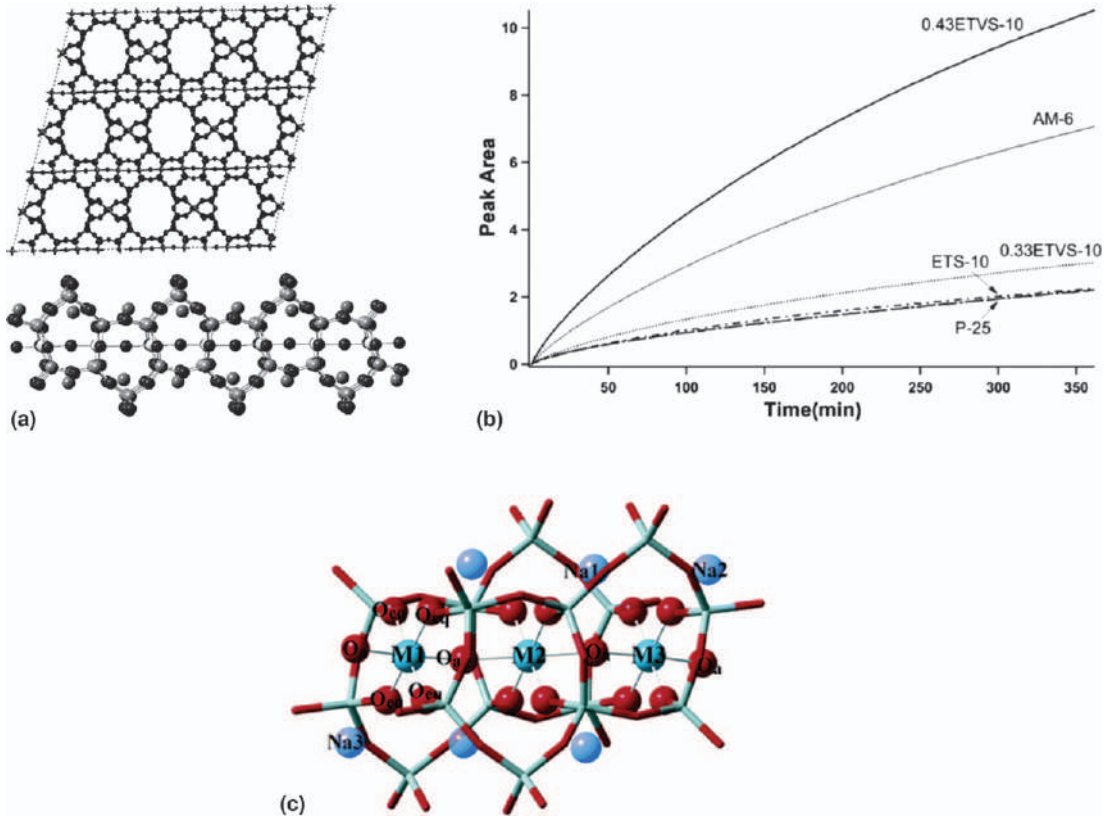

Figure 14.9 (a) Section of the titanium chain of ETS-10 with $SiO_{4/2}$ tetrahedra and Na cations surrounding the $TiO_{6/2}$ units. (b). Peak area of polyethylene *versus* reaction time for ETS-10, 0.43ETVS-10, 0.33ETVS-10, AM-6, and P-25 samples. Reproduced from ref. 77 with permission from American Chemical Society, Copyright 2007. (c) DFT cluster region for ONIOM models. Reproduced from ref. 78 with permission from American Chemical Society, Copyright 2007.

which increases with increasing vanadium content reaching a maximum for the 0.43 (V/V + Ti) ETVS-10 sample, decreasing again for AM-6. This behaviour as well as the lack of correlation between photocatalytic activity and photo-response in the visible range, resemble to that observed for the V-TiO_2 photocatalysts.

At this point it is apposite to comment briefly on some results from computational calculations performed by Sough *et al.*,[78] using a three-metal atoms cluster (M = Ti or V) isolated in a silica matrix (Figure 14.9c) simulating ETS-10, to assess the effect on the geometry and energy of system caused by replacing 1, 2, or 3 Ti(IV) ions by V(IV) and/or V(V). With respect to cluster geometry, it remains practically unaltered even after triple V(IV) substitution level suggesting that long chains V(IV)–O–V(IV) could be relatively stable. Meanwhile, V(V) substitution induces significant distortion that does increase with an increasing number of adjacent V(V) sites due to both smaller V(V) ionic-radius and counterion-rearrangement. Concerning substitution energetics, V(V) substitution is more favourable than the V(IV) even when the former requires charge balancing. However, the V(V) substitution level is limited due to the unfavourable interactions between adjacent V(V) sites. This contrasts with the stabilizing contribution of V(IV)–O–V(IV) conformations. Therefore, even at low vanadium loading, auspicious for V(V) substitution, V(V)-V(IV) mixed configuration results preferable, agreeing with experimental results. Additional calculations for assessing photocatalytic behaviour conclude that V(V) and V(IV) lead to electron and hole traps, respectively. However, at low-vanadium loading V-sites will be isolated, so e^-/h^+ recombination will be less probable, increasing catalyst activity.

Despite the simplicity of these models and numerous interrelated processes involved in the substitution of Ti(IV) with V, calculations reveal some tendencies and hints valuable for understanding the dispersion of experimental results concerning both valence state and activity of V-TiO_2 catalysts.

14.5 Vanadium Oxide Composite-based Photocatalysts

This section focuses on photocatalytic composites in which vanadium oxide mixed with other semiconductors contributes to improve the catalytic properties of the material without losing its crystallographic identity. Composite materials are essentially characterized by the synergy that arises from the creation of new electrically active interfaces between their components. Built-in electric fields by photocatalysts heterojunction affect the density and energy positions of surface redox-sites available for chemical work (Figure 14.1). Therefore, the design (composition and electronic structure) and construction (synthesis strategy) of this kind of photocatalysts are important.

In this context, we will discuss selected examples of composite catalysts, focusing particularly on the strategies used to obtain homogeneous and

intimate mixtures of α-V_2O_5 with metal oxide catalysts, as well as the performance of the heterocatalysts with respect to that of their components. In addition, we comment on some examples of V_2O_5 compounds with graphite-like materials, an incipient but quite promising field.

Table 14.4 summarizes the main characteristics of a selected group of heterocatalysts based on α-V_2O_5

Table 14.4 Summary of heterocatalysts based on α-V_2O_5.

Catalyst	Synthesis	Ratio	Illumination and reaction	Ref.
Binary composites of V_2O_5 and TiO_2				
V_2O_5-TiO_2	one-step mechanical	1 : 1	Vis, RhB	80
V_2O_5/N, S-TiO_2	solid state route	1 : 1	Vis, H_2, and phenol	81
V_2O_5-TiO_2 binary oxides and surfactants (CTAB, HTAB, or PVA)*	Solid state dispersion	1 : 1	UV, 2,4-dichlorophenol solution	82
V_2O_5 /TiO_2	one-step electrospinning process	1 : 1	Vis, RhB	83
V_2O_5-TiO_2	electrospinning	1 : 1	Vis, Ethanol oxidation	84
TiO_2/V_2O_5	solid-state dispersion method	1 : 1	UV and Vis, bisphenol	37
Binary composites of V_2O_5 and oxides				
V_2O_5–CeO_2	precipitation-thermal decomposition	0.15 : 1	Vis, MB	80
V_2O_5–Bi_2O_3 V_2O_5–ZnO V_2O_5–ZrO_2	solid-state dispersion	1 : 1	UV and Vis, bisphenol	37
HfO_2–V_2O_5	precipitation	1 : 0.5; 1 : 1; 1 : 2	Vis, MB	81
NiO/V_2O_5	stirred and calcined at 250 °C	—	Vis, MO	82
SnO_2-V_2O_5	SnO_2 wrapped by vanadium oxide heating at 500 °C	$\approx$ 5 : 1	Vis, RhB	83
Ternary composites of V_2O_5				
V_2O_5/$BiVO_4$/TiO_2	sequentially hydrothermal and adhering	—	Vis, conversion of toluene	84
TiO_2/MoO_3/V_2O_5	*via* controlled hydrolysis	$[TiO_2]:[MoO_3 + V_2O_5]$ 5 : 1	*In-situ* light excitation, Rh6G	85
Ce-TiO_2/V_2O_5 La-TiO_2/V_2O_5 Y-TiO_2/V_2O_5	sol-gel and heat-treated in air	$TiO_2 : V_2O_5$ 10 : 1	UV, MO	86
Bi/$BiVO_4$/V_2O_5	hydrothermal and annealing treatment	—	Vis, O_2 evolution	87
N-TiO_2/V_2O_5	impregnation calcination	N-TiO_2/V_2O_5 V is 0.01, 0.05, 0.2, 0.5 and 1.0 wt	Vis, toluene in air at ambient temperature	88

14.5.1 Vanadium Oxide–Metal Oxide Composites

Most research on V_2O_5 concerns harnessing the optical properties of this oxide to improve the naturally low capacity of broadband semiconductors to capture visible light. Our comments in this section refer only to some binary compounds of V_2O_5/TiO_2, which in general have received more attention. However also exist examples of binary catalysts of V_2O_5 with other metal oxides,[80–83] as well as of some ternary systems[84–88] (Table 14.4). Binary compounds V_2O_5/TiO_2 with V/Ti ratios close to one, giving rise to products that exhibit good catalytic activity under visible or UV light, can be prepared using a variety of methods.

Recently, Mandal *et al.*,[89] reported on the single-step synthesis of heteronanostructured V_2O_5/TiO_2 composites by milling mixtures of commercial precursor oxides. The mechanical alloy method performed at room temperature does not affect V_2O_5, but it alters the pristine structure of TiO_2-anatase. In the absence of any reagent, anatase is transformed into rutile TiO_2, while in presence of V_2O_5, anatase becomes the relatively rare phase of titania bruxite. This is possibly due to a slight V-substitution imperceptible by XRD. The compounds obtained by this method prove to be active in the degradation of RhB under visible light.

Highly stable composites can be prepared directly from metal-salt precursors of both oxides by solid-state synthesis at high temperature. For example, the composite with double-doped TiO_2, V_2O_5/TiO_2, which stabilizes at 500 °C and shows high photocatalytic activity for phenol degradation, as well as in the evolution of H_2. Among the peculiarities of this composite, is its high anatase-to-rutile ratio (16 : 63).[90]

The solid-dispersion method used to manufacture V_2O_5 nanoparticles (Section 14.2) produces V_2O_5 composites with different broadband semiconductors, including TiO_2. However, its photocatalytic activity is lower than that of pure V_2O_5. On the other hand, it confirms that anatase keeps its structure intact after the process. This corroborates the smoothness of the method observed by Sinirtas *et al.*,[91] who demonstrate the feasibility of working with organic compounds. In this way, the authors prepared V_2O_5/TiO_2 composites with different V/Ti ratios, including 1 : 1, the best photocatalytic performance (Table 14.4), which after being calcined, photocatalysts are mixed with a series of surfactants causing hybrid catalysts that after heat treatment at 150 °C proved to have a photocatalytic behaviour superior to the binary composites alone (Figure 14.10a)

Another technique for preparing binary composites is electrospinning. It is a more drastic method than solid dispersion due to thermal treatment of the fibres necessary to remove the organic support that leads to anatase–rutile mixtures. On the other hand, it is an appropriate method to obtain nanostructures with high-aspect ratios, nanorods and nanofibres,[37,92] with good activity for photodegradation of dyes.

Recently, Ghosh *et al.*,[93] reported the gas-phase photocatalytic oxidation reaction of ethanol under visible light assisted by V_2O_5/TiO_2 composites with

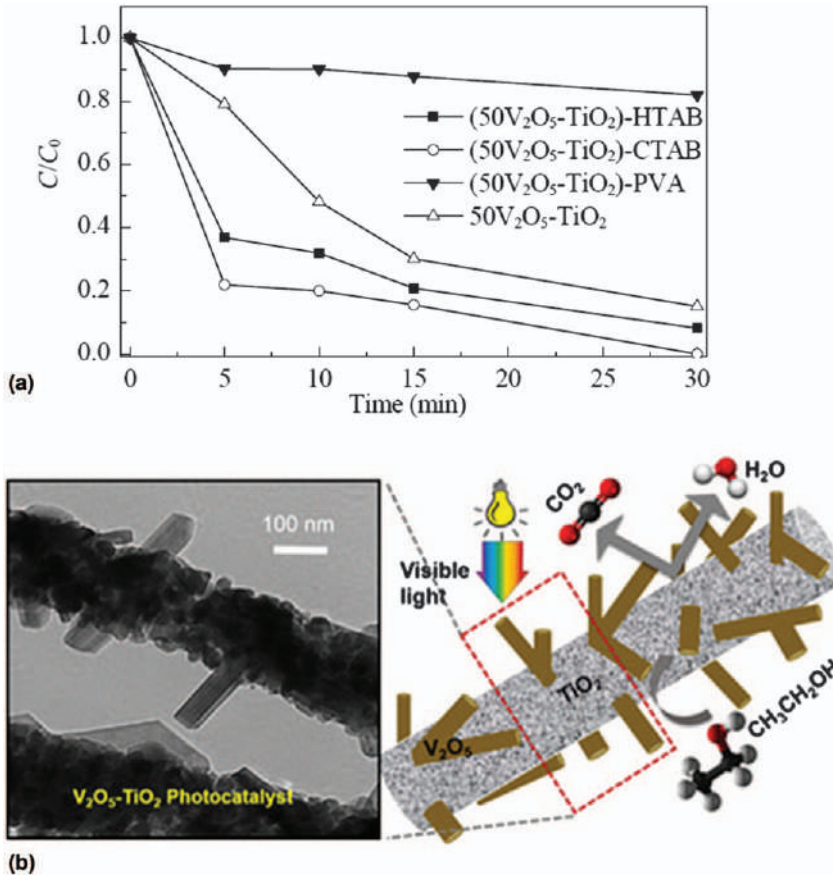

Figure 14.10 (a) Degradation activities of V_2O_5/TiO_2 and surfactant loaded V_2O_5/TiO_2 catalysts. Reproduced from ref. 91 with permission from Elsevier, Copyright 2016. (b) Hierarchical V_2O_5 nanorods on TiO_2 nanofibers.
Reproduced from ref. 93 with permission from John Wiley and Sons, © 2018 Wiley-VCH Verlag GmbH & Co. KGaA, Weinheim.

a peculiar hierarchical morphology, orthorhombic V_2O_5-nanorods emerging from the nanotube surface of anatase–rutile TiO_2 (Figure 14.10b). These hetero-nanostructures obtained from the calcination (400–600 °C) of fibres manufactured by gas jet electrospinning technique using sols containing polyvinylpyrrolidone and a 1 : 1 (w/w) mixture of the precursor metal oxides (vanadium oxytriisopropoxide and titanium tetraisopropoxide) in ethanol–acetic acid, show a high photocatalytic efficiency under visible light. The catalytic performance of calcined composite at 500 °C shows an initial ethanol conversion rate (1.59×10^{1} μmol g^{-1} min^{-1}) 2500-times greater than that of V_2O_5 (5.65×10^{-3} μmol g^{-1} min^{-1}), while TiO_2 is inactive under same conditions.

Monitoring the conversion of ethanol adsorbed in photocatalyst by *in-situ* DRIFTS shows the formation of intermediates such as acetaldehyde

(CH_3CHO), acetate (CH_3COO^-) together with CO_2 and H_2O, but also of formate ($HCOO^-$), in line with studies on its reaction under UV light catalyzed by TiO_2.[94] Ethyl derivatives may arise from the attack of photogenerated holes and/or hydroxyl $^{\bullet}OH$ radicals of water adsorbed on hydrogen at the α-carbon of adsorbed ethanol ($C^{\beta}H_3C^{\alpha}H_2OH$). However, attacking the hydrogen at β-C required for the C–C bond breakdown is only possible for $^{\bullet}OH$ radicals.[95] Therefore, the authors suggest the coexistence of both mechanisms.

14.5.2 Vanadium Oxide/Graphene-like-materials Composites

During the past decade, the use of graphite materials in metal broadband metal oxide-based heterogeneous photocatalysis expanded. In this section, we briefly describe some examples of V_2O_5 compounds with conductive and semiconductor carbon materials.

The formation of binary composites between graphene, or g-C_3N_4 (graphitic carbon nitride) and V_2O_5 nanostructures, based on their band alignments, is an effective strategy to improve the photocatalytic activity of vanadium oxide-based photocatalysts. For example, Liu *et al.*,[96] have reported the fabrication of g-C_3N_4-based nanosheets coupled with V_2O_5 to form a novel z-scheme heterojunction in order to explore the exfoliation and grafting effect of the g-C_3N_4-based layers on the photocatalytic activity. The improved photocatalytic activity for hydrogen evolution and organic pollutant degradation relies on the formation of a z-scheme mechanism, which improves the transfer and separation of the photoinduced electron – hole pairs. Another example to improve the photocatalytic activity is by the formation of Bi_2O_3/V_2O_5@g-C_3N_4 ternary heterojunctions. Vattikuti *et al.*,[97] integrated Bi_2O_3/V_2O_5 on the surface of the g-C_3N_4 nanosheets by an *in-situ* co-pyrolysis approach. The photodegradation efficiencies for the degradation of phenol red and the water reduction for H_2 production are higher than that of Bi_2O_3/V_2O_5 and pristine Bi_2O_3, respectively, under simulated solar light irradiation. The incorporation of g-C_3N_4 into Bi_2O_3/V_2O_5 shows a significant influence on the surface area, optical absorption spectra of the Bi_2O_3/V_2O_5 photocatalyst and the formation of oxygen vacancies during the synthesis process.

14.6 Layered Hybrid Vanadium Oxide Nanocomposite-based Photocatalyst

This section deals with the photocatalytic behaviour of VO_x layered organic–inorganic nanocomposites, where photocatalytic phenomena triggered by illumination of the inorganic core is transmitted target-species at fluid phase. First, after commenting briefly on the structure, morphology and

photocatalytic behaviour of these hybrid vanadium oxide-nanostructures, we comment on the possible origin of the photocatalytic activity of these materials. Thereafter we describe examples of hybrid VO_x nanocomposite–composites.

14.6.1 Inorganic–Organic Nanocomposites

Vanadium oxide xerogel-like hybrid nanostructures consist of a 2D metal-oxide layer protected on both sides with a long-chain organic amphiphilic (surfactant) monolayer. Hybrid organic–inorganic single-layers are commensurate species with a determined organic–inorganic stoichiometry ratio due specific interactions between the hydrophilic surfactant moiety and functional sites at metal oxide layer. In bulk, layers are stacked along the perpendicular direction to their basal plane, so these materials can be classified as an intercalation product resulting from exchanging water from hydrated V_2O_5-xerogel by surfactant molecules.[98]

Table 14.5 Band gap of layered nanocomposites and metal oxide.[98,99]

Catalyst	Band gap
ZnO	3.21
ZnO (stearic acid)	3.28
TiO_2 (anatasa)	3.20
TiO_2 (stearic acid)	3.28
V_2O_5	2.24
V_2O_5 (hexadecylamine)	2.28

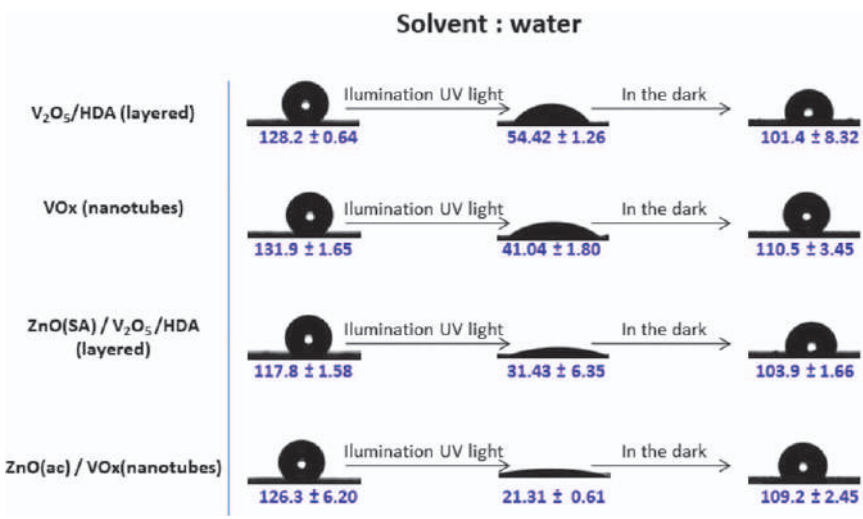

Figure 14.11 Photoinduced wettability transition of the samples (measurement performed with contact angles of the water in the samples).

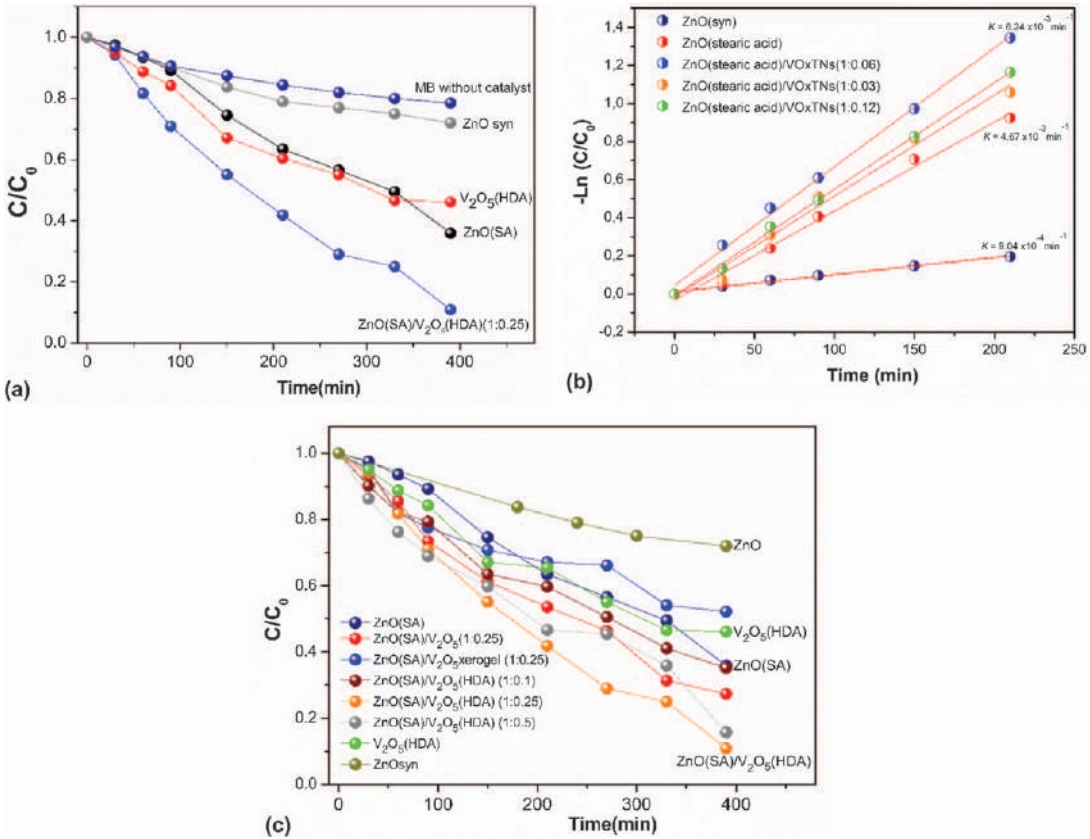

Figure 14.12 (a) Photocatalytic performance of samples ZnO(SA)/V_2O_5(HDA) in degradation of MB solution. (b) Photodegradation kinetics of samples ZnO(SA)/VO_x nanotubes. (c) Photocatalytic performance of the samples containing hybrid layered-vanadium for the degradation of MB solution.
Reproduced from ref. 98, https://doi.org/10.3390/catal8090374, under the terms of the CC BY 4.0 licence, https://creativecommons.org/licenses/by/4.0/.

The electronic spectra of layered nanocomposites are similar to that of V_2O_5 where the band-edge is blue-shifted due to 2D confinement. Layered nanocomposites from other metal oxides such as TiO_2[99] present similar behaviour. (Table 14.5).

Hydrothermal treatment of layered V_2O_5 nanocomposites leads to multi-wall nanotubes in which amine remains intercalated resulting in similar both stoichiometry and diffraction patterns.[100] However, their V–O network corresponds to mixed-valence species V_7O_{16}, similar to those in other VO_x hydrothermal products such as nanourchins[101] or the nanosquares[44] mentioned in Section 14.2.2.

Since the only photoactive component in these catalysts, the metal oxide, is completely covered by an aliphatic layer, degradation of the dye must occur at the catalyst–solution interface, at approximately 3 nm away from the metal-oxide layer. This was verified by positive photohydrophilising the catalyst surface (Figure 14.11). Results agree with the concept ''remote photocatalytic activity'' described for TiO_2 samples covered by either a grafted alkylsilane,[102] with a soot layer,[103] or in the composite V_2O_5/TiO_2 with alkyl amines[91] (see Figure 14.10a in Section 14.5.1).

14.6.2 Hybrid Vanadium Oxide-nanocomposite-based Composites

V_2O_5-amine nanocomposites show synergy-effects in binary composites. For instance, with hybrid-layered ZnO(SA) (SA: stearic acid) (Figure 14.12a) the observed photocatalytic activity suggests that the photocatalysis involves the processes described in Scheme 14.1.[98]

Layered V_2O_5 nanotube photocatalysts show regular behaviour leading to first order-dye degradation kinetics, which indicate that it is faster than the layered V_2O_5 photocatalyst, as both singly and composite in spite its contact surface with fluid phase is comparatively lower (Figure 14.12b).[104]

The activity of composite photocatalysts containing hybrid layered-vanadium increases with vanadium concentration (Figure 14.12c) reaching

$$\begin{aligned}
ZnO(SA)/V_2O_5(HDA) + h\nu\ (visible) &\rightarrow ZnO(SA)/V_2O_5(HDA)(h^+\ VB + e\text{-}\ CB)\\
ZnO(SA)(e^-\ CB) &\rightarrow V_2O_5(HDA)(e^-\ CB)\\
ZnO(SA)(h^+\ VB) &\rightarrow V_2O_5(HDA)(h^+\ VB)\\
V_2O_5(HDA)(e^-CB) + H^+ + O_2 &\rightarrow H_2O_2\\
H_2O_2 + e^- + h\nu\ (visible) &\rightarrow {}^{\bullet}OH + OH^-\\
{}^{\bullet}OH + h^+ + MB &\rightarrow \text{Degradation products}
\end{aligned}$$

Scheme 14.1 Proposed mechanism of the photocatalytic activity of ZnO(SA)/V_2O_5(HDA) for degradation of organic pollutants under visible light irradiation.
Reproduced from ref. 98, https://doi.org/10.3390/catal8090374, under the terms of the CC BY 4.0 licence, https://creativecommons.org/licenses/by/4.0/.

a maximum at a determined nanocomposite concentration, after which it again lowers – as often occurs for many of the different catalysis types discussed in this chapter.

14.7 Conclusions

Vanadium oxides have chemical and photophysical properties that give them high potential for the development of efficient photocatalysts under UV and visible light. Both the preparation of new materials and the creation of knowledge generated over the past decade portend a prompt possibility for the enormous potential of the possible applications of vanadium oxide photocatalysts.

In this way, it is worth highlighting:

Obtaining stoichiometric oxides of V(v) and V(iv) pure photocatalytically active.

Develop both synthesis strategies and design of photocatalysts that avoid excess structural water and/or strongly adsorbed detrimental to photocatalyst activity.

Prove the feasibility and the limitations to perform selective photocatalysis.

Study the effect of matrices to house active species of vanadium oxides.

Beginning to understand the strange balance between oxidation states of vanadium practically ungovernable by selecting precursors.

Beginning to understand the reason for the ''magic'' concentration of vanadium, but different for each system and/or condition, to which maximum activity is achieved.

Starting practicing interface and matching design of the electronic frontier bands of the components of composite catalysts to circumvent the recombination of photogenerated charge carriers as well as to achieve flows that allow the accumulation of charge in pre-determined energy levels for the redox processes that are to be triggered in the fluid phase.

Designing and use of composite catalysts with graphite materials, either conductive or semiconductor with energy levels by chemical modification of the carbonaceous component; studying easy-to-prepare systems that allow the study of its nature and scope, and to efficiently practice remote photocatalytic activity; *etc.*

These studies and developments would help to accumulate knowledge to face the challenge still pending to understand and, as far as possible, manage, the fluid nature of the surface of vanadium oxides under usual photocatalysis conditions.

References

1. J. Kou, C. Lu, J. Wang, Y. Chen, Z. Xu and R. S. Varma, *Chem. Rev.*, 2017, **117**, 1445–1514.

2. L. I. Granone, F. Sieland, N. Zheng, R. Dillert and D. W. Bahnemann, *Green Chem.*, 2018, **20**, 1169–1192.
3. J. Schneider, M. Matsuoka, M. Takeuchi, J. Zhang, Y. Horiuchi, M. Anpo and D. W. Bahnemann, *Chem. Rev.*, 2014, **114**, 9919–9986.
4. K. Nakata and A. Fujishima, *J. Photochem. Photobiol., C*, 2012, **13**, 169–189.
5. J. M. Herrmann, *Top. Catal.*, 2005, **34**, 49–65.
6. N. Serpone, A. V. Emeline, S. Horikoshi, V. N. Kuznetsov and V. K. Ryabchuk, *Photochem. Photobiol. Sci.*, 2012, **11**, 1121–1150.
7. A. O. Ibhadon and P. Fitzpatrick, *Catalysts*, 2013, **3**, 189–218.
8. U. I. Gaya, *Heterog. Photocatal. Using Inorg. Semicond. Solids*, 2014, **9789400777**, 1–213.
9. M. R. Hoffmann, S. T. Martin, W. Choi and D. W. Bahnemann, *Chem. Rev.*, 1995, **95**, 69–96.
10. D. Kong, Y. Zheng, M. Kobielusz, Y. Wang, Z. Bai, W. Macyk, X. Wang and J. Tang, *Mater. Today*, 2018, **21**, 897–924.
11. X. He and C. Zhang, *J. Mater. Sci.*, 2019, **54**, 8831–8851.
12. P. Riente and T. Noël, *Catal. Sci. Technol.*, 2019, **9**, 5186–5232.
13. A. V. Emeline, V. K. Ryabchuk and N. Serpone, *J. Phys. Chem. B*, 2005, **109**, 18515–18521.
14. C. Xu, P. Ravi Anusuyadevi, C. Aymonier, R. Luque and S. Marre, *Chem. Soc. Rev.*, 2019, **48**, 3868–3902.
15. K. Fujishima and A. Honda, *Nature*, 1972, **238**, 37–38.
16. A. Rani, R. Reddy, U. Sharma, P. Mukherjee, P. Mishra, A. Kuila, L. C. Sim and P. Saravanan, *J. Nanostruct. Chem.*, 2018, **8**, 255–291.
17. L. Caswell, *Bull. Hist. Chem.*, 2003, **28**, 35–41.
18. P. Shvets, O. Dikaya, K. Maksimova and A. Goikhman, *J. Raman Spectrosc.*, 2019, **50**, 1226–1244.
19. U. Schwingenschlögl and V. Eyert, *Ann. Phys.*, 2004, **13**, 475–510.
20. H. Katzke, P. Tolédano and W. Depmeier, *Phys. Rev. B: Condens. Matter Mater. Phys.*, 2003, **68**, 1–7.
21. A. Pergament, G. Stefanovich and A. Velichko, *J. Sel. Top. Nano Electron. Comput.*, 2013, **1**, 24–43.
22. J. Jin, D. Zhang, X. Qin, Y. Yang, Y. Huang, H. Guan, Q. He, P. Fan and W. Lv, *Nanomaterials*, 2019, **9**, 102.
23. Q. Kang, Y. Zhang, S. Bao and G. Zhang, *R. Soc. Open Sci.*, 2019, **6**, 181116.
24. R. Levi, M. Bar-Sadan, A. Albu-Yaron, R. Popovitz-Biro, L. Houben, Y. Prior and R. Tenne, *Materials*, 2010, **3**, 4428–4445.
25. Y. Zhang, Y. Luo, C. Fincher, S. Banerjee and M. Pharr, *J. Mater. Chem. A*, 2019, **7**, 23922–23930.
26. D. A. Semenenko, D. M. Itkis, E. A. Pomerantseva, E. A. Goodilin, T. L. Kulova, A. M. Skundin and Y. D. Tretyakov, *Electrochem. Commun.*, 2010, **12**, 1154–1157.
27. S. G. Wang, *ACS Nano*, 2013, **7**, 11218–11226.
28. H. Miyazaki, T. Matsuura and T. Ota, *RSC Adv.*, 2017, **7**, 2388–2391.

29. M. Alsawafta, A. Almoabadi, S. Badilescu and V. Van Truong, *J. Electrochem. Soc.*, 2015, **162**, H466–H472.
30. M. Aslam, I. M. I. Ismail, N. Salah, S. Chandrasekaran, M. T. Qamar and A. Hameed, *J. Hazard. Mater.*, 2015, **286**, 127–135.
31. X. Liu, J. Zeng, H. Yang, K. Zhou and D. Pan, *RSC Adv.*, 2018, **8**, 4014–4031.
32. M. Liu, B. Su, Y. Tang, X. Jiang and A. Yu, *Adv. Energy Mater.*, 2017, **7**, 1–34.
33. K. Zilberberg, S. Trost, J. Meyer, A. Kahn, A. Behrendt, D. Lützenkirchen-Hecht, R. Frahm and T. Riedl, *Adv. Funct. Mater.*, 2011, **21**, 4776–4783.
34. W. Avansi, V. R. De Mendonça, O. F. Lopes and C. Ribeiro, *RSC Adv.*, 2015, **5**, 12000–12006.
35. B. Li, Y. Xu, G. Rong, M. Jing and Y. Xie, *Nanotechnology*, 2006, **17**, 2560–2566.
36. J. H. Kim, D. Hansora, P. Sharma, J. W. Jang and J. S. Lee, *Chem. Soc. Rev.*, 2019, **48**, 1908–1971.
37. Y. Zengin and G. S. Pozan Soylu, *Environ. Eng. Sci.*, 2018, **35**, 323–332.
38. Y. Li, J. L. Kuang, Y. Lu and W. Bin Cao, *Acta Metall. Sin.*, 2017, **30**, 1017–1026.
39. H. Liu, Y. Gao, J. Zhou, X. Liu, Z. Chen, C. Cao, H. Luo and M. Kanehira, *J. Solid State Chem.*, 2014, **214**, 79–85.
40. T. Puangpetch, S. Chavadej and T. Sreethawong, *Powder Technol.*, 2011, **208**, 37–41.
41. Y. Wang, Z. Zhang, Y. Zhu, Z. Li, R. Vajtai, L. Ci and P. M. Ajayan, *Acs Nano*, 2008, **2**, 1492–1496.
42. S. Kajita, T. Yoshida, N. Ohno, Y. Ichino and N. Yoshida, *J. Phys. D: Appl. Phys.*, 2018, **51**, 215201.
43. B. Jiang, X. Peng, Y. Qu, H. Wang, C. Tian, Q. Pan, M. Li, W. Zhou and H. Fu, *ChemCatChem*, 2014, **6**, 2553–2559.
44. D. Navas, J. P. Donoso, C. Magon, C. M. Sotomayor-Torres, M. Moreno, H. Lozano, E. Benavente and G. González, *New J. Chem.*, 2019, **43**, 17548–17556.
45. A. M. Love, C. A. Carrero, A. Chieregato, J. T. Grant, S. Conrad, R. Verel and I. Hermans, *Chem. Mater.*, 2016, **28**, 5495–5504.
46. G. Deo and I. E. Wachs, *J. Phys. Chem.*, 1991, **95**, 5889–5895.
47. H. Tian, E. I. Ross and I. E. Wachs, *J. Phys. Chem. B*, 2006, **110**, 9593–9600.
48. I. E. Wachs, *Dalton Trans.*, 2013, **42**, 11762–11769.
49. B. M. Weckhuysen and D. E. Keller, *Catal. Today*, 2003, **78**, 25–46.
50. I. E. Wachs, Y. Chen, J. M. Jehng, L. E. Briand and T. Tanaka, *Catal. Today*, 2003, **78**, 13–24.
51. M. Badlani and I. E. Wachs, *Catal. Lett.*, 2001, **75**, 137–149.
52. B. Kortewille, I. E. Wachs, N. Cibura, O. Pfingsten, G. Bacher, M. Muhler and J. Strunk, *ChemCatChem*, 2018, **10**, 2360–2364.
53. B. Kortewille, I. E. Wachs, N. Cibura, O. Pfingsten, G. Bacher, M. Muhler and J. Strunk, *Eur. J. Inorg. Chem.*, 2018, 3725–3735.

54. N. R. Jaegers, C. Wan, M. Y. Hu, M. Vasiliu, D. A. Dixon, E. Walter, I. E. Wachs, Y. Wang and J. Z. Hu, *J. Phys. Chem. C*, 2017, **121**, 6246–6254.
55. D. Nitsche and C. Hess, *J. Phys. Chem. C*, 2016, **120**, 1025–1037.
56. M. El-Roz, L. Lakiss, I. Telegeiev, O. I. Lebedev, P. Bazin, A. Vicente, C. Fernandez and V. Valtchev, *ACS Appl. Mater. Interfaces*, 2017, **9**, 17846–17855.
57. T. Umebayashi, T. Yamaki, H. Itoh and K. Asai, *J. Phys. Chem. Solids*, 2002, **63**, 1909–1920.
58. W. Lin and Y. Lin, *Environ. Eng. Sci.*, 2012, **29**, 447–452.
59. B. Liu, X. Wang, G. Cai, L. Wen, Y. Song and X. Zhao, *J. Hazard. Mater.*, 2009, **169**, 1112–1118.
60. W. Chen, P. Koshy, L. Adler and C. C. Sorrell, *J. Aust. Ceram. Soc.*, 2017, **53**, 569–576.
61. S. Wang, W. Liu and D. Zhang, *Adv. Mater. Res.*, 2014, **959**, 2521–2525.
62. J. C. Wu and C. Chen, *J. Photochem. Photobiol. Chem., A*, 2004, **163**, 509–515.
63. O. Sacco, D. Sannino, M. Matarangolo and V. Vaiano, *Materials*, 2019, **12**, 911.
64. B. Tian, C. Li, F. Gu, H. Jiang, Y. Hu and J. Zhang, *Chem. Eng. J.*, 2009, **151**, 220–227.
65. R. Rahimi, M. M. Moghaddas, S. Zargari and R. Rahimi, *Adv. Mater. Res.*, 2013, **702**, 56–61.
66. X. Zhou, J. Wu, Q. Li, Y. Qi, Z. Ji, P. He and X. Qi, *Chem. Eng. J.*, 2017, **330**, 294–308.
67. S. P. Takle, S. D. Naik, S. K. Khore, S. A. Ohwal, N. M. Bhujbal, S. L. Landge, B. B. Kale and R. S. Sonawane, *RSC Adv.*, 2018, **8**, 20394–20405.
68. G. Rossi, L. Pasquini, D. Catone, A. Piccioni, N. Patelli, A. Paladini, A. Molinari, S. Caramori, P. O. Keeffe and F. Boscherini, *Appl. Catal., B*, 2018, **612**, 603–612.
69. A. Giannakas, F. Bairamis, I. Papakostas, T. Zerva and I. Konstantinou, *J. Ind. Eng. Chem.*, 2018, **65**, 370–379.
70. Y. Chen, J. Chang and B. Moongraksathum, *J. Taiwan Inst. Chem. Eng.*, 2015, **52**, 140–146.
71. K. Nagaveni, M. S. Hegde and G. Madras, *J. Phys. Chem. B*, 2004, **2**, 20204–20212.
72. Y. Izumi, K. Konishi, D. M. Obaid, T. Miyajima and H. Yoshitake, *Anal. Chem.*, 2007, **79**, 6933–6940.
73. A. I. Kokorin, V. I. Pergushov and A. I. Kulak, *Catal. Lett.*, 2020, **150**, 263–272.
74. Z. Zhang, C. Shao, L. Zhang, X. Li and Y. Liu, *J. Colloid Interface Sci.*, 2010, **351**, 57–62.
75. R. Jaiswal, N. Patel, D. C. Kothari and A. Miotello, *Appl. Catal., B*, 2012, **126**, 47–54.
76. H. Liu, Y. Wu and J. Zhang, *ACS Appl. Mater. Interfaces*, 2011, **3**, 1757–1764.

77. M. J. Nash, S. Rykov, R. F. Lobo, D. J. Doren, I. Wachs and V. Pennsyl, *J. Phys. Chem. C*, 2007, **111**, 7029–7037.
78. A. M. Shough, D. J. Doren, M. Nash and R. F. Lobo, *J. Phys. Chem. C*, 2007, **10**, 1776–1782.
79. L. Lv, F. Su and X. S. Zhao, *Micropor. Mesopor. Mater.*, 2004, **76**, 113–122.
80. M. A. Zeleke and D. H. Kuo, *Chemosphere*, 2019, **235**, 935–944.
81. I. Sari, T. Lu and Sang-hsuan, *J. Am. Ceram. Soc.*, 2020, **103**, 2252–2261.
82. S. A. Mohammed, L. Al Amouri, E. Yousif, A. A. Ali, F. Mabood, H. F. Abbas and S. Alyaqoobi, *Heliyon*, 2018, **4**, e00581.
83. M. Epifani, S. Kaciulis, A. Mezzi, D. Altamura, C. Giannini, R. Díaz, C. Force, A. Genç, J. Arbiol, P. Siciliano, E. Comini and I. Concina, *Sci. Rep.*, 2017, **7**, 1–13.
84. J. Sun, X. Li, Q. Zhao, J. Ke and D. Zhang, *J. Phys. Chem. C*, 2014, **118**, 10113–10121.
85. E. A. Konstantinova, A. I. Kokorin, A. A. Minnekhanov, T. V. Sviridova and D. V. Sviridov, *Catal. Lett.*, 2019, **149**, 2256–2267.
86. J. Liu, R. Yang and S. Li, *J. Rare Earths*, 2007, **25**, 173–178.
87. X. Xu, S. Kou, X. Guo, X. Li, X. Ma and H. Mao, *J. Phys. Chem. C*, 2017, **121**, 16257–16265.
88. F. Dong, Y. Sun and M. Fu, *Int. J. Photoenergy*, 2012, **569716**, 1–10.
89. R. K. Mandal, S. Kundu, S. Sain and S. K. Pradhan, *New J. Chem.*, 2019, **43**, 2804–2816.
90. S. Martha, D. P. Das, N. Biswal and K. Parida, *J. Mater. Chem.*, 2012, **22**, 10695–10703.
91. E. Sinirtas, M. Isleyen and G. S. P. Soylu, *Chin. J. Catal.*, 2016, **37**, 607–615.
92. Q. Su, J. Zhang, Y. Wang, M. Yu and C. Zhu, *J. Phys. Chem. Solids*, 2013, **74**, 1475–1481.
93. M. Ghosh, J. Liu, S. S. C. Chuang and S. C. Jana, *ChemCatChem*, 2018, **10**, 3305–3318.
94. Z. Yu and S. S. C. Chuang, *J. Catal.*, 2007, **246**, 118–126.
95. S. Gligorovski, R. Strekowski, S. Barbati and D. Vione, *Chem. Rev.*, 2015, **115**, 13051–13092.
96. B. Liu, D. Yin, F. Zhao, K. K. Khaing, T. Chen, C. Wu, L. Deng, L. Li, K. Huang and Y. Zhang, *J. Phys. Chem. C*, 2019, **123**, 4193–4203.
97. S. V. P. Vattikuti, A. K. R. Police, J. Shim and C. Byon, *Appl. Surf. Sci.*, 2018, **447**, 740–756.
98. J. Aliaga, N. Cifuentes, G. González, C. Sotomayor-Torres and E. Benavente, *Catalysts*, 2018, **8**, 1–13.
99. E. Benavente, C. Maldonado, S. Devis, L. Diaz, H. Lozano, C. Sotomayor-Torres and G. González, *RSC Adv.*, 2016, **6**, 18538–18541.
100. F. Krumeich, H. J. Muhr, M. Niederberger, F. Bieri, B. Schnyder and R. Nesper, *J. Am. Chem. Soc.*, 1999, **121**, 8324–8331.

101. C. O'Dwyer, D. Navas, V. Lavayen, E. Benavente, M. A. Santa Ana, G. González, S. B. Newcomb and C. M. Sotomayor Torres, *Chem. Mater.*, 2006, **18**, 3016–3022.
102. H. Haick and Y. Paz, *J. Phys. Chem. B*, 2001, **105**, 3045–3051.
103. M. C. Lee and W. Choi, *J. Phys. Chem. B*, 2002, **106**, 11818–11822.
104. E. Benavente, D. Navas, S. Devis, M. Segovia, C. Sotomayor-Torres and G. González, *Catalysts*, 2018, **8**, 93.

CHAPTER 15

Theoretical Mechanistic Analysis on Vanadium Oxidation Catalysis

M. L. KUZNETSOV

Centro de Química Estrutural, Instituto Superior Técnico, Universidade de Lisboa, Av. Rovisco Pais, 1049-001 Lisboa, Portugal
Email: max@mail.ist.utl.pt

15.1 Introduction

Knowledge of reaction mechanisms, intimate details and driving forces of chemical processes is extremely important for molecular design, optimisation of reaction conditions, understanding chemical reactivity, regulation of reaction course, regio- and stereoselectivity, tuning catalytic properties and development of new synthetic strategies towards novel materials with valuable properties. Theoretical methods of quantum chemistry represent one of the most powerful tools for the investigation of reaction mechanisms, in particular when chemical processes occur *via* formation of short-lived intermediates that cannot be detected experimentally. Mechanistic aspects of vanadium catalysed reactions were discussed recently in several reviews.[1–3] This chapter is focused on the analysis of mechanistic features of vanadium catalysed oxidation reactions, investigated using theoretical methods.

Catalysis Series No. 41
Vanadium Catalysis
Edited by Manas Sutradhar, José Armando L. da Silva and Armando J. L. Pombeiro

Published by the Royal Society of Chemistry, www.rsc.org

15.2 Oxidation and Oxidative Dehydrogenation of Alkanes

Alkanes (RH) represent the most abundant component of natural gas and their oxidation is of crucial industrial importance as they allow the synthesis of a great variety of valuable products, such as alcohols, esters, aldehydes, ketones, acids, amines and others.

15.2.1 Hydroperoxidation and Hydroxylation of Alkanes

Peroxides (H_2O_2, ^tBuOOH, SO_5^{2-}, $S_2O_8^{2-}$) are one of the most studied oxidants used for the V-catalysed homogeneous functionalisation of alkanes. Reactions of RH with aqueous H_2O_2 catalysed by various V(v) complexes usually lead to formation of alkyl hydroperoxides ROOH. The general mechanism is of a radical type including the generation of highly reactive $HO^\bullet$ radicals that abstract hydrogen from an alkane molecule to give $R^\bullet$ (Scheme 15.1). The latter reacts with molecular oxygen to produce ROOH.

Generation of $HO^\bullet$ in the "V(v) + H_2O_2" Fenton-like system is the rate-limiting step of the whole alkane oxidation reaction. The conventional mechanism for this process was supported by several Density Functional Theory (DFT) calculations[4–6] and includes coordination of H_2O_2 to the V atom in an active catalytic species, proton transfer from the coordinated H_2O_2 to (hydr)oxido or peroxido ligands, elimination of the $HOO^\bullet$ radical accompanied by the reduction of V(v) to V(iv), coordination of the second H_2O_2 molecule followed by another H-transfer and the O–O bond cleavage in the activated hydroperoxido ligand to give $HO^\bullet$ and the initial form of the catalyst (Scheme 15.2).

In accord with DFT calculations,[4,5] the rate-determining step of the $HO^\bullet$ generation is an H-transfer from H_2O_2. Since the reaction occurs much faster in the presence of pyrazine-2-carboxylic acid (pcaH) as an additive, Shul'pin and co-authors proposed that pcaH facilitates this H-transfer *via* a robot's arm mechanism acting as a proton shuttle on the way from H_2O_2 to the oxido-ligand (see Chapter 4). Subsequent DFT (B3LYP) calculations[4] confirmed that such pca-assisted H-transfer is by 4.3 kcal mol^{-1} more favourable than a direct one-step proton transfer. However, further calculations demonstrated that a water-assisted mechanism of the H-transfer is even more favourable than the robot's arm pathway (by 9.6 kcal mol^{-1}).[5] The reason is in the formation of a

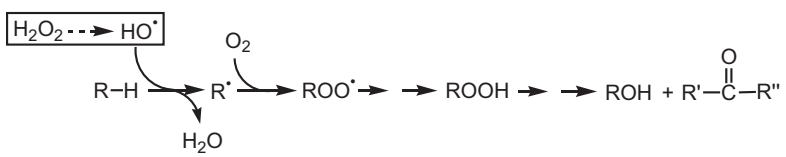

Scheme 15.1 Radical Mechanism of the Alkanes Oxidation with H_2O_2 (the rate-limiting step of the whole process is boxed).
Reproduced from ref. 80 with permission from American Chemical Society, Copyright 2013.

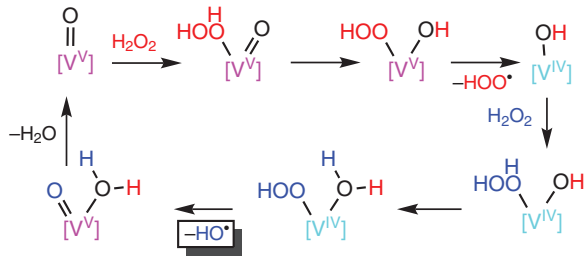

Scheme 15.2 Simplified mechanism of the HO• radical generation catalysed by V(v) complexes.
Adapted from ref. 80 with permission from American Chemical Society, Copyright 2013.

6-membered cyclic transition state (TS) in the former case and less stable 4-membered cyclic TS in the latter case. The proposed role of pcaH is the stabilisation of the V(IV) species involved in the rate-limiting step. However, further investigations are required to clarify this issue.

Complementary results were obtained for the alkane oxidation by the vanadate–H_2O_2 system in acidified acetonitrile.[6] Under acidic conditions, oligovanadates are the predominant V-species in solution. The divanadate active catalytic form $[\{V(O_2)(=O)(H_2O)\}_2\mu\text{-}O]$ is more active than the simple monovanadate $[V(O_2)(=O)(H_2O)_2(OH)]$ by a factor of *ca.* 1200. Such activation is due to the effect of the second V-moiety, which facilitates proton transfer in the rate-limiting step of the HO• generation.

A different mechanism was found for the V(v) catalyst $[V(=O)(OMe)(5\text{-Cl-quin})_2]$ (**1**) (quin = quinolin-8-olate) (Scheme 15.3).[7] The DFT (M06) calculations showed that H_2O_2 is tremendously activated by a simple coordination to vanadium in **2** and directly produces HO• upon the O–O bond cleavage. Such an activation is explained by the non-innocent character of the quinolin-8-olate ligand. Due to the ability of this ligand to be easily oxidised, one of two HO• radicals formed upon the O–O bond cleavage in **3** (*i.e.*, that coordinated to V) is immediately stabilised to the OH^- anion by reduction with the quinolin-8-olate ligand. Spin density in the O–O cleavage product **[4]L•** is significantly delocalised among the atoms of {5-Cl-quin}• (Figure 15.1). As a result, the oxidation state of V in this mechanism is not changed. Thus, in this catalytic system, the ligand plays the same role as a metal does in the conventional mechanisms proposed for the Fenton and Fenton-like systems.

The same mechanism was found by DFT calculations for a V(IV) catalyst bearing the 2,2′-bipyridine ligand.[8] However, in this case, the ligand is not redox-active, and easy oxidation of V(IV) to V(V) is responsible for the activation of coordinated H_2O_2, as in the conventional mechanism proposed by Haber and Weiss[9] for the Fenton system "Fe(II) + H_2O_2".

The mechanism of hydroxylation of propane into isopropanol with molecular oxygen and a vanadium bis(2-phenoxyl)-phosphinite pincer complex used as a catalyst was investigated by Fu *et al.*[10] The first step

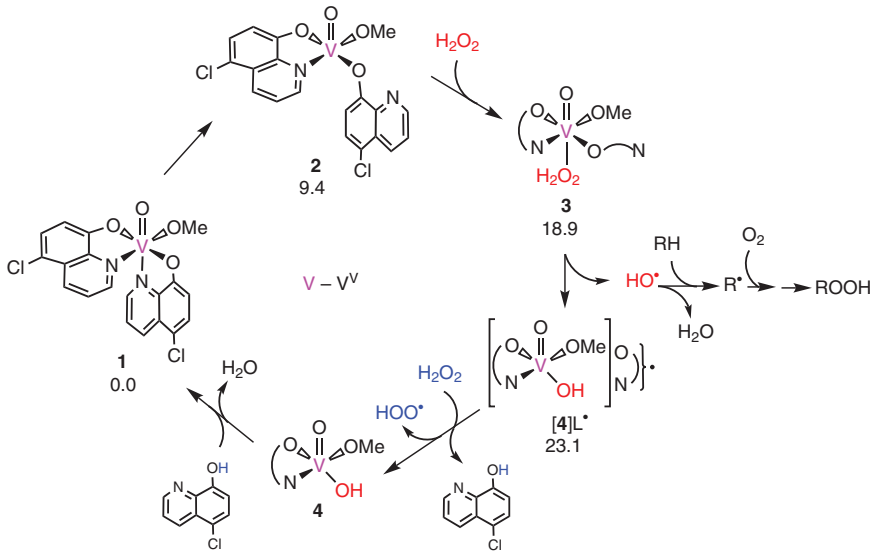

Scheme 15.3 Most favourable mechanism of HO• generation from H_2O_2 catalysed by complex **1** (relative ΔG_s values are indicated in kcal mol^{-1}). Adapted from ref. 7 with permission from American Chemical Society, Copyright 2018.

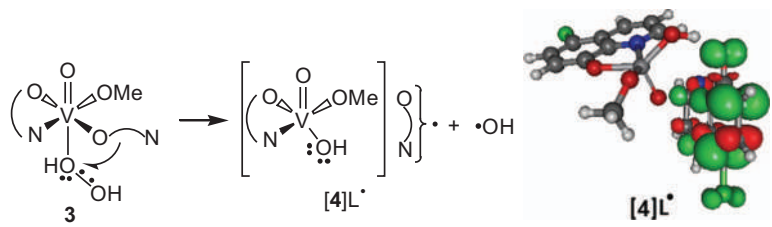

Figure 15.1 HO – OH bond cleavage and intramolecular electron transfer in complex **3** and spin density distribution in [**4**]L•. Adapted from ref. 7 with permission from American Chemical Society, Copyright 2018.

is H-abstraction by the P=O unit of a catalytic active form to give isopropyl radical (Scheme 15.4). This process is associated with one-electron reduction of the vanadium centre. The isopropyl radical then rebounds to the V=O group and, upon an H-transfer from the P–OH group, coordinated isopropanol is formed. After addition of molecular oxygen to give a peroxido V-complex, ^{i}PrOH is released from the V coordination sphere.

15.2.2 Carboxylation of Alkanes

Light alkanes (methane and ethane) undergo carboxylation to the corresponding carboxylic acids upon oxidation with $K_2S_2O_8$ catalysed by

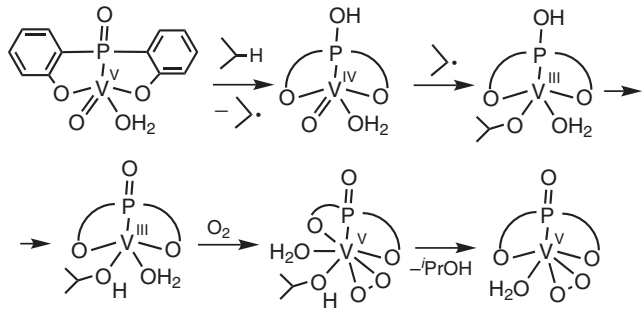

Scheme 15.4 Simplified mechanism of V-catalysed propane hydroxylation with O_2.

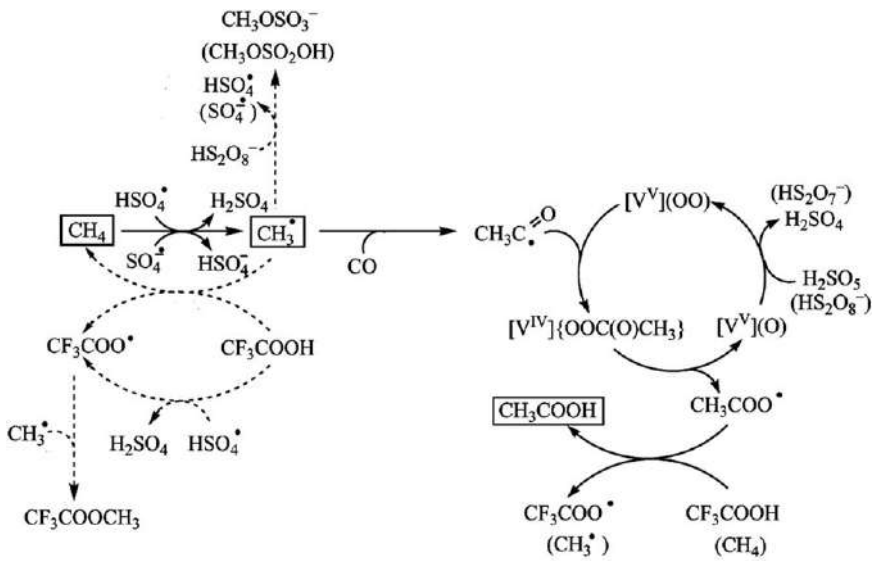

[V] = vanadium metal center namely V{N(CH2CH2O)3}.

Scheme 15.5 Mechanism of Radical Formation and Carboxylation of Methane to Acetic Acid and Side Reactions (Dotted Lines) in the system $CH_4/K_2S_2O_8$/CO/vanadatrane/TFA.
Adapted from ref. 11 with permission from American Chemical Society, Copyright 2007.

vanadatrane in the presence of CO.[11,12] The mechanism elucidated by DFT (B3LYP) includes thermic generation of the $HSO_4^{\bullet}$ of $SO_4^{\bullet -}$ radicals from peroxodisulphate and the hydrogen abstraction from RH to give $R^{\bullet}$ (Scheme 15.5). The alkyl radical reacts with CO affording $R(=O)C^{\bullet}$ which abstracts an oxygen atom in two steps from a V-peroxido active species. The final hydrogen abstraction from trifluoroacetic acid (TFA) used as solvent gives the final product.

15.2.3 Oxidative Dehydrogenation (ODH) of Alkanes

The oxidative dehydrogenation (ODH) of alkanes is of great industrial interest because it constitutes a direct route to alkenes, which are basic reactive precursors for a number of industrially valuable products. This process is thermodynamically favourable but requires a catalyst to accelerate the reaction and to avoid side reactions and overoxidation. One of the most efficient catalytic systems for the ODH of alkanes is based on vanadium oxides or species bearing the vanadyl group V=O.

Earlier experimental studies[13] indicate that the selective oxidation of alkanes over vanadium oxides occurs *via* a Mars–van Krevelen mechanism[14] that involves the catalyst surface as an active part of the reaction (Scheme 15.6). The vanadium oxide surface (usually, a V atom) is reduced by alkane to give alkene and water, followed by reoxidation of the surface with an oxidant (O_2, N_2O, CO_2, *etc.*).

The first step of alkane ODH is an abstraction of the hydrogen atom from RH (Scheme 15.7). This step is usually rate-limiting for the whole process,

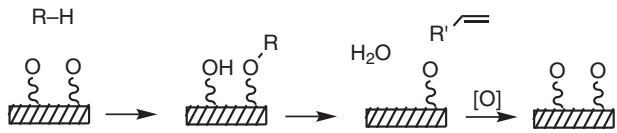

Scheme 15.6 Mars–van Krevelen mechanism of alkane dehydrogenation.

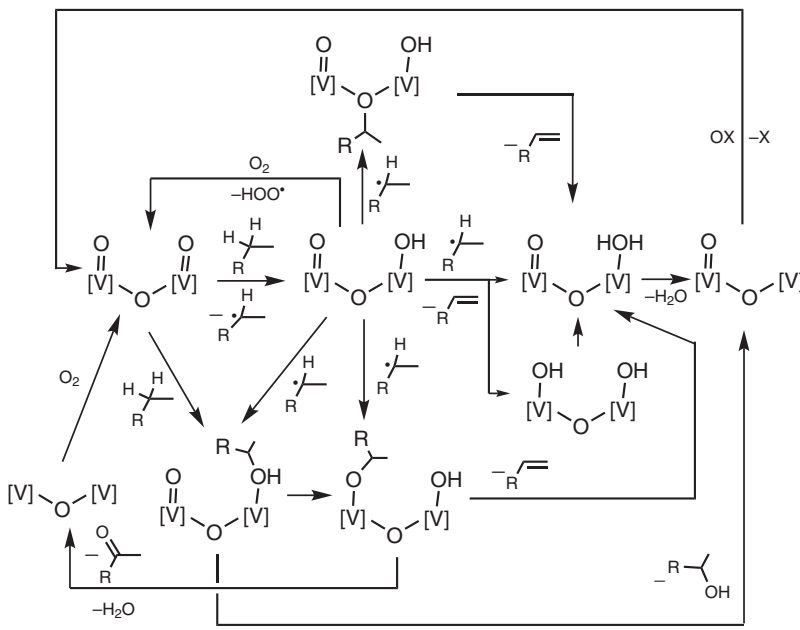

Scheme 15.7 Simplified mechanisms of alkane ODH catalysed by vanadium oxides (divanadyl fragment is shown, OX is an oxidant).

and the most active site for the H-abstraction is the vanadyl group V=O, while the bridging oxygen atoms are typically less active.[15–23] Stabilisation of the radical character of the surface oxygen atoms significantly decreases the activation barrier for the first H-abstraction step.[24] Most of the works suggest that the H-abstraction results in generation of the alkyl radical R• – free or weakly bound to the formed V–OH group and/or another part of the surface.[15,17–19,21–23,25,26] The generated alkyl radical can undergo a second, usually more facile H-abstraction by the V=O, V–OH or V–O–V oxygen atoms of the catalyst, depending on the catalytic system, to give alkene and water, which is formed either directly or upon H-transfer(s) and then eliminated from the catalyst's surface.[16,18,19,23,24]

Alternatively, R• can interact with the same V=O, V–OH or V–O–V groups affording adsorbed alkoxide or alcohol or the bridging V–O(R)–V fragment which undergo the second H-transfer to give alkene and water.[16,17,22,25,26] In side reactions, alcohol may desorb while alkoxide can lead to ketone or aldehyde upon an H-transfer and the V–O bond cleavage leaving vacancies on the catalyst surface.[16,17,27] Modification of V_2O_5 by its supporting on TiO_2 not only activates the catalyst towards ODH but improves the selectivity of alkene formation compared to the alcohol or ketone production.[16]

Meanwhile, the DFT calculations by Bell and co-authors[20] indicate that the dissociative adsorption of propane at the V=O site of V_2O_5 [(010) surface)] to give adsorbed activated propanol occurs in one step.

Curtiss and co-authors[28] proposed a mechanism involving the initial excitation of V_2O_5 to the triplet spin state. Propane interacts with the V=O group on the triplet surface giving the adsorbed isopropanol in one step. Initial excitation also makes the H-abstraction by the bridging O atoms to be even slightly more favourable than that by the vanadyl oxygen.

As a result of alkane dehydrogenation, reduced vanadium centres, V(IV) or V(III), are formed. At the next step, these centres undergo reoxidation (*e.g.*, by O_2, CO_2 or N_2O) associated with the oxygen migration to the vacancy at V, dehydrogenation of the OH ligand to generate the HOO• radical or formation of the peroxido ligand. In the latter case, the resulting V-peroxido species can be involved in the H-abstraction from alkane[21,22] or in the oxygen insertion into the R–H bond of alkane[15,27] in the second cycle of ODH.

Mechanism of the further deep oxidation of alkenes to CO_2 on V_2O_5 was described by Fan *et al.*, in a series of works.[17,29,30]

The Mo-V-Te-Nb-O mixed-metal oxide catalysts are successfully used for the ammoxidation of alkanes, ODH of RH being the first step of the process. According to DFT calculations,[31,32] the Te=O site is the most active towards the initial H-abstraction from the alkane molecule followed by the alkoxide formation at the V=O site and the second H-transfer to another Te=O group to give alkene (Scheme 15.8). Based on the computational results, Cheng and Goddard III[32] proposed a modification of the catalyst "maximizing the probability of having $Te_2V_5O_x$ sites ... but arranging them to be maximally distant from each other, while minimizing the probability of having V on all other Te". Yu *et al.*,[31] speculated that the high relative activity of the Te=O

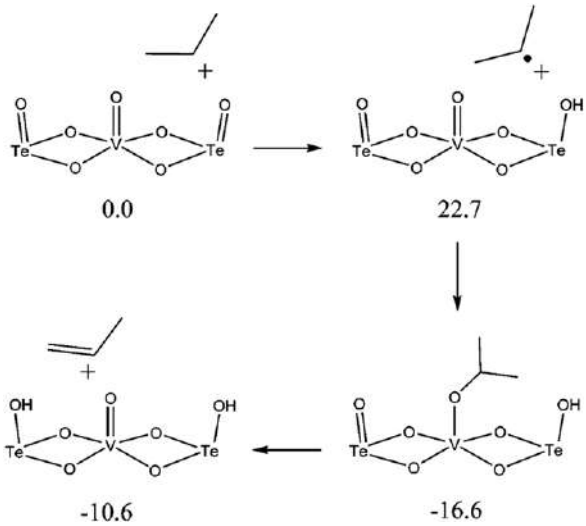

Scheme 15.8 Mechanism of propane ODH over a Mo-V-Te-Nb-O mixed-metal oxide catalyst (electronic energies are given in kcal mol^{-1}).
Adapted from ref. 32, https://pubs.acs.org/doi/10.1021/jacs.5b07073, with permission from American Chemical Society, Copyright 2015.

group may be due to inaccurate modelling of the catalyst surface, which, in reality, may be more complex than was assumed in calculations.

Vanadium phosphorus oxide is a catalyst able to convert *n*-butane to maleic anhydride. The mechanism of this process was theoretically investigated in several works.[33–37] The first step of the mechanism is an H-abstraction from *n*-butane. The most active site is the P=O group. However, the presence of the V(v) centre next to the P=O bond to couple to the latter by the bridging oxygen is crucial for the initial C–H activation of alkanes.[33–35] Goddard III *et al.*,[35] explained this finding by the so-called reduction-coupled oxo activation, *i.e.,* H-abstraction by the P=O group results in the electron transfer to the V centre though the O=P–O–V=O fragment reducing vanadium oxidation state to +4 (Figure 15.2). A plausible mechanism of the whole process proposed by Goddard III *et al.*, is shown in Scheme 15.9. The rate-limiting step is the H-abstraction from adsorbed 2,5-dihydrofuran. The calculated overall activation barrier is 21.7 kcal mol^{-1}, consistent with the experimental values of 12.9–23.6 kcal mol^{-1}.

15.3 Oxidation of Alkenes and Arenes

One of the most industrially important types of alkene transformation is their epoxidation. Typical catalytic systems used for this reaction are transition metal peroxido complexes formed in solution upon treatment of the initial pre-catalyst by peroxide. There are three main types of reaction mechanisms proposed for alkene epoxidation. First, a Mimoun-type

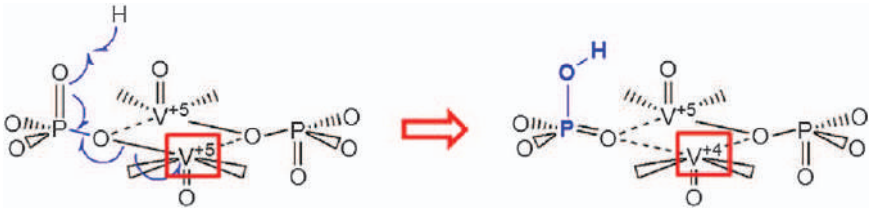

Figure 15.2 Reduction-coupled oxo activation upon hydrogen abstraction by vanadium phosphate oxide.
Reproduced from ref. 35 with permission from Springer Nature, Copyright 2014.

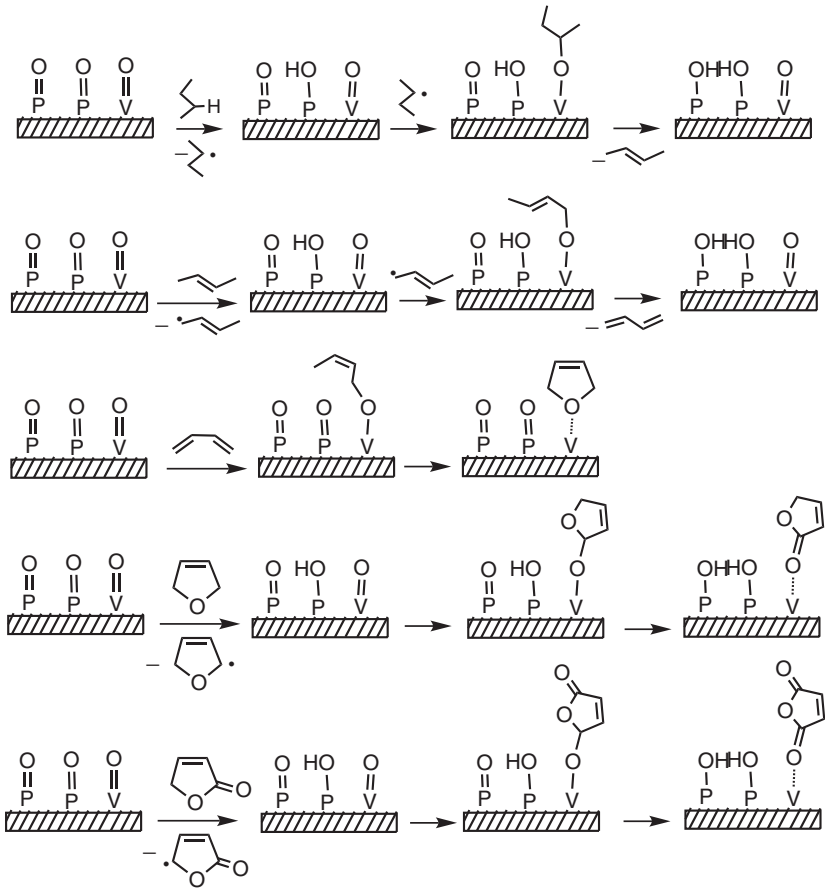

Scheme 15.9 Mechanism of n-butane oxidation to maleic anhydride catalysed by vanadium phosphate oxide.
Adapted from ref. 34 with permission from American Chemical Society, Copyright 2013.

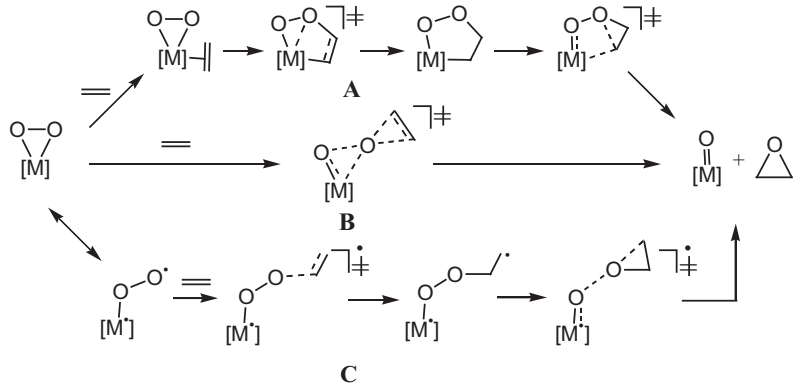

Scheme 15.10 Mechanisms of olefin epoxidation with peroxo complexes. Reproduced from ref. 41 with permission from the Royal Society of Chemistry.

mechanism that includes the coordination of alkene to a transition metal of the catalyst to give a π-complex (Scheme 15.10A). The peroxido ligand and alkene then undergo intramolecular cyclisation affording a penta- or tetra-cyclic intermediate, which finally transforms into epoxide. Second, a Sharpless-type mechanism, represents one-step oxygen transfer from the peroxido-ligand to the C=C double bond of alkene (Scheme 15.10B). Third, a diradical mechanism starts with the generation of a diradical peroxido complex with the end-on coordination of the O_2^- ligand, followed by attack of alkene to give diradical alkylperoxido intermediate (Scheme 15.10C).

Most of the publications support the Sharpless-type mechanism as the most favourable for the V-catalysed epoxidation (Scheme 15.11).[38–42] The reaction stars with coordination of peroxide to the metal centre of a catalyst, proton transfer from RO–OH to the V=O group[39] or to another ligand of the V-complex[40,41,43] to give the alkylperoxido, hydroperoxido or peroxido ligand and O-transfer to alkene. Meanwhile, Nunes *et al.*,[43] found that both Sharpless- and Mimoun-type mechanisms are competitive in ethylene epoxidation with the methylperoxido intermediate $[V(L)(=O)(MeOH)(OOMe)]^+$ (L = 1,2-bis[(phenyl)imino]-acenaphthene.

Vandichel *et al.*,[38] investigated in detail plausible catalytic species and the mechanism of cyclohexene epoxidation with ^{t}BuOOH catalysed by $[VO(acac)_2]$. It was shown that oxido-peroxido complexes of V(V) and V(IV) are the most abundant catalytic forms in solution. Cyclohexene efficiently undergoes epoxidation by V(V) and V(IV) catalysts.

Several works were devoted to theoretical mechanistic studies of ethylene epoxidation and arene hydroxylation with H_2O_2 catalysed by divanadium-substituted γ-Keggin polyoxotungstates $[\gamma\text{-}1,2\text{-}H_2SiV_2W_{10}O_{38}(\mu\text{-}OH)_2]^{4-}$ (ethylene)[44,45] and $[\gamma\text{-}PW_{10}O_{38}V_2(\mu\text{-}O)(\mu\text{-}OH)]^{4-}$ (arene).[46] The mechanisms

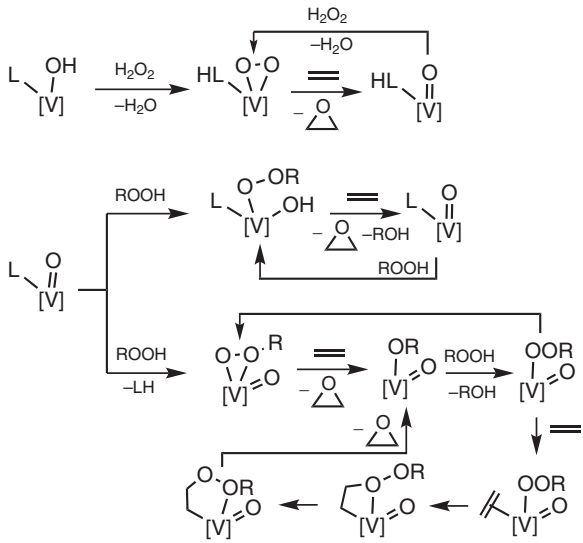

Scheme 15.11 The most favourable mechanisms of V-catalysed alkene epoxidation.

include the generation of peroxido complexes bearing the 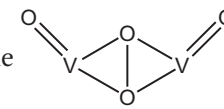 fragment upon treatment of the initial catalysts with H_2O_2. Then, one-step O-migration occurs *via* the Sharpless-type mechanism. Explicit accounting of the solvent effects by putting one water molecule in the second coordination sphere results in a lower activation barrier.[45] The origin of unusual regioselectivity observed in the case of pseudocumene hydroxylation is accounted for by steric hindrance imposed by the peroxido complex, while electronic factors are responsible for the regioselective *para*-hydroxylation of anisole and toluene.[46]

Apart from epoxides, treatment of alkenes with peroxides in the presence of V-complexes often leads to several other reaction products. For instance, formation of the C–C bond cleavage products such as benzaldehyde and benzoic acid upon oxidation of styrene indicates another competitive pathway. Indeed, the mechanism of the HO$^{\bullet}$ radical formation from H_2O_2 catalysed by complex [V(O)$_2$L] (L is a Schiff base) – similar to that shown in Scheme 15.2 – is by 5.3 kcal mol^{-1} more favourable than the Sharpless-type epoxidation.[47] The HO$^{\bullet}$ radicals then participate in the C–C bond cleavage of alkene.

Mechanism of the selective propene oxidation to acrolein on anionic $V_4O_{11}^-$ cluster includes an H-abstraction from the methyl group of propene by the vanadyl group to give a π-allyl intermediate, the C–O bond formation between the allyl anion and another O atom at the same V centre, second H-abstraction by another V=O centre (rate limiting step), desorption

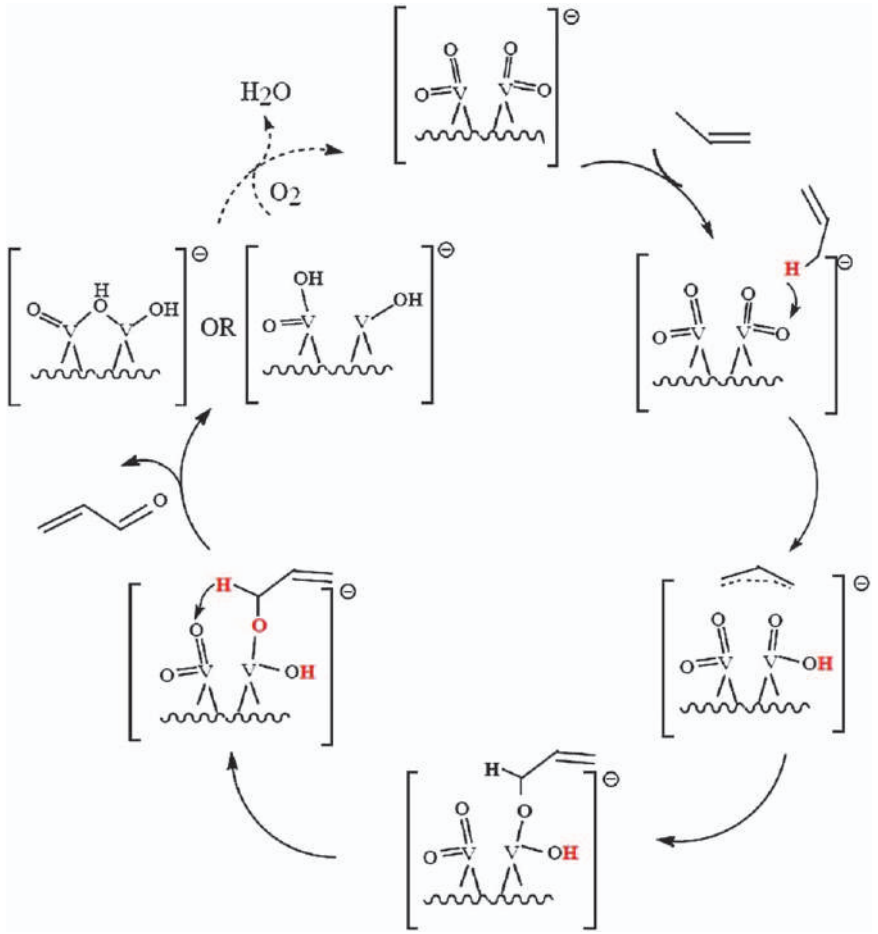

Scheme 15.12 Mechanism of the selective propene oxidation to acrolein on anionic $V_4O_{11}^-$ cluster.
Reproduced from ref. 48 with permission from American Chemical Society, Copyright 2010.

of acrolein and reoxidation of the catalyst by molecular oxygen (Scheme 15.12).[48] Various mechanisms of ethylene oxidation and propylene dehydrogenation over V_3O_8, VO_3^+ and $CeV_2O_7^+$ clusters were reported by He *et al.*[49–52]

Mechanism of benzene hydroxylation with H_2O_2 catalysed by mono- and dinuclear oxido-peroxido V complexes with acetonitrile ligand(s) was considered by Tang *et al.*[53] It includes formation of the η^1-benzene complex with the catalyst, proton transfer to the peroxido ligand to give a phenyl complex and OH-transfer from the hydroperoxido ligand to the phenyl one affording phenol. Dinuclear complexes were found to be more active than the mononuclear one. However, the calculated free-energy barriers relative

to the initial level seem to be too high (more than 40 kcal mol^{-1} for all pathways).

15.4 Oxidation of Methanol and Formaldehyde

The mechanism of the methanol oxidation into formaldehyde catalysed by V-species was a subject of a number of theoretical studies.[54–61] Models of pure vanadium oxide (represented as V(=O)(OH)$_3$) or that supported on TiO_2(110) or silica, vanadium-containing SiBEA zeolite and $[VO]^+$-ZSM-5 clusters were considered as catalysts. To summarise the results of these works, the general mechanism of the MeOH into $H_2C{=}O$ transformation may be represented by Scheme 15.13. At the first step, methanol undergoes a dissociative adsorption accompanied by an H-transfer to the V=O, V–OH or V–O–Si(Ti) sites and producing the corresponding methoxide intermediate. The second H-transfer from the methyl group to the V=O, V–OH, H–O–Ti or V–O–Ti sites gives the coordinated formaldehyde. After desorption of $H_2C{=}O$, the reduced V centre is reoxidised by molecular oxygen or another oxidant (*e.g.*, N_2O).

Formaldehyde may undergo further oxidation to formic acid. The mechanism of this reaction over the V_2O_5/TiO_2 catalyst includes co-adsorption of $H_2C{=}O$ and oxygen at V to give the H_2CO–peroxido intermediate, stepwise O-transfer from the peroxido ligand to the carbon atom of $H_2C{=}O$, H-transfer from H_2CO to the V=O group, another H-transfer from the V–OH group to the oxygen atom of formate and desorption of HCOOH (Scheme 15.14).[62] The first H-transfer is the rate-limiting step with

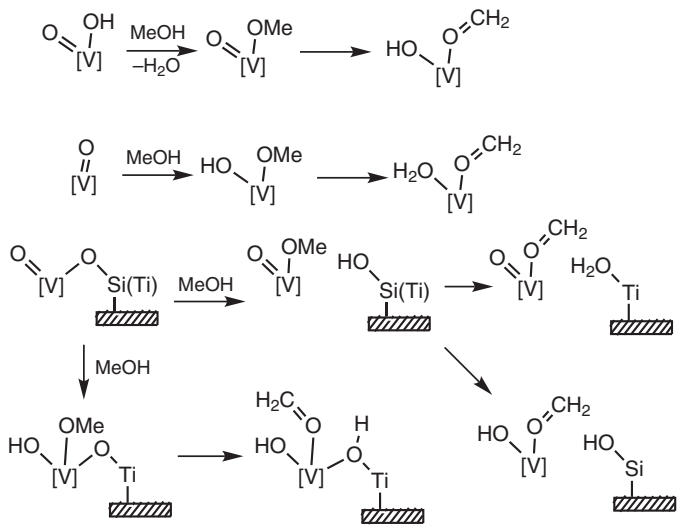

Scheme 15.13 Simplified mechanism of methanol to formaldehyde oxidation catalysed by V-species.

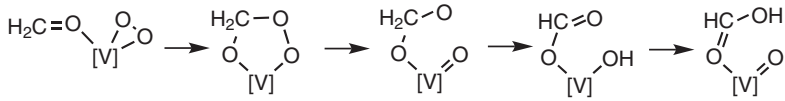

Scheme 15.14 Mechanism of oxidation of formaldehyde to formic acid over the V_2O_5–TiO_2 catalyst.

the activation barrier of 28 kcal mol^{-1} found at the B3LYP level of theory. This mechanism is more favourable than the redox Mars–van Krevelen pathway.

15.5 Oxidative C–C Bond Cleavage

In accord with the ^{13}C-labelling experiments, one of pathways of the ethane oxidation by $K_2S_2O_8$ in the presence of vanadatrane and CO in TFA solution is associated with C–C bond cleavage.[12] DFT calculations allowed to propose the following mechanisms for this process (Scheme 15.15,A). Peroxodisulphate undergoes thermal homolytic O–O bond cleavage to give sulphate or hydrosulphate radicals which can abstract proton from EtH to give ethyl radical (see Section 15.2.2). The latter reacts with the vanadyl group of the catalyst affording an intermediate with the ethoxide ligand. Consecutive reactions with $HSO_4^{\bullet}$ and CO give ketene, which, upon reaction with TFA, is converted into acetic acid. The C–C bond cleavage may also occur at later stages of the ethane oxidation, in accord with Scheme 15.15,B.

The C–C bond cleavage in vicinal diols catalysed by vanadium amino triphenolates leads to corresponding ketones or aldehydes. DFT (PBE-D3) calculations suggest the mechanism based on coordination of ethylene glycol to the V centre, hydrogen transfer to the V=O group to give alkoxide and water assisted H-transfer, leading to a chelate intermediate which undergoes the C–C bond cleavage (Figure 15.3).[63] Reoxidation of the catalyst occurs by molecular oxygen and it involves two molecules of the reduced catalyst.

15.6 Oxidation of CO

Mechanism of the carbon monoxide oxidation to CO_2 over vanadium-embedded graphene was investigated by Tang *et al.*, using the DFT (B3LYP) approach.[64] The Eley–Rideal mechanism was found to be more favourable than the Langmuir–Hinshelwood mechanism. The reaction starts with the molecular oxygen adsorption at the V site of the catalyst, the rate-limiting oxygen dissociative activation and addition of CO to the $V(O)_2$ group affording a carbonate complex (Scheme 15.16). The following CO and VO bond cleavages result in formation of CO_2 and the vanadyl surface group. Another CO molecule may interact with the V=O group to give CO_2 as a result of the oxygen transfer.

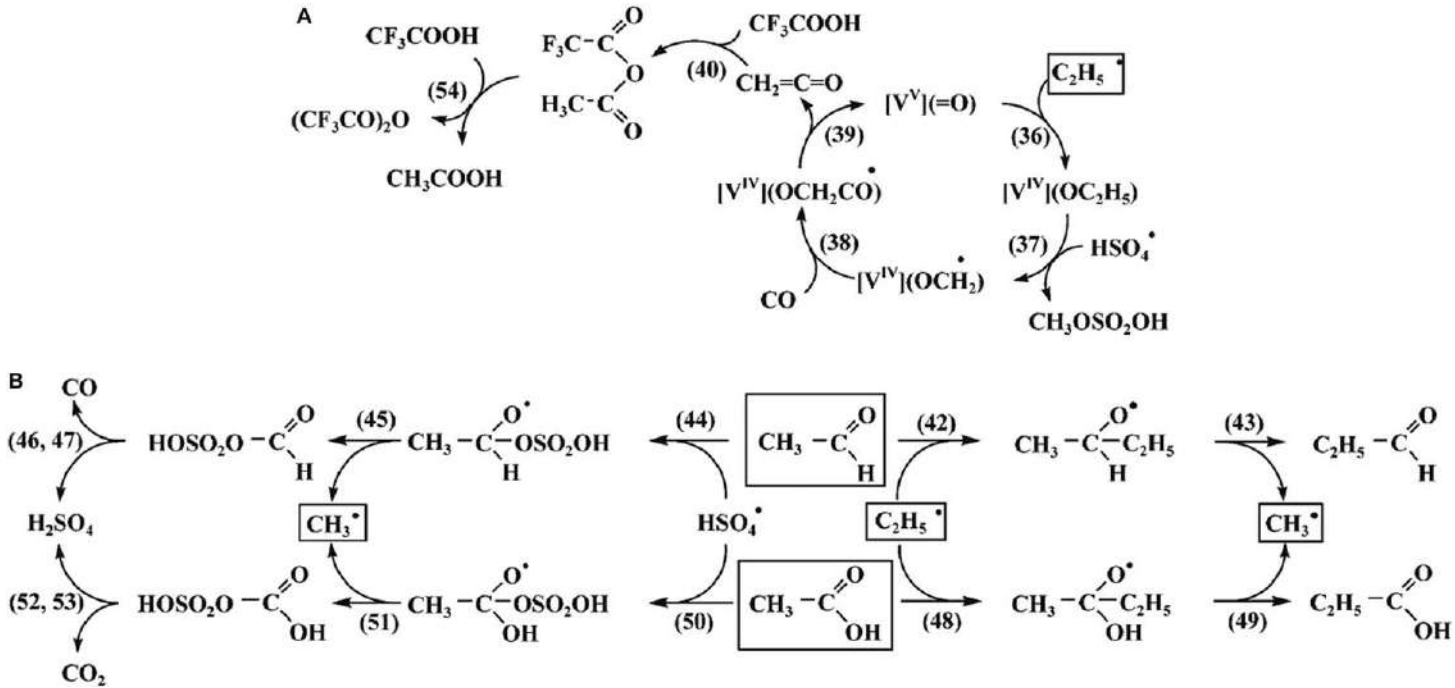

Scheme 15.15 Proposed mechanisms for ethane C–C bond cleavage in the system $C_2H_6/K_2S_2O_8/CO$/vanadatrane/TFA. Reproduced from ref. 12 with permission from John Wiley and Sons, Copyright © 2008 Wiley-VCH Verlag GmbH & Co. KGaA, Weinheim.

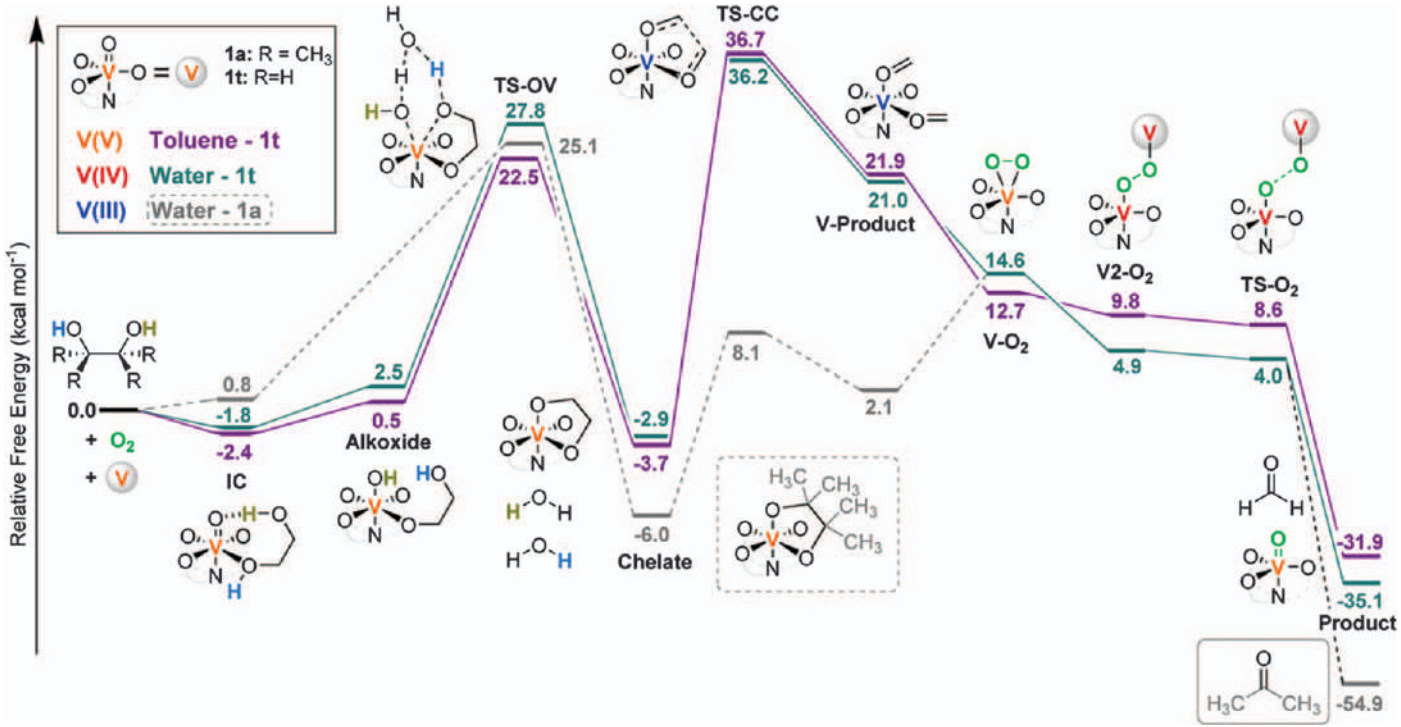

Figure 15.3 Energy profile of the oxidative C–C cleavage of ethylene glycol (**1t**) in water (green line) and in toluene (purple line) and of pinacol (**1a**) in water (grey line), catalysed by V-complexes using molecular oxygen as oxidant.
Reproduced from ref. 63 with permission from John Wiley and Sons, Copyright © 2018 Wiley-VCH Verlag GmbH & Co. KGaA, Weinheim.

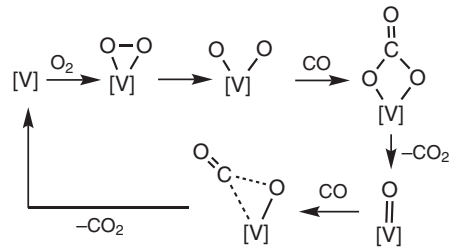

Scheme 15.16 Mechanism of CO oxidation over V-embedded graphene.

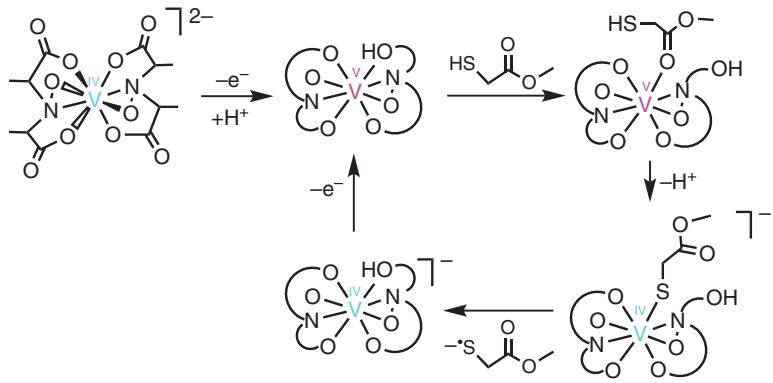

Scheme 15.17 Proposed mechanism of MMA oxidation to the methylmercaptoacetate radical catalysed by amavadin.

15.7 Oxidation of Thiols and Organic Sulphides

The mechanism of oxidation of methylmercaptoacetate $HSCH_2C(=O)OCH_3$ (MMA) into corresponding disulphide catalysed by amavadin was proposed by Zampella and co-authors[65] and includes oxidation of amavadin to the corresponding V(v) complex and protonation of one of the 2,2′-hydroxyimino-dipropionate ligand of the catalyst, coordination of MMA to vanadium by the carbonyl oxygen atom, recoordination of the thiol by the sulphur atom that is accompanied by the reduction of V(v) to V(iv) and oxidation of sulphur to give the $^{\bullet}SCH_2C(=O)OCH_3$ radical (Scheme 15.17). Coupling of this radical gives disulphide.

Further oxidation of organic sulphides or disulphides R_1–S–R_2 or R_1–S–S–R_2 into corresponding sulphoxides catalysed by V-complexes with bulky unreduced and reduced tridentate Schiff base ligands was investigated theoretically (DFT) by Maseras *et al.*,[66,67] and Adão *et al.*[68] The most plausible mechanism of this process is concerted oxygen transfer from the OO^{2-} or OOH^{-} ligand of the catalytic active species to the sulphur atom. In other words, this mechanism resembles that of the Sharpless-type for alkene epoxidation. The insertion mechanism involving coordination of sulphide to V and formation of a 4-membered metallocyclic intermediate (analogous of

the Mimoun-type mechanism) was found to be less favourable.[67] Similar results were obtained from the QM/MM calculations for sulphide oxidation with the SBA-15 supported vanadia catalyst.[69] A significant decrease of the activation barrier for the oxygen transfer was predicted when the peroxido ligand is protonated.[70] Vanadium complexes with unreduced iminoalcohol-derived Schiff base ligands (IASB) are more efficient catalysts in this process than the reduced aminoalcohol derivatives (AASB).[68] This effect was attributed to the different nature of active catalytic species, *i.e.,* V-peroxido- and V-hydroperoxido complexes for IASB and AASB, respectively. The nature of the enantioselectivity of sulphoxide formation is discussed in detail in these works.

15.8 Oxidation of SO_2

The mechanism of oxidation of sulphur dioxide into SO_3 over V_2O_5 supported on TiO_2 was investigated by Du *et al.*,[71] using periodical and finite boundary solid-state calculations. The general mechanistic scheme includes adsorption of SO_2 at the catalyst surface, one-step transfer of the surface oxygen to SO_2 and desorption of SO_3. It was found that the most favourable site of SO_2 adsorption is an uncovered TiO_2 surface. However, desorption of the formed SO_3 in this case is very energy-consuming. Therefore, the most plausible pathway is adsorption of SO_2 at the vanadia site to give a sulphate intermediate followed by the SO_3 elimination upon V–O and S–O bond cleavages and the catalyst reoxidation with oxygen (Scheme 15.18).

15.9 Bromoperoxidase Activity

Vanadium haloperoxidases are enzymes which catalyse the halide ion oxidation into the corresponding hypohalous acids (HOHal) by hydrogen peroxide. Theoretical calculations of the mechanism for this process are usually performed for V-complexes which mimic the vanadium cofactor of these enzymes. The overall mechanism includes coordination of H_2O_2 to the metal centre, water-assisted proton transfer to a co-ligand to give the hydroperoxido or peroxido complex representing an active catalytic species and concerted or stepwise OH group transfer to Br^- producing HOBr (Scheme 15.19).[70,72–76] The hydroperoxido complexes are significantly more active towards the Br^- oxidation than the corresponding peroxido species.[70,76]

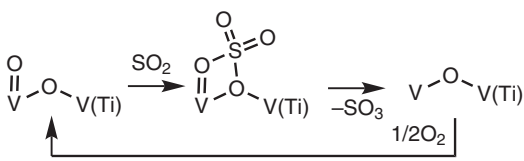

Scheme 15.18 Mechanism of SO_2 oxidation over V_2O_5 supported on TiO_2.

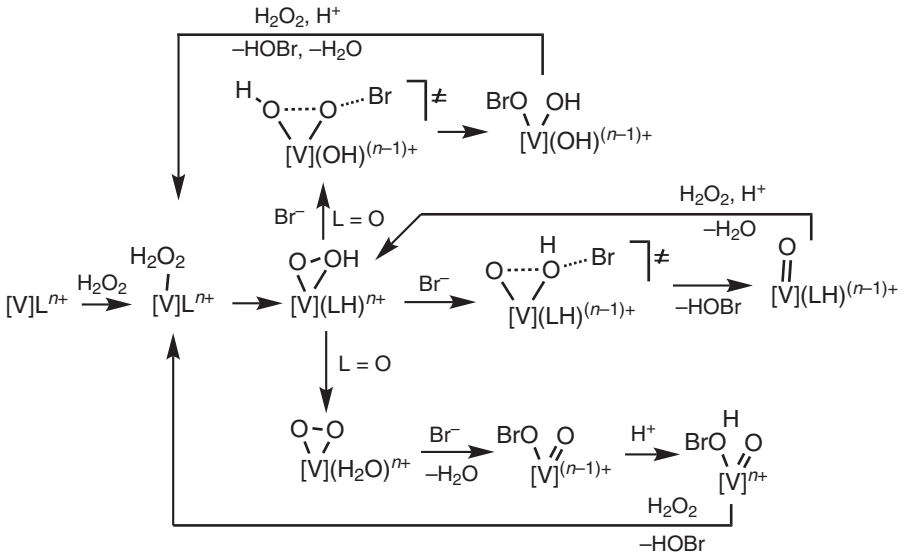

Scheme 15.19 Simplified mechanistic schemes proposed for the bromide oxidation with H_2O_2 catalysed by V-complexes.

15.10 Water Oxidation

Chemical water oxidation to O_2 is associated with an overall transfer of four electrons (reaction 15.1) and is usually considered as a two-step process involving sequential formation of the peroxido group and then molecular oxygen (reactions 15.2 and 15.3). Each step requires the transfer of two electrons.

$$2H_2O \rightarrow O_2 + 4H^+ + 4e^- \tag{15.1}$$

$$2H_2O \rightarrow H_2O_2 + 2H^+ + 2e^- \text{ or } 2H_2O \rightarrow OOH^- + 3H^+ + 2e^- \text{ or } 2H_2O \rightarrow OO^{2-} + 4H^+ + 2e^- \tag{15.2}$$

$$H_2O_2 \rightarrow O_2 + 2H^+ + 2e^- \text{ or } OOH^- \rightarrow O_2 + H^+ + 2e^- \text{ or } OO^{2-} \rightarrow O_2 + 2e^- \tag{15.3}$$

This process is typically catalysed by Ru complexes, although complexes of Co, Os, Ir and Mn were also used. It is proposed that an oxidant (*e.g.*, Ce^{4+} is often used as a model oxygen-free oxidant) oxidizes the transition metal centre of a catalyst to a sufficiently high oxidation state, and the oxidised form of the catalyst then participates in the water oxidation (Scheme 15.20). Vanadium complexes are not typical catalysts for homogeneous water oxidation because the two-electron oxidative strength of V(v) is not sufficient to oxidize water to peroxide ($E^\circ(H_2O_2/H_2O) = 1.78$ V and $E^\circ(VO_2{}^+/V^{3+}) = 0.67$ V). Meanwhile, it was reported that amavadin and its homologues are efficient catalysts for water oxidation to molecular oxygen with Ce^{4+}.[77]

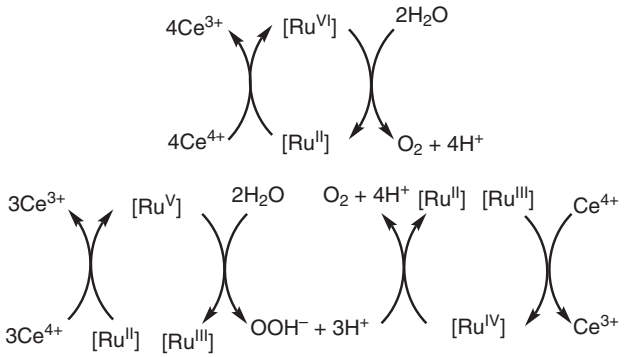

Scheme 15.20 Two general mechanisms of water oxidation with Ce^{4+} catalysed by a ruthenium complex.

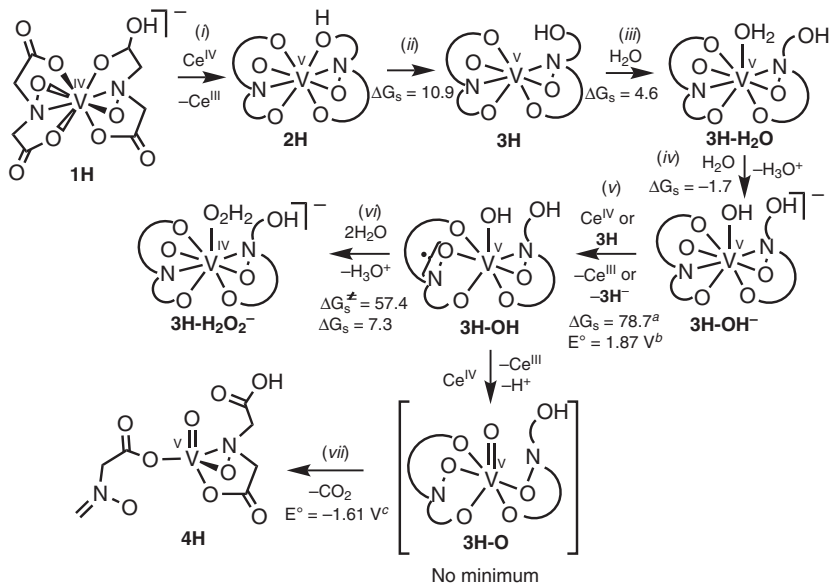

Scheme 15.21 Proposed mechanism of the O–O bond formation (i–vi) and complex degradation (vii). Gibbs free energies of activation and reaction are given in kJ mol^{-1}. [a]For the oxidation with **3H**. [b]For the process $\mathbf{3H–H_2O} \rightarrow \mathbf{3H–OH} + H^+ + 1e^-$. [c]For the process $\mathbf{3H–OH} \rightarrow \mathbf{[4H]CO_2} + H^+ + 1e^-$.
Reproduced from ref. 77 with permission from John Wiley and Sons, Copyright © 2016 Wiley-VCH Verlag GmbH & Co. KGaA, Weinheim.

The mechanism includes oxidation of the protonated amavadin (or its analogue **1H**) with Ce^{4+} to the corresponding complex of V(v) (**2H**) and water coordination to the vanadium atom (Scheme 15.21). Water ligated in $\mathbf{3H–H_2O}$ is highly acidic and undergoes facile deprotonation. The resulting

hydroxido intermediate **3H–OH**$^{-}$ can be relatively easy oxidised and, upon interaction with another H_2O molecule, give a hydrogen peroxide adduct **3H–H$_2$O$_2$**$^{-}$. Coordinated hydrogen peroxide can undergo a further metal-catalysed oxidation into O_2.

One of the most important features of this mechanism is the non-innocent character of the catalyst's *N*-hydroxyiminodiacetate (HIDA) ligand. Indeed, the oxidation of **3H–OH**$^{-}$ affects HIDA rather than the metal centre, which is in its highest oxidation state. Thus, the two-electron oxidation of water into hydrogen peroxide is associated with one-electron reduction of the vanadium(v) atom and one-electron transfer to the oxidised HIDA ligand.

15.11 Ammonia Oxidation

The mechanism of ammonia oxidation to N_2 over vanadium oxides depends on the availability of gaseous species.[78] The reaction starts with the activation of NH_3 on the surface *via* a single electron transfer to give the oxidised NH_3^{+} species that is adsorbed either through NH$\cdots$O=V hydrogen bonds or *via* formation of the H_3N–O=V bond. In the absence of molecular oxygen, hydrazine N_2H_4 is formed either from the $NH_3^{+} + NH_3$ coupling followed by the proton–hydrogen transfers to the vanadyl group of the surface or *via* formation and recombination of two NH_2 species (Scheme 15.22). N_2H_4 is oxidised to N_2 as a result of four consecutive hydrogen transfers to the V=O groups. In the presence of gaseous oxygen, the mechanism includes the formation of H_2NOO and HNOOH intermediates, which further lead to NO and, upon reaction with NH_3, to N_2.

15.12 Mercury Oxidation

Oxidation of Hg to $HgCl_2$ by HCl over the V_2O_5–TiO_2 catalyst was considered by Liu and co-authors.[79] Based on solid-state DFT periodic slab calculations, the mechanism is of the Eley–Rideal type including adsorption and dissociation of HCl on the V_2O_5–TiO_2 (001) surface, interaction of Hg with the V-bound Cl atom to give HgCl and interaction with the second HCl molecule accompanied by the H transfer to give coordinated H_2O and $HgCl_2$ which desorb from the surface (Scheme 15.23). Formation of $HgCl_2$ is the rate-determining step of the whole process.

15.13 Final Remarks

Vanadium compounds have broad, actual or potential applications as catalysts in various oxidative processes including those with great industrial significance. Tuning the catalytic activity and reaction course and optimisation of reaction conditions require knowledge of the reaction mechanism and driving forces of these processes. The analysis of numerous studies undertaken in this chapter clearly indicates that the computational

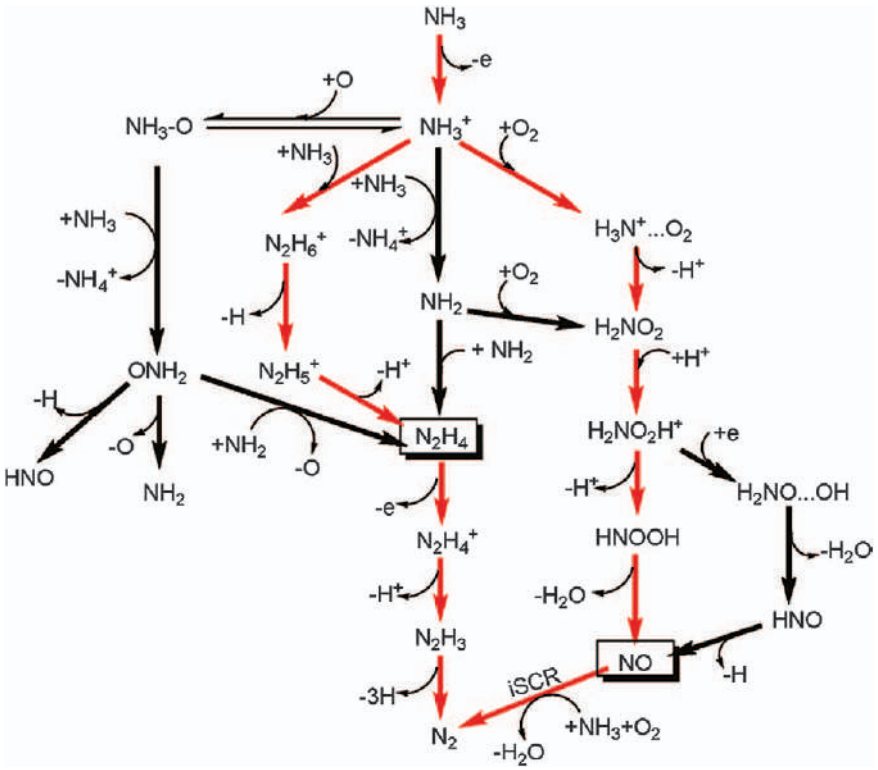

Scheme 15.22 Proposed mechanism of ammonia oxidation over vanadium oxide. Reproduced from ref. 78 with permission from American Chemical Society, Copyright 2011.

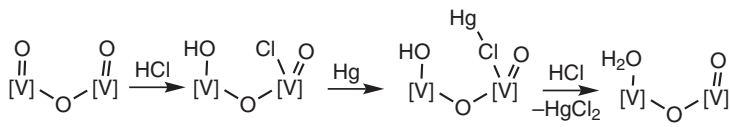

Scheme 15.23 Simplified mechanism of Hg oxidation over V_2O_5–TiO_2.

methods of quantum chemistry are indispensable for the understanding of intimate details of vanadium-catalysed reactions and for the development of new efficient catalytic systems based on vanadium.

Acknowledgements

The author thanks the Fundação para a Ciência e a Tecnologia (FCT), Portugal (projects PTDC/QEQ-QIN/3967/2014 and UID/QUI/00100/2019) for its financial support.

References

1. R. R. Langeslay, D. M. Kaphan, C. L. Marshall, P. C. Stair, A. P. Sattelberger and M. Delferro, *Chem. Rev.*, 2019, **119**, 2128.
2. V. Conte, A. Coletti, B. Floris, G. Licini and C. Zonta, *Coord. Chem. Rev.*, 2011, **255**, 2165.
3. M. Sutradhar, L. M. D. R. S. Martins, M. F. C. Guedes da Silva and A. J. L. Pombeiro, *Coord. Chem. Rev.*, 2015, **301–302**, 200.
4. R. Z. Khaliullin, A. T. Bell and M. Head-Gordon, *J. Phys. Chem. B*, 2005, **109**, 17984.
5. M. V. Kirillova, M. L. Kuznetsov, V. B. Romakh, L. S. Shul'pina, J. J. R. Fraústo da Silva, A. J. L. Pombeiro and G. B. Shul'pin, *J. Catal.*, 2009, **267**, 140.
6. M. V. Kirillova, M. L. Kuznetsov, Y. N. Kozlov, L. S. Shul'pina, A. Kitaygorodskiy, A. J. L. Pombeiro and G. B. Shul'pin, *ACS Catal.*, 2011, **1**, 1511.
7. I. Gryca, K. Czerwińska, B. Machura, A. Chrobok, L. S. Shul'pina, M. L. Kuznetsov, D. S. Nesterov, Y. N. Kozlov, A. J. L. Pombeiro, I. A. Varyan and G. B. Shul'pin, *Inorg. Chem.*, 2018, **57**, 1824.
8. I. S. Fomenko, A. L. Gushchin, P. A. Abramov, M. N. Sokolov, L. S. Shul'pina, N. S. Ikonnikov, M. L. Kuznetsov, A. J. L. Pombeiro, Y. N. Kozlov and G. B. Shul'pin, *Catalysts*, 2019, **9**, 217.
9. F. Haber and J. Weiss, *Naturwissemschaften*, 1932, **20**, 948.
10. R. Fu, W. A. Goddard, III, M.-J. Cheng and R. J. Nielsen, *ACS Catal.*, 2017, **7**, 356.
11. M. V. Kirillova, M. L. Kuznetsov, P. M. Reis, J. A. L. da Silva, J. J. R. Fraústo da Silva and A. J. L. Pombeiro, *J. Am. Chem. Soc.*, 2007, **129**, 10531.
12. M. V. Kirillova, M. L. Kuznetsov, J. A. L. da Silva, M. F. C. Guedes da Silva, J. J. R. Fraústo da Silva and A. J. L. Pombeiro, *Chem. – Eur. J.*, 2008, **14**, 1828.
13. K. Chen, A. Khodakov, J. Yang, A. T. Bell and E. Iglesia, *J. Catal.*, 1999, **186**, 325.
14. P. Mars and D. W. van Krevelen, *Chem. Eng. Sci. Spec. Suppl.*, 1954, **3**, 41.
15. X. Rozanska, E. V. Kondratenko and J. Sauer, *J. Catal.*, 2008, **256**, 84.
16. K. Alexopoulos, M.-F. Reyniers and G. B. Marin, *J. Catal.*, 2012, **289**, 127.
17. G.-L. Dai, Z.-P. Liu, W.-N. Wang, J. Lu and K.-N. Fan, *J. Phys. Chem. C*, 2008, **112**, 3719.
18. N. E. Damoyi, H. B. Friedrich, G. H. Kruger and D. Willock, *Mol. Catal.*, 2018, **452**, 83.
19. I. Ascoop, V. V. Galvita, K. Alexopoulos, M.-F. Reyniers, P. Van Der Voort, V. Bliznuk and G. B. Marin, *J. Catal.*, 2016, **335**, 1.
20. F. Gilardoni, A. T. Bell, A. Chakraborty and P. Boulet, *J. Phys. Chem. B*, 2000, **104**, 12250.
21. M.-J. Cheng, K. Chenoweth, J. Oxgaard, A. van Duin and W. A. Goddard III, *J. Phys. Chem. C*, 2007, **111**, 5115.

22. J. M. H. Lo, Z. A. Premji, T. Ziegler and P. D. Clark, *J. Phys. Chem. C*, 2013, **117**, 11258.
23. S. Wannakao, B. Boekfa, P. Khongpracha, M. Probst and J. Limtrakul, *ChemPhysChem*, 2010, **11**, 3432.
24. V. I. Avdeev and A. F. Bedilo, *Res. Chem. Intermed.*, 2016, **42**, 5237.
25. H. Fu, Z.-P. Liu, Z.-H. Li, W.-N. Wang and K.-N. Fan, *J. Am. Chem. Soc.*, 2006, **128**, 11114.
26. X. Rozanska, R. Fortrie and J. Sauer, *J. Phys. Chem. C*, 2007, **111**, 6041.
27. B. Liu and D. Wang, *Kinet. Catal.*, 2018, **59**, 393.
28. P. C. Redfern, P. Zapol, M. Sternberg, S. P. Adiga, S. A. Zygmunt and L. A. Curtiss, *J. Phys. Chem. B*, 2006, **110**, 8363.
29. G.-L. Dai, Z.-H. Li, J. Lu, W.-N. Wang and K.-N. Fan, *J. Phys. Chem. C*, 2012, **116**, 807.
30. D. Guoliang, L. Zhenhua, W. Wenning, L. Jing and F. Kangnian, *Chin. J. Catal.*, 2013, **34**, 906.
31. J. Yu, Y. Xu and V. V. Guliants, *Catal. Today*, 2014, **238**, 28.
32. M.-J. Cheng and W. A. Goddard III, *J. Am. Chem. Soc.*, 2015, **137**, 13224.
33. G. Fu, R. Yuan, P. Wang and H. Wan, *Chin. J. Catal.*, 2015, **36**, 1528.
34. M.-J. Cheng and W. A. Goddard III, *J. Am. Chem. Soc.*, 2013, **135**, 4600.
35. M.-J. Cheng, W. A. Goddard III and R. Fu, *Top. Catal.*, 2014, **57**, 1171.
36. D. Thompson and B. K. Hodnett, *Top. Catal.*, 2008, **50**, 116.
37. R. Shimizu and T. Fuchikami, *Catal. Today*, 2001, **71**, 137.
38. M. Vandichel, K. Leus, P. Van Der Voort, M. Waroquier and V. Van Speybroeck, *J. Catal.*, 2012, **294**, 1.
39. J. Pisk, J.-C. Daran, R. Poli and D. Agustin, *J. Mol. Catal. A*, 2015, **403**, 52.
40. P. Adão, J. C. Pessoa, R. T. Henriques, M. L. Kuznetsov, F. Avecilla, M. R. Maurya, U. Kumar and I. Correia, *Inorg. Chem.*, 2009, **48**, 3542.
41. M. L. Kuznetsov and J. C. Pessoa, *Dalton Trans.*, 2009, 5460.
42. M. Bühl, R. Schurhammer and P. Imhof, *J. Am. Chem. Soc.*, 2004, **126**, 3310.
43. C. D. Nunes, P. D. Vaz, V. Félix, L. F. Veiros, T. Moniz, M. Rangel, S. Realista, A. C. Mourato and M. J. Calhorda, *Dalton Trans.*, 2015, **44**, 5125.
44. Y. Nakagawa and N. Mizuno, *Inorg. Chem.*, 2007, **46**, 1727.
45. A. E. Kuznetsov, Y. V. Geletii, C. L. Hill, K. Morokuma and D. G. Musaev, *Inorg. Chem.*, 2009, **48**, 1871.
46. I. Y. Skobelev, V. Yu Evtushok, O. A. Kholdeeva, N. V. Maksimchuk, R. I. Maksimovskaya, J. M. Ricart, J. M. Poblet and J. J. Carbó, *ACS Catal.*, 2017, **7**, 8514.
47. M. R. Maurya, M. Bisht, A. Kumar, M. L. Kuznetsov, F. Avecilla and J. C. Pessoa, *Dalton Trans.*, 2011, **40**, 6968.
48. H.-B. Li, S. X. Tian and J. Yang, *J. Phys. Chem. A*, 2010, **114**, 6542.
49. Y.-P. Ma, X.-L. Ding, Y.-X. Zhao and S.-G. He, *ChemPhysChem*, 2010, **11**, 1718.
50. J.-B. Ma, Z. Yuan, J.-H. Meng, Q.-Y. Liu and S.-G. He, *ChemPhysChem*, 2014, **15**, 4117.

51. W. ZheChen, D. XunLei, M. YanPing, C. Hai, W. XiaoNan, Z. YanXia and H. ShengGui, *Chin. Sci. Bull.*, 2009, **54**, 2814.
52. J.-B. Ma, L.-L. Xu, J.-H. Meng and S.-G. He, *Int. J. Mass Spectrom.*, 2016, **401**, 39.
53. D. Tang, L. Zhu and C. Hu, *RSC Adv.*, 2012, **2**, 2329.
54. D. C. Tranca, F. J. Keil, I. Tranca, M. Calatayud, S. Dzwigaj, M. Trejda and F. Tielens, *J. Phys. Chem. C*, 2015, **119**, 13619.
55. M. F. Fellah and I. Onal, *Phys. Chem. Chem. Phys.*, 2013, **15**, 13969.
56. H. Y. Kim, H. M. Lee and H. Metiu, *J. Phys. Chem. C*, 2010, **114**, 13736.
57. H. Y. Kim, H. M. Lee, R. G. S. Pala and H. Metiu, *J. Phys. Chem. C*, 2009, **113**, 16083.
58. P. González-Navarrete, L. Gracia, M. Calatayud and J. Andrés, *J. Comput. Chem.*, 2010, **31**, 2493.
59. X.-L. Ding, W. Xue, Y.-P. Ma, Y.-X. Zhao, X.-N. Wu and S.-G. He, *J. Phys. Chem. C*, 2010, **114**, 3161.
60. J. Döbler, M. Pritzsche and J. Sauer, *J. Am. Chem. Soc.*, 2005, **127**, 10861.
61. A. Goodrow and A. T. Bell, *J. Phys. Chem. C*, 2007, **111**, 14753.
62. V. I. Avdeev and V. N. Parmon, *J. Phys. Chem. C*, 2009, **113**, 2873.
63. E. Amadio, J. González-Fabra, D. Carraro, W. Denis, B. Gjoka, C. Zonta, K. Bartik, F. Cavani, S. Solmi, C. Bo and G. Licini, *Adv. Synth. Catal.*, 2018, **360**, 3286.
64. J.-Y. Tang, J.-S. Shen, L. Chen, J.-W. Jiang, J. Lu, X. Zhao and G.-L. Dai, *Monatsh. Chem.*, 2018, **149**, 1349.
65. L. Bertini, V. Barbieri, P. Fantucci, L. De Gioia and G. Zampella, *Dalton Trans.*, 2011, **40**, 7704.
66. D. Balcells, F. Maseras and G. Ujaque, *J. Am. Chem. Soc.*, 2005, **127**, 3624.
67. D. Balcells, F. Maseras and A. Lledós, *J. Org. Chem.*, 2003, **68**, 4265.
68. P. Adão, M. L. Kuznetsov, S. Barroso, A. M. Martins, F. Avecilla and J. C. Pessoa, *Inorg. Chem.*, 2012, **51**, 11430.
69. N. Kaur, S. Gupta and N. Goel, *Phys. Chem. Chem. Phys.*, 2017, **19**, 25059.
70. G. Zampella, P. Fantucci, V. L. Pecoraro and L. De Gioia, *J. Am. Chem. Soc.*, 2005, **127**, 953.
71. X. Du, J. Xue, X. Wang, Y. Chen, J. Ran and L. Zhang, *J. Phys. Chem. C*, 2018, **122**, 4517.
72. H. Eshtiagh-Hosseini, M. Chahkandi, M. R. Housaindokht and M. Mirzaei, *Polyhedron*, 2013, **60**, 93.
73. G. Zampella, L. Bertini and L. De Gioia, *Chem. Commun.*, 2014, **50**, 304.
74. M. Debnath, M. Dolai, K. Pal, S. Bhunya, A. Paul, H. M. Lee and M. Ali, *Dalton Trans.*, 2018, **47**, 2799.
75. H. Eshtiagh-Hosseini, M. R. Housaindokht, M. Chahkandi and A. Morsali, *Transition Met. Chem.*, 2010, **35**, 939.
76. G. Zampella, P. Fantucci, V. L. Pecoraro and L. De Gioia, *Inorg. Chem.*, 2006, **45**, 7133.
77. M. Domarus, M. L. Kuznetsov, J. Marçalo, A. J. L. Pombeiro and J. A. L. da Silva, *Angew. Chem., Int. Ed.*, 2016, **55**, 1489.

78. R.-M. Yuan, G. Fu, X. Xu and H.-L. Wan, *J. Phys. Chem. C*, 2011, **115**, 21218.
79. B. Zhang, J. Liu, G. Dai, M. Chang and C. Zheng, *Proc. Combust. Inst.*, 2015, **35**, 2855.
80. A. S. Novikov, M. L. Kuznetsov, A. J. L. Pombeiro, N. A. Bokach and G. B. Shul'pin, *ACS Catal.*, 2013, **3**, 1195.

CHAPTER 16

Vanadium-catalyzed Olefin Oligomerization, Polymerization and Copolymerization

SHU ZHANG*[a] AND WENJUAN ZHANG[b]

[a] State Key Laboratory of Chemical Resource Engineering, Beijing University of Chemical Technology, Beijing 100029, China; [b] Beijing Key Laboratory of Clothing Materials R&D and Assessment, School of Materials Science and Engineering, Beijing Institute of Fashion Technology, Beijing 100029, China
*Email: zhangshu@mail.buct.edu.cn

16.1 Introduction

Ethylene is the simplest vinyl monomer that can be used to prepare various products ranging from linear α-olefins (LAOs) to high-density polyethylene (HDPE), linear low-density polyethylene (LLDPE), polyolefin elastomer (POE), ethylene-propylene-diene copolymer (so-called EPDM) and olefin block copolymer (OBC). LAOs are valuable building blocks for industrial products, including comonomers for polyolefins (LLDPE, POE and OBC), surfactants and synthetic lubricants.[1] Polyolefins are the largest volume and important commercial synthetic polymers in the plastics industry, which are widely used in our everyday life because of their excellent cost–performance value.[2] Polyolefins are either produced by using free-radical polymerization or coordination polymerization in a commercialized process. Compared to

Catalysis Series No. 41
Vanadium Catalysis
Edited by Manas Sutradhar, José Armando L. da Silva and Armando J. L. Pombeiro

Published by the Royal Society of Chemistry, www.rsc.org

the extreme conditions for free-radical polymerization, polyolefins could be produced by coordination polymerization under much lower temperature and pressure.[2] In olefin coordination polymerization, catalysts, which determine the catalytic activity and the microstructure of resulting polyolefins, play a critically important role. Since the pioneering work of Ziegler and Natta in coordination polymerization of olefins in 1950s, the development of effective catalysts for olefin polymerization with high catalytic activity and controlled molecular architectures of resulting polyolefin has been of great interest in fundamental research and industrial applications.[2] Remarkable progress has been made in achieving effective catalysts containing transition metals, such as metallocene catalysts (with Ti, Zr or Hf)[3] and post-metallocene catalysts (such as α-diimine Ni and Pd complex catalysts,[4] bisiminopyridine Fe and Co complex catalysts,[5] group 4 transition metal complex catalysts containing phenoxy-imine chelating ligands,[6] *etc.*). Each new progress in the development of catalysts has increased the possibility of a more precise control of the structure and properties of the resulting polyolefins. As one series of important catalysts, vanadium catalysts display unique characteristics in olefin polymerization,[7] affording amorphous polymers in ethylene/propylene/non-conjugated diene copolymerization and yield syndiotactic polypropylene in propylene polymerization.[7] Up to now, about 70% of commercial ethylene–propylene rubber is produced by using vanadium catalysts in the industry.[8] Ligand design plays a pivotal role in the development of catalysts with high catalytic activity and selectivity. The most efficient vanadium catalysts with various ligands for olefin oligomerization, polymerization and copolymerization will be introduced in this chapter.

16.2 Vanadium-catalyzed Ethylene Oligomerization

Since the discovery that iron or cobalt complexes bearing bis(imino)pyridine ligands are able to catalyze ethylene oligomerization and polymerization, considerable attention has been focused on the modification of transition-metal precatalysts containing bis(imino)pyridine ligands.[5] Vanadium(III) complexes bearing such ligands were prepared by Schmidt *et al.*[9] After activation with methyl aluminoxane (MAO), these vanadium(III) complexes **1** (see Scheme 16.1) were highly active for ethylene oligomerization (up to 1140 $kg\,g^{-1}$ of $V\,h^{-1}$) under mild conditions and the resulting oligomers follow a Schulz–Flory distribution with high α-olefin selectivity. It is worth noting that the substituents on phenyl rings significantly affect the catalytic behavior of the vanadium(III) complex.[10] An increase in the bulkiness of the alkyl-substituents in the 2-position of the phenyl ring leads to a decrease of catalytic activity, productivity of liquid products and α-olefin selectivity.[10]

Nomura *et al.* designed a series of (imido)vanadium(V) complexes containing (2-anilidomethyl)pyridine and other [NN] chelating ligands

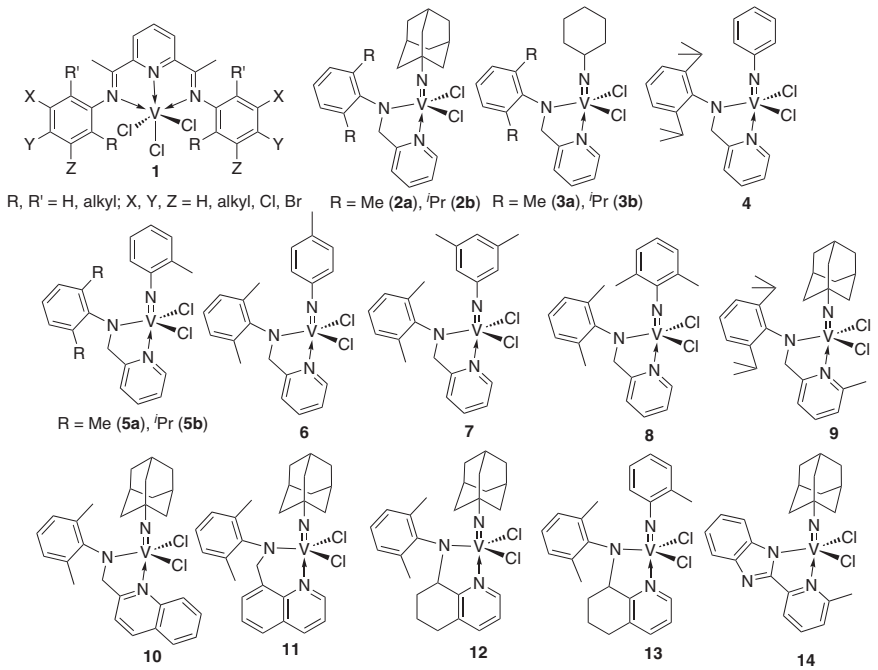

Scheme 16.1 Vanadium complexes for ethylene oligomerization.

Table 16.1 Ethylene oligomerization by imido vanadium(v) complexes **2–13**.[a]

Entry	Complex (μmol)	Al/V	Activity	C_4/%	C_6/%
1	**2a** (0.1)	1500	76 500	97.0	3.0
2	**2b** (0.5)	1000	35 700	92.1	7.9
3	**3a** (0.5)	200	28 200	93.2	6.8
4	**3b** (0.5)	200	32 300	95.9	4.1
5	**4** (0.5)	500	18 300	95.1	4.9
6	**5a** (0.2)	600	50 300	95.2	4.8
7	**5b** (0.2)	700	41 500	97.1	2.9
8	**6** (0.5)	200	15 100	94.0	6.0
9	**7** (0.5)	750	14 200	94.6	5.4
10	**9** (0.5)	2000	2100	95.9	4.1
11	**10** (2.0)	1500	249	92.0	8.0
12	**11** (5.0)	1000	43	71.6	28.4
13	**12** (0.1)	4000	274 000	97.7	2.3
14	**13** (0.2)	3000	80 900	97.3	2.7

[a]Conditions: toluene 30 mL, ethylene 8 atm, 25 °C, 10 min, d-MAO white solid was used as cocatalyst. Activity in $kg\,mol^{-1}$ of $V\,h^{-1}$.

(**2–14**, see Scheme 16.1), which showed significant catalytic activities for ethylene dimerization in the presence of MAO, affording 1-butene with high selectivity, as shown in Table 16.1.[11–17] The reactivity (dimerization or polymerization) and catalytic activity were affected by the steric bulkiness

and electronic nature of the imido ligand. At optimized polymerization conditions, the adamantylimido vanadium(v) complex **2a** (see Scheme 16.1) displayed the highest catalytic activity for ethylene oligomerization, affording 1-butadiene exclusively.[11] In comparison, the cyclohexylimido and phenyiimido analogs **3a** and **4** (see Scheme 16.1) exhibit relatively lower catalytic activity. The introduction of a methyl group to the 2-position of the phenyl ring in phenylimido vanadium(v) complexes leads to an increased catalytic activity (for complexes **5a** and **5b** in Scheme 16.1).[12] However, the methyl groups in the 4-position and 3,5-position of the phenyl ring in phenylimido vanadium complexes have no obvious effect on the catalytic activity (for complexes **6** and **7** in Scheme 16.1).[12] 1-butene was obtained in the ethylene oligomerization by using vanadium complexes **2–7** (see Scheme 16.1), whereas polyethylene was prepared by using the 2,6-dimethylphenylimido analog **8** (see Scheme 16.1).[13] These results, thus, clearly indicate that the steric bulkiness of the imido substituent plays an essential role in the selectivity (1-butene or polyethylene) of this catalysis.[12]

Catalytic behavior is also affected significantly by the structure of the [NN] chelating ligand. Ethylene oligomerization using the complex containing a methyl group in the ortho position of the pyridine ring (complex **9** in Scheme 16.1) affords a mixture of 1-butene and polyethylene with a low catalytic activity of 2100 $kg\,mol^{-1}$ of $V\,h^{-1}$.[11] Adamantlyimido vanadium(v) dichloride complexes containing 2- or 8-(anilidomethyl)quinoline ligands (complexes **10** and **11**, see Scheme 16.1) display much lower catalytic activity than complex **2a** containing (2-anilidomethyl)pyridine ligand. Moreover, the resultant products prepared by complexes **10** and **11** (see Scheme 16.1) were a mixture of oligomer (1-butene as the major product) and polyethylene.[12] If the [NN] chelating ligand is replaced by 8-(2,6-dimethylanilide) – 5,6,7-trihydroquinoline, the resulting imido vanadium(v) complexes **12** and **13** (see Scheme 16.1) exhibit remarkable catalytic activities, affording 1-butene as the major product. Notably, complex **12** displays a much higher catalytic activity (274 000 $kg\,mol^{-1}$ of $V\,h^{-1}$) than complex **2a** (76 500 $kg\,mol^{-1}$ of $V\,h^{-1}$) due to the effect of 8-(2,6-dimethylanilide) – 5,6,7-trihydroquinoline ligand.[14] If the [NN] chelating ligand is changed to 2-(′-benz-imidazolyl)-pyridine, the resulting imido vanadium(v) complexes **14** (see Scheme 16.1) show a moderate catalytic activity for ethylene oligomerization, affording a mixture of oligomers (C_4–C_{22}) and polymers.[15] The catalytic behavior of this catalytic system is also affected by the ethylene pressure. For example, a first-order relationship between the activity and the ethylene pressure was observed in ethylene oligomerization using the **2a**/MMAO catalytic system.[16] The investigation of active species by ESR, ^{51}V NMR and XANES indicates that cationic vanadium(v) alkyl–hydride species play a role in this catalysis.[16,17]

Although the reports on vanadium catalysts are still limited, these catalysts have the potential to be good candidates for future commercialization for the production of α-olefins from ethylene oligomerization.

16.3 Vanadium-catalyzed Olefin Polymerization

16.3.1 Vanadium-catalyzed Ethylene Polymerization

Ethylene polymerization by using vanadium catalysts has been a topic of active research in numerous groups and has been reviewed for several times concerning various aspects.[7] In this chapter, vanadium catalysts for ethylene polymerization, which have been reviewed previously, will be introduced briefly. Only some typical and recently reported vanadium catalysts will be introduced. In ethylene polymerization catalyzed by vanadium catalysts, vanadium(III) species are usually considered as active species. Vanadium(IV) and vanadium(V) were assumed to be reduced to vanadium(III) by alkyl aluminum cocatalysts. Next, according to the oxidation state of the vanadium metal, vanadium catalysts for ethylene polymerization will be discussed separately.

16.3.1.1 Vanadium(III)-catalyzed Ethylene Polymerization

Although traditional vanadium-based Ziegler–Natta catalysts exhibit unique characteristics in ethylene or propylene polymerization and copolymerization, catalyst deactivation is still a key problem in polymerization with vanadium catalysts due to reduction of catalytically active species to less-active or inactive low-valent species. Designing the chemical structure of ancillary ligands to stabilize active vanadium species is an effective approach to prolong the catalyst lifetime. Bidentate [N, O] chelating ligands including β-enaminoketonato, salicylaldiminato and iminopyrrolide ligands have been developed to stabilize vanadium(III) catalysts.[7d] The mono(β-enaminoketonato) vanadium(III) complex **15** (see Scheme 16.2) was designed and synthesized by Li *et al.*[18,19] The vanadium(III) center is coordinated by one β-enaminoketonato ligand, two chlorine atoms and two THF molecules. The two chlorine atoms are located in a *trans*-position, while two THF molecules are in a *cis*-position. In the presence of Et_2AlCl (cocatalyst) and trichloroacetate (promoter), a high catalytic activity up to 27 800 kg PE mol^{-1} of V h^{-1} bar^{-1} could be obtained for ethylene polymerization catalyzed by vanadium(III) complex **15** (see Scheme 16.2).[18] The introduction of two β-enaminoketonato ligands leads to a thermostable vanadium(III) complex in ethylene polymerization. Complex **16** (see Scheme 16.2) exhibits a high catalytic activity of 23 760 kg PE mol^{-1} of V h^{-1} bar^{-1} at 70 °C, affording

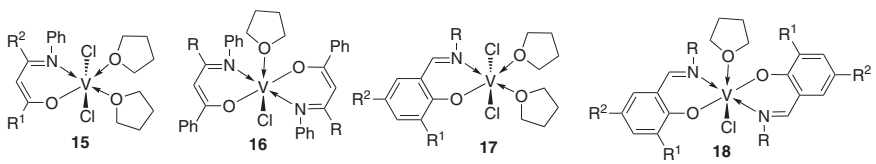

Scheme 16.2 Vanadium(III) complexes for ethylene polymerization.

polyethylene with M_w of 18.4 mol^{-1} and M_w/M_n of 2.24.[20] Vanadium(III) complex **17** (see Scheme 16.2) containing a salicylaldiminato ligand (see Scheme 16.2) was designed as precatalyst for ethylene polymerization. Although the chemical structure of the ligands was adjusted, comparable catalytic activity of 17 000–22 000 kg PE mol^{-1} of V h^{-1} bar^{-1} at 25 °C was observed during ethylene polymerization using complexes **17** as precatalysts.[21] Complex **18** (see Scheme 16.2) containing two salicylaldiminato ligands displays similar catalytic activity for ethylene polymerization to complex **17** containing one salicylaldiminato ligand. The chemical structure of the ligands in complex **18** significantly affect the catalytic activity.[21] Other vanadium(III) complexes containing α-diimine ligands,[22] bis(imidazole) ligands,[23] tris(imidazole) ligands,[23] bis(pyrozolyl)pyridine ligand,[24] bis(carbene)pyridine ligand[25] and phosphine ligands[26] show relatively lower catalytic activity for ethylene polymerization than complexes **15**–**18**.

16.3.1.2 Vanadium(IV)-catalyzed Ethylene Polymerization

Several (arylimido)vanadium(IV) complexes were reported as precatalysts for ethylene polymerization.[27,28] Activated by Et_2AlCl cocatalyst, (arylimido)vanadium(IV) complex **19** (see Scheme 16.3) shows a catalytic activity of 120 kg PE mol^{-1} of V h^{-1}.[27] Vanadium(IV) complexes containing two β-enaminoketonato ligands (complex **20** in Scheme 16.3) show similar catalytic activities to their vanadium(III) analogs in ethylene polymerization, affording polyethylene with similar molecular weight and molecular weight distribution to that prepared by their analogous vanadium(III) complexes.

16.3.1.3 Vanadium(V)-catalyzed Ethylene Polymerization

$VOCl_3$ was widely used in the industry to produce ethylene–propylene rubber. However, the unstable active centers bring low activity and the catalyst residues should be removed from the polymer product after deactivation. Therefore, several oxovanadium(V) complexes containing chelated aryloxo or alkoxo ligands, such as amine pyridine(s) phenolate ligands,[29,30] pyridylalkoxide ligand,[31] 2-(2-butoxyethoxy)ethanolate ligand,[32] [OSSO] type bis(phenolato) ligand[33] and C- and N-capped bi/tris(phenolate) ligands[34,35] have been designed and applied as precatalysts for ethylene polymerization.

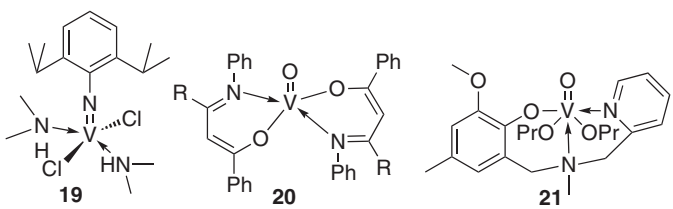

Scheme 16.3 Vanadium(IV and V) complexes for ethylene polymerization.

A series of oxovanadium(v) complexes containing amine pyridine(s) phenolate ligands [ONN] have been synthesized and their catalytic behavior for ethylene polymerization have been investigated.[29] Complex **21** exhibits a high catalytic activity of 66200 kg PE mol^{-1} of V h^{-1} for ethylene polymerization, affording polyethylene with M_w of 55.8 kg mol^{-1} and M_w/M_n of 2.4.[29] The introduction of another aryloxide group lead to oxovanadium(V) complexes containing [ONNO] ligand, which exhibits lower catalytic activity for ethylene polymerization than complex 21. The thermal stability during ethylene polymerization are enhanced, affording high molecular weight polyethylene ($M_w = 203$ kg mol^{-1}) with unimodal molecular weight distributions ($M_w/M_n = 2.2$).[30] Vanadium complexes containing a pyridylalkoxide ligand[31] and 2-(2-butoxyethoxy)ethanolate ligand[32] display relatively low catalytic activity for ethylene polymerization. Upon activation by MAO, vanadium(v) complex **22** (see Scheme 16.4) containing [OSSO] type bis(phenolato) ligand catalyzes ethylene polymerization with a catalytic activity of 774 kg PE mol^{-1} of V h^{-1}, producing polyethylene with a high molecular weight ($M_n = 560$ kg mol^{-1}) and M_w/M_n of 2.8.[33] Redshaw *et al.*, have reported that vanadyl precatalysts bearing chelating aryloxide ligands are found to polymerize ethylene with exceptionally high activities. Vanadium(v) complex **23** (see Scheme 16.4), activated by Me_2AlCl, exhibits a high activity of 122 900 kg PE mol^{-1} of V h^{-1} bar^{-1} at 80 °C for ethylene polymerization, which is much higher than that (*i.e.*, 22 300 kg PE mol^{-1} of V h^{-1} bar^{-1}) at 20 °C. Polyethylene with ultrahigh molecular weight ($M_w = 6860$ kg mol^{-1}) was obtained at 20 °C. A high catalytic activity of 96 500 kg PE mol^{-1} of V h^{-1} bar^{-1} was also observed when vanadium(v) complex **24** (see Scheme 16.4) was used as precatalyst.[34] Activated by Me_2AlCl, vanadium complex **25** (see Scheme 16.4) exhibits extremely high catalytic activity of 640 000 kg PE mol^{-1} of V h^{-1} bar^{-1} at high polymerization temperature of 80 °C.[35] Redshaw *et al.*, also designed many other vanadium(v) complexes containing mutiphenolate chelate ligands, which showed high catalytic activity for ethylene polymerization.[36–47]

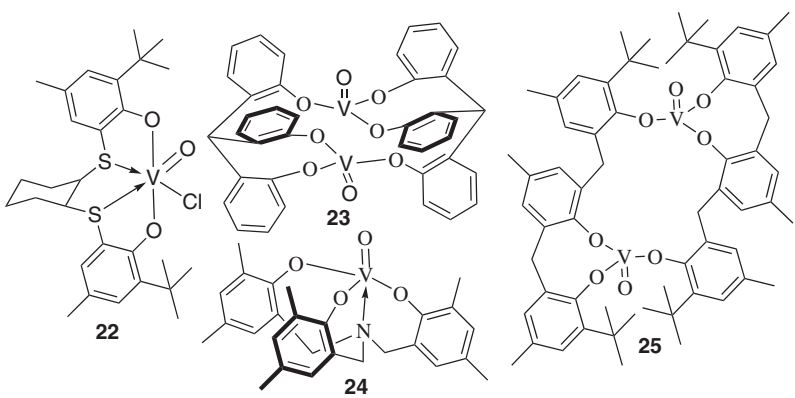

Scheme 16.4 Oxovanadium(v) complexes for ethylene polymerization.

The replacement of the oxygen atom in $VOCl_3$ by arylimido ligand results in (arylimido)vanadium(v) complexes with moderate thermal stability.[7a] In this case, (arylimido)vanadium(v) complexes containing cyclopentadienyl ligand[48] and hydrotris(pyrazolyl)borato ligand[49] were designed for ethylene polymerization. However, the catalytic activity of these vanadium(v) complexes is low. Nomura *et al.*, reported a series of imidovanadium(v) complexes containing anionic ancillary donor ligands for ethylene polymerization. Activated by MAO, the imidovanadium(v) complex **26** (R1 = Me, R^2 = H, see Scheme 16.5) exhibits a notable catalytic activity of 2930 kg PE mol^{-1} of V h^{-1} for ethylene polymerization. Ultrahigh molecular weight linear polyethylene with uniform molecular weight distributions ($M_n = 1750$ kg mol^{-1}, $M_w/M_n = 1.64$) was obtained.[50–52] In the presence of Et_2AlCl, complex **26** (see Scheme 16.5) displays a much higher catalytic activity of 11 700 kg PE mol^{-1} of V h^{-1} than that of the **26**/MAO catalytic system.

The catalytic behavior of imidovanadium(v) complexes is affected by the structure of the imido ligand. The (adamantylimido)vanadium(v) complex **27** (see Scheme 16.5) shows lower activity for ethylene polymerization than that of **26**, and the resulting polymer possesses bimodal or multimodal molecular weight distributions. The introduction of electron withdrawing groups of F and Cl in the imido ligand leads to an increase of catalytic activity. Vanadium(v) complexes **28a** or **28b**/Et_2AlCl catalytic systems could catalyze ethylene polymerization with catalytic activity of 55 800 and 31 900 kg PE mol^{-1} of V h^{-1}, respectively.[53] The catalytic behavior for ethylene polymerization is also affected by the chemical structure of anionic ancillary donor ligands. The catalytic activity of imidovanadium(v) complex containing a ketimide ligand **29** (see Scheme 16.5) is lower than that of complex **26** in the presence of MAO or Et_2AlCl. However, in the presence of Et_2AlCl, the ethylene polymerization activities of imidovanadium(v)

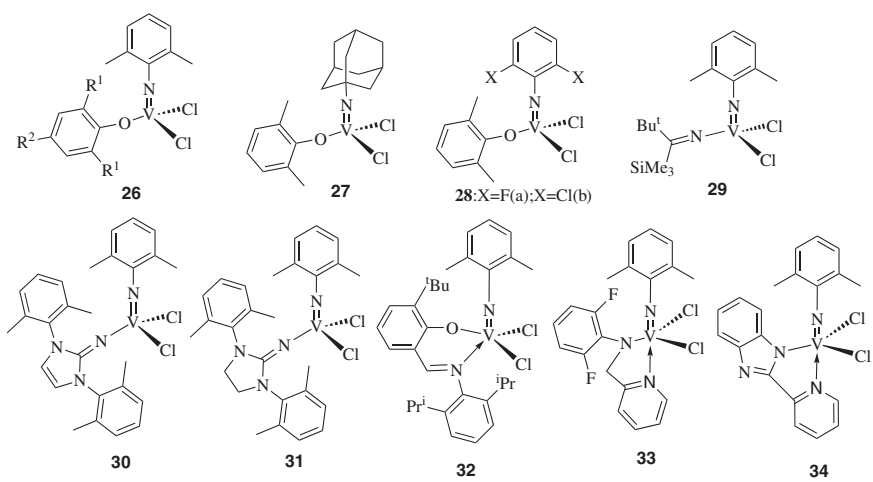

Scheme 16.5 Imidovanadium(v) complexes for ethylene polymerization.

complexes containing the imidazolin-2-iminato ligand **30** (see Scheme 16.4) and the imidazolidin-2-iminato ligand **31** (see Scheme 16.4) are 38 300 and 32 000 kg PE mol^{-1} of V h^{-1} respectively, which are much higher than that of complex **26.**[54] Activated by MAO, the imidovanadium(v) complex **32** (see Scheme 16.4) bearing a phenoxy-imine ligand exhibits high activity of 2150 kg PE mol^{-1} of V h^{-1}, affording polyethylene with high-molecular weight and unimodal molecular weight distribution.[55] In comparison, the catalytic activity of the imidovanadium(v) complex **33** (see Scheme 16.5) with the (2-anilidomethyl)pyridine ligand is lower (618 kg PE mol^{-1} of V h^{-1}) than that of complex **32**, although the resulting polyethylene possesses high molecular weight with unimodal molecular weight distribution.[13] In the presence of Me_2AlCl, the imidovanadium(v) complex **34** (see Scheme 16.5) displays high catalytic activity of 35 700 kg PE mol^{-1} of V h^{-1}. However, the mixture of polyethylene and oligomers of ethylene were obtained when MAO was used as catalyst.[15]

16.3.2 Vanadium-catalyzed Propylene Polymerization

The physical and mechanical properties of polypropylene are dependent on tactility. Isotactic, syndiotactic and atactic are three basic forms of polypropylene. It has been known that the use of a vanadium compound [$V(acac)_3$ or VCl_4] in the presence of an alkyl aluminum compound affords mainly syndiotactic polypropene.[56] Further, Doi *et al.*, found that the $V(acac)_3/Et_2AlCl$ catalyst system polymerizes propylene with living character, affording a syndiotactic polypropylene without any detectable chain termination as well as transfer reactions at temperatures below −65 °C.[57] The resulting polypropylene possessed narrow molecular weight distribution ($M_w/M_n = 1.05–1.20$).[57] The living catalytic system of $V(acac)_3/Et_2AlCl$ can also be used to prepare well-defined block copolymers. A diblock copolymer of polypropylene-*b*-poly(methyl methacrylate) was prepared by the combination of living coordination polymerization of propylene and anionic polymerization of methyl methacrylate by using the $V(acac)_3/Et_2AlCl$ catalytic system.[58] A propylene–tetrahydrofuran (THF) diblock copolymer was synthesized through the living polymerization of THF initiated by iodine functionalized polypropylene, which was prepared by the transformation of the living polypropylene ends into cationic polymer ends.[59]

As described in Section 16.3.1, the introduction of an electronic donor ligand can stabilize the active center and subsequently leads to a high catalytic activity. Vanadium complexes containing ancillary donor ligands were also reported and used as precatalysts for propylene polymerization. Vanadium(III) complex **35** (see Scheme 16.6) containing bis(phenoxy)pyridine ligand shows a catalytic activity of 803 kg PP mol^{-1} of V h^{-1} for propylene polymerization in the presence of MAO. The resulting polypropylene possesses high molecular weight ($M_w = 1170$ kg mol^{-1}) with uniform molecular weight distribution ($M_w/M_n = 2.03$).[47] However, a large extent of irregularity

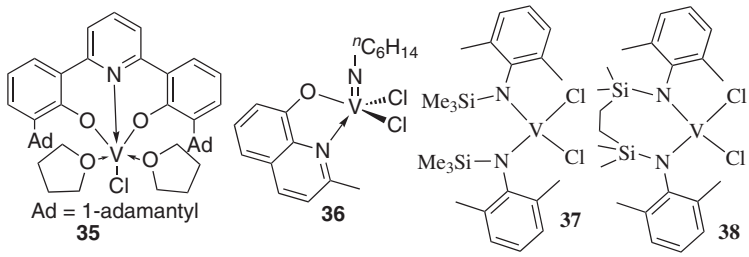

Scheme 16.6 Vanadium complexes for propylene polymerization.

was observed from the ^{13}C NMR spectra of the resulting polypropylene.[60] The (arylimido)vanadium(V) complex containing a hydrotris(pyrazolyl)borato (Tp) ligand or aryloxo ligand shows a low catalytic activity for propylene polymerization, which may be attributed to the bulky ligand around the vanadium center.[49,51] The *n*-hexylimido complex **36** (see Scheme 16.6) containing 2-methyl-8-quinolinolate ligand shows low catalytic activity (0.77 kg PP mol^{-1} of V h^{-1} atm^{-1}) for the polymerization of propylene, affording atactic polypropylene with M_n of 116 kg mol^{-1}.[61] Activated by $Et_3Al_2Cl_3$, syndiotactic specific propylene polymerization was successfully conducted by the vanadium(IV) amide complexes **37** and **38** (see Scheme 16.6) with catalytic activity of 7.0 and 16.9 kg PP mol^{-1} of V h^{-1}, respectively.[62]

16.3.3 Vanadium-catalyzed α-olefin Polymerization

Compared to polyethylene and polypropylene, other poly(α-olefin)s attract less attention. However, these polymeric materials based on α-olefins polymers can find various applications. For example, poly(1-octene) with low-molecular weight provides excellent fundamental material for lubricating oil formulation. Vanadium catalysts are also good candidates for the polymerization of α-olefins. Vanadium(IV) complex **39** containing phenoxyimine ligand promotes 1-octene polymerization with the catalytic activity of 5.5 kg polymer mol^{-1} of V at 19 °C, affording poly(1-octene) with M_w of 576 kg mol^{-1}. Poly(1-octene) with [mmmm] content of 70% could be prepared by decreasing polymerization temperature to 0.5 °C, but the catalytic activity also decreased to 0.7 kg polymer mol^{-1} of V.[63] Dichlorovanadium(IV) diamine-bis(phenolate) complex **40** (see Scheme 16.7), activated by MAO or $Al(^iBu)_3/Ph_3CB(C_6F_5)_4$, becomes an active catalyst for 1-octene polymerization, affording stereoregular polymers (mmmm ~90%). However, the conversion of 1-octene was low (2.2%–4.7%).[64] The vanadium(V) complex **41** (see Scheme 16.7) containing a [OSSO]-type ligand also shows a low catalytic activity (0.77 kg polymer mol^{-1} of V) for 1-hexene polymerization, affording poly(1-hexene) with low molecular weight ($M_w = 1.56$ kg mol^{-1}).[65] In the presence of binary cocatalyst ($Et_2AlCl/MgBu_2$), the vanadium(V) complex **42** (see Scheme 16.7) with the 2-[hydroxy(diaryl)methyl] – 8-hydroxyquinoline ligand promotes 1-hexene polymerization with high monomer conversion

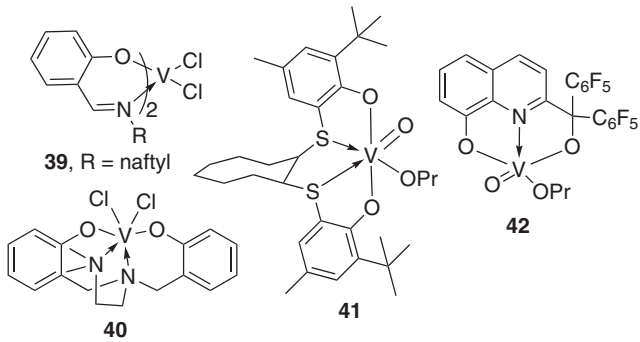

Scheme 16.7 Vanadium complexes for α-olefin polymerization.

(77%), affording oligomers of 1-hexene (82% of C_{12}–C_{18} oligomers and 18% of higher molecular weight ones) in aliphatic solvent.[66]

16.4 Vanadium-catalyzed Olefin Copolymerization

16.4.1 Vanadium-catalyzed Ethylene/Propylene Copolymerization

Ethylene–propylene rubber (EPR) or ethylene–propylene–diene rubber (EPDM) concern a rapidly growing class of elastomers prepared by the copolymerization of ethylene with propylene or their terpolymerization with a nonconjugated diene. Catalysts, which determine the catalytic activity and the microstructure of the copolymer, play an important role in the production of EPR or EPDM. Vanadium-based Ziegler–Natta catalysts were widely used in the industry for the production of about 70% of the commercial E/P copolymers.[8] However, the open active site of vanadium catalysts results in random E/P copolymers that prevent the formation of long crystallized ethylene sequences. The unstable active centers of traditional vanadium catalysts lead to low activity. In order to stabilize the active centers, good electron ligands are usually used. The coordination of a N-heterocyclic carbene (NHC) ligand to trichloro-oxo-vanadium(v) results in a highly stable vanadium(v) complex.[67] After activation by $Et_3Al_2Cl_3$, vanadium(v) complexes **43** exhibit moderate catalytic activity for ethylene–propylene copolymerization, affording ethylene–propylene copolymers with random monomer distribution.[8] The quasi-living copolymerization of ethylene with propylene was achieved by using **43c** as precatalyst. The ultra-high-molecular-weight ethylene-propylene copolymer ($M_w = 1612$ kg mol^{-1}) can be obtained by **43c**/$Et_3Al_2Cl_3$ catalytic system.[68] Vanadium(v) complexes bearing chelating aryloxides (**23** and **24** in Scheme 16.4, **44** and **45** in Scheme 16.8) display high catalytic activity for ethylene–propylene copolymerization, but the propylene content of the resulting ethylene-propylene copolymer is low.[34,35,38] For example, in the presence of Me_2AlCl, a catalytic activity up to 144 000 kg polymer mol^{-1} of V h^{-1} and a propylene content of 8.5 mol% in the resulting

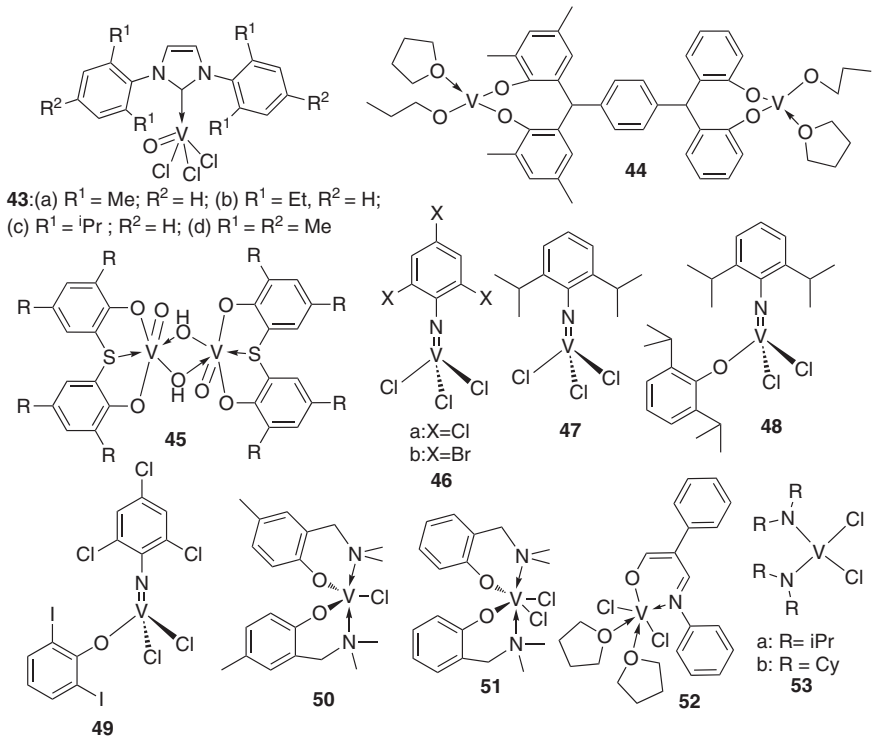

Scheme 16.8 Vanadium complexes for ethylene/propylene copolymerization.

copolymer were obtained by using vanadium(v) complex **44** as precatalys.[38] In contrast, imido vanadium(v) complexes **46** and **47** displayed a lower catalytic of 590–680 kg polymer mol^{-1} of V h^{-1}, but a much higher propylene content of about 43 mol% in the resulting ethylene-propylene copolymer was observed.[69] The introduction of a phenyl ligand (complex **48** and **49** in Scheme 16.8) leads to an increase in the catalytic activity and a similar propylene content in the resulting copolymer.[69] Vanadium(iv) and vanadium(iii) complexes were also used as precatalysts for ethylene–propylene copolymerization since vanadium(iii) species are usually considered as active species during olefin polymerization. Vanadium(iii) and vanadium(iv) complexes bearing ligands (**50** and **51** in Scheme 16.8) were prepared.[70] In the presence of $Et_3Al_2Cl_3$, the vanadium(iv) complex **50** showed a slightly higher catalytic activity (1800 kg polymer mol^{-1} of V h^{-1}) than that (1300 kg polymer mol^{-1} of V h^{-1}) of complex **51**. However, the propylene content of ethylene–propylene copolymer prepared by using complex **50** (37.5 wt%) is higher than that prepared by using complex **51** (32.3 wt%). Vanadium(iii) complexes **15** ($R^1 = Ph$, $R^2 = Me$, in Scheme 16.2), **17** ($R = Ph$, $R^1 = R^2 = H$, in Scheme 16.2) and **52** (see Scheme 16.8) exhibit similar catalytic activity (12 600–14 800 kg polymer mol^{-1} of V h^{-1}) toward ethylene–propylene copolymerization, affording ethylene–propylene copolymer with low propylene

content (6.2–7.4 mol%).[71] In the presence of $Et_3Al_2Cl_3$, the vanadium(IV) amide complexes **37**, **38** (see Scheme 16.6) and **53** (see Scheme 16.8) catalyze ethylene–propylene copolymerization with a high catalytic activity of 860 kg polymer mol^{-1} of V h^{-1}, affording ethylene-propylene copolymer with a propylene content of ~29 wt%.[62,72]

16.4.2 Vanadium-catalyzed Ethylene/α-olefin Copolymerization

Vanadium catalysts are also good catalysts for ethylene/α-olefin copolymerization, which have been introduced in several review articles. Therefore, represented vanadium catalysts and some recently reported vanadium catalysts will be discussed in this section. The ethylene/1-hexene copolymerization was investigated by the vanadium(III) complexes **15** (see Scheme 16.2) in the presence of Et_2AlCl. The catalytic activity of 3660–5820 kg polymer mol^{-1} of V h^{-1} was observed, with 1-hexene incorporation of 4.9–5.3 mol%. With an increase of comonomer in feed, the catalyst activity of ethylene/1-hexene copolymerization decreases rapidly, while the insertions of 1-hexene increases almost linearly. Ethylene-1-hexene copolymer with 1-hexene incorporation of 16 mol% could be obtained with M_w of 34 kg mol^{-1} and M_w/M_n of 1.84.[18] A similar catalytic behavior for ethylene/1-hexene copolymerization was observed by using the **16** (see Scheme 16.2)/Et_2AlCl catalytic system.[20] The investigation of ethylene/1-hexene copolymerization with **42** (see Scheme 16.7) showed that the high catalytic activity of 1400 kg polymer mol^{-1} of V h^{-1} and copolymer with high 1-hexene incorporation of 11.7 mol% could be obtained.[66] In the presence of Et_2AlCl, complex **40** (see Scheme 16.7) catalyzes ethylene/1-octene copolymerization with catalytic activity of 350 kg polymer mol^{-1} of V h^{-1}, affording ethylene-1-octene copolymer with M_w of 99 kg mol^{-1}, M_w/M_n of 2.3 and 1-octene incorporation of 4.1 mol%.[64]

16.5 Summary

In this chapter, we summarized a series of defined vanadium complexes and their application for olefin oligomerization, polymerization and copolymerization. Most of the examples focused on ethylene polymerization and copolymerization with α-olefins. Although the reported vanadium catalysts for ethylene oligomerization are still limited, they indicate their potential to be good candidates for ethylene oligomerization. Traditional vanadium Ziegler–Natta catalysts have been used widely in the production of commercial ethylene–propylene rubber. Vanadium complex catalysts have already shown their advantages in controlling the molecular weight, molecular weight distribution, sequence and topological structure of the resulting ethylene–propylene copolymer.

Note: After completion of this chapter, a review on vanadium-catalyzed olefin coordination polymerization appeared online.[73]

References

1. J. Skupiňska, *Chem. Rev.*, 1991, **91**, 613.
2. (a) D. S. McGuinness, *Chem. Rev.*, 2011, **111**, 2321; (b) M. Stürzel, S. Mihan and R. Mülhaupt, From Multisite Polymerization Catalysis to Sustainable Materials and All-Polyolefin Composites, *Chem. Rev.*, 2016, **116**, 1398; (c) M. C. Baier, M. A. Zuideveld and S. Mecking, *Angew. Chem., Int. Ed.*, 2014, **53**, 9722; (d) P. S. Chum and K. W. Swogger, *Prog. Polym. Sci.*, 2008, **33**, 797; (e) D. W. Sauter, M. Taoufik and C. Boisson, *Polymers*, 2017, **9**, 185.
3. (a) H. Sinn, W. Kaminsky, H. J. Vollmer and R. Woldt, *Angew. Chem.*, 1980, **92**, 396; (b) W. Kaminsky and A. Laban, *Appl. Catal., A*, 2001, **222**, 47; (c) H. G. Alt and A. Koppl, *Chem. Rev.*, 2000, **100**, 1205; (d) G. W. Coates, *Chem. Rev.*, 2000, **100**, 1223.
4. (a) L. K. Johnson, C. M. Killian and M. Brookhart, *J. Am. Chem. Soc.*, 1995, **117**, 6414; (b) S. Ittel, L. K. Johnson and M. Brookhart, *Chem. Rev.*, 2000, **100**, 1169; (c) I. E. Soshnikov, K. P. Bryliakov, A. A. Antonov, W.-H. Sun and E. P. Talsi, *Dalton Trans.*, 2019, **48**, 7974.
5. (a) B. L. Small, M. Brookhart and A. M. A. Bennett, *J. Am. Chem. Soc.*, 1998, **120**, 4049; (b) G. J. P. Britovsek, V. C. Gibson, B. S. Kimberley, P. J. Maddox, S. J. McTavish, G. A. Solan, A. J. P. White and D. J. Williams, *Chem. Commun.*, 1998, 849; (c) S. D. Ittel, L. K. Johnson and M. Brookhart, *Chem. Rev.*, 2000, **100**, 1169.
6. (a) T. Fujita, Y. Tohi, M. Mitani, S. Matsui, J. Saito, M. Nitabaru, K. Sugi, H. Makio, T. Tsutsui, *Eur. Pat.* 0874005, 1998;; (b) T. Matsugi and T. Fujita, *Chem. Soc. Rev.*, 2008, **37**, 1264; (c) H. Makio, N. Kashiwa and T. Fujita, *Adv. Synth. Catal.*, 2002, **344**, 477; (d) H. Makio and T. Fujita, *Acc. Chem. Res.*, 2009, **42**, 1532.
7. (a) K. Nomura and S. Zhang, *Chem. Rev.*, 2011, **111**, 2342; (b) H. Hagen, J. Boersma and G. van Koten, *Chem. Soc. Rev.*, 2002, **31**, 357; (c) S. Gambarotta, *Prog. Polym. Sci.*, 2008, **33**, 797; (d) J.-Q. Wu and Y.-S. Li, *Coord. Chem. Rev.*, 2011, **255**, 2303; (e) C. Redshaw, *Dalton Trans.*, 2016, **45**, 9018.
8. S. Zhang, W.-C. Zhang, D.-D. Shang, Z.-Q. Zhang and Y.-X. Wu, *Dalton Trans.*, 2015, **44**, 15264.
9. R. Schmidt, M. B. Welch, R. D. Knudsen, S. Gottfried and H. G. Alt, *J. Mol. Catal. A: Chem.*, 2004, **222**, 17.
10. R. Schmidt, M. B. Welch, R. D. Knudsen, S. Gottfried and H. G. Alt, *J. Mol. Catal. A: Chem.*, 2004, **222**, 9.
11. S. Zhang and K. Nomura, *J. Am. Chem. Soc.*, 2010, **132**, 4960.
12. K. Nomura, A. Igarashi, S. Katao, W. Zhang and W.-H. Sun, *Inorg. Chem.*, 2013, **52**, 2607.
13. S. Zhang, S. Katao, W.-H. Sun and K. Nomura, *Organometallics*, 2009, **28**, 5925.
14. X.-Y. Tang, A. Igarashi, W.-H. Sun, A. Inagaki, J. Liu, W. Zhang, Y.-S. Li and K. Nomura, *Organometallics*, 2014, **33**, 1053.

15. K. Nomura, M. Oshima, T. Mitsudome, H. Harakawa, P. Hao, K. Tsutsumi, G. Nagai, T. Ina, H. Takaya, W.-H. Sun and S. Yamazoe, *ACS Omega*, 2017, **2**, 8660.
16. A. Igarashi, S. Zhang and K. Nomura, *Organometallics*, 2012, **31**, 3575.
17. K. Nomura, T. Mitsudome, A. Igarashi, G. Nagai, K. Tsutsumi, T. Ina, T. Omiya, H. Takaya and S. Yamazoe, *Organometallics*, 2017, **36**, 530.
18. L. M. Tang, J. Q. Wu, Y. Q. Duan, L. Pan, Y. G. Li and Y. S. Li, *J. Polym. Sci., Part A: Polym. Chem.*, 2008, **46**, 2038.
19. J. S. Mu, J. Y. Liu, S. R. Liu and Y. S. Li, *Polymer*, 2009, **50**, 5059.
20. J. Q. Wu, B. X. Li, S. W. Zhang and Y. S. Li, *J. Polym. Sci., Part A: Polym. Chem.*, 2010, **48**, 3062.
21. J. Q. Wu, L. Pan, N. H. Hu and Y. S. Li, *Organometallics*, 2008, **27**, 3840.
22. S. Milione, G. Cavallo, C. Tedesco and A. Grassi, *J. Chem. Soc., Dalton Trans.*, 2002, 1839.
23. T. Ruther, K. J. Cavell, N. C. Braussaud, B. W. Skelton and A. H. White, *J. Chem. Soc., Dalton Trans.*, 2002, 4684.
24. H. S. Abbo, S. F. Mapolie, J. Darkwa and S. J. J. Titinchi, *J. Organomet. Chem.*, 2007, **692**, 5327.
25. D. S. McGuinness, V. C. Gibson and J. W. Steed, *Organometallics*, 2004, **23**, 6288.
26. (a) G. Zanchin, A. Gavezzoli, F. Bertini, G. Ricci and G. Leone, *Molecules*, 2019, **24**, 2088; (b) G. Zanchin, I. Pierro, E. Parisini, J. Martí-Rujas, G. Ricci and G. Leone, *J. Organomet. Chem.*, 2018, **861**, 142.
27. (a) C. Lorber, B. Donnadieu and R. Choukroun, *Dalton Trans.*, 2000, 4497; (b) C. Lorber, R. Choukroun and B. Donnadieu, *Inorg. Chem.*, 2002, **41**, 4217.
28. H. B. Bigmore, M. A. Zuideveld, R. M. Kowalczyk, A. R. Cowley, M. Kranenburg, E. J. L. McInnes and P. Mountford, *Inorg. Chem.*, 2006, **45**, 6411.
29. J.-B. Wang, L.-P. Lu, J.-Y. Liu and Y.-S. Li, *Dalton Trans.*, 2014, **43**, 12926.
30. J.-B. Wang, L.-P. Lu, J.-Y. Liu, H.-L. Mu and Y.-S. Li, *J. Mol. Catal. A: Chem.*, 2015, **398**, 289.
31. H. Hagen, C. Bezemer, J. Boersma, H. Kooijman, M. Lutz, A. L. Spek and G. van Koten, *Inorg.Chem.*, 2000, **39**, 3970.
32. E. C. E. Rosenthal, H. Cui and M. Mummert, *Inorg. Chem. Commun.*, 2008, **11**, 918.
33. G. M. Meppelder, T. S. Halbach, T. P. Spaniol, R. Mülhaupt and J. Okuda, *J. Organomet. Chem.*, 2009, **694**, 1235.
34. C. Redshaw, M. A. Rowan, D. M. Homden, S. H. Dale, M. R. J. Elsegood, S. Matsui and S. Matsuura, *Chem. Commun.*, 2006, 3329.
35. C. Redshaw, L. Warford, S. H. Dale and M. R. J. Elsegood, *Chem. Commun.*, 2004, 1954.
36. C. Redshaw, M. J. Walton, D. S. Lee, C. Y. Jiang, M. R. J. Elsegood and K. Michiue, *Chem. – Eur. J.*, 2015, **21**, 5199.
37. C. Redshaw, M. J. Walton, K. Michiue, Y. M. Chao, A. Walton, P. Elo, V. Sumerin, C. Y. Jiang and M. R. J. Elsegood, *Dalton Trans.*, 2015, **44**, 12292.

38. (a) C. Redshaw, M. J. Walton, T. J. Prior and K. Michiue, *RSC Adv.*, 2015, **5**, 89783; (b) J. Ma, K. Q. Zhao, M. J. Walton, J. A. Wright, J. W. A. Frese, M. R. J. Elsegood, Q. F. Xing, W.-H. Sun and C. Redshaw, *Dalton Trans.*, 2014, **43**, 8300.
39. J. Ma, K. Q. Zhao, M. J. Walton, J. A. Wright, D. L. Hughes, M. R. J. Elsegood, K. Michiue, X. S. Sun and C. Redshaw, *Dalton Trans.*, 2014, **43**, 16698.
40. C. Redshaw, L. Clowes, D. L. Hughes, M. R. J. Elsegood and T. Yamato, *Organometallics*, 2011, **30**, 5620.
41. L. Clowes and C. Redshaw, *Inorg. Chem.*, 2011, **50**, 7838.
42. C. Lorber, E. Despagnet-Ayoub, L. Vendier, A. Arbaoui and C. Redshaw, *Catal. Sci. Tech.*, 2011, **1**, 489.
43. C. Redshaw, *Dalton Trans.*, 2010, **39**, 5595.
44. A. Arbaoui, C. Redshaw, D. M. Homden, J. A. Wright and M. R. J. Elsegood, *Dalton Trans.*, 2009, **41**, 8911.
45. D. M. Homden, C. Redshaw, L. Warford, D. L. Hughes, J. A. Wright, S. H. Dale and M. R. J. Elsegood, *Dalton Trans.*, 2009, **41**, 8900.
46. D. M. Homden, C. Redshaw and D. L. Hughes, *Inorg. Chem.*, 2007, **46**, 10827.
47. C. Redshaw, M. A. Rowan, L. Warford, D. M. Homden, A. Arbaoui, M. R. J. Elsegood, S. H. Dale, T. Yamato, C. P. Casas, S. Matsui and S. Matsuura, *Chem. – Eur. J.*, 2007, **13**, 1090.
48. M. P. Coles, C. I. Dalby, V. C. Gibson, I. R. Little, E. L. Marshall, M. H. RibeirodaCosta and S. Mastroianni, *J. Organomet. Chem.*, 1999, **591**, 78.
49. S. Sheuer, J. Fischer and J. Kress, *Organometallics*, 1995, **14**, 2627.
50. K. Nomura, A. Sagara and Y. Imanishi, *Chem. Lett.*, 2001, 36.
51. K. Nomura, A. Sagara and Y. Imanishi, *Macromolecules*, 2002, **35**, 1583.
52. W. Wang and K. Nomura, *Macromolecules*, 2005, **38**, 5905.
53. N. Diteepeng, X. Tang, X. Hou, Y.-S. Li, K. Phomphraib and K. Nomura, *Dalton Trans.*, 2015, **44**, 12273.
54. K. Nomura, B. K. Bahuleyan, S. Zhang, P. M. V. Sharma, S. Katao, A. Igarashi, A. Inagaki and M. Tamm, *Inorg. Chem.*, 2014, **53**, 607.
55. Y. Onishi, S. Katao, M. Fujiki and K. Nomura, *Organometallics*, 2008, **27**, 2590.
56. G. Natta, I. Paquon and A. Zambelli, *J. Am. Chem. Soc.*, 1962, **84**, 1488.
57. Y. Doi, S. Ueki and T. Keii, *Macromolecules*, 1978, **12**, 814.
58. Y. Doi, T. Koyama and K. Soga, *Makromol. Chem.*, 1985, **186**, 11.
59. Y. Doi, Y. Watanabe, S. Ueki and K. Soga, *Makromol. Chem., Rapid Commun.*, 1983, **4**, 533.
60. S. R. Golisz and J. E. Bercaw, *Macromolecules*, 2009, **42**, 8751.
61. Y. Sato, Y. Nakayama and H. Yasuda, *J. Appl. Polym. Sci.*, 2005, **97**, 1008.
62. C. Cuomo, S. Milione and A. Grassi, *J. Polym. Sci., Part A: Polym. Chem.*, 2006, **44**, 3279.
63. M. Białek and E. Bisz, *J. Polym. Res.*, 2013, **20**, 164.
64. M. Białek and E. Bisz, *J. Catal.*, 2018, **362**, 65.

65. T. Toda, N. Nakata, T. Matsuo and A. Ishii, *ACS Catal.*, 2013, **3**, 1764.
66. N. A. Kolosov, V. A. Tuskaev, S. C. Gagieva, I. V. Fedyanin, V. N. Khrustalev, O. V. Polyakova and B. M. Bulychev, *Eur. Polym. J.*, 2017, **87**, 266.
67. C. D. Abernethy, G. M. Codd, M. D. Spicer and M. K. Taylor, *J. Am. Chem. Soc.*, 2003, **125**, 1128.
68. S. Zhang, W.-C. Zhang, D.-D. Shang and Y.-X. Wu, *J. Polym. Sci., Part A: Polym. Chem.*, 2019, **57**, 553.
69. A. R. Michael, H. Martin, S. Jörg, *Eur. Pat.* EP1284269-A, 2001.
70. H. Hagen, J. Boersma, M. Lutz, A. L. Spek and G. van Koten, *Eur. J. Inorg. Chem.*, 2001, 117.
71. J. S. Mu and Y.-S. Li, *Gaofenzi Xuebao*, 2013, **12**, 1492.
72. N. Desmangles, S. Gambarotta, C. Bensimon, S. Davis and H. Zahalka, *J. Organomet. Chem.*, 1998, **562**, 53.
73. A. M. F. Phillips, H. Suo, M. F. C. Guedes da Silva, A. J. L. Pombeiro and W.-H. Sun, *Coord. Chem. Rev.*, 2020, **416**, 213332.

CHAPTER 17

Vanadium-catalysed Olefin Metathesis and Related Chemistry

KOTOHIRO NOMURA

Department of Chemistry, Tokyo Metropolitan University, 1-1 Minami Osawa, Hachioji, Tokyo 192-0397, Japan
Email: ktnomura@tmu.ac.jp

17.1 Introduction

Olefin metathesis is an useful method applied for the synthesis of various organic compounds (basic, fine chemicals, pharmaceuticals *etc*.), polymers and advanced materials.[1–28] These reactions, such as ring-opening metathesis (ROM, reaction with cyclic olefins), ring closing metathesis (RCM, intramolecular reaction with acyclic diene) and acyclic diene metathesis (ADMET, intermolecular reaction with acyclic diene) as well as cross metathesis (CM, reaction with acyclic olefins) proceed *via* metallacycle intermediates (Scheme 17.1). Metal-carbene (alkylidene) species, thus, play a key role in this catalysis.[1–19] These carbon–carbon bond formations are widely recognised as one of the most effective and important methods employed in modern organic and polymer synthesis[20–27] in terms of better atom efficiency and construction of environmentally benign chemical processes, precise control of repeat units and of post (end) modifications (grafting). Ring-opening metathesis polymerisation (ROMP),[20–25] addition

Catalysis Series No. 41
Vanadium Catalysis
Edited by Manas Sutradhar, José Armando L. da Silva and Armando J. L. Pombeiro

Published by the Royal Society of Chemistry, www.rsc.org

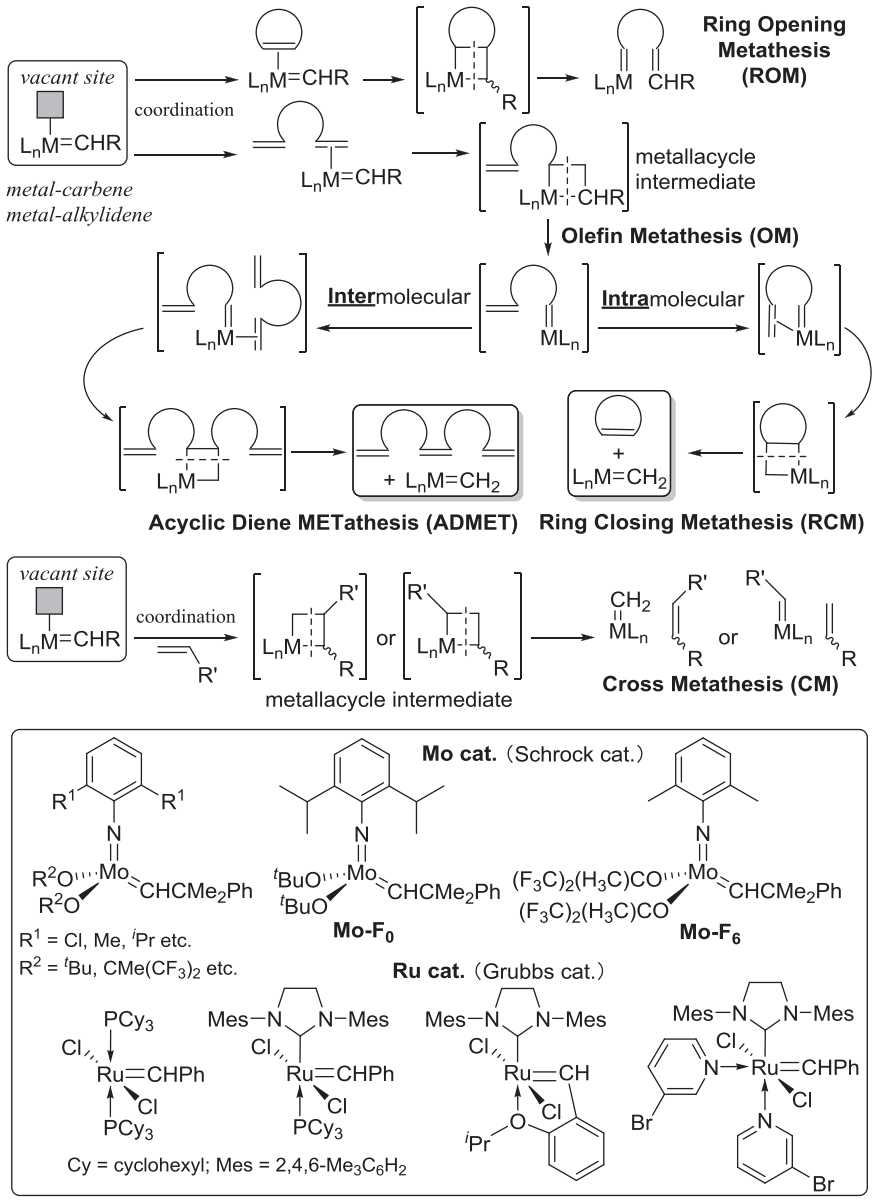

Scheme 17.1 Typical olefin metathesis reactions and their basic mechanisms.

type polymerisation induced by ring strain (ROMP) and ADMET polymerisation,[26–28] condensation polymerisation accompanied by-production of small molecule (such as ethylene or propylene), are widely used in the synthesis of advanced polymeric materials. Molybdenum- or tungsten-alkylidene (called Schrock type)[4–15] and ruthenium-carbene (called Grubbs type)[16–19] complexes, as shown in Scheme 17.1, have been

widely used as the catalysts. Catalyst development has been considered as an important topic because there are some concerns, such as thermal stability and catalyst deactivation over time (and subsequent isomerisation and/or generating radicals, *etc*., especially observed by ruthenium catalysts).

Studies on synthesis and reaction chemistry of vanadium–alkylidene complexes have been considered an attractive subject not only of fundamental importance in organometallic chemistry,[9,10,13,14,29,30] but also due to their potential in catalysis displayed by classical Ziegler-type, vanadium-catalyst systems in olefin coordination–insertion polymerisation (synthesis of ultrahigh molecular weight polymers).[31–40] However, limited examples were known for synthesis of vanadium–alkylidene (carbene) complexes,[13,14] in particular concerning olefin metathesis active vanadium–alkylidene complex catalysts until recently.[13,14,25]

One report from 1968 found that VCl_4-^{n}BuLi catalyst afforded ring-opened polymers in the polymerisation of cyclobutene [32% conv. after 20 h at -20 °C, monomer/V = 20 (molar ratio)], whereas the polymerisation using VCl_4-$AlEt_3$ catalyst proceeded in the vinyl addition manner under the same conditions (100% conv.). The catalyst also afforded ring-opened polymers in the polymerisation of 3-methylcyclobutene (3% conv.).[41] Although $MoCl_5$-$AlEt_3$ and WCl_6-$AlEt_3$ catalysts afforded ring-opened polymers in the polymerisation of cyclopentene, the activity using the vanadium catalysts were quite low.[42] These are, as far as we know, the first reports in olefin metathesis polymerisation using vanadium catalysts.[43] There had been no reports on this topic until 2002 when a study was published on ring-opening metathesis polymerisation (ROMP) of norbornene (NBE) using V(N-2,6-$Me_2C_6H_3$)(CH_2Ph)$_2$(O-2,6-^{i}Pr$_2C_6H_3$), V(N-2,6-$Me_2C_6H_3$)Cl_2(O-2,6-^{i}Pr$_2C_6H_3$) –$AlMe_3$ catalyst.[44] In 2005, ROMP of NBE using a vanadium(v)-alkylidene catalyst, V(CHSiMe_3)(N-2,6-$Me_2C_6H_3$)(N=C^{t}Bu$_2$)(PMe_3), was demonstrated for the first time.[45]

In this chapter, reports for synthesis of vanadium–alkylidene complexes and some reactions are reviewed and ring-opening metathesis polymerisation (ROMP) of cyclic olefins using (imido)vanadium(v)-alkylidene are summarised. In particular, reports in olefin metathesis have been limited mostly to the ROMP of cyclic olefins with a series of (imido)vanadium(v) complexes, thus the effects of (imido and anionic ancillary donor) ligands towards the activity and the stereo specific ROMP are summarised in this chapter.

17.2 Synthesis of Vanadium–Alkylidene Complexes and Some Reactions

17.2.1 Synthesis of Vanadium–Alkylidene Complexes

Scheme 17.2 summarises reported methods for the synthesis of vanadium–alkylidene complexes. α-Hydrogen elimination (abstraction) from metal

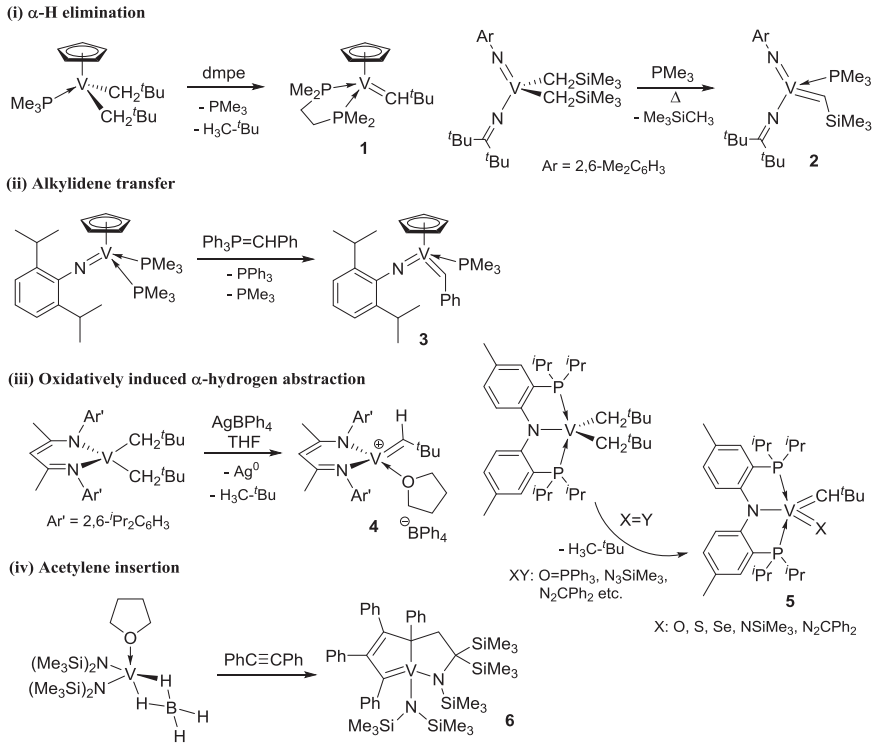

Scheme 17.2 Reported methods for synthesis of vanadium-alkylidene complexes.[45–49,53,54]

alkyl complexes lacking β-hydrogen is the most common method for preparation of high-oxidation state, early transition metal alkylidenes.[4–14] In order to induce or promote the reaction (abstraction or deprotonation), certain assistances, such as (i) addition of neutral donor ligand (*e.g.*, phosphine *etc.*) to increase the steric crowding, (ii) photochemical stimulation and (iii) addition of a base, are often employed.[5–14]

The synthesis of a vanadium(III)–alkylidene complex containing a cyclopentadienyl ligand CpV(CH^{t}Bu)(dmpe) [**1**, dmpe = bis(dimethylphosphino)-ethane] from the dialkyl analogue by α-hydrogen abstraction with addition of dmpe was demonstrated by Hessen and Teuben in 1989.[46,47] The (arylimido)vanadium(V)–alkylidene complex CpV(CHPh)(NAr′)(PMe_3) (**3**, Ar′ = 2,6-^{i}Pr$_2$C$_6$H$_3$) was then prepared from the vanadium(III) complex CpV(NAr′)(PMe_3)$_2$ by benzylidene transfer with $Ph_3P{=}CHPh$.[48] However, these complexes showed poor ability as olefin metathesis catalysts. Treatment of V(III) borohydride complex with excess diphenylacetylene afforded a bicyclic vanadium(V) complex containing a V=C double bond (**6**).[49] Metalacyclic vanadoxycarbene complexes were prepared by reaction of (butadiene)zirconocene or (butadiene)hafnocene with [CpV(CO)$_4$].[50,51]

Reaction of Cp*vanadium(η^6-naphthalene) with ^{t}BuC≡P afforded a partially cleaved 1,3,5-triphosphaprismane derivative containing the vanadium–carbon double bond,[52] which afforded 1,3,5-triphospha-Dewar benzene complex by treating with CO.

Synthesis of vanadium(IV)–alkylidene complexes, [(nacnac)V(CH^tBu)(THF)]$^+$[BPh_4]$^-$ [**4**, nacnac$^-$ = {Ar′N-C(Me)}$_2$CH$^-$], from the vanadium(III) dialkyl analogue, (nacnac)V($CH_2{}^tBu)_2$, *via* oxidatively induced α-hydrogen abstraction with $AgBPh_4$ was demonstrated by Mindiola in 2004.[53] A similar approach for the synthesis of a series of vanadium(V)-alkylidene from the vanadium(III) dialkyl complex that contains a monoanionic tridentate ligand V($CH_2{}^tBu)_2$(PNP) [PNP = N{4-Me-2-(P^iPr_2)C_6H_3}$_2^-$] was also demonstrated by treating with π-acids or two-electron oxidants.[54]

In 2005, it was demonstrated that α-hydrogen abstraction from the (arylimido)vanadium(V) dialkyl complex V(NAr)($CH_2SiMe_3)_2$(N=C$^tBu_2$) (Ar = 2,6-$Me_2C_6H_3$) with the addition of excess PMe_3 afforded the vanadium(V)–alkylidene V($CHSiMe_3$)(NAr)(N=C$^tBu_2$)(PMe_3) (**2**), which catalysed ring-opening metathesis polymerisation (ROMP) of norbornene (NBE) for the first time with a vanadium–alkylidene complex.[45] As described next, this method enables the synthesis of a series of (imido)vanadium(V)-alkylidene complexes containing anionic ancillary donor ligands, which act as catalysts for ROMP of cyclic olefins.[13,14,29,30]

α-Hydrogen elimination–abstraction is the common method for synthesis of metal-alkylidenes with early transition metals.[4–14] The method enables the synthesis of a series of (imido)vanadium(V)–alkylidenes containing anionic ancillary donor ligands from the corresponding dialkyl analogues in the presence of PMe_3 (Scheme 17.3).[13,29,45,55–61] The addition of PMe_3 is a prerequisite for proceeding the α-hydrogen abstraction by sterically crowding, and the reaction rate (and the optimised conditions for obtaining better yields) was affected by the ligand substituents. For instance, a steric bulkiness in the imido ligand affected the rate in the α-hydrogen abstraction in the iminoimidazolidide analogues (Scheme 17.3); the phenyl imido complex (**8c**) required longer reaction hours at high temperature (*i.e.*, 9–10 days at 70 °C for completion) than the adamantylimido analogue (**8b**) and the analogous arylimido (**8a**) (after 1 day at 60 °C).[58] The rate of α-hydrogen elimination was also affected by the electronic nature of the anionic donor ligand; the synthesis of the 2,6-diisopropylphenoxide analogue (**7**) required 80 °C for 5 h for completion,[55] whereas the synthesis of the similar pentafluorophenoxide analogue (**14**) required 12 h at 25 °C[59] and fluorinated alkoxo analogues (**20,21**) could be obtained upon heating (60 °C for 12 h).[59] Similarly, as shown in Scheme 17.4, reaction of V(NAd)($CH_2SiMe_3)_3$ in the presence of excess (12 equiv.) PMe_3 yielded the corresponding alkyl-alkylidene complex V($CHSiMe_3$)(NAd)(CH_2SiMe_3)($PMe_3)_2$ (**24**).[62] A *N*-heterocyclic carbene (NHC) was also used in place of PMe_3, and reactions of the trialkyl analogues in the presence of 1,3-bis(2,6-diisopropylphenyl)-imidazol-2-ylidene (NHC) gave the corresponding alkyl-alkylidene complexes, V($CHSiMe_3$)(NR)(CH_2SiMe_3)(NHC) (**25,26**).[63]

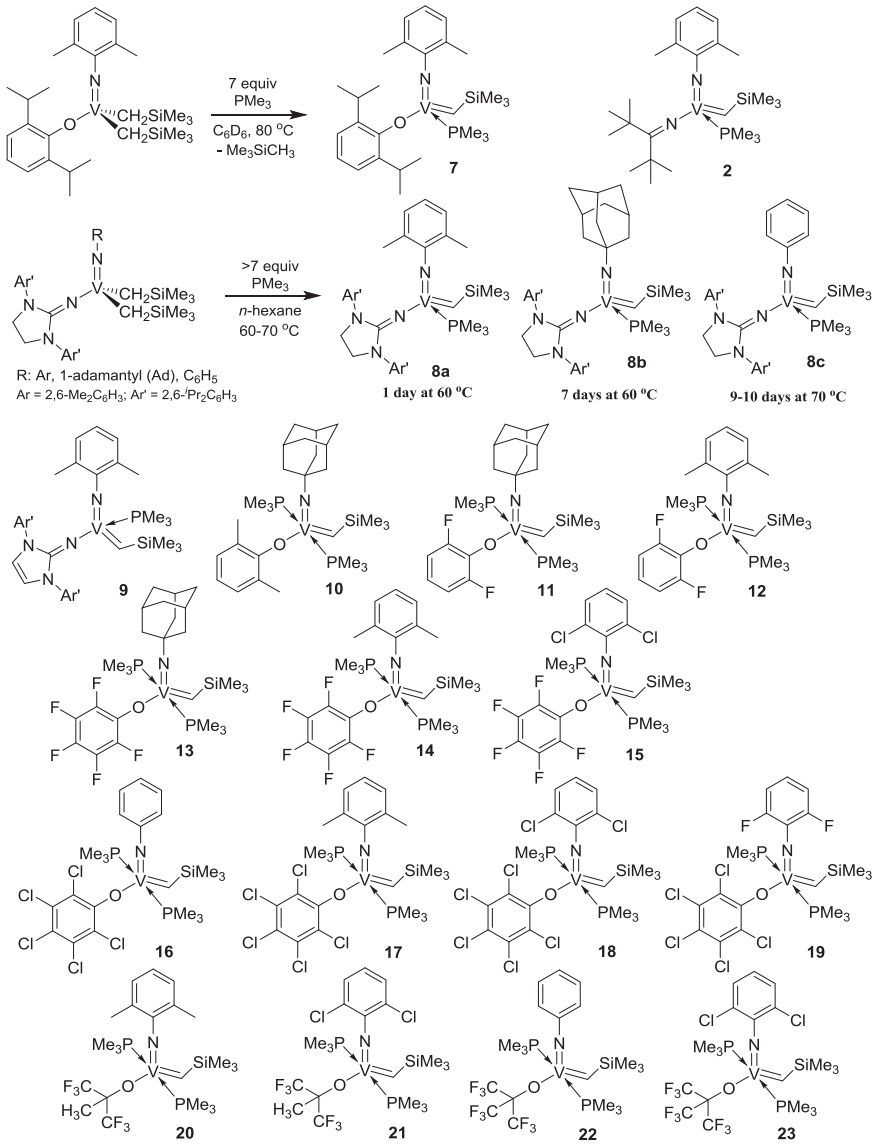

Scheme 17.3 Various (imido)vanadium(v)-alkylidene complexes prepared by α-hydrogen elimination–abstraction in the presence of PMe_3.[45,55–61]

17.2.2 Reaction Chemistry with Vanadium–Alkylidene Complexes

Treatment of the cationic vanadium(IV)-alkylidene, $[(nacnac)V(CH^tBu)(THF)]^+[BPh_4]^-$ (**4**), with MgI_2 or I_2 afforded the neutral alkylidene, (nacnac)V(CH^tBu)(I) (**27**) and the subsequent alkylation of **27** with $LiCH_2SiMe_3$ gave the vanadium(IV)-alkyl, alkylidene complex, (nacnac)V(CH^tBu)(CH_2SiMe_3)

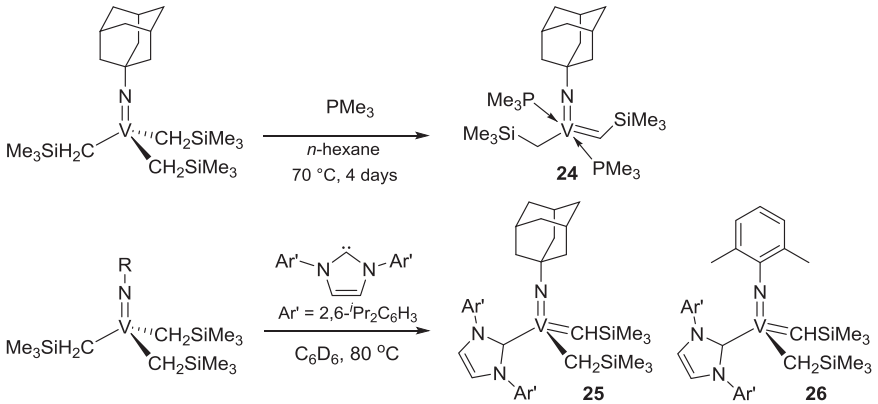

Scheme 17.4 Synthesis of (imido)vanadium(v)–alkyl, alkylidene complexes prepared by α-hydrogen elimination–abstraction.[62,63]

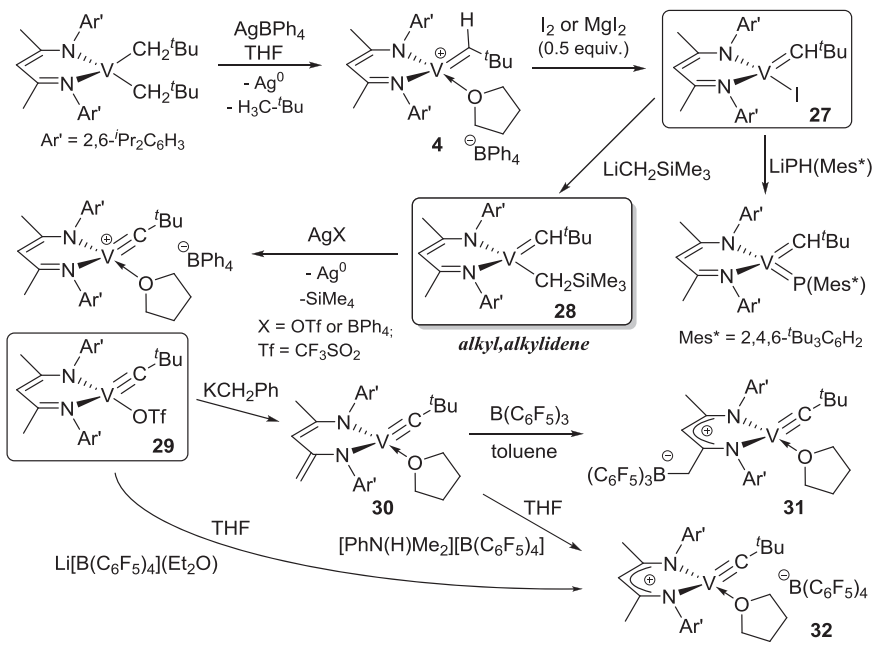

Scheme 17.5 Synthesis of vanadium(IV)–alkylidene and vanadium(v)–alkylidyne complexes and some reactions.[53,64,65]

(**28**), as shown in Scheme 17.5.[64] Treatment of **28** with AgOTf (Tf = CF_3SO_2) or $AgBPh_4$ afforded neutral or cationic vanadium(v)–alkylidyne complexes, $[(nacnac)V(C^tBu)(THF)]^+[BPh_4]^-$ or (nacnac)V(C^tBu)(OTf) (**29**).[53] Moreover, reaction of **27** with LiPH(Mes*) (Mes* = 2,4,6-^{t}Bu$_3$C$_6$H$_2$) or LiPH(2,4,6-^{i}Pr$_3$C$_6$H$_2$) afforded the corresponding vanadium(IV)–alkylidene, phosphinidene complexes.[65] Reaction of neutral vanadium(v)-alkylidyne (**29**)

with KCH_2Ph in THF resulted in another vanadium(v)-alkylidyne (**30**); the subsequent treatment with $B(C_6F_5)_3$ gave a zwitterionic vanadium(v)-alkylidyne complex (**31**) containing weakly coordinating borate moiety (WCA-nacnac).[65] The cationic vanadium(v)-alkylidyne complex (**32**) was obtained from **29** by reaction with $Li[B(C_6F_5)_4](Et_2O)$ and from **30** by treatment with $[PhN(H)Me_2][B(C_6F_5)_4]$.[65]

As shown in Scheme 17.6, addition of chalcogens to the vanadium(III) dialkyl complex containing the monoanionic chelate tridentate PNP ligand, $V(CH_2{}^tBu)_2(PNP)$ (**33**), gave the corresponding vanadium(v)–alkylidene chalcogenide species, $V(X)(CH^tBu)(PNP)$ (X = O, S, Se, Te, Scheme 17.6).[54] Similarly, treatment of **33** with N_2CPh_2 afforded the alkylidene-hydrazido complex, $V(CH^tBu)(=N\text{-}NCPh_2)(PNP)$[54] and the vanadium(v)-alkylidene, phosphinidene complex (**34**) was also obtained *via* phosphinidene-transfer with $Me_3P=PAr''$ ($Ar'' = 2,4,6\text{-}{}^tBu_3C_6H_2$).[66] The bridged end-on dinitrogen–alkylidene, $[(PNP)V(CH^tBu)]_2(\mu_2,\eta^1{:}\eta^1\text{-}N_2)$ (**35**) was formed when a toluene solution of **33** was placed under N_2 for several days or treating with 1 equiv. of $PhHC=PPh_3$ (or $Ph_3P=NPh$).[54] The related vanadium(III)–alkylidene complex was prepared upon addition of 2,2′-bipyridine (bpy) by α-hydrogen abstraction.[54] The reaction of **33** with 2 equiv. of ^{t}BuCN under N_2 afforded the bridged (imido)vanadium dinitrogen complex (**35**), whereas the reaction upon addition of excess ^{t}BuCN did not occur (even at 40 °C after 48 h).[67] These results suggest the presence of transient vanadium(III)–alkylidene intermediates.[66]

The ring-opened bis(imido) complexes $V(NAr)[NC(R)=CHSiMe_3](NC^tBu_2)(PMe_3)$ (**37**) were obtained (a mixture of *E*-, *Z*- isomers) by treating **2** with RC≡N (R = Me, ^{t}Bu, Ph, and the further nitrile insertion did not occur

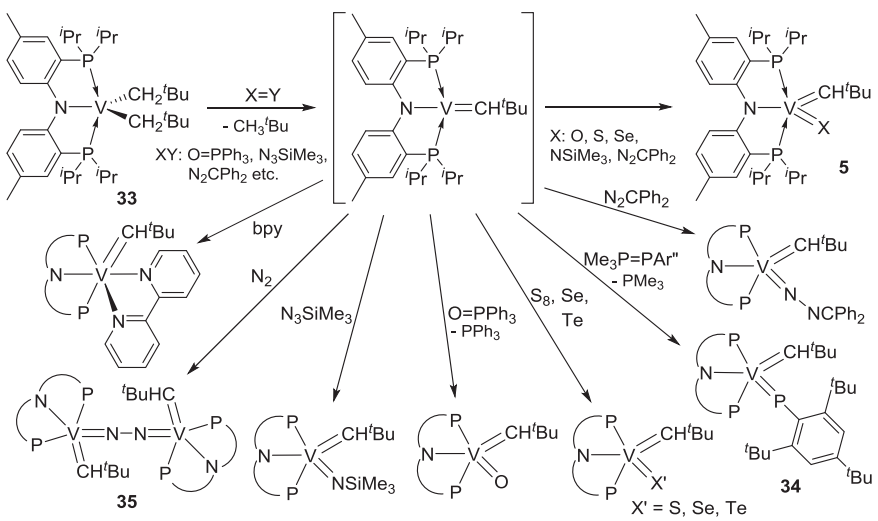

Scheme 17.6 Synthesis of various vanadium(v)-, vanadium(III)–alkylidene complexes via assumed $[(PNP)V(=CH^tBu)]$ intermediate.[54,66,67]

(Scheme 17.7).[68] CpV(CHCMe$_3$)(dmpe) (**1**) with ^{t}BuC≡N at 60 °C also afforded CpV[=NC(CMe$_3$)=CHCMe$_3$](dmpe) (**36**, 65% after 16 h).[46] Similar vinylimido complexes (a mixture of *E*-, *Z*- isomers) were obtained in the reactions of Ta(v)–alkylidenes, [Ta = CHR′] (R′ = ^{t}Bu, Ph), with nitriles,[69–71] and [Ti = CHR″] fragments (R″ = H, ^{t}Bu) with ^{t}BuC≡N[72,73] or (2,4,6-Me$_3$C$_6$H$_2$)CH$_2$CN;[74] the subsequent reaction with ^{t}BuC≡N (or reaction with 2 equiv. of PhC≡N) gave the diazatitanacyclohexadiene complex, assumed *via* azametalacyclobutene intermediate (and subsequent cross-metathesis).[72,73] It was assumed that the relatively small V centre in **1** caused the

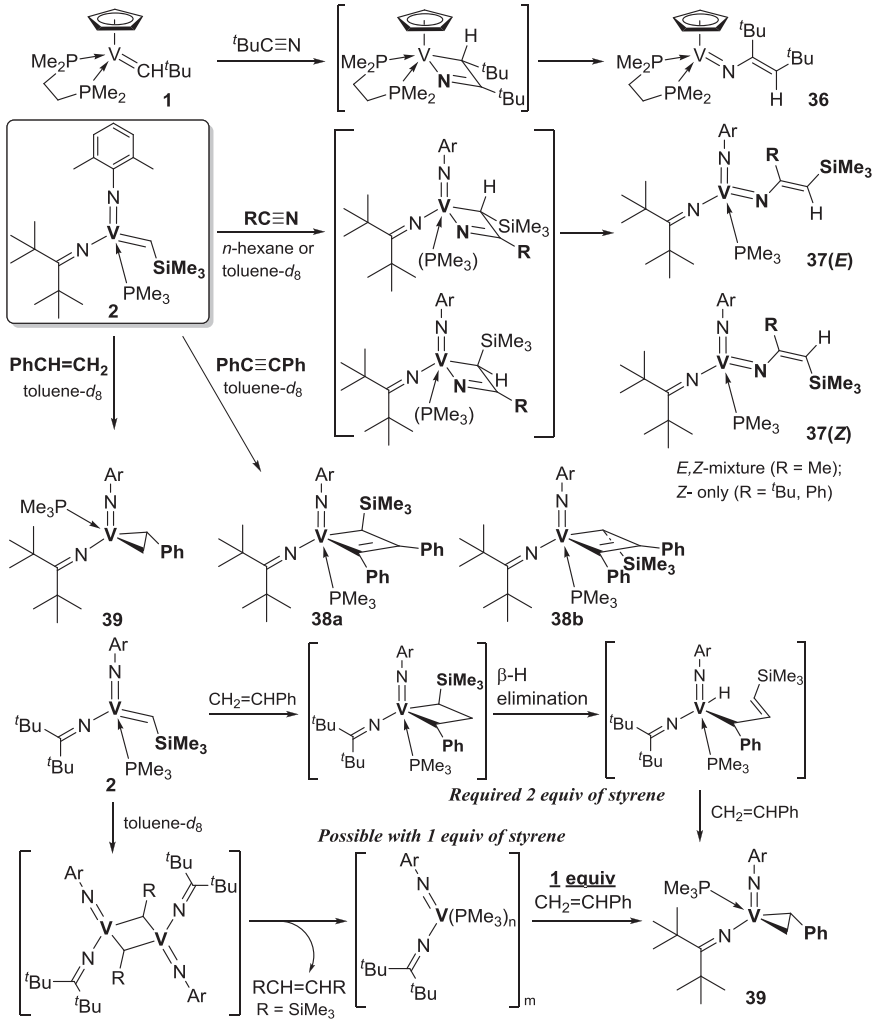

Scheme 17.7 Reactions of CpV(CH^{t}Bu)(dmpe) (**1**) or V(CHSiMe$_3$)(NAr)(N=C^{t}Bu$_2$) (**2**) with nitriles, and **2** with diphenyl acetylene, styrene.[46,68]

steric repulsion to prevail over the ^{t}Bu–^{t}Bu repulsion in the ring-opening step, thus affording the *Z* isomer exclusively.[46]

Reaction of **2** with 1.0 equiv. of PhC≡CPh afforded the corresponding metalacyclobutene analogue, (ArN)V[C(Ph)=C(Ph)CHSiMe$_3$)](NC^{t}Bu$_2$)(PMe$_3$) (**38a,b**).[68] The result seems to be analogous to that of the reaction of [Cp$_2$Ti=CH$_2$] with substituted acetylenes to form titanacylobutenes,[75] but could be a unique contrast to the reaction with CpTaCl$_2$(CHCMe$_3$) affording another alkylidene, CpTaCl$_2$[C(Ph)C(Ph)=CHCMe$_3$][70] and to the reaction of Ta(CHCMe$_3$)(O-2,6-^{i}Pr$_2$C$_6$H$_3$)$_3$(THF) yielding THF-free metallacyclobutene.[76]

Reaction of **2** with 1.0 equiv. of styrene afforded the metallacyclopropane analogue, V(NAr)(CH$_2$CHPh)(NC^{t}Bu$_2$) (**39**), exclusively under mild conditions. Two reaction pathways, formation of metallacylobutane and subsequent β-hydride elimination[77] or dimeric pathway by-producing Me$_3$SiHC=CHSiMe$_3$, could be considered; the latter pathway *via* vanadium(III) should be expected because the reaction with 1.0 equiv. of styrene yielded **39** exclusively.[68]

Reaction of the (imido)vanadium(v)-alkyl, alkylidene (**24**) with 1.0 equiv. of 2,6-Me$_2$C$_6$H$_3$OH (ArOH) gave V(CHSiMe$_3$)(NAd)(O-2,6-Me$_2$C$_6$H$_3$)(PMe$_3$)$_2$ (**40**) in high yield. In contrast, the reaction with C$_6$F$_5$OH in C$_6$D$_6$ afforded a mixture of the phenoxy-alkylidene (**41**) and the dialkyl analogue, V(NAd)(CH$_2$SiMe$_3$)$_2$(OC$_6$F$_5$), as well as the PMe$_3$ adduct. The conversion rate of **24** to form **41** was affected by addition of PMe$_3$ or use of C$_6$F$_5$OD in place of C$_6$F$_5$OH, and this strongly suggests that the reaction proceeds *via* coordination of C$_6$F$_5$OH after dissociation of one PMe$_3$ and subsequent reaction with the alkylidene or the alkyl moiety (Scheme 17.8).[62]

Reactions of V(NAr)(CH$_2$SiMe$_3$)$_3$ (Ar = 2,6-Me$_2$C$_6$H$_3$) with 1.0 equiv. of phenols and alcohols (with less steric bulkiness) took place cleanly at 25 °C

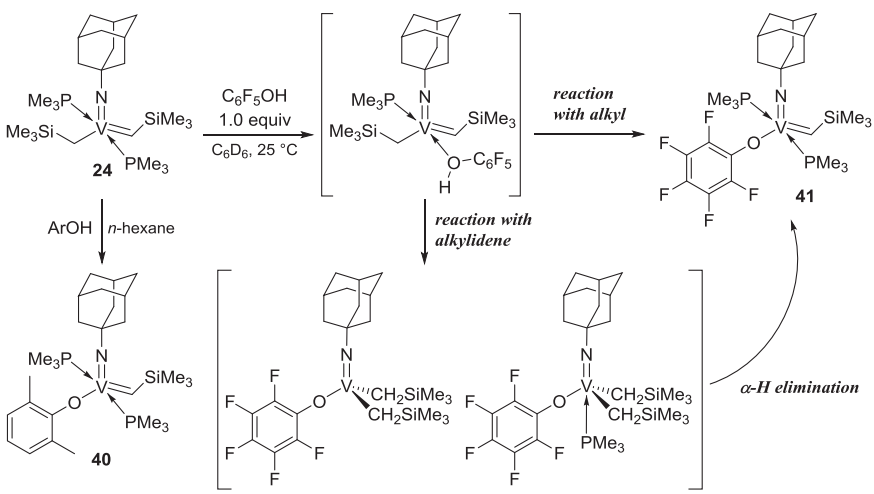

Scheme 17.8 Reaction of (imido)vanadium(v)-alkyl, alkylidene complexes (**24**) with phenols.[62]

to afford the corresponding dialkyl complexes in high yields (Scheme 17.9).[55] In contrast, the reaction with excess 2,6-^{t}Bu$_2$-4-MeC$_6$H$_2$OH did not take place (2.6 equiv. in $C_2D_2Cl_4$ at 50 °C).[55] Moreover, reaction of V(NAr)(CH$_2$SiMe$_3$)$_2$(OAr) with ArOH to yield V(NAr)(CH$_2$SiMe$_3$)(OAr)$_2$ required 50 h at 60 °C for completion, and no reaction took place at 25 °C.[78] Although early transition metal alkyls are in general more nucleophilic than those with late transition metals and are thus highly reactive towards Brönsted/Lewis acids, steric crowding contributes to their stability towards alcohols in some alkyl complexes with high oxidation state, such as tetrakis(alkyl)-chromium(IV)[79,80] and zirconium(IV)[81] complexes [exemplified as Cr^{t}Bu$_4$ and Zr(CH$_2$^{t}Bu)$_4$], and the (arylimido)vanadium(V) trialkyl complexes.[55,82]

In the reactions of V(NAr^1)(CH$_2$SiMe$_3$)$_3$ (Ar^1 = C$_6$H$_5$, 2-MeC$_6$H$_4$, 2,6-Me$_2$C$_6$H$_3$, 2,6-Cl$_2$C$_6$H$_3$) with 1.0 equiv. of various phenols (Ar^{2}OH, Ar^2 = 2,6-F$_2$C$_6$H$_3$, 2,6-Cl$_2$C$_6$H$_3$, 2,6-Me$_2$C$_6$H$_3$, 2,6-^{i}Pr$_2$C$_6$H$_3$, 2-^{t}BuC$_6$H$_4$, 2,6-^{t}Bu$_2$C$_6$H$_3$), the substitution rate was affected by the steric bulkiness in the arylimido ligand in the order: Ar^1 = 2,6-Me$_2$C$_6$H$_3$ < 2,6-Cl$_2$C$_6$H$_3$ < 2-MeC$_6$H$_4$ < C$_6$H$_5$.[82] The conversions in the reaction of V(NAr^1)(CH$_2$SiMe$_3$)$_3$ with various disubstituted phenols increased in the order: 2,6-^{i}Pr$_2$C$_6$H$_3$OH < 2,6-Me$_2$C$_6$H$_3$OH < 2,6-Cl$_2$C$_6$H$_3$OH < 2,6-F$_2$C$_6$H$_3$OH, irrespective of the kind of the aryl imido ligands present. In contrast, the reactions of V(NAr^1)(CH$_2$SiMe$_3$)$_3$ with 1.0 (and 3.0) equiv. of 2,6-^{t}Bu$_2$C$_6$H$_3$OH did not take place even at 60 °C. These results strongly suggest that the reactions proceed *via*

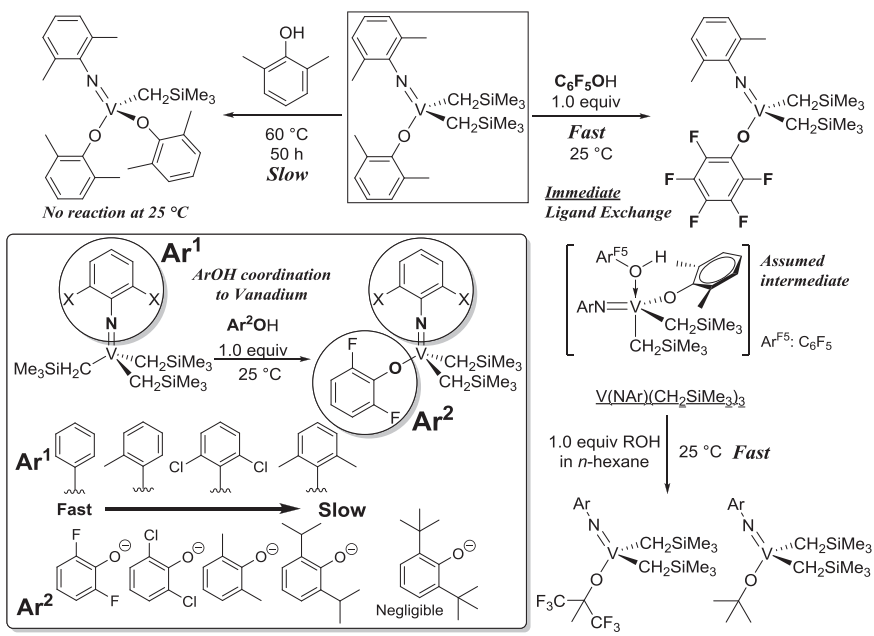

Scheme 17.9 Reactions of V(NAr)(CH$_2$SiMe$_3$)$_3$ with phenols, alcohols,[45,82] and fast phenoxy ligand exchange in V(NAr)(CH$_2$SiMe$_3$)$_2$(OAr) (Ar = 2,6-Me$_2$C$_6$H$_3$).[78]

coordination of ArOH to vanadium, and the reactivity is highly affected by a steric bulkiness of the arylimido ligand and the phenol. The hypothesis, *i.e.,* the reaction *via* coordination of phenol to vanadium, was also supported by the observed immediate phenoxide ligand exchange in $V(NAr)(CH_2SiMe_3)_2(OAr)$ with 1.0 equiv. of C_6F_5OH at 25 °C (Scheme 17.9).[78]

It turned out that 1,2-C–H (or C–D) activation occurred by simple thermolysis of (arylimido)vanadium(v) dialkyl precursors containing imidazolin-2-iminato or imidazolidine-2-iminato ligands in benzene,[56,58] whereas α-hydrogen abstraction–elimination is the common method[4–14] for synthesis of a series of (imido)vanadium(v)-alkylidenes (Scheme 17.10).[13,14,29] For instance, $V(NAr)(CHDSiMe_3)(C_6D_5)[1,3\text{-}Ar'_2(CHN)_2C{=}N]$ (**42-*d*$_6$**) was obtained quantitatively by thermolysis of the dialkyl complex in C_6D_6 (at 60 or 70 °C),[56] and the kinetic studies (conversion to **42-*d*$_6$**) at 70 °C revealed first-order kinetics; the result excluded a mechanism through a bimetallic

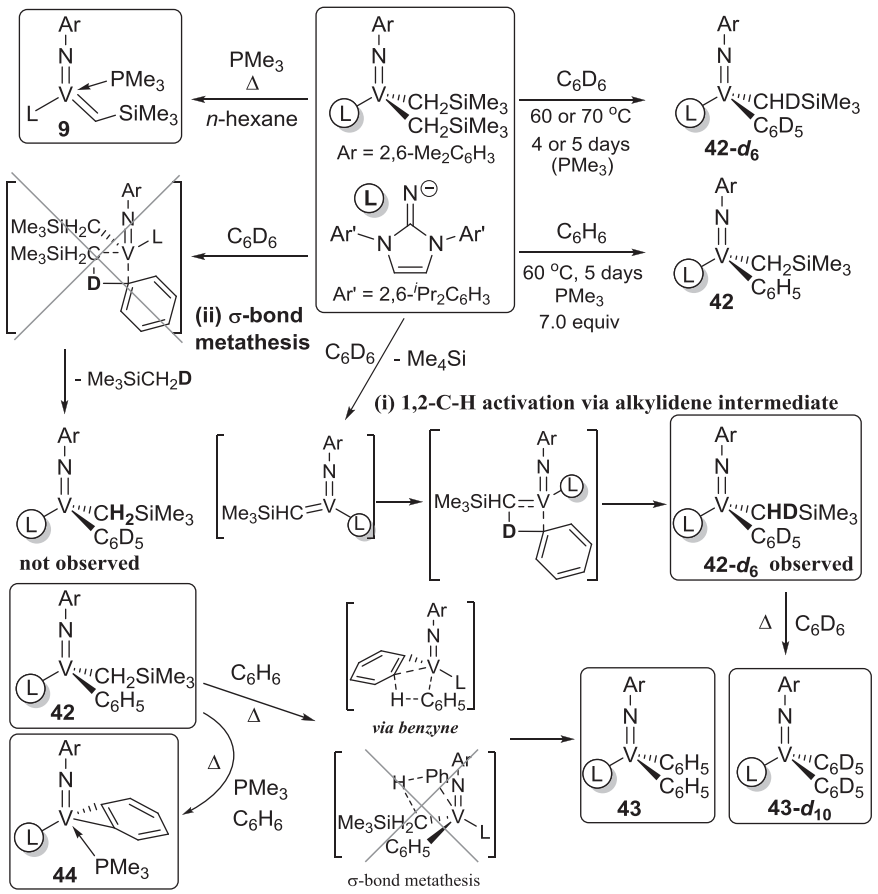

Scheme 17.10 1,2-C–H bond activation of benzene via vanadium(V)-alkylidene intermediate.[56]

intermediate. The corresponding alkylidene complex (**9**) was isolated by α-hydrogen abstractions in *n*-hexane in place of benzene upon addition of PMe_3. Two mechanisms, (i) 1,2-C–D activation *via* (initially generated) alkylidene intermediate or (ii) σ-bond metathesis between the dialkyl complex and C_6D_6, can be considered. The D atom in $CH\mathit{D}SiMe_3$ incorporated from C_6D_6 was confirmed in **42-*d*$_6$** by a ^{2}H NMR spectrum, whereas no resonances corresponding to D atoms in $C\mathit{D}_2SiMe_3$ (in the ^{2}H NMR spectrum) nor protons in $C\mathit{H}_2SiMe_3$ (in the ^{1}H NMR spectrum) were observed. The results strongly suggest that the reaction proceeds *via* 1,2-C–D bond activation of C_6D_6 *via* a vanadium(v)-alkylidene intermediate. This is in good agreement with a postulated mechanism in the reaction of (PNP)V($CH_2{}^t$Bu)$_2$ with C_6D_6 affording (PNP)V(C_6D_5)$_2$ [PNP = N{2-P^{i}Pr$_2$-4-Me-C_6H_3}$_2^-$] *via* a vanadium(III)–alkylidene intermediate.[83] Further reaction of **42** or **42-*d*$_6$** in C_6D_6 or C_6H_6 yielded the diphenyl complex (**43** or **43-*d*$_{10}$**). The same reaction in the presence of PMe_3 afforded the benzyne complex (**44**) as the proposed intermediate. It thus seems likely that the second C–H (C–D) activation would proceed via the benzyne intermediate.[56]

Thermolysis of the dialkyl complex (PNP)V($CH_2{}^t$Bu)$_2$ (**33**) in C_6D_6 afforded the assumed intermediate, (PNP)V[CH(D)^{t}Bu](C_6D_5), with monitoring formation of $CH_3{}^t$Bu and $CD_2H{}^t$Bu (by ^{1}H NMR and UV–VS spectroscopy and GC–MS) and subsequent oxidation with N_2O yielded a benzyne complex, (PNP)V=O(η^2-C_6D_4) (**45**), which was also prepared from thermolysis of **33** in C_6D_6 in the presence of N_2O.[83] The result suggests α-hydrogen abstraction to form [(PNP)N=CH^{t}Bu], prior to the C–H bond activation, and (PNP)V[CH(D)^{t}Bu](C_6D_5) could be an assumed intermediate generated by C–H bond activation. As considered in Scheme 17.10, a stepwise mechanism *via* a σ-bond metathesis of benzene (path 1, shown in Scheme 17.11) or a

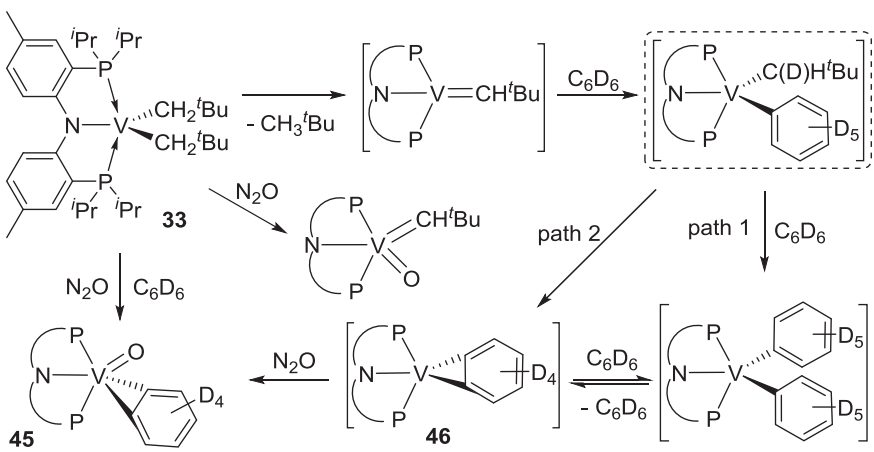

Scheme 17.11 1,2-C–H bond activation of benzene via vanadium(III)-alkylidene intermediate.[83]

concerted β-hydrogen abstraction step (path 2), were proposed to yield the vanadium(III) benzyne intermediate, (PNP)V(η^2-C_6D_4) (**46**).[83]

17.3 Ring-Opening Metathesis Polymerisation (ROMP) of Cyclic Olefins by Vanadium–Alkylidene Complex Catalysts

17.3.1 Ring-opening Metathesis Polymerisation (ROMP) of Norbornene (NBE) and the Derivative Using (Imido)Vanadium(V)–Alkylidene Complex Catalysts

Ring-opening metathesis polymerisation (ROMP) of cyclic olefins has been used as an efficient method especially for precision synthesis of advanced polymeric materials.[1–3,20–25] ROMP is the additional polymerisation induced by the release of the ring strain; norbornene derivatives have, thus, been employed as the monomers in most cases. As shown in Scheme 17.12, the polymerisation proceeds through coordination of cyclic olefin to the metal-alkylidene (carbene) and following formation of the ''metallacyclobutane'' intermediate for the subsequent (ring-opened) olefin metathesis. The ROMP proceeds in a living manner upon absence of chain-transfer process (inter/intra molecular olefin metathesis with international olefins in the resultant polymer) without catalyst deactivation; precise control of monomer repeat units and the end-group has thus been attained under certain optimised conditions.[20–25] ROMP demonstrated a tremendous utility as a powerful tool in preparing macromolecular materials displaying promising biological, electronic and mechanical properties.

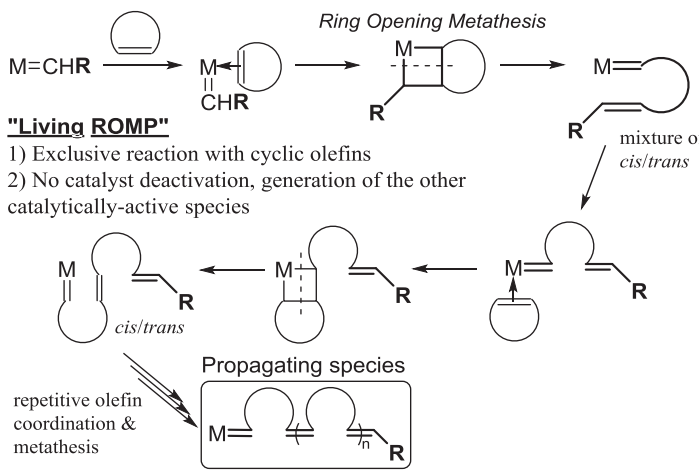

Scheme 17.12 General scheme for ring-opening metathesis polymerisation (ROMP).

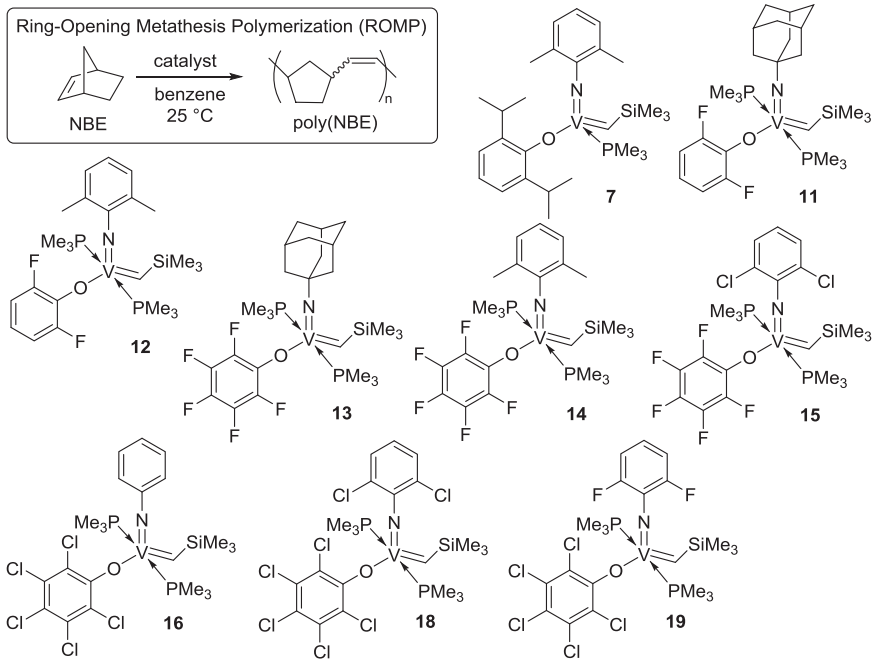

Scheme 17.13 Ring-opening metathesis polymerisation (ROMP) of norbornene (NBE) using $V(CHSiMe_3)(NR)(OR')(PMe_3)_n$ (**7**,**11-16**,**18**,**19**; R = Ad, C_6H_5, 2,6-$Me_2C_6H_3$, 2,6-$Cl_2C_6H_3$, 2,6-$F_2C_6H_3$; R′ = 2,6-$^i Pr_2C_6H_3$, 2,6-$F_2C_6H_3$, C_6F_5, C_6Cl_5; $n = 1$, 2).[55,59–61]

Reports on the synthesis of high oxidation state vanadium-alkylidene complexes that catalyse ROMP had been limited until recently.[13,14,25] (Imido)vanadium(v)–alkylidene complexes containing anionic ancillary donor ligands of the type, $V(CHSiMe_3)(NR)(X)(PMe_3)_n$ [R = adamantyl, aryl; X = phenoxide, alkoxide, ketimide, iminoimidazolide, iminoimidazolidide; $n = 1,2$; **2**,**7-23**, Scheme 17.13) exhibited moderate to high catalytic activities for ROMP of norbornene (NBE). The activities were affected by the imido and the anionic donor ligands.[55–61]

Table 17.1 summarises selected results in the ROMP of norbornene (NBE) using the phenoxide analogues of the type $V(CHSiMe_3)(NR)(OR')(PMe_3)_n$ [R = Ad, C_6H_5, 2,6-$Me_2C_6H_3$, 2,6-$Cl_2C_6H_3$, 2,6-$F_2C_6H_3$; R′ = 2,6-$^i Pr_2C_6H_3$, 2,6-$F_2C_6H_3$, C_6F_5, C_6Cl_5; $n = 1,2$]. The activity in the ROMP was affected by substituents on the phenoxide and the imido ligands employed; the OC_6F_5 analogues (**13–15**) showed higher activities than the O-2,6-$F_2C_6H_3$ (**11**,**12**) and the O-2,6-$^i Pr_2C_6H_3$ (**7**) analogues.[55,59,60] The activities by the OC_6F_5 analogues $V(CHSiMe_3)(NR)(OC_6F_5)(PMe_3)_2$ (**13–15**) increased in the order: R = Ad [**13**, TOF = 99 000 h^{-1} (27.5 s^{-1})] < 2,6-$Me_2C_6H_3$ [**14**, 230 000 (27.5)] < 2,6-$Cl_2C_6H_3$ [**15**, 552 000 (153)]. The activity by the 2,6-$Cl_2C_6H_3$ analogue (**15**) seemed improving upon addition of PMe_3, but the activity for the 2,6-$Me_2C_6H_3$ analogue (**14**) decreased even upon addition of a small

Table 17.1 Ring-opening metathesis polymerisation (ROMP) of norbornene (NBE) by V(CHSiMe$_3$)(NR)(OR′)(PMe$_3$)$_n$ [R = 1-adamantyl (Ad), C$_6$H$_5$, 2,6-Me$_2$C$_6$H$_3$, 2,6-Cl$_2$C$_6$H$_3$, 2,6-F$_2$C$_6$H$_3$; R' = 2,6-^{i}Pr$_2$C$_6$H$_3$, 2,6-F$_2$C$_6$H$_3$, C$_6$F$_5$, C$_6$Cl$_5$; n = 1,2] at 25 °C.[a,55,59–61]

Complex (μmol)	R	R′	PMe$_3$/equiv.	Time/min	TON[b]	TOF[b]/h^{-1} (s^{-1})	M_n[c]×10^{-4}	M_w/M_n[c]
7 (5.0)[d]	2,6-Me$_2$C$_6$H$_3$	2,6-^{i}Pr$_2$C$_6$H$_3$	—	60	150	150 (0.04)	3.1	1.1
11 (0.5)	Ad	2,6-F$_2$C$_6$H$_3$	—	5	1380	16 500 (4.58)	29	1.53
12 (0.5)	2,6-Me$_2$C$_6$H$_3$	2,6-F$_2$C$_6$H$_3$	—	5	3300	39 700 (11.0)	59	1.41
12 (0.3)	2,6-Me$_2$C$_6$H$_3$	2,6-F$_2$C$_6$H$_3$	—	3	3820	76 300 (21.2)	122	1.08
13 (0.3)	Ad	C$_6$F$_5$	—	3	4950	99 000 (27.5)	79	1.15
14 (0.1)	2,6-Me$_2$C$_6$H$_3$	C$_6$F$_5$	—	3	11 500	230 000 (63.9)	164	1.18
14 (0.3)	2,6-Me$_2$C$_6$H$_3$	C$_6$F$_5$	—	1	5650	339 000 (94.2)	117	1.22
14 (0.3)	2,6-Me$_2$C$_6$H$_3$	C$_6$F$_5$	0.1	3	1210	24 200 (6.7)	61.8	1.1
14 (0.3)	2,6-Me$_2$C$_6$H$_3$	C$_6$F$_5$	0.5	3	198	3960 (1.1)	12.4	1.03
15 (0.1)	2,6-Cl$_2$C$_6$H$_3$	C$_6$F$_5$	—	3	21 200[e]	424 000 (118)	110	1.27
15 (0.1)	2,6-Cl$_2$C$_6$H$_3$	C$_6$F$_5$	—	2	18 400	552 000 (153)	205	1.12
15 (0.1)	2,6-Cl$_2$C$_6$H$_3$	C$_6$F$_5$	3	2	20 100[e]	603 000 (168)	179	1.11
16 (0.1)	C$_6$H$_5$	C$_6$Cl$_5$	—	2	4000	120 000 (33.3)	107	1.61
16 (0.1)	C$_6$H$_5$	C$_6$Cl$_5$	—	3	5300	106 000 (29.5)	114	1.81
18 (0.1)	2,6-Cl$_2$C$_6$H$_3$	C$_6$Cl$_5$	—	2	16 600	498 000 (138)	128	1.57
18 (0.1)	2,6-Cl$_2$C$_6$H$_3$	C$_6$Cl$_5$	—	3	19 500	390 000 (108)	132	1.6
19 (0.1)	2,6-F$_2$C$_6$H$_3$	C$_6$Cl$_5$	—	2	15 900	477 000 (133)	152	1.55
19 (0.1)	2,6-F$_2$C$_6$H$_3$	C$_6$Cl$_5$	—	3	19 100	382 000 (106)	158	1.66
Mo-F$_0$ (1.0)[f]			—	10	1340	8040 (2.2)	19	1.02
Mo-F$_6$ (0.1)[f]			—	3	17 300	346 000 (96.1)	186	1.2

[a]Conditions: NBE 2.12 mmol, benzene 4.8 mL, initial NBE conc. 0.44 mmol mL^{-1}, 25 °C.
[b]TON (turnovers) = NBE reacted (mmol) V(mmol), TOF = TON per time.
[c]GPC data *vs.* polystyrene standards.
[d]Initial NBE 0.89 mmol mL^{-1}.
[e]Yield >85%
[f]In toluene. **Mo-F$_0$** = Mo(CHCMe$_2$Ph)(N-2,6-^{i}Pr$_2$C$_6$H$_3$)(O^{t}Bu)$_2$; **Mo-F$_6$** = Mo(CHCMe$_2$Ph)(N-2,6-Me$_2$C$_6$H$_3$)[OC(CH$_3$)(CF$_3$)$_2$]$_2$ (shown in Scheme 17.1).

amount of PMe_3.[59,60] The resultant polymers possessed ring-opened structure (confirmed by NMR spectra) with a mixture of *cis*- or *trans*-olefinic double bonds. Moreover, the resultant polymers exhibited ultrahigh molecular weights with low PDI (M_w/M_n) values, suggesting a possibility of living polymerisation. The activity by **15** was also higher than that by the known active molybdenum catalysts, **Mo-F$_6$** (TOF 346 000 h^{-1} after 3 min)[57] and **Mo-F$_0$** (8040 h^{-1} after 10 min).[59]

The activity of the OC_6Cl_5 analogues (**16**,**18**,**19**) was also affected by the imido ligand employed and the activity (after 2 min) increased in the order: R = Ph [**16**, TOF = 120 000 h^{-1} (33.3 s^{-1})] < 2,6-$Cl_2C_6H_3$ [**18**, 498 000 (138)], 2,6-$F_2C_6H_3$ [**19**, 477 000 (133)].[61] The activity by the 2,6-dimethylphenylimido analogue was low (TOF 48 000). The results suggest that an electronic factor in the arylimido ligand plays a role towards the activity,[59–61] as well as the introduction of electron-withdrawing groups on the imido and phenoxide ligands, generating electron deficient alkylidene species, leads to a higher activity; V(CHSiMe$_3$)(N-2,6-$Cl_2C_6H_3$)(OC_6F_5)(PMe_3)$_2$. Thus, (**15**) showed the highest activity for the ROMP of NBE.

Linear relationships between the polymer yield (TON; corresponding to conversion) and the M_n values were observed to be consistent with low PDI values (in all polymerisation runs conducted under the same initial NBE concentration conditions, Figure 17.1), irrespective of the kind of ligand set employed (**13**, **14**). Moreover, the first-order kinetics – linear relationships between $\ln[NBE]_t/[NBE]_0$ and the reaction time, where $[NBE]_0$, $[NBE]_t$ are the NBE concentration at the initial and at a certain time, respectively – without catalyst deactivation were also observed. These results thus clearly demonstrate that ROMPs proceeded in a living manner, affording ultrahigh

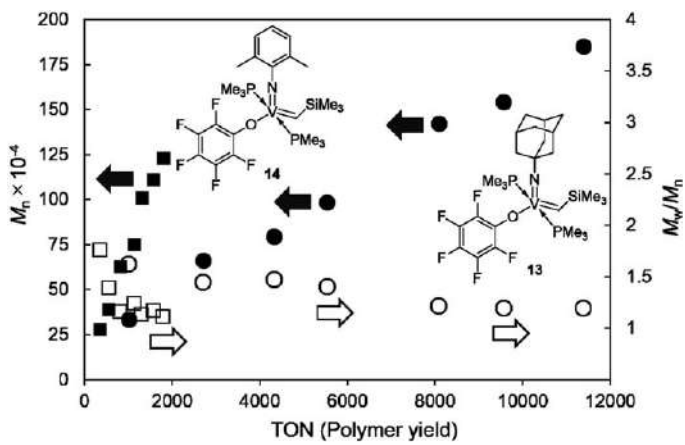

Figure 17.1 Plots of M_n and M_w/M_n *vs.* polymer yield (TON, turnover number) in ROMP of norbornene (NBE) using V(CHSiMe$_3$)(NR)(OC_6F_5)(PMe_3)$_2$ [R = 1-adamantyl (Ad, **13**), 2,6-$Me_2C_6H_3$ (Ar, **14**)]. Conditions: cat. 1.0 μmol (**13**) or 0.30 μmol (**14**), NBE 8.48 mmol in benzene, initial NBE concentration 0.22 mmol mL^{-1} at 25 °C.[60]

molecular weight polymers with narrow molecular weight distributions [low PDI (M_w/M_n) values].

Table 17.2 summarises selected results in the ROMP of norbornene (NBE) using the fluorinated alkoxide analogues of the type V(CHSi-Me_3)(NR)(OR′)(PMe_3)$_2$ [R = 2,6-$Me_2C_6H_3$ (Ar), 2,6-$Cl_2C_6H_3$ (Ar^{Cl}); R′ = C_6F_5, $C(CH_3)(CF_3)_2$ (F_6), $C(CF_3)_3$ (F_9)].[59,60] Note that olefinic double bonds in the resultant polymers prepared by the fluorinated alkoxide analogues (**22**,**23**) at 25 °C display a high *cis* selectivity (98%), although the resultant polymers prepared by the OC_6F_5 analogue (**15**) possess a mixture of *cis*- and *trans*-olefinic double bonds, confirmed by ^{1}H and ^{13}C NMR spectra. The $OC(CF_3)_3$ (F_9) analogues (**22**,**23**) showed much higher activity than that by the $OC(CH_3)(CF_3)_2$ (F_6) analogue (**21**). The activities by (**22**,**23**) increased with addition of PMe_3, but decreased by further additions. The activities by **22**,**23** increased by addition of PMe_3 even at 80 °C, probably due to improvement of stability of the active species by excess PMe_3, and the high *cis* percentages by **22**,**23** (97,98%) were maintained even at 50 and 80 °C in the presence of PMe_3. Although *cis* specific (*Z* selective) olefin metathesis reactions including ROMP using molybdenum[84–95] and ruthenium[96–107] complex catalysts have been known, these reactions were generally conducted at room temperature. Reports conducted at high temperature have been very limited so far, and the present catalysts (**22** and **23**) are rare examples as thermally robust, highly efficient *cis*-specific ROMP catalysts.

In the ROMP of NBE by **21**, the *cis* selectivities increased upon addition of PMe_3 (at 25 °C and 50 °C), and the resultant polymers by **20** at 25 °C exhibited bimodal molecular weight distributions with 85% of *cis* selectivity and the resultant polymers prepared at −20 °C possessed the unimodal distribution with high *cis* selectivity (96%). Taking into account these facts, it was assumed that coordination of NBE for subsequent metathesis would be controlled in this catalysis; NBE would coordinate to V *trans* (opposite) to PMe_3 and high *cis* selectivity would be achieved due to a proposed intermediate consisting of steric bulky small arylimido and large alkoxo ligands (Scheme 17.14).[60]

As summarised in Table 17.3, a highly efficient synthesis of end-functionalised ring-opened polymers has been achieved by combined *cis*-specific ROMP of NBE with terminal olefins [1-hexene, allyltrimethylsilane (ATMS) *etc*.] as the chain transfer (cross metathesis) agent in the presence of V($CHSiMe_3$)(N-2,6-$Cl_2C_6H_3$)[$OC(CF_3)_3$](PMe_3)$_2$ (**23**).[108] Although the activity in the ROMP at 25 °C (in the presence of PMe_3) slightly decreased upon addition of 1-hexene, the M_n values decreased upon increasing the 1-hexene concentration with broadening of the M_w/M_n values, clearly demonstrating that a certain degree of chain transfer (cross metathesis) reaction proceeded under these conditions. Moreover, the activity in the presence of 1-hexene at 80 °C was low in the absence of PMe_3, but it increased upon addition of this phosphine; both the activity and the M_n value were unchanged by varying the PMe_3/V molar ratios (10–100) under these conditions. The M_n values in the

Table 17.2 Ring-opening metathesis polymerisation (ROMP) of norbornene (NBE) by V(NR)(CHSiMe$_3$)(OR′)(PMe$_3$)$_2$ [R = 2,6-Me$_2$C$_6$H$_3$ (Ar), 2,6-Cl$_2$C$_6$H$_3$ (Ar^{Cl}); R′ = C$_6$F$_5$, C(CH$_3$)(CF$_3$)$_2$ (F$_6$), C(CF$_3$)$_3$ (F$_9$)].[a,59,60]

Complex (μmol)	R; R′	PMe$_3$/equiv.	Temp./°C	Time min^{-1}	TON[b]	TOF[b]/h^{-1} (s^{-1})	M_n[c]×10^{-24}	M_w/M_n[c]	*cis*/%
15 (0.1)	Ar^{Cl}; C$_6$F$_5$	—	25	3	21 200[e]	424 000 (118)	110	1.27	45
21 (1.0)	Ar^{Cl}; F$_6$	—	25	20	1000	3000	53	1.38	92
21 (1.0)	Ar^{Cl}; F$_6$	3	25	20	2090	6270	95	1.15	97
21 (1.0)	Ar^{Cl}; F$_6$	—	50	20	1460	4380	49	1.30	77
22 (1.0)	Ar^{Cl}; F$_6$	3	50	10	2120[e]	12 700 (3.52)	83	1.37	96
22 (0.3)	C$_6$H$_5$; F$_9$	—	25	3	4910	99 000 (27.5)	160	1.08	98
22 (0.3)	C$_6$H$_5$; F$_9$	3	25	3	6700	134 000 (37.2)	176	1.18	
22 (0.3)	C$_6$H$_5$; F$_9$	10	25	3	5990	120 000 (33.3)	139	1.22	98
22 (0.3)	C$_6$H$_5$; F$_9$	50	25	3	2110	42 200 (11.7)	79	1.15	
22 (0.3)	C$_6$H$_5$; F$_9$	—	50	3	5480	109 000 (30.3)	189	1.06	96
22 (0.3)	C$_6$H$_5$; F$_9$	3	50	3	7030[e]	141 000 (39.2)	168	1.17	95
22 (0.3)	C$_6$H$_5$; F$_9$	—	80	3	4670	93 400 (25.9)	156	1.09	93
22 (0.3)	C$_6$H$_5$; F$_9$	3	80	3	6900[e]	138 000 (38.3)	161	1.19	97
22 (0.3)	C$_6$H$_5$; F$_9$	10	80	3	6960[e]	139 000 (38.6)	146	1.2	97
23 (0.3)	Ar^{Cl}; F$_9$	—	25	3	3620	72 400 (20.1)	133	1.17	98
23 (0.3)	Ar^{Cl}; F$_9$	3	25	3	6250	125 000 (34.7)	142	1.23	98
23 (0.3)	Ar^{Cl}; F$_9$	10	25	3	4590	91 800 (25.5)	129	1.25	98
23 (0.3)	Ar^{Cl}; F$_9$	50	25	3	2160	43 200 (12.0)	86	1.22	98
23 (0.3)	Ar^{Cl}; F$_9$	—	80	3	4530	90 600 (25.2)	121	1.28	98
23 (0.3)	Ar^{Cl}; F$_9$	3	80	3	6850[e]	137 000 (38.1)	128	1.25	97

[a]Selected data cited from ref. 15, conditions: NBE 2.12 mmol, benzene 4.8 mL, initial NBE conc. 0.44 mmol mL^{-1}.
[b]TON (turnovers) = NBE reacted (mmol) V(mmol)$^{-1}$, TOF = TONper time.
[c]GPC data *vs.* polystyrene standards.
[d]*Cis* percentage (%) estimated by ^{1}H NMR spectra.
[e]Yield >97%.

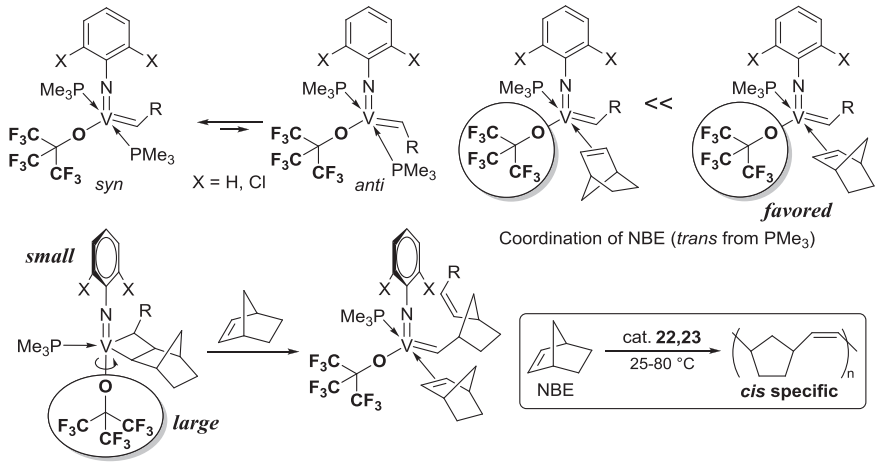

Scheme 17.14 *Cis*-specific ring-opening metathesis polymerisation (ROMP) of norbornene (NBE) by (imido)vanadium(v)–alkylidene catalysts.[59,60]

Table 17.3 Ring-opening metathesis polymerisation (ROMP) of norbornene (NBE) by V(CHSiMe$_3$)(N-2,6-Cl$_2$C$_6$H$_3$)[OC(CF$_3$)$_3$](PMe$_3$)$_2$ (**23**) in the presence of chain transfer agents (CTA).[a,108]

CTA (mol%)	PMe$_3$/ equiv.	Temp./ °C	TON[b]	TOF[b]/min^{-1} (s^{-1})	M_n[c]$\times10^{-4}$	M_w/M_n[c]	*cis*/ %
—	—	25	3620	1200 (20)	133	1.17	98
—	3	25	6270	2090 (35)	142	1.23	98
1-hexene (10.0)	—	25	3010	1000 (17)	8.67	1.67	
1-hexene (10.0)	10	25	4140	1380 (23)	7.64	1.79	
1-hexene (10.0)	—	80	1790	596 (9.9)	6.28	1.51	94
1-hexene (10.0)	3	80	3200	1070 (18)	4.80	1.74	97
1-hexene (10.0)	10	80	4350	1450 (24)	3.90	2.04	98
ATMS (5.0)	10	25	4890	1630 (27)	42.7	1.78	
ATMS (5.0)	10	80	5490	1830 (31)	15.2	2.46	
ATMS (10.0)	10	80	5590	1860 (31)	8.73	2.43	98
ATMS (30.0)	10	80	5740	1910 (32)	3.45	2.46	98
ATMS (50.0)	10	80	5590	1860 (31)	2.16	2.16	
ATMS (50.0)	10	80	5660	1890 (32)	1.94	2.43	97
1-octene (10.0)	10	80	2940	980 (16)	5.14	1.68	98
VCH (10.0)	10	80	6660	2220 (37)	9.85	2.35	98
VCHE (10.0)	10	80	5490	1830 (31)	9.97	1.95	98

[a]Conditions: complex 0.3 μmol, NBE 2.12 mmol, benzene 4.8 mL (initial NBE conc. 0.44 mmol mL^{-1}), 80 °C, 3 min.
[b]TON (turnovers) = NBE reacted (mmol) V(mmol)$^{-1}$, TOF = TON per time.
[c]GPC data in THF *vs.* polystyrene standards (M_n in g mol^{-1}).
[d]*Cis* percentage (%) estimated by ^{1}H NMR spectra. VCH = vinylcyclohexane, VCHE = 4-vinyl-1-cyclohexene.

polymers prepared at 80 °C (in the presence of 1-hexene) were lower than those prepared at 25 °C, suggesting that the degree of chain transfer (CM) was affected by the polymerisation temperature. The resultant polymers showed a high *cis* selectivity (97%–98%) if these chain-transfer ROMPs were conducted in the presence of PMe_3.[108]

The ROMP in the presence of ATMS proceeded with a high activity and a high *cis* selectivity (97%–98%) upon addition of PMe_3 and the M_n values could be controlled by varying the concentration of terminal olefins. The activity at 80 °C was not affected by the ATMS concentrations [5.0–50.0 mol%, TOF 1860–1890 min^{-1}].[108] Resonances corresponding to protons in the $SiMe_3$ and vinyl group (–CH=CH_2) were clearly observed with the integration ratios [9($SiMe_3$):3(–CH=CH_2)], strongly suggesting that the resultant polymers possessed $SiMe_3$ and the vinyl group at each polymer chain end. The ROMPs in the presence of vinylcyclohexane (VCH), 4-vinyl-1-cyclohexene (VCHE) also afforded the polymers with the M_n values that are close to those in the presence of ATMS, 1-hexene; protons corresponding to the vinyl group were also observed by their ^1H NMR spectra. The results suggest that the chain transfer ROMP (tandem ROMP and CM) proceeded in the presence of these olefins.[108]

Table 17.4 summarises selected results in ROMPs of 5-vinyl-2-norbornene (VNBE), 5-ethylidene-2-norbornene (ENB) and dicyclopentadiene (DCPD).[60] The catalytic activities in the ROMP of VNBE (without PMe_3 addition) increased in the order: TOF (h^{-1}) = 3240 (**22**) < 27 200 (**23**) < 167 000 (**15**). The activity by **23** showed to be much higher than that by **22** under the same conditions, as well as the activities upon addition of PMe_3. The activity by **15** was higher than those by the 2,6-dimethylphenylimido, adamantylimido analogues [TOF = 81 300 h^{-1} (**14**), 2770 (**13**), respectively].[59,60] The resultant polymer possessed low-molecular weights with rather broad molecular

Table 17.4 ROMP of 5-vinyl-2-norbornene (VNBE), 5-ethylidene-2-norbornene (ENB), dicyclopentadiene (DCPD) by $V(CHSiMe_3)(N\text{-}2,6\text{-}Cl_2C_6H_3)(OR')(PMe_3)_2$ [$R' = C_6F_5$ (**15**), $C(CF_3)_3$ (**23**)].[a,60]

Monomer	Cat. (μmol)	PMe_3 / equiv.	Time / min	Yield / %	TON[b]	TOF[b]/h^{-1} (s^{-1})	M_n[c]×10^{-4}	M_w/M_n[c]
VNBE	**15** (0.2)	—	3	79	8350	167 000 (46.3)	4.00	2.24
VNBE	**15** (0.2)	3.0	3	95	10000	200 000 (55.6)	3.18	2.37
VNBE	**23** (0.3)	—	3	19	1360	27 200 (7.6)	1.35	1.77
VNBE	**23** (0.3)	3.0	3	52	3730	74 600 (20.7)	1.69	1.56
ENB	**15** (0.2)	—	2	> 99	10600	318 000 (88.3)	80.5	1.34
ENB	**23** (0.5)	—	2	> 99	4240	127 000 (35.3)	12.8	2.39
DCPD	**15** (0.2)	—	3	48	5110	102 000 (28.3)	—[d]	—
DCPD	**23** (0.5)	—	3	73	3090	61 800 (17.2)	119	1.24

[a]Reaction conditions: monomer 2.12 mmol, total solvent (benzene) 4.8 mL (initial monomer conc. 0.44 mmol mL^{-1}), 25 °C.
[b]TON (turnovers) = monomer reacted (mmol) V(mmol)$^{-1}$, TOF = TON per time.
[c]GPC data in THF *vs.* polystyrene standards (M_n in g mol^{-1}).
[d]Insoluble (in THF, $CDCl_3$) for GPC measurement.

weight distributions ($M_w/M_n = 1.50–2.37$) suggesting the occurrence of certain chain transfer in this catalysis. In contrast, the M_n value in the resultant polymer in ROMP of ENB by **15** was an ultrahigh molecular weight with relatively narrow molecular weight distribution, and the observed activity was higher than those for VNBE conducted under the similar conditions. Moreover, **23** showed a higher activity than **22**, and dichlorophenylimido analogues (**15** and **23**) were thus effective for the ROMP of NBE derivatives.

Although the resultant polymers in the ROMP of DCPD prepared by **23** afforded high molecular weights with low PDI value ($M_w/M_n = 1.24$), the resultant polymer prepared by **15** was insoluble in ordinary GPC runs in THF (and ordinary GPC analysis in hot *o*-dichlorobenzene at 145 °C). The result with **15** clearly suggests the possibility of certain cross-linking by olefin metathesis of two olefinic double bonds (norbornene and cyclopentene units). It also suggests that **15** shows a higher reactivity than the others towards various cyclic olefins, as demonstrated next.

17.3.2 Ring-opening Metathesis Polymerisation (ROMP) of Cycloheptene (CHPE) and *Cis*-cyclooctene (COE) Using (Imido)Vanadium(V)–Alkylidene Complex Catalysts

The driving force in the ROMP has been invoked to be the release of the ring strain, and several reports concerning the effect of ring strain towards the activity in the ROMP – so-called low ring strain monomers, cyclopentene (CPE), cycloheptene (CHPE) and *cis*-cyclooctene (COE) – using neutral ruthenium-carbene catalysts[109,110] and Fischer-type tungsten–carbene catalyst[111] were known. However, reports in the ROMP of COE using early transition metal alkylidene complex catalysts were limited.

It was revealed that certain (arylimido)vanadium(v)–alkylidene catalysts are effective for ROMPs of low-ring strain monomers. As summarised in Table 17.5, the OC_6Cl_5 analogue (**18**) showed a higher activity than the OC_6F_5 analogue (**15**) in the ROMP of cycloheptene (CHPE) and the M_n value in the resultant polymer prepared by **18** increased upon increasing the polymer yields (TON) consistent with rather low PDI (M_w/M_n) values (Figure 17.2), demonstrating that the ROMPs proceeded in a living manner.[61] However, the polymer yields by the 2,6-difluorophenyl- imido (**19**) and the 2,6-dimethylphenylimido analogues were negligible.[61]

Selected results in ROMP of *cis*-cyclooctene (COE) using the OC_6F_5 analogue (**15**) or the OC_6Cl_5 analogue (**18**) in benzene are summarised in Table 17.6.[60,61,112] The activity by **18** was higher than that by **15**, and the observed activities based on the polymer yield became high when these ROMPs by **18** were conducted under low catalyst concentrations. The activity by **18** further increased at 100 °C and the initial activities by **18** at 120 °C seemed lower than that conducted at 100 °C (probably due to the catalyst

Table 17.5 ROMP of cycloheptene (CHPE) using $V(CHSiMe_3)(N\text{-}2,6\text{-}Cl_2C_6H_3)(OC_6F_5)(PMe_3)_2$ (**15**), $V(CHSiMe_3)(NR)(OC_6Cl_5)(PMe_3)_2$ [R = 2,6-$Cl_2C_6H_3$ (**18**), 2,6-$F_2C_6H_3$ (**19**)] at 25 °C.[a,61]

Catalyst	CHPE[b]/M	Time/min	TON[c]	TOF[d]/min^{-1} (s^{-1})	M_n[e]$\times10^{-4}$	M_w/M_n[e]
15	2.08	5	759	152 (2.53)	21.2	1.37
15	2.08	10	1330	133 (2.22)	35.3	1.4
15	2.08	15	1730	115 (1.92)	40	1.59
18	2.08	5	1340	268 (4.47)	31.6	1.55
18	2.08	10	2100	210 (3.50)	56.3	1.54
18	1.04	1	530	530 (8.83)	14.6	1.11
18	1.04	5	613	123 (2.05)	16.4	1.12
18	1.04	10	1200	120 (2.00)	42.9	1.31
18	1.04	15	1660	111 (1.85)	65.3	1.29
18	1.04	20	1780	89.0 (1.48)	80	1.38
19	1.04	30	510	17.0 (0.28)	17.2	1.55

[a]Conditions: catalyst 1.0 μmol, CHPE 10.0 mmol (initial conc. 2.08 M) or 5.0 mmol (initial conc. 1.04 M), CHPE + benzene total 4.8 mL.
[b]Initial CHPE conc. in mmol mL^{-1} (M).
[c]TON (turnover) = CHPE reacted (mmol) vanadium (mmol)$^{-1}$.
[d]TOF = TON per time.
[e]GPC data in THF *vs.* polystyrene standards.

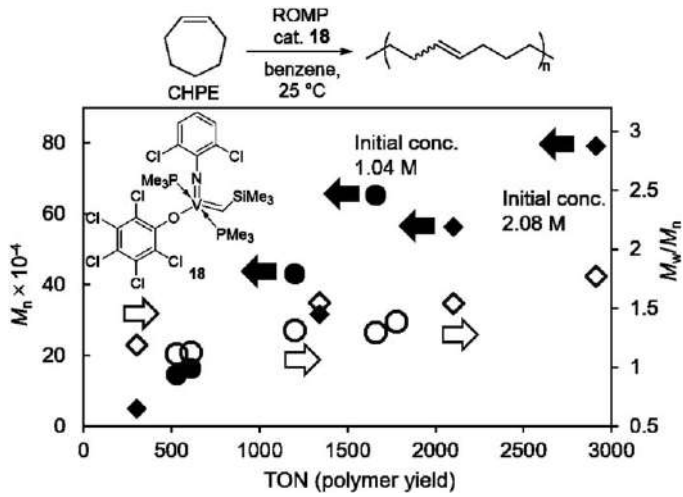

Figure 17.2 Plots of M_n and M_w/M_n *vs.* polymer yield (TON) in ROMP of cycloheptene (CHPE) using $V(CHSiMe_3)(N\text{-}2,6\text{-}Cl_2C_6H_3)(OC_6Cl_5)(PMe_3)_2$ (**18**). Conditions: cat. 1.0 μmol (**18**), 10.0 mmol (initial conc. 2.08 M) or 5.0 mmol (initial conc. 1.04 M) in benzene at 25 °C.

decomposition); however, the activity at 120 °C after 5 min improved with the presence of a small amount of PMe_3. In particular, the polymer yield in the ROMP by **18** increased over time and the activity increased at high temperature (25–80 °C). The M_n value in the resultant polymer increased with time, even at 50–80 °C (and 100 °C) without significant changes in the

Table 17.6 ROMP of *cis*-cyclooctene (COE) using V(CHSiMe$_3$)(N-2,6-Cl$_2$C$_6$H$_3$)(OC$_6$X$_5$)(PMe$_3$)$_2$ [X = F (**15**), Cl (**18**)].[a,60,61,112]

Cat. (μmol)	Temp./°C	Time/min	TON[b]	TOF[c]/min^{-1} (h^{-1})	M_n[d]×10^{-3}	M_w/M_n[d]
15 (20)	25	30	45	1.5 (90)	10.5	1.34
15 (20)	25	120	132	1.1 (66)	27	1.59
15 (10)	50	5	47	9.4 (564)	19.3	1.51
15 (10)	50	10	110	11.0 (660)	32	1.59
15 (10)	50	15	160	10.7 (640)	41.9	1.6
15 (10)	80	5	164	32.8 (1970)	52	1.46
15 (10)	80	10	259	25.9 (1550)	62.1	1.64
15 (10)	100	5	118	23.6 (1420)	42.2	1.6
15 (10)	100	10	140	14.0 (840)	54.6	1.36
18 (20)	50	1	83	83.0 (4980)	5.8	1.45
18 (20)	50	5	169	33.8 (2030)	28.2	1.51
18 (1.0)	50	5	889	178 (10 700)	55.4	1.45
18 (1.0)	50	10	1660	166 (9960)	80.3	1.47
18 (1.0)	50	15	1920	128 (7690)	90.1	1.49
18 (1.0)	80	2	1060	531 (31 900)	126	1.18
18 (1.0)	80	5	2490	497 (29 800)	226	1.24
18 (1.0)	100	5	2770	554 (33 200)	126	1.59
18 (1.0)	100	10	6450	645 (38 700)	509	1.32
18 (1.0)	120	2	2030	1020 (60 900)	44.4	1.55
18 (1.0)	120	5	2400	480 (28 800)	113	1.57
18 (1.0)[e]	120	5	2900	580 (34 800)	126	1.6

[a]Conditions: COE 10.0 mmol, benzene 0.5 mL.
[b]TON(turnover) = COE reacted (mmol) vanadium (mmol)$^{-1}$.
[c]TOF = TON per time.
[d]GPC data in THF *vs.* polystyrene standards (g mol^{-1}).
[e]Addition of PMe$_3$ (3.0 equiv.).

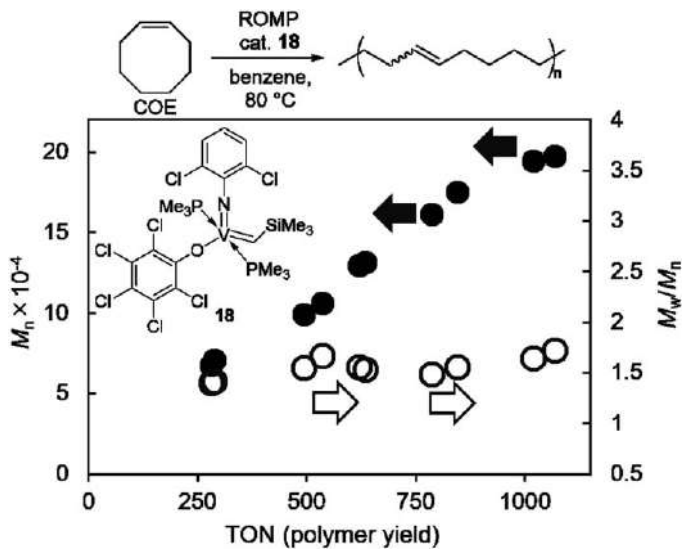

Figure 17.3 Plots of M_n and M_w/M_n *vs* TON (polymer yield) in ROMP of COE using V(CHSiMe$_3$)(N-2,6-Cl$_2$C$_6$H$_3$)(OC$_6$Cl$_5$)(PMe$_3$)$_2$ (**18**). Conditions: **18** 5.0 μmol, COE 10.0 mmol (initial conc. 2.08 M) in benzene at 80 °C.[61]

PDI (M_w/M_n) values. As shown in Figure 17.3, a linear relationship was demonstrated between the M_n values and the polymer yields (TON) till a relatively high COE conversion (*ca.* 50%), clearly demonstrating that the ROMP by **18** proceeded at 80 °C without catalyst decomposition and chain transfer. As far as we know, this is a very rare demonstration of high temperature (quasi) living ROMP using transition metal catalysts.[61]

17.4 Concluding Remarks

Reported examples for the synthesis of vanadium-alkylidene complexes and some reactions have been summarised in this chapter. There are several approaches for the synthesis of high oxidation state vanadium-alkylidenes (such as α-hydrogen elimination, benzylidene transfer, *etc.*) and α-hydrogen abstraction induced by oxidation or steric crowding (*e.g.*, addition of PMe_3, *etc.*) have been employed in the most recent examples. A series of (imido)vanadium(v)–alkylidene complexes, $V(CHSiMe_3)(NR)(Y)(PMe_3)_2$ – R = 1-adamantyl (Ad), 2,6-$X_2C_6H_3$ (X = H, Me, Cl, *etc.*); Y = aryloxide, alkoxide *etc.* – exhibit catalytic activities for ring-opening metathesis polymerisation (ROMP) of cyclic olefins. $V(CHSiMe_3)(N\text{-}2,6\text{-}Cl_2C_6H_3)(OC_6X_5)(PMe_3)_2$ [X = F (**15**), Cl (**18**)] displayed are markable activity, not only for ROMP of norbornene and the derivatives, but also for the ROMP of low-strained monomers such as cycloheptene and *cis*-cyclooctene. *Cis*-specific (living) ROMPs of NBE have been achieved with remarkable catalytic activities by the fluorinated alkoxide analogues, $V(CHSiMe_3)(N\text{-}2,6\text{-}X_2C_6H_3)[OC(CF_3)_3](PMe_3)_2$ [X = H (**22**), Cl (**23**)] and the activity increased upon addition of PMe_3 and/or at high temperature (50 and 80 °C) without decreasing the *cis* selectivity (98%) in the resultant polymers. The chain transfer ROMPs have also been demonstrated in the presence of terminal olefins. Thus, these catalysts should be promising candidates as thermally robust *cis*-specific (*Z* selective) metathesis catalysts. Although several concerns (*e.g.*, tacticity control, expansion of monomer scope, applications to the other olefin metathesis reactions such as cross metathesis,[113] ring-closing metathesis and acyclic diene metathesis, *etc.*) have to be explored along with the catalyst development, the promising potential of vanadium(v)–alkylidene complexes and of the organometallic chemistry including catalyst development are expected to be fruitful in the near future.

References

1. *Handbook of Metathesis*, ed. R. H. Grubbs, Wiley-VCH, Weinheim, Germany, 2003.
2. *Olefin Metathesis: Theory and Practice*, ed. K. Grela, John Wiley & Sons, Inc., Hoboken, New Jersey, USA, 2014.
3. *Handbook of Metathesis*, ed. R. H. Grubbs, A. G. Wenzel, D. J. O'Leary and E. Khosravi, Wiley-VCH, Weinheim, Germany, 2nd edn, 2015.
4. R. R. Schrock, *Acc. Chem. Res.*, 1979, **12**, 98.
5. R. R. Schrock, *Acc. Chem. Res.*, 1990, **23**, 158.

6. R. R. Schrock, in *Alkene Metathesis in Organic Synthesis*, ed. A. Fürstner, Springer, Berlin, Germany, 1998, p. 1.
7. R. R. Schrock, in *Handbook of Metathesis*, ed. R. H. Grubbs, Wiley-VCH, Weinheim, Germany, **vol. 1**, 2003, p. 8.
8. R. R. Schrock, *Chem. Rev.*, 2002, **102**, 145.
9. D. Mindiola, *Acc. Chem. Res.*, 2006, **39**, 813.
10. D. Mindiola, B. Bailey and F. Basuli, *Eur. J. Inorg. Chem.*, 2006, **16**, 3135.
11. R. R. Schrock, *Chem. Rev.*, 2009, **109**, 3211.
12. R. R. Schrock, *Acc. Chem. Res.*, 2014, **47**, 2457.
13. K. Nomura and X. Hou, *Dalton Trans.*, 2017, **46**, 12.
14. S. Zhang, W. Zhang and K. Nomura, *Adv. Organomet. Chem.*, 2017, **68**, 93.
15. A. Fürstner, *Angew. Chem., Int. Ed.*, 2000, **39**, 3012.
16. T. M. Trnka and R. H. Grubbs, *Acc. Chem. Res.*, 2001, **34**, 18.
17. R. R. Schrock and A. H. Hoveyda, *Angew. Chem., Int. Ed.*, 2003, **42**, 4592.
18. C. Samojzowicz, M. Bieniek and K. Grela, *Chem. Rev.*, 2009, **109**, 3708.
19. G. Vougioukalakis and R. H. Grubbs, *Chem. Rev.*, 2010, **110**, 1746.
20. M. R. Buchmeiser, *Chem. Rev.*, 2000, **100**, 1565.
21. *Handbook of Metathesis*, ed. R. H. Grubbs, Wiley-VCH, Weinheim, Germany, **vol. 3**, 2003.
22. K. Nomura and M. M. Abdellatif, *Polymer*, 2010, **51**, 1861.
23. A. Leitgeb, J. Wappel and C. Slugovc, *Polymer*, 2010, **51**, 2927.
24. *Handbook of Metathesis*, ed. R. H. Grubbs and E. Khosravi, Wiley-VCH, Weinheim, Germany, 2nd edn, **vol. 3**, 2015.
25. Y. Chen, M. M. Abdellatif and K. Nomura, *Tetrahedron*, 2018, **74**, 619.
26. H. Mutlu, L. M. de Espinosa and M. A. R. Meier, *Chem. Soc. Rev.*, 2011, **40**, 1404.
27. P. Atallah, K. B. Wagener and M. D. Schulz, *Macromolecules*, 2013, **46**, 4735.
28. L. Caire da Silva, G. Rojas, M. D. Schulz and K. B. Wagener, *Prog. Polym. Sci.*, 2017, **69**, 79.
29. K. Nomura and W. Zhang, *Chem. Sci.*, 2010, **1**, 161.
30. K. Nomura and S. Zhang, *Chem. Rev.*, 2011, **111**, 2342.
31. W. L. Carrick, *J. Am. Chem. Soc.*, 1958, **80**, 6455.
32. W. L. Carric, R. W. Kluiber, E. F. Bonner, L. H. Wartman, F. M. Rugg and J. J. Smyth, *J. Am. Chem. Soc.*, 1960, **82**, 3883.
33. G. W. Phillips and W. L. Carrick, *J. Polym. Sci.*, 1962, **59**, 401.
34. E. Junghanns, O. Gumboldt and G. Bier, *Makromol. Chem.*, 1962, **59**, 401.
35. G. Natta, G. Mazzanti, A. Valvassori, G. Sartori and D. Fiumani, *J. Polym. Sci.*, 1961, **51**, 411.
36. G. Natta, A. Zambelli, G. Lanzi, I. Pasquon, E. R. Mognaschi, A. L. Segre and P. Centola, *Makromol. Chem.*, 1965, **81**, 161.
37. A. Zambelli, I. Pasquon, R. Signorini and G. Natta, *Makromol. Chem.*, 1968, **112**, 160.
38. H. Hagen, J. Boersma and G. van Koten, *Chem. Soc. Rev.*, 2002, **31**, 357.

39. S. Gambarotta, *Coord. Chem. Rev.*, 2003, **237**, 229.
40. C. Redshaw, *Dalton Trans.*, 2010, **39**, 5595.
41. G. Dall'Asta, *J. Polym. Sci., Part A1*, 1968, **6**, 2397.
42. G. Natta, G. Dall'Asta and G. Mazzanti, *Angew. Chem.*, 1964, **76**, 765.
43. There is a description that homo- and heterogeneousvanadium catalysts (e.g. VCl3/AliBu3, VOCl3/AliBu3, VOCl3/Et3Al2Cl3) induced ROMP of norbornene instead of additionpolymerization, although no data were givenK. L. Makovetsky, L. I. Gorbachva, T. G. Golenko, I. Y. Ostrovskaya and G. N. Bondarenko, in *MetathesisPolymerization of Olefins and Polymerization of Alkynes*, ed. Y. Imamoglu, NATO ASI Series, Kluwer Academic Publishers, Dordrecht, Germany, 1988, p. 69.
44. K. Nomura and A. Sagara, *Macromolecules*, 2002, **35**, 1583.
45. J. Yamada and K. Nomura, *Organometallics*, 2005, **24**, 2248.
46. B. Hessen, A. Meetsma and J. H. Teuben, *J. Am. Chem. Soc.*, 1989, **111**, 5977.
47. B. Hessen, J.-K. F. Buijink, A. Meetsma, J. H. Teuben, G. Helgesson, M. Hakansson, S. Jagner and A. L. Spek, *Organometallics*, 1993, **12**, 2268.
48. J.-K. F. Buijink, J. H. Teuben, H. Kooijman and A. L. Spek, *Organometallics*, 1994, **13**, 2922.
49. M. Moore, S. Gambarotta, G. Yap, L. M. Liable-Sands and A. L. Rheingold, *Chem. Commun.*, 1997, 643.
50. G. Erker, R. Lecht, R. Schlund, K. Angermund and C. Krüger, *Angew. Chem., Int. Ed.*, 1987, **26**, 666.
51. M. Berlekamp, G. Erker and J. L. Petersen, *J. Organomet. Chem.*, 1993, **458**, 97.
52. R. Milczarek, W. Rüsseler, P. Binger, K. Jonas, K. Angermund, C. Kruger and M. Regitz, *Angew. Chem., Int. Ed.*, 1987, **26**, 908.
53. F. Basuli, U. J. Kilgore, X. Hu, K. Meyer, M. Pink, J. C. Huffman and D. J. Mindiola, *Angew. Chem., Int. Ed.*, 2004, **43**, 3156.
54. U. J. Kilgore, C. A. Sengelaub, M. Pink, A. R. Fout and D. J. Mindiola, *Angew. Chem., Int. Ed.*, 2008, **47**, 3769.
55. K. Nomura, Y. Onishi, M. Fujiki and J. Yamada, *Organometallics*, 2008, **27**, 3818.
56. S. Zhang, M. Tamm and K. Nomura, *Organometallics*, 2011, **30**, 2712.
57. K. Nomura, K. Suzuki, S. Katao and Y. Matsumoto, *Organometallics*, 2012, **31**, 5114.
58. K. Nomura, B. K. Bahuleyan, K. Tsutsumi and A. Igarashi, *Organometallics*, 2014, **33**, 6682.
59. X. Hou and K. Nomura, *J. Am. Chem. Soc.*, 2015, **137**, 4662.
60. X. Hou and K. Nomura, *J. Am. Chem. Soc.*, 2016, **138**, 11840.
61. S. Chaimongkolkunasin and K. Nomura, *Organometallics*, 2018, **37**, 2064.
62. K. Hatagami and K. Nomura, *Organometallics*, 2014, **33**, 6585.
63. W. Zhang and K. Nomura, *Organometallics*, 2008, **27**, 6400.

64. F. Basuli, B. C. Bailey, D. Brown, J. Tomaszewski, J. C. Huffman, M.-H. Baik and D. J. Mindiola, *J. Am. Chem. Soc.*, 2004, **126**, 10506.
65. F. Basuli, B. C. Bailey, J. C. Huffman, M.-H. Baik and D. J. Mindiola, *J. Am. Chem. Soc.*, 2004, **126**, 1924.
66. U. J. Kilgore, H. Fan, M. Pink, E. Urnezius, J. D. Protasiewicz and D. J. Mindiola, *Chem. Commun.*, 2009, 4521–4523.
67. U. J. Kilgore, C. A. Sengelaub, H. Fan, J. Tomaszewski, J. A. Karty, M.-H. Baik and D. J. Mindiola, *Organometallics*, 2009, **28**, 843.
68. W. Zhang, J. Yamada and K. Nomura, *Organometallics*, 2008, **27**, 5353.
69. R. R. Schrock and J. D. Fellmann, *J. Am. Chem. Soc.*, 1978, **100**, 3359.
70. C. D. Wood, S. J. McLain and R. R. Schrock, *J. Am. Chem. Soc.*, 1979, **101**, 3210.
71. K. Mashima, H. Yonekura, T. Yamagata and K. Tani, *Organometallics*, 2003, **22**, 3766.
72. K. M. Doxsee, J. B. Farahi and H. Hope, *J. Am. Chem. Soc.*, 1991, **113**, 8889.
73. H. van der Heiden and B. Hessen, *Inorg. Chim. Acta*, 2003, **345**, 27.
74. F. Basuli, B. C. Bailey, L. A. Watson, J. Tomaszewski, J. C. Huffman and D. J. Mindiola, *Organometallics*, 2005, **24**, 1886.
75. F. N. Tebbe and R. L. Harlow, *J. Am. Chem. Soc.*, 1980, **102**, 6149.
76. K. C. Wallace, A. H. Liu, W. M. Davis and R. R. Schrock, *Organometallics*, 1989, **8**, 644.
77. W. C. P. Tsang, J. Y. Jamieson, S. L. Aeilts, K. C. Hultzsch, R. R. Schrock and A. H. Hoveyda, *Organometallics*, 2004, **23**, 1997.
78. K. Nomura and Y. Matsumoto, *Organometallics*, 2011, **30**, 3610.
79. W. Kruse, *J. Organomet. Chem.*, 1972, **42**, C39.
80. W. Mowat, A. J. Shortland, N. J. Hill and G. Wilkinson, *J. Chem. Soc., Dalton Trans.*, 1973, 770.
81. T. V. Lubben, P. T. Wolczanski and G. D. van Duyne, *Organometallics*, 1984, **3**, 977.
82. H. Hayashibara, A. Ngamnithiporn and K. Nomura, *ACS Omega*, 2019, **4**, 5818.
83. J. G. Andino, U. J. Kilgore, M. Pink, A. Ozarowski, J. Krzystek, J. Telser, M.-H. Baik and D. J. Mindiola, *Chem. Sci.*, 2010, **1**, 351.
84. I. Ibrahem, M. Yu, R. R. Schrock and A. H. Hoveyda, *J. Am. Chem. Soc.*, 2009, **131**, 3844.
85. M. M. Flook, A. J. Jiang, R. R. Schrock, P. Muller and A. H. Hoveyda, *J. Am. Chem. Soc.*, 2009, **131**, 7962.
86. A. J. Jiang, Y. Zhao, R. R. Schrock and A. H. Hoveyda, *J. Am. Chem. Soc.*, 2009, **131**, 16630.
87. S. Torker, A. Müller and P. Chen, *Angew. Chem., Int. Ed.*, 2010, **49**, 3762.
88. M. M. Flook, L. C. H. Gerber, G. T. Debelouchina and R. R. Schrock, *Macromolecules*, 2010, **43**, 7515.
89. S. J. Meek, R. V. O'brien, J. Llaveria, R. R. Schrock and A. H. Hoveyda, *Nature*, 2011, **471**, 461.

90. M. M. Flook, V. W. L. Ng and R. R. Schrock, *J. Am. Chem. Soc.*, 2011, **132**, 1784.
91. S. C. Marinescu, R. R. Schrock, P. Müller, M. K. Takase and A. H. Hoveyda, *Organometallics*, 2011, **30**, 1780.
92. M. J. Koh, T. T. Nguyen, H. Zhang, R. R. Schrock and A. H. Hoveyda, *Nature*, 2016, **531**, 459.
93. J. Hyvl, B. Autenrieth and R. R. Schrock, *Macromolecules*, 2015, **48**, 3148.
94. B. Autenrieth, H. Jeong, W. P. Forrest, J. C. Axtell, A. Ota, T. Lehr, M. R. Buchmeiser and R. R. Schrock, *Macromolecules*, 2015, **48**, 2480.
95. M. J. Koh, T. T. Nguyen, J. K. Lam, S. Torker, J. Hyvl, R. R. Schrock and A. H. Hoveyda, *Nature*, 2017, **542**, 80.
96. K. Endo and R. H. Grubbs, *J. Am. Chem. Soc.*, 2011, **133**, 8525.
97. B. K. Keitz, K. Endo, M. B. Herbert and R. H. Grubbs, *J. Am. Chem. Soc.*, 2011, **133**, 9686.
98. B. K. Keitz, K. Endo, P. R. Patel, M. B. Herbert and R. H. Grubbs, *J. Am. Chem. Soc.*, 2012, **134**, 693.
99. B. K. Keitz, A. Fedorov and R. H. Grubbs, *J. Am. Chem.Soc.*, 2012, **134**, 2040.
100. V. M. Marx, M. B. Herbert, B. K. Keitz and R. H. Grubbs, *J. Am. Chem. Soc.*, 2013, **135**, 94.
101. L. E. Rosebrugh, M. B. Herbert, V. M. Marx, B. K. Keitz and R. H. Grubbs, *J. Am. Chem. Soc.*, 2013, **135**, 1276.
102. G. Occhipinti, F. R. Hansen, K. W. Törnroos and V. R. Jensen, *J. Am. Chem. Soc.*, 2013, **135**, 3331.
103. J. S. Cannon and R. H. Grubbs, *Angew. Chem., Int. Ed.*, 2013, **52**, 9001.
104. R. K. M. Khan, S. Torker and A. H. Hoveyda, *J. Am. Chem. Soc.*, 2013, **135**, 10258.
105. J. Hartung and R. H. Grubbs, *J. Am. Chem. Soc.*, 2013, **135**, 10183.
106. R. K. M. Khan, S. Torker and A. H. Hoveyda, *J. Am. Chem. Soc.*, 2014, **136**, 14337.
107. M. J. Koh, R. K. M. Khan, S. Torker, M. Yu, M. S. Mikus and A. H. Hoveyda, *Nature*, 2015, **517**, 181.
108. K. Nomura and X. Hou, *Organometallics*, 2017, **36**, 4103.
109. A. Hejl, O. A. Scherman and R. H. Grubbs, *Macromolecules*, 2005, **38**, 7214.
110. A. R. Hlil, J. Balogh, S. Moncho, H. L. Su, R. Tuba, E. N. Brothers, M. Al-Hashimi and H. S. Bazzi, *J. Polym. Sci., Part A: Polym. Chem.*, 2017, **55**, 3137.
111. T. J. Katz, S. J. Lee and N. Acton, *Tetrahedron Lett.*, 1976, **17**, 4247.
112. S. Chaimongkolkunasin, X. Hou and K. Nomura, *J. Polym. Sci., Part A: Polym. Chem.*, 2017, **55**, 3067.
113. W. S. Farrell, *Organometallics*, 2019, **38**, 3481.

CHAPTER 18

Vanadium-catalyzed Enantioselective C–C Bond-forming Reactions

MAKOTO SAKO, SHINOBU TAKIZAWA* AND HIROAKI SASAI*

The Institute of Scientific and Industrial Research (ISIR), Osaka University, Mihogaoka, Ibaraki-shi, Osaka 567-0047, Japan,
*Emails: taki@sanken.osaka-u.ac.jp; sasai@sanken.osaka-u.ac.jp

18.1 Introduction: Enantioselective Oxidative-coupling of Naphthol Derivatives

Metal-mediated carbon–carbon (C–C) bond-forming reactions concern the most important and straightforward methods used to construct complicated organic molecules such as fine chemicals, pharmaceuticals and natural products.[1] The impact of these methods was recognized by the 2010 Nobel Prize in Chemistry being awarded to Professors Negishi, Suzuki and Heck for their contributions toward the development of Pd-catalyzed cross-coupling reactions.[2] Currently, the primary goal for synthetic chemists is to provide efficient ways to perform chemo-, regio- and enantioselective C–C bond-forming reactions to avoid or minimize the formation of undesired side-products and toxic waste, thus leading to environmentally benign chemical syntheses.[3] Among them, vanadium complexes are recognized as green metal catalysts because of the high natural abundance of vanadium as well as its low toxicity when compared to other metals.[4] Over the past few decades, the use of chiral vanadium catalysts has been extended to a variety of

Catalysis Series No. 41
Vanadium Catalysis
Edited by Manas Sutradhar, José Armando L. da Silva and Armando J. L. Pombeiro

Published by the Royal Society of Chemistry, www.rsc.org

different and complementary enantioselective transformations,[5,6] such as C–C bond-forming reactions including cyanide addition to carbonyl compounds,[6a] Friedel–Crafts-type reactions,[6b] Diels–Alder reactions[6c] and pinacol coupling reactions.[6d] Inspired by the multiple activation of substrates in nature (*e.g.*, bromoperoxidase, nitrogenase, *etc.*), chiral dinuclear vanadium complexes have been mainly designed for use in the enantioselective coupling of 2-naphthol derivatives.[7,8]

In 1969, Carrick first reported that either VCl_4 or $VOCl_3$ can catalyze the coupling of 2-naphthol to produce 1,1′-bi-2-naphthol (BINOL),[9] which is utilized as an efficient building block in a wide range of highly stereoselective organic synthetic reactions.[10] Vanadium-mediated couplings, which occur *via* a favorable one-electron phenolic oxidation mechanism, proceed under mild reaction conditions and tolerate many functional groups, with water formed as the only side product in the reaction. A further advantage of vanadium complex-mediated enantioselective couplings is that neither a directing group nor bulky substituent at the 3-position of the 2-naphthol starting material is essential for high asymmetric induction when compared to that needed using other metal catalysts, such as Cu and Fe complexes.[11]

In 2001, Uang[12a] and Chen[13a] independently reported the first efficient chiral vanadium(IV) catalysts **1** and **2** (Figure 18.1). These vanadium catalysts showed good enantioselectivity (up to 68% ee) in the coupling of 2-naphthol derivatives **5**. Uang found that the activity of the vanadium catalyst could be improved by the addition of a Lewis[12a] or Brønsted acid.[12b]

In 2002, Chen[13b] achieved an enantioselectivity of 87% ee in coupling product **6** for the first time when using a ketopinidine-based vanadium catalyst **3**; however, a long reaction time was required.

An increased enantioselectivity (up to 98% ee) was achieved by Gong using 10 mol% of dinuclear vanadium catalyst **4** bearing a V–O–V linkage.[7a] However, a long reaction time (120–192 h) was still required and the use of 7-substituted 2-naphthol derivatives as starting materials was essential to establish excellent results; when the reaction of unsubstituted 2-naphthol was carried out using catalyst **4**, (*R*)-BINOL (**6a**, $R^n = H$) was obtained in 58% yield and 60% ee.

Thus, the development of a catalyst fulfilling the criteria of both high enantioselectivity and activity has remained a significant challenge for a considerable period of time. Inspired by enzymatic activation using multifunctional chiral catalysts, such as $LaLi_3$tris(binaphthoxide) (LLB) and AlLibis(binaphthoxide) (ALB),[14] Sasai and co-workers applied the dual activation concept to design dinuclear vanadium(IV) catalyst (R_a,*S,S*)-**7** (Figure 18.2)[8a] prepared from $VOSO_4$, 3,3′-formyl-(*R*)-BINOL and (*S*)-*tert*-leucine. In the presence of 5 mol% of (R_a,*S,S*)-**7**, (*S*)-BINOL was obtained in 76% yield with high enantioselectivity (91% ee) after 24 h. Since diastereomeric catalyst (S_a,*S*,*S*)-**7** is less active and represents a mismatched pair during the oxidative coupling reaction of **5**, (R_a,*S*,*S*)-**7** is a matched pair for the coupling.

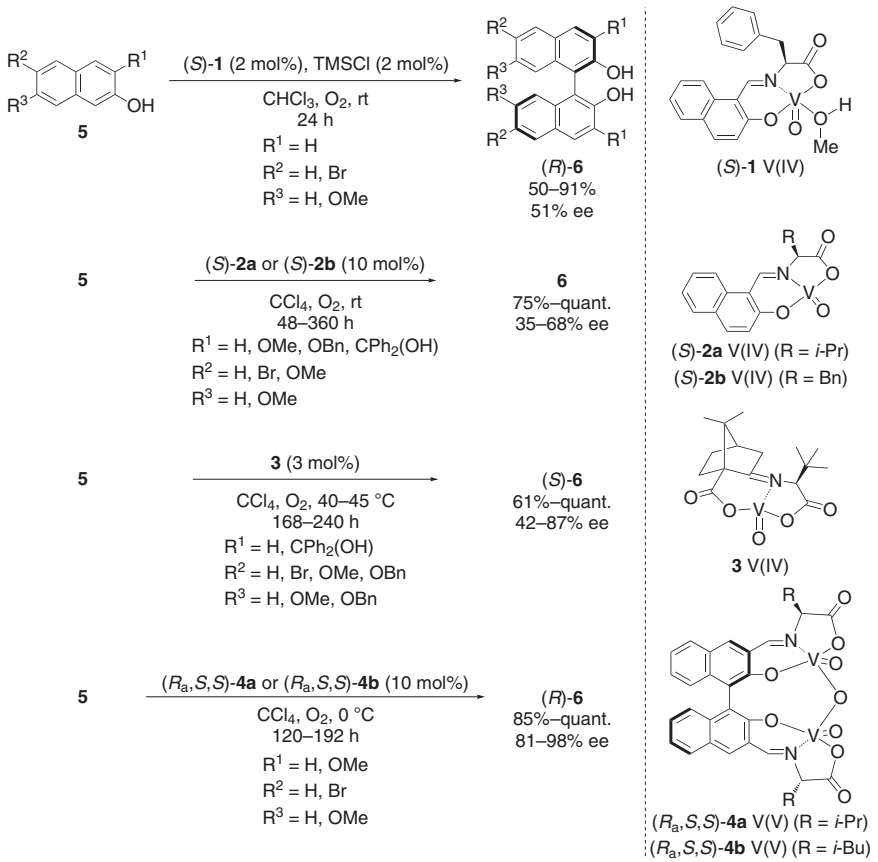

Figure 18.1 Catalytic and enantioselective oxidative coupling of 2-naphthol derivatives using vanadium complexes, independently reported by Uang, Chen and Gong.

Kinetic analysis showed that the reactions catalyzed by dinuclear vanadium complex (R_a,*S,S*)-**7** and mononuclear vanadium complex (*S*)-**9** obeyed a second-order kinetic model up to 15 h. Although mononuclear complex (*S*)-**9** gave racemic BINOL in low yield, the coupling rate in the presence of 5 mol% of (R_a,*S,S*)-**7** was found to be 48.3-times faster than that observed using 10 mol% of (*S*)-**9**.

During further investigations, single crystals suitable for X-ray analysis were obtained as an adduct with NaOH upon recrystallization of (R_a,*S,S*)-**7** from MeOH-Et_2O-H_2O in the presence of NaOAc.[8b] The X-ray structure suggested that the complexes had been oxidized into a distorted octahedral vanadium(v) species with one extra hydroxide on each vanadium center (Figure 18.3a). The hydroxide is *anti* to the imine nitrogen atom. The V=O bonds are *syn* to the *tert*-butyl groups in the template. The sodium cation is coordinated by the oxygen atoms of the two carboxylic groups in the (*S*)-*tert*-leucine moieties.

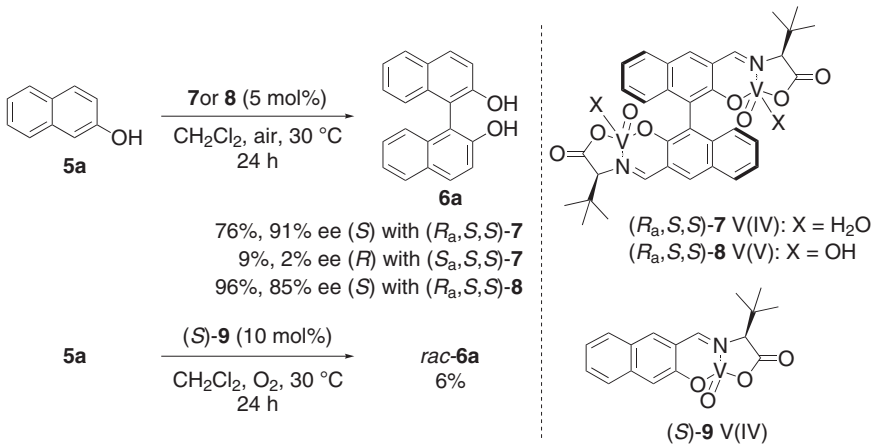

Figure 18.2 Enantioselective coupling of 2-naphthol using dinuclear and mononuclear vanadium catalysts, reported by Sasai.

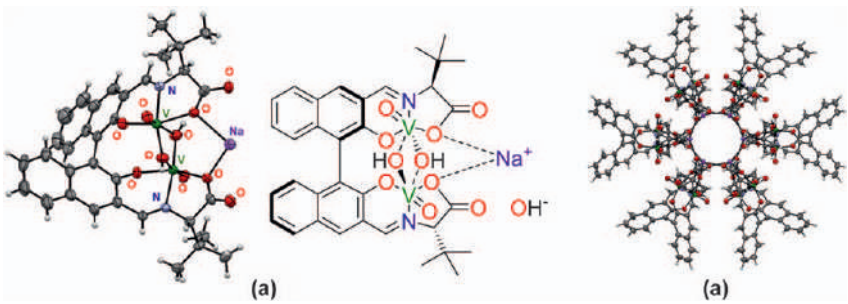

Figure 18.3 (a) The structure of dinuclear vanadium(v) complex (R_a,*S*,*S*)-7 as an adduct of NaOH. The OH^- counter anion and the hydrogen atom, which was not determined, are omitted for clarity. (b) A perspective view of the molecular aggregation in the vanadium(v) complex.

The oxygen atoms coordinated to the sodium cations construct a helical molecular aggregation in the crystal structure (Figure 18.3b).

Superconducted quantum interference device (SQUID) analysis was used to determine the oxidation state of dinuclear vanadium complex (R_a,*S*,*S*)-7 using $VOSO_4$ (line a) and V_2O_5 (line e) as standard vanadium(IV) and vanadium(v) samples, respectively (Figure 18.4).[8b] The magnetic susceptibility was 5 emu mol^{-1} at 5 K in 5 T when vanadium complex (R_a,*S*,*S*)-7 was prepared under an air atmosphere (line c). In contrast, the magnetic susceptibility of the vanadium complex prepared under an Ar atmosphere was 28 emu mol^{-1} (line b). The susceptibility of the single-crystals obtained *via* recrystallization (Figure 18.3) was 0 emu mol^{-1} which clearly indicates the vanadium(v) species (line d). These results suggested dinuclear vanadium(IV) complex (R_a,*S*,*S*)-7 was readily oxidized to afford a vanadium(v) complex species during its preparation under an air atmosphere. The coupling

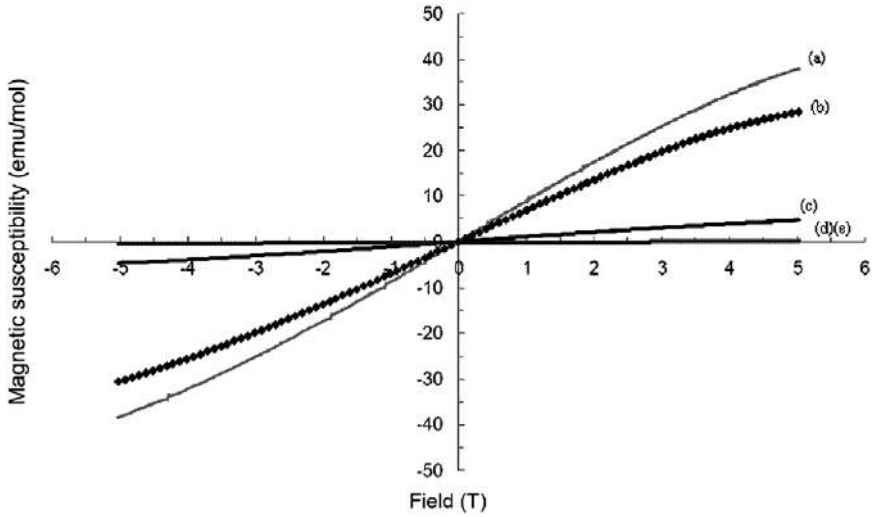

Figure 18.4 SQUID magnetometer plots of the vanadium magnetic susceptibility under a magnetic field at 5 K obtained for (a) $VOSO_4$, (b) (R_a,*S*,*S*)-**7** (prepared under an Ar atmosphere), (c) (R_a,*S*,*S*)-**7** (prepared under an air atmosphere), (d) single-crystals obtained upon the recrystallization of (R_a,*S*,*S*)-**7**. NaOH from $MeOH/Et_2O/H_2O$ containing NaOAc and (e) V_2O_5.

reaction of **5a** catalyzed by dinuclear vanadium(V) complex (R_a,*S*,*S*)-**8** prepared from $VOCl_3$ exhibited a 2.3-fold increase in the reaction rate when compared to dinuclear vanadium(IV) complex (R_a,*S*,*S*)-**7**, indicating that the vanadium(IV) complex most likely acts as a precatalyst.

A plausible reaction mechanism for (R_a,*S*,*S*)-**7** is shown in Figure 18.5. Auto-oxidation of the dinuclear vanadium(IV) complex under an air atmosphere forms the active vanadium(V) complex, (R_a,*S*,*S*)-**8**, which reacts with two molecules of 2-naphthol to form **Ia**. The C1-positions of the 2-naphthol moieties are in close proximity to one another *via* rotation of the binaphthyl axis, yielding **Ib**, which is then intramolecularly coupled after a single electron transfer process to form a vanadium(V) species. After the coupling and reoxidation of the vanadium(IV) species **II**, the vanadium(V) species is regenerated and (*S*)-BINOL is released. Since the catalytic activity of the dinuclear vanadium complex is significantly higher than that of mononuclear complex, the intermolecular coupling reaction proceeds as a minor pathway.

To date, significant research effort has been devoted to the development of highly active chiral vanadium catalysts (Figure 18.6) used for the oxidative-coupling of not only 2-naphthol derivatives, but also various arenols such as polycyclic phenols, hydroxycarbazoles and resorcinol derivatives.[7,8,12,13,15–19] Since many reviews and reports on the enantioselective oxidative-coupling of 2-naphthols have been presented,[20] we will mainly focus on the recent advances in the vanadium-mediated enantioselective coupling reaction of poly-, hetero- and monocyclic phenol derivatives in this chapter.

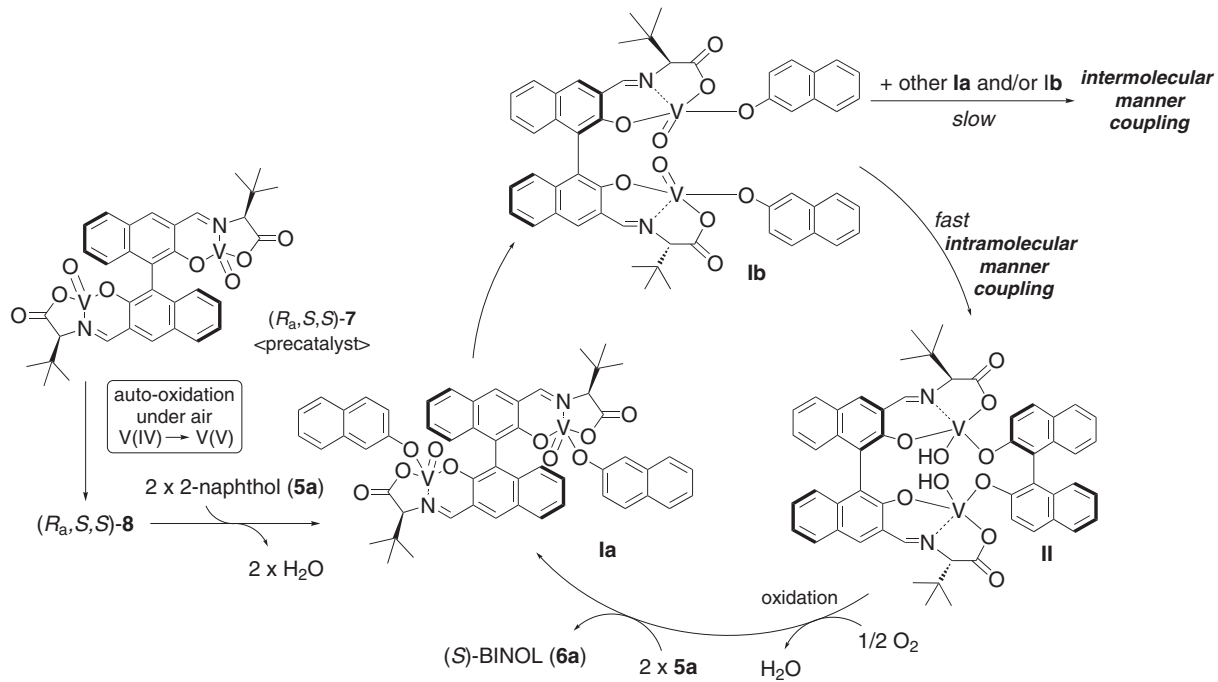

Figure 18.5 Plausible dual activation mechanism for the chiral dinuclear vanadium complex-catalyzed oxidative-coupling of 2-naphthol.

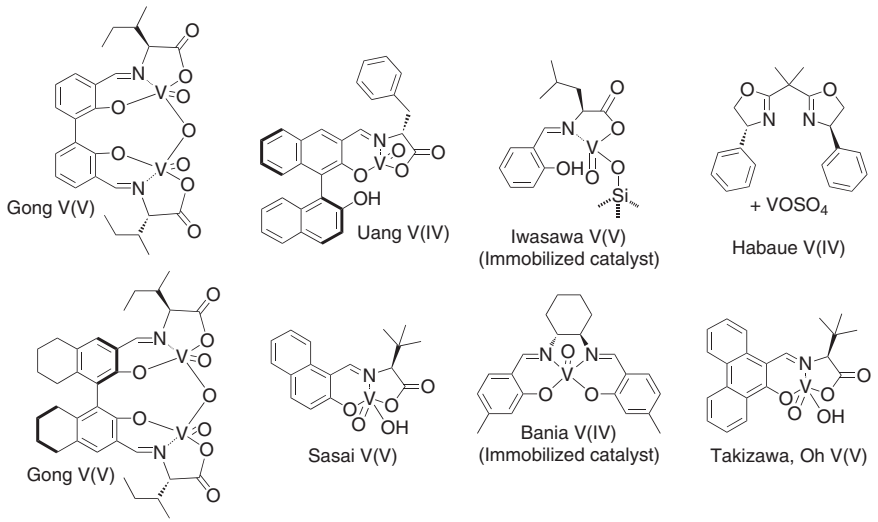

Figure 18.6 Previously reported highly active vanadium catalysts used for the enantioselective oxidative-coupling of 2-naphthol derivatives.

18.2 Enantioselective Oxidative-coupling of Polycyclic Phenols

Optically pure polycyclic biphenols, such as biphenanthrols and bianthracenol, are also useful as synthetic intermediates for chiral ligands and organocatalysts.[21] Despite their potential applications, no efficient catalytic enantioselective oxidative coupling of their corresponding polycyclic phenol precursors has been achieved due to the side-reaction of the substrate forming *ortho*-quinone **12** and/or the facile over-oxidation of the product such as xanthene **13** (Figure 18.7).

In 2009,[8d] Sasai and co-workers successfully extended the dual activation methodology to the enantioselective coupling of 9-phenanthrol (**10a**), which employed 5 mol% of dinuclear vanadium(v) catalyst (R_a,*S*,*S*)-**8** at –10 °C. As a result, the coupling product, 10,10′-bi(9-phenanthrol) (**11a**), was obtained in quantitative yield and 93% ee. Subsequently, they focused on the coupling reaction of 2-antracenol (**10b**) and 3-phenanthrol (**10c**) to give 1,1′-bi(2-anthracenol) (**11b**) and 4,4′-bi(3-phenanthrol) (**11c**), respectively, which can be readily used to construct hetero[7]helicenes.[21b] During the screening of the coupling reaction conditions for **10c**, the dinuclear vanadium(v) complex (R_a,*S*,*S*)-**14** containing a (*R*)-H_8-BINOL skeleton exhibited moderate reactivity to produce **11c** in 30% yield and 69% ee.[8e]

To date, the redox properties and Lewis acidity of chiral vanadium complexes have been utilized for other asymmetric reactions,[6] such as epoxidation,[6e] sulfoxidation,[6f] oxidation of α-hydroxy carbonyl compound,[6g] and ring-opening of *meso*-epoxides.[6h] However, there are few reports describing the cooperative effect of these two properties in vanadium-catalyzed

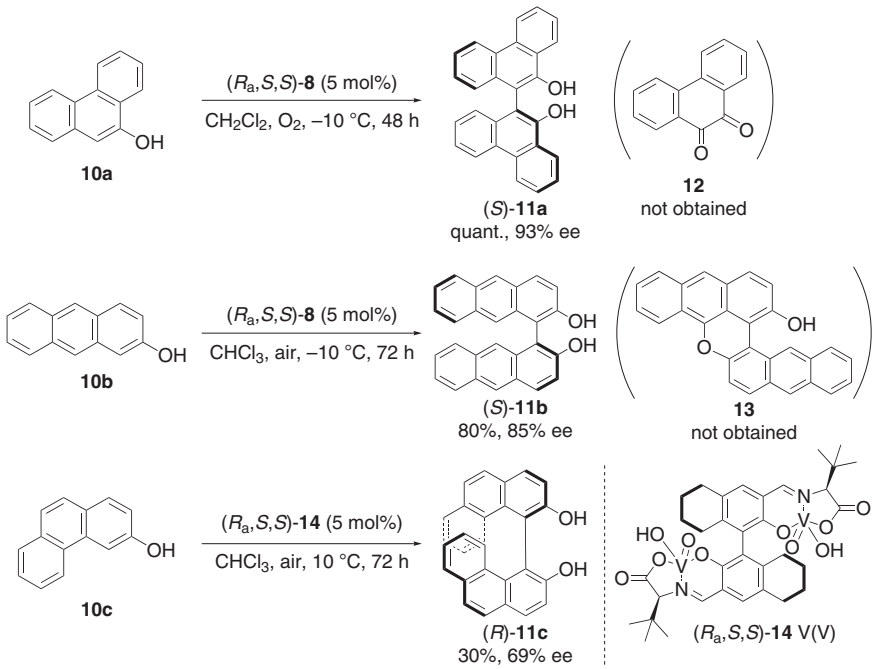

Figure 18.7 Enantioselective oxidative-coupling reaction of polycyclic phenols catalyzed by dinuclear vanadium complexes, reported by Sasai.

sequential reactions with an enantioselective epoxidation and ring-opening cascade reaction being the sole example reported to date.[22] In 2016, Takizawa and Sasai developed a novel vanadium complex, (R_a,*S*)-**15a**, which cooperatively functions as both a redox and Lewis acid catalyst to promote the sequential oxidative-coupling of 2-hydroxybenzo[*c*]phenanthrenes **16** and Lewis acid-mediated intramolecular dehydrative cyclization of the intermediate coupling products to form oxa[9]helicenes (*M*)-**17** in good yield (56%–86%) with up to 94% ee (Figure 18.8).[18a]

Since the sequential reaction was found to be first order with respect to (R_a,*S*)-**15a**, the oxidative-coupling reaction would occur with one molecule of the vanadium complex and not *via* a dual activation mechanism with the two vanadium centers;[8] the reaction of mononuclear vanadium(v) complex (R_a,*S*)-**15a** with substrate **16a** generates intermediate **A**. Intermediate **A** then promotes an intermolecular coupling with another molecule of **16a** after a single electron transfer to the vanadium(v) species, followed by oxidation of vanadium(iv) by O_2 to form intermediate **B**. Finally, a dehydrative cyclization assisted by the Lewis acidity of the vanadium(v) species affords the desired helicene (**17a**) with intermediate **A** regenerated. Since methyl-capped catalyst (R_a,*S*)-**15b** exhibits a low reaction rate without a decrease in the ee of the product, the hydroxy group in the binaphthyl ligand of the vanadium complex may increase the Lewis acidity of vanadium metal center *via* an intramolecular hydrogen bond (Figure 18.9).

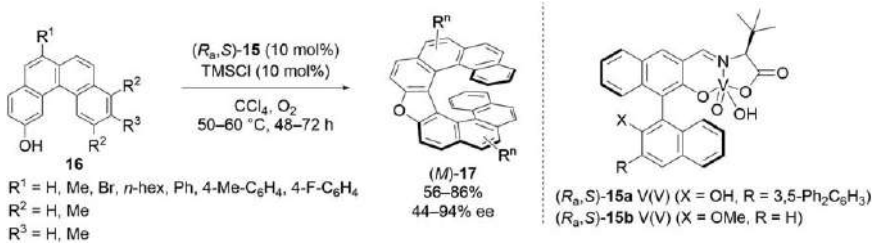

Figure 18.8 Chiral vanadium(v) complex-catalyzed oxidative-coupling/intramolecular cyclization sequence to produce oxa[9]helicenes, reported by Takizawa and Sasai.

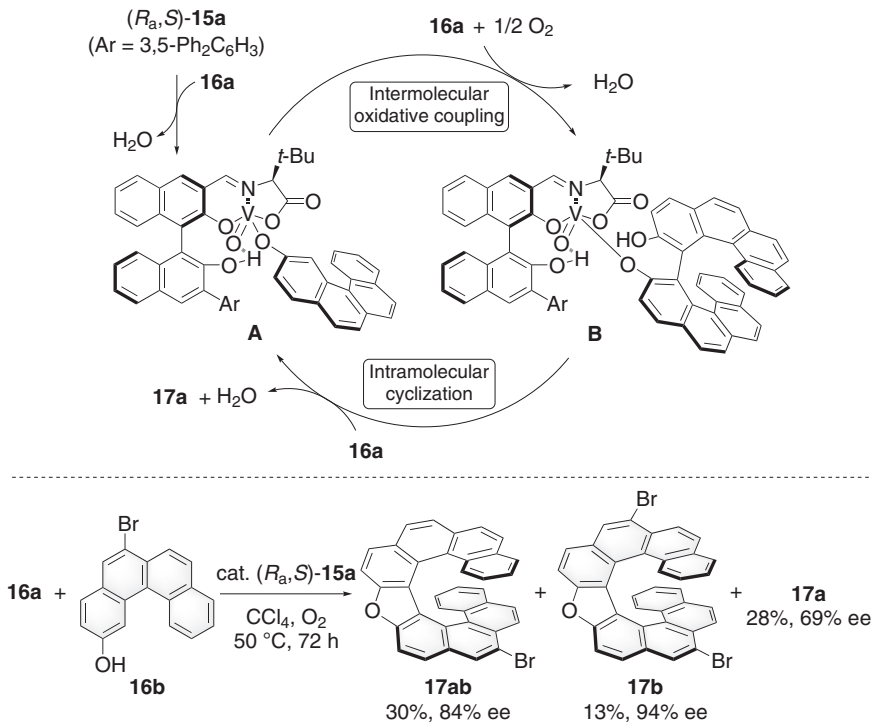

Figure 18.9 Reaction mechanism for the chiral vanadium(v) complex-catalyzed oxidative-coupling/dehydrative cyclization.

Treatment of a 1:1 mixture of electron-rich **16a** and electron-poor **16b** bearing a bromine group with (R_a,*S*)-**15a** (10 mol%) afforded a mixture of the hetero-coupling product **17ab** (30% yield, 84% ee) and homo-coupling products **17a** (28% yield, 69% ee) and **17b** (13% yield, 94% ee). Gong reported that the ratio of the product mixture in the vanadium-mediated

radical-radical hetero-coupling is in agreement with their relative reactivities.[7c] In principal, the redox potential of **16b** is higher than that of **16a**, which results in homo-coupling product **17a** being formed as the major product. These outcomes suggest that the coupling reaction of **16** likely proceeds *via* a radical-anion coupling mechanism, as shown in Figure 18.9.

18.3 Enantioselective Oxidative-coupling of Heterocyclic Phenols

Bi(hydroxycarbazole)s involving C–C and C–N linked biaryls have attracted considerable interest from many research groups because these alkaloids exhibit a broad range of biological properties, such as antimalarial, cytotoxic, anti-HIV and antimicrobial activities.[23] Sorazolon E and E2 (dimeric sorazolon E), which are isolated from *Sorangium cellulosum* strain soce375, exhibit antibacterial (Gram-positive and Gram-negative) and cytotoxic (mouse fibroblast cell line L929) activities.[23] In 2017,[18c] Takizawa and Sasai reported the first and short synthesis of 4-deoxycarbazomycin B and sorazolon E using cyclohexanone (**18**) and commercially available 4-methoxy-2,3-dimethylaniline (**19**) as starting materials (Figure 18.10). Chiral dinuclear vanadium(v) complex (R_a,*S*,*S*)-**8** was used as the catalyst in the enantioselective oxidative-coupling reaction of sorazolon E, giving (+)-sorazolon E2 in good yield and enantioselectivity. The absolute configuration of synthetic sorazolon E2 was assigned as *R* upon comparison

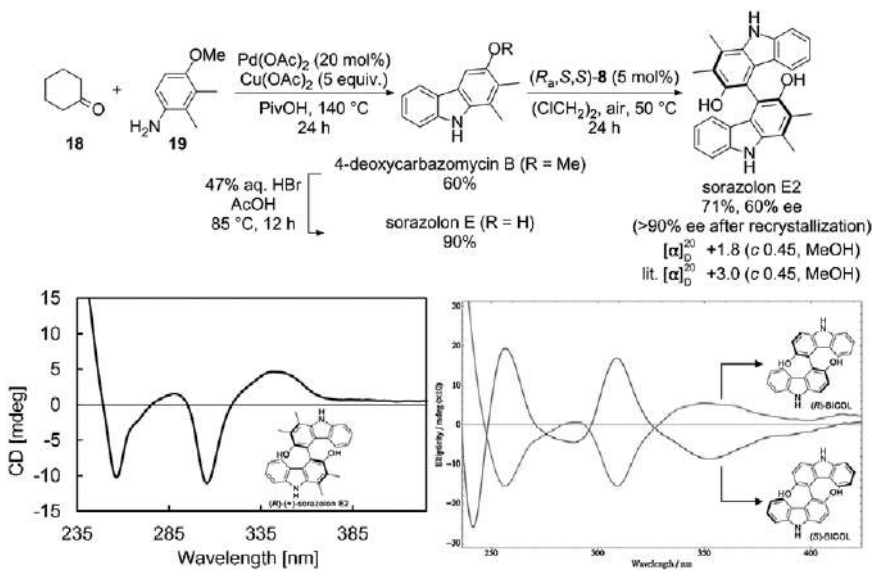

Figure 18.10 Short syntheses of 4-deoxycarbazomycin B, sorazolon E and (+)-sorazolon E2, reported by Takizawa and Sasai.

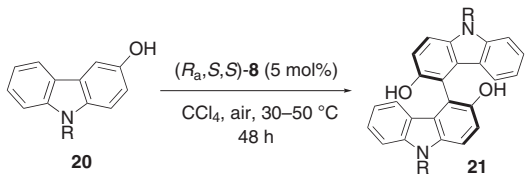

20 (R)	21
20a (Me)	**21a**, 20%, 65% ee
20b (Ac)	**21b**, no reaction
20c (Ph)	**21c**, 55%, 80% ee
20d (4-Cl-C_6H_4)	**21d**, 65%, 75% ee
20e (4-Me-C_6H_4)	**21e**, 65%, 80% ee

Figure 18.11 Chiral vanadium(v)-catalyzed oxidative-coupling reaction of 3-hydroxycarbazoles, reported by Takizawa.

with the circular dichroism (CD) spectrum obtained for optically pure 9*H*,9′*H*-[4,4′-*bi*carbazole]-3,3′-di*ol* (BICOL)[24] in 5% DMSO/H_2O. Hence, dinuclear vanadium complex (R_a,*S*,*S*)-**8** can be used to produce the natural form of sorazolon E2.

To improve the enantioselectivity of the oxidative-coupling reaction of 3-hydroxycarbazoles **20**, the effect of various protecting groups on the nitrogen atom was investigated (Figure 18.11).[18d] The methyl-substituted substrate **20a** underwent the coupling reaction at 50 °C to afford **21a** in 65% ee, but only 20% yield, which was attributed to the low reactivity of **20a**. In contrast, phenyl-, 4-Cl-C_6H_4- and 4-Me-C_6H_4-substituted substrates, **20c**, **20d** and **20e** afforded their corresponding products **21c**, **21d** and **21e**, respectively, in moderate yield (55%–65%) with good enantioselectivity (75%–80% ee). The reaction of **20b**, an acetyl-substituted substrate, did not proceed under the reaction conditions, indicating that the oxidative-coupling depends on electronically rich *N*-substituents.

Kozlowski attempted the catalytic oxidative-coupling of 2-hydroxycarbazole **25a** using chiral vanadium catalyst (*S*)-**22** under an oxygen atmosphere (Figure 18.12a). However, the regio- and enantioselective oxidative-coupling remains a challenge due to the high number of reactive sites leading to regioisomers **26a** and **27a** and tetramer **28a**, as well as the low atropisomerization barriers of their biaryl bonds, leading to easy racemization.[19a] In 2017, Kozlowski used 3-substituted 2-hydroxycarbazoles **25** bearing bulky benzyl substituents on the nitrogen atom to suppress the over-coupling reaction and racemization of **26**. Finally, the optimized conditions [20 mol% (*S*)-**23a**, 6.5 equiv. AcOH in chlorobenzene] provided bi(hydroxycarbazole)s **26** in up to 91% yield and 96% ee (Figure 18.12b).[19b,19c] Later, Takizawa also applied mononuclear vanadium(v) catalysts (R_a,*S*)-**24** bearing a chiral binaphthyl skeleton to synthesize (+)-bi-2-hydroxy-3-carbazole **26b**, a natural product, *via* the oxidative-coupling of **25b** (Figure 18.12c).[18d]

18.4 Enantioselective Oxidative-coupling of Monocyclic Phenols

Biresorcinols are also attractive compounds because of their great potential as bioactive and functional materials.[25] In 2017, Kozlowski demonstrated the first enantioselective oxidative-coupling reaction of resorcinols **29**, as

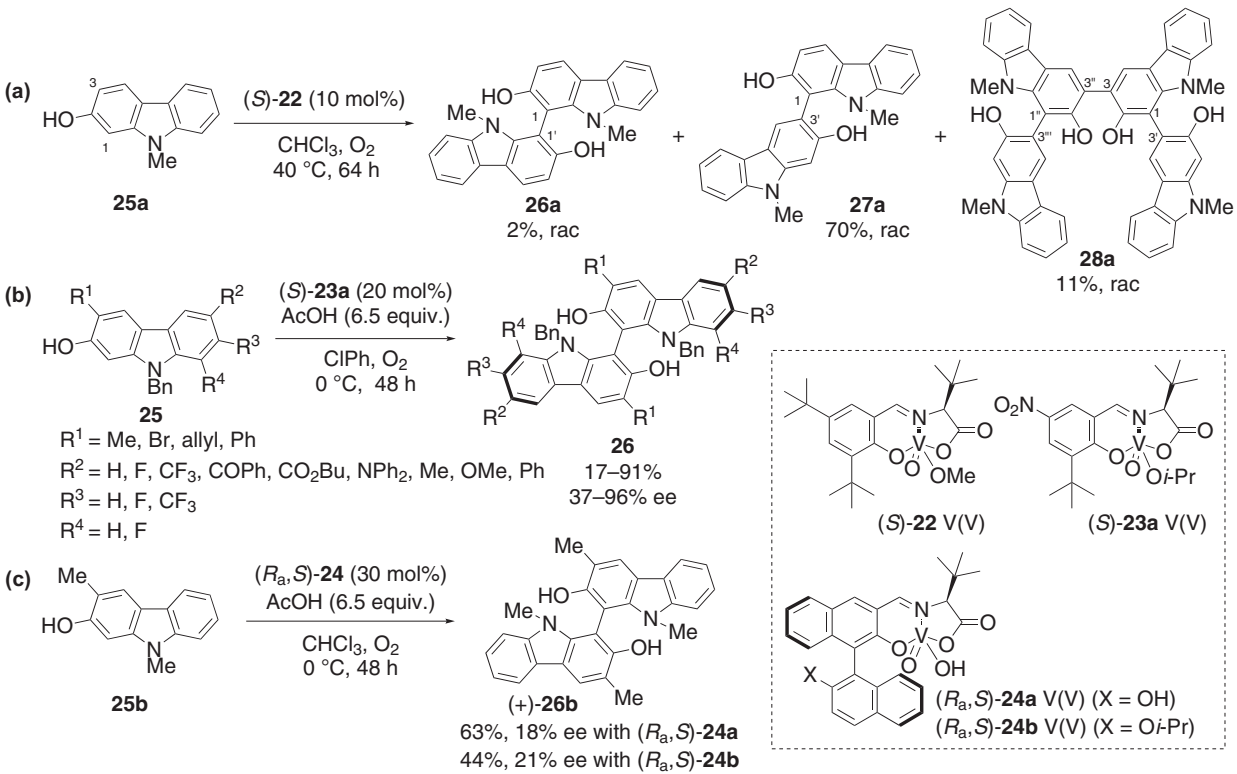

Figure 18.12 Chiral vanadium(v) complex-catalyzed oxidative-coupling of 2-hydroxycarbazoles, independently reported by Kozlowski and Takizawa.

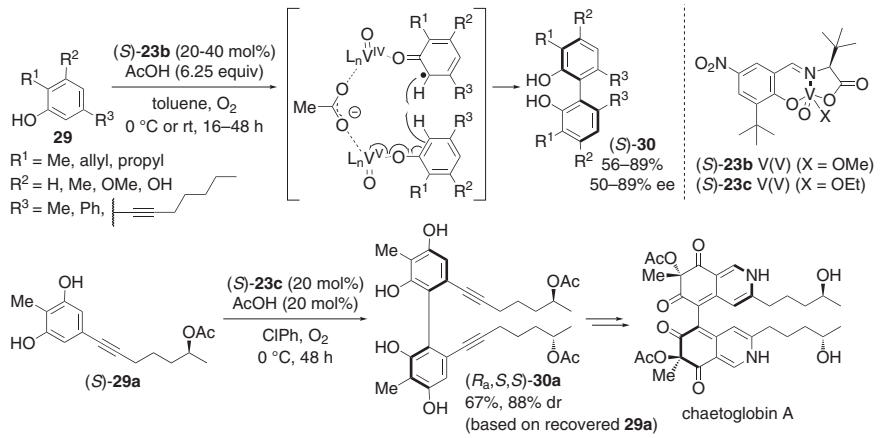

Figure 18.13 Chiral vanadium(v) complex-catalyzed oxidative-coupling of monocyclic phenols, reported by Kozlowski.

monocyclic phenol derivatives, using 20–40 mol% of chiral mononuclear vanadium(v) complex (*S*)-**23** and AcOH as an additive,[19b,c] as well as their application toward the total synthesis of chaetoglobin A.[19d] Experimental and DFT studies on the mechanism of the reaction indicated that AcOH promotes the aggregation of the vanadium monomers. In addition, a singlet to triplet crossover is implicated prior to the C–C bond-forming step. The two lowest energy diastereomeric transition states leading to the enantiomeric products differ substantially with the pathway to the minor enantiomer involving greater torsional strain between the two phenol moieties (Figure 18.13).

In 2019, Takizawa and Sasai extended this dual activation methodology to the enantioselective oxidative-coupling of resorcinols **29** to prepare biresorcinols **30** using the brominated chiral dinuclear vanadium(v) catalyst (*R*$_a$,*S*,*S*)-**31**. When resorcinols bearing an aryl substituent were applied, their corresponding biresorcinols were obtained as single regioisomers in up to 93% yield and 97% ee (Figure 18.14).[18e]

18.5 Conclusions

In this chapter, we have described the recent advances in vanadium-catalyzed oxidative-coupling reactions. Chiral vanadium complexes bearing Schiff base ligands act as remarkably active catalysts for regio- and enantioselective C–C bond-forming reactions. These catalytic systems have been applied to the synthesis of important chiral molecules, such as polycyclic biphenols, oxa[9]helicenes, bi(hydroxycarbazole)s and biresorcinols. In the field of oxidative reactions of arenols, it is crucial to suppress the side reaction forming regioisomers and over-oxidation of the desired product. The characteristic activity of vanadium metal enables efficient transformations to occur using mild reaction conditions under an air or oxygen

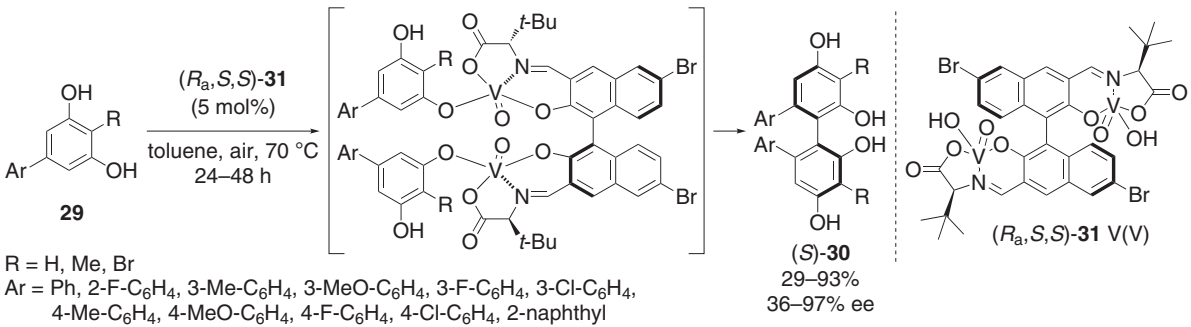

Figure 18.14 Chiral dinuclear vanadium(v) complex-catalyzed oxidative-coupling of resorcinols, reported by Takizawa and Sasai.

atmosphere, which exhibit good functional group tolerance. Continuous efforts should be made toward understanding the reaction mechanism including the activation mode and development of more challenging reactions, such as oxidative hetero-couplings. The combination of vanadium catalysts, biocatalysts and/or organocatalysts has been utilized to provide new reaction protocols that furnish important building blocks in a previously unknown fashion.[5g,26] Hence, vanadium-catalyzed reactions show new and promising aspects for further ground-breaking discoveries and applications in industrial processes.

References

1. A. de Meijere, S. Braese and M. Oestreich, *Metal Catalyzed Cross-coupling Reactions and More*, Wiley-VCH, Weinheim, 2014.
2. https://www.nobelprize.org/prizes/chemistry/2010/press-release/.
3. V. K. Ahluwalia, *Green Chemistry: Environmentally Benign Reactions*, CRC Press, Florida, 2018.
4. R. R. Langeslay, D. M. Kaphan, C. L. Marshall, P. C. Stair, A. P. Sattelberger and M. Delferro, *Chem. Rev.*, 2019, **119**, 2128.
5. Reviews on asymmetric vanadium catalyses:(a) C. Bolm, *Coord. Chem. Rev.*, 2003, **237**, 245; (b) M. North, D. L. Usanov and C. Young, *Chem. Rev.*, 2008, **108**, 5146; (c) K. P. Volcho and N. F. Salakhutdinov, *Russ. Chem. Rev.*, 2009, **78**, 457; (d) W. Plass, *Coord. Chem. Rev.*, 2011, **255**, 2378; (e) Z. Li and H. Yamamoto, *Acc. Chem. Res.*, 2013, **46**, 506; (f) H. Pellissier, *Coord. Chem. Rev.*, 2015, **284**, 93; (g) S. Takizawa, H. Gröger and H. Sasai, *Chem. – Eur. J.*, 2015, **21**, 8992.
6. Selected examples of chiral vanadium complex-mediated transformation (pioneering work), addition of cyanide ion:(a) Y. N. Belokon', M. North and T. Parsons, *Org. Lett.*, 2000, **2**, 1617; Friedel-Crafts-type reaction: (b) S. Takizawa, F. A. Arteaga, Y. Yoshida, J. Kodera, Y. Nagata and H. Sasai, *Dalton Trans.*, 2013, **42**, 11787; Diels-Alder reaction: (c) A. Togni, *Organometallics*, 1990, **9**, 3106; pinacol coupling: (d) R. Annuziata, M. Cinquini, F. Cozzi and P. Giaroni, *Tetrahedron: Asymmetry*, 1990, **1**, 355; (e) epoxidation:R. C. Michaelson, R. E. Palermo and K. B. Sharpless, *J. Am. Chem. Soc.*, 1977, **99**, 1990; sulfoxidation: (f) K. Nakajima, M. Kojima and J. Fujita, *Chem. Lett.*, 1986, 1483; oxidation of α-hydroxy carbonyl compounds: (g) A. T. Radosevich, C. Musich and F. D. Toste, *J. Am. Chem. Soc.*, 2005, **127**, 1090; ring-opening of meso-epoxides: (h) J. Sun, Z. Dai, M. Yang, X. Pan and C. Zhu, *Synthesis*, 2008, 2100.
7. (a) Z. Luo, Q. Liu, L. Gong, X. Cui, A. Mi and Y. Jiang, *Chem. Commun.*, 2002, 914; (b) Z. Luo, Q. Liu, L. Gong, X. Cui, A. Mi and Y. Jiang, *Angew. Chem., Int. Ed.*, 2002, **41**, 4532; (c) Q.-X. Guo, Z.-J. Wu, Z.-B. Luo, Q.-Z. Liu, J.-L. Ye, S.-W Luo, L.-F. Cun and L.-Z. Gong, *J. Am. Chem. Soc.*, 2007, **129**, 13927.

8. (a) H. Somei, Y. Asano, T. Yoshida, S. Takizawa, H. Yamataka and H. Sasai, *Tetrahedron Lett.*, 2004, **45**, 1841; (b) S. Takizawa, T. Katayama, C. Kameyama, K. Onitsuka, T. Suzuki, T. Yanagida, T. Kawai and H. Sasai, *Chem. Commun.*, 2008, 1810; (c) S. Takizawa, T. Katayama, H. Somei, Y. Asano, T. Yoshida, C. Kameyama, D. Rajesh, K. Onitsuka, T. Suzuki, M. Mikami, H. Yamataka, D. Jayaprakash and H. Sasai, *Tetrahedron*, 2008, **64**, 3361; (d) S. Takizawa, D. Rajesh, T. Katayama and H. Sasai, *Synlett*, 2009, 1667; (e) S. Takizawa, J. Kodera, Y. Yoshida, M. Sako, S. Breukers, D. Enders and H. Sasai, *Tetrahedron*, 2014, **70**, 1786; (f) M. Sako, S. Takizawa, Y. Yoshida and H. Sasai, *Tetrahedron: Asymmetry*, 2015, **26**, 613.
9. W. L. Carrick, G. L. Karapinka and G. T. Kwiatkowski, *J. Org. Chem.*, 1969, **34**, 2388.
10. Selected recent reviews on applications of BINOLs in stereoselective organic synthesis, see:(a) F. E. Held, D. Grau and S. B. Tsogoeva, *Molecules*, 2015, **20**, 16103; (b) G. Li, F. Liu and M. Wu, *ARKIVOC*, 2015, 140; (c) L. Pu, *Acc. Chem. Res.*, 2017, **50**, 1032; (d) T. N. Nguyen, P.-A. Chen, K. Setthakarn and J. A. May, *Molecules*, 2018, **23**, 2317.
11. Selected examples of chiral metal complex-mediated oxidative couplings of 3-substituted 2-naphthols, see:(a) M. Nakajima, I. Miyoshi, K. Kanayama, S.-I. Hashimoto, M. Noji and K. Koga, *J. Org. Chem.*, 1999, **64**, 2264; (b) X. Li, J. Yang and M. C. Kozlowski, *Org. Lett.*, 2001, **3**, 1137; (c) T. Temma and S. Habaue, *J. Polym. Sci., Part A: Polym. Chem.*, 2005, **43**, 6287; (d) H. Egami and T. Katsuki, *J. Am. Chem. Soc.*, 2009, **131**, 6082–6083.
12. (a) C.-Y. Chu, D.-R. Hwang, S.-K. Wang and B.-J. Uang, *Chem. Commun.*, 2001, 980; (b) C.-Y. Chu and B.-J. Uang, *Tetrahedron: Asymmetry*, 2003, **14**, 53.
13. (a) S.-W. Hon, C.-H. Li, J.-H. Kuo, N. B. Barhate, Y.-H. Liu, Y. Wang and C.-T. Chen, *Org. Lett.*, 2001, **3**, 869; (b) N. B. Barhate and C.-T. Chen, *Org. Lett.*, 2002, **4**, 2529.
14. Selected reviews on multifunctional chiral catalysts(a) M. Shibasaki, H. Sasai and T. Arai, *Angew. Chem., Int. Ed. Engl.*, 1997, **36**, 1236; (b) M. Ikunaka, *Org. Process Res. Dev.*, 2007, **11**, 495; (c) D. H. Paull, C. J. Abraham, M. T. Scerba, E. Alden-Danforth and T. Lectka, *Acc. Chem. Res.*, 2008, **41**, 655; (d) J. Park and S. Hong, *Chem. Soc. Rev.*, 2012, **41**, 6931; (e) J. Zhou, *Multicatalyst System in Asymmetric Catalysis*, John Wiley & Sons, New Jersey, 2014; (f) B. M. Trost and M. J. Bartlett, *Acc. Chem. Res.*, 2015, **48**, 688.
15. (a) M. Tada, T. Taniike, L. M. Kantam and Y. Iwasawa, *Chem. Commun.*, 2004, 2542; (b) M. Tada, N. Kojima, Y. Izumi, T. Taniike and Y. Iwasawa, *J. Phys. Chem. B*, 2005, **109**, 9905; (c) M. Tada and Y. Iwasawa, *Chem. Commun*, 2006, 2833.
16. (a) S. Habaue, S. Murakami and H. Higashimura, *J. Polym. Sci., Part A: Polym. Chem.*, 2005, **43**, 5872; (b) S. Murakami, S. Habaue and H. Higashimura, *Polymer*, 2007, **48**, 6565.

17. M. Mandal, V. Nagaraju, G. V. Karunakar, B. Sarma, B. J. Borah and K. K. Bania, *J. Phys. Chem. C*, 2015, **119**, 28854.
18. (a) M. Sako, Y. Takeuchi, T. Tsujihara, J. Kodera, T. Kawano, S. Takizawa and H. Sasai, *J. Am. Chem. Soc.*, 2016, **138**, 11481; (b) H. Y. Kim, S. Takizawa, H. Sasai and K. Oh, *Org. Lett.*, 2017, **19**, 3867; (c) M. Sako, K. Ichinose, S. Takizawa and H. Sasai, *Chem. – Asian J.*, 2017, **12**, 1305; (d) M. Sako, M. A. Sugizaki and S. Takizawa, *Bioorg. Med. Chem. Lett.*, 2018, **28**, 2751; (e) M. Sako, T. Aoki, N. Zumbrägel, L. Schober, H. Gröger, S. Takizawa and H. Sasai, *J. Org. Chem.*, 2019, **84**, 1580.
19. (a) L. Liu, P. J. Carroll and M. C. Kozlowski, *Org. Lett.*, 2015, **17**, 508; (b) H. Kang, Y. E. Lee, P. V. G. Reddy, S. Dey, S. E. Allen, K. A. Niederer, P. Sung, K. Hewitt, C. Torruellas, M. R. Herling and M. C. Kozlowski, *Org. Lett.*, 2017, **19**, 5505; (c) H. Kang, M. R. Herling, K. A. Niederer, Y. E. Lee, P. V. G. Reddy, S. Dey, S. E. Allen, P. Sung, K. Hewitt, C. Torruellas, G. J. Kim and M. C. Kozlowski, *J. Org. Chem.*, 2018, **83**, 14362; (d) H. Kang, C. Torruellas, J. Liu and M. C. Kozlowski, *Org. Lett.*, 2018, **20**, 5554.
20. (a) M. Smrćina, J. Poláková, S. Vyskoćil and P. Koćovský, *J. Org. Chem.*, 1993, **58**, 4534; (b) R. Irie, K. Masutani and T. Katsuki, *Synlett*, 2000, 1433; (c) J. Gao, J. H. Reibenspies and A. E. Martell, *Angew. Chem., Int. Ed.*, 2003, **42**, 6008; (d) P. P. Reddy, C.-Y. Chu, D.-R. Hwang, S.-K. Wang and B.-J. Uang, *Coord. Chem. Rev.*, 2003, **237**, 257; (e) S. Takizawa, T. Katayama and H. Sasai, *Chem. Commun.*, 2008, 4113; (f) S. Takizawa, *Chem. Pharm. Bull.*, 2009, **57**, 1179; (g) H. Wang, *Chirality*, 2010, **22**, 827; (h) S. Narute, R. Parnes, F. D. Toste and D. Pappo, *J. Am. Chem. Soc.*, 2016, **138**, 16553; (i) N. V. Tkachenko and K. P. Bryliakov, *Mini-Rev. Org. Chem.*, 2019, **16**, 392; (j) P. Adãoa, C. M. Teixeira, M. F. N. N. Carvalho, M. L. Kuznetsov, C. S. B. Gomes and J. C. Pessoa, *Mol. Catal.*, 2019, **475**, 110480; (k) J.-M. Tian, A.-F. Wang, J.-S. Yang, X.-J. Zhao, Y.-Q. Tu, S.-Y. Zhang and Z.-M. Chen, *Angew. Chem., Int. Ed.*, 2019, **58**, 11023; (l) T. Horibe, K. Nakagawa, T. Hazeyama, K. Takeda and K. Ishihara, *Chem. Commun.*, 2019, **55**, 13677.
21. (a) F. Bell and D. H. Waring, *J. Chem. Soc.*, 1949, 267; (b) K. Nakano, Y. Hidehira, K. Takahashi, T. Hiyama and K. Nozaki, *Angew. Chem., Int. Ed.*, 2005, **44**, 7136; (c) S. Zhang, Y. Wang, Z. Song, K. Nakajima and T. Takahashi, *Chem. Lett.*, 2013, **42**, 697; (d) Z. He, A. P. Pulis and D. J. Procter, *Angew. Chem., Int. Ed.*, 2019, **58**, 7813.
22. (a) A. Blanc and F. D. Toste, *Angew. Chem., Int. Ed.*, 2006, **45**, 2096; (b) L. Han, C. Liu, W. Zhang, X.-X. Shi and S.-L. You, *Chem. Commun.*, 2014, **50**, 1231; (c) L. Han, W. Zhang, X.-X. Shi and S.-L. You, *Adv. Synth. Catal.*, 2015, **357**, 3064.
23. (a) S. Karwehl, R. Jansen, V. Huch and M. Stadler, *J. Nat. Prod.*, 2016, **79**, 369; (b) C. Brütting, R. F. Fritsche, S. K. Kutz, C. Börger, A. W. Schmidt, O. Kataeva and H.-J. Knölker, *Chem. – Eur. J.*, 2018, **24**, 458.
24. M.-A. Dubois, A. Grandbois, S. K. Collins and A. R. Schmitzer, *J. Mol. Recognit.*, 2011, **24**, 288.

25. (a) Z. Xiao, Y. Li and S. Gao, *Org. Lett.*, 2017, **19**, 1834; (b) A. Richieu, P. A. Peixoto, L. Pouysegu, D. Deffieux and S. Quideau, *Angew. Chem., Int. Ed.*, 2017, **56**, 13833; (c) E. Chen, X. Chen, X. Yuan, S. Wei, L. Zhou, J. Zhou and J. Shen, *Dalton Trans.*, 2017, **46**, 5151.
26. (a) M. Andersson, A. Willetts and S. Allenmark, *J. Org. Chem.*, 1997, **62**, 8455; (b) H. B. ten Brink, A. Tuynman, H. L. Dekker, W. Hemrika, Y. Izumi, T. Oshiro, H. E. Schoemaker and R. Wever, *Inorg. Chem.*, 1998, **37**, 6780; (c) F. van de Velde, L. Könemann, F. van Rantwijk and R. A. Sheldon, *Chem. Commun.*, 1998, 1891–1892; (d) F. van de Velde, I. W. C. E. Arends and R. A. Sheldon, *J. Inorg. Biochem.*, 2000, **80**, 81; (e) S. Akai, K. Tanimoto, Y. Kanao, M. Egi, T. Yamamoto and Y. Kita, *Angew. Chem., Int. Ed.*, 2006, **45**, 2592; (f) I. Correia, S. Aksu, P. Adão, J. C. Pessoa, R. A. Sheldon and I. W. C. E. Arends, *J. Inorg. Biochem.*, 2008, **102**, 318; (g) S. Akai, R. Hanada, N. Fujiwara, Y. Kita and M. Egi, *Org. Lett.*, 2010, **12**, 4900; (h) M. Egi, K. Sugiyama, M. Saneto, R. Hanada, K. Kato and S. Akai, *Angew. Chem., Int. Ed.*, 2013, **52**, 3654; (i) S. Akai, *Chem. Lett.*, 2014, **43**, 746; (j) K. Sugiyama, Y. Oki, S. Kawanishi, K. Kato, T. Ikawa, M. Egi and S. Akai, *Catal. Sci. Technol.*, 2016, **6**, 5023; (k) S. Kawanishi, K. Sugiyama, Y. Oki, T. Ikawa and S. Akai, *Green Chem.*, 2017, **19**, 411; (l) S. Kawanishi, S. Oki, D. Kundu and S. Akai, *Org. Lett.*, 2019, **21**, 2978.

CHAPTER 19

Vanadium-induced Oxidative and Reductive Coupling

T. AMAYA*[a] AND T. HIRAO*[b]

[a] Graduate School of Engineering, Osaka University, Yamada-oka, Suita, Osaka 565-0871, Japan; [b] The Institute of Scientific and Industrial Research, Osaka University, Mihoga-oka, Ibaraki, Osaka 567-0047, Japan
*Emails: amaya@chem.eng.osaka-u.ac.jp; hirao@chem.eng.osaka-u.ac.jp

19.1 Introduction

Vanadium is a redox-active metal and generally converts between oxidation states *via* one-electron redox processes.[1,2] This versatility allows the development of a wide range of oxidative and reductive organic reactions. High valent vanadium(V) compounds can induce oxidative transformations including carbon–carbon bond formations based on the V(V)-V(IV) couple. The redox process based on the low valent vanadium species such as V(II) to V(III) can be used for one-electron reduction reactions, which has led to various synthetic methods. This chapter discusses oxidative and reductive carbon–carbon bond-forming coupling we have developed. For the transformations of functional groups such as dehydrogenation, oxygenation, oxidative decarboxylation and reductive dehalogenation using vanadium reagents, see the review article published in Chemical Review.[1]

Catalysis Series No. 41
Vanadium Catalysis
Edited by Manas Sutradhar, José Armando L. da Silva and Armando J. L. Pombeiro

Published by the Royal Society of Chemistry, www.rsc.org

19.2 Vanadium-induced Oxidative Coupling

19.2.1 Vanadium-induced Oxidative Coupling of Enolate Species

1,4-Dicarbonyl compounds are found in naturally occurring products and medicinal compounds.[3] Furthermore, they are also used as a precursor to synthesize furans, pyrolles and thiophens by the Paar-Knoll method[4] and even benzene rings.[5] Therefore, versatile methods to prepare various 1,4-dicarbonyl compounds are required. One of the most direct approaches is the oxidative coupling of enolates.[6–14] On the other hand, high valent oxovanadium(v) species permit the oxidative homo-coupling of carbanion species such as alkynyl, alkenyl and aryl lithium, alkyl Grignard reagents and lithium enolate.[15] In this section, V(v)-induced homo- and cross-coupling using silyl enol ethers and/or boron enolate is described.

Oxidative coupling of silyl enol ethers is induced by oxovanadium(v) species such as $VO(OEt)Cl_2$ to give the corresponding 1,4-diones. For example, oxidative homo-coupling of silyl enol ethers **1** derived from cyclic ketones proceeds smoothly to give the symmetric 1,4-diketones **2** in good yields, where a stoichiometric amount of $VO(OEt)Cl_2$ is used (Scheme 19.1).[16] A careful choice of substrates based on the redox potentials permits the oxidative cross-coupling in these reactions. More specifically, highly substituted silyl enol ethers **3** tend to be readily oxidized compared to the less-substituted ones **4**. So, the combination of **3** and **4** (2 equiv.) gives rise to the selective oxidative cross-coupling to form **5** (Scheme 19.2).[16] γ-Keto ester **11** is also synthesized by the cross-coupling of readily oxidizable silyl ketene acetal **9** and silyl enol ether **10** (Scheme 19.3).[16] An imidovanadium complex also induces this cross-coupling selectively.[17] The plausible mechanism is as follows (Scheme 19.2): (1) one-electron oxidation of silyl enol ether **3** to give a radical cation **6**, (2) desilylation to result in the carbonyl α-radical **7**, (3) radical addition to **4** to form **8** and (4) one-electron oxidation and desilylation to afford the 1,4-dicarbonyl compounds **5**.[16]

Treatment of silyl enol ethers **12** and allylsilanes **13** with $VO(OEt)Cl_2$ also undergoes oxidative cross-coupling to give the γ,δ-unsaturated ketones **14** (Scheme 19.4).[18] In every case, the selective cross-coupling is attained.

Boron enolate can be used for the V(v)-induced oxidative coupling (Scheme 19.5).[19] The (*Z*)-boron enolate **16** is selectively prepared by 1,4-hydroboration of enone **15** with 9-BBN. The homo-coupling reaction takes place to give the corresponding *dl*-1,4-diketone **17** as a main product.

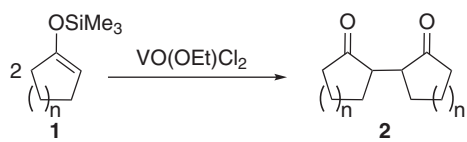

Scheme 19.1 Oxidative homo-coupling of silyl enol ethers **1**.

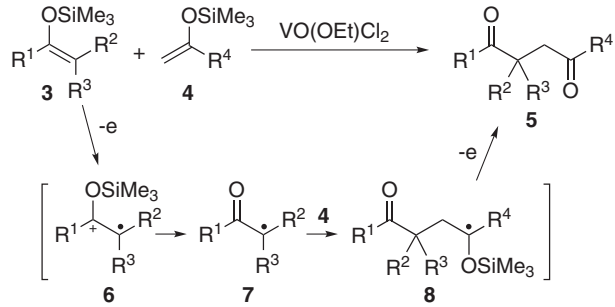

Scheme 19.2 Oxidative cross-coupling of silyl enol ethers **3** and **4**, and the proposed pathway.

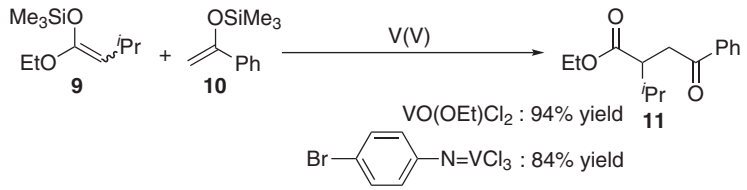

Scheme 19.3 Oxidative cross-coupling of silyl ketene acetal **9** and silyl enol ether **10**.

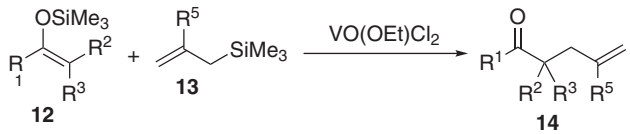

Scheme 19.4 Oxidative cross-coupling of silyl enol ethers **12** and allyl silanes **13**.

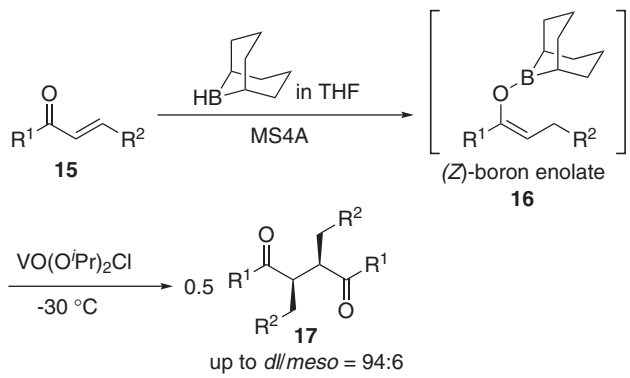

Scheme 19.5 Diastereoselective oxidative homo-coupling of boron enolates **16**.

The use of $VO(O^iPr)_2Cl$ at -30 °C is effective for higher selectivity (*dl* : *meso* ratio up to 94 : 6). The mechanism of the diastereoselectivity is not clear, but chelation of two enolates to vanadium is suggested to account for the

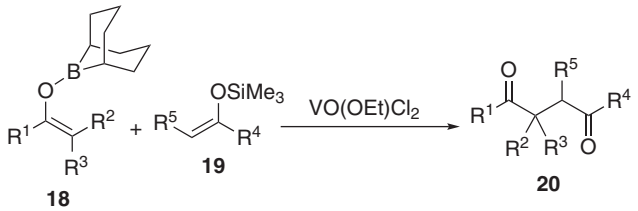

Scheme 19.6 Oxidative cross-coupling of boron enolates **18** and silyl enol ethers **19**.

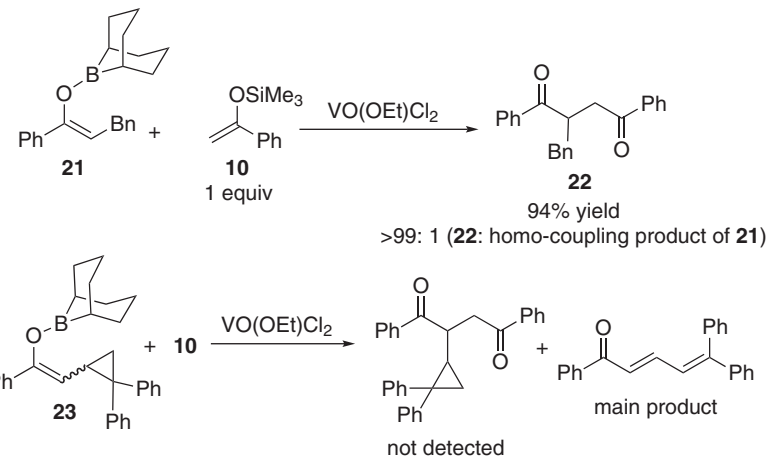

Scheme 19.7 Oxidative cross-coupling of boron enolate **21** and silyl enol ether **10**, and radical clock reaction.

selectivity. This is the first example using boron enolate for the oxidative formation of 1,4-dicarbonyl compounds.

The combination of boron enolate **18** and silyl enol ether **19** allows selective oxidative cross-coupling to form 1,4-dicarbonyl compounds **20** (Scheme 19.6).[14] The reactivity can be controlled by the metallic countercation of enolates. It should be noted that this metallic moiety (boron and silicon) is not included in the product. Although excess use of one enolate is required in the most general strategies in the oxidative cross-coupling of enolates, such a method is not necessary in this reaction. In the case of enolates **21** and **10**, 1,4-diketone **22** is obtained in an excellent yield and selectivity (Scheme 19.7), and can be scaled up without lowering the yield and selectivity. The proposed mechanism is as follows. Transmetallation of boron to V(v) followed by redox reaction results in carbonyl α-radical species, which may be activated by V(IV). Then, radical addition to silyl enol ether and subsequent oxidation occur to form the product. Generation of carbonyl α-radical species is confirmed by the radical clock reaction using cyclopropyl-substituted substrate **23** (Scheme 19.7).[14]

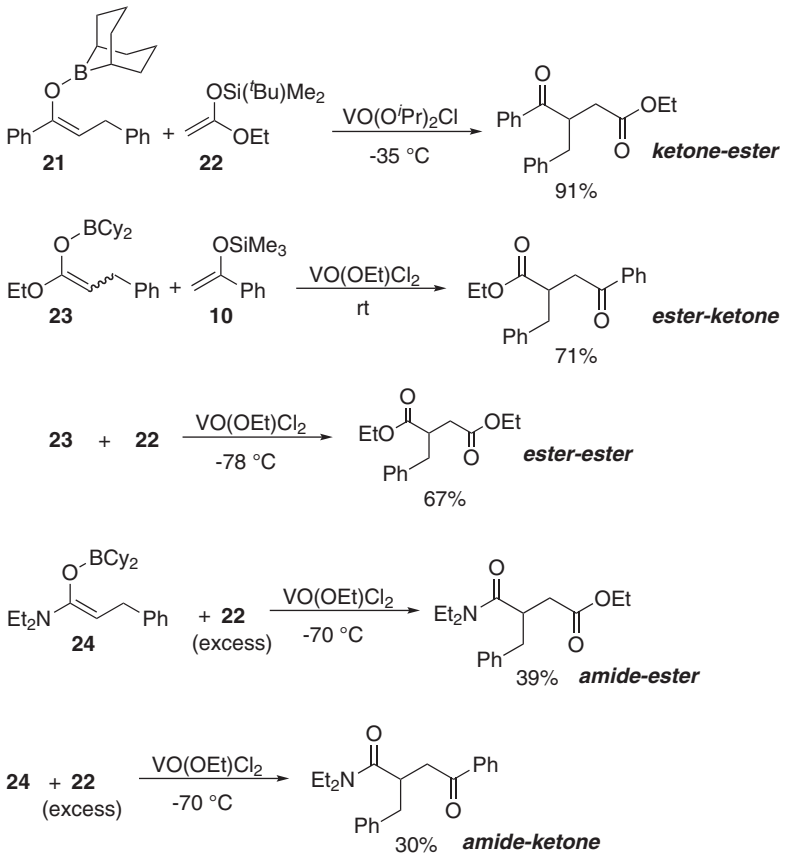

Scheme 19.8 Oxidative cross-coupling of various enolates derived from ketone, ester and amide.

This strategy for the oxidative cross-coupling can be extended to the combinations of various enolate species derived from ketone, ester and amide. Scheme 19.8 shows some examples for the enolate coupling of ketone–ester, ester–ketone, ester–ester, amide–ketone and amide–ester.[20]

19.2.2 Vanadium-induced Oxidative Ligand-coupling Reactions

As exemplified by Suzuki-Miyaura, Negishi and Stille cross-coupling reactions, the transition-metal-catalyzed cross-coupling of main-group organometallic compounds with organic halides is one of the most important and versatile synthetic methods in organic synthesis. The reaction pattern is considered as coupling between an electrophile and a nucleophile. On the other hand, the reactivity of main-group organometallic compounds can be widened by the transmetallation and/or electronic interaction of high-valent

metals. One-electron oxidation of d^0-transition metal compounds such as zirconocene[21] and titanocene[22] and platinum compounds[23] with a metallic oxidant permits selective coupling between two ligands on the transition metal, providing synthetically useful transformations. Such intramolecular coupling reactions of organic substituents on organometallic compounds are called ligand coupling. The oxovanadium(v)-induced oxidative ligand coupling on Al, Zn, Zr and B is described next (Scheme 19.9).

Oxidation of organoaluminum compounds usually gives alcohols, but the selective oxidative ligand coupling on aluminum has not been investigated. Treatment of aryldiethylaluminums **26**, prepared from aryllithiums **25** and diethylaluminum chloride, with $VO(OEt)Cl_2$ provides the oxidative cross-ligand coupling products, ethylarenes **27** (Scheme 19.10).[24] This is applicable to various arylaluminums **26** having an electron-donating group, allowing the selective cross-ligand coupling of the organic substituents on aluminum.

The ate complex **30** prepared from alkenylaluminum compound **28** and 1-alkynyllithium **29** can be similarly employed in the coupling of organic substituents on aluminum, leading to the *trans*-enyne **31** (Scheme 19.11).[24]

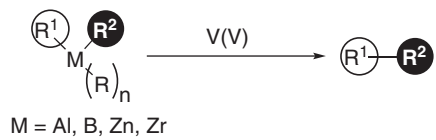

Scheme 19.9 Oxovanadium(v)-induced oxidative ligand coupling.

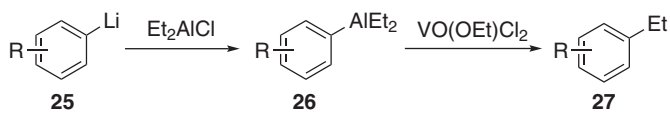

Scheme 19.10 Oxidative cross-ligand coupling on aluminum.

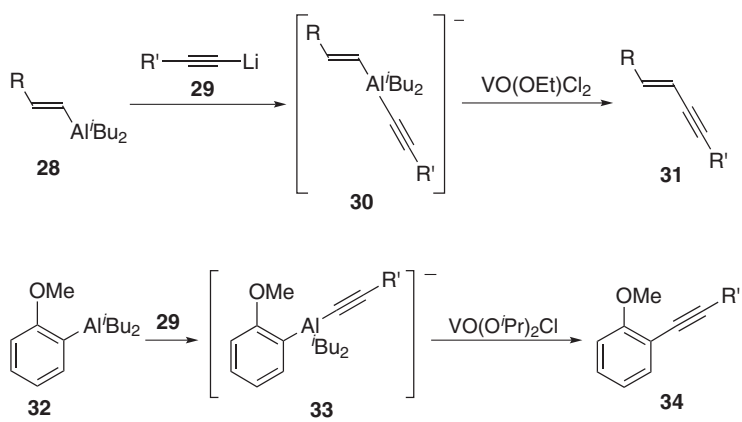

Scheme 19.11 Oxidative cross-ligand coupling from ate complex of aluminum for $sp–sp^2$ carbon–carbon bond formation.

It should be noted that this coupling reaction between sp and sp^2 carbons proceeds in the chemoselective and stereoselective manners. The ate complex **33** derived from the aryl-substituted aluminum compound **32** and 1-alkynyllithium **29** also undergoes the selective ligand coupling to give the aryl-1-alkynyl coupling product **34** (Scheme 19.11).[24] Although the reaction mechanism is not clear, oxovanadium(v)-involved electron transfer or transmetallation is considered to promote the oxidative ligand coupling. This transformation is regarded as the formal reductive elimination on aluminum.

Since organoborane compounds are readily available or prepared, their transformations, especially carbon–carbon bond-forming reactions, are important in organic synthesis. While most of the transformations employ them as a nucleophilic reagent, as exemplified by Suzuki-Miyaura cross-coupling, the oxidative ligand coupling between two nucleophilic substituents on boron is unique in the reactions of organoboron compounds.

In the case of organoborane **35,** which has two cyclohexyl and an (*E*)-alkenyl groups, $VO(OEt)Cl_2$-induced oxidative coupling takes place selectively between alkyl and alkenyl groups to give the corresponding cyclohexyl-substituted (*E*)-alkenyl compound **36** (Scheme 19.12),[25] where no homo-coupling products, dicyclohexyl and 1,3-bitadiene, are formed. Intramolecular coupling is indicated as a main pathway from the result of cross-over experiments.

Borate formation makes the V(v)-induced oxidative ligand coupling more facile, similar to the case of aluminum ate complexes. Borates **37** are formed by the reaction of dicyclohexyl(alkenyl)borane **35** with BuLi or CsF. The in-situ treatment with $VO(OEt)Cl_2$ results in the corresponding cyclohexyl substituted (*E*)-alkenyl compound **36** (Scheme 19.13).[25] A small amount of the (*Z*)-isomer is formed in the case using BuLi. But, when CsF is employed, the (*E*)-isomer is exclusively formed. As related reactions, alkenyltrialkylborates are known to be oxidized to alkylated alkenes with I_2 or BrCN.[26]

The catalytic use of oxovanadium(v) reagents is desirable. Such catalytic oxidative ligand coupling is achieved in the biaryl formation from tetra-arylborates under O_2. Tetra-arylborates **39** are prepared *via* the coupling of Ph_3B and ArLi **38**. The *in-situ* prepared borates **39** can be used for the catalytic oxidative ligand coupling to form biaryls **40** (Scheme 19.14).[27] It should be noted that unsymmetric biaryls **40** can be selectively obtained when an electron-rich Ar group is employed to prepare the corresponding

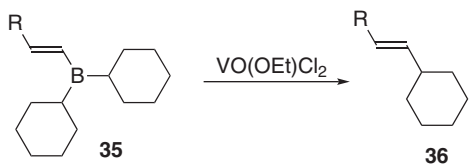

Scheme 19.12 Oxidative cross-ligand coupling on boron.

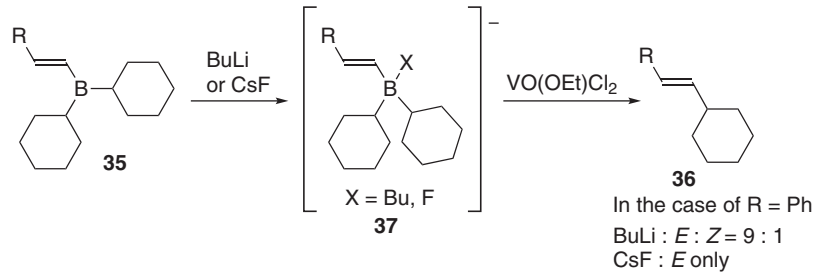

Scheme 19.13 Oxidative cross-ligand coupling from borate.

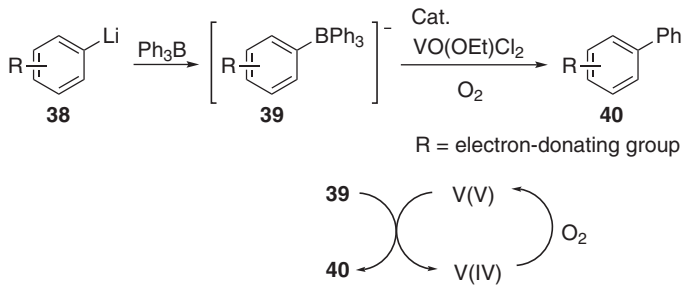

Scheme 19.14 Catalytic oxidative cross-ligand coupling from borate under O_2.

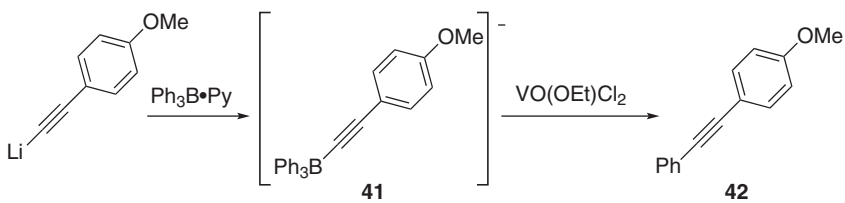

Scheme 19.15 Oxidative cross-ligand coupling from borate to form sp^2–sp carbon–carbon bond.

borate. Although the mechanism is not clear, the selectivity is based on the electron-rich Ar group. The crossover experiment indicates that this coupling proceeds in an intramolecular pathway. The catalytic cycle is likely to depend on the redox between V(IV) and V(V) under O_2. The evidence of V(IV) species is shown in the ESR spectrum. Other oxidative biaryl formations from tetraarylborates by photochemical, electrochemical and chemical oxidation using, *e.g.*, Ir(IV) oxidant, are also reported.[28–30]

The oxidative ligand coupling of borates also works to form an sp^2–sp carbon–carbon bond. The *in-situ* prepared triaryl(alkynyl)borate **41** is treated with a stoichiometric amount of $VO(OEt)Cl_2$, giving the corresponding aryl–alkynyl coupling product **42** selectively (Scheme 19.15).[31]

Organozinc compounds are useful carbanion equivalents because of the broad functional group tolerance. They have been employed for transition-

metal-catalyzed cross-coupling reactions with electrophiles such as organic halides (Negishi cross-coupling). On the other hand, the selective cross-coupling of two ligands on organozinc compounds are limited to a few examples, including 1,2-migration of zincate carbenoids and intramolecular coupling of organozinc compounds by organocopper reagents.[31–33]

The organozinc compound **44** for the oxidative ligand coupling is readily prepared by the reaction of MeZnCl and (2-methoxyphenyl)lithium derived from **43**. Treatment of **44** with $VO(OEt)Cl_2$ as an oxidant provides 1-methoxy-2-methylbenzene **45** as a ligand-coupling product (Scheme 19.16).[34] The cross-coupling between methyl and aryl groups takes place in preference to the homo-coupling of them in this oxidative ligand coupling. In the case of electron-rich aryl derivatives, for example bearing an *o*-methoxy, *o*-phenyl or *o*-methylthio group for a ligand of the zinc, the reaction proceeds well to afford the corresponding oxidative ligand coupling product. On the other hand, an electron-poor aryl derivative such as an *o*-cyano group shows lower reactivity. Instead of the methyl group, a 1-alkynyl group can be employed for this reaction to give the corresponding oxidative cross-coupling product.

Triorganozincates R_3ZnLi show a higher reactivity for the oxidative ligand coupling. Reaction of R_2Zn with ArLi forms the zincate $[(Ar)R_2Zn]^-$ **46**, followed by the treatment with $VO(OEt)Cl_2$ to afford the Ar-R compound **47** (Scheme 19.17).[34] The higher-order zincates $[ArMe_3Zn]^{2-}$ **48** generated by reaction of Me_4ZnLi_2 and ArBr also undergo the V(v)-induced oxidative cross-coupling to provide the corresponding Me-Ar **49** (Scheme 19.17).[35]

This method is applied to not only sp^3–sp^2 coupling but also sp^3–sp^3 coupling. Such a coupling is demonstrated by using the *gem*-dibromocyclopropane **50**. The higher-order zincate **51** is generated by bromine-zinc exchange of

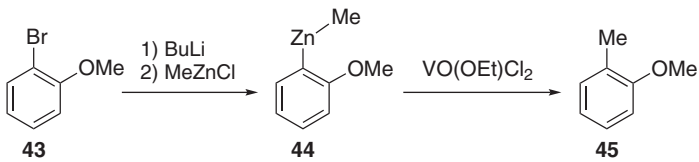

Scheme 19.16 Oxidative cross-ligand coupling on Zn.

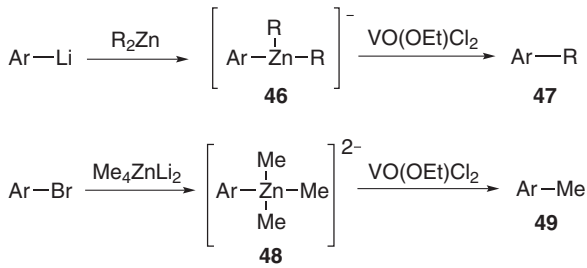

Scheme 19.17 Oxidative cross-ligand coupling from zincates.

50 with Me_4ZnLi_2 at –78 °C, where zinc takes at the *cis* position of phenyl group. Treatment of **51** with $VO(OEt)Cl_2$ leads to the oxidative cross-coupling product **52** stereoselectively with one bromide intact (Scheme 19.18).[36] On the other hand, dimethylated product **54** is formed *via* **53** by increasing the solution temperature of **51** to 0 °C, followed by treatment with $VO(OEt)Cl_2$.

1,4-Addition of R_2Zn to an α,β-unsaturated ketone requires the presence of a Lewis acid for the activation. The oxovanadium(v) compound with the properties of a Lewis acid and one-electron oxidant not only promotes 1,4-addition of R_2Zn to enone **55** but also the intramolecular oxidative cross-coupling of the resulting alkylzinc enolate species **56**. Consequently, the corresponding vicinally α,β-dialkylated compound **57** is formed (Scheme 19.19).[37] Two nucleophiles can be introduced at the α- and β-positions of enone **55**. Some examples are provided here. Treatment of 2-cyclohexenone and Me_2Zn with a stoichiometric amount of $VO(OEt)Cl_2$ provides 2,3-dimethylcyclohexanone **58** with 78% yield (Scheme 19.20).[37]

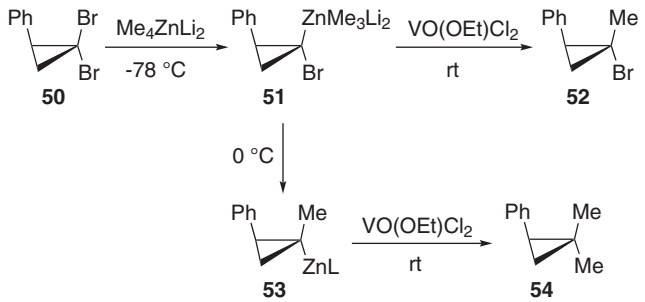

Scheme 19.18 Oxidative cross-ligand coupling from zincates to form sp^3–sp^3 carbon–carbon bond.

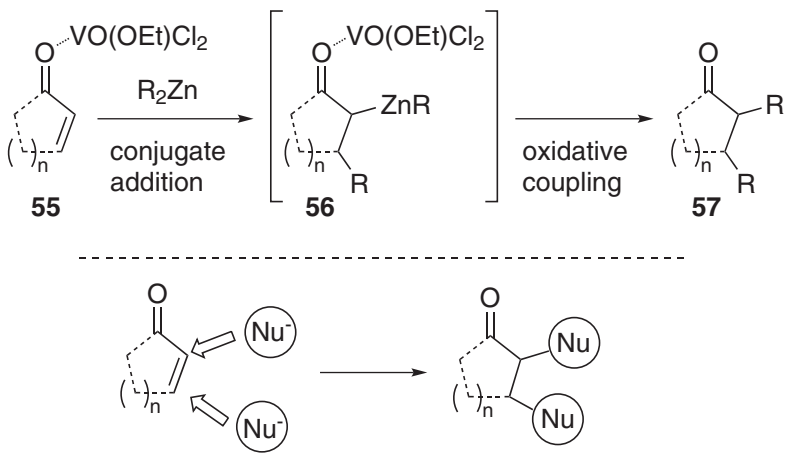

Scheme 19.19 Sequential conjugate addition to enone and oxidative cross-coupling to form vicinally α,β-disubstituted compound.

Instead of R_2Zn, AlR_3 and BR_3 can be used for this kind of reaction as well. Zincate R_3ZnLi undergoes 1,4-addition to enone without the assistance of Lewis acid. Furthermore, selective transfer of butyl group in $BuMe_3ZnLi$ is possible in this type of 1,4-addition. The introduction of two different alkyl groups at α- and β-positions of enone is allowed by the sequence of selective 1,4-addtion and intramolecular oxidative cross-coupling. As an example, the reaction of cyclohexenone with $BuMe_2ZnLi$, followed by treatment with $VO(OEt)Cl_2$ affords the corresponding 3-butyl-2-methlcycloalkanone **59** in a moderate yield.

Oxidative ligand coupling on Zr is also possible. (*E*)-1-Alkenyl-1-alkynylzirconocenes **61** can be formed by hydrozirconation of a terminal alkyne to give (*E*)-alkenylchlorozirconocenes **60**, followed by the reaction with alkynyl lithium. *In-situ* treatment of **61** with $VO(O^iPr)_2Cl$ induces oxidative ligand coupling on zirconium to give the (*E*)-enynes **62** stereoselectively and chemoselectively (Scheme 19.21).[38]

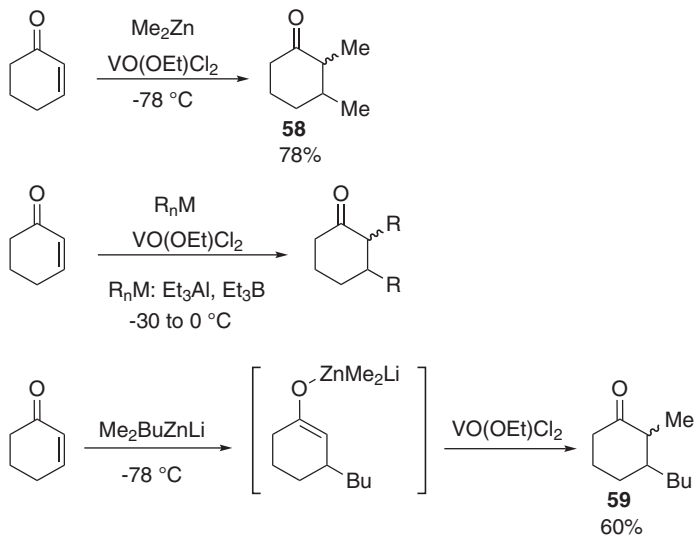

Scheme 19.20 Vicinal dialkylation of 2-cyclohexenone based on sequential conjugate addition to enone and oxidative cross-coupling.

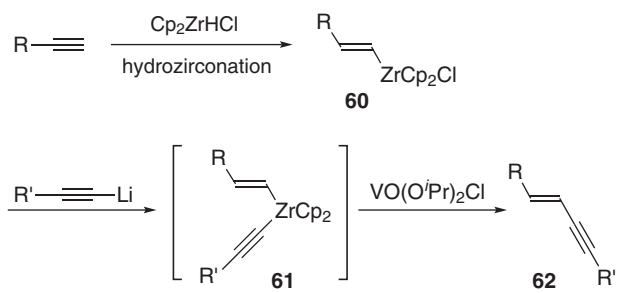

Scheme 19.21 Oxidative cross-ligand coupling on zirconium.

19.3 Vanadium-induced Reductive Coupling

The reductive coupling of carbonyl compounds is a useful synthetic method to form carbon–carbon bonds bearing vicinal functional groups. One-electron transfer from a metal to a carbonyl group generates the corresponding anion radical, which can dimerize to give 1,2-diol. The stoichiometric reductive dimerization has been carried out with low-valent metals such as aluminum amalgam, zinc, titanium, vanadium and samarium. For example, the pinacol coupling using $TiCl_3$/Zn-Cu or $[V_2Cl_3(THF)_6]_2[Zn_2Cl_6]$ has been employed for the synthesis of paclitaxel[39] or C_2-symmetrical HIV protease inhibitors,[40] respectively. To synthesize such complex compounds, control of the stereochemistry and construction of a catalytic system are important.[41] Furthermore, the cross-coupling is a challenging issue.

A catalytic system for a vanadium reagent is realized in the presence of chlorosilane and a stoichiometric co-reductant to induce the pinacol coupling.[42] A redox cycle consists of the generation (or regeneration) of low-valent vanadium species mediating the electron transfer from Zn and the low-valent vanadium-induced pinacol coupling in the presence of chlorosilane (Scheme 19.22).

Highly diastereoselective pinacol coupling of secondary aliphatic aldehydes takes place in the presence of Cp_2VCl_2 catalyst and stoichiometric amount of chlorosilane derivatives and Zn in THF to form *dl*-1,2-diols **63**

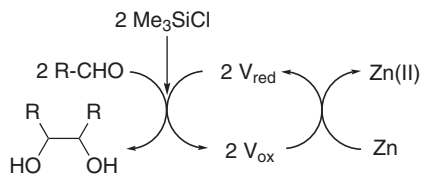

Scheme 19.22 Vanadium-catalyzed pinacol coupling assisted by chlorosilane.

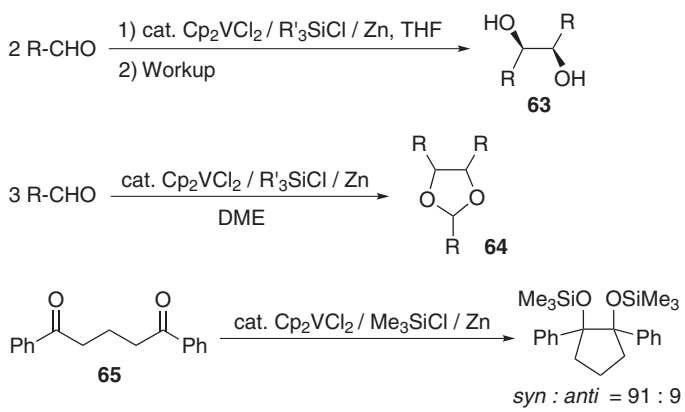

Scheme 19.23 Catalytic pinacol coupling reactions.

(Scheme 19.23).[43,44] The reaction in DME provides the 1,3-dioxolanes **64** *via* the pinacol coupling and acetal formation (Scheme 19.23).[45] The diastereoselectivity depends on substituent of chlorosilanes. $PhMe_2SiCl$ shows a higher selectivity as compared to Me_3SiCl. This implies its steric effect in the coupling step. In the absence of a chlorosilane, a catalytic reaction does not proceed. Silylation is likely to play a role for liberating the catalyst from the alkoxide intermediate. Chlorosilane is also assumed to facilitate the electron transfer to the carbonyl group as a Lewis acid, generating the stabilized silyloxyalkyl radical for dimerization. This catalytic system is applied to the selective intramolecular pinacol coupling reaction of the 1,5-diketone **65** (Scheme 19.23).[43] The $VOCl_3/Me_3SiCl/Al$ system also gives rise to the *dl*-selective reductive coupling of benzaldehydes.[46]

Instead of a chlorosilane, Ac_2O or AcCl can be used in the $VOCl_3$-catalyzed pinacol coupling of an aromatic aldehyde to provide the diacetate **66** (Scheme 19.24).[47]

The $Cp_2VCl_2/R_3SiCl/Zn$ catalytic system can be applicable to the reductive coupling of aldimine (Scheme 19.25).[48] Formation of *meso*-diamine **67** is favorable in this reaction compared to the *dl*-diamine. The diastereoselectivity depends on the substituents on the nitrogen and silicon atoms. The allyl or benzyl group on the nitrogen atom tends to raise *meso*-selectivity. Various catalytic systems have been investigated for the diastereoselective coupling.

Fürstner and co-workers have independently developed a similar catalytic method for the Ti-induced intramolecular McMurry-type coupling of the amide to give the indoles in the presence of Zn and chlorosilane.[49] Catalytic systems for the enantioselective pinacol coupling are also demonstrated by using a titanium or chromium catalyst with a chiral ligand.[50–54]

A ternary system such as cat. $Cp_2MCl_2/Me_3SiCl/Zn$ (M = V or Ti) allows other reductive carbon–carbon bond-forming reactions. The reaction of the δ,ε-unsaturated aldehyde **68** provides the cyclic alcohol **69** with excellent diastereoselectivity in the presence of Cp_2VCl_2 as a catalyst (Scheme 19.26).[43] The radical anion intermediate generated by one-electron reduction of aldehyde is likely to undergo 5-*exo*-cyclization followed by chlorination.

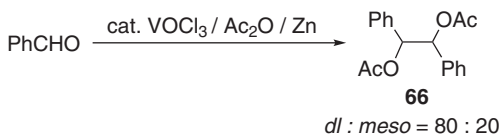

Scheme 19.24 Pinacol coupling reaction assisted by Ac_2O.

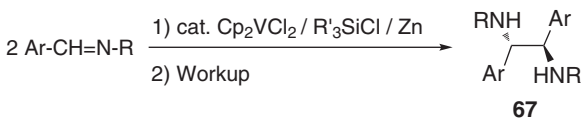

Scheme 19.25 Pinacol coupling reaction of aldimines.

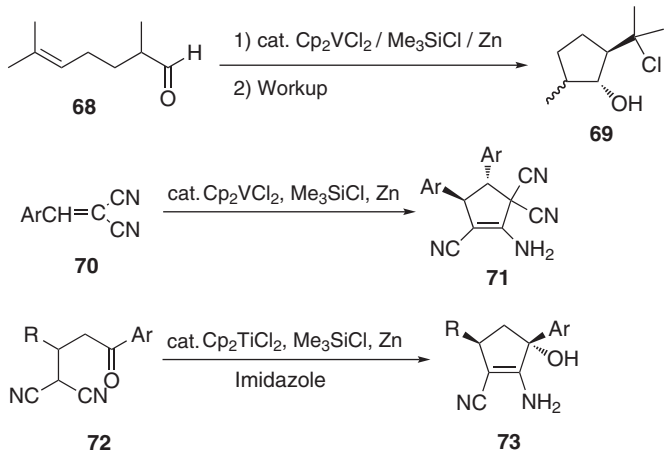

Scheme 19.26 Reductive carbon-carbon bond formations.

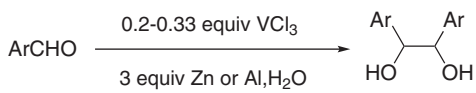

Scheme 19.27 Pinacol coupling reaction in water.

Arylidene malononitrile **70** also undergoes diastereoselective catalytic cyclodimerization to give **71** under similar conditions (Scheme 19.26).[55] The Cp_2TiCl_2-catalyzed reductive cyclization of the ketonitrile **72** affords the amino alcohol **73** with high *trans* selectivity (up to 94% *trans*) (Scheme 19.26).[56]

Surprisingly, vanadium-catalyzed pinacol coupling proceeds in water. It should be noted that chlorosilane is not necessary for the reaction in water, probably since a proton source is available in this catalytic system (Scheme 19.27).[57]

Selective intermolecular cross-pinacol coupling is a direct method to provide asymmetric 1,2-diols. However, the selective intermolecular cross-coupling is not as easily attained as the homo-coupling. Some examples have been reported so far.[41,58,59] For example, Pedersen *et al.,* have reported the cross-pinacol coupling between aldehydes using a stoichiometric dimeric vanadium complex.[60–62] The key point in cross-selectivity is that one aldehyde has a chelating moiety to metal, such as amide, to increase its reactivity. The difference of reactivity between two aldehydes allows the cross-coupling. Namely, the selectivity is controlled by the substrate.

Cross-pinacol coupling by control of spatially regulated reaction sites in the catalysts has been studied. The dinuclear complex consisting of three-dimensionally arranged bis-biphenol ligand on a hexaaryl benzene scaffold **74** has been developed for this purpose (Scheme 19.28).[63] The cross-selectivity is not high in the case of this homo-dinuclear complex with Ti, but the effect of the homo-dinuclear complex is clearly exhibited.

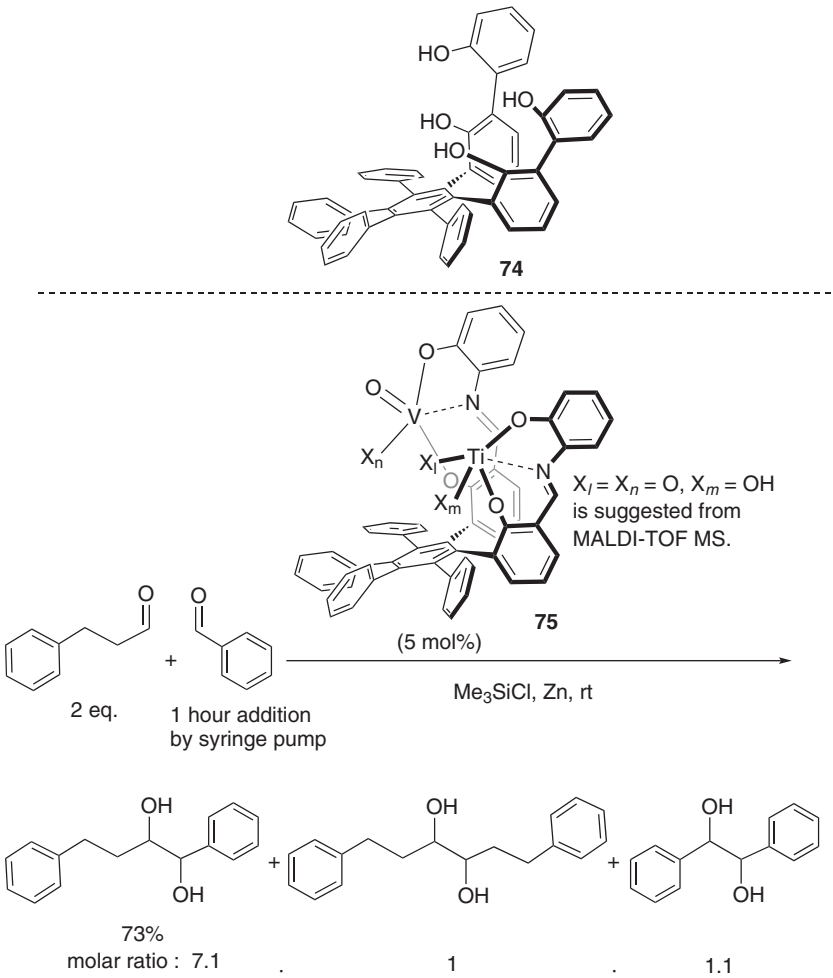

Scheme 19.28 Cross-pinacol coupling reaction catalyzed by hetero dinuclear complex catalyst with V(v) and Ti(iv).

As an advanced version of this ligand for the dinuclear complex, the dihemisalen complex **75** has been applied.[59,64] Notably, a hetero dinuclear complex can be designed, namely by the combination of V and Ti. The hetero-dinuclear complex catalyst with V(v) and Ti(iv) permits the selective intermolecular cross-pinacol coupling reaction between aliphatic and aromatic aldehydes in the presence of Me_3SiCl and Zn (Scheme 19.28), where aromatic aldehydes are dropwise added over 1 h by syringe pump.[59] A model study using the corresponding mononuclear hemisalen complex indicates that the vanadium complex does not activate aliphatic aldehydes but aromatic ones. On the other hand, the titanium complex can activate both. Therefore, the observed cross-selectivity can be explained by the individual

activation of two aldehydes (the aliphatic one by titanium and the aromatic one by vanadium species) that are placed in suitable spaces on the rigid scaffold.

19.4 Conclusion

This chapter surveys the vanadium-induced oxidative and reductive coupling developed in our group. One-electron oxidation capability with Lewis acidity of oxovanadium(v) compounds allows oxidative carbon–carbon bond formation. V(v) can work well as an oxidant for the homo- and cross-coupling of enolate species such as silyl enol ether. The redox potential of silyl enol ether is a key feature for the susceptibility to oxidation. A careful choice of the combination with the redox potential in mind leads to the successful oxidative cross-coupling. Combination of boron enolate and silyl enol ether is even more effective for the selective oxidative coupling. Ligand coupling reactions, which are coupling reactions of organic substituents on main-group organometallic compounds, are also induced by oxidation with oxovanadium(v) compounds, where main-group metals, Al, Zn, B, *etc*., can be used in these reactions. Low-valent vanadiums or titaniums contribute to reductive coupling reactions as a catalyst, as exemplified by pinacol coupling reactions, which require the presence of chlorosilane and a co-reductant, zinc. The use of the heterobimetallic catalyst consisting of vanadium and titanium permits the selective cross-coupling between aryl and aliphatic aldehydes.

Abbreviations

Ac	acetyl
Ar	aryl
Bu	butyl
9-BBN	9-borabicyclo[3.3.1]nonane
Cp	cyclopentadienyl
Cy	cyclohexyl
DME	1,2-dimethoxyethane
Et	ethyl
^{i}Pr	isopropyl
L	ligand
Me	methyl
CN	nitrile
Ph	phenyl
THF	tetrahydrofuran

References

1. T. Hirao, *Chem. Rev.*, 1997, **97**, 2707.
2. T. Hirao, T. Moriuchi, T. Amaya, A. Ogawa and A. Nomoto, Synthetic Methods for Redox Reactions Using Phosphorus, Vanadium and

Samarium Compounds, in *Functionalized Redox Systems: Synthetic Reactions and Design of π- and Bio-Conjugates*, ed. T. Hirao, Springer, Tokyo, 2015, pp. 5–50.
3. F. Guo, M. D. Clift and R. J. Thomson, *Eur. J. Org. Chem.*, 2012, 4881.
4. S. Khaghaninejad and M. M Heravi, *Adv. Heterocycl. Chem.*, 2014, **111**, 95.
5. V. E. Ziffle, P. Cheng and D. L. J. Clive, *J. Org. Chem.*, 2010, **75**, 8024.
6. Y. Ito, T. Konoike and T. Saegusa, *J. Am. Chem. Soc.*, 1975, **97**, 649.
7. Y. Ito, T. Konoike and T. Saegusa, *J. Am. Chem. Soc.*, 1975, **97**, 2912.
8. K. Narasaka, T. Okauchi, K. Tanaka and M. Murakami, *Chem. Lett.*, 1992, **21**, 2099.
9. Y. Kohno and K. Narasaka, *Bull. Chem. Soc. Jpn.*, 1995, **68**, 322.
10. K. Ryter and T. Livinghouse, *J. Am. Chem. Soc.*, 1998, **120**, 2658.
11. M. Schmittel and A. Haeuseler, *J. Organomet. Chem.*, 2002, **661**, 169.
12. M. P. DeMartino, K. Chen and P. S. Baran, *J. Am. Chem. Soc.*, 2008, **130**, 11546.
13. X. Huang, Q. Zhang, J. Lin, K. Harms and E. Meggers, *Nat. Chem.*, 2019, **2**, 34.
14. T. Amaya, Y. Maegawa, T. Masuda, Y. Osafune and T. Hirao, *J. Am. Chem. Soc.*, 2015, **137**, 10072. And other related references are cited in this report.
15. T. Ishikawa, A. Ogawa and T. Hirao, *Organometallics*, 1998, **17**, 5713.
16. T. Fujii, T. Hirao and Y. Ohshiro, *Tetrahedron Lett.*, 1992, **33**, 5823.
17. M. Nishina, T. Moriuchi and T. Hirao, *Dalton Trans.*, 2010, **39**, 9936.
18. T. Hirao, T. Fujii and Y. Ohshiro, *Tetrahedron*, 1994, **50**, 10207.
19. T. Amaya, T. Masuda, Y. Maegawa and T. Hirao, *Chem. Commun.*, 2014, **50**, 2279.
20. T. Amaya, Y. Osafune, Y. Maegawa and T. Hirao, *Chem. – Asian J.*, 2017, **12**, 1301.
21. R. F. Jordan, R. E. LaPointe, C. S. Bajgur, S. F. Echols and R. Willet, *J. Am. Chem. Soc.*, 1987, **109**, 4111.
22. M. J. Burk, W. Tumas, M. D. Ward and D. R. Wheeler, *J. Am. Chem. Soc.*, 1990, **112**, 6133.
23. M. Sato and E. Mogi, *Otganometallics*, 1995, **14**, 3157.
24. T. Ishikawa, A. Ogawa and T. Hirao, *J. Am. Chem. Soc.*, 1998, **120**, 5124.
25. T. Ishikawa, S. Nonaka, A. Ogawa and T. Hirao, *Chem. Commun.*, 1998, 1209.
26. A. Pelter, K. Smith and H. C. Brown, *Borane Reagents*, Academic Press, London, 1988.
27. H. Mizuno, H. Sakurai, T. Amaya and T. Hirao, *Chem. Commun.*, 2006, 5042.
28. D. H. Geske, *J. Phys. Chem.*, 1959, **63**, 1062, 1962, 66, 1743.
29. A. Pelter, R. T. Pardasani and P. Pardasani, *Tetrahedron*, 2000, **56**, 7339.
30. P. Abley and J. Halpern, *J. Chem. Soc. D, Chem. Commun.*, 1971, 1238.

31. T. Amaya, Y. Tsukamura and T. Hirao, *Adv. Synth. Catal.*, 2009, **351**, 1025.
32. M. Iyoda, S. M. H. Kabir, A. Vorasingha, Y. Kuwatani and M. Yosihda, *Tetrahedron Lett.*, 1998, **39**, 5393.
33. T. Harada, T. Kaneko, T. Fujiwara and A. Oku, *J. Org. Chem.*, 1997, **62**, 8966.
34. T. Harada, T. Katsuhira, A. Osada, K. Iwazaki, K. Maejima and A. Oku, *J. Am. Chem. Soc.*, 1996, **118**, 11377.
35. T. Hirao, T. Takada and A. Ogawa, *J. Org. Chem.*, 2000, **65**, 1511.
36. T. Takada, H. Sakurai and T. Hirao, *J. Org. Chem.*, 2001, **66**, 300.
37. T. Hirao, T. Takada and H. Sakurai, *Org. Lett.*, 2000, **2**, 3659.
38. T. Ishikawa, A. Ogawa and T. Hirao, *J. Organometal. Chem.*, 1999, **575**, 76.
39. K. C. Nicolaou, J.-J. Liu, Z. Yang, H. Ueno, E. J. Sorensen, C. F. Claiborne, R. K. Guy, C.-K Hwang, M. Nakada and P. G. Nantermet, *J. Am. Chem. Soc.*, 1995, **117**, 634.
40. B. Kammermeier, G. Beck, D. Jacobi and H. Jendralla, *Angew. Chem., Int. Ed. Engl.*, 1994, **33**, 685.
41. A. Chatterjee and N. N. Joshi, *Tetrahedron*, 2006, **62**, 12137.
42. T. Hirao, *Synlett*, 1999, 175.
43. T. Hirao, M. Asahara, Y. Muguruma and A. Ogawa, *J. Org. Chem.*, 1998, **63**, 2812.
44. T. Hirao, A. Ogawa, M. Asahara, Y. Muguruma and H. Sakurai, *Org. Synth.*, 2005, **81**, 26.
45. T. Hirao, T. Hasegawa, Y. Muguruma and I. Ikeda, *J. Org. Chem.*, 1996, **61**, 366.
46. T. Hirao, B. Hatano, Y. Imamoto and A. Ogawa, *J. Org. Chem.*, 1999, **64**, 7665.
47. B. Hatano, A. Ogawa and T. Hirao, *J. Org. Chem.*, 1998, **63**, 9421.
48. T. Hirao, H. Takeuchi, A. Ogawa and H. Sakurai, *Synlett*, 2000, 1658.
49. A. Fürstner and A. Hupperts, *J. Am. Chem. Soc.*, 1995, **117**, 4468.
50. R. L. Halterman, C. Zhu, Z. Chen, M. S. Dunlap, M. A. Khan and K. M. Nicholas, *Organometallics*, 2000, **19**, 3824.
51. A. Bensari, J.-L. Renaud and O. Riant, *Org. Lett.*, 2001, **3**, 3863.
52. A. Chatterjee, T. H. Bennur and N. N. Joshi, *J. Org. Chem.*, 2003, **68**, 5668.
53. N. Takenaka, G. Xia and H. Yamamoto, *J. Am. Chem. Soc.*, 2004, **126**, 13198.
54. Y.-G. Li, Q.-S. Tian, J. Zhao, Y. Feng, M.-J. Li and T.-P. You, *Tetrahedron: Asymmetry*, 2004, **15**, 1707.
55. L. Zhou and T. Hirao, *Tetrahedron Lett.*, 2000, **41**, 8517.
56. L. Zhou and T. Hirao, *Tetrahedron*, 2001, **57**, 6927.
57. X. Xu and T. Hirao, *J. Org. Chem.*, 2005, **70**, 8594.
58. B. S. Terra and F. Macedo Jr., *ARKIVOC*, 2012, **i**, 134.
59. A. Miyasaka, T. Amaya and T. Hirao, *Chem. – Eur. J.*, 2014, **20**, 1615. And references are cited in this report.

60. J. H. Freudenberger, A. W. Konradi and S. F. Pedersen, *J. Am. Chem. Soc.*, 1989, **111**, 8014.
61. J. Park and S. F. Pedersen, *J. Org. Chem.*, 1990, **55**, 5924.
62. A. W. Konradi, S. J. Kemp and S. F. Pedersen, *J. Am. Chem. Soc.*, 1994, **116**, 1316.
63. T. Amaya, A. Miyasaka and T. Hirao, *Tetahedron Lett.*, 2011, **52**, 4567.
64. A. Miyasaka, T. Amaya and T. Hirao, *Tetahedron Lett.*, 2012, **53**, 5589.

CHAPTER 20

Vanadium-catalyzed Transformations of Selected Functional Groups

T. MORIUCHI*[a] AND T. HIRAO*[b]

[a] Division of Molecular Materials Science, Graduate School of Science, Osaka City University, 3-3-138 Sugimoto, Sumiyoshi-ku, Osaka 558-8585, Japan; [b] The Institute of Scientific and Industrial Research, Osaka University, Mihoga-oka, Ibaraki, Osaka 567-0047, Japan
*Emails: moriuchi@sci.osaka-cu.ac.jp; hirao@chem.eng.osaka-u.ac.jp

20.1 Vanadium-catalyzed Oxidative Halogenation under Molecular Oxygen

20.1.1 Vanadium-catalyzed Oxidative Chlorination and Iodination under Molecular Oxygen

The bromination reaction is one of the most fundamental reactions in organic synthesis, affording important precursors for various transformations. The combination of commercially available inexpensive NH_4VO_3, Bu_4NBr and a Brønsted acid (TFA or PTS·H_2O) or a Lewis acid ($AlCl_3$ or $AlBr_3$) under molecular oxygen is demonstrated to induce an efficient oxidative bromination reaction (Scheme 20.1).[1–4] This method is successfully applied to vanadium-catalyzed oxidative chlorination and iodination under molecular oxygen.[5]

Catalysis Series No. 41
Vanadium Catalysis
Edited by Manas Sutradhar, José Armando L. da Silva and Armando J. L. Pombeiro

Published by the Royal Society of Chemistry, www.rsc.org

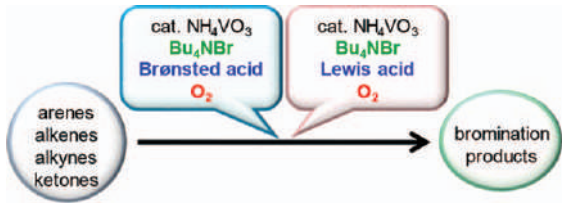

Scheme 20.1 Oxovanadium(v)-catalyzed bromination under molecular oxygen.

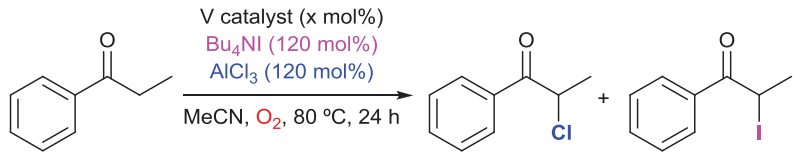

V catalyst =		1	2
	NH_4VO_3 (10 mol%)	60%	0%
	NH_4VO_3 (20 mol%, 36 h)	98%	0%
	$VO(O^iPr)_3$ (20 mol%)	90%	3%

Scheme 20.2 Catalytic chlorination of propiophenone.

Table 20.1 Catalytic chlorination of alkenes.[a]

Entry	Substrate	Time (h)	Product NMR yield[b]	Entry	Substrate	Time (h)	Product NMR yield[b]
1	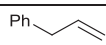	24	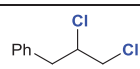 **3**, 87% (66%)	3	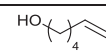	24	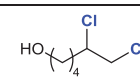 **5**, 78% (65%)
2		30	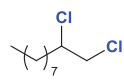 **4**, 72% (66%)				

[a]Conditions: 0.25 mmol of substrate, 25 mol% $VO(O^iPr)_3$, 220 mol% Bu_4NI, 220 mol% $AlCl_3$, 1 mL acetnitrile, under molecular oxygen, 80 °C.
[b]Isolated yields in parentheses.

The catalytic chlorination reaction of propiophenone by using NH_4VO_3 (10 mol%) catalyst combined with Bu_4NI (120 mol%) and $AlCl_3$ (120 mol%) as a Lewis acid in MeCN at 80 °C for 24 h under molecular oxygen proceeds well to afford the α-chlorocarbonyl product **1** in 60% yield. (Scheme 20.2).[5] Longer reaction time affords the α-chlorocarbonyl product **1** quantitatively. A high catalytic activity is observed with $VO(O^iPr)_3$ as a catalyst. This catalytic chlorination system can be applied to the chlorination of alkenes (Table 20.1).[5] Allylbenzene undergoes the selective *vic*-chlorination to give the dichloride **3** in 87% yield (Entry 1). 1-Decene is converted into 1,2-dichlorodecane (**4**) in 72% yield (Entry 2). Catalytic chlorination of 5-hexene-1-ol affords the dichlorinated product **5** in 78% yield with the hydroxy group intact (Entry 3).

Scheme 20.3 Gram-scale catalytic chlorination reaction of propiophenone.

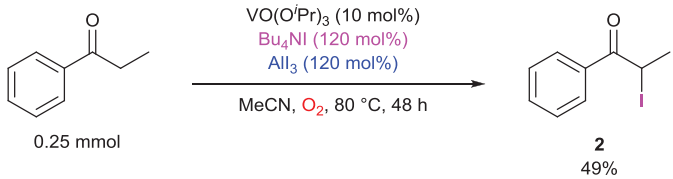

Scheme 20.4 Catalytic iodination of propiophenone.

Gram-scale reaction of the α-chlorination of propiophenone is successfully allowed to give the expected chlorinated product **1** in 78% isolated yield as shown in Scheme 20.3.[5]

The combination of Bu_4NI and AlI_3 induces the α-iodination of propiophenone to give **2** in 49% yield (Scheme 20.4).[5]

20.1.2 Vanadium-catalyzed Oxidative Aromatization of 2-cyclohexenones under Molecular Oxygen

Catalytic dehydrogenative aromatization of α,β-unsaturated cyclohexenones has attracted much attention for the synthesis of phenols.[6–9] However, severe reaction conditions or a long reaction time are required in these catalytic dehydrogenative aromatization systems. The aerobic vanadium-catalyzed oxidation system is applicable to the catalytic oxidative aromatization of α,β-unsaturated cyclohexenones.[10]

The catalytic oxidative aromatization reaction of 2-cyclohexen-1-one by using NH_4VO_3 (5 mol%) catalyst combined with Bu_4NBr (300 mol%) and TFA (300 mol%) in 1,4-dioxane at 80 °C for 6 h under molecular oxygen proceeds smoothly to give the corresponding phenol **6a** in 80% yield with *p*-benzoquinone **7** in 7% yield (Table 20.2, Entry 1).[10] $VO(acac)_2$ shows a similar catalytic activity (Entry 2). A high catalytic activity is achieved with $VOSO_4$ to afford the further monobrominated product **6b** (Entry 3). The catalytic oxidative aromatization is effectively demonstrated even under air to give the phenol **6a** in 75% yield, although a longer reaction time is required (Entry 4).

The catalyst loading can be successfully reduced to 1 mol% in a gram-scale catalytic oxidative aromatization of 4-carboethoxy-3-methyl-2-cyclohexen-1-one to afford the phenol **6c** in 81% isolated yield as shown in Scheme 20.5.[10]

Table 20.2 Catalytic oxidative aromatization of 2-cyclohexen-1-one.[a]

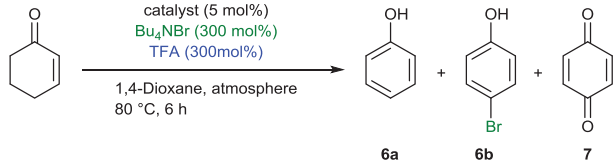

Entry	Catalyst	Atmosphere	NMR yield (%) 6a	6b	7	Entry	Catalyst	Atmosphere	NMR yield (%) 6a	6b	7
1	NH_4VO_3	O_2	80	0	7	3	$VOSO_4$	O_2	64	24	4
2	$VO(acac)_2$	O_2	86	0	6	4[b]	$VOSO_4$	air	75	0	14

[a]Conditions: 0.50 mmol of 2-cyclohexen-1-one, 5 mol% catalyst, 300 mol% Bu_4NBr, 300 mol% TFA, 1.5 mL 1,4-dioxane.
[b]Reaction time: 21 h.

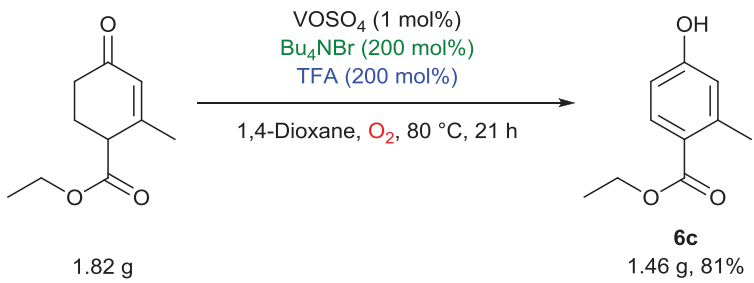

Scheme 20.5 Gram-scale catalytic oxidative aromatization of 4-carboethoxy-3-methyl-2-cyclohexen-1-one.

Table 20.3 Catalytic oxidative aromatization of 2-cyclohexen-1-one by using HBr aq (48%) as bromide and proton sources.[a]

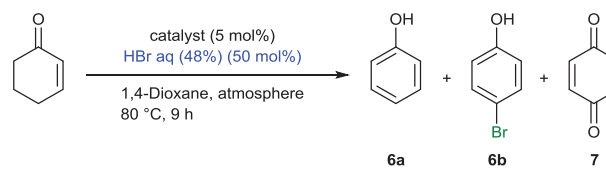

Entry	Catalyst	Atmosphere	NMR yield (%) 6a	6b	7	Entry	Catalyst	Atmosphere	NMR yield (%) 6a	6b	7
1	NH_4VO_3	O_2	71	0	5	3	$VOSO_4$	O_2	77	0	10
2	$VO(acac)_2$	O_2	72	0	8	4[b]	$VOSO_4$	air	73	0	10

[a]Conditions: 0.50 mmol of 2-cyclohexen-1-one, 5 mol% catalyst, 50 mol% HBr aq (48%), 1.5 mL 1,4-dioxane.
[b]Reaction time: 47 h.

The catalytic oxidative aromatization of 2-cyclohexen-1-one is also performed by a combination of NH_4VO_3 (5 mol%) and HBr aq (48%) (50 mol%) to afford the phenol **6a** in 71% yield, indicating that HBr serves as both a bromide source and Brønsted acid (Table 20.3, Entry 1).[10] A similar catalytic activity is observed with $VO(acac)_2$ as a catalyst (Entry 2). $VOSO_4$ exhibits a high catalytic activity (Entry 3). The catalytic oxidative aromatization proceeds well even under air with a longer reaction time (Entry 4).

20.2 Vanadium(v)-catalyzed Direct Amination of Allyl Alcohols

Allyl amines are important precursors and building blocks for the synthesis of biologically active compounds.[11,12] One reliable method for the synthesis of allyl amines is the direct amination of allyl alcohols because water is the only by-product.[13–16] Generally, precious transition metal catalysts have been utilized to achieve direct amination of allyl alcohols.[13,14,17–19] Only some examples of direct amination of allyl alcohols using non-precious metal-catalysts have been reported.[20–24] In this section, direct amination of allyl alcohols using the advantages of Lewis acidity and oxophilicity of the economical oxovanadium(v) compound is described.[25]

The direct amination reaction of 1,3-diphenylprop-2-en-1-ol (**8a**) with *p*-anisidine (**9a**) in the presence of $VO(OSiPh_3)_3$ (5 mol%) as a catalyst and MS3A as a dehydrating reagent at 50 °C gives the corresponding allyl amine **10aa** in 85% yield (Table 20.4, Entry 1).[25] This oxovanadium(v)-catalyzed direct amination system can be applied to the catalytic amination with *p*-substituted aniline derivatives **9b–e** having either electron-rich or electron-deficient substituents, affording the desired allyl amines **10ab–ae** in good yields. The desired allyl amine **10af** is also obtained in an excellent yield in the direct amination reaction with an *o*-substituted aniline such as *o*-nitroaniline (**9f**).

Table 20.4 Substrate scope in the amination of 1,3-diphenylprop-2-en-1-ol (**8a**) with aniline derivatives.[a,b]

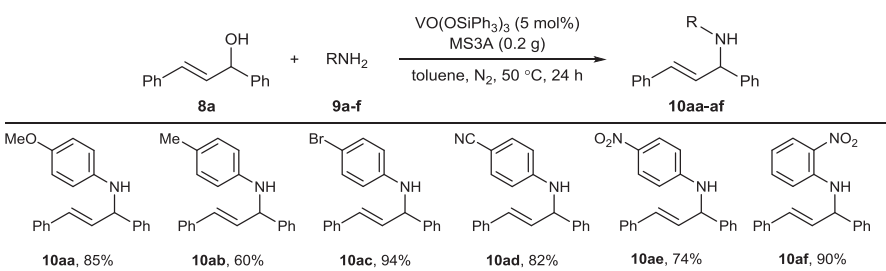

[a]Reaction conditions: 0.20 mmol of amine and 1,3-diphenylprop-2-en-1-ol (**8a**), 5 mol% of $VO(OSiPh_3)_3$, 0.2 g MS3A, 2.0 mL toluene, under nitrogen atmosphere.
[b]The yield was determined by ^1H NMR.

The oxovanadium(v)-catalyzed direct amination of **8a** with various aliphatic amines **9g–o** can be induced by performing the reaction with 10 mol% of $VO(OSiPh_3)_3$ and 1.0 g of MS3A at 100 °C to produce the desired allyl amines (Table 20.5).[25] A bulky amine such as 1-adamantylamine (**9j**) undergoes the catalytic direct amination to afford the desired allyl amine **10aj** in 88% yield. Even in the case of secondary aliphatic amines **9k-n**, the desired allyl amines **10ak–an** are produced. By using 300 mol% of *p*-toluenesulfonamide **9o**, the corresponding allyl amine **10ao** can be also obtained in 35% yield.

This oxovanadium(v)-catalyzed direct amination system can be applied to a variety of allyl alcohols (Table 20.6).[25] The catalytic direct amination reaction of the allyl alcohols with *p*-substitutions **8b–c** proceeds moderately. The catalytic direct amination reaction of the α-methylated allyl alcohol **8d** is also performed to afford the desired allyl amine **10da** in 77% yield. The allyl amines **10ea** and **10fa** are produced in 31% and 14% yields, respectively, from the catalytic direct amination reaction of 4-phenyl-3-buten-2-ol (**8e**) at 80 °C. By elevating the reaction temperature to 100 °C with 200 mol% of **8e**, the allyl amine **10ea** is obtained selectively in 78% yield. The catalytic direct amination reaction of 1-phenyl-2-buten-1-ol (**8f**) at 80 °C also leads to the formation of the allyl amines **10ea** and **10fa** in 24% and 9% yields, respectively. At 100 °C, the allyl amine **10ea** is produced regioselectively in 81% yield by using 200 mol% of **8f**.

Gram-scale oxovanadium(v)-catalyzed direct amination of **8a** with **9a** is successfully performed, leading to the formation of the amination product **10aa** in 84% isolated yield with a trace amount of compound **11** as a by-product (Scheme 20.6).[25]

Table 20.5 Substrate scope in the amination of 1,3-diphenylprop-2-en-1-ol (**8a**) with aliphatic amines.[a,b]

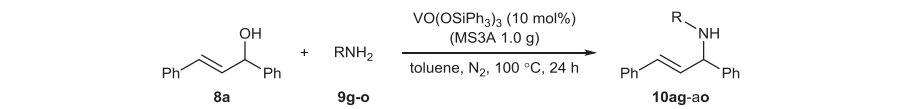

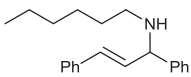

10ag, 85%

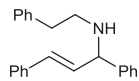

10ah, 69%

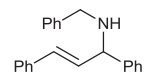

10ai, 85%

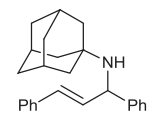

10aj, 88%

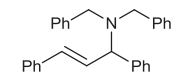

10ak, 69%

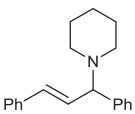

10al, 56%

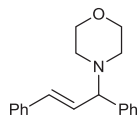

10am, 79%

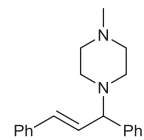

10an, 59%

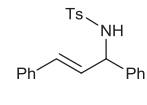

10ao, 35%[c]

[a]Reaction conditions: 0.20 mmol of amines and 1,3-diphenylprop-2-en-1-ol (**8a**), 10 mol% of $VO(OSiPh_3)_3$, 1.0 g MS3A, 2.0 mL toluene, under a nitrogen atmosphere.
[b]The yield was determined by ^1H NMR.
[c]300 mol% of *p*-toluenesulfonamide was used.

Table 20.6 Substrate scope in the amination of allyl alcohols with *p*-anisidine (**9a**).[a,b]

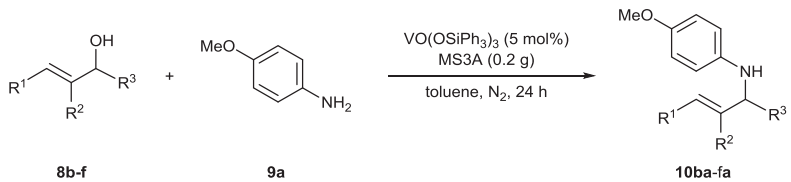

8b-f **9a** **10ba-fa**

Substrate	Temperature (°C)	Products
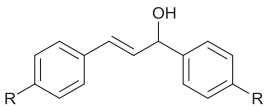 **8b-c**		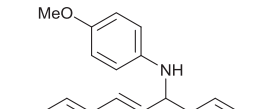 **10ba-ca**
R = F (**8b**)	50	R = F (**10ba**) 64%
OMe (**8c**)	50	OMe (**10ca**) 68%[c]
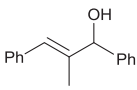 **8d**		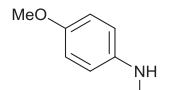 **10da**
	100	77%
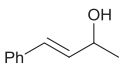 **8e**		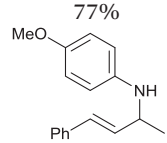 **10ea** 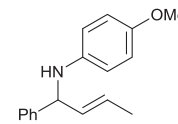 **10fa**
	80	31% 14%
	100[d]	78% trace
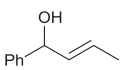 **8f**		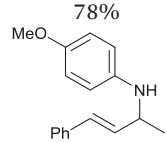 **10ea** 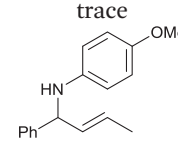 **10fa**
	80	24% 9%
	100[d]	81% trace

[a]Reaction conditions: 0.20 mmol of *p*-anisidine (**9a**) and allyl alcohols, $VO(OSiPh_3)_3$, 0.2 g MS3A, 2.0 mL toluene, under nitrogen atmosphere.
[b]The yield was determined by ^1H NMR.
[c]150 mol% of allyl alcohol was used.
[d]200 mol% of allyl alcohol was used, reaction time was 34 h.

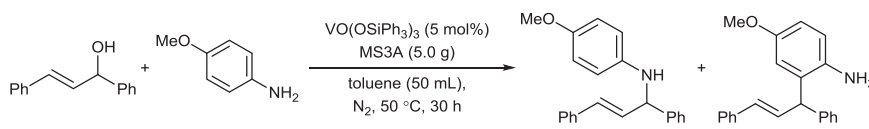

8a 100 mol% (1.05 g) **9a** 5.0 mmol (0.616 g) **10aa** 84% (isolated yield) (4.22 mmol, 1.33 g) **11** trace

Scheme 20.6 Gram-scale oxovanadium(v)-catalyzed direct amination.

20.3 Vanadium(v)-catalyzed Deoxygenative Homocoupling Reaction of Alcohols

Development of efficient synthetic methods for 1,5-diene derivatives has attracted much attention[26–28] because the 1,5-diene structure is an important skeleton for the synthesis of natural products.[29,30] The utilization of allyl

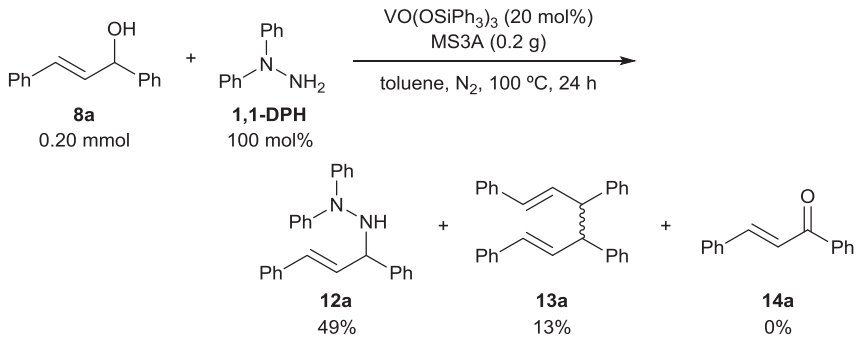

Scheme 20.7 Direct hydrazination reaction of allyl alcohol **8a** with **1,1-DPH**.

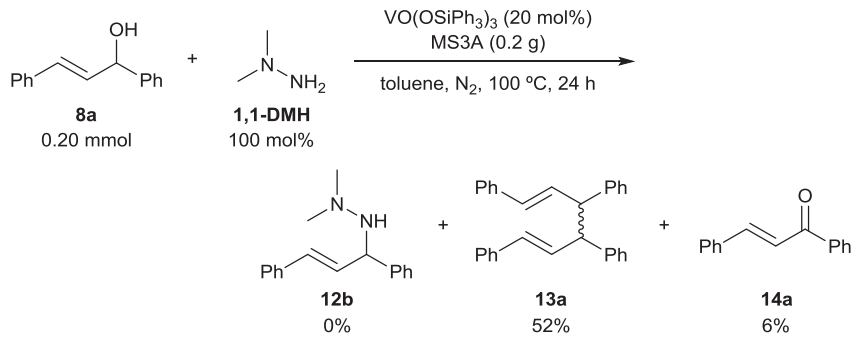

Scheme 20.8 Deoxygenative homocoupling reaction of allyl alcohol **8a** in the presence of **1,1-DPH**.

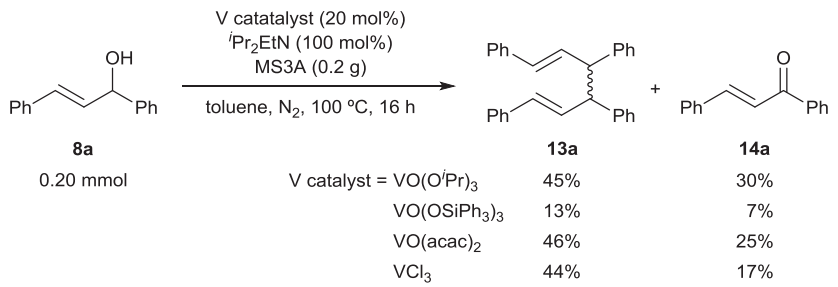

Scheme 20.9 The effect of vanadium catalyst for deoxygenative homcoupling reaction od 1,3-diphenylprop-2-en-1-ol (**8a**).

Table 20.7 The vanadium-catalyzed deoxygenative homocoupling reaction of 1,3-diphenylprop-2-en-1-ol (**8a**) in the presence of reductants.[a,b]

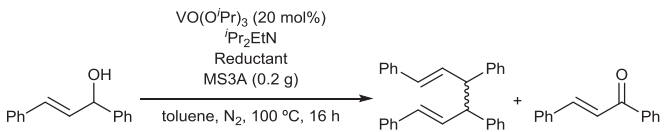

Entry	Reductant (mol%)	^{i}Pr$_2$EtN (mol %)	Yield of **13a**[c] (%)	Yield of **14a** (%)
1	none	100	45	30
2	**DPPDA** (50 mol%)	100	38	24
3	ascorbic acid (50 mol%)	100	42	29
4	**1,1-DMH** (50 mol%)	100	54	15
5	**1,2-DPH** (50 mol%)	100	65	14
6	**1,2-DPH** (50 mol%)	10	73	11

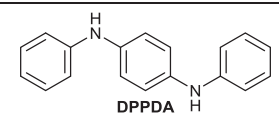

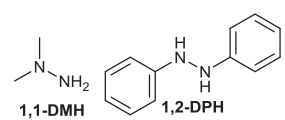

[a]Reaction conditions: 0.20 mmol of 1,3-diphenylprop-2-en-1-ol (**8a**), VO(O^{i}Pr)$_3$, 50 mmol% of reductant, ^{i}Pr$_2$EtN, 0.2 g MS3A, 1.0 mL toluene, under nitrogen atmosphere.
[b]The yield was determined by ^{1}H NMR.
[c]NMR yield (%) = [product (mmol)×2/substrate (mmol)]×100.

alcohols as a reliable starting material, which is cheap and easily obtainable, is considered to be a convenient approach to the synthesis of 1,5-diene structures. Deoxygenative homocoupling reaction is regarded as one of the reliable strategies to construct 1,5-diene structures from the view point of biomass conversion. Deoxygenative homocoupling reaction of allyl alcohols has been performed by using $TiCl_3$,[26] $NbCl_5$[27] or La[28] for the synthesis of 1,5-dienes. However, these reactions require additional metal salts. Also, oxovanadium(v) complexes have been demonstrated to catalyze the deoxygenative homocoupling reaction of alcohols,[31,32] wherein ketones are generated as by-products through oxidation of alcohols used as substrates. In the previous section, the oxovanadium(v) compound is shown to catalyze the direct amination of allyl alcohols. Direct hydrazination of an allyl alcohol and deoxygenative homocoupling reaction of alcohols using oxovanadium(v) catalysts are discussed in this section.[33]

The reaction of 1,3-diphenylprop-2-en-1-ol (**8a**) with 1,1-diphenylhydrazine (**1,1-DPH**) in the presence of 20 mol% of $VO(OSiPh_3)_3$ catalyst and MS3A (0.2 g) as a dehydrating reagent at 100 °C leads to the formation of the corresponding allyl hydrazine **12a** in 49% yield as a major product accompanied with the deoxygenative homocoupling product 1,5-diene **13a** in 13% yield (Scheme 20.7).[33] In the case of 1,1-dimethylhydrazine (**1,1-DMH**), the deoxygenative homocoupling product, 1,5-diene **13a** is obtained in 52% yield (*dl*/*meso* = 1 : 1) as a major product with a small amount of *E*-chalcone (**14a**), the oxidized product of allyl alcohol **8a** (Scheme 20.8).[33]

The utilization of $VO(O^iPr)_3$ as a catalyst in the deoxygenative homocoupling reaction of **8a** shows a higher efficiency than $VO(OSiPh_3)_3$ (Scheme 20.9).[33] A similar reactivity is also observed with $VO(acac)_2$. The formation of the oxidized product **14a** can be suppressed a little by using low-valent VCl_3 catalyst.

N,*N*′-Diphenyl-*p*-phenylenediamine (**DPPDA**) and ascorbic acid are not effective as an organic reductant (Table 20.7, Entries 2–3).[33] Hydrazine derivatives are effective for the deoxygenative homocoupling reaction. With 50 mol% of **1,1-DMH**, the deoxygenative homocoupling reaction of **8a** proceeds moderately to give 1,5-diene **13a** in 54% yield (Entry 4), wherein the yield of **14a** is lower than the reaction without **1,1-DMH** (Entry 1). The

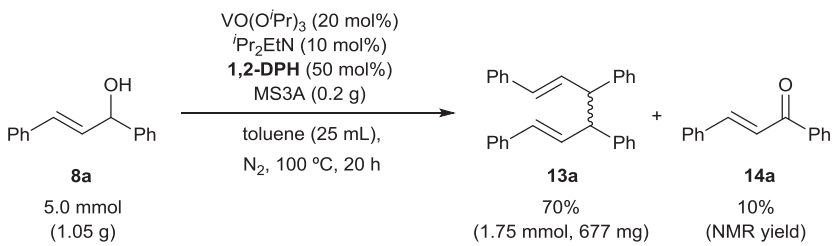

Scheme 20.10 Gram-scale oxovanadium(v)-catalyzed deoxygenative homocoupling reaction pf allyl alcohol **8a** in the presence of **1,2-DPH**.

Table 20.8 Substrate scope in the vanadium-catalyzed deoxygenative homocoupling reaction of alcohols.[a,b]

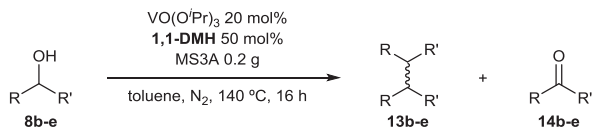

Entry	Substrate	Products		Entry	Substrate	Products	
1	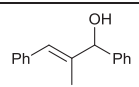 **8b**	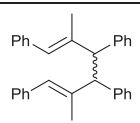 **13b** 46%[c] ($dl/meso = 1:1$)[c]	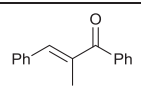 **14b** 13%	3	 **8d**	 **13d** 42%[c] ($dl/meso = 1:1$)[c]	 **14d** 5%
2	 **8c**	 **13c** 65%[c]	 **14c** 26%	4	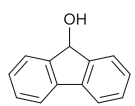 **8e**	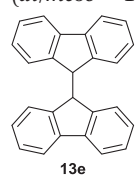 **13e** 36%[c]	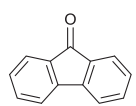 **14e** trace

[a]Reaction conditions: 0.20 mmol of alcohols, 20 mmol% of VO(O^{i}Pr)$_3$, 50 mmol% of **1,1-DMH**, 0.2 g MS3A, 1.0 mL toluene, under nitrogen atmosphere.
[b]The yield was determined by ^{1}H NMR.
[c]NMR yield (%) = [product (mmol)×2/substrate (mmol)]×100.

utilization of 1,2-diphenylhydrazine (**1,2-DPH**) in place of **1,1-DMH** shows a higher efficiency in the deoxygenative homocoupling reaction of **8a** to afford 1,5-diene **13a** in 65% yield (Entry 5). 1,5-Diene **13a** can be produced in 73% yield by performing the deoxygenative homocoupling reaction in the presence of 20 mol% of $VO(O^iPr)_3$, 10 mol% of $^iPr_2EtN$, 50 mol% of **1,2-DPH** and 0.2 g of MS3A (Entry 6).

The oxovanadium(v)-catalyzed deoxygenative homocoupling reaction of **8a** with **1,2-DPH** as a reductant can be performed in a gram-scale to afford the 1,5-diene **13a** in 70% isolated yield (Scheme 20.10).[33]

Starting from 1,3-diphenyl-2-methylprop-2-en-1-ol (**8b**), 1,5-diene **13b** (*dl*/*meso* = 1 : 1) is obtained in 46% yield (Table 20.8, Entry 1).[33] This oxovanadium(v)-catalyzed deoxygenative homocoupling reaction system is applicable to the deoxygenative homocoupling reaction of benzyl alcohols. The desired coupling product **13c** is achieved in 65% yield from the catalytic reaction of diphenylmethanol (**8c**) as shown in Entry 2. The catalytic reaction of 1-phenylethan-1-ol (**8d**) proceeds moderately to produce the corresponding coupling product **13d** (*dl*/*meso* = 1 : 1) (Entry 3). 9*H*-Fluoren-9-ol (**8e**) undergoes the deoxygenative homocoupling reaction, affording 9*H*,9′*H*-9,9′-bifluorene (**13e**) as a coupling product in 36% yield (Entry 4).

20.4 Conclusion

Economical oxovanadium(v) compounds can induce a variety of catalytic reactions based on the advantages of Lewis acidity, oxophilicity, and redox properties. Catalytic oxidative halogenation and aromatization systems are realized by the redox interaction of oxovanadium(v) catalysts with molecular oxygen. Lewis acidity and oxophilicity of oxovanadium(v) catalysts also permit the catalytic direct amination and hydrazination of allyl alcohols. The advantages of Lewis acidity, oxophilicity and redox properties of economical oxovanadium(v) catalysts enables not only oxidation reactions but also reduction reactions, as exemplified by the deoxygenative homocoupling reaction of alcohols. The results provided in this chapter are envisioned to provide fundamental insight not only into the catalytic ability of oxovanadium(v) compounds but also into the usability of Lewis acidity, oxophilicity and redox properties of oxovanadium(v) compounds.

Abbreviations

1,1-DMH	1,1-dimethylhydrazine
1,1-DPH	1,1-diphenylhydrazine
1,2-DPH	1,2-diphenylhydrazine
DPPDA	*N*,*N*′-diphenyl-*p*-phenylenediamine
$PTS{\cdot}H_2O$	*p*-toluenesulfonic acid monohydrate
TFA	trifluoroacetic acid
VBrPO	vanadium bromoperoxidase

References

1. K. Kikushima, T. Moriuchi and T. Hirao, *Chem. – Asian J.*, 2009, **4**, 1213.
2. Synthetic Methods for Redox Reactions Using Phosphorus, Vanadium and Samarium Compounds in *Functionalized Redox Systems: Synthetic Reactions and Design of π- and Bio-Conjugates*, ed. T. Hirao, T. Moriuchi, T. Amaya, A. Ogawa and A. Nomoto, Springer, Tokyo, 2015, pp. 5–50.
3. K. Kikushima, T. Moriuchi and T. Hirao, *Tetrahedron Lett.*, 2010, **51**, 340.
4. K. Kikushima, T. Moriuchi and T. Hirao, *Tetrahedron*, 2010, **66**, 6906.
5. T. Moriuchi, Y. Fukui, S. Kato, T. Kajikawa and T. Hirao, *J. Inorg. Biochem.*, 2015, **147**, 177.
6. M. Hayashi, K. Yamada and S. Nakayama, *J. Chem. Soc., Perkin Trans. 1*, 2000, 1501.
7. S. Kamiguchi, S. Nishida, M. Kodomari and T. Chihara, *J. Clust. Sci.*, 2005, **16**, 77.
8. C. S. Yi and D. W. Lee, *Organometallics*, 2009, **28**, 947.
9. Y. Izawa, D. Pun and S. S. Stahl, *Science*, 2011, **333**, 209.
10. T. Moriuchi, K. Kikushima, T. Kajikawa and T. Hirao, *Tetrahedron Lett.*, 2009, **50**, 7385.
11. B. M. Trost and M. L. Crawley, *Chem. Rev.*, 2003, **103**, 2921.
12. S. Nag and S. Batra, *Tetrahedron*, 2011, **67**, 8959.
13. B. Sundararaju, M. Achard and C. Bruneau, *Chem. Soc. Rev.*, 2012, **41**, 4467.
14. N. A. Butt and W. Zhang, *Chem. Soc. Rev.*, 2015, **44**, 7929.
15. Y. Kita, H. Sakaguchi, Y. Hoshimoto, D. Nakauchi, Y. Nakahara, J. F. Carpentier, S. Ogoshi and K. Mashima, *Chem. – Eur. J.*, 2015, **21**, 14571.
16. M. S. Azizi, Y. Edder, A. Karim and M. Sauthier, *Eur. J. Org. Chem.*, 2016, 3796.
17. P. Mukherjee and R. A. Widenhoefer, *Org. Lett.*, 2010, **12**, 1184.
18. T. Ohshima, Y. Nakahara, J. Ipposhi, Y. Miyamoto and K. Mashima, *Chem. Commun.*, 2011, **47**, 8322.
19. G. Hirata, H. Satomura, H. Kumagae, A. Shimizu, G. Onodera and M. Kimura, *Org. Lett.*, 2017, **19**, 6148.
20. H. Qin, N. Yamagiwa, S. Matsunaga and M. Shibasaki, *Angew. Chem. Int. Ed.*, 2007, **46**, 409.
21. S. Haubenreisser and M. Niggemann, *Adv. Synth. Cat.*, 2011, **353**, 469.
22. T. Ohshima, J. Ipposhi, Y. Nakahara, R. Shibuya and K. Mashima, *Adv. Synth. Catal.*, 2012, **354**, 2447.
23. Z. Wang, S. Li, B. Yu, H. Wu, Y. Wang and X. Sun, *J. Org. Chem.*, 2012, **77**, 8615.
24. P. Trillo, A. Baeza and C. Nájera, *ChemCatChem*, 2013, **5**, 1538.
25. T. Sakuramoto, T. Hirao, M. Tobisu and T. Moriuchi, *ChemCatChem*, 2019, **11**, 1175.
26. J. E. McMurry and M. Silvestri, *J. Org. Chem.*, 1975, **40**, 2687.
27. M. Sato and K. Oshima, *Chem. Lett.*, 1982, **11**, 157.

28. T. Nishino, Y. Nishiyama and N. Sonoda, *Bull. Chem. Soc. Jpn.*, 2003, **76**, 635.
29. N. S. Sheikh, *Org. Biomol. Chem.*, 2014, **12**, 9492.
30. J. Adrian, L. J. Gross and C. B. W. Stark, *Beilstein J. Org. Chem.*, 2016, **12**, 2104.
31. E. Steffensmeier and K. M. Nicholas, *Chem. Commun.*, 2018, **54**, 790.
32. E. Steffensmeier, M. T. Swann and K. M. Nicholas, *Inorg. Chem.*, 2019, **58**, 844.
33. T. Sakuramoto, Y. Donaka, M. Tobisu and T. Moriuchi, *New J. Chem.*, 2019, **43**, 17571–17576.

CHAPTER 21

Vanadium Compounds as Indirect Activators of a G Protein-coupled Receptor

DUAA ALTHUMAIRY,[a,b] HEIDE A. MURAKAMI,[c] RACHEL COLCLOUGH,[c] B. GEORGE BARISAS,[a,c] DEBORAH A. ROESS[a,d] AND DEBBIE C. CRANS*[a,c]

[a] Cell and Molecular Biology Program, Colorado State University Fort Collins, CO 80523, USA; [b] Department of Biological Sciences, King Faisal University, Al-Ahsa 31982, Saudi Arabia; [c] Department of Chemistry, Colorado State University Fort Collins, CO 80523, USA; [d] Department of Biomedical Sciences, Colorado State University Fort Collins, CO 80523, USA
*Email: Debbie.Crans@colostate.edu

21.1 Introduction

Catalysis in biology is critical to cell function in numerous ways. Although the reactions involved in catalysis most commonly involved protein-based enzymes,[1,2] nucleic acid- and lipid-based systems have also been identified. Proteins, functioning as enzymes, will catalyze the conversion of substrates to products. Co-factors or other ligands can affect an enzyme's ability to carry out catalysis by functioning either as inhibitors of enzyme function or as enhancers or initiators of enzyme activity. Vanadium is known to bind to several classes of enzymes as cofactors including the vanadium-containing peroxidases,[3,4] the vanadium-containing nitrogenases[4,5] and the vanadium-binding proteins, vanabins.[4,6] In addition to these classes of enzymes,

Catalysis Series No. 41
Vanadium Catalysis
Edited by Manas Sutradhar, José Armando L. da Silva and Armando J. L. Pombeiro

Published by the Royal Society of Chemistry, www.rsc.org

phosphatases and phosphorylates are strongly inhibited by vanadate,[7,8] which serves as a structural and electronic analog of phosphorus – vanadate can bind as a transition state analog or a substrate–product analog.[3,7] Although these actions of vanadium compounds can occur as a result of their direct effects on enzymes, vanadium-containing compounds can also act indirectly to affect chemical reactions mediated by proteins. We have described such a mechanism for a number of vanadium compounds that indirectly activate cell signaling mediated by plasma membrane receptors including receptors involved in immune system function[9] and glucose metabolism.[10] Here we describe time-dependent, indirect effects of a simple vanadate salt and a vanadium coordination complex on a membrane-bound protein receptor, specifically the luteinizing hormone receptor (LHR),[11,12] which belongs to the large family of G protein-coupled receptors (GPCR).[13]

To examine the indirect effects of vanadium compounds on the relationship between plasma membrane lipid packing and aggregation of a G protein-coupled receptor, we monitored time-dependent changes in both parameters following pretreatment of CHO cells expressing luteinizing hormone receptors (LHR) with BMOV or $VOSO_4$. The structures of these compounds are shown in Figure 21.1. LHR are involved in the reproductive function in both males and females[14] and are structurally related to rhodopsin, a G protein-coupled receptor for which a crystal structure together with an associated G protein is available.[15] These receptors bind a ligand at an extracellular binding site that initiates transduction of signal across the plasma membrane where intracellular receptor structures activate G proteins and intracellular signaling cascades.[14] As part of hormone-mediated signaling, LHR translocate to plasma membrane microdomains[16,17] where locally higher concentrations of LHR results in aggregation of these receptors and initiation of signal transduction to the cell cytoplasm.[18] Important to these studies, cells lines are available that stably express human luteinizing hormone receptors at low, physiologic

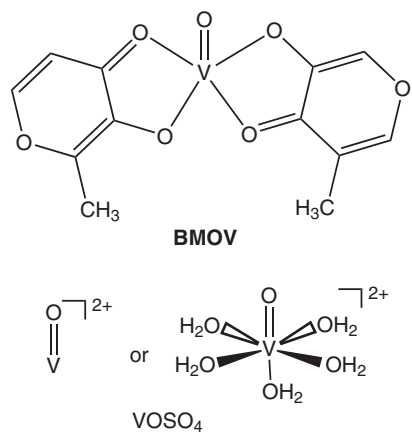

Figure 21.1 Schematic structures for BMOV and the cation in $VOSO_4$.

numbers, approximately 10 000 LHR per cell, as well as over-express the receptor which leads to receptor crowding and constitutive receptor aggregation.[12]

We have previously shown that treatment of cells expressing 10 000 LHR with BMOV or $VOSO_4$ can, like hormones, induce formation of receptor clusters in homo-transfer fluorescence resonance energy transfer studies.[12] The formation of these receptor clusters is required for initiation of signal transduction by LHR. When receptor density is low, LHR receptor aggregation appears to occur in response to BMOV or $VOSO_4$ interactions with the plasma membrane lipid bilayer as assessed using Di-4 ANEPPDHQ, a lipid targeted dye.[19] Importantly, LHR aggregation in response to BMOV or $VOSO_4$ does not require binding of ligand to receptor for receptor activation, as is normally the case. Thus, signaling is achieved through the indirect effects of BMOV or $VOSO_4$ on membrane lipid packing. Di-4 ANEPPDHQ, which readily associates with biological membranes, has a peak emission wavelength that depends on the relative order of surrounding lipid molecules. Treatment of cells with BMOV increases the ratio of fluorescence emission indicating that membrane lipids have become less densely packed. These results in cells are consistent with known interactions of bismaltolatodioxovanadium(IV) (BMOV) and its oxidation product $[VO(Malto)_2]^-$ with AOT-reverse micellar interfaces.[10]

The question addressed here is whether the indirect effects of BMOV or $VOSO_4$ on aggregation of LHR persists in cells after removing BMOV or $VOSO_4$ from the cell medium. *We hypothesize that direct interactions of vanadium-containing compounds with cell-membrane lipids are necessary for indirect effects of vanadium-containing compounds on LHR aggregation. Moreover, V-compound interactions with membrane lipids persist for hours after removing either BMOV or $VOSO_4$ from the cell medium.* These studies also provide information on the rate of BMOV or $VOSO_4$ clearance from the plasma membrane that may occur *via* internalization of these compounds by cells, metabolism within the membrane or equilibration of the V-compound with the cell medium. Each of these mechanisms for clearing V-compounds from the cell membrane will be affected by changes in speciation of BMOV and $VOSO_4$ in cell medium at pH 7.3 over 24 h.

21.2 Materials and Methods

21.2.1 Materials

Chinese Hamster Ovary cells, CHO-K1, were kindly provided by Dr. Takamitsu Kato at Colorado State University. Dulbecco's Modified Eagle medium (DMEM) and geneticin were purchased from Corning Cellgro. Penicillin–streptomycin and L-glutamine solution were purchased from Gemini Bio-Products (West Sacramento, CA). Fetal bovine serum (FBS) was purchased from Atlas Biologicals (Fort Collins, CO). 100X MEM nonessential amino acid solution, bovine albumin and $VOSO_4$ were purchased from

Sigma-Aldrich (St. Louis, MO). Trypsin-EDTA (0.25%) was purchased from Fisher Scientific Co (Pittsburgh, PA). Optimal-MEM was purchased from Life Technologies – Carlsbad, CA35 mm diameter glass-bottom cell culture dishes were purchased from In Vitro Scientific (Sunnyvale, CA).

21.2.2 Stock Solutions of BMOV and VOSO4

A stock solution of 1.0 mM BMOV was prepared by dissolving the BMOV in powder form in $<0.5\%$ DMSO and then adding phosphate-buffered saline (PBS) containing 1.0 mM $CaCl_2$ and 0.50 mM $MgCl_2$. A stock solution of $VOSO_4$ was made by dissolving $VOSO_4$ in powder form into PBS, pH 7.3. For homo-transfer fluorescence resonance energy transfer (homo-FRET) studies to assess LHR aggregation, dilution of stock solutions into serum-free media (500 mL of DMEM, 5 mL of 100×nonessential amino acid solution, 5 mL of penicillin–streptomycin and 5 mL of L-glutamine solution) to obtain a 10 mM solution were done immediately before beginning cell studies.

21.2.3 Cell Viability Assay

To verify effects of BMOV and $VOSO_4$ on CHO cell growth and to select appropriate concentrations of these vanadium compounds for further cell studies, growth inhibition assays were carried on using resazurin-based fluorometric assay and serial dilutions of BMOV (or $VOSO_4$ in a second experiment). This assay effectively counts the number of viable cells in a fixed volume. Approximately 20 000 cells per well were seeded in 96 well plates in 100 μl free serum media and allowed to attach for 3 h. This was designated as time 0. One group of cells were treated with BMOV (or $VOSO_4$ in a second experiment) (100, 50, 10, 5 or 1 μM) together with 10% resazurin for 3 h to obtain a baseline value for cell number at time 0. A separate population of cells was treated with BMOV (or $VOSO_4$ in a second experiment) and incubated for 12 h before addition of 10% resazurin for an additional 3 h (total time = 15 h). After the incubation with resazurin, fluorescence measurements at time 0 and time 15 to assess cell number were made using an excitation wavelength of 530 nm and measuring emission at 590 nm. To establish control rates of cells growth, the estimated number of live cells at time 0 and the estimated number of cells after exposure to BMOV (or $VOSO_4$ in a second experiment) for a total of 15 h, the last 3 h with 10% resazurin, the number of cells was expressed as a ratio of values at time 15 h to time 0 and expressed as a percentage of control cell numbers. Inhibitory concentrations at which 50% of cells died (IC_{50}) in either BMOV (or $VOSO_4$ in a second experiment) treated CHO cells were calculated by fitting curves to log values for the V compound. Values shown are the averaged triplicate responses from three separate experiments using nonlinear regression with three parameters and GraphPad Prism 8. The concentration of either BMOV (or $VOSO_4$ in a second experiment) used in subsequent cell experiments was 10 μM.

21.2.4 Membrane Retention of BMOV or $VOSO_4$ as Assessed by Membrane Lipid Order

Untransfected CHO cells were grown to 80%–90% confluence in 25 cm^2 culture flasks and then incubated with 1.0 mL trypsin-EDTA (0.25%) for 3 min. Cells (0.5 mL) were seeded into six of a 35 mm glass-bottom petri dish. After 12 h, cells were washed twice with 1 x PBS (pH 7.3) then five of them were suspended in medium with appropriate treatment. The first dish was immediately labeled with 200 μL of 1.5 μM environmentally sensitive dye di-4-ANEPPDHQ for 15 min, washed and immersed in 1 x PBS buffer for imaging using a Zeiss Axiovert 200 M inverted microscope.[12] The remaining five dishes were incubated with 10 μM BMOV (or 10 μM $VOSO_4$ in a second experiment) for 10 h. After taking the dishes from the incubator, cells were washed once, resuspended in medium free serum and imaged at time 0, 1, 2, 6 and 24 h after labeling with di-4-ANEPPDHQ using a Zeiss Axiovert 200 M inverted microscope equipped with a 63×1.2 NA water objective and an Andor Du897E EMCCD camera. Cell samples were illuminated with an arc lamp with a 480/30x or 495/20x excitation filter. Fluorescence emission was collected simultaneously in channel 1 using a 535/40 nm filter and in channel 2 using a 620/40 nm filter. MetaFluor software was used to observe and image cells during experiments. Background correction for each image and fluorescence intensity ratio of 620 : 535 nm calculation was performed using Image J.

21.2.5 Polarized Homo-fluorescence Resonance Energy Transfer Measurements

Stable cell lines expressing either 10 000 LHR or 560 000 LHR per cell were grown to 80%–90% confluence in 25 cm culture flasks and then incubated with 1.0 mL trypsin-EDTA (0.25%) for 3 min. These human LHR were tagged on their intracellular *C*-terminus with an enhanced yellow fluorescence protein to provide a fluorescence signal (hLHR-eYFP) for homo-transfer fluorescence energy transfer (homo-FRET) studies.[12] Cells (0.5 mL) were plated in 35 mm glass-bottom petri dishes. After 12 h, the cells were washed twice with 1×phosphate buffered saline (PBS; pH 7.3). Cells were then treated with 10 μM BMOV (or $VOSO_4$ in a second experiment). One group of cells was imaged immediately using a Zeiss Axiovert 200 M inverted microscope to establish the baseline values for the extent of LHR aggregation. The remaining cell populations were preincubated with 10 μM BMOV (or 10 μM $VOSO_4$ in a second experiment) for 10 h. Cells were then washed once to remove the vanadium compound, resuspended in serum-free medium and imaged homo-FRET methods at 0, 1, 2, 3, 6 and 24 h after removing BMOV (or $VOSO_4$ in a second experiment) from the cell medium. About 5–7 cells were examined from each petri dish and at least 30 cells were examined for each treatment. To avoid internalization of LHR-eYFP, data were acquired after no more than 30 min.

Energy transfer between chromophores of the same type is termed polarized homo-transfer fluorescence resonance energy transfer (homo-FRET) and occurs to a significant extent when donor eYFP and acceptor eYFP moieties are within 2–10 nm of each other.[20] In these studies, homo-FRET imaging data were collected using a Zeiss Axiovert 200 M inverted microscope with an Andor Du897E EMCCD camera and MetaMorph software. Arc lamp illumination passing through a vertically-polarized filter provided polarized excitation. Approximately 16 images were acquired at a rate of one image per minute with a 15 sec exposure time. This exposure typically bleaches the eYFP tag covalently attached to the *C*-terminus of the LHR to ~10% of its initial fluorescence intensity. A Princeton Instruments Dual View image splitter created side-by-side images of fluorescence polarized parallel or perpendicular to the excitation polarization. Backgrounds were subtracted from fluorescence emission images and a g-factor was calculated to correct for efficiency differences in instrument optics, as previously described.[21] The G-factor constitutes the instrument-specific correction for different detection sensitivities for vertically and horizontally polarized fluorescence. The intrinsic anisotropy of a single eYFP fluorophore is 0.38.[21] We assumed monomeric LHR tagged with eYFP exhibited this value and set to 0.38 the apparent anisotropy upon complete bleaching. Homo-FRET results were expressed as mean ± SEM. Statistical evaluation of mean differences in untreated and treatments groups was analyzed by one-way ANOVA followed by the Tukey multiple comparison test and Student's t-test to compare between two groups using R version 3.3.1. P values <0.05 were statistically significant.

21.2.6 Ambient Temperature EPR Measurements

Electron paramagnetic resonance (EPR) was used to record characterize the vanadium complexes formed in DMEM media and aqueous solution. Spectra were recorded at ambient temperature in aqueous solution using a Bruker ESR-300 spectrometer and previously described methods.[22] The solutions were made at 1 mM concentrations and were recorded in 1 mm glass capillary tubes placed in 2 mm quartz tubes. A powder sample of 2,2-diphenyl-1-picrylhydrazyl (DPPH, $g = 2.0037$) was used as an external standard.[22] The spectra were recorded at 9.84 GHz frequency and 20.00 mW (microwave) power with modulation frequency 100.00 kHz, modulation amplitude 10.00 G, time constant 5.12 ms, sweep width 1000.00 G, sweep time 5.24 s, resolution 1048 points and 10 scans with a central field 3511.20 G.

21.2.7 Speciation Calculations

Solution speciation was measured using methods and known speciation parameters. The resulting quantification of species needed modeling of a defined stoichiometry using formation constants.[23–27] Details in the speciation of BMOV have been reported previously.[26,27] In brief, the complexes are defined by the notation (p, q, r). Eqn (21.1) shows H^+, a metal ion (M^{2+}), and

a ligand (L^-) forming a complex with the stoichiometry defined by p, q and r in an equilibrium reaction, respectively.[23–25,27] The resulting formation constant β (p, q, r) is shown in eqn (21.2), where the concentrations of H^+, M^{2+} and L^-, which together form the BMOV complex described here, are multiplied with each other and divided by the concentration of the BMOV complex originally added to the solution.

$$pH^+ + qM^{2+} + rL^- \rightleftharpoons (H^+)_p (M^{2+})_q (L^-)_r \tag{21.1}$$

$$\beta(p, q, r) = \frac{[(H^+)_p (M^{2+})_q (L^-)_r]}{[H^+]^p [M^{2+}]^q [L^-]^r} \tag{21.2}$$

Because the cell assays were carried out at an ionic strength of 0.17, similar parameters were used for these calculations.[28] The intact coordination complex, BMOV, can be described by a series of equations and the associated formation constants that represent the entire system.[12,25–27,29] Using the reported constants shown in Table 21.1,[12,25–27] we can describe the species distribution under conditions similar to those found in cell media.

21.2.8 Spectroscopic Investigation of Vanadium Species

The nature of the V-species in solution was determined using both electron paramagnetic resonance (EPR) and NMR spectroscopy. BMOV and $VOSO_4$ are vanadium compounds with vanadium in oxidation state IV. However, under the conditions used in cell studies, the vanadium(IV) compounds oxidize to form vanadium(V) compounds. It is therefore important that the vanadium(IV) compounds are monitored using EPR spectroscopy and the vanadium(V) compounds are monitored using ^{51}V NMR spectroscopy because both oxidation states are likely to be present in these samples.

Table 21.1 Formation constants (log β) of vanadium(IV) hydrolysis and complexes of maltol at 25 °C.[12,23–27]

Binary system [H^+–VO^{2+}]			
(p, q)	Notation	log β	Citations
(−1, 1)	$[VO(OH)]^+$	− 5.94	12, 23–25
(−2, 2)	$[(VO)_2(OH)_2]^{2+}$	− 6.95	12, 23–25
(−3, 1)	$[VO(OH)_3]^-$	− 18.2	12, 23–25
(−5, 2)	$[(VO)_2(OH)_5]^-$	− 22.3	12, 23–25
Ternary System [H^+-VO^{2+}-Mal]			
(p, q, r)	Notation	log β	Citations
(1, 0, 1)	HMa	8.44	12, 26–27
(0, 1, 1)	[VOMa] +	8.69	12, 26–27
(0, 1, 2)	$[VO(Ma)_2]$	16.29	12, 26–27
(−1, 1, 2)	$[H_{-1}VO(Ma)_2]^-$	7.51	12, 26–27
(−2, 2, 2)	$[H_{-2}(VO)2(Ma)2]$ 9.88		12, 26–27

21.2.8.1 EPR Spectroscopic Studies

Electron paramagnetic resonance (EPR) was used to record characterize the vanadium complexes formed in DMEM media and aqueous solution. Spectra were recorded at ambient temperature in aqueous solution using a Bruker ESR-300 spectrometer and previously described methods.[22] BMOV and $VOSO_4$ were prepared at 1.0 mM concentrations in serum-free media as described. The solutions, prepared at 1 mM concentrations, were recorded in 1 mm glass capillary tubes placed in 2 mm quartz tubes. A powder sample of 2,2-diphenyl-1-picrylhydrazyl (DDPH, $g = 2.0037$) was used as an external standard. The spectra were recorded at 9.84 GHz frequency and 25.00 mW (microwave) power with modulation frequency 100.00 kHz, modulation amplitude 10.00 G, time constant 5.12 ms, sweep width 1000.00 G, sweep time 5.24 s, resolution 1048 points and 16 scans with a central field 3511.20 G. An EPR spectra were recorded every hour for 10 hours, followed by a 24-hour time point.

21.2.8.2 NMR Spectroscopic Studies

Solutions containing paramagnetic materials can be nontrivial to record on because of the presence of the paramagnetic compounds. However, after 3 h, the ^{51}V NMR was recorded for the $VOSO_4$ sample for every time point. The parameters used for the ^{51}V studies were similar to those reported previously.[12,22] ^{51}V NMR spectra for the BMOV sample was recorded at the 24 hour time point.

21.3 Results

21.3.1 Concentration-dependent Effects of BMOV or $VOSO_4$

Initial studies were performed to evaluate effects of BMOV and $VOSO_4$ on CHO cell viability. The goal of these studies was to identify a concentration of these vanadium compounds that was less than the IC_{50} for BMOV or $VOSO_4$ at a time approximating the incubation time used in measurements of membrane lipid packing in CHO cells and homo-FRET studies of LHR aggregation in cells expressing LHR-eYFP. All concentrations greater than 1 μM BMOV or 1 μM $VOSO_4$ decreased CHO cell viability over the timescale of this experiment. The IC_{50} for BMOV was estimated to be 34 μM while the IC_{50} for $VOSO_4$ was 65 μM indicating that BMOV was a slightly more potent inhibitor of cell growth than $VOSO_4$ at comparable concentrations (Figure 21.2). A concentration of 10 μM BMOV (or $VOSO_4$ in a separate experiment) – less than the IC_{50} for either V-compound – was selected for use in subsequent experiments.

21.3.2 Effects of BMOV and $VOSO_4$ on Lipid Packing in CHO Cell Plasma Membranes

A 10 h preincubation of CHO cells with 10 μM BMOV or $VOSO_4$, lipid packing was decreased when compared to untreated cells as indicated by an increase

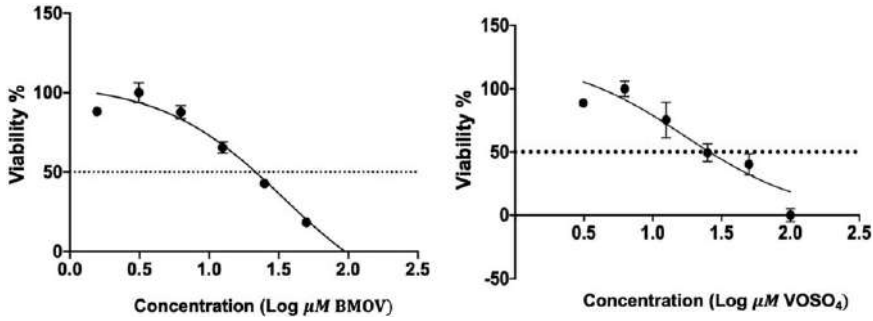

Figure 21.2 Effects of BMOV (left panel) and $VOSO_4$ (right panel) on CHO cell viability. The dashed line at 50% viability was used to establish the IC_{50} for these compounds.

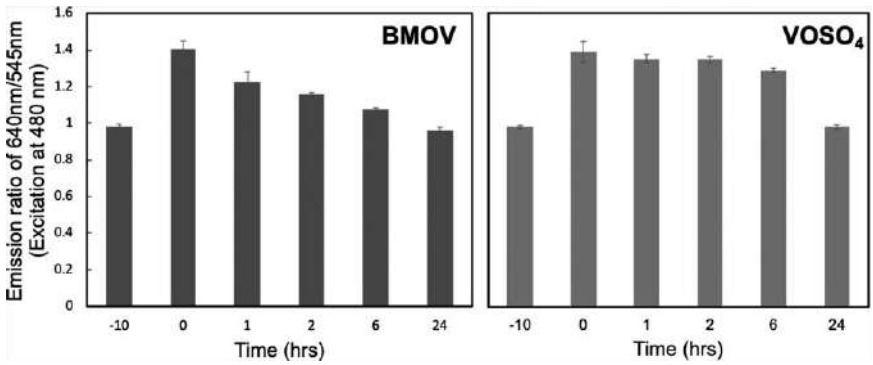

Figure 21.3 Membrane retention of BMOV or $VOSO_4$ as measured by an assay of membrane lipid order. Cells were preincubated with BMOV (left panel) or $VOSO_4$ (right panel) for 10 h and then washed once to remove vanadium compounds from the cell medium. The extent of lipid packing as indicated by the emission ratio at 640 nm/545 nm was monitored over 24 hours. Increased emission at 640 nm relative to emission at 545 nm is indicative of a decrease in lipid order.

in the ratio of emission at 640 nm : 545 nm. After washing cells once to remove BMOV or $VOSO_4$ from the cell medium, lipid packing was monitored for 24 h. After 24 h, lipid packing returned to baseline values suggesting that, under these conditions, BMOV or $VOSO_4$ lipid interactions with the plasma decreased steadily over this time, with a slightly faster decrease in cells pretreated with $VOSO_4$ (Figure 21.3).

21.3.3 BMOV and VOSO4 Effects on LHR Aggregation

Effects of BMOV or $VOSO_4$ pretreatment on LHR aggregation were examined using CHO cell lines stably expressing 10 000 LHR per cell or 560 0000 LHR per cell. When cells expressed 10 000 LHR per cell, preincubation of cells with either 10 mM BMOV or 10 mM $VOSO_4$ produced extensive aggregation

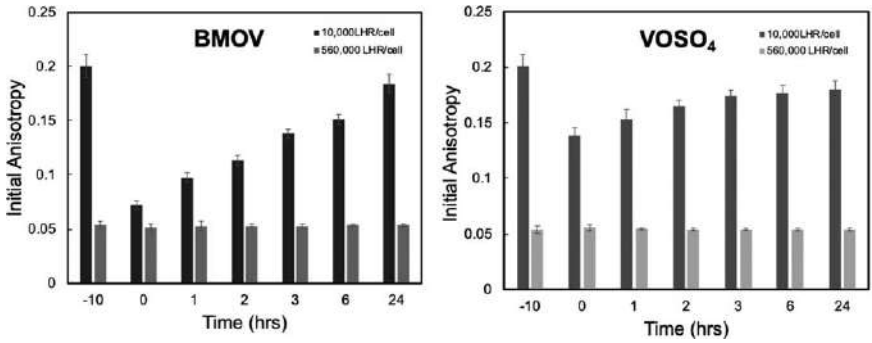

Figure 21.4 Values for the initial anisotropy measured for eYFP covalently linked to LHR using polarized homo-FRET methods. Smaller values for initial anisotropy are indicative of LHR aggregation. Treatment of cells with BMOV (left panel) or $VOSO_4$ (right panel), decreased values for initial anisotropy for receptors on cells expressing 10 000 LHR per cell. After removing BMOV or $VOSO_4$ at time 0, the extent of LHR aggregation decreased over time as indicated by increased values for initial anisotropy. When cells expressing 560 000 LHR per cell were examined using homo-FRET methods, there was no change in initial anisotropy in response to either BMOV or $VOSO_4$. This result indicates that overexpressed LHR are extensively clustered and that receptors are not affected by changes in lipid packing.

of LHR, conditions that also decreased membrane lipid order. Previous studies have shown that this extent of LHR aggregation is accompanied by activation of LHR and increased in intracellular signaling.[12] Removing BMOV or $VOSO_4$ from the cell medium resulted in a slow reduction in the extent of receptor aggregation which returned to baseline values in 24 h (Figure 21.4). Effects of $VOSO_4$ on the extent of LHR aggregation were slightly less than that of BMOV-treated cells and recovery to baseline anisotropy values was slightly faster.

In contrast to results with 10 000 LHR per cell, overexpression of LHR was associated with constitutive aggregation of the receptors. There was no further aggregation of LHR when cells were pretreated with either BMOV (or $VOSO_4$ in a separate experiment) despite the increase in lipid disorder caused by these V-compounds. Removing BMOV (or $VOSO_4$ in a separate experiment) from the cell medium did not alter the extent of LHR aggregation over 24 h (Figure 21.4).

21.3.4 Monitoring the Stability of BMOV and $VOSO_4$ in Media

The stability of BMOV and the oxidation of $VOSO_4$ was monitored in media since it was not possible to monitor compound stability in the cell membrane. In Figure 21.5 the EPR the spectra of 1.0 mM of $VOSO_4$ and BMOV compounds are shown in media. The bottom panel shows the 10.0 mM

$VOSO_4$ reference at pH 3.0 in aqueous solution used to normalize the spectra. The middle and top panels show the EPR spectra from the 1.0 mM $VOSO_4$ and 1.0 mM BMOV immediately after sample preparation and normalized to the reference spectrum. It was anticipated that the VO^{2+} at pH 7.4 will complex to media components, dimerize or oxidize to form vanadium(v) species and no longer show an EPR spectrum. As a result, the EPR signal intensities are low and we also recorded the ^{51}V NMR spectra, which are shown in Figure 21.6. Vanadate was observed at the 3 h time-point in the 1.0 mM $VOSO_4$ sample. Similar spectra were recorded at the time points up until 24 h. These spectra show that both V(IV) and V(V) species are present in the $VOSO_4$ media sample under the conditions of the experiment, and that, at the low vanadium(IV) concentrations, the conversion to the mixture of species was observed at 1–3 h and continued to be observed throughout the entire experiment. Considering that the G-value for the $VOSO_4$ sample and the BMOV sample is similar but different than that observed for the reference $VOSO_4$ at pH 3.0, we conclude that the vanadium(IV) formed is an adduct with phosphates, amino acids and other prevalent media components and not the free VO^{2+} observed in aqueous solution (as represented by the reference compound).

In Figure 21.6 top, the spectrum of 1.0 mM BMOV is shown in media. The bottom panel is showing 7.0 mM $VOSO_4$ reference at pH 3.0 to which the spectrum is normalized against. Although there is more vanadium(IV) in the

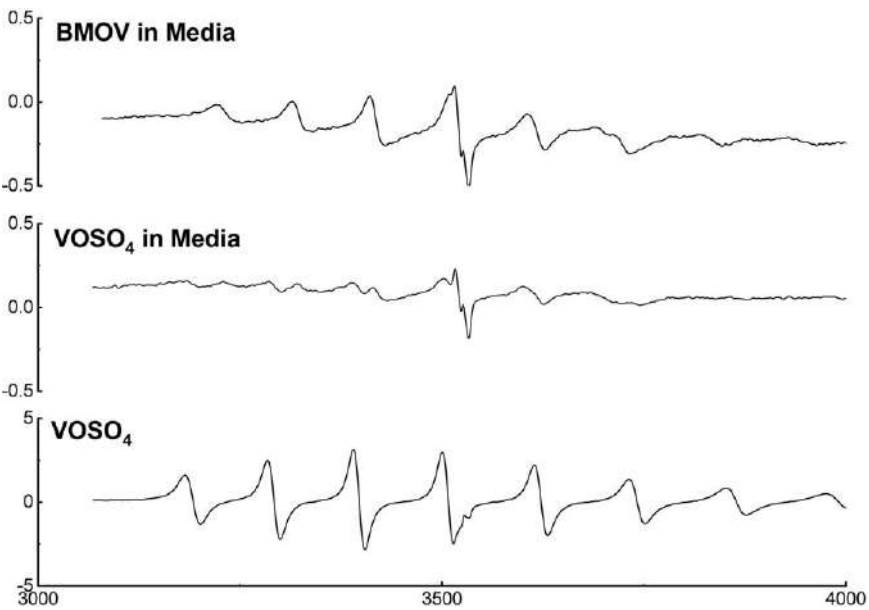

Figure 21.5 EPR spectra are shown for 1.0 mM BMOV in media (top panel), 1.0 mM $VOSO_4$ in media (middle panel) and 10.0 mM $VOSO_4$ in aqueous solution at pH 3.0. The spectra are normalized to the 7.0 mM spectrum shown for reference spectrum for $VOSO_4$ at pH 3.0 (bottom panel).

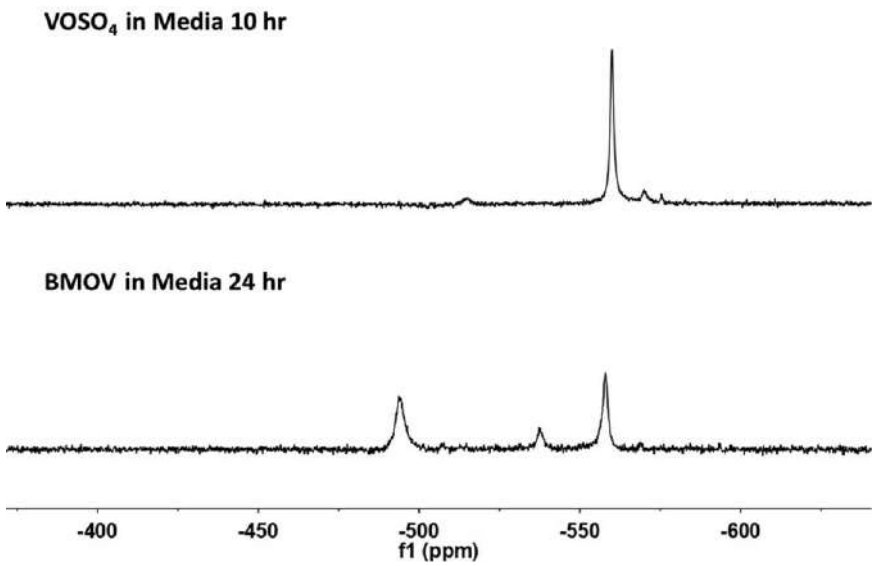

Figure 21.6 Representative ^{51}V NMR spectra are recorded to measure the oxidation of the V(IV) compounds in media in a time-dependent manner. The NMR spectrum of the $VOSO_4$ sample is shown after 10 h of incubation showing the presence of vanadate oligomers (left). Then ^{51}V NMR of BMOV in media after 24 h of incubation (left).

1.0 mM BMOV sample than the 1.0 mM VOSO4 sample some of the BMOV had oxidized. Furthermore, the spectrum of the BMOV sample appears to contain two species, one similar to that in the $VOSO_4$ sample and another broader peak which is attributed to an oxidized BMOV species and similar to the parameters reported for stability studies on BMOV.[27] This is consistent with the BMOV sample partially hydrolyzing forming some aqueous V(IV) as well as some remaining as BMOV. The corresponding NMR spectra show that at the 24 h time point the BMOV sample contains a significant fraction of oxidized BMOV, $[VO(malto)_2]^-$. In the case of the BMOV sample, the vanadium(IV) complex form some vanadium(V) complex, but hydrolyze more than expected compared to stability studies in aqueous solution. This is consistent with the report that BMOV hydrolyze as it approaches the interface.[30]

21.4 Discussion

Both BMOV and $VOSO_4$ interact with membrane lipids and decrease lipid packing, an effect that is diminished over time after removal of these V-compounds from the cell medium. The timeframe for cell recovery from effects on lipid packing is about 24 h. At any time during recovery from V-compound exposure, increased lipid disorder over baseline values appears to affect the extent of LHR aggregation when LHR is expressed at physiologically relevant receptor numbers, *i.e.*, 10 000 LHR per cell.

There are no effects of lipid disorder on LHR aggregation when receptors are overexpressed in CHO cells and receptor crowding has occurred. From these and other results, it appears that LHR migrate from the bulk membrane, the site of V compound interactions with membrane lipids, to membrane microdomains that have more densely packed lipids and where receptors are concentrated. This concentration of receptors in membrane microdomains produces LHR aggregation and activation of receptors which then signal intracellularly.[12] Although it appears that BMOV and $VOSO_4$ are cleared from the membrane in approximately 24 h, it is less clear what happens to V-compounds over this time. We can monitor V-compounds in the media using both EPR and NMR spectroscopies but not monitor events in the membrane. V-compounds may be released back into the cell medium, taken up by the cell or, less likely, metabolized to products that no longer affect lipid packing. A schematic model summarizing these results for CHO cells expressing low- and high-LHR density is shown in Figure 21.7.

It seems most likely from studies of model membrane systems and from measurements effects on lipid packing in intact cells that these compounds interact with the extracellular surface of the lipid bilayer after which the V-compound is internalized (see Figure 21.5). Vanadium compounds such as BMOV and a related compound BEOV have been explored clinically as glucose-regulating drugs for oral use.[31–33] In accordance with Lipinski's rules[34,35] describing requirements for an ideal drug capable of crossing membranes, small, neutral compounds such as BMOV can penetrate membranes.[10] In addition to interacting with membrane surfaces if sufficiently hydrophilic, vanadium compounds such as BMOV may also dissolve in the hydrophobic core of the bilayer. $VOSO_4$, on the other hand. is known to readily penetrate interfaces over the course of a few minutes using available cation transporters.[36] If BMOV or $VOSO_4$ are transiently associated with membrane lipids and then internalized, clearing remaining BMOV or $VOSO_4$, after washing cells, is slow.

Internalization of these V-compounds is attractive from a functional perspective given phosphatase targets for these compounds are found in the cell cytoplasm.[7] More importantly, it is not possible to rule out membrane transport, *via* an unidentified mechanism, into the CHO cell interior. For many compounds functioning as drugs, the ability to transit the plasma membrane, enter the cell cytoplasm and then target intracellular functions or structures, is critical to their action.[37] Transport of V-compounds across a membrane would likely depend on available membrane proteins that were adapted for transport of these V-compounds.[37] In the case of the erythrocyte membrane, the addition of DIDS stopped the internalization of the V-compounds.[38,39] Alternatively, lipoidal diffusion is commonly considered as an alternative explanation for drug movement across membrane barriers (reviewed in ref. 8 and 40). Drugs proposed to use lipoidal transport display, in monolayers, approximately equal rates of flux across the monolayer in either direction. These compounds have ''intrinsic permeability'' in cell lines expressing membrane transporters used for passive diffusion.

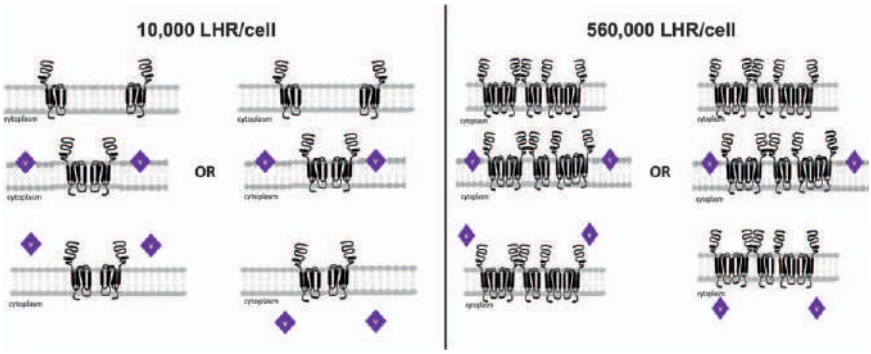

Figure 21.7 Models for the effects of BMOV or VOSO4 on cell membranes. The panels on the left show vanadium compounds interacting CHO cell membranes in cells expressing 10 000 LHR per cell. V-compounds in the plasma membrane, after removing extracellular C-compounds by washing the cell, are either released back into the extracellular environment or are internalized by the cell. While V-compounds are present in the membrane, lipids are arranged in a more disordered fashion and LHR, as a result of changes in their lipid environment, become aggregated in small membrane microdomains. For CHO cells overexpressing LHR (560 000 LHR per cell), changes in membrane lipid order have no effect on LHR aggregation. As in the left panels, V-compounds are either released into the extracellular environment or are internalized.

Speciation studies of suggest that BMOV and $VOSO_4$, and their oxidized products, are present in media solution and that this mixture of V-compounds is responsible for the initiation of receptor aggregation on the cell membrane. Although it is not possible to assess speciation of V-compounds within the membrane's lipid environment or once the V-compound internalized, it is possible to examine changes in V-compound speciation in the cell medium. Considering how readily these molecules traverse the lipid interface, the V-compound content in the media is likely to impact its content in the lipid interface. This may be particularly critical given changes in V-species during their association with the membrane. Speciation of the V-compounds in the media is, therefore, very important to understand the mode of action of these V-compounds.

The NMR and EPR spectra (Figures 21.6 and 21.7) show that V(IV) and V(V) species are present in the $VOSO_4$ media sample under the conditions of the experiment and that at the low vanadium concentrations the conversion to the mixture of species observed after 1–3 h continue to be observed throughout the entire experiment. Similarly, the results shown in Figures 21.6 and 21.7 are consistent with the BMOV sample partially hydrolyzing and forming some aqueous hydrolyzed V(IV) and some V(V). Furthermore, it appears that at 24 h the BMOV has directly oxidized and formed $[VO(malto)_2]^-$. The NMR spectra show that a significant fraction of oxidized vanadium, about 50%, is present in the form of $[VO(malto)_2]^-$. In the case of the BMOV sample, the vanadium(IV) complex forms some

vanadium(v) complex and $VOSO_4$ hydrolyzes more than expected based on stability studies in aqueous solution. This is consistent with the report that BMOV hydrolyzes as it approaches an interface. Considering that the G-value for the $VOSO_4$ sample and one of the two signals observed in the BMOV spectrum are similar and also similar to the reference $VOSO_4$ at pH 3.0, we conclude that vanadium(IV) is formed in the media. The EPR spectrum recorded from the media shows that there is still some intact BMOV in the media. Combined, these studies show that the media contains V(IV) and V(V) species and that BMOV and $[VO(malto)_2]^-$ are present and their combination is responsible for the inhibition of growth effect that we observe.

21.5 Conclusions

The interactions of BMOV and $VOSO_4$ with the eukaryotic cell plasma membrane directly decrease packing of membrane lipids and, as an indirect effect, drive aggregation of LHR, a G protein-coupled receptor in CHO cells. LHR continue to be aggregated when the lipid order is decreased in the presence of either BMOV or $VOSO_4$ in the cell medium and after the V-compounds have been removed. These BMOV or $VOSO_4$ effects are only observed on cells where LHR density is low; when LHR are overexpressed, receptor density is high and the receptors are constitutively aggregated regardless of V-compound effects on membrane lipid packing. In the case of these small V-compounds and their known ability to traverse membranes, we anticipate that these vanadium compounds are taken up by cells and appear in the cell cytoplasm. However, this process may be slow. It is also expected that there will be changes in speciation of the V-compounds in the medium over time and that such speciation may potentially affect lipid packing in the membrane. The V-compounds present in the cell medium interact with lipids in model membranes since the V-compounds readily traverse the membrane and move in and out between the aqueous phase and into the interface.

Acknowledgements

D. A. would like to thank King Faisal University and the Saudi Arabian Cultural Mission for her fellowship to study at Colorado State University. D. C. C. and D. R. thank Colorado State University for support. D. C. C. also thanks the Author Cope Scholar Foundations administered by the American Chemical Society for partial support. We thank Professor Sandra Eaton for assistance with the EPR spectroscopy.

References

1. X. Zhao, K. Gentile, F. Mohajerani and A. Sen, *Acc. Chem. Res.*, 2018, **51**, 373.
2. M. O. Ross and A. C. Rosenzweig, *J. Biol. Inorg. Chem.*, 2017, **22**, 307.

3. C. C. McLauchlan, H. A. Murakami, C. A. Wallace and D. C. Crans, *J. Inorg. Biochem.*, 2018, **186**, 267.
4. J. C. Pessoa, S. Etcheverry and D. Gambino, *Coord. Chem. Rev.*, 2015, **301**, 24.
5. C. C. Lee, Y. Hu and M. W. Ribbe, *Science*, 2010, **329**, 642.
6. H. Michibata and T. Ueki, *Biomol. Concepts*, 2010, **1**, 97.
7. D. C. Crans, *J. Org. Chem.*, 2015, **80**, 11899.
8. C. C. McLauchlan, B. J. Peters, G. R. Willsky and D. C. Crans, *Coord. Chem. Rev.*, 2015, **301–302**, 163–199.
9. A. Al-Qatati, F. L. Fontes, B. G. Barisas, D. Zhang, D. A. Roess and D. C. Crans, *Dalton Trans.*, 2013, **42**, 11912.
10. P. W. Winter, A. Al-Qatati, A. L. Wolf-Ringwall, S. Schoeberl, P. B. Chatterjee, B. G. Barisas, D. A. Roess and D. C. Crans, *Dalton Trans.*, 2012, **41**, 6419.
11. N. Samart, D. Althumairy, D. Zhang, D. A. Roess and D. C. Crans, *Coord. Chem. Rev.*, 2020, **416**, 213286.
12. D. Althumairy, H. A. Murakami, D. Zhang, B. G. Barisas, D. A. Roess and D. C. Crans, *J. Inorg. Biochem.*, 2020, **203**, 110873.
13. S. P. H. Alexander, A. Christopoulos, A. P. Davenport, E. Kelly, N. V. Marrion, J. A. Peters, E. Faccenda, S. D. Harding, A. J. Pawson and J. L. Sharman, *Br. J. Pharmacol.*, 2017, **174**, S17–S129.
14. M. Ascoli, *Luteinizing Hormone Action and Receptors*, CRC Press, 2019.
15. Y. Kang, O. Kuybeda, P. W. de Waal, S. Mukherjee, N. Van Eps, P. Dutka, X. E. Zhou, A. Bartesaghi, S. Erramilli and T. Morizumi, *Nature*, 2018, **558**, 553.
16. S. M. Smith, Y. Lei, J. Liu, M. E. Cahill, G. M. Hagen, B. G. Barisas and D. A. Roess, *Endocrinology*, 2006, **147**, 1789.
17. Y. Lei, G. M. Hagen, S. M. L. Smith, J. Liu, B. G. Barisas and D. A. Roess, *Mol. Cell. Endocrinol.*, 2007, **260–262**, 65.
18. A. L. Wolf-Ringwall, P. W. Winter, D. A. Roess and B. G. Barisas, *Cell Biochem. Biophys.*, 2014, **68**, 561.
19. D. M. Owen, P. M. P. Lanigan, C. Dunsby, I. Munro, D. Grant, M. A. A. Neil, P. M. W. French and A. I. Magee, *Biophys. J.*, 2006, **90**, L80.
20. D. W. Piston and M. A. Rizzo, Fluorescent Proteins, in *Methods in Cell Biology*, 2nd edn, ed. K. F. Sullivan, **vol. 85**, 2008, pp. 415–430.
21. E. K. L. Yeow and A. H. A. Clayton, *Biophys. J.*, 2007, **92**, 3098.
22. S. S. Amin, K. Cryer, B. Zhang, S. K. Dutta, S. S. Eaton, O. P. Anderson, S. M. Miller, B. A. Reul, S. M. Brichard and D. C. Crans, *Inorg. Chem.*, 2000, **39**, 406.
23. T. Kiss, E. Kiss, G. Micera and D. Sanna, *Inorg. Chim. Acta*, 1998, **283**, 202–210.
24. J. C. Pessoa, I. Tomaz, T. Kiss and P. Buglyó, *J. Inorg. Biochem.*, 2001, **84**, 259–270.
25. J. C. Pessoa, *J. Inorg. Biochem.*, 2015, **147**, 4–24.
26. A. G. Baró, I. Andersson, L. Pettersson and A. Gorzsás, *Dalton Trans.*, 2008, 1095.

27. C. Orvig, P. Caravan, L. Gelmini, N. Glover, F. G. Herring, H. C. Li, J. H. McNeill, S. J. Rettig and I. A. Setyawati, *J. Am. Chem. Soc.*, 1995, **117**, 12759.
28. A. Bergeron, K. Kostenkova, M. Selman, H. A. Murakami, E. Owens, N. Haribabu, R. Arulanandam, J.-S. Diallo and D. C. Crans, *Biometals*, 2019, 1.
29. J. C. Pessoa, *J. Inorg. Biochem.*, 2015, **147**, 4.
30. D. C. Crans, S. Schoeberl, E. Gaidamauskas, B. Baruah and D. A. Roess, *J. Biol. Inorg. Chem.*, 2011, **16**, 961.
31. D. C. Crans, L. Henry, G. Cardiff and B. I. Posner, *Met. Ions Life Sci.*, 2019, 203.
32. T. Scior, J. A. Guevara-Garcia, Q.-T. Do, P. Bernard and S. Laufer, *Curr. Med. Chem.*, 2016, **23**, 2874.
33. K. H. Thompson and C. Orvig, *J. Inorg. Biochem.*, 2006, **100**, 1925.
34. C. Lipinski and A. Hopkins, *Nature*, 2004, **432**, 855.
35. C. A. Lipinski, L. Lombardo, B. W. Dominy and P. J. Feeney, *Adv. Drug Delivery Rev.*, 1997, **23**, 3.
36. G. R. Willsky, D. A. White and B. C. McCabe, *J. Biol. Chem.*, 1984, **259**, 13273.
37. T. Peck, S. Hill and M. Williams, *Pharmacology for Anaesthesia and Intensive Care*, 2nd edn, Greenwich Medical Media, London, 2003, pp. 3–10.
38. X. Yang, K. Wang, J. Lu and D. C. Crans, *Coord. Chem. Rev.*, 2003, **237**, 103.
39. X.-G. Yang, X.-D. Yang, L. Yuan, K. Wang and D. C. Crans, *Pharm. Res.*, 2004, **21**, 1026.
40. D. Smith, P. Artursson, A. Avdeef, L. Di, G. F. Ecker, B. Faller, J. B. Houston, M. Kansy, E. H. Kerns, S. D. Krämer, H. Lennernäs, H. van de Waterbeemd, K. Sugano and B. Testa, *Mol. Pharm.*, 2014, **11**, 1727.

CHAPTER 22

Reductive Dioxygen Activation by Biomimetic Vanadium Complexes

C. DROUZA[a] AND A. KERAMIDAS*[b]

[a] Department of Agricultural Sciences, Biotechnology and Food Science, Cyprus University of Technology, Limassol 3036, Cyprus; [b] Department of Chemistry, University of Cyprus, Nicosia 2109, Cyprus
*Email: akeramid@ucy.ac.cy

22.1 Introduction

The reductive activation of dioxygen (O_2) *via* oxidative addition of O_2 to transition metal complexes,[1] a well-known process encountered in biological systems, promoted extensive studies in the area of biomimetic activation of molecular oxygen by metal complexes over the past few years.[2–14]

Electron–proton coupled transfer reactions between transition metal centers and O_2 are vital for all life occurring in key biological processes as diverse as the oxidative maintenance of biological amine levels[15,16] and aerobic (mitochondrial) respiration.[17,18] The chemistry of synthetic analogs of the active sites of the metal proteins participating in these processes followed a general evolution, with important advances in the chemistry of high-valent species. In parallel, the use of small coordination complexes led to the evolution of applications such as the homogeneous oxidative alkane functionalization, the production of hydrogen peroxide and emerging energy technologies. Fuel cells and metal–air batteries are emerging energy technologies using O_2 as an oxidant, combining the reduction of O_2 with the

Catalysis Series No. 41
Vanadium Catalysis
Edited by Manas Sutradhar, José Armando L. da Silva and Armando J. L. Pombeiro

Published by the Royal Society of Chemistry, www.rsc.org

oxidation of fuel, such as Zn, H_2, *etc.*, to generate electricity powering houses or vehicles.[19–30] Dioxygen, after its activation, can be used as a green oxidant and in the facile on-site production of H_2O_2. H_2O_2 is also a powerful green oxidant[11,31] and can be used for clean energy storage.[32,33] These complexes, producers of reactive oxygen species (ROS), are also potential anticancer drugs, which induce apoptosis of cancer cells.[34–36] There is, however, a fundamental difference between biological systems and synthetic analogs. The former use O_2 in an efficient way (including the formation of ROS). The best synthetic biomimetic complexes involved as oxidation catalysts are active in the presence of already reduced forms of O_2, such as peroxides. Thus, the extensive research in the field of biomimetic oxidation chemistry has not yet allowed the delineation of an efficient biomimetic strategy to address points for the efficient utilization of O_2 which is of crucial economic and ecological relevance.

Molecular oxygen is a strong but kinetically inert oxidant. The triplet electronic structure of O_2 ground state, the complicated two-electron oxidations of the diamagnetic organic substrates and the unfavorable thermodynamically initial one electron reduction of O_2 (Figure 22.1) accounted for the sluggish oxidative activity of the molecular oxygen. Several research groups have studied the use of transition-metal complexes as activating agents to overcome these kinetic barriers in order to activate the reduction of the molecular oxygen, therefore, replacing the unsafe and waste-generating oxidants with the ''green'' and economic O_2. A particular active research area focuses on heme and non-heme iron, cobalt and copper complexes as models for metalloenzymes, while the mechanisms on the reductive activation of O_2 have been recently reviewed.[12,13,37]

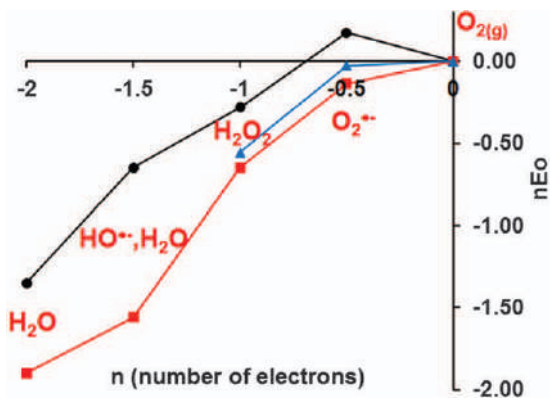

Figure 22.1 (Black circles): Frost diagram of O_2 at pH = 7.0, showing the least facile, first, step-one electron O_2 reduction to $O_2^{\bullet -}$. (Red squares): Frost diagram of O_2 coordinated to Cr_{aq}^{3+}.[1] (Blue triangles): Frost diagram of O_2 coordinated to $[V^{IV}O(pbq)(H_2O)_2]$ (Hpbq = *N*-(8-quinolyl)pyridine-2-carboxamide) measurements in CH_3CN solutions.[39]

The activation of O_2 by transition-metal complexes may involve either the coordination and partial reduction of O_2 or, in rare cases, the attack of O_2 on the organic ligand activated by the ligation to metal ion.[38] Coordination of O_2 to metal ions affects the thermodynamics of each of the four steps of O_2 reduction (Figure 22.1). For example, the first electron can be removed more easily ($E_0 = 0.27$ V) at the Cr_{aq}^{3+}-O_2 than in free O_2, and the superoxido-chromium complex $Cr_{aq}OO^{2+}$ ($E_0 = 1.03$ V) is a significantly weaker oxidant than HOO· ($E_0 = 1.44$ V). On the other hand, the hydroperoxido-chromium complex $Cr_{aq}OOH^{2+}$ ($E_0 = 2.09$ V) is a much stronger oxidant than H_2O_2 (0.80 V). Despite its large reduction potential ($E_0 = 1.71$ V), $Cr^{IV}aqO^{2+}$ is a much weaker oxidizing agent than HO· ($E_0 = 2.72$ V) (Figure 22.1).[1] Coordination of O_2 on $[V^{I}{}^{V}O(pbq)(H_2O)_2]$ (Hpbq = *N*-(8-quinolyl)pyridine-2-carboxamide) complex affects the potentials of O_2 reduction in a similar way (Figure 22.1).[39]

The vanadium-dioxygen compounds are of particular interest because vanadium complexes take part in various catalytic oxidation reactions including industrial processes, organic synthesis, electrochemical cells, pharmaceutical applications and enzymatic reactions.[40–66] In many of these applications, vanadium-peroxido complexes are utilized – vanadium-peroxido compounds are synthesized by the reaction of V^V complexes with peroxides (ROOH, R = H- or alkyl-). Despite the economic and environmental benefits of using O_2 instead of peroxides as an oxidant, the understanding of the reductive activation of O_2 by vanadium complexes still remains limited. Recently, An *et al.*,[66] demonstrated a cheap, high-performance zinc-hydrogen peroxide fuel cell, designed to propel vehicles, which consisted of a redox flow cell with the redox couples V(II)/V(III) at the anode and V(IV)/V(V) at the cathode regenerated by zinc and hydrogen peroxide, respectively (Figure 22.2). These processes in fuel cells and metal–air batteries convert chemical to electrical energy and it is desirable to replace H_2O_2 by O_2. For such a goal to be achieved, a catalyst with high rates, selectivity and energy efficiency is required. Needless to say, the reported catalysts up to date are slow, unstable and expensive.

The activation of the reduction of O_2 by vanadium in protic media can proceed through $2H^+/2e^-$ reduction to H_2O_2 or by $4H^+/4e^-$ reduction to H_2O (reactions 1 and 2 in Scheme 22.1). Even though both processes look simple, they involve several one-electron steps and might involve a combination of these two half-reactions in an either competitively or sequentially mode. Oxidation of vanadium proceeds with one-electron change (V^{IV} to V^V and V^{III} to V^{IV}), while O_2 to $O_2{}^{2-}$ and O^{2-} involve two- and four-electron processes. This makes things more complicated because of the mismatch in redox stoichiometry.

This chapter covers the field of soluble molecular oxygen reductive activation by vanadium (III/IV), both in aqueous and nonaqueous media. The $2e^-$ and $4e^-$ reduction of O_2 by vanadium complexes is presented from the mechanistic point of view in a comprehensive way. A separate section is included for the reduction of O_2 by the vanadium–"non-innocent" ligand complexes because of their particular reactivity.

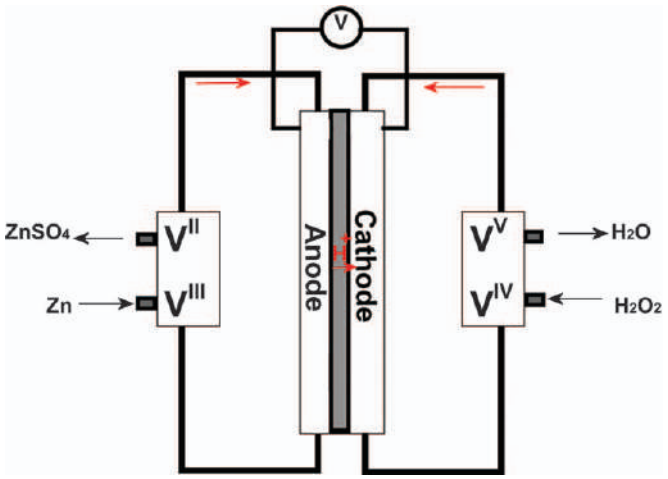

Figure 22.2 A catalyst-free, high-performance, zinc-hydrogen peroxide fuel cell consisting of a redox flow cell with the respective redox couple at the anode [V(II)/V(III)] and cathode [V(IV)/V(V)] regenerated by the fuel (zinc) and the oxidant (hydrogen peroxide).
Reproduced from ref. 66 with permission from Elsevier, Copyright 2015.

$$O_2 + 2H^+ + 2e^- \longrightarrow H_2O_2 \quad (1)$$

$$O_2 + 4H^+ + 4e^- \longrightarrow 2H_2O \quad (2)$$

Scheme 22.1 Half-reactions for O_2 reduction to H_2O_2 (1) and H_2O (2).

22.2 Reductive Activation of O_2 to O_2^{2-} by Direct Binding of O_2 on Vanadium(IV) Ion

Reduction of dioxygen to the level of peroxide dianion (O_2^{2-}) is typically accomplished in chemical and biological systems by the ligation of O_2 to a transition-metal center.[38,67–70] Only few reactions of O_2 with vanadium(IV) complexes yielding vanadium(V)-peroxido species have been reported so far.[13,71–75]

A mechanism proposed for these type of reactions is the direct binding of O_2 to vanadium(IV) complex to form an intermediate superoxido radical that is reduced to peroxide vanadium complex by subtracting a $H^\bullet$ from a reducing agent according to Scheme 22.2; the first step (**i**) has been found to be much faster than the second (**ii**). This results in accumulation of the intermediate species $[V^VO(O–O)(L)_x]^{\bullet n+}$ for a period of time (lag time) prior the formation of $[V^VO(O–O)(L)_x]^{(n-1)+}$ takes place. The lag time ranges from 0.5–24 h depending on the conditions of the reaction (*i.e.*, ligand, concentration of the reagents, solvent).

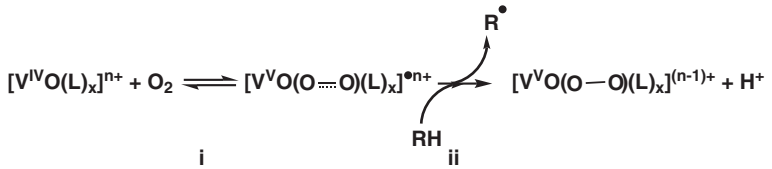

Scheme 22.2 Mechanism proposed for the reductive activation of O_2 to O_2^{2-} by direct binding of O_2 on vanadium(IV) ion.

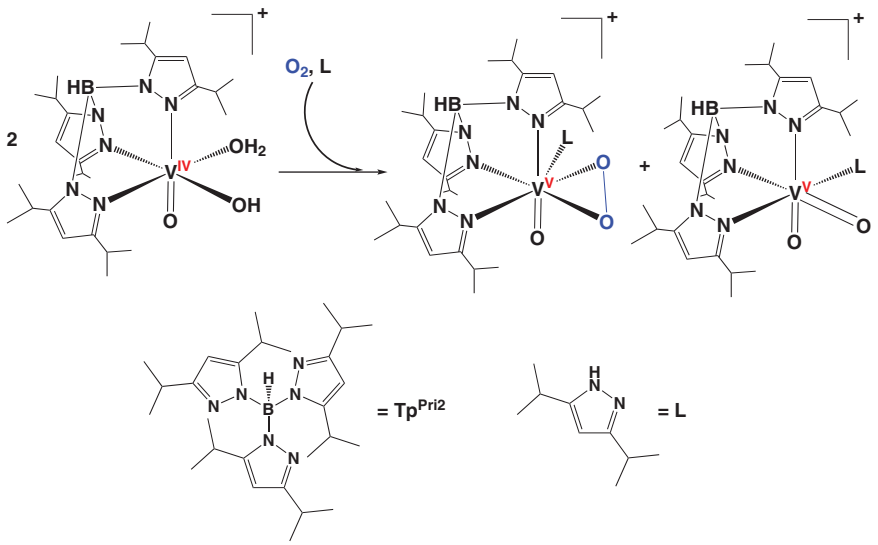

Scheme 22.3 Reaction of *cis*-$[V^{IV}O(OH)(Tp^{Pri2})]$ with O_2 in the toluene solution.[73]

The first example of a vanadium-peroxide species, $[V^{V}O(O_2)(Tp^{Pri2})]^+$ {Tp^{Pri2} = hydrotris(3,5-diisopropylpyrazol-1-yl)borate} from the reaction of *cis*-$[V^{IV}O(OH)(Tp^{Pri2})]^+$ with O_2 was reported by Kosugi *et al.* (Scheme 22.3).[73] Reaction of a toluene solution of *cis*-$[V^{IV}O(OH)(Tp^{Pri2})]^+$ with O_2 yielded equimolar quantities of *cis*-$[V^{V}O_2(Tp^{Pri2})(L)]^+$ and $[V^{V}O(O_2)(Tp^{Pri2})]^+$. Experiments with $^{18}O_2$ showed that the peroxide group was originated from the external O_2 while the origin of the oxido groups from oxido and OH^- groups. The authors noticed that the reaction system of *cis*-$[V^{IV}O(OH)(Tp^{Pri2})]/O_2$ was a stronger oxidant than $[V^{V}O(O_2)(Tp^{Pri2})]^+$ and this was assigned to the formation of an unknown intermediate.

The hypothesis of a superoxido-vanadium(V) radical intermediate for these types of reactions has been based on the existence of the electrochemically prepared $[V^{V}O(O_2)(L\text{-}N4Me_2)]^{\bullet 2+}$ superoxy centered radical species {L-N4Me$_2$ = 3,7-dimethyl-3,7-diaza-1,5(2,6)-dipyridinacyclooctaphane} produced from the oxidation of $[V^{V}O(O_2)(L\text{-}N4Me_2)]^+$ at −30 °C, identified by EPR spectroscopy (Scheme 22.4a, Figure 22.3).[72] $[V^{V}O(O_2)(L\text{-}N4Me_2)]^{\bullet 2+}$ is decomposed at room temperature resulting in $[V^{IV}O(L\text{-}N4Me_2)(CH_3CN)]^{2+}$ and

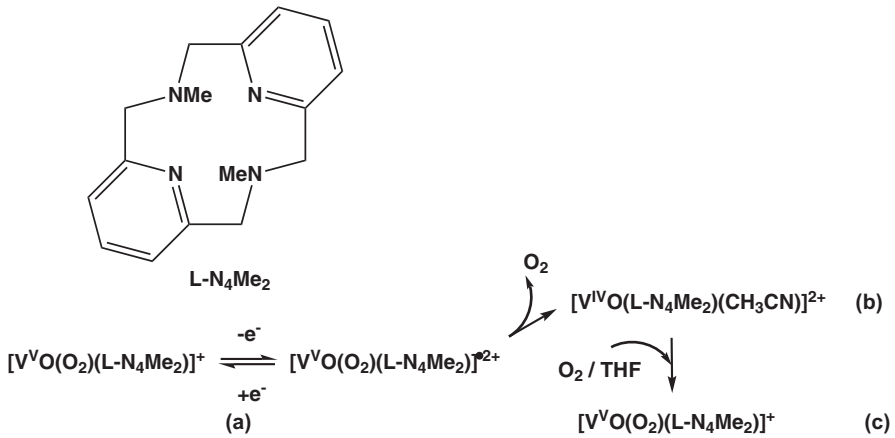

Scheme 22.4 (a) Electrochemical synthesis of $[V^{V}O(O_2)(L\text{-}N4Me_2)]^{\bullet 2+}$ at −30 °C. (b) Decomposition $[V^{V}O(O_2)(L\text{-}N4Me_2)]^{\bullet 2+}$ at room temperature. (c) Reduction of O_2 by $[V^{IV}O(L\text{-}N4Me_2)(CH_3CN)]^{2+}$ in the presence of THF.[72]

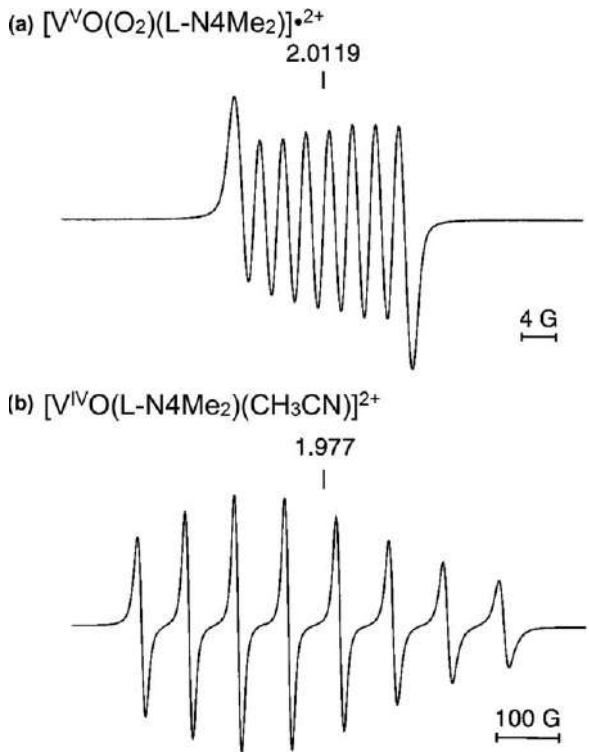

Figure 22.3 cw X-Band EPR spectra of (a) a CH_3CN solution of $[V^{V}O(O_2)(L\text{-}N4Me_2)]^{\bullet 2+}$ at −30 °C electrochemically generated from $[V^{V}O(O_2)(L\text{-}N4Me_2)]^{+}$ (electrolyte 0.2 M But_4NClO_4, electrolysis at 1.85 V *vs.* NHE), (b) a CH_3CN solution of $[V^{V}O(O_2)(L\text{-}N4Me_2)]^{\bullet 2+}$ at room temperature, the signal is assigned to $[V^{IV}O(L\text{-}N4Me_2)(CH_3CN)]^{2+}$.
Reproduced from ref. 72 with permission from John Wiley and Sons, © 2001 WILEY-VCH Verlag GmbH, Weinheim, Fed. Rep. of Germany.

O_2 (Scheme 22.4b). Kelm and Kruger[72] trials to reduce $[V^{V}O(O_2)(L\text{-}N4Me_2)]^{\bullet 2+}$ to the peroxido vanadium complex $[V^{V}O(O_2)(L\text{-}N4Me_2)]^{+}$ were unsuccessful. On the other hand, the reaction of $[V^{IV}O(L\text{-}N4Me_2)(CH_3CN)]^{2+}$ with oxygen in the presence of tetrahydrofuran (THF) resulted in $[V^{V}O(O_2)(L\text{-}N4Me_2)]^{+}$ (Scheme 22.4c). Kelm and Kruger[72] assigned the formation of $[V^{V}O(O_2)(L\text{-}N4Me_2)]^{+}$ to the abstraction of a $H^{\bullet}$ from THF by the $[V^{V}O(O_2)(L\text{-}N4Me_2)]^{\bullet 2+}$ intermediate yielded from the reaction of $[V^{IV}O(L\text{-}N4Me_2)(CH_3CN)]^{2+}$ with O_2. However, this is in contrast to the unsuccessful synthesis of $[V^{V}O(O_2)(L\text{-}N4Me_2)]^{+}$ from the electrochemically synthesized $[V^{V}O(O_2)(L\text{-}N4Me_2)]^{\bullet 2+}$ and does not justify the presence of $[V^{V}O(O_2)(L\text{-}N4Me_2)]^{\bullet 2+}$ as intermediate.

Tagika *et al.*,[71] observed the formation of $[V^{V}O(O_2)(tpa)]^{+}$ [tpa = tris(2-pyridylmethyl)amine] from $[V^{IV}O(tpa)]^{2+}$ in the presence of THF and other ethers. They attributed the formation of $[V^{V}O(O_2)(tpa)]^{+}$ to the peroxide contaminants of the solvents.

Mayer and co-workers[76] found out that the compound *cis*-$[V^{IV}O(OH)(t\text{-}Bu_2bpy)_2]^{+}$ (*t*-Bu_2bpy = 4,4′-di-*tert*-butyl-2,2′-dipyridyl) was also oxidized to $[V^{V}O(O_2)(t\text{-}Bu_2bpy)_2]^{+}$ in the presence of ethers. They proved that the oxidation was a result of the reaction of the complex *cis*-$[V^{IV}O(OH)(t\text{-}Bu_2bpy)_2]^{+}$ with atmospheric O_2. They proposed a mechanism based on Kelm's and Kruger's V^{V} superoxido O_2 center radical. According to that, initially O_2 binds to *cis*-$[V^{IV}O(OH)(t\text{-}Bu_2bpy)_2]^{+}$ to form a $[V^{V}O(O_2)(t\text{-}Bu_2bpy)_2]^{\bullet 2+}$ intermediate.[13,29,37] They claimed that the oxidation of CH_3CN/THF solutions of *cis*-$[V^{IV}O(OH)(t\text{-}Bu_2bpy)_2]^{+}$ by O_2 is light dependent. However, the acceleration might be due to the peroxide formation caused by the degradation of THF present in solution. It is known that THF starts to form peroxides under O_2 within three days and this reaction is accelerated under light, in particular in the presence of metal ions.[77]

McKenzie and co-workers[74] investigated the air oxidation of the dinuclear vanadium(IV) $[(V^{IV}O)_2(pbbp)(OH_2)_2]^{3+}$ complex (bpbp = 2,6-bis{[*N*,*N*-bis(2-pyridylmethyl)amino]methyl}-4-*tert*-butylphenolato) that yields two dinuclear species, a diperoxido $[(V^{V}O)_2(O_2)_2(pbbp)]^{+}$ and a mixed valence $[(V^{V}O)(V^{IV}O)(pbbp)(OH_2)]^{2+}$ complexes (Scheme 22.5). The reaction of $[(V^{IV}O)_2(pbbp)(OH_2)_2]^{3+}$ with O_2 exhibits a lag time ranging from 6 to 24 hours prior to the formation of $[(V^{V}O)_2(O_2)_2(pbbp)]^{+}$. During that time, an EPR silent intermediate species have been formed and assigned to vanadium(V)-superoxido radical. The authors suggested that the vanadium(V)-superoxido radical subtract a $H^{\bullet}$ from the solvent (CH_3OH) toward the formation of the peroxide-V^{V} complex $[(V^{V}O)_2(O_2)_2(pbbp)]^{+}$.

Keramidas and co-workers designed a tridentate ligand that contains nitrogen donor atoms (Hpbq; Scheme 22.6) targeting the stabilization of the intermediate species through delocalization of the radical in the extended π-system of the ligand (Scheme 22.6).[39] Reaction of methanolic solutions of $[V^{IV}O(pbq)(H_2O)_2]^{+}$ with O_2 yielded the peroxide $[V^{V}O(O_2)(pbq)(H_2O)]$ and dioxido *cis*-$[V^{V}O_2(pbq)]$ complexes.

Based on the experimental data and computational calculations, the authors proposed the mechanism shown in Scheme 22.6. Despite of the

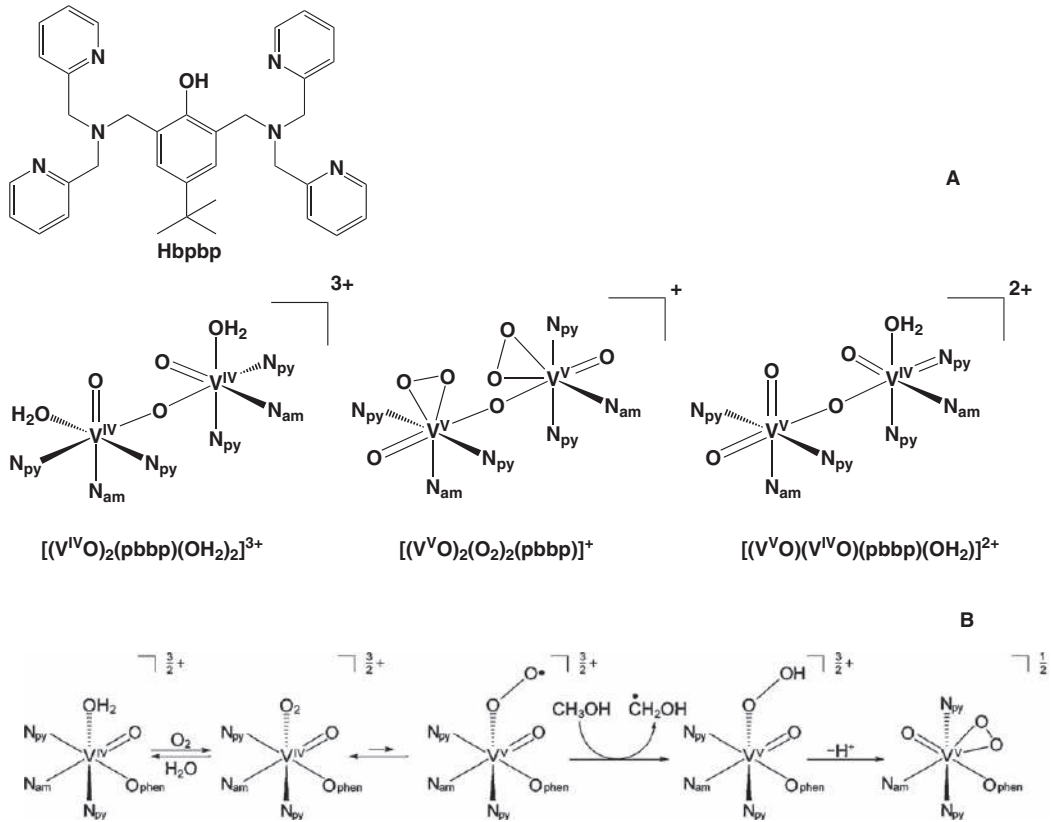

Scheme 22.5 (A) Structure of the dinuclear $pbbp^{-}$ complexes. (B) Partial drawings of half of the $[(VO)_2bpbp(OH_2)_2]^{3+}$ system, showing the proposed mechanism for formation of a peroxido ligand. The nonintegral charges represent the fact that the phenolate bridges the two V ions.
Reproduced from ref. 74 with permission from the Royal Chemical Society.

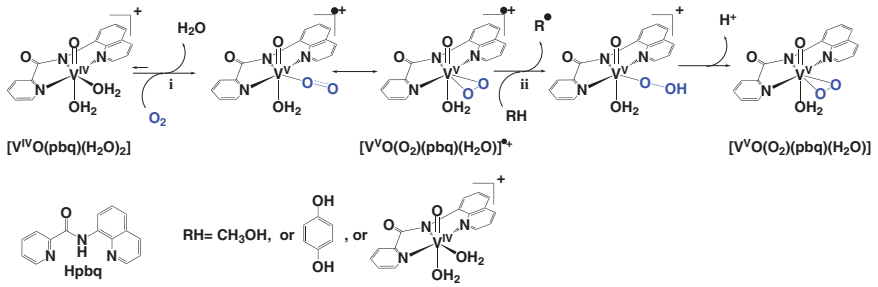

Scheme 22.6 The sequence of reactions for the exposure of $[V^{IV}O(pbq)(H_2O)_2]^+$ to O_2.

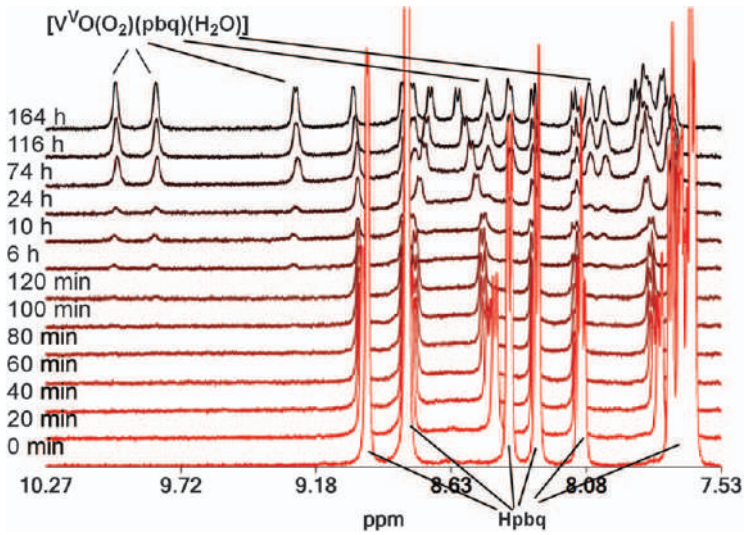

Figure 22.4 ^{1}H NMR spectra of a $V^{IV}OSO_4$ (0.0144 M)-Hpbq (0.0138 M) solution [D_2O:CD_3OD; 25:75, v/v] *vs.* time (first 164 min) and proton assignments.

paramagnetic character of the intermediate species $[V^{V}O(O_2)(pbq)(H_2O)]^{\bullet+}$, it was characterized by ^{1}H NMR. In the first two hours after mixing an aqueous solution of $V^{IV}OSO_4$ with a Hpbq solution in CD_3OD, a broadening of the peaks and a shift to lower field were observed by ^{1}H NMR spectroscopy (Figure 22.4). The signal of one of the quinolone protons of the ligand appeared as a broad peak at ~8.5 ppm with a line width of ~650 Hz, which almost collapses within the baseline. The broadening and the change of the chemical shift of the ligand peaks have been assigned to the paramagnetic intermediate $[V^{V}O(O_2)(pbq)(H_2O)]^{\bullet+}$. $[V^{V}O(O_2)(pbq)(H_2O)]^{\bullet+}$ has been found to be thermodynamically stable with $K_{eq} = [V^{V}O(O_2)(pbq)(H_2O)^{\bullet+}]/([V^{IV}O(pbq)(H_2O)^{+}]\times[O_2]) = 4.5\times10^4 \pm 0.5\ M^{-1}$ at 22 °C.

Based on the experimental data, Keramidas and co-workers have shown the first step **i** in Scheme 22.6 to be ~1000-times faster than the second **ii**. The rate of step **i** is dependent on the concentrations of $[V^{IV}O(pbq)(H_2O)_2]^+$ and $[O_2]$ while the rate of step **ii** is dependent on concentration of both the $[V^{V}O(\eta^2\text{-}O_2)(pbq)(H_2O)]^{\bullet+}$ and the molecule ($[V^{IV}O(pbq)(H_2O)_2]^+$, or CH_3OH or hydroquinone) that reduces the radical. Lag time from 30 to 120 min is required prior to the formation of $[V^{V}O(\eta^2\text{-}O_2)(pbq)(H_2O)]$ – which is the shortest lag time reported so far for these type of reactions.[73,74,76] Zero-order pO_2-dependence has also been reported for the reduction of O_2 to O_2^{2-} from the Co^{II}-salophen catalyst.[37,78] In contrast to $[V^{IV}O(pbq)(H_2O)]^+$, the Co^{II}-salophen's [salophen = *N,N′*- bis(salicylidene)-1,2-phenylenediamine] rate for the O_2 reduction to O_2^{2-} is first order with respect to $[H^+]$ and it was assigned to a protonated intermediate $(salophen)Co^{III}(\kappa^1\text{-}O\text{-}OH)$. It is worth noting here that in the reduction of O_2 to H_2O by the related Fe^{II}(porphyrin) complex, the rate of the reaction is first order with respect to both $[H^+]$ and $[O_2]$. The proposed mechanism includes a pre-equilibrium of O_2 bonding to the metal ion and a protonation rate-determining step. Apparently, in the $2e^-$ O_2 reduction by V^{IV}-Hpbq, the $[V^{V}O(\eta^2\text{-}O_2)(pbq)(H_2O)]^{\bullet+}$ protonation is not a rate-determining step of the reaction.[12] The high reactivity of $[V^{IV}O(pbq)(H_2O)_2]^+$ toward the $2e^-$ reductive activation of O_2 has been attributed to the thermodynamic stabilization of both the intermediate $[V^{V}O(\eta^2\text{-}O_2)(pbq)(H_2O)]^{\bullet+}$ and the $[V^{V}O(\eta^2\text{-}O_2)(pbq)(H_2O)]$ through the radical delocalization on the pbq^- and the coordination of the V^V metal ion with nitrogen donor atoms, respectively.

DFT calculations have suggested that compound $[V^{V}O(O_2)(pbq)(H_2O)]$ can be formed by an initial end-on binding of O_2 to complex $[V^{IV}O(pbq)(H_2O)_2]^+$ followed by a low-barrier isomerization to give the side-on $[V^{V}O(\eta^2\text{-}O_2)(pbq)(H_2O)]^{\bullet+}$ valence tautomer. The potential energy surface for the $[V^{V}O(\eta^2\text{-}O_2)(pbq)(H_2O)]^{\bullet+} \rightarrow [V^{V}O(\eta^2\text{-}O_2)(pbq)(H_2O)]^{\bullet+}$ isomerization plotted *vs.* the V–O–O bond angle from 180° to 67° shows a transition state located at a V–O–O bond angle of 158° surmounting an activation barrier of 2.05 kcal mol^{-1} (Figure 22.5).

Further investigation of the reactivity of other V^{IV} complexes with tridentate containing nitrogen donor atom ligands toward the O_2 to O_2^{2-} conversion has shown that despite the lack of publications in the field, this reaction is common among these types of compounds.

22.3 Reductive Activation of O_2 to O_2^{2-} by Direct Binding of O_2 on Vanadium(III) Ion

In the case of V^{III} complexes, oxidation of the metal ion by O_2 typically produces a V^V *cis*-diooxido species resulting from a bimetallic, four-electron reduction of O_2.[79,80] Cozzolino *et al.*, have investigated the reaction of $V^{III}(N[tBu]Ar)_3$ with O_2.[81] At room temperature, the reduction of O_2 by $V^{III}(N[tBu]Ar)_3$ gives $V^{V}O(N[tBu]Ar)_3$. However, at −78 °C, $V^{III}(N[tBu]Ar)_3$ dissolved in toluene reacts with excess of O_2 to give the nonoxido peroxide

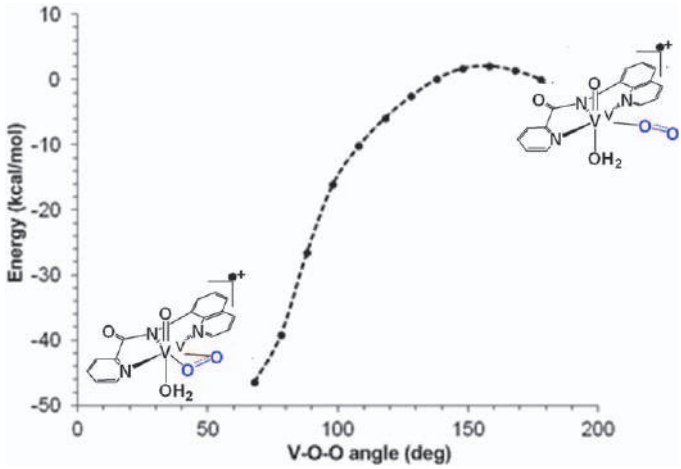

Figure 22.5 DFT-calculated potential energy surface for isomerization of $[VO(pbq)(OH_2)(\eta^1\text{-}O_2)]^{\bullet+}$ to $[VO(pbq)(OH_2)(\eta^2\text{-}O_2)]^{\bullet+}$.

vanadium complex $V^V(\eta^2\text{-}O_2)(N[tBu]Ar)_3$. ^{51}V NMR spectroscopy showed a peak at 198 ppm originated from $V^V(\eta^2\text{-}O_2)(N[tBu]Ar)_3$. This is a very high frequency relative to those for known V^V peroxides (−520 to −650 ppm)[82] and reflects the unique ligand environment used to support the vanadium peroxide moiety in $V^V(\eta^2\text{-}O_2)(N[tBu]Ar)_3$, including the lack of a vanadyl moiety. DFT calculations support an initial attack of O_2 on V^{III} ion and formation of the end on $V^V(\eta^1\text{-}O_2)(N[tBu]Ar)_3$ (Scheme 22.7).

The calculated potential energy surface for the isomerization of $V^V(\eta^1\text{-}O_2)(N[tBu]Ar)_3$ to $V^V(\eta^2\text{-}O_2)(N[tBu]Ar)_3$ shows the transition state to be located at a V–O–O bond angle of 110° surmounting an activation barrier of 12.2 kcal mol^{-1} (Figure 22.6), which is higher than the activation barrier of 2.05 kcal mol^{-1} calculated for the $[V^VO(\eta^1\text{-}O_2)(pbq)(OH_2)]^{\bullet+} \rightarrow [V^VO(\eta^2\text{-}O_2)(pbq)(OH_2)]^{\bullet+}$ isomerization. The large steric interactions of O–O with the bulky $N[tBu]Ar^-$ compared with pbq^- might account for the larger activation barrier.

22.4 Four-electron Reduction of O_2 by Vanadium Complexes

Considering that the reduction of O_2 to H_2O requires $4e^-$ while V^{IV} catalysts are able to provide only one e^-, these catalysts might not be considered efficient. The oxidation of V^{III} to V^V is a two-electron process. Presumably a dinuclear V^{III} can offer the $4e^-$ electrons required for the full reduction of O_2. Myser and Shepherd synthesized the dinuclear $[V^{III}_2O(ttha)]^{2-}$ (ttha = triethylenetertraminehexacetate) and studied the mechanism of O_2 reduction by the complex.[83] They proposed that initially $[V^{III}_2O(ttha)]^{2-} \equiv [V^{III},V^{III}]$ binds O_2 to form a superoxido $[V^{III},V^{IV}\ O_2^{\bullet-}]$ and then the coordinated $O_2^{\bullet-}$ is reduced by three $[V^{III},V^{III}]$ complexes to result in water

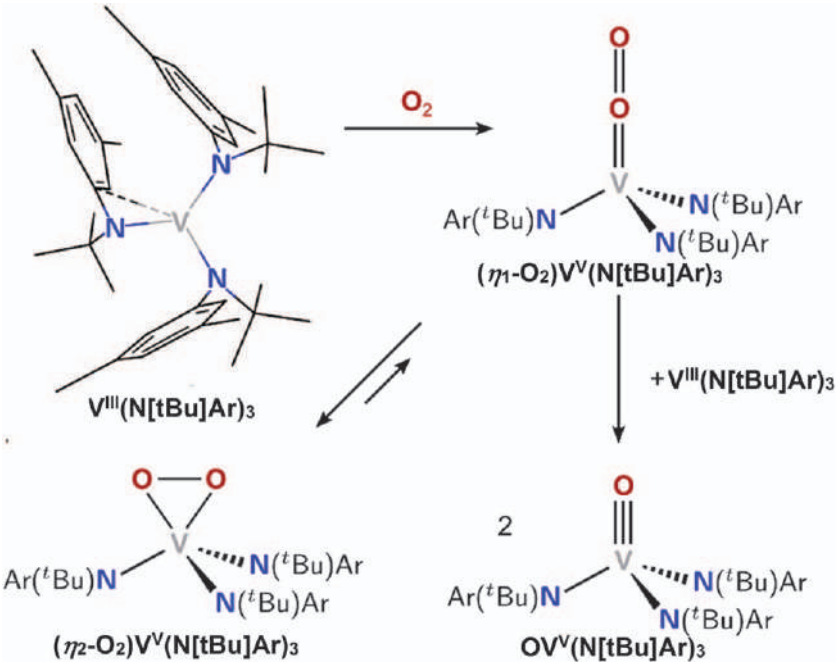

Scheme 22.7 The sequence of reactions for the exposure of $V^{III}(N[tBu]Ar)_3$ to O_2. Reproduced from ref. 81 with permission from American Chemical Society, Copyright 2012.

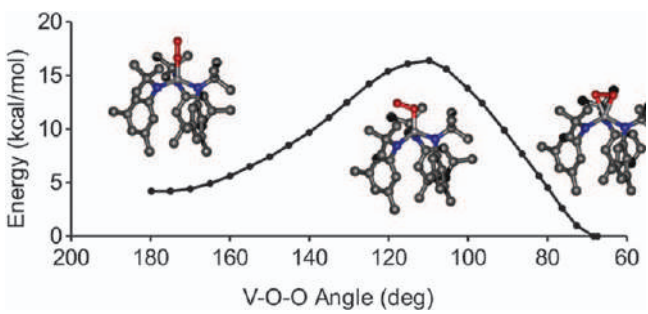

Figure 22.6 DFT-calculated potential energy surface for isomerization of $(\eta^1\text{-}O_2)V^V(N[tBu]Ar)_3$ to $(\eta^2\text{-}O_2)V^V(N[tBu]Ar)_3$. Reproduced from ref. 81 with permission from American Chemical Society, Copyright 2012.

and more dinuclear oxidized vanadium species [V^{III},V^{IV}], [V^{IV},V^{IV}]. They could not detect $O_2^{\bullet -}$ in solutions, which was attributed to the inner sphere superoxido [V^{III},V^{IV} $O_2^{\bullet -}$] complex in which the superoxido is ligated to both vanadium atoms.

[V^{IV}O(salen)] (salen = *N*,*N*′-bis(salicylidene)-1,2-ethylenediamine) has been investigated extensively for its use as a $4e^-$ O_2 reductive electrocatalyst.[84–87]

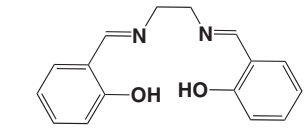

Hsalen

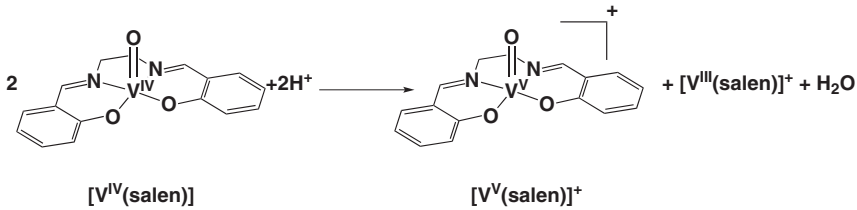

[V IV(salen)] [V V(salen)]+

Scheme 22.8 Disproportionation reaction of $[V^{IV}(salen)]$.

$$[V^{III}(salen)]^+ + O_2 \rightleftharpoons [O_2V(salen)]^+$$

$$[O_2V(salen)]^+ + [V^{III}(salen)]^+ \longrightarrow [(salen)VOOV(salen)]^{2+}$$

$$[(salen)VOOV(salen)]^{2+} \longrightarrow 2[V^{V}O(salen)]^+$$

Scheme 22.9 Mechanism of the O_2 electrocatalytic reduction by $[V^{III}(salen)]$.[84]

Most of the studies were based on the observation of Carrano, Pecoraro and co-workers that $[V^{IV}O(salen)]$ disproportionates to $[V^{V}O(salen)]^+$ and $[V^{III}(salen)]^+$ under acidic conditions (Scheme 22.8)[88,89] and then $[V^{III}(salen)]^+$ can reduce O_2. Although acids such as $HClO_4$ disproportionate $[V^{IV}O(salen)]$, reaction of $[V^{IV}O(salen)]$ with HCl gives $[V^{IV}Cl_2(salen)]$. These reactions suggest that protonation of the oxido V=O atom is involved in the reaction mechanism.

Anson and co-workers have investigated the mechanism of O_2 electrocatalytic reduction by $[V^{IV}O(salen)]$.[84] In acidic condition they reduced $[V^{V}O(salen)]$ electrochemically to $[V^{III}(salen)]^+$. $[V^{III}(salen)]^+$ reacts with O_2 and forms a V-O_2 adduct presumably of the same nature as this reported by Cozzolino *et al.*[81] The $[O_2V(salen)]^+$ reacts with a $[V^{III}(salen)]^+$ molecule to form a binuclear peroxo species which decomposes fast to $[V^{V}O(salen)]^+$. Tusida *et al.*,[80,86] isolated several $[(salen)VOV(O)_{0or1}(salen)]^{1+or2+}$ ($V^{III–V}$) species from the reaction of $[V^{IV}O(salen)]$ with O_2 in dichloromethane in acidic conditions, supporting the mechanism in Scheme 22.9. However, they figured out that only the $[V^{III}(salen)]^+$ is an active electrocatalyst for the $4e^-$ O_2 reduction.

22.5 Reductive Activation of O_2 by Vanadium – "Non-innocent" Ligand Complexes

22.5.1 Vanadium-catecholates

Vanadium compounds have been found to exhibit catechol-dioxygenase like catalytic activity.[90–94] Pierpont and co-workers have observed that the

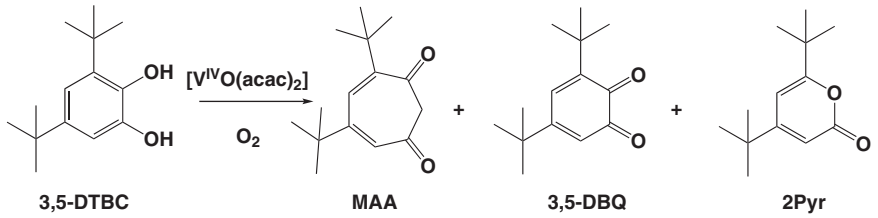

Scheme 22.10 Catalytic oxidation of 3,5-DTBC by $[V^{IV}O(acac)_2]$ (acac$^-$ = acateylacetonate) and O_2

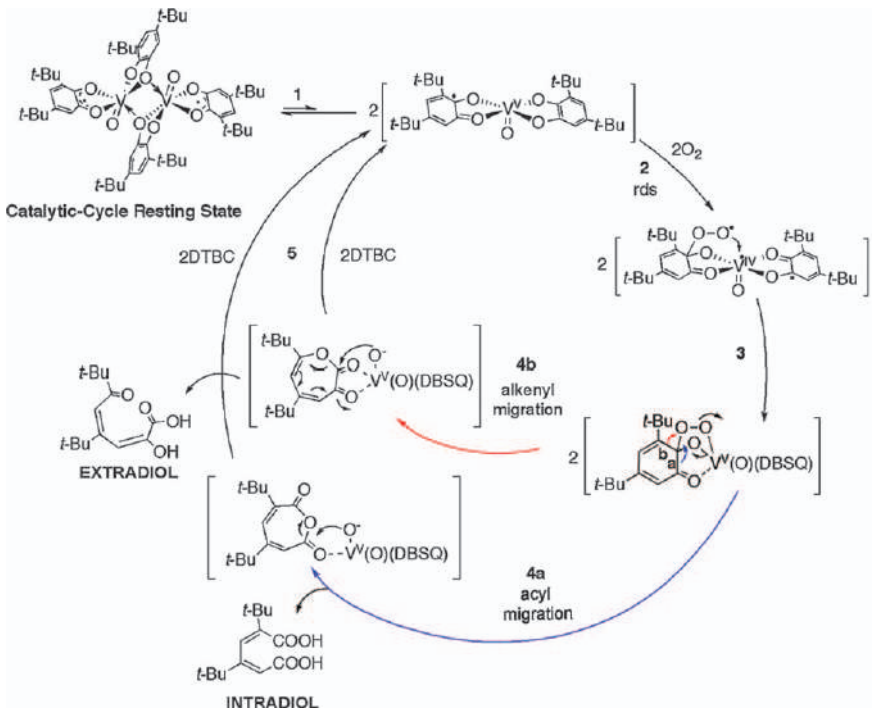

Figure 22.7 Mechanism of the oxygenation of 3,5-DTBC by vanadium catalysts. Reproduced from ref. 96 with permission from American Chemical Society, Copyright 2005.

reaction of $[V^{III}(3,5\text{-DBSQ})_3]$ (3,5-DBSQ = 3,5-di-*tert*-butyl-semiquinone) with O_2 results in the formation of $[V^{V}O(3,5\text{-DBSQ})(3,5\text{-DTBC})]$ (3,5-DTBC = 3,5-di-*tert*-butyl-catechol) and 3,5-DBQ (3,5-DBQ = 3,5-di-*tert*-butyl-quinone).[95] Tatsuno *et al.*, and others found out that when catalytic quantities of V^{III} or V^{IV} compounds react with 3,5-DTBC yield 41% 4,6-di-*tert*-butylcyclohepta-4,6-diene-1,3-dione (MAA) and the 15% 4,6-di-*tert*-butyl-2*H*-pyran-2-one (2Pyr) together with 3,5-DBQ (27%) (Scheme 22.10).[90,92]

Finke and co-workers have investigated this mechanism, examining the kinetics of the reduction of dioxygen by $[V^{V}O(3,5\text{-DBSQ})(3,5\text{-DTBC})]$ (Figure 22.7).[96] They have suggested that a possible mechanism proceeds

through the electrophilic attack of O_2 to the 3,5-DBSQ ligand of the valence tautomer of $[V^{V}O(3,5\text{-DBSQ})(3,5\text{-DTBC})]$, *i.e.*, $[V^{IV}O(3,5\text{-DBSQ})_2]$, as the initial step. A subsequent V–OO bond formation step is required in order for the O–O bond cleavage to occur eventually as a required step to account for the observed products. Steps 3 and 4 of the mechanism in Figure 22.7 have been drawn in analogy to the iron-catechol dioxygenase mechanism.

22.5.2 Vanadium-hydroquinonates

Organic–inorganic vanadium-hydroquinonate binary redox systems have been found to exhibit oxidase-like properties.[75,97] The tetranuclear $[V^{IV}{}_4O_4(\mu\text{-}O)_2(\mu\text{-bicas})_2]^{6-}$ ($bicas^{\bullet 5-}$ = 2,5-bis[*N,N*-bis(carboxymethyl) aminomethyl]-*p*-semiquinonate) exhibits a proton-induced electron transfer from the metal ion to the ligand (Scheme 22.11).[97] At pH = 3.8 one of the two semiquinonates bridges ($bicas^{5-}$) of the complex oxidizes one of the V^{IV} to V^{V} while $bicas^{5-}$ is reduced to hydroquinonate ($bicah^{6-}$) (H_6bicah = 2,5-bis[*N,N*-bis(carboxymethyl)aminomethyl]hydroquinone). The second V^{IV} ion with coordinated $bicah^{6-}$ is oxidized by the atmospheric O_2 yielding $[V^{IV}{}_2V^{V}{}_2O_4(\mu\text{-}O)_2(\mu\text{-bicas})(\mu\text{-bicah})]^{5-}$. At pH = 2.8, $[V^{IV}{}_2V^{V}{}_2O_4(\mu\text{-}O)_2(\mu\text{-bicas})(\mu\text{-bicah})]^{5-}$ is converted to $[V^{V}{}_4O_4(\mu\text{-}O)_2(\mu\text{-bicah})_2]^{4-}$ following the same mechanism. In contrast to the previous examples, the reduction of O_2 by these tetranuclear V^{IV} complexes is instantaneous. The oxidation of the $bicah^{6-}$ coordinated V^{IV} to V^{V} by O_2 has been attributed to the higher affinity of V^{V} than V^{IV} for the hydroquinonate oxygen donor atoms.[98] H_2O_2 was not detected in the reaction, depicting a $4e^-$ reduction of O_2.

Stylianou *et al.*, replaced the carboxylate group with a pyridine targeting to the stabilization of the vanadium in oxidation state IV by introducing more nitrogen donor atoms in the vanadium coordination sphere.[75] The dinuclear

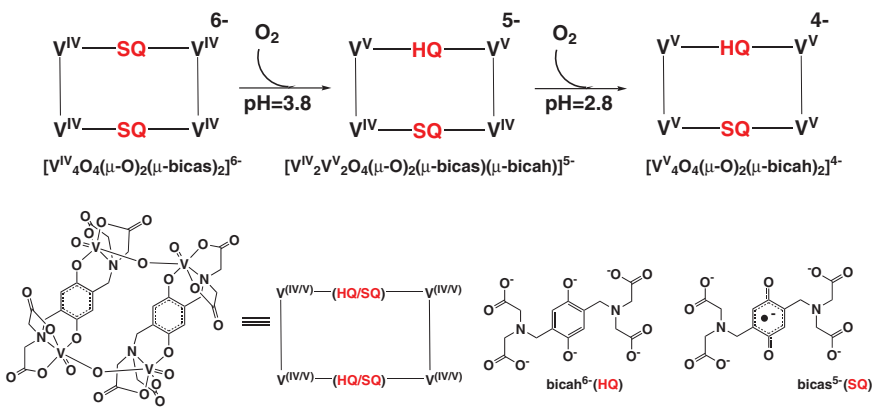

Scheme 22.11 pH-induced redox changes of the tetranuclear vanadium-$bicah^{6-}$ complexes.
Reproduced from ref. 97 with permission from American Chemical Society, Copyright 2008.

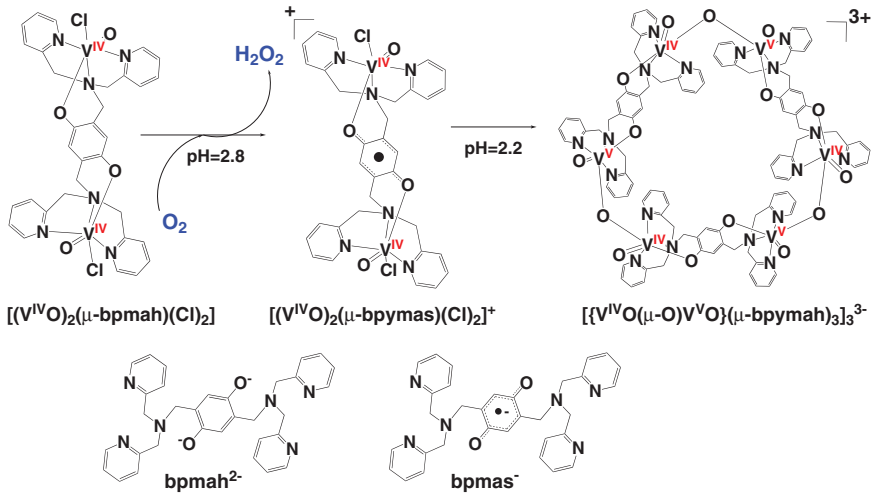

Scheme 22.12 pH-induced redox changes of the dinuclear vanadium-bpmah^{2-} complexes.
Reproduced from ref. 75 with permission from American Chemical Society, Copyright 2015.

vanadium complex $[(V^{IV}O)_2(\mu\text{-bpmah})(Cl)_2]$ (H_2bpmah = 2,5-bis[*N*,*N*′-bis(2-pyridyl-aminomethyl)aminomethyl]-*p*-hydroquinone) at pH = 2.8 in CH_3CN spontaneously reduces O_2 to H_2O_2 yielding the semiquinonate ligated to V^{IV} radical $[(V^{IV}O)_2(\mu\text{-bpmas})(Cl)_2]^+$ (Scheme 22.12). At pH = 2.2, the bpmas$^-$ bridge oxidizes one of the ligated radical V^{IV} ions to V^V, resulting in the hexanuclear $[\{V^{IV}O(\mu\text{-O})V^{V}O\}(\mu\text{-bpymah})_3]_3{}^{3-}$. Similarly to the bicah^{6-} vanadium complexes described, the reduction of O_2 by $[(V^{IV}O)_2(\mu\text{-bpmah})(Cl)_2]$ is almost instantaneous. The reduction of O_2 to H_2O_2 by $[(V^{IV}O)_2(\mu\text{-bpmas})(Cl)_2]^+$ is catalytic at the expense of a reducing agent.

22.6 Conclusions

Studies of homogeneous vanadium dioxygen reductive activators provide important knowledge and valuable insight for understanding the O_2 reduction in biological systems, utilizing O_2 as oxidant in catalytic oxidation of organic substrates and developing effective O_2-based energy sources. The design of more efficient O_2 reductive activators requires the complete understanding of the thermodynamic parameters governing the individual mechanistic steps in aqueous and nonaqueous solutions. Oxygen reduction activation can proceed by one of two pathways: *via* initial O_2 binding to a V(III/IV) center to form a V-O_2 adduct, or *via* an initial binding to the ligated to vanadium ion organic ligand. However, the former pathway dominates the O_2 reductive activation in vanadium literature. The V^{III} mononuclear complexes reduce O_2 by a 4e$^-$ process, with vanadium to be oxidized mainly to the respective $V^VO_2{}^+$ compounds in both aqueous and nonaqueous solutions. In

nonaqueous solutions, $V^{IV}O^{2+}$ mononuclear complexes reduce O_2 selectively to O_2^{2-}, a $2e^-$ process. In acidic solutions, $V^{IV}O^{2+}$ compounds completely reduce O_2 to H_2O; however, this reaction has been attributed to the V^{III} species that are present in the solution after acidification of $V^{IV}O^{2+}$ complexes. In $V^{IV}O^{2+}$-catecholate and -hydroquinonate complexes, both the organic and inorganic redox systems participate in O_2 reduction. In organic solvents these compounds reduce O_2 to H_2O_2 while in aqueous solutions to H_2O.

Experimental and computational data support that initially O_2 binds V^{IV} or V^{III} atom to form the $V^{V}O(\eta^2-O_2)^{\bullet+}$ or $V^{V}(\eta^1-O_2)^{3+}$ complexes respectively. $V^{V}O(\eta^2-O_2)^{\bullet 2+}$ subtracts a $H^{\bullet}$ from a reducing reagent such as methanol to form $V^{V}O(\eta^2-O_2)^{+}$ while $V^{V}(\eta^1-O_2)^{3+}$ at room temperature reacts with another V^{III} to form 2 $V^{V}O^{3+}$ complexes.

Although the formation of $V^{V}O(\eta^2\text{-}O_2)^{+}$ from the exposure of $V^{IV}O^{2+}$ complexes to atmospheric O_2 is slow, it can be accelerated by stabilization of the $OV^{V}(\eta^2-O_2)^{\bullet 2+}$, for example by coordinating vanadium with a ligand able to stabilize the radical through spin delocalization. However, $VO^{V}(\eta^2-O_2)^{\bullet 2+}$ is better oxidant and is formed faster than $V^{V}O(\eta^2-O_2)^{+}$. Thus, $VO^{V}(\eta^2-O_2)^{\bullet 2+}$ may be a more suitable oxidative reagent than the peroxide-vanadium complexes in applications such as homogeneous oxidation of hydrocarbons and energy production from fuel cells. V^{IV}-hydroquinonate complexes are much more effective toward O_2 reduction; however, they are oxidative unstable.

The biomimetic activation of molecular oxygen by vanadium complexes remains a difficult research field. The few studies on O_2 reductive activation by vanadium complexes show that V^{III}, V^{IV} compounds can be efficient catalysts for $2e^-$ and $4e^-$ O_2 reduction. Careful comparisons among different systems will allow for better understanding of how the catalyst, with the use of new ligands or modification of the experimental conditions, can be tuned to achieve enhanced O_2 reduction efficiency and activity.

References

1. A. Bakac, *Inorg. Chem.*, 2010, **49**, 3584–3593.
2. W. Nam, *Acc. Chem. Res.*, 2007, **40**, 465.
3. E. I. Solomon, T. C. Brunold, M. I. Davis, J. N. Kemsley, S.-K. Lee, N. Lehnert, F. Neese, A. J. Skulan, Y.-S. Yang and J. Zhou, *Chem. Rev.*, 2000, **100**, 235–350.
4. E. G. Kovaleva and J. D. Lipscomb, *Nat. Chem. Biol.*, 2008, **4**, 186–193.
5. A. T. Fiedler and A. A. Fischer, *J. Biol. Inorg. Chem.*, 2017, **22**, 407–424.
6. S. Sahu and D. P. Goldberg, *J. Am. Chem. Soc.*, 2016, **138**, 11410–11428.
7. G. M. Yee and W. B. Tolman, *Transition Metal Complexes and the Activation of Dioxygen*, 2015.
8. M. L. Neidig and E. I. Solomon, *Chem. Commun.*, 2005, 5843–5863.
9. I. V. Korendovych, S. V. Kryatov and E. V. Rybak-Akimova, *Acc. Chem. Res.*, 2007, **40**, 510–521.

10. X. Shan and L. Que, *PNAS*, 2005, **102**, 5340.
11. R. Hage and A. Lienke, *Angew. Chem., Int. Ed.*, 2006, **45**, 206–222.
12. M. L. Pegis, D. J. Martin, C. F. Wise, A. C. Brezny, S. I. Johnson, L. E. Johnson, N. Kumar, S. Raugei and J. M. Mayer, *J. Am. Chem. Soc.*, 2019, **141**, 8315–8326.
13. M. L. Pegis, C. F. Wise, D. J. Martin and J. M. Mayer, *Chem. Rev.*, 2018, **118**, 2340–2391.
14. D. Mandon, H. Jaafar and A. Thibon, *New J. Chem.*, 2011, **35**, 1986–2000.
15. D. M. Dooley, R. A. Scott, P. F. Knowles, C. M. Colangelo, M. A. McGuirl and D. E. Brown, *J. Am. Chem. Soc.*, 1998, **120**, 2599.
16. J. P. Klinman, *Chem. Rev.*, 1996, **96**, 2541.
17. D. G. Nichols and S. J. Ferguson, *Bioenergetics 2*, Academic Press, New York, 1992.
18. S. Iwata, L. W. Lee, K. Okada, J. K. Lee, M. Iwata, B. Rasmussen, T. A. Link, S. Ramaswamy and B. K. Jap, *Science*, 1998, **281**, 64.
19. D. Munz and T. Strassner, *Inorg. Chem.*, 2015, **54**, 5043–5052.
20. Y. Liang, J. Wei, X. Qiu and N. Jiao, *Chem. Rev.*, 2018, **118**, 4912–4945.
21. C. J. Allpress and L. M. Berreau, *Coord. Chem. Rev.*, 2013, **257**, 3005–3029.
22. E. G. Chepaikin, *J. Mol. Catal. A: Chem.*, 2014, **385**, 160–174.
23. D. M. Boghaei and S. Mohebi, *J. Mol. Catal. A: Chem.*, 2002, **179**, 41–51.
24. S. Hazra, P. Pilania, M. Deb, A. K. Kushawaha and A. J. Elias, *Chem. – Eur. J.*, 2018, **24**, 15766–15771.
25. J. Sun, Z. Ou, R. Guo, Y. Fang, M. Chen, Y. Song and K. M. Kadish, *J. Porphyrins phthalocyanines*, 2016, **20**, 456–464.
26. E. Anxolabéhère-Mallart, J. Bonin, C. Fave and M. Robert, *Dalton Trans.*, 2019, **48**, 5869–5878.
27. D. Liu, L. Tao, D. Yan, Y. Zou and S. Wang, *ChemElectroChem*, 2018, **5**, 1775–1785.
28. Y. M. Zhao, G. Q. Yu, F. F. Wang, P. J. Wei and J. G. Liu, *Chem. – Eur. J.*, 2019, **25**, 3726–3739.
29. K. Mase, M. Yoneda, Y. Yamada and S. Fukuzumi, *Nat. Commun.*, 2016, **7**, 1–7.
30. P. Vanýsek and V. Novák, *J. Energy Storage*, 2017, **13**, 435–441.
31. J. M. Campos-Martin, G. Blanco-Brieva and J. L. G. Fierro, *Angew. Chem., Int. Ed.*, 2006, **45**, 6962–6984.
32. R. S. Disselkamp, *Appl. Energy*, 2011, **88**, 4214–4217.
33. Y. G. Zhang, A. M. Pang, J. W. Xiao, W. B. Li, H. Yuan and D. W. Zeng, *Proceedings of the International Astronautical Congress, IAC*, 2013, **9**, 7010–7016.
34. Z. Liu and P. J. Sadler, *Acc. Chem. Res.*, 2014, **47**, 1174–1185.
35. C. Santini, M. Pellei, V. Gandin, M. Porchia, F. Tisato and C. Marzano, *Chem. Rev.*, 2014, **114**, 815–862.
36. G. Lenaz, *Journal*, 2012, **942**, 93–136.
37. Y.-H. Wang, M. L. Pegis, J. M. Mayer and S. S. Stahl, *J. Am. Chem. Soc.*, 2017, **139**, 16458–16461.

38. M. G. Papanikolaou, S. Hadjithoma, D. S. Chatzikypraiou, D. Papaioannou, C. Drouza, A. C. Tsipis, H. N. Miras, A. D. Keramidas and T. A. Kabanos, *Dalton Trans.*, 2018, **47**, 16242–16254.
39. S. Hadjithoma, M. Papanikolaou, A. Kartakoullis, S. C. Hayes, C. Drouza, P. Lianos, A. C. Tsipis, T. A. Kabanos and A. D. Keramidas, Submited for Publication, 2019.
40. D. Rehder, *Coord. Chem. Rev.*, 1999, **182**, 297–322.
41. D. Rehder, *Bioinorganic Vanadium Chemistry*, John Wiley & Sons, Ltd., 2008.
42. C. R. Cornman, G. J. Colpas, J. D. Hoeschele, J. Kampf and V. L. Pecoraro, *J. Am. Chem. Soc.*, 1992, **114**, 9925–9933.
43. C. J. Schneider, J. E. Penner-Hahn and V. L. Pecoraro, *J. Am. Chem. Soc.*, 2008, **130**, 2712–2713.
44. T. Hirao, *Chem. Rev.*, 1997, **97**, 2707.
45. S. K. Hanson, T. R. Baker, J. C. Gordon, B. L. Scott and D. L. Thorn, *Inorg. Chem.*, 2010, **49**, 5611–5618.
46. G. H. Spikes, S. Sproules, E. Bill, T. Weyhermuller and K. Wieghardt, *Inorg. Chem.*, 2008, **47**, 10935–10944.
47. C. Mukherjee, T. Weyhermuller, E. Bothe and P. Chaudhuri, *Inorg. Chem.*, 2008, **47**, 11620–11632.
48. C. J. Chang, J. A. Labinger and H. B. Gray, *Inorg. Chem.*, 1997, **36**, 5927–5930.
49. P. B. Chatterjee, K. Bhattacharya, N. Kundu, K. Y. Choi, R. Clérac and M. Chaudhury, *Inorg. Chem.*, 2009, **48**, 804–806.
50. V. Conte and B. Floris, *Dalton Trans.*, 2011, 1419–1436.
51. G. J. Colpas, B. J. Hamstra, J. W. Kampf and V. L. Pecoraro, *J. Am. Chem. Soc.*, 1996, **118**, 3469–3478.
52. A. G. L. Ligtenbarg, R. Hage and B. L. Feringa, *Coord. Chem. Rev.*, 2003, **237**, 89–101.
53. D. C. Crans, B. Zhang, E. Gaidamauskas, A. D. Keramidas, G. R. Willsky and C. R. Roberts, *Inorg. Chem.*, 2010, **49**, 4245–4256.
54. M. Sutradhar, N. V. Shvydkiy, M. F. C. Guedes Da Silva, M. V. Kirillova, Y. N. Kozlov, A. J. L. Pombeiro and G. B. Shul'Pin, *Dalton Trans.*, 2013, **42**, 11791–11803.
55. J. A. L. Da Silva, J. J. R. Fraústo da Silva and A. J. L. Pombeiro, *Coord. Chem. Rev.*, 2013, **257**, 2388–2400.
56. G. B. Shul'pin, *J. Mol. Catal. A: Chem.*, 2002, **189**, 39–66.
57. A. Messerschmidt, L. Prade and R. Wever, *Biol. Chem.*, 1997, **378**, 309–315.
58. D. C. Crans, L. Henry, G. Cardiff and B. I. Posner, *Met. Ions Life Sci.*, 2019, **19**, 359–392.
59. M. V. Kirillova, M. L. Kuznetsov, Y. N. Kozlov, L. S. Shul'Pina, A. Kitaygorodskiy, A. J. L. Pombeiro and G. B. Shul'Pin, *ACS Catal.*, 2011, **1**, 1511–1520.
60. D. Wischang, O. Brücher and J. Hartung, *Coord. Chem. Rev.*, 2011, **255**, 2204–2217.

61. I. E. León, S. B. Etcheverry, B. S. Parajón-Costa and E. J. Baran, *Biol. Trace Elem. Res.*, 2013, **155**, 295–300.
62. M. R. Maurya, *J. Chem. Sci.*, 2006, **118**, 503–511.
63. D. Rehder, M. Ebel, C. Wikete, G. Santoni and J. Gätjens, *Pure Appl. Chem.*, 2005, **77**, 1607–1616.
64. G. Saikia, S. R. Gogoi, J. J. Boruah, B. M. Ram, P. Begum, K. Ahmed, M. Sharma, G. Ramakrishna, T. Ramasarma and N. S. Islam, *ChemistrySelect*, 2017, **2**, 5838–5848.
65. N. Tanaka and R. Wever, *J. Inorg. Biochem.*, 2004, **98**, 625–631.
66. L. An, T. S. Zhao, X. L. Zhou, X. H. Yan and C. Y. Jung, *J. Power Sources*, 2015, **275**, 831–834.
67. R. A. Baglia, J. P. T. Zaragoza and D. P. Goldberg, *Chem. Rev.*, 2017, **117**, 13320–13352.
68. D. E. DeRosha, B. Q. Mercado, G. Lukat-Rodgers, K. R. Rodgers and P. L. Holland, *Angew. Chem., Int. Ed.*, 2017, **56**, 3211–3215.
69. S. Hong, Y. M. Lee and W. Nam, *Coord. Chem. Rev.*, 2017, **334**, 25–42.
70. H. Zhang, G. P. Hatzis, C. E. Moore, D. A. Dickie, M. W. Bezpalko, B. M. Foxman and C. M. Thomas, *J. Am. Chem. Soc.*, 2019, **141**, 19516–19520.
71. Y. Tajika, K. Tsuge and Y. Sasaki, *Dalton Trans.*, 2005, 1438–1447.
72. H. Kelm and H. J. Krüger, *Angew. Chem., Int. Ed.*, 2001, **40**, 2344–2348.
73. M. Kosugi, S. Hikichi, M. Akita and Y. Moro-oka, *J. Chem. Soc., Dalton Trans.*, 1999, 1369–1371.
74. R. Kirk Egdal, A. D. Bond and C. J. McKenzie, *Dalton Trans.*, 2009, 3833–3839.
75. M. Stylianou, C. Drouza, J. Giapintzakis, G. I. Athanasopoulos and A. D. Keramidas, *Inorg. Chem.*, 2015, **54**, 7218–7229.
76. C. R. Waidmann, A. G. Dipasquale and J. M. Mayer, *Inorg. Chem.*, 2010, **49**, 2383–2391.
77. P. G. Klimko, *CRC Handbook of Laboratory Safety*, 5th edn, ed. A. Keith Furr, CRC Press, Boca Raton, FL, 2000, p. xvii 2001.
78. C. W. Anson, S. Ghosh, S. Hammes-Schiffer and S. S. Stahl, *J. Am. Chem. Soc.*, 2016, **138**, 4186–4193.
79. S. Groysman, I. Goldberg, Z. Goldschmidt and M. Kol, *Inorg. Chem.*, 2005, **44**, 5073–5080.
80. E. Tsuchida and K. Oyaizu, *Coord. Chem. Rev.*, 2003, **237**, 213–228.
81. A. F. Cozzolino, D. Tofan, C. C. Cummins, M. Temprado, T. D. Palluccio, E. V. Rybak-Akimova, S. Majumdar, X. Cai, B. Captain and C. D. Hoff, *J. Am. Chem. Soc.*, 2012, **134**, 18249–18252.
82. D. Rehder, C. Weidemann, A. Duch and W. Priebsch, *Inorg. Chem.*, 1988, **27**, 584–587.
83. T. K. Myser and R. E. Shepherd, *Inorg. Chem.*, 1987, **26**, 1544–1555.
84. Z. Liu and F. C. Anson, *Inorg. Chem.*, 2000, **39**, 274–280.
85. Z. Liu and F. C. Anson, *Inorg. Chem.*, 2001, **40**, 1329–1333.
86. E. Tsuchida, K. Oyaizu, E. L. Dewi, T. Imai and F. C. Anson, *Inorg. Chem.*, 1999, **38**, 3704–3708.

87. K. Yamamoto, K. Oyaizu and E. Tsuchida, *J. Am. Chem. Soc.*, 1996, **118**, 12665–12672.
88. J. A. Bonadies, W. M. Butler, V. L. Pecoraro and C. J. Carrano, *Inorg. Chem.*, 1987, **26**, 1218–1222.
89. J. A. Bonadies, V. L. Pecoraro and C. J. Carrano, *J. Chem. Soc., Chem. Commun.*, 1986, 1218–1219.
90. B. Galeffi, M. Postel, A. Grand and P. Rey, *Inorg. Chim. Acta*, 1987, **129**, 1–5.
91. A. M. Morris, C. G. Pierpont and R. G. Finke, *Inorg. Chem.*, 2009, **48**, 3496–3498.
92. Y. Tatsuno, M. Tatsuda and S. Otsuka, *J. Chem. Soc., Chem. Commun.*, 1982, 1100–1101.
93. C.-X. Yin and R. G. Finke, *J. Am. Chem. Soc.*, 2005, **127**, 9003–9013.
94. A. M. Morris, C. G. Pierpont and R. G. Finke, *J. Mol. Catal. A: Chem.*, 2009, **309**, 137–145.
95. M. E. Cass, D. L. Green, R. M. Buchanan and C. G. Pierpont, *J. Am. Chem. Soc.*, 1983, **105**, 2680–2686.
96. C.-X. Yin and R. G. Finke, *J. Am. Chem. Soc.*, 2005, **127**, 13988–13996.
97. C. Drouza and A. D. Keramidas, *Inorg. Chem.*, 2008, **47**, 7211–7224.
98. C. Drouza, M. Stylianou, P. Papaphilippou and A. D. Keramidas, *Pure Appl. Chem.*, 2013, **85**, 329–342.

CHAPTER 23

Vanadium in Catalytically Proceeding Natural Processes

DIETER REHDER

Chemistry Department, University of Hamburg, D-20367 Hamburg, Germany
Email: rehder@chemie.uni-hamburg.de

23.1 Introduction

To date, two vanadium-dependent enzymatic reactions are well established, *viz*. (1) the reduction of dinitrogen (by nitrogen-fixing bacteria) in the presence of protons to ammonium ions by vanadium nitrogenase (VNase) and (2) the oxidation (with hydrogen peroxide) of halides (chloride, bromide and iodide) and pseudohalides by vanadate-dependent haloperoxidases (VHPO) present in marine algae and bacteria associated with these algae, and in certain lichens and mould – enzymatic processes that will be treated in some detail in this chapter. The (structural) similarity between vanadate $H_2VO_4^-$ and phosphate $HPO_4^{2-}/H_2PO_4^-$ suggests the role of vanadate also as an antagonist, substitute or amplifier of phosphate in biological processes operated by phosphatases and kinases. In addition, inorganic vanadium – in the form of vanadate(V) and oxidovanadium(IV) – has been reported to adopt a potential role in bacterial nitrate reduction.[1] Investigations carried out with amavadin and its homologues (amavadin is a vanadium coordination compound originally isolated from the fly agaric *Amanita muscaria*) have shown that this species, with a non-oxido vanadium(IV) centre, can be an effective catalysts in the redox conversion of, *inter alia*, nitrite (which is

Catalysis Series No. 41
Vanadium Catalysis
Edited by Manas Sutradhar, José Armando L. da Silva and Armando J. L. Pombeiro

Published by the Royal Society of Chemistry, www.rsc.org

reduced to N_2O) and water (which is oxidised to O_2)[2,3] – presumably, therefore, amavadin can convey appropriate functions in nature.[4]

In this chapter, the naturally occurring enzymes VHPO and VNase will be addressed in some detail. In addition, the potentiality of amavadin (and its synthetic analogues) will be envisaged, as will the vanadate–phosphate antagonism in the context of physiologically active enzymes based on phosphate.

23.2 Vanadate-dependent Haloperoxidases

Along with the vanadate-dependent haloperoxidases (HPOs), iron-haem and flavin-based HPOs have been characterised.[5] Haem-type and vanadate-dependent peroxidases are responsible for a broad variety of halogenations of (essentially) organic compounds. Haloperoxidases based on vanadium (VHPOs) in the active centre (for recent review see ref. 6,7) primarily catalyse the oxidation, by (hydro)peroxide, of halides (I^-, Br^-, Cl^-; X^-) to hypohalous acids HXO (or their corresponding anions XO^-) (see eqn (23.1)) and thus play an important role in the release of these oxidatively active compounds into the environment. They are commonly named according to the most electronegative halide they can oxidise. Pseudohalides such as cyanide and thiocyanate, (eqn (23.2)) can also be substrates for the VHPOs. The primary oxidation product of the halide is then involved in the oxidative protection of its direct producer, and the halogenation of organics (for a basic example, see eqn (23.3). In 1929, H. Kylin addressed the occurrence of a vanadium-dependent iodide-oxidase in marine algae,[8] which later turned out to be an iodide-peroxidase. In this report, Kylin notes ''that *Ascophyllum nodosum* and several species of the genus *Laminaria* can demerge iodine from iodide to a great extent''. In 1983, Hans Vilter and co-authors presented the first isolation and detailed characterisation of a bromoperoxidase with vanadate in the active centre, extracted from the marine brown alga *Ascophyllum nodosum* (also known as pig weed or knobbed wreck).[9] A detailed X-ray structure analysis of the *A. nodosum* enzyme has been published two decades ago.[10*a*] For crystal structure analyses of the bromoperoxidases from the mould *Curvularia inaequalis* and the red alga *Corallina officinalis* see ref. 10*b,c*. Vanadate-dependent chloroperoxidases can further occur in marine bacteria of the genus *Streptomyces*[11] and in the terrestrial lichen *Xanthoria parietina*.[12] In the case of streptomycetes, VHPOs are involved in the synthesis of chlorinated compounds acting as antibodies.[13] Finally, certain cyanobacteria apparently also contain a vanadate-dependent iodoperoxidase[14*a*] and cyanobacterial blooms have been shown to be responsible for the formation of halocarbons such as $CHBr_3$ and $CHBr_2Cl$[14*b*] (discussed further in Chapter 24).

Hypohalous acids protect the algae against parasitic and bacterial infections. On the other hand, HClO, produced by, *e.g.*, *Curvularia inaequalis*, helps to oxidatively degrade lignocellulose and thus facilitates access for the fungus to the cell walls of the host's tissues. The *in-situ* generation of the

highly oxidative hypohalous acids can be deployed in the oxidative halogenation (and thus biodegradation) of various organic substrates, which also has implications for the potentiality of these enzymes in industrial processes. An example is the oxidative decarboxylation of glutamic acid by H_2O_2 in the presence of VClPO.[15] An intricate consequence of halide oxidation by marine algae (marine phytoplankton) is the impact on atmospheric – in particular tropospheric – chemistry,[16,17] in as far as bromination of organics by hypobromous acid or hypobromite, formed according to eqn (23.1), can occur, which in turn gives rise to the formation of brominated methanes $CH_{4-x}Br_x$ (eqn (23.3)). More generally, the VHPOs are thus employed as an additional or alternative enzyme for halogenations – alternative with respect to halogenases depending on iron.[17]

$$Br^- + H_2O_2 + H^+ \rightarrow HOBr + H_2O \quad (23.1a)$$

$$Br^- + H_2O_2 \rightarrow BrO^- + H_2O \quad (23.1b)$$

$$SCN^- + H_2O_2 + H^+ \rightarrow HOSCN + 2H_2O \quad (23.2)$$

$$CH_4 + xHOBr \rightarrow CH_{4-x}Br_x + xH_2O \quad (23.3)$$

Photolysis of bromomethanes, in turn, gives rise to the formation of highly reactive bromine radicals (eqn (23.4)) that are released into the atmosphere where they are oxidised (by ozone) to form BrO (eqn (23.5)).[15] BrO, in turn, can oxidise nitrous oxide NO to NO_2 eqn (23.6). Similarly, dimethylsulphide can be subject to oxidation eqn (23.7). Finally, the hypobromous acid formed according to eqn. (23.1a) may brominate diverse organic substrates RH eqn (23.8). Analogous reactions, in particular with respect to the depletion of atmospheric ozone (eqn (23.5)) have been discussed for fungal chloroperoxidases.[18,19]

$$CH_3Br + h\nu \rightarrow Br^\bullet + CH_3^\bullet \ (\times 2 \rightarrow C_2H_6) \quad (23.4)$$

$$Br^\bullet + O_3 \rightarrow BrO + O_2; \quad (23.5)$$

$$NO + BrO \rightarrow NO_2 + Br^\bullet \quad (23.6)$$

$$(CH_3)_2S + H_2O_2 + H^+ \rightarrow (CH_3)_2SO + H_2O \quad (23.7)$$

$$HOBr + RH \rightarrow RBr + H_2O \quad (23.8)$$

The structure of the active centre of the *A. nodosum* enzyme and its immediate surroundings are shown in Figure 23.1; a more general picture of the structural features at the active sites of two VHPOs (from a fungus and an alga) is depicted in Figure 23.2. An essentially superimposable structure has been established for the iodoperoxidase of *Zobiella galactanivorans*, a marine flavobacterium associated with macroalgae.[20]

Contrasting many haem-based peroxidases, VHPOs are generally stable during turnover. In the course of the primary reaction (*i.e.*, the one-electron oxidation of halide or pseudohalide) catalysed by VHPOs, a peroxido intermediate is formed, in which vanadium – in its originally trigonal-bipyramidal

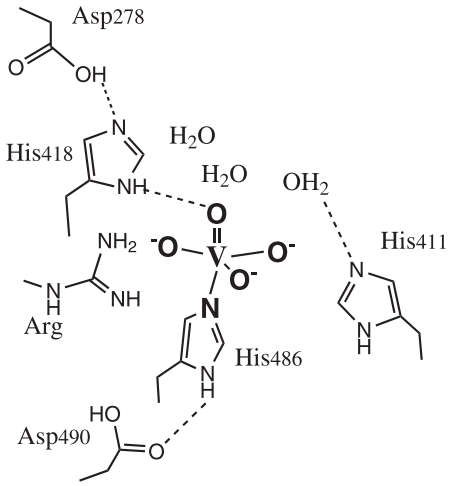

Figure 23.1 The structure at the active site of the haloperoxidase from the seaweed *Ascophyllum nodosum*, including parts of the network around the vanadate-His centre.

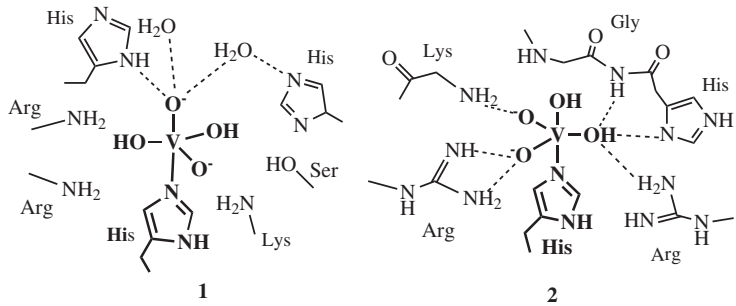

Figure 23.2 The active centres of the chloroperoxidase VClPO from the fungus *Curvularia inaequalis* (**1**)[9b] and the bromoperoxidase VBrPO from the brown alga *Ascophyllum nodosum* (**2**),[9a] based on X-ray structure determinations. Hydrogen-bonding interactions are depicted by broken lines. For a similar structure of the dodecameric VBrPO from the red alga Corallina officinalis, see ref. 9*c*. Depending on the pH, doubly and trebly protonated vanadate centres (*i.e.*, $H_2VO_4\{N\}$ and $H_3VO_4\{N\}$) have been suggested for the chloroperoxidase from *C. inaequalis*, based on ^{51}V NMR evidence.[21]

coordination environment – attains a configuration reminiscent of a distorted square pyramid,[21] with the peroxido ligand in the basal plane, as shown in Figure 23.3. After coordinative interaction with the halide, hypohalous acid is released and the catalytically active centre is reconstituted.

There are also structural and functional similarities between VHPOs and phosphatases, a feature that reflects the vanadate–phosphate antagonism in living organisms, *i.e.*, the fact that vanadate can act as an inhibitor

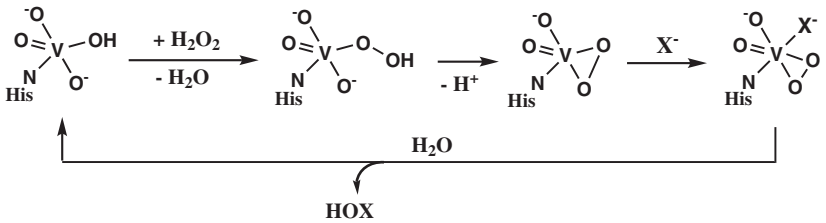

Figure 23.3 Probable mechanism for the formation of hypohalous acid (HOX) at the active centre of VHPOs, based on the proposal (X-ray structural evidence) for the generation of HClO by the chloroperoxidase from the fungus *Curvularia inaequalis*.[22]

as well as an analogue or even amplifier of the phosphatase activity[22,23] – low physiological vanadate concentrations presupposed. The trigonal-pentagonal *transition* state in the active centre is stabilized as phosphate HPO_4^{2-} is replaced by vanadate $H_2VO_4^-$, with V in a *stable* trigonal-bipyramidal configuration comparable to the steric situation of vanadium in VHPOs.

Quite interestingly, the chloroperoxidase of the *C. inaequalis* peroxidase is also active as vanadate is replaced by boric acid $B(OH)_3$.[24]

23.3 Vanadium Nitrogenase

Dinitrogen (N_2) is a limiting nutrient for biomass production due to its lacking polarisation and polarizability as well as its overall low reactivity, induced by the particularly strong N≡N triple bond (bond energy 946 kJ). Nitrogen – in its reduced and thus reactive form NH_3/NH_4^+ – is an essential building block for organic matter and several organisms, thus, dispose of an enzyme that reductively fixes N_2 via reduction to ammonia. A role for vanadium in the fixation of nitrogen – *i.e.*, the reduction of (aerial) N_2 to NH_3/NH_4^+ – was originally mentioned by Bortels[25*a*] who noted: ''I found out in 1930 that vanadium compounds almost match molybdenum with respect to their positive effect on nitrogen fixation.'' Three years later, a more detailed report appeared, where Bortels notes that ''without molybdenum or vanadium there is no possibility for any appreciable nitrogen fixation''.[25*b*] The final breakthrough goes back to the Sussex Nitrogen Fixation group in the 1980s,[26] where an alternative (with respect to the more common molybdenum variant) nitrogen-fixing system depending on vanadium – vanadium nitrogenase, VNase – present in the bacterium *Azotobacter chroococcum* – is described. Both enzymes, the vanadium- and the (more common) molybdenum-dependent nitrogenases, are homodimers (consisting of an α and β subunit; the VNase contains, in addition, two small δ subunits) of *ca.* 60 kDa, and share about 90% sequence identity. In addition to the reduction of N_2 to ammonia (and some hydrazine), protons are reduced to hydrogen. Carbon monoxide commonly acts as an inhibitor of nitrogenases.[27] The realisation of the fact that legumes can use atmospheric

dinitrogen for growth by means of bacteria in the root nodules of the legumes goes back to the 1980s.[28] Along with *Azotobacter*, bacterial strains such as *Rhodopseudomonas* and *Anabaena* can express a VNase.

For the uptake of vanadium, *Azotobacter vinelandii* produces azobactin (particularly released under iron limitations), an oligopeptide that – *via* its chelating residues provided by hydroxyaspartate, catecholate and hydroxamates – strongly binds vanadate, the vanadium of which is then delivered and made available in the course of the formation of the nitrogenase.[27]

Biogenic N_2 fixation (eqn (23.9)), to some extent an equivalent to the industrial Haber-Bosch process, is part of the global nitrogen cycle and a precondition for plants to dispose of nitrogen in their life cycles. H_2 is a by-product of the naturally occurring N_2 reduction.[29] In the absence of N_2, only H_2 is formed. Other substrates can also be reduced: Ethyne (acetylene) is reduced to ethene (ethylene), eqn (23.10), while carbon monoxide CO, which is isoelectronic to N_2 and commonly acts as an inhibitor for nitrogenases,[30] can also be reduced to hydrocarbons; *e.g.*, see eqn (23.11).[31] Further, CO_2 can be a substrate for the nitrogenases,[31c] a fact of particular interest in the context of the ''bio-conversion'' of atmospheric carbon dioxide to, *e.g.*, fuels. In this respect, VNase is more ''effective'' than the molybdenum-based and iron-only nitrogenases.[31b] Along with the free-living diazotrophic bacteria of the genus *Azotobacter*, the bacterial strains *Clostridium*, *Klebsiella*, *Rhodospirillum* and *Rhodopseudomonas* and the symbionts *Rhizobium* and *Francia* are examples for bacteria that can convert dinitrogen to ammonia (ammonium ions). *Azotobacter vinelandii* is particularly well adapted to reduce N_2 to ammonium ions in soils with a metal-limited environment,[32] as is the cyanobacterium *Anabaena variabilis*, which is effective under conditions of both nitrogen and molybdenum deficiency.[33] The high altitude cyanolichen *Peltigera aphthosa* also disposes of a vanadium-dependent nitrogenase.[34] More generally, plant endosymbiosis with N_2-fixing cyanobacteria has evolved in several plant lineages.[35] The process is part of the complex system resulting in the reduction of N_2 in the *M* cluster (the iron-vanadium cofactor, Figure 23.4); the electrons are delivered to the cofactor via a [4Fe,4S]-protein. Once dinitrogen N_2 approaches the active site of the *M* cluster, it is integrated and reduced via the formation of an N-bridged intermediate (Figure 23.4b). For the steps of the reduction of N_2 to NH_3 (NH_4^+), a reaction path corresponding to that shown in Figure 23.4b has been proposed.[36,37]

$$N_2 + 10H^+ + 8e^- \rightarrow 2NH_4^+ + H_2 \quad \text{(ATP-fuelled)} \tag{23.9}$$

$$C_2H_2 + H_2 \rightarrow C_2H_4\ (\rightarrow\ C_2H_6) \tag{23.10}$$

$$2CO + 5H_2 \rightarrow C_2H_6 + 2H_2O;\ 2CO + 8H^+ \rightarrow C_2H_4 + 2H_2O \tag{23.11}$$

The overall process of N_2 reduction at the catalytic site of the nitrogenase (*i.e.*, the successive delivery of the electrons to the substrate N_2) is preceded by a complementary reductase based on an iron protein containing a [4Fe,4S] cluster, a site where also the energy for the reduction of N_2 via the hydrolysis of adenosine triphosphate (ATP) to adenosine diphosphate

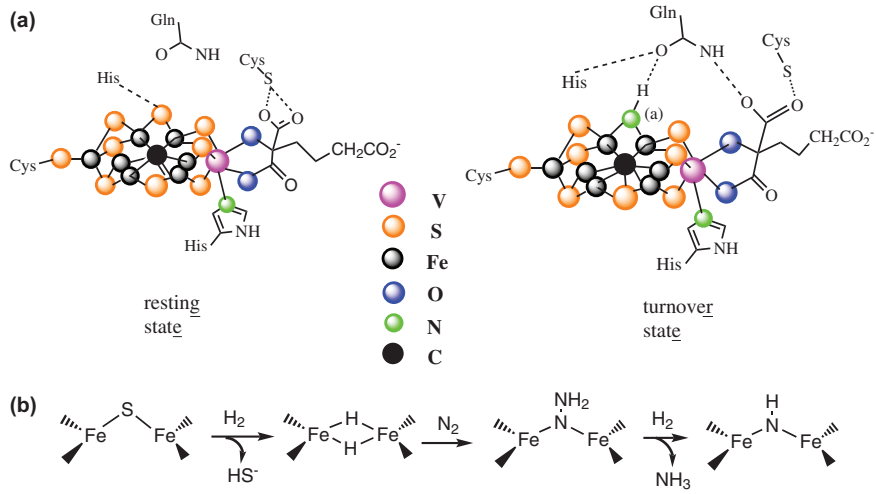

Figure 23.4 (a) Structural features of the active centre of the M cluster of vanadium nitrogenase in resting state (left) and in turn-over state (right).[36,37] In the turn-over state, a bridging NH group (position (a)) crops up; two one-electron reduction steps finally deliver ammonia. The position (a) can also be occupied by a bridging OH group[36a] or by bridging carbonate[36b] (and thus intermittently be blocked). The interstitial carbon actually is carbide.[38] (b) Reduction of N_2 at the reaction site of the M cluster.

(ADP) + phosphate is delivered.[37] Further involved in this overall reduction process, and the site which *directly* relays electrons to the *M* cluster, is a [8Fe,7S] protein, the so-called *P* cluster. For the consecutive steps of the electron transfer see eqn (23.12),[31b] where Δ stands for energy delivery.

$$2\mathrm{ATP}(\mathrm{Mg}^{2+}) \xrightarrow{\Delta} [\mathrm{Fe_4S_4}] \xrightarrow{e^-} [\mathrm{Fe_8S_7}] \xrightarrow{e^-} \{\mathrm{Fe\,V-cofactor}\} \xrightarrow{N_2,e^-,H^+} \mathrm{NH_4^+} \tag{23.12}$$

23.4 Catalytic Activity of Vanadium in Fungi

Bromoperoxidase activity has also been noted for amavadin, a non-oxidovanadium(IV) compound isolated from several *Amanita* mushrooms. As early as in 1931, Ter Meulen mentioned the relatively high amount of vanadium (in a compound later-on termed amavadin) present in the fungus *Amanita muscaria* (fly agaric, toad-stool);[39] several other species of the genus *Amanita* can also contain amavadin. The name "amavadin" goes back to Bayer, who was the first to isolate and characterize the compound;[40] he was also the first to assign the correct structure[41] (see Figure 23.5).

In amavadin, the non-oxidovanadium(IV) centre is in a coordination environment made up of two ligand functions provided by two (*S*,*S*′)-*N*-oxyimino(2,2′)-dipropionate ligands. Similarly built ligands, such as

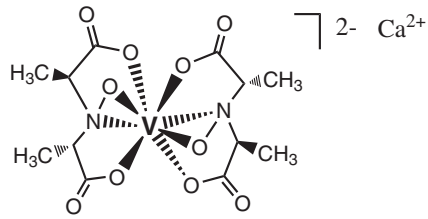

Figure 23.5 The structure of amavadin as isolated from the mushroom *Amanita muscaria*.

N-oxyiminodiacetate (where the methyl groups are missing), provide properties similar to those characteristics of amavadin. Thus, amavadin displays catalase- and peroxidase-type activity[42] (for examples see eqn (23.13) and (23.14)). Its major function in nature appears to be the (light-induced) reduction of nitrite to dinitrogen oxide (*i.e.*, laughing gas) (eqn (23.13)),[43,44] and – in the presence of nitrite as a comparatively weak oxidant – the oxidation of water to dioxygen (eqn (23.14)).[42] Apparently, vanadium(IV) in amavadin becomes intermittently oxidised to vanadium(V), which then mediates the oxidation of the substrate.

$$NO_2^- \rightarrow (NO,\ ONNO^-) \rightarrow N_2O \qquad (23.13)$$

$$2H_2O\ [+\ NO_2^-] \rightarrow O_2 + 4H^+ \qquad (23.14)$$

One of the biological functions of amavadin thus might stem from its involvement in the nitrogen metabolism of the fungus as well as in its role as a mediator of water oxidation. In addition, amavadin and models thereof have proven efficient catalysts for the oxidative conversion of ethane, by peroxodisulfate, to organic acids such as acetic and propionic acid.[45] For an example, see the non-stoichiometric eqn (23.15).

$$C_2H_6 + CO + S_2O_8^{2-} \rightarrow H_3C\text{–}(CH_2)_n\text{–}CO_2H\ (n = 0,\ 1) \qquad (23.15)$$

Comparatively high vanadate concentrations (up to about 3 mM) have also been found in the fungus *Coprinus comatus*. Here, vanadate initiates an increase of the sugar phosphate level.[46]

23.5 The Phosphate–Vanadate Antagonism in Physiological Functions

The amino acid environment of vanadate in vanadate-dependent haloperoxidases shares homology with several families of acid phosphatases, enzymes that catalyse, at a pH of 4 to 5, the hydrolysis of phosphoesters (eqn (23.16)).[47] The resemblance of vanadate and phosphate, and consequentially the role of vanadate as a phosphate antagonist or substitute in life processes, will briefly be addressed. Physiological conditions provided, *i.e.*, at a pH of ~7.5 (in blood), the predominant forms of phosphate and vanadate as the tetrahedrally built species HPO_4^{2-} and $H_2VO_4^-$, respectively. Both anions

also tend to form dimers, where the formation of $H_2V_2O_7^{2-}$ is clearly more pronounced (eqn (23.17)) than that of its phosphorus analogue.

$$H_2PO_3(OR) + H_2O \rightarrow H_2PO_4^- + ROH \quad (23.16)$$

$$H_2VO_4^{2-} \leftrightarrows H_2V_2O_7^{2-} + H_2O + 2H^+ \quad (23.17)$$

Given the similarity between phosphate and vanadate, in size, geometry and protonation state, vanadate can thus act as an antagonist of phosphate, in particular when it comes to the interaction with (phosphate-dependent) proteins or enzymes, which commonly exhibit a higher binding affinity to vanadate (forming *stable* penta-coordinate complexes) when compared to phosphate, for which the formation of *labile* penta-coordinate structures occurs intermittently only; see Figures 23.6. (**a**) and (**b**). A well-documented example is the binding of vanadate to the active site of the protein tyrosine-phosphatase, a fact that plays a key role in fighting diabetes with medications based on vanadium compounds – such as oxidovanadium(IV)maltolate.[48] The maltolato complex delivers vanadate at physiological conditions, which blocks protein-tyrosine-phosphatase, thus enabling the cellular insulin transporter to trigger glucose intake across the cell membrane.[49] In addition, mixed vanadate-phosphate anhydrides, (**c**) in Figure 23.6, and esters thereof can form. Another example is the incorporation of vanadate into the active site of phytase, an enzyme that naturally catalyses the hydrolysis of inositol hexa-phosphate; for the active centre of the vanadate analogue of phytase see Figure 23.7.[50] On the other hand, vanadate may also act as an efficient inhibitor of otherwise phosphate-dependent enzymes, such as protein-tyrosine-phosphatases,[51] ATPases, ribonucleases[52] and phosphodiesterases.[53]

Contrasting phosphate, vanadate can form multinuclear species at physiological conditions, sufficiently high – and consequently potentially toxic – vanadate concentrations provided.[49,52] Examples are tetravanadate, pentavanadate and decavanadate. Tetravanadate $V_4O_{12}^{4-}$ actively promotes

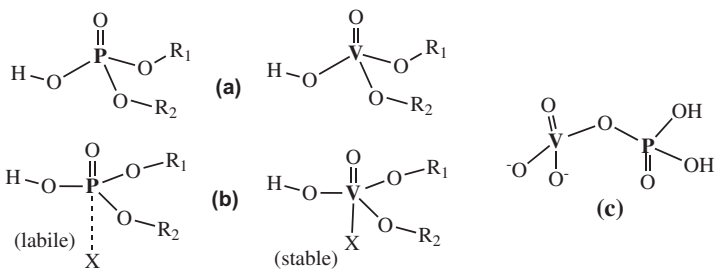

Figure 23.6 Stable tetrahedral configurations of phosphate and vanad**a**te (**a**); and the penta-coordinate transition states of phosphate and vanadate (**b**). X is, *e.g.*, a carbonic acid anion, an alcoholate function, or a sulphide RS^- residue of an amino acid, commonly connecting the phosphate or, more efficiently, vanadate to an amino acid side chain of a protein. (**c**) A mixed vanadate-phosphate anhydride.

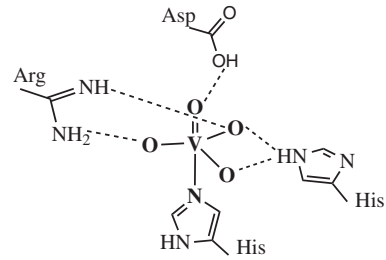

Figure 23.7 The active centre of phytase with incorporated vanadate.[50]

the hydrolysis of the phophodiester bond at physiological pH.[50] Incorporation of vanadate into phytase results in a semi-synthetic peroxidase that catalyses the (enantio-selective) oxidation, by H_2O_2, of sulphides to sulphoxides (eqn (23.18)).

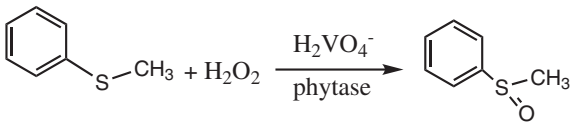

(23.18)

23.6 Conclusion

The catalytic potentiality of vanadium in industrial processes directed towards oxidation (such as the production of sulphuric acid, the conversion of methanol to formaldehyde and the oxidative ''detoxification'' of organic sulphur compounds in crude oil and diesel fuels) against reduction (*e.g.*, of NO in exhaust gases) is paralleled in naturally proceeding cycles. These include (1) the reduction of N_2, CO and alkynes by vanadium-dependent haloperoxidase provided by *Azotobacter vinelandii*, (2) the oxidation of bromide and iodide (and, eventually, also chloride and pseudohalides) by vanadate-dependent haloperoxidases in, *e.g.*, marine algae, and (3) the catalase and peroxidase activity of amavadin, an ingredient in the fly agaric mushroom.

The similarity between vanadate ($H_2VO_4^-$) and phosphate (HPO_4^{2-}) accounts for additional biological (including physiological) functions of vanadate in as far as vanadate acts as a phosphate analogue–antagonist.

References

1. (a) A. N. Antipov, D. Y. Sorokin, N. P. L'Vov and J. G. Kuenen, *Biochem. J.*, 2003, **369**, 185–189; (b) A. N. Antipov, N. L. Lyalikova, T. V. Khijniak, N. P. L'Vov and A. N. Bach, *IUBMB Life*, 2000, **50**, 39–42.
2. L. Dias, N. Bekhti, M. L. Kuznetzov, J. A. B. Ferreia, M. N. C. Bacariza and J. A. L. da Silva, *Chem. Eur. J.*, 2018, **24**, 1–10.
3. M. Domarus, M. L. Kuznetsov, J. Marçalo, A. J. L. Pombeiro and J. A. L. da Silva, *Angew. Chem., Int. Ed.*, 2016, **55**, 1489–1492.

4. J. A. L. da Silva, J. J. R. Fraústo da Silva and A. J. L. Pombeiro, *Coord. Chem. Rev.*, 2013, **257**, 2388–2400.
5. A. Timmins and S. P. de Visser, *Catalysts*, 2018, **8**, 314.
6. C. Leblanc, H. Vilter, J. Fournier, L. Delage, P. Potin, E. Rebuffet, G. Michel, P. L. Solari, M. C. Feiters and M. Czjzek, *Coord. Chem. Rev.*, 2015, **301–302**, 134–146.
7. R. Wever, B. E. Krenn and R. Renirie, *Methods Enzymol.*, 2018, **605**, 141–201.
8. H. Kylin, *Hoppe-Seyler's Z. Physiol. Chem.*, 1929, **186**, 50–84.
9. (a) H. Vilter, K.-W. Glombitza and A. Grawe, *Bot. Mar.*, 1983, **26**, 331–340; (b) H. Vilter, *Phytochem.*, 1984, **23**, 1387–1390.
10. (a) M. Weyand, H.-J. Hecht, M. Kiess, M.-F. Liaud, H. Vilter and D. Schomburg, *J. Mol. Biol.*, 1999, **293**, 595–611; (b) A. Messerschmidt and R. Wever, *Proc. Natl. Acad. Sci. U. S. A.*, 1996, **93**, 392–396; (c) M. N. Isopov, A. R. Dalby, A. A. Brindley, Y. Izumi, T. Tanabe, G. N. Murshodov and J. A. Littlechild, *J. Mol. Biol.*, 2000, **299**, 1035–1049.
11. P. Bernhardt, T. Okino, J. M. Winter, A. Miyanaga and B. S. Moore, *J. Am. Chem. Soc.*, 2011, **133**, 4268–4270.
12. H. Plat, B. E. Krenn and R. Wever, *Biochem. J.*, 1987, **248**, 277–279.
13. S. Diethelm, R. Teufel, L. Kaysser and B. S. Moore, *Angew. Chem., Int. Ed.*, 2014, **53**, 11203–11206.
14. (a) M. Bernroitner, M. Zamocky, P. G. Furtmüller, G. A. Peschek and C. Obinger, *J. Exp. Bot.*, 2009, **60**, 423–440; (b) T. L. Johnson, B. Brahamsha, B. Palenik and J. Mühle, *Limnol. Oceanogr.*, 2015, **60**, 1823–1835.
15. A. Butler, J. Le Notre, E. L. Scott, R. Wever and J. P. M. Sanders, *ChemSusChem*, 2012, **5**, 199–1202.
16. D. Rehder, *Oceanography*, 2014, **2**, 1000121.
17. R. Wever and M. A. van der Horst, *Dalton Trans*, 2013, **42**, 11778–11786.
18. R. Wever and P. Barnett, *Chem. Asian J.*, 2017, **12**, 1997–2007.
19. R. Gupta, G. Hou, R. Renirie, R. Wever and T. Polenova, *J. Am. Chem. Soc.*, 2015, **137**, 5618–5628.
20. J.-B. Fournier, E. Rebuffet, L. Delage, R. Grijol, L. Meslet-Cladière, J. Rzonca, P. Potin, G. Michel, M. Czjzek, C. Leblanc and C. R. Lovell, *Appl. Environment. Microbiol*, 2014, **80**, 7561–7573.
21. C. C. McLauchlan, H. A. Murakami, C. A. Wallace and D. C. Crans, *J. Inorg. Biochem.*, 2018, **186**, 267–279.
22. A. Messerschmidt, L. Prade and R. Wever, *Biol. Chem.*, 1997, **278**, 309–315.
23. W. Hemrika, R. Renirie, S. Macedo-Ribeiro, A. Messerschmidt and R. Wever, *J. Biol. Chem.*, 1999, **274**, 23820–23827.
24. F. Natalio, S. Wiese, W. Brandt and L. Wessjohann, *Chem. Eur. J.*, 2017, **23**, 1–9.
25. (a) H. Bortels, *Zentralbl. Bakteriol. Parasitenkd. Infektionskr.*, 1933, **87**, 476–477; (b) H. Bortels, *Zentralbl. Bakteriol. Parasitenkd. Infektionskr.*, 1936, **95**, 193–217.

26. (a) R. L. Robson, R. R. Eady, T. H. Richardson, R. W. Miller, M. Hawkins and J. R. Postgate, *Nature*, 1986, **322**, 388–390; (b) R. Cammack, *Nature*, 1986, **322**, 312.
27. (a) T. Spatzal, K. A. Perez, O. Einsle, J. B. Howard and D. C. Rees, *Science*, 2014, **345**, 1620–1623; (b) T. Wichard, J.-P. Bellenger, F. M. M. Morel and A. M. E. Kraepiel, *Environ. Sci. Technol.*, 2009, **43**, 7218–7224.
28. Y. Hu and M. W. Ribbe, *Methods Molecul. Biol.*, 2011, **766**, 3–7.
29. F. B. Simpson and R. H. Burris, *Science*, 1984, **224**, 1095–1097.
30. C. C. Lee, A. W. Fay, T.-C. Weng, C. M. Krest, B. Hedmann, K. O. Hodgson, Y. Hu and M. W. Ribbe, *Proc. Natl. Acad. Sci. U. S. A.*, 2015, **112**, 13845–13849.
31. (a) Y. Hu, C. C. Lee and M. W. Ribbe, *Science*, 2011, **333**, 753–755; (b) C. C. Lee, Y. Hu and M. W. Ribbe, *Angew. Chem., Int. Ed.*, 2011, **50**, 5545–5547; (c) Y. Hu, C. C. Lee and W. Ribbe, *Dalton Trans.*, 2012, **41**, 1118–1127; (d) J. G. Rebelein, Y. Hu and M. W. Ribbe, *Angew. Chem., Int. Ed.*, 2014, **53**, 11543–11546.
32. J.-P. Bellenger, T. Wichard, X. Yu and A. M. L. Kraepiel, *Environment. Microbiol.*, 2011, **13**, 1395–1411.
33. B. S. Pratte, R. Sheridan, J. A. James and T. Thiel, *Molecul. Microbiol.*, 2013, **88**, 413–424.
34. (a) R. Darnajoux, J. Constantin, J. Miadlikowska, F. Lutzoni and J.-P. Bellenger, *New Phytol.*, 2014, **202**, 765–771; (b) B. D. Hotkinson, J. L. Allen, L. R. Forrest, B. Goffinet, E. Sérusiaux, O. S. Andrésson, V. Miao, J.-P. Belliger and F. Lutzoni, *Eur. J. Physiol*, 2014, **49**, 11–19.
35. J. M. Nelson, D. A. Hauser, J. A. Gudiño, Y. A. Guadalupe, J. C. Meeks, N. S. Allen, J. C. Villarreal and F.-W. Li, *Genome Biol. Evolv.*, 2019, **11**, 1959–1964.
36. (a) B. Benediktsson, A. T. Thorhallsson and R. Bjornsson, *Chem. Commun.*, 2018, **53**, 7265–7280; (b) D. Sippel and O. Einsle, *Nat. Chem. Biol.*, 2017, **13**, 956–960; (c) D. Sippel, M. Rohde, J. Netzer, C. Trncik, J. Gies, K. Grunau, I. Djurdjevic, L. Decamps, S. L. Andrade and O. Einsle, *Science*, 2018, **359**, 1484–1489.
37. M. Rohde, C. Trncik, D. Sippel, S. Gerhardt and O. Einsle, *J. Biol. Inorg. Chem.*, 2018, **23**, 1049–1056.
38. J. A. Rees, R. Bjornsson, J. Schlesier, D. Sippel, O. Einsle and S. DeBeer, *Angew. Chem., Int. Ed.*, 2015, **54**, 13249–13252.
39. G. Zampella, L. Bertini and L. De Goia, *Chem. Commun.*, 2014, **50**, 304–307.
40. (a) H. Ter Meulen, *Rec. Trav. Chim. Pays-Bas*, 1931, **50**, 491–405; (b) E. Bayer and H. Kneifel, *Z. Naturforsch.*, 1972, **27b**, 207.
41. (a) E. Bayer and H. Kneifel, *Z. Naturforsch.*, 1972, **27b**, 207; (b) E. Bayer, E. Koch and G. Anderegg, *Angew. Chem., Int. Ed. Engl.*, 1997, **26**, 454–457.
42. L. Dias, N. Bekhti, M. L. Kusnetzov, J. A. B. Ferreira, M. C. Bacariza and J. A. L. daSilva, *Chem. Eur. J.*, 2018, **24**, 2474–2482.
43. C. Buchwald, K. Grabb, C. M. Hansel and S. D. Wankel, *Geochim. Cosmochim. Acta*, 2016, **186**, 1–12.

44. M. Domarus, M. L. Kuznetsov, J. Marçalo, A. J. L. Pombeiro and J. A. L. da Silva, *Angew. Chem., Int. Ed.*, 2016, **55**, 1489–1492.
45. M. V. Kirillova, M. L. Kuznetsov, J. A. da Silva, M. F. Guedes da Silva, J. J. Frausto da Silva and A. J. Pombeiro, *Chemistra*, 2008, **14**, 1828–1842.
46. J. Zakrzewska, K. Tešanović, E. Bošković, M. Nešković and M. Karaman, *J. Trace Metal Med. Biol.*, 2018, **50**, 320–326.
47. (a) J. M. Winter and B. S. Moore, *J. Biol. Chem.*, 2009, **284**, 18577–18581; (b) J. Littlechild, E. Garcia-Rodriguez, A. Dalby and M. Isupov, *J. Mol. Recognit.*, 2002, **15**, 291–296; (c) G. Xu and B.-G. Wang, *PLoS One*, 2016, **11**, e0154619.
48. K. H. Thomson, J. Lichter, C. LeBel, M. C. Scaife, J. H. McNeill and C. Orvig, *J. Inorg. Biochem.*, 2009, **103**, 554–558.
49. D. Rehder, *Future Med. Chem.*, 2016, **8**, 325–338.
50. F. van de Velde, I. W. C. E. Arends and R. A. Sheldon, *J. Inorg. Biochem.*, 2000, **80**, 81–89.
51. E. Irvig and A. W. Stoker, *Molecules*, 2017, **22**, 2229.
52. D. Rehder, *Elsev. Rev. Mod. Chem. Mol. Sci. Chem. Engin.*, 2015, 1–11.
53. N. Steens, A. M. Ramadan and T. N. Parac-Vogt, *Chem. Commun.*, 2009, 965–967.

CHAPTER 24

Vanadium Chloroperoxidases as Versatile Biocatalysts

RON WEVER,*[a] ROKUS RENIRIE[a] AND FRANK HOLLMANN[b]

[a] Van 't Hoff Institute for Molecular Sciences (HIMS), Faculty of Science, University of Amsterdam, The Netherlands; [b] Department of Biotechnology, Delft University of Technology, van der Maasweg 9, 2629 HZ Delft, The Netherlands
*Email: r.wever@uva.nl

24.1 Introduction

The vanadate-dependent haloperoxidases are enzymes that catalyse a rather simple reaction – the two-electron oxidation of a halide by hydrogen peroxide resulting in the formation of hypohalous acids, according to eqn (24.1).

$$Cl^- + H_2O_2 + H^+ \longrightarrow HOCl + H_2O \quad (24.1)$$

These hypohalous acids are very reactive and are able to halogenate a broad range of organic substrates. In the absence of organic compounds, the formed HOX will non-enzymatically react with the substrate hydrogen peroxide resulting in the formation of singlet oxygen ($^1O_2$, eqn (24.2). The rate of the non-catalytic reaction between HOCl and H_2O_2 is pH dependent and decreases strongly at low pH (<7).[1]

$$HOCl + H_2O_2 \longrightarrow {}^1O_2 + H_2O + HCl \quad (24.2)$$

Catalysis Series No. 41
Vanadium Catalysis
Edited by Manas Sutradhar, José Armando L. da Silva and Armando J. L. Pombeiro

Published by the Royal Society of Chemistry, www.rsc.org

Haloperoxidases able to catalyse the oxidation of chloride, bromide or iodide are named chloroperoxidases and enzymes able to oxidise bromide and iodide are characterised as bromoperoxidases. The iodoperoxidases are only able to oxidise iodide and, thus, will not be discussed here. Since a bromoperoxidase may also oxidise chloride, albeit with low specificity constant, the distinction between the haloperoxidases is somewhat arbitrary. The vanadium bromo- and iodoperoxidases (VBPO's, VIPO's) are mostly found in the marine environment (macro-algae and cyanobacteria) and are involved in the production of large amounts of brominated and iodinated compounds that are released in the marine environment.[2,3] These BPO's produce oxidised bromine species (HOBr, Br_2 and Br_3^-) that will react selectively with a range of organic molecules and organic matter.[4–6] However, there is some evidence that some VBPO's from red seaweeds are selective since they show diastereoselectivity in the bromohydrin formation.[7,8] The VBPO's are highly stable and the peroxidases from the brown seaweed *Ascophyllum nodosum* have been used in the biosynthesis of brominated compounds. The many properties and successful use of this enzyme in bromination reactions are described in detail elsewhere[9,10] and will only be discussed here shortly.

The vanadium chloroperoxidases (VCPO's) are especially interesting because of their ability to oxidise Cl^-. They are found in a group of terrestrial fungi, the so-called dematiaceous hyphomycetes belonging to the phylum *Ascomycota*. These fungal VPO's probably function in the decay of plant debris and have a possible role in the degradation of the cell walls of the plant host via the formation of HOCl.[11] These enzymes just release HOCl in solution and there is no evidence for regio- or stereoselective halogenation catalysed by these fungal VCPOs.

In contrast, the vanadium peroxidases NapH1 and Mcl24 from the marine prokaryote *Streptomyces* bacteria *Streptomyces* sp. CNQ-525 and *Streptomyces* sp. CNH-189, respectively, catalyse stereoselective halogenation of merochlorin and napyradiomycin molecules. These enzymes do not form free diffusible HOCl as judged from their inability to chlorinate monochlorodimedone, a widely used assay[10] to asses halogenating activity, but instead are able to specifically catalyse the stereoselective chlorination-cyclisation of their natural substrates. This suggests a very specific binding of the substrate to the active site of these enzymes. A detailed description of the properties of these enzymes and their dedicated role in the biosynthetic route to the napyradiomycin family of bacterial meroterpenoids can be found elsewhere.[12,13]

There are a number of other enzyme classes that are able to carry out halogenations reactions and are, or maybe become, synthetically useful. These are the heme-dependent haloperoxidases, the non-heme α-keto glutarate-dependent halogenases and the flavin-dependent halogenases. This chapter focuses on the use of the fungal VCPOs that are more stable than enzymes from the other classes in biocatalytic halogenation reactions. For information on these classes, the reader is referred to several reviews.[14–16]

24.2 Fungal Vanadium Chloroperoxidases

Many mechanistic and molecular details are available for vanadium chloroperoxidases. Most studies have been done with the enzyme from the fungus *Curvularia inaequalis*, though enzymes from other species have also been studied, *e.g.*, those from *Drechslera biseptata*[17] and *Embellisia didymospora.*[18] This includes detailed structural data of the enzyme,[19] the nature of the active site, the nature of the peroxido intermediate that is formed during catalysis[20] and the role of the various amino acids ligated and coordinated to the vanadate.[21,22]

24.2.1 Stability of the VCPO

Early on it was discovered that the fungal VCPO is unusually stable, like the VBPOs from the marine environment. The enzyme can be stored for weeks in water-miscible and immiscible solvents such as methanol, ethanol, 2-propanol or ethylacetate,[23,24] and also remains active when used as a cosolvent.[24] The enzyme is also resistant towards chaotropic agents. For example, at incubation in guanidine-HCl only at a concentration of 2 M the enzyme starts to lose activity[23] and at 3.7 M, only half the original activity is lost. At these concentrations most enzymes have lost their activity completely. Also, the VCPO remains catalytically active in a polydisperse nonionic surfactant, for at least 10 h, converting H_2O_2 into a constant flow of $^1O_2$.[25] The thermostability as shown in Figure 24.1 is also very high and close to that of thermostable enzymes. The midpoint temperature of denaturation of the CPO's *from Curvularia inaequalis* and *Drechslera biseptata* are about 90 and 82 °C, respectively.

These midpoint temperatures of thermal denaturation are close to those found for thermophilic enzymes. The enzyme structure of VCPO from *C. inaequalis* is mainly α helical with two four-helix bundles and some antiparallel beta sheets. The high stability is probably due to the very compact packing of the helices and the hydrophobic interaction in the middle of these bundles. There are no disulphide bridges.[19]

Currently five VHPO crystal structures are available[13,15] and the active site in all these enzymes consists of negatively charged vanadate held in place by positively charged amino acids lysine and two arginines. Further, there is a covalent bond to the $N\varepsilon_2$ of a histidine and two hydrogen bonds to a serine and a glycine residue. Finally, there is a hydrogen bond of the axial oxygen atom to the $N\varepsilon_1$ atom of a histidine. The active site, as illustrated in Figure 24.2, is conserved in all vanadium haloperoxidases known to date, with some minor differences.

Thus, the vanadium enzymes differ significantly in their active site structure from the well-known heme peroxidases. These enzymes and their prosthetic group the oxido-metallate are very resistant towards oxidative inactivation by both substrate (hydrogen peroxide) and products (hypohalous acids and singlet oxygen) as will be discussed in some detail. This

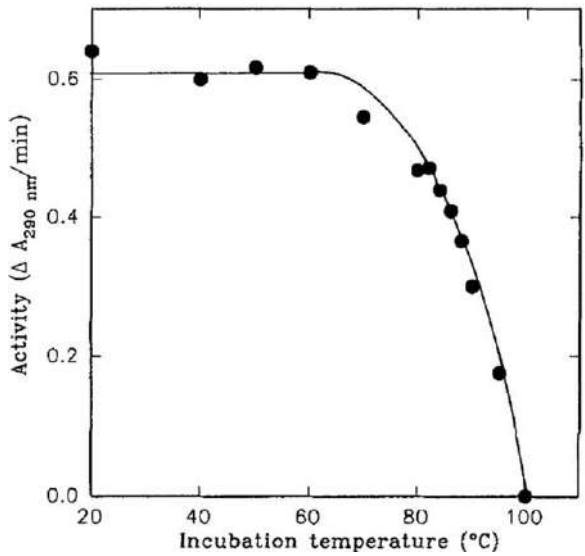

Figure 24.1 The thermostability of VCPO. Samples of VCPO were incubated for 5 min in Tris-buffer (pH 8.3) after which time the chlorinating activity was measured. Prolonged incubation for 15 min did not affect the midpoint temperature.
Reproduced from ref. 23 with permission form John Wiley and Sons, © 2020 Federation of European Biochemical Societies.

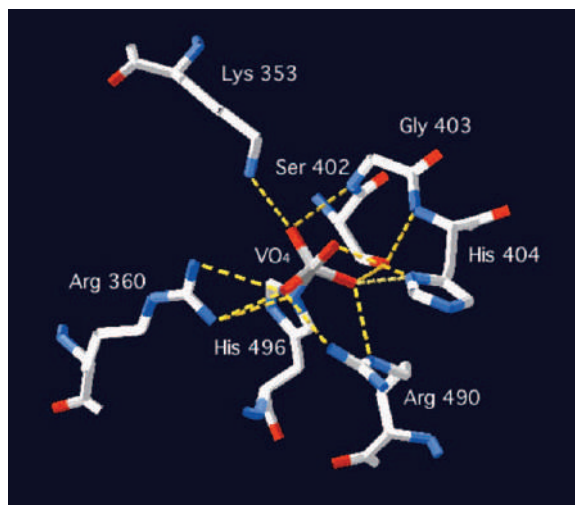

Figure 24.2 The active site of VCPO from Curvularia inaequalis (PDB accession number 1IDQ).
Adapted from ref. 26 with permission from John Wiley and Sons, © 2020 Federation of European Biochemical Societies.

resistance towards inactivation[23–27] is in strong contrast to heme-containing enzymes which are rapidly inactivated even at micromolar concentrations presumably by the oxidation of the labile cofactor.

24.2.2 Kinetic Properties Vanadium Chloroperoxidase from *Curvularia inaequalis*

This enzyme shows a pH optimum in the bromination or chlorination varying from pH 5 to 5.5 depending on the concentration of hydrogen peroxide, the halide used and its concentration.[28] Steady-state kinetic studies[23] on the oxidation of chloride by VCPO reveal a mechanism in which hydrogen peroxide binds first to the enzyme forming a peroxido intermediate which oxidises the halide. High halide concentrations inhibit the enzyme strongly whereas high peroxide concentrations have hardly any effect.[23,29] This substrate inhibited Bi Bi Ping-Pong mechanism resembles that of the VBPOs. At pH values below the pH optimum the chlorinating activity is inhibited by chloride whereas higher pH values chloride oxidation follows a Michaelis–Menten type of curve. As Table 24.1 shows, the K_m value for chloride oxidation is strongly dependent on pH and its value increases nearly linearly with pH. The kinetics of bromide oxidation is similar to that of the chloride oxidation.[23,29]

However, the K_m for bromide in the order of μmolar is surprisingly small (<10 μM) in the pH range 4.2–6.3 and it is much less dependent upon pH. Bromide is much more inhibitory than chloride.[29] This should be kept in mind when applying the enzyme in synthetic halogenation procedures. It should be noted that the turnover frequencies (k_{cat} values) mentioned in Table 24.1 have been obtained for pure enzyme and are derived from V_{max} values from Lineweaver–Burk plots. These values are in general significantly higher than those obtained at a fixed halide and H_2O_2 concentrations. Table 24.1 also shows that the K_m values for H_2O_2 are in the μmolar range. Inhibition by H_2O_2 even at high concentrations has not been reported so, again, in preparative purposes the H_2O_2 concentration is not crucial. The specificity constants (k_{cat}/K_m) for the oxidation of Br^- are about 5–10-times

Table 24.1 Kinetic parameters of the oxidation of Br^- and Cl^- catalysed by VCPO.

		X^-			H_2O_2		
Halide	pH	K_m (μM)	k_{cat} (s^{-1})	k_{cat}/K_m ($M^{-1}\,s^{-1}$)	K_m (μM)	k_{cat} (s^{-1})	k_{cat}/K_m ($M^{-1}\,s^{-1}$)
Br^- [21,30]	4.2	<5	253	$>5.1\times10^7$	90	250	2.6×10^6
	5.2	9	248	2.8×10^7	35	203	5.8×10^6
	6.3	7	37	5.3×10^6	<5	33	6.6×10^6
	8.0	120	1	8.3×10^3	<5	1	$>2\times10^5$
Cl^- [23,29]	5.0	1.1×10^3	23	2.0×10^4	49	183	3.7×10^6
	6.3	1.0×10^4	7.3	7.1×10^2	2.6	152	5.8×10^6
	8.0	1.1×10^5	n.d.	n.d.	n.d.	n.d.	n.d.

higher than those for chloride oxidation, in part reflecting the ease of oxidation of Br^-.

24.2.3 Use of the VCPO in the Production of Singlet Oxygen

In fact, the VCPO can be used as a highly efficient catalyst for the production of singlet oxygen[27] under mildly acidic conditions according to eqn (24.1) and (24.2). In these reactions the halide is regenerated and the process is catalytic, resulting in slow and controlled formation of $^1O_2$. To minimise the side reactions of $^1O_2$ with compounds other than HOCl, high H_2O_2 concentration (0.1 M–1.0 M) should be used.

Figure 24.3 illustrates the surprising stability of VCPO against 0.5 M H_2O_2 under continuous turnover producing $^1O_2$ for at least one hour in the presence of 5 mM chloride. This system under appropriate conditions may function as efficient catalytic system for the generation of $^1O_2$ under slightly acidic conditions.[27] Chloride should be used as substrate rather than bromide since with the latter formation of side products is observed. The VBPO from *Ascophyllum nodosum* has also been tested as singlet oxygen producer. Unlike the VCPO, this enzyme though it initially produces singlet oxygen, is inactivated in time. Using anthracene-9,10-bis(ethane sulphonate) as a singlet oxygen trap full conversion is observed into the corresponding endoperoxide. During the conversion[27] the enzyme activity is not affected for 25 000 turnovers within 75 minutes with a turnover frequency of 5.6 s^{-1}. The rate is about 10^4-times higher than those based on Na_2MoO_4 or $La(NO_3)_3$/NaOH and which are not effective at slightly acidic pH values. The enzyme is also active in singlet oxygen formation in non-ionic micro-

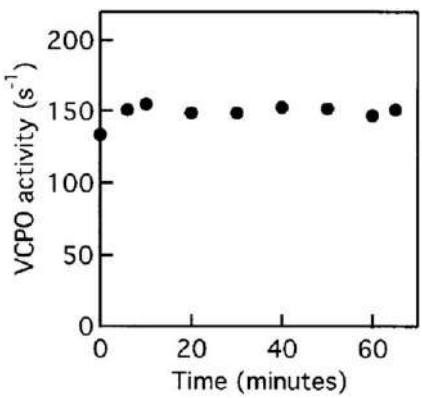

Figure 24.3 Resistance of the VCPO against inactivation by H_2O_2 and $^1O_2$. The formation of $^1O_2$ was initiated by the addition of 0.5 M H_2O_2 and 5 mM Cl^-. At selected time intervals samples were taken and the brominating activity of the VCPO assayed.
Reproduced from ref. 27 with permission from John Wiley and Sons, Copyright © 2003 WILEY-VCH Verlag GmbH & Co. KGaA, Weinheim.

emulsions and fully stable for at least 10 h converting H_2O_2 in a constant flow of $^1O_2$.[25] This makes the enzyme a viable alternative for inorganic systems.

24.2.4 Use of VCPO in Decarboxylation of Amino Acids

Nitriles are important building blocks in the synthesis of a variety of pharmaceuticals, in polymer production or as industrial solvents such as acetonitrile. Many methods to produce them are available but they are either energy-intensive or use toxic chemicals (*e.g.*, HCN) and there is clearly a need for greener alternatives. In this respect, VCPO may be a viable alternative. When the amino acid phenylalanine and glutamate are exposed to the enzyme in the presence of Br^- and H_2O_2 at pH 5.6 the amino acids are decarboxylated[31] resulting in the formation of the corresponding nitriles (phenylacetonitrile and 3-cyanopropanoic acid). The amino group of the amino acid reacts with HOBr forming a N-bromo-intermediate that decays to 3-cyanopropanoic acid and CO_2 (Scheme 24.1).

This scheme shows that Br^- is regenerated and thus the reaction is catalytic in bromide. Since the K_m for bromide oxidation is very small (<10 μM, see Table 24.1) only a catalytic amount of bromide is needed. Other amino acids are also converted by this enzymatic system, *e.g.*, phenylalanine into phenylacetonitrile. However, in this conversion not only phenylacetonitrile is formed but also the corresponding aldehyde as a side product. This oxidative decarboxylation catalysed *via* formation of HOBr may have a potential application in the valorisation of biomass that is rich in glutamic acid.[31]

24.2.5 Sulphoxidation by VBPO and VCPO

Optically active sulphoxides are important synthons in particular for the preparation of biologically active compounds and they also function as carriers of chiral information in asymmetric transformations. No general method is available to synthesise these compounds. Several oxidoreductases catalyse the enantioselective sulphoxidation of a variety of sulphides and also the VBPO's have been successfully used in this reaction[10] though the k_{cat} values of enantioselective sulphoxidations (1 min^{-1}) are in general much slower than the k_{cat} of the brominating activity (166 s^{-1}) of for example the VBPO from *A. nodosum.*[32] In contrast to VBPO, VCPO is not capable of a direct and selective oxygen transfer to methyl phenyl sulphide and a racemic mixture is formed. It has been suggested[33] that the aromatic sulphide is directly oxidised by the very reactive peroxido enzyme intermediate by one

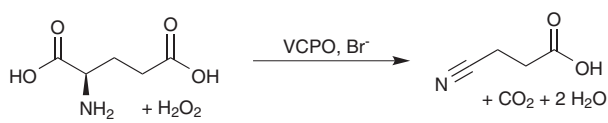

Scheme 24.1 Enzymatic oxidative decarboxylation of glutamic acid into 3-cyanopropanoic acid by vanadium chloroperoxidase from *C. inaequalis*.

electron and the formed positively charged sulphur radical decays to the racemic sulphoxide.

24.2.6 Halogenation of Phenolics and Alkenes by Haloperoxidases

Chemical halogenation of organic compounds by elementary halogens or hypohalous acids suffers from the high reactivity of the reagents leading to unwanted side products and the direct use of these reagents requires special non-corrosive equipment. *N*-halocompounds as halogenating agents may also be used but these need to be halogenated as well, causing significant organic waste. Similarly, vanadium-based catalysts may be used,[34] but in general the turnover is low. Transition metals such as W and V and vanadium peroxides have been shown to be useful in the conversion of olefins to halohydrines.[35–37] The best method from a green-chemistry perspective would be the generation of halogenating species from halides by the oxidant H_2O_2 or O_2.[38] Alternatively oxone[39] (potassium monopersulphate) in the presence of alkali metal bromides may be used to obtain brominated compounds. Given the importance of organohalogens, the use of enzymes able to halogenate compounds under mild conditions is becoming more and more attractive since the process may be greener and more selective. Several studies and reviews have appeared[14,40–43] in which the application of the heme chloroperoxidase form *Caldariomyces fumago* in halogenation of several compounds is discussed. The popularity of using this enzyme in conversions is mainly due to the fact that it is commercially available and its initial high turnover frequency (1000 s^{-1}) but it is rapidly inactivated by moderate peroxide concentrations.[44] In addition, the activity of the heme CPO is readily eliminated at temperatures above 50 °C and storage at slightly elevated temperatures leads to inactivation.[45]

Alternatively, the VBPO from *Ascophyllum nodosum* can be used in the synthesis of brominated organic compounds and several studies have appeared[10] of the successful application of this enzyme in the synthesis of brominated phenols, barbituric derivatives and pyrroles. In particular, the controlled and slow generation of HOBr in solution allows more specific bromination of a susceptible site on the organic substrate.[46] However, though the VBPO may be purified in pretty large amounts[10] from its natural source (*e.g.*, the seaweed *Ascophyllum nodosum)* this source is not universally accessible. To date, successful methods to express this enzyme or other VBPO's in sufficient amounts from seaweeds have failed due to the formation of insoluble inclusion bodies from which it is difficult to obtain active enzyme. Also, this VBPO is only moderately resistant towards oxidative inactivation by H_2O_2.[27,47]

A much better alternative may be the VCPO considering its superb stability and the fact that it can easily expressed in sufficient amounts in convenient hosts.[21,30,48] Recently the VCPO was also successfully His-tagged without any effect on known enzymatic parameters (unpublished results). Despite this

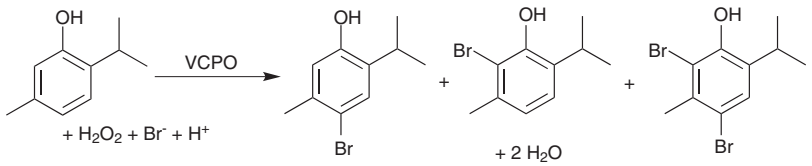

Scheme 24.2 Bromination of thymol to 2-bromo, 4-bromo and 2,4-dibromothymol by VCPO.

only a few studies have appeared on the use of the enzyme in conversions. To investigate the feasibility of the VCPO in bromination and chlorination reactions, the electrophilic halogenation of thymol was chosen as model substrate.[24] Since the kinetic properties of the VCPO towards bromide or chloride (Table 24.1) differ it is difficult to compare the efficiency and specificity at the same pH or substrate concentrations. For example, it was observed that when using 10 mM of each halide at pH 5 and dosing the incubation every 30 min for 6 h with 1 mM H_2O_2 complete conversion of the thymol in brominated compounds was observed (see Scheme 24.2) whereas when chloride was used the conversion was only 50%. In this bromination reaction an apparent turnover frequency of 55 s^{-1} was found.

This bromination process is kinetically controlled. In the initial stage of the reaction first 2-bromo- and 4-bromo thymol are formed which are subsequently converted into the 2,4-dibromothymol. Up-scaling the process to obtain synthetic useful amounts is hampered by the fact that high bromide concentrations (>10 mM) inhibit the reaction[29] and bromide was added continuously to the incubation. Further thymol poorly dissolves in water and 50% of ethanol had to be used as co-solvent. This semi-preparative method yielded 0.09, 0.69 and 0.14 g of 2-bromo-,4-bromo- and 2,4-dibromothymol, respectively. The turnover frequencies obtained[24] are high, up to 55 s^{-1} and close to the maximum value of 250 s^{-1} that can be obtained for the enzyme under optimal conditions (see Table 24.1). A total turnover number of 2×10^6 can be calculated from the data. This illustrates the robustness of this enzyme and its insensitivity to hydrogen peroxide which makes this enzyme a better catalyst than the heme-containing chloroperoxidase from *Caldariomyces fumago* for which the concentration of added hydrogen peroxide has to be carefully controlled,[40] and an even better catalyst than the vanadium bromoperoxidase.[46]

24.2.7 Formation of Halohydrins and Epoxides

Halohydrins are useful intermediates in the synthesis of more complex compounds and can easily be converted into epoxides. Classical chemical methods to obtain halohydrins suffer from the formation of side products and the corrosive conditions that have to be used. Haloperoxidases have been used early on[49] to produce α,β halohydrins on an analytical scale from gaseous alkenes (ethylene, propylene, 1-butene, 2-butene, isobutylene,

butadiene and allene) using the heme CPO from *Caldariomyces fumago* and bovine lactoperoxidase. These enzymes are very susceptible to hydrogen peroxide and the concentration used (30 mM) prevented long incubation times and sufficient yields. In 1988 the formation of the bromohydrins by a peroxidase[50] – later shown to be a VBPO[51] from the red seaweed *Corallina pilulifera* – was reported. Substrates were substituted alkenes, including cyclohexene, styrene, transcinnamyl alcohol, trans-cinnamic acid and *cis*-propenylphosphonic acid. The results showed that the products formed result from hypohalous addition across the carbon–carbon bond forming a bromonium intermediate. As shown in Section 24.2.6, the use of vanadium CPO may be a much better biocatalytic alternative and this was evaluated[52] using the halohydroxylation of styrene as a model reaction (see Scheme 24.3).

Indeed, full conversion and formation of bromohydrin were obtained at the pH optimum of the enzyme (pH 5) with only traces of side products. When chloride was used as a substrate, the corresponding chlorohydrin was formed. As expected from a process in which the enzyme produces HOBr or HOCl, enantioselectivity is not observed. At more alkaline pH values more epoxide is formed in line with the base-catalysed intramolecular ring closure. In the presence of 170 mM hydrogen peroxide and 160 mM KBr 40 mM water soluble styrene-4-sulphonate was easily converted within 6.5 h into it the corresponding bromohydrin by 0.1 μM VCPO. The data showed that the VCPO performed 0.4×10^6 catalytic turnovers which could be increased to 1.3×10^6 by increasing the concentration of both the styrene-4-sulphonate and the KBr concentrations. The turnover frequency initially was 69 s^{-1} but decreased to 15 s^{-1} at a later stage of the reaction. The values of these kinetic parameters are close to those obtained in bromination of thymol by VCPO. The substrate scope of the enzymatic halogenation is large. In the presence of ethanol as a co-solvent for the poorly soluble substrates, various aromatic and aliphatic alkenes were converted into the corresponding halohydrins with satisfactory yields (60–88%). In general, at the same halide concentration the yields with bromide are higher. Preparative scale (1.1 g) reactions of some alkenes were also reported.[52]

Transformation of the formed halohydrins into the corresponding epoxides is also possible. This ring closure occurs spontaneously at alkaline pH. However, the VCPO (pH optimum 5) is only active at slightly acidic pH values. A two-step procedure was carried out[52] in which first the halohydrin is formed enzymatically followed by a pH increase to pH 10. This approach was successful for most of the aromatic and aliphatic alkenes.

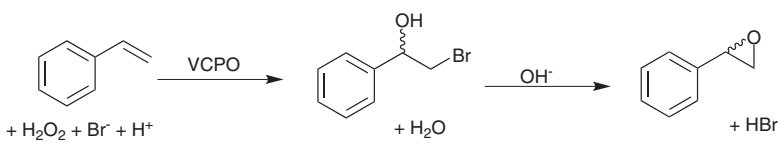

Scheme 24.3 Enzymatic formation of α,β-bromohydrin from styrene.

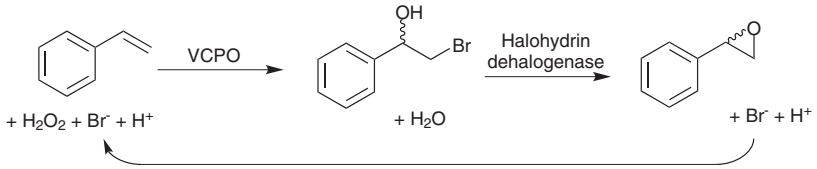

Scheme 24.4 Enzymatic cascade for the conversion of alkenes into epoxides.

An enzymatic cascade in a one-pot procedure was also developed[52] using the halohydrin dehalogenase that will catalyse the ring closure at more neutral pH values (pH 7, see Scheme 24.4). Only 33% of the styrene was converted into the epoxide. However, the low yield is due to a mismatch of the pH optima, the dehalogenase has a pH optimum of 8–9 whereas that of VCPO is 5–5.5. Combining a halohydrin dehalogenase with haloperoxidase to obtain epoxides *via* an alternate pathway has been proposed before.[49] However, details of this study are lacking.

This enzymatic cascade has the advantage that bromide is regenerated in the reaction and, thus, catalytically present.

The group of Dordick[53] reported a very peculiar reaction. VCPO from *C. inaequalis* was shown to catalyse the hydroxylation, bromination and demethylation of 2,4,6-trinitrotoluene (TNT) in the presence of H_2O_2 and Br^- under alkaline conditions (pH 8). This is a surprising result considering the pH optimum of the enzyme (5–5.5) and the very low brominating activity at pH 8 (1 s^{-1}, See Table 24.1). No follow-up study has been reported.

24.2.8 Haloetherification by Bromoperoxidases

Using the VBPO's from marine red algae it was shown that the monoterpene nerol and sesquiterpene (*E*)-(+)-nerolidol were brominated and cyclised to a cyclic ether.[54,55] However, the yield (5%) was low and bromohydrins and epoxides were also formed. It is likely the enzymes form a bromonium ion that reacts at the alkene to form a bromonium intermediate, which, by a nucleophilic reaction with a nearby alcohol group, results in a cyclic bromoether structure.

24.2.8.1 Halolactonisation of Unsaturated Carboxylic Acids by VCPO

Bromolactonisation has been studied[56–58] in the past using the heme lactoperoxidase from milk and a bromoperoxidase (BPO) from *Laurencia nipponica*. In these studies, it was shown that these enzymes catalysed the intramolecular cyclisation of (3*E*)- and (3*Z*)-laurediol to the 8-membered bromoethers (*E*)-deacetyllaurencin and (*Z*)-prelaureatin. However, the yields of brominated cyclic lactones were very low. Bromolactonisation of 4-pentynoic acid and formation of a brominated furanone using the VBPO from the red alga *Delisea pulchra* was also reported.[59]

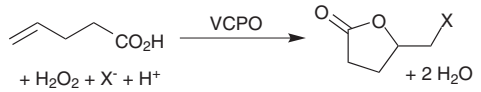

Scheme 24.5 Halolactonisation of 4-pentenoic acid into 5-(bromomethyl)dihydro-2(3*H*)-furanone.

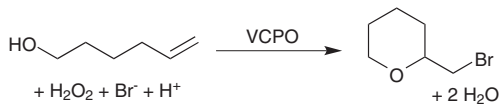

Scheme 24.6 The etherification 40 mM of 5-hexen-1-ol into 2-(bromomethyl)tetrahydro-2*H*-pyran.

Recently it was shown that γ,δ-unsaturated carboxylic could also be halocyclised by VCPO.[48] Using 4-pentenoic acid as a substrate (Scheme 24.5) the corresponding halolactones could easily be obtained.

It was possible to prepare 0.91 and 1.4 g of the chloro-and bromolactone products from 10 mMol 4-pentenoic acid corresponding to 70% and 80% isolated yield. Also, a number of γ,δ unsaturated carboxylic acids were converted into the corresponding brominated or chlorinated cyclic lactones. As could be expected, the reaction proceeded optimally at pH 5. In most cases the conversion was 100%.

24.2.8.2 Conversions of Alkenols into Haloethers by VCPO

Haloetherification was also studied[48] using 5-hexen-1-ol as a substrate (see Scheme 24.6) and could be converted into 36 mM 2-(bromomethyl)tetrahydro-2*H*-pyran within 24 h.

This corresponds to a total turnover number of 360 000. It was possible to convert several other alkenols into the corresponding chloro- or bromoethers with good selectivity. The potential environmental benefits of the enzymatic process compared to the chemical proces using bromosuccinimide as a brominating agent were also demonstrated.[48] The mass intensities are comparable, but the chemical process yielded more waste.

24.2.9 Achmatowicz Reaction Catalysed by VCPO

The Achmatowicz reaction in which α-heterosubstituted furfural derivatives are oxidatively converted into six-membered O- or N-heterocyclic building blocks gives access to range of useful building blocks. In this reaction the furan ring is oxidatively activated using for example *m*-chloroperbenzoic acid or bromine.[60,61] Also biocatalytic conversions have been reported. For example, the heme chloroperoxidase from *Caldariomyces fumago* has been used in the selective oxidation of furfuryl alcohols.[62] However, the supply of H_2O_2 has to be carefully tuned in order to avoid oxidative inactivation of the

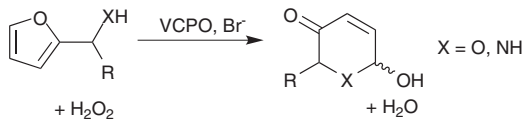

Scheme 24.7 The (aza)-Achmatowicz conversion mediated by VCPO.

peroxidase. The very robust VCPO has been exploited[63] in an (aza)-Achmatowicz reaction in which functionalised piperidinones or substituted pyranones are formed (see Scheme 24.7).

As expected, the oxidation of furfural derivatives proceeded optimally at pH 5 and for the aza-Achmatowicz reaction to proceed only low amounts of bromide were needed. This prompted the group[63] to carry out the reaction in seawater which was buffered 1 : 1 with 0.1 M citrate buffer (pH 5) as a source of bromide. Indeed, conversion of *N*-Boc protected 3-aminofuran was observed though the rate was significantly slower than in defined buffers. This was attributed to the high concentration of chloride in seawater and its inhibitory effect. Several furanyl derivatives[63] were fully converted into substituted piperidinones and prepared on a semi-preparative scale (about 0.2 g) using a reaction medium of ethanol with 100 mM citrate buffer at pH 5 [1 : 1 (v/v)] to solubilise the substrates. The turnover frequency was 8.7 s^{-1} and the total turnover number was larger than 10^6. It was also possible to obtain a substituted pyranone *via* the Achmatowicz rearrangement of a furfural alcohol. The use of VCPO in these rearrangements has several advantages. Since the enzyme remains active in mixtures of water and water-soluble organics high concentrations of the substrates can be reached. In contrast, the heme chloroperoxidase from *C. fumago* rapidly denatures in these mixtures. Further, unlike the heme chloroperoxidase from *C. fum*ago,[62] there is no need to control the H_2O_2 concentration.

24.3 Conclusion and Prospects

In many pharmaceuticals, halogens are introduced to increase their activity and halogenated compounds are intermediates in the synthesis of more complex molecules, *e.g.*, the Suzuki-Miyaura palladium catalysed cross-coupling of brominated compounds. In general, the halogenation processes require deleterious reagent, most reaction conditions are corrosive and waste is formed. There is clearly a need for other methods that are more environment-friendly and can be carried out under mild conditions. The research by the Hollmann group on the VCPO illustrates that such a viable enzymatic halogenation method exists and that the enzymatic halogenating methods can be carried out under very mild condtions. The only drawback of the enzymatic halogenation using this class of enzymes is that the halogenation of organic compounds by the hypohalous acids formed will not be regio- or stereoselective. Further the enzyme is not yet commercially available. Nevertheless, the results show that enzymatic halogenation should be

part of the toolbox of organic chemists. Other applications of these VCPOs have also been envisaged based on their stability and on the formation of HOCl and HOBr. Hypohalites have antimicrobial and bleaching properties and patent applications describing the use of VCPO on these subjects are abundant.[64]

References

1. A. M. Held, D. J. Halko and J. K. Hurst, *J. Am. Chem. Soc.*, 1978, **100**, 5732.
2. R. Wever, M. G. M. Tromp, B. E. Krenn, A. Marjani and M. van Tol, *Environ. Sci. Technol.*, 1991, **25**, 446.
3. R. Wever and M. A. van der Horst, *Dalton Trans.*, 2013, **42**, 11778.
4. E. de Boer and R. Wever, *J. Biol. Chem.*, 1988, **263**, 12326.
5. V. Martínez Martínez, G. De Cremer, M. B. J. Roeffaers, M. Sliwa, M. Mukulesh, D. E. De Vos, J. Hofkens and B. F. Sels, *J. Am. Chem. Soc.*, 1988, **130**, 13192.
6. Y. Liu, D. C. O. Thornton, T. S. Bianchi, W. A. Arnold, M. R. Shields, J. Chen and S. A. Yvon-Lewis, *Environ. Sci. Technol.*, 2015, **49**, 3366.
7. P. Coughlin, S. Roberts, C. Rush and A. Willets, *Biotechnol. Lett.*, 1993, **15**, 907.
8. A. Butler and J. N. Carter-Franklin, *Nat. Prod. Rep.*, 2004, **211**, 180.
9. R. Wever, in *Vanadium Biochemical and Molecular Biological Approaches*, ed. H. Michibata, Springer, Dordrecht, Heidelberg, London, New York, ch. 5, 2012, p. 95.
10. R. Wever, B. E. Krenn and R. Renirie, *Methods Enzymol.*, 2018, **605**, 141.
11. R. Wever and P. Barnett, *Chem. – Asian, J.*, 2017, **12**, 1997.
12. S. M. K. McKinnie, Z. D. Miles and B. S. Moore, *Methods Enzymol.*, 2018, **604**, 405.
13. V. Agarwal, Z. D. Miles, J. M. Winter, A. S. Eustaq́uio, A. El Gamal and S. M. Moore, *Chem. Rev.*, 2017, **117**, 5619.
14. J. Latham, E. Brandenburger, S. A. Shepherd, B. R. K. Menon and J. Micklefield, *Chem. Rev.*, 2018, **118**, 232.
15. C. Leblanc, H. Vilter, J. B. Fournier, L. Delage, P. Potin, E. Rebuffet, G. Michel, P. L. Solari, M. C. Feiters and M. Czjzek, *Coord. Chem. Rev.*, 2015, **301–302**, 134.
16. G. Xu and B.-G. Wang, *PLoS One*, 2016, **11**, e0154619.
17. E. G. M. Vollenbroek, L. H. Simons, J. W. P. M. van Schijndel, P. Barnett, M. Balzar, H. L. Dekker, C. van der Linden and R. Wever, *Biochem. Soc. Trans.*, 1995, **23**, 267.
18. P. Barnett, W. Hemrika, H. L. Dekker, A. O. Muijsers, R. Renirie and R. Wever, *J. Biol. Chem.*, 1998, **273**, 23381.
19. A. Messerschmidt and R. Wever, *Proc. Natl. Acad. Sci. U. S. A.*, 1996, **93**, 392.
20. A. Messerschmidt, L. Prade and R. Wever, *Biol. Chem.*, 1997, **378**, 309.
21. W. Hemrika, R. Renirie, S. Macedo-Ribeiro, A. Messerschmidt and R. Wever, *J. Biol. Chem.*, 1999, **274**, 23820.

22. S. Macedo-Ribeiro, W. Hemrika, R. Renirie, R. Wever and A. Messerschmidt, *J. Biol. Inorg. Chem.*, 1999, **4**, 209.
23. J. W. M. Van Schijndel, P. Barnett, J. Roelse, E. G. M. Vollenbroek and R. Wever, *Eur. J. Biochem.*, 1994, **225**, 151.
24. E. Fernández-Fueyo, M. van Wingerden, R. Renirie, R. Wever, Y. Ni, D. Holtmann and F. Hollmann, *ChemCatChem*, 2015, **7**, 4035.
25. R. Renirie, C. Pierlot, R. Wever and J.-M. Aubry, *J. Mol. Catal. B: Enzym.*, 2009, **56**, 259.
26. N. Tanaka, V. Dumay, Q. Liao, A. J. Lange and R. Wever, *Eur. J. Biochem.*, 2002, **269**, 2162.
27. R. Renirie, C. Pierlot, J.-M. Aubry, A. F. Hartog, H. E. Schoemaker, P. L. Alsters and R. Wever, *Adv. Synth. Catal.*, 2003, **345**, 849.
28. J. W. M. Van Schijndel, E. G. M. Vollenbroek and R. Wever, *Biochim. Biophys. Acta*, 1993, **1161**, 249.
29. N. Tanaka, Z. Hasan and R. Wever, *Inorg. Chim. Acta*, 2003, **356**, 288.
30. Z. Hasan, R. Renirie, R. Kerkman, H. J. Ruijssenaars, A. F. Hartog and R. Wever, *J. Biol. Chem.*, 2006, **281**, 9738.
31. A. But, J. Le Nôtre, E. L. Scott, R. Wever and J. P. M. Sanders, *ChemSusChem*, 2012, **5**, 1199.
32. H. B. Ten Brink, A. Tuynman, H. L. Dekker, W. Hemrika, Y. Izumi, T. Oshiro, H. E. Schoemaker and R. Wever, *Inorg. Chem.*, 1998, **37**, 6780.
33. H. B. Ten Brink, H. E. Schoemaker and R. Wever, *Eur. J. Biochem.*, 2001, **268**, 132.
34. S. Patra, S. Chatterjee, T. K. Si and K. K. Mukherje, *Dalton Trans.*, 2013, **42**, 13425.
35. B. F. Sels, D. E. De Vos and P. A. Jacobs, *J. Am. Chem. Soc.*, 2001, **123**, 8350.
36. M. Ghiacia, M. E. Sedaghata, S. Ranjbaria and A. Gilb, *Appl. Catal., A*, 2010, **384**, 18.
37. V. Conte and B. Floris, *Inorg. Chim. Acta*, 2010, **363**, 1935.
38. A. Podgorsek, M. Zupan and J. Iskra, *Angew. Chem., Int. Ed.*, 2009, **48**, 8424.
39. K. Moriyama, C. Nishinohara, T. Sugiue and H. Togo, *RSC Adv.*, 2015, **5**, 85.
40. L. Getrey, T. Krieg, F. Hollmann, J. Schrader and D. Holtmann, *Green Chem.*, 2014, **16**, 1104.
41. K. M. Manoj and L. P. Hager, *Biochemistry*, 2008, **47**, 2997.
42. R. Vazquez, M. Ayala and F. J. Marquez- Rocha, *Phytochemistry*, 2001, **58**, 929.
43. G. T. Höffler, A. But and F. Hollmann, *Org. Biomol. Chem.*, 2019, **17**, 9267.
44. M. Ayala, C. V. Batista and R. Vazquez-Duhalt, *J. Biol. Inorg. Chem.*, 2011, **16**, 63.
45. M. A. Pickard and A. Hashimoto, *Can. J. Microbiol.*, 1988, **34**, 998.
46. F. Sabuzi, E. Churakova, P. Galloni, R. Wever, F. Hollmann, B. Floris and V. Conte, *Eur. J. Inorg. Chem.*, 2015, 3519.

47. R. R. Everett, J. R. Kanofsky and A. Butler, *J. Biol. Chem.*, 1990, **265**, 4908.
48. S. H. H. Younes, F. Tieves, D. Lan, Y. Wang, P. Süss, H. Brundiek, R. Wever and F. Hollmann, *ChemSusChem*, 2020, **13**, 97–101.
49. J. Geigert, S. L. Neidleman, D. J. Dalietos and S. K. DeWittt, *Appl. Environ. Microbiol.*, 1983, **45**, 366.
50. N. Itoh, A. K. M. Q. Hasan, Y. Izumi and H. Yamada, *Eur. J. Biochem.*, 1988, **172**, 477.
51. B. E. Krenn, Y. Izumi, H. Yamada and R. Wever, *Biochim. Biophys. Acta*, 1989, **998**, 63.
52. J. J. Dong, E. Fernández-Fueyo, J. Li, Z. Guo, R. Renirie, R. Wever and F. Hollmann, *Chem. Commun.*, 2017, **53**, 6207.
53. I. Z. Munir, S. Hu and J. S. Dordick, *Adv. Synth. Catal.*, 2002, **344**, 1097.
54. N. Carter-Franklin, J. D. Parrish, R. A. Tschirret-Guth, R. D. Little and A. Butler, *J. Am. Chem. Soc.*, 2003, **125**, 3688.
55. J. N. Carter-Franklin and A. Butler, *J. Am. Soc.*, 2004, **126**, 15060.
56. A. Fukuzawa, Y. Takasugi, A. Murai, M. Nakamura and M. Tamura, *Tetrahedron Lett.*, 1992, **33**, 2017.
57. A. Fukuzawa, M. Aye, Y. Takasugi, M. Nakamura, M. Tamura, M. Tamura and A. Murai, *Chem. Lett.*, 1994, **23**, 2307.
58. J. Ishihara, N. Kanoh and A. Murai, *Tetrahedron Lett.*, 1995, **36**, 737.
59. M. Sandy, J. N. Carter-Franklin, J. D. Martiny and A. Butler, *Chem. Commun.*, 2011, **47**, 12086.
60. D. Thiel, F. Blume, C. Jäger and J. Deska, *Eur. J. Org. Chem.*, 2018, 2717.
61. F. van der Pijl, F. L. van Delft and F. P. J. T. Rutjes, *Eur. J. Org. Chem.*, 2015, 4811.
62. D. Thiel, F. Blume, C. Jäger and J. Deska, *Eur. J. Org. Chem.*, 2018, 2717.
63. E. Fernández-Fueyo, S. H. H. Younes, S. van Rootselaar, R. W. M. Aben, R. Renirie, R. Wever, D. Holtmann, F. P. J. T. Rutjes and F. Hollmann, *ACS Catal.*, 2016, **6**, 5904.
64. R. Wever, in *Peroxidases and Catalases: Biochemistry, Biophysics, Biotechnology, and Physiology*, 2nd edn, ed. H. B. Dunford, John Wiley & Sons, Inc., ch. 25, 2010, p. 403.

CHAPTER 25

Vanadium Catalysis Relevant to Nitrogenase

HUNG-RUEI PAN AND HUA-FEN HSU*

Department of Chemistry, National Cheng Kung University, No.1, University Road, Tainan City 701, Taiwan
*Email: konopka@mail.ncku.edu.tw

25.1 Vanadium Nitrogenase

25.1.1 Introduction

Dinitrogen forms a triple bond with a bond energy of -946 kJ mol^{-1} which makes it a very difficult chemical bond to activate.[1] In contrast to the Haber–Bosch process utilized in industry to produce ammonia by reacting dinitrogen with hydrogen in the presence of iron at high pressures and temperatures,[2] biological nitrogen fixation is accomplished by nitrogenase conducted at ambient temperature and pressure.[3–5] The enzyme catalyzes the reduction of N_2 to NH_4^+ through the hydrolysis of ATP with the concomitant production of H_2.[6] According to the metal composition in the cofactor, it is generally categorized to three classes: molybdenum nitrogenase, vanadium nitrogenase and iron-only nitrogenase.[7,8] The three types of enzymes are highly homologous to each other and share similar structural features and functionality.[9–14] Mo-nitrogenase has been identified and studied more extensively compared to others.[4,15–18] However, over the past decade, studies of V-nitrogenase have provided important revelations regarding its structural and catalytic aspects. These two nitrogenases are very similar in their primary sequences.[14] The component proteins and the

Catalysis Series No. 41
Vanadium Catalysis
Edited by Manas Sutradhar, José Armando L. da Silva and Armando J. L. Pombeiro

Published by the Royal Society of Chemistry, www.rsc.org

cluster compositions of the cofactors are also very alike.[10] Vanadium ion was first known to enhance nitrogen fixation by diazotrophic microorganisms much earlier.[19] However, V-nitrogenase was confirmed in the 1980s through the generation of the protein strains lacking the structural genes of Mo-nitrogenase.[20,21] With these deletion strains, vanadium nitrogenase was isolated afterwards from *Azotobactor vinelandii*[22] and *Azotobactor chroococcum*.[23] Later on, Ribbe and co-workers were able to prepare the enzyme on a large scale by using a variant strain with a histidine-tagged VFe protein, further providing the basis for extensive biochemical studies.[10,24,25] More recently, Einsle and co-workers isolated an unmodified vanadium nitrogenase from molybdenum-depleted, actively nitrogen-fixing *A. vinelandii* wild-type cells.[26] This native protein can provide high-quality single crystals for X-ray diffraction analysis.[27–29]

25.1.2 Structure of V-nitrogenase

Vanadium nitrogenase, like its molybdenum counterpart, contains two protein components, the Fe protein and the VFe protein (see Figure 25.1).[27–29] The Fe protein structure was determined in the ADP-bound state and consists of homodimers.[29] The cuboidal-like [4Fe : 4S] cluster was located at the dimeric interface with the coordination of two cysteines from each monomer, analogous to the Fe protein found in Mo-nitrogenase (see Figure 25.2A). It is believed that two protein components form a complex to allow the ATP-dependent interprotein electron transfer from Fe protein to VFe protein for substrate reduction.

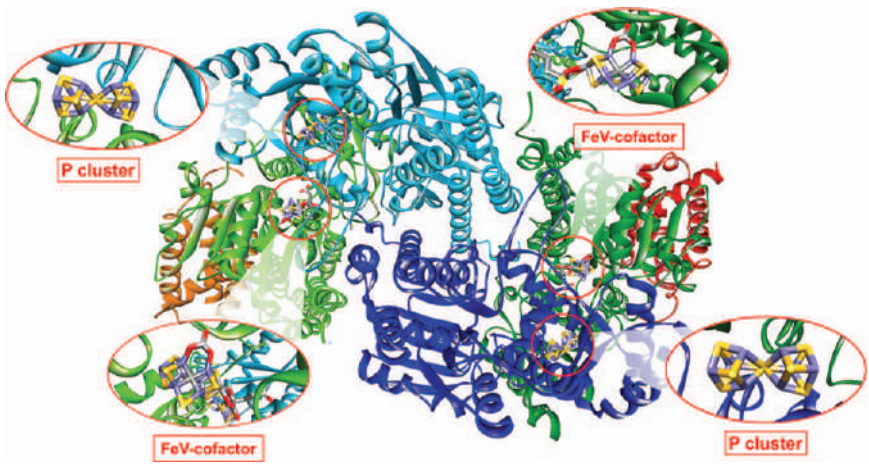

Figure 25.1 Crystal structure shown as ribbon diagrams of VFe protein in vanadium nitrogenase (pdb 5N6Y) with enlargements of P-cluster and FeV-cofactor. Each subunit of the hexamers is shown in a different color: VnfDD′ (light-green and emerald-green); VnfKK′ (sky-blue and primary-blue); VnfGG′ (red and orange).

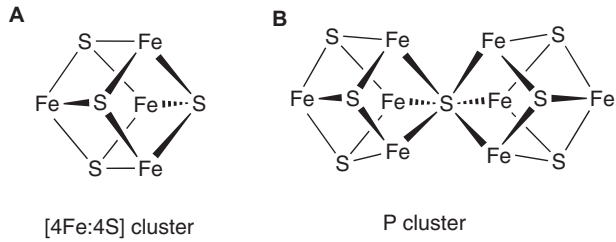

Figure 25.2 Structural drawings of [4Fe : 4S] cluster in Fe protein (A), and P-cluster in VFe protein (B).

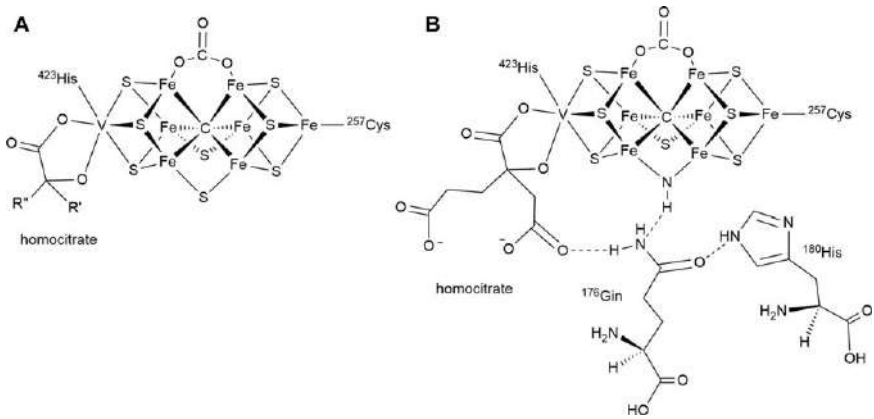

Figure 25.3 Structural drawings of FeV-cofactor in the resting state (based on pdb 5N6Y) (A), and an intermediate-bound state (based on pdb6FEA) (B).

The structure of VFe protein in the resting state has been resolved by X-ray crystallography with 1.35 Å resolution.[27] It consists of the $VnfD_2K_2G_2$ heterohexamer (see Figure 25.1). It is different from the MoFe protein of Mo-nitrogenase present in the same organism that the tetramer was found.[4] Two VnfG subunits are adjacent with VnfD subunits and with almost no contact with VnfK subunits. The role of VnfG for the reactivity of the VFe protein is not defined but is likely associated with the transfer of the FeV cofactor to the apoenzyme. The protein contains a P cluster and a FeV-cofactor. The P cluster is located in the interface of VnfD and VnfK subunits and has an [8Fe : 7S] moiety. The motif of the [8Fe : 7S] cluster can be considered as two [4Fe : 4S] clusters fused *via* a shared sulfide ion (see Figure 25.2). P cluster facilitates the electron transfer between the [4Fe4S] cluster in the Fe protein and catalytic site, FeV-cofactor.

The FeV-cofactor resides within the VnfD subunit and is the site where catalytic reactions occur. The cluster of the cofactor can be viewed as two cubanes, [4Fe–3S] and [V–3Fe–3S], bridged by two sulfide ions and one η^2-carbonate (see Figure 25.3). A carbonate ligand is not present in the X-ray structure of FeMo-cofactor where two cubanes are bridged by three sulfides.

However, like FeMo-cofactor, a μ^6-carbide is found inside the cluster, leading to a cluster composition of $[V:7Fe:8S:C:CO_3]$.[30,31] The cluster is linked to the protein backbone *via* a cysteine and a histidine binding to Fe and V on the apical positions of the cluster, respectively. Other than three bridging sulfides and one N_{His} donor, the six-coordinate vanadium center also binds to a η^2-homocitrate.

Very recently, an X-ray structure of vanadium nitrogenase with a bound intermediate was obtained.[28] Compared to the structure in the resting state, a μ^2-S is dissociated and the bridge is replaced by a N_2 reduced intermediate, a protonated nitrogen atom (see Figure 25.3). The bound NH moiety and dissociated HS^- ion have weak interaction through the hydrogen bonding network generated by neighboring amino acids and vanadium-bound homocitrate.

Interestingly, this labile bridging sulfide can be exchanged by CO in Mo-nitrogenase and was demonstrated in the X-ray structure of CO-bound Mo-nitrogenase.[17,32] According to these two structures, an intermediate (NH) bound VFe protein and an inhibitor (CO) bound MoFe protein, the NH- and CO-bound diiron site is likely the core for dinitrogen binding and activation.[33] A stepwise pathway of N_2 reduction on this diiron site of the FeMo-cofactor has been proposed based on spectroscopic investigation.[17] The intermediate-bound FeV-cofactor is likely associated with the E6 state in this proposed model.

25.1.3 Catalytic Features of V-nitrogenase

The catalytic efficiency of V-nitrogenase for the reduction of dinitrogen to ammonia is not as efficient as Mo-nitrogenase. In V-nitrogenase, 12 electrons are needed in order to reduce one N_2 molecule to two NH_3 molecules with the concomitant generation of three H_2 molecules from protons. The reaction accompanies the hydrolysis of ATPs to ADPs for electron transfer (see Reaction 25.1 in Scheme 25.1). Half of the electron flux is used in the production of H_2, burdening the enzyme with inefficiency. In contrast, Mo-nitrogenase is relatively more capable where only one hydrogen molecule is produced with one dinitrogen reduction (see Reaction 25.2 in Scheme 25.1).

Other than the reduction of dinitrogen to ammonia, nitrogenases can also reduce other substrates, such as H^+, C_2H_2 and HCN/CN^-. However, the catalytic profile varies between these two versions of enzymes (see Figure 25.4).[34–36] The reduction of H^+ is similar under Ar, but the product formation under C_2H_2 atmosphere is different. In the latter, V-nitrogenase has more H_2 forming and generates C_2H_4 and C_2H_6, in contrast to

$$N_2 + 12\ e^- + 12\ H^+ \longrightarrow 2\ NH_3 + 3\ H_2 \quad (25.1)$$

$$N_2 + 8\ e^- + 8\ H^+ \longrightarrow 2\ NH_3 + H_2 \quad (25.2)$$

Scheme 25.1

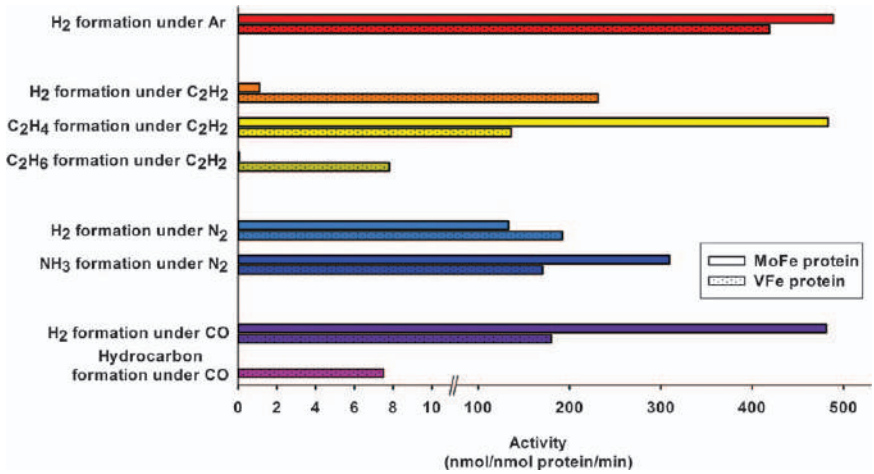

Figure 25.4 Catalytic features of vanadium and molybdenum nitrogenases for the reduction of H^+, N_2, C_2H_2 and CO.
Reproduced from ref. 36 with permission form John Wiley and Sons, Copyright © 2015 Wiley-VCH Verlag GmbH & Co. KGaA.

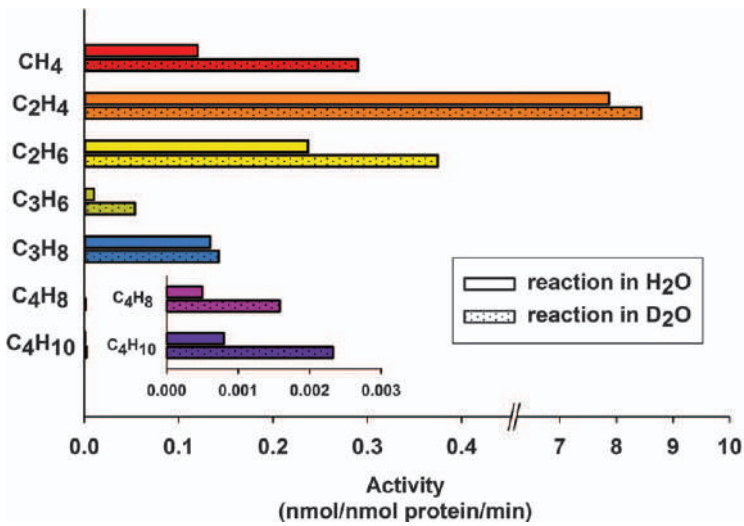

Figure 25.5 Activity of vanadium nitrogenases for hydrocarbon formation from CO in H_2O and D_2O.[38]

Mo-nitrogenase that generates less H_2, more C_2H_4 and no C_2H_6. Importantly, V-nitrogenase catalyzes the formation of hydrocarbons from CO. Such reactivity occurs much less in Mo-nitrogenase. The reduction of CO catalyzed by V-nitrogenase leads to the formation of CH_4, as well as C2–C4 hydrocarbons where C_2H_4 is the major species (see Figure 25.5).[37,38] The composition of the products is slightly different for the reactions carried in

H_2O and D_2O. Another exciting feature of V-nitrogenase is its capability of CO_2 reduction to generate CO, CD_4, C_2D_4 and C_2D_6.[39,40] Furthermore, the C3–C4 hydrocarbons are found when the reactions are conducted with isolated VFe protein and extracted FeV-cofactor.[41]

25.2 Vanadium Complexes as Catalysts for Substrates Relevant to Nitrogenase

25.2.1 Introduction

The Haber–Bosch process has been used for almost 100 years in industry for the synthesis of ammonia from dinitrogen and dihydrogen with an iron-based catalyst. It is very important for the further synthesis of fertilizers. However, the reaction runs at high temperature and pressure and is considered highly inefficient; it also contributes significantly to CO_2 emission and energy consumption.[42] Thus, it is an important topic to develop other nitrogen-fixation catalysts that are more advantageous than the Haber–Bosch process.[43] Transition-metal complexes are likely to serve this purpose. Aimed toward this goal, many examples have been shown to bind and activate dinitrogen and substrates relevant to nitrogenase. However, only a few cases show capability of fixing dinitrogen catalytically.[44] The first reported complex based on a well-defined metal center binding with a tetradentate triamidoamine ligand was developed by Schrock and co-workers (see Figure 25.6A).[45,46] The reaction is run at ambient temperature and pressure with mild reductants and four turnover number of catalysis is achieved. Several intermediates of this catalytic reaction were isolated and well characterized, indicating that N_2 was reduced at a sterically protected single Mo center with the oxidation state changing between III and VI. The catalytic N^2 reduction also occurs on dimolybdenum sites supported by PNP pincer ligand derivatives (see Figure 25.6B–D).[47–49] Another successful example reported earlier on is a *tris*(phosphine)borane iron(I) complex developed by Peters and co-workers. (see Figure 25.6E).[50] Considering N_2 is likely bound and activated at iron sites of FeMo and FeV cofactors in nitrogenases, the system demonstrated the likelihood that a single iron center can reduce N_2 catalytically. In addition, Ru and Os complexes bearing tris (phosphine)silyl ligands were also reported to be catalysts of N_2 reduction.[51]

25.2.2 Vanadium Catalyst for N_2 Reduction into NH_3 and N_2H_4

The development of synthetic vanadium complexes that serve as catalysts of nitrogen fixation is taking longer than molybdenum and iron complexes, which were established in 2003 and 2013, respectively.[45,50,52] Recently, Nishibayashi and co-workers reported a class of vanadium complexes that reduced N_2 to NH_3 and N_2H_4, serving as the first successful example of

vanadium-catalyzed dinitrogen reduction under mild conditions (see Figure 25.7).[53] The reaction occurs in Et_2O at low temperature (–78 °C) with KC_8 and $[H(OEt_2)_2][BAr^F{}_4]$ as external electron and proton sources, respectively. The best-performing catalyst in this system contains a four-coordinate vanadium(II) center bearing with a tridentate pyrrole-based PNP pincer ligand and and an aryloxy ligand. (see Figure 25.7A). When 200 equiv. reductants and 184 equiv. protons were used, 12 equiv. NH_3 and 2 equiv. N_2H_4 were produced, together yielding 16 equiv. fixed-N atoms based on the vanadium atom of the catalyst. Five-coordinate vanadium(III) complexes binding with the same PNP ligand and aryloxyl ligands, as well as a fifth donor, Cl^- or $NH_2{}^-$, produced less NH_3 and N_2H_4 with fixed N atom equivalents in the range of 2–8 (see Figure 25.7B-C). With the same supported ligand, a divanadium complex bridged by a μ-N_2 also demonstrated similar catalytic reactivity (see Figure 25.7D). It is worth mentioning that introducing an aryloxy ligand to the coordination sphere of the metal center is necessary for catalysis because the bulky effect of the ligand likely helps to stabilize N_2 binding at the V(II) center of the complex. A reaction pathway for the reduction of dinitrogen by this system was proposed according to the experimental observations combined with DFT calculations (see Figure 25.7). A V-NH_2 species such as complex **B** should likely prove to be one of the key intermediates.

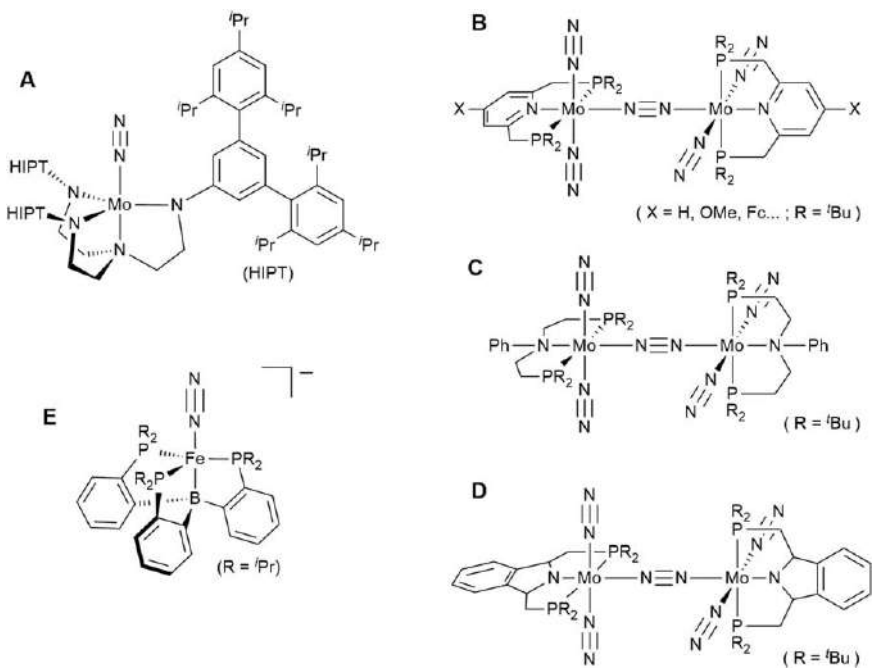

Figure 25.6 Examples of iron and molybdenum complexes serving as catalysts for N_2 reduction.

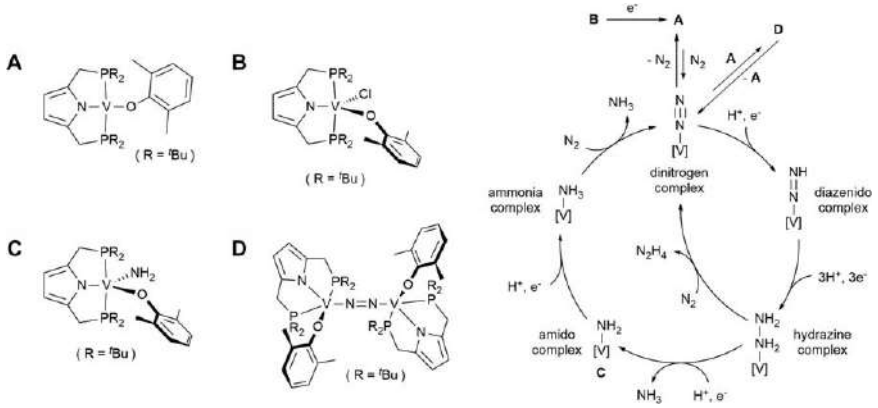

Figure 25.7 Examples of vanadium complexes serving as catalysts for N_2 reduction (left); and the proposed catalytic pathway for the reaction (right).[53]

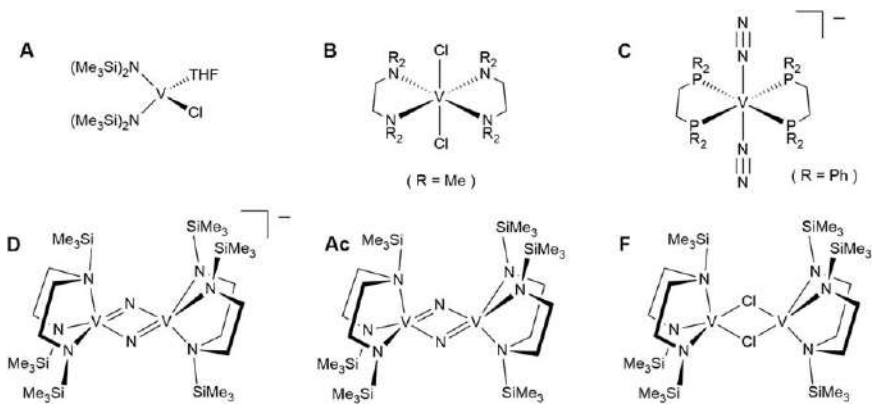

Figure 25.8 Examples of vanadium complexes serving as catalysts for silylation of N_2 into silylamine.

25.2.3 Vanadium Catalyst for Silylation of N_2 into Silylamine

Some vanadium complexes that fail to reduce dinitrogen to ammonia were found by Nishibayashi and coworkers to catalyze silylation of N_2 into silylamine under mild conditions (see Figure 25.8).[54] These include mononuclear *trans*-[VCl{N(SiMe$_3$)$_2$}$_2$(thf)] (**A**), *trans*-[VCl$_2$(tmeda)$_2$] (**B**) and [V(N$_2$)$_2$(dppe)$_2$]$^-$ (**C**), as well as bis(μ-nitrido)divanadium and bis(μ-Cl)divanadium complexes binding with silylamino(disilylamido) ligands (**D**–**F**). The reactions were carried out at room temperature with the addition of 600 equiv. Na and 600 equiv. (Me$_3$Si)Cl, giving (Me$_3$Si)$_3$N with turnover number in the range of 11–24.

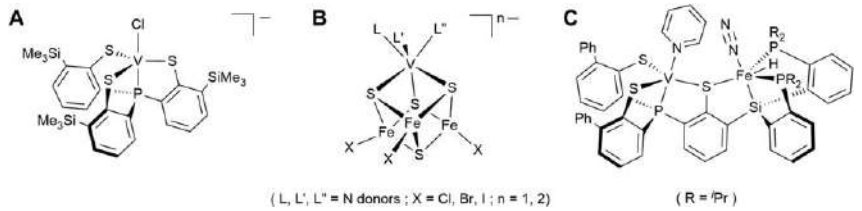

Figure 25.9 Examples of vanadium complexes serving as catalysts for reduction and disproportionation of N_2H_4 into NH_3.

25.2.4 Vanadium Catalyst for Reduction and Disproportionation of N_2H_4 into NH_3

Hydrazine is considered as a substrate as well as an intermediate of nitrogenase.[55,56] A combined biochemical-genetic investigative strategy revealed intermediates trapped in the catalytic cycle and were identified as N_2H_2 and N_2H_4 bound FeMo-cofactor through ENDOR/ESEEM spectroscopies – these are associated with the middle and late stages of nitrogen fixation, respectively.[16] The catalytic reduction of hydrazine to ammonia is likely associated with the late stage of biological nitrogen fixation. Synthetic examples that catalyzed such reactions are limited.[57–63] Only two examples exist where the catalytic reaction occurs at the vanadium center. One of them is a V(III) complex binding with a tetradentate tris(benzenethiolato)phosphine ligand with a chloride ion in the axial position (see Figure 25.9A).[64] This complex serves as a precursor for reducing N_2H_4 to NH_3 catalytically. With the presence of reductant and proton source, cobaltocene and 2,6-lutidinium chloride, respectively, the reaction can reach up to five turnovers in 48 hours. However, in the absence of an external proton source and reducing agent, the reaction of the complex and N_2H_4 does not produce ammonia. This indicates that the complex does not assist the disproportionation of N_2H_4. According to spectroscopic and electrochemical studies, it was proposed that hydrazine is bound and activated in a V(II) state. The other example for the catalytic reduction of N_2H_4 to NH_3 is a class of synthetic Fe/V/S clusters that contain the $[VFe^3S^4]^{2+}$ cuboidal core (see Figure 25.9B).[61] With the presence of cobaltocene and 2,6-lutidine hydrochloride as reductant and proton source, respectively, NH^3 was generated with the best efficiency of approximately 32 turnovers. The reaction rate varies with different V-coordinated terminal ligands, strongly suggesting that the V site of the $[VFe^3S^4]^{2+}$ cuboidal core is likely the center for substrate binding and activation. A heterobimetallic VFe complex with supporting thiolate, phosphine and silyl donors is demonstrated to have catalytic reactivity of N_2H_4 disproportionation with more than 500 turnovers (see Figure 25.9C). In contrast, monometallic analogues of V and Fe show poor activity, implying the catalytic reactivity is facilitated by bimetallic cooperativity.[65]

25.3 Conclusions

Vanadium ions have been found to associate with biological nitrogen fixation for almost a century; however, progress for understanding vanadium nitrogenase has been moving slowly, partially because of the challenge of isolating pure protein.[66] During the past decade, the understanding of vanadium nitrogenase in various aspects such as its function, structure and mechanism has been increasing much more due to the finding of protocols to prepare pure protein on a good scale. The enzyme not only catalyzes nitrogen fixation that converts dinitrogen to ammonia, but also catalytically reduces CO and CO_2 to various C2–C4 hydrocarbons, providing a potential application for renewable fuel generation. Although structural information by X-ray analysis including the enzyme in a resting state and an intermediate-bound state has been resolved recently, many questions remain, including a detailed stepwise mechanism for N_2 binding and activation.[33] Furthermore, whether the reduction of CO and CO_2 share a common pathway with N_2 reduction is unclear. In addition, although the diron site of the FeV-cofactor might be a potential binding pocket for substrate and intermediate, the role of the vanadium site is not yet well understood. It is noteworthy that the catalytic features in vanadium and molybdenum nitrogenases have different profiles; even FeV- and FeMo-cofactors have high degree of similarity. Perhaps the nature of heterometallic ions (V *versus* Mo) might be the key contributing to the differences between these two systems.

Although synthetic vanadium complexes are known to have a variety of catalytic applications,[67] the first series of vanadium catalysts for dinitrogen reduction was only reported recently by Nishibayashi and co-workers. Although the catalytic efficiency is poor, the example demonstrates that a vanadium ion in a well-tuned coordination environment has the ability of serving as a catalyst for N_2 reduction. Furthermore, several synthetic vanadium complexes have shown to catalyze the reduction and disproportionation of hydrazine to ammonia, which is associated with the late stage of biological fixation. Taken together, the examples of vanadium catalysts that carry the reactions relevant to nitrogenase are still very rare. It remains a great challenge to develop more systems that are capable of fixing dinitrogen. The optimal goals for investigating such systems are to provide a mechanistic understanding of nitrogenase, considering that vanadium is a key element in the enzyme, as well as an industrial application for ammonia synthesis and renewable energy generation.

References

1. T. A. Bazhenova and A. E. Shilov, *Coord. Chem. Rev.*, 1995, **144**, 69–145.
2. V. Smil, *Enriching the Earth: Fritz Haber, Carl Bosch, and the transformation of World Food Production*; The MIT Press: Cambridge, MA, 2004.
3. R. R. Eady, *Chem. Rev.*, 1996, **96**, 3013–3030.

4. J. B. Howard and D. C. Rees, *Chem. Rev.*, 1996, **96**, 2965–2982.
5. B. K. Burgess and D. J. Lowe, *Chem. Rev.*, 1996, **96**, 2983–3012.
6. L. C. Seefeldt, B. M. Hoffman, J. W. Peters, S. Raugei, D. N. Beratan, E. Antony and D. R. Dean, *Acc. Chem. Res.*, 2018, **51**, 2179–2186.
7. R. R. Eady and G. J. Leigh, *J. Chem. Soc., Dalton Trans.*, 1994, 2739–2747.
8. B. E. Smith, in *Advances in Inorganic Chemistry*, ed. A. G. Sykes, Academic Press, **vol. 47**, 1999, pp. 159–218.
9. Y. Hu and M. W. Ribbe, *Biochim. Biophys. Acta – Bioenerg.*, 2013, **1827**, 1112–1122.
10. Y. Hu and M. W. Ribbe, *JBIC, J. Biol. Inorg. Chem.*, 2015, **20**, 435–445.
11. X. Zhang, D. L. McRose, R. Darnajoux, J. P. Bellenger, F. M. M. Morel and A. M. L. Kraepiel, *Biogeochemistry*, 2016, **127**, 189–198.
12. D. L. McRose, X. Zhang, A. M. L. Kraepiel and F. M. M. Morel, *Front. Microbiol.*, 2017, 8.
13. D. F. Harris, D. A. Lukoyanov, S. Shaw, P. Compton, M. Tokmina-Lukaszewska, B. Bothner, N. Kelleher, D. R. Dean, B. M. Hoffman and L. C. Seefeldt, *Biochemistry*, 2018, **57**, 701–710.
14. F. Mus, A. B. Alleman, N. Pence, L. C. Seefeldt and J. W. Peters, *Metallomics*, 2018, **10**, 523–538.
15. D. Lawson and B. Smith, *Met. Ions Biol. Syst.*, 2002, **39**, 75–119.
16. B. M. Hoffman, D. R. Dean and L. C. Seefeldt, *Acc. Chem. Res.*, 2009, **42**, 609–619.
17. B. M. Hoffman, D. Lukoyanov, Z.-Y. Yang, D. R. Dean and L. C. Seefeldt, *Chem. Rev.*, 2014, **114**, 4041–4062.
18. B. M. Hoffman, D. Lukoyanov, D. R. Dean and L. C. Seefeldt, *Acc. Chem. Res.*, 2013, **46**, 587–595.
19. H. Bortels, *Zentralbl Bakt II Abt*, 1933, **87**, 476–477.
20. P. E. Bishop, R. Premakumar, D. R. Dean, M. R. Jacobson, J. R. Chisnell, T. M. Rizzo and J. Kopczynski, *Science*, 1986, **232**, 92–94.
21. P. E. Bishop, M. E. Hawkins and R. R. Eady, *Biochem. J.*, 1986, **238**, 437–442.
22. B. J. Hales, E. E. Case, J. E. Morningstar, M. F. Dzeda and L. A. Mauterer, *Biochemistry*, 1986, **25**, 7251–7255.
23. R. R. Eady, R. L. Robson, T. H. Richardson, R. W. Miller and M. Hawkins, *Biochem. J.*, 1987, **244**, 197–207.
24. C. C. Lee, Y. Hu and M. W. Ribbe, *Proc. Natl. Acad. Sci. U. S. A.*, 2009, **106**, 9209–9214.
25. Y. Hu, C. C. Lee and M. W. Ribbe, *Dalton Trans.*, 2012, **41**, 1118–1127.
26. D. Sippel, J. Schlesier, M. Rohde, C. Trncik, L. Decamps, I. Djurdjevic, T. Spatzal, S. L. A. Andrade and O. Einsle, *J. Biol. Inorg. Chem.*, 2017, **22**, 161–168.
27. D. Sippel and O. Einsle, *Nat. Chem. Biol.*, 2017, **13**, 956–960.
28. D. Sippel, M. Rohde, J. Netzer, C. Trncik, J. Gies, K. Grunau, I. Djurdjevic, L. Decamps, S. L. A. Andrade and O. Einsle, *Science*, 2018, **359**, 1484–1489.

29. M. Rohde, C. Trncik, D. Sippel, S. Gerhardt and O. Einsle, *JBIC, J. Biol. Inorg. Chem.*, 2018, **23**, 1049–1056.
30. T. Spatzal, M. Aksoyoglu, L. Zhang, S. L. A. Andrade, E. Schleicher, S. Weber, D. C. Rees and O. Einsle, *Science*, 2011, **334**, 940.
31. J. A. Rees, R. Bjornsson, J. Schlesier, D. Sippel, O. Einsle and S. DeBeer, *Angew. Chem., Int. Ed.*, 2015, **54**, 13249–13252.
32. T. Spatzal, K. A. Perez, O. Einsle, J. B. Howard and D. C. Rees, *Science*, 2014, **345**, 1620–1623.
33. K. L. Skubi and P. L. Holland, *Biochemistry*, 2018, **57**, 3540–3541.
34. R. R. Eady, T. H. Richardson, R. W. Miller, M. Hawkins and D. J. Lowe, *Biochem. J.*, 1988, **256**, 189–196.
35. M. J. Dilworth, R. R. Eady and M. E. Eldridge, *Biochem. J.*, 1988, **249**, 745–751.
36. C. C. Lee, J. A. Wiig, Y. Hu and M. W. Ribbe, in *Bioinspired Catalysis*, ed. W. Weigand and P. Schollhammer, , DOI: 10.1002/9783527664160.ch8, 2014, pp. 199–224.
37. C. C. Lee, Y. Hu and M. W. Ribbe, *Science*, 2010, **329**, 642.
38. Y. Hu, C. C. Lee and M. W. Ribbe, *Science*, 2011, **333**, 753–755.
39. J. G. Rebelein, Y. Hu and M. W. Ribbe, *Angew. Chem., Int. Ed.*, 2014, **53**, 11543–11546.
40. N. S. Sickerman, Y. Hu and M. W. Ribbe, *Chem. – Asian J.*, 2017, **12**, 1985–1996.
41. J. G. Rebelein, Y. Hu and M. W. Ribbe, *ChemBioChem*, 2015, **16**, 1993–1996.
42. J. W. Erisman, M. A. Sutton, J. Galloway, Z. Klimont and W. Winiwarter, *Nat. Geosci.*, 2008, **1**, 636–639.
43. S. D. Minteer, P. Christopher and S. Linic, *ACS Energy Lett.*, 2019, **4**, 163–166.
44. Y. Nishibayashi, *Dalton Trans.*, 2018, **47**, 11290–11297.
45. D. V. Yandulov and R. R. Schrock, *Science*, 2003, **301**, 76–78.
46. R. R. Schrock, *Angew. Chem., Int. Ed.*, 2008, **47**, 5512–5522.
47. K. Arashiba, Y. Miyake and Y. Nishibayashi, *Nat. Chem.*, 2011, **3**, 120; (a) S. Kuriyama, K. Arashiba, K. Nakajima, H. Tanaka, N. Kamaru, K. Yoshizawa and Y. Nishibayashi, *J. Am. Chem. Soc.*, 2014, **136**, 9719–9731; (b) S. Kuriyama, K. Arashiba, K. Nakajima, H. Tanaka, K. Yoshizawa and Y. Nishibayashi, *Chem. Sci.*, 2015, **6**, 3940–3951.
48. K. Arashiba, E. Kinoshita, S. Kuriyama, A. Eizawa, K. Nakajima, H. Tanaka, K. Yoshizawa and Y. Nishibayashi, *J. Am. Chem. Soc.*, 2015, **137**, 5666–5669.
49. A. Eizawa, K. Arashiba, H. Tanaka, S. Kuriyama, Y. Matsuo, K. Nakajima, K. Yoshizawa and Y. Nishibayashi, *Nat. Commun.*, 2017, **8**, 14874.
50. J. S. Anderson, J. Rittle and J. C. Peters, *Nature*, 2013, **501**, 84–87.
51. J. Fajardo and J. C. Peters, *J. Am. Chem. Soc.*, 2017, **139**, 16105–16108.
52. Y. Tanabe and Y. Nishibayashi, *Coord. Chem. Rev.*, 2019, **381**, 135–150.
53. Y. Sekiguchi, K. Arashiba, H. Tanaka, A. Eizawa, K. Nakajima, K. Yoshizawa and Y. Nishibayashi, *Angew. Chem., Int. Ed.*, 2018, **57**, 9064–9068.

54. R. Imayoshi, K. Nakajima and Y. Nishibayashi, *Chem. Lett.*, 2017, **46**, 466–468.
55. R. N. F. Thorneley, R. R. Eady and D. J. Lowe, *Nature*, 1978, **272**, 557–558.
56. B. M. Barney, T.-C. Yang, R. Y. Igarashi, P. C. Dos Santos, M. Laryukhin, H.-I. Lee, B. M. Hoffman, D. R. Dean and L. C. Seefeldt, *J. Am. Chem. Soc.*, 2005, **127**, 14960–14961.
57. R. R. Schrock, T. E. Glassman and M. G. Vale, *J. Am. Chem. Soc.*, 1991, **113**, 725–726.
58. E. Block, G. Ofori-Okai, H. Kang and J. Zubieta, *J. Am. Chem. Soc.*, 1992, **114**, 758–759.
59. R. R. Schrock, T. E. Glassman, M. G. Vale and M. Kol, *J. Am. Chem. Soc.*, 1993, **115**, 1760–1772.
60. D. Coucouvanis, P. E. Mosier, K. D. Demadis, S. Patton, S. M. Malinak, C. G. Kim and M. A. Tyson, *J. Am. Chem. Soc.*, 1993, **115**, 12193–12194.
61. S. M. Malinak, K. D. Demadis and D. Coucouvanis, *J. Am. Chem. Soc.*, 1995, **117**, 3126–3133.
62. Y. Chen, Y. Zhou, P. Chen, Y. Tao, Y. Li and J. Qu, *J. Am. Chem. Soc.*, 2008, **130**, 15250–15251.
63. M. Yuki, Y. Miyake and Y. Nishibayashi, *Organometallics*, 2012, **31**, 2953–2956.
64. W.-C. Chu, C.-C. Wu and H.-F. Hsu, *Inorg. Chem.*, 2006, **45**, 3164–3166.
65. N. X. Gu, G. Ung and J. C. Peters, *Chem. Commun.*, 2019, **55**, 5363–5366.
66. R. R. Eady, *Coord. Chem. Rev.*, 2003, **237**, 23–30.
67. R. R. Langeslay, D. M. Kaphan, C. L. Marshall, P. C. Stair, A. P. Sattelberger and M. Delferro, *Chem. Rev.*, 2019, **119**, 2128–2191.

Subject Index